Synthesis of $P2Y_{12}$ receptor antagonists as therapeutics and diagnostics

DISSERTATION

zur

Erlangung des Doktorgrades (Dr. rer. nat.)

der

Mathematisch-Naturwissenschaftlichen Fakultät

der

Rheinischen Friedrich-Wilhelms-Universität Bonn

vorgelegt von

Hashem Ali M. Al Musawi

aus

Al Hassa, Königreich Saudi-Arabien

Bonn 2025

Angefertigt mit Genehmigung der Mathematisch-Naturwissenschaftlichen

Fakultät der Rheinischen Friedrich-Wilhelms-Universität Bonn

Gutachterin/Betreuerin: Prof. Dr. Christa E. Müller

Gutachter: Prof. Dr. Finn Hansen

Tag der Promotion: 30.01.2026

Erscheinungsjahr: 2026

Die vorliegende Arbeit wurde in der Zeit von Januar 2020 bis August 2025 am Pharmazeutischen Institut der Rheinischen Friedrich-Wilhelms-Universität Bonn unter der Leitung von Frau Prof. Dr. Christa E. Müller angefertigt.

Table of contents

Abstract……1

1 Introduction……..……...3

1.1 G protein-coupled receptors (GPCRs) in drug discovery and development……....3

1.1.1 Structural features and roles of GPCRs in signal transduction…….……..…4

1.1.2 Classification of GPCRs……...…7

1.2 Purinergic signaling……8

1.3 P2Y receptors……...…9

1.4 $P2Y_{12}$ receptor……...……....11

1.4.1 $P2Y_{12}$ receptor antagonists..……...13

1.4.2 Anthraquinones as $P2Y_{12}$ receptor antagonists……...……15

1.4.3 Development of a $P2Y_{12}$ receptor antagonist radioligand……...16

1.5 The central nervous system (CNS) as a drug target……17

1.6 Passive diffusion and CNS penetration filtering……...……18

2 Aims of the study……...…...20

2.1 Improvement of the anthraquinone scaffold……..20

2.2 Research and development of potentially brain-permeable $P2Y_{12}$ receptor antagonists or radiolabeling……..……...……..21

3 Results and discussion……..24

3.1 Chapter I: Synthesis of anthraquinone-based $P2Y_{12}$ receptor antagonists: Structure-activity relationships……24

3.1.1 Introduction……..…..24

3.1.2 Results and discussion……....26

3.1.3 Conclusion and outlook……..35

3.1.4 Experimental part……...37

3.1.5 Supporting information……..42

3.2 Chapter II: Systematic development of anthraquinone-derived $P2Y_{12}$ receptor antagonists as radioligand candidates (Manuscript I)..……..……....61

3.2.1 Author contributions……...61

3.2.2 Abstract……..…61

3.2.3 Introduction……..……..62

3.2.4 Results and discussion……....63

3.2.5 Conclusions and outlook……..……..…69
3.2.6 Experimental part……..……69
3.2.7 Supporting information……..……75
3.3 Chapter III: $P2Y_{12}$ receptor antagonists: Evaluation of their potential as lead structures for brain therapeutics and diagnostics (Manuscript II)..……....81
3.3.1 Author contributions……...81
3.3.2 Abstract……..……82
3.3.3 Introduction……..……..82
3.3.4 Results and discussion……....84
3.3.5 Conclusions and outlook……..……..…..105
3.3.6 Supporting information……..……..107
3.4 Chapter IV: Selective, non-nucleotidic radiotracer for $P2Y_{12}$ receptors: Design, synthesis, characterization, and imaging of brain slices (Publication I)……...180
3.4.1 Publication summary……...….181
3.4.2 Author contributions……...……..182
3.5 Chapter V**:** Design, synthesis, and properties of brain-permeable $P2Y_{12}$ receptor antagonists for neuroinflammation diseases (Manuscript III)..……..…183
3.5.1 Author contributions…….....183
3.5.2 Abstract……...……183
3.5.3 Introduction……..184
3.5.4 Results and discussion……..…186
3.5.5 Conclusions and outlook……..……..……..193
3.5.6 Experimental part……..…...194
3.5.7 Supporting information……..……..210
4 Conclusions and outlook……...…….236
5 List of abbreviations…….…..……...…241
6 References……...……245
7 Appendices……...……...…259
7.1 Appendix I: Synthesis of anthraquinone-based $P2Y_{12}$ receptor antagonists: Structure-activity relationships……..….259
7.2 Appendix II: Systematic development of anthraquinone-derived $P2Y_{12}$ receptor antagonists as radioligand candidates (Manuscript I)..……....319
7.3 Appendix III: Selective, non-nucleotidic radiotracer for $P2Y_{12}$ receptors:

Design, synthesis, characterization, and imaging of brain slices (Publication I)..…530

7.4 Appendix IV: Design, synthesis, and properties of brain-permeable $P2Y_{12}$ receptor antagonists for neuroinflammation diseases (Manuscript III)..……..627

8 Acknowledgments……...……...……779

Abstract

The $P2Y_{12}$ receptor ($P2Y_{12}R$), a G protein-coupled receptor activated by adenosine diphosphate (ADP), has traditionally been associated with platelet aggregation and targeted for antithrombotic therapy. More recently, its expression on microglial cells in the central nervous system (CNS) has attracted considerable interest, as it plays a central role in neuroinflammatory processes and represents a promising biomarker for neurodegenerative diseases including Alzheimer's disease, Parkinson's disease, multiple sclerosis, and epilepsy. Targeting microglial $P2Y_{12}Rs$ enables modulation of its function and offers an avenue for imaging neuroinflammatory processes. In this context, the present dissertation focuses on the design, synthesis, characterization, and evaluation of novel $P2Y_{12}R$ antagonists, with particular emphasis on radiolabeled ligands, and blood-brain barrier (BBB)-permeable compounds for both therapeutic and diagnostic applications.

The first part of this work explores structural modifications of anthraquinone derivatives guided by molecular docking studies performed on sodium 1-amino-9,10-dioxo-4-((4-(phenylamino)-3-sulfonatophenyl)amino)-9,10-dihydroanthracene-2-sulfonate (**PSB-0739**), a potent and selective $P2Y_{12}R$ antagonist. These studies highlighted synthetic strategies to enable substitution at the C6- and C7-positions of the anthraquinone core and to modify the aniline moiety, followed by the synthesis of the targeted final compounds via Ullmann coupling. This systematic structure-activity relationship (SAR) study provided new insights into the chemical space surrounding the anthraquinone scaffold within the binding pocket and led to the synthesis of novel $P2Y_{12}R$ antagonist radioligand precursors as a basis for the development of radioligands.

In the second part, efforts were directed towards the development of radiolabeled anthraquinone-based $P2Y_{12}R$ antagonists. Radioligands hold promise as diagnostic tools for non-invasive imaging of microglial activation, thereby supporting early detection and monitoring of neurodegenerative disorders. However, the chemical instability of the 2-sulfo- and 2-carboxyanthraquinone derivatives, particularly the release of the C2-sulfonate or carboxylic acid groups under palladium-catalyzed hydrogenation conditions, has limited their use as indicated by three synthetic trials starting with three different precursors. To address this challenge, a model compound was developed and investigated to optimize key reaction parameters, including catalyst type, solvent system, and hydrogen pressure. These studies identified suitable conditions, thus laying the foundation for the preparation of radioligands suitable for imaging applications.

The third part of this dissertation shifts focus from anthraquinones to a systematic evaluation of published $P2Y_{12}R$ antagonists with regard to their suitability as CNS-permeable lead structures. Since microglial $P2Y_{12}Rs$ provide an attractive marker for imaging neuroinflammation through positron emission tomography (PET), identifying scaffolds with favorable BBB-penetration is of high relevance. A comprehensive review of available antagonists was performed, combining physicochemical property analysis with *in silico* CNS penetration filters and SAR assessment. This approach identified a pyrazolyl-phenyl-carbamoyl-indole scaffold as particularly promising. Within this series, substitution patterns were defined that improve potency and hold potential of CNS bioavailability. These findings provide a roadmap for the rational design of novel $P2Y_{12}R$ antagonists optimized for CNS applications.

Building on these evaluations, the fourth part of the work describes the development and pharmacological characterization of [^{3}H]PSB-22219, a novel non-nucleotidic $P2Y_{12}R$ antagonist radioligand. The unlabeled compound demonstrated high metabolic stability in rat liver microsomes and selectivity over other ADP-activated receptors. [^{3}H]PSB-22219 exhibited high-affinity binding to human $P2Y_{12}Rs$ expressed in recombinant cell systems (K_D = 4.57 nM) with very low nonspecific binding. Importantly, radioligand binding assays confirmed nanomolar affinity to native receptors in human platelets (K_D = 2.53 nM), rat brain cortex (K_D = 5.35 nM), and mouse microglia (K_D = 269 nM), with microglia displaying exceptionally high receptor density. Autoradiography studies further demonstrated visualization of human $P2Y_{12}R$ expression in the brain of a humanized rat model. Together, these results establish [^{3}H]PSB-22219 as a valuable pharmacological tool for probing $P2Y_{12}R$ biology and as a promising candidate for radiodiagnostic development.

Finally, the lead structure [^{3}H]PSB-22219 was taken as a starting point for the design, synthesis, and establishment of structure-property relationship (SPR) studies to identify novel, potent, selective, and metabolically stable $P2Y_{12}R$ antagonists with favorable permeability properties. The identified candidates present opportunities for direct application as $P2Y_{12}$-targeted therapeutics as well as for chemical radiolabeling to enable CNS imaging.

1. Introduction

1.1 G protein-coupled receptors (GPCRs) in drug discovery and development

The G protein-coupled receptor (GPCR) superfamily represents a diverse class of transmembrane proteins, comprising more than 800 members in the human genome.[1] GPCRs play a fundamental role in various physiological processes, including sensory perception (e.g. vision, taste, and olfaction) as well as the regulation of critical organ functions such as those of the heart, liver, lungs, kidneys, brain, and immune system.[2] Due to their pivotal role in signal transduction and disease pathophysiology, GPCRs have emerged as highly attractive therapeutic targets.[1,2] One of the characteristics of GPCRs is their broad ligand-binding capacity, exhibiting high affinity for structurally diverse chemical modulators, including proteins, lipids, and small molecules.[1,2] These modulators interact specifically with certain GPCRs or GPCR subfamilies, each possessing distinct properties that affect receptor activity.[2] Modifications of these chemical ligands and the discovery of novel ligands represent a key aspect of drug discovery and development.[2]

The hit-to-lead optimization process is a crucial stage in the multi-step drug discovery process. It follows target identification and validation, which involves defining a disease-relevant target through pathophysiological studies or high-throughput screening (HTS) methodologies. The subsequent target-to-hit stage focuses on identifying biologically active chemical compounds (hit compounds) that demonstrate promising activity against the target. In the hit-to-lead phase, these initial hit compounds are subjected to structural modifications to improve their potency, selectivity, and pharmacokinetic properties. This process includes chemical synthesis of optimized analogs based on the initial hit compound structure, biological and pharmacological evaluation to assess receptor activity and efficacy, as well as structure-activity relationship (SAR) analysis to correlate molecular modifications with biological outcomes. Following successful hit-to-lead optimization, candidate compounds progress through preclinical evaluation, including in vivo animal studies, before advancing into clinical trials (Phase I− III) and ultimately undergoing regulatory approval for market availability (Figure 1).[3] Notably, GPCRs represent the primary target for over 30% of all approved drugs, with many additional candidates currently in preclinical development.[1] This underscores their significant impact on pharmaceutical research and their continued relevance in the discovery of novel therapeutics.

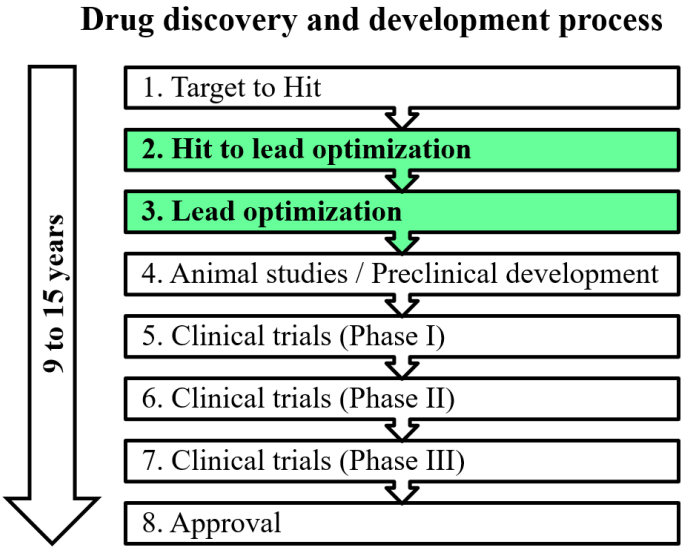


Figure 1. Drug discovery and development process highlighting the two major stages associated with the current study.

1.1.1 Structural features and roles of GPCRs in signal transduction

The structural framework of GPCRs is defined by seven α-helical, hydrophobic transmembrane (7TM) domains, an N-terminal extracellular region, and a C-terminal intracellular region. Each of the 7TM domains consists of 25-35 consecutive amino acid residues, forming a compact and highly conserved structure.[4] The N-terminal domain and the extracellular loops (ECL1−ECL3) serve as the primary ligand-recognition and binding sites. These regions facilitate the interaction with physiological ligands or external stimuli, including hormones, neurotransmitters, ions, and photons, enabling the receptor to mediate diverse cellular responses. The C-terminal domain and intracellular loops (ICL1−ICL3) are responsible for intracellular signal transduction through their association with heterotrimeric guanine nucleotide-binding proteins (G proteins). These proteins consist of three subunits (α, β, γ), where the α-subunit binds guanosine diphosphate (GDP) in its inactive state, often forming a stable $G\alpha_{GDP}\beta\gamma$ complex.[5,6]

The activation of GPCRs and their associated G protein subunits is primarily mediated by structural rearrangements in specific domains. For example, the sixth transmembrane domain (TM6), the extracellular loop 2 (ECL2) and 3 (ECL3) are essential for the conformational changes required for rhodopsin-receptor activation and subsequent intracellular signaling.[6] Structural studies have revealed that the structure of GPCRs can be stabilized through covalent linkages between the domains such as the conserved disulfide bond between TM3 and ECL2 or by palmitate attached to an eighth helix that interacts with the cell membraine.[5] Figure 2 illustrates the structure

of the β_2-adrenergic receptor (PDB ID: 2RH1), highlighting the architectural features of a GPCR, including the 7TM helical core, the N- and C-terminal regions, the extracellular and intracellular loops, as well as the covalently attached palmitate at the eighth helix.

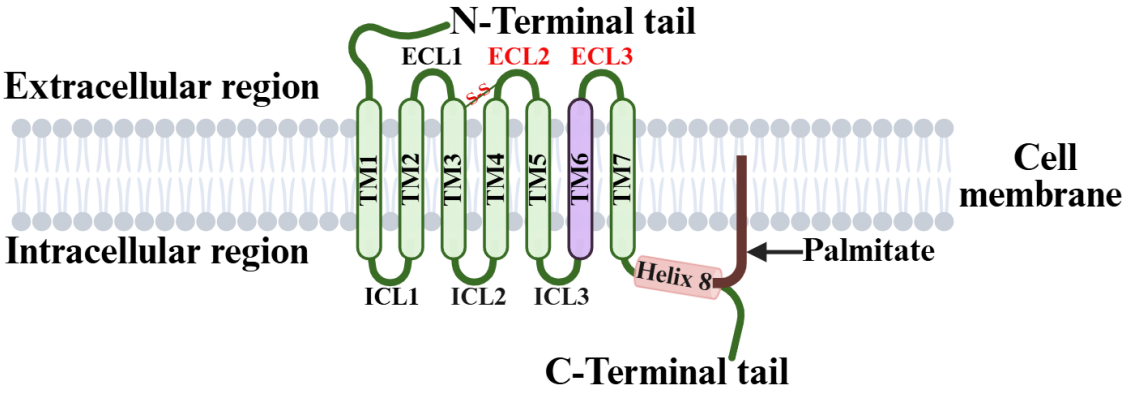


Figure 2. Structure of a typical class A GPCR (the β_2-adrenergic receptor) with a disulfide bond between TM3 and ECL2, and a covalently attached palmitate linked to an eighth helix; TM = transmembrane domain, ECL = extracellular loops, ICL = intracellular loops.

GPCRs undergo conformational rearrangements upon agonist binding, initiating intracellular signaling cascades that are dependent on the specific heterotrimeric G protein subunit (α, β, γ) that is activated. Upon receptor activation, a conformational shift in the G_α-subunit facilitates the exchange of GDP for guanosine triphosphate (GTP), leading to the dissociation of the heterotrimeric G protein complex ($G\alpha_{GDP}\beta\gamma$) into two active signaling components, the activated $G\alpha_{GTP}$-subunit and an activated Gβγ-subunit. The activated $G\alpha_{GTP}$-subunit subsequently regulates membrane-bound enzymes, catalyzing the production of second messengers that act as signal amplifiers, propagating the ligand-receptor response through the activation of protein kinases (PKs), which phosphorylate intracellular target proteins, thereby modulating their function and eliciting specific cellular responses.[2,7]

The G_α-protein family consists of four major classes: $G_{\alpha s}$, $G_{\alpha i}$, $G_{q/11}$ and $G_{12/13}$ (Table 1).[2] Each subtype regulates distinct intracellular signaling pathways: The $G_{\alpha s}$-protein activates adenylate cyclase (AC), catalyzing the cyclization of adenosine triphosphate (ATP) to generate the second messenger cyclic adenosine monophosphate (cAMP). cAMP interacts with protein kinase A (PKA) to activate the phosphorylation of intracellular targets, driving downstream effects. Phosphodiesterases hydrolyze cAMP to terminate its effect.[2] The $G_{\alpha i}$-subunit functions as a

negative regulator of adenylate cyclase (AC), leading to inhibition of cAMP production, thereby counteracting $G_{\alpha s}$-mediated signaling.[2] The $G_{q/11}$-subunit is responsible for phospholipase C (PLC) stimulation which catalyzes the breakdown of the membrane lipid phosphatidylinositol-4,5-bisphosphate (PIP_2) into diacylglycerol (DAG), which remains membrane-bound, and inositol trisphosphate (IP_3), which diffuses into the cytosol and binds to IP_3-gated Ca^{2+}-release channels on the endoplasmic reticulum (ER) allowing the release of stored calcium ions (Ca^{2+}). Both DAG and calcium ions (Ca^{2+}) act as second messengers. Activation of the calcium-dependent protein kinase C (PKC) phosphorylates cellular targets, modulating biological responses.[7] The $G_{12/13}$-subunit is responsible for the activation of Rho family monomeric GTPases via RhoGTPase nucleotide exchange factors (Rho-GEF) to regulate actin cytoskeleton rearrangement.[7] Figure 3 illustrates the complexity of GPCR-mediated signal transduction, highlighting the diverse ligands, effectors, and signaling pathways.

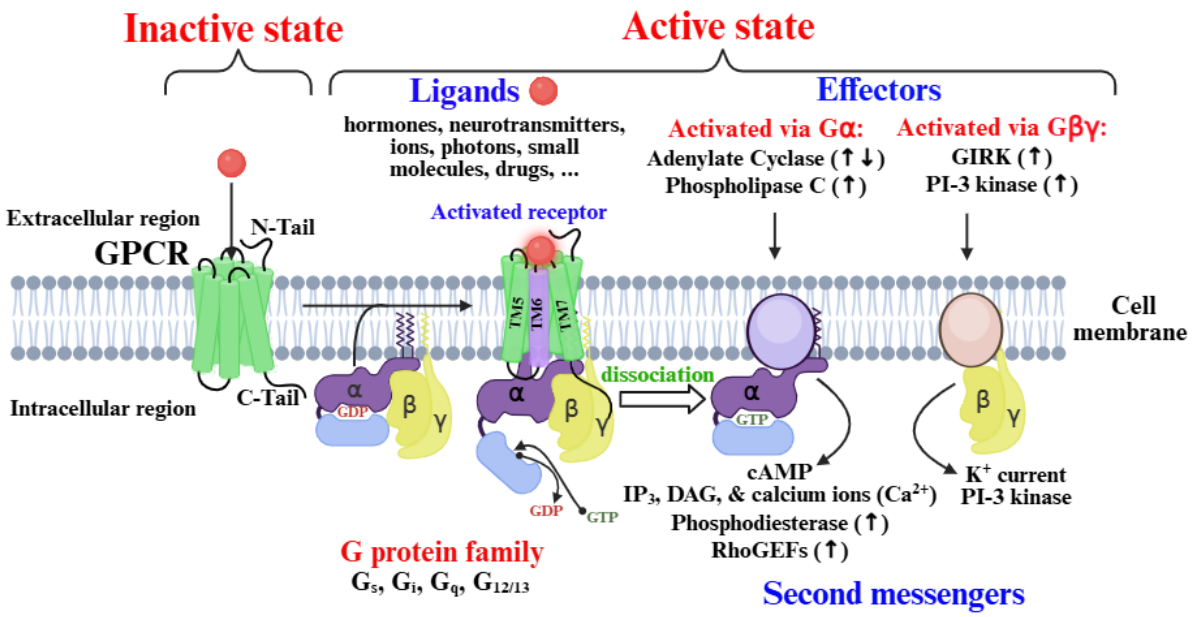


Figure 3. A brief illustration of G protein-coupled receptor signaling. GIRK = G protein-regulated inwardly rectifying potassium channels, PI-3 kinase = phosphoinositide 3-kinases, GDP = guanosine diphosphate, GTP = guanosine triphosphate, cAMP = cyclic adenosine monophosphate, IP_3 = inositol trisphosphate, DAG = diacylglycerol, PIP_2 = phosphatidylinositol-4-5-bisphosphate.

1.1.2 Classification of GPCRs

GPCRs are classified into distinct families based on sequence homology and functional similarity. One of the most recognized classification systems is the GRAFS classification, introduced by Fredriksson et al. (2003). This system is based on phylogenetic analyses of GPCRs in the human genome and categorizes these receptors into five major families Glutamate (G), Rhodopsin (R), Adhesion (A), Frizzled/Taste2 (F), and Secretin (S). Additionally, the GRAFS classification system subdivides the large Rhodopsin class (R) into 13 subclasses.[8,9]

The glutamate (G) family comprises 16 receptors, subdivided into 8 metabotropic glutamate receptors (GRM), two γ-aminobutyric acid (GABA) receptors, a single calcium-sensing receptor (CASR), and 5 taste receptors. The Adhesion class (A) consists of 33 receptors characterized by long N-terminal domains enriched with epidermal growth factor (EGF) domains, mucin-like regions, and conserved cysteine-bridges. The Frizzled/Taste2 (F) class contains 24 receptors that are responsible for regulation of cell fate, proliferation, and polarity during metazoan development by mediating signals from secreted glycoproteins termed Wnt-signaling pathway. The secretin family (S) includes 15 receptors that predominantly bind large peptide ligands. The N terminal region of these receptors contains conserved cysteine-bridges, which are crucial for ligand-receptor interactions and receptor activation.[8,9]

Rhodopsin family (R) represents the largest class within the GPCR superfamily. It is further divided into four main branches: α-, β-, γ-, and δ-branch. Except for the β-branch each of these subclasses has its own sub-classification. While the α-branch contains 89 members and is subdivided into five main branches: the prostaglandin receptor cluster (15), the amine receptor cluster (40), the opsin receptor cluster (9), the melatonin receptor cluster (3) and the MECA receptor cluster (Melanocortin, Endothelial differentiation, Cannabinoid, and Adenosine binding) (22), the β-branch has no main branches and contains 35 members. Peptides are the only ligand type that is known for this branch.[8,9] 59 members belong to the γ -branch and they are distributed into three main branches: the somatostatin, opioids, and galanin (SOG) receptor cluster (15), the melanin-concentrating hormone (MCH) receptor cluster (2) and the chemokine receptor cluster (42).[8,9] The δ-branch consists of three main branches that involve 58 members, besides the branch of the 460 olfactory receptors. The first branch is the MAS-related receptor cluster (8), the second is the glycoprotein receptor cluster (8) and the third is the purine receptor cluster (42). The purine receptor cluster represents an important subclass, since it contains a large variety of activating

ligands (for example, nucleotides (P2Y receptors), lipids and peptides) as well as many orphan receptors such as GPR17 and GPR34, whose endogenous ligands remain unidentified.[8,9] Certain seven transmembrane (7TM) receptors identified in phylogenetic analysis do not exhibit a clear evolutionary relationship to any of the five major GPCR families and remain unclassified.[8,9]

P2Y receptors, which are involved in purinergic signaling, are further categorized into two functional subgroups based on their G protein coupling specificity: the $P2Y_1$-like (G_q-coupled) receptors, which consists of five P2Y receptors ($P2Y_1$, $P2Y_2$, $P2Y_4$, $P2Y_6$, and $P2Y_{11}$), and the $P2Y_{12}$-like (G_i-coupled) subclass, which includes three receptors ($P2Y_{12}$, $P2Y_{13}$, and $P2Y_{14}$) (Figure 4).[10–12]

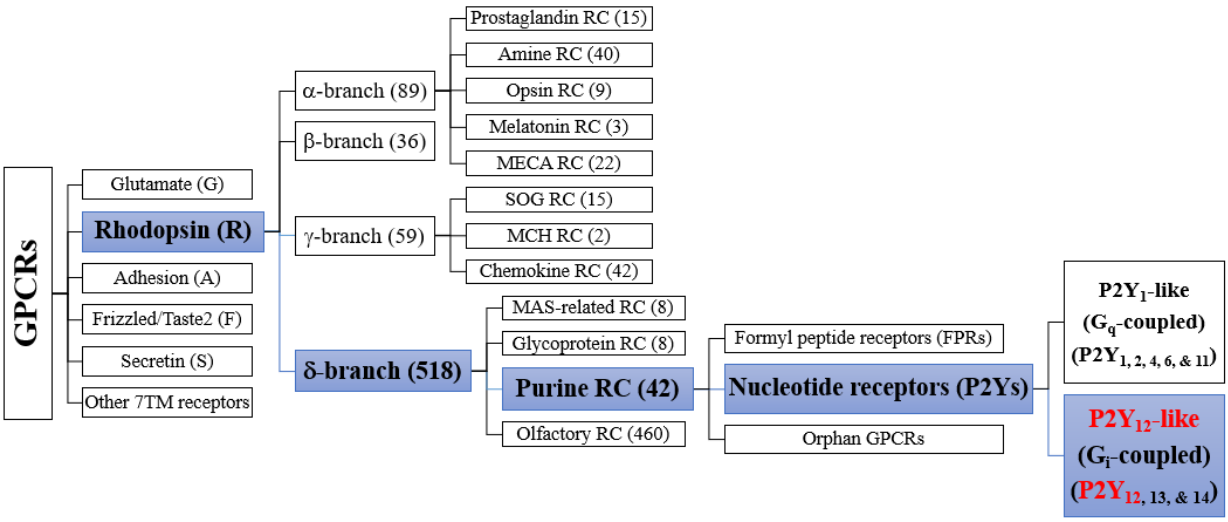


Figure 4. Classification of GPCRs, highlighting the classification of the P2Y receptors and their respective signaling mechanisms. RC (receptor cluster), MECA (Melanocortin-, Endothelial differentiation-, Cannabinoid-, and Adenosine binding-receptors), SOG (Somatostatin-, Opioid-, and Galanin binding-receptors), MCH (Melanin-Concentrating Hormone).[8,9,11]

1.2 Purinergic signaling

The concept of purinergic signaling was first described in 1929 by Drury and Szent-Györgyi, who identified the extracellular actions of purines.[10] Nearly five decades later, in 1976, Geoffrey Burnstock successfully characterized purinergic receptors, which were subsequently classified based on their endogenous activating ligands into three major families: P0 receptors activated by adenine (**1**), P1 receptors, which are activated by adenosine (**2**), and P2 receptors, that are activated by adenosine triphosphate (ATP) and related nucleotides (**3**-**7**, Figure 5).[10,13,14] This classification

system proposed by Burnstock in 1978, was initially limited to P1 and P2 receptors, as P0 receptors had not yet been identified at that time.[10]

In 1985, Burnstock and Kennedy further refined the classification of P2 receptors by dividing them into two distinct families based on their pharmacological properties: P2X family, which contains the ligand-gated ion channels or ionotropic receptors, and P2Y family, which comprises the G protein-coupled or metabotropic receptors. This classification was later confirmed through molecular cloning, which provided insights into the structural and functional properties of P2 receptors, establishing their distinct transduction mechanisms.[10,14]

The P2X family consists of seven members (P2X1−P2X7) which are endogenously activated by adenosine triphosphate (ATP) (**3**, Figure 5). The P2Y family comprises eight members ($P2Y_1$, $P2Y_2$, $P2Y_4$, $P2Y_6$, $P2Y_{11}$, $P2Y_{12}$, $P2Y_{13}$, and $P2Y_{14}$).[10,11] The numerical gaps in the P2Y receptor family (e.g., missing $P2Y_3$, $P2Y_5$, $P2Y_{7–10}$) are explained as follows: First, some of the missing P2Y receptors correspond to nonmammalian orthologs that do not have direct counterparts in human physiology. Second, these receptors share sequence similarity with P2Y receptors, however their functional response to nucleotides has not been definitively established.[10]

1.3 P2Y receptors

The purinergic P2Y receptors belong to the GPCRs, that structurally share functionally important positively charged residues within transmembrane domains TM3, 6, and 7 as confirmed by site-directed mutagenesis studies applied on $P2Y_1$ and $P2Y_2$ receptors.[10] These basic amino acid residues interact with the negatively charged phosphate groups of endogenous nucleotides, facilitating ligand binding and receptor activation. The H-X-X-R/K motif in TM6 is a typical feature across all P2Y receptors, playing a fundamental role in nucleotide binding. $P2Y_1$- like receptors share the Q/K-X-X-R motif in TM7, which is essential for their ligand specificity. $P2Y_{12}$-like receptors are characterized by a KEXXL motif in TM7 and an additional lysine (K) residue in extracellular loop 2 (ECL2), which significantly enhance ligand-receptor interactions.[10] Among P2Y receptors, $P2Y_{12}$ and $P2Y_{13}$ share the highest sequence identity of 48%, indicating structural and functional similarities within this receptor subgroup.[10,15–17]

Endogenously, P2Y receptors are targeted by adenine and uracil nucleotides with different degrees of selectivity and potency. Some P2Y receptors are selectively activated by adenosine nucleotides. Adenosine diphosphate (ADP) is the most potent and selective ligand for $P2Y_1$, $P2Y_{12}$, and $P2Y_{13}$

receptors (**4**). Some other P2Y receptors are activated selectively by uracil nucleotides. Uridine triphosphate (UTP), uridine diphosphate (UDP), and uridine diphosphate-glucose are the most potent and selective ligands for human $P2Y_{4(UTP)}$, $P2Y_{6(UDP)}$, and $P2Y_{14(UDP/UDP\text{-}glucose)}$ receptors (**5-7**, Figure 5). [14–17]

P2Y receptors are functionally categorized into two major subgroups based on their G protein-coupling specificity. While the $P2Y_1$-like subgroup primarily couples to $G_{q/11}$ to stimulate the phospholipase C (PLC)/inositol trisphosphate (IP_3) signaling pathway and subsequently the release of the intracellular calcium (Ca^{2+}) to mediate various physiological responses, the $P2Y_{12}$-like subgroup couples to the $G_{\alpha i}$ subunit to inhibit adenylate cyclase (AC) leading to a subsequent decrease in cyclic adenosine monophosphate (cAMP) levels, which results in the inhibition of protein kinase A (PKA), modulating downstream signaling pathways.[15–18]

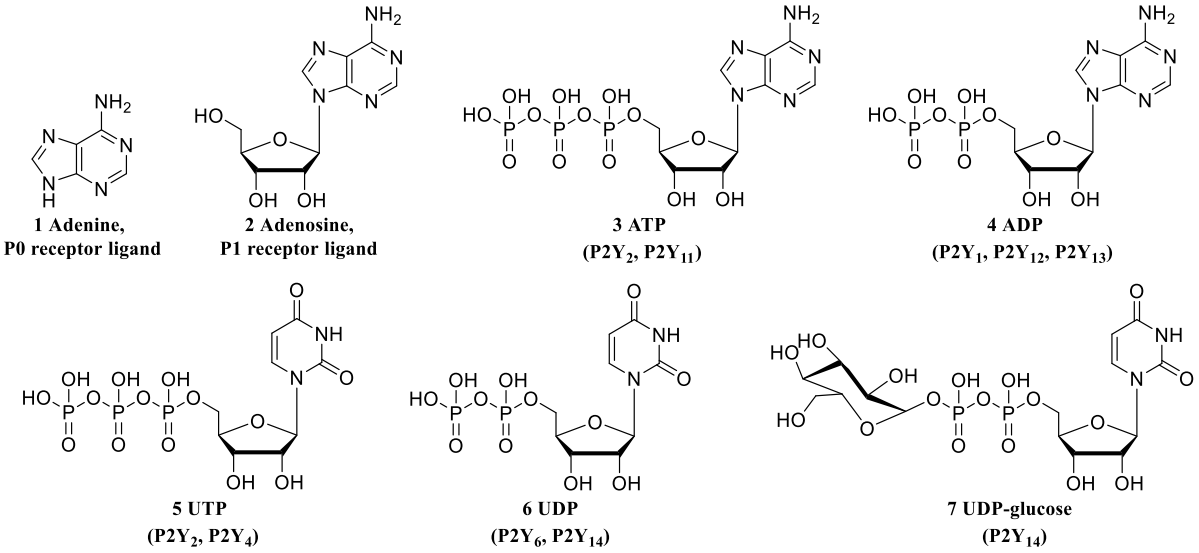


Figure 5. Chemical structures for the most potent and selective endogenous ligands for purinergic GPCRs. **1** Adenine (P0 receptor ligand), **2** adenosine (P1 receptor ligand), **3** ATP ($P2Y_2$, $P2Y_{11}$), **4** ADP ($P2Y_1$, $P2Y_{12}$, $P2Y_{13}$), **5** UTP: uridine triphosphate ($P2Y_2$, $P2Y_4$), **6** UDP: uridine diphosphate ($P2Y_6$, $P2Y_{14}$), **7** UDP-glucose: uridine diphosphate glucose ($P2Y_{14}$).

P2Y receptors are widely expressed across various human tissues, where they regulate numerous biological processes. Due to their diverse physiological roles, they have been identified as promising therapeutic targets for several pathological conditions, including neurodegenerative disorders (e.g., Alzheimer's and Parkinson's disease), cardiovascular diseases (e.g., thrombosis and hypertension), pain modulation, and cancer progression and metastasis.[19–21] The broad tissue

distribution and functional diversity of P2Y receptors make them valuable drug targets, with ongoing research focusing on the development of selective agonists and antagonists for therapeutic intervention.

1.4 $P2Y_{12}$ receptor

The human $P2Y_{12}$ receptor is composed of 342 amino acids, with a molecular weight of 39 kDa. Structurally, it features four extracellular cysteine residues located at positions 17, 97, 175, and 270, which play a crucial role in receptor expression, stability, and ligand interaction. These cysteine residues contribute to disulfide bond formation, linking the N-terminal domain with extracellular loop 3 (ECL3), and the extracellular loop 2 (ECL2) with extracellular loop 1 (ECL1). The $P2Y_{12}$ receptor was cloned in 2001, and its high expression on blood platelets and its presence in brain microglia was confirmed.[22–25]

While the platelet-expressed $P2Y_{12}$ receptor is primarily involved in arterial thrombosis and acute coronary syndrome (ACS), the microglial $P2Y_{12}$ receptor has been implicated in neuroinflammatory and neurodegenerative processes.[26–33] Additionally, nonplatelet $P2Y_{12}$ receptors have been identified in immune cells and vascular smooth muscle cells, where they modulate inflammatory responses.[23–25]

The $P2Y_{12}$ receptor gene is located on chromosome 3q24–25, adjacent to the $P2Y_{14}$ and $P2Y_1$ genes.[22] Endogenously, ADP serves as the primary physiological agonist, activating both Gq-coupled $P2Y_1$ and G_i-coupled $P2Y_{12}$ receptors. ADP-interaction with the $P2Y_1$ receptor activates the PLC/IP_3 pathway, leading to intracellular Ca^{2+} release. This transient calcium mobilization induces a reversable shape change in platelets, initiating platelet aggregation. ADP-$P2Y_{12}$ receptor interaction inhibits the adenylate cyclase (AC) pathway, reducing cyclic adenosine monophosphate (cAMP) levels. This suppression prevents protein kinase A (PKA)-mediated phosphorylation of vasodilator-stimulated phosphoprotein (VASP-P), thereby amplifying and sustaining platelet aggregation.[23–25,34] In addition, the $P2Y_{12}$ receptor modulates the phosphoinositide-3-kinase-(PI_3K)/Akt (PKB) pathway through interaction of the dissociated dimeric Gβγ-subunit. This pathway enhances intracellular Ca^{2+} mobilization, promoting platelet secretion and stabilization of aggregation, which contributes to vascular occlusion and stroke development.[34] Figure 6 illustrates the molecular mechanisms underlying ADP-induced platelet aggregation.

Given its critical function in thrombosis and hemostasis, the $P2Y_{12}$ receptor is a major pharmacological target in antiplatelet therapy.[35] Well-established $P2Y_{12}$ receptor antagonists, such as clopidogrel, effectively inhibit ADP-induced platelet aggregation, reducing the risk of cardiovascular events. Similarly, MRS 2500, a $P2Y_1$ receptor antagonist, prevents platelet shape change, further disrupting the thrombotic cascade.[36] Notably, clopidogrel functions as a prodrug, requiring hepatic enzymatic activation via cytochrome P450 before exerting its inhibitory effects, a process that will be discussed in later sections.

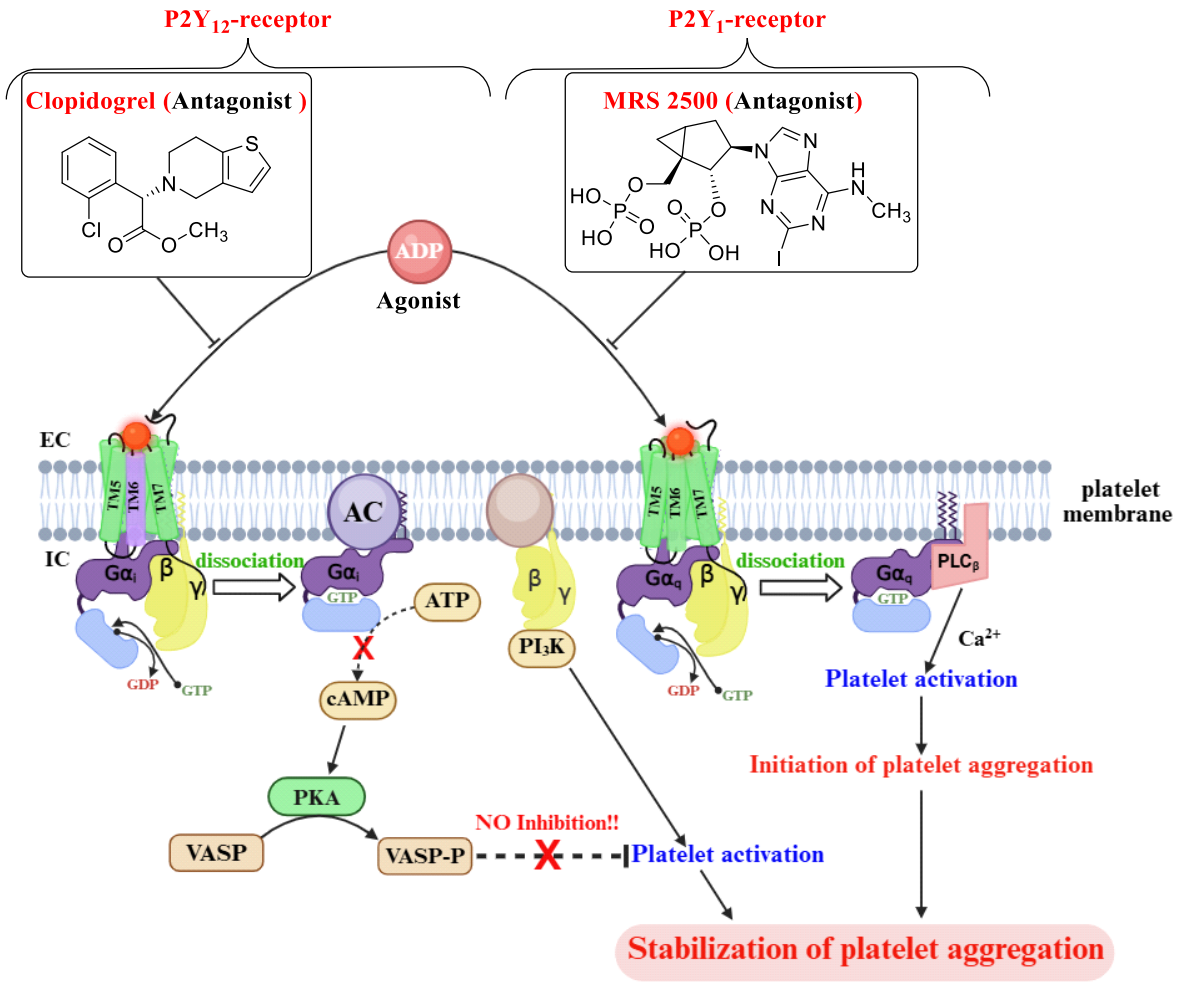


Figure 6. Platelet activation (initiation and stabilization). $P2Y_1$ and $P2Y_{12}$ receptors are involved in the adenosine diphosphate (ADP)-induced platelet aggregation. EC = extracellular, IC = intracellular, TM = transmembrane, AC = adenylate cyclase, PLC = phospholipase C, GDP = guanosine diphosphate, GTP = guanosine triphosphate, ATP = adenosine triphosphate, cAMP = cyclic adenosine monophosphate, PKA = protein kinase A, VASP = vasodilator-stimulated phosphoprotein, PI-3 kinase = Phosphoinositide 3-kinases.

$P2Y_{12}$ receptor expression by microglia has been demonstrated in vivo, particularly in a non-activated state. While microglia can exhibit pro-inflammatory properties, activated $P2Y_{12}$ receptors have been implicated in neuroprotection and modulation of central nervous system (CNS) inflammatory responses.[26–33]

This discovery positions the $P2Y_{12}$ receptor as a promising biomarker for monitoring microglial cells, enabling brain inflammation imaging through advanced techniques such as positron emission tomography (PET).[33] However, a major challenge in PET imaging studies is the development of novel, selective, high-affinity $P2Y_{12}$ receptor ligands that exhibit nanomolar binding affinity, are bioavailable to the CNS, and demonstrate metabolic stability. Despite the availability of potent $P2Y_{12}$ receptor antagonists, most have been specifically optimized to target platelet $P2Y_{12}$ receptors, highlighting the need for brain-penetrant $P2Y_{12}$ receptor antagonists.

The current study focuses on the systematic optimization of $P2Y_{12}$ receptor PET tracers, leveraging existing $P2Y_{12}$ receptor ligand scaffolds to develop CNS-permeable imaging agents. Such advancements could significantly enhance our understanding of microglial function in neuroinflammatory and neurodegenerative conditions, ultimately facilitating therapeutic interventions for CNS disorders.

1.4.1 $P2Y_{12}$ receptor antagonists

Structural studies have provided insights into $P2Y_{12}$ receptor activation and inhibition.[37–39] So far, a variety of $P2Y_{12}$ receptor antagonists has been developed, particularly as antithrombotic agents targeting platelet $P2Y_{12}$ receptors. Among these, the thienopyridine derivatives, such as clopidogrel (**8**), and prasugrel (**9**), have demonstrated significant therapeutic efficacy in the treatment of arterial thrombosis.[25,34,35,40] These compounds function as prodrugs, requiring bioactivation before irreversibly binding to platelet $P2Y_{12}$ receptors via covalent disulfide bond formation (Figure 7). Despite their clinical utility, thienopyridine derivatives present several limitations, including slow onset of action due to the necessity of metabolic activation, irreversible inhibition which results in prolonged platelet suppression, potential for drug resistance, moderate potency, and difficulties in dose adjustment. These challenges have driven efforts to develop reversible $P2Y_{12}$ receptor antagonists that can effectively modulate platelet aggregation without the drawbacks associated with irreversible inhibitors.[25]

Several reversible and competitive antithrombotic $P2Y_{12}$ receptor antagonists have been synthesized using adenine nucleotide-based scaffolds, derived from the physiological $P2Y_{12}$ receptor antagonist ATP (**3**, Figure 5). Examples include cangrelor (AR-C69931MX, **10**), and AR-C67085MX (**11**), both of which exhibit high selectivity (>10^4-fold) for $P2Y_{12}$ receptors over other P2Y and P2X receptor subtypes (Figure 7).[41–45] Despite their high potency, these nucleotide-based antagonists suffer from several drawbacks, such as poor oral bioavailability due to their high polarity and negative charge at physiological pH (7.4).[25]

To overcome these issues, orally active, reversible nucleoside analogues with antithrombotic properties have been developed. One of the prominent drugs in this class is ticagrelor (AZD6140, **12**),[42,44,45] which has demonstrated high efficacy in clinical settings. However, ticagrelor is associated with adverse effects in some patients (dyspnea and bradycardia). Its complex stereochemistry makes its synthesis challenging (Figure 7).[46,47]

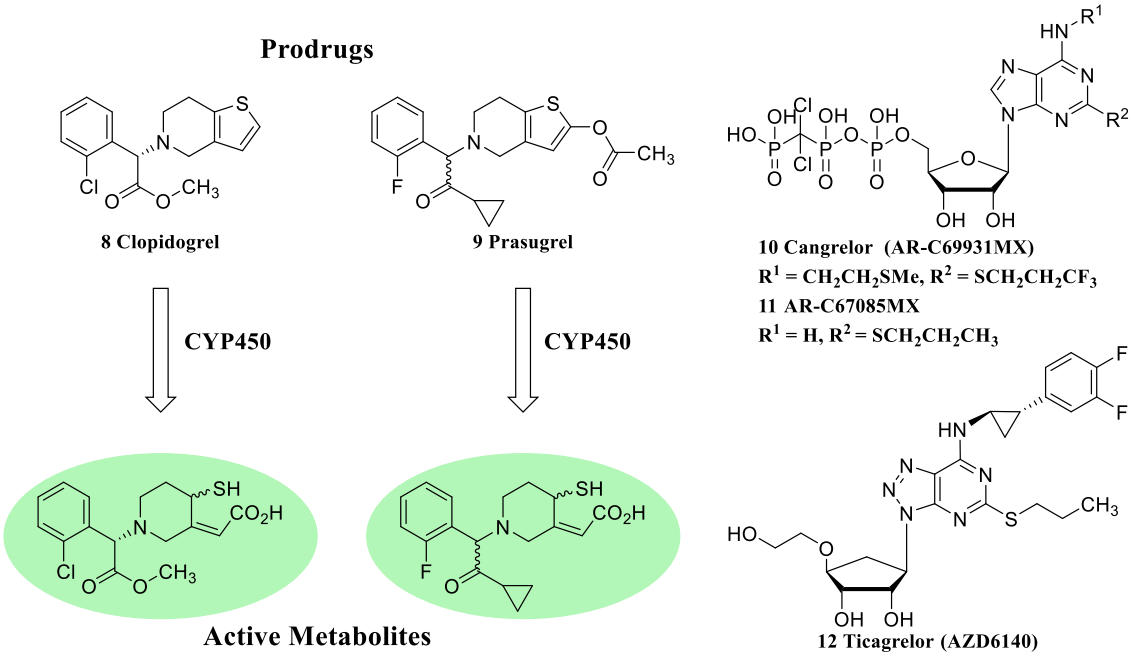


Figure 7. Structures of $P2Y_{12}$ receptor antagonists with antithrombotic activity.

In addition to nucleoside analogues, several alternative scaffolds have been developed and modified to target $P2Y_{12}$ receptors with high potency and selectivity such as anthraquinone derivatives,[35,48] piperazinyl-glutamate derivatives (e.g., phenylpyrimidines,[49–52] phenylpyridines,[53,54] phenylpyrazoles,[55] quinolines[56]), Azetidinyl- and piperidinyl-cyano-

nicotinate derivatives,[57,58] biphenylpiperazinylethylthienopyrimidine analogues,[59–61] pyrazolyl-phenyl-carbamoyl-indole derivatives,[62–64] and pyrazolidinedione derivatives.[65,66] These scaffolds, which will be analyzed in detail in the data analysis section, represent reversible $P2Y_{12}$ receptor antagonists, offering potential for their improvement regarding potency, selectivity, metabolic stability, oral bioavailability, and CNS permeability.

1.4.2 Anthraquinones as $P2Y_{12}$ receptor antagonists

Anthraquinones represent a class of organic compounds, structurally defined by a rigid planar three-ring aromatic system (anthracene) functionalized with two ketone groups at the C9- and C10-positions (Figure 8). This distinct quinone-based core confers unique chemical and biological properties, making anthraquinones valuable for various scientific and industrial applications.[67]

The anthraquinone family encompasses multiple compound subclasses, many of which exhibit bioactive properties. These compounds are derived from various natural sources, including plants (e.g., aloe), where they have been traditionally used in folk medicine for thousands of years, and from fungi and insects.[68–70] Beyond their biological significance, anthraquinones are of considerable importance in various industrial sectors such as pharmaceuticals, textile dying, painting, and food industries as additives, as well as catalysis due to their redox properties.[71–75]

One of the best-known anthraquinone derivatives is Reactive Blue 2 (RB-2) (**13**, Figure 8), a synthetic anthraquinone dye extensively utilized in textile industry. Beyond its industrial applications, RB-2 has been identified as a biologically active compound capable of modulating purinergic signaling pathways. Specifically, RB-2 functions as a $P2Y_{12}$ receptor antagonist.[76,77]

Our research group has explored anthraquinone-based scaffolds, particularly derivatives and analogs of RB-2, for their potential as $P2Y_{12}$ receptor antagonists. RB-2 has been reported to inhibit $P2Y_{12}$ receptor activation with a K_i value of 1.3 μM, which is consistent with our findings, where we determined a K_i value of 0.68 μM.[35,77] Further research led to the development of two novel ligands by our group, belonging to the most potent $P2Y_{12}$ receptor antagonists, **PSB-0739** (sodium 1-amino-9,10-dioxo-4-((4-(phenylamino)-3-sulfonatophenyl)amino)-9,10-dihydroanthracene-2-sulfonate, **14**, Figure 8), and **PSB-0702** (sodium 5-((4-amino-3-carboxy-9,10-dioxo-9,10-dihydroanthracen-1-yl)amino)-2-(phenylamino)benzenesulfonate, **15**, Figure 8), with K_i values of 24.9 nM and 21.0 nM, respectively, determined in radioligand binding studies.[35,77] These novel ligands were synthesized using an Ullmann coupling reaction.[35,77]

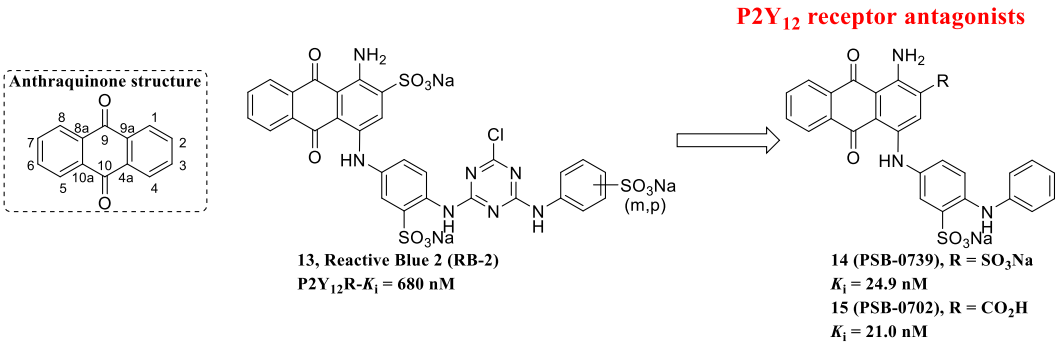


Figure 8. Structures of RB-2 and the most potent $P2Y_{12}$ receptor antagonists of the anthraquinone scaffold, K_i values at the human $P2Y_{12}$ receptor were determined in radioligand binding assays.[35,77]

1.4.3 Development of a $P2Y_{12}$ receptor antagonist radioligand

The development of a potent and selective $P2Y_{12}$ receptor antagonist radioligand remains a key area of interest, as such tools enable studies on platelet and microglial $P2Y_{12}$ receptors. Such radioligands serve as essential tools for medical imaging techniques, particularly PET, and play a critical role in the drug development process, notably enabling radioligand binding assays for assessing receptor-ligand interactions.[26,33,78–82]

Various methodologies have been explored for the synthesis of radioligands incorporating radioactive isotopes of specific elements, such as tritium (^{3}H or T), fluorine-18 (^{18}F), or carbon-11 (^{11}C).[78,83–87] Among these, tritiation of organic molecules has been extensively investigated.[87] Tritium labeling is particularly advantageous due to its low-energy β-emission (18.6 keV) and relatively long half-life (12.3 years), making it a preferred choice over other radiolabeling techniques.[88] Furthermore, tritium-labeled compounds can achieve high specific activity with relative ease, further enhancing their utility in radiolabeling applications.[88] These characteristics make tritium-labeled radioligands highly suitable for in vitro studies, such as the establishment of radioligand binding assays. However, their toxicity and low signal limit their applicability in in vivo studies. In contrast, fluorine-18 (^{18}F) and carbon-11 (^{11}C) are more appropriate for in vivo applications, as PET-tracers for imaging studies.

Several $P2Y_{12}$ receptor antagonist radioligands have been synthesized for both in vitro or in vivo studies as will be discussed in Chapter 3.[64,66,83–86,88–91,72] However, none have demonstrated optimal efficacy in fulfilling their intended applications, highlighting the inherent challenges and complexities associated with their development. These limitations underscore the need for continued research in this field. Given these challenges, ongoing research aims to develop next-

generation radioligands with improved pharmacokinetic properties, enhanced metabolic stability, optimized synthetic accessibility, and high capability of crossing the blood-brain barrier (BBB). Such CNS-permeable $P2Y_{12}$ receptor antagonists could serve as PET tracers to investigate the anti-inflammatory role of microglia, providing valuable insights into neuroinflammatory mechanisms. Developing brain-penetrant $P2Y_{12}$ receptor antagonists hold significant therapeutic potential, particularly for chronic neurodegenerative diseases such as Alzheimer's and Parkinson's disease, multiple scleroses, and epilepsy.[27−32] By targeting $P2Y_{12}$ receptors in microglia, these agents could help elucidate the reported neuroprotective versus pro-inflammatory roles of microglial activation,[92−96] paving the way for novel therapeutic and diagnostic strategies.

A comprehensive understanding of CNS protective mechanisms including the structural and functional characteristics of the BBB as well as its permeability requirements is essential for the systematic evaluation of $P2Y_{12}$ receptor ligands for brain applications to facilitate the rational design and optimization of $P2Y_{12}$ receptor-targeted PET tracers and therapeutics, contributing to the advancement of CNS drug discovery.

1.5 The central nervous system (CNS) as a drug target

Achieving CNS penetration in drug discovery is a formidable challenge due to the brain's complex structure and its robust protective systems designed to shield the internal physiological environment from harmful external substances. Three primary barriers contribute to CNS protection: the BBB, the choroid plexus blood-cerebrospinal fluid barrier (B-CSFB), and the arachnoid blood-cerebrospinal fluid barrier. Among these, the BBB, with the largest blood-CNS interface surface area, is the most critical consideration for CNS drug design and delivery.[97,98]

The BBB consists of tightly packed endothelial cells connected via tight junctions, forming a physical barrier supported by the phospholipid bilayer of the cell membrane. While lipid-soluble and non-polar molecules can passively diffuse across this barrier, most other substances require active transport mechanisms. The transport barrier is mediated by two primary systems: First, the active efflux carriers, which are ATP-binding cassette (ABC) transporters, such as P-glycoprotein (P-gp), breast cancer resistance protein (BCRP), and multidrug resistance proteins (MRPs), actively expel a wide range of substrates, including molecules with diverse ionization states, hydrophobicity, and amphipathic properties, e.g. anticancer drugs, chemical toxins, and nucleoside analogs.[99,100] Second, the enzymatic carriers "solute carriers (SLCs)" which are regulating the transport of polar molecules like glucose, amino acids, and nucleosides into the CNS, alongside

maintaining ion gradients, nutrient uptake, and waste removal. Their function can be unidirectional or bidirectional, depending on substrate concentrations and electrochemical gradients.[101] Additional mechanisms include receptor-mediated transport (RMT), which is a specific binding of ligands such as transferrin, insulin, or leptin to facilitate their transport across the BBB.[97] Adsorptive-mediated transport (AMT) represents charge-based interactions enable the absorption of cationized proteins like albumin into the CNS.[97] The immunological barrier regulates leukocyte trafficking through either transcellular migration or modulation of tight junctions (Figure 9).[97]

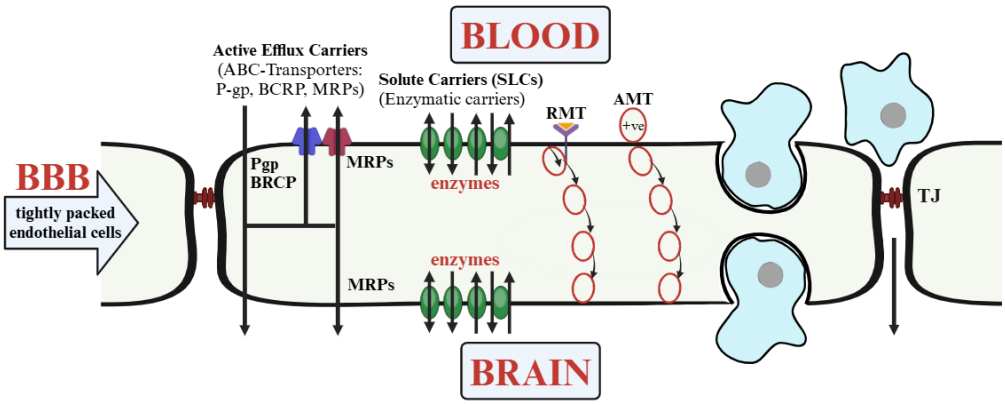


Figure 9. BBB-structure and function. ATP-binding cassette (ABC); P-glycoprotein (P-gp); breast cancer resistance protein (BCRP); multidrug resistance proteins (MRPs); receptor-ligand mediated transport (RMT); absorptive mediated transport (AMT); tight junctions (TJ); The arrows show the transport direction of each permeability pathway; blue shapes represent the leucocytes.[97]

1.6 Passive diffusion and CNS penetration filtering

Passive diffusion remains the straightforward mechanism by which molecules traverse the BBB. This process heavily depends on modulating the physicochemical properties of synthesized ligands while simultaneously refining their affinity and selectivity for the target receptor ($P2Y_{12}$). According to the central nervous system multiparameter optimization (CNS-MPO) framework, six key parameters must remain within specific thresholds to observe BBB permeability. These include the partition coefficient (clogP < 5), the distribution coefficient at physiological pH 7.4 (clogD < 4), the topological polar surface area (TPSA < 120 Å²), molecular weight (MW < 500 g/mol), the number of hydrogen bond donors (HBDs < 3), and the dissociation constant (pKa) for the most basic (< 10) center.[102,103] The probability of BBB penetration increases as these values approach lower limits of their respective thresholds. Passive diffusion remains the simplest yet

most fundamental pathway for enabling molecular transport across the BBB, making it a critical consideration in the development of CNS-active $P2Y_{12}$ receptor ligands.

Different reported biological assays have been employed to determine the affinity and selectivity of synthesized $P2Y_{12}$ receptor antagonists. This study primarily focuses on ADP-induced platelet aggregation assays in rat (rPRP) or human (hPRP) platelet-rich plasma, where IC_{50} values (µM) serve as key indicators of reported antagonist potency. Additionally, radioligand binding assays (K_i values (nM)) are utilized for the precise evaluation and optimization of novel $P2Y_{12}$ receptor antagonists. To assess the CNS permeability of candidate molecules, both affinity and permeability probabilities are classified into three categories: high (green), medium (yellow), or low (red), based on predefined threshold values for these parameters, as outlined in Table 1.

Table 1. The assigned CNS penetration filters.[102,103]

Properties[a]	**Predicted brain permeability**		
	High	**Middle**	**Low**
IC_{50} (h/rPRP, µM)	<0.07	0.07– 0.10	>0.10
K_i or IC_{50} (affinity, nM)	<11	11– 50	>50
clogD	1.00– 2.99	3.00– 3.99	>4.00
TPSA (Å²)	<90	90– 110	>110
MW (g/mol)	<450	450– 500	>500
N_{HBDs}	<2	2– 3	>3
pK_a (most acidic center)	>7	6– 7	<6
pK_a (most basic center)	<9	9– 10	>10

[a] **h/rPRP**: Inhibition of ADP-induced platelet aggregation in human/rat platelet-rich-plasma; **TPSA**: topological polar surface area; **MW**: molecular weight; **N_{HBDs}**: number of hydrogen-bond donors.

Establishment of CNS penetration filters provides a structured framework for systematically evaluating and optimizing $P2Y_{12}$ receptor antagonists. By applying these criteria to data analysis outcomes, the development process can identify promising BBB-permeable candidates, enabling the design of PET tracers and advancing CNS-targeted therapeutic strategies. This systematic approach ensures efficient refinement of drug properties for both imaging and therapeutic applications.

2 Aims of the study

The current study is focused on two main aims.

2.1 Improvement of the anthraquinone scaffold to increase affinity, and its radiolabeling to establish a radioligand binding assay

2.1.1 Synthesis of anthraquinone-based $P2Y_{12}$ receptor antagonists: structure-activity relationships (**Chapter I**)

The published structure-activity relationship (SAR) studies of the anthraquinone scaffold have not yet explored modifications of ring **A**, ring **E**, or the nitrogen atom **X** of the aniline moiety, which could significantly influence receptor binding affinity and other properties (Figure 10).[35] The present study aims to address this gap by systematically investigating those unexplored regions, providing valuable insights for optimizing the potency, selectivity, and stability of anthraquinone-based compounds.

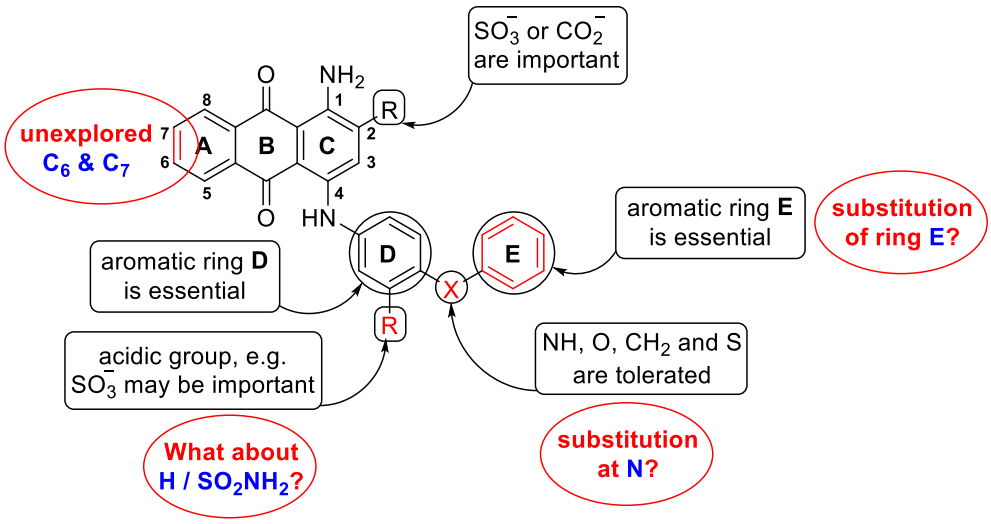


Figure 10. Analysis of published structure-activity relationships of the anthraquinone scaffold.[35] Targeted optimization positions are assigned in red.

2.1.2 Trials to obtain an anthraquinone-based radioligand (**Chapter II**)

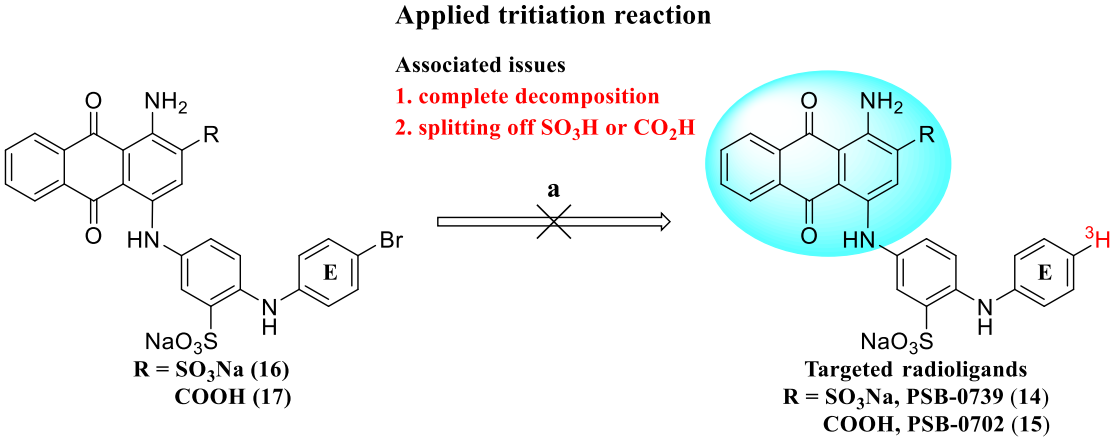
Compounds **PSB-0739** and **PSB-0702** (**14**, **15**, Figure 8) had been selected as promising candidates for the development of anthraquinone-based tritium-labeled radioligands, with the goal to establish a reliable radioligand binding assay. To ensure the retention of potency and selectivity within this scaffold, dehalogenative tritiation was pursued as a labeling strategy. This approach involved the

introduction of a halogen (Br or I) at the terminal phenyl ring of the aniline moiety, which would later be replaced by the hydrogen isotope tritium (^{3}H) during the labeling process.

The brominated precursors **16** and **17** of the most potent and selective anthraquinone-based P2Y$_{12}$ receptor antagonists **PSB-0739** (**14**) and **PSB-0702** (**15**) were successfully synthesized (Scheme 1) and subsequently subjected to heterogeneous catalytic dehalogenative tritiation under three different reaction conditions as described in Scheme 1 using a palladium catalyst and a stream of tritium gas to generate the desired radiolabeled P2Y$_{12}$ receptor antagonists (Scheme 1).

However, during the hydrogenation/dehalogenation process, the anthraquinone moiety exhibited significant instability toward Pd-catalyzed reactions. Complete degradation of the anthraquinone moiety or the release of the sulfonate or carboxylic acid from the C2-position was observed. Extensive optimization of the reaction conditions was therefore performed and described in detail in Chapter II, which covers the trials for the development of anthraquinone-based P2Y$_{12}$ receptor antagonist radioligands.

Scheme 1. Structure and design of the targeted P2Y$_{12}$ receptor radioligands with an AQs scaffold and the applied tritiation reaction conditions.[a]



[a]Reaction conditions: The three reactions were performed under tritium gas (a. 1. Pd/C, *N*,*N*-dimethylformamide (DMF), 25 °C, 4 h; 2. Pd/C, DMF, 25 °C, 11 min; 3. *Lindlar* catalyst, DMF, 25 °C, 16 h) (failed trials).

2.2 Research and development of potentially brain-permeable P2Y$_{12}$ receptor antagonists for radiolabeling

Beyond the challenging anthraquinone scaffold modifications, the present study focuses on the research and development of P2Y$_{12}$ receptor antagonists with the goal to improve potency,

selectivity, metabolic stability, oral bioavailability, and in particular, central nervous system (CNS) permeability. Moreover, the establishment of a radioligand binding assay, the development of $P2Y_{12}$ receptor-targeted positron emission tomography (PET) tracers, as well as the development of therapeutics for inflammatory brain diseases are planned. The overall systematic strategy employed to achieve this objective is summarized in Figure 11.

To systematically identify the most promising $P2Y_{12}$ receptor antagonists for PET-tracer development, an extensive data analysis was conducted, encompassing nearly all reported $P2Y_{12}$ receptor antagonists (**Chapter III**). The analysis began with the classification of compounds based on the biological assays used to determine receptor affinity. Subsequently, these compounds were categorized into three groups based on their activity: Class A (highly active) with K_i/IC_{50} values lower than 11 nM, Class B (moderately active) with K_i/IC_{50} values between 11 and 50 nM, Class C (moderately active to inactive) with K_i/IC_{50} values above 50 nM.

Following affinity-based classification, Class A compounds were further grouped according to their structural scaffolds, resulting in five major scaffolds. These scaffolds were then subjected to a CNS-permeability filtering process to identify candidates suitable for BBB penetration. Among the evaluated scaffolds, the pyrazolyl-phenyl-carbamoyl-indole scaffold was selected as the most promising one for the development of tritium-labeled radioligands to allow the establishment of radioligand binding assays (**Chapter IV**).

To refine the selection process, a secondary data analysis was conducted specifically on the aforementioned reported indole-based $P2Y_{12}$ receptor antagonists, taking into consideration the primary biological assay used for their characterization, namely the inhibition of ADP-induced platelet aggregation in rat platelet-rich plasma (rPRP), reported as IC_{50} values in μM. The classification scheme for these compounds was adjusted accordingly: Class A (highly active) with IC_{50} values lower than 0.07 μM, Class B (moderately active) with IC_{50} values between 0.07 and 0.10 μM, Class C (moderately active to inactive) with IC_{50} values above 0.10 μM)) (**Chapter III**). This refined analysis led to the determination of the most promising indole sub-scaffold, which was then utilized in a design and optimization workflow, including a structure–property relationship (SPR) analysis, to fine-tune the biological activity and physicochemical properties of newly designed and synthesized compounds (**Chapter V**) with the aim to develop novel $P2Y_{12}$ receptor antagonists with enhanced potency, selectivity, metabolic stability, and potential BBB permeability. These optimized compounds will be further investigated for their applicability in the

development of ^{18}F- or ^{11}C-labeled radioligands, enabling their use as P2Y$_{12}$-targeted PET tracers for monitoring active microglia in neuroinflammatory conditions (Figure 11).

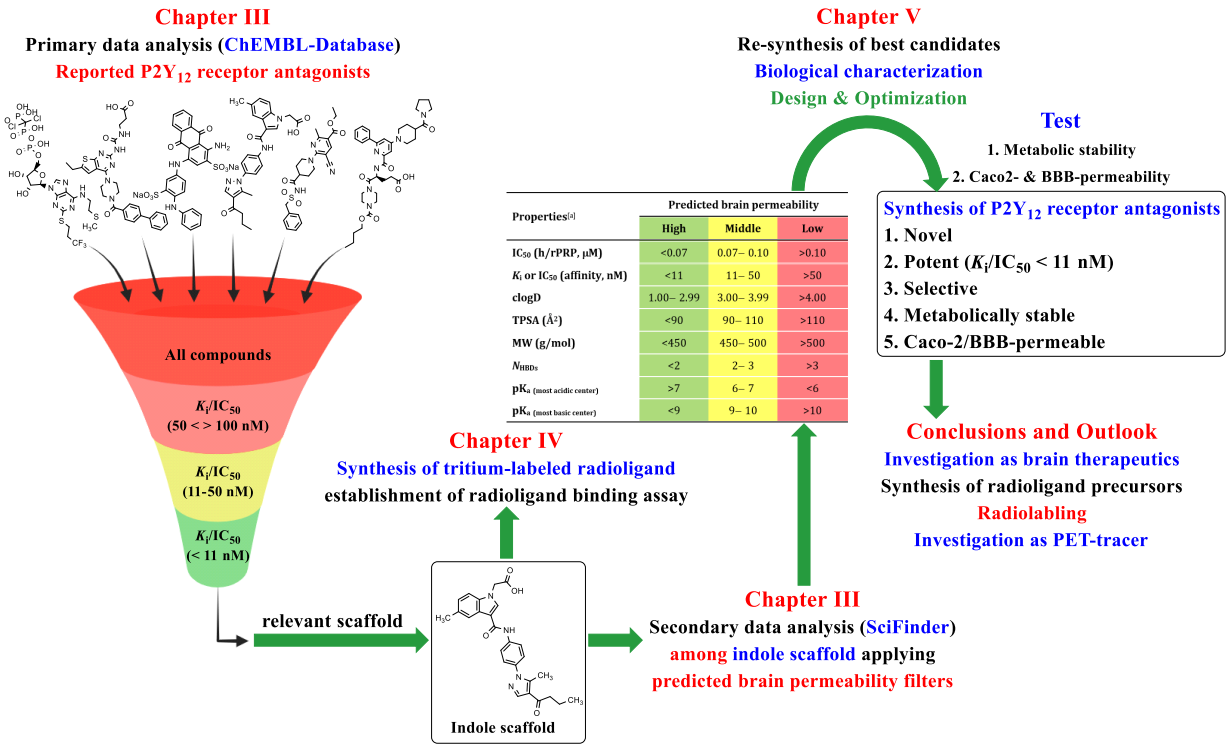


Figure 11. Research and development processes toward the synthesis of P2Y$_{12}$ receptor-targeted PET tracers and potential therapeutics (**Chapters III–V**).

3 Results and discussion

3.1 Chapter I: Synthesis of anthraquinone-based P2Y$_{12}$ receptor antagonists: Structure-activity relationships

3.1.1 Introduction

Exploration of rings **A** and **E** of the anthraquinone derivatives was guided by molecular docking studies conducted on the potent and selective anthraquinone **14** (**PSB-0739**, Figure 12) and its interaction with the P2Y$_{12}$ receptor.[77] These studies provided valuable insights into ligand-receptor interactions, highlighting the potential for modifications at the C6- and C7-positions. The analysis revealed that these positions lie within a vacant space in the receptor binding pocket, suggesting that appropriate substitutions could establish favorable interactions with surrounding amino acid residues, such as S156, H187, and V190 (Figure 12). Similarly, the study indicated that ring **E** and the nitrogen atom of the secondary amine attached to it could be further optimized to enhance receptor binding. Notably, interactions with amino acid residues R256, Y259, and L276 were suggested as potential targets for further modification (Figure 12).

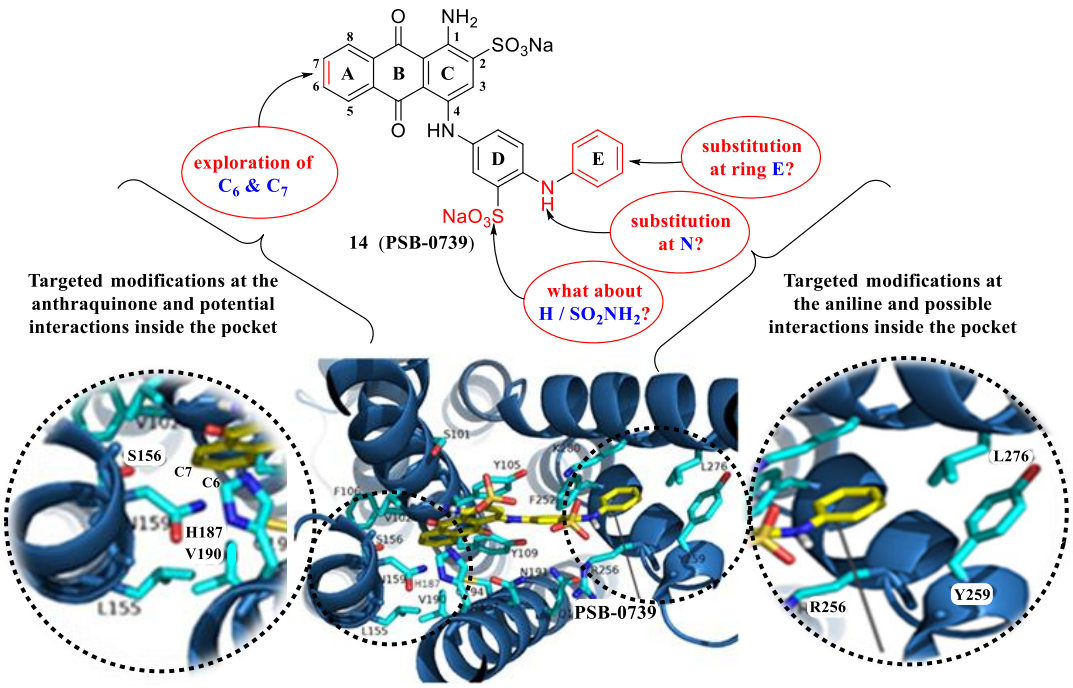


Figure 12. Docking of **PSB-0739** (**2**) into the P2Y$_{12}$ receptors pocket and a close-up to illustrate the residues at the transmembrane domains (TMs) and the vacant space surrounding ring **A**, ring

E, and the ***N***-aniline. Targeted optimization positions are assigned in red at the structure of **14** (**PSB-0739**). The docking study is based on the published X-ray structure.[37–39]

Thus, the current study aims to expand the structure-activity relationship (SAR) studies of the anthraquinone scaffold focusing on two key regions: first, exploration of the C6- and C7-positions of the anthraquinone (**18**, Figure 13), which represents a significant synthetic challenge, as it requires the reconstruction of tailored bromaminc acid derivatives required for the Ullmann-coupling reaction; second, modifications at the aniline moiety (**19**, Figure 13), particularly substitutions at the terminal phenyl ring and its attached secondary amine. This is especially relevant for the development of a radiolabeled ligand. In addition, elimination of the sulfonate at ring **D** or replacing it by a sulfonamide was to be performed. All modified intermediates, including the C2-carboxylic acid-substituted bromaminic acid **20**, were coupled with the appropriate moieties to obtain the final anthraquinone derivatives (Figure 13).

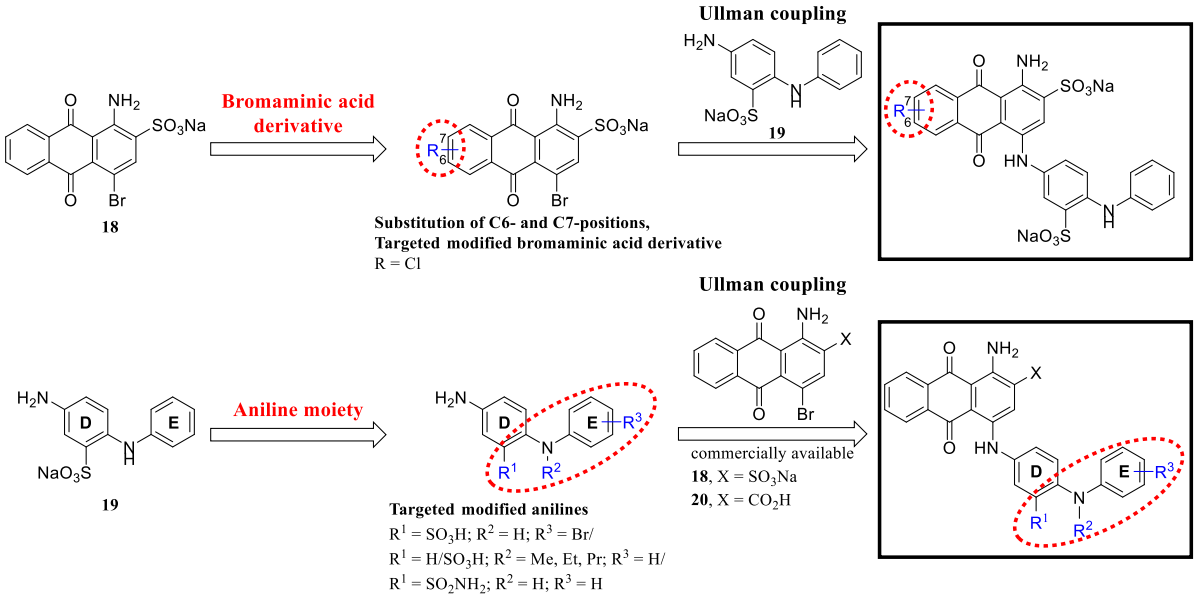


Figure 13. Targeted final anthraquinone-based $P2Y_{12}$ receptor antagonists.

3.1.2 Results and discussion

i. Chemistry

Synthesis of the modified bromaminic acid derivative sodium 1-amino-4-bromo-6/7-chloro-9,10-dioxo-9,10-dihydroanthracene-2-sulfonate (21)

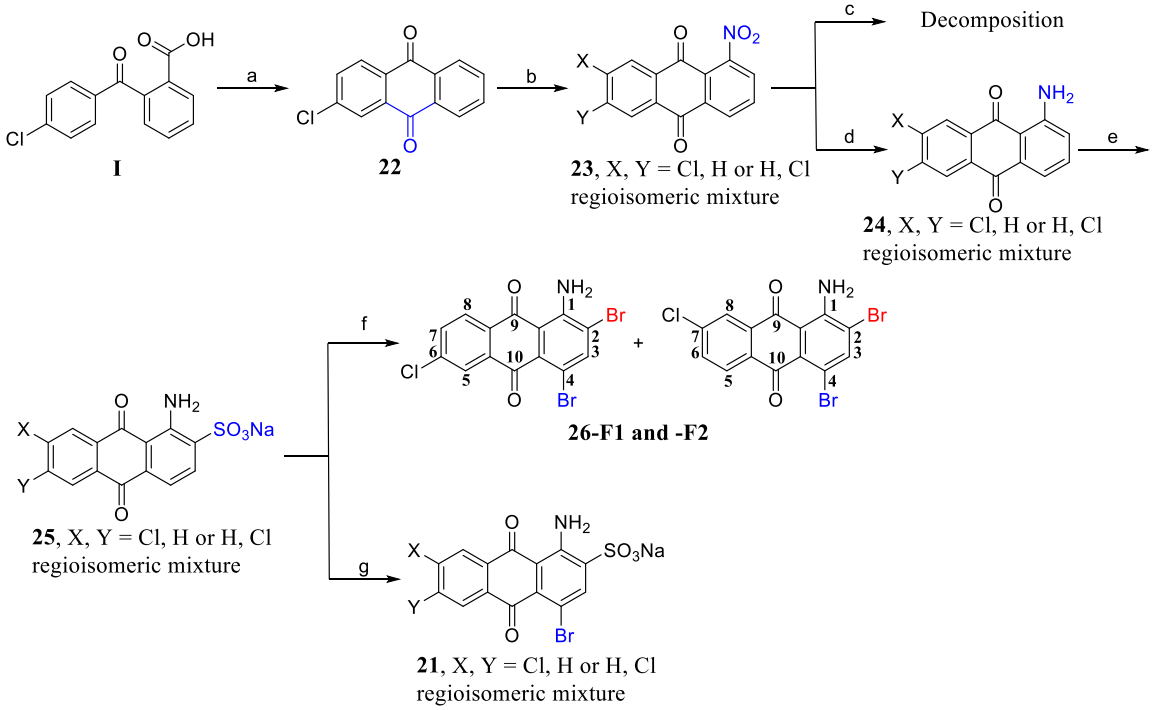
The C6- and C7-position of the anthraquinone core are considered relatively unreactive compared to other positions, necessitating their selective functionalization prior to the final construction of the anthraquinone scaffold. To achieve this, two synthetic strategies were designed, with the following pathway being outlined below.

Pathway A: Five-step synthetic route starting with 2-(4-chlorobenzoyl)benzoic acid (I)

The synthesis began with the investigation of the commercially available compound 2-(4-chlorobenzoyl)benzoic acid derivative (**I**, Scheme 2) in a five-step synthetic sequence: (i) **Acid-mediated cyclization to obtain the anthraquinone core.** Compound **I** was subjected to intramolecular cyclization under harsh acidic conditions using concentrated sulfuric acid (H_2SO_4) under an argon atmosphere at 135 °C for 4 hours to ensure complete cyclization, yielding the modified anthraquinone derivative 2-chloroanthracene-9,10-dione (**22**, Scheme 2). (ii) **Selective nitration at the C1-position.** Electrophilic nitration was carried out on compound **22** using a mixture of fuming nitric acid (HNO_3), sulfuric acid (H_2SO_4), and phosphoric acid (H_3PO_4) in carbon tetrachloride (CCl_4) at 25 °C for 6 hours. This process yielded a regioisomeric mixture of 6-chloro-1-nitroanthracene-9,10-dione and 7-chloro-1-nitroanthracene-9,10-dione (**23**, Scheme 2). (iii) **Reduction of the nitro group.** Two strategies were explored to reduce the nitro group of compounds **23** to form the corresponding regioisomeric mixture of 6-/7-chloro-1-aminoanthracene-9,10-dione (**24**, Scheme 2). First, hydrogenation using Pd/C, 35 psi, in methanol at 25 °C for 2 hours was performed leading to complete decomposition of **23**. Second, stannous chloride reduction using $SnCl_2 \cdot 2H_2O$ in ethanol at 70 °C for 1 hour was tried. This method was effective and reproducibly yielded the regioisomeric mixture of 6-/7-chloro-1- aminoanthracene-9,10-dione (**24**, Scheme 2). (iv) **Sulfonation at the C2-position.** Compounds **24** were sulfonated at the C2-position using chlorosulfonic acid ($HClSO_3$) in nitrobenzene at 130 °C for 90 minutes. After cooling, the reaction mixture was quenched with aqueous sodium carbonate (Na_2CO_3) solution, leading to the formation of the regioisomeric mixture of the C2-sulfonated sodium salts of 1-amino-6-/7-chloro-9,10-dioxo-9,10-dihydroanthracene-2-sulfonate (**25**, Scheme 2). (v) **Bromination at the C4-position.** Bromination of **25** using 2 equivalents of bromine water (Br_2)

in *N*,*N*-dimethylformamide (DMF) at 25 °C for 2 hours led to the substitution at both the targeted C4-position and the C2-sulfonyl position, forming the regioisomeric mixture of 1-amino-2,4-dibromo-6/7-chloroanthracene-9,10-dione derivatives (**26**, Scheme 2). Separation of the mixture has been performed using column chromatography, however differentiation between the 6-chloro- and 7-chloro-substituted derivatives is still challenging. Adjustment of the bromine water equivalency to 0.5, its slow addition over 30 minutes, and minimizing the total reaction time to one hour led to the successful formation of the targeted modified bromaminic acid, sodium 1-amino-4-bromo-6/7-chloro-9,10-dioxo-9,10-dihydroanthracene-2-sulfonate (**21**, Scheme 2).

Scheme 2. Synthesis of sodium 1-amino-4-bromo-6/7-chloro-9,10-dioxo-9,10-dihydroanthracene-2-sulfonate (**21**).[a]



[a]Reaction conditions: a. H_2SO_4, 135 °C, 4 h; b. HNO_3, H_2SO_4, H_3PO_4, CCl_4, 25 °C, 6 h; c. Pd/C, MeOH, H_2 (35 psi), 25 °C, 2 h; d. $SnCl_2 \cdot 2\,H_2O$, EtOH, 70 °C, 1 h; e. $ClSO_3H$, $BzNO_2$, 85 °C, 10 min; 130 °C, 90 min, Na_2CO_3, H_2O, 25 °C; f. Br_2 (2 equiv.), DMF, 25 °C, 2 h; f. Br_2 (0.5 equiv.), DMF, 25 °C, 1 h.

This optimized synthetic route was also tried to introduce further substituents such as F, CH_3, or di-Cl at the unreactive C6- and C7-position of the anthraquinone core. However, none of the trials led to the formation of the desired key-intermediate. Further details are depicted in Scheme S1 in the Supporting Information. In addition, two alternative strategies failed (Pathways B and C,

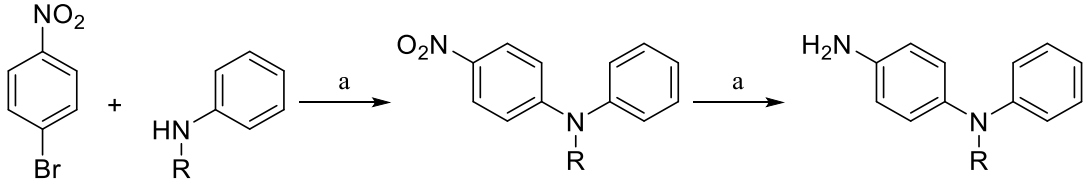
Scheme S2) that were applied to circumvent the regioselectivity challenges encountered during the nitration step (Step 2 of Pathway A), particularly at the C1-position of the anthraquinone scaffold. These routes aimed to introduce the nitro group at an earlier stage by utilizing nitrated benzoylbenzoic acid precursors, thereby enhancing positional control and synthetic efficiency.

Synthesis of modified aniline derivatives

Structure-activity relationship (SAR) analyses demonstrated that the aniline moiety in the C4-position of the anthraquinone scaffold plays a role in modulating the biological activity of anthraquinone-based $P2Y_{12}$ receptor antagonists. Accordingly, a range of substituted aniline derivatives were synthesized to explore this moiety systematically.

Buchwald-Hartwig coupling. Direct alkylation of commercially available aniline derivatives poses selectivity challenges due to the presence of a reactive primary amine ($–NH_2$). To circumvent this, Buchwald–Hartwig cross-coupling was employed using 4-nitrobromobenzene and various secondary amines (*N*-methyl-, *N*-ethyl-, and *N*-propylaniline). The reactions were catalyzed by tris(dibenzylideneacetone)dipalladium (0) ($Pd_2(dba)_3$), in the presence of the Xantphos ligand and cesium carbonate (Cs_2CO_3) in tetrahydrofuran (THF) at 70 °C overnight, affording the desired nitro-substituted derivatives **27**–**29** in good yields (66–84%). Subsequent reduction of these nitro intermediates using $SnCl_2{\cdot}2H_2O$ in refluxing ethanol yielded the corresponding amine intermediates **30**–**32** (Scheme 5).

Scheme 3. Synthesis of the targeted modified aniline intermediates **30**–**32**.[a]



R = Me, Et, Propyl

27, R = Me
28, R = Et
29, R = Pr

30, R = Me
31, R = Et
32, R = Pr

[a]Reaction conditions: a. Cs_2CO_3, THF, Xantphos, $Pd_2(dba)_3$, 70 °C, 16 h; b. $SnCl_2{\cdot}2\,H_2O$, EtOH, 80 °C, 16 h.

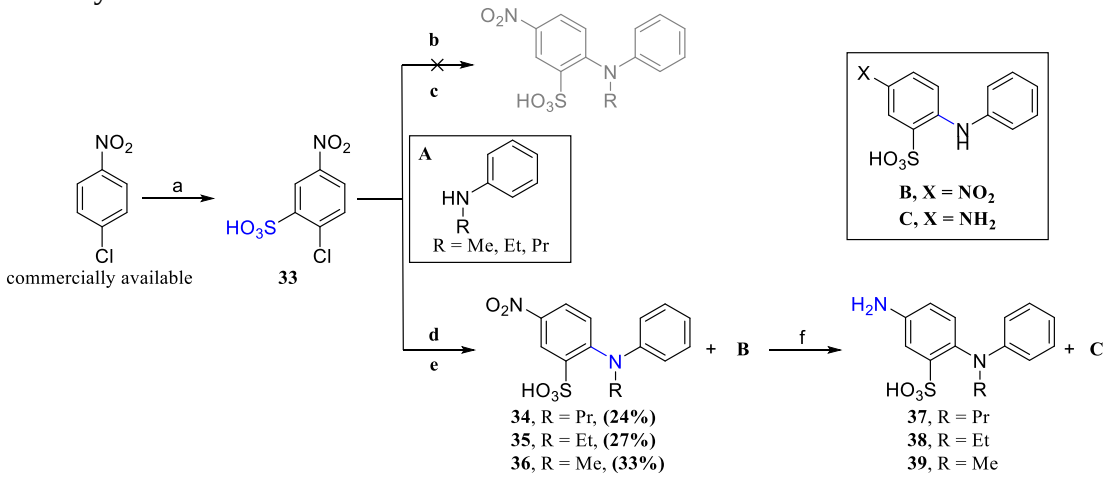
Incorporation of the sulfonic acid functionality. To enhance the potency of the compounds, a sulfonic acid moiety was introduced at the *meta*-position relative to the nitro group. For this

purpose, 4-nitrochlorobenzene was sulfonated using 20% oleum ($SO_3 \cdot H_2SO_4$) at 140 °C under argon for 16 hours, yielding 2-chloro-5-nitrobenzenesulfonic acid (**33**, Scheme 4).

Attempts to couple **33** with secondary amines (*N*-methyl-, *N*-ethyl-, and *N*-propylaniline) under Buchwald–Hartwig conditions failed, likely due to (i) the poor leaving ability of the chloro group, and (ii) the strong electron-withdrawing effect of the adjacent sulfonic acid group, which further deactivates the aromatic ring. Multiple trials using microwave or thermal conditions with various bases such as Et_3N, Cs_2CO_3 were unsuccessful (Scheme 4). Scheme S3 displays two strategies to overcome the deactivation effect of the sulfonic acid group, either by protecting it or the replacement of the leaving group (chloro) by a better one (bromo).

Amination and reduction. To overcome these limitations, **33** was reacted with an excess of liquid secondary aniline derivatives under microwave irradiation (300 W, 150 °C, 3 h). While minimal yield was observed (e.g., ~5% yield for **33** with *N*-propylaniline), improved yields (24–33%) were achieved via thermal reactions in a pressure tube at 150 °C over 3 days. Products **34** (*N*-propyl), **35** (*N*-ethyl), and **36** (*N*-methyl) were obtained alongside a side-product, the corresponding primary aniline (**B**), indicating cleavage of the alkyl group. Due to inseparable by-product contamination, crude products were directly subjected to zinc/ammonium chloride-mediated reduction in EtOH/H_2O (1:1) at 100 °C for 1 hour, affording **37** (*N*-propyl), **38** (*N*-ethyl), and **39** (*N*-methyl) beside their analogs (**C**) (Scheme 4), which were subsequently used with bromaminic acid **18** in the Ullmann-coupling reaction.

Scheme 4. Synthesis of **33** and the modified aniline derivatives **37**–**39**.[a]



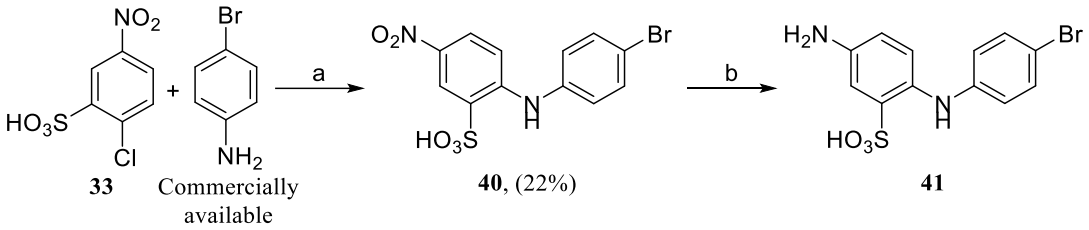
[a]Reaction conditions: a. 20% $SO_3.H_2SO_4$, 0 °C; 140 °C, 16 h; b. Cs_2CO_3, THF, **A**, Xantphos, $Pd_2(dba)_3$, 70 °C, 16 h; c. **A**, NEt_3/Cs_2CO_3/NaH, microwave or thermal at 120 °C $SnCl_2 \cdot 2\ H_2O$,

EtOH, 80 °C, 16 h; d. **A**, microwave (300 W, 150 °C, 15 mbr, 3 h (~5% of **34**)); e. **A**, 150 °C, 3 d; f. Zn, NH_4Cl, EtOH:H_2O (1:1), 100 °C, 1 h.

Radioligand precursors

To prepare precursors for radiolabeled derivatives, solid halogenated anilines were reacted with **33** in DMF at 150 °C for 3 days. Of five trials, only the reaction with 4-bromoaniline yielded a product, 2-((4-bromophenyl)amino)-5-nitrobenzenesulfonic acid **40** (22%) (Scheme 7), which was reduced to **41** using zinc powder. Compound **41** (Scheme 7) served as a key intermediate for the potential radioligand precursors **16** and **17** (Scheme 1).

Scheme 5. Synthesis of the modified aniline derivative **41** as an intermediate for the synthesis of potential radioligand precursors.[a]

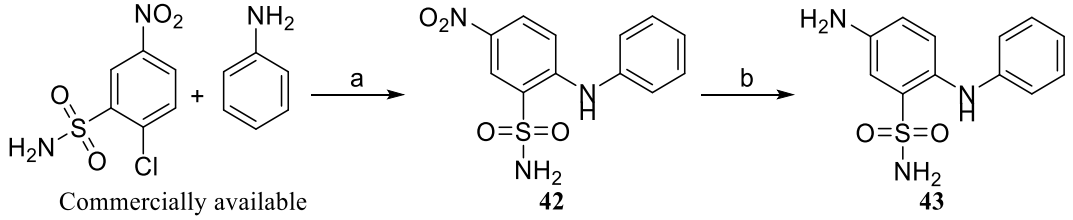


[a]Reaction conditions: a. DMF, 150 °C, 3 d; b. Zn, NH_4Cl, EtOH:H_2O (1:1), 100 °C, 1 h.

Sulfonamide substitution strategy

To reduce deactivation while retaining hydrophilicity, the sulfonic acid was replaced with a sulfonamide. Commercially available 2-chloro-5-nitrobenzenesulfonamide was reacted with aniline in 3-chlorotoluene at 160 °C for 2 days, affording 5-nitro-2-(phenylamino)benzenesulfonamide **42**, which was then reduced using zinc to give **43** (Scheme 6).

Scheme 6. Synthesis of the modified aniline 5-amino-2-(phenylamino)benzenesulfonamide (**43**).[a]

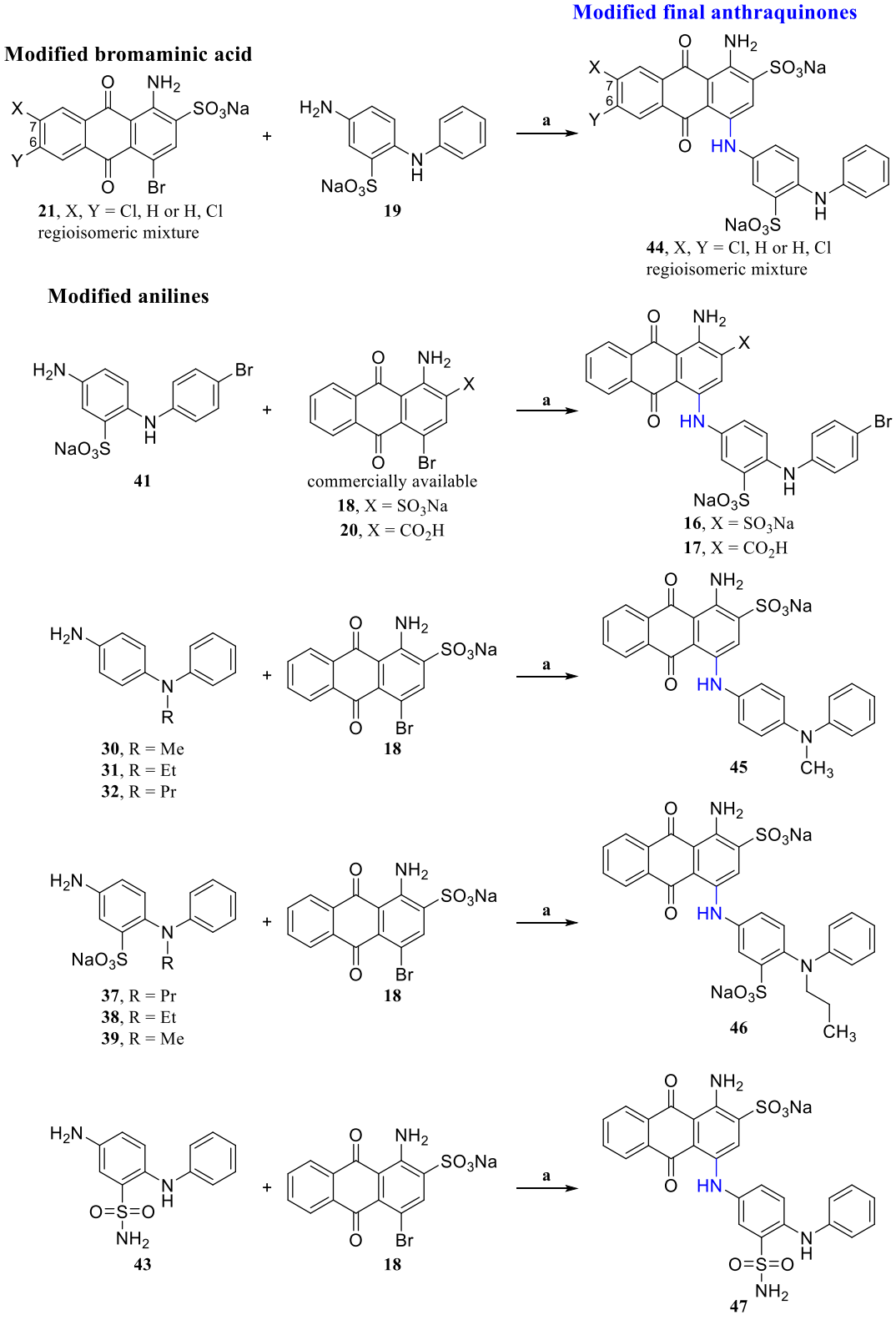


[a]Reaction conditions: a. 3-chlorotoluene, 160 °C, 2 d; b. Zn, NH_4Cl, EtOH:H_2O (1:1), 100 °C, 1 h.

Synthesis of final anthraquinone derivatives 16, 17 and 44−47

The anthraquinone derivatives were obtained by an Ullmann-coupling reaction to form a C−N-bond between the modified bromaminic acid **21** and the aniline (sodium 5-amino-2-(phenylamino)benzenesulfonate) **19** using elemental copper powder (Cu^0) as a catalyst in phosphate buffer (pH 6− 7). The reaction was performed under microwave irradiation at 100−120 °C to afford a regioisomeric mixture (83:13%) of C6- and C7-chloro-substituted final compounds **44** (Scheme 7). The same reaction conditions were applied to couple the commercially available bromaminic acids sodium 1-amino-4-bromo-9,10-dioxo-9,10-dihydroanthracene-2-sulfonate (**18**) and 1-amino-4-bromo-9,10-dioxo-9,10-dihydroanthracene-2-carboxylic acid (**20**) to the previously prepared aniline 5-amino-2-((4-bromophenyl)amino)benzenesulfonic acid (**41**), which resulted in the formation of the two radioligand precursors **16** and **17** (Scheme 7). Compound **18** was further investigated in the coupling to the synthesized anilines N^1-methyl-N^1-phenylbenzene-1,4-diamine (**30**), N^1-ethyl-N^1-phenylbenzene-1,4-diamine (**31**), N^1-phenyl-N^1-propylbenzene-1,4-diamine (**32**), 5-amino-2-(phenyl(propyl)amino)benzenesulfonic acid (**37**), 5-amino-2-(ethyl(phenyl)amino)benzenesulfonic acid (**38**), 5-amino-2-(methyl(phenyl)amino)benzenesulfonic acid (**39**), and 5-amino-2-(phenylamino)benzenesulfonamide (**43**) to afford the final compounds **45− 47** (Scheme 7). Coupling reactions involving the aniline intermediates **31**, **32**, **38**, and **39** were not completed due to byproduct formation or purification issues.

Scheme 7. Synthesis of the final anthraquinone derivatives **16**, **17** and **44**–**47**.[a]



[a]Reaction conditions: a. Cu^0, phosphate buffer, microwave, 100–120 °C.

i. Biological activity

All synthesized final compounds **16**, **17** and **44**–**47** (Scheme 7) were investigated at the human $P2Y_{12}$ receptor in two different biological assays, a ***radioligand binding assay*** using the recently developed antagonist radioligand **[^{3}H]PSB-22219** (**48**, **A**, Figure 14, Chapter 5),[86] and a functional assay measuring ***ß-arrestin recruitment*** by enzyme (galactosidase) complementation,[104,105] where the antagonistic activity was tested versus 2-methylthioadenosine diphosphate (2-MeSADP) (**49**, **B**, Figure 14) as an agonist. The approved antithrombotic $P2Y_{12}$ receptor antagonist ticagrelor was tested in the same assay for comparison (**48**, **B**, Figure 14).

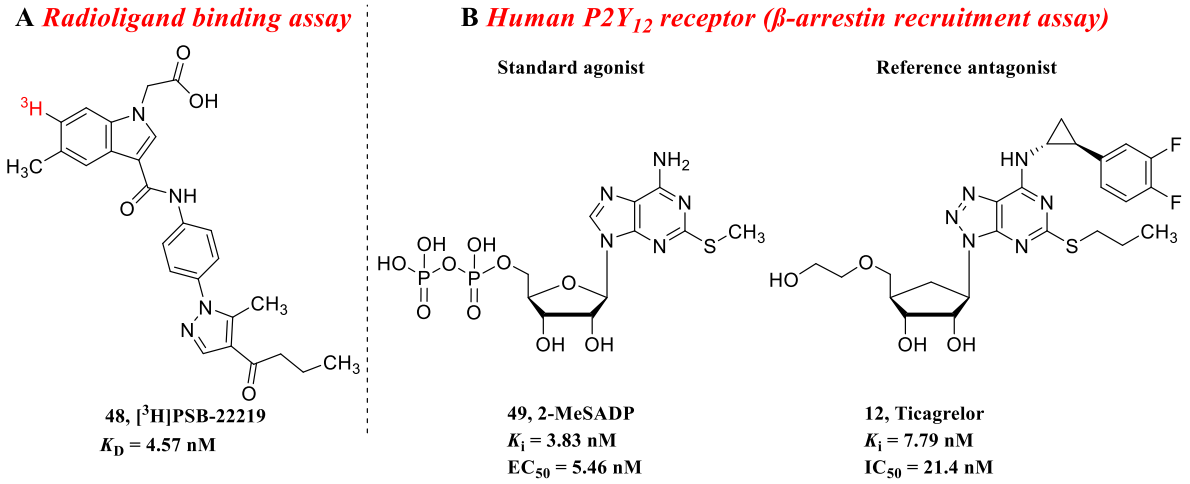
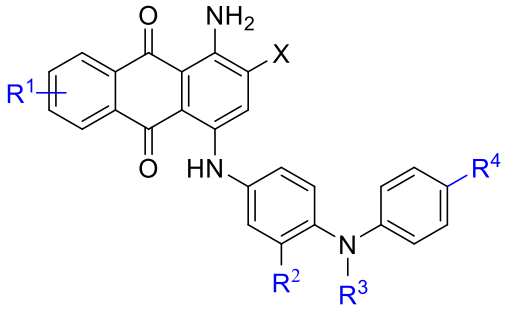


Figure 14. Structures of the $P2Y_{12}$ receptor antagonist radioligand [^{3}H]PSB-22219, the agonist 2-MeSADP, and the antagonist ticagrelor.

The most potent anthraquinone-based $P2Y_{12}$ receptor antagonists PSB-0739 (**14**) and PSB-0702 (**15**) were tested as well and demonstrated their high potency in both assays. Table 2 displays the affinity and potency values for all final compounds.

Table 2. Biological results of the developed anthraquinone-based $P2Y_{12}$-receptor antagonists. Affinities of compounds at human $P2Y_{12}$ receptor determined in [^{3}H]PSB-22219 radioligand binding assay (K_i-values), compared to the data from β-arrestin recruitment assays (IC_{50}-values).



Compd.	X	R¹	R²	R³	R⁴	K_i (µM)[a]	IC_{50} (µM)[b]
14 PSB-0739	SO_3Na	H	SO_3Na	H	H	**0.00431**	**0.0613**
15 PSB-0702	CO_2H	H	SO_3Na	H	H	**0.0146**	**1.21**
16	SO_3Na	H	SO_3Na	H	Br	**0.0182**	**1.52**
17	CO_2H	H	SO_3Na	H	Br	**0.0197**	**2.41**
44	SO_3Na	6/7-Cl regioisomeric mixture 83:13%	SO_3Na	H	H	**0.0718**	**2.56**
45	SO_3Na	H	H	CH_3	H	**0.0597**	**0.931**
46	SO_3Na	H	SO_3Na	C_3H_7	H	**1.3430**	**> 10**
47	SO_3Na	H	SO_2NH_2	H	H	**0.0813**	**3.89**

[a] Human $P2Y_{12}$ receptor vs. [^{3}H]PSB-22219 in recombinantly expressing CHO cell membrane preparations. Data represent mean ± SEM of 3-4 independent experiments each in duplicates.
[b] Human $P2Y_{12}$ receptor *β*-arrestin assay (IC_{50} or % inhibition vs an EC_{80} concentration of the standard agonist 2-MeSADP (25 nM)). Data represent mean ± SEM of 3-4 independent experiments each in duplicates.

Structure-activity relationship study

The C6- and C7- regioisomeric mixture of **44** showed a decrease in potency. More potential for high potency has the modifications at the aniline moiety. The free nitrogen (NH) of the secondary amine between the rings **D** and **E** represents the best substituent (**14, PSB-0739**), an attached methyl was found to be tolerated (**45**), however the propyl led to a loss in potency (**46**). The sulfonate attached to ring **D** remains the best substituent (**14**, **PSB-0739**) in comparison to its unsubstituted or sulfonamide-substituted analogs (**45** and **47**). In addition, the 4-Br-substituted ring E of **16** and **17** showed good tolerability compared to their analogs **14** (**PSB-0739**) and **15** (**PSB-0702**), respectively (Figure 15).

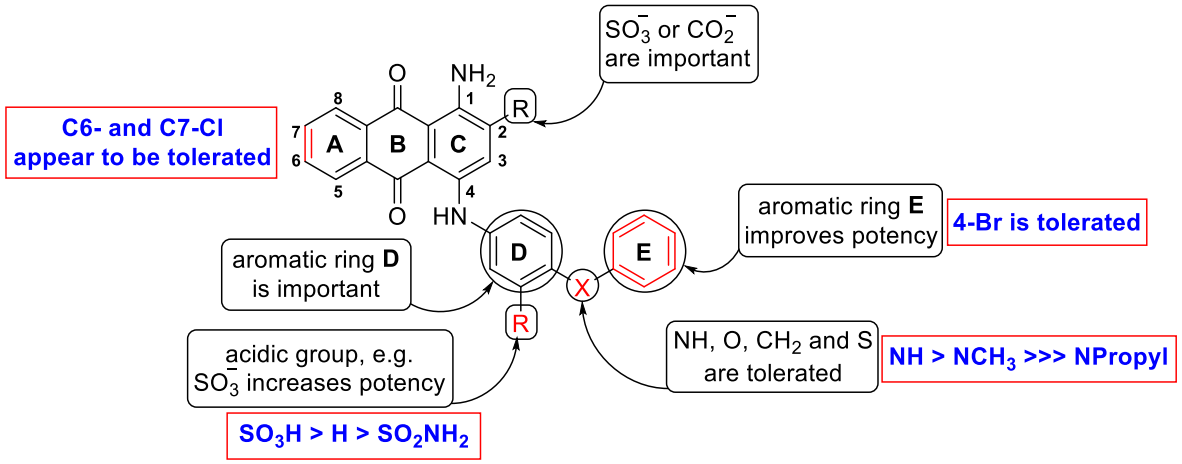
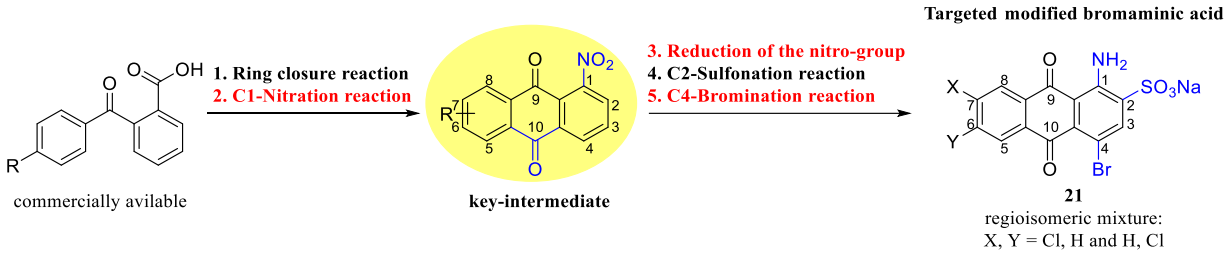


Figure 15. Update of the published structure-activity relationship analysis of the anthraquinone scaffold.[35] Positions modified in the present study are assigned in red.

3.1.1 Conclusions and outlook

Through extensive experimentation and multiple synthetic trials, successful approaches for synthesizing the targeted intermediates and subsequently the final compounds were developed. Three critical observations emerged during the reconstruction of bromaminic acid: First, the non-selective nitration step led to the synthesis of unwanted by-products. Second, the anthraquinone demonstrated instability under Pd-catalyzed hydrogenation conditions, resulting in a complete degradation of the nitroanthraquinone derivative. Third, sulfonate group elimination at the C2-position during the bromination step complicated the synthetic process (Scheme 8). Despite these challenges we succeeded in the synthesis of a regioisomeric mixture of C6- and C7-chloro-substituted bromaminic acid (**21**, Scheme 8).

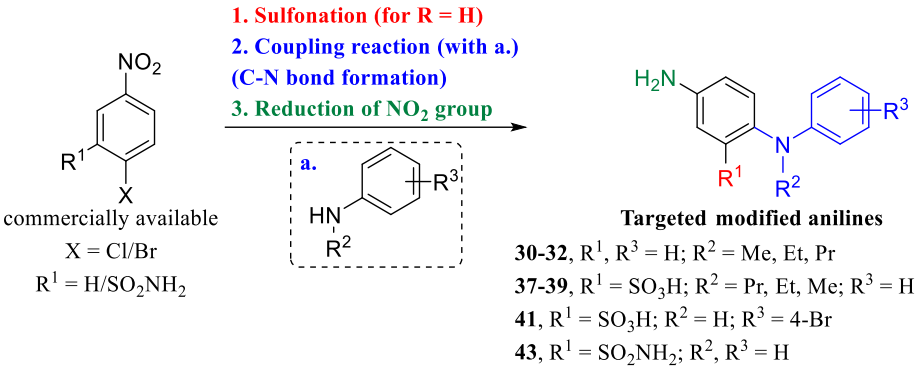
Scheme 8. Outlined synthesis pathway for the modified bromaminic acid derivatives. Challenging steps were highlighted in red.



Beyond the synthesis of the substituted bromaminic acid, modifications of the aniline moiety represented an important strategy for studying the structure-activity relationships (SARs) of the

anthraquinone scaffold. This aspect was especially relevant for the development of radiolabeled ligands within this series. A synthetic pathway to achieve the desired modifications was established leading to the formation of the targeted modified aniline derivatives **30**–**32**, **37**–**39**, **41**, and **43** (Scheme 9). These advancements may be beneficial for the continued development of novel anthraquinone-based $P2Y_{12}$ receptor antagonists with improved pharmacokinetic properties and as potential precursors for the synthesis of a radioligand.

Scheme 9. Synthesis pathway of the targeted modified aniline derivatives.



Reaction of the aforementioned intermediates (Scheme 8 and 9) by Ullmann-coupling reaction to the appropriate aniline (**19**, Scheme 7) or bromaminic acid (**18** or **20**, Scheme 7) led to the formation of the targeted modified final anthraquinone-based $P2Y_{12}$ receptor antagonists **16**, **17**, and **44**–**47** (Figure 16).

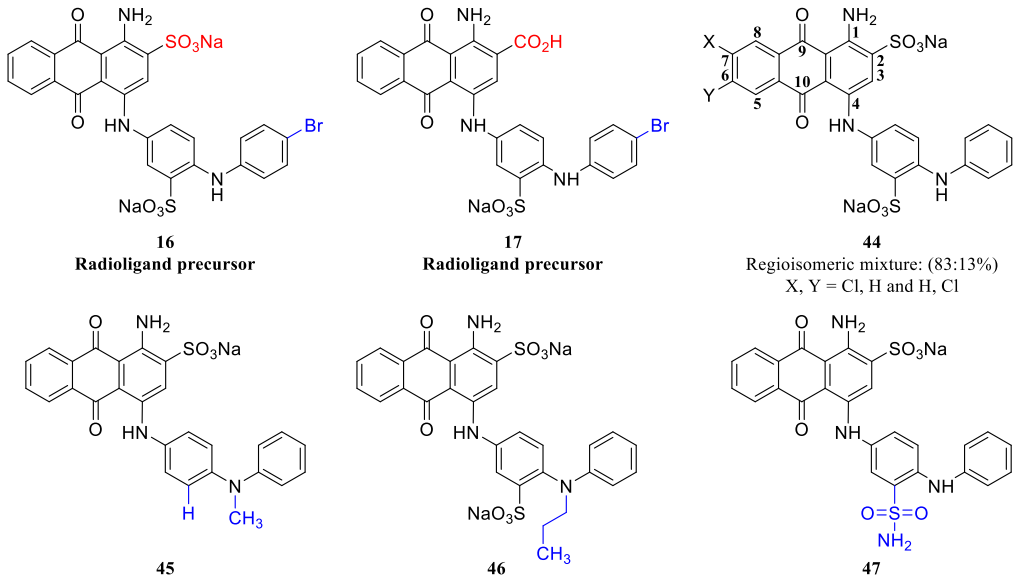


Figure 16. Structures of synthesized modified anthraquinone derivatives **16**, **17**, and **44**–**47**.

Future work will be focusing on the optimization of these synthesis pathways to expand the SAR-study and enhance the synthesis of anthraquinone-based potent and selective $P2Y_{12}$ receptor antagonists.

3.1.4 Experimental part

Materials and reagents

All commercially available reagents were used as purchased (abcr, Acros, Alfa Aesar, BLDpharm, Sigma-Aldrich, or TCI). Solvents were used without additional purification or drying. Thin-layer chromatography (TLC) and reversed phase thin-layer chromatography (RP-18-TLC) using aluminum sheets with silica gel 60 F_{254} and RP silica gel 18 F_{254} were utilized to monitor the reactions (Merck). Colored compounds were visible at daylight; other compounds were visualized under UV light (254 nm). Flash chromatography was performed on a Büchi system using silica gel RP-18 (Merck). All synthesized compounds were finally dried in vacuum at 8−12 Pa (0.08−0.12 mbar) using a sliding vane rotary vacuum pump (Vacuubrand GmbH). A freeze-dryer (CHRIST ALPHA 1-4 LSC) was used for lyophilization. ^{1}H and ^{13}C NMR data were collected on a Bruker Avance 500 MHz NMR spectrometer at 500 MHz (^{1}H) or 126 MHz (^{13}C), respectively. If indicated, NMR data were collected on a Bruker Ascend 600 MHz NMR spectrometer at 600 MHz (^{1}H) or 151 MHz (^{13}C). DMSO-d_6 was used as a solvent at 303 K. Chemical shifts are reported in parts per million (ppm) relative to the deuterated solvent: DMSO, δ ^{1}H: 2.49 ppm; ^{13}C: 39.7 ppm. Coupling constants *J* are given in Hertz, and spin multiplicities are given as s (singlet), d (doublet), dd (doublet of doublet), t (triplet), q (quartet), sext (sextet), m (multiplet), and br (broad). The purities of all isolated products were determined by an HPLC 1260 Infinity II (Agilent) using an EC 50/2 Nucleodur C18 Gravity 3 μm column (Macherey-Nagel), coupled to a UV/vis diode array detector, and a mass spectrometer (Infinity Lab LC MSD system, Agilent, with an EC 50/2 Nucleodur C18 Gravity 3 μm column, Machery-Nagel). All compounds are >95% pure by HPLC/UV. The column temperature was 40 degrees. The compounds were dissolved at a concentration of 1.0 mg/mL in water, methanol, or acetonitrile. Then, 2 μL of the sample solution was injected to a flow of 0.5 mL/min. Elution started with a gradient of water containing 2 mM ammonium acetate/acetonitrile from 90:10 to 0:100 for 10 min, and then, it was flushed with 100% acetonitrile for an additional 5 min. Positive total ion scans were observed from 100−1000 *m*/*z* (or more if necessary). UV absorption was detected from 190 to 600 nm using a diode array detector

(DAD). The purity of all compounds was determined at 220−600 nm. For microwave reactions a CEM Focused Microwave Synthesis type Discover apparatus was used. The general procedure for the synthesis of final compounds is described below. Following compounds were reported previously: **14**, **15**,[35] **22**,[106] **23**, **24**,[107,108] **27**, **28**, **30**, **31**,[109] **33**,[110] **42**,[111,112] however they were prepared by other procedures. Thus, comprehensive synthesis of both reported and novel intermediates, as well as the analytical characterization of all compounds, are provided in the Supporting Information (SI).

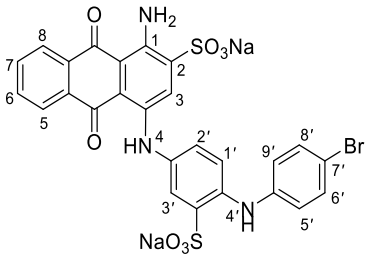
Synthesis of the desired final anthraquinone derivatives

General procedure A[35]

A 10 mL microwave reaction vessel equipped with a magnetic stir bar was charged with sodium 1-amino-4-bromo-9,10-dioxo-9,10-dihydroanthracene-2-sulfonate (**18**) (1.0 equiv.) as the aryl halide coupling partner. For the synthesis of the radioligand precursor **17**, 1-amino-4-bromo-9,10-dioxo-9,10-dihydroanthracene-2-carboxylic acid (1.0 equiv.) (**20**) was used instead. To the vessel, the desired aniline derivative (2.0 equiv.), elemental copper (Cu^0) powder (catalytic amount), and a phosphate buffer system comprising Na_2HPO_4 (pH 9.6, 4.5 mL) and NaH_2PO_4 (pH 4.2, 0.5 mL) were added. The reaction mixture was sealed and subjected to microwave irradiation at 80–100 W for 5–10 minutes at 120 °C.

Upon completion, the reaction mixture was allowed to cool to room temperature and filtered to remove residual copper. The filtrate was extracted with dichloromethane (ca. 200 mL) and water. The aqueous phase was concentrated under reduced pressure to a volume of 10–20 mL and subsequently purified by flash chromatography using RP-18 reversed-phase silica gel with water as the initial eluent. Stepwise increases in eluent polarity were achieved by adding acetone or methanol at concentrations of 5%, 10%, 20%, 40%, and 60%. Fractions containing the desired blue-colored product were combined and subjected to rotary evaporation to remove organic solvents and reduce the aqueous volume. Final drying was achieved by lyophilization to afford the pure products as solid blue powders:

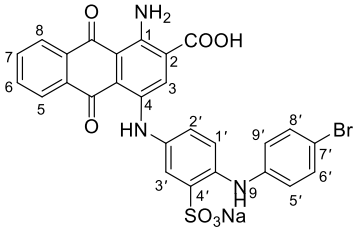
Sodium 1-amino-4-((4-((4-bromophenyl)amino)-3-sulfonatophenyl)amino)-9,10-dioxo-9,10-dihydroanthracene-2-sulfonate (**16**)



Chemical formula: $C_{26}H_{16}BrN_3Na_2O_8S_2$
Molecular weight: 688.43 g/mol
Calculations: Reactants: bromaminic acid (0.05 g, 0.13 mmol), aniline (0.09 g, 0.26 mmol)
Reaction conditions: 11 min, 120 °C, 100 W; pressure up to 10 bar.
Purification: Purification step has been repeated five times. Polarity of the eluent was decreased by the addition of acetone in the following steps: 5, 10, 20, 40, and 60%.
Yield: 31%, as blue powder (26.00 mg, 0.04 mmol)
LC-MS (m/z): 642.97 $[M-2Na^+ + 2H]^+$ (purity: 97%)
Mp: >300 °C

^{1}H NMR (600 MHz, DMSO-d_6) δ 12.12 (s, 1H, 4-NH), 8.63 (s, 1H, 4'-NH), 8.29 (dt, J = 6.8, 1.6 Hz, 2H, 6-H, 7-H), 7.90 – 7.78 (m, 3H, 3-H, 5-H, 8-H), 7.50 (d, J = 2.6 Hz, 2H, 6'-H, 8'-H), 7.42 (d, J = 8.8 Hz, 1H, 3'-H), 7.34 (d, J = 8.6 Hz, 1H, 1'-H), 7.17 (dd, J = 8.6, 2.7 Hz, 2H, 5'-H, 9'-H), 7.07 (d, J = 8.8 Hz, 1H, 2'-H); ^{13}C NMR (151 MHz, DMSO) δ 181.97, 181.75, 144.32, 143.14, 142.44, 141.95, 136.93, 135.92, 134.25, 133.82, 133.05, 132.79, 132.13, 130.17, 126.12, 125.79, 123.91, 122.68, 119.65, 116.53, 111.50, 110.56, 109.07.

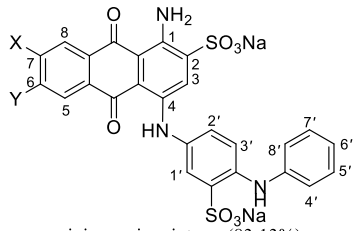
Sodium 5-((4-amino-3-carboxy-9,10-dioxo-9,10-dihydroanthracen-1-yl)amino)-2-((4-bromophenyl)amino)benzenesulfonate (**17**)



Chemical formula: $C_{27}H_{17}BrN_3NaO_7S$
Molecular weight: 630.40 g/mol
Calculations: Reactants: bromaminic acid (0.04 g, 0.115 mmol), aniline (0.08 g, 0.23 mmol)
Reaction conditions: 10 min, 120 °C, 100 W; pressure up to 10 bar.
Purification: Purification step has been repeated four times. Polarity of the eluent was decreased by the addition of acetone in the following steps: 5, 10, 20, 40, and 60%.
Yield: 29%, as blue powder (18.00 mg, 0.03 mmol)
LC-MS (m/z): 608.10 $[M - Na^+ + H]^+$ (purity: 95%)
Mp: >300 °C

^{1}H NMR (600 MHz, DMSO-d_6) δ 11.77 (s, 1H, 4-NH), 8.61 (s, 1H, 9-NH), 8.29 (ddd, J = 6.2, 3.7, 1.6 Hz, 2H, 6-H, 7-H), 8.19 (s, 1H, 3-H), 7.86 (p, J = 7.5, 6.9 Hz, 2H, 5-H, 8-H), 7.54 (d, J = 2.4 Hz, 1H, 2'-H), 7.42 (d, J = 8.7 Hz, 2H, 6'-H, 8'-H), 7.34 (d, J = 8.5 Hz, 1H, 3'-H), 7.21 (dd, J = 8.5, 2.5 Hz, 1H, 1'-H), 7.07 (d, J = 8.7 Hz, 2H, 5'-H, 9'-H); ^{13}C NMR (151 MHz, DMSO) δ 182.89, 181.95, 167.63, 142.05, 136.80, 135.98, 134.29, 133.58, 133.45, 132.99, 132.17, 130.49, 126.23, 126.15, 125.71, 123.52, 119.63, 116.57, 111.50.

Sodium 1-amino-6-chloro-9,10-dioxo-4-((4-(phenylamino)-3-sulfonatophenyl)amino)-9,10-dihydroanthracene-2-sulfonate (**44**)

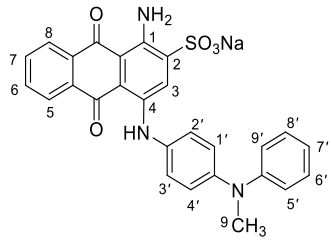


regioisomeric mixture: (83:13%)
X, Y = Cl, H and H, Cl

Chemical formula: $C_{26}H_{16}ClN_2NaO_5S_2$
Molecular weight: 558.99 g/mol
Calculations: Reactants: modified bromaminic acid (0.065 g, 0.156 mmol), aniline (0.08 g, 0.31 mmol)
Reaction conditions: 10 min, 120 °C, 100 W; pressure up to 10 bar.
Purification: Purification step has been repeated three times. Polarity of the eluent was decreased by the addition of acetone in the following steps: 5, 10, 20, 40, and 60%. HPLC-purification showed one clear peak.
Combined yield: 14% (over two steps), as blue powder (11.50 mg, 0.02 mmol).
LC-MS (m/z): 598.20 $[M - 2Na^+ + H]^+$, 83%:13% is the best purity measured so far.

(The compound has been registered as two isomers (83:13) due to the NMR-analysis that confirmed the existence of another compound)

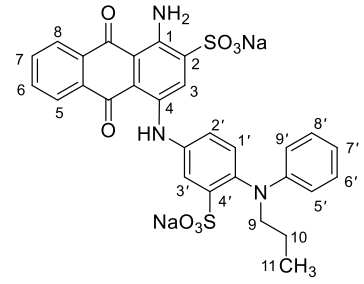
Sodium 1-amino-4-((4-(methyl(phenyl)amino)phenyl)amino)-9,10-dioxo-9,10-dihydroanthracene-2-sulfonate (**45**)



Chemical formula: $C_{27}H_{20}N_3NaO_5S$
Molecular weight: 521.52 g/mol
Calculations: Reactants: bromaminic acid **4** (0.1 g, 0.26 mmol), aniline **12** (0.10 g, 0.52 mmol)
Reaction conditions: 8 min, 120 °C, 100 W; pressure up to 10 bar.
Purification: Purification step has been repeated three times. Polarity of the eluent was decreased by the addition of acetone in the following steps: 5, 10, 20, 40, and 60%.
Yield: 18%, as blue powder (24.00 mg, 0.047 mmol)
LC-MS (m/z): 500.30 $[M - Na^+ + H]^+$ (purity: 95%)
Mp: >300 °C

^{1}H NMR (600 MHz, DMSO-d_6) δ 12.11 (s, 1H, 4-NH), 8.27 (ddt, J = 6.1, 4.2, 2.4 Hz, 2H, 6-H, 7-H), 7.95 (s, 1H, 3-H), 7.88 – 7.81 (m, 2H, 5-H, 8-H), 7.30 (dd, J = 8.5, 7.4 Hz, 2H, 2'-H, 3'-H), 7.20 (d, J = 8.8 Hz, 2H, 6'-H, 8'-H), 7.08 – 7.03 (m, 4H, 1'-H, 4'-H, 5'-H, 9'-H), 6.96 (t, J = 7.3 Hz, 1H, 7'-H), 3.25 (s, 3H, 9-H); ^{13}C NMR (151 MHz, DMSO) δ 182.00, 181.76, 148.67, 145.91, 144.38, 143.13, 142.09, 134.28, 133.84, 133.11, 132.83, 132.26, 129.46, 126.17, 126.04, 124.97, 122.78, 121.55, 121.00, 120.56, 110.71, 109.11, 40.23.

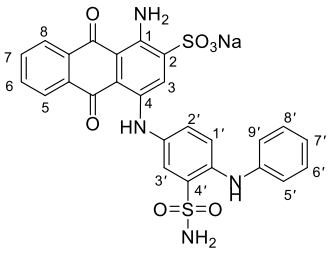
Sodium 1-amino-9,10-dioxo-4-((4-(phenyl(propyl)amino)-3-sulfonatophenyl)amino)-9,10-dihydroanthracene-2-sulfonate (**46**)



Chemical formula: $C_{29}H_{23}N_3Na_2O_8S_2$
Molecular weight: 629.63 g/mol
Calculations: Reactants: bromaminic acid (0.07 g, 0.18 mmol), aniline (0.112 g, 0.37 mmol)
Reaction conditions: 8 min, 120 °C, 100 W; pressure up to 10 bar.
Purification: Purification step has been repeated five times. Polarity of the eluent was decreased by the addition of acetone in the following steps: 5, 10, 20, 40, and 60%.
Yield: 2%, as blue powder (2.34 mg, 3.60 μmol)
The best registered LC-MS (m/z): 607.11 $[M - 2Na^+ + 2H]^+$ (purity: 98%)
Mp: >300 °C

^{1}H NMR (600 MHz, DMSO-d_6) δ 12.15 (s, 1H, 4-NH), 8.32 – 8.26 (m, 2H, 6-H, 7-H), 8.07 (s, 1H, 3-H), 7.86 (ddd, J = 6.6, 4.0, 1.8 Hz, 2H, 5-H, 8-H), 7.76 (d, J = 2.7 Hz, 1H, 3'-H), 7.27 (dd, J = 8.3, 2.7 Hz, 1H, 2'-H), 7.06 – 6.97 (m, 3H, 1'-H, 6'-H, 8'-H), 6.50 (t, J = 7.2 Hz, 1H, 7'-H), 6.41 (d, J = 8.2 Hz, 2H, 5'-H, 9'-H) , 3.63 – 3.57 (m, 2H, 9-H), 1.62 (dq, J = 15.1, 7.5 Hz, 2H), 1.24 (d, J = 14.0 Hz, 2H, 10-H), 0.87 (t, J = 7.4 Hz, 3H, 11-H).

Sodium 1-amino-9,10-dioxo-4-((4-(phenylamino)-3-sulfamoylphenyl)amino)-9,10-dihydroanthracene-2-sulfonate (**47**)



Chemical formula: $C_{26}H_{19}N_4NaO_7S_2$
Molecular weight: 586.57 g/mol
Calculations: Reactants: bromaminic acid (0.1 g, 0.26 mmol), aniline (0.14 g, 0.52 mmol)
Reaction conditions: 17 min, 120 °C, 100 W; pressure up to 10 bar.
Purification: Purification step has been repeated three times. Polarity of the eluent was decreased by the addition of acetone in the following steps: 5, 10, 20, and 40%.
Yield: 45%, as blue powder (69.00 mg, 0.12 mmol)
LC-MS (m/z): 565.20 $[M-Na^+ + H]^+$ (purity: 98%)
Mp: >300 °C

^{1}H NMR (500 MHz, DMSO-d_6) δ 12.00 (s, 1H, 4-NH), 8.33 – 8.23 (m, 2H, 6-H, 7-H), 7.87 – 7.84 (m, 2H, 5-H, 8-H), 7.83 (s, 1H, 3-H), 7.67 (d, J = 2.0 Hz, 1H, 3'-H), 7.39 – 7.33 (m, 4H, 5'-H, 6'-H, 8'-H, 9'-H), 7.23 – 7.19 (m, 2H, 1'-H, 2'-H), 7.05 (t, J = 7.3 Hz, 1H, 7'-H); ^{13}C NMR (126 MHz, DMSO) δ 182.35, 181.88, 144.36, 143.13, 142.13, 141.38, 138.75, 134.29, 133.76, 133.23, 132.88, 130.45, 130.10, 129.57, 129.45, 126.18, 126.07, 124.70, 122.60, 122.50, 120.53, 117.24, 110.95, 109.20.

3.1.5 Supporting information

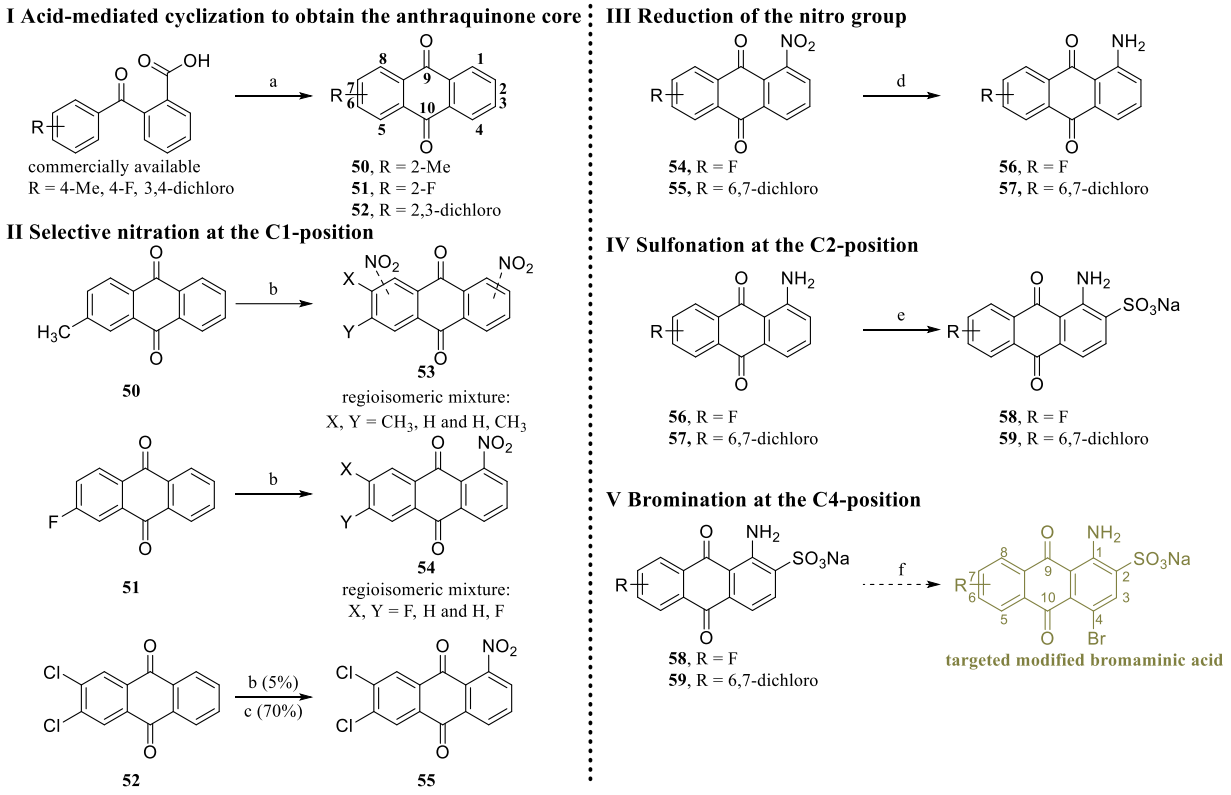
Modifications of C6- and C-7 at anthraquinone core: CH_3, F, and di-Cl (Scheme S1)

In addition to the synthesized C6- and C7-chloro-substituted key intermediate **21**, three uncompleted trials to introduce a methyl, a fluoro-, or dichloro-substitution at the C6- and C7-position of the anthraquinone core were performed according to the aforementioned synthesis pathway A (Scheme S1). The synthesis began with the investigation of the commercially available functionalized 2-(benzoyl)benzoic acid derivatives bearing C6- or C7-substituents (CH_3, F, and di-Cl) in the following five-step synthetic sequence:

1. **Acid-mediated cyclization to obtain the anthraquinone core.** 2-(4-Fluoro/methylbenzoyl)benzoic acid and 2-(3,4-dichlorobenzoyl)benzoic acid were subjected to intramolecular cyclization under harsh acidic conditions using concentrated sulfuric acid (H_2SO_4) under an argon atmosphere at 135 °C for overnight to ensure complete cyclization, yielding the modified anthraquinone derivatives **50**–**51** (**I**, Scheme S1).
2. **Selective nitration at the C1-position.** Electrophilic nitration was carried out on compound **50** using a mixture of fuming nitric acid (HNO_3), sulfuric acid (H_2SO_4), and phosphoric acid (H_3PO_4) in carbon tetrachloride (CCl_4) at 25 °C for 6 hours and resulted in the formation of dinitro-regioisomers **53**-F1 and -F2. This result prevented the investigation of the compound in the optimization process. Application of the same nitration conditions to compound **51** yielded regioisomers of nitro-anthraquinone, **54**-F1/F2. However, these conditions were ineffective for the dichlorinated anthraquinone **52**, leading to minimal conversion after stirring at 50 °C for two days. Improved nitration of the dichloro-anthraquinone was achieved using $NaNO_3$ in H_2SO_4 at 25 °C for 16 hours, resulting in the formation of **55** in an isolated yield of 70%, with reduced by-product formation (**II**, Scheme S1).
3. **Reduction of the nitro group.** Stannous chloride reduction using $SnCl_2 \cdot 2H_2O$ in ethanol at 70 °C for 1 hour was applied on the compounds **54** and **55** and found to be an effective and reproducible method which yielded the compounds **56** and **57**, respectively (**III**, Scheme S1).
4. **Sulfonation at the C2-position.** The 1-aminoanthraquinones **56** and **57** were sulfonated at the C2-position using chlorosulfonic acid ($HClSO_3$) in nitrobenzene at 130 °C for 90 minutes. After cooling, the reaction mixtures were quenched with aqueous sodium carbonate (Na_2CO_3), leading to the formation of sulfonated anthraquinone sodium salts **58** and **59**, respectively (**IV**, Scheme S1).

5. **Bromination at the C4-position:** Bromination step found to be critical as mentioned in the synthesis of compound **21** because of the potential additional substitution at the C2-sulfonyl position, which will lead to the formation of the 2,4-dibromo derivatives. Future work will focus on the application of the optimized bromination conditions on both compounds **58** and **59** using 0.5 equivalents of bromine water (Br_2) in *N*,*N*-dimethylformamide (DMF) at 25 °C for 30 minutes (**V**, Scheme S1).

Scheme S1. Modifications of C6- and C-7 at anthraquinone core: CH_3, F, di-Cl.[a]



[a]Reaction conditions: a. H_2SO_4, 135 °C, 16 h; b. HNO_3, H_2SO_4, H_3PO_4, CCl_4, 25 °C, 6 h; c. H_2SO_4, $NaNO_3$, 25 °C, 16 h, (70%); d. $SnCl_2 \cdot 2\,H_2O$, EtOH, 70 °C, 1 h (90-95%); e. $ClSO_3H$, $BzNO_2$, 85 °C, 10 min; 130 °C, 90 min, Na_2CO_3, H_2O, 25 °C; f. Br_2 (0.5 equiv.), DMF, 25 °C, 1 h.

Alternative synthesis pathways of modified bromaminic acid derivatives via pre-functionalized nitrated intermediates (Failed trials) (Scheme S2)

Alternative strategies were applied to circumvent the regioselectivity challenges encountered during the nitration step (Step 2 of Pathway A), particularly at the C1-position of the anthraquinone scaffold. These routes aimed to introduce the nitro group at an earlier stage by utilizing nitrated

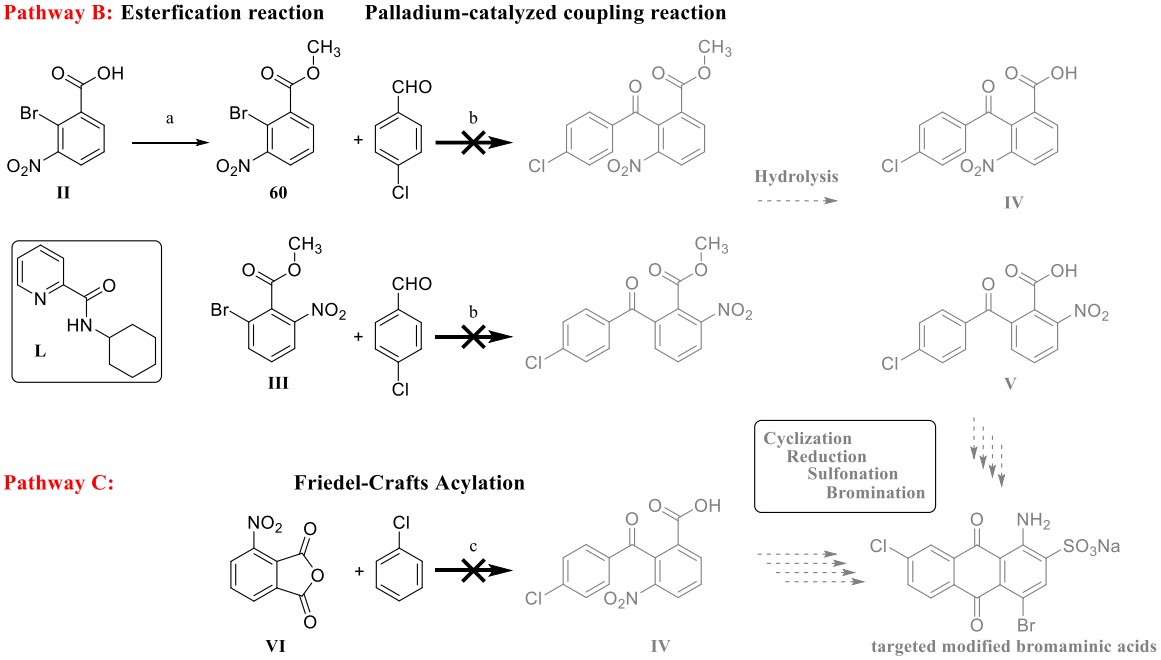
benzoylbenzoic acid precursors, thereby enhancing positional control and synthetic efficiency. The overall sequences are outlined in Scheme S2 and comprise the following steps:

Pathway B: This pathway started with the esterification of the commercially available nitrobenzoic acid derivative 2-bromo-3-nitrobenzoic acid (**II**, Scheme S2) using potassium carbonate (K_2CO_3) and methyl iodide (MeI) in acetone at 60 °C for 16 hours. This reaction afforded the corresponding methyl ester methyl 2-bromo-3-nitrobenzoate (**60**, Scheme S2) in good yield. Additionally, the isomeric methyl 2-bromo-6-nitrobenzoate (**III**, Scheme S2) was commercially obtained and used as an alternative substrate for subsequent coupling steps. Next step in this pathway was the palladium-catalyzed carbon–carbon coupling, whereas both esters **60** and **III** were subjected to palladium-catalyzed carbon–carbon bond formation with 4-chloro benzaldehyde using palladium acetate ($Pd(OAc)_2$) as a catalyst, potassium hydrogen carbonate ($KHCO_3$) as a base, and the ligand *N*-cyclohexylpicolinamide (**L**) in 2-methyl-2-butanol (^{t}AmylOH) at 150 °C for 24 hours. Coupling using compound **60** with 4-chlorobenzaldehyde failed, likely due to significant steric hindrance due to the proximity of the bromine atom to both the nitro group and the ester moiety. As a result, **III** was tested as a more accessible alternative. However, coupling of **III** with 4-chlorobenzaldehyde did also not proceed (Scheme S2). Had the coupling worked, the synthetic plan would have continued with the hydrolysis of the methyl ester to form the corresponding benzoic acid derivatives (**IV** or **V**, Scheme S2).

Pathway C: Another failed pathway was the one-step reaction based on the Friedel-Crafts acylation of chlorobenzene using the commercially available compound 3-nitrophthalic anhydride (**VI**, Scheme S2) in the presence of the Luis acid aluminum chloride.

A successful synthesis of nitrated benzoylbenzoic acids (**IV** or **V**, Scheme S2) would allow its further investigation in the cyclization, reduction, sulfonation, and bromination reactions which ultimately could furnish the targeted modified bromaminic acid analogs, consistent with the products synthesized via Pathway A.

Scheme S2. Alternative synthesis pathways for the exploration of C6- and C7-positions of anthraquinone derivatives (failed trials).[a]



[a]Reaction conditions: a. Na_2CO_3, DMF, 60 °C, 8 h, (99%); b. $Pd(OAc)_2$ (5.0 mol%), $KHCO_3$ (2.5 equiv), Ligand (**L**) (6.0 mol%), ^{t}AmylOH, 150 °C, 24 h; c. $AlCl_3$, PhCl,100 °C, 8 h.

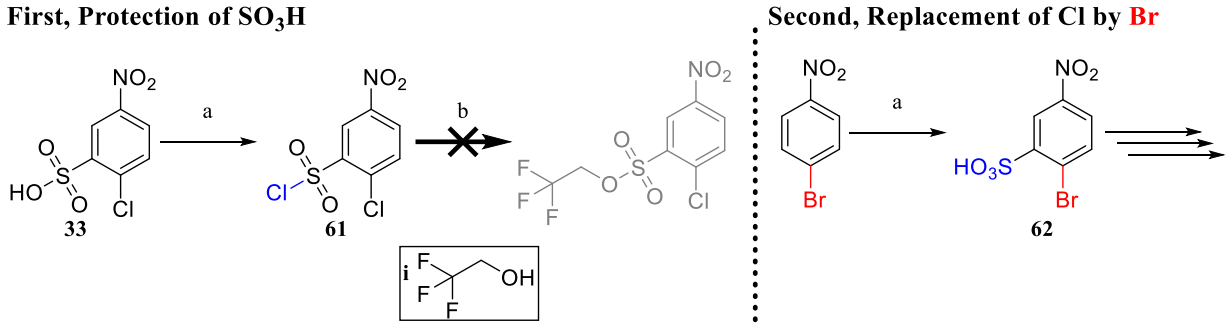
Although Pathway B and C offered theoretically attractive routes by introducing the nitro group early on to avoid regioselectivity issues during nitration, attempts were not successful. As such, Pathway A remained the more feasible and robust approach for accessing the desired C6-/C7-substituted bromaminic acid derivatives.

Two strategies to overcome the deactivation effect of the sulfonic acid group (Scheme S3)

First, protection of the sulfonic acid group: Compound **33** was converted to the corresponding acid chloride **61** using $POCl_3$ in the presence of sulfolane and dimethylacetamide (DMAc) in acetonitrile under reflux for 3 hours. Attempts to generate sulfonic acid esters using trifluoroethanol and Et_3N with or without 4-dimethylaminopyridine (4-DMAP) failed to yield the desired products (Scheme S3).

Second, replacement of Cl with a better leaving group (e.g., Br): The sulfonation of 4-nitrobromobenzene yielded 2-bromo-5-nitrobenzenesulfonic acid **62**, which allows for milder amination conditions. Applications of the aforementioned reactions on **62** allow further optimization of anthraquinone-based $P2Y_{12}$ receptor antagonists.

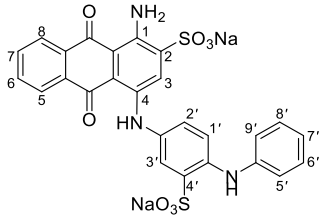
Scheme S3. Trials to overcome the deactivation effect of the sulfonic acid group: First, protection of SO_3H at **33**. Second, replacement of Cl by Br **62**.[a]



[a]Reaction conditions: a. DMAc, $POCl_3$, Sulfolane, MeCN, 85 °C, 3 h; b. **i**, Et_3N, CH_2Cl_2, 1 h, 0 °C; 0 °C to 25 °C, 24 h/**i**, Et_3N, 4-DMAP, CH_2Cl_2, 25 °C,10 h; c. 20% $SO_3.H_2SO_4$, 0 °C; 140 °C, 16 h.

Synthesis of the reported final compounds (General procedure A)[35]

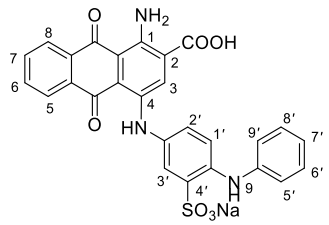
Sodium 1-amino-9,10-dioxo-4-((4-(phenylamino)-3-sulfonatophenyl)amino)-9,10-dihydroanthracene-2-sulfonate (**14**, **PSB-0739**)[35]



Chemical formula: $C_{26}H_{17}N_3Na_2O_8S_2$
Molecular weight: 609,53 g/mol
Calculations: Reactants: bromaminic acid (0.1 g, 0.26 mmol), aniline (0.14 g, 0.52 mmol)
Reaction conditions: 9 min, 120 °C, 100 W; pressure up to 10 bar.
Purification: Purification step has been repeated three times. Polarity of the eluent was decreased by the addition of acetone in the following steps: 5, 10, 20, 40, and 60%.
Yield: 4%, as blue powder (6.00 mg, 0.01 mmol)
LC-MS (m/z): 566.10 $[M - 2Na^+ + 2H]^+$ (purity: 99%)
Mp: >300 °C

^{1}H NMR (500 MHz, DMSO-d_6) δ 12.13 (s, 1H, 4-NH), 8.36 – 8.18 (m, 2H, 6-H, 7-H), 7.85 (dd, J = 9.0, 5.1 Hz, 3H, 3-H, 5-H, 8-H), 7.51 (s, 1H, 3'-H), 7.32 (dt, J = 15.6, 8.0 Hz, 3H, 6'-H, 8'-H, 9'-H), 7.14 (dt, J = 13.1, 5.1 Hz, 3H, 1'-H, 2'-H, 5'-H), 6.92 (t, J = 7.2 Hz, 1H, 7'-H); ^{13}C NMR (151 MHz, DMSO) δ 183.35, 183.24, 144.39, 142.84, 142.47, 141.99, 141.95, 138.84, 134.79, 134.44, 134.40, 134.21, 133.86, 130.53, 130.00, 127.69, 127.10, 127.06, 124.55, 124.02, 122.69, 119.70, 117.00, 111.78, 110.30.

Sodium 5-((4-amino-3-carboxy-9,10-dioxo-9,10-dihydroanthracen-1-yl)amino)-2-(phenylamino)benzenesulfonate (**15**, **PSB-0702**)[35]



Chemical formula: $C_{27}H_{18}N_3NaO_7S$
Molecular weight: 551,50 g/mol
Calculations: Reactants: bromaminic acid (0.08 g, 0.23 mmol), aniline (0.12 g, 0.46 mmol)
Reaction conditions: 8 min, 120 °C, 100 W; pressure up to 10 bar.
Purification: Purification step has been repeated four times. Polarity of the eluent was decreased by the addition of acetone in the following steps: 5, 10, 20, 40, and 60%.
Yield: 3.7%, as blue powder (4.50 mg, 8.50 μmol)
LC-MS (m/z): 530.20 $[M - Na^+ + H]^+$ (purity: 95%)
Mp: >300 °C

^{1}H NMR (500 MHz, DMSO-d_6) δ 12.06 (s, 1H, 4-NH), 8.54 (s, 1H, 3-H), 8.29 (d, *J* = 7.0 Hz, 2H, 6-H, 7-H), 7.83 (p, *J* = 7.3 Hz, 2H, 5-H, 8-H), 7.55 (s, 1H, 3'-H), 7.32 (dt, *J* = 15.2, 7.9 Hz, 3H, 6'-H, 8'-H, 9'-H), 7.18 (d, *J* = 7.9 Hz, 1H, 5'-H), 7.12 (d, *J* = 7.8 Hz, 2H, 1'-H, 2'-H), 6.93 (t, *J* = 7.3 Hz, 1H, 7'-H); ^{13}C NMR (126 MHz, DMSO) δ 181.72, 180.99, 142.27, 137.45, 134.94, 134.40, 133.65, 132.73, 132.26, 129.72, 129.33, 126.03, 125.80, 123.78, 120.78, 118.01, 115.85, 111.11, 108.62.

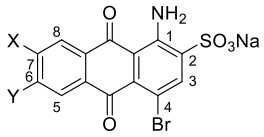
Synthesis of modified bromaminic acid derivatives for C6- and C7-functionalization

Bromination at the C4-position (21)

Synthesis of sodium 1-amino-4-bromo-6/7-chloro-9,10-dioxo-9,10-dihydroanthracene-2-sulfonate (21-F1 & F2)

Procedure:

In a 100 mL round-bottom flask, a mixture containing 1.0 equivalent of 1-amino-6- and 7-chloro-9,10-dioxo-9,10-dihydroanthracene-2-sulfonic acid (**25-F1 & F2**) was dissolved in 8 mL of anhydrous *N*,*N*-dimethylformamide (DMF) and stirred at 0 °C. Subsequently, **0.5 equivalents** of bromine dissolved in DMF (1 mL) were added dropwise over 30 minutes. The reaction mixture was then stirred at room temperature for an additional 30 minutes. To quench the reaction, an aqueous solution of sodium bisulfite ($NaHSO_3$, 1 g in 3 mL demineralized water) was added, and the mixture was extracted with dichloromethane (4 × 50 mL). The aqueous phase was concentrated under reduced pressure to yield a reddish, elastic mixture of brominated isomers sodium 1-amino-4-bromo-6/7-chloro-9,10-dioxo-9,10-dihydroanthracene-2-sulfonate (**21-F1 & F2**) which was used for the coupling reaction without purification:



X, Y = Cl, H or H, Cl
regioisomeric mixture

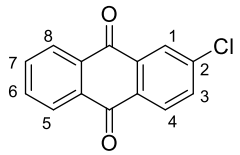
Chemical formula: $C_{14}H_6BrClNNaO_5S$
Molecular weight: 416.63 g/mol
Calculations: Reactant: compound **25** (0.05 g, 0.14 mmol), Br_2 (0.011 g, 0.07 mmol)
LC-MS (m/z): 417.90 $[M - Na^+ + H]^+$ (purity: 96%)

Cyclization to anthraquinone core

General procedure B

In a sealed reaction tube, 1.0 equivalent of 2-(4-substitutedbenzoyl)benzoic acid was dissolved in 12 mL of concentrated sulfuric acid (H_2SO_4) under an inert argon atmosphere. The reaction mixture was heated to 135 °C and stirred vigorously for 4 hours to promote intramolecular cyclization. The progress of the reaction was monitored by thin-layer chromatography (TLC) using a mobile phase of cyclohexane:ethyl acetate (9:1), confirming the formation of the cyclized anthraquinone derivative. After completion, the reaction mixture was allowed to cool to room temperature (25 °C) and then carefully poured onto crushed ice, resulting in the precipitation of the crude product. The mixture was subsequently neutralized with a saturated aqueous solution of sodium carbonate (Na_2CO_3) to complete precipitation and quench residual acid. The resulting solid was collected by Büchner filtration and dried under high vacuum to afford the desired anthraquinone compounds (**22, 50–52**) as solid products:

2-Chloroanthracene-9,10-dione (22) (according to general procedure **B)**



Chemical formula: $C_{14}H_7ClO_2$
Molecular weight: 242.66 g/mol
Calculations: Reactant: 2-(4-chlorobenzoyl)benzoic acid (1 g, 3.8 mmol)
TLC-MS (m/z): 242.90 $[M+H]^+$ (purity: 99%)
Mp: 210–212 °C (literature mp: 211–213 °C)[6]
R_f = 0.51 (eluent: cyclohexane : ethyl acetate; 9 : 1)
Yield: 81%, as yellowish-white powder (0.75 g, 3.1 mmol).

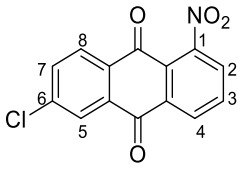
^{1}H NMR (600 MHz, Chloroform-*d*) δ 8.29 (dt, *J* = 7.0, 2.8 Hz, 2H, 6-H, 7-H), 8.24 (dd, *J* = 5.2, 3.0 Hz, 2H, 1-H, 4-H), 7.85 – 7.78 (m, 2H, 5-H, 8-H), 7.74 (dd, *J* = 8.3, 2.1 Hz, 1H, 3-H); ^{13}C NMR (151 MHz, $CDCl_3$) δ 182.07, 181.98, 141.07, 134.56, 134.39, 134.23, 134.09, 133.20, 133.14, 131.63, 128.96, 127.30, 127.27, 127.10.

Selective nitration at the C1-position
General Procedure C

In a 100 mL round-bottom flask, 1.0 equivalent of substituted anthraquinone derivative **27** or **28** was dissolved in 14 mL of tetrachloromethane (CCl_4). To the stirred solution, a nitrating mixture consisting of fuming nitric acid (HNO_3, 7.0 equiv.), concentrated sulfuric acid (H_2SO_4, 7.0 equiv.), and phosphoric acid (H_3PO_4, 2.0 equiv.) was added dropwise at room temperature (25 °C). The

reaction mixture was stirred vigorously for 6 hours. The progress of the nitration was monitored by thin-layer chromatography (TLC), confirming the formation of the desired regioisomeric products. After completion, the reaction mixture was slowly poured onto crushed ice with continuous stirring to quench the reaction and induce precipitation. The solid product was collected by Büchner filtration, washed thoroughly with cold water, and extracted with ethyl acetate. The organic phase was dried over anhydrous magnesium sulfate ($MgSO_4$), filtered, and concentrated under reduced pressure. The crude product was purified by column chromatography (eluent: cyclohexane:ethyl acetate, 9:1) to afford a mixture of regioisomeric mono-nitrated products:

6-/7-Chloro-1-nitroanthracene-9,10-dione (**23-F1**/**F2**)

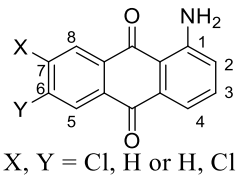


Chemical formula: $C_{14}H_6ClNO_4$
Molecular weight: 287.65 g/mol
Calculations: Reactant: 2-chloroanthracene-9,10-dione (**22**) (0.75 g, 3.1 mmol), nitrating mixture: HNO_3 (0.90 mL), H_2SO_4 (1.15 mL), H_3PO_4 (0.32 mL).
TLC-MS (m/z): 287.90 $[M+H]^+$ (purity: 95%)
$\mathbf{R}_{f\text{-}23\text{-}F1,\ F2}$ = 0.22, 0.16 (eluent: cyclohexane:ethyl acetate; 9:1)
Combined yield: 64%, as yellowish powder (0.57 g, 1.98 mmol).

Reduction of the nitro group
General procedure D

In a 250 mL round-bottom flask, 1.0 equivalent of the nitroanthraquinone derivatives **23**, **54**, or **55** was dissolved in 20 mL of absolute ethanol. To the stirred solution, 5.0 equivalents of tin(II) chloride dihydrate ($SnCl_2 \cdot 2H_2O$) were added. The reaction mixture was then heated to 80 °C and stirred vigorously for an hour. Progress of the reaction was monitored via thin-layer chromatography (TLC). After cooling the reaction mixture to room temperature, it was quenched by the slow addition of 200 mL of 20% aqueous sodium carbonate solution. The resulting mixture was extracted three times using ethyl acetate and 1 N sodium hydroxide. The combined organic extracts were dried over anhydrous magnesium sulfate ($MgSO_4$), filtered, and concentrated under reduced pressure. The crude products were obtained as reddish powders corresponding to compounds **24**, **56**, and **57**:

1-Amino-6/7-chloroanthracene-9,10-dione (**24-F1**/**F2**) **(**according to general procedure **D)**



X, Y = Cl, H or H, Cl
regioisomeric mixture

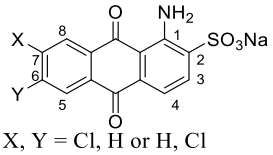
Chemical formula: $C_{14}H_8ClNO_2$
Molecular weight: 257.67 g/mol
Calculations: Reactant: compound **23** (0.57 g, 1.98 mmol), $SnCl_2 \cdot 2H_2O$ (2.24 g, 9.91 mmol)
TLC-MS (m/z): 258.67 $[M+H]^+$ (purity: 97%)
$\mathbf{R}_f$ = 0.4 (eluent: cyclohexane:ethyl acetate; 9:1)
Yield: 94%, as reddish powder (0.48 g, 1.86 mmol)

Sulfonation at the C2-position

General procedure E

In a 250 mL round-bottom flask, 1.0 equivalent of the respective 1-aminoanthraquinone derivative (compounds **24**, **56**, and **57**) was dissolved in 25 mL of nitrobenzene and stirred vigorously. Subsequently, 1.3 equivalents of chlorosulfonic acid ($HClSO_3$) were added dropwise over 10 minutes under continuous stirring. The reaction mixture was then heated to 130 °C and maintained at this temperature for 1.5 hours. Reaction progress was monitored via thin-layer chromatography (TLC) using a cyclohexane:ethyl acetate (9:1) mobile phase, confirming complete consumption of the starting material. Upon completion, the reaction mixture was cooled to room temperature and quenched by slow addition of 200 mL of 20% aqueous sodium carbonate solution. The resulting mixture was subjected to triple extraction using ethyl acetate and 1 N sodium hydroxide (NaOH). The combined aqueous layer was concentrated under reduced pressure to a final volume of 10–20 mL and purified via flash chromatography on RP-18 reversed-phase silica gel using water as the initial eluent. The polarity of the mobile phase was subsequently adjusted by incremental addition of acetone in concentrations of 5%, 10%, and 20%. Fractions containing the dark red product were pooled, and residual solvents were removed via rotary evaporation. Final traces of water were eliminated by lyophilization to afford the sulfonated aminoanthraquinone derivatives **25**, **58**, and **59**:

Sodium 1-amino-6/7-chloro-9,10-dioxo-9,10-dihydroanthracene-2-sulfonate (**25**) **(**according to general procedure **E)**



X, Y = Cl, H or H, Cl
regioisomeric mixture

Chemical formula: $C_{14}H_7ClNNaO_5S$
Molecular weight: 337.74 g/mol
Calculations: Reactant: compound **24** (0.48 g, 1.86 mmol), $HClSO_3$ (0.28 g, 2.42 mmol)
TLC-MS (m/z): 338 $[M-Na^+ + H]^+$ (purity: 46:21%)
Combined yield: 52%, as a dark reddish powder (0.35 g, 0.97 mmol)

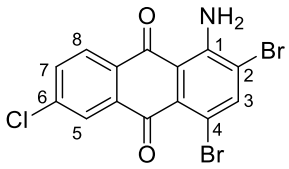
Synthesis of 1-amino-2,4-dibromo-6/7-chloroanthracene-9,10-dione (26-F1 & F2)

Procedure

In a 100 mL round-bottom flask, a mixture containing 1.0 equivalent of 1-amino-6- and 7-chloro-9,10-dioxo-9,10-dihydroanthracene-2-sulfonic acid (**25-F1 & F2**), was dissolved in 8 mL of anhydrous *N*,*N*-dimethylformamide (DMF) and stirred at 0 °C. Subsequently, **2.0 equivalents** of bromine dissolved in DMF (1 mL) were added dropwise over 30 minutes. The reaction mixture was then stirred at room temperature for an additional 30 minutes. To quench the reaction, an aqueous solution of sodium bisulfite ($NaHSO_3$, 1 g in 3 mL demineralized water) was added, and

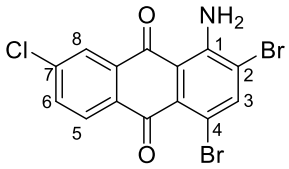
the mixture was extracted with dichloromethane (4 × 50 mL). The organic layer was collected, dried over magnesium sulfate ($MgSO_4$). The solvent was removed under reduced pressure to afford a mixture of the regioisomers **26-F1** and **-F2** as orang powder. Separation of the two regioisomers was successfully achieved through repeated flash column chromatography (three cycles) using cyclohexane:ethyl acetate (9:1) as the eluent, affording the isomer:

1-Amino-2,4-dibromo-6-chloroanthracene-9,10-dione (26-F1)



Chemical formula: $C_{14}H_6Br_2ClNO_2$
Molecular weight: 415.46 g/mol
Calculations: Reactant: compound **25** (0.10 g, 0.28 mmol), Br_2 (0.089 g, 0.56 mmol)
TLC-MS (m/z): 416 $[M+H]^+$ (purity: 95%)
R_f = 0.28 (eluent: cyclohexane:ethyl acetate; 95:5)
Yield: 63%, as orang powder (0.073 g, 0.18 mmol)

1-Amino-2,4-dibromo-7-chloroanthracene-9,10-dione (26-F2)



Chemical formula: $C_{14}H_6Br_2ClNO_2$
Molecular weight: 415.46 g/mol
Calculations: Reactant: compound **25** (0.10 g, 0.28 mmol), Br_2 (0.089 g, 0.56 mmol)
TLC-MS (m/z): 416 $[M+H]^+$ (purity: 98%)
R_f = 0.20 (eluent: cyclohexane:ethyl acetate; 95:5)
Yield: 35%, as orang powder (0.041 g, 0.098 mmol)

^{1}H NMR (600 MHz, DMSO-d_6) δ 8.23 (s, 1H, 3-H), 8.10 (d, J = 8.3 Hz, 1H, 8-H), 8.08 (d, J = 2.1 Hz, 1H, 5-H), 7.91 (dd, J = 8.3, 2.2 Hz, 1H, 7-H); ^{13}C NMR (151 MHz, DMSO) δ 182.42, 180.91, 148.60, 143.89, 139.48, 134.62, 133.89, 131.73, 130.16, 128.94, 125.71, 117.43, 114.45, 107.54. and / or

^{1}H NMR (600 MHz, DMSO-d_6) δ 8.24 (s, 1H, 3-H), 8.18 (d, J = 8.3 Hz, 1H, 5-H), 8.05 (s, 1H, 8-H), 7.94 (dd, J = 8.4, 1.7 Hz, 1H, 6-H); ^{13}C NMR (151 MHz, DMSO) δ 182.58, 180.46, 148.28, 143.46, 138.91, 134.28, 133.91, 131.52, 129.98, 128.49, 125.65, 117.31, 114.16, 107.26.

Synthesis of targeted modified aniline derivatives

Synthesis of the anilines 30−32

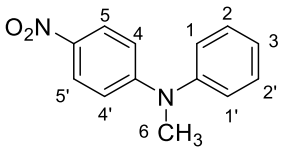
First: alkylation via Buchwald-Hartwig coupling 27−29

General procedure F

In a sealed reaction tube under an argon atmosphere, 3.0 equivalents of cesium carbonate (Cs_2CO_3) were added to a solution of the corresponding aniline derivative (1.0 equiv.) in 12 mL of anhydrous tetrahydrofuran (THF). After stirring the suspension for 1 minute, 4-nitrobromobenzene (1.0 equiv.), Xantphos (0.06 equiv.), and $Pd_2(dba)_3$ (0.02 equiv.) were sequentially introduced. The reaction mixture was stirred at 70 °C overnight under argon. Upon completion (monitored by

TLC), the solvent was removed under reduced pressure. The resulting residue was dissolved in ethyl acetate and washed sequentially with 0.03 M sodium diethyldithiocarbamate solution (5 × 15 mL) and brine (1 × 15 mL). The organic layer was dried over anhydrous magnesium sulfate ($MgSO_4$), filtered through celite, and concentrated under vacuum. The crude product was purified by flash column chromatography on silica gel using cyclohexane:ethyl acetate (75:25) as the eluent, affording the target compounds **27**–**29**:

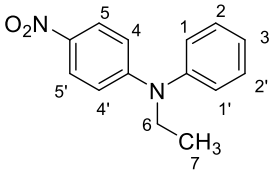
N-Methyl-4-nitro-*N*-phenylaniline (**27**) **(**according to general procedure **F)**



Chemical formula: $C_{13}H_{12}N_2O_2$
Molecular weight: 228.25 g/mol
Calculations: Reactants: *N*-methylaniline (0.50 g, 4.67 mmol), 1-bromo-4-nitrobenzene (0.94 g, 4.67 mmol), Reagents: Cs_2CO_3 (4.56 g, 14.00 mmol), Xantphos (0.16 g, 0.28 mmol), $Pd_2(dba)_3$ (0.092 g, 0.09 mmol)
TLC-MS (m/z): 228.90 $[M+H]^+$ (purity: 90%)
R_f = 0.33 (eluent: cyclohexane:ethyl acetate; 9:1)
Yield: 79%, as yellow powder (0.84 g, 3.68 mmol)

^{1}H NMR (500 MHz, DMSO-d_6) δ 8.05 (d, *J* = 9.4 Hz, 1H, 5-H), 7.83 – 7.76 (m, 1H, 5′-H), 7.53 – 7.45 (m, 2H, 2-H, 2′-H), 7.39 – 7.28 (m, 3H, 3-H, 4-H, 4′-H), 6.76 (d, *J* = 9.4 Hz, 2H, 1-H, 1′-H), 3.39 (s, 3H, 6-H); ^{13}C NMR (126 MHz, DMSO) δ 153.68, 145.97, 142.70, 137.11, 134.69, 130.45, 130.16, 128.92, 128.48, 126.65, 126.48, 125.60, 112.57, 40.37.

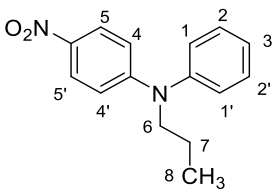
1. *N*-Ethyl-4-nitro-*N*-phenylaniline (**28**) **(**according to general procedure **F)**



Chemical formula: $C_{14}H_{14}N_2O_2$
Molecular weight: 242.28 g/mol
Calculations: Reactants: *N*-ethylaniline (0.50 g, 4.13 mmol), 1-bromo-4-nitrobenzene (0.83 g, 4.13 mmol), Reagents: Cs_2CO_3 (4.04 g, 12.39 mmol), Xantphos (0.15 g, 0.25 mmol), $Pd_2(dba)_3$ (0.084 g, 0.08 mmol)
TLC-MS (m/z): 243.10 $[M+H]^+$ (purity: 98%)
R_f = 0.36 (eluent: cyclohexane:ethyl acetate; 9:1)
Yield: 84%, as yellow powder (0.84 g, 3.47 mmol)

^{1}H NMR (500 MHz, DMSO-d_6) δ 8.02 (d, *J* = 9.4 Hz, 2H, 5-H, 5′-H), 7.52 (t, *J* = 7.8 Hz, 2H, 2-H, 2′-H), 7.37 (t, *J* = 7.5 Hz, 1H, 3-H), 7.29 (d, *J* = 7.4 Hz, 2H, 4-H, 4′-H), 6.69 (d, *J* = 9.4 Hz, 2H, 1-H, 1′-H), 3.83 (q, *J* = 7.1 Hz, 2H, 6-H), 1.18 (t, *J* = 7.1 Hz, 3H, 7-H); ^{13}C NMR (126 MHz, DMSO) δ 152.94, 144.33, 136.73, 130.31, 127.51, 127.00, 125.78, 112.39, 46.68, 12.00.

2. *N*-Propyl-4-nitro-*N*-phenylaniline (**29**) **(**according to general procedure **F)**



Chemical formula: $C_{15}H_{16}N_2O_2$
Molecular weight: 256.30 g/mol
Calculations: Reactants: *N*-propylaniline (0.50 g, 3.70 mmol), 1-bromo-4-nitrobenzene (0.75 g, 3.70 mmol), Reagents: Cs_2CO_3 (3.62 g, 11.10 mmol), Xantphos (0.13 g, 0.22 mmol), $Pd_2(dba)_3$ (0.078 g, 0.07 mmol)
TLC-MS (m/z): 257.10 $[M+H]^+$ (purity: 99%)
R_f = 0.44 (eluent: cyclohexane:ethyl acetate; 9:1)
Yield: 66%, as yellow powder (0.63 g, 2.46 mmol)

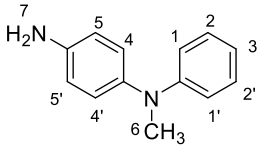
^{1}H NMR (500 MHz, DMSO-d_6) δ 8.01 (d, J = 9.4 Hz, 2H, 5-H, 5′-H), 7.52 (t, J = 7.8 Hz, 2H, 2-H, 2′-H), 7.36 (t, J = 7.4 Hz, 1H, 3-H), 7.30 (d, J = 7.5 Hz, 2H, 4-H, 4′-H), 6.70 (d, J = 9.4 Hz, 2H, 1-H, 1′-H), 3.83 – 3.59 (m, 2H, 6-H), 1.61 (q, J = 7.5 Hz, 2H, 7-H), 0.90 (t, J = 7.4 Hz, 3H, 8-H); ^{13}C NMR (126 MHz, DMSO) δ 153.55, 144.78, 136.92, 130.48, 127.62, 127.11, 125.91, 112.64, 53.79, 20.14, 11.07.

Second: reduction to form 30−32

General procedure G

In a 250 mL round-bottom flask, 1.0 equivalent of the respective 4-nitro-*N*-phenylaniline derivative **27−29** was dissolved in 20 mL of ethanol and treated with 5.0 equivalents of tin(II) chloride dihydrate ($SnCl_2 \cdot 2H_2O$). The reaction mixture was heated to 80 °C and stirred vigorously for 30 minutes. Progress of the reaction was monitored by thin-layer chromatography (TLC), confirming the formation of the desired aniline product. After completion, the mixture was cooled to room temperature (25 °C) and quenched with 200 mL of 20% aqueous sodium carbonate (Na_2CO_3). The resulting solution was extracted three times with ethyl acetate, followed by an additional wash with 1 N sodium hydroxide to ensure complete removal of tin residues. The combined organic layers were dried over anhydrous magnesium sulfate ($MgSO_4$), filtered, and the solvent was removed under reduced pressure to yield the corresponding aniline derivative **30−32**:

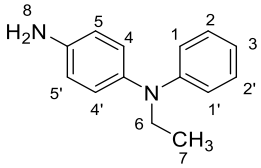
1. N^1-Methyl-N^1-phenylbenzene-1,4-diamine (**30**) **(**according to general procedure **G)**



Chemical formula: $C_{13}H_{14}N_2$
Molecular weight: 198.26 g/mol
Calculations: Reactant: *N*-methyl-4-nitro-*N*-phenylaniline (**27**) (0.84 g, 3.68 mmol), $SnCl_2 \cdot 2H_2O$ (4.13 g, 18.30 mmol)
TLC-MS (m/z): 199.10 $[M+H]^+$ (purity: %)
R_f = 0.3 (eluent: cyclohexane:ethyl acetate; 7.5:2.5)
Yield: 98.5%, as a brown oily substance (0.72 g, 3.63 mmol)

^{1}H NMR (500 MHz, DMSO-d_6) δ 7.14 – 7.03 (m, 2H, 5-H, 5′-H), 6.86 – 6.78 (m, 2H, 2-H, 2′-H), 6.66 – 6.51 (m, 5H, 1-H, 1′-H, 3-H, 4-H, 4′-H), 4.98 (s, 2H, 7-NH_2), 3.11 (s, 3H, 6-H); ^{13}C NMR (126 MHz, DMSO) δ 150.00, 146.14, 137.19, 128.58, 126.93, 116.53, 114.78, 113.61, 40.16.

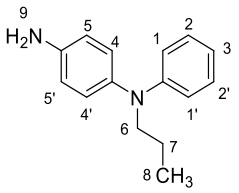
2. N^1-Ethyl-N^1-phenylbenzene-1,4-diamine (**31**) **(**according to general procedure **G)**



Chemical formula: $C_{14}H_{16}N_2$
Molecular weight: 212.29 g/mol
Calculations: Reactant: *N*-ethyl-4-nitro-*N*-phenylaniline (**28**) (0.50 g, 2.06 mmol), $SnCl_2 \cdot 2H_2O$ (2.33 g, 10.32 mmol)
TLC-MS (m/z): 213,10 $[M+H]^+$ (purity: %)
R_f = 0.34 (eluent: cyclohexane:ethyl acetate; 7.5:2.5)
Yield: 95.45%, as a brown oily substance (0.42 g, 1.95 mmol)

^{1}H NMR (500 MHz, DMSO-d_6) δ 7.12 – 7.00 (m, 2H, 5-H, 5′-H), 6.81 (dd, J = 8.5, 1.3 Hz, 2H, 2-H, 2′-H), 6.60 (dd, J = 8.5, 1.3 Hz, 2H, 4-H, 4′-H), 6.55 (d, J = 7.8 Hz, 3H, 1-H, 1′-H, 3-H), 5.01 (s, 2H, 8-NH_2), 3.56 (q, J = 7.0 Hz, 2H, 6-H), 1.08 (t, J = 7.0 Hz, 2H, 7-H); ^{13}C NMR (126 MHz, DMSO) δ 148.95, 146.40, 134.90, 128.66, 128.35, 115.89, 114.88, 113.22, 45.61, 12.27.

3. N^1-Phenyl-N^1-propylbenzene-1,4-diamine (**32**) **(**according to general procedure **G)**



Chemical formula: $C_{15}H_{18}N_2$
Molecular weight: 226.32 g/mol
Calculations: Reactant: *N*-propyl-4-nitro-*N*-phenylaniline (**29**) (0.50 g, 1.95 mmol), $SnCl_2 \cdot 2H_2O$ (2.20 g, 9.75 mmol)
TLC-MS (m/z): 227.10 $[M+H]^+$ (purity: %)
R$_f$ = 0.35 (eluent: cyclohexane:ethyl acetate; 7.5:2.5)
Yield: 94%, as a brown oily substance (0.415 g, 1.83 mmol)

^{1}H NMR (500 MHz, DMSO-d_6) δ 7.04 (t, J = 7.6 Hz, 2H, 5-H, 5′-H), 6.81 (d, J = 8.4 Hz, 2H, 2-H, 2′-H), 6.59 (d, J = 8.4 Hz, 2H, 4-H, 4′-H), 6.54 (t, J = 8.9 Hz, 3H, 1-H, 1′-H, 3-H), 4.99 (s, 2H, 9-NH_2), 3.53 – 3.36 (m, 2H, 6-H), 1.53 (h, J = 7.4 Hz, 2H, 7-H), 0.86 (t, J = 7.4 Hz, 3H, 8-H); ^{13}C NMR (126 MHz, DMSO) δ 149.56, 146.51, 135.47, 128.81, 128.41, 116.08, 115.06, 113.43, 53.45, 20.27, 11.33.

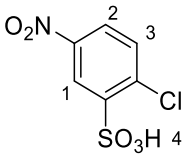
Synthesis of the anilines 37−39 and 41

1. Incorporation of the sulfonic acid functionality

General procedure H[113]

In a sealed reaction tube, 1.0 equivalent of 4-nitrochloro- or 4-nitrobromobenzene was dissolved in 5.1 equivalent of oleum (fuming sulfuric acid containing 20% SO_3) under an argon atmosphere at 0 °C. The mixture was then heated to 110 °C and stirred vigorously for 16 hours. Reaction progress was monitored by thin-layer chromatography (TLC), confirming the formation of the desired sulfonated product. Upon completion, the reaction mixture was cooled to room temperature (25 °C) and carefully poured onto crushed ice, resulting in the precipitation of the crude product. The suspension was neutralized with saturated sodium carbonate (Na_2CO_3) solution. The precipitate was collected by Büchner filtration, washed thoroughly with water, and dried under high vacuum to afford the corresponding sulfonic acid derivatives **33** and **62**:

1. 2-Chloro-5-nitrobenzenesulfonic acid (**33**) **(**according to general procedure **H)**



Chemical formula: $C_6H_4ClNO_5S$
Molecular weight: 237.61 g/mol
Calculations: Reactant: 4-Nitrochlorobenzene (1.00 g, 6.35 mmol), 20% oleum (5.77 g, 32.37 mmol, 3.3 mL)
TLC-MS (m/z): 238.20 $[M+H]^+$ (purity: 99%)
R_f = 0.14 (eluent: DCM : MeOH; 86:14)
Yield: 40%, as grey powder (0.60 g, 2.54 mmol)

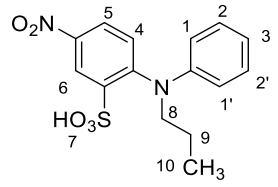
^{1}H NMR (500 MHz, DMSO-d_6) δ 8.62 (d, *J* = 2.9 Hz, 1H, 1-H), 8.16 (dd, *J* = 8.7, 2.9 Hz, 1H, 3-H), 7.70 (d, *J* = 8.7 Hz, 1H, 2-H); ^{13}C NMR (126 MHz, DMSO) δ 146.50, 145.46, 137.82, 132.06, 124.70, 123.52.

2. Amination

General procedure I (Thermal amination, 34−36 and 40)

In a sealed reaction tube, 1.0 equivalent of 2-chloro-5-nitrobenzenesulfonic acid **33** was dissolved in 6.0 equivalents of the required liquid aniline or 3.0 equivalents of solid aniline in *N*,*N*-dimethylformamide (DMF) under an argon atmosphere. The reaction mixture was stirred at 150 °C until completion, as confirmed by thin-layer chromatography (TLC). Upon completion, the mixture was cooled to room temperature, diluted with dichloromethane (DCM), and washed with water. A 2.5 M aqueous solution of sodium hydroxide (NaOH) was added to transfer the product into the aqueous phase. After confirming complete transfer by TLC, the aqueous layer was neutralized with concentrated sulfuric acid (H_2SO_4) to approximately pH 7. Water was removed under reduced pressure, and the residue was dissolved in warm ethanol, followed by vacuum filtration and washing with additional warm ethanol. The filtrate was then concentrated under vacuum to yield the desired products as greenish-yellow powders **34−36** and **40**, that were used in the next step without further purification:

2-(Propyl(phenyl)amino)-5-nitrobenzenesulfonic acid (**34**) **(**according to general procedure **I)**

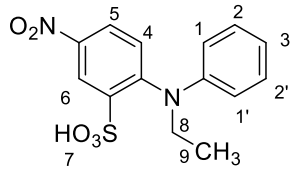


Chemical formula: $C_{15}H_{16}N_2O_5S$
Molecular weight: 336.36 g/mol
Calculations: Reactants: 2-chloro-5-nitrobenzenesulfonic acid **33** (0.50 g, 2.10 mmol), *N*-propylaniline (1.71 g, 12.63 mmol)
TLC-MS (m/z): 337.20 $[M+H]^+$ (purity: 94%)
R_f = 0.24 (eluent: DCM:MeOH ; 86:14)
Yield: 24%, as greenish-yellow powder (0.17 g, 0.51 mmol)

^{1}H NMR (500 MHz, DMSO-d_6) δ 8.76 (d, *J* = 2.9 Hz, 1H, 6-H), 8.13 (dd, *J* = 8.7, 3.0 Hz, 1H, 5-H), 7.23 (d, *J* = 8.7 Hz, 1H, 4-H), 7.10 (dd, *J* = 8.6, 7.3 Hz, 2H, 2-H, 2′-H), 6.68 (t, *J* = 7.3 Hz, 1H, 3-H), 6.58 (d, *J* = 7.9 Hz, 2H, 1-H, 1′-H), 3.84 – 3.70 (m, 2H, 8-H), 1.58 (dq, *J* = 15.1, 7.5 Hz, 2H, 9-H), 0.82 (t, *J* = 7.4 Hz, 3H, 10-H); ^{13}C NMR (126 MHz, DMSO) δ

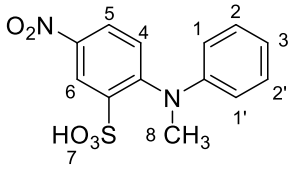
150.58, 148.11, 146.73, 143.60, 132.55, 128.56, 125.52, 124.67, 117.60, 115.43, 52.51, 19.29, 11.12.

2-(Ethyl(phenyl)amino)-5-nitrobenzenesulfonic acid (**35**) **(**according to general procedure **I)**



Chemical formula: $C_{14}H_{14}N_2O_5S$
Molecular weight: 322.34 g/mol
Calculations: Reactants: 2-chloro-5-nitrobenzenesulfonic acid **33** (0.50 g, 2.10 mmol), *N*-ethylaniline (1.53 g, 12.63 mmol)
TLC-MS (m/z): 323.10 $[M+H]^+$ (purity: 98%)
R_f = 0.23 (eluent: DCM:MeOH ; 86:14)
Yield: 27%, as greenish-yellow powder (0.18 g, 0.57 mmol)

2-(Methyl(phenyl)amino)-5-nitrobenzenesulfonic acid (**36**) **(**according to general procedure **I)**



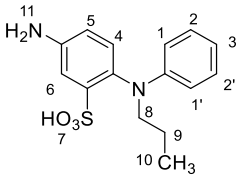
Chemical formula: $C_{13}H_{12}N_2O_5S$
Molecular weight: 308.31 g/mol
Calculations: Reactants: 2-chloro-5-nitrobenzenesulfonic acid **33** (0.50 g, 2.10 mmol), *N*-methylaniline (1.35 g, 12.63 mmol)
TLC-MS (m/z): 309.10 $[M+H]^+$ (purity: 99%)
R_f = 0.21 (eluent: DCM:MeOH ; 86:14)
Yield: 33%, as greenish-yellow powder (0.21 g, 0.69 mmol)

3. Reduction of the nitro group (37–39 and 41)

General procedure J

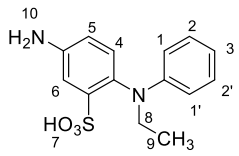
In a sealed reaction tube, 1.0 equivalent of 2-(alkyl(phenyl)amino)-5-nitrobenzenesulfonic acid derivatives **34**–**36** and **40** with 0.5 equivalent of ammonium chloride (NH_4Cl) were dissolved in a 12 mL mixture of ethanol and water (1:1, v/v). The reaction mixture was heated to 100 °C, followed by the portionwise addition of 3.0 equivalents of zinc powder. The suspension was stirred at 100 °C for 1 hour, and the reaction progress was monitored by thin-layer chromatography (TLC). After completion, the reaction mixture was cooled to room temperature and filtered over a pad of celite to remove residual zinc. The filtrate was washed with ethanol and water, and the solvents were removed under reduced pressure to afford the target 5-amino-2-substituted benzenesulfonic acids as grey powders, that were used in the coupling step without further purification:

5-Amino-2-(propyl(phenyl)amino)benzenesulfonic acid (**37**) **(**according to general procedure **J)**



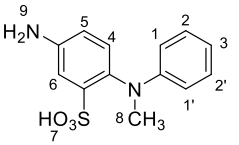
Chemical formula: $C_{15}H_{18}N_2O_3S$
Molecular weight: 306.38 g/mol
Calculations: Reactants: compound **34** (0.13 g, 0.38 mmol), NH_4Cl (10.34 mg, 0.19 mmol), Zn (0.076 g, 1.16 mmol)
TLC-MS (m/z): 307.10 $[M+H]^+$ (purity: 65%)
R_f = 0.09 (eluent: DCM:MeOH ; 86:14)

5-Amino-2-(ethyl(phenyl)amino)benzenesulfonic acid (**38**) **(**according to general procedure **J)**



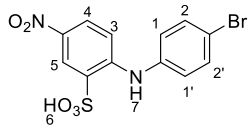
Chemical formula: $C_{14}H_{16}N_2O_3S$
Molecular weight: 292.35 g/mol
Calculations: Reactants: compound **35** (1.00 g, 3.42 mmol), NH_4Cl (91.48 mg, 1.71 mmol), Zn (0.67 g, 10.26 mmol)
TLC-MS (m/z): 293.10 $[M+H]^+$ (purity: 25%)
R_f = 0.11 (eluent: DCM:MeOH ; 86:14)

5-Amino-2-(methyl(phenyl)amino)benzenesulfonic acid (**39**) **(**according to general procedure **J)**



Chemical formula: $C_{13}H_{14}N_2O_3S$
Molecular weight: 278.33 g/mol
Calculations: Reactants: compound **36** (1.00 g, 3.59 mmol), NH_4Cl (96.09 mg, 1.80 mmol), Zn (0.70 g, 10.78 mmol)
TLC-MS (m/z): 279.10 $[M+H]^+$ (purity: 39%)
R_f = 0.11 (eluent: DCM:MeOH ; 86:14)

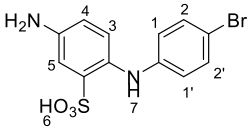
2-((4-Bromophenyl)amino)-5-nitrobenzenesulfonic acid (**40**) **(**according to general procedure **I)**



Chemical formula: $C_{12}H_9BrN_2O_5S$
Molecular weight: 373.18 g/mol
Calculations: Reactants: 2-chloro-5-nitrobenzenesulfonic acid **33** (0.50 g, 2.10 mmol), 4-bromoaniline (1.09 g, 6.31 mmol)
TLC-MS (m/z): 375.00 $[M+H]^+$ (purity: 99%)
R_f = 0.22 (eluent: DCM:MeOH ; 86:14)
Yield: 22%, as greenish-yellow powder (0.17 g, 0.46 mmol)

^{1}H NMR (500 MHz, DMSO-d_6) δ 9.32 (s, 1H, 7-NH), 8.44 (d, J = 2.8 Hz, 1H, 5-H), 8.06 (dd, J = 9.2, 2.8 Hz, 1H, 4-H), 7.63 – 7.48 (m, 2H, 2-H, 2′-H), 7.24 (d, J = 9.2 Hz, 1H, 3-H), 7.23 – 7.21 (m, 2H, 1-H, 1′-H); ^{13}C NMR (126 MHz, DMSO) δ 146.37, 139.00, 137.51, 132.69, 132.63, 126.41, 123.88, 123.54, 115.72, 112.75.

5-Amino-2-((4-bromophenyl)amino)benzenesulfonic acid (**41**) **(**according to general procedure **J)**



Chemical formula: $C_{12}H_9BrN_2O_5S$
Molecular weight: 343.20 g/mol
Calculations: Reactants: compound **40** (0.17 g, 0.46 mmol), NH_4Cl (12.20 mg, 0.23 mmol), Zn (0.09 g, 1.37 mmol)
TLC-MS (m/z): 344.90 $[M+H]^+$ (purity: 70%)
R_f = 0.09 (eluent: DCM:MeOH ; 86:14)

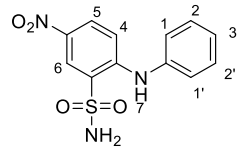
Synthesis of the sulfonamide-substituted aniline 43

Synthesis of 5-nitro-2-(phenylamino)benzenesulfonamide (42)

Procedure

In a sealed reaction tube, 0.76 g of 2-chloro-5-nitrobenzenesulfonamide (3.23 mmol) and 1.50 g of aniline (16.10 mmol) were dissolved in 3-chlorotoluene (12 mL) and the mixture was refluxed for 48 hours. The progress of the reaction was monitored by thin-layer chromatography (TLC), confirming complete consumption of the starting material. After completion, the reaction mixture was evaporated to dryness under reduced pressure. The residue was dissolved in an aqueous solution of sodium hydroxide (2 N) and extracted with diethyl ether to remove organic impurities.

The aqueous layer was separated and acidified to pH 1 with 2 M hydrochloric acid. The resulting precipitate was collected by filtration, washed thoroughly with water, and dried under vacuum to yield **42** as greenish yellow powder.



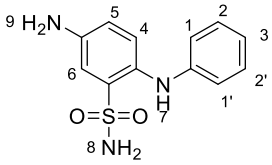
Chemical formula: $C_{12}H_{11}N_3O_4S$
Molecular weight: 293.30 g/mol
TLC-MS (m/z): 294.00 $[M+H]^+$ (purity: 99%)
R_f = 0.83 (eluent: DCM:ethyl acetate; 8:2)
Yield: 79%, as greenish yellow powder (0.75 g, 2.55 mmol)

^{1}H NMR (500 MHz, DMSO-d_6) δ 8.59 (d, *J* = 2.8 Hz, 1H, 6-H), 8.19 (dd, *J* = 9.3, 2.8 Hz, 1H, 5-H), 7.48 (dd, *J* = 8.3, 7.5 Hz, 2H, 1-H, 1′-H), 7.36 – 7.32 (m, 2H, 2-H, 2′-H), 7.28 (t, *J* = 7.4 Hz, 1H, 3-H), 7.18 (d, *J* = 9.3 Hz, 1H, 4-H); ^{13}C NMR (126 MHz, DMSO) δ 147.07, 138.33, 136.78, 129.75, 128.67, 126.20, 125.76, 125.30, 123.93, 113.99.

Synthesis of 5-amino-2-(phenylamino)benzenesulfonamide (43)

Procedure

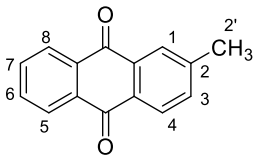
Compound **43** was synthesized according to the general procedure J.



Chemical formula: $C_{12}H_{13}N_3O_2S$
Molecular weight: 263.32 g/mol
Calculations: Reactants: compound **42** (0.40 g, 1.36 mmol), NH_4Cl (29.00 mg, 0.55 mmol), Zn (0.383 g, 5.86 mmol)
TLC-MS (m/z): 264.20 $[M+H]^+$ (purity: 98%)
R_f = 0.20 (eluent: DCM : ethyl acetate; 8 : 2)
Yield: 95%, as grey powder (0.34 g, 1.29 mmol)

^{1}H NMR (500 MHz, DMSO-d_6) δ 7.18 – 7.14 (m, 4H, 2-H, 2′-H, 8-NH_2), 7.11 (d, *J* = 2.7 Hz, 1H, 4-H), 7.08 (d, *J* = 8.6 Hz, 1H, 5-H), 6.97 (s, 1H, 6-H), 6.85 (d, *J* = 7.7 Hz, 1H, 3-H), 6.78 – 6.70 (m, 2H, 1-H, 1′-H), 5.19 (s, 2H, 9-NH_2); ^{13}C NMR (126 MHz, DMSO) δ 145.06, 143.71, 134.68, 128.90, 128.73, 123.71, 118.88, 118.32, 116.07, 112.51.

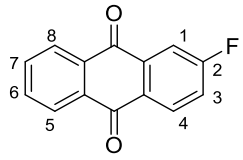
2-Methylanthracene-9,10-dione (50) (according to general procedure **B)**



Chemical formula: $C_{15}H_{10}O_2$
Molecular weight: 222.24 g/mol
Calculations: Reactant: 2-(4-methylbenzoyl)benzoic acid (1 g, 4.16 mmol)
TLC-MS (m/z): 223.10 $[M+H]^+$ (purity: 91%)
Mp: 175–176 (literature mp: 174–175 °C)[7]
R_f = 0.42 (eluent: cyclohexane : ethyl acetate; 9 : 1)
Yield: 83%, as yellow powder (0.77 g, 3.46 mmol).

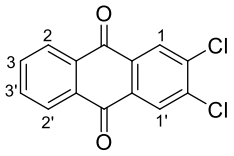
^{1}H NMR (500 MHz, DMSO-d_6) δ 8.23 – 8.12 (m, 2H, 6-H, 7-H), 8.08 (d, *J* = 7.9 Hz, 1H, 4-H), 7.98 (s, 1H, 1-H), 7.95 – 7.88 (m, 2H, 5-H, 8-H), 7.71 (ddd, *J* = 7.9, 1.8, 0.9 Hz, 1H, 3-H), 2.50 (s, 3H, 2'-H); ^{13}C NMR (126 MHz, DMSO) δ 182.41, 182.03, 145.17, 135.00, 134.33, 134.23, 132.86, 132.74, 130.60, 126.79, 126.72, 126.54, 126.49, 21.20.

2-Fluoroanthracene-9,10-dione (51) (according to general procedure **B)**



Chemical formula: $C_{14}H_7FO_2$
Molecular weight: 226.20 g/mol
Calculations: Reactant: 2-(4-fluorobenzoyl)benzoic acid (1 g, 4.09 mmol)
TLC-MS (m/z): 227.1 $[M+H]^+$ (purity: 96%)
Mp: 231–232 (literature mp: 230–232 °C)[8]
R_f = 0.39 (eluent: cyclohexane : ethyl acetate; 9 : 1)
Yield: 76%, as light brown powder (0.70 g, 3.09 mmol)

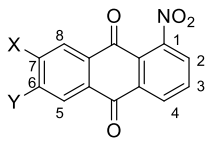
2,3-Dichloroanthracene-9,10-dione (52) (according to general procedure **B)**



Chemical formula: $C_{14}H_6Cl_2O_2$
Molecular weight: 277.10 g/mol
Calculations: Reactant: 2-(3,4-dichlorobenzoyl)benzoic acid (1 g, 3.39 mmol)
TLC-MS (m/z): 276.97 $[M+H]^+$ (purity: 98%)
Mp: 269–271 °C
R_f = 0.52 (eluent: cyclohexane : ethyl acetate; 9 : 1)
Yield: 92%, as yellowish-white powder (0.86 g, 3.10 mmol).

^{1}H NMR (500 MHz, DMSO-d_6) δ 8.32 (s, 2H, 1-H, 1′-H), 8.25 – 8.22 (m, 2H, 3-H, 3′-H), 7.99 – 7.96 (m, 2H, 2-H, 2′-H); ^{13}C NMR (126 MHz, DMSO) δ 180.82, 137.48, 134.85, 132.83, 128.59, 126.87.

6-Fluoro-1-nitroanthracene-9,10-dione (**54-F1**/**F2) (**according to general procedure **C)**



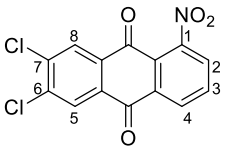
X, Y = F, H or H, F
regioisomeric mixture

Chemical formula: $C_{14}H_6FNO_4$
Molecular weight: 271.03 g/mol
Calculations: Reactant: 2-fluoroanthracene-9,10-dione (**51**) (0.70 g, 3.09 mmol), nitrating mixture: HNO_3 (0.9 mL), H_2SO_4 (1.15 mL), H_3PO_4 (0.32 mL).
TLC-MS (m/z): 272.03 $[M+H]^+$ (purity: 61:27%)
$R_{f\text{-}31\text{-}F1,\ F2}$ = 0.14, 0.11 (eluent: cyclohexane:ethyl acetate; 9:1)
Combined yield: 60%, as yellowish powder (0.50 g, 1.85 mmol)

6,7-Dichloro-1-nitroanthracene-9,10-dione **(55)**

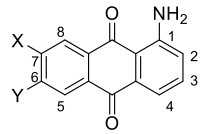
Procedure

In a sealed reaction tube, 1.0 equivalent of 2,3-dichloroanthraquinone (**30**) (0.2 g, 0.72 mmol) was suspended in 9 mL of concentrated sulfuric acid (H_2SO_4). To this mixture, 6.5 equivalents of potassium nitrate (KNO_3) (0.5 g, 4.7 mmol) were carefully added in portions under stirring at room temperature (25 °C). The resulting suspension was stirred vigorously for 16 hours. Upon completion, the reaction mixture was slowly poured into a beaker containing crushed ice under continuous stirring to quench the reaction and induce precipitation of the product. The resulting solid was collected by Büchner filtration, washed thoroughly with cold distilled water, and extracted with ethyl acetate. The organic phase was separated, dried over anhydrous magnesium sulfate ($MgSO_4$), filtered, and concentrated under reduced pressure. The crude product was subjected to purification by column chromatography using cyclohexane:ethyl acetate (9:1) as the eluent to afford the desired nitrated product **(55)**:



Chemical formula: $C_{14}H_5Cl_2NO_4$
Molecular weight: 322.10 g/mol
TLC-MS (m/z): 323.00 $[M+H]^+$ (purity: 95%)
Calculations: Reactant: 2,3-Dichloroanthracene-9,10-dione (**52**) (0.20 g, 0.72 mmol), potassium nitrate KNO_3 (0.50 g, 4.70 mmol).
Yield: 69%, as yellowish powder (0.16 g, 0.5 mmol)

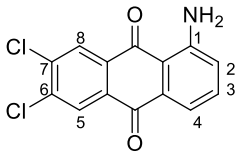
1-Amino-6-fluoroanthracene-9,10-dione (**56-F1**/**F2) (**according to general procedure **D)**



X, Y = F, H or H, F
regioisomeric mixture

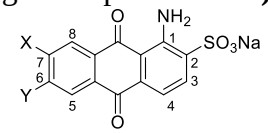
Chemical formula: $C_{14}H_8FNO_2$
Molecular weight: 241.22 g/mol
Calculations: Reactant: compound **54** (0.50 g, 1.85 mmol), $SnCl_2 \cdot 2H_2O$ (2.08 g, 9.25 mmol)
TLC-MS (m/z): 242.03 $[M+H]^+$ (purity: 92%)
Combined yield: 90%, as reddish powder (0.40 g, 1.66 mmol)

1-Amino-6,7-dichloroanthracene-9,10-dione **(57) (**according to general procedure **D)**



Chemical formula: $C_{14}H_7Cl_2NO_2$
Molecular weight: 292.12 g/mol
Calculations: Reactant: 6/7-Dichloro-1-nitroanthraquinone (0.16 g, 0.5 mmol), $SnCl_2 \cdot 2H_2O$ (0.56 g, 2.5 mmol)
TLC-MS (m/z): 293.03 $[M+H]^+$ (purity: 92%)
Yield: 92%, as reddish powder (0.135 g, 0.46 mmol)

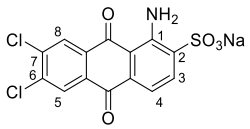
Sodium 1-amino-6/7-fluoro-9,10-dioxo-9,10-dihydroanthracene-2-sulfonate **(58) (**according to general procedure **E)**



X, Y = F, H or H, F
regioisomeric mixture

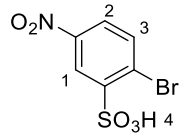
Chemical formula: $C_{14}H_7FNNaO_5S$
Molecular weight: 321.28 g/mol
Calculations: Reactant: compound **56** (0.40 g, 1.66 mmol), $HClSO_3$ (0.25 g, 2.16 mmol)
TLC-MS (m/z): 322.01 $[M-Na^+ + H]^+$ (purity: 94%)
Combined yield: 60%, as a dark reddish powder (0.35 g, 0.99 mmol)

Sodium 1-amino-6,7-dichloro-9,10-dioxo-9,10-dihydroanthracene-2-sulfonate **(59) (**according to general procedure **E)**



Chemical formula: $C_{14}H_6Cl_2NNaO_5S$
Molecular weight: 372.18 g/mol
Calculations: Reactant: compound **57** (0.135 g, 0.46 mmol), $HClSO_3$ (0.07 g, 0.60 mmol)
TLC-MS (m/z): 373.03 $[M-Na^+ + H]^+$ (purity: 97%)
Yield: 50%, as a dark reddish powder (0.091 g, 0.22 mmol)

2-Bromo-5-nitrobenzenesulfonic acid (**62**) **(**according to general procedure **H)**



Chemical formula: $C_6H_4BrNO_5S$
Molecular weight: 282.06 g/mol
Calculations: Reactant: 4-Nitrobromobenzene (1.00 g, 4.95 mmol), 20% oleum (4.49 g, 25.25 mmol, 2.36 mL)
TLC-MS (m/z): 283.20 $[M+H]^+$ (purity: 92%)
Yield: 57%, as grey powder (0.80 g, 2.82 mmol)

^{1}H NMR (500 MHz, DMSO-d_6) δ 8.62 (d, J = 2.9 Hz, 1H, 1-H), 8.04 (dd, J = 8.6, 2.9 Hz, 1H, 3-H), 7.89 (d, J = 8.6 Hz, 1H, 2-H); ^{13}C NMR (126 MHz, DMSO) δ 148.55, 146.29, 135.78, 127.47, 124.74, 123.50.

The analytical data is provided in **Appendix I.**

3.2 Chapter II: Systematic development of anthraquinone-derived $P2Y_{12}$ receptor antagonists as radioligand candidates (Manuscript I)

Hashem Ali M. Al Musawi[1], Younis Baqi[1,2], and Christa E. Müller[1,*]

1 PharmaCenter Bonn, Department of Pharmaceutical & Medicinal Chemistry, Pharmaceutical Institute at University of Bonn, Bonn, Germany

2 Department of Chemistry, Faculty of Science at Sultan Qaboos University, Muscat, Oman

*Correspondence:

Prof. Dr. Christa E. Müller, PharmaCenter Bonn, Pharmaceutical Institute, Pharmaceutical and Medicinal Chemistry, University of Bonn, An der Immenburg 4, 53121 Bonn, Germany

Email: christa.mueller@uni-bonn.de

3.2.1 Author contributions

The author synthesized the radioligand precursors **5** and **6**, and the model compound **7**, performed the optimization at the hydrogenation reaction conditions, determined the analytical data (LC/MS and NMR) of the developed compounds, and wrote the manuscript in close collaboration with the corresponding author Prof. Dr. Christa E. Müller.

3.2.2 Abstract

The $P2Y_{12}$ receptor is expressed in microglial cells in the central nervous system. Radiolabeled antagonists targeting this receptor are of particular interest as therapeutics for neurodegenerative diseases and as diagnostics enabling non-invasive imaging of microglial activation. The potent anthraquinone-based $P2Y_{12}$ receptor antagonists such as PSB-0739 (**1**) and PSB0702 (**2**) were selected for radiolabeling. However, tritiation has been limited by chemical instability, particularly the release of the C2-sulfonate or carboxylate moieties under palladium-catalyzed hydrogenation condition. In this study, we describe three synthetic trials aimed at developing anthraquinone-based $P2Y_{12}$ receptor antagonist radioligands. A model compound **7** was synthesized to systematically optimize key reaction parameters, including catalyst type, solvent system, and hydrogen pressure. These results provide critical insights into the reactions of anthraquinone core and its substituents and lay the groundwork for future radioligand development to advance neuroimaging of the $P2Y_{12}$ receptor.

3.2.3 Introduction

Anthraquinones represent a class of organic compounds, structurally defined by a rigid planar three-ring aromatic system (anthracene) functionalized with two ketone groups at the C9- and C10-positions (Figure 16). This distinct quinone-based core confers unique chemical and biological properties, making anthraquinones valuable across various scientific and industrial applications.[67] The anthraquinone family encompasses multiple compound subclasses, many of which are of considerable importance in various industrial sectors such as pharmaceuticals, textile dying, painting, and food industries as additives, as well as catalysis due to their redox properties.[71–75] Beyond their industrial significance, several anthraquinones possess well-known bioactive properties. These compounds are derived from various natural sources, including plants (e.g., aloe), where they have been traditionally used in folk medicine for thousands of years, fungi and insects.[68–70] Clinically approved anthraquinone derivatives include anthracyclines such as doxorubicin, daunorubicin, and epirubicin, which remain among the most effective chemotherapeutic agents in oncology. Anthrones (e.g., anthraquinone glycosides such as sennosides), widely used as stimulant laxatives.[67]

One of the best-known anthraquinone derivatives is Reactive Blue 2 (RB-2) (**I**, Figure 1), a synthetic anthraquinone dye extensively utilized in textile industry. In addition, RB-2 has been identified as a biologically active compound capable of modulating purinergic signaling pathways. Specifically, RB-2 functions as a P2Y receptor antagonist, interfering with adenosine diphosphate (ADP)-mediated receptor activation.[76,77] Our research group has explored anthraquinone-based scaffolds, particularly derivatives and analogs of RB-2, for their potential as $P2Y_{12}$ receptor antagonists. RB-2 has been reported to inhibit $P2Y_{12}$ receptor activation with a K_i value of 1.3 μM, which is consistent with our findings, where we determined a K_i value of 0.68 μM.[35] Further research led to the development of two novel ligands by our group, belonging to the most potent $P2Y_{12}$ receptor antagonists, the sodium 1-amino-9,10-dioxo-4-((4-(phenylamino)-3-sulfonatophenyl)amino)-9,10-dihydroanthracene-2-sulfonate (**1** (**PSB-0739**), Figure 1), and sodium 5-((4-amino-3-carboxy-9,10-dioxo-9,10-dihydroanthracen-1-yl)amino)-2-(phenylamino)benzenesulfonate, (**2** (**PSB-0702**), Figure 1), with K_i values of 24.9 nM and 21.0 nM, respectively, determined in radioligand binding studies.[23] These novel ligands were synthesized using an Ullman-coupling reaction.[35]

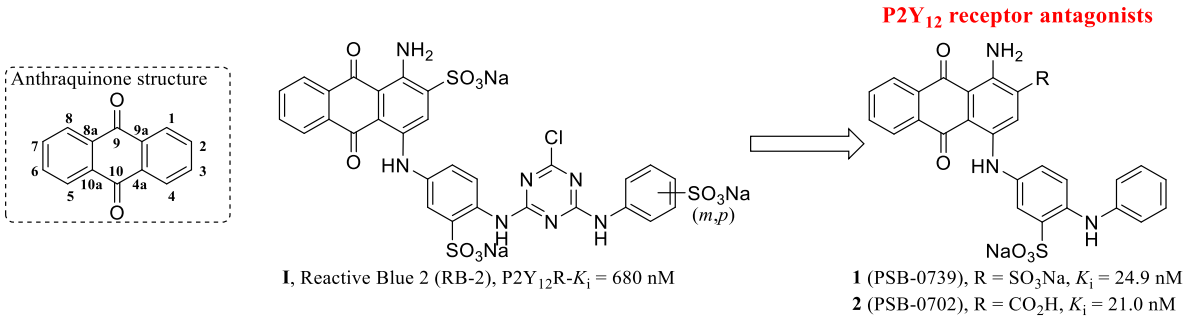


Figure 17. Structures of RB-2 (**I**) and the most potent $P2Y_{12}$ receptor antagonists of the anthraquinone scaffold (**1** and **2**), K_i values at the human $P2Y_{12}$ receptor were determined in radioligand binding assays.[35]

The purinergic $P2Y_{12}$ receptor is a G protein–coupled receptor (GPCR) that is activated endogenously by adenosine diphosphate (ADP). It is highly expressed in the blood platelets and essential in mediating platelet aggregation. Antagonizing ADP-induced activation of $P2Y_{12}$ receptor contributes in the regulation of thrombotic disorders.[22] In addition, $P2Y_{12}$ receptor is expressed in microglial cells within the central nervous system, where it serves as a reliable biomarker of microglial activation and plays a critical role in the progression of neurodegenerative diseases, including Alzheimer's disease, Parkinson's disease, and multiple sclerosis.[23,26]

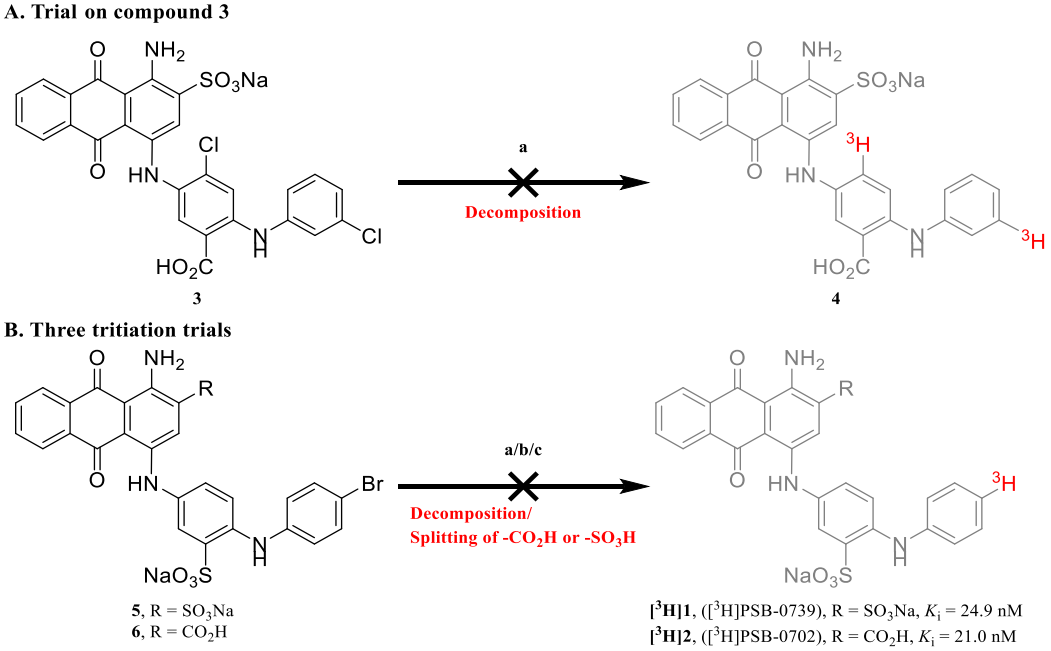
Our aim has been to develop a tritium-labeled antagonist radioligand for $P2Y_{12}$ receptors based on compounds 1 and 2 (Figure 1). Our approach has been to introduce a chlorine or a bromine atom and to subsequent perform dehalogenative tritiation.

3.2.4 Results and discussion

Palladium over carbon (Pd/C) was used for the reduction of the previously synthesized chloro-substituted radioligand precursor **3** (Scheme S4) of the $P2Y_{12}$ receptor antagonist **4**, where a complete decomposition had been observed (**A**, Scheme 10). Recently, we observed another instability issue during the three tritiation trials of the synthesized novel bromo-substituted precursors **5** and **6** (**B**, Scheme 10) of the most potent and selective anthraquinone-based $P2Y_{12}$ receptor antagonists (**1** (**PSB-0739**) and (**2** (**PSB-0702**), **B**, Scheme 10), respectively. Both novel precursors were synthesized (Scheme S4) and subjected to heterogeneous catalytic dehalogenative tritiation using palladium as a catalyst and a stream of tritium gas to generate the desired radiolabeled analogs (**B**, Scheme 10). In both, the first and the second trial, Pd/C was used as a catalyst in DMF; the only difference was the reaction time which was decreased from 4 h in the

first trial to 11 min in the second trial. In both trials, a complete degradation was observed. Thus, the *Lindlar*-catalyst was used in the third trial as a milder palladium catalyst. In this trial, partial degradation of the starting material and elimination of the sulfonate or carboxylate from the C2-position were observed (**B**, Scheme 10).

Scheme 10. Instability cases: **A**. Tritiation trial of **3** (failed trial) ; **B**. Tritiation trials of the novel $P2Y_{12}$ receptor antagonist radioligand precursors **5** and **6** (failed trials); Associated challenges are a complete decomposition or splitting of the sulfonate or carboxylic acid from the C2-position.[a]

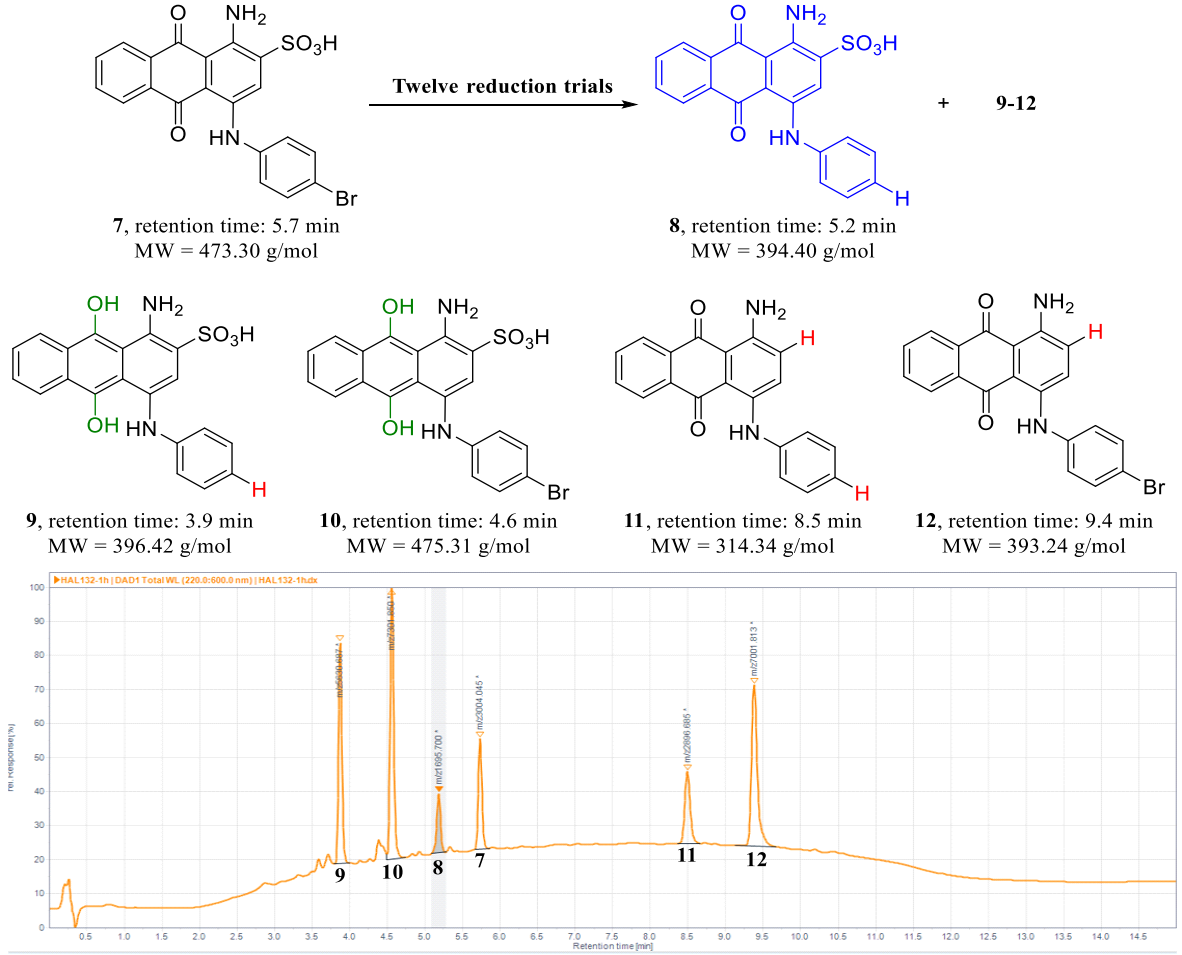


[a]Reaction conditions: The three reactions were performed under tritium gas (a. Pd/C, DMF, 25 °C, 4 h; b. Pd/C, DMF, 25 °C, 11 min; c. *Lindlar* catalyst, DMF, 25 °C, 16 h) (failed trials).

Subsequently, we performed a systematic optimization of the reaction. For this purpose, a simple model compound, **7**, structurally analogous to **5** and **6**, was synthesized and purified to be used in the systematic optimization of the reduction strategy (Scheme S1). Twelve reduction trials were conducted using two milder palladium-based catalysts, palladium hydroxide on carbon ($Pd(OH)_2/C$), or palladium on calcium carbonate ($Pd/CaCO_3$). Reactions were carried out under varying hydrogen pressures (5−8 psi (34.5−55.2 kPa)/atmospheric via a balloon) and in different solvent systems (methanol, ethanol, 1,4-dioxane, a 1:1 mixture of water and 1,4-dioxane, and dichloromethane). The reaction duration ranged from 2 to 12 h using a hydrogen generator and up to 7 days when applying hydrogen-filled balloons. The reaction progress was monitored by LC/MS at regular intervals (Scheme 11). LC/MS analysis revealed the formation of trace amounts of the

desired product **8**, along with four distinct side products: The hydroquinone analog **9** of the desired product **8**, which should be reoxidizable to **8**, the hydroquinone analog **10** of the starting material **7**, the de-sulfonated derivative of **8** (**11**), and the de-sulfonated derivative of **7** (**12**) (Scheme 11). Table 3 summarizes the dehalogenative hydrogenation trials and their associated results.

Scheme 11. Reduction of the model compound **7** and the formed products **8**– **12**. Reaction conditions, retention time, and molecular weight are given, along with an example of the LCMS-DAD-total wavelength diagram highlighting the peaks (related response) of each compound **7**–**12** at the measured retention time.[a]



[a]Reaction conditions: H_2-pressure: 5-8 psi (34.5–55.2 kPa) or atmospheric; catalyst type: $Pd(OH)_2/C$ or $Pd/CaCO_3$; solvent system: MeOH, EtOH, 1,4-dioxane, CH_2Cl_2, or 1,4-dioxane:H_2O (1:1); reaction time: 2h to 7d; temperature: 25 °C.

Different solvent systems previously described for palladium-catalyzed hydrogenations were employed in this study based on *SciFinder*-platform. Methanol (MeOH) was identified as the most suitable solvent for the reduction reaction, consistently resulting in near-complete conversion of

the starting material and the highest combined yield of the desired compound **8** and its analog **9** (Scheme 11) (Trials **I**−**IV** and **X**−**XII**; Table 3).

Comparison of catalysts showed the best performance for $Pd/CaCO_3$ in terms of selectivity. $Pd(OH)_2/C$ appeared to be too reactive, promoting rapid degradation of the starting material and extensive de-sulfonation, as evidenced by a 34% combined yield of by-products **11** and **12** (Scheme 2) after 2 h (Trial **I**, Table 3). Catalyst loading may affect the reduction process as reducing the amount of $Pd/CaCO_3$ catalyst to 10% led to increased de-sulfonation and formation of **11** and **12** (75% combined; Trial **IV**, Table 3) under conditions applying of 8 psi (55.2 kPa) H_2 pressure in methanol.

Studying the hydrogen pressure was performed under constant conditions of 30% of $Pd/CaCO_3$ and methanol at room temperature in the trials **II**, **III**, and **X**−**XII**. Comparative analysis of these trials (Trials **II**, **III**, and **X**−**XII**; Table 3) illustrates the significant influence of H_2 pressure on reaction selectivity. At **5 psi** (34.5 kPa), the major product was the hydroquinone **10** (56%), indicating predominant quinone reduction (Scheme 11). In addition, formation of the undesired by-products **11** and **12** (Scheme 11) was observed (17% combined; Trial **II**, Table 3). At **6 psi** (41.4 kPa), simultaneous quinone reduction and dehalogenation occurred, yielding 70% of **11** (Scheme 11) after 3 h. However, 10% of combined undesired by-products **11** and **12** (Scheme 11) were observed (Trial **III**, Table 3). Increasing the pressure to **8 psi** (55.2 kPa) (in a 25 mL hydrogenation flask) improved the yield of compound **8** to 32% after 6 h, although 58% of the starting material **7** remained unreacted (Trial **IV**, Table 3). Notably, performing the same reaction in a **smaller 10 mL flask** (Trial **XI**, Table 3) caused de-sulfonation, yielding **12** as the main product (65%) and leaving 16% of unreacted **7** (Scheme 11). Conducting the reaction under atmospheric hydrogen pressure using a hydrogen-filled balloon resulted in a gradual formation of the desired product **8**, while effectively suppressing the formation of the undesired by-products **11** and **12** (Trial **XII**, Table 3). The slower reaction kinetics under these conditions enabled clearer observation of the dynamic equilibrium between the starting material **7** and its hydroquinone analog **10**, as well as between the target compound **8** and its reduced analog **9** (Scheme 11). Moreover, it was clearly observed that the reduction to the hydroquinone analog occurred prior to the dehalogenation step as expected. Further optimization of this reaction setup, such as increasing the catalyst loading or maintaining a constant atmospheric hydrogen pressure, holds potential for

improving the stability and selectivity of anthraquinone derivatives during palladium-catalyzed hydrogenation processes.

Table 3. Summary of the twelve reduction experiments applied on the model compound **7**.

Trial (reactor size) (% of 7/at the end (h))	**Reactions' conditions at 25 °C**			**Observations (based on LC/MS results)**			
	Solvent	Catalyst	H_2 (psi/ kPa)/ atmospheric pressure	Maximum yield (% of **8**/time (h))	Maximum yield (% of **9**/time (h))	Maximum yield (% of **10**/ at the end)	Maximum yield (% of **11** + **12**/ at the end)
I (25 mL) (0/2)	MeOH	$Pd(OH)_2/C$ (0.2 equiv.)	5/34.5	18/2	18/1	25	34
II (25 mL) (9/9)	MeOH	$Pd/CaCO_3$ (30%)	5/34.5	12/2	8/9	56	17
III (25 mL) (0/7)	MeOH	$Pd/CaCO_3$ (30%)	6/41.4	**9/3**	**70/3**	1	10
IV (25 mL) (1.3/10)	MeOH	$Pd/CaCO_3$ (10%)	8	5/2	3/10	1	75
V (25 mL) (63/8)	1,4-Dioxan	$Pd(OH)_2/C$ (0.2 equiv.)	5/34.5	6/5	3/8	16	6
VI (25 mL) (60/6)	EtOH	$Pd(OH)_2/C$ (0.2 equiv.)	5/34.5	6/5	3/6	9	4
VII (25 mL) (44/7)	Water:1,4-dioxan (1:1)	$Pd(OH)_2/C$ (0.2 equiv.)	5/34.5	4/2	3/7	4	25
VIII (25 mL) (52/12)	EtOH	$Pd/CaCO_3$ (30%)	5/34.5	5/4	2/12	5	22
IX (25 mL) (99/7)	CH_2Cl_2	$Pd/CaCO_3$ (30%)	5/34.5	–	–	–	–
X (25 mL) (58/6)	MeOH	$Pd/CaCO_3$ (30%)	8/55.2	32/6	2/6	0	5
XI (10 mL) (16/9)	MeOH	$Pd/CaCO_3$ (30%)	8/55.2	15/2	1/2	4	65
XII (25 mL) (round-bottom flask) (70/7d)	MeOH	$Pd/CaCO_3$ (30%)	atmospheric pressure	27/7d	16/27	–	–

The maximum yield observed of the desired compound **8** (Scheme 11) (8%) alongside 70% of its hydroquinone analog **9** (Scheme 11) was achieved under the conditions applied in Trial **III** (Table 3), with a reaction time of 3 h. However, reproduction of this condition was found to be challenging, and the oxidation of the hydroquinone analog **9** to the quinone **8** was not completely achieved. Stirring the reaction mixtures for an extra 24 or 55 h under ambient atmosphere was performed with the aim to reoxidize the hydroquinone byproduct **9** to the desired product **8**. In general, a reoxidization could be observed, however elimination of the sulfonate at the C2-position was observed as well.

Table 4 provides the results for the reoxidization reactions of the four trials: **II**, **III**, **X**, and **XI** and allows the comparison between both the formation of the desired product **8** (de-brominated quinone), its de-brominated hydroquinone analog **9** and the de-brominated and de-sulfonated byproduct **11** or the formation of **7**, **10**, and **12**.

In trial three **III**, the percentage of hydroquinone **9** was 66%; after stirring for 55 h under ambient atmosphere it becomes 44%. As a result, the amount of the desired quinone product **8** increased from 8 to 17% as was expected, however the de-sulfonated analog **11** was increased from 9 to 17% as well (Table 4). Another example is trial **X**, where the 33% of **8** became 4% after 24 h of stirring under ambient atmosphere, leading to the formation of 34% of the de-sulfonated analog **11**, which amounts to 4% at the end of the trial, but a low increase in the percentage of the hydroquinone **9** (from 2 to 4%). Comparison of the compounds **7**, **10**, and **12** in the same trial emphasize this result whereas 36% of the starting material **7** was converted after stirring to the de-sulfonated analog, and only 3% to the hydroquinone analog (Table 4). The de-sulfonated product **12** of the starting material **7** and its hydroquinone analog **10** was also observed in trial **II** leading to an increase of up to 29% in the formation of **12** (Table 4). Trial **XI** confirms the effect of the high hydrogen pressure on the direct de-sulfonation of the starting material **7** to form **12**, which correlated to the mentioned results after 24 h (Table 4).

Table 4. Observations of the reoxidization and de-sulfonation percentages of **7**−**12** at the end of the trials **II**, **III**, **X**, and **XI** or after 24 to 55 h of stirring under ambient conditions.

Trial (reactor size) (reaction time)	H_2-pressure (psi/kPa)	Percentage (%) of **7**−**12** at the end of the trials/after 24 to 55 h of stirring under ambient conditions					
		7	**8**	**9**	**10**	**11**	**12**
II (25 mL) (7 h)	5/34.5	8.7/7.6	2.2/2.5	7.8/5.3	56.0/13.2	2.3/11.3	14.5/43.4
III (25 mL) (7 h)	6/41.4	−	8.3/17.5	66.0/44.8	−	9.1/17.3	−
X (25 mL) (6 h)	8/55.2	58.0/6.7	32.6/4.5	2.0/3.7	0.7/4.0	3.6/33.9	1.8/38.3
XI (10 mL) (9 h)	8/55.2	16.2/15.7	7.8/7.4	1.1/1.4	4.2/1.8	12.0/11.1	53.3/58.8

In conclusion, the sulfonate group at the C2-position appears to be a more labile leaving group than the bromine at the aniline moiety. The tendency for SO_3H release is hydrogen pressure-dependent and it might be catalyst-dependent as it was exacerbated by prolonged stirring under ambient conditions in the presence of $Pd/CaCO_3$, despite trial **XII**, where the reaction time was prolonged to 7 days without any observation of de-sulfonation.

3.2.5 Conclusions and outlook

In the present study, we synthesized the novel anthraquinone-based $P2Y_{12}$ receptor antagonist radioligand precursors **3**, **5** and **6**, and extensively studied the instability of the anthraquinone core and sulfonate or carboxylate elimination from the C2-position during palladium-catalyzed dehalogenative reduction. Subsequently, compound **7** was developed and employed as a model compound for optimizing the catalytic hydrogenation conditions. Through systematic investigation, it was determined that $Pd/CaCO_3$ in methanol at 5 psi (34.5 kPa) of hydrogen gas at room temperature offered the most favorable conditions. Further experiments revealed that the reactor size (25 mL vs. 10 mL hydrogenation flasks) significantly affected the reaction outcome, likely due to variations in effective hydrogen pressure. Continued optimization efforts were taken in consideration included reducing the reaction rate by applying atmospheric hydrogen pressure via a balloon. Under these conditions, the formation of undesired byproducts was suppressed, and the reduction to the hydroquinone analog was found to precede the dehalogenation step, providing valuable mechanistic insights.

Future work will prioritize further optimization of this reaction setup, such as increasing the catalyst loading or maintaining a constant atmospheric hydrogen pressure, which holds potential for improving the palladium-catalyzed hydrogenation of the anthraquinone derivatives. Regarding the relative stability of sulfonate versus carboxylate groups at the C2-position, the optimized reduction conditions should be applied on the C2-carboxyl-substituted anthraquinone derivatives. These advancements are expected to support the development of novel, stable anthraquinone-based P2-purinergic receptor ligands and to contribute to the study of $P2Y_{12}$ receptors through the use of robust chemical tools.

3.2.6 Experimental part

Materials and reagents

All commercially available reagents were used as purchased (abcr, Acros, Alfa Aesar, BLDpharm, Sigma-Aldrich, or TCI). Solvents were used without additional purification or drying. Thin-layer chromatography (TLC) and reversed phase thin-layer chromatography (RP-18-TLC) using aluminum sheets with silica gel 60 F_{254} and RP silica gel 18 F_{254} were utilized to monitor the reactions (Merck). Colored compounds were visible at daylight; other compounds were visualized under UV light (254 nm). Flash chromatography was performed on a Büchi system using silica

gel RP-18 (Merck). All synthesized compounds were finally dried in vacuum at 8−12 Pa (0.08−0.12 mbar) using a sliding vane rotary vacuum pump (Vacuubrand GmbH). A freeze-dryer (CHRIST ALPHA 1-4 LSC) was used for lyophilization. ^{1}H and ^{13}C NMR data were collected on a Bruker Avance 500 MHz NMR spectrometer at 500 MHz (^{1}H) or 126 MHz (^{13}C), respectively. If indicated, NMR data were collected on a Bruker Ascend 600 MHz NMR spectrometer at 600 MHz (^{1}H) or 151 MHz (^{13}C). DMSO-d_6 was used as a solvent at 303 K. Chemical shifts are reported in parts per million (ppm) relative to the deuterated solvent: DMSO, δ ^{1}H: 2.49 ppm; ^{13}C: 39.7 ppm. Coupling constants *J* are given in Hertz, and spin multiplicities are given as s (singlet), d (doublet), dd (doublet of doublet), t (triplet), q (quartet), sext (sextet), m (multiplet), and br (broad). The purities of all isolated products were determined by an HPLC 1260 Infinity II (Agilent) using an EC 50/2 Nucleodur C18 Gravity 3 μm column (Macherey-Nagel), coupled to a UV/vis diode array detector, and a mass spectrometer (Infinity Lab LC MSD system, Agilent, with an EC 50/2 Nucleodur C18 Gravity 3 μm column, Machery-Nagel). All compounds are >95% pure by HPLC/UV. The column temperature was 40 degrees. The compounds were dissolved at a concentration of 1.0 mg/mL in water, methanol, or acetonitrile. Then, 2 μL of the sample solution was injected to a flow of 0.5 mL/min. Elution started with a gradient of water containing 2 mM ammonium acetate/acetonitrile from 90:10 to 0:100 for 10 min, and then, it was flushed with 100% acetonitrile for an additional 5 min. Positive total ion scans were observed from 100−1000 *m*/*z* (or more if necessary). UV absorption was detected from 190 to 600 nm using a diode array detector (DAD). The purity of all compounds was determined at 220−600 nm. For microwave reactions a CEM Focused Microwave Synthesis type Discover apparatus was used. The procedures of the twelfth optimization trials along with their LC/MS-results are described below in table 5. Comprehensive synthesis procedures for the radioligand precursors **3**, **5**, and **6**, the model compound **7**, and the reported intermediates, as well as the analytical characterization of all trials and compounds, are provided in the Supporting Information (SI).

Optimization of the reduction conditions (Change of catalyst, H_2-pressure, or solvent) of the model compound 7

Table 5 summarizes the reduction protocols applied to compound **7** and presents the corresponding LC/MS-analysis of the resulting products, including their retention times (RT) and relative formation percentages (Area%). The retention time of the target compound **8** was identified as

5.18 min. The retention times of the additionally detected byproducts were as follows: 5.73 min for the unreacted starting material **7**, 3.87 min for the hydroquinone analog of the desired product **9**, 4.56 min for the hydroquinone analog of the starting material **10**, 8.49 min for the desired product analog without the sulfonate salt **11**, and 9.38 min for the reactant analog without the sulfonate **12**.

Table 5. Experimental protocols and interpretation of LC/MS-results for the optimized conditions.

First method: In a 25 mL hydrogenation flask, 1.0 equivalent (20 mg, 0.04 mmol) of compound **7** was dissolved in 5 mL of methanol under an argon atmosphere. To the solution, 1.3 mg (7,67 μmol) of $Pd(OH)_2/C$ was added. The reaction mixture was stirred under a hydrogen atmosphere (5 psi (34.5 kPa) H_2 pressure) for 2 h. Samples were withdrawn for LC/MS analysis at hourly intervals. An additional sample was collected after 24 h to monitor further reaction progress.						
LC/MS-analysis of Experiment I (2 h)						
Cpd. [RT in min]	**9** [3.87]	**10** [4.56]	**8** [5.18]	**7** [5.73]	**11** [8.49	**12** [9.38]
Trial-Time	Area%					
I-1h	18.45	22.83	5.56	9.84	9.49	22.94
I-2h	6.30	24.82	18.39	–	26.55	7.95
I-(55h O_2)	1.07	4.68	24.57	12.79	27.37	13.92
Second method: In a 25 mL hydrogenation flask, 1.0 equivalent (10 mg, 0.02 mmol) of compound **7** was dissolved in 5 mL of methanol under an argon atmosphere. Subsequently, 30% per weight of $Pd/CaCO_3$ (3 mg) was added. The reaction mixture was stirred under a hydrogen atmosphere (5 psi (34.5 kPa) H_2 pressure) for 9 h. LC/MS samples were collected at hourly intervals to monitor the reaction progress. An additional sample was taken after 24 h to assess extended reaction outcomes.						
LC/MS-analysis of Experiment II (9 h)						
Cpd. [RT in min]	**9** [3.87]	**10** [4.56]	**8** [5.18]	**7** [5.73]	**11** [8.49]	**12** [9.38]
Trial-Time	Area%					
II-1h		0.15	11.91	78.45	0.65	7.15
II-2h	0.11	1.11	12.27	59.08	1.87	20.04
II-3h	1.89	12.49	9.61	42.95	2.42	21.69
II-4h	2.92	22.13	7.22	34.14	2.36	22.37
II-5h	4.55	38.16	5.75	26.35	1.87	14.70
II-6h	5.15	37.10	5.12	22.51	2.09	16.76
II-7h	5.70	45.58	4.43	19.01	196	13.92
II-8h	7.39	55.20	3.14	12.29	1.95	12.81
II-9h	7.84	55.96	2.15	8.69	2.34	14.49
II-(24h O_2)	5.30	13.15	2.48	7.60	11.26	43.43
Third method: In a 25 mL hydrogenation flask, 1.0 equivalent (10 mg, 0.02 mmol) of compound **7** was dissolved in 5 mL of methanol under an argon atmosphere. Subsequently, 30% per weight of $Pd/CaCO_3$ (3 mg) was added. The reaction mixture was stirred under a hydrogen atmosphere (6 psi (41.4 kPa) H_2 pressure) for 7 h. LC/MS samples were collected at hourly intervals to monitor the reaction progress. An additional sample was taken after 55 h to assess extended reaction outcomes.						
LC/MS-analysis of Experiment III (7 h)						
Cpd. [RT in min]	**9** [3.87]	**10** [4.56]	**8** [5.18]	**7** [5.73]	**11** [8.49]	**12** [9.38]
Trial-Time	Area%					
III-1h	**50.38**	23.19	**4.94**	3.24	6.88	4.44

III-2h	**65.69**	3.45	**8.75**	0.97	10.81	1.18
III-3h	**69.89**	0.67	**8.50**	**0.41**	10.38	0.48
III-4h	68.44	0.03	8.27	0.25	9.90	0.35
III-5h	68.42	0.78	7.29	0.08	10.55	0.34
III-6h	66.80	0.74	8.02	0.10	9.42	0.27
III-7h	66.04	0.91	8.26	0.10	9.13	0.31
III-(55h O_2)	44.81	0.10	17.54	0.47	17.33	0.38

Fourth method: In a 25 mL hydrogenation flask, 1.0 equivalent (10 mg, 0.02 mmol) of compound **7** was dissolved in 5 mL of methanol under an argon atmosphere. Subsequently, 10% per weight of $Pd/CaCO_3$ (1 mg) was added. The reaction mixture was stirred under a hydrogen atmosphere (8 psi (55.2 kPa) H_2 pressure) for 10 h. LC/MS samples were collected at hourly intervals to monitor the reaction progress.

LC/MS-analysis of Experiment IV (10 h)

Cpd. [RT in min]	**9** [3.87]	**10** [4.56]	**8** [5.18]	**7** [5.73]	**11** [8.49]	**12** [9.38]
Trial-Time	Area%					
IV-2h	–	–	4.76	69.69	1.32	19.28
IV-4h	1.47	1.89	3.43	45.21	1.59	37.13
IV-6h	1.32	1.16	1.86	16.92	1.54	62.83
IV-8h	2.79	0.22	0.73	3.10	3.50	70.62
IV-10h	2.93	0.68	0.11	1.35	2.75	71.97

Fifth method: In a 25 mL hydrogenation flask, 1.0 equivalent (10 mg, 0.02 mmol) of compound **7** was dissolved in 5 mL of 1,4-dioxan under an argon atmosphere. To the solution, 0.65 mg (3,84 μmol) of $Pd(OH)_2/C$ was added. The reaction mixture was stirred under a hydrogen atmosphere (5 psi (34.5 kPa) H_2 pressure) for 8 h. Samples were withdrawn for LC/MS analysis at hourly intervals. An additional sample was collected after 24 h to monitor further reaction progress.

LC/MS-analysis of Experiment V (8 h)

Cpd. [RT in min]	**9** [3.87]	**10** [4.56]	**8** [5.18]	**7** [5.73]	**11** [8.49]	**12** [9.38]
Trial-Time	Area%					
V-1h	0.06	0.18	0.33	97.64	–	–
V-2h	0.07	0.21	0.39	97.47	–	–
V-3h	0.08	0.16	0.33	97.58	–	–
V-4h	–	0.07	5.59	83.93	–	1.70
V-5h	0.48	0.10	5.84	76.76	0.31	4.36
V-7h	2.50	14.25	5.39	65.80	0.49	6.55
V-8h	2.94	16.55	5.08	63.04	0.58	6.51
V-(24h O_2)	3.13	16.28	5.43	62.79	0.59	6.03

Sixth method: In a 25 mL hydrogenation flask, 1.0 equivalent (10 mg, 0.02 mmol) of compound **7** was dissolved in 5 mL of ethanol under an argon atmosphere. To the solution, 0.65 mg (3,84 μmol) of $Pd(OH)_2/C$ was added. The reaction mixture was stirred under a hydrogen atmosphere (5 psi (34.5 kPa) H_2 pressure) for 6 h. Samples were withdrawn for LC/MS analysis at hourly intervals. An additional sample was collected after 24 h to monitor further reaction progress.

LC/MS-analysis of Experiment VI (6 h)

Cpd. [RT in min]	**9** [3.87]	**10** [4.56]	**8** [5.18]	**7** [5.73]	**11** [8.49]	**12** [9.38]
Trial-Time	Area%					
VI-10min	–	3.13	0.29	92.98	–	–
VI-1h	0.73	3.66	4.32	88.12	–	0.73
VI-2h	1.02	4.23	5.05	84.81	0.32	1.13
VI-4h	1.51	6.32	5.96	81.54	0.50	2.29
VI-5h	1.10	7.61	6.03	79.31	0.67	2.67
VI-6h	2.93	8.70	5.28	60.55	0.63	4.01
VI-(24h O_2)	2.94	5.19	7.32	61.12	2.14	12.56

Seventh method: In a 25 mL hydrogenation flask, 1.0 equivalent (10 mg, 0.02 mmol) of compound **7** was dissolved in 5 mL mixture of water:1,4-dioxan (1:1) under an argon atmosphere, then 0.65 mg (3,84 μmol) of $Pd(OH)_2/C$ was added to the solution,. The reaction mixture was stirred under a hydrogen atmosphere (5 psi (34.5 kPa) H_2 pressure) for 7 h. Samples were withdrawn for LC/MS analysis at hourly intervals.

LC/MS-analysis of Experiment VII (7 h)

Cpd. [RT in min]	**9** [3.87]	**10** [4.56]	**8** [5.18]	**7** [5.73]	**11** [8.49]	**12** [9.38]
Trial-Time	Area%					
VII-10min	–	5.86	–	91.78	–	–
VII-2h	0.74	5.85	3.67	76.89	0.56	6.06
VII-4h	1.60	5.48	3.65	63.12	0.90	14.12
VII-6h	2.20	4.42	2.92	48.60	0.96	21.11
VII-7h	2.55	3.89	2.83	44.04	0.89	23.99

Eighth method: In a 25 mL hydrogenation flask, 1.0 equivalent (10 mg, 0.02 mmol) of compound 7 was dissolved in 5 mL of ethanol under an argon atmosphere. Subsequently, 30% per weight of $Pd/CaCO_3$ (3 mg) was added. The reaction mixture was stirred under a hydrogen atmosphere (5 psi (34.5 kPa) H_2 pressure) for 12 h. LC/MS samples were collected at hourly intervals to monitor the reaction progress.

LC/MS-analysis of Experiment VIII (12 h)

Cpd. [RT in min]	**9** [3.87]	**10** [4.56]	**8** [5.18]	**7** [5.73]	**11** [8.49]	**12** [9.38]
Trial-Time	Area%					
VIII-15min	–	2.27	1.02	96.45	–	–
VIII-1h	–	4.72	4.72	87.01	–	3.54
VIII-2h	–	4.31	4.68	85.59	–	5.13
VIII-3h	0.22	4.35	4.88	82.44	–	6.09
VIII-4h	0.72	4.75	5.15	74.91	–	10.71
VIII-5h	1.03	5.74	4.62	66.96	–	12.92
VIII-6h	1.22	5.98	4.76	67.30	–	13.95
VIII-7h	1.48	5.68	3.83	60.42	0.31	16.78
VIII-8h	1.35	4.64	4.40	59.50	0.32	17.01
VIII-12h	2.00	5.40	3.83	52.06	0.24	21.34

Ninth method: In a 25 mL hydrogenation flask, 1.0 equivalent (10 mg, 0.02 mmol) of compound **7** was dissolved in 5 mL of dichloromethane under an argon atmosphere. Subsequently, 30% per weight of $Pd/CaCO_3$ (3 mg) was added. The reaction mixture was stirred under a hydrogen atmosphere (5 psi (34.5 kPa) H_2 pressure) for 7 h. LC/MS samples were collected at hourly intervals to monitor the reaction progress. No reaction has been observed

Tenth method: In a 25 mL hydrogenation flask, 1.0 equivalent (10 mg, 0.02 mmol) of compound **7** was dissolved in 5 mL of methanol under an argon atmosphere. Subsequently, 30% per weight of $Pd/CaCO_3$ (3 mg) was added. The reaction mixture was stirred under a hydrogen atmosphere (8 psi (55.2 kPa) H_2 pressure) for 6 h. LC/MS samples were collected at hourly intervals to monitor the reaction progress. An additional sample was collected after 24 h to monitor further reaction progress.

LC/MS-analysis of trial X (6 h)

Cpd. [RT in min]	**9** [3.87]	**10** [4.56]	**8** [5.18]	**7** [5.73]	**11** [8.49]	**12** [9.38]
Trial-Time	Area%					
X-20 min	0.44	–	12.67	84.35	–	–
X-2h	2.07	0.33	25.60	64.82	2.31	3.57
X-3h	2.09	0.45	26.97	64.11	3.36	2.45
X-4h	2.10	0.70	29.30	61.80	3.72	1.35
X-5h	1.93	0.77	31.15	60.48	3.13	1.49
X-6h	2.00	0.66	32.64	58.04	3.55	1.84
X-24h	3.72	3.97	4.46	6.65	33.92	38.32

Eleventh method: In a 10 mL hydrogenation flask, 1.0 equivalent (10 mg, 0.02 mmol) of compound **7** was dissolved in 5 mL of methanol under an argon atmosphere. Subsequently, 30% per weight of $Pd/CaCO_3$ (3 mg) was added. The reaction mixture was stirred under a hydrogen atmosphere (8 psi (55.2 kPa) H_2 pressure) for 9 h. LC/MS samples were collected at hourly intervals to monitor the reaction progress. An additional sample was collected after 24 h to monitor further reaction progress.

LC/MS-analysis of trial XI (9 h)

Cpd. [RT in min]	**9** [3.87]	**10** [4.56]	**8** [5.18]	**7** [5.73]	**11** [8.49]	**12** [9.38]
Trial-Time	Area%					
XI-2h	1.29	0.37	14.87	42.71	6.25	34.51
XI-4h	1.27	1.44	13.18	31.17	8.13	44.82
XI-6h	1.28	2.99	12.26	26.15	10.07	46.47
XI-7h	1.13	4.03	8.80	18.26	8.81	57.59
XI-8h	0.92	5.79	6.73	14.00	8.43	59.56
XI-9h	1.07	4.19	7.81	16.23	11.96	53.29
XI-24h	1.41	1.77	7.36	15.67	11.14	58.79

Twelfth method: In a 25 mL round-bottom flask, 1.0 equivalent (10 mg, 0.02 mmol) of compound **7** was dissolved in 5 mL of methanol under an argon atmosphere. Subsequently, 30% per weight of $Pd/CaCO_3$ (3 mg) was added. The reaction mixture was stirred under a hydrogen atmosphere (balloon pressure) for 7 days. LC/MS samples were collected at defined intervals to monitor the reaction progress.

LC/MS-analysis of trial XII (7 days)

Cpd. [RT in min]	**9** [3.87]	**10** [4.56]	**8** [5.18]	**7** [5.73]	**11** [8.49]	**12** [9.38]
Trial-Time	Area%					
XII-1h	–	31.03	2.09	63.49	–	–
XII-2.5h	–	17.30	8.52	71.34	–	–
XII-4h	4.52	25.67	6.39	61.24	–	–
XII-7.5h	–	–	17.55	81.54	–	–
XII-9h	–	7.35	16.81	74.96	–	–
XII-11h	5.23	15.68	13.10	64.79	–	–
XII-27h	16.11	39.31	5.10	36.97	–	–
XII-28.5h	15.54	38.48	5.62	38.17	–	–
XII-31.5h	6.11	16.69	15.50	58.22	–	–
XII-33.5h	6.10	15.08	15.82	61.42	–	–
XII-36h	6.68	14.25	16.89	60.50	–	–
XII-51.5h	4.42	12.30	18.57	63.50	–	–
XII-54h	5.77	12.45	18.28	62.13	–	–
XII-59h	–	–	25.10	71.32	–	–
XII-76h	3.70	9.74	20.67	64.86	–	–
XII-82h	–	–	25.86	70.35	–	–
XII-5d & 9h	2.58	7.04	21.60	68.30	–	–
XII-6d & 5h	2.65	7.38	21.17	68.74	–	–
XII-7d & 3h	–	–	26.70	68.91	–	–

Acknowledgements

H.A.M.A.M. is grateful for a PhD scholarship from the Saudi Ministry of Education, Saudi Arabia. This study was supported by the Deutsche Forschungsgemeinschaft (DFG) and the Agence Nationale de la Recherche (ANR); MU 1665/12-1, project 1291 number 471773752 and ANR-21-CE18-0067-01, project 'PURImaging'.

Conflict of interest

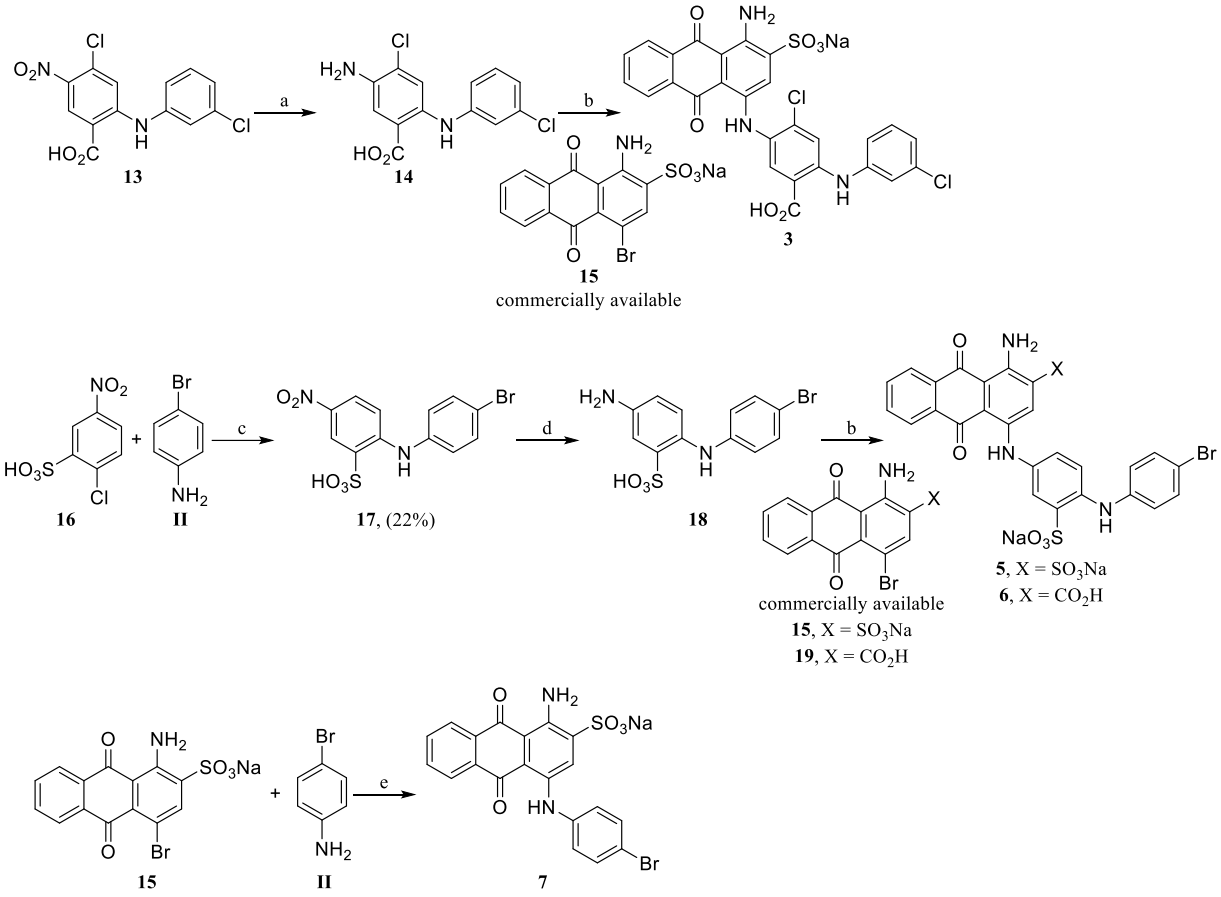
The authors declare no conflict of interest

3.2.7 Supporting information

Synthesis of the anthraquinone-based $P2Y_{12}$ receptor antagonist radioligand precursors 3, 5, 6, and the model compound 7

To prepare the precursor **3**, the intermediate 4-chloro-2-((3-chlorophenyl)amino)-5-nitrobenzoic acid (**13**, Scheme S4) was reduced using zinc powder in a mixture of acetic acid and water (1:1) at room temperature. The resulted product 14 was subsequently coupled by Ullman-coupling reaction under microwave irradiation to the commercially available bromaminic acid 15 to afforded **3**. A similar synthesis pathway was performed to prepare the precursors **5** and **6**, whereas the commercially available 4-bromoaniline (**II**, Scheme S4) was reacted with the synthesized compound 2-chloro-5-nitrobenzenesulfonic acid[1] (**16**, Scheme S4) in *N*,*N*-dimethylformamide (DMF, bp = 153 °C) at 150 °C for 3 days to yield the 2-((4-bromophenyl)amino)-5-nitrobenzenesulfonic acid (**17**, Scheme S4), which was reduced to **18** using zinc powder and ammonium chloride in a mixture of ethanol and water (1:1) at 100 °C (Scheme S4). Compound **18** served as a key-intermediate which was reacted with the anthraquinone key-intermediates **15** and **19** in an Ullman-coupling reaction under microwave irradiation, leading to the formation of both potential $P2Y_{12}$ receptor antagonists radioligand precursors **5** and **6**, respectively (Scheme S4). The model compound **7** was synthesized using the same procedure of the coupling between the anthraquinone key-intermediate **15** and the 4-bromoaniline **II** (Scheme S4).

Scheme S4. Synthesis of the radioligand precursors **3**, **5**, and **6**, as well as the model compound **7**.[a]



[a]Reaction conditions: a. Zn, AcOH:H_2O (1:1), 25 °C, 3 h; b. **15**/**19**, microwave irradiation: Cu^0, phosphate buffer, 100-120 °C; c. DMF, 150 °C, 3 d; d. Zn, NH_4Cl, EtOH:H_2O (1:1), 100 °C, 1 h; e. microwave irradiation: Cu^0, phosphate buffer, 100-120 °C.

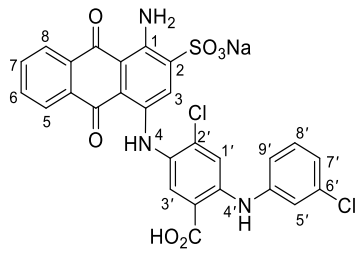
Synthesis of the desired anthraquinone-derived P2Y$_{12}$ receptor antagonist radioligand precursors 3, 5, and 6, as well as the model compound 7

General procedure A[35]

A 10 mL microwave reaction vessel equipped with a magnetic stir bar was charged with sodium 1-amino-4-bromo-9,10-dioxo-9,10-dihydroanthracene-2-sulfonate (**15**) (1.0 equiv.) as the aryl halide coupling partner. For the synthesis of the radioligand precursor **6**, 1-amino-4-bromo-9,10-dioxo-9,10-dihydroanthracene-2-carboxylic acid (1.0 equiv.) (**19**) was used instead. To the vessel, the desired aniline derivative (1.0 to 2.0 equiv.), elemental copper (Cu^0) powder (catalytic amount), and a phosphate buffer system comprising Na_2HPO_4 (pH 9.6, 4.5 mL) and NaH_2PO_4 (pH 4.2, 0.5 mL) were added. The reaction mixture was sealed and subjected to microwave irradiation at 80–100 W for 5–10 min at 120 °C.

Upon completion, the reaction mixture was allowed to cool to room temperature and filtered to remove residual copper. The filtrate was extracted with dichloromethane (ca. 200 mL) and water. The aqueous phase was concentrated under reduced pressure to a volume of 10–20 mL and subsequently purified by flash chromatography using RP-18 reversed-phase silica gel with water as the initial eluent. Stepwise increases in eluent polarity were achieved by adding acetone or methanol at concentrations of 5%, 10%, 20%, 40%, and 60%. Fractions containing the desired blue-colored product were combined and subjected to rotary evaporation to remove organic solvents and reduce the aqueous volume. Final drying was achieved by lyophilization to afford the pure products as solid blue powders:

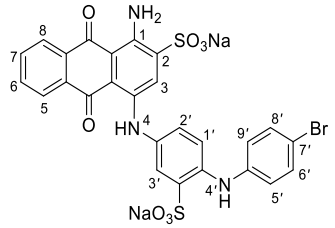
Sodium 1-amino-4-((5-carboxy-2-chloro-4-((3-chlorophenyl)amino)phenyl)amino)-9,10-dioxo-9,10-dihydroanthracene-2-sulfonate (**3**)



Chemical formula: $C_{27}H_{16}Cl_2N_3NaO_7S$
Molecular weight: 620.39 g/mol
Calculations: Reactants: bromaminic acid (0.12 g, 0.29 mmol), aniline (0.09 g, 0.29 mmol)
Reaction conditions: 5 min, 120 °C, 100 W; pressure up to 10 bar.
Purification: Purification step has been repeated twice. Polarity of the eluent was decreased by the addition of acetone in the following steps: 5, 10, 20, 40, and 60%.
Yield: 8%, as blue powder (15.00 mg, 0.024 mmol)
LC-MS (m/z): 599.4 $[M-Na^+ + H]^+$ (purity: 96%)
Mp: >300 °C

^{1}H NMR (600 MHz, DMSO-d_6) δ 12.46 (s, 1H, 4'-NH), 11.92 (s, 1H, 4-NH), 10.10 (s, 1H, CO_2H), 8.29 – 8.28 (m, 2H, 6-H, 7-H), 7.96 (s, 1H, 3'-H), 7.87 – 7.82 (m, 2H, 5-H, 8-H), 7.64 (s, 1H, 3-H), 7.34 – 7.31 (m, 2H, 1'-H, 5'-H), 7.16 (dd, J = 8.6, 2.7 Hz, 2H, 7'-H, 9'-H), 6.97 – 6.95 (m, 1H, 8'-H); ^{13}C NMR (151 MHz, DMSO) δ 182.38, 181.84, 169.30, 144.29, 143.80, 143.34, 143.11, 142.72, 134.32, 133.97, 133.78, 133.17, 132.83, 131.19, 130.70, 130.57, 126.17, 126.11, 125.54, 122.57, 120.82, 118.28, 117.23, 113.74, 110.70, 109.13.

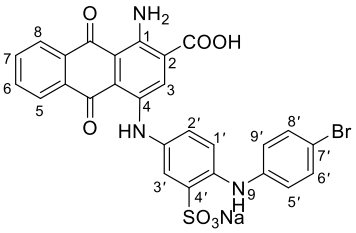
Sodium 1-amino-4-((4-((4-bromophenyl)amino)-3-sulfonatophenyl)amino)- 9,10-dioxo-9,10-dihydroanthracene-2-sulfonate (**5**)



Chemical formula: $C_{26}H_{16}BrN_3Na_2O_8S_2$
Molecular weight: 688.43 g/mol
Calculations: Reactants: bromaminic acid (0.05 g, 0.13 mmol), aniline (0.09 g, 0.26 mmol)
Reaction conditions: 10 min, 120 °C, 100 W; pressure up to 10 bar.
Purification: Purification step has been repeated five times. Polarity of the eluent was decreased by the addition of acetone in the following steps: 5, 10, 20, 40, and 60%.
Yield: 31%, as blue powder (26.00 mg, 0.04 mmol)
LC-MS (m/z): 642.97 $[M-2Na^+ + 2H]^+$ (purity: 97%)
Mp: >300 °C

^{1}H NMR (600 MHz, DMSO-d_6) δ 12.12 (s, 1H, 4-NH), 8.63 (s, 1H, 4'-NH), 8.29 (dt, J = 6.8, 1.6 Hz, 2H, 6-H, 7-H), 7.90 – 7.78 (m, 3H, 3-H, 5-H, 8-H), 7.50 (d, J = 2.6 Hz, 2H, 6'-H, 8'-H), 7.42 (d, J = 8.8 Hz, 1H, 3'-H), 7.34 (d, J = 8.6 Hz, 1H, 1'-H), 7.17 (dd, J = 8.6, 2.7 Hz, 2H, 5'-H, 9'-H), 7.07 (d, J = 8.8 Hz, 1H, 2'-H); ^{13}C NMR (151 MHz, DMSO) δ 181.97, 181.75, 144.32, 143.14, 142.44, 141.95, 136.93, 135.92, 134.25, 133.82, 133.05, 132.79, 132.13, 130.17, 126.12, 125.79, 123.91, 122.68, 119.65, 116.53, 111.50, 110.56, 109.07.

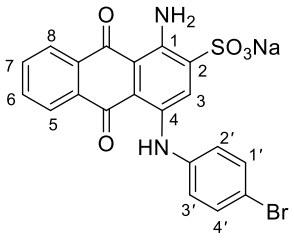
Sodium 5-((4-amino-3-carboxy-9,10-dioxo-9,10-dihydroanthracen-1-yl)amino)-2-((4-bromophenyl)amino)benzenesulfonate (**6**)



Chemical formula: $C_{27}H_{17}BrN_3NaO_7S$
Molecular weight: 630.40 g/mol
Calculations: Reactants: bromaminic acid (0.04 g, 0.115 mmol), aniline (0.08 g, 0.23 mmol)
Reaction conditions: 10 min, 120 °C, 100 W; pressure up to 10 bar.
Purification: Purification step has been repeated four times. Polarity of the eluent was decreased by the addition of acetone in the following steps: 5, 10, 20, 40, and 60%.
Yield: 29%, as blue powder (18.00 mg, 0.03 mmol)
LC-MS (m/z): 608.10 $[M - Na^+ + H]^+$ (purity: 95%)
Mp: >300 °C

^{1}H NMR (600 MHz, DMSO-d_6) δ 11.77 (s, 1H, 4-NH), 8.61 (s, 1H, 9-NH), 8.29 (ddd, J = 6.2, 3.7, 1.6 Hz, 2H, 6-H, 7-H), 8.19 (s, 1H, 3-H), 7.86 (p, J = 7.5, 6.9 Hz, 2H, 5-H, 8-H), 7.54 (d, J = 2.4 Hz, 1H, 2'-H), 7.42 (d, J = 8.7 Hz, 2H, 6'-H, 8'-H), 7.34 (d, J = 8.5 Hz, 1H, 3'-H), 7.21 (dd, J = 8.5, 2.5 Hz, 1H, 1'-H), 7.07 (d, J = 8.7 Hz, 2H, 5'-H, 9'-H); ^{13}C NMR (151 MHz, DMSO) δ 182.89, 181.95, 167.63, 142.05, 136.80, 135.98, 134.29, 133.58, 133.45, 132.99, 132.17, 130.49, 126.23, 126.15, 125.71, 123.52, 119.63, 116.57, 111.50.

Sodium 1-amino-9,10-dioxo-4-((4-(phenylamino)-3-sulfonatophenyl)amino)-9,10-dihydroanthracene-2-sulfonate (**7**)



Chemical formula: $C_{20}H_{12}BrN_2NaO_5S$
Molecular weight: 495.28 g/mol
Calculations: Reactants: bromaminic acid **4** (0.1 g, 0.26 mmol), 4-bromoaniline (0.09 g, 0.52 mmol)
Reaction conditions: 9 min, 120 °C, 100 W; pressure up to 10 bar.
Purification: Purification step has been repeated twice. Polarity of the eluent was decreased by the addition of acetone in the following steps: 5, 10, 20, and 40%.
Yield: 42%, as blue powder (54.50 mg, 0.11 mmol)
LC-MS (m/z): 473.20 $[M-Na^+ + H]^+$ (purity: 99%)
Mp: >300 °C

^{1}H NMR (500 MHz, DMSO-d_6) δ 11.85 (s, 1H, 4-NH), 8.35 – 8.18 (m, 2H, 6-H, 7-H), 7.99 (s, 1H, 3-H), 7.85 (p, J = 7.2 Hz, 2H, 5-H, 8-H), 7.60 (d, J = 8.5 Hz, 2H, 1'-H, 4'-H), 7.25 (d, J = 8.6 Hz, 2H, 2'-H, 3'-H); ^{13}C NMR (126 MHz, DMSO) δ 182.63, 181.75, 144.26, 142.40, 139.58, 138.77, 133.92, 133.26, 133.13, 132.65, 132.25, 125.85, 125.77, 124.49, 122.48, 115.76, 112.02, 109.14.

Synthesis of 5-amino-4-chloro-2-((3-chlorophenyl)amino)benzoic acid (14)

Procedure

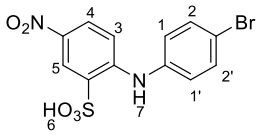
The 4-chloro-2-((3-chlorophenyl)amino)-5-nitrobenzoic acid (**13**) (0.33 g, 1.0 mmol) was suspended in 15 mL of AcOH:H_2O (1:1, v/v) and stirred for 5 min at room temperature, followed by the addition of zinc (0.65 g, 10.0 mmol). The reaction mixture was then stirred for further 2.5 h. After completion as indicated by thin-layer chromatography (TLC), $NaHCO_3$ was portion wise added to pH of 4−5 followed by 10 mL of water to observe the formation of white precipitation. This was extracted using 100 mL of ethyl acetate, washed with brine and water, dried over magnesium sulfate, and evaporated under reduced pressure to afford the desired aniline **14** as gray powder (0.09 g, 0.29 mmol, 29%), that was used in the Ullman-coupling reaction without further purification.

Synthesis of 5-amino-2-((4-bromophenyl)amino)benzenesulfonic acid (18)

Procedure (thermal amination)

In a sealed reaction tube, 0.50 g of 2-chloro-5-nitrobenzenesulfonic acid **16** (2.10 mmol) and 1.09 g of 4-bromoaniline (6.31 mmol) were dissolved in 9 mL of *N*,*N*-dimethylformamide (DMF) under an argon atmosphere. The reaction mixture was stirred at 150 °C until completion, as confirmed by TLC. Upon completion, the mixture was cooled to room temperature, diluted with dichloromethane (DCM), and washed with water. A 2.5 M aqueous solution of sodium hydroxide

(NaOH) was added to transfer the product into the aqueous phase. After confirming complete transfer by TLC, the aqueous layer was neutralized with concentrated sulfuric acid (H_2SO_4) to approximately pH 7. Water was removed under reduced pressure, and the residue was dissolved in warm ethanol, followed by vacuum filtration and washing with additional warm ethanol. The filtrate was then concentrated under vacuum to yield the desired product 2-((4-bromophenyl)amino)-5-nitrobenzenesulfonic acid (**17**) as greenish-yellow powder (0.17 g, 0.46 mmol, 22%), that was used in the next step without further purification:

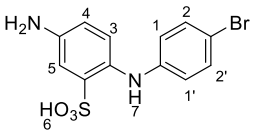


Chemical formula: $C_{12}H_9BrN_2O_5S$
Molecular weight: 373.18 g/mol
TLC-MS (m/z): 375.00 $[M+H]^+$ (purity: 99%)
R_f = 0.22 (eluent: DCM:MeOH ; 86:14)
Yield: 22%, as greenish-yellow powder (0.17 g, 0.46 mmol)

^{1}H NMR (500 MHz, DMSO-d_6) δ 9.32 (s, 1H, 7-NH), 8.44 (d, J = 2.8 Hz, 1H, 5-H), 8.06 (dd, J = 9.2, 2.8 Hz, 1H, 4-H), 7.63 – 7.48 (m, 2H, 2-H, 2′-H), 7.24 (d, J = 9.2 Hz, 1H, 3-H), 7.23 – 7.21 (m, 2H, 1-H, 1′-H); ^{13}C NMR (126 MHz, DMSO) δ 146.37, 139.00, 137.51, 132.69, 132.63, 126.41, 123.88, 123.54, 115.72, 112.75.

Procedure (Reduction of nitro group)

In a sealed reaction tube, 0.17 g of 2-((4-bromophenyl)amino)-5-nitrobenzenesulfonic acid (**17**) (0.46 mmol) with 0.012 g of ammonium chloride (NH_4Cl) (0.23 mmol) were dissolved in a 12 mL mixture of ethanol and water (1:1, v/v). The reaction mixture was heated to 100 °C, followed by the portion wise addition of 0.09 g of zinc powder (1.37 mmol). The suspension was stirred at 100 °C for 1 h, and the reaction progress was monitored by TLC. After completion, the reaction mixture was cooled to room temperature and filtered over a pad of celite to remove residual zinc. The filtrate was washed with ethanol and water, and the solvents were removed under reduced pressure to afford the target compound 5-amino-2-((4-bromophenyl)amino)benzenesulfonic acid (**18**) as grey powder (0.14 g, 0.41 mmol, 89%), that was used in the coupling step without further purification:



Chemical formula: $C_{12}H_9BrN_2O_5S$
Molecular weight: 343.20 g/mol
TLC-MS (m/z): 344.90 $[M+H]^+$ (purity: 70%)
R_f = 0.09 (eluent: DCM:MeOH ; 86:14)

The analytical data is provided in **Appendix II**.

3.3 Chapter III: $P2Y_{12}$ receptor antagonists: Evaluation of their potential as lead structures for brain therapeutics and diagnostics (Manuscript II)

Hashem Ali M. Al Musawi[1], Nader M. Boshta[1], Alexandra Winkeler[2], Bertrand Kuhnast[2], Christa E. Müller[1]

[1]PharmaCenter Bonn, Pharmaceutical Institute, Department of Pharmaceutical & Medicinal Chemistry, University of Bonn, An der Immenburg 4, 53121 Bonn, Germany
[2]Laboratoire d'Imagerie Biomédicale Multimodale (BioMaps), CEA, CNRS, Inserm, Université Paris-Saclay, Orsay, France

Corresponding Author
Prof. Dr. Christa E. Müller
PharmaCenter Bonn
Pharmaceutical Institute
Pharmaceutical & Medicinal Chemistry
University of Bonn
An der Immenburg 4, 53121 Bonn, Germany
Phone: +49-228-73-2301
Fax: +49-228-73-2567
E-mail: christa.mueller@uni-bonn.de

3.3.1 Author contributions

The author performed the data analysis process starting with collecting the data, followed by classification, selection of the scaffolds, analysis by applying the central nervous system filters, and discussing the physicochemical properties, the reported metabolic stability and Caco-2 permeability, in addition to the design and writing of this manuscript in a close collaboration with the corresponding author Prof. Dr. Christa E. Müller.

3.3.2 Abstract

$P2Y_{12}$ receptors ($P2Y_{12}Rs$) are activated by adenosine diphosphate (ADP) and predominantly recognized for their role in platelet aggregation. They are additionally expressed on microglia in the central nervous system (CNS) and involved in neuroinflammation. Microglial $P2Y_{12}Rs$ represent a promising marker to monitor neuroinflammatory processes by applying imaging techniques such as positron emission tomography (PET). This study presents a systematic analysis of published $P2Y_{12}R$ antagonists, evaluating their potential as CNS-permeable lead structures for brain therapeutics and diagnostics. As a result, it led to the identification of promising scaffolds by assessment of their physicochemical properties, applying in silico CNS penetration filters, and by analysis of their structure-activity relationships (SARs). A pyrazolyl-phenyl-carbamoyl-indole scaffold, in particular 2-(3-((4-(4-butyryl-5-methyl-1*H*-pyrazol-1-yl)phenyl)carbamoyl)-5-methyl-1*H*-indol-1-yl)acetic acid, emerged as a starting point for developing CNS-permeable $P2Y_{12}R$ antagonists. Detailed SAR-analysis of this scaffold allowed the identification of promising substitution patterns to guide the design of novel $P2Y_{12}R$ antagonists with potential for brain bioavailability. This analysis provides a basis for advancing $P2Y_{12}R$-targeted therapeutics and diagnostics for inflammatory CNS disorders including Alzheimer's and Parkinson's disease.

3.3.3 Introduction

G protein-coupled $P2Y_{12}Rs$ are endogenously activated by the nucleotide ADP (**I**, Figure 18). Adenosine triphosphate (ATP, **II**, Figure 18), on the other hands, represents a $P2Y_{12}R$ antagonist. These receptors are expressed on microglia and play pivotal roles in neuroinflammation and neurodegeneration. While $P2Y_{12}Rs$ expressed on blood platelets are critical for blood coagulation and play a role in arterial thrombosis formation and acute coronary syndrome, microglial $P2Y_{12}Rs$ represent a novel, promising biomarker for monitoring microglial activity via advanced brain imaging techniques, such as positron emission tomography (PET).[26–33] Moreover, antagonists of brain $P2Y_{12}Rs$ have potential as therapeutics for inflammatory disorders, including Alzheimer's and Parkinson's disease.[26]

The current challenge lies in developing $P2Y_{12}R$ antagonists with blood-brain barrier (BBB) permeability. Reported and approved $P2Y_{12}R$ antagonists primarily target platelet receptors, lacking brain penetration which is not desired for antithrombotic drugs. This study aims to identify

scaffolds with potential for CNS penetration while retaining $P2Y_{12}R$ potency and selectivity. To this end, we analyzed published $P2Y_{12}R$ antagonist scaffolds.

Numerous $P2Y_{12}R$ antagonists have been developed to date as antithrombotic drugs. Among these, thienopyridine derivatives such as clopidogrel (**III**, Figure 18) and prasugrel (**IV**, Figure 18) have demonstrated significant efficacy in managing arterial thrombosis. Both compounds are prodrugs requiring bioactivation, enabling covalent disulfide bond formation with a peripheral allosteric site on the platelet $P2Y_{12}R$.[25,34,35,40]

Several competitive reversible $P2Y_{12}R$ antagonists have been published based on scaffolds, either derived from the physiological $P2Y_{12}R$ agonist adenosine diphosphate (ADP**, I**, Figure 18) or the antagonist adenosine triphosphate (ATP, **II**, Figure 18). An important example is the intravenous antithrombotic drug cangrelor (AR-C69931MX, **V**, Figure 18).[41–45] However, this compound is unsuitable for oral administration due to its negative charge and the resulting high polarity at physiological pH of 7.4.[35] The nucleoside analog ticagrelor is orally bioavailable (**VI**, Figure 18),[42] clinically used as an antithrombotic drug, but displays poor penetration into the brain.[47] Beyond these classes of compounds, various further heterocyclic antagonist scaffolds have been developed and optimized to achieve reversible $P2Y_{12}R$ inhibition.

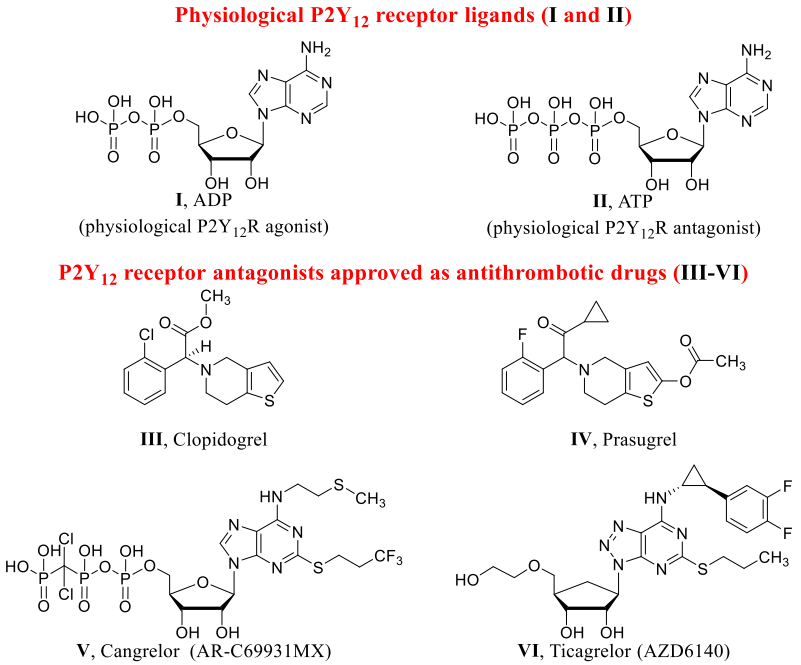


Figure 18. Structure of the physiological $P2Y_{12}R$ agonist adenosine diphosphate (ADP**, I**), the antagonist adenosine triphosphate (ATP, **II**), the prodrugs clopidogrel (**III**) and prasugrel (**IV**),

and the reversible competitive antagonists cangrelor (AR-C69931MX, **V**) and ticagrelor (AZD6140, **VI**).

For CNS drugs, two primary routes of brain permeation have been observed: passive diffusion and transporter-mediated blood-brain barrier (BBB) penetration.[97] Among these, passive diffusion is considered the most straightforward mechanism. The efficiency of this process is largely determined by the compounds' physicochemical properties. To optimize CNS permeability, the central nervous system multiparameter optimization (CNS MPO) approach[102,103] recommends the systematic modulation of six key physicochemical parameters: (1) partition coefficient (logP), (2) distribution coefficient at physiological pH 7.4 (logD), (3) topological polar surface area (TPSA), (4) molecular weight (MW), (5) number of hydrogen bond donors (HBDs), and (6) dissociation constant of the most basic center (pK_a). These parameters are evaluated along with the affinity and selectivity for the target protein, in this case the $P2Y_{12}R$.[102,103] In addition, this study includes discussion of ADME (absorption, distribution, metabolism, excretion) parameters such as metabolic stability and intestinal cell permeability determined in Caco-2 cells, which provides primary insights for potential brain permeability. Thus, the aim of the present study was the identification of potentially brain-permeable $P2Y_{12}R$ antagonists among the published $P2Y_{12}R$ antagonists, which could serve as lead structures to develop CNS-therapeutics and diagnostics.

3.3.4 Results and discussion

Search for $P2Y_{12}$ receptor antagonists and analysis of their properties

The *ChEMBL* database was utilized to search for $P2Y_{12}R$ antagonists, and their properties were analyzed by application of predefined CNS penetration filters to identify promising lead compounds. This approach involved a structured workflow beginning with the collection of all available $P2Y_{12}R$ antagonists, including those published in patents (2,180 compounds), followed by sequential classification, and ending with the selection of the most relevant scaffolds and identification of promising lead structures. Figure 19 provides an overview of the data analysis process employed in this study.

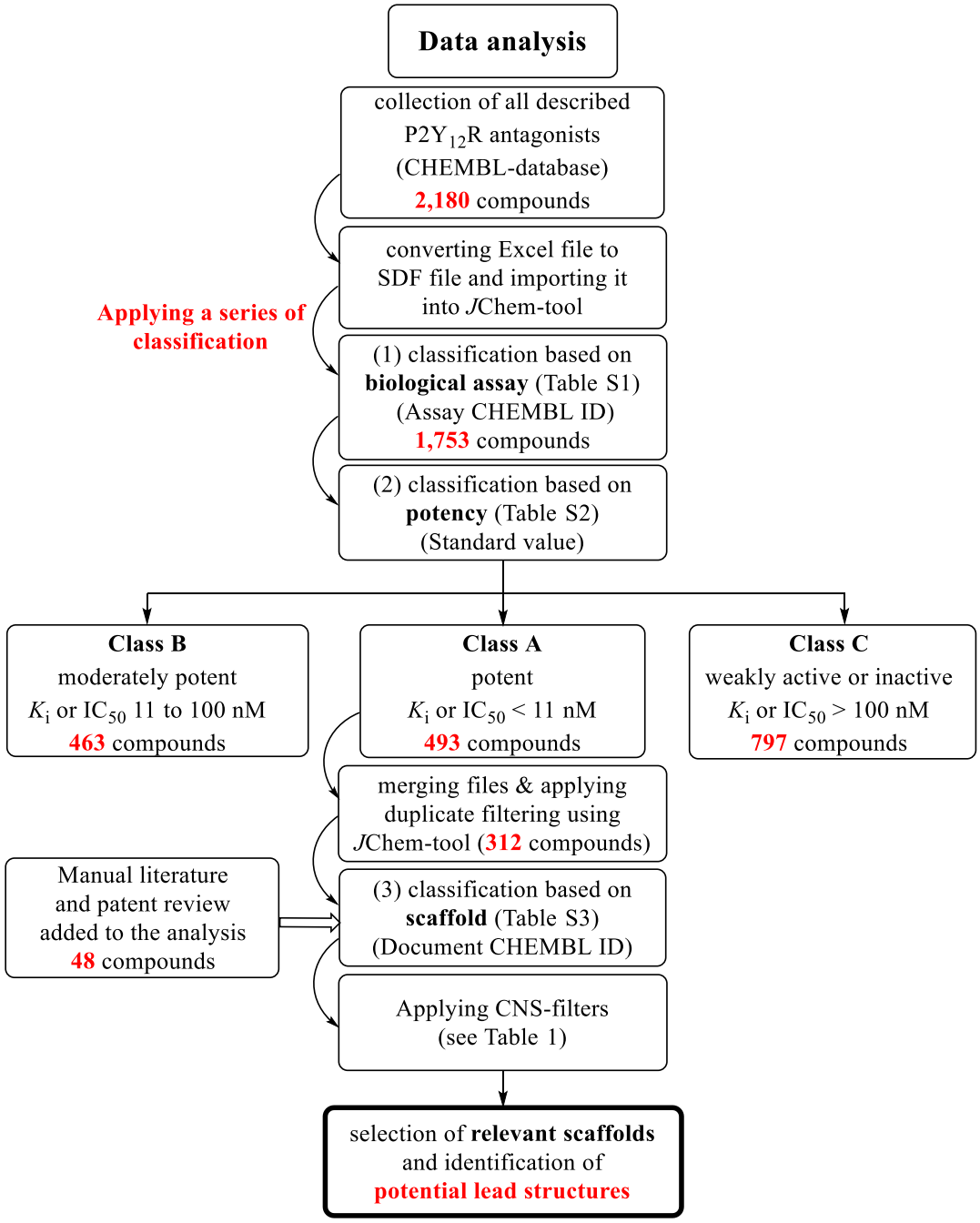


Figure 19. Flow chart for analysis of $P2Y_{12}R$ antagonists.

Classification of collected compounds

Compounds were grouped by biological assay type, potency, and structural similarity (type of scaffold). Using *Instant JChem* compounds were first grouped according to the biological assays used to evaluate their $P2Y_{12}R$ potency and selectivity. A [^{33}P]ADP radioligand binding assay (CHEMBL ID 1064897) has been used to measure the potency of 258 compounds. Radioligand

binding ([^{33}P]2MeS-ADP) and aggregometry assays (CHEMBL IDs 1042521 and 1042522) were applied to 105 compounds. [^{33}P]2MeS-ADP (CHEMBL ID 3367077) was used as a radioligand for affinity measurement of 91 compounds. Additional assays assessing IC_{50} ratios relative to thienopyrimidine or ticagrelor (CHEMBL IDs 1042523 and 1042524) for inhibition of ADP-induced platelet aggregation in human platelet rich plasma, provided insights into 86 compounds. This classification covered 1,753 compounds as summarized in **Table S1**. Compounds were classified by affinity or potency (K_i- or IC_{50}-value) into three classes. **Class A** includes highly potent compounds (K_i- or IC_{50}-values ≤10 nM). **Class B** represents moderately active compounds (K_i- or IC_{50}-values >10 and ≤100 nM). **Class C** comprises weakly active or inactive compounds (>100 nM). This process identified 493 active compounds (Class A) across all assays and scaffolds with a final count of 312 unique potent compounds after removing duplicates using *Instant JChem's* filtering options (**Table S2**). The 312 potent compounds of class A were found in 12 publications using their Document CHEMBL IDs and structural similarity (**Table S3**). Four extra patents and recent publications were analyzed to identify 58 compounds reported as potent thienopyrimidine-based, anthraquinone-based, or pyrazolidinedione-based $P2Y_{12}R$ antagonists to complete the search (**Table S3**).

Application of CNS penetration filters

Molecular descriptors, such as computed partition coefficient (clogP < 4) , calculated distribution coefficient (clogD < 4) at physiological pH of 7.4, topological polar surface area (TPSA < 110 Å²), molecular weight (MW < 500 g/mol), number of hydrogen bond donors (HBDs < 3) and dissociation constant (pK_a) of the most acidic (> 6) or basic (< 10) center were employed to identify molecules that have potential to cross the BBB via passive diffusion.[102,103] It is worth mentioning that hydrogen bond acceptors (HBAs) should not be neglected, since they are affecting the CNS-penetration indirectly by increasing TPSA. We considered clogD rather than clogP to account for protonation or deprotonation at a blood pH of 7.4.

Different biological assays were used to determine the affinity and selectivity of the synthesized $P2Y_{12}R$ antagonists (**Table S1**). We considered results from ADP-induced platelet aggregation assays in human (hPRP) or rat (rPRP) platelet-rich plasma (**IC_{50}-values** (µM)), or radioligand binding assay slots (***K_i*-/IC_{50}-values** (nM)). To assess the CNS permeability of candidate

molecules, affinity and permeability probabilities are categorized as high (green), medium (yellow), or low (red), based on defined thresholds for these parameters, as outlined in Table 6.

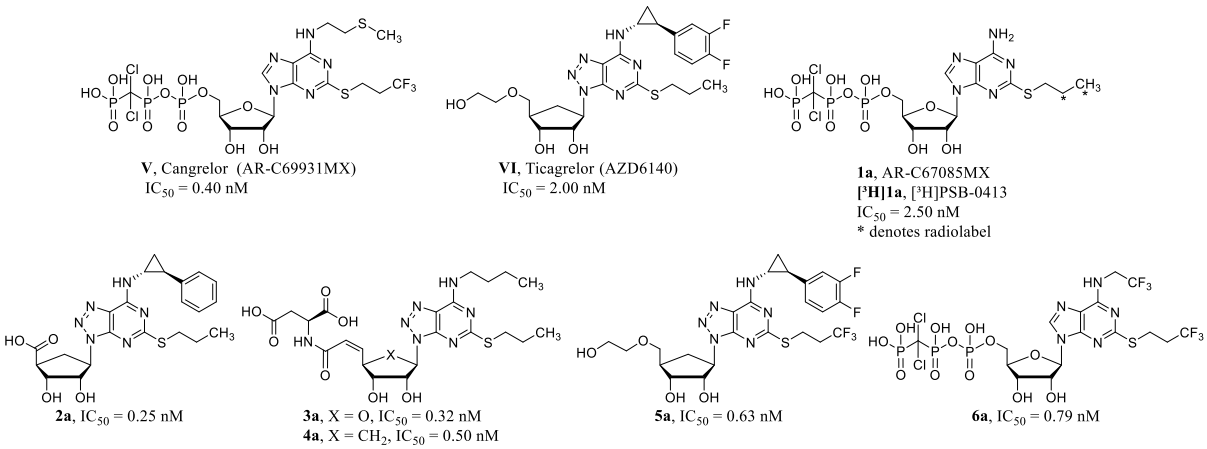
Table 6. Applied CNS penetration filters.[102,103]

Properties[a]	Predicted brain permeability		
	High	Middle	Low
IC_{50} (h/rPRP, μM)	<0.07	0.07– 0.10	>0.10
K_i or IC_{50} (affinity, nM)	<11	11– 50	>50
clogD	1.00– 2.99	3.00– 3.99	>4.00
TPSA (Å²)	<90	90– 110	>110
MW (g/mol)	<450	450– 500	>500
N_{HBDs}	<2	2– 3	>3
pK_a (most acidic center)	>7	6– 7	<6
pK_a (most basic center)	<9	9– 10	>10

[a] **h/rPRP**: Inhibition of ADP-induced platelet aggregation in human/rat platelet-rich-plasma; **TPSA**: topological polar surface area; **MW**: molecular weight; N_{HBDs}: number of hydrogen bond donors.

Identified scaffolds

Scaffold I: Adenine nucleotides and analogs. The first scaffold[42,43] with eighteen compounds included cangrelor (**V**, Figure 18) and ticagrelor (**VI**, Figure 18). This scaffold was not further considered due to the high molecular weight, high TPSA value, and high polarity resulting from the acidic phosphonate or carboxylate groups in most of the compounds. Compounds **V**, **VI**, and **1a**–**6a** (Figure 20) represent the most potent compounds in this class. Based on compound **1a**, our group synthesized the first potent and selective $P2Y_{12}R$ antagonist radioligand [^{3}H]PSB-0413 (**[^{3}H]1a**, Figure 20), through tritiation of a precursor with a triple bond.[83] Despite its utility, [^{3}H]PSB-0413 suffers from significant limitations, in particular, low metabolic stability, and moderate selectivity. Other adenine- or nucleoside-based compounds were reported to block the $P2Y_{12}R$ and act as antithrombotic drugs.[25] **Table S4** provides a brief structure-properties relationship analysis for this scaffold.

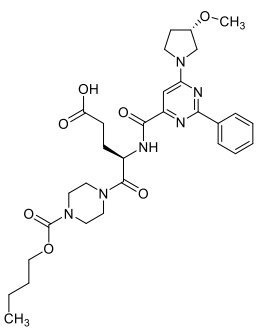


Property[a]	V	VI	1a	2a	3a	4a	5a	6a
IC_{50} (affinity, nM)	0.40	2.00	2.50	0.25	0.32	0.50	0.63	0.79
clogD	-5.3	2.4	-6.5	-0.8	-4.5	-4.3	2.4	-5.1
TPSA (Å²)	256	138	270	146	222	213	138	256
MW (g/mol)	776.4	536.6	648.2	470.6	553.6	551.6	590.6	784.2
N_{HBD}	3	4	4	3	4	4	4	3
pK_a (most acidic center)	0.8	>7.0	0.8	3.4	3.2	-2.2	>7.0	0.8

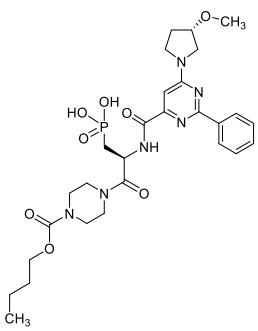
Figure 20. Structures and properties of the most potent nucleotide-based $P2Y_{12}$ receptor antagonists **V**, **VI**, **1a** (AR-C67085MX), [^{3}H]PSB-0413 (**[^{3}H]1a**), and **2a– 6a**; [a] **TPSA**: topological polar surface area; **MW**: molecular weight; N_{HBDs}: number of hydrogen bond donors.

Scaffold II: Piperazinyl-glutamate derivatives. This class represents a scaffold with a total of 281 compounds,[49–56] that was further divided into four distinct sub-scaffolds. The first subclass contains a phenyl-pyrimidine moiety and consists of 80 compounds.[49–52] Compound **1b** (Figure 21) represents the most potent member in this sub-scaffold with an IC_{50}-value of 3.0 nM.[50] A subcutaneously applied $P2Y_{12}R$ antagonist that was clinically evaluated is selatogrel (ACT-246475, **2b**, Figure 21), which belongs to the phenyl-pyrimidine sub-scaffold and contains a phosphonic acid instead of a carboxylic acid residue.[51,52] Its bis[(isopropoxycarbonyl)oxy]methyl ester prodrug (ACT-281959, **3b**, Figure 21) was developed to increase oral bioavailability.[25] Compound **1c** (Figure 21) is the most potent member of this class with a K_i-value of 2.1 nM belonging to the second sub-scaffold which includes 183 phenyl-pyridine-substituted compounds.[53,54] The third subclass are phenyl-pyrazole-based compounds comprising 10 members with compound **1d** (Figure 21) being the most potent candidate (K_i-value of 0.8 nM).[55] The fourth sub-scaffold are quinoline-based compounds containing 8 members that show high potency, the most potent member **1e** (Figure 21) displaying an IC_{50}-value of 3.0 nM.[56] Despite their potent

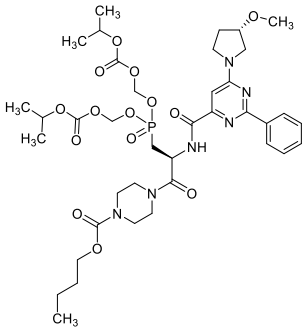
$P2Y_{12}R$ antagonistic activity, good water solubility, chemical stability, and mostly high metabolic stability, these sub-scaffolds were excluded from further analysis due to several limitations, including their high molecular weight (exceeding 550 g/mol for most derivatives), high topological polar surface area (TPSA), high acidity resulting from glutamate's carboxylic acid group or bioisosteric phosphonate, and poor Caco-2 permeability.[49,50,55] These factors rendered them unsuitable for CNS penetration (see **Tables S5–S8** for details).



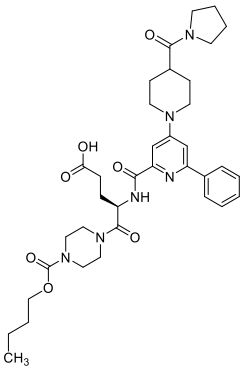
1b (11x), IC_{50} = 3.0 nM
Phenylpyrimidine
CHEMBL3351863



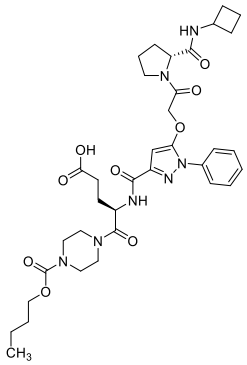
2b, ACT-246475,
Selatogrel
IC_{50} = 1.0 nM



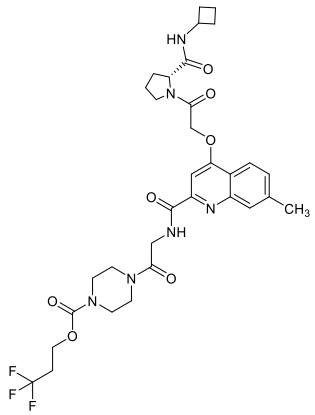
3b, ACT-281959,
IC_{50} = 1.0 nM



1c (4t), K_i = 2.1 nM
Phenylpyridine
CHEMBL1156904



1d (19k), K_i = 0.8 nM, IC_{50} = 19 nM
Phenylpyrazole
CHEMBL2169809



1e (BDBM119428), IC_{50} = 3 nM
Quinoline
CHEMBL3639290

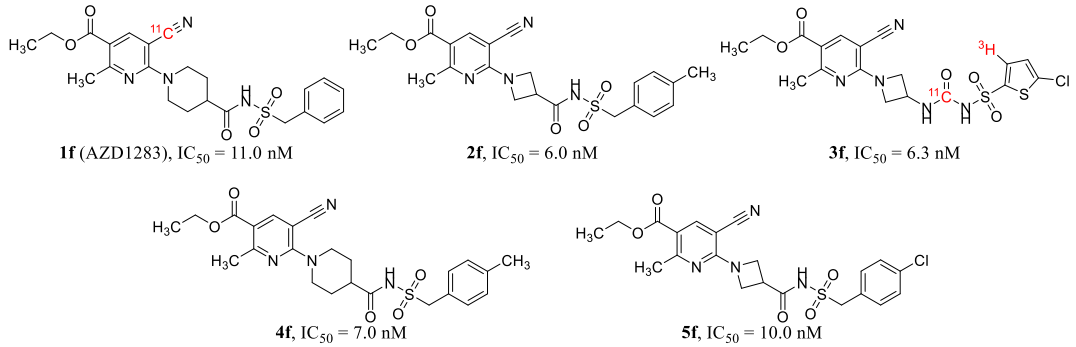
Property[a]	**1b**	**2b**	**3b**	**1c**	**1d**	**1e**
K_i or IC_{50} (affinity, nM)	3.00	1.00	1.00	2.10	0.80	3.00
clogD	-0.4	-0.9	5.2	-0.3	-1.9	1.4
TPSA (Å²)	155	175	224	153	193	151
MW (g/mol)	596.7	618.6	850.9	676.8	709.8	676.7
N_{HBD}	1	1	1	1	2	2
pK_a (most acidic center)	3.9	1.8	>7.0	3.8	3.8	>7.0

Figure 21. Structures and properties of the most potent members of the four piperazinyl-glutamate sub-scaffolds **1b–1e**; [a] **TPSA**: topological polar surface area; **MW**: molecular weight; N_{HBDs}: number of hydrogen bond donors.

Although adenine nucleotide analogs and piperazinyl-glutamate derivatives appear to be unsuitable as lead structures for direct modification to develop $P2Y_{12}R$ antagonists able to penetrate into the CNS via passive diffusion, they should not be entirely disregarded.

Scaffold III: 6-Azetidin-1-yl nicotinate and analogs. Compound **AZD1283** (**1f**, Figure 22)[57] serves as the lead structure for the third scaffold[57,58] possessing an IC_{50}-value of 11 nM. Efforts to optimize AZD1283 have been undertaken by several research groups, including replacement of the ester moiety by a ketone, conducting a ring-closing reaction between the methyl group and the oxygen atom on the pyridine ring, replacement of the central piperidine ring by an azetidine, or removal of the sulfonamide moiety.[58,114–116] These modifications led to the identification of very potent $P2Y_{12}R$ antagonists **2f–5f** (Figure 22). However, they exceed the required topological polar surface area (TPSA = 120 to 141 Å²), and the dissociation constant of the most acidic center, namely the sulfonamide (pKa = 3.92 to 5.82). In addition, urea-based compounds among this scaffold such as **3f** are generally associated with low water solubility, low metabolic stability, and low to moderate Caco-2 permeability.[57] High metabolic stability and Caco-2 permeability have been reported for compound **4f** (piperidine derivative), whereas moderate values were reported for **5f** (azetidine derivative).[58] Compound **2f** (azetidine analog of **4f**) showed high metabolic stability but moderate Caco-2 permeability, whereas low metabolic stability and high Caco-2 permeability were identified for **1f**.[58]

Radiolabeled analogs of **1f** and **3f** have recently been reported as candidates for the development of $P2Y_{12}R$ PET tracers.[85,88–91] However, none of the developed radioligands showed any significant brain uptake. **Table S9** provides more details about this scaffold.



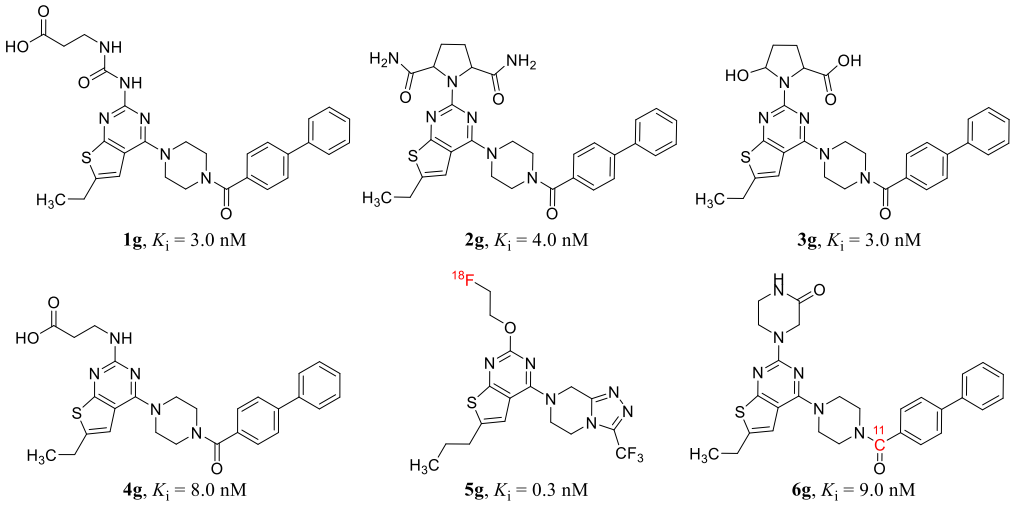
Property[a]	1f	2f	3f	4f	5f
IC_{50} (affinity, nM)	11.00	6.00	6.30	7	10
clogD	1.5	1.4	1.8	2.0	1.5
TPSA (Å²)	129	129	141	129	129
MW (g/mol)	470.5	456.5	484.0	484.6	476.9
N_{HBD}	1	1	2	1	1
pK_a (most acidic center)	4.0	4.0	5.8	4.0	4.0

Figure 22. Structures and properties of the most potent $P2Y_{12}R$ antagonists among the **AZD1283**-derived scaffold **1f**–**5f**. Radioactive atoms of radioligands are colored red; [a] **TPSA**: topological polar surface area; **MW**: molecular weight; N_{HBDs}: number of hydrogen bond donors.

Scaffold IV: Thienopyrimidines. The fourth scaffold are the thienopyrimidine-based $P2Y_{12}R$ antagonists.[59–61] Data analysis identified four compounds with this scaffold, **1g**–**4g**[59] (Figure 23), with high $P2Y_{12}R$ affinity determined in binding studies. However, potency assessments using human platelet-rich plasma (hPRP) aggregation assays revealed low efficacy, with IC_{50}-values in the micromolar range.[59] Two additional derivatives, compounds **5g** (K_i-value = 0.3 nM)[59] and **6g** (K_i-value = 9 nM)[61] (Figure 23), have recently been radiolabeled and proposed as promising $P2Y_{12}R$ PET tracers to monitor active microglial inflammation in the brain. However, both compounds demonstrated low brain exposure. Nonetheless, their partly favorable physicochemical properties provide a basis for further optimization to develop brain-penetrating $P2Y_{12}R$ antagonists.[85]

In the context of CNS filtering, all analyzed compounds still exhibit significant limitations that hinder their potential as brain-penetrant candidates. Compounds **1g**–**4g** and **6g** have high molecular weights (MW > 500 g/mol), exceeding the acceptable threshold for CNS penetration. Additionally, compounds **1g**–**3g** and **6g** display a high topological polar surface area (TPSA > 110 Å²), further

reducing their likelihood of crossing the blood-brain barrier. High acidity due to a carboxylate moiety is a notable drawback for compounds **1g**, **3g**, and **4g**, with pK_a values below 6. Critical values for clogD of > 5 is observed for **6g**. Compound **2g** is characterized by an excessive number of hydrogen bond donors. However, experimental logD values of 2.06 and 2.66 were reported for compounds **5g** and **6g**, respectively,[85] suggesting that the predicted logD values using the *Instant Jchem*-tool are overestimated. **Table S10** provides more details on compounds **1g**–**6g** and related patented compounds of this scaffold.

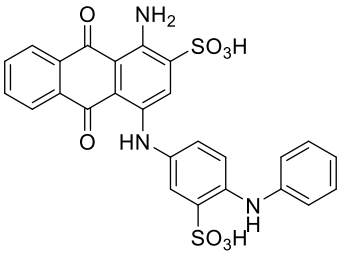


Property[a]	1g	2g	3g	4g	5g	6g
K_i (affinity, nM)	3.00	4.00	3.00	8.00	0.30	9.00
clogD	2.1	4.6	2.9	2.6	4.7	5.2
TPSA (Å²)	128	139	110	99	69	110
MW (g/mol)	558.7	583.7	557.7	515.6	430.4	526.7
N_{HBD}	2	4	1	1	0	1
pK_a (most acidic center)	4.2	>7.0	3.8	3.8	>7.0	>7.0

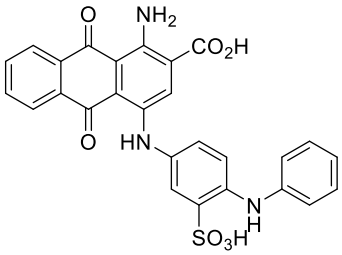
Figure 23. Structures and properties of the most potent $P2Y_{12}R$ antagonists among scaffold IV **1g**–**6g**.[59–61] Radioactive atoms of radioligands are colored red; [a] **TPSA**: topological polar surface area; **MW**: molecular weight; N_{HBDs}: number of hydrogen bond donors.

Scaffold V: Anthraquinones. The most promising compound with this scaffold is PSB-0739[48] (**1h**, Figure 24) which possesses a K_i-value of 4.31 nM according to a recently published binding study,[86] followed by PSB-0702 (**2h**, Figure 24) with K_i-value of 14.6 nM. Both compounds possess a high molecular weight (MW > 500 g/mol), a high topological polar surface area (TPSA > 110 Å²), high acidity due to sulfonate or carboxylate moieties with pK_a values below 6, and an

excessive number of hydrogen bond donors thus exceeding the acceptable thresholds for CNS penetration.



1h, PSB-0739, K_i = 4.31 nM

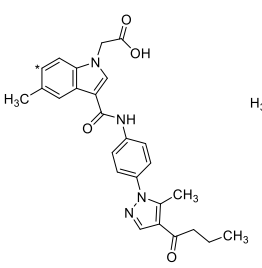


2h, PSB-0702, K_i = 14.6 nM

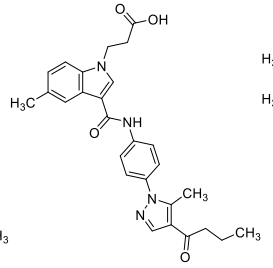
Property[a]	1h	2h
K_i (affinity, nM)	4.31	14.6
clogD	0.5	1.6
TPSA (Å²)	193	176
MW (g/mol)	565.6	529.5
N_{HBD}	4	4
pK_a (most acidic center)	3.2	4.9

Figure 24. Structures and properties of the most potent $P2Y_{12}R$ antagonists with an anthraquinone scaffold V **1h** and **2h**.[48] [a] **TPSA**: topological polar surface area; **MW**: molecular weight; N_{HBDs}: number of hydrogen bond donors.

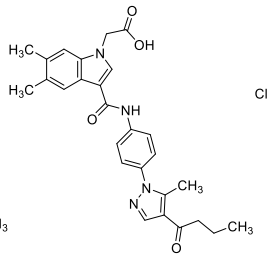
Scaffold VI: Pyrazolyl-phenyl-carbamoyl-indoles. Compounds **1i–5i** (Figure 25) represent the most promising candidates of this scaffold.[62–64] High affinity and high metabolic stability are reported, and the predicted physicochemical properties are promising, except for compounds **4i** and **5i**, which have high molecular weights, and compound **5i** additionally exhibiting a high topological polar surface area (TPSA = 112.78 Å²). Compounds **1i–3i** share structural similarities. They exhibit relatively high acidity, with pK_a values below 6. Among these, compound **1i** appears to be most promising due to its high potency, metabolic stability, and favorable physicochemical properties. However, it showed no permeability in a Caco-2 cell assay.[62] **Table S11** provides details on compounds **1i**–**5i**. We recently prepared **1i** in its tritium-labeled form, **[^{3}H]1i** ([^{3}H]PSB-22219, Figure 25), which is useful for in vitro radioligand binding studies.[86]



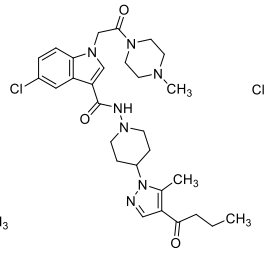
1i, IC_{50} = 0.9 nM
[^{3}**H]1i**, ([^{3}H]PSB-22219)
* denotes radiolabel



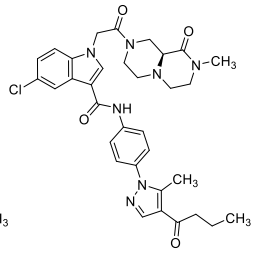
2i, IC_{50} = 7.0 nM



3i, IC_{50} = 5.1 nM



4i, IC_{50} = 7.0 nM

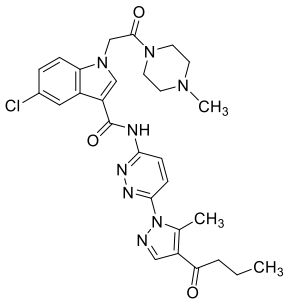


5i, IC_{50} = 7.0 nM

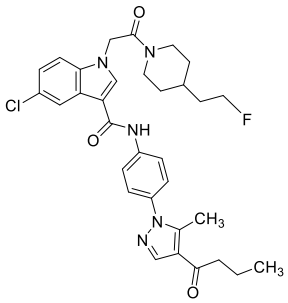
Property[a]	**1i**	**2i**	**3i**	**4i**	**5i**
IC_{50} (affinity, nM)	0.90	7.00	5.10	7.00	7.00
clogD	1.2	1.6	1.7	1.6	3.1
TPSA (Å²)	106	106	106	96	113
MW (g/mol)	458.5	472.6	472.6	568.1	630.2
N_{HBD}	1	1	1	1	1
pK_a (most acidic center)	3.9	4.2	4.0	>7.0	>7.0

Figure 25. Structures and properties of the most potent $P2Y_{12}R$ antagonists among scaffold VI, including the radioligand **[^{3}H]1i** ([^{3}H]PSB-22219);[86,62,63] [a] **TPSA**: topological polar surface area; **MW**: molecular weight; N_{HBDs}: number of hydrogen bond donors.

SAR216471 (**6i**, Figure 26) is a promising preclinical candidate of this scaffold which was reported as a potent and highly selective $P2Y_{12}R$ antagonist.[62,117] A [^{11}C]-labeled version of SAR216471 ([^{11}C]**6i**, Figure 26) has recently been reported as a PET tracer along with another, ^{18}F-based radioligand ([^{18}F]**7i**, Figure 26).[64] Despite the reported affinity, high selectivity, and good to high metabolic stability, [^{11}C]**6i** was not able to cross the BBB, and limitations of brain penetration were also observed for [^{18}F]**7i**, indicating its behavior as a substrate of efflux transporters.[64] Both compounds show a high molecular weight.



6i, SAR216471, IC_{50} = 17.0 nM
[^{11}**C]6i**, ([^{11}C]SAR216471)

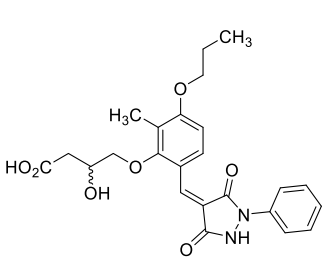


7i, IC_{50} = 17.1 nM
[^{18}**F]7i**

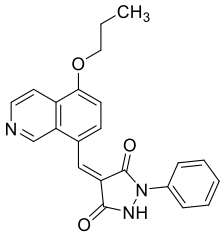
Property[a]	**6i**	**7i**
K_i or IC_{50} (affinity, nM)	17.0	17.1
clogD	2.8	5.1
TPSA (Å²)	118	89
MW (g/mol)	563.1	592.1
N_{HBD}	1	1
pK_a (most acidic center)	>7.0	>7.0

Figure 26. Structures and properties of SAR216471 (**6i**), its [^{11}C]**6i**-radioligand analog, **7i**, and its [^{18}F]**7i**-radioligand analog;[62–64] [a] **TPSA**: topological polar surface area; **MW**: molecular weight; N_{HBDs}: number of hydrogen bond donors.

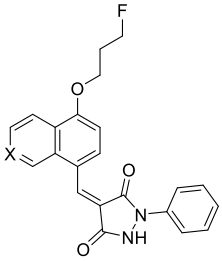
Scaffold VII: Pyrazolidinediones. Compounds **1j** (*S*) and (*R*) (Figure 27) represent the most promising candidates of this scaffold regarding the potency.[65,66] Compound **2j** was recently further modified to produce the compounds **3j**–**6j** (Figure 27), radiolabeling **4j** with ^{18}F and investigating it in PET-imaging. Low brain uptake has been observed and referred to the deprotonation of this scaffold in vivo, in addition to the rapid metabolism.[66] **Table S12** provides details on the promising compounds among this scaffold.



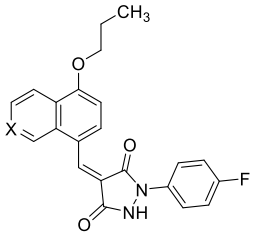
1j, IC_{50} = 0.8 nM (S), 1.0 nM (*R*)



2j, IC_{50} = 10.0 nM



3j, X = N, K_i = 1.2 nM
4j, X = CH, K_i = 5.3 nM
[^{18}F]4j



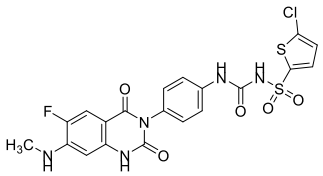
5j, X = N, K_i = 5.7 nM
6j, X = CH, K_i = 1.9 nM

Property[a]	**1j**	**2j**	**3j**	**4j**	**5j**	**6j**
K_i or IC_{50} (affinity, nM)	0.8/1.0	10.0	1.2	5.3	5.7	1.9
clogD	-1.59	2.0	1.4	2.6	2.1	2.6
TPSA (Å²)	125	72	72	59	72	59
MW (g/mol)	454.5	373.4	391.4	390.4	391.4	390.4
N_{HBD}	1	0	0	0	0	0
pK_a (most acidic center)	2.8	2.6	2.6	3.1	1.9	3.1

Figure 27. Structures and properties of pyrazolidinedione derivatives **1j**–**6j**, including the [^{18}F]**4j**-radioligand;[65,66] [a] **TPSA**: topological polar surface area; **MW**: molecular weight; N_{HBDs}: number of hydrogen bond donors.

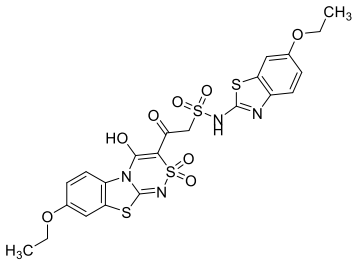
Other heterocyclic compound classes[25] such as quinazoline-2,4-diones and benzothiazolo[2,3-*c*]thiadiazines were reported to block $P2Y_{12}$Rs. Compound **1k** (elinogrel) and **1l** (CT50547) (Figure 28), are among the most promising candidates of these scaffolds regarding potency.

Quinazoline-2,4-dione scaffold



1k, Elinogrel
K_i = 23.0 nM

Benzothiazolo[2,3-*c*]thiadiazine scaffold



1l, (CT50547)
IC_{50} = 170.0 nM

Property[a]	1k	1l
K_i or IC_{50} (affinity, nM)	23.0	170.0
clogD	2.5	0.1
TPSA (Å²)	137	165
MW (g/mol)	523.9	596.7
N_{HBD}	3	0
pK_a (most acidic center)	5.2	4.1

Figure 28. Structures and properties of the most potent $P2Y_{12}R$ antagonists among various scaffolds **1k** and **1l**;[25] [a] **TPSA**: topological polar surface area; **MW**: molecular weight; N_{HBDs}: number of hydrogen bond donors.

Among all aforementioned scaffolds, the pyrazolyl-phenyl-carbamoyl-indole was selected as the most promising scaffold, since it matches almost all CNS-filtering thresholds (see Figure 25 and 9). Therefore, a more comprehensive data analysis was conducted using *Scifinder* to explore all reported compounds with this scaffold.

Extended data analysis of the pyrazolyl-phenyl-carbamoyl-indole scaffold

A second round of data analysis was conducted on the pyrazolyl-phenyl-carbamoyl-indole scaffold to identify non-acidic, potentially CNS-permeable $P2Y_{12}R$ antagonists. *Scifinder* was utilized to identify $P2Y_{12}R$ antagonists having the same scaffold (Figure 29). Two key references containing over 900 structurally related compounds were identified and filtered according to molecular weight. The molecular weight of the smallest derivative *N*-(4-(4-butyryl-5-methyl-1*H*-pyrazol-1-yl)phenyl)-1*H*-indole-3-carboxamide (**8i**, Figure 29) (MW = 386 g/mol), was selected as a threshold to exclude irrelevant substances and building blocks with no biological data. The remaining 555 compounds were downloaded as SDF files and imported into *Instant JChem* for further analysis. Stepwise systematic compound classification was applied to refine the dataset starting with chemical structure filtering. Compounds with structural similarity to compound **8i** and its pyridazinyl analog **9i** (Figure 29) were retained, reducing the dataset to 484 compounds. Finally, compounds lacking biological data or including undesirable functional groups and physicochemical properties such as NH-free indoles (15 compounds), acetyl-protected *N*-indoles (10 compounds), Boc-protected nitrogens (41 compounds), and esters (64 compounds) in pre-final structures were excluded. This reduced the dataset to 313 compounds. Three biological parameters were considered for analysis: $P2Y_{12}$ binding assay using [^{33}P]2MeS-ADP on $P2Y_{12}R$-transfected

CHO cells, referred to as Bnd-assay in the original publication (Bnd/IC_{50} in nM), inhibition of ADP-induced platelet aggregation in human platelet-rich plasma (hPRP, µM), and inhibition of ADP-induced platelet aggregation in rat platelet-rich plasma (rPRP, µM).[62,63] Since Bnd-values were incomplete and hPRP values were not concretely reported (0.1–2.0 µM), rPRP inhibition was selected as the primary potency parameter, as it was available for most compounds. The 313 compounds were sorted in ascending order of molecular weight to facilitate duplicate filtering, further reducing the dataset to 258 compounds. The SAR analysis of this scaffold was then conducted on the remaining 258 compounds to identify the most promising sub-scaffolds. This analysis yielded 236 compounds grouped into five major sub-scaffolds (**A**–**E**, Figure 29) that were investigated using the CNS-penetration filters to identify the relevant substituents and assist in the subsequent design of suitable $P2Y_{12}R$ antagonists with brain penetration. **Figure S2** provides a detailed description of the data analysis.

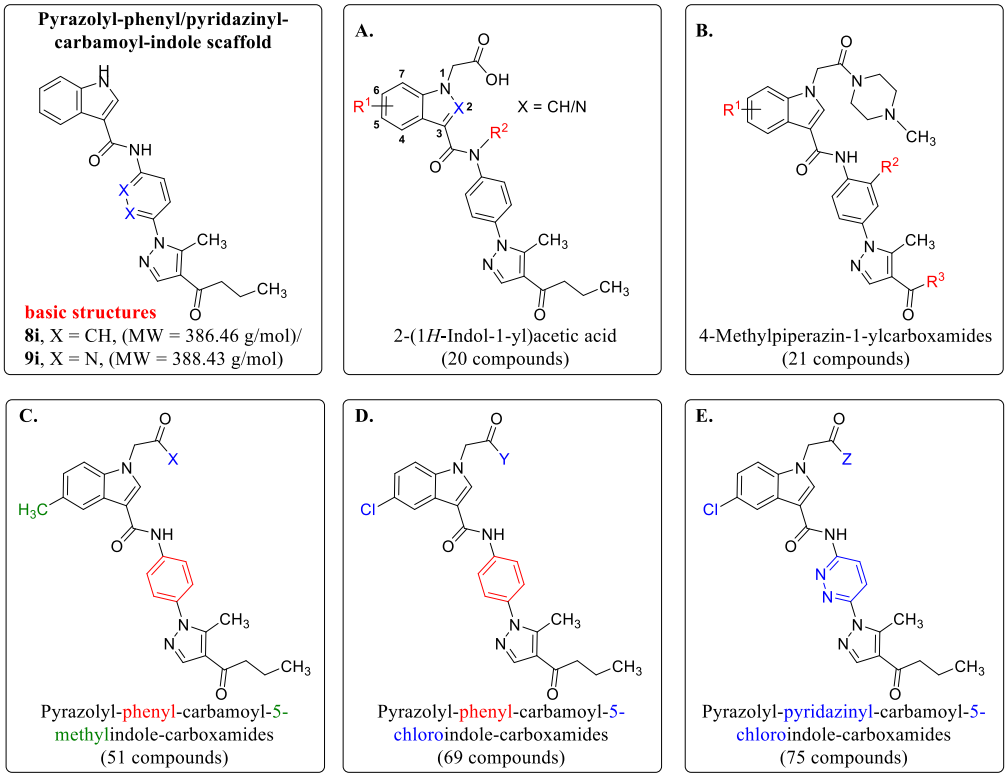


Figure 29. Structures of pyrazolyl-phenyl-carbamoyl-indoles: phenyl-based structure **8i**, its pyridazinyl analog **9i**, the carboxylic acid sub-scaffold **A**, and the four carboxamide sub-classes **B**–**E**.[62–64] For $R^{1–3}$, **X**, **Y**, and **Z** see Figures 13–16 and 17. Tables S13–S17 provide SAR analysis of all sub-classes.

The first sub-scaffold is the pyrazolyl-phenyl-carbamoyl-indole **acetic acid** with 20 compounds (**A**, Figure 30). The primary limitation of this scaffold is the presence of the carboxylic acid group, which results in high acidity (pKa < 6) which significantly contributes to an elevated TPSA value (ca. 106 Å²). The C5- and C6-positions of the indole ring were identified as the most favorable sites for substitution, particularly with small groups such as methyl. In contrast, introducing a methyl group at the C5-position in combination with methylation of the amide nitrogen or substitutions at the C2- or C4-position resulted in a significant loss of potency. Replacement of the 5-methylindole by a 5-methylindazole ring system led to a notable decrease in potency and increased the overall polarity of the molecule due to the higher number of hydrogen bond acceptors. The introduction of bulky substituents such as phenyl, bromine (Br), or trifluoromethyl (CF_3) resulted in a substantial increase in molecular weight (MW > 500 g/mol), potentially impeding CNS penetration. **Table S13** provides the biological data for the SAR analysis of this sub-scaffold shown in Figure 30.

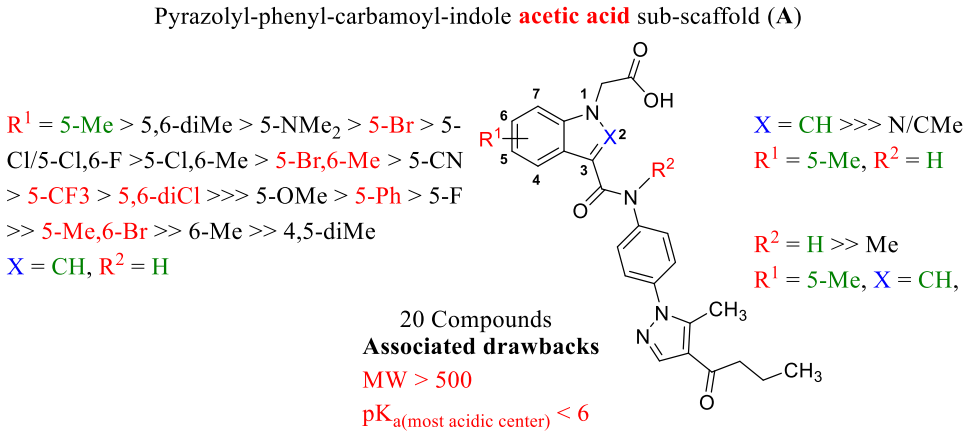


Figure 30. SAR analysis of pyrazolyl-phenyl-carbamoyl-indole **acetic acid** sub-scaffold (**A**). Substituents of the most potent compounds are labeled in green, whereas substituents of compounds that exceed the molecular weight threshold (MW > 500 g/mol) are labeled in red.[62,63]

The pyrazolyl-phenyl-carbamoyl-indole-**4-methylpiperazin-1-yl carboxamide** sub-scaffold with 21 compounds (**B**, Figure 31) is no longer acidic and therefore less polar. However, all compounds within this series exhibit high molecular weights. In terms of potency, substitution at the C5-position of the indole ring consistently resulted in the highest activity. No significant difference in potency was observed between 5-methyl and 5-chloro substitution; the lower mass of a methyl group in comparison to a chloro-substituent may render 5-methyl substitution more favorable over 5-chloro substitution. However, 5-chloro substituted indoles of this sub-class were found to

possess better metabolic stability than their 5-methyl substituted analogs.[62] Substitution on the phenyl ring led to a noticeable decrease in potency while further increasing the molecular weight. The propyl group at the ketone moiety was identified as the best substituent in this series, balancing potency and physicochemical properties. **Table S14** provides the biological data for the SAR analysis of this sub-scaffold.

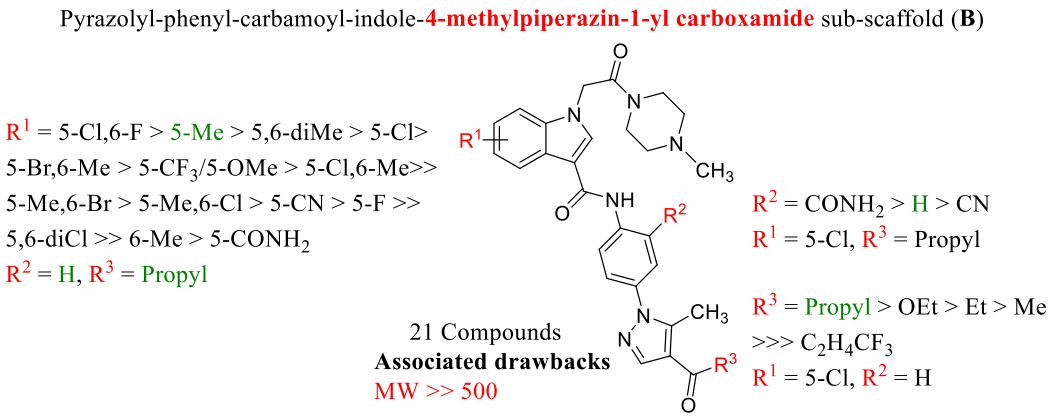


Figure 31. SAR analysis of pyrazolyl-phenyl-carbamoyl-indole-**4-methylpiperazin-1-yl carboxamide** sub-scaffold **(B)**.[62–64]

Pyrazolyl-**phenyl**-carbamoyl-**5-methyl**indole-carboxamides with 51 compounds (**C**, Figure 32) represent the third sub-scaffold. All compounds within this scaffold fail to meet the required potency threshold (K_i/IC_{50} < 10 nM or $IC_{50(rPRP)}$ < 0.10 µM) and significantly exceed the acceptable molecular weight limit (MW > 500 g/mol). As a result, they are unsuitable for further modification to achieve blood-brain barrier (BBB) permeability. However, certain compounds may still serve as reference points for comparison with structurally similar compounds in the following scaffold, particularly to help identify the optimal substituent at the indole-C5-position (CH_3 vs. Cl). **Table S15** provides the biological data for the SAR analysis of this sub-scaffold.

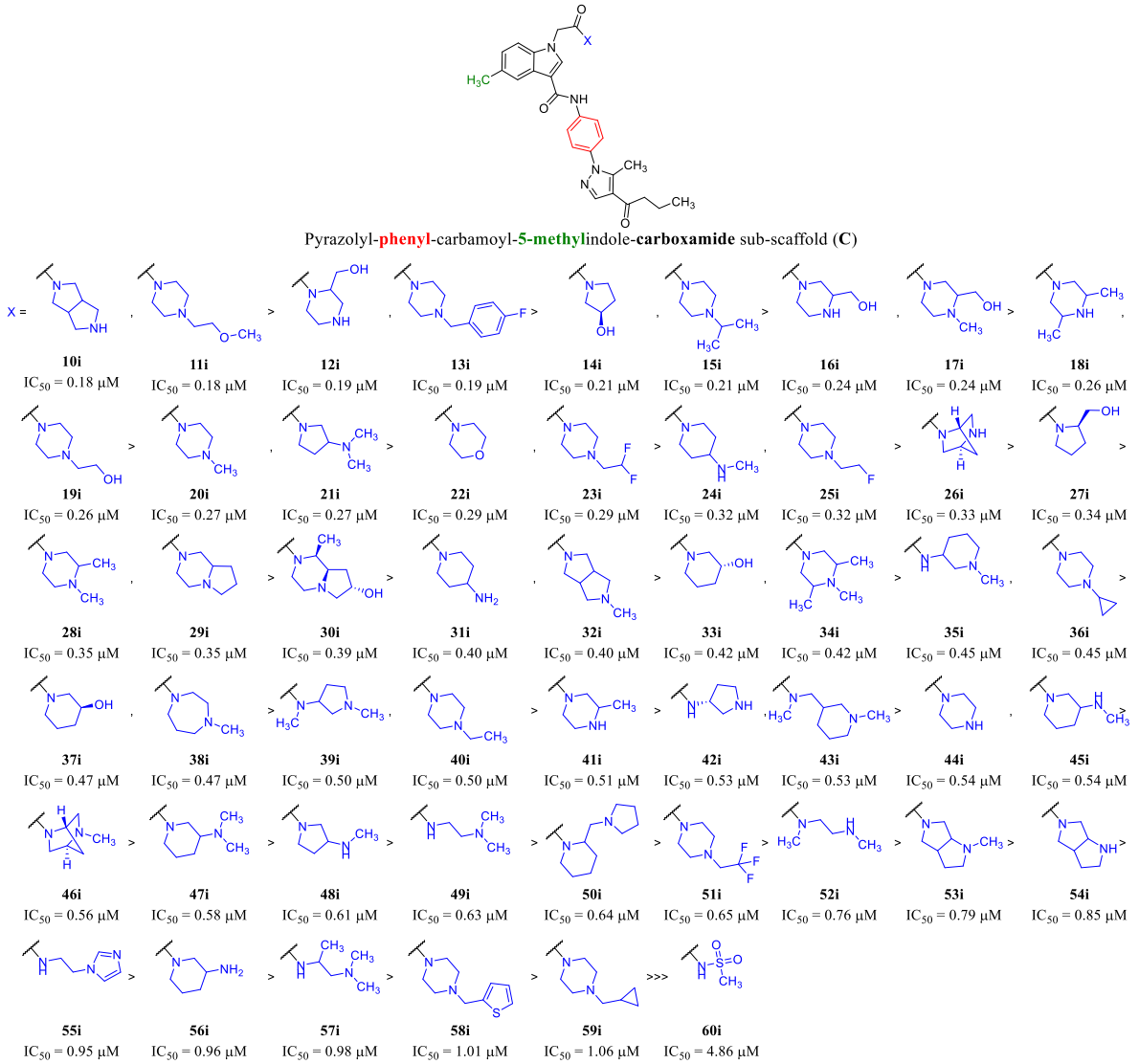


Figure 32. Structures and SAR analysis based on the IC_{50}-values derived from the inhibition of ADP-induced platelet aggregation in rat platelet-rich-plasma (rPRP) of pyrazolyl-**phenyl**-carbamoyl-**5-methyl**indole-carboxamide sub-scaffold **(C).**[62,63]

The pyrazolyl-**phenyl**-carbamoyl-**5-chloro**indole-carboxamide sub-scaffold with 69 compounds (**D**, Figure 33) demonstrates improved potency compared to the previous scaffolds, several examples approaching or meeting the required threshold of potency (K_i/IC_{50} < 10 nM or $IC_{50(rPRP)}$ < 0.10 µM). However, they exhibit significantly higher molecular weights than compounds of the aforementioned scaffold (**C**), primarily due to the contribution of the high mass of chlorine. **Table S16** provides the biological data for the SAR analysis of this sub-scaffold.

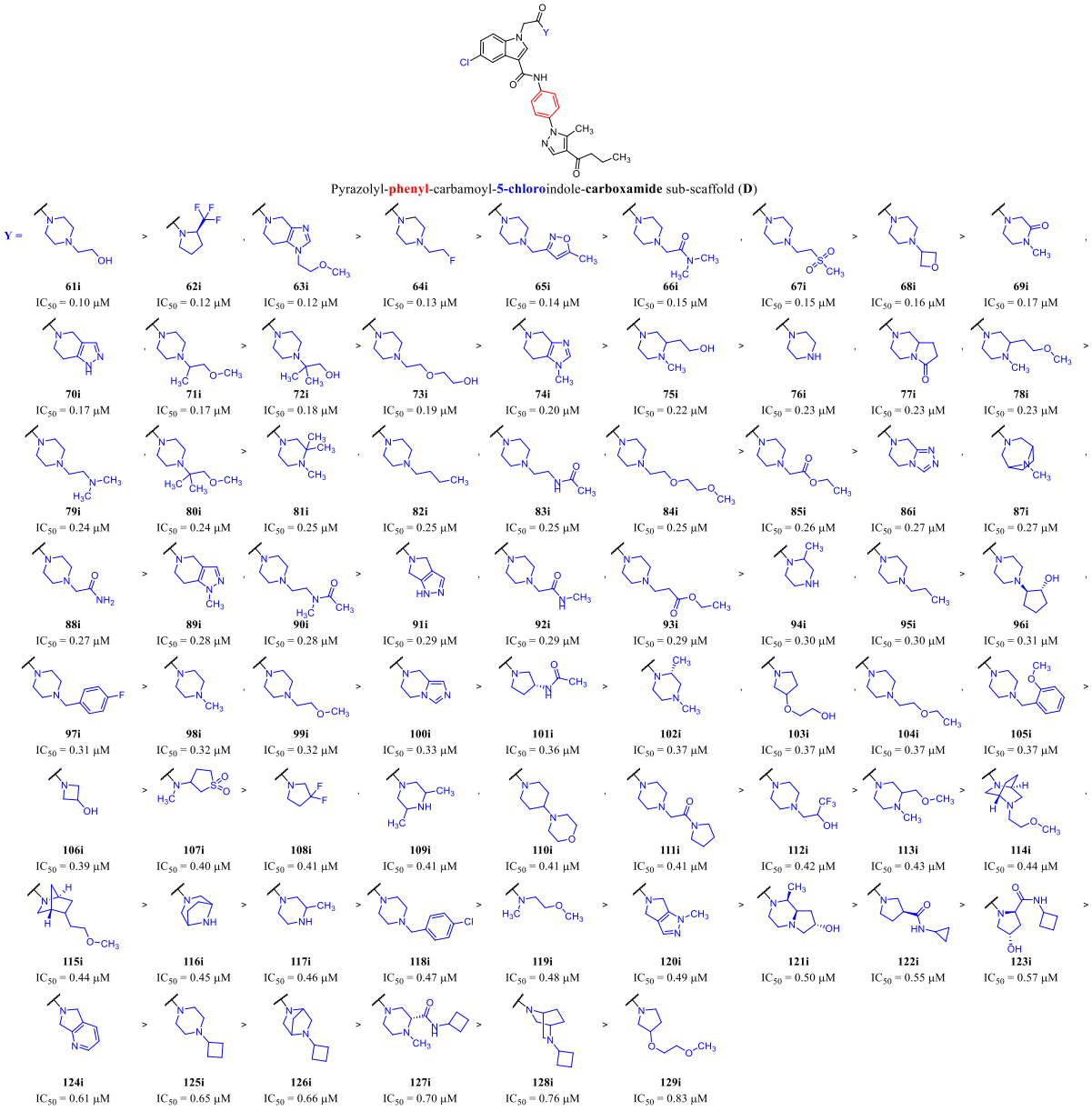
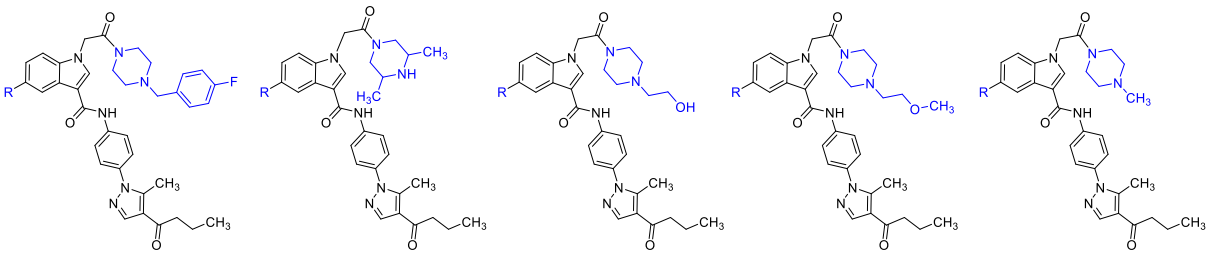


Figure 33. Structures and SAR analysis based on the IC_{50}-values derived from the inhibition of ADP-induced platelet aggregation in rat platelet-rich-plasma (rPRP) of pyrazolyl-**phenyl**-carbamoyl-**5-chloro**indole-carboxamide sub-scaffold **(D)**.[62,63]

A detailed comparison of structurally similar compounds from both scaffolds **C** and **D** revealed no clear preference for the 5-chloro or 5-methyl substituent in terms of potency. For instance, compounds **13i** and **18i** with 5-CH_3 substitution showed superior potency (IC_{50}-values of rPRP) compared to their 5-Cl analogs **97i** and **109i** (Figure 34), respectively. Conversely, compound **61i** (5-Cl) outperformed its 5-CH_3 analog **19i** (Figure 34). A comparison between **11i** (5-CH_3) and **99i**

(5-Cl) or between **20i** (5-CH_3) and **98i** (5-Cl) (Figure 34) produced inconsistent results depending on the biological assay (K_i/IC_{50}-values of binding-assay vs. IC_{50}-values of rPRP assay).

In terms of metabolic stability and Caco-2 permeability, the reported data showed no differences regarding metabolic stability between the compounds **20i** and **98i** determined in human liver microsomes during 20 min of incubation in the presence of NADPH, 61% of **20i** and 64% of **98i** remaining intact.[62] However, compound **98i** appeared to be metabolically more stable than its 5-methylindole analog **20i** in rat (% of unchanged compound: **20i** (59%), **98i** (86%).[62] In contrast, compound **20i** showed a higher degree of Caco-2 permeation in comparison to its 5-chloroindole analog **98i**.[62] The same results were observed for the 5-methylindole derivatives **11i** and **19i** compared to their 5-chloroindole analogs **99i** and **61i**, respectively. In conclusion, both substituents should be considered in the development of brain-permeable $P2Y_{12}R$ antagonists, despite the potentially lower metabolic stability of 5-methylindole derivatives and the potentially poorer Caco-2 permeation of 5-chloroindole derivatives that possess a higher molecular weight.[62]



13i, R = CH_3 **97i**, R = Cl | **18i**, R =CH_3 **109i**, R = Cl | **19i**, R = CH_3 **61i**, R = Cl | **11i**, R = CH_3 **99i**, R = Cl | **20i**, R = CH_3 **98i**, R = Cl

Property[a]	**13i**	**97i**	**18i**	**109i**	**19i**	**61i**	**11i**	**99i**	**20i**	**98i**
R	CH_3	Cl	CH_3	Cl	CH_3	Cl	CH_3	Cl	CH_3	Cl
IC_{50} (rPRP, nM)	0.19	0.31	0.26	0.41	0.26	0.10	0.18	0.32	0.27	0.32
IC_{50} (affinity, nM)	12	n.d	102	n.d	41	11	20	15	31	27
MW (g/mol)	634.8	655.2	554.7	575.1	570.7	591.1	584.7	605.1	540.7	561.1

Figure 34. Comparison of 5-methyl- and 5-chloro-indole substituted derivatives. [a] **rPRP**: inhibition of ADP-induced platelet aggregation in rat platelet-rich-plasma; **MW**: molecular weight.[62,63]

The pyrazolyl-**pyridazinyl**-carbamoyl-**5-chloro**indole-carboxamide sub-scaffold contains 75 compounds (**E**, Figure 35) and represents the final sub-scaffold. 40 Compounds with this sub-scaffold exhibit the required potency (K_i/IC_{50} < 10 nM or $IC_{50(rPRP)}$ < 0.10 µM), highlighting the high tolerability of the pyridazinyl ring. **Table S17** provides the biological data for the SAR analysis of this sub-scaffold.

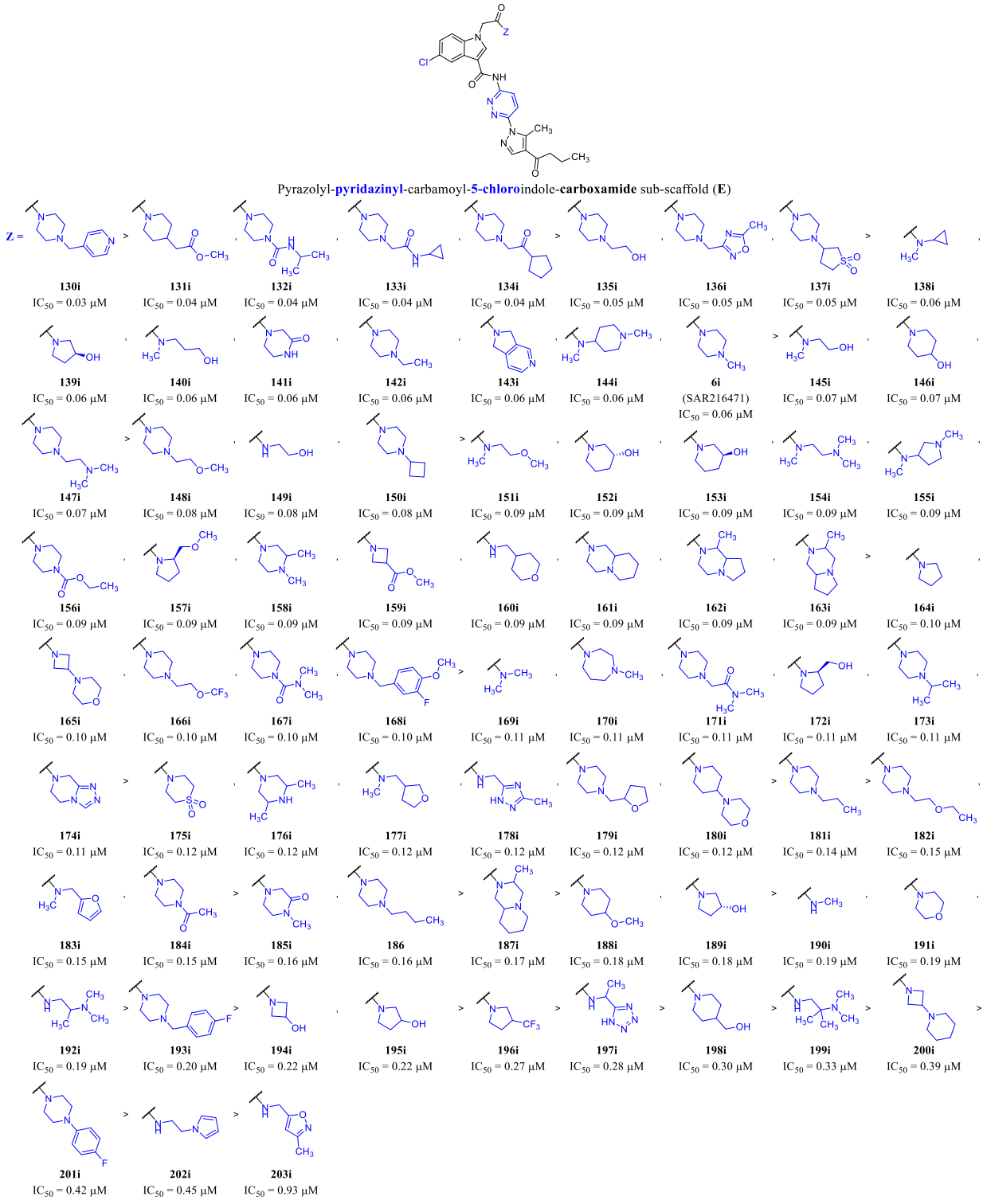
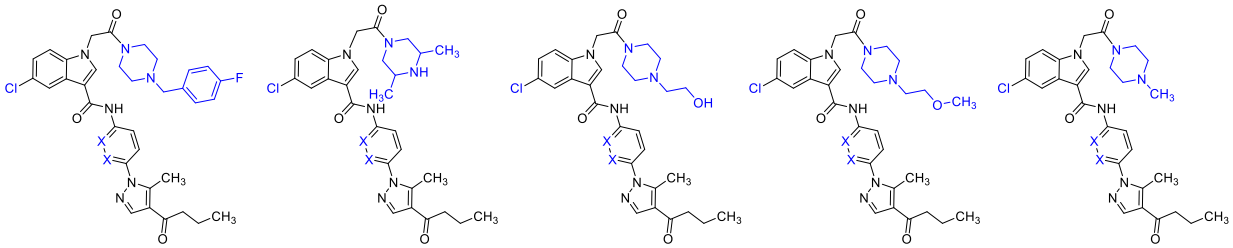


Figure 35. Structures and SAR analysis based on the IC_{50}-values derived from the inhibition of ADP-induced platelet aggregation in rat platelet-rich-plasma (rPRP) of pyrazolyl-**pyridazinyl**-carbamoyl-**5-chloro**indole-carboxamide sub-scaffold **(E)**.[62,63]

Notable examples include compounds **6i**, **135i**, **148i**, **176i**, and **193i** (Figure 35), which demonstrate superior potency compared to their analogs with the previous scaffold D (**98i**, **61i**, **99i**, **109i**, and **97i**, Figure 33). Figure 36 displays a comparison between these analogs to highlight the differences between the phenyl- and pyridazinyl-containing compounds. Despite the improved potency of the pyridazinyl derivatives of scaffold E, they are less favorable than their phenyl counterparts in scaffold D with respect to topological polar surface area (TPSA). The presence of additional hydrogen bond acceptors in the pyridazinyl ring increases the TPSA by approximately 26 units and decreases the distribution coefficient (clogD) by approximately 1.01 units compared to the corresponding phenyl-containing compounds. Consequently, while the pyridazinyl ring improves potency, the phenyl ring remains more favorable overall due to its lower TPSA and better physicochemical profile. Almost all compounds with this scaffold exceed the acceptable molecular weight threshold.



97i, X = CH
193i, X = N

109i, X = CH
176i, X = N

61i, X = CH
135i, X = N

99i, X = CH
148i, X = N

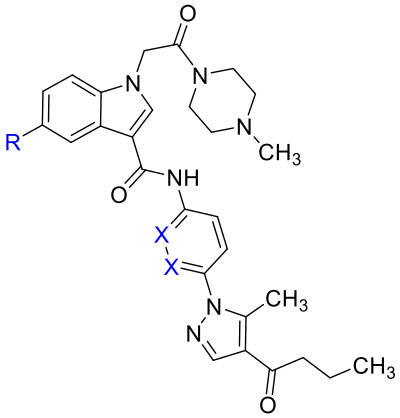
98i, X = CH
6i, (SAR216471), X = N

Property[a]	97i	193i	109i	176i	61i	135i	99i	148i	98i	6i (SAR216471)
X	CH	N	CH	N	CH	N	CH	N	CH	N
IC_{50} (rPRP, nM)	0.31	0.20	0.41	0.12	0.10	0.05	0.32	0.08	0.32	0.06
IC_{50} (affinity, nM)	n.d	n.d	n.d	n.d	11	n.d	15	n.d	27	n.d
TPSA (Å²)	92	118	101	127	113	138	102	127	92	118
clogD	5.8	4.8	3.7	2.7	3.2	2.2	3.8	2.8	3.8	2.8
MW (g/mol)	655.2	657.2	575.1	577.1	591.1	593.1	605.1	607.1	561.1	563.1

Figure 36. Comparison between phenyl- and pyridazinyl-derivatives. [a] **rPRP**: inhibition of ADP-induced platelet aggregation in rat platelet-rich-plasma; **TPSA**: topological polar surface area; **MW**: molecular weight.[62,63]

To validate the reported potency values, K_i-values for the compounds **6i** (SAR216471), **20i**, **98i**, and the recently synthesized pyridazinyl-carbamoyl-5-methylindole-4-methylpiperazin-1-yl carboxamide **204i**[64] (Figure 37) were determined using a radioligand binding assay[86] to allow for the direct comparison between phenyl and pyridazinyl derivatives, in addition to the 5-

methylindole and 5-chloroindole substitution. No significant difference in the potency between pyridazinyl-containing compounds versus phenyl-containing compounds was observed (Figure 37) except for **6i** (SAR216471), but the value might be incorrect due to its poor solubility.[64] No significant differences regarding metabolic stability in rat and human liver microsomes after 60 min of incubation (unchanged compounds: 88-98%) were observed. These values confirm the conclusion that the pyrazolyl-**phenyl**-carbamoyl-**5-methyl**indole represents the most promising sub-scaffold and should be further explored for the design and synthesis of new potent, selective, metabolically stable, and BBB-penetrant $P2Y_{12}R$ antagonists.



Property[a]	20i	204i	98i	6i (SAR216471)
R	CH_3	CH_3	Cl	Cl
X	CH	N	CH	N
IC_{50} (rPRP, nM)	0.27	n.d	0.32	0.06
K_i (affinity, nM)	10.4	11.5	12.1	43.8
clogD	3.7	2.7	3.8	2.8
TPSA (Å²)	92	118	92	118
MW (g/mol)	540.7	542.6	561.1	563.1

Figure 37. Comparison between phenyl ring-containing compounds **20i**, **98i** and pyridazinyl ring-containing compounds **6i** (SAR216471) and **204i**. [a] **rPRP**: inhibition of ADP-induced platelet aggregation in rat platelet-rich-plasma; **TPSA**: topological polar surface area; **MW**: molecular weight.[62–64]

In general, the high molecular weight (MW > 500 g/mol) emerged as the most challenging parameter across all sub-scaffolds, presenting a key hurdle for CNS permeability. This systematic data analysis highlights the critical steps taken to identify and refine the pyrazolyl-phenyl-carbamoyl-indole scaffold for the development of novel $P2Y_{12}R$ antagonists. The SAR insights and application of CNS penetration filters lay the foundation for further optimization toward brain-permeable $P2Y_{12}R$ antagonists.

3.3.5 Conclusions and outlook

The systematic analysis and classification of $P2Y_{12}R$ antagonists has successfully identified promising scaffolds for CNS-targeted applications. These scaffolds can serve as lead structures for direct modification or as references for comparative studies, modeling, and fragmentation-based

optimization approaches. Among the identified scaffolds, the **pyrazolyl-phenyl-carbamoyl-indole scaffold**, particularly compound **1i** (2-(3-((4-(4-butyryl-5-methyl-1*H*-pyrazol-1-yl)phenyl)carbamoyl)-5-methyl-1*H*-indol-1-yl)acetic acid), emerged as a promising candidate for the development of blood-brain barrier (BBB)-penetrable $P2Y_{12}R$ antagonists. Compound **1i** demonstrates high affinity (K_i < 10 nM), high selectivity, metabolic stability, and met the majority of the CNS penetration criteria. Future research will focus on optimization of compound **1i** through extended and focused SAR studies.

Preliminary SAR analysis identified essential substituents and moieties within this scaffold and allowed for the direct comparison between final compounds. No significant affinity differences were observed comparing 5-chloroindole derivatives to their 5-methylindole analogs, or the pyridazinyl-containing compounds to their phenyl-containing analogs. However, 5-chloro compounds appears to be metabolically more stable than their 5-methyl analogs and may therefore be preferable despite their higher molecular weight. Otherwise, the 5-methyl derivatives showed high degrees of permeability in Caco-2 cells. The two hydrogen bond acceptors (nitrogen atoms) of the pyridazinyl ring contribute to increasing the TPSA by ca. 26 units compared to a phenyl ring, which renders the pyridazinyl-containing compounds less favorable as brain-permeable agents in comparison to their phenyl-containing analogs. Thus, our future work will focus on the development of novel pyrazolyl-**phenyl**-carbamoyl-**5-methyl/chloroindole**-derived $P2Y_{12}R$ antagonists with high potency, selectivity, metabolic stability, and BBB-permeation potential.

3.3.6 Supporting information

Table S1. Classification of the collected $P2Y_{12}R$ ligands based on the applied biological assay.

No.	Assay CHEMBL ID	Assay description	No. of compounds
1	CHEMBL1064897	Displacement of [^{33}P]ADP from human recombinant $P2Y_{12}$ receptor expressed in CHO cells	258
2	CHEMBL1042521	Binding affinity at human recombinant $P2Y_{12}$ receptor expressed in CHO cells by radioligand binding assay ([^{33}P]2MeS-ADP)	105
3	CHEMBL1042522	Antagonist activity at $P2Y_{12}$ receptor in human platelet rich plasma assessed as inhibition of ADP-induced platelet aggregation by light transmission aggregometry	105
4	CHEMBL3367077	Displacement of [^{33}P]2MeS-ADP from $P2Y_{12}$ receptor transfected in CHO cells after 30 mins by scintillation counting analysis	91
5	CHEMBL1042523	Ratio of compound IC_{50} to thienopyrimidine IC_{50} for $P2Y_{12}$ receptor in human platelet rich plasma assessed as inhibition of ADP-induced platelet aggregation by light transmission aggregometry	86
6	CHEMBL1042524	Ratio of compound IC_{50} to AZD-6140 IC_{50} for $P2Y_{12}$ receptor in human platelet rich plasma assessed as inhibition of ADP-induced platelet aggregation by light transmission aggregometry	86
7	CHEMBL1064501	Inhibition of human $P2Y_{12}$ receptor expressed in CHO cells	84
8	CHEMBL1060022	Binding affinity to human recombinant $P2Y_{12}$ receptor expressed in CHO cells	76
9	CHEMBL1060023	Antagonist activity at human $P2Y_{12}$ receptor assessed as inhibition of ADP-induced platelet-rich plasma aggregation by turbidimetric method	74
10	CHEMBL767230	Inhibition of platelet aggregation using Adenosine diphosphate (ADP) as activating agent in rabbit platelet rich plasma (PRP)	74
11	CHEMBL1786558	Displacement of [^{125}I]AZ11931285 from human recombinant $P2Y_{12}$ receptor expressed in platelet cell membrane after 1 h by scintillation counting	73
12	CHEMBL1786559	Antagonist activity at human recombinant $P2Y_{12}$ receptor expressed in platelet cell membrane by [^{35}S] GTPγS binding assay	73
13	CHEMBL2175134	Displacement of [^{33}P]2-MeS-ADP from human recombinant $P2Y_{12}$ receptor expressed in CHO cell membranes by scintillation counting method	62
14	CHEMBL2404824	Antagonist activity at $P2Y_{12}$ receptor assessed as inhibition of GTPγS binding after 1 h by scintillation counting analysis	53
15	CHEMBL2404825	Displacement of [^{125}I]AZ11931285 from $P2Y_{12}$ receptor after 1 h by scintillation counting analysis	53
16	CHEMBL3369059	Displacement of [^{3}H]2-methyl-thio-adenosine 5'-diphosphate from human recombinant $P2Y_{12}$ expressed in CHO cell membranes by scintillation counting method	51
17	CHEMBL995340	Displacement of [^{3}H]PSB-0413 from human platelet $P2Y_{12}$ receptor	49
18	CHEMBL842944	In vitro inhibitory activity against ADP-induced human platelet aggregation	42
19	CHEMBL2404822	Antagonist activity at $P2Y_{12}$ receptor in human washed platelets assessed as inhibition of fibrinogen-induced aggregation	40
20	CHEMBL4223325	Displacement of [^{3}H]2MeSADP from $P2Y_{12}$ receptor in human platelets after 60 mins by Top Count scintillation counting method	35
21	CHEMBL696422	Inhibition of platelet aggregation using adenosine diphosphate (ADP) as activating agent in human platelet rich plasma PRP	31
22	CHEMBL1050572	Binding affinity to human recombinant $P2Y_{12}$ receptor expressed on CHO cell membrane	31
23	CHEMBL931130	Antagonist activity at $P2Y_{12}$ receptor assessed as inhibition of ADP-induced human platelet aggregation by washed platelet assay	30
24	CHEMBL3367078	Antagonist activity at $P2Y_{12}$ receptor in human platelet rich plasma assessed as inhibition of ADP-induced aggregation	29
25	CHEMBL1050573	Binding affinity to human recombinant $P2Y_{12}$ receptor expressed in CHO cell membrane in presence of HSA and human AGP	23
26	CHEMBL933022	Antagonist activity at $P2Y_{12}$ receptor assessed as platelet aggregation by washed platelet assay	22

27	CHEMBL 3705643	Binding Assay: The ability of a test compound to bind to the $P2Y_{12}$ receptor was evaluated in a recombinant cell membrane binding assay. In this competitive binding assay, the test compound competed against a radiolabeled agonist for binding to the $P2Y_{12}$ receptor, expressed on the cell membrane. Inhibition of binding of the labeled material was measured and correlated to the amount and potency of the test compound. This binding assay is a modification of the procedure described by Takasaki, J. et. al, Mol. Pharmacol., 2001, Vol. 60, pg. 432.	17
	Total no. of classified compounds		1753
28	Several different unclassified compounds		427
	Total no. of compounds		2180

Table S2. Classification of the collected $P2Y_{12}R$ ligands according to the potency values gained from each biological assay.

No.	Assay CHEMBL ID	Total number of compounds	Class A[a]	Class B[b]	Class C[c]
1	CHEMBL1064897	258	121	88	49
2	CHEMBL1042521	105	74	29	2
3	CHEMBL1042522	105	25	78	2
4	CHEMBL3367077	91	7	63	21
5	CHEMBL1042523	86	86	-	-
6	CHEMBL1042524	86	85	-	1
7	CHEMBL1064501	84	58	24	2
8	CHEMBL1060022	76	5	46	25
9	CHEMBL1060023	74	-	-	74
10	CHEMBL767230	74	4	11	59
11	CHEMBL1786558	73	-	-	73
12	CHEMBL1786559	73	-	2	71
13	CHEMBL2175134	62	10	25	27
14	CHEMBL2404824	53	-	11	42
15	CHEMBL2404825	53	1	13	39
16	CHEMBL3369059	51	4	28	19
17	CHEMBL995340	49	-	4	45
18	CHEMBL842944	42	-	-	42
19	CHEMBL2404822	40	1	7	32
20	CHEMBL4223325	35	-	1	34
21	CHEMBL696422	31	-	1	30
22	CHEMBL1050572	31	4	10	17
23	CHEMBL931130	30	-	8	22
24	CHEMBL3367078	29	-	-	29
25	CHEMBL1050573	23	-	5	18
26	CHEMBL933022	22	-	2	20
27	CHEMBL3705643	17	8	7	2
Total No. of classified compounds		1753	**493**	463	797
Number of potent compounds after "Duplicate Filtering**"**			**312**	-	-

[a] Highly potent compounds (K_i- or IC_{50}-values ≤10 nM)

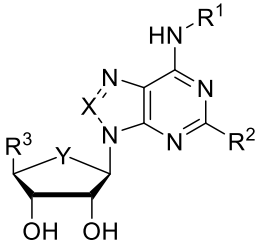
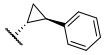
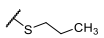
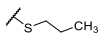
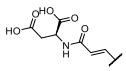
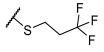
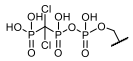
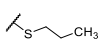
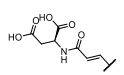
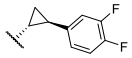
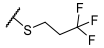
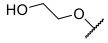
[b] Moderately active compounds (K_i- or IC_{50}-values >10 and ≤100 nM)

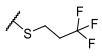
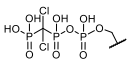
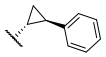
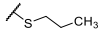
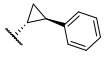
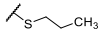
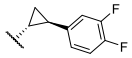
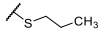
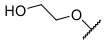
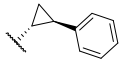
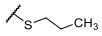
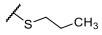
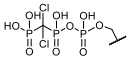
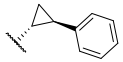
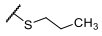
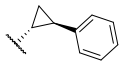
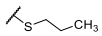
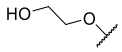
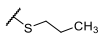
[c] weakly active or inactive compounds (>100 nM)

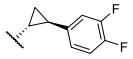
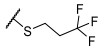
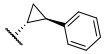
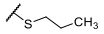
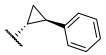
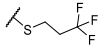
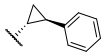
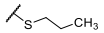
Table S3. Resulted seven main $P2Y_{12}R$ antagonists' scaffolds (classification based on **Document CHEMBL ID**), anthraquinone, and pyrazolidinedione scaffolds.

No.	Document CHEMBL ID	No. of compd.	Descriptions of the scaffold
Scaffold I. Adenine nucleotides and analogs			
1	CHEMBL1140463[42]	15	Not suitable for brain penetration: • High degree of polarity • Synthesis and stereochemical complexity • Lack of metabolic stability
2	CHEMBL3797132[43]	3	
	Total number among the scaffold	**18**	
Scaffold II. Piperazinyl-glutamate derivatives			
3	CHEMBL1156077[49]	76	Not suitable for brain penetration: • High degree of polarity (carboxylic acids) • High molecular weight • Poor Caco-2-permeability
4	CHEMBL3351863[50]	4	
5	CHEMBL1157562[53]	127	
6	CHEMBL1156904[54]	56	
7	CHEMBL2169809[55]	10	
8	CHEMBL3639290[56]	8	
	Total number among the scaffold	**281**	
Scaffold III. 6-Azetidin-1-yl, nicotinate (AZD1283)			
9	CHEMBL2401653[57]	1	Selected for CNS filtering
10	CHEMBL2417494[58]	3	
	Total number among the scaffold	**4**	
Scaffold IV. Thienopyrimidines			
11	CHEMBL1156059[59]	4 + 50[60] + 1[61]	Selected for CNS filtering
	Total number among the scaffold	**50**	
Scaffold V. Anthraquinones.			
12	–	**2**[48]	Not suitable for brain penetration: • High degree of polarity (sulfonic/carboxylic acids) • High molecular weight
Scaffold VI. Pyrazolyl-phenyl-carbamoyl-indole			
13	CHEMBL3352233[62,63]	**5**	Selected for CNS filtering
Scaffold VII. Pyrazolidinedione			
14	–	**10**[65,66]	Selected for CNS filtering

Table S4. Scaffold I: Adenine nucleotide analogs (18 compounds).[42,43]

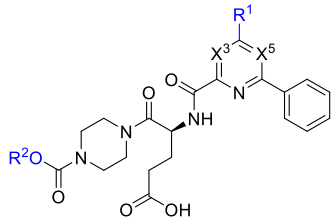
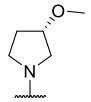
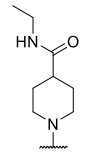
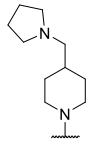
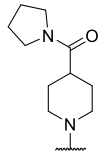
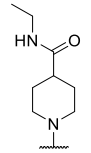
ID	Smiles	Chemical formula	MW (g/mol)	#RO5 Violation	AlogP	Structure				Affinity (IC_{50}) in nM	Compound number in original publication
											
						R^1	**R^2**	**R^3**	**X, Y**		
2a	CCCSC1=NC2=C(N=NN2[C@@H]3C[C@H](C(O)=O)[C@H]([C@H]3O)O)C(N[C@@H]4C[C@H]4C5=CC=CC=C5)=N1	$C_{22}H_{26}N_6O_4S$	470.55	0	2.06				N, CH_2	0.25	8
3a	CCCCNC1=NC(SCCC)=NC2=C1N=NN2[C@@H]3O[C@@H]([C@H]([C@H]3O)O)/C=C/C(N[C@H](C(O)=O)CC(O)=O)=O	$C_{22}H_{31}N_7O_8S$	553.59	3	0.15	^{n}Bu			N, O	0.32	3
V	CSCCNC1=NC(SCCC(F)(F)F)=NC2=C1N=CN2[C@@H]3O[C@@H]([C@H]([C@H]3O)O)COP(O)(OP(O)(C(Cl)(P(O)(O)=O)Cl)=O)=O	$C_{17}H_{25}Cl_2F_3N_5O_{12}P_3S_2$	776.36	3	2.85				CH, O	0.40	Cangrelor
4a	CCCCNC1=NC(SCCC)=NC2=C1N=NN2[C@@H]3C[C@@H]([C@H]([C@H]3O)O)/C=C/C(N[C@H](C(O)=O)CC(O)=O)=O	$C_{23}H_{33}N_7O_7S$	551.62	3	0.82	^{n}Bu			N, CH_2	0.50	4
5a	OCCO[C@H]1C[C@@H](N2N=NC3=C2N=C(SCCC(F)(F)F)N=C3N[C@@H]4C[C@H]4C5=CC=C(C(F)=C5)F)[C@@H]([C@@H]1O)O	$C_{23}H_{25}F_5N_6O_4S$	576.54	2	2.56				N, CH_2	0.63	18

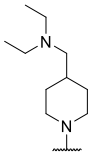
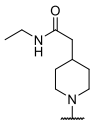
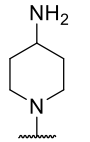
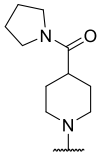
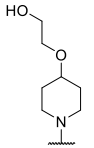
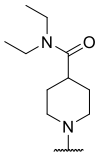
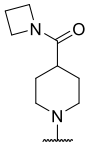
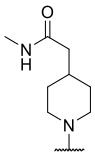
6a	O[C@@H]1[C@H](O[C@@H](N2C=NC3=C2N=C(SCCC(F)(F)F)N=C3NCC(F)(F)F)[C@@H]1O)COP(O)(OP(O)(C(Cl)(P(O)(O)=O)Cl)=O)=O	$C_{16}H_{20}Cl_2F_6N_5O_{12}P_3S$	784.24	3	3.05				CH, O	0.79	1C
7a	CCCSC1=NC2=C(N=NN2[C@@H]3C[C@H](C(N)=O)[C@H]([C@H]3O)O)C(N[C@@H]4C[C@H]4C5=CC=CC=C5)=N1	$C_{22}H_{27}N_7O_3S$	469.56	0	1.46				N, CH_2	1.59	9
8a	CCCSC1=NC2=C(N=NN2[C@@H]3C[C@@H]([C@H]([C@H]3O)O)O)C(N[C@@H]4C[C@H]4C5=CC=CC=C5)=N1	$C_{21}H_{26}N_6O_3S$	442.54	0	1.72			OH	N, CH_2	2.00	12
VI	CCCSC1=NC2=C(N=NN2[C@@H]3C[C@@H]([C@H]([C@H]3O)O)OCCO)C(N[C@@H]4C[C@H]4C5=CC=C(C(F)=C5)F)=N1	$C_{23}H_{28}F_2N_6O_4S$	536.60	2	2.01				N, CH_2	2.00	17, Ticagrelor (AZD-6140)
9a	CCCSC1=NC2=C(N=NN2[C@@H]3C[C@H](C4=NN=NN4)[C@H]([C@H]3O)O)C(N[C@@H]5C[C@H]5C6=CC=CC=C6)=N1	$C_{22}H_{26}N_{10}O_2S$	494.57	1	1.65				N, CH_2	2.00	3A
1a	CCCSC1=NC2=C(N=CN2[C@@H]3O[C@@H]([C@H]([C@H]3O)O)COP(O)(OP(O)(C(Cl)(P(O)(O)=O)Cl)=O)=O)C(N)=N1	$C_{14}H_{22}Cl_2N_5O_{12}P_3S$	648.24	3	1.12	H			CH, O	2.50	1B
10a	CCCSC1=NC2=C(N=NN2[C@@H]3CC[C@H]([C@H]3O)O)C(N[C@@H]4C[C@H]4C5=CC=CC=C5)=N1	$C_{21}H_{26}N_6O_2S$	426.54	0	2.75			H	N, CH_2	2.51	14
11a	CCCSC1=NC2=C(N=NN2[C@@H]3C[C@@H]([C@H]([C@H]3O)O)OCCO)C(N[C@@H]4C[C@H]4C5=CC=CC=C5)=N1	$C_{23}H_{30}N_6O_4S$	486.59	1	1.74				N, CH_2	3.16	11
12a	CCCCNC1=NC(SCCC)=NC2=C1N=NN2[C@@H]3C[C@H](C(O)=O)[C@H]([C@H]3O)O	$C_{17}H_{26}N_6O_4S$	410.49	0	1.3	^{n}Bu			N, CH_2	5.01	5

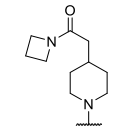
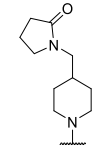
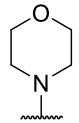
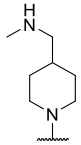
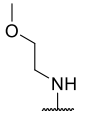
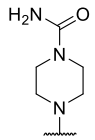
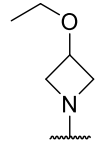
13a	OC[C@H]1C[C@@H](N2N=NC3=C2N=C(SCCC(F)(F)F)N=C3N[C@@H]4C[C@H]4C5=CC=C(C(F)=C5)F)[C@@H]([C@@H]1O)O	$C_{22}H_{23}F_5N_6O_3S$	546.51	1	2.79				N, CH_2	5.01	16
14a	CCCSC1=NC2=C(N=NN2[C@@H]3C[C@@H]([C@H]([C@H]3O)O)CO)C(N[C@@H]4C[C@H]4C5=CC=CC=C5)=N1	$C_{22}H_{28}N_6O_3S$	456.56	0	1.97				N, CH_2	5.01	10
15a	OC[C@H]1C[C@@H](N2N=NC3=C2N=C(SCCC(F)(F)F)N=C3N[C@@H]4C[C@H]4C5=CC=CC=C5)[C@@H]([C@@H]1O)O	$C_{22}H_{25}F_3N_6O_3S$	510.53	1	2.51				N, CH_2	5.01	15
16a	CCCSC1=NC2=C(N=CN2[C@@H]3C[C@@H]([C@H]([C@H]3O)O)CO)C(N[C@@H]4C[C@H]4C5=CC=CC=C5)=N1.Cl	$C_{22}H_{29}ClN_6O_3S$	493.02	0	1.97				CH, CH_2	6.31	13

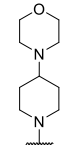
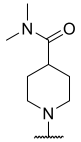
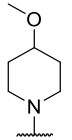
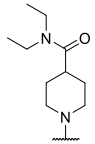
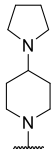
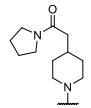
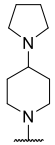
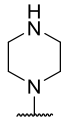
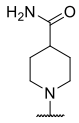
Compounds 8a and 15a were found to be metabolically stable in the presence of NADPH but unstable with UDPGA, whereas the opposite was observed for compounds 4a and 13a.

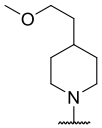
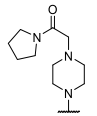
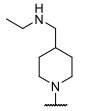
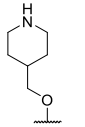
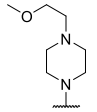
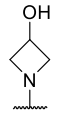
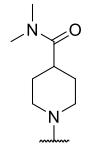
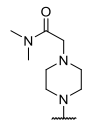
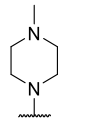
Table S5. Scaffold II: Piperazinyl-glutamate-**phenyl-pyrimidine** derivatives (80 compounds).[49,50]

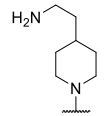
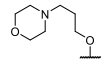
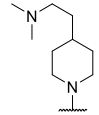
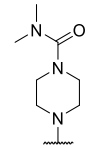
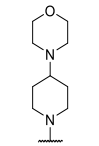
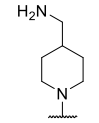
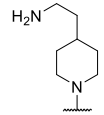
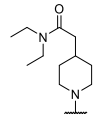
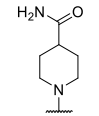
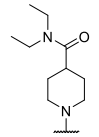
ID	Smiles	Chemical formula	MW (g/mol)	#RO5 Violation	AlogP	Structure & SAR-analysis				Affinity (K_i/(IC_{50})) in nM	Compound number in original publication
											
						R^1	**R^2**	**X^3**	**X^5**		
1b	CCCCOC(N1CCN(C([C@@H](NC(C2=NC(C3=CC=CC=C3)=NC(N4CC[C@H](OC)C4)=C2)=O)CCC(O)=O)=O)CC1)=O	$C_{30}H_{40}N_6O_7$	596.67	1	2.41		^{n}Bu	CH	N	(3)	11x
4b	CCCCOC(N1CCN(C([C@@H](NC(C2=NC(C3=CC=CC=C3)=NC([C@H]4C[C@@H]4COC)=C2)=O)CCC(O)=O)=O)CC1)=O	$C_{30}H_{39}N_5O_7$	581.66	1	2.94		^{n}Bu	CH	N	(4.8)	23u
5b	CCCCOC(N1CCN(C([C@@H](NC(C2=NC(C3=CC=CC=C3)=NC(N4CCC(C(NCC)=O)CC4)=C2)=O)CCC(O)=O)=O)CC1)=O	$C_{34}H_{46}N_6O_7$	650.77	1	3.15		^{n}Bu	CH	N	0.38	25V
6b	CCCCCOC(N1CCN(C([C@@H](NC(C2=NC(C3=CC=CC=C3)=NC(N4CCC(CC4)CN5CCCC5)=C2)=O)CCC(O)=O)=O)CC1)=O	$C_{36}H_{51}N_7O_6$	677.83	1	3.89		Pentyl	CH	N	0.4	25h
7b	CCCCCOC(N1CCN(C([C@@H](NC(C2=NC(C3=CC=CC=C3)=NC(N4CCC(C(N5CCCC5)=O)CC4)=C2)=O)CCC(O)=O)=O)CC1)=O	$C_{36}H_{49}N_7O_7$	691.82	1	3.42		Pentyl	CH	N	0.46	25y
8b	CCCCCOC(N1CCN(C([C@@H](NC(C2=NC(C3=CC=CC=C3)=NC(N4CCC(C(NCC)=O)CC4)=C2)=O)CCC(O)=O)=O)CC1)=O	$C_{34}H_{47}N_7O_7$	665.78	1	2.93		Pentyl	CH	N	0.6	25v

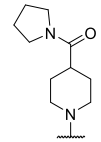
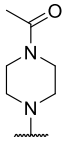
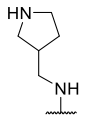
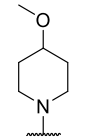
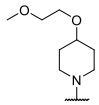
9b	CCCCCOC(N1CCN(C([C@@H](NC(C2=NC(C3=CC=CC=C3)=NC(N4CCC(CC4)CN(CC)CC)=C2)=O)CCC(O)=O)=O)CC1)=O	$C_{36}H_{53}N_7O_6$	679.85	1	4.14		Pentyl	CH	N	0.61	25g
10b	CCCCCOC(N1CCN(C([C@@H](NC(C2=NC(C3=CC=CC=C3)=NC(N4CCC(CC4)CC(NCC)=O)=C2)=O)CCC(O)=O)=O)CC1)=O	$C_{35}H_{49}N_7O_7$	679.81	1	3.32		Pentyl	CH	N	0.67	25bb
11b	CCCCCOC(N1CCN(C([C@@H](NC(C2=NC(C3=CC=CC=C3)=NC(N4CCC(CC4)N)=C2)=O)CCC(O)=O)=O)CC1)=O	$C_{31}H_{43}N_7O_6$	609.72	1	2.51		Pentyl	CH	N	0.69	9i
12b	CCCCOC(N1CCN(C([C@@H](NC(C2=NC(C3=CC=CC=C3)=NC(N4CCC(C(N5CCCC5)=O)CC4)=C2)=O)CCC(O)=O)=O)CC1)=O	$C_{35}H_{47}N_7O_7$	677.79	1	3.03		^{n}Bu	CH	N	0.7	25Y
13b	CCCCCOC(N1CCN(C([C@@H](NC(C2=NC(C3=CC=CC=C3)=NC(N4CCC(OCCO)CC4)=C2)=O)CCC(O)=O)=O)CC1)=O	$C_{33}H_{46}N_6O_8$	654.75	1	2.56		Pentyl	CH	N	0.71	25o
14b	CCCCOC(N1CCN(C([C@@H](NC(C2=NC(C3=CC=CC=C3)=NC(N4CCC(C(N(CC)CC)=O)CC4)=C2)=O)CCC(O)=O)=O)CC1)=O	$C_{35}H_{49}N_7O_7$	679.81	1	3.27		^{n}Bu	CH	N	0.79	25W
15b	CCCCCOC(N1CCN(C([C@@H](NC(C2=NC(C3=CC=CC=C3)=NC(N4CCC(C(N5CCC5)=O)CC4)=C2)=O)CCC(O)=O)=O)CC1)=O	$C_{35}H_{47}N_7O_7$	677.79	1	3.03		Pentyl	CH	N	0.83	25x
16b	CCCCCOC(N1CCN(C([C@@H](NC(C2=NC(C3=CC=CC=C3)=NC(N4CCC(CC4)CC(NC)=O)=C2)=O)CCC(O)=O)=O)CC1)=O	$C_{34}H_{47}N_7O_7$	665.78	1	2.93		Pentyl	CH	N	0.9	25aa

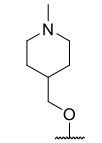
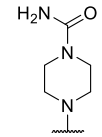
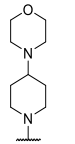
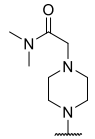
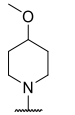
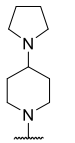
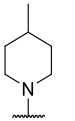
17b	CCCCCOC(N1CCN(C([C@@H](NC(C2=NC(C3=CC=CC=C3)=NC(N4CCC(CC4)CC(N5CCC5)=O)=C2)=O)CCC(O)=O)=O)CC1)=O	$C_{36}H_{49}N_7O_7$	691.82	1	3.42		Pentyl	CH	N	0.92	25dd
18b	CCCCCOC(N1CCN(C([C@@H](NC(C2=NC(C3=CC=CC=C3)=NC(N4CCC(CC4)CN5CCCC5=O)=C2)=O)CCC(O)=O)=O)CC1)=O	$C_{36}H_{49}N_7O_7$	691.82	1	3.42		Pentyl	CH	N	0.99	25s
19b	CCCCCOC(N1CCN(C([C@@H](NC(C2=NC(C3=CC=CC=C3)=NC(N4CCOCC4)=C2)=O)CCC(O)=O)=O)CC1)=O	$C_{30}H_{40}N_6O_7$	596.67	1	2.41		Pentyl	CH	N	1	9b
20b	CCCCCOC(N1CCN(C([C@@H](NC(C2=NC(C3=CC=CC=C3)=NC(N4CCC(CC4)CNC)=C2)=O)CCC(O)=O)=O)CC1)=O	$C_{33}H_{47}N_7O_6$	637.77	1	3.01		Pentyl	CH	N	1.2	25e
21b	CCCCCOC(N1CCN(C([C@@H](NC(C2=NC(C3=CC=CC=C3)=NC(NCCOC)=C2)=O)CCC(O)=O)=O)CC1)=O	$C_{29}H_{40}N_6O_7$	584.66	1	2.64		Pentyl	CH	N	1.2	9a
22b	CCCCCOC(N1CCN(C([C@@H](NC(C2=NC(C3=CC=CC=C3)=NC(N4CCN(C(N)=O)CC4)=C2)=O)CCC(O)=O)=O)CC1)=O	$C_{31}H_{42}N_8O_7$	638.71	1	1.78		Pentyl	CH	N	1.2	23c
23b	CCCCCOC(N1CCN(C([C@@H](NC(C2=NC(C3=CC=CC=C3)=NC(N4CCC(OCC)C4)=C2)=O)CCC(O)=O)=O)CC1)=O	$C_{31}H_{42}N_6O_7$	610.70	1	2.8		Pentyl	CH	N	1.2	9d
24b	CCCCCOC(N1CCN(C([C@@H](NC(C2=NC(C3=CC=CC=C3)=CC(OCCOC)=N2)=O)CCC(O)=O)=O)CC1)=O	$C_{29}H_{39}N_5O_8$	585.65	1	2.6		Pentyl	N	CH	1.2	22a
25b	CCCCCOC(N1CCN(C([C@@H](NC(C2=NC(C3=CC=CC=C3)=NC(OCCOC)=C2)=O)CCC(O)=O)=O)CC1)=O	$C_{29}H_{39}N_5O_8$	585.65	1	2.6		Pentyl	CH	N	1.2	14a

26b	CCCCOC(N1CCN(C([C@@H](NC(C2=NC(C3=CC=CC=C3)=NC(N4CCC(N5CCOCC5)CC4)=C2)=O)CCC(O)=O)=O)CC1)=O	$C_{34}H_{47}N_7O_7$	665.78	1	2.49		^{n}Bu	CH	N	1.3	25C
27b	CCCCOC(N1CCN(C([C@@H](NC(C2=NC(C3=CC=CC=C3)=NC(N4CCC(C(N(C)C)=O)CC4)=C2)=O)CCC(O)=O)=O)CC1)=O	$C_{33}H_{45}N_7O_7$	651.75	1	2.49		^{n}Bu	CH	N	1.3	25U
28b	CCCCOC(N1CCN(C([C@@H](NC(C2=NC(C3=CC=CC=C3)=NC(N4CCC(OC)CC4)=C2)=O)CCC(O)=O)=O)CC1)=O	$C_{31}H_{42}N_6O_7$	610.70	1	2.8		^{n}Bu	CH	N	1.4	25M
29b	CCCCCOC(N1CCN(C([C@@H](NC(C2=NC(C3=CC=CC=C3)=NC(N4CCC(C(N(CC)CC)=O)CC4)=C2)=O)CCC(O)=O)=O)CC1)=O	$C_{36}H_{51}N_7O_7$	693.83	1	3.66		Pentyl	CH	N	1.5	25w
30b	CCCCCOC(N1CCN(C([C@@H](NC(C2=NC(C3=CC=CC=C3)=NC(N4CCC(N5CCCC5)CC4)=C2)=O)CCC(O)=O)=O)CC1)=O	$C_{35}H_{49}N_7O_6$	663.81	1	3.64		Pentyl	CH	N	1.5	25b
31b	CCCCCOC(N1CCN(C([C@@H](NC(C2=NC(C3=CC=CC=C3)=NC(N4CCC(CC4)CC(N5CCCC5)=O)=C2)=O)CCC(O)=O)=O)CC1)=O	$C_{37}H_{51}N_7O_7$	705.84	1	3.81		Pentyl	CH	N	1.6	25ee
32b	CCCCOC(N1CCN(C([C@@H](NC(C2=NC(C3=CC=CC=C3)=NC(N4CCC(N5CCCC5)CC4)=C2)=O)CCC(O)=O)=O)CC1)=O	$C_{34}H_{47}N_7O_6$	649.78	1	3.25		^{n}Bu	CH	N	1.7	25B
33b	CCCCCOC(N1CCN(C([C@@H](NC(C2=NC(C3=CC=CC=C3)=NC(N4CCNCC4)=C2)=O)CCC(O)=O)=O)CC1)=O	$C_{30}H_{41}N_7O_6$	595.69	1	1.99		Pentyl	CH	N	2	23a
34b	CCCCCOC(N1CCN(C([C@@H](NC(C2=NC(C3=CC=CC=C3)=NC(N4CCC(C(N)=O)CC4)=C2)=O)CCC(O)=O)=O)CC1)=O	$C_{32}H_{43}N_7O_7$	637.73	1	2.28		Pentyl	CH	N	2	25t

35b	CCCCOC(N1CCN(C([C@@H](NC(C2=CC(N3CCC(CC3)CCOC)=NC(C4=CC=CC=C4)=N2)=O)CCC(O)=O)=O)CC1)=O	$C_{33}H_{46}N_6O_7$	638.75	1	3.44		^{n}Bu	CH	N	2	25R
36b	CCCCCOC(N1CCN(C([C@@H](NC(C2=NC(C3=CC=CC=C3)=NC(N4CCC(CC4)CCN5CCCC5)=C2)=O)CCC(O)=O)=O)CC1)=O	$C_{37}H_{53}N_7O_6$	691.86	1	4.28		Pentyl	CH	N	2.1	25k
37b	CCCCCOC(N1CCN(C([C@@H](NC(C2=NC(C3=CC=CC=C3)=NC(N4CCN(CC4)CC(N5CCCC5)=O)=C2)=O)CCC(O)=O)=O)CC1)=O	$C_{36}H_{50}N_8O_7$	706.83	1	2.32		Pentyl	CH	N	2.1	23f
38b	CCCCCOC(N1CCN(C([C@@H](NC(C2=NC(C3=CC=CC=C3)=NC(N4CCC(CC4)CNCC)=C2)=O)CCC(O)=O)=O)CC1)=O	$C_{34}H_{49}N_7O_6$	651.80	1	3.4		Pentyl	CH	N	2.2	25f
39b	CCCCCOC(N1CCN(C([C@@H](NC(C2=NC(C3=CC=CC=C3)=NC(OCC4CCNCC4)=C2)=O)CCC(O)=O)=O)CC1)=O	$C_{32}H_{44}N_6O_7$	624.73	1	2.96		Pentyl	CH	N	2.2	14g
40b	CCCCCOC(N1CCN(C([C@@H](NC(C2=NC(C3=CC=CC=C3)=NC(N4CCN(CC4)CCOC)=C2)=O)CCC(O)=O)=O)CC1)=O	$C_{33}H_{47}N_7O_7$	653.77	1	2.35		Pentyl	CH	N	2.3	23g
41b	CCCCCOC(N1CCN(C([C@@H](NC(C2=NC(C3=CC=CC=C3)=NC(N4CC(C4)O)=C2)=O)CCC(O)=O)=O)CC1)=O	$C_{29}H_{38}N_6O_7$	582.65	1	1.76		Pentyl	CH	N	2.5	9c
42b	CCCCCOC(N1CCN(C([C@@H](NC(C2=NC(C3=CC=CC=C3)=NC(N4CCC(C(N(C)C)=O)CC4)=C2)=O)CCC(O)=O)=O)CC1)=O	$C_{34}H_{47}N_7O_7$	665.78	1	2.88		Pentyl	CH	N	2.5	25u
43b	CCCCCOC(N1CCN(C([C@@H](NC(C2=NC(C3=CC=CC=C3)=NC(N4CCN(CC4)CC(N(C)C)=O)=C2)=O)CCC(O)=O)=O)CC1)=O	$C_{34}H_{48}N_8O_7$	680.79	1	1.79		Pentyl	CH	N	2.6	23e
44b	CCCCCOC(N1CCN(C([C@@H](NC(C2=NC(C3=CC=CC=C3)=NC(N4CCN(CC4)C)=C2)=O)CCC(O)=O)=O)CC1)=O	$C_{31}H_{43}N_7O_6$	609.72	1	2.33		Pentyl	CH	N	2.7	9h

45b	CCCCCOC(N1CCN(C([C@@H](NC(C2=NC(C3=CC=CC=C3)=NC(N4CCC(CC4)CCN)=C2)=O)CCC(O)=O)=O)CC1)=O	$C_{33}H_{47}N_7O_6$	637.77	1	3.14		Pentyl	CH	N	2.7	25i
46b	CCCCCOC(N1CCN(C([C@@H](NC(C2=NC(C3=CC=CC=C3)=NC(OCCCN4CCOCC4)=C2)=O)CCC(O)=O)=O)CC1)=O	$C_{33}H_{46}N_6O_8$	654.75	1	2.68		Pentyl	CH	N	2.8	14d
47b	CCCCCOC(N1CCN(C([C@@H](NC(C2=NC(C3=CC=CC=C3)=NC(N4CCC(CC4)CCN(C)C)=C2)=O)CCC(O)=O)=O)CC1)=O	$C_{35}H_{51}N_7O_6$	665.82	1	3.75		Pentyl	CH	N	2.8	25j
48b	CCCCCOC(N1CCN(C([C@@H](NC(C2=NC(C3=CC=CC=C3)=NC(N4CCN(C(N(C)C)=O)CC4)=C2)=O)CCC(O)=O)=O)CC1)=O	$C_{33}H_{46}N_8O_7$	666.77	1	2.38		Pentyl	CH	N	2.9	23d
49b	CCCCCOC(N1CCN(C([C@@H](NC(C2=NC(C3=CC=CC=C3)=NC(N4CCC(N5CCOCC5)CC4)=C2)=O)CCC(O)=O)=O)CC1)=O	$C_{35}H_{49}N_7O_7$	679.81	1	2.88		Pentyl	CH	N	2.9	25c
50b	CCCCCOC(N1CCN(C([C@@H](NC(C2=NC(C3=CC=CC=C3)=NC(N4CCC(CC4)CN)=C2)=O)CCC(O)=O)=O)CC1)=O	$C_{32}H_{45}N_7O_6$	623.74	1	2.75		Pentyl	CH	N	3	25d
51b	CCCCCOC(N1CCN(C([C@@H](NC(C2=NC(C3=CC=CC=C3)=CC(N4CCC(CC4)CCN)=N2)=O)CCC(O)=O)=O)CC1)=O	$C_{33}H_{47}N_7O_6$	637.77	1	3.14		Pentyl	N	CH	3	26i
52b	CCCCCOC(N1CCN(C([C@@H](NC(C2=NC(C3=CC=CC=C3)=NC(N4CCC(CC4)CC(N(CC)CC)=O)=C2)=O)CCC(O)=O)=O)CC1)=O	$C_{37}H_{53}N_7O_7$	707.86	1	4.05		Pentyl	CH	N	3.1	25cc
53b	CCCCCOC(N1CCN(C([C@@H](NC(C2=NC(C3=CC=CC=C3)=CC(N4CCC(C(N)=O)CC4)=N2)=O)CCC(O)=O)=O)CC1)=O	$C_{32}H_{43}N_7O_7$	637.73	1	2.28		Pentyl	N	CH	3.5	26t
54b	CCCCCOC(N1CCN(C([C@@H](NC(C2=NC(C3=CC=CC=C3)=CC(N4CCC(C(N(CC)CC)=O)CC4)=N2)=O)CCC(O)=O)=O)CC1)=O	$C_{36}H_{51}N_7O_7$	693.83	1	3.66		Pentyl	N	CH	3.6	26w

55b	CCCCCOC(N1CCN(C([C@@H](NC(C2=NC(C3=CC=CC=C3)=CC(N4CCC(C(N5CCCC5)=O)CC4)=N2)=O)CCC(O)=O)=O)CC1)=O	$C_{36}H_{49}N_7O_7$	691.82	1	3.42		Pentyl	N	CH	3.6	26y
56b	CCCCCOC(N1CCN(C([C@@H](NC(C2=NC(C3=CC=CC=C3)=NC(N4CCN(C(C)=O)CC4)=C2)=O)CCC(O)=O)=O)CC1)=O	$C_{32}H_{43}N_7O_7$	637.73	1	2.25		Pentyl	CH	N	3.7	23b
57b	CCCCCOC(N1CCN(C([C@@H](NC(C2=NC(C3=CC=CC=C3)=NC(NCC4CCNC4)=C2)=O)CCC(O)=O)=O)CC1)=O	$C_{31}H_{43}N_7O_6$	609.72	1	2.6		Pentyl	CH	N	4.1	9f
58b	CCCCCOC(N1CCN(C([C@@H](NC(C2=NC(C3=CC=CC=C3)=CC(N4CCC(CC4)CCN5CCCC5)=N2)=O)CCC(O)=O)=O)CC1)=O	$C_{37}H_{53}N_7O_6$	691.86	1	4.28		Pentyl	N	CH	4.2	26k
59b	CCCCCOC(N1CCN(C([C@@H](NC(C2=NC(C3=CC=CC=C3)=NC(N4CCC(CC4)COCCOC)=C2)=O)CCC(O)=O)=O)CC1)=O	$C_{35}H_{50}N_6O_8$	682.81	1	3.46		Pentyl	CH	N	4.3	25q
60b	CCCCCOC(N1CCN(C([C@@H](NC(C2=NC(C3=CC=CC=C3)=NC(SCCO)=C2)=O)CCC(O)=O)=O)CC1)=O	$C_{28}H_{37}N_5O_7S$	587.69	1	2.66		Pentyl	CH	N	4.5	10b
61b	CCCCCOC(N1CCN(C([C@@H](NC(C2=NC(C3=CC=CC=C3)=NC(NCCCN(C)C)=C2)=O)CCC(O)=O)=O)CC1)=O	$C_{31}H_{45}N_7O_6$	611.73	1	2.94		Pentyl	CH	N	4.8	9e
62b	CCCCCOC(N1CCN(C([C@@H](NC(C2=NC(C3=CC=CC=C3)=NC(N4CCC(OC)CC4)=C2)=O)CCC(O)=O)=O)CC1)=O	$C_{32}H_{44}N_6O_7$	624.73	1	3.19		Pentyl	CH	N	5	25m
63b	CCCCCOC(N1CCN(C([C@@H](NC(C2=NC(C3=CC=CC=C3)=CC(NCCOC)=N2)=O)CCC(O)=O)=O)CC1)=O	$C_{29}H_{40}N_6O_7$	584.66	1	2.64		Pentyl	N	CH	5.2	20a
64b	CCCCCOC(N1CCN(C([C@@H](NC(C2=NC(C3=CC=CC=C3)=NC(N4CCC(OCCOC)CC4)=C2)=O)CCC(O)=O)=O)CC1)=O	$C_{34}H_{48}N_6O_8$	668.78	1	3.21		Pentyl	CH	N	5.3	25n

65b	CCCCCOC(N1CCN(C([C@@H](NC(C2=NC(C3=CC=CC=C3)=NC(OCC4CCN(CC4)C)=C2)=O)CCC(O)=O)=O)CC1)=O	$C_{33}H_{46}N_6O_7$	638.75	1	3.3		Pentyl	CH	N	5.7	14h
66b	CCCCCOC(N1CCN(C([C@@H](NC(C2=NC(C3=CC=CC=C3)=CC(N4CCN(C(N)=O)CC4)=N2)=O)CCC(O)=O)=O)CC1)=O	$C_{31}H_{42}N_8O_7$	638.71	1	1.78		Pentyl	N	CH	5.8	24c
67b	CCCCCOC(N1CCN(C([C@@H](NC(C2=NC(C3=CC=CC=C3)=CC(N4CCC(N5CCOCC5)CC4)=N2)=O)CCC(O)=O)=O)CC1)=O	$C_{35}H_{49}N_7O_7$	679.81	1	2.88		Pentyl	N	CH	5.9	26c
68b	CCCCCOC(N1CCN(C([C@@H](NC(C2=NC(C3=CC=CC=C3)=CC(N4CCN(CC4)CC(N(C)C)=O)=N2)=O)CCC(O)=O)=O)CC1)=O	$C_{34}H_{48}N_8O_7$	680.79	1	1.79		Pentyl	N	CH	6.8	24e
69b	CCCCCOC(N1CCN(C([C@@H](NC(C2=NC(C3=CC=CC=C3)=CC(N4CCC(OCCOC)CC4)=N2)=O)CCC(O)=O)=O)CC1)=O	$C_{34}H_{48}N_6O_8$	668.78	1	3.21		Pentyl	N	CH	7.1	26n
70b	CCCCCOC(N1CCN(C([C@@H](NC(C2=NC(C3=CC=CC=C3)=CC(N4CCC(OC)CC4)=N2)=O)CCC(O)=O)=O)CC1)=O	$C_{32}H_{44}N_6O_7$	624.73	1	3.19		Pentyl	N	CH	7.4	26m
71b	CCCCCOC(N1CCN(C([C@@H](NC(C2=NC(C3=CC=CC=C3)=CC(N4CCC(N5CCCC5)CC4)=N2)=O)CCC(O)=O)=O)CC1)=O	$C_{35}H_{49}N_7O_6$	663.81	1	3.64		Pentyl	N	CH	7.4	26b
72b	CCCCCOC(N1CCN(C([C@@H](NC(C2=CC(N3CCC(CC3)C)=NC(C4=CC=CC=C4)=N2)=O)CCC(O)=O)=O)CC1)=O	$C_{32}H_{44}N_6O_6$	608.73	1	3.81		Pentyl	CH	N	7.5	25a
73b	CCCCCOC(N1CCN(C([C@@H](NC(C2=NC(C3=CC=CC=C3)=CC(N4CCC(CC4)COCCOC)=N2)=O)CCC(O)=O)=O)CC1)=O	$C_{35}H_{50}N_6O_8$	682.81	1	3.46		Pentyl	N	CH	8.1	26q

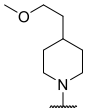
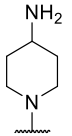
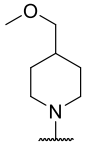
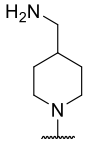
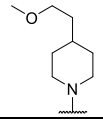
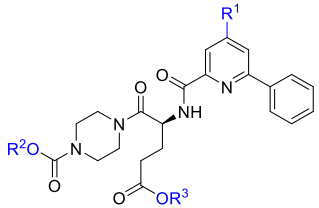
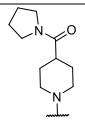
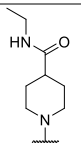
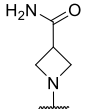
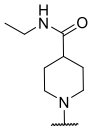
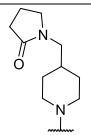
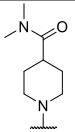
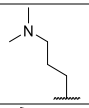
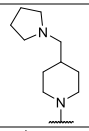
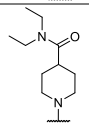
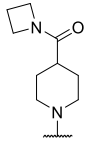
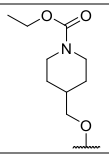
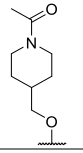
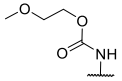
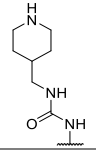
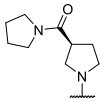
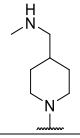
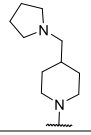
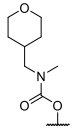
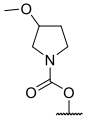
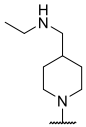
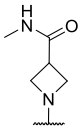
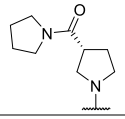
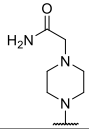
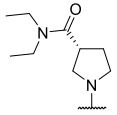
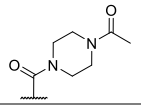
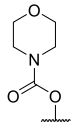
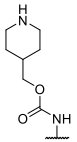
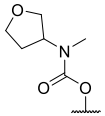
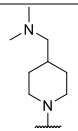
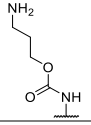
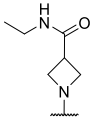
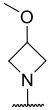
74b	CCCCCOC(N1CCN(C([C@@H](NC(C2=NC(C3=CC=CC=C3)=CC(N4CCC(CC4)CCOC)=N2)=O)CCC(O)=O)=O)CC1)=O	$C_{34}H_{48}N_6O_7$	652.78	1	3.83		Pentyl	N	CH	8.4	26r
75b	CCCCCOC(N1CCN(C([C@@H](NC(C2=NC(C3=CC=CC=C3)=CC(N4CCC(CC4)N)=N2)=O)CCC(O)=O)=O)CC1)=O	$C_{31}H_{43}N_7O_6$	609.72	1	2.51		Pentyl	N	CH	8.4	20i
76b	CCCCCOC(N1CCN(C([C@@H](NC(C2=NC(C3=CC=CC=C3)=NC(N4CCC(CC4)COC)=C2)=O)CCC(O)=O)=O)CC1)=O	$C_{33}H_{46}N_6O_7$	638.75	1	3.44		Pentyl	CH	N	8.4	25p
77b	CCCCCOC(N1CCN(C([C@@H](NC(C2=NC(C3=CC=CC=C3)=CC(N4CCC(CC4)CN)=N2)=O)CCC(O)=O)=O)CC1)=O	$C_{32}H_{45}N_7O_6$	623.74	1	2.75		Pentyl	N	CH	9.4	26d
78b	CCCCCOC(N1CCN(C([C@@H](NC(C2=NC(C3=CC=CC=C3)=NC(NC4CCN(C(C)C)CC4)=C2)=O)CCC(O)=O)=O)CC1)=O	$C_{34}H_{49}N_7O_6$	651.80	1	3.86		Pentyl	CH	N	9.4	9g
79b	CCCCCOC(N1CCN(C([C@@H](NC(C2=NC(C3=CC=CC=C3)=CC(N4CCC(OCCO)CC4)=N2)=O)CCC(O)=O)=O)CC1)=O	$C_{33}H_{46}N_6O_8$	654.75	1	2.56		Pentyl	N	CH	10	26o
80b	CCCCCOC(N1CCN(C([C@@H](NC(C2=NC(C3=CC=CC=C3)=NC(N4CCC(CC4)CCOC)=C2)=O)CCC(O)=O)=O)CC1)=O	$C_{34}H_{48}N_6O_7$	652.78	1	3.83		Pentyl	CH	N	10.2	25r

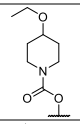
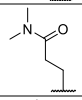
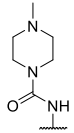
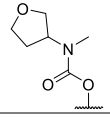
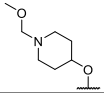
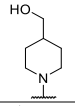
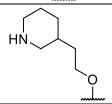
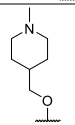
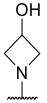
Table S6. Scaffold II: Piperazinyl-glutamate-**phenyl-pyridine** derivatives (183 compounds).[53,54]

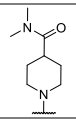
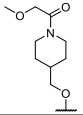
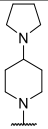
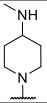
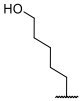
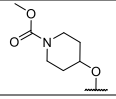
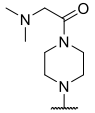
ID	Smiles	Chemical formula	MW (g/mol)	#RO5 Violation	AlogP	Structure & SAR-analysis		Affinity (K_i/(IC_{50})) in nM	Compound number in original publication
									
						R^1	**R^2, R^3**		
1c	CCCCOC(N1CCN(C([C@@H](NC(C2=CC(N3CCC(C(N4CCCC4)=O)CC3)=CC(C5=CC=CC=C5)=N2)=O)CCC(O)=O)=O)CC1)=O	$C_{36}H_{48}N_6O_7$	676.80	1	3.63		^{n}Bu, H	2.10 (360)	4t
2c	CCCCCOC(N1CCN(C([C@@H](NC(C2=CC(N3CCC(C(NCC)=O)CC3)=CC(C4=CC=CC=C4)=N2)=O)CCC(O)=O)=O)CC1)=O	$C_{35}H_{48}N_6O_7$	664.80	1	3.54		Pentyl, H	0.58 (650)	5o
3c	CCCCCOC(N1CCN(C([C@@H](NC(C2=CC(N3CC(C(N)=O)C3)=CC(C4=CC=CC=C4)=N2)=O)CCC(O)=O)=O)CC1)=O	$C_{31}H_{40}N_6O_7$	608.70	1	2.1		Pentyl, H	0.64	9f
4c	CCCCOC(N1CCN(C([C@@H](NC(C2=CC(N3CCC(C(NCC)=O)CC3)=CC(C4=CC=CC=C4)=N2)=O)CCC(O)=O)=O)CC1)=O	$C_{34}H_{46}N_6O_7$	650.78	1	3.15		^{n}Bu, H	0.68	4o
5c	CCCCOC(N1CCN(C([C@@H](NC(C2=CC(N3CCC(CC3)CN4CCCC4=O)=CC(C5=CC=CC=C5)=N2)=O)CCC(O)=O)=O)CC1)=O	$C_{36}H_{48}N_6O_7$	676.82	1	3.63		^{n}Bu, H	0.79	4l
6c	CCCCCOC(N1CCN(C([C@@H](NC(C2=CC(N3CCC(C(N(C)C)=O)CC3)=CC(C4=CC=CC=C4)=N2)=O)CCC(O)=O)=O)CC1)=O	$C_{35}H_{48}N_6O_7$	664.80	1	3.49		Pentyl, H	0.98	5q

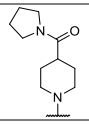
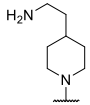
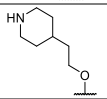
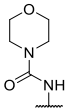
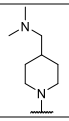
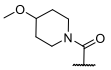
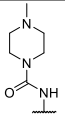
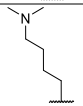
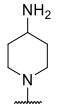
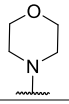
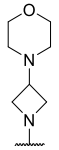
7c	CCCCCOC(N1CCN(C([C@@H](NC(C2=CC(CCCN(C)C)=CC(C3=CC=CC=C3)=N2)=O)CCC(O)=O)=O)CC1)=O	$C_{32}H_{45}N_5O_6$	595.74	1	3.68		Pentyl, H	1.00	83h
8c	CCCCCOC(N1CCN(C([C@@H](NC(C2=CC(N3CCC(CC3)CN4CCCC4)=CC(C5=CC=CC=C5)=N2)=O)CCC(O)=O)=O)CC1)=O	$C_{37}H_{52}N_6O_6$	676.86	1	4.5		Pentyl, H	1.10	47x
9c	CCCCOC(N1CCN(C([C@@H](NC(C2=CC(N3CCC(C(N(CC)CC)=O)CC3)=CC(C4=CC=CC=C4)=N2)=O)CCC(O)=O)=O)CC1)=O	$C_{36}H_{50}N_6O_7$	678.83	1	3.88		^{n}Bu, H	1.10	4r
10c	CCCCCOC(N1CCN(C([C@@H](NC(C2=CC(N3CCC(C(N4CCC4)=O)CC3)=CC(C5=CC=CC=C5)=N2)=O)CCC(O)=O)=O)CC1)=O	$C_{36}H_{48}N_6O_7$	676.80	1	3.63		Pentyl, H	1.20	5s
11c	CCCCCOC(N1CCN(C([C@@H](NC(C2=CC(OCC3CCN(C(OCC)=O)CC3)=CC(C4=CC=CC=C4)=N2)=O)CCC(O)=O)=O)CC1)=O	$C_{36}H_{49}N_5O_9$	695.80	1	4.43		Pentyl, H	1.30	72g
12c	CCCCCOC(N1CCN(C([C@@H](NC(C2=CC(OCC3CCN(C(C)=O)CC3)=CC(C4=CC=CC=C4)=N2)=O)CCC(O)=O)=O)CC1)=O	$C_{35}H_{47}N_5O_8$	665.78	1	3.82		Pentyl, H	1.30	72d
13c	CCCCCOC(N1CCN(C([C@@H](NC(C2=CC(NC(OCCOC)=O)=CC(C3=CC=CC=C3)=N2)=O)CCC(OC(C)(C)C)=O)=O)CC1)=O	$C_{35}H_{49}N_5O_9$	683.79	1	4.63		Pentyl, ^{ter}Bu	1.40	77b
14c	CCCCCOC(N1CCN(C([C@@H](NC(C2=CC(NC(NCC3CCNCC3)=O)=CC(C4=CC=CC=C4)=N2)=O)CCC(OC(C)(C)C)=O)=O)CC1)=O	$C_{38}H_{55}N_7O_7$	721.89	1	4.56		Pentyl, ^{ter}Bu	1.40	76b
15c	CCCCCOC(N1CCN(C([C@@H](NC(C2=CC(N3CC[C@@H](C(N4CCCC4)=O)C3)=CC(C5=CC=CC=C5)=N2)=O)CCC(O)=O)=O)CC1)=O	$C_{36}H_{48}N_6O_7$	676.80	1	3.63		Pentyl, H	1.40	8k, (S,R)diastereomer2

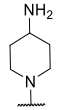
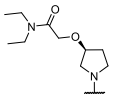
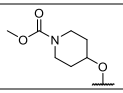
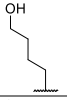
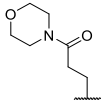
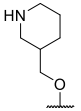
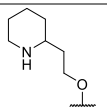
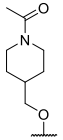
16c	CCCCCOC(N1CCN(C([C@@H](NC(C2=CC(N3CCC(CC3)CNC)=CC(C4=CC=CC=C4)=N2)=O)CCC(O)=O)=O)CC1)=O	$C_{34}H_{48}N_6O_6$	636.78	1	3.62		Pentyl, H	1.50	47v
17c	CCCCOC(N1CCN(C([C@@H](NC(C2=CC(N3CCC(CC3)CN4CCCC4)=CC(C5=CC=CC=C5)=N2)=O)CCC(O)=O)=O)CC1)=O	$C_{36}H_{50}N_6O_6$	662.82	1	4.1		^{n}Bu, H	1.50	46x
18c	CCCCOC(N1CCN(C([C@@H](NC(C2=CC(OC(N(CC3CCOCC3)C)=O)=CC(C4=CC=CC=C4)=N2)=O)CCC(O)=O)=O)CC1)=O	$C_{34}H_{45}N_5O_9$	667.75	1	3.65		^{n}Bu, H	1.50	56b
19c	CCCCOC(N1CCN(C([C@@H](NC(C2=CC(OC(N3CCC(OC)C3)=O)=CC(C4=CC=CC=C4)=N2)=O)CCC(O)=O)=O)CC1)=O	$C_{32}H_{41}N_5O_9$	639.70	1	3.01		^{n}Bu, H	1.50	56g
20c	CCCCCOC(N1CCN(C([C@@H](NC(C2=CC(N3CCC(CC3)CNCC)=CC(C4=CC=CC=C4)=N2)=O)CCC(O)=O)=O)CC1)=O	$C_{35}H_{50}N_6O_6$	650.81	1	4.01		Pentyl, H	1.50	5c
21c	CCCCCOC(N1CCN(C([C@@H](NC(C2=CC(N3CC(C(NC)=O)C3)=CC(C4=CC=CC=C4)=N2)=O)CCC(O)=O)=O)CC1)=O	$C_{32}H_{42}N_6O_7$	622.71	1	2.37		Pentyl, H	1.70	9g
22c	CCCCCOC(N1CCN(C([C@@H](NC(C2=CC(N3CC[C@H](C(N4CCCC4)=O)C3)=CC(C5=CC=CC=C5)=N2)=O)CCC(O)=O)=O)CC1)=O	$C_{36}H_{48}N_6O_7$	676.80	1	3.63		Pentyl, H	1.70	8j, (S,S)diastereomer1
23c	CCCCCOC(N1CCN(C([C@@H](NC(C2=CC(N3CCN(CC3)CC(N)=O)=CC(C4=CC=CC=C4)=N2)=O)CCC(O)=O)=O)CC1)=O	$C_{33}H_{45}N_7O_7$	651.75	1	1.79		Pentyl, H	1.70	12k
24c	CCCCCOC(N1CCN(C([C@@H](NC(C2=CC(N3CC[C@H](C(N(CC)CC)=O)C3)=CC(C4=CC=CC=C4)=N2)=O)CCC(O)=O)=O)CC1)=O	$C_{36}H_{50}N_6O_7$	678.82	1	3.88		Pentyl, H	1.70	8h, (S,S)diastereomer1

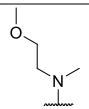
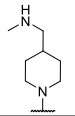
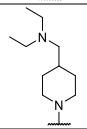
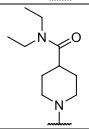
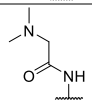
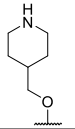
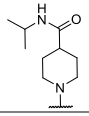
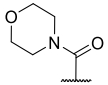
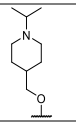
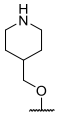
25c	CCCCCOC(N1CCN(C([C@@H](NC(C2=CC(C(N3CCN(C(C)=O)CC3)=O)=CC(C4=CC=CC=C4)=N2)=O)CCC(O)=O)=O)CC1)=O	$C_{34}H_{44}N_6O_8$	664.75	1	2.49		Pentyl, H	1.70	80s
26c	CCCCOC(N1CCN(C([C@@H](NC(C2=CC(OC(N3CCOCC3)=O)=CC(C4=CC=CC=C4)=N2)=O)CCC(O)=O)=O)CC1)=O	$C_{31}H_{39}N_5O_9$	625.67	1	2.62		^{n}Bu, H	1.70	56f
27c	CCCCCOC(N1CCN(C([C@@H](NC(C2=CC(NC(OCC3CCNCC3)=O)=CC(C4=CC=CC=C4)=N2)=O)CCC(OC(C)(C)C)=O)=O)CC1)=O	$C_{38}H_{54}N_6O_8$	722.87	1	4.99		Pentyl, ^{ter}Bu	1.70	77d
28c	CCCCOC(N1CCN(C([C@@H](NC(C2=CC(OC(N(C3CCOC3)C)=O)=CC(C4=CC=CC=C4)=N2)=O)CCC(O)=O)=O)CC1)=O	$C_{32}H_{41}N_5O_9$	639.70	1	3.01		^{n}Bu, H	1.80	56c
29c	CCCCCOC(N1CCN(C([C@@H](NC(C2=CC(N3CCC(CC3)CN(C)C)=CC(C4=CC=CC=C4)=N2)=O)CCC(O)=O)=O)CC1)=O	$C_{35}H_{50}N_6O_6$	650.81	1	3.96		Pentyl, H	1.90	47w
30c	CCCCCOC(N1CCN(C([C@@H](NC(C2=CC(NC(OCCCN)=O)=CC(C3=CC=CC=C3)=N2)=O)CCC(OC(C)(C)C)=O)=O)CC1)=O	$C_{35}H_{50}N_6O_8$	682.81	1	4.34		Pentyl, ^{ter}Bu	1.90	77c
31c	CCCCOC(N1CCN(C([C@@H](NC(C2=CC(OC(N(C)C)=O)=CC(C3=CC=CC=C3)=N2)=O)CCC(O)=O)=O)CC1)=O	$C_{29}H_{37}N_5O_8$	583.63	1	2.85		^{n}Bu, H	2.00	56a
32c	CCCCCOC(N1CCN(C([C@@H](NC(C2=CC(N3CC(C(NCC)=O)C3)=CC(C4=CC=CC=C4)=N2)=O)CCC(O)=O)=O)CC1)=O	$C_{33}H_{44}N_6O_7$	636.74	1	2.76		Pentyl, H	2.00	9h
33c	CCCCCOC(N1CCN(C([C@@H](NC(C2=CC(N3CC(OC)C3)=CC(C4=CC=CC=C4)=N2)=O)CCC(O)=O)=O)CC1)=O	$C_{31}H_{41}N_5O_7$	595.69	1	3.02		Pentyl, H	2.00	9b
34c	CCCCCOC(N1CCN(C([C@@H](NC(C2=CC(N(CCOC)C)=CC(C3=CC=CC=C3)=N2)=O)CCC(O)=O)=O)CC1)=O	$C_{31}H_{43}N_5O_7$	597.70	1	3.27		Pentyl, H	2.10	47h

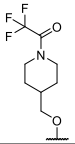
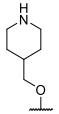
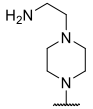
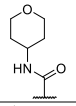
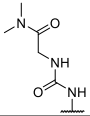
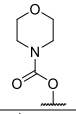
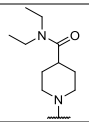
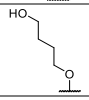
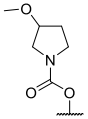
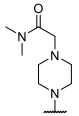
35c	CCCCOC(N1CCN(C([C@@H](NC(C2=CC(OC(N3CCC(OCC)CC3)=O)=CC(C4=CC=CC=C4)=N2)=O)CCC(O)=O)=O)CC1)=O	$C_{34}H_{45}N_5O_9$	667.75	1	3.79		^{n}Bu, H	2.10	56h
36c	CCCCCOC(N1CCN(C([C@@H](NC(C2=CC(CCC(N(C)C)=O)=CC(C3=CC=CC=C3)=N2)=O)CCC(O)=O)=O)CC1)=O	$C_{32}H_{43}N_5O_7$	609.71	1	3.2		Pentyl, H	2.10	83k
37c	CCCCCOC(N1CCN(C([C@@H](NC(C2=CC(NC(N3CCN(CC3)C)=O)=CC(C4=CC=CC=C4)=N2)=O)CCC(OC(C)(C)C)=O)=O)CC1)=O	$C_{37}H_{53}N_7O_7$	707.86	1	4.22		Pentyl, ^{ter}Bu	2.30	75e
38c	CCCCCOC(N1CCN(C([C@@H](NC(C2=CC(OC(N(C3CCOC3)C)=O)=CC(C4=CC=CC=C4)=N2)=O)CCC(O)=O)=O)CC1)=O	$C_{33}H_{43}N_5O_9$	653.72	1	3.4		Pentyl, H	2.30	57c
39c	CCCCOC(N1CCN(C([C@@H](NC(C2=CC(OC3CCN(CC3)COC)=CC(C4=CC=CC=C4)=N2)=O)CCC(O)=O)=O)CC1)=O	$C_{33}H_{45}N_5O_8$	639.74	1	3.24		^{n}Bu, H	2.40	69f
40c	CCCCCOC(N1CCN(C([C@@H](NC(C2=CC(C(N(C)C)=O)=CC(C3=CC=CC=C3)=N2)=O)CCC(O)=O)=O)CC1)=O	$C_{30}H_{39}N_5O_7$	581.66	1	2.88		Pentyl, H	2.40	80e
41c	CCCCOC(N1CCN(C([C@@H](NC(C2=CC(NCCOC)=CC(C3=CC=CC=C3)=N2)=O)CCC(O)=O)=O)CC1)=O	$C_{29}H_{39}N_5O_7$	569.65	1	2.85		^{n}Bu, H	2.40	46g
42c	CCCCCOC(N1CCN(C([C@@H](NC(C2=CC(N3CCC(CC3)CO)=CC(C4=CC=CC=C4)=N2)=O)CCC(O)=O)=O)CC1)=O	$C_{33}H_{45}N_5O_7$	623.74	1	3.39		Pentyl, H	2.40	47r
43c	CCCCOC(N1CCN(C([C@@H](NC(C2=CC(OCCC3CCCNC3)=CC(C4=CC=CC=C4)=N2)=O)CCC(O)=O)=O)CC1)=O	$C_{33}H_{45}N_5O_7$	623.74	1	3.56		^{n}Bu, H	2.50	51u
44c	CCCCOC(N1CCN(C([C@@H](NC(C2=CC(OCC3CCN(CC3)C)=CC(C4=CC=CC=C4)=N2)=O)CCC(O)=O)=O)CC1)=O	$C_{33}H_{45}N_5O_7$	623.74	1	3.51		^{n}Bu, H	2.50	71a
45c	CCCCCOC(N1CCN(C([C@@H](NC(C2=CC(C(N(CC)C)=O)=CC(C3=CC=CC=C3)=N2)=O)CCC(O)=O)=O)CC1)=O	$C_{32}H_{43}N_5O_7$	609.71	1	3.27		^{n}Bu, H	2.50	69a
46c	CCCCCOC(N1CCN(C([C@@H](NC(C2=CC(N3CC(C3)O)=CC(C4=CC=CC=C4)=N2)=O)CCC(O)=O)=O)CC1)=O	$C_{30}H_{39}N_5O_7$	581.66	1	2.36		Pentyl, H	2.50	9a

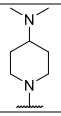
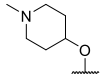
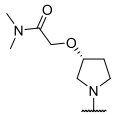
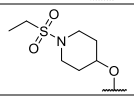
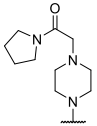
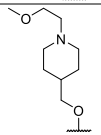
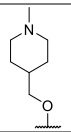
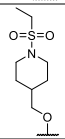
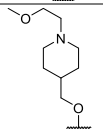
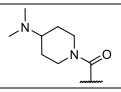
47c	CCCCCOC(N1CCN(C([C@@H](NC(C2=CC(N3CC[C@@H](C(N(CC)CC)=O)C3)=CC(C4=CC=CC=C4)=N2)=O)CCC(O)=O)=O)CC1)=O	$C_{36}H_{50}N_6O_7$	678.82	1	3.88		Pentyl, H	2.60	8i, (S,R)diastereomer2
48c	CCCCOC(N1CCN(C([C@@H](NC(C2=CC(N3CCC(C(N(C)C)=O)CC3)=CC(C4=CC=CC=C4)=N2)=O)CCC(O)=O)=O)CC1)=O	$C_{34}H_{46}N_6O_7$	650.77	1	3.1		^{n}Bu, H	2.60	4q
49c	CCCCCOC(N1CCN(C([C@@H](NC(C2=CC(C(N(CC)C)=O)=CC(C3=CC=CC=C3)=N2)=O)CCC(O)=O)=O)CC1)=O	$C_{31}H_{41}N_5O_7$	595.69	1	3.27		Pentyl, H	2.60	80f
50c	CCCCOC(N1CCN(C([C@@H](NC(C2=CC(OCC3CCN(C(COC)=O)CC3)=CC(C4=CC=CC=C4)=N2)=O)CCC(O)=O)=O)CC1)=O	$C_{35}H_{47}N_5O_9$	681.78	1	3.06		^{n}Bu, H	2.60	71f
51c	CCCCCCOC(N1CCN(C([C@@H](NC(C2=CC(N3CCC(N4CCCC4)CC3)=CC(C5=CC=CC=C5)=N2)=O)CCC(O)=O)=O)CC1)=O	$C_{37}H_{52}N_6O_6$	676.85	1	4.64		Hexyl, H	2.60	48p
52c	CCCCCOC(N1CCN(C([C@@H](NC(C2=CC(C(N(CCCOC)C)=O)=CC(C3=CC=CC=C3)=N2)=O)CCC(O)=O)=O)CC1)=O	$C_{33}H_{45}N_5O_8$	639.74	1	3.29		Pentyl, H	2.60	80k
53c	CCCCOC(N1CCN(C([C@@H](NC(C2=CC(N3CCC(NC)CC3)=CC(C4=CC=CC=C4)=N2)=O)CCC(O)=O)=O)CC1)=O	$C_{32}H_{44}N_6O_6$	608.73	1	2.98		^{n}Bu, H	2.70	46n
54c	CCCCCOC(N1CCN(C([C@@H](NC(C2=CC(NC(NC(C)C)=O)=CC(C3=CC=CC=C3)=N2)=O)CCC(OC(C)(C)C)=O)=O)CC1)=O	$C_{35}H_{50}N_6O_7$	666.81	1	4.97		Pentyl, ^{ter}Bu	2.70	76a
55c	CCCCCOC(N1CCN(C([C@@H](NC(C2=CC(CCCCCO)=CC(C3=CC=CC=C3)=N2)=O)CCC(O)=O)=O)CC1)=O	$C_{32}H_{44}N_4O_7$	596.71	1	3.89		Pentyl, H	2.80	83d
56c	CCCCCOC(N1CCN(C([C@@H](NC(C2=CC(C(N3CCCCC3)=O)=CC(C4=CC=CC=C4)=N2)=O)CCC(O)=O)=O)CC1)=O	$C_{33}H_{43}N_5O_7$	621.72	1	3.81		Pentyl, H	2.80	80n
57c	CCCCOC(N1CCN(C([C@@H](NC(C2=CC(OC3CCN(C(OC)=O)CC3)=CC(C4=CC=CC=C4)=N2)=O)CCC(O)=O)=O)CC1)=O	$C_{33}H_{43}N_5O_9$	653.72	1	3.4		^{n}Bu, H	2.80	69d
58c	CCCCCOC(N1CCN(C([C@@H](NC(C2=CC(N3CCN(C(CN(C)C)=O)CC3)=CC(C4=CC=CC=C4)=N2)=O)CCC(O)=O)=O)CC1)=O	$C_{35}H_{49}N_7O_7$	679.81	1	2.39		Pentyl, H	2.80	12q

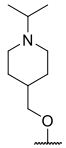
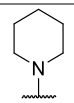
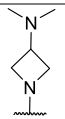
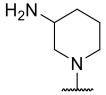
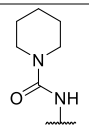
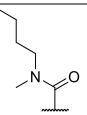
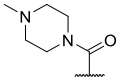
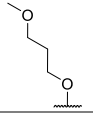
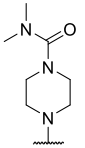
59c	CCCCCOC(N1CCN(C([C@@H](NC(C2=CC(N3CCC(C(N4CCCC4)=O)CC3)=CC(C5=CC=CC=C5)=N2)=O)CCC(O)=O)=O)CC1)=O	$C_{37}H_{50}N_6O_7$	690.83	1	4.02		Pentyl, H	2.80	5t
60c	CCCCCOC(N1CCN(C([C@@H](NC(C2=CC(N3CCC(CC3)CCN)=CC(C4=CC=CC=C4)=N2)=O)CCC(O)=O)=O)CC1)=O	$C_{34}H_{48}N_6O_6$	636.78	1	3.75		Pentyl, H	2.80	5h
61c	CCCCOC(N1CCN(C([C@@H](NC(C2=CC(OCCC3CCNCC3)=CC(C4=CC=CC=C4)=N2)=O)CCC(O)=O)=O)CC1)=O	$C_{33}H_{45}N_5O_7$	623.74	1	3.56		^{n}Bu, H	3.00	51t
62c	CCCCCOC(N1CCN(C([C@@H](NC(C2=CC(NC(N3CCOCC3)=O)=CC(C4=CC=CC=C4)=N2)=O)CCC(OC(C)(C)C)=O)=O)CC1)=O	$C_{36}H_{50}N_6O_8$	694.82	1	4.3		Pentyl, ^{ter}Bu	3.00	75d
63c	CCCCOC(N1CCN(C([C@@H](NC(C2=CC(N3CCC(CC3)CN(C)C)=CC(C4=CC=CC=C4)=N2)=O)CCC(O)=O)=O)CC1)=O	$C_{34}H_{48}N_6O_6$	636.78	1	3.57		^{n}Bu, H	3.20	46w
64c	CCCCCOC(N1CCN(C([C@@H](NC(C2=CC(C(N3CCC(OC)CC3)=O)=CC(C4=CC=CC=C4)=N2)=O)CCC(O)=O)=O)CC1)=O	$C_{34}H_{45}N_5O_8$	651.75	1	3.43		Pentyl, H	3.20	80p
65c	CCCCCOC(N1CCN(C([C@@H](NC(C2=CC(NC(N3CCN(CC3)C)=O)=CC(C4=CC=CC=C4)=N2)=O)CCC(O)=O)=O)CC1)=O	$C_{33}H_{45}N_7O_7$	651.75	1	2.96		Pentyl, H	3.20	76e
66c	CCCCCOC(N1CCN(C([C@@H](NC(C2=CC(CCCCN(C)C)=CC(C3=CC=CC=C3)=N2)=O)CCC(O)=O)=O)CC1)=O	$C_{33}H_{47}N_5O_6$	609.76	1	4.07		Pentyl, H	3.30	83j
67c	CCCCCCOC(N1CCN(C([C@@H](NC(C2=CC(N3CCC(CC3)N)=CC(C4=CC=CC=C4)=N2)=O)CCC(O)=O)=O)CC1)=O	$C_{33}H_{46}N_6O_6$	622.75	1	3.5		Hexyl, H	3.30	48m
68c	CCCCOC(N1CCN(C([C@@H](NC(C2=CC(N3CCOCC3)=CC(C4=CC=CC=C4)=N2)=O)CCC(O)=O)=O)CC1)=O	$C_{30}H_{39}N_5O_7$	581.66	1	2.63		^{n}Bu, H	3.30	46j
69c	CCCCCOC(N1CCN(C([C@@H](NC(C2=CC(N3CC(N4CCOCC4)C3)=CC(C5=CC=CC=C5)=N2)=O)CCC(O)=O)=O)CC1)=O	$C_{34}H_{46}N_6O_7$	650.77	1	2.7		Pentyl, H	3.30	9d

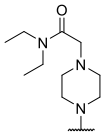
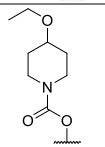
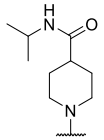
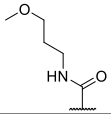
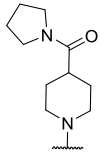
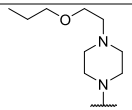
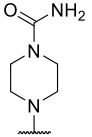
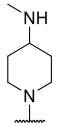
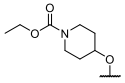
70c	CCCCOC(N1CCN(C([C@@H](NC(C2=CC(N3CCC(CC3)N)=CC(C4=CC=CC=C4)=N2)=O)CCC(O)=O)=O)CC1)=O	$C_{31}H_{42}N_6O_6$	594.70	1	2.72		^{n}Bu, H	3.50	46m
71c	CCCCCOC(N1CCN(C([C@@H](NC(C2=CC(OC3CCNCC3)=CC(C4=CC=CC=C4)=N2)=O)CCC(O)=O)=O)CC1)=O	$C_{32}H_{43}N_5O_7$	609.71	1	3.31		Pentyl, H	3.50	52n
72c	CCCCCOC(N1CCN(C([C@@H](NC(C2=CC(N3CC[C@@H](OCC(N(CC)CC)=O)C3)=CC(C4=CC=CC=C4)=N2)=O)CCC(O)=O)=O)CC1)=O	$C_{37}H_{52}N_6O_8$	708.84	1	3.65		Pentyl, H	3.50	8c, (S,R)diastereomer1
73c	CCCCCOC(N1CCN(C([C@@H](NC(C2=CC(OC3CCN(C(OC)=O)CC3)=CC(C4=CC=CC=C4)=N2)=O)CCC(O)=O)=O)CC1)=O	$C_{34}H_{45}N_5O_9$	667.75	1	3.79		Pentyl, H	3.60	70d
74c	CCCCCOC(N1CCN(C([C@@H](NC(C2=CC(CCCCO)=CC(C3=CC=CC=C3)=N2)=O)CCC(O)=O)=O)CC1)=O	$C_{31}H_{42}N_4O_7$	582.69	1	3.5		Pentyl, H	3.60	83c
75c	CCCCCOC(N1CCN(C([C@@H](NC(C2=CC(CCC(N3CCOCC3)=O)=CC(C4=CC=CC=C4)=N2)=O)CCC(O)=O)=O)CC1)=O	$C_{34}H_{45}N_5O_8$	651.75	1	2.97		Pentyl, H	3.70	83l
76c	CCCCOC(N1CCN(C([C@@H](NC(C2=CC(OC3CCNC3)=CC(C4=CC=CC=C4)=N2)=O)CCC(O)=O)=O)CC1)=O	$C_{30}H_{39}N_5O_7$	581.66	1	2.53		^{n}Bu, H	3.70	51p
77c	CCCCOC(N1CCN(C([C@@H](NC(C2=CC(OCC3CCCNC3)=CC(C4=CC=CC=C4)=N2)=O)CCC(O)=O)=O)CC1)=O	$C_{32}H_{43}N_5O_7$	609.71	1	3.17		^{n}Bu, H	3.70	51r
78c	CCCCOC(N1CCN(C([C@@H](NC(C2=CC(OCCC3CCCCN3)=CC(C4=CC=CC=C4)=N2)=O)CCC(O)=O)=O)CC1)=O	$C_{33}H_{45}N_5O_7$	623.74	1	3.7		^{n}Bu, H	3.70	51v
79c	CCCCCOC(N1CCN(C([C@@H](NC(C2=CC(CCCO)=CC(C3=CC=CC=C3)=N2)=O)CCC(O)=O)=O)CC1)=O	$C_{30}H_{40}N_4O_7$	568.66	1	3.11		Pentyl, H	3.80	83b
80c	CCCCOC(N1CCN(C([C@@H](NC(C2=CC(OCC3CCN(C(C)=O)CC3)=CC(C4=CC=CC=C4)=N2)=O)CCC(O)=O)=O)CC1)=O	$C_{34}H_{45}N_5O_8$	651.75	1	3.43		^{n}Bu, H	3.90	71d

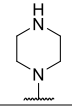
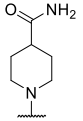
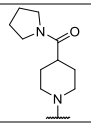
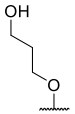
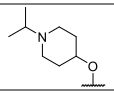
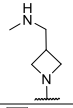
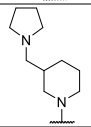
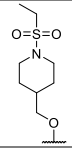
81c	CCCCOC(N1CCN(C([C@@H](NC(C2=CC(N(CCOC)C)=CC(C3=CC=CC=C3)=N2)=O)CCC(O)=O)=O)CC1)=O	$C_{30}H_{41}N_5O_7$	583.68	1	2.88		^{n}Bu, H	4.00	46h
82c	CCCCOC(N1CCN(C([C@@H](NC(C2=CC(N3CCC(CC3)CNC)=CC(C4=CC=CC=C4)=N2)=O)CCC(O)=O)=O)CC1)=O	$C_{33}H_{46}N_6O_6$	622.75	1	3.23		^{n}Bu, H	4.00	46v
83c	CCCCCOC(N1CCN(C([C@@H](NC(C2=CC(N3CCC(CC3)CN(CC)CC)=CC(C4=CC=CC=C4)=N2)=O)CCC(O)=O)=O)CC1)=O	$C_{37}H_{54}N_6O_6$	678.86	1	4.74		Pentyl, H	4.00	5e
84c	CCCCCOC(N1CCN(C([C@@H](NC(C2=CC(N3CCC(C(N(CC)CC)=O)CC3)=CC(C4=CC=CC=C4)=N2)=O)CCC(O)=O)=O)CC1)=O	$C_{37}H_{52}N_6O_7$	692.84	1	4.27		Pentyl, H	4.00	5r
85c	CCCCCOC(N1CCN(C([C@@H](NC(C2=CC(NC(CN(C)C)=O)=CC(C3=CC=CC=C3)=N2)=O)CCC(OC(C)(C)C)=O)=O)CC1)=O	$C_{35}H_{50}N_6O_7$	666.81	1	3.94		Pentyl, ^{ter}Bu	4.10	75h
86c	CCCCOC(N1CCN(C([C@@H](NC(C2=CC(OCC3CCNCC3)=CC(C4=CC=CC=C4)=N2)=O)CCC(O)=O)=O)CC1)=O	$C_{32}H_{43}N_5O_7$	609.71	1	3.17		^{n}Bu, H	4.20	51q
87c	CCCCOC(N1CCN(C([C@@H](NC(C2=CC(N3CCC(C(NC(C)C)=O)CC3)=CC(C4=CC=CC=C4)=N2)=O)CCC(O)=O)=O)CC1)=O	$C_{35}H_{48}N_6O_7$	664.79	1	3.53		^{n}Bu, H	4.30	4p
88c	CCCCCOC(N1CCN(C([C@@H](NC(C2=CC(C(N3CCOCC3)=O)=CC(C4=CC=CC=C4)=N2)=O)CCC(O)=O)=O)CC1)=O	$C_{32}H_{41}N_5O_8$	623.70	1	2.66		Pentyl, H	4.40	80o
89c	CCCCOC(N1CCN(C([C@@H](NC(C2=CC(OCC3CCN(C(C)C)CC3)=CC(C4=CC=CC=C4)=N2)=O)CCC(O)=O)=O)CC1)=O	$C_{35}H_{49}N_5O_7$	651.79	1	4.29		^{n}Bu, H	4.50	71b
90c	CCCCCOC(N1CCN(C([C@@H](NC(C2=CC(OCC3CCNCC3)=CC(C4=CC=CC=C4)=N2)=O)CCC(O)=O)=O)CC1)=O	$C_{33}H_{45}N_5O_7$	623.74	1	3.56		Pentyl, H	4.50	52q

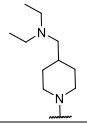
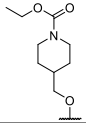
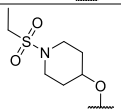
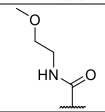
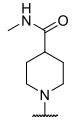
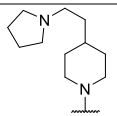
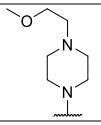
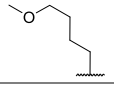
91c	CCCCCOC(N1CCN(C([C@@H](NC(C2=CC(OCC3CCN(C(C(F)(F)F)=O)CC3)=CC(C4=CC=CC=C4)=N2)=O)CCC(O)=O)=O)CC1)=O	$C_{35}H_{44}F_3N_5O_8$	719.75	1	4.36		Pentyl, H	4.50	72e
92c	CCCCCCOC(N1CCN(C([C@@H](NC(C2=CC(OCC3CCNCC3)=CC(C4=CC=CC=C4)=N2)=O)CCC(O)=O)=O)CC1)=O	$C_{34}H_{47}N_5O_7$	637.77	1	3.95		Hexyl, H	4.50	53q
93c	CCCCCOC(N1CCN(C([C@@H](NC(C2=CC(N3CCN(CC3)CCN)=CC(C4=CC=CC=C4)=N2)=O)CCC(O)=O)=O)CC1)=O	$C_{33}H_{47}N_7O_6$	637.77	1	2.26		Pentyl, H	4.50	12g
94c	CCCCCOC(N1CCN(C([C@@H](NC(C2=CC(C(NC3CCOCC3)=O)=CC(C4=CC=CC=C4)=N2)=O)CCC(O)=O)=O)CC1)=O	$C_{33}H_{43}N_5O_8$	637.72	1	3.09		Pentyl, H	4.60	80j
95c	CCCCCOC(N1CCN(C([C@@H](NC(C2=CC(NC(NCC(N(C)C)=O)=O)=CC(C3=CC=CC=C3)=N2)=O)CCC(OC(C)(C)C)=O)=O)CC1)=O	$C_{36}H_{51}N_7O_8$	709.83	1	3.65		Pentyl, ^{ter}Bu	4.70	76c
96c	CCCCCOC(N1CCN(C([C@@H](NC(C2=CC(OC(N3CCOCC3)=O)=CC(C4=CC=CC=C4)=N2)=O)CCC(O)=O)=O)CC1)=O	$C_{32}H_{41}N_5O_9$	639.70	1	3.01		Pentyl, H	4.80	57f
97c	CCCCCCOC(N1CCN(C([C@@H](NC(C2=CC(N3CCC(C(N(CC)CC)=O)CC3)=CC(C4=CC=CC=C4)=N2)=O)CCC(O)=O)=O)CC1)=O	$C_{38}H_{54}N_6O_7$	706.87	1	4.66		Hexyl, H	4.80	6r
98c	CCCCOC(N1CCN(C([C@@H](NC(C2=CC(OCCCCO)=CC(C3=CC=CC=C3)=N2)=O)CCC(O)=O)=O)CC1)=O	$C_{30}H_{40}N_4O_8$	584.66	1	2.94		^{n}Bu, H	4.90	51h
99c	CCCCCOC(N1CCN(C([C@@H](NC(C2=CC(OC(N3CCC(OC)C3)=O)=CC(C4=CC=CC=C4)=N2)=O)CCC(O)=O)=O)CC1)=O	$C_{33}H_{43}N_5O_9$	653.72	1	3.4		Pentyl, H	4.90	57g
100c	CCCCCOC(N1CCN(C([C@@H](NC(C2=CC(N3CCN(CC3)CC(N(C)C)=O)=CC(C4=CC=CC=C4)=N2)=O)CCC(O)=O)=O)CC1)=O	$C_{35}H_{49}N_7O_7$	679.81	1	2.39		Pentyl, H	4.90	12l

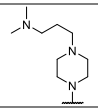
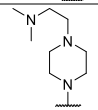
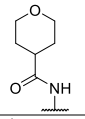
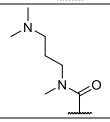
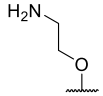
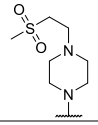
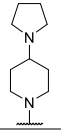
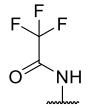
101c	CCCCOC(N1CCN(C([C@@H](NC(C2=CC(N3CCC(N(C)C)CC3)=CC(C4=CC=CC=C4)=N2)=O)CCC(O)=O)=O)CC1)=O	$C_{33}H_{46}N_6O_6$	622.75	1	3.32		^{n}Bu, H	5.00	46o
102c	CCCCCOC(N1CCN(C([C@@H](NC(C2=CC(OC3CCN(CC3)C)=CC(C4=CC=CC=C4)=N2)=O)CCC(O)=O)=O)CC1)=O	$C_{33}H_{45}N_5O_7$	623.74	1	3.66		Pentyl, H	5.00	70a
103c	CCCCCOC(N1CCN(C([C@@H](NC(C2=CC(N3CC[C@H](OCC(N(C)C)=O)C3)=CC(C4=CC=CC=C4)=N2)=O)CCC(O)=O)=O)CC1)=O	$C_{35}H_{48}N_6O_8$	680.79	1	2.87		Pentyl, H	5.00	8b, (S,S)diastereomer1
104c	CCCCCOC(N1CCN(C([C@@H](NC(C2=CC(OC3CCN(S(=O)(CC)=O)CC3)=CC(C4=CC=CC=C4)=N2)=O)CCC(O)=O)=O)CC1)=O	$C_{34}H_{47}N_5O_9S$	701.83	1	3.38		Pentyl, H	5.10	70h
105c	CCCCCOC(N1CCN(C([C@@H](NC(C2=CC(N3CCN(CC3)CC(N4CCCC4)=O)=CC(C5=CC=CC=C5)=N2)=O)CCC(O)=O)=O)CC1)=O	$C_{37}H_{51}N_7O_7$	705.84	1	2.93		Pentyl, H	5.20	12n
106c	CCCCCOC(N1CCN(C([C@@H](NC(C2=CC(OCC3CCN(CC3)CCOC)=CC(C4=CC=CC=C4)=N2)=O)CCC(O)=O)=O)CC1)=O	$C_{36}H_{51}N_5O_8$	681.82	1	3.92		Pentyl, H	5.30	72c
107c	CCCCCOC(N1CCN(C([C@@H](NC(C2=CC(OCC3CCN(CC3)C)=CC(C4=CC=CC=C4)=N2)=O)CCC(O)=O)=O)CC1)=O	$C_{34}H_{47}N_5O_7$	637.77	1	3.9		Pentyl, H	5.30	72a
108c	CCCCOC(N1CCN(C([C@@H](NC(C2=CC(OCC3CCN(S(=O)(CC)=O)CC3)=CC(C4=CC=CC=C4)=N2)=O)CCC(O)=O)=O)CC1)=O	$C_{34}H_{47}N_5O_9S$	701.83	1	3.23		^{n}Bu, H	5.30	71h
109c	CCCCOC(N1CCN(C([C@@H](NC(C2=CC(OCC3CCN(CC3)CCOC)=CC(C4=CC=CC=C4)=N2)=O)CCC(O)=O)=O)CC1)=O	$C_{35}H_{49}N_5O_8$	667.79	1	3.53		^{n}Bu, H	5.30	71c
110c	CCCCCOC(N1CCN(C([C@@H](NC(C2=CC(C(N3CCC(N(C)C)CC3)=O)=CC(C4=CC=CC=C4)=N2)=O)CCC(O)=O)=O)CC1)=O	$C_{35}H_{48}N_6O_7$	664.79	1	3.35		Pentyl, H	5.40	80q
111c	CCCCCOC(N1CCN(C([C@@H](NC(C2=CC(OC(N(C)C)=O)=CC(C3=CC=CC=C3)=N2)=O)CCC(O)=O)=O)CC1)=O	$C_{30}H_{39}N_5O_8$	597.66	1	3.24		Pentyl, H	5.50	57a

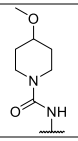
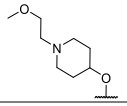
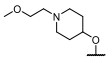
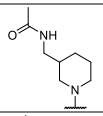
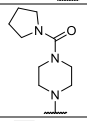
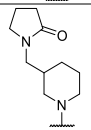
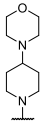
112c	CCCCCOC(N1CCN(C([C@@H](NC(C2=CC(OCC3CCN(C(C)C)CC3)=CC(C4=CC=CC=C4)=N2)=O)CCC(O)=O)=O)CC1)=O	$C_{36}H_{51}N_5O_7$	665.82	1	4.68		Pentyl, H	5.50	72b
113c	CCCCCOC(N1CCN(C([C@@H](NC(C2=CC(N3CCCCC3)=CC(C4=CC=CC=C4)=N2)=O)CCC(O)=O)=O)CC1)=O	$C_{32}H_{43}N_5O_6$	593.71	1	4.17		Pentyl, H	5.50	47i
114c	CCCCCOC(N1CCN(C([C@@H](NC(C2=CC(N3CC(N(C)C)C3)=CC(C4=CC=CC=C4)=N2)=O)CCC(O)=O)=O)CC1)=O	$C_{32}H_{44}N_6O_6$	608.73	1	2.93		Pentyl, H	5.50	9c
115c	CCCCCOC(N1CCN(C([C@@H](NC(C2=CC(N3CCCC(C3)N)=CC(C4=CC=CC=C4)=N2)=O)CCC(O)=O)=O)CC1)=O	$C_{32}H_{44}N_6O_6$	608.73	1	3.11		Pentyl, H	5.50	7e
116c	CCCCCOC(N1CCN(C([C@@H](NC(C2=CC(NCCO)=CC(C3=CC=CC=C3)=N2)=O)CCC(O)=O)=O)CC1)=O	$C_{29}H_{39}N_5O_7$	569.65	1	2.59		Pentyl, H	5.70	47e
117c	CCCCCOC(N1CCN(C([C@@H](NC(C2=CC(NC(CNC)=O)=CC(C3=CC=CC=C3)=N2)=O)CCC(OC(C)(C)C)=O)=O)CC1)=O	$C_{34}H_{48}N_6O_7$	652.78	1	3.6		Pentyl, ^{ter}Bu	5.70	75g
118c	CCCCCOC(N1CCN(C([C@@H](NC(C2=CC(NC(N3CCCCC3)=O)=CC(C4=CC=CC=C4)=N2)=O)CCC(OC(C)(C)C)=O)=O)CC1)=O	$C_{37}H_{52}N_6O_7$	692.84	2	5.46		Pentyl, ^{ter}Bu	5.80	76d
119c	CCCCCOC(N1CCN(C([C@@H](NC(C2=CC(C(N(CCCC)C)=O)=CC(C3=CC=CC=C3)=N2)=O)CCC(O)=O)=O)CC1)=O	$C_{33}H_{45}N_5O_7$	623.74	1	4.05		Pentyl, H	5.80	80g
120c	CCCCCOC(N1CCN(C([C@@H](NC(C2=CC(C(N3CCN(CC3)C)=O)=CC(C4=CC=CC=C4)=N2)=O)CCC(O)=O)=O)CC1)=O	$C_{33}H_{44}N_6O_7$	636.74	1	2.57		Pentyl, H	5.80	80r
121c	CCCCOC(N1CCN(C([C@@H](NC(C2=CC(OCCCOC)=CC(C3=CC=CC=C3)=N2)=O)CCC(O)=O)=O)CC1)=O	$C_{30}H_{40}N_4O_8$	584.66	1	3.21		^{n}Bu, H	5.90	51j
122c	CCCCCOC(N1CCN(C([C@@H](NC(C2=CC(N3CCN(C(N(C)C)=O)CC3)=CC(C4=CC=CC=C4)=N2)=O)CCC(O)=O)=O)CC1)=O	$C_{34}H_{47}N_7O_7$	665.78	1	2.99		Pentyl, H	5.90	12s

123c	CCCCCOC(N1CCN(C([C@@H](NC(C2=CC(N3CCN(CC3)CC(N(CC)CC)=O)=CC(C4=CC=CC=C4)=N2)=O)CCC(O)=O)=O)CC1)=O	$C_{37}H_{53}N_7O_7$	707.86	1	3.17		Pentyl, H	5.90	12m
124c	CCCCCOC(N1CCN(C([C@@H](NC(C2=CC(OC(N3CCC(OCC)CC3)=O)=CC(C4=CC=CC=C4)=N2)=O)CCC(O)=O)=O)CC1)=O	$C_{35}H_{47}N_5O_9$	681.78	1	4.18		Pentyl, H	6.00	57h
125c	CCCCCOC(N1CCN(C([C@@H](NC(C2=CC(N3CCC(C(NC(C)C)=O)CC3)=CC(C4=CC=CC=C4)=N2)=O)CCC(O)=O)=O)CC1)=O	$C_{36}H_{50}N_6O_7$	678.82	1	3.92		Pentyl, H	6.00	5p
126c	CCCCCOC(N1CCN(C([C@@H](NC(C2=CC(C(NCCCOC)=O)=CC(C3=CC=CC=C3)=N2)=O)CCC(O)=O)=O)CC1)=O	$C_{32}H_{43}N_5O_8$	625.71	1	2.95		Pentyl, H	6.10	80i
127c	CCCCCOC(N1CCN(C([C@@H](NC(C2=CC(NC(C)=O)=CC(C3=CC=CC=C3)=N2)=O)CCC(OC(C)(C)C)=O)=O)CC1)=O	$C_{33}H_{45}N_5O_7$	623.74	1	4.4		Pentyl, ^{ter}Bu	6.20	75a
128c	CCCCOC(N1CCN(C([C@@H](NC(C2=CC(N3CCC(C(N4CCCC4)=O)CC3)=CC(C5=CC=CC=C5)=N2)=O)CCC(O)=O)=O)CC1)=O	$C_{36}H_{48}N_6O_7$	676.80	1	3.63		^{n}Bu, H	6.30	4t
129c	CCCCCOC(N1CCN(C([C@@H](NC(C2=CC(N3CCN(CC3)CCOCCC)=CC(C4=CC=CC=C4)=N2)=O)CCC(O)=O)=O)CC1)=O	$C_{36}H_{52}N_6O_7$	680.83	1	3.73		Pentyl, H	6.30	12f
130c	CCCCCOC(N1CCN(C([C@@H](NC(C2=CC(N3CCN(C(N)=O)CC3)=CC(C4=CC=CC=C4)=N2)=O)CCC(O)=O)=O)CC1)=O	$C_{32}H_{43}N_7O_7$	637.73	1	2.38		Pentyl, H	6.30	12r
131c	CCCCCOC(N1CCN(C([C@@H](NC(C2=CC(N3CCC(NC)CC3)=CC(C4=CC=CC=C4)=N2)=O)CCC(O)=O)=O)CC1)=O	$C_{33}H_{46}N_6O_6$	622.75	1	3.37		Pentyl, H	6.50	47n
132c	CCCCCOC(N1CCN(C([C@@H](NC(C2=CC(OC3CCN(C(OCC)=O)CC3)=CC(C4=CC=CC=C4)=N2)=O)CCC(O)=O)=O)CC1)=O	$C_{35}H_{47}N_5O_9$	681.78	1	4.18		Pentyl, H	6.50	70g

133c	CCCCCOC(N1CCN(C([C@@H](NC(C2=CC(N3CCNCC3)=CC(C4=CC=CC=C4)=N2)=O)CCC(O)=O)=O)CC1)=O	$C_{31}H_{42}N_6O_6$	594.70	1	2.59		Pentyl, H	6.50	12a
134c	CCCCCOC(N1CCN(C([C@@H](NC(C2=CC(N3CCC(C(N)=O)CC3)=CC(C4=CC=CC=C4)=N2)=O)CCC(O)=O)=O)CC1)=O	$C_{33}H_{44}N_6O_7$	636.74	1	2.88		Pentyl, H	6.50	5m
135c	CCCCCOC(N1CCN(C([C@@H](NC(C2=CC(N3CCC(C(N4CCCC4)=O)CC3)=CC(C5=CC=CC=C5)=N2)=O)CCC(O)=O)=O)CC1)=O	$C_{37}H_{50}N_6O_7$	690.83	1	4.02		Pentyl, H	6.70	5t
136c	CCCCOC(N1CCN(C([C@@H](NC(C2=CC(OCCCO)=CC(C3=CC=CC=C3)=N2)=O)CCC(O)=O)=O)CC1)=O	$C_{29}H_{38}N_4O_8$	570.63	1	2.55		^{n}Bu, H	6.90	51g
137c	CCCCOC(N1CCN(C([C@@H](NC(C2=CC(OC3CCCNC3)=CC(C4=CC=CC=C4)=N2)=O)CCC(O)=O)=O)CC1)=O	$C_{31}H_{41}N_5O_7$	595.69	1	2.92		^{n}Bu, H	6.90	51o
138c	CCCCCCCOC(N1CCN(C([C@@H](NC(C2=CC=CC(C3=CC=CC=C3)=N2)=O)CCC(O)=O)=O)CC1)=O	$C_{29}H_{38}N_4O_6$	538.64	1	3.96		Heptyl, H	7.00	26f
139c	CCCCCOC(N1CCN(C([C@@H](NC(C2=CC(OC3CCN(C(C)C)CC3)=CC(C4=CC=CC=C4)=N2)=O)CCC(O)=O)=O)CC1)=O	$C_{35}H_{49}N_5O_7$	651.79	1	4.43		Pentyl, H	7.00	70b
140c	CCCCCOC(N1CCN(C([C@@H](NC(C2=CC(N3CC(C3)CNC)=CC(C4=CC=CC=C4)=N2)=O)CCC(O)=O)=O)CC1)=O	$C_{32}H_{44}N_6O_6$	608.73	1	2.84		Pentyl, H	7.10	9e
141c	CCCCCOC(N1CCN(C([C@@H](NC(C2=CC(N3CCCC(C3)CN4CCCC4)=CC(C5=CC=CC=C5)=N2)=O)CCC(O)=O)=O)CC1)=O	$C_{37}H_{52}N_6O_6$	676.85	1	4.5		Pentyl, H	7.30	7g
142c	CCCCCOC(N1CCN(C([C@@H](NC(C2=CC(OCC3CCN(S(=O)(CC)=O)CC3)=CC(C4=CC=CC=C4)=N2)=O)CCC(O)=O)=O)CC1)=O	$C_{35}H_{49}N_5O_9S$	715.86	1	3.62		Pentyl, H	7.40	72h
143c	CCCCCOC(N1CCN(C([C@@H](NC(C2=CC(C(N)=O)=CC(C3=CC=CC=C3)=N2)=O)CCC(O)=O)=O)CC1)=O	$C_{28}H_{35}N_5O_7$	553.61	1	2.28		Pentyl, H	7.50	80a

144c	CCCCOC(N1CCN(C([C@@H](NC(C2=CC(N3CCC(CC3)CN(CC)CC)=CC(C4=CC=CC=C4)=N2)=O)CCC(O)=O)=O)CC1)=O	$C_{36}H_{52}N_6O_6$	664.83	1	4.35		^{n}Bu, H	7.50	4e
145c	CCCCOC(N1CCN(C([C@@H](NC(C2=CC(OCC3CCN(C(OCC)=O)CC3)=CC(C4=CC=CC=C4)=N2)=O)CCC(O)=O)=O)CC1)=O	$C_{35}H_{47}N_5O_9$	681.78	1	4.04		^{n}Bu, H	7.60	71g
146c	CCCCOC(N1CCN(C([C@@H](NC(C2=CC(OC3CCN(S(=O)(CC)=O)CC3)=CC(C4=CC=CC=C4)=N2)=O)CCC(O)=O)=O)CC1)=O	$C_{33}H_{45}N_5O_9S$	687.80	1	2.99		^{n}Bu, H	7.60	69h
147c	CCCCCOC(N1CCN(C([C@@H](NC(C2=CC(OC(N3CCCC3)=O)=CC(C4=CC=CC=C4)=N2)=O)CCC(O)=O)=O)CC1)=O	$C_{32}H_{41}N_5O_8$	623.70	1	3.78		Pentyl, H	7.70	57d
148c	CCCCCOC(N1CCN(C([C@@H](NC(C2=CC(C(NCCOC)=O)=CC(C3=CC=CC=C3)=N2)=O)CCC(O)=O)=O)CC1)=O	$C_{31}H_{41}N_5O_8$	611.69	1	2.56		Pentyl, H	7.90	80h
149c	CCCCCOC(N1CCN(C([C@@H](NC(C2=CC(OCC)=CC(C3=CC=CC=C3)=N2)=O)CCC(O)=O)=O)CC1)=O	$C_{29}H_{38}N_4O_7$	554.63	1	3.58		Pentyl, H	7.90	52c
150c	CCCCCOC(N1CCN(C([C@@H](NC(C2=CC(N3CCC(C(NC)=O)CC3)=CC(C4=CC=CC=C4)=N2)=O)CCC(O)=O)=O)CC1)=O	$C_{34}H_{46}N_6O_7$	650.77	1	3.15		Pentyl, H	7.90	5n
151c	CCCCCOC(N1CCN(C([C@@H](NC(C2=CC(N3CCC(CC3)CCN4CCCC4)=CC(C5=CC=CC=C5)=N2)=O)CCC(O)=O)=O)CC1)=O	$C_{38}H_{54}N_6O_6$	690.87	1	4.89		Pentyl, H	8.00	5j
152c	CCCCCOC(N1CCN(C([C@@H](NC(C2=CC(N3CCN(CC3)CCOC)=CC(C4=CC=CC=C4)=N2)=O)CCC(O)=O)=O)CC1)=O	$C_{34}H_{48}N_6O_7$	652.78	1	2.95		Pentyl, H	8.30	12e
153c	CCCCCOC(N1CCN(C([C@@H](NC(C2=CC(CCCCOC)=CC(C3=CC=CC=C3)=N2)=O)CCC(O)=O)=O)CC1)=O	$C_{32}H_{44}N_4O_7$	596.71	1	4.15		Pentyl, H	8.30	83f
154c	CCCCCCOC(N1CCN(C([C@@H](NC(C2=CC(OCCN)=CC(C3=CC=CC=C3)=N2)=O)CCC(O)=O)=O)CC1)=O	$C_{30}H_{41}N_5O_7$	583.68	1	2.91		Hexyl, H	8.40	53m

155c	CCCCCOC(N1CCN(C([C@@H](NC(C2=CC(CCCOC)=CC(C3=CC=CC=C3)=N2)=O)CCC(O)=O)=O)CC1)=O	$C_{31}H_{42}N_4O_7$	582.69	1	3.76		Pentyl, H	8.40	83e
156c	CCCCCOC(N1CCN(C([C@@H](NC(C2=CC(N3CCN(CC3)CCCN(C)C)=CC(C4=CC=CC=C4)=N2)=O)CCC(O)=O)=O)CC1)=O	$C_{36}H_{53}N_7O_6$	679.85	1	3.26		Pentyl, H	8.40	12i
157c	CCCCCOC(N1CCN(C([C@@H](NC(C2=CC(N3CCN(CC3)CCN(C)C)=CC(C4=CC=CC=C4)=N2)=O)CCC(O)=O)=O)CC1)=O	$C_{35}H_{51}N_7O_6$	665.82	1	2.87		Pentyl, H	8.50	12h
158c	CCCCCOC(N1CCN(C([C@@H](NC(C2=CC(NC(C3CCOCC3)=O)=CC(C4=CC=CC=C4)=N2)=O)CCC(OC(C)(C)C)=O)=O)CC1)=O	$C_{34}H_{47}N_5O_7$	693.83	1	4.81		Pentyl, ^{ter}Bu	8.50	75c
159c	CCCCCOC(N1CCN(C([C@@H](NC(C2=CC(C(N(CCCN(C)C)C)=O)=CC(C3=CC=CC=C3)=N2)=O)CCC(O)=O)=O)CC1)=O	$C_{37}H_{51}N_5O_8$	652.78	1	3.21		Pentyl, H	8.60	80l
160c	CCCCCOC(N1CCN(C([C@@H](NC(C2=CC(CC3CCCCC3)=CC(C4=CC=CC=C4)=N2)=O)CCC(O)=O)=O)CC1)=O	$C_{34}H_{48}N_6O_7$	606.75	2	5.31		Pentyl, H	8.60	83a
161c	CCCCCOC(N1CCN(C([C@@H](NC(C2=CC(OCCN)=CC(C3=CC=CC=C3)=N2)=O)CCC(O)=O)=O)CC1)=O	$C_{34}H_{46}N_4O_6$	569.65	1	2.52		Pentyl, H	8.80	52m
162c	CCCCCOC(N1CCN(C([C@@H](NC(C2=CC(N3CCN(CC3)CCS(C)(=O)=O)=CC(C4=CC=CC=C4)=N2)=O)CCC(O)=O)=O)CC1)=O	$C_{34}H_{48}N_6O_8S$	700.85	1	2.35		Pentyl, H	8.90	12j
163c	CCCCCOC(N1CCN(C([C@@H](NC(C2=CC(N3CCC(N4CCCC4)CC3)=CC(C5=CC=CC=C5)=N2)=O)CCC(O)=O)=O)CC1)=O	$C_{29}H_{39}N_5O_7$	662.82	1	4.25		Pentyl, H	9.00	47p
164c	CCCCCOC(N1CCN(C([C@@H](NC(C2=CC(NC(C(F)(F)F)=O)=CC(C3=CC=CC=C3)=N2)=O)CCC(OC(C)(C)C)=O)=O)CC1)=O	$C_{28}H_{37}N_5O_4S$	677.71	1	4.94		Pentyl, ^{ter}Bu	9.10	75b

165c	CCCCCOC(N1CCN(C([C@@H](NC(C2=CC(NC(N3CCC(OC)CC3)=O)=CC(C4=CC=CC=C4)=N2)=O)CCC(OC(C)(C)C)=O)=O)CC1)=O	$C_{33}H_{42}F_3N_5O_7$	722.87	2	5.08		Pentyl, *ter*Bu	9.20	76f
166c	CCCCOC(N1CCN(C([C@@H](NC(C2=CC(OC3CCN(CC3)CCOC)=CC(C4=CC=CC=C4)=N2)=O)CCC(O)=O)=O)CC1)=O	$C_{38}H_{54}N_6O_8$	653.77	1	3.28		nBu, H	9.40	69c
167c	CCCCCCOC(N1CCN(C([C@@H](NC(C2=CC(OC3CCNCC3)=CC(C4=CC=CC=C4)=N2)=O)CCC(O)=O)=O)CC1)=O	$C_{34}H_{47}N_5O_8$	623.74	1	3.7		nHex, H	9.40	53n
168c	CCCCCOC(N1CCN(C([C@@H](NC(C2=CC(NCCOC)=CC(C3=CC=CC=C3)=N2)=O)CCC(O)=O)=O)CC1)=O	$C_{33}H_{45}N_5O_7$	583.68	1	3.24		Pentyl, H	9.80	47g
169c	CCCCCOC(N1CCN(C([C@@H](NC(C2=CC(OCCOC)=CC(C3=CC=CC=C3)=N2)=O)CCC(O)=O)=O)CC1)=O	$C_{30}H_{41}N_5O_7$	584.66	1	3.21		Pentyl, H	9.90	52i
170c	CCCCCOC(N1CCN(C([C@@H](NC(C2=CC(OC3CCN(CC3)CCOC)=CC(C4=CC=CC=C4)=N2)=O)CCC(O)=O)=O)CC1)=O	$C_{30}H_{40}N_4O_8$	667.79	1	3.67		Pentyl, H	9.90	70c
171c	CCCCCOC(N1CCN(C([C@@H](NC(C2=CC(N3CCCC(C3)CNC(C)=O)=CC(C4=CC=CC=C4)=N2)=O)CCC(O)=O)=O)CC1)=O	$C_{35}H_{48}N_6O_7$	664.79	1	3.54		Pentyl, H	9.90	7h
172c	CCCCCOC(N1CCN(C([C@@H](NC(C2=CC(N3CCN(C(N4CCCC4)=O)CC3)=CC(C5=CC=CC=C5)=N2)=O)CCC(O)=O)=O)CC1)=O	$C_{36}H_{49}N_7O_7$	691.82	1	3.52		Pentyl, H	10.00	12u
173c	CCCCCOC(N1CCN(C([C@@H](NC(C2=CC(N3CCCC(C3)CN4CCCC4=O)=CC(C5=CC=CC=C5)=N2)=O)CCC(O)=O)=O)CC1)=O	$C_{37}H_{50}N_6O_7$	690.83	1	4.02		Pentyl, H	10.00	7i
174c	CCCCOC(N1CCN(C([C@@H](NC(C2=CC(OC3CCN(C(C)C)CC3)=CC(C4=CC=CC=C4)=N2)=O)CCC(O)=O)=O)CC1)=O	$C_{35}H_{49}N_5O_8$	637.77	1	4.04		nBu, H	10.00	69b
175c	CCCCCOC(N1CCN(C([C@@H](NC(C2=CC(C(NC)=O)=CC(C3=CC=CC=C3)=N2)=O)CCC(O)=O)=O)CC1)=O	$C_{34}H_{47}N_5O_7$	567.63	1	2.54		Pentyl, H	10.00	80b
176c	CCCCCOC(N1CCN(C([C@@H](NC(C2=CC(N3CCC(N4CCOCC4)CC3)=CC(C5=CC=CC=C5)=N2)=O)CCC(O)=O)=O)CC1)=O	$C_{29}H_{37}N_5O_7$	678.82	1	3.48		Pentyl, H	10.00	47q

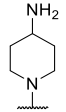
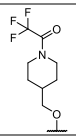
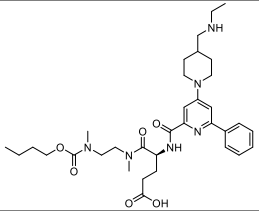
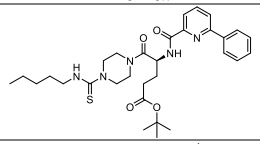
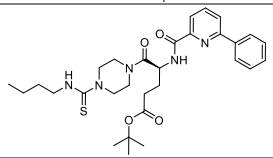
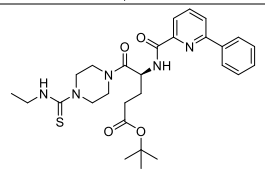
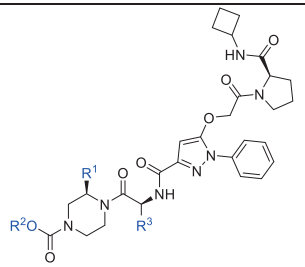
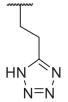
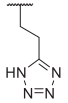
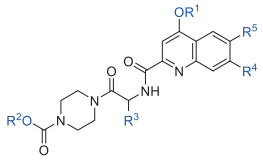
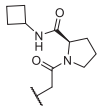
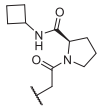
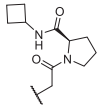
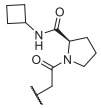
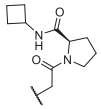
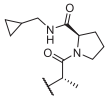
177c	CCCCOC(N1CCN(C([C@@H](NC(C2=CC(OC3CCOCC3)=CC(C4=CC=CC=C4)=N2)=O)CCC(O)=O)=O)CC1)=O	$C_{36}H_{50}N_6O_7$	596.67	1	3.35		^{n}Bu, H	10.00	51k
178c	CCOC(N1CCN(C([C@@H](NC(C2=CC(N3CCC(CC3)N)=CC(C4=CC=CC=C4)=N2)=O)CCC(O)=O)=O)CC1)=O	$C_{31}H_{40}N_4O_8$	566.65	1	1.94		Et, H	10.00	45m
179c	CCCCOC(N1CCN(C([C@@H](NC(C2=CC(OCC3CCN(C(C(F)(F)F)=O)CC3)=CC(C4=CC=CC=C4)=N2)=O)CCC(O)=O)=O)CC1)=O	$C_{29}H_{38}N_6O_6$	705.72	1	3.97		^{n}Bu, H	10.00	71e
180c	CCCCOC(N(CCN(C([C@@H](NC(C1=CC(N2CCC(CC2)CNCC)=CC(C3=CC=CC=C3)=N1)=O)CCC(O)=O)=O)C)C)=O	$C_{34}H_{50}N_6O_6$	638.81	1	3.62			3.80	4c
181c	CCCCCNC(N1CCN(C([C@@H](NC(C2=CC=CC(C3=CC=CC=C3)=N2)=O)CCC(OC(C)(C)C)=O)=O)CC1)=S	$C_{31}H_{43}N_5O_4S$	581.77	1	4.18			6.00	20aa
182c	CCCCNC(N1CCN(C([C@@H](NC(C2=CC=CC(C3=CC=CC=C3)=N2)=O)CCC(OC(C)(C)C)=O)=O)CC1)=S	$C_{30}H_{41}N_5O_4S$	567.74	1	3.79			8.00	20z
183c	CCNC(N1CCN(C([C@@H](NC(C2=CC=CC(C3=CC=CC=C3)=N2)=O)CCC(OC(C)(C)C)=O)=O)CC1)=S	$C_{36}H_{50}N_6O_6$	539.69	1	3.01			9.00	20x

Table S7. Scaffold II: Piperazinyl-glutamate-**phenyl-pyrazole** derivatives (10 compounds).[55]

ID	Smiles	Chemical formula	MW (g/mol)	#RO5 Violation	AlogP	Structure		Affinity (K_i) in nM	Compound number in original publication
									
						R^1, R^2	**R^3**		
1d	CCCCOC(N1CCN(C([C@@H](NC(C2=NN(C3=CC=CC=C3)C(OCC(N4CCC[C@@H]4C(NC5CCC5)=O)=O)=C2)=O)CCC(O)=O)=O)CC1)=O	$C_{35}H_{47}N_7O_9$	709.79	1	1.95	H, ^{n}Bu		0.8	19k
2d	CCCCOC(N1CCN(C([C@@H](NC(C2=NN(C3=CC=CC=C3)C(OCC(N4CCC[C@H]4C(NC5CCC5)=O)=O)=C2)=O)CCC6=NN=NN6)=O)CC1)=O	$C_{35}H_{47}N_{11}O_7$	733.82	2	1.24	H, ^{n}Bu		1.5	20d
3d	CCCOC(N1CCN(C([C@@H](NC(C2=NN(C3=CC=CC=C3)C(OCC(N4CCC[C@H]4C(NC5CCC5)=O)=O)=C2)=O)CCC(O)=O)=O)CC1)=O	$C_{34}H_{45}N_7O_9$	695.76	1	1.56	H, Propyl		3.1	19j
4d	CCOC(N1CCN(C([C@@H](NC(C2=NN(C3=CC=CC=C3)C(OCC(N4CCC[C@H]4C(NC5CCC5)=O)=O)=C2)=O)CCC6=NN=NN6)=O)CC1)=O	$C_{33}H_{43}N_{11}O_7$	705.76	2	0.46	H, Et		5	20c
5d	OC(CC[C@@H](C(N1CCN(C(OC2CCC2)=O)CC1)=O)NC(C3=NN(C4=CC=CC=C4)C(OCC(N5CCC[C@H]5C(NC6CCC6)=O)=O)=C3)=O)=O	$C_{35}H_{45}N_7O_9$	707.77	1	1.71	H, ^{Cyc}Bu		5	19l
6d	OC(CC[C@@H](C(N1CCN(C(OCC2=CC=CC=C2)=O)CC1)=O)NC(C3=NN(C4=CC=CC=C4)C(OCC(N5CCC[C@H]5C(NC6CCC6)=O)=O)=C3)=O)=O	$C_{38}H_{45}N_7O_9$	743.81	1	2.36	H, Benzyl (Bn)		5.7	19h
7d	CCCCOC(N1CCN(C([C@@H](NC(C2=NN(C3=CC=CC=C3)C(OCC(N4CCC[C@H]4C(NC5CCC5)=O)=O)=C2)=O)CCCO)=O)CC1)=O	$C_{35}H_{49}N_7O_8$	695.81	1	1.86	H, ^{n}Bu		6.5	20h
8d	CCOC(N1CCN(C([C@@H](NC(C2=NN(C3=CC=CC=C3)C(OCC(N4CCC[C@H]4C(NC5CCC5)=O)=O)=C2)=O)CCC(O)=O)=O)CC1)=O	$C_{33}H_{43}N_7O_9$	681.74	1	1.17	H, Et		7.3	18i

9d	CCCCOC(N1CCN(C(CNC(C2=NN(C3=CC=CC=C3)C(OCC(N4CCC[C@H]4C(NC5CCC5)=O)=O)=C2)=O)=O)CC1)=O	$C_{32}H_{43}N_7O_7$	637.73	1	1.72	H, ^{n}Bu	H	7.7	20o
10d	CCOC(N1CCN(C([C@@H](NC(C2=NN(C3=CC=CC=C3)C(OCC(N4CCC[C@H]4C(NC5CCC5)=O)=O)=C2)=O)CCC(O)=O)=O)[C@@H](C1)C)=O	$C_{34}H_{45}N_7O_9$	695.76	1	1.56	CH_3, Et		7.7	19m

Table S8. Scaffold II: Piperazinyl-glutamate-**quinoline** derivatives (8 compounds).[56]

ID	Smiles	Chemical formula	MW (g/mol)	#RO5 Violation	AlogP	Structure				Affinity (IC_{50}) in nM	Compound number in original publication
											
						R^1	**R^2**	**R^3**	**R^4, R^5**		
1e	CC1=CC2=C(C(OCC(N3CCC[C@@H]3C(NC4CCC4)=O)=O)=CC(C(NCC(N5CCN(C(OCCC(F)(F)F)=O)CC5)=O)=O)=N2)C=C1	$C_{32}H_{39}F_3N_6O_7$	676.69	1	2.54			H	CH_3, H	3	BDBM1194 28
2e	CCCCOC(N1CCN(C([C@@H](NC(C2=NC3=C(C=CC(C)=C3)C(OCC(N4CCC[C@H]4C(NC5CCC5)=O)=O)=C2)=O)CCO)=O)CC1)=O	$C_{35}H_{48}N_6O_8$	680.79	1	2.14		^{n}Bu		CH_3, H	4	BDBM1194 26
3e	CCCCOC(N1CCN(C([C@@H](NC(C2=NC3=C(C=CC(C)=C3)C(OCC(N4CCC[C@H]4C(NC5CCC5)=O)=O)=C2)=O)CO)=O)CC1)=O	$C_{34}H_{46}N_6O_8$	666.76	1	1.75		^{n}Bu		CH_3, H	4	BDBM1194 31
4e	CCCOC(N1CCN(C([C@@H](NC(C2=NC3=C(C=CC(C)=C3)C(OCC(N4CCC[C@H]4C(NC5CCC5)=O)=O)=C2)=O)CCC(OC)=O)=O)CC1)=O	$C_{36}H_{48}N_6O_9$	708.80	1	2.32		Propyl		CH_3, H	5	BDBM1194 27
5e	CCCCOC(N1CCN(C(CNC(C2=NC3=C(C=CC=C3)C(OCC(N4CCC[C@H]4C(NC5CCC5)=O)=O)=C2)=O)=O)CC1)=O	$C_{32}H_{42}N_6O_7$	622.71	1	2.08		^{n}Bu	H	H, H	5	BDBM1194 29
6e	CCOC(N1CCN(C([C@@H](NC(C2=NC3=C(C=CC(C)=C3)C(O[C@@H](C(N4CCC[C@H]4C(NCC5CC5)=O)=O)C)=C2)=O)CCC(O)=O)=O)CC1)=O	$C_{35}H_{46}N_6O_9$	694.77	1	2.09		Et		CH_3, H	5	BDBM1194 24
7e	CCOC(N1CCN(C([C@@H](NC(C2=NC3=C(C=CC(C)=C3)C(OC(C)(C(O)=O)C)=C2)=O)CCC(O)=O)=O)CC1)=O	$C_{27}H_{34}N_4O_9$	558.58	1	2.05		Et		CH_3, H	5.30	BX048

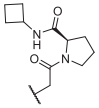
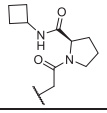
8e	CCCCOC(N1CCN(C([C@@H](NC(C2=NC3=C(C=CC(C)=C3)C(OCC(N4CCC[C@H]4C(NC5CCC5)=O)=O)=C2)=O)CCC6=NN=NN6)=O)CC1)=O	$C_{36}H_{48}N_{10}O_7$	732.83	2	1.91		^{n}Bu		CH_3, H	8	BDBM119430
9e	CCOC(N1CCN(C([C@@H](NC(C2=NC3=C(C=C(C(C)=C3)F)C(OCC(N4CCC[C@H]4C(NC5CCC5)=O)=O)=C2)=O)CC(O)=O)=O)CC1)=O	$C_{33}H_{41}FN_6O_9$	684.71	1	1.59		Et		CH_3, F	9	BDBM119422

Table S9. Scaffold III: 6-Azetidin-1-yl nicotinate derivatives (5 compounds).[57,58]

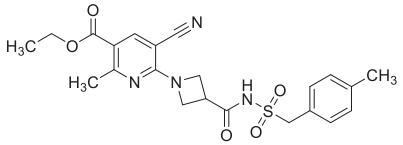
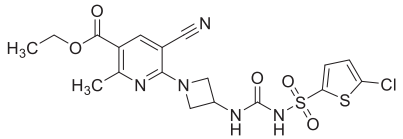
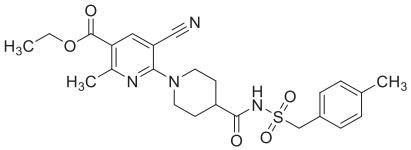
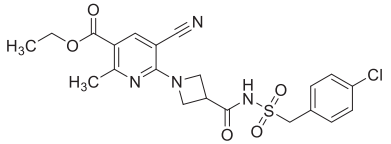
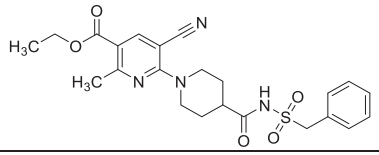
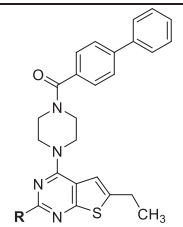
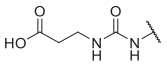
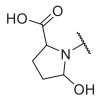
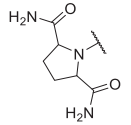
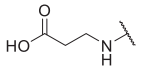
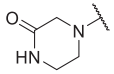
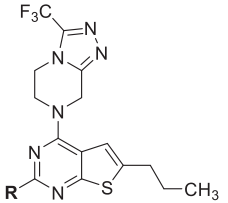
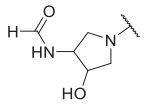
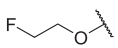
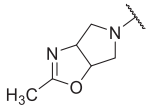
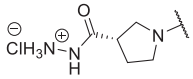
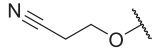
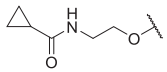
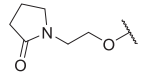
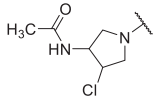
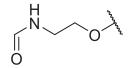
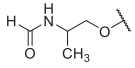
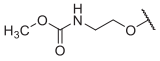
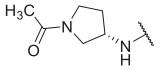
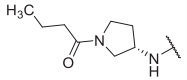
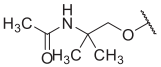
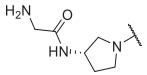
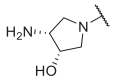
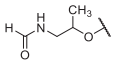
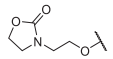
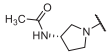
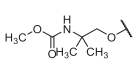
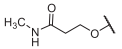
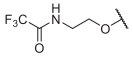
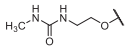
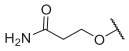
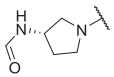
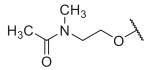
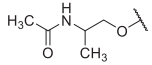
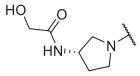
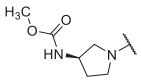
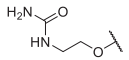
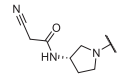
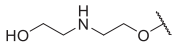
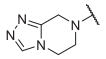
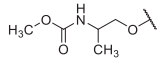
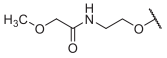
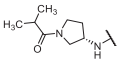
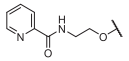
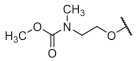
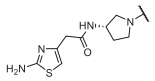
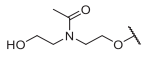
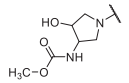
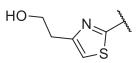
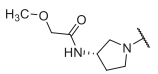
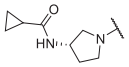
ID	Smiles	Chemical formula	MW (g/mol)	#RO5 Violation	AlogP	Structure	Affinity (IC_{50}) in nM	Compound number in original publication
2f	CCOC(C1=C(C)N=C(N2CC(C(NS(=O)(CC3=CC=C(C)C=C3)=O)=O)C2)C(C#N)=C1)=O	$C_{22}H_{24}N_4O_5S$	456.52	0	1.83		6	21
3f	CCOC(C1=C(C)N=C(N2CC(NC(NS(=O)(C3=CC=C(S3)Cl)=O)=O)C2)C(C#N)=C1)=O	$C_{18}H_{18}ClN_5O_5S_2$	483.95	0	2.03		6.3	3
4f	CCOC(C1=C(C)N=C(N2CCC(C(NS(=O)(CC3=CC=C(C)C=C3)=O)=O)CC2)C(C#N)=C1)=O	$C_{24}H_{28}N_4O_5S$	484.57	0	2.61		7	27
5f	CCOC(C1=C(C)N=C(N2CC(C(NS(=O)(CC3=CC=C(Cl)C=C3)=O)=O)C2)C(C#N)=C1)=O	$C_{21}H_{21}ClN_4O_5S$	476.93	0	2.17		10	19
1f	CCOC(C1=C(C)N=C(N2CCC(C(NS(=O)(CC3=CC=CC=C3)=O)=O)CC2)C(C#N)=C1)=O	$C_{23}H_{26}N_4O_5S$	470.54	0	2.3		11	3

Table S10. Scaffold IV: Piperazinyl thienopyrimidine derivatives (55 compounds).[59–61]

ID	Smiles	Chemical formula	MW (g/mol)	#RO5 Violation	AlogP	Structure	Affinity (IC_{50}) in nM	Compound number in original publication
						 **R**		
1g	CCC1=CC2=C(S1)N=C(NC(NCCC(O)=O)=O)N=C2N3CCN(C(C4=CC=C(C5=CC=CC=C5)C=C4)=O)CC3	$C_{29}H_{30}N_6O_4S$	558.65	1	4.48		3	21k
3g	CCC1=CC2=C(S1)N=C(N3C[C@H](C[C@H]3C(O)=O)O)N=C2N4CCN(C(C5=CC=C(C6=CC=CC=C6)C=C5)=O)CC4	$C_{30}H_{31}N_5O_4S$	557.66	1	3.91		3	15h
2g	CCC1=CC2=C(S1)N=C(N3[C@@H](C(N)=O)CC[C@H]3C(N)=O)N=C2N4CCN(C(C5=CC=C(C6=CC=CC=C6)C=C5)=O)CC4	$C_{31}H_{33}N_7O_3S$	583.70	1	3.19		4	15k
4g	CCC1=CC2=C(S1)N=C(NCCC(O)=O)N=C2N3CCN(C(C4=CC=C(C5=CC=CC=C5)C=C4)=O)CC3	$C_{28}H_{29}N_5O_3S$	515.63	1	4.77		8	15c
6g	CCC1=CC2=C(S1)N=C(N3CC(NCC3)=O)N=C2N4CCN(CC4)C(C5=CC=C(C=C5)C6=CC=CC=C6)=O	$C_{29}H_{30}N_6O_2S$	526.66	–	–		9	23
						 **R**		

7g	CCCC1=CC2=C(N3CC4=NN=C(C(F)(F)F)N4CC3)N=C(N5CC(O)C(NC([H])=O)C5)N=C2S1	$C_{20}H_{23}F_3N_8O_2S$	496.51	–	–		0.16	9-28
5g	CCCC1=CC2=C(N3CC4=NN=C(C(F)(F)F)N4CC3)N=C(OCCF)N=C2S1	$C_{17}H_{18}F_4N_6OS$	430.43	–	–		0.3	9-83
8g	CCCC1=CC2=C(N3CC4=NN=C(C(F)(F)F)N4CC3)N=C(N5CC6C(N=C(C)O6)C5)N=C2S1	$C_{21}H_{23}F_3N_8OS$	492.53	–	–		0.3	9-30
9g	CCCC1=CC2=C(N3CC4=NN=C(C(F)(F)F)N4CC3)N=C(N5C[C@@H](C(N[NH3+])=O)CC5)N=C2S1.[Cl-]	$C_{20}H_{25}ClF_3N_9OS$	531.99	–	–		0.6	9-72
10g	CCCC1=CC2=C(N3CC4=NN=C(C(F)(F)F)N4CC3)N=C(OCCC#N)N=C2S1	$C_{18}H_{18}F_3N_7OS$	437.45	–	–		0.7	9-71
11g	CCCC1=CC2=C(N3CC4=NN=C(C(F)(F)F)N4CC3)N=C(OCCNC(C5CC5)=O)N=C2S1	$C_{21}H_{24}F_3N_7O_2S$	495.53	–	–		1.5	3-59
12g	CCCC1=CC2=C(N3CC4=NN=C(C(F)(F)F)N4CC3)N=C(OCCN5CCCC5=O)N=C2S1	$C_{21}H_{24}F_3N_7O_2S$	495.53	–	–		1.9	3-62
13g	CCCC1=CC2=C(N3CC4=NN=C(C(F)(F)F)N4CC3)N=C(N5CC(Cl)C(NC(C)=O)C5)N=C2S1	$C_{21}H_{24}ClF_3N_8OS$	528.98	–	–		2.2	9-29
14g	CCCC1=CC2=C(N3CC4=NN=C(C(F)(F)F)N4CC3)N=C(OCCNC=O)N=C2S1	$C_{18}H_{20}F_3N_7O_2S$	455.46	–	–		3.0	9-23
15g	CCCC1=CC2=C(N3CC4=NN=C(C(F)(F)F)N4CC3)N=C(OCC(C)NC([H])=O)N=C2S1	$C_{19}H_{22}F_3N_7O_2S$	469.49	–	–		3.0	9-75
16g	CCCC1=CC2=C(N3CC4=NN=C(C(F)(F)F)N4CC3)N=C(OCCNC(OC)=O)N=C2S1	$C_{19}H_{22}F_3N_7O_3S$	485.49	–	–		3.0	9-19
17g	CCCC1=CC2=C(N3CC4=NN=C(C(F)(F)F)N4CC3)N=C(N[C@H]5CCN(C(C)=O)C5)N=C2S1	$C_{21}H_{25}F_3N_8OS$	494.54	–	–		3.0	8-13
18g	CCCC1=CC2=C(N3CC4=NN=C(C(F)(F)F)N4CC3)N=C(N[C@H]5CCN(C(CCC)=O)C5)N=C2S1	$C_{23}H_{29}F_3N_8OS$	522.60	–	–		3.0	8-14
19g	CCCC1=CC2=C(N3CC4=NN=C(C(F)(F)F)N4CC3)N=C(OCC(C)(C)NC(C)=O)N=C2S1	$C_{21}H_{26}F_3N_7O_2S$	497.54	–	–		3.4	9-79
20g	CCCC1=CC2=C(N3CC4=NN=C(C(F)(F)F)N4CC3)N=C(N5C[C@@H](NC(CN)=O)CC5)N=C2S1	$C_{21}H_{26}F_3N_9OS$	509.56	–	–		3.5	1-101

21g	CCCC1=CC2=C(N3CC4=NN=C(C(F)(F)F)N4CC3)N=C(N5C[C@@H](N)[C@@H](O)C5)N=C2S1	$C_{19}H_{23}F_3N_8OS$	468.50	–	–		3.8	1-114
22g	O=C([H])NCC(C)OC1=NC(N2CC3=NN=C(C(F)(F)F)N3CC2)=C4C(SC(CCC)=C4)=N1	$C_{19}H_{22}F_3N_7O_2S$	469.49	–	–		3.8	9-74
23g	CCCC1=CC2=C(N3CC4=NN=C(C(F)(F)F)N4CC3)N=C(N5CCS(CC5)(=O)=O)N=C2S1	$C_{19}H_{22}F_3N_7O_2S_2$	501.55	–	–		3.9	1-124
24g	CCCC1=CC2=C(N3CC4=NN=C(C(F)(F)F)N4CC3)N=C(OCCN5CCOC5=O)N=C2S1	$C_{20}H_{22}F_3N_7O_3S$	497.50	–	–		4.0	9-99
25g	CCCC1=CC2=C(N3CC4=NN=C(C(F)(F)F)N4CC3)N=C(CC(N)=O)N=C2S1	$C_{17}H_{18}F_3N_7OS$	425.43	–	–		4.2	4-55
26g	CCCC1=CC2=C(N3CC4=NN=C(C(F)(F)F)N4CC3)N=C(N5C[C@@H](NC(C)=O)CC5)N=C2S1	$C_{21}H_{25}F_3N_8OS$	494.54	–	–		4.4	1-105
27g	CCCC1=CC2=C(N3CC4=NN=C(C(F)(F)F)N4CC3)N=C(OCC(C)(C)NC(OC)=O)N=C2S1	$C_{21}H_{26}F_3N_7O_3S$	513.54	–	–		5.0	9-82
28g	CCCC1=CC2=C(N3CC4=NN=C(C(F)(F)F)N4CC3)N=C(OCCC(NC)=O)N=C2S1	$C_{19}H_{22}F_3N_7O_2S$	469.49	–	–		5.2	9-66
29g	CCCC1=CC2=C(N3CC4=NN=C(C(F)(F)F)N4CC3)N=C(OCCNC(C(F)(F)F)=O)N=C2S1	$C_{19}H_{19}F_6N_7O_2S$	523.46	–	–		5.4	3-61
30g	CCCC1=CC2=C(N3CC4=NN=C(C(F)(F)F)N4CC3)N=C(OCCNC(NC)=O)N=C2S1	$C_{19}H_{23}F_3N_8O_2S$	484.50	–	–		5.7	9-25
31g	CCCC1=CC2=C(N3CC4=NN=C(C(F)(F)F)N4CC3)N=C(OCCC(N)=O)N=C2S1	$C_{18}H_{20}F_3N_7O_2S$	455.46	–	–		6.0	9-70
32g	CCCC1=CC2=C(N3CC4=NN=C(C(F)(F)F)N4CC3)N=C(N5C[C@@H](NC=O)CC5)N=C2S1	$C_{20}H_{23}F_3N_8OS$	480.51	–	–		6.0	9-21
33g	CCCC1=CC2=C(N3CC4=NN=C(C(F)(F)F)N4CC3)N=C(OCCN(C)C(C)=O)N=C2S1	$C_{20}H_{24}F_3N_7O_2S$	483.51	–	–		6.0	9-97
34g	CCCC1=CC2=C(N3CC4=NN=C(C(F)(F)F)N4CC3)N=C(OCC(C)NC(C)=O)N=C2S1	$C_{20}H_{24}F_3N_7O_2S$	483.51	–	–		6.0	9-77
35g	CCCC1=CC2=C(N3CC4=NN=C(C(F)(F)F)N4CC3)N=C(N5C[C@@H](NC(CO)=O)CC5)N=C2S1	$C_{21}H_{25}F_3N_8O_2S$	510.54	–	–		6.0	1-100
36g	CCCC1=CC2=C(N3CC4=NN=C(C(F)(F)F)N4CC3)N=C(N5C[C@H](NC(OC)=O)CC5)N=C2S1	$C_{21}H_{25}F_3N_8O_2S$	510.54	–	–		6.0	9-20
37g	CCCC1=CC2=C(N3CC4=NN=C(C(F)(F)F)N4CC3)N=C(CC(N)=S)N=C2S1	$C_{17}H_{18}F_3N_7S_2$	441.50	–	–		6.4	4-56

38g	CCCC1=CC2=C(N3CC4=NN=C(C(F)(F)F)N4CC3)N=C(OCCNC(N)=O)N=C2S1	$C_{18}H_{21}F_3N_8O_2S$	470.48	–	–		6.5	9-27
39g	CCCC1=CC2=C(N3CC4=NN=C(C(F)(F)F)N4CC3)N=C(N5C[C@@H](NC(CC#N)=O)CC5)N=C2S1	$C_{22}H_{24}F_3N_9OS$	519.55	–	–		6.6	1-103
40g	CCCC1=CC2=C(N3CC4=NN=C(C(F)(F)F)N4CC3)N=C(NC5CNC5)N=C2S1	$C_{18}H_{21}F_3N_8S$	438.48	–	–		7.0	1-83
41g	CCCC1=CC2=C(N3CC4=NN=C(C(F)(F)F)N4CC3)N=C(OCCNCCO)N=C2S1	$C_{19}H_{24}F_3N_7O_2S$	471.50	–	–		7.0	3-60
42g	CCCC1=CC2=C(N3CC4=NN=C(C(F)(F)F)N4CC3)N=C(N5CC6=NN=CN6CC5)N=C2S1	$C_{20}H_{21}F_3N_{10}S$	490.51	–	–		7.0	1-75
43g	CCCC1=CC2=C(N3CC4=NN=C(C(F)(F)F)N4CC3)N=C(OCC(C)NC(OC)=O)N=C2S1	$C_{20}H_{24}F_3N_7O_3S$	499.51	–	–		7.0	9-81
44g	CCCC1=CC2=C(N3CC4=NN=C(C(F)(F)F)N4CC3)N=C(OCCNC(COC)=O)N=C2S1	$C_{20}H_{24}F_3N_7O_3S$	499.51	–	–		7.0	3-63
45g	CCCC1=CC2=C(N3CC4=NN=C(C(F)(F)F)N4CC3)N=C(N[C@H]5CCN(C(C(C)C)=O)C5)N=C2S1	$C_{23}H_{29}F_3N_8OS$	522.60	–	–		7.0	8-15
46g	CCCC1=CC2=C(N3CC4=NN=C(C(F)(F)F)N4CC3)N=C(OCCNC(C5=CC=CC=N5)=O)N=C2S1	$C_{23}H_{23}F_3N_8O_2S$	532.55	–	–		7.0	3-70
47g	CCCC1=CC2=C(N3CC4=NN=C(C(F)(F)F)N4CC3)N=C(OCCN(C)C(OC)=O)N=C2S1	$C_{20}H_{24}F_3N_7O_3S$	499.51	–	–		7.2	9-95
48g	CCCC1=CC2=C(N3CC4=NN=C(C(F)(F)F)N4CC3)N=C(N5C[C@@H](NC(CC6=CSC(N)=N6)=O)CC5)N=C2S1	$C_{24}H_{27}F_3N_{10}OS_2$	592.66	–	–		7.2	1-119
49g	CCCC1=CC2=C(N3CC4=NN=C(C(F)(F)F)N4CC3)N=C(OCCN(CCO)C(C)=O)N=C2S1	$C_{21}H_{26}F_3N_7O_3S$	513.54	–	–		8.0	9-102
50g	CCCC1=CC2=C(N3CC4=NN=C(C(F)(F)F)N4CC3)N=C(N5CC(O)C(NC(OC)=O)C5)N=C2S1	$C_{21}H_{25}F_3N_8O_3S$	526.54	–	–		8.0	9-2
51g	CCCC1=CC2=C(N3CC4=NN=C(C(F)(F)F)N4CC3)N=C(C5=NC(CCO)=CS5)N=C2S1	$C_{20}H_{20}F_3N_7OS_2$	495.54	–	–		8.4	4-59
52g	CCCC1=CC2=C(N3CC4=NN=C(C(F)(F)F)N4CC3)N=C(N5C[C@@H](NC(COC)=O)CC5)N=C2S1	$C_{22}H_{27}F_3N_8O_2S$	524.57	–	–		8.6	1-102
53g	CCCC1=CC2=C(N3CC4=NN=C(C(F)(F)F)N4CC3)N=C(N5C[C@@H](NC(C6CC6)=O)CC5)N=C2S1	$C_{23}H_{27}F_3N_8OS$	520.58	–	–		9.3	1-108

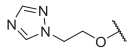
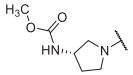
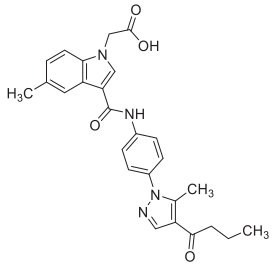
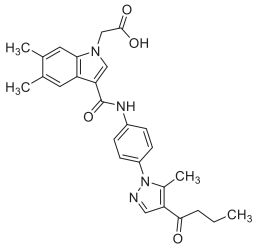
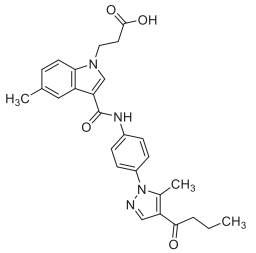
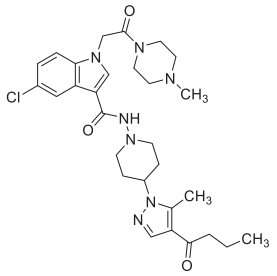
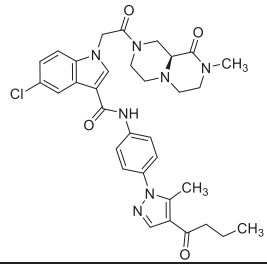
54g	CCCC1=CC2=C(N3CC4=NN=C(C(F)(F)F)N4CC3)N=C(OCCN5N=CN=C5)N=C2S1	$C_{19}H_{20}F_3N_9OS$	479.49	–	–		9.8	9-44
55g	CCCC1=CC2=C(N3CC4=NN=C(C(F)(F)F)N4CC3)N=C(N5C[C@@H](NC(OC)=O)CC5)N=C2S1	$C_{21}H_{25}F_3N_8O_2S$	510.54	–	–		10.0	9-18

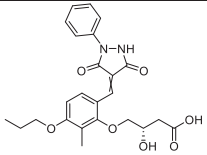
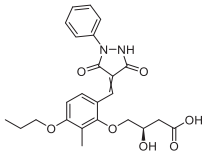
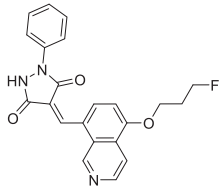
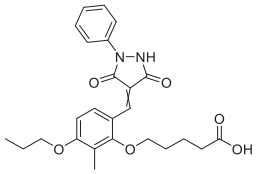
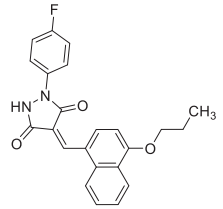
Table S11. Scaffold VI: Pyrazolyl-phenyl-carbamoyl-indole derivatives (5 compounds).[62,63]

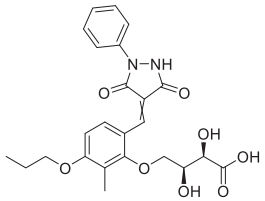
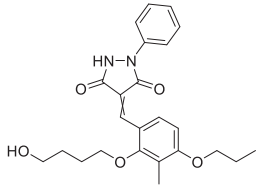
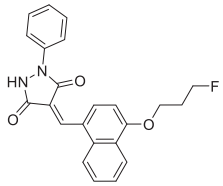
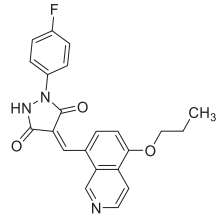
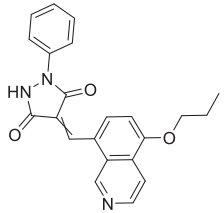
ID	Smiles	Chemical formula	MW (g/mol)	#RO5 Violation	AlogP	Structure	Affinity[a] (IC_{50}) in nM	Compound number in original publication
1i	CCCC(C1=C(C)N(C2=CC=C(C=C2)NC(C3=CN(C4=C3C=C(C)C=C4)CC(O)=O)=O)N=C1)=O	$C_{26}H_{26}N_4O_4$	458.51	0	4.76		0.9	50a
3i	CCCC(C1=C(C)N(C2=CC=C(C=C2)NC(C3=CN(C4=C3C=C(C)C(C)=C4)CC(O)=O)=O)N=C1)=O	$C_{27}H_{28}N_4O_4$	472.54	1	5.07		5.1	50c
2i	CCCC(C1=C(C)N(C2=CC=C(C=C2)NC(C3=CN(C4=C3C=C(C)C=C4)CCC(O)=O)=O)N=C1)=O	$C_{27}H_{28}N_4O_4$	472.54	1	5.15		7	49
4i	CCCC(C1=C(C)N(C2CCN(NC(C3=CN(C4=C3C=C(Cl)C=C4)CC(N5CCN(CC5)C)=O)=O)CC2)N=C1)=O	$C_{29}H_{38}ClN_7O_3$	568.11	1	3.54		7	52ae

5i	CCCC(C1=C(C)N(C2=CC=C(C=C2)NC(C3=CN(C4=C3C=C(Cl)C=C4)CC(N5CCN6CCN(C(C6C5)=O)C)=O)=O)N=C1)=O	$C_{33}H_{36}ClN_7O_4$	630.14	1	4.01		8	102

[a] Displacement of [^{33}P]2MeS-ADP from P2Y$_{12}$ receptor transfected in CHO cells after 30 mins by scintillation counting analysis.

Table S12. Scaffold VII: Pyrazolidinedione derivatives (10 compounds).[65,66]

ID	Smiles	Chemical formula	MW (g/mol)	Structure	Affinity (IC_{50}/K_i) in nM	Compound number in original publication
1k (*S*)	O=C(C1=CC2=CC=C(OCCC)C(C)=C2OC[C@@H](O)CC(O)=O)NN(C3=CC=CC=C3)C1=O	$C_{24}H_{26}N_2O_7$	454.48		0.8	2a64
1k (*R*)	O=C(C1=CC2=CC=C(OCCC)C(C)=C2OC[C@H](O)CC(O)=O)NN(C3=CC=CC=C3)C1=O	$C_{24}H_{26}N_2O_7$	454.48		1.0	2a63
3k	O=C(NN(C1=CC=CC=C1)C/2=O)C2=C\C3=CC=C(OCCCF)C4=C3C=NC=C4	$C_{22}H_{18}FN_3O_3$	391.40		1.2	6
7k	O=C(C1=CC2=CC=C(OCCC)C(C)=C2OCCCCC(O)=O)NN(C3=CC=CC=C3)C1=O	$C_{25}H_{28}N_2O_6$	452.51		1.6	2a52
6k	CCCOC1=CC=C(/C=C2C(NN(C3=CC=C(F)C=C3)C/2=O)=O)C4=C1C=CC=C4	$C_{23}H_{19}FN_2O_3$	390.41		1.9	9

8k	O=C(C1=CC2=CC=C(OCCC)C(C)=C2OC[C@H](O)[C@H](C(O)=O)O)NN(C3=CC=CC=C3)C1=O	$C_{24}H_{26}N_2O_8$	470.48		3.0	2a71
9k	O=C(C1=CC2=CC=C(OCCC)C(C)=C2OCCCCO)NN(C3=CC=CC=C3)C1=O	$C_{24}H_{28}N_2O_5$	424.50		5.0	2a43
4k	O=C(NN(C1=CC=CC=C1)C/2=O)C2=C\C3=CC=C(OCCCF)C4=C3C=CC=C4	$C_{23}H_{19}FN_2O_3$	390.41		5.3	8
5k	CCCOC1=CC=C(/C=C2C(NN(C3=CC=C(F)C=C3)C/2=O)=O)C4=C1C=CN=C4	$C_{22}H_{18}FN_3O_3$	391.40		5.7	7
2k	O=C(C1=CC2=CC=C(OCCC)C3=C2C=NC=C3)NN(C4=CC=CC=C4)C1=O	$C_{22}H_{19}N_3O_3$	373.41		10	2a30

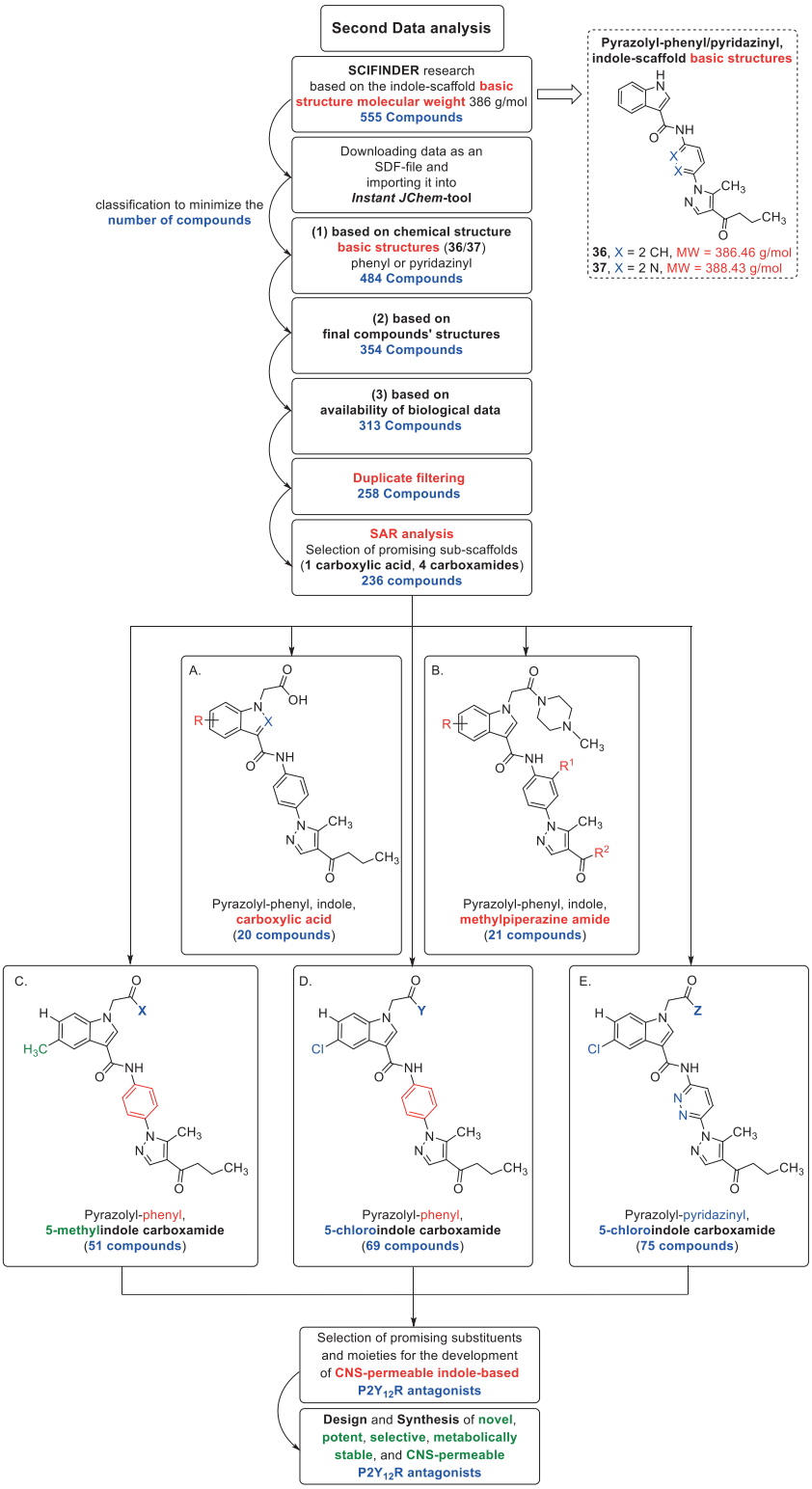
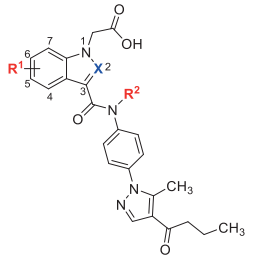


Figure S1. Description of the second data analysis process within pyrazolyl-phenyl-carbamoyl-indole scaffold.[38,39]

Table S13. SAR Analysis of pyrazolyl-phenyl-carbamoyl-indole-**acetic acid** sub-scaffold **(A)** (20 compounds).[62,63]

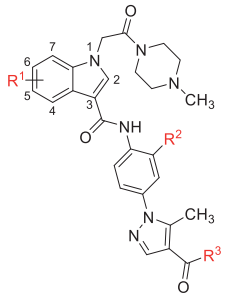
ID	Smiles	Chemical formula	MW (g/mol)	Structure			Affinity[a] (IC_{50}) in nM	hPRP[b] (IC_{50}) in µM	rPRP[b] (IC_{50}) in µM	Compound number in original publication
										
				R^1	**X**	**R^2**				
1i	CCCC(C1=C(C)N(C2=CC=C(C=C2)NC(C3=CN(C4=C3C=C(C)C=C4)CC(O)=O)=O)N=C1)=O	$C_{26}H_{26}N_4O_4$	458.51	5-Me	CH	H	0.9	1.8	9.6	**50a/11**
3i	CCCC(C1=C(C)N(C2=CC=C(C=C2)NC(C3=CN(C4=C3C=C(C)C(C)=C4)CC(O)=O)=O)N=C1)=O	$C_{27}H_{28}N_4O_4$	472.54	5,6-diMe	CH	H	5.1	0.4	4.6	**50c/16**
205i	O=C(O)CN1C(C(C(C(NC2=CC=C(N(N=C3)C(C)=C3C(CCC)=O)C=C2)=O)=C1)=C4)=CC([H])=C4N(C)C	$C_{27}H_{29}N_5O_4$	487.56	5-NMe_2	CH	H	–	–	1.2	**22**
206i	O=C(O)CN1C(C(C(C(NC2=CC=C(N(N=C3)C(C)=C3C(CCC)=O)C=C2)=O)=C1)=C4)=CC([H])=C4Br	$C_{25}H_{23}BrN_4O_4$	523.39	5-Br	CH	H	–	–	1.9	**14**
207i	O=C(O)CN1C(C(C(C(NC2=CC=C(N(N=C3)C(C)=C3C(CCC)=O)C=C2)=O)=C1)=C4)=CC([H])=C4Cl	$C_{25}H_{23}ClN_4O_4$	478.93	5-Cl	CH	H	–	–	2.8	**3**
208i	O=C(O)CN1C(C(C(C(NC2=CC=C(N(N=C3)C(C)=C3C(CCC)=O)C=C2)=O)=C1)=C4)=CC(F)=C4Cl	$C_{25}H_{22}ClFN_4O_4$	496.92	5-Cl,6-F	CH	H	–	–	2.8	**21**
209i	O=C(O)CN1C(C(C(C(NC2=CC=C(N(N=C3)C(C)=C3C(CCC)=O)C=C2)=O)=C1)=C4)=CC(C)=C4Cl	$C_{26}H_{25}ClN_4O_4$	492.96	5-Cl,6-Me	CH	H	–	–	3.3	**4**
210i	O=C(O)CN1C(C(C(C(NC2=CC=C(N(N=C3)C(C)=C3C(CCC)=O)C=C2)=O)=C1)=C4)=CC(C)=C4Br	$C_{26}H_{25}BrN_4O_4$	537.41	5-Br,6-Me	CH	H	–	–	3.9	**20**
211i	O=C(O)CN1C(C(C(C(NC2=CC=C(N(N=C3)C(C)=C3C(CCC)=O)C=C2)=O)=C1)=C4)=CC([H])=C4C#N	$C_{26}H_{23}N_5O_4$	469.50	5-CN	CH	H	–	–	4.1	**23**
212i	O=C(O)CN1C(C(C(C(NC2=CC=C(N(N=C3)C(C)=C3C(CCC)=O)C=C2)=O)=C1)=C4)=CC([H])=C4C(F)(F)F	$C_{26}H_{23}F_3N_4O_4$	512.49	5-CF_3	CH	H	–	–	4.6	**13**

213i	O=C(O)CN1C(C(C(C(NC2=CC=C(N(N=C3)C(C)=C3C(CCC)=O)C=C2)=O)=C1)=C4)=CC(Cl)=C4Cl	$C_{25}H_{22}Cl_2N_4O_4$	513.38	5,6-diCl	CH	H	–	–	7.3	**17**
214i	O=C(O)CN1C(C(C(C(NC2=CC=C(N(N=C3)C(C)=C3C(CCC)=O)C=C2)=O)=C1)=C4)=CC([H])=C4OC	$C_{26}H_{26}N_4O_5$	474.52	5-OMe	CH	H	–	–	17	**12**
215i	O=C(O)CN1C(C(C(C(NC2=CC=C(N(N=C3)C(C)=C3C(CCC)=O)C=C2)=O)=C1)=C4)=CC([H])=C4C5=CC=CC=C5	$C_{31}H_{28}N_4O_4$	520.59	5-Ph	CH	H	–	–	25	**15**
216i	O=C(O)CN1C(C(C(C(NC2=CC=C(N(N=C3)C(C)=C3C(CCC)=O)C=C2)=O)=C1)=C4)=CC([H])=C4F	$C_{25}H_{23}FN_4O_4$	462.48	5-F	CH	H	–	–	36	**18**
217i	O=C(O)CN1C(C(C(C(NC2=CC=C(N(N=C3)C(C)=C3C(CCC)=O)C=C2)=O)=C1)=C4)=CC(Br)=C4C	$C_{26}H_{25}BrN_4O_4$	537.41	5-Me,6-Br	CH	H	–	–	42	**19**
218i	O=C(O)CN1C(C(C(C(NC2=CC=C(N(N=C3)C(C)=C3C(CCC)=O)C=C2)=O)=C1)=C4)=CC(C)=C4[H]	$C_{26}H_{26}N_4O_4$	458.52	6-Me	CH	H	–	–	63	**8**
219i	O=C(C1=CN(CC(O)=O)C2=CC=C(C)C(C)=C12)NC3=CC=C(N(N=C4)C(C)=C4C(CCC)=O)C=C3	$C_{27}H_{28}N_4O_4$	472.55	4,5-diMe	CH	H	272	>30	>30	**50d**
220i	O=C(C(C1=CC(C)=CC=C1N2CC(O)=O)=C2C)NC3=CC=C(N(N=C4)C(C)=C4C(CCC)=O)C=C3	$C_{27}H_{28}N_4O_4$	472.55	5-Me	CH	H	84	15	16	**50e**
221i	O=C(O)CN1C(C(C(C(NC2=CC=C(N(N=C3)C(C)=C3C(CCC)=O)C=C2)=O)=N1)=C4)=CC([H])=C4C	$C_{25}H_{25}N_5O_4$	459.51	5-Me	N	H	–	–	37	**24**
222i	O=C(C(C1=CC(C)=CC=C12)=CN2CC(O)=O)N(C3=CC=C(N(N=C4)C(C)=C4C(CCC)=O)C=C3)C	$C_{27}H_{28}N_4O_4$	472.55	5-Me	CH	Me	304	>30	>30	**50b**

[a] Displacement of [^{33}P]2MeS-ADP from $P2Y_{12}$ receptor transfected in CHO cells after 30 mins by scintillation counting analysis.

[b] Inhibition of ADP-induced platelet aggregation in human (hPRP) or rat (rPRP) platelet-rich-plasma.

Table S14. SAR Analysis of pyrazolyl-phenyl-carbamoyl-indole-**4-methylpiperazin-1-yl carboxamide** sub-scaffold **(B)** (21 compounds).[62,63]

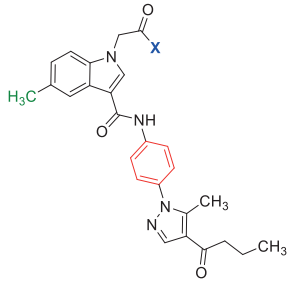
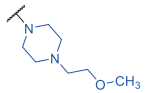
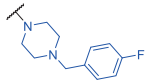
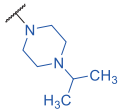
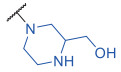
ID	Smiles	Chemical formula	MW (g/mol)	Structure			Affinity[a] (IC_{50}) in nM	hPRP[b] (IC_{50}) in µM	rPRP[b] (IC_{50}) in µM	Compound number in original publication
										
				R^1	**R^2**	**R^3**				
223i	O=C(N1CCN(C)CC1)CN2C(C(C(C(NC3=CC=C(N(N=C4)C(C)=C4C(CCC)=O)C=C3)=O)=C2)=C5)=CC(F)=C5Cl	$C_{30}H_{32}ClFN_6O_3$	579.07	5-Cl,6-F	H	^{n}Pr	48	–	0.18	**52l/157**
20i	O=C(N1CCN(C)CC1)CN2C(C(C(C(NC3=CC=C(N(N=C4)C(C)=C4C(CCC)=O)C=C3)=O)=C2)=C5)=CC([H])=C5C	$C_{31}H_{36}N_6O_3$	540.67	5-Me	H	^{n}Pr	31	–	0.27	**114**
224i	O=C(N(CC1)CCN1C)CN2C(C(C(C(NC3=CC=C(N(N=C4)C(C)=C4C(CCC)=O)C=C3)=O)=C2)=C5)=CC(C)=C5C	$C_{32}H_{38}N_6O_3$	554.70	5,6-diMe	H	^{n}Pr	39	–	0.30	**52c/107**
98i	O=C(N1CCN(C)CC1)CN2C(C(C(C(NC3=CC=C(N(N=C4)C(C)=C4C(CCC)=O)C=C3)=O)=C2)=C5)=CC([H])=C5Cl	$C_{30}H_{33}ClN_6O_3$	568.12	5-Cl	H	^{n}Pr	27	–	0.32	**115**
225i	O=C(N1CCN(C)CC1)CN2C(C(C(C(NC3=CC=C(N(N=C4)C(C)=C4C(CCC)=O)C=C3)=O)=C2)=C5)=CC(C)=C5Br	$C_{31}H_{35}BrN_6O_3$	619.56	5-Br,6-Me	H	^{n}Pr	48	–	0.36	**52m/112**
226i	O=C(N1CCN(C)CC1)CN2C(C(C(C(NC3=CC=C(N(N=C4)C(C)=C4C(CCC)=O)C=C3)=O)=C2)=C5)=CC([H])=C5C(F)(F)F	$C_{31}H_{33}F_3N_6O_3$	594.64	5-CF_3	H	^{n}Pr	50	–	0.40	**52n/203**
227i	O=C(C(C1=CC(OC)=C([H])C=C12)=CN2CC(N(CC3)CCN3C)=O)NC4=CC=C(N(N=C5)C(C)=C5C(CCC)=O)C=C4	$C_{31}H_{36}N_6O_4$	556.67	5-OMe	H	^{n}Pr	22	–	0.40	**52g/136**
228i	O=C(N1CCN(C)CC1)CN2C(C(C(C(NC3=CC=C(N(N=C4)C(C)=C4C(CCC)=O)C=C3)=O)=C2)=C5)=CC(C)=C5Cl	$C_{31}H_{35}ClN_6O_3$	575.11	5-Cl,6-Me	H	^{n}Pr	34	–	0.62	**52o/113**

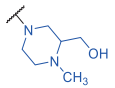
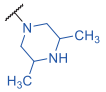
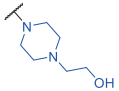
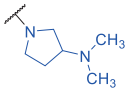
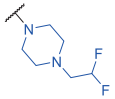
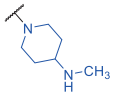
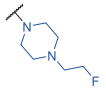
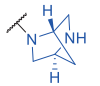
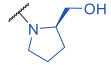
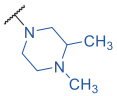
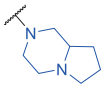
229i	O=C(N(CC1)CCN1C)CN2C(C(C(C(NC3=CC=C(N(N=C4)C(C)=C4C(CCC)=O)C=C3)=O)=C2)=C5)=CC(Br)=C5C	$C_{31}H_{35}BrN_6O_3$	619.56	5-Me,6-Br	H	^{n}Pr	118	–	1.7	**52q**
230i	O=C(N(CC1)CCN1C)CN2C(C(C(C(NC3=CC=C(N(N=C4)C(C)=C4C(CCC)=O)C=C3)=O)=C2)=C5)=CC(Cl)=C5C	$C_{31}H_{35}ClN_6O_3$	575.11	5-Me,6-Cl	H	^{n}Pr	138	–	2.0	**52r**
231i	O=C(N1CCN(C)CC1)CN2C(C(C(C(NC3=CC=C(N4C(C)=C(C(CCC)=O)C=N4)C=C3)=O)=C2)=C5)=CC([H])=C5C#N	$C_{31}H_{33}N_7O_3$	551.65	5-CN	H	^{n}Pr	76	–	2.30	**52p/160**
232i	O=C(C(C1=CC(F)=C([H])C=C12)=CN2CC(N(CC3)CCN3C)=O)NC4=CC=C(N(N=C5)C(C)=C5C(CCC)=O)C=C4	$C_{30}H_{33}FN_6O_3$	544.63	5-F	H	^{n}Pr	142	–	2.70	**52t**
233i	O=C(N(CC1)CCN1C)CN2C(C(C(C(NC3=CC=C(N(N=C4)C(C)=C4C(CCC)=O)C=C3)=O)=C2)=C5)=CC(Cl)=C5Cl	$C_{30}H_{32}Cl_2N_6O_3$	595.53	5,6-diCl	H	^{n}Pr	99	–	3.70	**52s/111**
234i	O=C(CN1C2=CC(C)=CC=C2C(C(NC(C=C3)=CC=C3N4N=CC(C(CCC)=O)=C4C)=O)=C1)N5CCN(C)CC5	$C_{31}H_{36}N_6O_3$	540.67	6-Me	H	^{n}Pr	–	–	5.4	**52u**
235i	O=C(C(C1=CC(C(N)=O)=CC=C12)=CN2CC(N(CC3)CCN3C)=O)NC4=CC=C(N(N=C5)C(C)=C5C(CCC)=O)C=C4	$C_{31}H_{35}N_7O_4$	569.67	5-$CONH_2$	H	^{n}Pr	–	–	5.9	**52p'**
236i	O=C(N1CCN(C)CC1)CN2C(C(C(C(NC3=CC=C(N(N=C4)C(C)=C4C(CCC)=O)C=C3C(N)=O)=O)=C2)=C5)=CC([H])=C5Cl	$C_{31}H_{34}ClN_7O_4$	604.11	5-Cl	$CONH_2$	^{n}Pr	–	–	0.22	**220**
237i	O=C(N1CCN(C)CC1)CN2C(C(C(C(NC3=CC=C(N(N=C4)C(C)=C4C(CCC)=O)C=C3C#N)=O)=C2)=C5)=CC([H])=C5Cl	$C_{31}H_{32}ClN_7O_3$	586.09	5-Cl	CN	^{n}Pr	–	–	0.54	**219**
238i	O=C(N1CCN(C)CC1)CN2C(C(C(C(NC3=CC=C(N(N=C4)C(C)=C4C(OCC)=O)C=C3)=O)=C2)=C5)=CC([H])=C5Cl	$C_{29}H_{31}ClN_6O_4$	563.06	5-Cl	H	OEt	–	–	0.56	**218**
239i	O=C(N1CCN(C)CC1)CN2C(C(C(C(NC3=CC=C(N(N=C4)C(C)=C4C(CC)=O)C=C3)=O)=C2)=C5)=CC([H])=C5Cl	$C_{29}H_{31}ClN_6O_3$	547.06	5-Cl	H	Et	336	–	0.60	**217**
240i	O=C(N1CCN(C)CC1)CN2C(C(C(C(NC3=CC=C(N(N=C4)C(C)=C4C(C)=O)C=C3)=O)=C2)=C5)=CC([H])=C5Cl	$C_{28}H_{29}ClN_6O_3$	533.03	5-Cl	H	Me	143	–	0.73	**216**
241i	O=C(C(C1=CC(Cl)=CC=C12)=CN2CC(N(CC3)CCN3C)=O)NC4=CC=C(N(N=C5)C(C)=C5C(CCC(F)(F)F)=O)C=C4	$C_{30}H_{30}ClF_3N_6O_3$	615.05	5-Cl	H	$C_2H_4CF_3$	574	–	8	**52k**

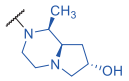
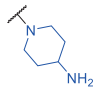
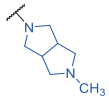
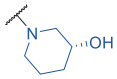
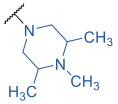
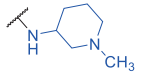
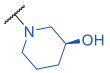
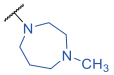
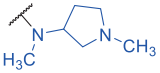
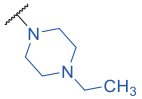
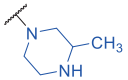
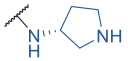
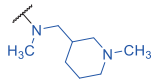
[a] Displacement of [^{33}P]2MeS-ADP from $P2Y_{12}$ receptor transfected in CHO cells after 30 mins by scintillation counting analysis.

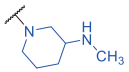
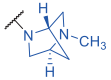
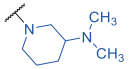
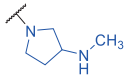
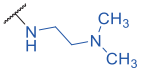
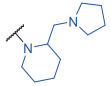
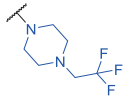
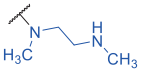
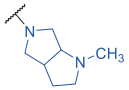
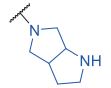
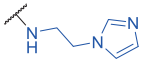
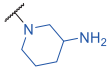
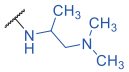
[b] Inhibition of ADP-induced platelet aggregation in human (hPRP) or rat (rPRP) platelet-rich-plasma

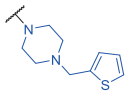
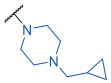
Table S15. SAR Analysis of pyrazolyl-**phenyl**-carbamoyl-**5-methyl**indole-**carboxamide** sub-scaffold (**C**) (51 compounds).[62,63]

ID	Smiles	Chemical formula	MW (g/mol)	Structure	Affinity[a] (IC_{50}) in nM	rPRP[b] (IC_{50}) in μM	Compound number in original publication
							
10i	O=C(CN1C2=CC([H])=C(C)C=C2C(C(NC3=CC=C(C=C3)N4N=CC(C(CCC)=O)=C4C)=O)=C1)N5CC6CNCC6C5	$C_{32}H_{36}N_6O_3$	552.68		106	0.18	255
11i	O=C(N1CCN(CCOC)CC1)CN2C(C(C(C(NC3=CC=C(N(N=C4)C(C)=C4C(CCC)=O)C=C3)=O)=C2)=C5)=CC([H])=C5C	$C_{33}H_{40}N_6O_4$	584.72		20	0.18	119
12i	O=C(N1CCNCC1CO)CN2C(C(C(C(NC3=CC=C(N(N=C4)C(C)=C4C(CCC)=O)C=C3)=O)=C2)=C5)=CC([H])=C5C	$C_{31}H_{36}N_6O_4$	556.67		–	0.19	254
13i	O=C(N1CCN(CC2=CC=C(F)C=C2)CC1)CN3C(C(C(C(NC4=CC=C(N(N=C5)C(C)=C5C(CCC)=O)C=C4)=O)=C3)=C6)=CC([H])=C6C	$C_{37}H_{39}FN_6O_3$	634.76		12	0.19	147
14i	O=C(N1C[C@H](O)CC1)CN2C(C(C(C(NC3=CC=C(N(N=C4)C(C)=C4C(CCC)=O)C=C3)=O)=C2)=C5)=CC([H])=C5C	$C_{30}H_{33}N_5O_4$	527.63		–	0.21	135
15i	O=C(N1CCN(C(C)C)CC1)CN2C(C(C(C(NC3=CC=C(N(N=C4)C(C)=C4C(CCC)=O)C=C3)=O)=C2)=C5)=CC([H])=C5C	$C_{33}H_{40}N_6O_3$	568.72		82	0.21	124
16i	O=C(N1CCNC(CO)C1)CN2C(C(C(C(NC3=CC=C(N(N=C4)C(C)=C4C(CCC)=O)C=C3)=O)=C2)=C5)=CC([H])=C5C	$C_{31}H_{36}N_6O_4$	556.67		–	0.24	249

17i	O=C(N1CCN(C)C(CO)C1)CN2C(C(C(C(NC3=CC=C(N(N=C4)C(C)=C4C(CCC)=O)C=C3)=O)=C2)=C5)=CC([H])=C5C	$C_{32}H_{38}N_6O_4$	570.69		–	0.24	268
18i	O=C(N1CC(C)NC(C)C1)CN2C(C(C(C(NC3=CC=C(N(N=C4)C(C)=C4C(CCC)=O)C=C3)=O)=C2)=C5)=CC([H])=C5C	$C_{32}H_{38}N_6O_3$	554.70		102	0.26	247
19i	O=C(N1CCN(CCO)CC1)CN2C(C(C(C(NC3=CC=C(N(N=C4)C(C)=C4C(CCC)=O)C=C3)=O)=C2)=C5)=CC([H])=C5C	$C_{32}H_{38}N_6O_4$	570.69		41	0.26	116
20i	O=C(N1CCN(C)CC1)CN2C(C(C(C(NC3=CC=C(N(N=C4)C(C)=C4C(CCC)=O)C=C3)=O)=C2)=C5)=CC([H])=C5C	$C_{31}H_{36}N_6O_3$	540.67		31	0.27	114
21i	O=C(N1CCC(N(C)C)C1)CN2C(C(C(C(NC3=CC=C(N(N=C4)C(C)=C4C(CCC)=O)C=C3)=O)=C2)=C5)=CC([H])=C5C	$C_{32}H_{38}N_6O_3$	554.70		87	0.27	120
22i	O=C(N1CCOCC1)CN2C(C(C(C(NC3=CC=C(N(N=C4)C(C)=C4C(CCC)=O)C=C3)=O)=C2)=C5)=CC([H])=C5C	$C_{30}H_{33}N_5O_4$	527.63		–	0.29	128
23i	O=C(N1CCN(CC(F)F)CC1)CN2C(C(C(C(NC3=CC=C(N(N=C4)C(C)=C4C(CCC)=O)C=C3)=O)=C2)=C5)=CC([H])=C5C	$C_{32}H_{36}F_2N_6O_3$	590.68		19	0.29	118
24i	O=C(N1CCC(NC)CC1)CN2C(C(C(C(NC3=CC=C(N(N=C4)C(C)=C4C(CCC)=O)C=C3)=O)=C2)=C5)=CC([H])=C5C	$C_{32}H_{38}N_6O_3$	554.70		115	0.32	248
25i	O=C(N1CCN(CCF)CC1)CN2C(C(C(C(NC3=CC=C(N(N=C4)C(C)=C4C(CCC)=O)C=C3)=O)=C2)=C5)=CC([H])=C5C	$C_{32}H_{37}FN_6O_3$	572.69		19	0.32	133
26i	O=C(N1[C@]2([H])CN[C@](C2)([H])C1)CN3C(C(C(C(NC4=CC=C(N(N=C5)C(C)=C5C(CCC)=O)C=C4)=O)=C3)=C6)=CC([H])=C6C	$C_{31}H_{34}N_6O_3$	538.65		86	0.33	253
27i	O=C(N1CCC[C@@H]1CO)CN2C(C(C(C(NC3=CC=C(N(N=C4)C(C)=C4C(CCC)=O)C=C3)=O)=C2)=C5)=CC([H])=C5C	$C_{31}H_{35}N_5O_4$	541.65		–	0.34	140
28i	O=C(N1CCN(C)C(C)C1)CN2C(C(C(C(NC3=CC=C(N(N=C4)C(C)=C4C(CCC)=O)C=C3)=O)=C2)=C5)=CC([H])=C5C	$C_{32}H_{38}N_6O_3$	554.70		27	0.35	269
29i	O=C(N1CCN(CCC2)C2C1)CN3C(C(C(C(NC4=CC=C(N(N=C5)C(C)=C5C(CCC)=O)C=C4)=O)=C3)=C6)=CC([H])=C6C	$C_{33}H_{38}N_6O_3$	566.71		76	0.35	123

30i	O=C(N1CCN2C[C@@H](O)C[C@@H]2[C@@H]1C)CN3C(C(C(C(NC4=CC=C(N(N=C5)C(C)=C5C(CCC)=O)C=C4)=O)=C3)=C6)=CC([H])=C6C	$C_{34}H_{40}N_6O_4$	596.73		15	0.39	137
31i	O=C(N1CCC(N)CC1)CN2C(C(C(C(NC3=CC=C(N(N=C4)C(C)=C4C(CCC)=O)C=C3)=O)=C2)=C5)=CC([H])=C5C	$C_{31}H_{36}N_6O_3$	540.67		71	0.40	252
32i	O=C(N1CC(CN(C)C2)C2C1)CN3C(C(C(C(NC4=CC=C(N(N=C5)C(C)=C5C(CCC)=O)C=C4)=O)=C3)=C6)=CC([H])=C6C	$C_{33}H_{38}N_6O_3$	566.71		33	0.40	266
33i	O=C(N1CCC[C@@H](O)C1)CN2C(C(C(C(NC3=CC=C(N(N=C4)C(C)=C4C(CCC)=O)C=C3)=O)=C2)=C5)=CC([H])=C5C	$C_{31}H_{35}N_5O_4$	541.65		–	0.42	138
34i	O=C(N1CC(C)N(C)C(C)C1)CN2C(C(C(C(NC3=CC=C(N(N=C4)C(C)=C4C(CCC)=O)C=C3)=O)=C2)=C5)=CC([H])=C5C	$C_{33}H_{40}N_6O_3$	568.72		28	0.42	263
35i	O=C(NC1CN(C)CCC1)CN2C(C(C(C(NC3=CC=C(N(N=C4)C(C)=C4C(CCC)=O)C=C3)=O)=C2)=C5)=CC([H])=C5C	$C_{32}H_{38}N_6O_3$	554.70		71	0.45	267
36i	O=C(N1CCN(C2CC2)CC1)CN3C(C(C(C(NC4=CC=C(N(N=C5)C(C)=C5C(CCC)=O)C=C4)=O)=C3)=C6)=CC([H])=C6C	$C_{33}H_{38}N_6O_3$	566.71		44	0.45	122
37i	O=C(N1CCC[C@H](O)C1)CN2C(C(C(C(NC3=CC=C(N(N=C4)C(C)=C4C(CCC)=O)C=C3)=O)=C2)=C5)=CC([H])=C5C	$C_{31}H_{35}N_5O_4$	541.65		–	0.47	139
38i	O=C(N1CCN(C)CCC1)CN2C(C(C(C(NC3=CC=C(N(N=C4)C(C)=C4C(CCC)=O)C=C3)=O)=C2)=C5)=CC([H])=C5C	$C_{32}H_{38}N_6O_3$	554.70		95	0.47	130
39i	O=C(N(C)C1CN(C)CC1)CN2C(C(C(C(NC3=CC=C(N(N=C4)C(C)=C4C(CCC)=O)C=C3)=O)=C2)=C5)=CC([H])=C5C	$C_{32}H_{38}N_6O_3$	554.70		47	0.50	127
40i	O=C(N1CCN(CC)CC1)CN2C(C(C(C(NC3=CC=C(N(N=C4)C(C)=C4C(CCC)=O)C=C3)=O)=C2)=C5)=CC([H])=C5C	$C_{32}H_{38}N_6O_3$	554.70		66	0.50	117
41i	O=C(N1CCNC(C)C1)CN2C(C(C(C(NC3=CC=C(N(N=C4)C(C)=C4C(CCC)=O)C=C3)=O)=C2)=C5)=CC([H])=C5C	$C_{31}H_{36}N_6O_3$	540.67		46	0.51	242
42i	O=C(N[C@H]1CNCC1)CN2C(C(C(C(NC3=CC=C(N(N=C4)C(C)=C4C(CCC)=O)C=C3)=O)=C2)=C5)=CC([H])=C5C	$C_{30}H_{34}N_6O_3$	526.64		61	0.53	245
43i	O=C(N(C)CC1CCCN(C)C1)CN2C(C(C(C(NC3=CC=C(N(N=C4)C(C)=C4C(CCC)=O)C=C3)=O)=C2)=C5)=CC([H])=C5C	$C_{34}H_{42}N_6O_3$	582.75		–	0.53	143

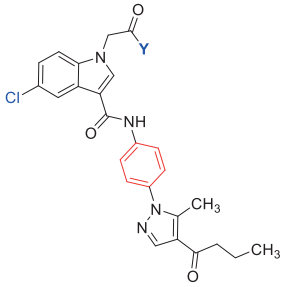
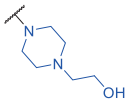
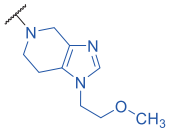
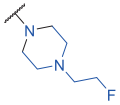
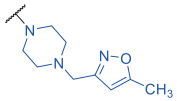
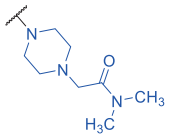
44i	O=C(N1CCNCC1)CN2C(C(C(C(NC3=CC=C(N(N=C4)C(C)=C4C(CCC)=O)C=C3)=O)=C2)=C5)=CC([H])=C5C	$C_{30}H_{34}N_6O_3$	526.64		26	0.54	243
45i	O=C(N1CCCC(NC)C1)CN2C(C(C(C(NC3=CC=C(N(N=C4)C(C)=C4C(CCC)=O)C=C3)=O)=C2)=C5)=CC([H])=C5C	$C_{32}H_{38}N_6O_3$	554.70		65	0.54	251
46i	O=C(N1[C@]2([H])CN(C)[C@](C2)([H])C1)CN3C(C(C(C(NC4=CC=C(N(N=C5)C(C)=C5C(CCC)=O)C=C4)=O)=C3)=C6)=CC([H])=C6C	$C_{32}H_{36}N_6O_3$	552.68		70	0.56	264
47i	O=C(N1CCCC(N(C)C)C1)CN2C(C(C(C(NC3=CC=C(N(N=C4)C(C)=C4C(CCC)=O)C=C3)=O)=C2)=C5)=CC([H])=C5C	$C_{33}H_{40}N_6O_3$	568.72		73	0.58	125
48i	O=C(N1CCC(NC)C1)CN2C(C(C(C(NC3=CC=C(N(N=C4)C(C)=C4C(CCC)=O)C=C3)=O)=C2)=C5)=CC([H])=C5C	$C_{31}H_{36}N_6O_3$	540.67		94	0.61	250
49i	O=C(NCCN(C)C)CN1C(C(C(C(NC2=CC=C(N(N=C3)C(C)=C3C(CCC)=O)C=C2)=O)=C1)=C4)=CC([H])=C4C	$C_{30}H_{36}N_6O_3$	528.66		92	0.63	131
50i	O=C(N1CCCCC1CN2CCCC2)CN3C(C(C(C(NC4=CC=C(N(N=C5)C(C)=C5C(CCC)=O)C=C4)=O)=C3)=C6)=CC([H])=C6C	$C_{36}H_{44}N_6O_3$	608.79		100	0.64	141
51i	O=C(N1CCN(CC(F)(F)F)CC1)CN2C(C(C(C(NC3=CC=C(N(N=C4)C(C)=C4C(CCC)=O)C=C3)=O)=C2)=C5)=CC([H])=C5C	$C_{32}H_{35}F_3N_6O_3$	608.67		66	0.65	129
52i	O=C(N(C)CCNC)CN1C(C(C(C(NC2=CC=C(N(N=C3)C(C)=C3C(CCC)=O)C=C2)=O)=C1)=C4)=CC([H])=C4C	$C_{30}H_{36}N_6O_3$	528.66		94	0.76	126
53i	O=C(N1CC(CCN2C)C2C1)CN3C(C(C(C(NC4=CC=C(N(N=C5)C(C)=C5C(CCC)=O)C=C4)=O)=C3)=C6)=CC([H])=C6C	$C_{33}H_{38}N_6O_3$	566.71		89	0.79	265
54i	O=C(N1CC(CCN2)C2C1)CN3C(C(C(C(NC4=CC=C(N(N=C5)C(C)=C5C(CCC)=O)C=C4)=O)=C3)=C6)=CC([H])=C6C	$C_{32}H_{36}N_6O_3$	552.68		117	0.85	246
55i	O=C(NCCN1C=CN=C1)CN2C(C(C(C(NC3=CC=C(N(N=C4)C(C)=C4C(CCC)=O)C=C3)=O)=C2)=C5)=CC([H])=C5C	$C_{31}H_{33}N_7O_3$	551.65		61	0.95	134
56i	O=C(N1CCCC(N)C1)CN2C(C(C(C(NC3=CC=C(N(N=C4)C(C)=C4C(CCC)=O)C=C3)=O)=C2)=C5)=CC([H])=C5C	$C_{31}H_{36}N_6O_3$	540.67		46	0.96	244
57i	O=C(NC(C)CN(C)C)CN1C(C(C(C(NC2=CC=C(N(N=C3)C(C)=C3C(CCC)=O)C=C2)=O)=C1)=C4)=CC([H])=C4C	$C_{31}H_{38}N_6O_3$	542.68		88	0.98	132

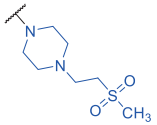
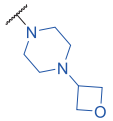
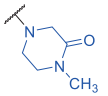
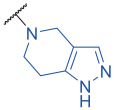
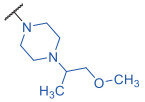
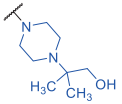
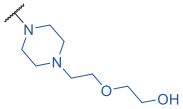
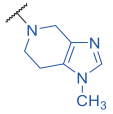
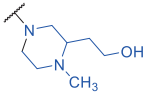
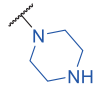
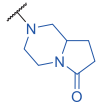
58i	O=C(N1CCN(CC2=CC=CS2)CC1)CN3C(C(C(C(NC4=CC=C(N(N=C5)C(C)=C5C(CCC)=O)C=C4)=O)=C3)=C6)=CC([H])=C6C	$C_{35}H_{38}N_6O_3S$	622.79		–	1.01	164
59i	O=C(N1CCN(CC2CC2)CC1)CN3C(C(C(C(NC4=CC=C(N(N=C5)C(C)=C5C(CCC)=O)C=C4)=O)=C3)=C6)=CC([H])=C6C	$C_{34}H_{40}N_6O_3$	580.73		29	1.06	121
60i	O=C(NS(C)(=O)=O)CN1C(C(C(C(NC2=CC=C(N(N=C3)C(C)=C3C(CCC)=O)C=C2)=O)=C1)=C4)=CC([H])=C4C	$C_{27}H_{29}N_5O_5S$	535.62		–	4.86	213

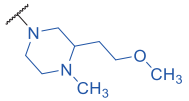
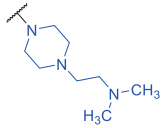
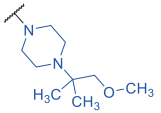
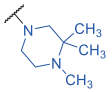
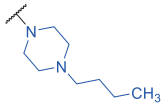
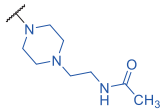
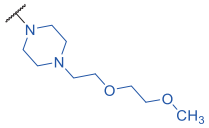
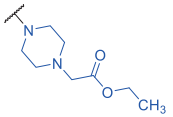
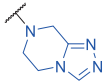
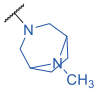
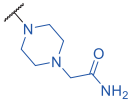
[a] Displacement of [^{33}P]2MeS-ADP from P2Y$_{12}$ receptor transfected in CHO cells after 30 mins by scintillation counting analysis.

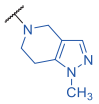
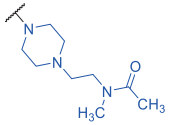
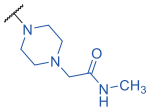
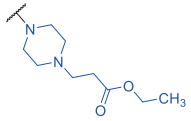
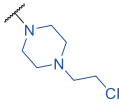
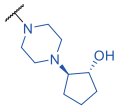
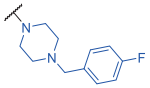
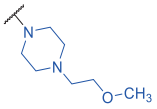
[b] Inhibition of ADP-induced platelet aggregation in rat (rPRP) platelet-rich-plasma.

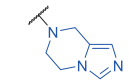
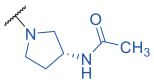
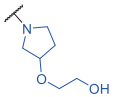
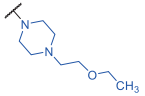
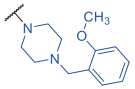
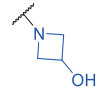
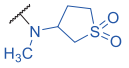
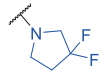
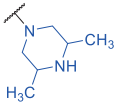
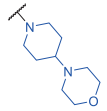
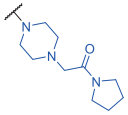
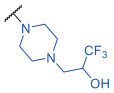
Table S16. SAR Analysis of pyrazolyl-**phenyl**-carbamoyl-**5-chloro**indole-**carboxamide** sub-scaffold (**D**) (69 compounds).[62,63]

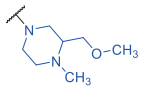
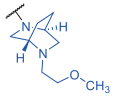
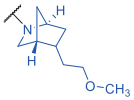
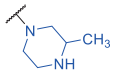
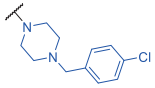
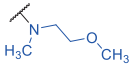
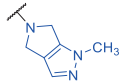
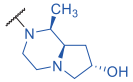
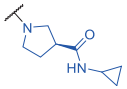
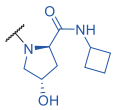
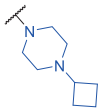
ID	Smiles	Chemical formula	MW (g/mol)	Structure	Affinity[a] (IC_{50}) in nM	rPRP[b] (IC_{50}) in µM	Compound number in original publication
				 **Y**			
61i	OCCN1CCN(C(CN2C(C(C(C(NC3=CC=C(N(N=C4)C(C)=C4C(CCC)=O)C=C3)=O)=C2)=C5)=CC([H])=C5Cl)=O)CC1	$C_{31}H_{35}ClN_6O_4$	591.11		11	0.10	146
62i	O=C(N1CCC[C@@H]1C(F)(F)F)CN2C(C(C(C(NC3=CC=C(N(N=C4)C(C)=C4C(CCC)=O)C=C3)=O)=C2)=C5)=CC([H])=C5Cl	$C_{30}H_{29}ClF_3N_5O_3$	600.04		–	0.12	170
63i	O=C(N1CCC(N(CCOC)C=N2)=C2C1)CN3C(C(C(C(NC4=CC=C(N(N=C5)C(C)=C5C(CCC)=O)C=C4)=O)=C3)=C6)=CC([H])=C6Cl	$C_{34}H_{36}ClN_7O_4$	642.16		–	0.12	193
64i	O=C(N1CCN(CCF)CC1)CN2C(C(C(C(NC3=CC=C(N(N=C4)C(C)=C4C(CCC)=O)C=C3)=O)=C2)=C5)=CC([H])=C5Cl	$C_{31}H_{34}ClFN_6O_3$	593.10		–	0.13	142
65i	O=C(N1CCN(CC2=NOC(C)=C2)CC1)CN3C(C(C(C(NC4=CC=C(N(N=C5)C(C)=C5C(CCC)=O)C=C4)=O)=C3)=C6)=CC([H])=C6Cl	$C_{34}H_{36}ClN_7O_4$	628.13		11	0.14	166
66i	O=C(N1CCN(CC(N(C)C)=O)CC1)CN2C(C(C(C(NC3=CC=C(N(N=C4)C(C)=C4C(CCC)=O)C=C3)=O)=C2)=C5)=CC([H])=C5Cl	$C_{33}H_{38}ClN_7O_4$	632.16		11	0.15	154

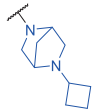
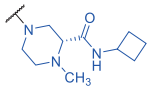
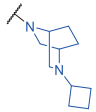
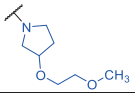
67i	O=C(N1CCN(CCS(=O)(C)=O)CC1)CN2C(C(C(C(NC3=CC=C(N(N=C4)C(C)=C4C(CCC)=O)C=C3)=O)=C2)=C5)=CC([H])=C5Cl	$C_{32}H_{37}ClN_6O_5S$	653.20		–	0.15	148
68i	O=C(N1CCN(C2COC2)CC1)CN3C(C(C(C(NC4=CC=C(N(N=C5)C(C)=C5C(CCC)=O)C=C4)=O)=C3)=C6)=CC([H])=C6Cl	$C_{32}H_{35}ClN_6O_4$	603.12		–	0.16	191
69i	O=C(N1CCN(C)C(C1)=O)CN2C(C(C(C(NC3=CC=C(N(N=C4)C(C)=C4C(CCC)=O)C=C3)=O)=C2)=C5)=CC([H])=C5Cl	$C_{30}H_{31}ClN_6O_4$	575.07		–	0.17	184
70i	O=C(N1CCC(NN=C2)=C2C1)CN3C(C(C(C(NC4=CC=C(N(N=C5)C(C)=C5C(CCC)=O)C=C4)=O)=C3)=C6)=CC([H])=C6Cl	$C_{31}H_{30}ClN_7O_3$	584.08		–	0.17	173
71i	O=C(N1CCN(C(C)COC)CC1)CN2C(C(C(C(NC3=CC=C(N(N=C4)C(C)=C4C(CCC)=O)C=C3)=O)=C2)=C5)=CC([H])=C5Cl	$C_{33}H_{39}ClN_6O_4$	619.16		–	0.17	179
72i	O=C(N1CCN(C(C)(C)CO)CC1)CN2C(C(C(C(NC3=CC=C(N(N=C4)C(C)=C4C(CCC)=O)C=C3)=O)=C2)=C5)=CC([H])=C5Cl	$C_{33}H_{39}ClN_6O_4$	619.16		–	0.18	181
73i	O=C(N1CCN(CCOCCO)CC1)CN2C(C(C(C(NC3=CC=C(N(N=C4)C(C)=C4C(CCC)=O)C=C3)=O)=C2)=C5)=CC([H])=C5Cl	$C_{33}H_{39}ClN_6O_5$	635.16		–	0.19	144
74i	O=C(N1CCC(N(C)C=N2)=C2C1)CN3C(C(C(C(NC4=CC=C(N(N=C5)C(C)=C5C(CCC)=O)C=C4)=O)=C3)=C6)=CC([H])=C6Cl	$C_{32}H_{32}ClN_7O_3$	598.10		–	0.20	194
75i	O=C(N1CCN(C)C(CCO)C1)CN2C(C(C(C(NC3=CC=C(N(N=C4)C(C)=C4C(CCC)=O)C=C3)=O)=C2)=C5)=CC([H])=C5Cl	$C_{32}H_{37}ClN_6O_4$	605.14		–	0.22	152
76i	O=C(N1CCNCC1)CN2C(C(C(C(NC3=CC=C(N(N=C4)C(C)=C4C(CCC)=O)C=C3)=O)=C2)=C5)=CC([H])=C5Cl	$C_{29}H_{31}ClN_6O_3$	547.06		–	0.23	256
77i	O=C(N1CCN(C(CC2)=O)C2C1)CN3C(C(C(C(NC4=CC=C(N(N=C5)C(C)=C5C(CCC)=O)C=C4)=O)=C3)=C6)=CC([H])=C6Cl	$C_{32}H_{33}ClN_6O_4$	601.10		–	0.23	183

78i	O=C(N1CCN(C)C(CCOC)C1)CN2C(C(C(C(NC3=CC=C(N(N=C4)C(C)=C4C(CCC)=O)C=C3)=O)=C2)=C5)=CC([H])=C5Cl	$C_{33}H_{39}ClN_6O_4$	605.14		–	0.23	196
79i	O=C(N1CCN(CCN(C)C)CC1)CN2C(C(C(C(NC3=CC=C(N(N=C4)C(C)=C4C(CCC)=O)C=C3)=O)=C2)=C5)=CC([H])=C5Cl	$C_{33}H_{40}ClN_7O_3$	618.18		–	0.24	150
80i	O=C(N1CCN(C(C)(C)COC)CC1)CN2C(C(C(C(NC3=CC=C(N(N=C4)C(C)=C4C(CCC)=O)C=C3)=O)=C2)=C5)=CC([H])=C5Cl	$C_{34}H_{41}ClN_6O_4$	633.19		–	0.24	180
81i	O=C(N1CCN(C)C(C)(C)C1)CN2C(C(C(C(NC3=CC=C(N(N=C4)C(C)=C4C(CCC)=O)C=C3)=O)=C2)=C5)=CC([H])=C5Cl	$C_{32}H_{37}ClN_6O_3$	589.14		–	0.25	186
82i	O=C(N1CCN(CCCC)CC1)CN2C(C(C(C(NC3=CC=C(N(N=C4)C(C)=C4C(CCC)=O)C=C3)=O)=C2)=C5)=CC([H])=C5Cl	$C_{33}H_{39}ClN_6O_3$	603.16		–	0.25	151
83i	O=C(N1CCN(CCNC(C)=O)CC1)CN2C(C(C(C(NC3=CC=C(N(N=C4)C(C)=C4C(CCC)=O)C=C3)=O)=C2)=C5)=CC([H])=C5Cl	$C_{33}H_{38}ClN_7O_4$	632.16		–	0.25	197
84i	O=C(N1CCN(CCOCCOC)CC1)CN2C(C(C(C(NC3=CC=C(N(N=C4)C(C)=C4C(CCC)=O)C=C3)=O)=C2)=C5)=CC([H])=C5Cl	$C_{34}H_{41}ClN_6O_5$	649.19		–	0.25	145
85i	O=C(N1CCN(CC(OCC)=O)CC1)CN2C(C(C(C(NC3=CC=C(N(N=C4)C(C)=C4C(CCC)=O)C=C3)=O)=C2)=C5)=CC([H])=C5Cl	$C_{33}H_{37}ClN_6O_5$	633.15		–	0.26	155
86i	O=C(N1CCN2C=NN=C2C1)CN3C(C(C(C(NC4=CC=C(N(N=C5)C(C)=C5C(CCC)=O)C=C4)=O)=C3)=C6)=CC([H])=C6Cl	$C_{30}H_{29}ClN_8O_3$	585.07		–	0.27	182
87i	O=C(N1CC(CC2)N(C)C2C1)CN3C(C(C(C(NC4=CC=C(N(N=C5)C(C)=C5C(CCC)=O)C=C4)=O)=C3)=C6)=CC([H])=C6Cl	$C_{32}H_{35}ClN_6O_3$	587.12		–	0.27	192
88i	O=C(N1CCN(CC(N)=O)CC1)CN2C(C(C(C(NC3=CC=C(N(N=C4)C(C)=C4C(CCC)=O)C=C3)=O)=C2)=C5)=CC([H])=C5Cl	$C_{31}H_{34}ClN_7O_4$	604.11		–	0.27	199

89i	O=C(N1CCC(N(C)N=C2)=C2C1)CN3C(C(C(C(NC4=CC=C(N(N=C5)C(C)=C5C(CCC)=O)C=C4)=O)=C3)=C6)=CC([H])=C6Cl	$C_{32}H_{32}ClN_7O_3$	598.10		–	0.28	195
90i	O=C(N1CCN(CCN(C)C(C)=O)CC1)CN2C(C(C(C(NC3=CC=C(N(N=C4)C(C)=C4C(CCC)=O)C=C3)=O)=C2)=C5)=CC([H])=C5Cl	$C_{34}H_{40}ClN_7O_4$	646.19		–	0.28	211
91i	O=C(N1CC(NN=C2)=C2C1)CN3C(C(C(C(NC4=CC=C(N(N=C5)C(C)=C5C(CCC)=O)C=C4)=O)=C3)=C6)=CC([H])=C6Cl	$C_{30}H_{28}ClN_7O_3$	570.05		–	0.29	175
92i	O=C(N1CCN(CC(NC)=O)CC1)CN2C(C(C(C(NC3=CC=C(N(N=C4)C(C)=C4C(CCC)=O)C=C3)=O)=C2)=C5)=CC([H])=C5Cl	$C_{32}H_{36}ClN_7O_4$	618.14		–	0.29	163
93i	O=C(N1CCN(CCC(OCC)=O)CC1)CN2C(C(C(C(NC3=CC=C(N(N=C4)C(C)=C4C(CCC)=O)C=C3)=O)=C2)=C5)=CC([H])=C5Cl	$C_{34}H_{39}ClN_6O_5$	647.17		–	0.29	153
94i	O=C(N1CCNCC1C)CN2C(C(C(C(NC3=CC=C(N(N=C4)C(C)=C4C(CCC)=O)C=C3)=O)=C2)=C5)=CC([H])=C5Cl	$C_{30}H_{33}ClN_6O_3$	561.08		–	0.30	258
95i	O=C(N1CCN(CCC)CC1)CN2C(C(C(C(NC3=CC=C(N(N=C4)C(C)=C4C(CCC)=O)C=C3)=O)=C2)=C5)=CC([H])=C5Cl	$C_{32}H_{37}ClN_6O_3$	575.11		–	0.30	156
96i	O=C(N1CCN([C@@H]2CCC[C@H]2O)CC1)CN3C(C(C(C(NC4=CC=C(N(N=C5)C(C)=C5C(CCC)=O)C=C4)=O)=C3)=C6)=CC([H])=C6Cl	$C_{34}H_{39}ClN_6O_4$	631.17		–	0.31	207
97i	O=C(N1CCN(CC2=CC=C(F)C=C2)CC1)CN3C(C(C(C(NC4=CC=C(N(N=C5)C(C)=C5C(CCC)=O)C=C4)=O)=C3)=C6)=CC([H])=C6Cl	$C_{36}H_{36}ClFN_6O_3$	655.17		–	0.31	165
98i	O=C(N1CCN(C)CC1)CN2C(C(C(C(NC3=CC=C(N(N=C4)C(C)=C4C(CCC)=O)C=C3)=O)=C2)=C5)=CC([H])=C5Cl	$C_{30}H_{33}ClN_6O_3$	561.08		27	0.32	115
99i	O=C(N1CCN(CCOC)CC1)CN2C(C(C(C(NC3=CC=C(N(N=C4)C(C)=C4C(CCC)=O)C=C3)=O)=C2)=C5)=CC([H])=C5Cl	$C_{32}H_{37}ClN_6O_4$	605.14		15	0.32	105

100i	O=C(N1CCN2C(C1)=CN=C2)CN3C(C(C(C(NC4=CC=C(N(N=C5)C(C)=C5C(CCC)=O)C=C4)=O)=C3)=C6)=CC([H])=C6Cl	$C_{31}H_{30}ClN_7O_3$	584.08		–	0.33	172
101i	O=C(N1CC[C@@H](NC(C)=O)C1)CN2C(C(C(C(NC3=CC=C(N(N=C4)C(C)=C4C(CCC)=O)C=C3)=O)=C2)=C5)=CC([H])=C5Cl	$C_{31}H_{33}ClN_6O_4$	589.09		–	0.36	190
102i	O=C(N1CCN(C)C[C@H]1C)CN2C(C(C(C(NC3=CC=C(N(N=C4)C(C)=C4C(CCC)=O)C=C3)=O)=C2)=C5)=CC([H])=C5Cl	$C_{31}H_{35}ClN_6O_3$	575.11		–	0.37	177
103i	O=C(N1CCC(OCCO)C1)CN2C(C(C(C(NC3=CC=C(N(N=C4)C(C)=C4C(CCC)=O)C=C3)=O)=C2)=C5)=CC([H])=C5Cl	$C_{31}H_{34}ClN_5O_5$	592.09		–	0.37	208
104i	O=C(N1CCN(CCOCC)CC1)CN2C(C(C(C(NC3=CC=C(N(N=C4)C(C)=C4C(CCC)=O)C=C3)=O)=C2)=C5)=CC([H])=C5Cl	$C_{33}H_{39}ClN_6O_4$	619.16		–	0.37	161
105i	O=C(N1CCN(CC2=CC=CC=C2OC)CC1)CN3C(C(C(C(NC4=CC=C(N(N=C5)C(C)=C5C(CCC)=O)C=C4)=O)=C3)=C6)=CC([H])=C6Cl	$C_{37}H_{39}ClN_6O_4$	667.21		–	0.37	168
106i	O=C(N1CC(O)C1)CN2C(C(C(C(NC3=CC=C(N(N=C4)C(C)=C4C(CCC)=O)C=C3)=O)=C2)=C5)=CC([H])=C5Cl	$C_{28}H_{28}ClN_5O_4$	519.99		–	0.39	176
107i	O=C(N(C)C1CS(CC1)(=O)=O)CN2C(C(C(C(NC3=CC=C(N(N=C4)C(C)=C4C(CCC)=O)C=C3)=O)=C2)=C5)=CC([H])=C5Cl	$C_{30}H_{32}ClN_5O_5S$	610.13		–	0.40	169
108i	O=C(N1CCC(F)(F)C1)CN2C(C(C(C(NC3=CC=C(N(N=C4)C(C)=C4C(CCC)=O)C=C3)=O)=C2)=C5)=CC([H])=C5Cl	$C_{29}H_{28}ClF_2N_5O_3$	568.02		–	0.41	189
109i	O=C(N1CC(C)NC(C)C1)CN2C(C(C(C(NC3=CC=C(N(N=C4)C(C)=C4C(CCC)=O)C=C3)=O)=C2)=C5)=CC([H])=C5Cl	$C_{31}H_{35}ClN_6O_3$	575.11		–	0.41	159
110i	O=C(N1CCC(N2CCOCC2)CC1)CN3C(C(C(C(NC4=CC=C(N(N=C5)C(C)=C5C(CCC)=O)C=C4)=O)=C3)=C6)=CC([H])=C6Cl	$C_{34}H_{39}ClN_6O_4$	631.17		–	0.41	149
111i	O=C(N1CCN(CC(N2CCCC2)=O)CC1)CN3C(C(C(C(NC4=CC=C(N(N=C5)C(C)=C5C(CCC)=O)C=C4)=O)=C3)=C6)=CC([H])=C6Cl	$C_{35}H_{40}ClN_7O_4$	658.20		–	0.41	198
112i	O=C(N1CCN(CC(C(F)(F)F)O)CC1)CN2C(C(C(C(NC3=CC=C(N(N=C4)C(C)=C4C(CCC)=O)C=C3)=O)=C2)=C5)=CC([H])=C5Cl	$C_{32}H_{34}ClF_3N_6O_4$	659.11		–	0.42	209

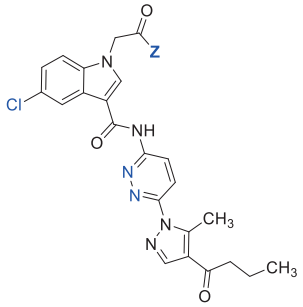
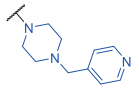
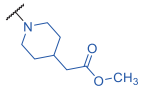
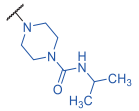
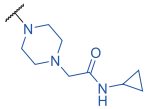
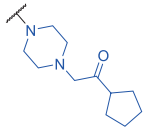
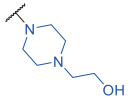
113i	O=C(N1CCN(C)C(COC)C1)CN2C(C(C(C(NC3=CC=C(N(N=C4)C(C)=C4C(CCC)=O)C=C3)=O)=C2)=C5)=CC([H])=C5Cl	$C_{32}H_{37}ClN_6O_4$	605.14		–	0.43	202
114i	O=C(N1C[C@@]2([H])N(CCOC)C[C@]1([H])CC2)CN3C(C(C(C(NC4=CC=C(N(N=C5)C(C)=C5C(CCC)=O)C=C4)=O)=C3)=C6)=CC([H])=C6Cl	$C_{34}H_{39}ClN_6O_4$	631.17		–	0.44	204
115i	O=C(N1C[C@@]2([H])[C@@H](CCOC)C[C@]1([H])C2)CN3C(C(C(C(NC4=CC=C(N(N=C5)C(C)=C5C(CCC)=O)C=C4)=O)=C3)=C6)=CC([H])=C6Cl	$C_{34}H_{38}ClN_5O_4$	616.16		–	0.44	205
116i	O=C(N1CC2NC(CC2)C1)CN3C(C(C(C(NC4=CC=C(N(N=C5)C(C)=C5C(CCC)=O)C=C4)=O)=C3)=C6)=CC([H])=C6Cl	$C_{31}H_{33}ClN_6O_3$	573.09		–	0.45	259
117i	O=C(N1CCNC(C)C1)CN2C(C(C(C(NC3=CC=C(N(N=C4)C(C)=C4C(CCC)=O)C=C3)=O)=C2)=C5)=CC([H])=C5Cl	$C_{30}H_{33}ClN_6O_3$	561.08		–	0.46	257
118i	O=C(N1CCN(CC2=CC=C(Cl)C=C2)CC1)CN3C(C(C(C(NC4=CC=C(N(N=C5)C(C)=C5C(CCC)=O)C=C4)=O)=C3)=C6)=CC([H])=C6Cl	$C_{36}H_{36}Cl_2N_6O_3$	671.62		–	0.47	167
119i	O=C(N(CCOC)C)CN1C(C(C(C(NC2=CC=C(N(N=C3)C(C)=C3C(CCC)=O)C=C2)=O)=C1)=C4)=CC([H])=C4Cl	$C_{29}H_{32}ClN_5O_4$	550.06		–	0.48	200
120i	O=C(N1CC(C=NN2C)=C2C1)CN3C(C(C(C(NC4=CC=C(N(N=C5)C(C)=C5C(CCC)=O)C=C4)=O)=C3)=C6)=CC([H])=C6Cl	$C_{31}H_{30}ClN_7O_3$	584.08		–	0.49	174
121i	O=C(N1CCN2C[C@@H](O)C[C@@H]2[C@@H]1C)CN3C(C(C(C(NC4=CC=C(N(N=C5)C(C)=C5C(CCC)=O)C=C4)=O)=C3)=C6)=CC([H])=C6Cl	$C_{33}H_{37}ClN_6O_4$	617.15		–	0.50	162
122i	O=C(N1CC[C@H](C(NC2CC2)=O)C1)CN3C(C(C(C(NC4=CC=C(N(N=C5)C(C)=C5C(CCC)=O)C=C4)=O)=C3)=C6)=CC([H])=C6Cl	$C_{33}H_{35}ClN_6O_4$	615.13		–	0.55	188
123i	O=C(N1C[C@@H](O)C[C@@H]1C(NC2CCC2)=O)CN3C(C(C(C(NC4=CC=C(N(N=C5)C(C)=C5C(CCC)=O)C=C4)=O)=C3)=C6)=CC([H])=C6Cl	$C_{34}H_{37}ClN_6O_5$	645.16		–	0.57	171
124i	O=C(N1CC(N=CC=C2)=C2C1)CN3C(C(C(C(NC4=CC=C(N(N=C5)C(C)=C5C(CCC)=O)C=C4)=O)=C3)=C6)=CC([H])=C6Cl	$C_{32}H_{29}ClN_6O_3$	581.07		–	0.61	187
125i	O=C(N1CCN(C2CCC2)CC1)CN3C(C(C(C(NC4=CC=C(N(N=C5)C(C)=C5C(CCC)=O)C=C4)=O)=C3)=C6)=CC([H])=C6Cl	$C_{33}H_{37}ClN_6O_3$	601.15		–	0.65	201

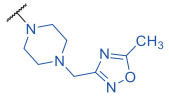
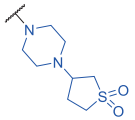
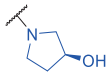
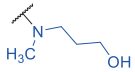
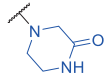
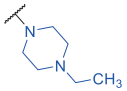
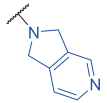
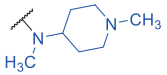
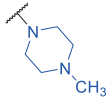
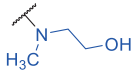
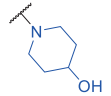
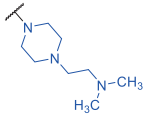
126i	O=C(N1CC2N(C3CCC3)CC1C2)CN4C(C(C(C(NC5=CC=C(N(N=C6)C(C)=C6C(CCC)=O)C=C5)=O)=C4)=C7)=CC([H])=C7Cl	$C_{34}H_{37}ClN_6O_3$	613.16		–	0.66	214
127i	O=C(N1CCN(C)[C@@H](C(NC2CCC2)=O)C1)CN3C(C(C(C(NC4=CC=C(N(N=C5)C(C)=C5C(CCC)=O)C=C4)=O)=C3)=C6)=CC([H])=C6Cl	$C_{35}H_{40}ClN_7O_4$	658.20		–	0.70	210
128i	O=C(N1C(CN2C3CCC3)CCC2C1)CN4C(C(C(C(NC5=CC=C(N(N=C6)C(C)=C6C(CCC)=O)C=C5)=O)=C4)=C7)=CC([H])=C7Cl	$C_{35}H_{39}ClN_6O_3$	627.19		–	0.76	215
129i	O=C(N1CCC(OCCOC)C1)CN2C(C(C(C(NC3=CC=C(N(N=C4)C(C)=C4C(CCC)=O)C=C3)=O)=C2)=C5)=CC([H])=C5Cl	$C_{32}H_{36}ClN_5O_5$	592.09		–	0.83	206

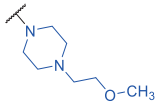
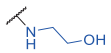
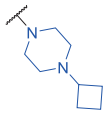
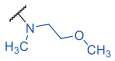
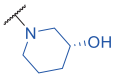
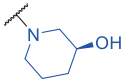
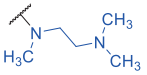
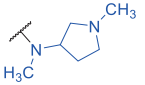
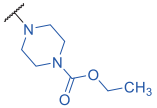
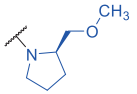
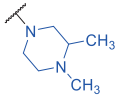
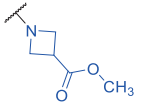
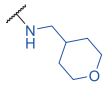
[a] Displacement of [^{33}P]2MeS-ADP from P2Y$_{12}$ receptor transfected in CHO cells after 30 mins by scintillation counting analysis.

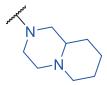
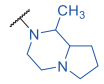
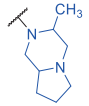
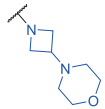
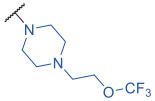
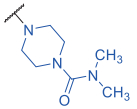
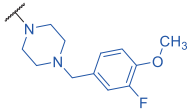
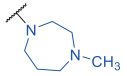
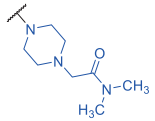
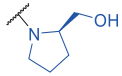
[b] Inhibition of ADP-induced platelet aggregation in rat (rPRP) platelet-rich-plasma.

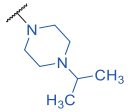
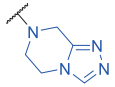
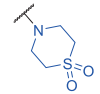
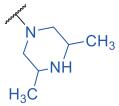
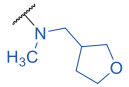
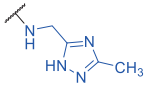
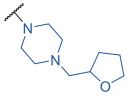
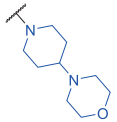
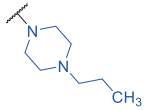
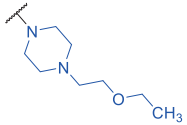
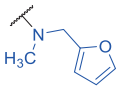
Table S17. SAR Analysis of pyrazolyl-**pyridazinyl**-carbamoyl-**5-chloro**indole-**carboxamide** sub-scaffold (**E**) (75 compounds).[62,63]

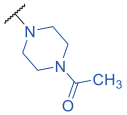
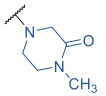
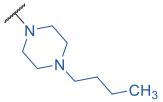
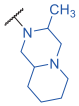
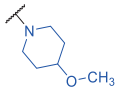
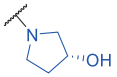
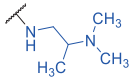
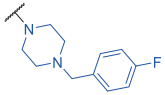
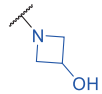
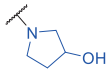
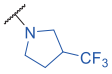
ID	Smiles	Chemical formula	MW (g/mol)	Structure	Affinity[a] (IC_{50}) in nM	rPRP[b] (IC_{50}) in µM	Compound number in original publication
				 **Z**			
130i	O=C(N1CCN(CC2=CC=NC=C2)CC1)CN3C(C(C(C(NC4=NN=C(N(N=C5)C(C)=C5C(CCC)=O)C=C4)=O)=C3)=C6)=CC([H])=C6Cl	$C_{33}H_{34}ClN_9O_3$	640.15		–	0.03	102
131i	O=C(N1CCN(CC(OC)=O)CC1)CN2C(C(C(C(NC3=NN=C(N(N=C4)C(C)=C4C(CCC)=O)C=C3)=O)=C2)=C5)=CC([H])=C5Cl	$C_{30}H_{33}ClN_8O_5$	605.10		–	0.04	87
132i	O=C(N1CCN(C(NC(C)C)=O)CC1)CN2C(C(C(C(NC3=NN=C(N(N=C4)C(C)=C4C(CCC)=O)C=C3)=O)=C2)=C5)=CC([H])=C5Cl	$C_{31}H_{36}ClN_9O_4$	634.14		–	0.04	39
133i	O=C(N1CCN(CC(NC2CC2)=O)CC1)CN3C(C(C(C(NC4=NN=C(N(N=C5)C(C)=C5C(CCC)=O)C=C4)=O)=C3)=C6)=CC([H])=C6Cl	$C_{32}H_{36}ClN_9O_4$	646.15		–	0.04	81
134i	O=C(N1CCN(CC(C2CCCC2)=O)CC1)CN3C(C(C(C(NC4=NN=C(N(N=C5)C(C)=C5C(CCC)=O)C=C4)=O)=C3)=C6)=CC([H])=C6Cl	$C_{34}H_{39}ClN_8O_4$	659.19		–	0.04	46
135i	O=C(N1CCN(CCO)CC1)CN2C(C(C(C(NC3=NN=C(N(N=C4)C(C)=C4C(CCC)=O)C=C3)=O)=C2)=C5)=CC([H])=C5Cl	$C_{29}H_{33}ClN_8O_4$	593.09		–	0.05	50

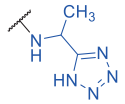
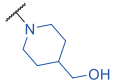
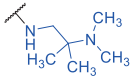
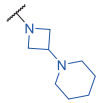
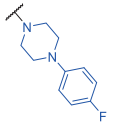
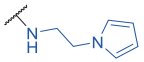
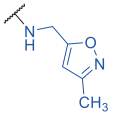
136i	O=C(N1CCN(CC2=NOC(C)=N2)CC1)CN3C(C(C(C(NC4=NN=C(N(N=C5)C(C)=C5C(CCC)=O)C=C4)=O)=C3)=C6)=CC([H])=C6Cl	$C_{31}H_{33}ClN_{10}O_4$	645.12		–	0.05	82
137i	O=C(N1CCN(C2CCS(C2)(=O)=O)CC1)CN3C(C(C(C(NC4=NN=C(N(N=C5)C(C)=C5C(CCC)=O)C=C4)=O)=C3)=C6)=CC([H])=C6Cl	$C_{31}H_{35}ClN_8O_5S$	667.18		–	0.05	73
138i	O=C(N(C)C1CC1)CN2C(C(C(C(NC3=NN=C(N(N=C4)C(C)=C4C(CCC)=O)C=C3)=O)=C2)=C5)=CC([H])=C5Cl	$C_{27}H_{28}ClN_7O_3$	534.02		–	0.06	90
139i	O=C(N1CC[C@H](O)C1)CN2C(C(C(C(NC3=NN=C(N(N=C4)C(C)=C4C(CCC)=O)C=C3)=O)=C2)=C5)=CC([H])=C5Cl	$C_{27}H_{28}ClN_7O_4$	550.02		–	0.06	57
140i	O=C(N(C)CCCO)CN1C(C(C(C(NC2=NN=C(N(N=C3)C(C)=C3C(CCC)=O)C=C2)=O)=C1)=C4)=CC([H])=C4Cl	$C_{27}H_{30}ClN_7O_4$	552.03		–	0.06	72
141i	O=C(N1CCNC(C1)=O)CN2C(C(C(C(NC3=NN=C(N(N=C4)C(C)=C4C(CCC)=O)C=C3)=O)=C2)=C5)=CC([H])=C5Cl	$C_{27}H_{27}ClN_8O_4$	563.02		–	0.06	64
142i	O=C(N1CCN(CC)CC1)CN2C(C(C(C(NC3=NN=C(N(N=C4)C(C)=C4C(CCC)=O)C=C3)=O)=C2)=C5)=CC([H])=C5Cl	$C_{29}H_{33}ClN_8O_3$	577.09		–	0.06	47
143i	O=C(N1CC(C=CN=C2)=C2C1)CN3C(C(C(C(NC4=NN=C(N(N=C5)C(C)=C5C(CCC)=O)C=C4)=O)=C3)=C6)=CC([H])=C6Cl	$C_{30}H_{27}ClN_8O_3$	583.05		–	0.06	76
144i	O=C(N(C1CCN(C)CC1)C)CN2C(C(C(C(NC3=NN=C(N(N=C4)C(C)=C4C(CCC)=O)C=C3)=O)=C2)=C5)=CC([H])=C5Cl	$C_{30}H_{35}ClN_8O_3$	591.11		–	0.06	52
6i	O=C(N1CCN(C)CC1)CN2C(C(C(C(NC3=NN=C(N(N=C4)C(C)=C4C(CCC)=O)C=C3)=O)=C2)=C5)=CC([H])=C5Cl	$C_{28}H_{31}ClN_8O_3$	563.06		–	0.06	28
145i	O=C(N(CCO)C)CN1C(C(C(C(NC2=NN=C(N(N=C3)C(C)=C3C(CCC)=O)C=C2)=O)=C1)=C4)=CC([H])=C4Cl	$C_{26}H_{28}ClN_7O_4$	538.01		–	0.07	38
146i	O=C(N1CCC(O)CC1)CN2C(C(C(C(NC3=NN=C(N(N=C4)C(C)=C4C(CCC)=O)C=C3)=O)=C2)=C5)=CC([H])=C5Cl	$C_{28}H_{30}ClN_7O_4$	564.04		–	0.07	68
147i	O=C(N1CCN(CCN(C)C)CC1)CN2C(C(C(C(NC3=NN=C(N(N=C4)C(C)=C4C(CCC)=O)C=C3)=O)=C2)=C5)=CC([H])=C5Cl	$C_{31}H_{38}ClN_9O_3$	620.16		–	0.07	98

148i	O=C(N1CCN(CCOC)CC1)CN2C(C(C(C(NC3=NN=C(N(N=C4)C(C)=C4C(CCC)=O)C=C3)=O)=C2)=C5)=CC([H])=C5Cl	$C_{30}H_{35}ClN_8O_4$	607.11		–	0.08	29
149i	O=C(NCCO)CN1C(C(C(C(NC2=NN=C(N(N=C3)C(C)=C3C(CCC)=O)C=C2)=O)=C1)=C4)=CC([H])=C4Cl	$C_{25}H_{26}ClN_7O_4$	523.98		–	0.08	33
150i	O=C(N1CCN(C2CCC2)CC1)CN3C(C(C(C(NC4=NN=C(N(N=C5)C(C)=C5C(CCC)=O)C=C4)=O)=C3)=C6)=CC([H])=C6Cl	$C_{31}H_{35}ClN_8O_3$	603.12		–	0.08	79
151i	O=C(N(C)CCOC)CN1C(C(C(C(NC2=NN=C(N(N=C3)C(C)=C3C(CCC)=O)C=C2)=O)=C1)=C4)=CC([H])=C4Cl	$C_{27}H_{30}ClN_7O_4$	552.03		–	0.09	61
152i	O=C(N1CCC[C@@H](O)C1)CN2C(C(C(C(NC3=NN=C(N(N=C4)C(C)=C4C(CCC)=O)C=C3)=O)=C2)=C5)=CC([H])=C5Cl	$C_{28}H_{30}ClN_7O_4$	564.04		–	0.09	87
153i	O=C(N1CCC[C@H](O)C1)CN2C(C(C(C(NC3=NN=C(N(N=C4)C(C)=C4C(CCC)=O)C=C3)=O)=C2)=C5)=CC([H])=C5Cl	$C_{28}H_{30}ClN_7O_4$	564.04		–	0.09	59
154i	O=C(N(C)CCN(C)C)CN1C(C(C(C(NC2=NN=C(N(N=C3)C(C)=C3C(CCC)=O)C=C2)=O)=C1)=C4)=CC([H])=C4Cl	$C_{28}H_{33}ClN_8O_3$	565.08		–	0.09	97
155i	O=C(N(C)C1CCN(C)C1)CN2C(C(C(C(NC3=NN=C(N(N=C4)C(C)=C4C(CCC)=O)C=C3)=O)=C2)=C5)=CC([H])=C5Cl	$C_{29}H_{33}ClN_8O_3$	577.09		–	0.09	53
156i	O=C(N1CCN(C(OCC)=O)CC1)CN2C(C(C(C(NC3=NN=C(N(N=C4)C(C)=C4C(CCC)=O)C=C3)=O)=C2)=C5)=CC([H])=C5Cl	$C_{30}H_{33}ClN_8O_5$	621.10		–	0.09	34
157i	O=C(N1CCC[C@@H]1COC)CN2C(C(C(C(NC3=NN=C(N(N=C4)C(C)=C4C(CCC)=O)C=C3)=O)=C2)=C5)=CC([H])=C5Cl	$C_{29}H_{32}ClN_7O_4$	578.07		–	0.09	37
158i	O=C(N1CCN(C)C(C)C1)CN2C(C(C(C(NC3=NN=C(N(N=C4)C(C)=C4C(CCC)=O)C=C3)=O)=C2)=C5)=CC([H])=C5Cl	$C_{29}H_{33}ClN_8O_3$	577.09		–	0.09	77
159i	O=C(N1CC(C(OC)=O)C1)CN2C(C(C(C(NC3=NN=C(N(N=C4)C(C)=C4C(CCC)=O)C=C3)=O)=C2)=C5)=CC([H])=C5Cl	$C_{28}H_{28}ClN_7O_5$	578.03		–	0.09	103
160i	O=C(NCC1CCOCC1)CN2C(C(C(C(NC3=NN=C(N(N=C4)C(C)=C4C(CCC)=O)C=C3)=O)=C2)=C5)=CC([H])=C5Cl	$C_{29}H_{32}ClN_7O_4$	578.07		–	0.09	60

161i	O=C(N1CCN(CCCC2)C2C1)CN3C(C(C(C(NC4=NN=C(N(N=C5)C(C)=C5C(CCC)=O)C=C4)=O)=C3)=C6)=CC([H])=C6Cl	$C_{31}H_{35}ClN_8O_3$	603.12		–	0.09	67
162i	O=C(N1CCN(CCC2)C2C1C)CN3C(C(C(C(NC4=NN=C(N(N=C5)C(C)=C5C(CCC)=O)C=C4)=O)=C3)=C6)=CC([H])=C6Cl	$C_{31}H_{35}ClN_8O_3$	603.12		–	0.09	84
163i	O=C(N1CC(CCC2)N2CC1C)CN3C(C(C(C(NC4=NN=C(N(N=C5)C(C)=C5C(CCC)=O)C=C4)=O)=C3)=C6)=CC([H])=C6Cl	$C_{31}H_{35}ClN_8O_3$	603.12		–	0.09	88
164i	O=C(N1CCCC1)CN2C(C(C(C(NC3=NN=C(N(N=C4)C(C)=C4C(CCC)=O)C=C3)=O)=C2)=C5)=CC([H])=C5Cl	$C_{27}H_{28}ClN_7O_3$	534.02		–	0.10	40
165i	O=C(N1CC(N2CCOCC2)C1)CN3C(C(C(C(NC4=NN=C(N(N=C5)C(C)=C5C(CCC)=O)C=C4)=O)=C3)=C6)=CC([H])=C6Cl	$C_{30}H_{33}ClN_8O_4$	605.10		–	0.10	104
166i	O=C(N1CCN(CCOC(F)(F)F)CC1)CN2C(C(C(C(NC3=NN=C(N(N=C4)C(C)=C4C(CCC)=O)C=C3)=O)=C2)=C5)=CC([H])=C5Cl	$C_{30}H_{32}ClF_3N_8O_4$	661.08		–	0.10	30
167i	O=C(N1CCN(C(N(C)C)=O)CC1)CN2C(C(C(C(NC3=NN=C(N(N=C4)C(C)=C4C(CCC)=O)C=C3)=O)=C2)=C5)=CC([H])=C5Cl	$C_{30}H_{34}ClN_9O_4$	620.11		–	0.10	69
168i	O=C(N1CCN(CC2=CC(F)=C(OC)C=C2)CC1)CN3C(C(C(C(NC4=NN=C(N(N=C5)C(C)=C5C(CCC)=O)C=C4)=O)=C3)=C6)=CC([H])=C6Cl	$C_{35}H_{36}ClFN_8O_4$	687.17		–	0.10	85
169i	O=C(N(C)C)CN1C(C(C(C(NC2=NN=C(N(N=C3)C(C)=C3C(CCC)=O)C=C2)=O)=C1)=C4)=CC([H])=C4Cl	$C_{25}H_{26}ClN_7O_3$	507.98		–	0.11	36
170i	O=C(N1CCCN(C)CC1)CN2C(C(C(C(NC3=NN=C(N(N=C4)C(C)=C4C(CCC)=O)C=C3)=O)=C2)=C5)=CC([H])=C5Cl	$C_{29}H_{33}ClN_8O_3$	577.09		–	0.11	99
171i	O=C(N1CCN(CC(N(C)C)=O)CC1)CN2C(C(C(C(NC3=NN=C(N(N=C4)C(C)=C4C(CCC)=O)C=C3)=O)=C2)=C5)=CC([H])=C5Cl	$C_{31}H_{36}ClN_9O_4$	634.14		–	0.11	101
172i	O=C(N1CCC[C@@H]1CO)CN2C(C(C(C(NC3=NN=C(N(N=C4)C(C)=C4C(CCC)=O)C=C3)=O)=C2)=C5)=CC([H])=C5Cl	$C_{28}H_{30}ClN_7O_4$	564.04		–	0.11	41

173i	O=C(N1CCN(C(C)C)CC1)CN2C(C(C(C(NC3=NN=C(N(N=C4)C(C)=C4C(CCC)=O)C=C3)=O)=C2)=C5)=CC([H])=C5Cl	$C_{30}H_{35}ClN_8O_3$	591.11		–	0.11	54
174i	O=C(N1CCN2C(C1)=NN=C2)CN3C(C(C(C(NC4=NN=C(N(N=C5)C(C)=C5C(CCC)=O)C=C4)=O)=C3)=C6)=CC([H])=C6Cl	$C_{28}H_{27}ClN_{10}O_3$	587.04		–	0.11	70
175i	O=C(N1CCS(CC1)(=O)=O)CN2C(C(C(C(NC3=NN=C(N(N=C4)C(C)=C4C(CCC)=O)C=C3)=O)=C2)=C5)=CC([H])=C5Cl	$C_{27}H_{28}ClN_7O_5S$	598.08		–	0.12	71
176i	O=C(N1CC(C)NC(C)C1)CN2C(C(C(C(NC3=NN=C(N(N=C4)C(C)=C4C(CCC)=O)C=C3)=O)=C2)=C5)=CC([H])=C5Cl	$C_{29}H_{33}ClN_8O_3$	577.09		–	0.12	43
177i	O=C(N(C)CC1CCOC1)CN2C(C(C(C(NC3=NN=C(N(N=C4)C(C)=C4C(CCC)=O)C=C3)=O)=C2)=C5)=CC([H])=C5Cl	$C_{29}H_{32}ClN_7O_4$	578.07		–	0.12	91
178i	O=C(NCC1=NC(C)=NN1)CN2C(C(C(C(NC3=NN=C(N(N=C4)C(C)=C4C(CCC)=O)C=C3)=O)=C2)=C5)=CC([H])=C5Cl	$C_{27}H_{27}ClN_{10}O_3$	575.03		–	0.12	74
179i	O=C(N1CCN(CC2OCCC2)CC1)CN3C(C(C(C(NC4=NN=C(N(N=C5)C(C)=C5C(CCC)=O)C=C4)=O)=C3)=C6)=CC([H])=C6Cl	$C_{32}H_{37}ClN_8O_4$	633.15		–	0.12	63
180i	O=C(N1CCC(N2CCOCC2)CC1)CN3C(C(C(C(NC4=NN=C(N(N=C5)C(C)=C5C(CCC)=O)C=C4)=O)=C3)=C6)=CC([H])=C6Cl	$C_{32}H_{37}ClN_8O_4$	633.15		–	0.12	65
181i	O=C(N1CCN(CCC)CC1)CN2C(C(C(C(NC3=NN=C(N(N=C4)C(C)=C4C(CCC)=O)C=C3)=O)=C2)=C5)=CC([H])=C5Cl	$C_{30}H_{35}ClN_8O_3$	591.11		–	0.14	48
182i	O=C(N1CCN(CCOCC)CC1)CN2C(C(C(C(NC3=NN=C(N(N=C4)C(C)=C4C(CCC)=O)C=C3)=O)=C2)=C5)=CC([H])=C5Cl	$C_{31}H_{37}ClN_8O_4$	621.14		–	0.15	93
183i	O=C(N(C)CC1=CC=CO1)CN2C(C(C(C(NC3=NN=C(N(N=C4)C(C)=C4C(CCC)=O)C=C3)=O)=C2)=C5)=CC([H])=C5Cl	$C_{29}H_{28}ClN_7O_4$	574.04		–	0.15	62

184i	O=C(N1CCN(C(C)=O)CC1)CN2C(C(C(C(NC3=NN=C(N(N=C4)C(C)=C4C(CCC)=O)C=C3)=O)=C2)=C5)=CC([H])=C5Cl	$C_{29}H_{31}ClN_8O_4$	591.07		–	0.15	42
185i	O=C(N1CCN(C)C(C1)=O)CN2C(C(C(C(NC3=NN=C(N(N=C4)C(C)=C4C(CCC)=O)C=C3)=O)=C2)=C5)=CC([H])=C5Cl	$C_{28}H_{29}ClN_8O_4$	577.04		–	0.16	44
186i	O=C(N1CCN(CCCC)CC1)CN2C(C(C(C(NC3=NN=C(N(N=C4)C(C)=C4C(CCC)=O)C=C3)=O)=C2)=C5)=CC([H])=C5Cl	$C_{31}H_{37}ClN_8O_3$	605.14		–	0.16	55
187i	O=C(N1CC(CCCC2)N2CC1C)CN3C(C(C(C(NC4=NN=C(N(N=C5)C(C)=C5C(CCC)=O)C=C4)=O)=C3)=C6)=CC([H])=C6Cl	$C_{32}H_{37}ClN_8O_3$	617.15		–	0.17	89
188i	O=C(N1CCC(OC)CC1)CN2C(C(C(C(NC3=NN=C(N(N=C4)C(C)=C4C(CCC)=O)C=C3)=O)=C2)=C5)=CC([H])=C5Cl	$C_{29}H_{32}ClN_7O_4$	578.07		–	0.18	94
189i	O=C(N1CC[C@@H](O)C1)CN2C(C(C(C(NC3=NN=C(N(N=C4)C(C)=C4C(CCC)=O)C=C3)=O)=C2)=C5)=CC([H])=C5Cl	$C_{27}H_{28}ClN_7O_4$	550.02		–	0.18	51
190i	O=C(NC)CN1C(C(C(C(NC2=NN=C(N(N=C3)C(C)=C3C(CCC)=O)C=C2)=O)=C1)=C4)=CC([H])=C4Cl	$C_{24}H_{24}ClN_7O_3$	493.95		–	0.19	32
191i	O=C(N1CCOCC1)CN2C(C(C(C(NC3=NN=C(N(N=C4)C(C)=C4C(CCC)=O)C=C3)=O)=C2)=C5)=CC([H])=C5Cl	$C_{27}H_{28}ClN_7O_4$	550.02		–	0.19	35
192i	O=C(NCC(C)N(C)C)CN1C(C(C(C(NC2=NN=C(N(N=C3)C(C)=C3C(CCC)=O)C=C2)=O)=C1)=C4)=CC([H])=C4Cl	$C_{28}H_{33}ClN_8O_3$	565.08		–	0.19	100
193i	O=C(N1CCN(CC2=CC=C(F)C=C2)CC1)CN3C(C(C(C(NC4=NN=C(N(N=C5)C(C)=C5C(CCC)=O)C=C4)=O)=C3)=C6)=CC([H])=C6Cl	$C_{34}H_{34}ClFN_8O_3$	657.15		–	0.20	92
194i	O=C(N1CC(O)C1)CN2C(C(C(C(NC3=NN=C(N(N=C4)C(C)=C4C(CCC)=O)C=C3)=O)=C2)=C5)=CC([H])=C5Cl	$C_{26}H_{26}ClN_7O_4$	535.99		–	0.22	66
195i	O=C(N1CCC(O)C1)CN2C(C(C(C(NC3=NN=C(N(N=C4)C(C)=C4C(CCC)=O)C=C3)=O)=C2)=C5)=CC([H])=C5Cl	$C_{27}H_{28}ClN_7O_4$	550.02		–	0.22	49
196i	O=C(N1CCC(C(F)(F)F)C1)CN2C(C(C(C(NC3=NN=C(N(N=C4)C(C)=C4C(CCC)=O)C=C3)=O)=C2)=C5)=CC([H])=C5Cl	$C_{28}H_{27}ClF_3N_7O_3$	602.02		–	0.27	75

197i	O=C(NC(C)C1=NN=NN1)CN2C(C(C(C(NC3=NN=C(N(N=C4)C(C)=C4C(CCC)=O)C=C3)=O)=C2)=C5)=CC([H])=C5Cl	$C_{26}H_{26}ClN_{11}O_3$	576.02		–	0.28	78
198i	O=C(N1CCC(CO)CC1)CN2C(C(C(C(NC3=NN=C(N(N=C4)C(C)=C4C(CCC)=O)C=C3)=O)=C2)=C5)=CC([H])=C5Cl	$C_{29}H_{32}ClN_7O_4$	578.07		–	0.30	56
199i	O=C(NCC(N(C)C)(C)C)CN1C(C(C(C(NC2=NN=C(N(N=C3)C(C)=C3C(CCC)=O)C=C2)=O)=C1)=C4)=CC([H])=C4Cl	$C_{29}H_{35}ClN_8O_3$	579.10		–	0.33	83
200i	O=C(N1CC(N2CCCCC2)C1)CN3C(C(C(C(NC4=NN=C(N(N=C5)C(C)=C5C(CCC)=O)C=C4)=O)=C3)=C6)=CC([H])=C6Cl	$C_{31}H_{35}ClN_8O_3$	603.12		–	0.39	86
201i	O=C(N1CCN(C2=CC=C(F)C=C2)CC1)CN3C(C(C(C(NC4=NN=C(N(N=C5)C(C)=C5C(CCC)=O)C=C4)=O)=C3)=C6)=CC([H])=C6Cl	$C_{33}H_{32}ClFN_8O_3$	643.12		–	0.42	45
202i	O=C(NCCN1C=CC=C1)CN2C(C(C(C(NC3=NN=C(N(N=C4)C(C)=C4C(CCC)=O)C=C3)=O)=C2)=C5)=CC([H])=C5Cl	$C_{29}H_{29}ClN_8O_3$	573.05		–	0.45	58
203i	O=C(NCC1=CC(C)=NO1)CN2C(C(C(C(NC3=NN=C(N(N=C4)C(C)=C4C(CCC)=O)C=C3)=O)=C2)=C5)=CC([H])=C5Cl	$C_{28}H_{27}ClN_8O_4$	575.03		–	0.93	96

[a] Displacement of [^{33}P]2MeS-ADP from $P2Y_{12}$ receptor transfected in CHO cells after 30 mins by scintillation counting analysis.

[b] Inhibition of ADP-induced platelet aggregation in rat (rPRP) platelet-rich-plasma.

Acknowledgment

H.A.M.A.M. is grateful for a PhD scholarship from the Saudi Ministry of Education, Saudi Arabia. This study was supported by the Deutsche Forschungsgemeinschaft (DFG) and the Agence Nationale de la Recherche (ANR); MU 1665/12-1, project 1291 number 471773752 and ANR-21-CE18-0067-01, project 'PURImaging'.

Conflicts of interest

The authors declare no conflict of interest

3.4 Chapter IV: Selective, non-nucleotidic radiotracer for $P2Y_{12}$ receptors: Design, synthesis, characterization, and imaging of brain slices (Publication I)

*Haneen Al-Hroub, **Hashem Ali M Al Musawi**, Aliaa Abdelrahman, Vigneshwaran Namasivayam, Margot Corbel, Fanny Petit, Gunes Aksyote, Fabrice Beau, Caroline Jan, Alexis-Pierre Bemelmans, Nadja Van Camp, Marie-Anne Peyronneau, Alexandra Winkeler and Christa E. Müller*

Published in: *Journal of Medicinal Chemistry **2025**, 68, 11279–11298, doi: 10.1021/acs.jmedchem.5c00213*

Appendix III: Original publication and supporting information

Introduction

The $P2Y_{12}$ receptor ($P2Y_{12}R$) is a G protein-coupled receptor (GPCR) within the P2Y family, activated by adenosine diphosphate (ADP).[23,34] ADP-induced activation leads to the reduction of intracellular cAMP levels and subsequently the modulation of multiple cellular processes that contribute in the stabilization of platelet aggregation.[23–25,34] Structural studies have provided insight in the binding modus and identified different nucleotidic and non-nucleotidic $P2Y_{12}R$ antagonists. Several irreversible antagonists such as clopidogrel or prasugrel, as well as reversible ones such as cangrelor or ticagrelor are used clinically as antiplatelet drugs to prevent thrombotic events.[25,34,35,40–45]

Beyond its role in platelet aggregation, $P2Y_{12}R$ is expressed on microglial cells of the central nervous system (CNS).[26–33] Microglial cells represent the first defender of the CNS by responding to any dysregulation, and their response is shifting between pro- and anti-inflammatory.[92– 96] $P2Y_{12}R$ is essential for microglial chemotaxis toward extracellular ATP/ADP signals and for regulation of cytokine release, thereby playing a central role in neuroinflammatory responses. Dysregulation of $P2Y_{12}R$ has been implicated in neurodegenerative disorders such as Alzheimer's disease, Parkinson's disease, multiple sclerosis, and epilepsy.[27–32] Consequently, $P2Y_{12}R$ has emerged as both a therapeutic target for controlling excessive inflammation and a promising biomarker for in vivo imaging of neurodegeneration.[26–33]

Imaging of $P2Y_{12}R$ offers potential for early diagnosis and monitoring of disease progression, as well as evaluation of therapeutic interventions. While [^{11}C]- and [^{18}F]-labeled $P2Y_{12}R$ antagonists have been developed as PET tracers, they have shown poor brain uptake or metabolic instability. Similarly, tritium-labeled nucleotide derivatives have demonstrated limitations in selectivity and stability.[64,66,83–85,88–91]

3.4.1 Publication summary

To address the aforementioned challenges, we designed and synthesized the $P2Y_{12}R$ antagonist radioligand **[^{3}H]18** (**[^{3}H]PSB-22219**), followed by investigating its binding properties across different species using radioligand binding studies, and finally evaluating its utility for autoradiography in brain slices. In addition, we explored the metabolic stability of **[^{3}H]18** (**[^{3}H]PSB-22219**), studied structure-activity relationships (SARs), and performed modeling studies.

1. Design and synthesis of $P2Y_{12}R$ antagonist radioligand

The systematic comprehensive data analysis of reported $P2Y_{12}R$ antagonists (Chapter III) led to the identification of the pyrazolyl-phenyl-carbamoyl-indole series of compounds as a promising scaffold for the development of potent and selective $P2Y_{12}R$ antagonist radioligand candidates as tracers for imaging applications such as positron emission tomography (PET) and autoradiography or for radioligand binding studies. The unlabeled antagonist **18** (**Figure 38**) was selected as the most promising ligand for the development of a $P2Y_{12}R$ antagonist radioligand. Dehalogenative tritiation was applied as radiolabeling strategy using palladium over carbon (Pd/C) and a stream of tritium gas at an appropriate pressure to substitute the bromo atom at the C6-position of the indole of precursor **41** by tritium (**Figure 38**).

Both unlabeled ligand **18** and radioligand precursor **41** were synthesized as reported[62] in 13, and 14 synthesis steps, respectively. Key optimizations were undertaken, particularly in the synthesis of compound **18**, to reduce the number of synthesis steps, optimizing the reaction conditions and increasing the yields. Compound **41** was subsequently radiolabeled in a dehalogenative tritiation reaction to form the selective, non-nucleotidic $P2Y_{12}R$ radiotracer **[^{3}H]18** (**[^{3}H]PSB-22219**) with a specific activity of **17.4** Ci/mmol (**Figure 38**). Custom labeling was performed by a specialized compony (Tritec, Switzerland).

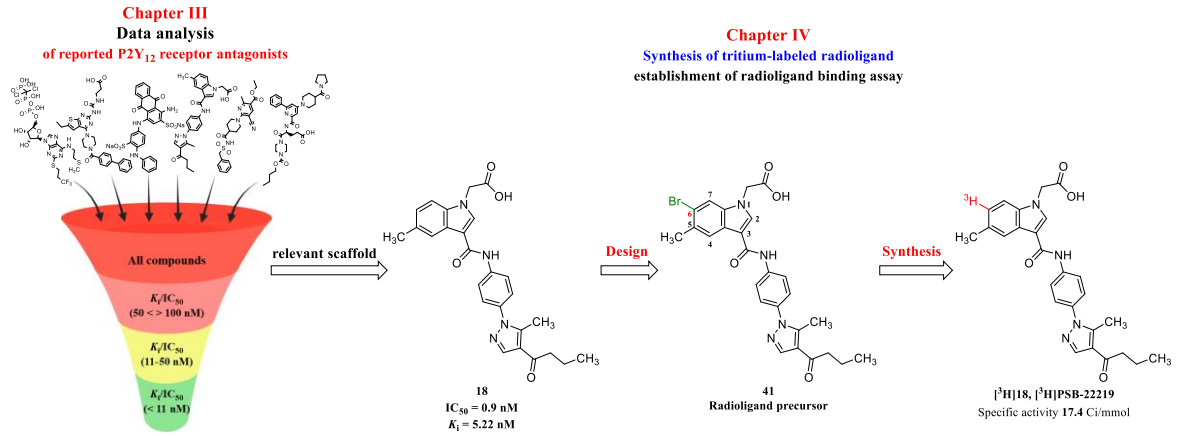


Figure 38. Design and synthesis of the unlabeled potent and selective $P2Y_{12}R$ antagonist **18**, its designed radioligand precursor **41** and the resulting radioligand **[^{3}H]18** (**[^{3}H]PSB-22219**).

2. Radioligand binding studies

Compound **[^{3}H]18** (**[^{3}H]PSB-22219**) was utilized for the establishment of radioligand binding studies which demonstrated remarkably high affinity and selectivity with K_D-values of **4.57** nM for human recombinant $P2Y_{12}R$ membranes, **2.53** nM for natively expressed $P2Y_{12}R$ on human platelets, **5.35** nM for rat brain cortex, and **269** nM for mouse microglial cell preparations, reflecting very high $P2Y_{12}R$ density in microglia.

3. Application in brain imaging (autoradiography)

Autoradiographic studies visualized $P2Y_{12}R$ expression in the brains of a humanized rat model, confirming that our radioligand **[^{3}H]18** (**[^{3}H]PSB-22219**) can clearly map receptor distribution in situ. Thus, it has been positioned as a powerful pharmacological tool for preclinical imaging of $P2Y_{12}R$ in brain tissues.

3.4.2 Author contributions

The author performed the chemistry part of this study (design, synthesis, purification, analytical characterization of LCMS and NMR data, SAR analysis, and the comparison between the radioligand **[^{3}H]18** (**[^{3}H]PSB-22219**) and other reported radioligands). In addition, he wrote the chemistry part in a close collaboration with the first author Haneen Al-Hroub and the corresponding author Prof. Dr. Christa E. Müller.

3.5 Chapter V: Design, synthesis, and properties of brain-permeable $P2Y_{12}$ receptor antagonists for neuroinflammation diseases (Manuscript III)

Hashem Ali M. Al Musawi[1], Haneen Al-Hroub[1], Marie-Anne Peyronneau[2], Alexandra Winkeler[2], Bertrand Kuhnast[2], Christa E. Müller[1]

[1]PharmaCenter Bonn, Pharmaceutical Institute, Department of Pharmaceutical & Medicinal Chemistry, University of Bonn, An der Immenburg 4, 53121 Bonn, Germany
[2]Laboratoire d'Imagerie Biomédicale Multimodale (BioMaps), CEA, CNRS, Inserm, Université Paris-Saclay, Orsay, France

Corresponding Author
Prof. Dr. Christa E. Müller
PharmaCenter Bonn
Pharmaceutical Institute
Pharmaceutical & Medicinal Chemistry
University of Bonn
An der Immenburg 4, 53121 Bonn, Germany
Phone: +49-228-73-2301
Fax: +49-228-73-2567
E-mail: christa.mueller@uni-bonn.de

3.5.1 Author contributions

The author performed the design, synthesis, purification, analytical characterization of LCMS and NMR data, as well as the discussion of the structure-property relationship (SPR), metabolic stability, and Caco-2 permeation data. In addition, he wrote the manuscript in a close collaboration with the corresponding author Prof. Dr. Christa E. Müller.

3.5.2 Abstract

Microglial cells are key players in the central nervous system (CNS). They are involved in neurodegenerative and neuroinflammatory diseases such as Alzheimer's disease (AD),

Parkinson's disease (PD), multiple sclerosis (MS) and epilepsy. $P2Y_{12}$ receptors ($P2Y_{12}Rs$) expressed on microglial cells have important roles in neuroinflammation, and therefore represent promising biomarkers for monitoring microglial function by imaging neuroinflammatory processes using imaging techniques such as positron emission tomography (PET). This study focuses on the design, synthesis and structure-property relationship (SPR) analysis of potent, selective, metabolically stable, Caco-2 permeable and potentially blood-brain barrier-permeable $P2Y_{12}$ receptor antagonists, which can be used either directly as $P2Y_{12}$-targeted therapeutics or as diagnostics after radiolabeling to perform central nervous system (CNS) imaging.

3.5.3 Introduction

Central nervous system (CNS) neurodegenerative and neuroinflammatory diseases such as Alzheimer's disease (AD), Parkinson's disease (PD), multiple sclerosis (MS) and epilepsy represent a major global health burden.[27,28] These diseases are typically characterized by progressive and irreversible neuronal loss, synaptic dysfunction, chronic neuroinflammation, and glial cell activation.[27–32] Despite extensive research, the precise mechanisms driving CNS degeneration remain incompletely understood.[27–32]

Microglia are essential brain and spinal cord cells, which constantly survey the CNS environment, and respond to injury or pathological stimuli. Their activation could be anti-inflammatory, represented in defense against disturbances, regulation of inflammatory responses, clearance of debris and pathogens, as well as developing and regulating synaptic plasticity to support neuronal functions.[29–32] However, chronic or dysregulated activation complicates neurodegeneration through sustained release of pro-inflammatory mediators such as cytokines that can lead to neurotoxicity.[92–96] Understanding the molecular mechanisms that govern microglial behavior is therefore crucial for identifying novel therapeutic targets.

The $P2Y_{12}$ receptors ($P2Y_{12}Rs$) expressed on microglial cells are reported to play a crucial role in the regulation of neuroinflammatory and neurodegenerative processes.[26] They enable the migration of microglial cells toward the injured or diseased cells as a result of an emitted signal from the physiological $P2Y_{12}R$ agonist adenosine diphosphate (ADP), which facilitates the role of microglial cells in chemotaxis and help them to modulate the release of various cytokines.[24,118–121] While $P2Y_{12}Rs$ on platelets are well-established mediators of arterial thrombosis and acute coronary syndromes (ACS), microglial $P2Y_{12}Rs$ have recently emerged as novel and promising

biomarkers for assessing microglial activation.[26,118,122–125] This has opened new avenues for non-invasive brain imaging using advanced modalities such as positron emission tomography (PET). PET-based visualization of $P2Y_{12}R$ expression may enable real-time monitoring of microglial activation, thus offering valuable insights for the diagnosis and therapeutic evaluation of CNS disorders.[26–33]

Data analysis of reported $P2Y_{12}$ receptor ($P2Y_{12}R$) antagonists identified the pyrazolyl-phenyl-carbamoyl-indole scaffold, particularly the 2-(3-((4-(4-butyryl-5-methyl-1*H*-pyrazol-1-yl)phenyl)carbamoyl)-5-methyl-1*H*-indol-1-yl)acetic acid (**1**, Figure 39), as the most promising candidate for developing CNS-penetrable $P2Y_{12}R$ antagonists. Compound **1** demonstrated high metabolic stability but no Caco-2 cell permeation which could be referred to the high polarity due to the negative charge caused by its carboxylic acid.[62,86] Nevertheless, this compound has been selected as a lead structure to develop potent, selective, metabolically stable, and potentially blood-brain barrier (BBB) penetrant $P2Y_{12}R$ antagonists. Design and synthesis of optimized analogs of compound **1** taking established CNS-filters in consideration (Table 7) represent the backbone of the current study.

Table 7. Applied CNS penetration filters.[103,104]

Properties[a]	Predicted brain permeability		
	High	Middle	Low
K_i (affinity, nM)	<11	11– 50	>50
clogD	1.00– 2.99	3.00– 3.99	>4.00
TPSA (Å²)	<90	90– 110	>110
MW (g/mol)	<450	450– 500	>500
N_{HBDs}	<2	2– 3	>3
pK_a (most acidic center)	>7	6– 7	<6

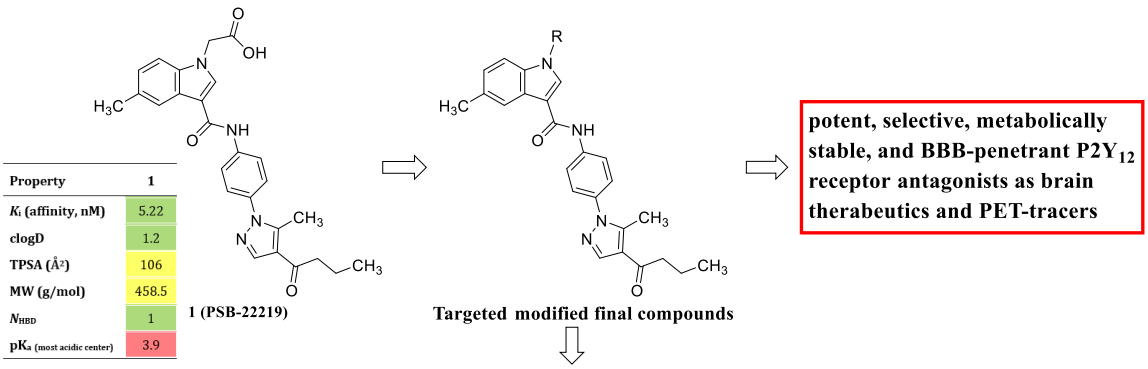
[a] **TPSA**: Topological polar surface area; **MW**: molecular weight; N_{HBDs}: number of hydrogen bond donors.

Novel pyrazolyl-phenyl-carbamoyl-indole-based compounds were designed, synthesized, and evaluated leading to potent and selective $P2Y_{12}R$ antagonists with increased lipophilicity as

compared to lead structure **1**. All predicted physicochemical properties were calculated using the *Instant JChem* tool.

3.5.4 Results and discussion

Design. Our previous data analysis study (Chapter III) identified compound **1** as a lead structure for the development of novel and potentially CNS-penetrant $P2Y_{12}R$ antagonists. Replacement of the acetic acid residue attached to the indole-nitrogen atom by small branched and unbranched substituted-alkyl chains or heterocycles, including cyclobutane, tetrahydrofuran, and fluoro-, chloro-, or methoxy substituted-alkyl residues, as well as carboxamides and ketones were targeted (Figure 39). Selection of the final compounds was based on the calculation and prediction of their physicochemical properties using the *Instant JChem* tool prior to synthesis. We focused on adjusting the pKa-values and decreasing both the molecular weight (MW) and the topological polar surface area (TPSA) to match the required prerequisite values for CNS penetration (Table 7). Replacement of the pyrazole ring by a pyrrole does not significantly affect the molecular weight (MW), which will differ just in one Dalton, however it will decrease the topological polar surface area (TPSA) by around 13 units being a hydrogen bond acceptor (HBA).



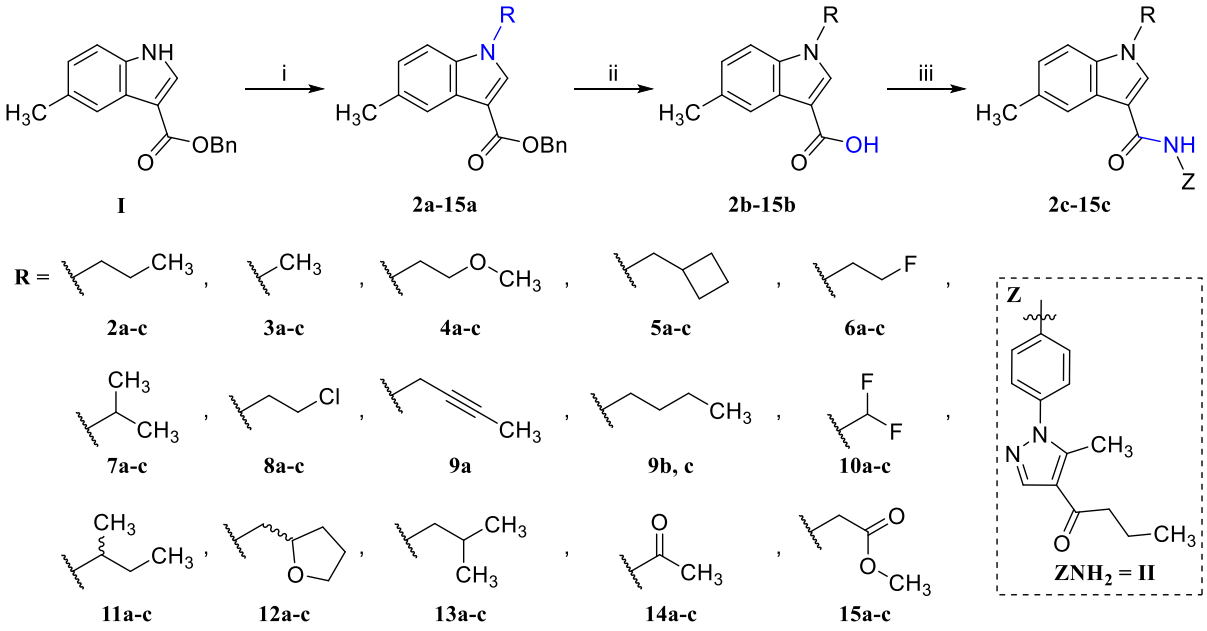
Property	1
K_i (affinity, nM)	5.22
clogD	1.2
TPSA (Å²)	106
MW (g/mol)	458.5
N_{HBD}	1
pK_a (most acidic center)	3.9

ID	R	K_i (affinity, nM)	MW (g/mol)	TPSA (Å²)	pK_a (most acidic center)	ID	R	K_i (affinity, nM)	MW (g/mol)	TPSA (Å²)	pK_a (most acidic center)
2c		–	442.6	69	>7	10c		–	450.5	69	>7
3c		–	414.5	69	>7	11c		–	456.6	69	>7
4c		–	458.6	78	>7	12c		–	484.6	78	>7
5c		–	468.6	69	>7	17		–	456.6	86	>7
6c		–	446.5	69	>7	19		–	485.6	89	>7
7c		–	442.6	69	>7	35		–	471.6	98	>7

Figure 39. Design of the targeted modified novel *N*-indole-substituted final compounds. **MW**: molecular weight; **TPSA**: topological polar surface area.

Chemistry. A total of **36** final compounds, **31** of which are novel (**2c−13c**, **17−34**, **44**, and **45**), were synthesized as depicted in Schemes 12−15. Our previously published novel intermediate **I**[86] was scaled up and utilized as starting material for the 3-step synthesis pathway. Compound **I** was alkylated using the appropriate alkyl halide in the presence of sodium hydride (NaH) in *N*,*N*-dimethylformamide (DMF) at room temperature to yield the *N*-alkylated benzyl esters (**2a−15a**, Scheme 12). Deprotection by catalytic hydrogenation using palladium over carbon (Pd/C) with H_2-gas (35 psi, 241.3 kPa) afforded the key carboxylic acids (**2b−15b**, Scheme 12), which were subsequently subjected to the amide coupling with the scaled-up aniline **II** (**ZNH$_2$**)[86] in the presence of 1-(3-dimethylaminopropyl)-3-ethylcarbodiimide hydrochloride (EDC·HCl) and 4-dimethylaminopyridine (4-DMAP) in CH_2Cl_2 yielding the targeted final compounds **2c− 15c** (Scheme 12).

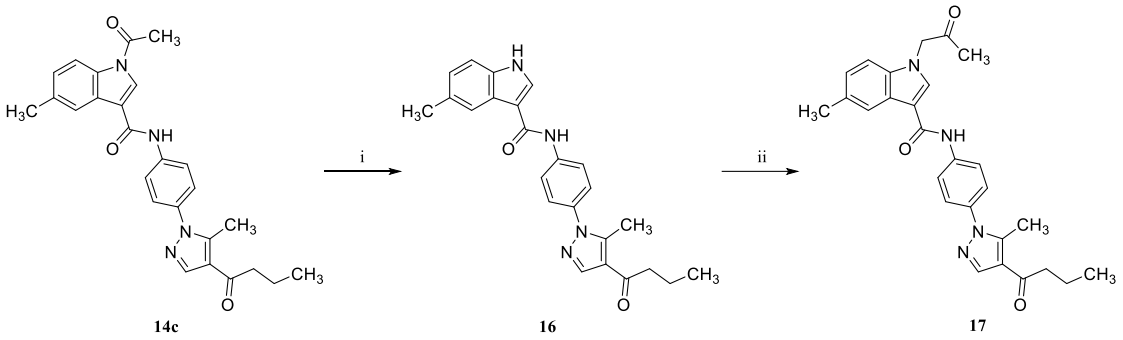
Scheme 12. Synthesis of the targeted *N*-indole substituted final compounds **2c−15c**.[a]



[a]Reagents and conditions: (i) NaH, dimethylformamide (DMF), 0 °C, 30 min; **RX**, 25 °C, 24 h (57–96%); (ii) Pd/C (10%), MeOH, H_2 (35 psi = 241.3 kPa), 25 °C, 2 h (75–100%); (iii) **ZNH$_2$** (**II**), 4-DMAP, EDC·HCl, CH_2Cl_2, 0 °C; 25 °C, 24 h (51–83%).

Deacetylation of compound **14c**[86] (Scheme 13) under basic conditions using potassium carbonate (K_2CO_3) in methanol produced **16**[86], which was further alkylated with chloroacetone in DMF in the presence of NaH to form the novel ketone final compound **17** (Scheme 13).

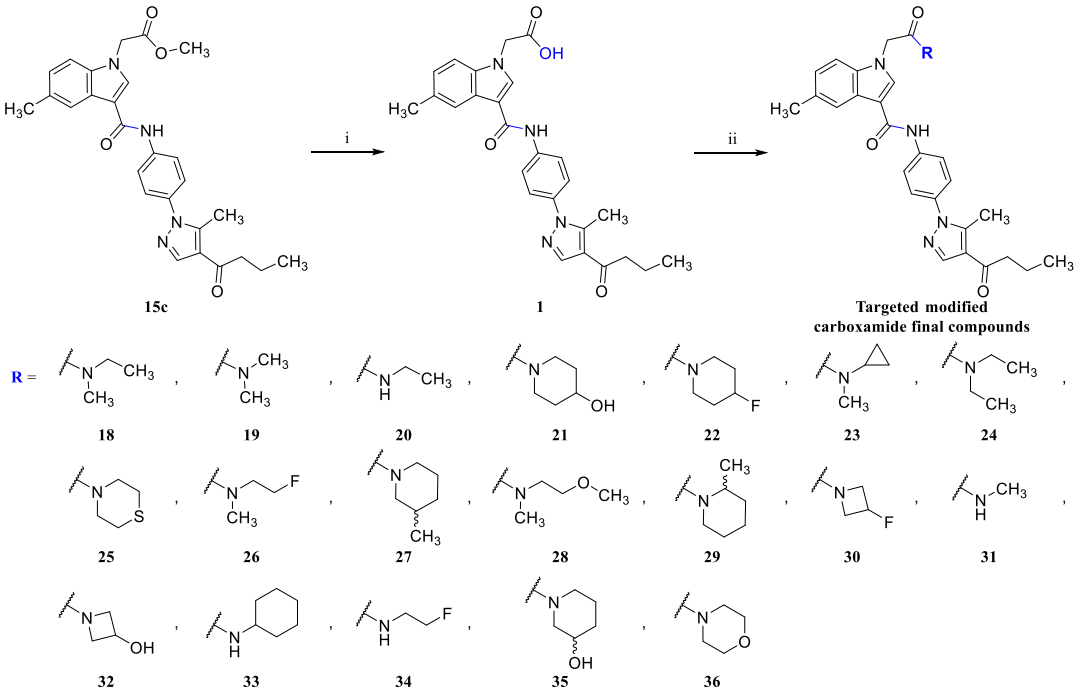
Scheme 13. Synthesis of the targeted ketone-based *N*-indole substituted final compound **17**.[a]



[a]Reagents and conditions: (i) K_2CO_3, MeOH, 25 °C, 24 h (72%)[86]; (ii) NaH, dimethylformamide (DMF), 0 °C, 30 min; **ClCH$_2$COCH$_3$**, 25 °C, 24 h (9%).

The ester **15c** (Scheme 14) was scaled-up and hydrolyzed using aqueous 2N sodium hydroxide (NaOH) in methanol at 25 °C for overnight to yield compound **1** (Scheme 14), which represents the starting material for the synthesis of the carboxamide final compounds (**18**−**37**, Scheme 14) using a selection of commercially available *N*-substituted amines in the presence of *o*-(7-azabenzotriazol-1-yl)-*N*,*N*,*N*′,*N*′-tetramethyluronium hexafluorophosphate (HATU) and *N*,*N*-diisopropylethylamine (DIPEA) in DMF at 25 °C for overnight.

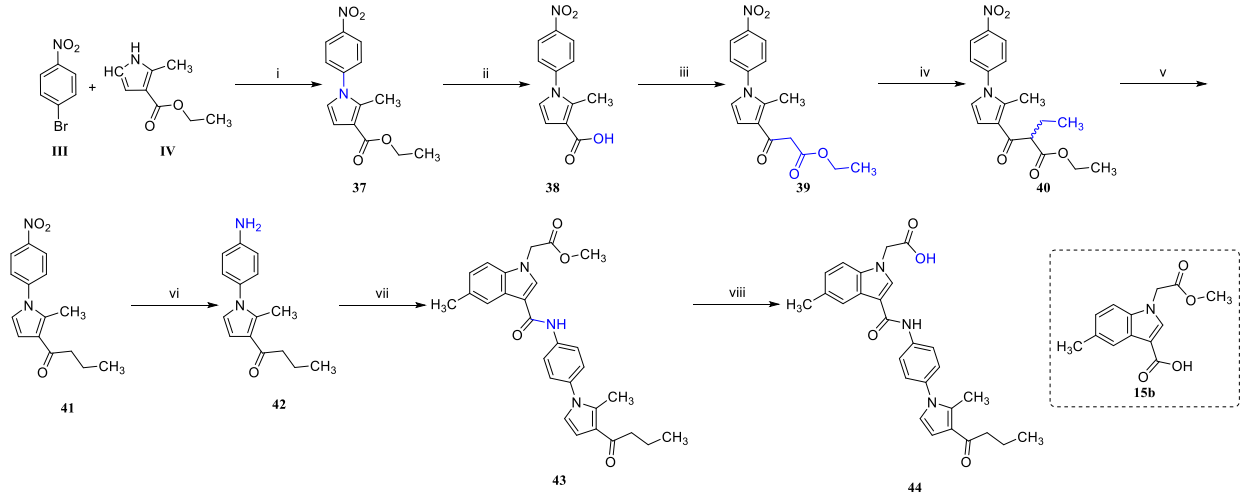
Scheme 14. Synthesis of the targeted carboxamide-based *N*-indole substituted final compounds.[a]



[a]Reagents and conditions: (i) NaOH, MeOH, 25 °C, 24 h (62%)[86]; (ii) **HR**, DIPEA, HATU, dimethylformamide (DMF), 25 °C, 24 h (53–93%).

Replacement of the pyrazolyl ring by pyrrolyl requires the synthesis of the novel aniline key-intermediate **42** (Scheme 15), which started with a copper catalyzed carbon-nitrogen coupling reaction between the commercially available compounds 4-nitrobromobenzene (**III**, Scheme 15) and ethyl 2-methyl-1*H*-pyrrole-3-carboxylate (**IV**, Scheme 15) using copper iodide (CuI), in the presence of potassium carbonate (K_2CO_3) and *N*,*N'*-Dimethylethylenediamine (DMEDA) in 1,4-Dioxane at 100 °C for overnight to afford **37**. Compound **37** was subsequently hydrolyzed using aqueous potassium hydroxide in a 1:1 mixture of tetrahydrofuran (THF) and ethanol under reflux to produce the carboxylic acid **38**. Treating **38** with carbonyldiimidazole (CDI) in THF at 25 °C for 16 hours, and subsequent addition of anhydrous magnesium chloride and potassium malonate and stirring the mixture at 55 °C for further 6 hours led to the formation of the novel β-keto ester analog **39**. Ethyl iodide was used to alkylate the active methylene in the presence of NaH in THF to form the novel compound **40**. Acidic decarboxylation of **40** with refluxed concentrated HCl for 2 hours produced **41**. This nitrophenyl derivative was subsequently reduced to the corresponding novel aniline **42** using Pd/C in methanol under H_2 at atmospheric pressure overnight (Scheme 15). Amide coupling of the aniline **42** with the carboxylic acid key-intermediate (**15b**, Scheme 15) under the above-mentioned EDC·HCl reaction conditions led to the formation of the novel methyl ester **43**, which was subsequently hydrolyzed according to the aforementioned NaOH hydrolysis procedure to synthesize the novel pyrrolyl-based final compound **44**.

Scheme 15. Synthesis of the targeted novel pyrrolyl-based carboxylic acid final compound **44**.[a]



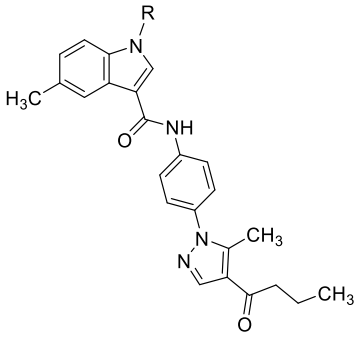
[a]Reagents and conditions: i. K_2CO_3, 1,4-dioxane, 0 °C; DMEDA, CuI, 100 °C, 24 h (93%); ii. aq. KOH, THF:EtOH (1:1), 100 °C, 2 h (82%); iii. carbonyldiimidazole (CDI), THF, 25 °C, 16 h;

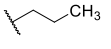
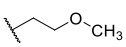
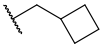
anhydrous $MgCl_2$, ethyl potassium malonate, 55 °C, 6 h (72%); iv. NaH, THF, 0 °C, 30 min; CH_3CH_2I, 25 °C, 24 h (59%); v. aq. HCl 37%, 105 °C, 2 h (99%); vi. Pd/C, H_2-gas (1 atm), MeOH, 25 °C, 4 h (100%); vii. **15b**, 4-DMAP, EDC·HCl, CH_2Cl_2, 0 °C; 25 °C, 24 h (62%); viii. NaOH, MeOH, 25 °C, 24 h (40%).

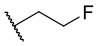
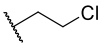
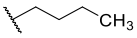
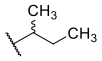
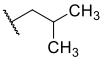
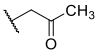
Biology and Structure-Property Relationships. The first biological evaluation of *N*-indole substituted final compounds showed that branched alkyl-chains such as compounds **7c**, **11c**, and **13c** (Table 8) possess better affinity than unbranched alkyl-chains **2c**, **3c**, and **9c** (Table 8). The longer the alkyl-chain is, the weaker the affinity becomes. Fluoro- or chloro-ethyl substituents **6c** and **8c** (Table 8) showed affinity in between, whereas cyclobutylmethyl and difluoromethyl showed better K_i-values **5c** and **10c** (Table 8). Compounds **4c**, **12c**, and **17** with the substituents methoxyethyl, 2-tetrahydrofuryl-methyl, acetonyl, (Table 8) represent the most potent $P2Y_{12}R$ antagonists in this series. This first biological evaluation concluded that the closer the substituent to the acetic acid of the lead structure **1**, the better the affinity will be.

Metabolic stability of these $P2Y_{12}R$ antagonists was acquired using LC/MS after incubation with human liver microsomes (HLM) in the presence of NADPH-regenerating system. The metabolism found to be high in the majority of compounds and the percentage of parent ligands remaining after 60 min varied from 0 to 35% (Table 8), much lower in comparison to the lead structure **1** (78%).

Table 8. Optimization of *N*-indole substituents.[a]



Compound	R	K_i (affinity, nM)	MW (g/mol)	TPSA	Metabolic stability (human)[b]
1		**5.2** ± 0.5	458.5	106	78%
2c		**80.9** ± 10.9	442.6	69	n.d.
3c		**68.5** ± 9.0	414.5	69	19%
4c		**32.2** ± 3.2	458.6	78	0%
5c		**37.7** ± 4.9	468.6	69	24%

6c		**58.3** ± 0.6	446.5	69	33%
7c		**51.5** ± 2.4	442.6	69	15%
8c		**60.1** ± 2.3	463.0	69	35%
9c		**90.4** ± 1.6	456.6	69	n.d.
10c		**44.9** ± 5.4	450.5	69	30%
11c		**52.8** ± 3.6	456.6	69	23%
12c		**22.5** ± 1.5	484.6	78	0%
13c		**77.3**[c]	456.6	69	1%
17		**28.5** ± 4.3	456.6	86	8%

[a]**MW**: molecular weight; **TPSA**: topological polar surface area, [b]% of remaining compound after 60 min incubation [c]the experiment was performed once (n = 1).

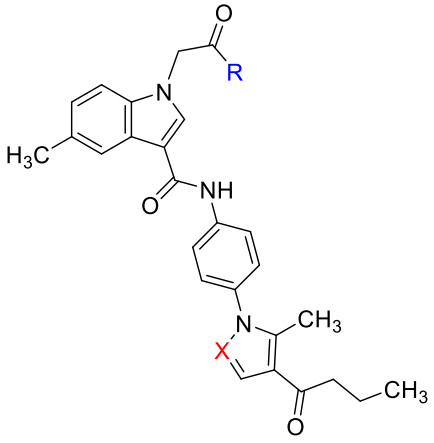
Thus, a second biological evaluation based on the synthesis of the carboxamide final compounds taking the acetic acid moiety in consideration has been performed and resulted in the identification of promising, novel, potent, and selective $P2Y_{12}R$ antagonists. Thirteen compounds possess K_i-values below 10 nM (**18**−**27**, and **34**−**36**, Table 9). The best three compounds of which possess promising physicochemical properties (**18**−**20**, Table 9). The rest have molecular weight above 500 g/mol. The high molecular weight was unavoidable issue taking in consideration to maintain the high affinity.

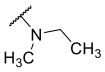
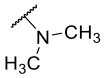
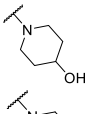
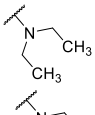
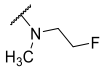
Metabolic Stability of these compounds was carried out using both human and rat liver microsomes (HLM and RLM), whereas the compounds were incubated in the presence of an NADPH-generating system and subsequently assessed through LC/MS. After 60 min of incubation, compound **20** showed the highest stability with $70\%_{human}$ and $98\%_{rat}$ of parent compound remaining intact, followed by **19** with $46\%_{human}$ and $87\%_{rat}$, Then, **21** with $42\%_{human}$ and $84\%_{rat}$. The metabolic stability results allowed the direct comparison between the 4-hydroxypiperidinyl **21** with its 4-fluoro analog **22**, as well as between the 3-hydroxyazetidinyl **32** and its 3-fluoroazetidinyl analog **30**. In both cases, the hydroxy group showed higher metabolic stability (Table 9). The mass spectrometry chromatogram and fragmentation tables are provided in the SI.

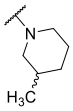
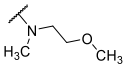
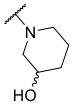
In general, this class of compound found to be associated with solubility issues as has been discussed in the SI. The solubility issues were confirmed during the Caco-2 permeability

measurements, which were performed for the compounds **19**, **20**, **22**, and **34**. Both compounds **19** and **22** showed moderate permeability and found to undergoe active efflux, whereas the other compounds **20** and **34** possess low permeability and did not undergo active efflux. Solubility check was suggested for all four compounds. All information regarding the Caco-2 permeability measurements are provided in the SI.

Table 9. Optimized carboxamide-based final compounds.[a]



Compound	X	R	K_i (affinity, nM)	MW (g/mol)	TPSA	Metabolic stability	
						human[b]	Rat[b]
1	N	OH	**5.2** ± 0.5	458.5	106	78%	99%[86]
18	N		**3.2** ± 0.3	499.6	89	11%	n.d.
19	N		**4.9** ± 0.5	485.6	89	46%	87%
20	N		**5.1** ± 0.4	485.6	98	70%	98%
21	N		**5.3** ± 0.7	541.7	109	42%	84%
22	N		**5.4** ± 0.1	543.6	89	38%	n.d.
23	N		**5.6** ± 0.5	511.6	89	0%	87%
24	N		**6.3** ± 0.6	513.6	89	n.d.	n.d.
25	N		**6.8** ± 0.5	543.7	89	n.d.	35%
26	N		**7.2** ± 0.3	517.6	89	12%	n.d.

27	N		**9.1** ± 0.8	539.7	89	n.d.	n.d.
28	N		**10.9** ± 0.9	529.6	98	n.d.	n.d.
29	N		**11.8** ± 1.1	539.7	89	n.d.	n.d.
30	N		**12.0** ± 2.1	515.6	89	36%	n.d.
31	N		**12.4** ± 0.4	471.6	98	7%	77%
32	N		**13.6** ± 0.8	513.6	109	50%	n.d.
33	N		**20.2** ± 3.1	539.7	98	n.d.	n.d.
34	N		**5.3** ± 0.4	503.6	98	18%	n.d.
35	N		**5.7** ± 0.9	541.7	109	n.d.	n.d.
36	N		**8.7** ± 1.0	527.6	98	n.d.	70%
43	CH		**64.6** ± 26.9	471.6	82	0%	n.d.
44	CH	OH	**24.1**[c]	457.5	93	65%	n.d.

[a]**MW**: molecular weight; **TPSA**: topological polar surface area, [b]% of remaining compound after 60 min incubation, [c]the experiment was performed once (n = 1).

3.5.5 Conclusions and outlook

The current study comprises the systematic design, synthesis, and structure-property relationship analysis of 36 potent and selective $P2Y_{12}R$ antagonists. The *N*-indole-substituted final compounds seem to be less potent than the carboxamide-derived compounds despite their better TPSA and MW values. All carboxamide-based compounds possess high affinity with K_i-values between 3.2 nM and 20.2 nM. The best compounds among these are **19** with a dimethylamide, and **20** with an ethylamide substitution. Both compounds have the same molecular weight and almost the same affinity, however compound **19** has a better TPSA value. The metabolically most stable compound in both human and rat liver microsomes was found to be **20** with 70% and 98% parent compound remaining intact after 60 min of incubation with liver microsomes and an NADPH-generating system, followed by **19**. With regard to the Caco-2 permeability, compound **19** showed moderate permeability, and was found to undergo active efflux, whereas compound **20** demonstrated low permeability and did not undergo active efflux. Despite the more favorable TPSA values observed

for the pyrrole-containing compounds **43** and **44** compared to their pyrazole-containing analogs (**15c**[86] and **1**), compounds **43** and **44** exhibited lower binding affinities, with K_i-values of 64.6 nM and 24.1 nM, respectively.

Future work will focus not only on the further optimization of pyrazole-based $P2Y_{12}R$ antagonists, but also on the solubility adjustment among this scaffold and replacement of the 5-methylindole moiety by 5-chloroindole, which holds potential for higher metabolic stability and maybe better permeability. In addition, application of the synthesized final compounds such as **19** and **20** or **22** and **30** as therapeutics or as diagnostics after radiolabeling with ^{11}C or ^{18}F will be performed.

3.5.6 Experimental part

Chemistry

General Methods. All commercially available reagents were used as purchased (BLDpharm, Acros, Alfa Aesar, Sigma-Aldrich, abcr or TCI). Solvents were used without additional purification or drying. Thinlayer chromatography (TLC) using aluminum sheets with silica gel 60 F254 were utilized to monitor the reactions (Merck). Column chromatography was performed with silica gel 0.060−0.200 mm, pore diameter ca. 6 nm. All synthesized compounds were finally dried in vacuum at 8 −12 Pa (0.08−0.12 mbar) using a sliding vane rotary vacuum pump (Vacuubrand GmbH). ^1H and ^{13}C NMR data were collected on a Bruker Avance 500 MHz NMR spectrometer at 500 MHz (^1H), or 126 MHz (^{13}C), respectively. If indicated, NMR data were collected on a Bruker Ascend 600 MHz NMR spectrometer at 600 MHz (^1H) or 151 MHz (^{13}C), respectively. DMSO-d_6 was employed as a solvent at 303 K. Chemical shifts are reported in parts per million (ppm) relative to the deuterated solvent: DMSO, δ ^1H: 2.49 ppm; ^{13}C: 39.7 ppm. Coupling constants *J* are given in Hertz and spin multiplicities are given as *s* (singlet, *d* (doublet) *dd* (doublet of doublet), *t* (triplet), *q* (quartet), *sext.* (sextet), *m* (multiplet), *br* (broad). The purities of isolated products were determined and proven to be >95% by ESI-mass spectra obtained on an Infinity Lab LC/MSD-system (Agilent) with ESI-source coupled with an HPLC 1260 Infinity II (Agilent) using an EC50/2 Nucleodur C18 Gravity 3 µm column (Macherey-Nagel). The column temperature was 40 degree. The compounds were dissolved at a concentration of 1.0 mg/mL in water, methanol or acetonitril. Then, 2 µL of the sample solution was injected to a flow of 0.5 ml/min. Elution started with a gradient of water containing 2 mM ammoniumacetate/acetonitrile from 90:10 to 0:100 for 10 min, and then it was flushed with 100% acetonitrile for additional 5 min. Positive total ion scans

were observed from 100 - 1000 m/z (or more if necessary). UV absorption was detected from 190 to 600 nm using a diode array detector (DAD). Purity of all compounds was determined at 220 to 600 nm. Synthesis of the final compounds **2c− 13c**, **17− 36**, **43**, and **44** is described below. Comprehensive synthesis procedures for all novel and reported intermediates are provided in the Supporting Information (SI) and the analytical characterization of all compounds in Appendix IV.

Amide coupling I: General Procedure A

In a sealed tube, 1.20 equiv. of 1-(1-(4-aminophenyl)-5-methyl-1*H*-pyrazol-4-yl)butan-1-one **(II)**, 1.50 equiv. of 4-dimethylaminopyridine (**4-DMAP**), and 1.10 equiv. of 1-ethyl-3-(3'-dimethylaminopropyl)carbodiimide hydrochloride (**EDC·HCl**) were added to a solution of carboxylic acid **2b−15b** in dichloromethane (**DCM**) (10−30 mL) at 0 °C. Then, the reaction mixture was stirred at room temperature overnight. The mixture was then washed sequentially with 1 N HCl, water, and brine. The organic layer was dried over $MgSO_4$, evaporated under reduced pressure, and the residue purified via silica gel column chromatography (DCM, followed by DCM/EtOAc, 8/2 v/v)

Synthesis of *N*-(4-(4-butyryl-5-methyl-1*H*-pyrazol-1-yl)phenyl)-5-methyl-1-propyl-1*H*-indole-3-carboxamide (2c)

General procedure A, calculations: **2b** (0.19 g, 0.87 mmol) in DCM (25 mL), **II** (0.26 g, 1.05 mmol), **4-DMAP** (0.16 g, 1.31 mmol), and **EDC·HCl** (0.38 g, 0.96 mmol); Purification: silica gel chromatography, eluent DCM, followed by DCM/EtOAc, 8/2 v/v to afford **2c** as white-yellowish powder (0.32 g, 0.72 mmol, 83%). ^{1}H NMR (600 MHz, DMSO-d_6) δ 9.91 (s, 1H, 8-H), 8.29 (s, 1H, 10-H), 8.24 (s, 1H, 9-H), 8.03 (s, 1H, 4-H), 7.95 (d, *J* = 8.5 Hz, 2H, 7-H, 7′-H), 7.48 (d, *J* = 8.6 Hz, 3H, 13-H, 6-H, 6′-H), 7.07 (d, *J* = 8.4 Hz, 1H, 12-H), 4.20 (t, *J* = 6.9 Hz, 2H, 14-H), 2.81 (t, *J* = 7.2 Hz, 2H, 3-H), 2.52 (s, 3H, 5-H), 2.43 (s, 3H, 11-H), 1.85 (h, *J* = 7.1 Hz, 2H, 15-H), 1.64 (h, *J* = 7.2 Hz, 2H, 2-H), 0.94 (t, *J* = 7.4 Hz, 3H, 1-H), 0.89 (t, *J* = 7.3 Hz, 3H, 16-H); ^{13}C NMR (151 MHz, DMSO) δ 195.47, 163.09, 142.11, 141.45, 140.14, 134.72, 132.62, 131.72, 129.77, 127.05, 125.69, 123.79, 120.98, 120.22, 119.68, 110.23, 108.81, 47.67, 41.96, 22.94, 21.24, 17.39, 13.68, 11.91, 11.12. m.p. = 156 −158 °C. LC-MS (*m*/*z*): positive mode 443.20 $[M + H]^{1+}$; purity by HPLC UV (254 nm)-ESI-MS: 98.0%.

Synthesis of *N*-(4-(4-butyryl-5-methyl-1*H*-pyrazol-1-yl)phenyl)-1,5-dimethyl-1*H*-indole-3-carboxamide (3c)

General procedure A, calculations: **3b** (0.057 g, 0.30 mmol) in DCM (10 mL), **II** (0.088 g, 0.36 mmol), **4-DMAP** (0.055 g, 0.45 mmol), and **EDC·HCl** (0.052 g, 0.33 mmol); Purification: silica gel chromatography, eluent DCM, followed by DCM/EtOAc, 8/2 v/v to afford **3c** as white powder (96 mg, 0.23 mmol, 70%). ^{1}H NMR (500 MHz, DMSO-d_6) δ 9.92 (s, 1H, 8-H), 8.23 (s, 2H, 9-H, 10-H), 8.02 (s, 1H, 4-H), 7.94 (d, *J* = 8.9 Hz, 2H, 7-H, 7′-H), 7.47 (d, *J* = 8.8 Hz, 2H, 6-H, 6′-H), 7.43 (d, *J* = 8.4 Hz, 1H, 13-H), 7.10 (d, *J* = 9.5 Hz, 1H, 12-H), 3.87 (s, 3H, 14-H), 2.81 (t, *J* = 7.2 Hz, 2H, 3-H), 2.52 (s, 3H, 5-H), 2.43 (s, 3H, 11-H), 1.64 (h, *J* = 7.3 Hz, 2H, 2-H), 0.94 (t, *J* = 7.4 Hz, 3H, 1-H); ^{13}C NMR (126 MHz, DMSO) δ 195.45, 163.05, 142.11, 141.43, 140.16, 135.31, 132.68, 129.80, 126.95, 125.68, 123.82, 120.85, 120.22, 119.63, 119.54, 110.07, 108.75, 41.95, 33.09, 21.25, 17.38, 13.67, 11.89. m.p. = 225−227 °C. LC-MS (*m*/*z*): positive mode 415.20 $[M + H]^{1+}$; purity by HPLC UV (254 nm)-ESI-MS: 98.0%.

Synthesis of *N*-(4-(4-butyryl-5-methyl-1*H*-pyrazol-1-yl)phenyl)-1-(2-methoxyethyl)-5-methyl-1*H*-indole-3-carboxamide (4c)

General procedure A, calculations: **4b** (0.16 g, 0.69 mmol) in DCM (25 mL), **II** (0.20 g, 0.84 mmol), **4-DMAP** (0.13 g, 1.05 mmol), and **EDC·HCl** (0.13 g, 0.77 mmol); Purification: silica gel chromatography, eluent DCM, followed by DCM/EtOAc, 8/2 v/v to afford **P316** as pale-yellow powder (0.18 g, 0.40 mmol, 57%). ^{1}H NMR (500 MHz, DMSO-d_6) δ 9.94 (s, 1H, 8-H), 8.27 (s, 1H, 10-H), 8.23 (s, 1H, 9-H), 8.03 (s, 1H, 4-H), 7.96 (dd, *J* = 9.0, 2.4 Hz, 2H, 7-H, 7′-H), 7.48 (dd, *J* = 8.6, 4.7 Hz, 3H, 6-H, 6′-H, 13-H), 7.07 (dd, *J* = 8.4, 1.3 Hz, 1H, 12-H), 4.40 (t, *J* = 5.1 Hz, 2H, 14-H), 3.71 (t, *J* = 5.1 Hz, 2H, 15-H), 3.25 (s, 3H, 16-H), 2.81 (t, *J* = 7.2 Hz, 2H, 3-H), 2.52 (s, 3H, 5-H), 2.43 (s, 3H, 11-H), 1.64 (h, *J* = 7.3 Hz, 2H, 2-H), 0.94 (t, *J* = 7.4 Hz, 3H, 1-H); ^{13}C NMR (126 MHz, DMSO) δ 195.46, 163.06, 142.11, 141.43, 140.13, 134.74, 132.63, 132.31, 129.80, 127.06, 125.66, 123.77, 120.96, 120.22, 119.72, 119.62, 110.28, 108.93, 70.56, 58.14, 46.14, 41.95, 21.22, 17.38, 13.67, 11.90. m.p. = 103 −105 °C. LC-MS (*m*/*z*): positive mode 459.20 $[M + H]^{1+}$; purity by HPLC UV (254 nm)-ESI-MS: 99.0%.

Synthesis of *N*-(4-(4-butyryl-5-methyl-1*H*-pyrazol-1-yl)phenyl)-1-(cyclobutylmethyl)-5-methyl-1*H*-indole-3-carboxamide (5c)

General procedure A, calculations: **5b** (0.19 g, 0.78 mmol) in DCM (25 mL), **II** (0.23 g, 0.94 mmol), **4-DMAP** (0.14 g, 1.17 mmol), and **EDC·HCl** (0.13 g, 0.86 mmol); Purification: silica gel

chromatography, eluent DCM, followed by DCM/EtOAc, 8/2 v/v to afford **5c** as white-yellowish powder (0.19 g, 0.41 mmol, 53%). ^{1}H NMR (500 MHz, DMSO-d_6) δ 9.90 (s, 1H, 8-H), 8.27 (s, 1H, 10-H), 8.23 (s, 1H, 9-H), 8.02 (s, 1H, 4-H), 7.94 (d, *J* = 8.9 Hz, 2H, 7-H, 7′-H), 7.48 (d, *J* = 8.9 Hz, 3H, 6-H, 6′-H, 13-H), 7.07 (d, *J* = 9.4 Hz, 1H, 12-H), 4.25 (d, *J* = 7.3 Hz, 2H, 14-H), 2.87 – 2.77 (m, 3H, 3-H, 15-H), 2.52 (s, 3H, 5-H), 2.42 (s, 3H, 11-H), 2.06 – 1.97 (m, 2H, 16-H), 1.93 – 1.83 (m, 2H, 16′-H), 1.86 – 1.75 (m, 2H, 17-H), 1.64 (h, *J* = 7.3 Hz, 2H, 2-H), 0.94 (t, *J* = 7.4 Hz, 3H, 1-H); ^{13}C NMR (126 MHz, DMSO) δ 195.46, 163.06, 142.11, 141.43, 140.10, 134.89, 132.64, 131.59, 129.76, 126.96, 125.66, 123.78, 120.92, 120.22, 119.74, 110.25, 108.81, 50.90, 41.96, 35.17, 25.42, 21.22, 17.64, 17.38, 13.67, 11.90. m.p. = 161 −163 °C. LC-MS (*m*/*z*): positive mode 469.20 $[M + H]^{1+}$; purity by HPLC UV (254 nm)-ESI-MS: 97.0%.

Synthesis of *N*-(4-(4-butyryl-5-methyl-1*H*-pyrazol-1-yl)phenyl)-1-(2-fluoroethyl)-5-methyl-1*H*-indole-3-carboxamide (6c)

General procedure A, calculations: **6b** (0.17 g, 0.78 mmol) in DCM (25 mL), **II** (0.23 g, 0.94 mmol), **4-DMAP** (0.14 g, 1.17 mmol), and **EDC·HCl** (0.13 g, 0.86 mmol); Purification: silica gel chromatography, eluent DCM, followed by DCM/EtOAc, 8/2 v/v to afford **6c** as white powder (0.23 g, 0.52 mmol, 67%). ^{1}H NMR (500 MHz, DMSO-d_6) δ 9.98 (s, 1H), 8.31 (s, 1H), 8.23 (s, 1H), 8.05 (s, 1H), 7.95 (d, *J* = 8.9 Hz, 2H), 7.49 (dd, *J* = 11.9, 8.7 Hz, 3H), 7.09 (d, *J* = 9.6 Hz, 1H), 4.84 (t, *J* = 4.6 Hz, 1H), 4.75 (t, *J* = 4.6 Hz, 1H), 4.61 (t, *J* = 4.5 Hz, 1H), 4.56 (t, *J* = 4.6 Hz, 1H), 2.81 (t, *J* = 7.2 Hz, 2H), 2.52 (s, 3H), 2.43 (s, 3H), 1.64 (h, *J* = 7.3 Hz, 2H), 0.94 (t, *J* = 7.4 Hz, 3H); ^{13}C NMR (126 MHz, DMSO) δ 195.46, 163.00, 142.11, 141.44, 140.09, 134.75, 132.68, 132.08, 129.99, 127.07, 125.67, 123.95, 121.00, 120.23, 119.74, 110.28, 109.43, 83.11, 81.78, 46.74, 46.58, 41.96, 21.22, 17.38, 13.67, 11.90. m.p. = 187 −189 °C. LC-MS (*m*/*z*): positive mode 447.20 $[M + H]^{1+}$; purity by HPLC UV (254 nm)-ESI-MS: 99.0%.

Synthesis of *N*-(4-(4-butyryl-5-methyl-1*H*-pyrazol-1-yl)phenyl)-1-isopropyl-5-methyl-1*H*-indole-3-carboxamide (7c)

General procedure A, calculations: **7b** (0.08 g, 0.36 mmol) in DCM (15 mL), **II** (0.11 g, 0.43 mmol), **4-DMAP** (0.07 g, 0.54 mmol), and **EDC·HCl** (0.06 g, 0.40 mmol); Purification: silica gel chromatography, eluent DCM, followed by DCM/EtOAc, 8/2 v/v to afford **7c** as yellow powder (0.11 g, 0.25 mmol, 69%). ^{1}H NMR (600 MHz, DMSO-d_6) δ 9.88 (s, 1H), 8.43 (s, 1H), 8.24 (s, 1H), 8.04 (s, 1H), 7.94 (d, *J* = 8.7 Hz, 2H), 7.49 (t, *J* = 8.3 Hz, 3H), 7.08 (d, *J* = 8.4 Hz, 1H), 4.81 (hept, *J* = 6.5 Hz, 1H), 2.81 (t, *J* = 7.1 Hz, 2H), 2.53 (s, 3H), 2.43 (s, 3H), 1.64 (h, *J* = 7.3 Hz, 2H),

1.53 (d, *J* = 6.6 Hz, 6H), 0.94 (t, *J* = 7.4 Hz, 3H); ^{13}C NMR (151 MHz, DMSO) δ 195.47, 163.08, 142.11, 141.46, 140.11, 134.20, 132.63, 129.86, 128.10, 127.19, 125.69, 123.73, 121.02, 120.23, 119.71, 110.25, 108.99, 47.18, 41.96, 22.43, 21.24, 17.39, 13.68, 11.92. m.p. = 189 −191 °C. LC-MS (*m*/*z*): positive mode 443.50 $[M + H]^{1+}$; purity by HPLC UV (254 nm)-ESI-MS: 98.0%.

Synthesis of *N*-(4-(4-butyryl-5-methyl-1*H*-pyrazol-1-yl)phenyl)-1-(2-chloroethyl)-5-methyl-1*H*-indole-3-carboxamide (8c)

General procedure A, calculations: **8b** (0.06 g, 0.25 mmol) in DCM (15 mL), **II** (0.07 g, 0.30 mmol), **4-DMAP** (0.05 g, 0.38 mmol), and **EDC·HCl** (0.04 g, 0.28 mmol); Purification: silica gel chromatography, eluent DCM, followed by DCM/EtOAc, 8/2 v/v to afford **8c** as white-yellowish powder (0.08 g, 0.17 mmol, 69%). ^{1}H NMR (600 MHz, DMSO-d_6) δ 9.97 (s, 1H), 8.33 (s, 1H), 8.24 (s, 1H), 8.04 (s, 1H), 7.95 (d, *J* = 7.7 Hz, 2H), 7.53 (d, *J* = 8.4 Hz, 1H), 7.48 (d, *J* = 7.9 Hz, 2H), 7.10 (d, *J* = 8.4 Hz, 1H), 4.62 (t, *J* = 5.3 Hz, 2H), 4.04 (t, *J* = 5.4 Hz, 2H), 2.81 (t, *J* = 7.1 Hz, 2H), 2.52 (s, 3H), 2.43 (s, 3H), 1.64 (h, *J* = 7.3 Hz, 2H), 0.94 (t, *J* = 7.4 Hz, 3H); ^{13}C NMR (151 MHz, DMSO) δ 195.48, 163.00, 142.12, 141.46, 140.05, 134.58, 132.71, 132.32, 130.07, 127.09, 125.69, 123.98, 121.03, 120.23, 119.76, 119.66, 110.29, 109.34, 47.89, 43.74, 41.96, 21.23, 17.39, 13.68, 11.92. m.p. = 172 −174 °C. LC-MS (*m*/*z*): positive mode 463.70 $[M + H]^{1+}$; purity by HPLC UV (254 nm)-ESI-MS: 99.5%.

Synthesis of 1-butyl-*N*-(4-(4-butyryl-5-methyl-1*H*-pyrazol-1-yl)phenyl)-5-methyl-1*H*-indole-3-carboxamide (9c)

General procedure A, calculations: **9b** (0.10 g, 0.43 mmol) in DCM (20 mL), **II** (0.11 g, 0.52 mmol), **4-DMAP** (0.08 g, 0.65 mmol), and **EDC·HCl** (0.08 g, 0.48 mmol); Purification: silica gel chromatography, eluent DCM, followed by DCM/EtOAc, 8/2 v/v to afford **9c** as beige powder (0.12 g, 0.26 mmol, 61%). ^{1}H NMR (600 MHz, DMSO-d_6) δ 9.90 (s, 1H), 8.29 (s, 1H), 8.24 (s, 1H), 8.03 (s, 1H), 7.94 (dd, *J* = 9.0, 2.8 Hz, 2H), 7.47 (dd, *J* = 8.5, 5.3 Hz, 3H), 7.14 – 7.02 (m, 1H), 4.23 (t, *J* = 7.1 Hz, 2H), 2.81 (t, *J* = 7.2 Hz, 2H), 2.52 (s, 3H), 2.43 (s, 3H), 1.81 (p, *J* = 7.2 Hz, 2H), 1.64 (h, *J* = 7.3 Hz, 2H), 1.31 (h, *J* = 7.4 Hz, 2H), 0.93 (dt, *J* = 12.2, 7.4 Hz, 6H); ^{13}C NMR (151 MHz, DMSO) δ 195.65, 163.25, 142.29, 141.63, 140.31, 134.86, 132.81, 131.81, 129.95, 127.23, 125.86, 123.98, 121.17, 120.40, 119.87, 110.38, 109.01, 46.00, 42.14, 31.85, 21.42, 19.64, 17.57, 13.86, 13.70, 12.09. m.p. = 143 −145 °C. LC-MS (*m*/*z*): positive mode 457.20 $[M + H]^{1+}$; purity by HPLC UV (254 nm)-ESI-MS: 98.0%.

Synthesis of *N*-(4-(4-butyryl-5-methyl-1*H*-pyrazol-1-yl)phenyl)-1-(difluoromethyl)-5-methyl-1*H*-indole-3-carboxamide (10c)

General procedure A, calculations: **10b** (0.07 g, 0.31 mmol) in DCM (15 mL), **II** (0.08 g, 0.37 mmol), **4-DMAP** (0.06 g, 0.47 mmol), and **EDC·HCl** (0.05 g, 0.34 mmol); Purification: silica gel chromatography, eluent DCM, followed by DCM/EtOAc, 8/2 v/v to afford **10c** as beige powder (0.08 g, 0.18 mmol, 58%). ^{1}H NMR (500 MHz, DMSO-d_6) δ 10.26 (s, 1H), 8.52 (s, 1H), 8.24 (s, 1H), 8.14 (t, *J* = 59.5 Hz, 1H), 8.06 (s, 1H), 7.95 (dd, *J* = 9.0, 2.3 Hz, 2H), 7.65 (d, *J* = 8.4 Hz, 1H), 7.54 – 7.48 (m, 2H), 7.23 (dd, *J* = 8.5, 1.3 Hz, 1H), 2.81 (t, *J* = 7.2 Hz, 2H), 2.53 (s, 3H), 2.45 (s, 3H), 1.64 (h, *J* = 7.3 Hz, 2H), 0.94 (t, *J* = 7.4 Hz, 3H); ^{13}C NMR (126 MHz, DMSO) δ 195.47, 162.21, 142.15, 141.50, 139.53, 133.17, 132.14, 127.40, 127.00, 125.77, 125.68, 121.54, 120.27, 119.89, 113.58, 112.31, 111.03, 110.36, 108.40, 41.96, 21.12, 17.37, 13.67, 11.89. m.p. = 181 − 183 °C. LC-MS (*m*/*z*): positive mode 451.30 $[M + H]^{1+}$; purity by HPLC UV (254 nm)-ESI-MS: 97.0%.

Synthesis of (*R*,*S*)-1-(*sec*-butyl)-*N*-(4-(4-butyryl-5-methyl-1*H*-pyrazol-1-yl)phenyl)-5-methyl-1*H*-indole-3-carboxamide (11c)

General procedure A, calculations: **11b** (0.10 g, 0.43 mmol) in DCM (20 mL), **II** (0.11 g, 0.52 mmol), **4-DMAP** (0.08 g, 0.65 mmol), and **EDC·HCl** (0.07 g, 0.47 mmol); Purification: silica gel chromatography, eluent DCM, followed by DCM/EtOAc, 8/2 v/v to afford **11c** as white-reddish powder (0.10 g, 0.22 mmol, 51%). ^{1}H NMR (500 MHz, DMSO-d_6) δ 9.86 (s, 1H), 8.40 (s, 1H), 8.24 (s, 1H), 8.04 (s, 1H), 7.94 (dd, *J* = 9.0, 2.4 Hz, 2H), 7.53 – 7.46 (m, 3H), 7.06 (dd, *J* = 8.5, 1.5 Hz, 1H), 4.58 (h, *J* = 6.7 Hz, 1H), 2.81 (t, *J* = 7.2 Hz, 1H), 2.53 (s, 3H), 2.42 (s, 3H), 1.89 (p, *J* = 7.0 Hz, 2H), 1.64 (h, *J* = 7.3 Hz, 2H), 1.52 (d, *J* = 6.7 Hz, 3H), 0.94 (t, *J* = 7.4 Hz, 3H), 0.79 (t, *J* = 7.4 Hz, 3H); ^{13}C NMR (126 MHz, DMSO) δ 195.64, 163.26, 142.28, 141.62, 140.26, 134.96, 132.81, 129.97, 128.62, 127.14, 125.85, 123.89, 121.16, 120.40, 119.90, 119.80, 110.44, 109.31, 53.06, 42.13, 29.58, 21.39, 20.78, 17.56, 13.85, 12.08, 10.66. m.p. = 202 −204 °C. LC-MS (*m*/*z*): positive mode 457.30 $[M + H]^{1+}$; purity by HPLC UV (254 nm)-ESI-MS: 98.0%.

Synthesis of (*R*,*S*)-*N*-(4-(4-butyryl-5-methyl-1*H*-pyrazol-1-yl)phenyl)-5-methyl-1-((tetrahydrofuran-2-yl)methyl)-1*H*-indole-3-carboxamide (12c)

General procedure A, calculations: **12b** (0.07 g, 0.27 mmol) in DCM (15 mL), **II** (0.08 g, 0.32 mmol), **4-DMAP** (0.05 g, 0.40 mmol), and **EDC·HCl** (0.05 g, 0.30 mmol); Purification: silica gel chromatography, eluent DCM, followed by DCM/EtOAc, 8/2 v/v to afford **12c** as white-yellowish

powder (0.08 g, 0.17 mmol, 63%). ^{1}H NMR (500 MHz, DMSO-d_6) δ 9.95 (s, 1H), 8.29 (s, 1H), 8.23 (s, 1H), 8.03 (s, 1H), 7.96 (d, *J* = 8.9 Hz, 2H), 7.49 (dd, *J* = 14.6, 8.6 Hz, 3H), 7.07 (dd, *J* = 8.4, 1.3 Hz, 1H), 4.36 (d, *J* = 11.1 Hz, 1H), 4.26 – 4.16 (m, 2H), 3.77 (q, *J* = 7.0 Hz, 1H), 3.65 (q, *J* = 7.6 Hz, 1H), 2.81 (t, *J* = 7.2 Hz, 2H), 2.52 (s, 3H), 2.43 (s, 3H), 2.06 – 1.94 (m, 1H), 1.86 – 1.69 (m, 2H), 1.65 (h, *J* = 7.3 Hz, 2H), 1.61 – 1.52 (m, 1H), 0.94 (t, *J* = 7.4 Hz, 3H); ^{13}C NMR (126 MHz, DMSO) δ 195.46, 163.08, 142.11, 141.43, 140.13, 135.12, 132.63, 132.48, 129.75, 126.90, 125.65, 123.76, 120.89, 120.22, 119.74, 110.45, 108.98, 77.24, 67.38, 49.98, 41.95, 28.41, 25.08, 21.22, 17.38, 13.67, 11.90. m.p. = 173 −175 °C. LC-MS (*m*/*z*): positive mode 485.50 $[M + H]^{1+}$; purity by HPLC UV (254 nm)-ESI-MS: 97.9%.

Synthesis of *N*-(4-(4-butyryl-5-methyl-1*H*-pyrazol-1-yl)phenyl)-1-isobutyl-5-methyl-1*H*-indole-3-carboxamide (13c)

General procedure A, calculations: **13b** (0.11 g, 0.48 mmol) in DCM (25 mL), **II** (0.12 g, 0.57 mmol), **4-DMAP** (0.09 g, 0.71 mmol), and **EDC·HCl** (0.09 g, 0.52 mmol); Purification: silica gel chromatography, eluent DCM, followed by DCM/EtOAc, 8/2 v/v to afford **13c** as white-yellowish powder (0.13 g, 0.29 mmol, 60%). ^{1}H NMR (600 MHz, DMSO-d_6) δ 9.90 (s, 1H), 8.26 (s, 1H), 8.24 (s, 1H), 8.03 (s, 1H), 7.94 (d, *J* = 8.9 Hz, 2H), 7.48 (d, *J* = 8.8 Hz, 3H), 7.10 – 7.04 (m, 1H), 4.04 (d, *J* = 7.3 Hz, 2H), 2.81 (t, *J* = 7.2 Hz, 2H), 2.52 (s, 3H), 2.42 (s, 3H), 2.17 (dp, *J* = 13.4, 6.7 Hz, 1H), 1.64 (h, *J* = 7.3 Hz, 2H), 0.94 (t, *J* = 7.4 Hz, 3H), 0.91 (d, *J* = 6.6 Hz, 6H); ^{13}C NMR (151 MHz, DMSO) δ 195.47, 163.08, 142.11, 141.45, 140.11, 135.01, 132.64, 132.10, 129.74, 126.95, 125.68, 123.80, 120.97, 120.22, 119.71, 110.43, 108.79, 53.39, 41.96, 29.03, 21.23, 19.83, 17.39, 13.68, 11.92. m.p. = 85−87 °C. LC-MS (*m*/*z*): positive mode 457.80 $[M + H]^{1+}$; purity by HPLC UV (254 nm)-ESI-MS: 98.0%.

Synthesis of *N*-(4-(4-butyryl-5-methyl-1*H*-pyrazol-1-yl)phenyl)-5-methyl-1-(2-oxopropyl)-1*H*-indole-3-carboxamide (17)

In a sealed tube, **16** (50.0 mg, 0.13 mmol) was added to a mixture of dissolved **sodium hydride** (6.0 mg, 0.25 mmol) in 10 mL of DMF and stirred at 0 °C for 30 minutes. Then, (17.3 mg, 0.19 mmol) of **1-chloropropan-2-one** was added dropwise to the mixture. The reaction mixture was allowed to stir at 25 °C for overnight. TLC-control was performed to confirm the formation of the desired product. The reaction mixture was poured into 25 mL of water and extracted with ethyl acetate (3x 20 mL). The organic phase was dried over $MgSO_4$, evaporated under reduced pressure, and then submitted to a column chromatography (silica gel chromatography, eluent: petroleum

ether:ethyl acetate; 8:2) to afford the desired compound **17** as white powder (5.5 mg, 0.01 mmol, 9%). ^{1}H NMR (600 MHz, DMSO-d_6) δ 10.01 (s, 1H), 8.23 (s, 1H), 8.12 (s, 1H), 8.01 (s, 1H), 7.95 (d, *J* = 8.9 Hz, 2H), 7.47 (d, *J* = 8.8 Hz, 2H), 7.34 (d, *J* = 8.4 Hz, 1H), 7.05 (dd, *J* = 8.4, 1.3 Hz, 1H), 5.30 (s, 2H), 2.81 (t, *J* = 7.2 Hz, 2H), 2.52 (s, 3H), 2.43 (s, 3H), 2.24 (s, 3H), 1.64 (q, *J* = 7.3 Hz, 2H), 0.94 (t, *J* = 7.4 Hz, 3H); ^{13}C NMR (151 MHz, DMSO) δ 202.77, 195.49, 163.07, 142.13, 141.46, 140.14, 135.31, 132.76, 132.68, 129.88, 126.77, 125.69, 123.88, 120.87, 120.23, 119.72, 110.22, 109.57, 55.41, 41.97, 27.00, 21.23, 17.40, 13.69, 11.92. m.p. = 136−138 °C. LC-MS (*m*/*z*): positive mode 457.30 $[M + H]^{1+}$; purity by HPLC UV (254 nm)-ESI-MS: 96.2%.

Amide coupling II: General Procedure B

In a sealed tube, 1.5 equiv. of ***N*-substituted amine**, (25.0 mg, 0.065 mmol) of **HATU**, and (24.7 mg, 0.190 mmol) of **DIPEA** to a mixture of **1** (25.0 mg, 0.055 mmol) in 5 mL of **DMF**. The reaction mixture was allowed to stir at room temperature under argon for overnight. After TLC-control, water was added to the mixture. In the case of precipitation, the mixture was filtered washed with water and recrystallized under sonication using Et_2O to afford the targeted final compounds after decantation of the separated Et_2O phase. If no precipitation has been observed, the mixture was diluted with ethyl acetate and washed with 1N aqueous HCl solution and water. It was then extracted, dried over $MgSO_4$ and concentrated under vacuum. The crude compounds were submitted to column chromatography (silica gel chromatography, eluent: DCM (100%) or DCM:MeOH; 99:1) to afford the targeted final compounds:

Synthesis of *N*-(4-(4-butyryl-5-methyl-1*H*-pyrazol-1-yl)phenyl)-1-(2-(ethyl(methyl)amino)-2-oxoethyl)-5-methyl-1*H*-indole-3-carboxamide (18)

General procedure B, calculations: ***N*-methylethanamine** (5.7 mg, 0.083 mmol); Purification: silica gel chromatography (eluent DCM, followed by DCM:MeOH, 99:1), to afford **18** as white-yellowish powder (20 mg, 0.041 mmol, 73%). ^{1}H NMR (500 MHz, DMSO-d_6) δ 9.98 (d, *J* = 7.2 Hz, 1H), 8.23 (s, 1H), 8.18 (d, *J* = 7.6 Hz, 1H), 8.03 (s, 1H), 7.96 (d, *J* = 8.7 Hz, 2H), 7.47 (d, *J* = 8.7 Hz, 2H), 7.34 (dd, *J* = 14.1, 8.4 Hz, 1H), 7.05 (d, *J* = 8.3 Hz, 1H), 5.24 (d, *J* = 16.2 Hz, 2H), 3.43 (dq, *J* = 76.1, 7.1 Hz, 2H), 2.99 (d, *J* = 130.4 Hz, 3H), 2.81 (t, *J* = 7.1 Hz, 2H), 2.52 (s, 3H), 2.43 (s, 3H), 1.64 (h, *J* = 7.2 Hz, 2H), 1.14 (dt, *J* = 92.7, 6.9 Hz, 3H), 0.94 (t, *J* = 7.4 Hz, 3H); ^{13}C NMR (126 MHz, DMSO) δ 195.46, 166.18, 163.12, 142.11, 141.43, 140.20, 135.61, 133.35, 133.31, 132.61, 129.65, 126.83, 125.67, 123.66, 120.83, 120.22, 119.66, 110.28, 110.22, 109.23,

109.19, 47.54, 47.19, 42.99, 42.16, 41.95, 33.40, 32.52, 21.23, 17.38, 13.67, 13.27, 12.18, 11.90. m.p. = 102 −104 °C. LC-MS (*m*/*z*): positive mode 500.90 $[M + H]^{1+}$; purity by HPLC UV (254 nm)-ESI-MS: 97.0%.

Synthesis of *N*-(4-(4-butyryl-5-methyl-1*H*-pyrazol-1-yl)phenyl)-1-(2-(dimethylamino)-2-oxoethyl)-5-methyl-1*H*-indole-3-carboxamide (19)

General procedure B, calculations: **dimethylamine** (3.0 mg, 0.083 mmol); Purification: silica gel chromatography (eluent DCM, followed by DCM:MeOH, 99:1), to afford **19** as white-yellowish powder (16 mg, 0.033 mmol, 60%). ^{1}H NMR (500 MHz, DMSO-d_6) δ 9.98 (s, 1H), 8.23 (s, 1H), 8.16 (s, 1H), 8.02 (s, 1H), 7.98 – 7.93 (m, 2H), 7.50 – 7.44 (m, 2H), 7.36 (d, *J* = 8.4 Hz, 1H), 7.05 (dd, *J* = 8.4, 1.5 Hz, 1H), 5.25 (s, 2H), 3.14 (s, 3H), 2.89 (s, 3H), 2.81 (t, *J* = 7.2 Hz, 2H), 2.52 (s, 3H), 2.43 (s, 3H), 1.64 (h, *J* = 7.3 Hz, 2H), 0.94 (t, *J* = 7.4 Hz, 3H); ^{13}C NMR (151 MHz,) δ 195.66, 166.93, 163.31, 142.31, 141.63, 140.38, 135.81, 133.47, 132.80, 129.84, 126.99, 125.86, 123.83, 121.00, 120.41, 119.86, 110.50, 109.42, 47.60, 42.14, 40.24, 36.13, 35.51, 21.43, 17.58, 13.87, 12.09. m.p. = 112 −114 °C. LC-MS (*m*/*z*): positive mode 486.50 $[M + H]^{1+}$; purity by HPLC UV (254 nm)-ESI-MS: 98.0%.

Synthesis of *N*-(4-(4-butyryl-5-methyl-1*H*-pyrazol-1-yl)phenyl)-1-(2-(ethylamino)-2-oxoethyl)-5-methyl-1*H*-indole-3-carboxamide (20)

General procedure B, calculations: **ethanamine** (3.3 mg, 0.083 mmol); Purification: silica gel chromatography (eluent DCM, followed by DCM:MeOH, 99:1), to afford **20** as white-yellowish powder (17 mg, 0.035 mmol, 64%). ^{1}H NMR (500 MHz,) δ 9.99 (s, 1H), 8.29 (t, *J* = 5.4 Hz, 1H), 8.23 (d, *J* = 9.6 Hz, 2H), 8.03 (s, 1H), 7.96 (dd, *J* = 9.0, 2.3 Hz, 2H), 7.46 (d, *J* = 8.8 Hz, 2H), 7.34 (d, *J* = 8.4 Hz, 1H), 7.12 – 7.01 (m, 2H), 4.86 (s, 2H), 3.18 – 3.08 (m, 3H), 2.80 (t, *J* = 7.2 Hz, 2H), 2.51 (s, 3H), 2.42 (s, 3H), 1.63 (h, *J* = 7.3 Hz, 2H), 1.05 (t, *J* = 7.2 Hz, 3H), 0.93 (t, *J* = 7.4 Hz, 3H); ^{13}C NMR (126 MHz,) δ 195.64, 166.54, 163.23, 142.29, 141.61, 140.34, 135.38, 133.25, 132.82, 130.07, 127.19, 125.85, 124.04, 121.15, 120.40, 119.87, 110.17, 109.43, 49.27, 42.14, 33.82, 21.40, 17.56, 14.75, 13.85, 12.08. m.p. = 272 −274 °C. LC-MS (*m*/*z*): positive mode 486.10 $[M + H]^{1+}$; purity by HPLC UV (254 nm)-ESI-MS: 99.0%.

Synthesis *N*-(4-(4-butyryl-5-methyl-1*H*-pyrazol-1-yl)phenyl)-1-(2-(4-hydroxypiperidin-1-yl)-2-oxoethyl)-5-methyl-1*H*-indole-3-carboxamide (21)

General procedure B, calculations: **piperidin-4-ol** (6.0 mg, 0.083 mmol); Purification: recrystallization to afford **21** as white powder (23 mg, 0.042 mmol, 77%). ^{1}H NMR (600 MHz,)

δ 9.98 (s, 1H), 8.23 (s, 1H), 8.19 (s, 1H), 8.02 (s, 1H), 7.96 (d, *J* = 8.8 Hz, 2H), 7.47 (d, *J* = 8.8 Hz, 2H), 7.35 (d, *J* = 8.4 Hz, 1H), 7.05 (d, *J* = 8.4 Hz, 1H), 5.35 – 5.22 (m, 2H), 4.79 (d, *J* = 3.9 Hz, 1H), 3.92 – 3.86 (m, 1H), 3.85 – 3.79 (m, 1H), 3.76 (dq, *J* = 8.0, 4.1 Hz, 1H), 3.08 (t, *J* = 9.9 Hz, 1H), 2.81 (t, *J* = 7.2 Hz, 2H), 2.52 (s, 3H), 2.43 (s, 3H), 1.89 – 1.79 (m, 1H), 1.77 – 1.68 (m, 1H), 1.64 (h, *J* = 7.3 Hz, 2H), 1.52 – 1.41 (m, 1H), 1.34 – 1.20 (m, 2H), 0.94 (t, *J* = 7.4 Hz, 3H); ^{13}C NMR (151 MHz,) δ 195.66, 165.28, 163.30, 142.30, 141.63, 140.39, 135.81, 133.51, 132.79, 129.85, 127.02, 125.86, 123.84, 121.02, 120.40, 119.84, 110.45, 109.40, 65.51, 47.55, 42.14, 42.06, 40.24, 34.65, 33.98, 21.43, 17.58, 13.87, 12.09. m.p. = 122 −124 °C. LC-MS (*m*/*z*): positive mode 542.50 $[M + H]^{1+}$; purity by HPLC UV (254 nm)-ESI-MS: 99.0%.

Synthesis *N*-(4-(4-butyryl-5-methyl-1*H*-pyrazol-1-yl)phenyl)-1-(2-(4-fluoropiperidin-1-yl)-2-oxoethyl)-5-methyl-1*H*-indole-3-carboxamide (22)

General procedure B, calculations: **4-fluoropiperidine** (8.5 mg, 0.083 mmol); Purification: silica gel chromatography (eluent DCM, followed by DCM:MeOH, 99:1), to afford **22** as white-yellowish powder (22.3 mg, 0.041 mmol, 75%). ^{1}H NMR (600 MHz, DMSO-d_6) δ 9.99 (s, 1H), 8.23 (s, 1H), 8.18 (s, 1H), 8.02 (s, 1H), 7.96 (d, *J* = 8.9 Hz, 2H), 7.47 (d, *J* = 8.8 Hz, 2H), 7.36 (d, *J* = 8.4 Hz, 1H), 7.08 – 7.02 (m, 1H), 5.32 (d, *J* = 2.6 Hz, 2H), 4.94 (dtt, *J* = 48.4, 6.9, 3.4 Hz, 1H), 3.76 – 3.66 (m, 1H), 3.64 – 3.52 (m, 2H), 3.53 – 3.45 (m, 1H), 2.81 (t, *J* = 7.2 Hz, 2H), 2.52 (s, 3H), 2.43 (s, 3H), 2.02 (ddd, *J* = 21.2, 11.3, 5.5 Hz, 1H), 1.85 (dd, *J* = 17.0, 7.2 Hz, 2H), 1.65 (qd, *J* = 14.6, 12.0, 5.4 Hz, 3H), 0.94 (t, *J* = 7.4 Hz, 3H); ^{13}C NMR (151 MHz, DMSO) δ 195.48, 165.37, 163.12, 142.12, 141.45, 140.20, 135.64, 133.29, 132.63, 129.69, 126.82, 125.68, 123.68, 120.84, 120.23, 119.67, 110.31, 109.30, 88.66, 87.53, 47.34, 41.96, 40.67, 40.63, 40.06, 38.06, 38.02, 31.41, 31.28, 30.78, 30.65, 21.24, 17.40, 13.68, 11.91. m.p. = 132−134 °C. LC-MS (*m*/*z*): positive mode 544.20 $[M + H]^{1+}$; purity by HPLC UV (254 nm)-ESI-MS: 98.0%.

Synthesis of *N*-(4-(4-butyryl-5-methyl-1*H*-pyrazol-1-yl)phenyl)-1-(2-(cyclopropyl(methyl)amino)-2-oxoethyl)-5-methyl-1*H*-indole-3-carboxamide (23)

General procedure B, calculations: ***N*-methylcyclopropanamine** (7.0 mg, 0.083 mmol); Purification: silica gel chromatography (eluent DCM, followed by DCM:MeOH, 99:1), to afford **23** as pale yellow powder (26 mg, 0.051 mmol, 92%). ^{1}H NMR (600 MHz, DMSO-d_6) δ 9.99 (s, 1H), 8.24 (s, 1H), 8.20 (s, 1H), 8.02 (s, 1H), 7.96 (d, *J* = 8.9 Hz, 2H), 7.47 (d, *J* = 8.8 Hz, 2H), 7.37 (d, *J* = 8.4 Hz, 1H), 7.10 – 6.99 (m, 1H), 5.34 (s, 2H), 3.03 – 2.96 (m, 1H), 2.86 (s, 3H), 2.81 (t, *J* = 7.2 Hz, 2H), 2.52 (s, 3H), 2.43 (s, 3H), 1.64 (h, *J* = 7.3 Hz, 2H), 1.27 – 1.23 (m, 2H), 0.97−

0.94 (m, 5H); ^{13}C NMR (151 MHz, DMSO) δ 195.48, 169.19, 163.15, 142.12, 141.45, 140.20, 135.61, 133.36, 132.62, 129.68, 126.82, 125.68, 123.67, 120.81, 120.23, 119.69, 110.36, 109.25, 48.24, 41.96, 33.62, 30.04, 21.25, 17.40, 13.68, 11.91, 8.41. m.p. = 98 −100 °C. LC-MS (*m*/*z*): positive mode 512.80 $[M + H]^{1+}$; purity by HPLC UV (254 nm)-ESI-MS: 98.0%.

Synthesis of *N*-(4-(4-butyryl-5-methyl-1*H*-pyrazol-1-yl)phenyl)-1-(2-(diethylamino)-2-oxoethyl)-5-methyl-1*H*-indole-3-carboxamide (24)

General procedure B, calculations: **diethylamine** (4.3 mg, 0.083 mmol); Purification: silica gel chromatography (eluent DCM, followed by DCM:MeOH, 99:1), to afford **24** as white-yellowish powder (15 mg, 0.029 mmol, 53%). ^{1}H NMR (500 MHz, DMSO-d_6) δ 9.98 (s, 1H), 8.23 (s, 1H), 8.20 (s, 1H), 8.03 (s, 1H), 7.96 (d, *J* = 8.9 Hz, 2H), 7.47 (d, *J* = 8.9 Hz, 2H), 7.31 (d, *J* = 8.4 Hz, 1H), 7.05 (dd, *J* = 8.4, 1.3 Hz, 1H), 5.24 (s, 2H), 3.49 (q, *J* = 7.1 Hz, 2H), 2.87 (d, *J* = 15.1 Hz, 3H), 2.81 (t, *J* = 7.2 Hz, 2H), 2.52 (s, 3H), 2.43 (s, 3H), 1.64 (h, *J* = 7.3 Hz, 2H), 1.25 (t, *J* = 7.0 Hz, 3H), 1.06 (t, *J* = 7.1 Hz, 3H), 0.94 (t, *J* = 7.4 Hz, 3H); ^{13}C NMR (126 MHz, DMSO) δ 195.47, 165.70, 163.13, 142.12, 141.44, 140.20, 135.59, 133.40, 132.62, 129.67, 126.87, 125.67, 123.69, 120.86, 120.22, 119.67, 110.18, 109.18, 47.34, 42.96, 41.96, 40.75, 21.23, 17.39, 14.13, 13.68, 12.94, 12.79, 11.90. m.p. = 95−97 °C. LC-MS (*m*/*z*): positive mode 514.40 $[M + H]^{1+}$; purity by HPLC UV (254 nm)-ESI-MS: 97.0%.

Synthesis of *N*-(4-(4-butyryl-5-methyl-1*H*-pyrazol-1-yl)phenyl)-5-methyl-1-(2-oxo-2-thiomorpholinoethyl)-1*H*-indole-3-carboxamide (25)

General procedure B, calculations: **thiomorpholine** (6.0 mg, 0.083 mmol); Purification: recrystallization to afford **25** as white-yellowish powder (27.2 mg, 0.05 mmol, 91%). ^{1}H NMR (600 MHz, DMSO-d_6) δ 9.99 (s, 1H), 8.23 (s, 1H), 8.18 (s, 1H), 8.02 (s, 1H), 7.96 (d, *J* = 8.8 Hz, 2H), 7.47 (d, *J* = 8.8 Hz, 2H), 7.37 (d, *J* = 8.4 Hz, 1H), 7.05 (d, *J* = 8.4 Hz, 1H), 5.30 (s, 2H), 3.80 (d, *J* = 58.8 Hz, 4H), 2.81 (t, *J* = 7.2 Hz, 2H), 2.76 (s, 2H), 2.59 (s, 2H), 2.52 (s, 3H), 2.43 (s, 3H), 1.64 (q, *J* = 7.3 Hz, 2H), 0.94 (t, *J* = 7.4 Hz, 3H); ^{13}C NMR (151 MHz, DMSO) δ 195.62, 165.67, 163.26, 142.26, 141.59, 140.33, 135.78, 133.43, 132.77, 129.84, 126.95, 125.82, 123.84, 120.97, 120.36, 119.82, 110.48, 109.48, 48.70, 47.66, 47.33, 44.39, 42.10, 27.07, 26.65, 21.38, 17.53, 13.82, 12.05. m.p. = 138 −140 °C. LC-MS (*m*/*z*): positive mode 544.20 $[M + H]^{1+}$; purity by HPLC UV (254 nm)-ESI-MS: 94.1%.

Synthesis of *N*-(4-(4-butyryl-5-methyl-1*H*-pyrazol-1-yl)phenyl)-1-(2-((2-fluoroethyl)(methyl)amino)-2-oxoethyl)-5-methyl-1*H*-indole-3-carboxamide (26)

General procedure B, calculations: **2-fluoro-*N*-methylethan-1-amine** (6.8 mg, 0.083 mmol); Purification: silica gel chromatography (eluent DCM, followed by DCM:MeOH, 99:1), to afford **26** as white powder (20.5 mg, 0.04 mmol, 72%). ^{1}H NMR (600 MHz, DMSO-d_6) δ 9.99 (d, *J* = 16.3 Hz, 1H), 8.23 (s, 1H), 8.18 (d, *J* = 3.6 Hz, 1H), 8.03 (s, 1H), 7.96 (d, *J* = 8.4 Hz, 2H), 7.47 (d, *J* = 8.8 Hz, 2H), 7.32 (dd, *J* = 60.0, 8.4 Hz, 1H), 7.05 (d, *J* = 8.4 Hz, 1H), 5.28 (d, *J* = 30.2 Hz, 2H), 4.74 (dt, *J* = 47.5, 4.6 Hz, 1H), 4.55 (dt, *J* = 47.5, 4.9 Hz, 1H), 3.85 (dt, *J* = 27.0, 4.6 Hz, 1H), 3.65 (dt, *J* = 26.7, 4.9 Hz, 1H), 3.07 (d, *J* = 170.6 Hz, 3H), 2.81 (t, *J* = 7.2 Hz, 2H), 2.52 (s, 3H), 2.43 (s, 3H), 1.64 (h, *J* = 7.3 Hz, 2H), 0.94 (t, *J* = 7.4 Hz, 3H); ^{13}C NMR (151 MHz, DMSO) δ 195.48, 167.26, 167.01, 163.09, 142.12, 141.45, 140.19, 135.63, 135.56, 133.37, 132.63, 129.70, 125.68, 123.68, 120.89, 120.83, 120.23, 119.68, 110.32, 110.01, 109.28, 82.40, 82.29, 81.30, 81.19, 48.49, 48.37, 48.00, 47.87, 47.55, 47.31, 41.96, 40.06, 35.13, 33.49, 21.24, 17.40, 13.68, 11.91. m.p. = 132 −134 °C. LC-MS (*m*/*z*): positive mode 518.30 $[M + H]^{1+}$; purity by HPLC UV (254 nm)-ESI-MS: 95.0%.

Synthesis of (*R*,*S*)-*N*-(4-(4-butyryl-5-methyl-1*H*-pyrazol-1-yl)phenyl)-5-methyl-1-(2-(3-methylpiperidin-1-yl)-2-oxoethyl)-1*H*-indole-3-carboxamide (27)

General procedure B, calculations: **3-methylpiperidine** (6.0 mg, 0.083 mmol); Purification: silica gel chromatography (eluent DCM, followed by DCM:MeOH, 99:1), to afford **27** as white-yellowish powder (19.5 mg, 0.036 mmol, 66%). ^{1}H NMR (500 MHz, DMSO-d_6) δ 9.97 (s, 1H), 8.23 (s, 1H), 8.19 (s, 1H), 8.03 (s, 1H), 7.96 (d, *J* = 8.9 Hz, 2H), 7.47 (d, *J* = 8.9 Hz, 2H), 7.34 (d, *J* = 8.4 Hz, 1H), 7.05 (d, *J* = 8.5 Hz, 1H), 5.39 – 5.16 (m, 2H), 4.16 (t, *J* = 14.9 Hz, 1H), 3.89 (t, *J* = 11.5 Hz, 1H), 2.88 – 2.76 (m, 3H), 2.71 – 2.62 (m, 1H), 2.52 (s, 3H), 2.43 (s, 3H), 1.83 – 1.70 (m, 2H), 1.64 (h, *J* = 7.3 Hz, 2H), 1.50 (dd, *J* = 15.4, 12.1 Hz, 1H), 1.38 – 1.22 (m, 1H), 1.22 – 1.11 (m, 1H), 0.94 (t, *J* = 7.4 Hz, 3H), 0.85 (dd, *J* = 17.1, 6.6 Hz, 3H); ^{13}C NMR (126 MHz, DMSO) δ 195.46, 164.96, 163.11, 142.11, 141.43, 140.19, 135.60, 133.31, 132.61, 129.65, 126.83, 125.66, 123.65, 120.84, 120.21, 119.66, 110.23, 109.21, 51.56, 48.80, 47.43, 44.80, 41.95, 32.30, 31.22, 30.57, 25.22, 24.48, 21.23, 18.79, 18.58, 17.38, 13.67, 11.90. LC-MS (*m*/*z*): positive mode 539.7 $[M + H]^{1+}$; purity by HPLC UV (254 nm)-ESI-MS: 96.0%.

Synthesis of *N*-(4-(4-butyryl-5-methyl-1*H*-pyrazol-1-yl)phenyl)-1-(2-((2-methoxyethyl)(methyl)amino)-2-oxoethyl)-5-methyl-1*H*-indole-3-carboxamide (28)

General procedure B, calculations: **2-methoxy-*N*-methylethan-1-amine** (5.7 mg, 0.083 mmol); Purification: silica gel chromatography (eluent DCM, followed by DCM:MeOH, 99:1), to afford **28** as yellow powder (21.2 mg, 0.04 mmol, 73%). ^{1}H NMR (600 MHz, DMSO-d_6) δ 9.99 (d, *J* = 13.5 Hz, 1H), 8.23 (s, 1H), 8.17 (s, 1H), 8.02 (s, 1H), 7.96 (d, *J* = 8.7 Hz, 2H), 7.47 (d, *J* = 8.7 Hz, 2H), 7.31 (dd, *J* = 51.8, 8.4 Hz, 1H), 7.05 (d, *J* = 8.5 Hz, 1H), 5.28 (s, 2H), 3.64 (dt, *J* = 35.2, 4.9 Hz, 2H), 3.53 – 3.43 (m, 2H), 3.33 (d, *J* = 91.0 Hz, 3H), 3.03 (d, *J* = 168.7 Hz, 3H), 2.81 (q, *J* = 6.5, 5.8 Hz, 2H), 2.52 (s, 3H), 2.43 (s, 3H), 1.64 (h, *J* = 7.3 Hz, 2H), 0.94 (t, *J* = 7.4 Hz, 3H); ^{13}C NMR (151 MHz, DMSO) δ 195.47, 167.03, 166.83, 163.11, 142.12, 141.45, 140.20, 135.57, 133.40, 133.29, 132.61, 129.67, 126.83, 125.68, 123.65, 120.88, 120.22, 119.67, 110.31, 110.00, 109.18, 69.51, 69.47, 58.56, 58.01, 48.16, 47.56, 47.41, 47.00, 41.96, 35.07, 33.32, 21.24, 17.39, 13.68, 11.91. m.p. = 163 −165 °C. LC-MS (*m*/*z*): positive mode 530.80 $[M + H]^{1+}$; purity by HPLC UV (254 nm)-ESI-MS: 95.0%.

Synthesis of (*R*,*S*)-*N*-(4-(4-butyryl-5-methyl-1*H*-pyrazol-1-yl)phenyl)-5-methyl-1-(2-(2-methylpiperidin-1-yl)-2-oxoethyl)-1*H*-indole-3-carboxamide (29)

General procedure B, calculations: **2-methylpiperidine** (6.0 mg, 0.083 mmol); Purification: silica gel chromatography (eluent DCM, followed by DCM:MeOH, 99:1), to afford **29** as white-yellowish powder (16.5 mg, 0.03 mmol, 56%). ^{1}H NMR (600 MHz, DMSO-d_6) δ 9.97 (s, 1H), 8.23 (s, 1H), 8.19 (s, 1H), 8.03 (s, 1H), 7.96 (d, *J* = 8.5 Hz, 2H), 7.47 (d, *J* = 8.4 Hz, 2H), 7.34 (d, *J* = 8.4 Hz, 1H), 7.05 (d, *J* = 8.4 Hz, 1H), 5.49 – 5.08 (m, 2H), 4.72 – 4.59 (m, 1H), 4.27 (dd, *J* = 55.8, 11.8 Hz, 1H), 3.80 (d, *J* = 11.3 Hz, 1H), 2.81 (t, *J* = 7.2 Hz, 2H), 2.52 (s, 3H), 2.43 (s, 3H), 1.77 – 1.43 (m, 7H), 1.39 – 1.21 (m, 3H), 1.19 – 1.06 (m, 2H), 0.94 (t, *J* = 7.4 Hz, 3H); ^{13}C NMR (151 MHz, DMSO) δ 195.47, 165.08, 163.12, 142.12, 141.44, 140.21, 135.63, 133.36, 132.60, 129.64, 126.85, 125.68, 123.65, 120.84, 120.22, 119.64, 110.25, 109.17, 41.96, 21.24, 18.23, 17.39, 13.68, 11.91. m.p. = 218 −220 °C. LC-MS (*m*/*z*): positive mode 540.50 $[M + H]^{1+}$; purity by HPLC UV (254 nm)-ESI-MS: 99.0%.

Synthesis of *N*-(4-(4-butyryl-5-methyl-1*H*-pyrazol-1-yl)phenyl)-1-(2-(3-fluoroazetidin-1-yl)-2-oxoethyl)-5-methyl-1*H*-indole-3-carboxamide (30)

General procedure B, calculations: **3-fluoroazetidine** (6.7 mg, 0.083 mmol); Purification: silica gel chromatography (eluent DCM, followed by DCM:MeOH, 99:1), to afford **30** as white-

yellowish powder (15.8 mg, 0.03 mmol, 56%). ^{1}H NMR (600 MHz, DMSO-d_6) δ 10.01 (s, 1H), 8.23 (s, 1H), 8.19 (s, 1H), 8.03 (s, 1H), 7.96 (d, *J* = 8.7 Hz, 2H), 7.48 (d, *J* = 8.7 Hz, 2H), 7.38 (d, *J* = 8.4 Hz, 1H), 7.08 (d, *J* = 8.4 Hz, 1H), 5.46 (ddt, *J* = 57.1, 5.9, 2.9 Hz, 1H), 5.05 (d, *J* = 5.3 Hz, 2H), 4.56 (ddd, *J* = 21.2, 10.4, 6.0 Hz, 1H), 4.40 – 4.19 (m, 2H), 3.99 (dd, *J* = 25.0, 11.5 Hz, 1H), 2.81 (t, *J* = 7.2 Hz, 2H), 2.52 (s, 3H), 2.43 (s, 3H), 1.64 (h, *J* = 7.3 Hz, 2H), 0.94 (t, *J* = 7.4 Hz, 3H); ^{13}C NMR (151 MHz, DMSO) δ 195.48, 167.03, 163.03, 142.12, 141.45, 140.12, 135.36, 132.97, 132.68, 129.93, 126.82, 125.69, 123.89, 120.92, 120.23, 119.72, 110.23, 109.55, 83.55, 82.22, 57.56, 56.16, 46.25, 41.96, 21.23, 17.39, 13.68, 11.91. m.p. = 120 −122 °C. LC-MS (*m*/*z*): positive mode 516.30 $[M + H]^{1+}$; purity by HPLC UV (254 nm)-ESI-MS: 97.5%.

Synthesis of *N*-(4-(4-butyryl-5-methyl-1*H*-pyrazol-1-yl)phenyl)-5-methyl-1-(2-(methylamino)-2-oxoethyl)-1*H*-indole-3-carboxamide (31)

General procedure B, calculations: **methanamine·hydrochloride** (4.0 mg, 0.083 mmol); Purification: recrystallization to afford **31** as pale-yellow powder (22.0 mg, 0.047 mmol, 85%). ^{1}H NMR (600 MHz, DMSO-d_6) δ 10.01 (s, 1H), 8.25 (s, 1H), 8.23 (s, 1H), 8.20 (d, *J* = 4.6 Hz, 1H), 8.04 (s, 1H), 7.96 (d, *J* = 8.8 Hz, 2H), 7.47 (d, *J* = 8.8 Hz, 2H), 7.35 (d, *J* = 8.4 Hz, 1H), 7.07 (d, *J* = 8.4 Hz, 1H), 4.88 (s, 2H), 2.81 (t, *J* = 7.2 Hz, 2H), 2.65 (d, *J* = 4.6 Hz, 3H), 2.52 (s, 3H), 2.43 (s, 3H), 1.64 (q, *J* = 7.3 Hz, 2H), 0.94 (t, *J* = 7.4 Hz, 3H); ^{13}C NMR (151 MHz, DMSO) δ 195.51, 167.21, 163.08, 142.14, 141.47, 140.17, 135.21, 133.03, 132.67, 129.95, 127.03, 125.70, 123.92, 120.99, 120.24, 119.72, 110.04, 109.35, 49.04, 48.58, 41.98, 25.66, 21.25, 17.41, 13.70, 11.93. m.p. = 264 −266 °C. LC-MS (*m*/*z*): positive mode 472.20 $[M + H]^{1+}$; purity by HPLC UV (254 nm)-ESI-MS: 95.0%.

Synthesis of *N*-(4-(4-butyryl-5-methyl-1*H*-pyrazol-1-yl)phenyl)-1-(2-(3-hydroxyazetidin-1-yl)-2-oxoethyl)-5-methyl-1*H*-indole-3-carboxamide (32)

General procedure B, calculations: **azetidin-3-ol** (7.0 mg, 0.083 mmol); Purification: silica gel chromatography (eluent DCM, followed by DCM:MeOH, 99:1), to afford **32** as white-yellowish powder (0.02 g, 0.039 mmol, 71%). ^{1}H NMR (600 MHz, DMSO-d_6) δ 10.01 (s, 1H), 8.23 (s, 1H), 8.20 (s, 1H), 8.02 (s, 1H), 7.96 (d, *J* = 8.5 Hz, 2H), 7.47 (d, *J* = 8.5 Hz, 2H), 7.37 (d, *J* = 8.4 Hz, 1H), 7.07 (d, *J* = 8.4 Hz, 1H), 5.78 (d, *J* = 5.8 Hz, 1H), 5.00 (d, *J* = 4.8 Hz, 2H), 4.52 (h, *J* = 5.8 Hz, 1H), 4.39 (t, *J* = 7.9 Hz, 1H), 4.14 – 4.09 (m, 1H), 3.96 (dd, *J* = 9.0, 4.2 Hz, 1H), 3.66 (dd, *J* = 10.2, 4.1 Hz, 1H), 2.81 (t, *J* = 7.2 Hz, 2H), 2.52 (s, 3H), 2.43 (s, 3H), 1.64 (h, *J* = 7.3 Hz, 2H), 0.94 (t, *J* = 7.4 Hz, 3H); ^{13}C NMR (151 MHz, DMSO) δ 195.48, 166.60, 163.03, 142.12, 141.45, 140.13,

135.34, 133.01, 132.66, 129.89, 126.83, 125.69, 123.86, 120.91, 120.23, 119.71, 110.20, 109.45, 60.27, 59.51, 58.03, 46.28, 41.96, 21.24, 17.39, 13.68, 11.91. LC-MS (*m*/*z*): positive mode 514.80 $[M + H]^{1+}$; purity by HPLC UV (254 nm)-ESI-MS: 99.0%.

Synthesis of *N*-(4-(4-butyryl-5-methyl-1*H*-pyrazol-1-yl)phenyl)-1-(2-(cyclohexylamino)-2-oxoethyl)-5-methyl-1*H*-indole-3-carboxamide (33)

General procedure B, calculations: **cyclohexanamine** (7.1 mg, 0.083 mmol); Purification: silica gel chromatography (eluent DCM, followed by DCM:MeOH, 99:1), to afford **33** as white powder (16.0 mg, 0.03 mmol, 54%). ^{1}H NMR (600 MHz,) δ 10.01 (s, 1H), 8.27 (s, 1H), 8.25 (d, *J* = 1.7 Hz, 1H), 8.23 (s, 1H), 8.03 (s, 1H), 7.97 (dd, *J* = 9.0, 2.7 Hz, 2H), 7.47 (d, *J* = 8.8 Hz, 2H), 7.34 (d, *J* = 8.4 Hz, 1H), 7.07 (d, *J* = 8.4 Hz, 1H), 4.86 (s, 2H), 3.56 (s, 1H), 2.81 (t, *J* = 7.2 Hz, 2H), 2.52 (s, 3H), 2.43 (s, 3H), 1.80 – 1.74 (m, 2H), 1.69 (dt, *J* = 10.5, 5.1 Hz, 2H), 1.63 (p, *J* = 7.3 Hz, 2H), 1.58 – 1.52 (m, 1H), 1.23 (qd, *J* = 22.8, 22.3, 12.2 Hz, 5H), 0.94 (t, *J* = 7.4 Hz, 3H); ^{13}C NMR (151 MHz,) δ 195.65, 165.72, 163.24, 142.30, 141.63, 140.35, 135.35, 133.34, 132.81, 130.06, 127.21, 125.85, 124.00, 121.16, 120.40, 119.86, 110.16, 109.30, 49.37, 47.95, 47.84, 42.14, 40.23, 32.44, 25.31, 24.52, 21.41, 17.57, 13.86, 12.09. m.p. = 299 −301 °C. LC-MS (*m*/*z*): positive mode 540.30 $[M + H]^{1+}$; purity by HPLC UV (254 nm)-ESI-MS: 97.0%.

Synthesis of *N*-(4-(4-butyryl-5-methyl-1*H*-pyrazol-1-yl)phenyl)-1-(2-((2-fluoroethyl)amino)-2-oxoethyl)-5-methyl-1*H*-indole-3-carboxamide (34)

General procedure B, calculations: **2-fluoroethan-1-amine** (6.0 mg, 0.083 mmol); Purification: silica gel chromatography (eluent DCM, followed by DCM:MeOH, 99:1), to afford **34** as white powder (21 mg, 0.042 mmol, 76%). ^{1}H NMR (500 MHz, DMSO-d_6) δ 10.01 (s, 1H), 8.61 (t, *J* = 5.5 Hz, 1H), 8.26 (s, 1H), 8.23 (s, 1H), 8.04 (s, 1H), 7.96 (d, *J* = 8.9 Hz, 2H), 7.47 (d, *J* = 8.8 Hz, 2H), 7.35 (d, *J* = 8.4 Hz, 1H), 7.13 – 7.01 (m, 1H), 4.95 (s, 2H), 4.52 (t, *J* = 5.0 Hz, 1H), 4.42 (t, *J* = 5.0 Hz, 1H), 3.47 (q, *J* = 5.1 Hz, 1H), 3.41 (q, *J* = 5.1 Hz, 1H), 2.81 (t, *J* = 7.2 Hz, 2H), 2.52 (s, 3H), 2.43 (s, 3H), 1.64 (h, *J* = 7.3 Hz, 2H), 0.94 (t, *J* = 7.4 Hz, 3H); ^{13}C NMR (126 MHz, DMSO) δ 195.46, 167.14, 163.04, 142.11, 141.43, 140.15, 135.21, 133.07, 132.65, 129.92, 127.00, 125.67, 123.89, 120.97, 120.22, 119.70, 109.99, 109.33, 82.94, 81.62, 48.92, 41.95, 21.22, 17.38, 13.67, 11.90. m.p. = 256−258 °C. LC-MS (*m*/*z*): positive mode 504.20 $[M + H]^{1+}$; purity by HPLC UV (254 nm)-ESI-MS: 98.0%.

Synthesis of (*R*,*S*)-*N*-(4-(4-butyryl-5-methyl-1*H*-pyrazol-1-yl)phenyl)-1-(2-(3-hydroxypiperidin-1-yl)-2-oxoethyl)-5-methyl-1*H*-indole-3-carboxamide (35)

General procedure B, calculations: **piperidin-3-ol** (6.0 mg, 0.083 mmol); Purification: silica gel chromatography (eluent DCM, followed by DCM:MeOH, 99:1), to afford **35** as white powder (22.3 mg, 0.041 mmol, 75%). ^{1}H NMR (500 MHz, DMSO-d_6) δ 9.97 (s, 1H), 8.23 (s, 1H), 8.18 (d, *J* = 3.7 Hz, 1H), 8.03 (s, 1H), 7.96 (d, *J* = 8.9 Hz, 2H), 7.47 (d, *J* = 8.8 Hz, 2H), 7.33 (t, *J* = 7.7 Hz, 1H), 7.04 (d, *J* = 8.4 Hz, 1H), 5.26 (s, 2H), 4.96 (dd, *J* = 43.0, 4.0 Hz, 1H), 4.10 – 4.04 (m, 1H), 3.75 (d, *J* = 13.3 Hz, 1H), 3.66 – 3.56 (m, 1H), 3.53 – 3.45 (m, 1H), 3.41 (dd, *J* = 13.4, 5.6 Hz, 2H), 3.21 – 3.12 (m, 1H), 2.81 (t, *J* = 7.2 Hz, 2H), 2.74 – 2.64 (m, 1H), 2.52 (s, 3H), 2.43 (s, 3H), 1.95 – 1.67 (m, 2H), 1.64 (h, *J* = 7.3 Hz, 2H), 1.60 – 1.30 (m, 2H), 1.25 (d, *J* = 11.2 Hz, 1H), 0.94 (t, *J* = 7.4 Hz, 3H); ^{13}C NMR (126 MHz, DMSO) δ 195.47, 165.69, 165.31, 163.11, 142.12, 141.43, 140.20, 135.62, 133.37, 132.61, 129.66, 126.86, 125.67, 123.65, 120.84, 120.22, 119.66, 110.23, 109.22, 64.94, 64.59, 51.22, 48.89, 47.42, 44.44, 42.31, 41.96, 32.77, 31.87, 23.34, 21.24, 17.39, 13.68, 11.90. m.p. = 166−168 °C. LC-MS (*m*/*z*): positive mode 542.70 $[M + H]^{1+}$; purity by HPLC UV (254 nm)-ESI-MS: 99.0%.

Synthesis of *N*-(4-(4-butyryl-5-methyl-1*H*-pyrazol-1-yl)phenyl)-5-methyl-1-(2-morpholino-2-oxoethyl)-1*H*-indole-3-carboxamide (36)

General procedure B, calculations: **morpholine** (6.0 mg, 0.083 mmol); Purification: recrystallization to afford **36** as white powder (27.0 mg, 0.051 mmol, 93%). ^{1}H NMR (600 MHz, DMSO-d_6) δ 9.98 (s, 1H), 8.23 (s, 1H), 8.18 (s, 1H), 8.02 (s, 1H), 7.96 (d, *J* = 8.6 Hz, 2H), 7.47 (d, *J* = 8.6 Hz, 2H), 7.37 (d, *J* = 8.4 Hz, 1H), 7.06 (d, *J* = 8.3 Hz, 1H), 5.30 (s, 2H), 3.70 (s, 2H), 3.61 (s, 4H), 3.48 (s, 2H), 2.81 (t, *J* = 7.1 Hz, 2H), 2.52 (s, 3H), 2.43 (s, 3H), 1.64 (h, *J* = 7.2 Hz, 2H), 0.94 (t, *J* = 7.4 Hz, 3H); ^{13}C NMR (151 MHz, DMSO) δ 195.47, 165.68, 163.10, 142.12, 141.45, 140.19, 135.64, 133.26, 132.63, 129.71, 126.81, 125.68, 123.69, 120.84, 120.22, 119.67, 110.30, 109.33, 66.05, 65.99, 64.87, 47.25, 44.81, 41.96, 21.24, 17.39, 15.12, 13.68, 11.91. m.p. = 145 −147 °C. LC-MS (*m*/*z*): positive mode 528.30 $[M + H]^{1+}$; purity by HPLC UV (254 nm)-ESI-MS: 95.0%.

Synthesis of methyl 2-(3-((4-(3-butyryl-2-methyl-1*H*-pyrrol-1-yl)phenyl)carbamoyl)-5-methyl-1*H*-indol-1-yl)acetate (43)

General procedure A, calculations: **15b** (0.06 g, 0.24 mmol) in DCM (25 mL), **42** (0.07 g, 0.29 mmol), **4-DMAP** (0.38 g, 0.05 mmol), and **EDC·HCl** (0.38 g, 0.05 mmol); Purification: silica gel

chromatography, eluent DCM, followed by DCM/EtOAc, 8/2 v/v to afford **43** as a beige powder (0.07 g, 0.15 mmol, 62%). ^{1}H NMR (600 MHz, DMSO-d_6) δ 9.99 (s, 1H), 8.20 (s, 1H), 8.00 (s, 1H), 7.91 (d, *J* = 8.8 Hz, 2H), 7.38 (d, *J* = 8.4 Hz, 1H), 7.34 (d, *J* = 8.7 Hz, 2H), 7.12 – 7.03 (m, 1H), 6.86 (d, *J* = 3.1 Hz, 1H), 6.68 (d, *J* = 3.1 Hz, 1H), 5.25 (s, 2H), 3.70 (s, 3H), 2.72 (t, *J* = 7.2 Hz, 2H), 2.42 (s, 3H), 2.39 (s, 3H), 1.61 (h, *J* = 7.3 Hz, 2H), 0.92 (t, *J* = 7.4 Hz, 3H); ^{13}C NMR (151 MHz, DMSO) δ 196.47, 169.21, 163.13, 139.74, 135.39, 134.37, 132.91, 132.83, 130.22, 126.98, 126.41, 124.25, 121.76, 121.34, 121.10, 120.17, 110.34, 110.15, 110.00, 52.44, 47.53, 41.88, 40.24, 21.40, 17.83, 14.00, 12.54. m.p. = 170 −172 °C. LC-MS (*m*/*z*): positive mode 472.20 $[M + H]^{1+}$; purity by HPLC UV (254 nm)-ESI-MS: 95.0%.

Synthesis of 2-(3-((4-(3-butyryl-2-methyl-1*H*-pyrrol-1-yl)phenyl)carbamoyl)-5-methyl-1*H*-indol-1-yl)acetic acid (44)

In a sealed tube, aqueous 2 N NaOH (0.1 mL, 0.12 mmol) was added to a solution of **43** (0.05 g, 0.11 mmol) in MeOH (5 mL). The reaction mixture was stirred at room temperature overnight. Then, it was concentrated under vacuum and neutralized via aqueous 1N HCl. The observed precipitation was filtered, washed with water and dried under high vacuum to afford the targeted unlabeled ligand **44** as white powder (0.02 g, 0.04 mmol, 40%). ^{1}H NMR (600 MHz, DMSO-d_6) δ 9.98 (s, 1H), 8.22 (s, 1H), 8.01 (s, 1H), 7.93 (d, *J* = 8.7 Hz, 2H), 7.39 (d, *J* = 8.4 Hz, 1H), 7.35 (d, *J* = 8.7 Hz, 2H), 7.07 (d, *J* = 8.4 Hz, 1H), 6.87 (d, *J* = 3.1 Hz, 1H), 6.69 (d, *J* = 3.1 Hz, 1H), 5.12 (s, 2H), 2.73 (t, *J* = 7.2 Hz, 2H), 2.43 (s, 3H), 2.40 (s, 3H), 1.62 (h, *J* = 7.3 Hz, 2H), 0.93 (t, *J* = 7.4 Hz, 3H); ^{13}C NMR (151 MHz, DMSO) δ 196.29, 169.95, 163.02, 139.62, 135.27, 134.20, 132.79, 132.69, 129.89, 126.82, 126.23, 123.95, 121.58, 121.16, 120.89, 119.97, 110.14, 109.82, 109.67, 47.55, 41.71, 40.06, 21.23, 17.65, 13.83, 12.37. m.p. = 127−129 °C. LC-MS (*m*/*z*): positive mode 458.20 $[M + H]^{1+}$; purity by HPLC UV (254 nm)-ESI-MS: 94.4%.

3.5.7 Supporting information

Chemistry

Synthesis of the intermediates (*N*-Alkylation of the 3-benzyl protected carboxylic acid indoles (2a−13a)

General procedure A

In a sealed tube, 1.0 equiv. of **I** was added to a mixture of dissolved **2.0 equiv.** of **sodium hydride** (NaH) in 10 mL of DMF and stirred for 30 minutes at 0 °C. Then **2.0 equiv.** of **alkyl halide** was

added dropwise to the mixture. The reaction mixture was allowed to stir at 25 °C for overnight. TLC-control was performed to confirm the formation of the desired product. The reaction mixture was poured into 25 mL of water and extracted with ethyl acetate 3x. The organic phase was dried over $MgSO_4$, evaporated under reduced pressure, and then submitted to a column chromatography (silica gel chromatography, eluent either DCM (100%) or petroleum ether:ethyl acetate mixture (8:2)) to afford the desired compounds:

Synthesis of benzyl 5-methyl-1-propyl-1*H*-indole-3-carboxylate (2a)

General procedure A, calculations: **I** (0.30 g, 1.13 mmol), NaH (0.054 g, 2.26 mmol), 1-iodopropane (0.38 g, 2.26 mmol); Purification: column chromatography (silica gel chromatography, eluent DCM) to afford **2a** as white powder (0.26 g, 0.85 mmol, 75%), ^{1}H NMR (500 MHz, DMSO-d_6) δ 8.13 (s, 1H), 7.82 (s, 1H), 7.48 (d, J = 8.4 Hz, 3H), 7.40 (t, J = 7.4 Hz, 2H), 7.34 (t, J = 7.3 Hz, 1H), 7.10 – 7.04 (m, 1H), 5.32 (s, 2H), 4.18 (t, J = 7.0 Hz, 2H), 2.40 (s, 3H), 1.78 (h, J = 7.3 Hz, 2H), 0.82 (t, J = 7.4 Hz, 3H); ^{13}C NMR (126 MHz, DMSO) δ 163.81, 137.01, 135.43, 134.73, 130.38, 128.40, 127.75, 126.46, 123.88, 120.30, 110.63, 104.52, 64.42, 47.56, 22.80, 21.20, 10.91. LC-MS (*m*/*z*): positive mode 308.20 $[M + H]^{1+}$; purity by HPLC UV (254 nm)-ESI-MS: 99.8%.

Synthesis of benzyl 1,5-dimethyl-1*H*-indole-3-carboxylate (3a)

General procedure A, calculations: **I** (0.30 g, 1.13 mmol), NaH (0.054 g, 2.26 mmol), iodomethane (0.32 g, 2.26 mmol); Purification: column chromatography (silica gel chromatography, eluent DCM) to afford **3a** as a white powder (0.21 g, 0.76 mmol, 67%),^{1}H NMR (500 MHz, DMSO-d_6) δ 8.10 (s, 1H), 7.81 (s, 1H), 7.47 (d, J = 7.3 Hz, 2H), 7.41 (q, J = 7.9 Hz, 3H), 7.34 (t, J = 7.3 Hz, 1H), 7.14 – 7.05 (m, 1H), 5.32 (s, 2H), 3.83 (s, 3H), 2.41 (s, 3H); ^{13}C NMR (126 MHz, DMSO) δ 163.75, 137.03, 136.26, 135.44, 130.45, 128.40, 127.76, 127.68, 126.36, 123.90, 120.16, 110.45, 104.39, 64.38, 33.00, 21.23. LC-MS (*m*/*z*): positive mode 280.10 $[M + H]^{1+}$; purity by HPLC UV (254 nm)-ESI-MS: 99.9%.

Synthesis of benzyl 1-(2-methoxyethyl)-5-methyl-1*H*-indole-3-carboxylate (4a)

General procedure A, calculations: **I** (0.20 g, 0.75 mmol), NaH (0.04 g, 1.51 mmol), 1-bromo-2-methoxyethane (0.31 g, 1.51 mmol) to afford **4a** as white powder (0.23 g, 0.72 mmol, 96%), ^{1}H NMR (500 MHz, DMSO-d_6) δ 8.07 (s, 1H), 7.82 (s, 1H), 7.48 (t, J = 7.9 Hz, 3H), 7.40 (t, J = 7.4 Hz, 2H), 7.34 (t, J = 7.3 Hz, 1H), 7.10 – 7.03 (m, 1H), 5.32 (s, 2H), 4.39 (t, J = 5.2 Hz, 2H), 3.81 (d, J = 14.8 Hz, 1H), 3.66 (t, J = 5.2 Hz, 2H), 3.20 (s, 3H), 2.40 (s, 3H); ^{13}C NMR (126 MHz,

DMSO) δ 163.79, 137.00, 135.83, 134.88, 130.42, 128.41, 127.79, 127.75, 126.36, 123.88, 120.21, 110.73, 104.72, 70.45, 64.44, 58.02, 45.85, 21.20. LC-MS (*m*/*z*): positive mode 324.20 $[M + H]^{1+}$; purity by HPLC UV (254 nm)-ESI-MS: 81.1%.

Synthesis of benzyl 1-(cyclobutylmethyl)-5-methyl-1*H*-indole-3-carboxylate (5a)

General procedure A, calculations: **I** (0.20 g, 0.75 mmol), NaH (0.04 g, 1.51 mmol), (bromomethyl)cyclobutane (0.34 g, 1.51 mmol) to afford **5a** as white powder (0.22 g, 0.66 mmol, 88%), ^{1}H NMR (500 MHz, DMSO-d_6) δ 8.11 (s, 1H), 7.81 (s, 1H), 7.48 (d, *J* = 3.1 Hz, 1H), 7.47 – 7.45 (m, 2H), 7.40 (t, *J* = 7.4 Hz, 2H), 7.33 (dd, *J* = 14.4, 6.0 Hz, 1H), 7.09 – 7.05 (m, 1H), 5.32 (s, 2H), 4.24 (d, *J* = 7.4 Hz, 2H), 2.78 (hept, *J* = 8.6, 8.0 Hz, 1H), 2.40 (s, 3H), 1.92 (qd, *J* = 8.7, 8.0, 3.3 Hz, 2H), 1.86 – 1.80 (m, 2H), 1.80 – 1.71 (m, 2H); ^{13}C NMR (126 MHz, DMSO) δ 164.00, 137.19, 135.45, 135.08, 130.56, 128.58, 127.96, 127.92, 126.54, 124.05, 120.42, 110.86, 104.75, 64.61, 50.94, 35.23, 25.46, 21.37, 17.75. LC-MS (*m*/*z*): positive mode 334.20 $[M + H]^{1+}$; purity by HPLC UV (254 nm)-ESI-MS: 89.0%.

Synthesis of benzyl 1-(2-fluoroethyl)-5-methyl-1*H*-indole-3-carboxylate (6a)

General procedure A, calculations: **I** (0.30 g, 1.13 mmol), NaH (0.054 g, 2.26 mmol), 1-fluoro-2-iodoethane (0.39 g, 2.26 mmol); Purification: column chromatography (silica gel chromatography, eluent DCM) to afford **6a** as white powder (0.26 g, 0.84 mmol, 74%), ^{1}H NMR (500 MHz, DMSO-d_6) δ 8.39 (s, 1H), 8.02 (d, *J* = 58.9 Hz, 2H), 7.62 (d, *J* = 8.4 Hz, 1H), 7.49 (d, *J* = 7.3 Hz, 2H), 7.41 (t, *J* = 7.4 Hz, 2H), 7.35 (t, *J* = 7.3 Hz, 1H), 7.26 – 7.19 (m, 1H), 5.36 (s, 2H), 2.42 (s, 3H); ^{13}C NMR (126 MHz, DMSO) δ 163.12, 136.42, 132.76, 131.99, 131.62, 128.46, 127.99, 127.90, 126.78, 125.83, 120.89, 111.87, 110.83, 109.04, 65.21, 21.11. m.p. = 90−92 °C. LC-MS (*m*/*z*): positive mode 312.10 $[M + H]^{1+}$; purity by HPLC UV (254 nm)-ESI-MS: 99.8%.

Synthesis of benzyl 1-isopropyl-5-methyl-1*H*-indole-3-carboxylate (7a)

General procedure A, calculations: **I** (0.30 g, 1.13 mmol), NaH (0.054 g, 2.26 mmol), 2-iodopropane (0.38 g, 2.26 mmol) to afford **7a** as white powder (0.28 g, 0.92 mmol, 82%), ^{1}H NMR (500 MHz, DMSO-d_6) δ 8.16 (s, 1H), 7.83 (s, 1H), 7.52 (d, *J* = 8.4 Hz, 1H), 7.48 (d, *J* = 7.2 Hz, 2H), 7.40 (t, *J* = 7.4 Hz, 2H), 7.33 (t, *J* = 7.3 Hz, 1H), 7.11 – 7.05 (m, 1H), 5.33 (s, 2H), 4.78 (hept, *J* = 6.6 Hz, 1H), 2.40 (s, 3H), 1.48 (d, *J* = 6.7 Hz, 6H); ^{13}C NMR (126 MHz, DMSO) δ 163.83, 137.05, 134.23, 131.63, 130.47, 128.40, 127.76, 126.48, 123.85, 120.35, 110.67, 104.99, 64.40, 47.56, 22.08, 21.19. LC-MS (*m*/*z*): positive mode 308.20 $[M + H]^{1+}$; purity by HPLC UV (254 nm)-ESI-MS: 87.0%.

Synthesis of benzyl 1-(2-chloroethyl)-5-methyl-1*H*-indole-3-carboxylate (8a)

General procedure A, calculations: **I** (0.20 g, 0.75 mmol), NaH (0.04 g, 1.51 mmol), 1-bromo-2-chloroethane (0.22 g, 1.51 mmol); Purification: column chromatography (silica gel chromatography, eluent DCM) to afford **8a** as a white powder (0.16 g, 0.50 mmol, 67%), ^{1}H NMR (600 MHz, DMSO-d_6) δ 8.18 (s, 1H), 7.83 (s, 1H), 7.54 (d, *J* = 8.4 Hz, 1H), 7.48 (d, *J* = 7.6 Hz, 2H), 7.41 (t, *J* = 7.5 Hz, 2H), 7.34 (t, *J* = 7.3 Hz, 1H), 7.09 (d, *J* = 8.4 Hz, 1H), 5.33 (s, 2H), 4.60 (t, *J* = 5.8 Hz, 2H), 4.02 (t, *J* = 5.8 Hz, 2H), 2.41 (s, 3H); ^{13}C NMR (151 MHz, DMSO) δ 163.77, 136.94, 135.88, 134.75, 130.68, 128.43, 127.83, 127.80, 126.41, 124.09, 120.31, 110.69, 105.13, 64.55, 47.50, 43.50, 21.20. m.p. = 86–88 °C. LC-MS (*m*/*z*): positive mode 328.10 $[M + H]^{1+}$; purity by HPLC UV (254 nm)-ESI-MS: 92.6%.

Synthesis of benzyl 1-(but-2-yn-1-yl)-5-methyl-1*H*-indole-3-carboxylate (9a)

General procedure A, calculations: **I** (0.30 g, 1.13 mmol), NaH (0.054 g, 2.26 mmol), 1-bromobut-2-yne (0.23 g, 1.70 mmol) to afford **9a** as white powder (0.29 g, 0.90 mmol, 79%), ^{1}H NMR (600 MHz, DMSO-d_6) δ 8.15 (s, 1H), 7.83 (s, 1H), 7.50 (d, *J* = 8.4 Hz, 1H), 7.47 (d, *J* = 7.5 Hz, 2H), 7.40 (t, *J* = 7.6 Hz, 2H), 7.34 (t, *J* = 7.3 Hz, 1H), 7.16 – 7.08 (m, 1H), 5.33 (s, 2H), 5.09 (d, *J* = 2.4 Hz, 2H), 2.41 (s, 3H), 1.79 (t, *J* = 2.4 Hz, 3H); ^{13}C NMR (151 MHz, DMSO) δ 163.67, 136.95, 134.85, 134.36, 130.82, 128.43, 127.82, 127.74, 126.52, 124.16, 120.32, 110.85, 105.16, 81.48, 73.68, 64.54, 36.09, 21.23, 2.97. LC-MS (*m*/*z*): positive mode 318.20 $[M + H]^{1+}$; purity by HPLC UV (254 nm)-ESI-MS: 96.1%.

Synthesis of benzyl 1-(difluoromethyl)-5-methyl-1*H*-indole-3-carboxylate (10a)

General procedure A, calculations: **I** (0.20 g, 0.75 mmol), NaH (0.04 g, 1.51 mmol), difluoroiodomethane (0.27 g, 1.51 mmol); Purification: column chromatography (silica gel chromatography, eluent: petroleum ether:ethyl acetate mixture (8:2)) to afford **10a** as white powder (0.15 g, 0.48 mmol, 63%), ^{1}H NMR (500 MHz, DMSO-d_6) δ 8.39 (s, 1H), 8.02 (d, *J* = 58.9 Hz, 1H), 7.62 (d, *J* = 8.4 Hz, 1H), 7.49 (d, *J* = 7.3 Hz, 2H), 7.41 (t, *J* = 7.4 Hz, 2H), 7.35 (t, *J* = 7.3 Hz, 1H), 7.26 – 7.19 (m, 2H), 5.36 (s, 2H), 2.42 (s, 3H); ^{13}C NMR (126 MHz, DMSO) δ 163.12, 136.42, 132.76, 131.99, 131.62, 128.46, 127.99, 127.90, 126.78, 125.83, 120.89, 111.87, 110.83, 109.04, 65.21, 21.11. LC-MS (*m*/*z*): positive mode 316.00 $[M + H]^{1+}$; purity by HPLC UV (254 nm)-ESI-MS: 98.4%.

Synthesis of (*R*,*S*)-benzyl 1-(*sec*-butyl)-5-methyl-1*H*-indole-3-carboxylate (11a)

General procedure A, calculations: **I** (0.20 g, 0.75 mmol), NaH (0.04 g, 1.51 mmol), 2-iodobutane (0.28 g, 1.51 mmol); Purification: column chromatography (silica gel chromatography, eluent DCM) to afford **11a** as white powder (0.15 g, 0.46 mmol, 61%), ^{1}H NMR (500 MHz, DMSO-d_6) δ 8.15 (s, 1H), 7.83 (s, 1H), 7.53 (d, *J* = 8.5 Hz, 1H), 7.48 (d, *J* = 7.3 Hz, 2H), 7.40 (t, *J* = 7.5 Hz, 2H), 7.34 (t, *J* = 7.3 Hz, 1H), 7.06 (dd, *J* = 8.5, 1.5 Hz, 1H), 5.33 (s, 2H), 4.62 – 4.49 (m, 1H), 2.40 (s, 3H), 1.87 (ddt, *J* = 30.4, 14.9, 7.5 Hz, 2H), 1.48 (d, *J* = 6.8 Hz, 3H), 0.71 (t, *J* = 7.4 Hz, 3H); ^{13}C NMR (126 MHz, DMSO) δ 163.86, 137.03, 134.78, 132.15, 130.40, 128.40, 127.79, 126.32, 123.84, 120.33, 110.75, 105.11, 64.43, 53.37, 28.98, 21.18, 20.28, 10.45. LC-MS (*m*/*z*): positive mode 322.10 $[M + H]^{1+}$; purity by HPLC UV (254 nm)-ESI-MS: 98.9%.

Synthesis of (*R*,*S*)-benzyl 5-methyl-1-((tetrahydrofuran-2-yl)methyl)-1*H*-indole-3-carboxylate (12a)

General procedure A, calculations: **I** (0.20 g, 0.75 mmol), NaH (0.04 g, 1.51 mmol), 2-(bromomethyl)tetrahydrofuran (0.25 g, 1.51 mmol); Purification: column chromatography (silica gel chromatography, eluent DCM) to afford **12a** as white powder (0.15 g, 0.43 mmol, 57%), ^{1}H NMR (500 MHz, DMSO-d_6) δ 8.08 (s, 1H), 7.81 (s, 1H), 7.51 (d, *J* = 8.4 Hz, 1H), 7.47 (d, *J* = 7.3 Hz, 2H), 7.40 (t, *J* = 7.4 Hz, 2H), 7.34 (t, *J* = 7.3 Hz, 1H), 7.07 (dd, *J* = 8.4, 1.3 Hz, 1H), 5.32 (s, 2H), 4.33 (dd, *J* = 14.0, 3.4 Hz, 1H), 4.25 – 4.09 (m, 2H), 3.78 – 3.68 (m, 1H), 3.60 (q, *J* = 7.0 Hz, 1H), 2.40 (s, 3H), 1.94 (dq, *J* = 13.6, 6.8 Hz, 1H), 1.81 – 1.69 (m, 2H), 1.59 – 1.45 (m, 1H); ^{13}C NMR (126 MHz, DMSO) δ 163.81, 137.00, 135.98, 135.17, 130.37, 128.41, 127.79, 127.76, 126.23, 123.86, 120.13, 110.93, 104.73, 77.07, 67.25, 64.45, 49.81, 28.33, 24.98, 21.20. LC-MS (*m*/*z*): positive mode 350.20 $[M + H]^{1+}$; purity by HPLC UV (254 nm)-ESI-MS: 99.3%.

Synthesis of benzyl 1-isobutyl-5-methyl-1*H*-indole-3-carboxylate (13a)

General procedure A, calculations: **I** (0.20 g, 0.75 mmol), NaH (0.04 g, 1.51 mmol), 1-iodo-2-methylpropane (0.28 g, 1.51 mmol); Purification: column chromatography (silica gel chromatography, eluent DCM) to afford **13a** as a pale brown powder (0.17 g, 0.53 mmol, 71%), ^{1}H NMR (500 MHz, DMSO-d_6) δ 8.10 (s, 1H), 7.82 (s, 1H), 7.49 (d, *J* = 2.7 Hz, 1H), 7.48 – 7.46 (m, 2H), 7.40 (t, *J* = 7.4 Hz, 2H), 7.34 (t, *J* = 7.3 Hz, 1H), 7.07 (dd, *J* = 8.4, 1.4 Hz, 1H), 5.32 (s, 2H), 4.04 (d, *J* = 7.4 Hz, 2H), 2.40 (s, 3H), 2.13 (dp, *J* = 13.7, 6.9 Hz, 1H), 0.84 (s, 3H), 0.82 (s, 3H); ^{13}C NMR (126 MHz, DMSO) δ 163.84, 136.99, 135.75, 135.02, 130.36, 128.41, 127.79,

127.77, 126.36, 123.88, 120.27, 110.85, 104.51, 64.45, 53.16, 28.71, 21.19, 19.62. LC-MS (*m*/*z*): positive mode 322.10 $[M + H]^{1+}$; purity by HPLC UV (254 nm)-ESI-MS: 99.6%.

Synthesis of the carboxylic acid key-intermediates (2b−13b)

General procedure B

In a 25 mL hydrogenation flask, 1.0 equiv. of benzyl ester (**2a−13a**) was dissolved in 10 mL of MeOH and stirred, before the addition of Pd/C (0.1 equiv.) under argon atmosphere. 35 psi of H_2 was applied and the reaction mixture was stirred at 25 °C for 2 hours. TLC-control indicated the deprotection of the benzyl alcohol. The reaction mixture was then filtered over a pad of celite washed with methanol and evaporated under reduced pressure to form the desired key-intermediate **2b−13b**:

Synthesis of 5-methyl-1-propyl-1*H*-indole-3-carboxylic acid (2b)

General procedure B, **2a** (0.26 g, 0.85 mmol) to afford **2b** as beige powder (0.18 g, 0.84 mmol, 99%), ^{1}H NMR (500 MHz, DMSO-d_6) δ 11.86 (s, 1H), 7.98 (s, 1H), 7.82 (s, 1H), 7.43 (d, *J* = 8.3 Hz, 1H), 7.04 (d, *J* = 8.2 Hz, 1H), 4.16 (t, *J* = 6.7 Hz, 2H), 2.41 (s, 3H), 1.78 (q, *J* = 7.0 Hz, 2H), 0.82 (t, *J* = 7.2 Hz, 3H); ^{13}C NMR (126 MHz, DMSO) δ 165.68, 135.09, 134.75, 129.95, 126.76, 123.59, 120.52, 110.37, 105.76, 47.48, 22.80, 21.17, 10.94. m.p. = 180 −182 °C. LC-MS (*m*/*z*): positive mode 218.10 $[M + H]^{1+}$; purity by HPLC UV (254 nm)-ESI-MS: 99.8%.

Synthesis of 1,5-dimethyl-1*H*-indole-3-carboxylic acid (3b)

General procedure B, **3a** (0.10 g, 0.38 mmol) to afford **3b** as beige powder (0.06 g, 0.33 mmol, 87%), ^{1}H NMR (500 MHz, DMSO-d_6) δ 7.95 (s, 1H), 7.82 (s, 1H), 7.38 (d, *J* = 8.3 Hz, 1H), 7.06 (d, *J* = 8.2 Hz, 1H), 3.81 (s, 3H), 2.41 (s, 3H); ^{13}C NMR (126 MHz, DMSO) δ 165.68, 135.86, 135.44, 129.96, 126.67, 123.58, 120.42, 110.17, 105.83, 32.91, 21.19. m.p. = 233 −235 °C. LC-MS (*m*/*z*): positive mode 190.10 $[M + H]^{1+}$; purity by HPLC UV (254 nm)-ESI-MS: 98.9%.

Synthesis of 1-(2-methoxyethyl)-5-methyl-1*H*-indole-3-carboxylic acid (4b)

General procedure B, **4a** (0.23 g, 0.71 mmol) to afford **4b** as beige powder (0.17 g, 0.71 mmol, 100%), ^{1}H NMR (500 MHz, DMSO-d_6) δ 7.94 (s, 1H), 7.82 (s, 1H), 7.45 (d, *J* = 8.4 Hz, 1H), 7.04 (d, *J* = 8.5 Hz, 1H), 4.36 (t, *J* = 4.9 Hz, 2H), 3.66 (t, *J* = 4.9 Hz, 2H), 3.21 (s, 3H), 2.41 (s, 3H); ^{13}C NMR (126 MHz, DMSO) δ 165.66, 135.48, 134.88, 129.97, 126.67, 123.58, 120.44, 110.45, 106.00, 70.49, 58.03, 45.73, 32.91, 21.16. LC-MS (*m*/*z*): positive mode 234.00 $[M + H]^{1+}$; purity by HPLC UV (254 nm)-ESI-MS: 78.5%.

Synthesis of 1-(cyclobutylmethyl)-5-methyl-1*H*-indole-3-carboxylic acid (5b)

General procedure B, **5a** (0.28 g, 0.84 mmol) to afford **5b** as oily brown substance (0.20 g, 0.83 mmol, 99%), ^{1}H NMR (500 MHz, DMSO-d_6) δ 7.96 (s, 1H), 7.81 (s, 1H), 7.44 (d, J = 8.3 Hz, 1H), 7.04 (d, J = 8.3 Hz, 1H), 4.21 (d, J = 7.3 Hz, 2H), 2.78 (hept, J = 7.0 Hz, 1H), 2.40 (s, 3H), 1.99 – 1.88 (m, 2H), 1.88 – 1.80 (m, 2H), 1.80 – 1.70 (m, 2H); ^{13}C NMR (126 MHz, DMSO) δ 165.69, 134.91, 134.88, 129.91, 126.67, 123.56, 120.46, 110.40, 105.90, 50.69, 35.07, 25.29, 21.16, 17.59. LC-MS (*m*/*z*): positive mode 244.00 $[M + H]^{1+}$; purity by HPLC UV (254 nm)-ESI-MS: 91.8%.

Synthesis of 1-(2-fluoroethyl)-5-methyl-1*H*-indole-3-carboxylic acid (6b)

General procedure B, **6a** (0.26 g, 0.84 mmol) to afford **6b** as oily brown substance (0.18 g, 0.83 mmol, 99%), ^{1}H NMR (500 MHz,) δ 11.95 (s, 1H), 8.00 (s, 1H), 7.84 (s, 1H), 7.47 (d, J = 8.3 Hz, 1H), 7.07 (d, J = 8.3 Hz, 1H), 4.88 – 4.66 (m, 2H), 4.63 – 4.45 (m, 2H), 2.42 (s, 3H); ^{13}C NMR (126 MHz,) δ 165.77, 135.50, 135.11, 130.35, 126.88, 123.94, 120.66, 110.64, 106.68, 83.27, 81.93, 46.63, 46.47, 21.33. LC-MS (*m*/*z*): positive mode 222.10 $[M + H]^{1+}$; purity by HPLC UV (254 nm)-ESI-MS: 99.2%.

Synthesis of 1-isopropyl-5-methyl-1*H*-indole-3-carboxylic acid (7b)

General procedure B, **7a** (0.28 g, 0.92 mmol) to afford **7b** as oily brown substance (0.17 g, 0.78 mmol, 85%), ^{1}H NMR (500 MHz, DMSO-d_6) δ 11.88 (s, 1H), 8.05 (s, 1H), 7.83 (s, 1H), 7.48 (d, J = 8.4 Hz, 1H), 7.05 (dd, J = 8.4, 1.4 Hz, 1H), 4.76 (hept, J = 6.7 Hz, 1H), 2.41 (s, 3H), 1.48 (d, J = 6.7 Hz, 6H); ^{13}C NMR (126 MHz, DMSO) δ 165.60, 134.26, 131.31, 130.04, 126.75, 123.56, 120.51, 110.40, 106.11, 47.29, 22.15, 21.15. LC-MS (*m*/*z*): positive mode 218.10 $[M + H]^{1+}$; purity by HPLC UV (254 nm)-ESI-MS: 94.7%.

Synthesis of 1-(2-chloroethyl)-5-methyl-1*H*-indole-3-carboxylic acid (8b)

General procedure B, **8a** (0.16 g, 0.50 mmol) to afford **8b** as oily brown substance (0.12 g, 0.49 mmol, 99%), ^{1}H NMR (500 MHz, DMSO-d_6) δ 8.04 (s, 1H), 7.83 (s, 1H), 7.50 (d, J = 8.4 Hz, 1H), 7.06 (d, J = 8.3 Hz, 1H), 4.57 (t, J = 5.7 Hz, 3H), 4.01 (t, J = 5.7 Hz, 2H), 2.41 (s, 3H); ^{13}C NMR (126 MHz, DMSO) δ 165.60, 135.52, 134.73, 130.22, 126.71, 123.77, 120.52, 110.40, 106.39, 47.44, 43.54, 21.15. LC-MS (*m*/*z*): positive mode 238.00 $[M + H]^{1+}$; purity by HPLC UV (254 nm)-ESI-MS: 96.0%.

Synthesis of 1-butyl-5-methyl-1*H*-indole-3-carboxylic acid (9b)

General procedure B, **9a** (0.29 g, 0.90 mmol) to afford **9b** as beige powder (0.20 g, 0.87 mmol, 97%), ^{1}H NMR (600 MHz, DMSO-d_6) δ 11.86 (s, 1H), 7.98 (s, 1H), 7.81 (s, 1H), 7.44 (d, J = 8.4

Hz, 1H), 7.05 (dd, *J* = 8.4, 1.3 Hz, 1H), 4.20 (t, *J* = 7.0 Hz, 2H), 2.41 (s, 3H), 1.74 (p, *J* = 7.2 Hz, 2H), 1.23 (h, *J* = 7.4 Hz, 2H), 0.87 (t, *J* = 7.4 Hz, 3H); ^{13}C NMR (151 MHz, DMSO) δ 165.67, 135.06, 134.70, 129.96, 126.75, 123.61, 120.51, 110.38, 105.73, 45.68, 31.54, 21.18, 19.32, 13.44. LC-MS (*m*/*z*): positive mode 232.10 $[M + H]^{1+}$; purity by HPLC UV (254 nm)-ESI-MS: 92.2%.

Synthesis of 1-(difluoromethyl)-5-methyl-1*H*-indole-3-carboxylic acid (10b)

General procedure B, **10a** (0.15 g, 0.48 mmol) to afford **10b** as oily brown substance (0.08 g, 0.36 mmol, 75%), ^{1}H NMR (600 MHz, DMSO-d_6) δ 8.22 (s, 1H), 8.08 – 7.85 (m, 2H), 7.60 (d, *J* = 8.4 Hz, 1H), 7.19 (d, *J* = 8.4 Hz, 1H), 2.43 (s, 3H); ^{13}C NMR (151 MHz, DMSO) δ 164.98, 132.34, 131.75, 131.22, 127.20, 125.50, 121.19, 112.44, 111.62, 110.81, 110.77, 109.19, 21.09. LC-MS (*m*/*z*): positive mode 226.00 $[M + H]^{1+}$; purity by HPLC UV (254 nm)-ESI-MS: 97.9%.

Synthesis of (*R*,*S*)-1-(*sec*-butyl)-5-methyl-1*H*-indole-3-carboxylic acid (11b)

General procedure B, **11a** (0.14 g, 0.45 mmol) to afford **11b** as oily brown substance (0.10 g, 0.43 mmol, 96%), ^{1}H NMR (600 MHz,) δ 8.02 (s, 1H), 7.83 (s, 1H), 7.48 (d, *J* = 8.4 Hz, 1H), 7.03 (d, *J* = 9.6 Hz, 1H), 4.53 (h, *J* = 6.7 Hz, 1H), 2.40 (s, 3H), 1.95 – 1.74 (m, 2H), 1.47 (d, *J* = 6.7 Hz, 3H), 0.71 (t, *J* = 7.4 Hz, 3H); ^{13}C NMR (151 MHz,) δ 165.95, 135.01, 131.88, 130.07, 126.83, 123.67, 120.73, 110.62, 106.77, 53.23, 29.25, 21.34, 20.55, 10.63. LC-MS (*m*/*z*): positive mode 232.10 $[M + H]^{1+}$; purity by HPLC UV (254 nm)-ESI-MS: 99.6%.

Synthesis of (*R*,*S*)-5-methyl-1-((tetrahydrofuran-2-yl)methyl)-1*H*-indole-3-carboxylic acid (12b)

General procedure B, **12a** (0.10 g, 0.29 mmol) to afford **12b** as oily brown substance (0.07 g, 0.27 mmol, 93%), ^{1}H NMR (600 MHz, DMSO-d_6) δ 7.94 (s, 1H), 7.81 (s, 1H), 7.47 (d, *J* = 8.4 Hz, 1H), 7.04 (dd, *J* = 8.4, 1.2 Hz, 1H), 4.31 (dd, *J* = 13.9, 3.2 Hz, 1H), 4.21 – 4.12 (m, 2H), 3.73 (q, *J* = 6.9 Hz, 1H), 3.61 (q, *J* = 7.4 Hz, 1H), 2.40 (s, 3H), 1.94 (dq, *J* = 12.5, 6.5 Hz, 1H), 1.76 (th, *J* = 12.2, 6.6, 5.9 Hz, 2H), 1.53 (dq, *J* = 14.5, 7.7 Hz, 1H); ^{13}C NMR (151 MHz, DMSO) δ 165.70, 135.68, 135.19, 129.91, 126.54, 123.56, 120.37, 110.65, 77.13, 67.26, 49.69, 28.34, 25.00, 21.17. LC-MS (*m*/*z*): positive mode 260.10 $[M + H]^{1+}$; purity by HPLC UV (254 nm)-ESI-MS: 88.5%.

Synthesis of 1-isobutyl-5-methyl-1*H*-indole-3-carboxylic acid (13b)

General procedure B, **13a** (0.17 g, 0.53 mmol) to afford **13b** as oily brown substance (0.12 g, 0.50 mmol, 94%), LC-MS (*m*/*z*): positive mode 232.00 $[M + H]^{1+}$; purity by HPLC UV (254 nm)-ESI-MS: 99.5%.

Synthesis of ethyl 2-methyl-1-(4-nitrophenyl)-1*H*-pyrrole-3-carboxylate (37)

In a flame-dried 100 mL Schlenk flask, 1-bromo-4-nitrobenzene (**III**) (3.0 g, 14.85 mmol), ethyl 2-methyl-1*H*-pyrrole-3-carboxylate (**IV**) (4.55 g, 29.7 mmol), CuI (0.17 g, 0.89 mmol) and K_2CO_3 (4.37 g, 31.19 mmol) were added sequentially under argon atmosphere, followed by the addition of anhydrous 1,4-dioxane (40 mL) and dimethylethylenediamine (0.50 mL, 4.46 mmol). The mixture was heated-up under stirring at 110 °C for overnight. The mixture was cooled down to the room temperature and filtered through a pad of Celite using ethyl acetate. The solvent was removed under reduced pressure and the crude compound was submitted to a column chromatography (silica gel chromatography, eluent: DCM:ethyl acetate; 9:1) to afford **37** as bright brown powder (3.8 g, 13.87 mmol, 93%), ^{1}H NMR (500 MHz, DMSO-d_6) δ 8.37 (d, *J* = 9.0 Hz, 2H), 7.74 (d, *J* = 9.0 Hz, 2H), 7.04 (d, *J* = 3.2 Hz, 1H), 6.60 (d, *J* = 3.2 Hz, 1H), 4.22 (q, *J* = 7.1 Hz, 2H), 2.46 (s, 3H), 1.28 (t, *J* = 7.1 Hz, 3H); ^{13}C NMR (126 MHz, DMSO) δ 164.24, 146.31, 143.72, 135.14, 126.80, 124.79, 121.77, 113.81, 110.61, 59.07, 14.35, 12.00. LC-MS (*m*/*z*): positive mode 275.10 $[M + H]^{1+}$; purity by HPLC UV (254 nm)-ESI-MS: 93.8%.

Synthesis of 2-methyl-1-(4-nitrophenyl)-1*H*-pyrrole-3-carboxylic acid (38)

A solution of **37** (3.8 g, 13.87 mmol) in a mixture of solvents 100 mL (THF/EtOH; 1:1) was treated in a 250 mL round-bottom flask with a solution of KOH (3.9 g, 69.35 mmol) in water (50 mL). The mixture was refluxed for 2h. Then, the organic solvents were removed under reduced pressure and the resulting aqueous phase was neutralized by slow addition of 6 N HCl. The precipitate formed was filtered, washed with water and dried under ultra-high vacuum to afford **38** as brown powder (2.8 g, 11.41 mmol, 82%), that has been used for next step without further purification. ^{1}H NMR (500 MHz, DMSO-d_6) δ 11.97 (s, 1H), 8.36 (d, *J* = 9.0 Hz, 2H), 7.73 (d, *J* = 9.0 Hz, 2H), 7.01 (d, *J* = 3.1 Hz, 1H), 6.57 (d, *J* = 3.1 Hz, 1H), 2.46 (s, 3H); ^{13}C NMR (126 MHz, DMSO) δ 165.88, 146.21, 143.89, 134.90, 126.71, 124.78, 121.45, 114.60, 111.09, 11.98. LC-MS (*m*/*z*): positive mode 247.30 $[M + H]^{1+}$; purity by HPLC UV (254 nm)-ESI-MS: 82.8%.

Synthesis of ethyl 3-(2-methyl-1-(4-nitrophenyl)-1*H*-pyrrol-3-yl)-3-oxopropanoate (39)

In a 250 mL round-bottom flask, **38** (2.8 g, 11.41 mmol) was dissolved in THF (150 mL) and treated with 1,1'-carbonyldiimidazole (2.8 g, 17.12 mmol). The mixture was stirred at room temperature for 16 hours, followed by the addition of anhydrous $MgCl_2$ (4.35 g, 45.64 mmol) and potassium malonate (7.77 g, 45.64 mmol). The mixture was stirred at 55 °C for 6 hours. After concentration under reduced pressure, the residue was extracted with EtOAc (100 mL), washed

with aqueous 1 N NaOH and brine, dried over $MgSO_4$, evaporated to dryness, and submitted to a column chromatography (silica gel chromatography, eluent: DCM:ethyl acetate; 9:1) to yield **39** as brown powder (2.6 g, 8.22 mmol, 72%). ^{1}H NMR (500 MHz, DMSO-d_6) δ 8.38 (d, J = 9.0 Hz, 2H), 7.75 (d, J = 9.0 Hz, 2H), 7.07 (d, J = 3.3 Hz, 1H), 6.79 (d, J = 3.3 Hz, 1H), 4.12 (q, J = 7.1 Hz, 2H), 3.90 (s, 2H), 2.45 (s, 3H), 1.20 (t, J = 7.1 Hz, 3H); ^{13}C NMR (126 MHz, DMSO) δ 188.98, 167.85, 146.50, 143.31, 135.31, 126.91, 124.81, 121.95, 121.55, 111.29, 60.34, 47.41, 14.03, 12.44. LC-MS (*m*/*z*): positive mode 317.1 $[M + H]^{1+}$; purity by HPLC UV (254 nm)-ESI-MS: 93.6%.

Synthesis of (*R*,*S*)-ethyl 2-(2-methyl-1-(4-nitrophenyl)-1*H*-pyrrole-3-carbonyl)butanoate (40)

In a 250 mL round-bottom flask, a solution of **39** (1.7 g, 5.37 mmol) in THF was cooled down to 0 °C and treated in portions with NaH (0.15 g, 6.45 mmol). The mixture was stirred for 30 minutes before the dropwise addition of iodoethane (1.3 g, 8.06 mmol, 0.65 mL). Then it was stirred at room temperature for overnight. Water was slowly added to the mixture and the organic solvent was removed under reduced pressure. The residue was then extracted using dichloromethane (3x), washed with water, dried over $MgSO_4$, and evaporated to dryness. The residue was purified via column chromatography (silica gel chromatography, eluent DCM, then DCM/MeOH mixture (95/5; v/v)) to afford **40** as bright brown crystals (1.1 g, 3.19 mmol, 59%). ^{1}H NMR (500 MHz, DMSO-d_6) δ 8.37 (d, J = 9.0 Hz, 2H), 7.76 (d, J = 9.0 Hz, 2H), 7.08 (d, J = 3.3 Hz, 1H), 6.85 (d, J = 3.3 Hz, 1H), 4.14 (t, J = 7.1 Hz, 1H), 4.12 – 4.06 (m, 2H), 2.46 (s, 3H), 1.83 (p, J = 7.3, 6.8 Hz, 2H), 1.15 (t, J = 7.1 Hz, 3H), 0.91 (t, J = 7.4 Hz, 3H); ^{13}C NMR (126 MHz, DMSO) δ 191.47, 169.99, 146.48, 143.32, 135.71, 126.90, 124.78, 121.93, 121.52, 111.03, 60.33, 56.56, 22.10, 13.99, 12.55, 11.77. LC-MS (*m*/*z*): positive mode 345.5 $[M + H]^{1+}$; purity by HPLC UV (254 nm)-ESI-MS: 98.7%.

Synthesis of 1-(2-methyl-1-(4-nitrophenyl)-1*H*-pyrrol-3-yl)butan-1-one (41)

In a 250 mL round-bottom flask, a vigorously stirred solution of **40** (1.0 g, 2.90 mmol) in aqueous 37% HCl was heated up to 105 °C for 2 hours. The mixture was then cooled down to 0 °C and neutralized using aqueous 2N NaOH. EtOAc was added to the neutralized mixture for extraction (3x). The organic phase was washed with water, dried over $MgSO_4$, and evaporated to dryness. The residue was further dried under ultra-high vacuum and submitted to a column chromatography (silica gel chromatography, eluent: DCM:ethyl acetate; 9:1) to afford **41** as bright brown crystals

(0.78 g, 2.86 mmol, 99%). ^{1}H NMR (500 MHz, DMSO-d_6) δ 8.36 (d, J = 9.0 Hz, 2H), 7.73 (d, J = 9.0 Hz, 2H), 7.04 (d, J = 3.2 Hz, 1H), 6.78 (d, J = 3.2 Hz, 1H), 2.75 (t, J = 7.2 Hz, 2H), 2.46 (s, 3H), 1.61 (h, J = 7.3 Hz, 2H), 0.92 (t, J = 7.4 Hz, 3H); ^{13}C NMR (126 MHz, DMSO) δ 196.53, 146.32, 143.58, 134.01, 126.80, 124.77, 122.28, 121.52, 110.91, 41.89, 17.51, 13.74, 12.45. m.p. = 138 −140 °C. LC-MS (*m*/*z*): positive mode 273.2 $[M + H]^{1+}$; purity by HPLC UV (254 nm)-ESI-MS: 97.9%.

Synthesis of 1-(1-(4-aminophenyl)-2-methyl-1*H*-pyrrol-3-yl)butan-1-one (42)

In a 250 mL round-bottom flask, compound **41** (0.45 g, 1.65 mmol) was dissolved in methanol (35 mL) and stirred, before the addition of Pd/C (10%) (0.08 g) under argon atmosphere. The mixture was then thrice evacuated and flushed with H_2-gas (hydrogen-filled balloon) at 25 °C for 4 hours. After TLC-analysis, the reaction mixture was filtered over celite, washed with methanol, and evaporated under reduced pressure to form the desired key-intermediate **42** as pale brown powder (0.41 g, 1.65 mmol, 100%). LC-MS (*m*/*z*): positive mode 243.4 $[M + H]^{1+}$; purity by HPLC UV (254 nm)-ESI-MS: 92.3%.

Biology

Cell culture.

The recombinant Chinese hamster ovary (CHO) cell line expressing the human $P2Y_{12}$ receptor (CHO-h$P2Y_{12}$R), incorporating a β-galactosidase fragment and β-arrestin with the complementary fragment for β-arrestin recruitment assays (PathHunter®, DiscoverX), was generated as previously described.[105] CHO-h$P2Y_{12}$R cells were maintained at 37 °C in a humidified atmosphere with 5% CO_2 in Ham's F-12 Nutrient Mix medium (F12; #11765054, Thermo Fisher Scientific, MA, USA) supplemented with 10% fetal bovine serum (FBS; #P30-1502, PAN Biotech, Germany), penicillin (100 U/mL) and streptomycin (100 µg/mL) (#P06-07100, PAN Biotech, Germany), 300 µg/mL hygromycin (#P06-08020, PAN Biotech, Germany), and 800 µg/mL G418 (#P06-07100, PAN Biotech, Germany). Upon reaching 80–90% confluency, the culture medium was removed, and the cell monolayer was rinsed with phosphate-buffered saline (PBS; 137 mM NaCl, 2.7 mM KCl, 4.3 mM Na_2HPO_4, 1.47 mM KH_2PO_4). Cells were then detached using trypsin–ethylenediaminetetraacetic acid (EDTA) solution (0.05%/0.6 mM) and subcultured at a 1:10 ratio into new flasks. Mycoplasma contamination was routinely monitored via polymerase chain reaction (PCR) analysis.

Membrane preparations of recombinant CHO cells

When CHO-β-arrestin-hP2Y$_{12}$R cells reached approximately 90% confluency, the contents of one 175 cm^2 flask were seeded into twenty sterile 150 mm culture dishes and incubated at 37 °C in a humidified atmosphere with 5% CO_2 for four days. Upon reaching ~90% confluency again, the culture medium was removed, each dish was rinsed with 5 mL phosphate-buffered saline (PBS), and the plates were frozen at -20 °C. Frozen cells were harvested by scraping with 1 mL ice-cold buffer (25 mM Tris-HCl, 1 mM EDTA, 0.32 M sucrose, pH 7.4) using a rubber cell scraper; this step was repeated to ensure complete recovery. The contents from all dishes were combined in a beaker and homogenized twice for 30 s each at speed level 4 using an UltraTurrax® (IKA Labortechnik, Staufen, Germany). The homogenate was centrifuged at 1,000 g for 10 min at 4 °C to remove nuclei, large organelles, and debris. The resulting pellet (P1) was discarded, and the supernatant (S1) was centrifuged at 48,000 *g* for 1 h at 4 °C. The supernatant (S2) was discarded, and the resulting pellet (P2) was resuspended in 25 mL washing buffer (50 mM Tris-HCl, pH 7.4) and centrifuged again at 48,000 *g* for 30 min at 4 °C. Following two additional washing steps, the final pellet was resuspended in 0.1 mL buffer (50 mM Tris-HCl, pH 7.4) per dish. Crude membrane preparations were aliquoted and stored at -80 °C until use. All procedures were performed rapidly at 4 °C to minimize receptor internalization.

Determination of protein concentration

Protein concentrations were determined using the Lowry method.[126] A 2% (w/v) $NaHCO_3$ solution in NaOH was prepared and mixed at a 50:1 ratio with an aqueous solution containing 0.5% (w/v) $CuSO_4$ and 1% (w/v) sodium tartrate. One milliliter of this reagent mixture was added to 200 µL of the sample (diluted 1:20 in 50 mM Tris-HCl buffer, pH 7.4). After incubation for 20 min at room temperature, 100 µL of Folin phenol reagent (18 mL Folin reagent diluted in 90 mL distilled water) was added, and the solution was vortexed thoroughly. Following a further 30 min incubation at room temperature, absorbance was measured at 750 nm and 500 nm using a DU® 530 spectrophotometer (Beckman-Coulter, Krefeld, Germany). Calibration was performed with bovine serum albumin (BSA) as the standard, using a concentration range of 0.1–0.5 mg/mL.

Radioligand competition binding assays

Binding experiments were performed in 50 mM Tris-HCl buffer (pH 7.4) in a final assay volume of 500 µL.[86] Each assay contained 5 µL of test compound (serially diluted to the desired

concentrations), 100 µL of [^{3}H]PSB-22219 in buffer (final concentration 2 nM), and 100 µL of CHO-human $P2Y_{12}R$ membrane preparation (5 µg protein). Nonspecific binding was determined in the presence of 1 µM PSB-0739. Reactions were initiated by adding the membrane preparation and incubated for 1 h at 18 °C in polypropylene test tubes (Cat. No. 55.535, SARSTEDT, Nümbrecht, Germany). Bound and free radioligand were separated by rapid filtration through GF/B glass fiber filters using a Brandel M-48 cell harvester (Brandel, MD, USA). Filters were washed three times with 3 mL of ice-cold 50 mM Tris-HCl containing 0.1% Tween 20 (pH 7.4), then transferred to scintillation vials. Each vial received 2.5 mL scintillation cocktail (ProSafe FC+, Triskem) and was incubated for 9 h before radioactivity measurement using a Hidex 600 SL Automatic TDCR Liquid Scintillation Counter (counting efficiency: 53–55%). All experiments were performed independently three times, each in duplicate. Affinity values were determined using one-site homologous or one-site-fit K_i models in GraphPad Prism (version 8.4.2; GraphPad Software Inc., San Diego, CA, USA).

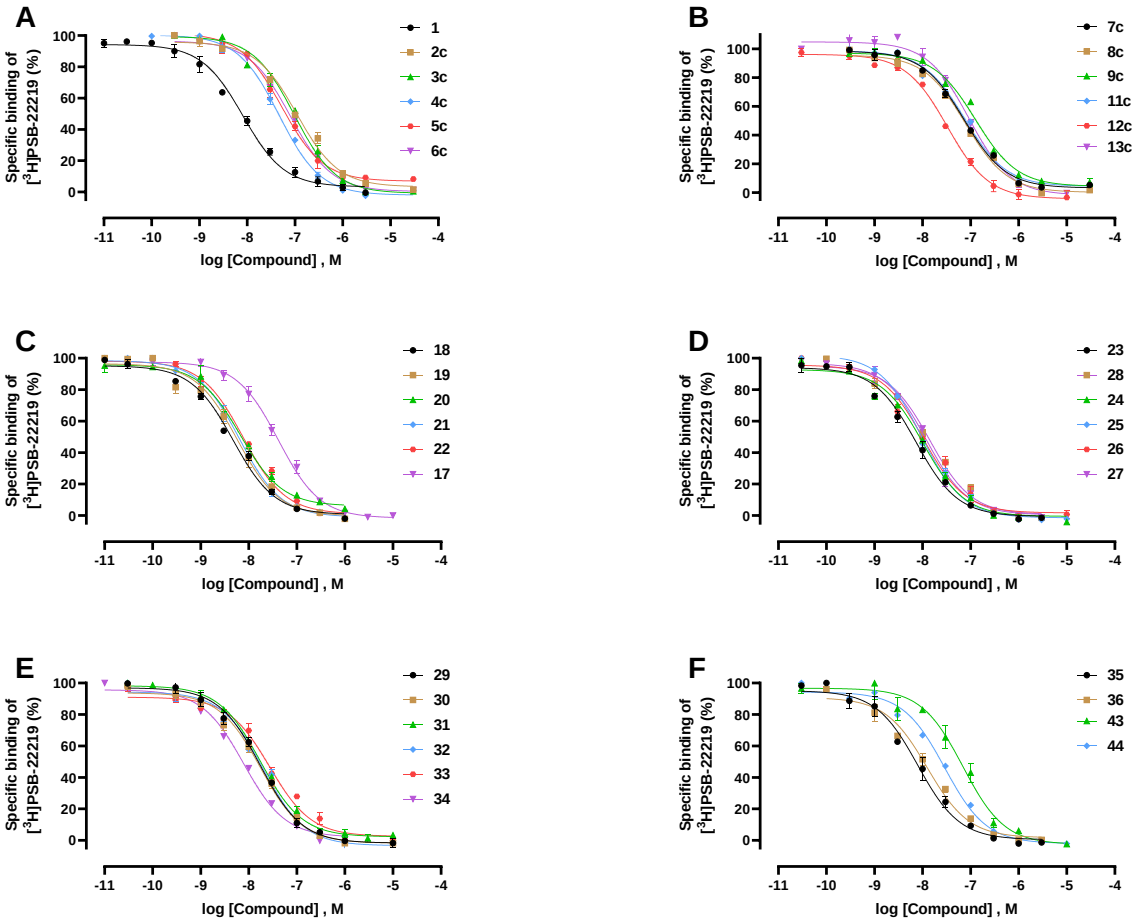


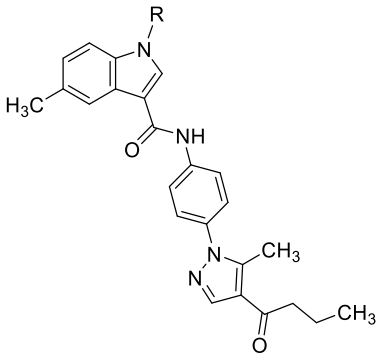
Figure S2. Concentration-response curves were carried out with serial dilutions of each competitor that were incubated with 2 nM [^{3}H]PSB-22219 and membrane preparations of CHO-hP2Y$_{12}$ (5 µg of protein) for 60 min at 18 °C. Nonspecific binding was assessed in the presence of 1 µM PSB-0739. 10c curve was not shown (maximum inhibition % is 73%). Data are presented as means ± SEM from at least three independent experiments, each conducted in duplicate.

Metabolic stability in human liver microsomes

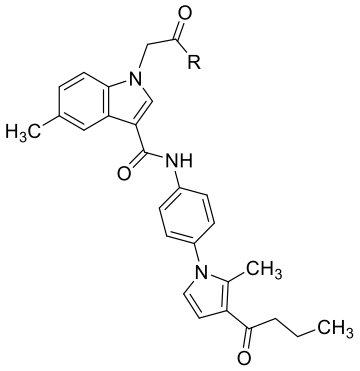
Pooled human liver microsomes were obtained from Sigma-Aldrich. Metabolic stability assays were conducted in the presence of an NADPH-regenerating system comprising 5 mM glucose-6-phosphate, 5 U/mL glucose-6-phosphate dehydrogenase, and 1 mM $NADP^+$. Liver microsomes (20 mg/mL), the NADPH-regenerating system, and 0.1 M phosphate buffer (pH 7.4) were preincubated at 37 °C and 450 rpm for 5 min. Reactions were initiated by adding preheated test compound (1 mM stock solution) to achieve a final concentration of 5 µM. At predetermined time points (0, 15, 30, 45, and 60 min), reactions were quenched with acetonitrile, vortexed for 30 s, and centrifuged at 15,000 × *g* for 15 min at 4 °C. Supernatants were directly subjected to LC-MS

analysis. All assays were performed in at least duplicate. Controls included a negative control (without liver microsomes) and a positive control with verapamil. The organic solvent content during incubation did not exceed 0.5%. Chromatographic separation and detection were performed using an Infinity Lab LC-MSD system (Agilent) equipped with an ESI source and coupled to a 1260 Infinity II HPLC (Agilent). An EC50/2 Nucleodur C18 Gravity column (3 µm; Macherey-Nagel) was maintained at 40 °C. The HPLC mobile phase consisted of 90% water with 2 mM ammonium acetate and 10% acetonitrile at the start. A linear gradient to 100% acetonitrile was applied over 7.5 min, followed by a 4 min wash at 100% acetonitrile. The injection volume was 4 µL with a flow rate of 0.5 mL/min. Table S18 summarizes all results, including the $T_{1/2}$ and Cl_{int}.

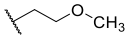
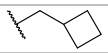
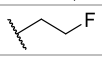
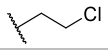
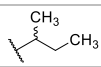
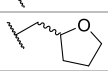
Table S18. Microsomal stability results (human).

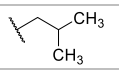
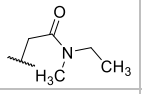
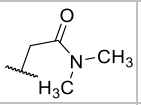
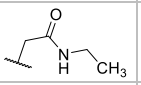
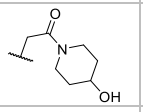
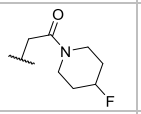
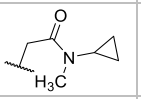
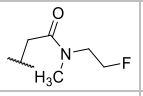
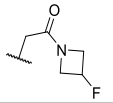
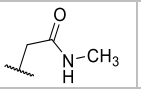
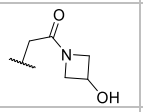
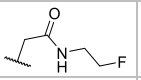


1 to 34



43 and 44

Microsomal stability results (human)						
Compound	**R**	***K*i (affinity, nM)**	**MW (g/mol)**	**Parent compound[b]**	**$T_{1/2}$ (min)**	**Cl_{int} (µl/min/mg protein)**
1		**5.20** ± 0.5	458.5	78%	163	8.5
3c		**68.5** ± 9.0	414.5	19%	25	54.4
4c		**32.2** ± 3.2	458.6	0%	9	162.3
5c		**37.7** ± 4.9	468.6	24%	27	51.1
6c		**58.3** ± 0.6	446.5	33%	35	39.3
7c		**51.5** ± 2.4	442.6	15%	22	62.7
8c		**60.1** ± 2.3	463.0	35%	43	32.1
10c		**44.9** ± 5.4	450.5	30%	34	41.0
11c		**52.8** ± 3.6	456.6	23%	26	53.2
12c		**22.5** ± 1.5	484.6	0%	–	–

13c		**77.3**[c]	456.6	1%	8	141.5
17		**28.5** ± 4.3	456.6	8%	18	76.8
18		**3.20** ± 0.3	499.6	11%	19	73.5
19		**4.90** ± 0.5	485.6	46%	46.5	29.7
20		**5.10** ± 0.4	485.6	70%	114	12.1
21		**5.30** ± 0.7	541.7	42%	48	29.1
22		**5.40** ± 0.1	543.6	38%	40	34.3
23		**5.60** ± 0.5	511.6	0%	–	–
26		**7.20** ± 0.3	517.6	12%	18	75.4
30		**12.0** ± 2.1	515.6	36%	40	35.4
31		**12.4** ± 0.4	471.6	7%	30	46.3
32		**13.6** ± 0.8	513.6	50%	60	23.0
34		**5.30** ± 0.4	503.6	18%	25	55.7
43		**64.6** ± 26.9	471.6	0%	–	–
44	OH	**24.1**[c]	457.5	65%	107	13.0

[a]**MW**: molecular weight, [b]% of remaining compound after 60 min incubation, [c]the experiment was performed once (n = 1).

Metabolic stability in rat liver microsomes

In vitro metabolism of P2Y$_{12}$ receptor antagonist

Rat liver microsomes (RLM), fully characterized for their protein content, P450s concentration, and catalytic activities, were obtained from Corning (France) and stored at -80 °C prior to use. Stock solutions (10 mM) of the P2Y$_{12}$R antagonists were prepared in DMSO. The incubation mixtures containing 1 mg of microsomal proteins (RLM), an NADPH-generating system (10 mM

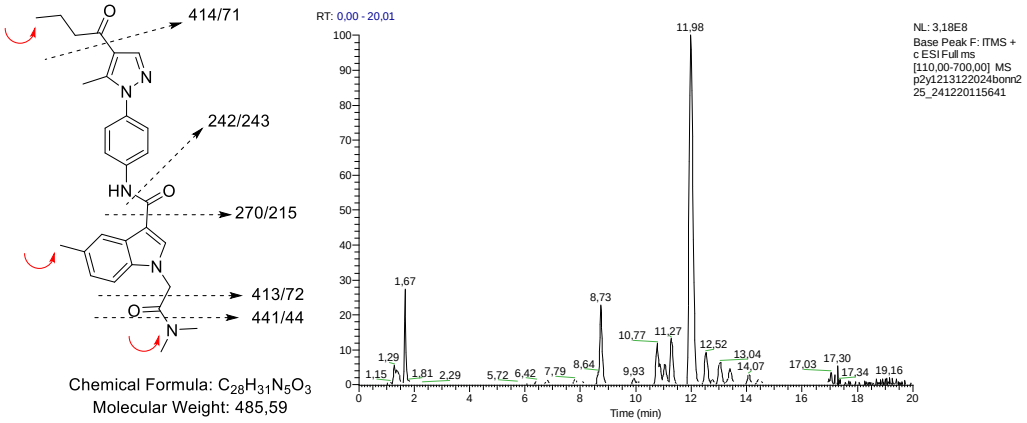
glucose-6-phosphate, 1.3 mM $NADP^+$, 2 IU/assay of glucose-6-phosphate dehydrogenase), the $P2Y_{12}R$ antagonist at a final concentration of 100 µM, and 0.1 M aqueous potassium phosphate buffer, pH 7.4 in a final volume of 1 mL, were pre-incubated for 2 min at 37 °C. The reaction was started by the addition of the NADPH-generating system (200 µL) and conducted in a water bath at 37 °C for 60 min. The reaction was stopped by the addition of an equal volume of acetonitrile (1 mL). The mixtures were centrifuged at 4 °C for 5 min at 10,000 g. The resulting supernatants were analyzed by LC/MS as described below. In control assays, the mixtures were incubated without the NADPH-generating system or without microsomes to confirm the stability of the ligand under the experimental conditions. The percentage of each metabolite was determined as a percentage of the total peak area (UV detection).

Identification of metabolites by LC-MS

The main metabolites of the $P2Y_{12}$ ligands generated in rat liver microsomes were identified by LC-MS and MS2 analyses. All incubation mixtures containing liver microsomes were deproteinated with an equal volume of acetonitrile and filtered (Vecta Spin Micro, 0.2 µm, Whatman, France) prior to extract analysis by LC-MS-MS. The main oxidative metabolites generated upon P450 oxidation in microsomal incubates were characterized by LC-MS in the positive mode using an Ion Trap LTQ VelosPro ion mass spectrometer equipped with an electrospray source (Thermo Fisher Scientific, France). The Ultimate 3000 UPLC system interfaced with the LTQ consisted of LC pumps (HPG3400RS series N°8041829), PDA (DAD3000 Series N°8041519) and autosampler (WPS3000TRS Series N°8043592). Pressurized nitrogen was used as sheath gas with a flow rate of 25 units (arbitrary units for sheath gas pressure as defined by the manufacturer). The source voltage for electrospray ionization was 4 kV; source temperature was 250 °C; capillary voltage was 40 V and capillary temperature was 350 °C. The parent ligands and their metabolites were separated on a reverse phase UPLC Atlantis C18, 1.8 µm, 2.1x100 mm column (Waters, France). The mobile phase consisted of A: water containing 0.05% formic acid and B: acetonitrile containing 0.05% formic acid. A linear gradient from 20 to 100% of B in 20 minutes was applied to the column at a flow rate of 300 µL/min. The full scan MS acquisition mode was set up to detect ions in the range of *m/z* 50-600. The MS was set up in the MS-MS mode for acquiring, isolating with a mass width of 1-3 amu (Cl) and dissociating the ions *m/z* = 459 (**1**), *m/z* = 472 (**31**), *m/z* = 528 (**37**), *m/z* = 544 (**25**), *m/z* = 486 (**19**), *m/z* = 486 (**20**), *m/z* = 542 (**21**), *m/z* = 512 (**23**) and their main metabolites by Collision Induced Dissociation and in the ion trap using

helium as the collision gas with an energy of 35%. Data acquisition and processing were performed with Xcalibur™ software (version 2.2) with the assistance of Mass Frontier™ software (version 7.0) for proposed fragmentation mechanisms (Thermo Fisher Scientific, France). Total analysis is provided below:

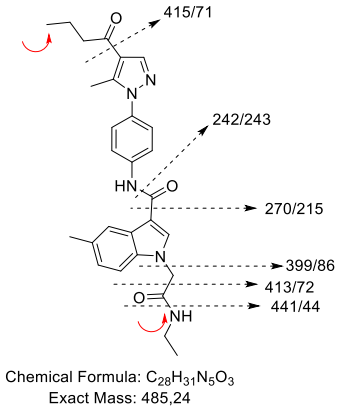
Compound **19 (**PSB-24383)**:**

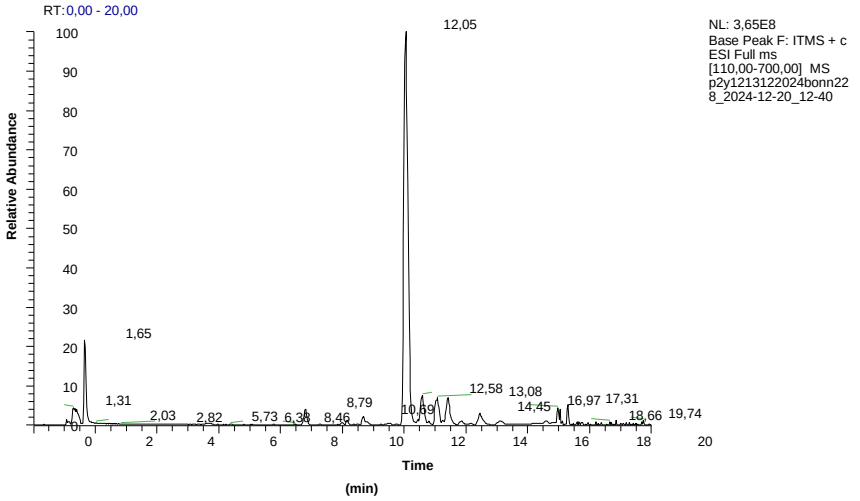


Parent 19 ***m/z* [M+H$^+$]** **Rt 11.98**	**Metabolite Mono-hydroxylation Rt 8.73**	**Metabolite Di-hydroxylation Rt 11.04**	**Metabolite *N*-demethylation Rt 11.27**
486	**502 (+16)**	**518 (+32)**	**472 (-14)**
468 (-H_2O)	**484**	**500**	**454**
442	**458**	**473**	**427**
413	**429**	**445**	**413**
416 (-butanone)	416	–	**402**
270	**286**	270	270
243	243	–	**229**
217	217	–	**203**
200	200	–	**200**
172	172	188	–
144	144	–	144

	%	Time (min)		
–	0	15	30	60
M1	0	4,31310514	5,59509704	6,9694127
M2	0	3,23990764	4,27598126	4,9754812
M3	0	0,43678753	0,40628153	0,59144929
19	100	92,0101997	89,7226402	87,4636568

Compound **20 (**PSB-24355**):**

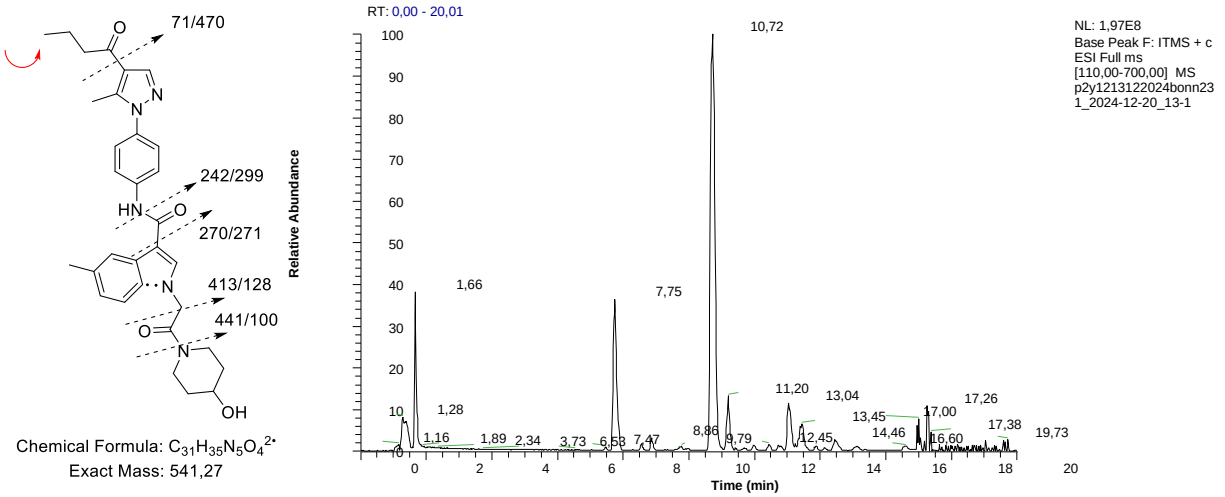




Parent 20 ***m/z* [M+H$^+$]** **Rt 12.05**	**Metabolite M1** **Hydroxylation** **Rt 8.79**	**Metabolite M2** ***N*-deethylation** **Rt 10.69**
486	**502 (+16)**	**458 (-28)**
468 (-H_2O)	**484**	**440**
441	**457**	441
413	**429**	413
416 (-butanone)	416	**388**
270	**286**	270
243	243	**215**
217	217	**189**
200	200	200
158	158	158
144	144	144

	%	Time (min)		
−	0	15	30	60
M1	0	1,23908453	1,45584992	1,56392359
M2	0	0,45382118	0,48144472	0,51772629
20	100	98,3070943	98,0627054	**97,9183501**

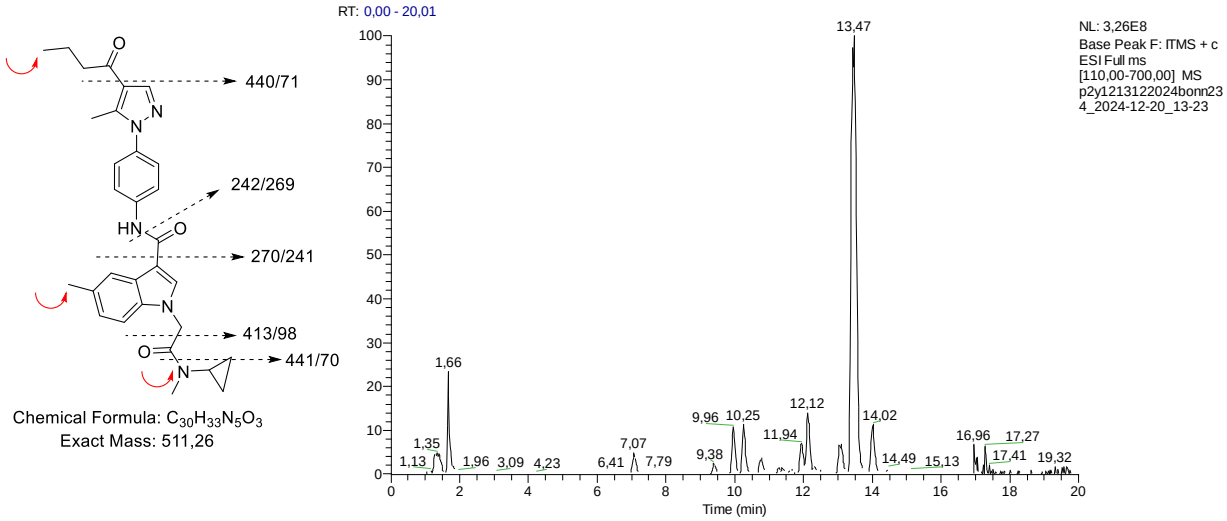
Compound **21 (**PBS-24382**):**



Parent 21 ***m/z* [M+H⁺]** **Rt 10.72**	**Metabolite M1** **Mono-hydroxylation** **Rt 7.75**
542	**558 (+16)**
524 (-H_2O)	**540**
472 (-butanone)	472
441	**457**
413	**429**
299	299
270	**286**
255	255
200	200
184	184
172	172
158	–

	%	Time (min)		
–	0	15	30	60
M1	0	8,02487207	11,4340061	16,3837814
21	100	91,9751279	88,5659939	**83,6162186**

Compound **23 (**PSB-24380**):**

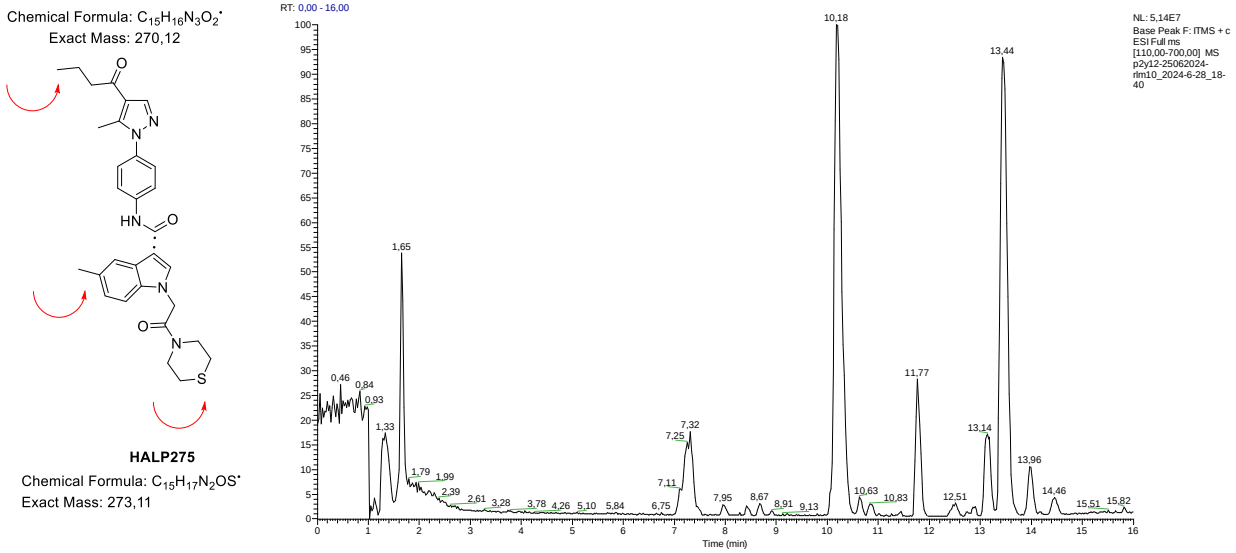


Parent 23 ***m/z* [M+H⁺]** **Rt 13.47**	**Metabolite Mono-hydroxylation Rt 10.27**	**Metabolite N-demethylation Rt 12.12**	**Metabolite N-dealkylation Rt 11.28**	**Metabolite Di-hydroxylation Rt 12.31**
512	**528 (+16)**	**498 (-14)**	**472 (-40)**	**544 (+32)**
494 (-H_2O)	**510**	**480**	**454**	**526**
468	**484**	**454**	**428**	**500**
441 (-butanone)	**441**	**427**	**402**	**473**
442	**468**	441	441	**473**
413	**429**	413	413	**445**
270	**286**	270	270	–
243	243	**229**	**203**	**258**
227	227	227	227	–
215	215	**201**	–	**226**
200	200	200	200	**216**
184	184	184	–	**200**
172	172	172	172	**188**
144	–	144	144	**160**

	%	Time (min)		
–	0	15	30	60
M1	0	1,21826147	1,77014366	2,62676492
M2	0	1,17678322	1,66046465	2,33400433
M3	0	0,40157515	0,37855487	0,41614063

M4	0	2,80212586	3,98611558	6,01382725
M5	0	0,32802897	0,34087135	0,34743387
M6	–	–	–	1,50586797
M7	–	–	–	0,41479397
23	100	94,0732253	91,8638499	**86,548564**

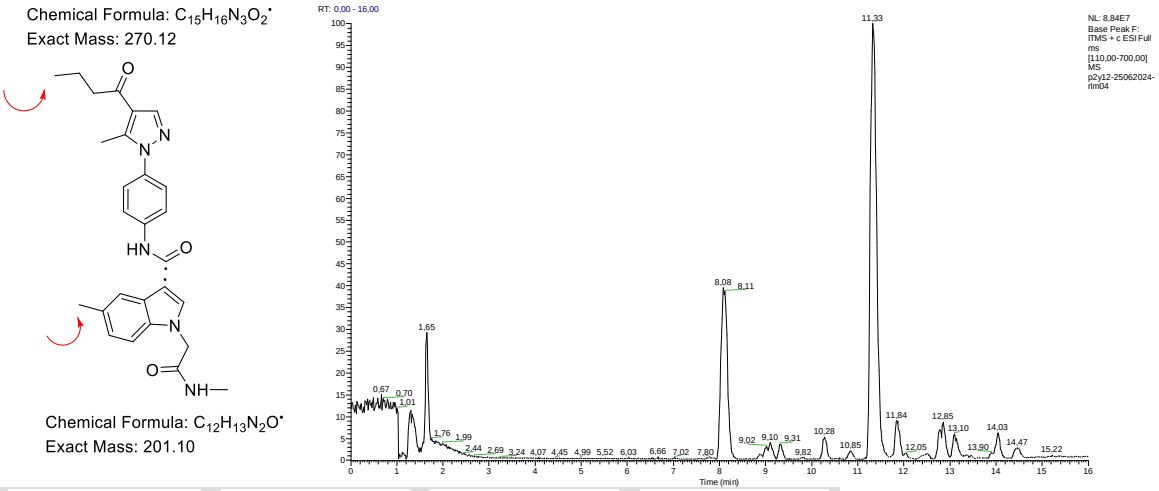
Compound **25:**



Parent 25 Rt13.44	**Metabolite Di-hydroxylation Rt7.32**	**Metabolite Mono-hydroxylation Rt10.18**	**Metabolite Di-hydroxylation Rt11.77**
544	**576 (+32)**	**560 (+16)**	**576 (+32)**
526 (-H2O)	**558**	**542**	**558**
474 (-butanone)	**490**	**490**	**506**
441	**457**	441	441 ring S
413	**429**	413	413 ring S
301	**317**	**317**	**333**
275	**291**	**291**	**307**
270	**286**	270	270
200	**216**	**216**	–
184	**198**	**200**	**200**
172	**188**	**188**	–
158	**174**	–	–

PEAK LIST			25	
Apex Rt	Start Rt	End Rt	Area	%Area
7,15	6,94	7,39	224505,946	7,34866246
10,15	9,87	10,48	1663040,81	54,4356431
11,72	11,61	11,89	105780,452	3,46246881
12,72	12,64	12,8	4767,995	0,15606885
13,4	13,29	13,58	1056963,42	**34,5971568**

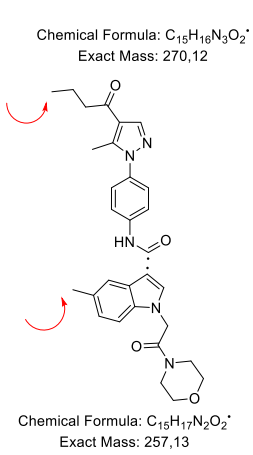
Compound **31:**

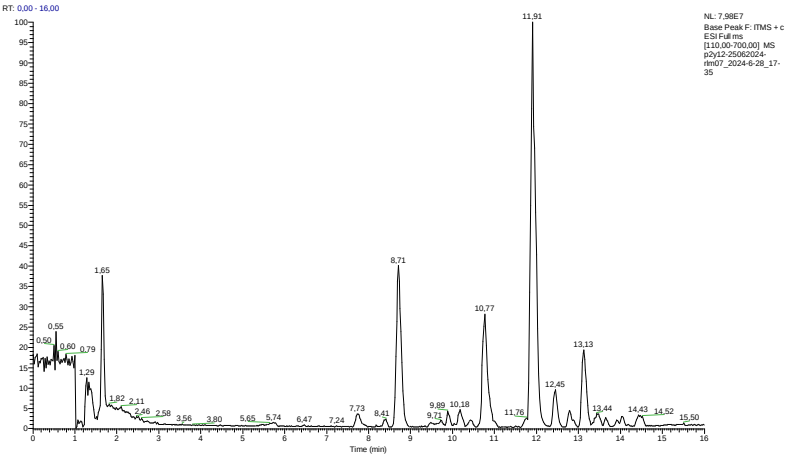


Parent 31 Rt11.33	**Metabolite Hydroxylation Rt8.08**	**Metabolite Hydroxylation Rt9.10**	**Metabolite Hydroxylation Rt10.28**
472	**488 (+16)**	**488 (+16)**	**488 (+16)**
454 (-H2O)	**470**	**470**	**470**
441	**457**	**457**	**457**
413	**429**	**429**	**429**
402 (-butanone)	402	402	**418**
270	**286**	**286**	270
244	**260**	–	–
229	**245**	229	**245**
203	203	203	**219**
200	200	200	–
172	–	–	**188**
158	158	158	–
144	144	144	**160**

PEAK LIST			31	
Apex Rt	Start Rt	End Rt	Area	%Area
8,06	7,89	8,35	708026,328	21,4916489
9,05	8,9	9,14	31157,163	0,94575411
10,23	10,15	10,33	28524,794	0,86585037
11,29	11,11	11,54	2526717,06	**76,6967467**

Compound **36:**





Parent 36 Rt11.91	**Metabolite Hydroxylation Rt8.71**	**Metabolite Hydroxylation Rt10.77**
528	**544 (+16)**	**544 (+16)**
510 (-H2O)	**526**	**526**
458 (-butanone)	458	**474**
441	**457**	**457**
413	**429**	**429**
285	285	**301**
270	**286**	270
259	259	**275**
200	200	**216**
172	172	**188**
158	–	–

PEAK LIST			36	
Apex Rt	Start Rt	End Rt	Area	%Area
8,66	8,5	8,81	502394,306	19,6726536

10,71	10,6	10,91	276387,05	10,8227076
11,86	11,72	12	1774988,55	**69,5046388**

Caco-2 Cell Culture and Permeability Assay

Caco-2 cells were cultured in 75 cm² flasks under standard conditions (37 °C, 5% CO_2, humidified atmosphere) to 80–90% confluence in accordance with ATCC and Millipore recommendations.[127] Cells were detached using trypsin/EDTA, resuspended in complete growth medium [DMEM high glucose (4,500 mg/L) supplemented with 4 mM L-glutamine, 10% heat-inactivated fetal bovine serum, 1% non-essential amino acids, and 730 nM puromycin], and seeded at a density of 5×10^5 cells per 75 cm^2 flask.[128] After 5 days, cells were harvested, adjusted to 6×10^5 cells/mL, and 400 µL of the suspension was seeded into each well of a 24-well HTS Multiwell Insert System. The feeder tray contained 25 mL of pre-warmed complete medium. Cultures were maintained for 6–10 days prior to transport experiments, with medium renewed every other day. Monolayer integrity was assessed before transport assays by measuring transepithelial electrical resistance (TEER) using a Millicell-ERS system, with values ranging between 150 and 600 $\Omega \cdot cm^2$, consistent with accepted assay standards.[129]

For permeability experiments, the insert plate was transferred to a sterile 24-well transport plate and washed with PBS. In apical-to-basolateral transport studies, 300 µL of the test compound solution (10 µM in transport buffer: 9.5 g/L Hanks' BSS, 0.35 g/L $NaHCO_3$, 0.81 mM $MgSO_4$, 1.26 mM $CaCl_2$, 25 mM HEPES, pH 7.4) was added to the apical compartment, and 1000 µL of transport buffer was added to the basolateral compartment. In basolateral-to-apical experiments, 1000 µL of the test compound solution was placed in the basolateral compartment, and 300 µL of transport buffer was added to the apical compartment. To evaluate P-glycoprotein-mediated efflux, bidirectional assays were repeated in the presence of verapamil (100 µM). Cells were pre-incubated with verapamil for 30 min at 37 °C in both compartments, followed by addition of the test compound solution (10 µM final concentration) containing verapamil to the donor compartment, with the corresponding receiver compartment filled with transport buffer containing the same concentration of inhibitor.

Plates were incubated at 37 °C under continuous shaking (100 rpm) for 90 min. Following incubation, 75 µL aliquots were withdrawn from both donor and receiver compartments and processed for LC-MS-MS analysis. Samples were mixed with two volumes of acetonitrile, proteins were precipitated by centrifugation (10,000 rpm, 10 min), and supernatants were analyzed by HPLC

coupled with tandem mass spectrometry. Ketoprofen, atenolol, and quinidine were employed as reference compounds. All test and reference solutions (10 μM) were prepared manually, and subsequent handling and liquid transfers were automated using an Opentrons robotic platform.

Analytical data of synthesized compounds are provided in **Appendix IV**.

4 Conclusions and outlook

The $P2Y_{12}$ receptor ($P2Y_{12}R$) is a promising drug target that has traditionally been associated with platelet aggregation and targeted for antithrombotic therapy.[23–25] More recently, its expression on microglial cells in the CNS has emerged as a promising area of research. Its involvement in neuroinflammatory processes positions $P2Y_{12}R$ both as a biomarker of neurodegeneration (e.g., Alzheimer's disease, Parkinson's disease, multiple sclerosis, and epilepsy) and as a target for therapeutic intervention. Modulating microglial $P2Y_{12}Rs$ thus provides opportunities for both therapy and imaging of neuroinflammatory conditions.[26–33] In this context, the present dissertation focuses on the design, synthesis, characterization, and evaluation of novel $P2Y_{12}R$ antagonists, with particular emphasis on radiolabeled ligands, and blood-brain barrier (BBB)-permeable compounds for both therapeutic and diagnostic applications.

The first two chapters deal with the synthesis of anthraquinone-derived $P2Y_{12}R$ antagonists to expand structure-activity relationships (SARs) of this class of compounds (Chapter I) and to foster radioligand development (Chapter II). A synthetic strategy was developed for anthraquinone-derived $P2Y_{12}R$ antagonists, focusing on critical intermediates and final compounds. Key synthetic challenges included nonselective nitration (leading to by-products), instability of the substituted anthraquinone scaffold under Pd-catalyzed hydrogenation condition, and sulfonate elimination during bromination reactions. Despite these hurdles, regioisomeric mixtures of C6- and C7-chloro-substituted bromaminic acid derivatives were successfully obtained. Further modifications of the aniline moiety enabled exploration of SARs and provided precursors for radioligand development. Using a previously optimized Ullmann coupling reaction, a series of modified anthraquinone-based $P2Y_{12}R$ antagonists was synthesized (**16**, **17**, and **44**–**47**, Figure 40). These results expand SARs and provide a basis for further optimizing the anthraquinone scaffold toward potent and selective $P2Y_{12}R$ antagonists with improved pharmacokinetic properties.

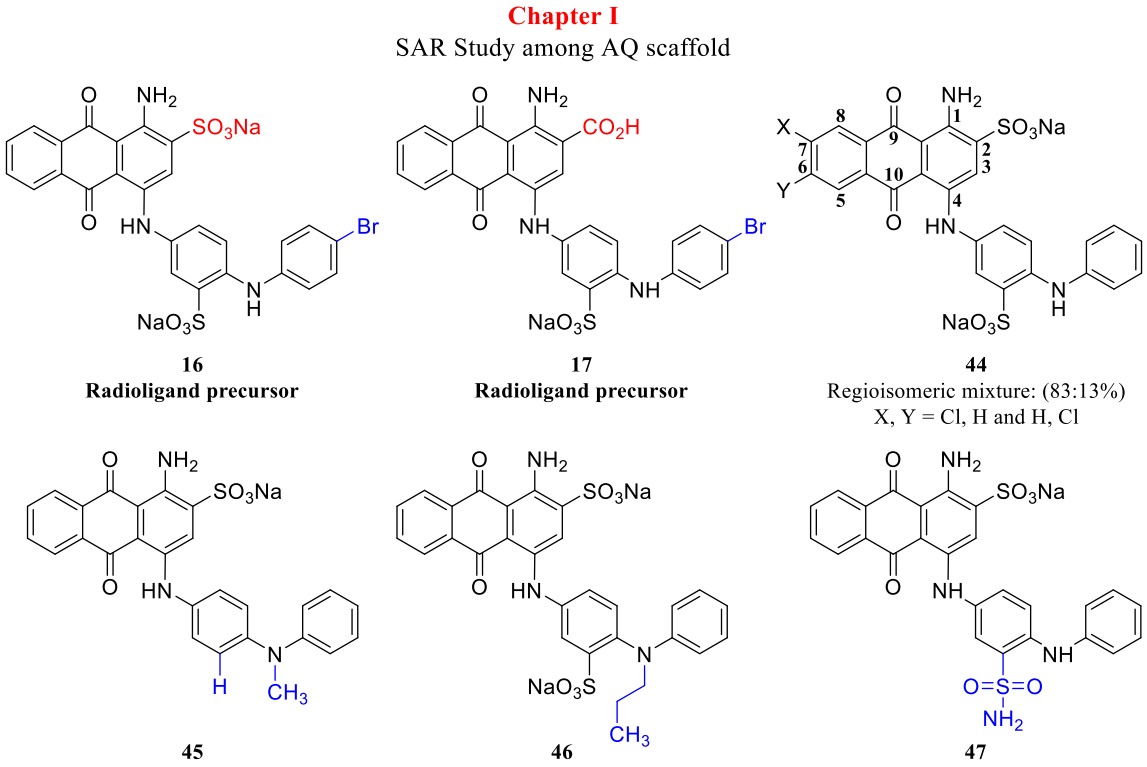


Figure 40. Structures of the modified anthraquinone derivatives **16**, **17**, and **44**–**47** (Chapter I).

In Chapter 2, we study the instability of the anthraquinone core and sulfonate or carboxylic acid elimination from the C2-position upon palladium-catalyzed reduction during the dehalogenation reaction of the aforementioned radioligand precursors **16** and **17** (Figure 40). Systematic optimization using a model compound (**7**, Figure 40) revealed that Pd/$CaCO_3$ in methanol at room temperature under low hydrogen pressure was the most favorable condition, although reactor size and hydrogen pressure significantly influenced the outcome. Continued optimization efforts included reducing the reaction rate by applying atmospheric hydrogen pressure via a balloon. Under these conditions, the formation of undesired byproducts was suppressed, and the reduction to the hydroquinone analog was found to precede the dehalogenation step, providing valuable mechanistic insight. Application of these optimized conditions to C2-carboxylate-substituted derivatives is expected to improve stability and enhance the development of an anthraquinone-based $P2Y_{12}R$ antagonist radioligand.

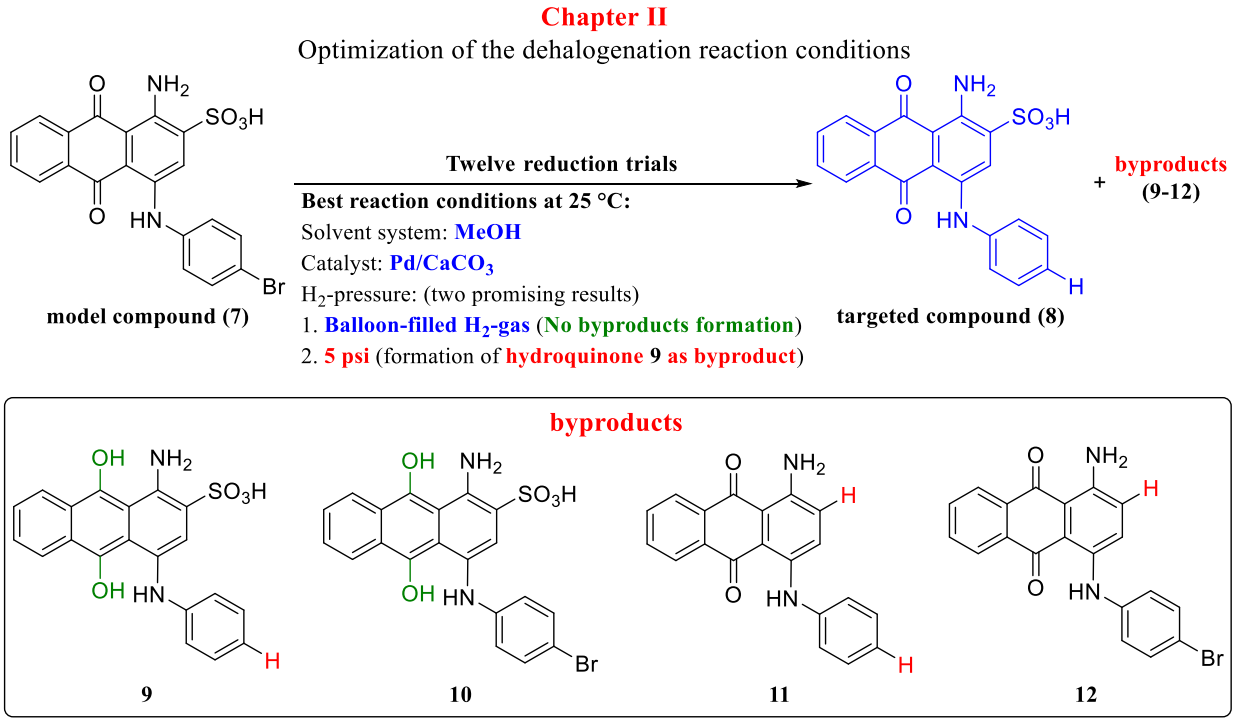


Figure 41. Summary of the systematic optimization of the dehalogenation reaction conditions applied on model compound **7**, and the resulted byproducts **8**–**12** (Chapter II).

The third part of the thesis is aimed at putting together a comprehensive collection of all reported $P2Y_{12}R$ antagonists, including patent literature, and to evaluate their potential as lead structures for the development of brain therapeutics and diagnostics. It has to be noted that all of these compounds have been developed as antithrombotic drugs, for which brain penetration is undesired. Systematic analysis and classification performed in this study has successfully identified promising scaffolds for CNS-targeted applications. These scaffolds can serve as lead structures for direct modification or as references for comparative studies, modeling, and fragmentation-based optimization approaches. In addition, this review represents an essential database for applying artificial intelligence (AI) in subsequent drug discovery and development processes targeting $P2Y_{12}Rs$, and accelerate the development of novel, more efficient antithrombotics as well as CNS-therapeutics and diagnostics. Among all identified scaffolds, the pyrazolyl-phenyl-carbamoyl-indole scaffold, particularly compound **1i** (2-(3-((4-(4-butyryl-5-methyl-1*H*-pyrazol-1-yl)phenyl)carbamoyl)-5-methyl-1*H*-indol-1-yl)acetic acid) (Figure 42), demonstrated high affinity (K_i < 10 nM), selectivity, metabolic stability, and favorable BBB penetration properties.

Preliminary SARs revealed that 5-chloroindole derivatives offered better metabolic stability compared to their 5-methyl analogs, but possess slightly higher molecular weights. Pyridazinyl-containing compounds display increased polarity and reduced brain permeability relative to phenyl analogs. Future efforts will therefore prioritize the optimization of pyrazolyl–phenyl–carbamoyl–5-methyl/chloroindole scaffolds to balance potency, selectivity, metabolic stability, and BBB permeability.

Chapter IV was based on compound **1i** identified in the aforementioned data analysis (Chapter III). A novel radioligand, **[^{3}H]PSB-22219** (**18**, Figure 42), was synthesized and shown to bind competitively and reversibly with high affinity to recombinant and native human, rat, and mouse $P2Y_{12}$Rs. It demonstrated minimal nonspecific binding, high selectivity versus related ADP-activated receptors, and high metabolic stability as determined in rat liver microsomes. Docking studies revealed key binding interactions (Tyr105, Asn159, Lys280, Trp260, Arg256). Autoradiography studies confirmed its utility for detecting $P2Y_{12}$Rs in brain sections of a humanized rat model. Compared to previously published radiotracers, **[^{3}H]PSB-22219** combines nanomolar affinity, reduced lipophilicity, low nonspecific binding, and high selectivity**,** making it a superior research tool for in vitro and ex vivo studies.

Although compound **1i** (Figure 42) possesses limited brain penetration as indicated in Chapter IV, it has been taken as a lead structure in Chapter V for the design, synthesis, and application of structure-property relationship studies. The polar carboxylic acid group was reacted by amides or ketones and the potential of the newly synthesized compounds as brain-permeable $P2Y_{12}$R antagonists was evaluated.

Altogether, a library of 31 novel $P2Y_{12}$R antagonists was synthesized and evaluated. Carboxamide derivatives showed superior potency (K_i 3.2−20.2 nM) compared to *N*-substituted analogs lacking a carbonyl group. Among these, compound **19** (dimethylamido) and **20** (ethylamido) (Figure 42) demonstrated the most favorable profile. Compound **20** exhibited exceptional metabolic stability in both human and rat liver microsomes, while compound **19** showed better Caco-2 permeability but was subject to active efflux.

Additionally, pyrrole-based compounds **43** and **44** exhibited lower binding affinities than their pyrazole-containing analogs (**15c**[86] and **1**) with K_i-values of 64.6 nM and 24.1 nM, respectively.

Future work will address sufficient water solubility, incorporation of 5-chloroindole moieties for improved metabolic stability, investigation of the best compounds as brain therapeutics, and radiolabeling (^{11}C or ^{18}F) of lead candidates for diagnostic applications in neuroinflammation.

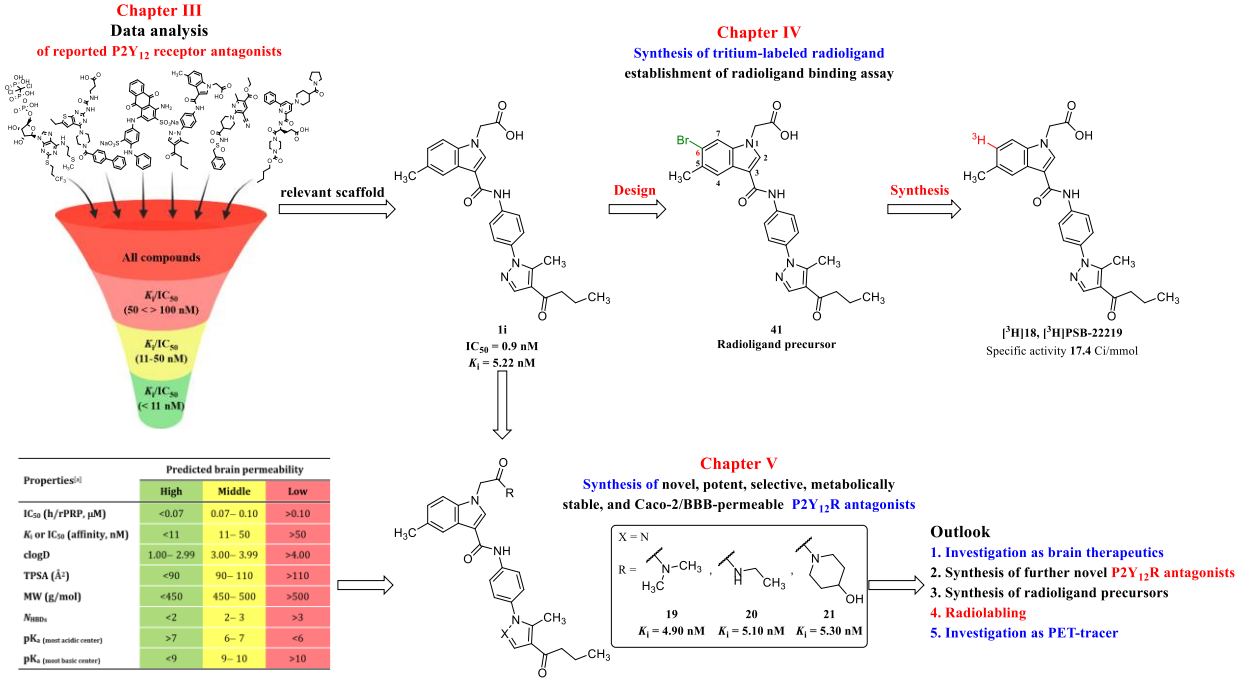


Figure 42: Summary of the systematic development of novel, potent, selective, metabolically stable, and Caco-2-permeable P2Y$_{12}$R antagonists, starting with data analysis and identification of compound **1i** (Chapter III), synthesis of its radioligand **[^{3}H]18** (**[^{3}H]PSB-22219**, Chapter IV), and finally the synthesis of targeted final compounds with the three best P2Y$_{12}$R antagonists **19**−**21** (Chapter V). Future directions were included as an outlook.

In conclusion, the present PhD thesis contributed significantly to the development of therapeutic and diagnostic drugs for P2Y$_{12}$ receptor expressed in brain, which play an important role in neuroinflammatory and neurodegenerative diseases.

5 List of abbreviations

2-MeSADP	2-Methylthioadenosine diphosphate
4-DMAP	4-Dimethylaminopyridine
7TM	Seven transmembrane
ABC	ATP-Binding cassette
AC	Adenylate cyclase
ACS	Acute coronary syndrome
AD	Alzheimer's disease
ADME	Absorption, distribution, metabolism, excretion
ADP	Adenosine diphosphate
AGP	α1-Acid glycoprotein
AMT	Adsorptive-mediated transport
AQ	Anthraquinone
ATCC	American type culture collection
ATP	Adenosine triphosphate
BBB	Blood-brain barrier
BCRP	Breast cancer resistance protein
B-CSFB	Blood-cerebrospinal fluid barrier
br	Broad
BSA	Bovine serum albumin
$BzNO_2$	Nitrobenzene
cAMP	Cyclic adenosine monophosphate
CASR	Calcium-sensing receptor
CDI	Carbonyldiimidazole
CHO cells	Chinese hamster ovary cells
CNS	Central nervous system
CNS-MPO	Central nervous system multiparameter optimization
DAD	Diode array detector
DAG	Diacylglycerol

DCM	Dichloromethane
dd	Doublet of doublet
DIPEA	*N*,*N*-Diisopropylethylamine
DMAc	Dimethylacetamide
DMEDA	*N*,*N'*-Dimethylethylenediamine
DMEM	Dulbecco's modified eagle medium
DMF	*N*,*N*-Dimethylformamide
DMSO	Dimethyl-sulfonamide
ECL	Extracellular loop
EDC·HCl	1-(3-Dimethylaminopropyl)-3-ethylcarbodiimide hydrochloride
EDTA	Ethylenediaminetetraacetic acid
EGF	Epidermal growth factor
ER	Endoplasmic reticulum
GABA	γ-Aminobutyric acid
GDP	Guanosine diphosphate
GIRK	G Protein-regulated inwardly rectifying potassium channels
GPCRs	G Protein-coupled receptors
GRAFS	Glutamate, Rhodopsin, Adhesion, Frizzled, and Secretin
GRM	Metabotropic glutamate receptors
GTP	Guanosine triphosphate
HATU	*o*-(7-Azabenzotriazol-1-yl)-*N*,*N*,*N'*,*N'* tetramethyluronium hexafluorophosphate
HBAs	Hydrogen bond acceptors
HBDs	Hydrogen bond donors
HEPES	4-(2-Hydroxyethyl)-1-piperazineethanesulfonic acid
HLM	Human liver microsomes
HPLC	High-performance liquid chromatography
hPRP:	Human platelet-rich-plasma
HSA	Human serum albumin
HTS	High-throughput screening

ICL	Intracellular loops
IP_3	Inositol trisphosphate
LC/MS	Liquid chromatography/mass spectrometry
m	Multiplet
MCH	Melanin-concentrating hormone
MECA	Melanocortin, Endothelial differentiation, Cannabinoid, and Adenosine binding
MRPs	Multidrug resistance proteins
MS	Multiple sclerosis
MW	Molecular weight
NADPH	Nicotinamide adenine dinucleotide phosphate
N_{HBDs}	Number of hydrogen-bond donors
NMR	Nuclear magnetic resonance
$P2Y_{12}Rs$	$P2Y_{12}$ Receptors
PBS	Phosphate-buffered saline
PCR	Polymerase chain reaction
PD	Parkinson's disease
PET	Positron emission tomography
P-gp	P-Glycoprotein
PI_3K	Phosphoinositide-3-kinase
PIP_2	Phosphatidylinositol-4,5-bisphosphate
PKA	Protein kinase A
PKC	Protein kinase C
PKs	Protein kinases
PLC	Phospholipase C
q	Quartet
RB-2	Reactive Blue 2
RC	Receptor cluster
RLM	Rat liver microsomes
RMT	Receptor-mediated transport

RP-18-TLC	Reversed phase-18-thin-layer chromatography
rPRP:	Rat platelet-rich-plasma
Rt	Retention times
s	Singlet
SAR	Structure-activity relationship
sext	Sextet
SI	Supporting Information
SLCs	Solute carriers
SOG	Somatostatin, opioids, and galanin
SPR	Structure-property relationship
t	Triplet
TDCR	Triple-to-double coincidence ratio
TEER	Transepithelial electrical resistance
THF	Tetrahydrofuran
TJ	Tight junctions
TLC	Thin-layer chromatography
TPSA	Topological polar surface area
UDP	Uridine diphosphate
UDPGA	Uridine diphosphate glucuronic acid
UDP-glucose	Uridine diphosphate-glucose
UTP	Uridine triphosphate
UV	Ultra-violate
VASP-P	Vasodilator-stimulated phosphoprotein

6 References

(1) Lorente, J. S.; Sokolov, A. V.; Ferguson, G.; Schioth, H. B.; Hauser, A. S.; Gloriam, D. E. GPCR drug discovery: new agents, targets and indications. *Nat. Rev. Drug Discov.* **2025**, *24*, 458−479.

(2) Zhang, M.; Chen, T.; Lu, X.; Lan, X.; Chen, Z.; Lu, S. G protein-coupled receptors (GPCRs): advances in structures, mechanisms, and drug discovery. *Signal Transduct. Target Ther.* **2024**, *9*, 88.

(3) Mohs, R. C.; Greig, N. H. Drug discovery and development: Role of basic biological research. *Alzheimers Dement. (N Y)* **2017**, *3*, 651−657.

(4) Trzaskowski, B.; Latek, D.; Yuan, S.; Ghoshdastider, U.; Debinski, A.; Filipek, S. Action of molecular switches in GPCRs--theoretical and experimental studies. *Curr. Med. Chem.* **2012**, *19*, 1090−1109.

(5) Erlandson, S. C.; McMahon, C.; Kruse, A. C. Structural basis for G protein-coupled receptor signaling. *Annu. Rev. Biophys.* **2018**, *47*, 1−18.

(6) Cheng, L.; Xia, F.; Li, Z.; Shen, C.; Yang, Z.; Hou, H.; Sun, S.; Feng, Y.; Yong, X.; Tian, X.; Qin, H.; Yan, W.; Shao, Z. Structure, function and drug discovery of GPCR signaling. *Mol. Biomed.* **2023**, *4*, 46.

(7) Hilger, D.; Masureel, M.; Kobilka, B. K. Structure and dynamics of GPCR signaling complexes. *Nat. Struct. Mol. Biol.* **2018**, *25*, 4−12.

(8) Fredriksson, R.; Lagerstrom, M. C.; Lundin, L. G.; Schioth, H. B. The G-protein-coupled receptors in the human genome form five main families. Phylogenetic analysis, paralogon groups, and fingerprints. *Mol. Pharmacol.* **2003**, *63*, 1256−1272.

(9) Schioth, H. B.; Fredriksson, R. The GRAFS classification system of G-protein coupled receptors in comparative perspective. *Gen. Comp. Endocrinol.* **2005**, *142*, 94−101.

(10) Abbracchio, M. P.; Burnstock, G.; Boeynaems, J. M.; Barnard, E. A.; Boyer, J. L.; Kennedy, C.; Knight, G. E.; Fumagalli, M.; Gachet, C.; Jacobson, K. A.; Weisman, G. A. International Union of Pharmacology LVIII: update on the P2Y G protein-coupled nucleotide receptors: from molecular mechanisms and pathophysiology to therapy. *Pharmacol. Rev.* **2006**, *58*, 281−341.

(11) Jacobson, K. A.; Müller, C. E. Medicinal chemistry of adenosine, P2Y and P2X receptors. *Neuropharmacology* **2016**, *104*, 31−49.

(12) Von Kügelgen, I. Pharmacological characterization of P2Y receptor subtypes − an update. *Purinergic Signalling* **2024**, *20*, 99−108.

(13) Brunschweiger, A.; Müller, C. E. P2 receptors activated by uracil nucleotides--an update. *Curr. Med. Chem.* **2006**, *13*, 289−312.

(14) Zarrinmayeh, H.; Territo, P. R. Purinergic receptors of the central nervous system: biology, PET ligands, and their applications. *Mol. Imaging* **2020**, *19*, 1−26.

(15) Erb, L.; Weisman, G. A. Coupling of P2Y receptors to G proteins and other signaling pathways. *Wiley Interdiscip. Rev. Membr. Transp. Signal.* **2012**, *1*, 789−803.

(16) Guo, X.; Li, Q.; Pi, S.; Xia, Y.; Mao, L. G protein-coupled purinergic P2Y receptor oligomerization: Pharmacological changes and dynamic regulation. *Biochem. Pharmacol.* **2021**, *192*, No. 114689.

(17) Jacobson, K. A.; Delicado, E. G.; Gachet, C.; Kennedy, C.; von Kügelgen, I.; Li, B.; Miras-Portugal, M. T.; Novak, I.; Schöneberg, T.; Perez-Sen, R.; Thor, D.; Wu, B.; Yang, Z.; Müller, C. E. Update of P2Y receptor pharmacology: IUPHAR review 27. *Br. J. Pharmacol.* **2020**, *177*, 2413−2433.

(18) Atkinson, B. N.; Chudasama, V.; Browne, L. E. Controlling engineered P2X receptors with light. *Methods Mol. Biol.* **2020**, *2041*, 301−309.

(19) Burnstock, G. Introduction: P2 receptors. *Curr. Top. Med. Chem.* **2004**, *4*, 793−803.

(20) Jacobson, K. A.; Jarvis, M. F.; Williams, M. Purine and pyrimidine (P2) receptors as drug targets. *J. Med. Chem.* **2002**, *45*, 4057−4093.

(21) Jacob, F.; Perez Novo, C.; Bachert, C.; Van Crombruggen, K. Purinergic signaling in inflammatory cells: P2 receptor expression, functional effects, and modulation of inflammatory responses. *Purinergic Signal.* **2013**, *9*, 285−306.

(22) Hollopeter, G.; Jantzen, H. M.; Vincent, D.; Li, G.; England, L.; Ramakrishnan, V.; Yang, R. B.; Nurden, P.; Nurden, A.; Julius, D.; Conley, P. B. Identification of the platelet ADP receptor targeted by antithrombotic drugs. *Nature* **2001**, *409*, 202−207.

(23) Mansour, A.; Bachelot-Loza, C.; Nesseler, N.; Gaussem, P.; Gouin-Thibault, I. $P2Y_{12}$ inhibition beyond thrombosis: effects on inflammation. *Int. J. Mol. Sci.* **2020**, *21*.

(24) Entsie, P.; Kang, Y.; Amoafo, E. B.; Schöneberg, T.; Liverani, E. The signaling pathway of the ADP receptor $P2Y_{12}$ in the immune system: Recent discoveries and new challenges. *Int. J. Mol. Sci.* **2023**, *24*, 6709.

(25) Baqi, Y.; Müller, C. E. Antithrombotic $P2Y_{12}$ receptor antagonists: recent developments in drug discovery. *Drug Discov. Today* **2019**, *24*, 325−333.

(26) Mildner, A.; Huang, H.; Radke, J.; Stenzel, W.; Priller, J. $P2Y_{12}$ receptor is expressed on human microglia under physiological conditions throughout development and is sensitive to neuroinflammatory diseases. *Glia* **2017**, *65*, 375−387.

(27) Feigin, V. L.; Vos, T.; Nichols, E.; Owolabi, M. O.; Carroll, W. M.; Dichgans, M.; Deuschl, G.; Parmar, P.; Brainin, M.; Murray, C. The global burden of neurological disorders: translating evidence into policy. *Lancet Neurol.* **2020**, *19*, 255−265.

(28) Erkkinen, M. G.; Kim, M.-O.; Geschwind, M. D. Clinical neurology and epidemiology of the major neurodegenerative diseases. *Cold Spring Harb. Perspect. Biol.* **2018**, *10*, a033118.

(29) Illes, P.; Rubini, P.; Ulrich, H.; Zhao, Y.; Tang, Y. Regulation of microglial functions by purinergic mechanisms in the healthy and diseased CNS. *Cells* **2020**, *9*, 1108.

(30) Kitaoka, S. Microglia regulate neuronal and behavioural functions under physiological and pathological conditions. *J. Biochem* **2023**, *173*, 153−157.

(31) Soares, N. L.; Vieira, H. L. A. Microglia at the centre of brain research: Accomplishments and challenges for the future. *Neurochem. Res.* **2022**, *47*, 218−233.

(32) Wake, H.; Moorhouse, A. J.; Nabekura, J. Functions of microglia in the central nervous system − beyond the immune response. *Neuron Glia Biol.* **2011**, *7*, 47−53.

(33) Uff, C. E. G.; Patel, K.; Yeung, C.; Yip, P. K. Advances in Visualizing Microglial Cells in Human Central Nervous System Tissue. *Biomolecules* **2022**, *12*, 603.

(34) Wallentin, L. $P2Y_{12}$ inhibitors: differences in properties and mechanisms of action and potential consequences for clinical use. *Eur. Heart J.* **2009**, *30*, 1964−1977.

(35) Baqi, Y.; Atzler, K.; Köse, M.; Glänzel, M.; Müller, C. E. High-affinity, non-nucleotide-derived competitive antagonists of platelet $P2Y_{12}$ receptors. *J. Med. Chem.* **2009**, *52*, 3784−3793.

(36) Burnstock, G. Purinergic signaling in the cardiovascular system. *Circ. Res.* **2017**, *120*, 207−228.

(37) Paoletta, S.; Sabbadin, D.; von Kügelgen, I.; Hinz, S.; Katritch, V.; Hoffmann, K.; Abdelrahman, A.; Straßburger, J.; Baqi, Y.; Zhao, Q.; Stevens, R. C.; Moro, S.; Müller, C. E.; Jacobson, K. A. Modeling ligand recognition at the $P2Y_{12}$ receptor in light of X-ray structural information. *J. Comput.-Aided Mol. Des.* **2015**, *29*, 737−756.

(38) Zhang, J.; Zhang, K.; Gao, Z.-G.; Paoletta, S.; Zhang, D.; Han, G. W.; Li, T.; Ma, L.; Zhang, W.; Müller, C. E.; Yang, H.; Jiang, H.; Cherezov, V.; Katritch, V.; Jacobson, K. A.; Stevens, R. C.; Wu, B.; Zhao, Q. Agonist-bound structure of the human $P2Y_{12}$ receptor. *Nature* **2014**, *509*, 119−122.

(39) Zhang, K.; Zhang, J.; Gao, Z.; Zhang, D.; Zhu, L.; Han, G. W.; Moss, S. M.; Paoletta, S.; Kiselev, E.; Lu, W.; Fenalti, G.; Zhang, W.; Müller, C. E.; Yang, H.; Jiang, H.; Cherezov, V.; Katritch, V.; Jacobson, K. A.; Stevens, R. C.; Wu, B.; Zhao, Q. Structure of the human P2Y12 receptor in complex with an antithrombotic drug, *Nature* **2014**, *509*, 115−118.

(40) Savi, P.; Pereillo, J. M.; Uzabiaga, M. F.; Combalbert, J.; Picard, C.; Maffrand, J. P.; Pascal, M.; Herbert, J. M. Identification and biological activity of the active metabolite of clopidogrel. *Thromb. Haemost.* **2000**, *84*, 891−896.

(41) Ingall, A. H.; Dixon, J.; Bailey, A.; Coombs, M. E.; Cox, D.; McInally, J. I.; Hunt, S. F.; Kindon, N. D.; Teobald, B. J.; Willis, P. A.; Humphries, R. G.; Leff, P.; Clegg, J. A.; Smith, J. A.; Tomlinson, W. Antagonists of the platelet P2T receptor: a novel approach to antithrombotic therapy. *J. Med. Chem.* **1999**, *42*, 213−220.

(42) Springthorpe, B.; Bailey, A.; Barton, P.; Birkinshaw, T. N.; Bonnert, R. V.; Brown, R. C.; Chapman, D.; Dixon, J.; Guile, S. D.; Humphries, R. G.; Hunt, S. F.; Ince, F.; Ingall, A. H.; Kirk, I. P.; Leeson, P. D.; Leff, P.; Lewis, R. J.; Martin, B. P.; McGinnity, D. F.; Mortimore, M. P.; Paine, S. W.; Pairaudeau, G.; Patel, A.; Rigby, A. J.; Riley, R. J.; Teobald, B. J.; Tomlinson, W.; Webborn, P. J.; Willis, P. A. From ATP to AZD6140: The discovery of an orally active reversible $P2Y_{12}$ receptor antagonist for the prevention of thrombosis. *Bioorg. Med. Chem. Lett.* **2007**, *17*, 6013−6018.

(43) Zetterberg, F.; Svensson, P. State of affairs: design and structure-activity relationships of reversible $P2Y_{12}$ receptor antagonists. *Bioorg. Med. Chem. Lett.* **2016**, *26*, 2739−2754.

(44) Jacobson, K. A.; Ivanov, A. A.; de Castro, S.; Harden, T. K.; Ko, H. Development of selective agonists and antagonists of P2Y receptors. *Purinergic Signalling* **2009**, *5*, 75−89.

(45) Kerru, N.; Gummidi, L.; Maddila, S.; Gangu, K. K.; Jonnalagadda, S. B. A Review on recent advances in nitrogen-containing molecules and their biological applications. *Molecules* **2020**, *25*, 1909.

(46) Serebruany, V. L.; Stebbing, J.; Atar, D. Dyspnoea after antiplatelet agents: the AZD6140 controversy. *Int. J. Clin. Pract.* **2007**, *61*, 529−533.

(47) Weitz, J. I.; Hirsh, J.; Samama, M. M. New antithrombotic drugs: American college of chest physicians evidence-based clinical practice guidelines (8th Edition). *Chest* **2008**, *133*, 234S−256S.

(48) Baqi, Y.; Müller, C. E. Synthesis of alkyl- and aryl-amino-substituted anthraquinone derivatives by microwave-assisted copper(0)-catalyzed Ullmann coupling reactions. *Nat. Protoc.* **2010**, *5*, 945−953.

(49) Parlow, J. J.; Burney, M. W.; Case, B. L.; Girard, T. J.; Hall, K. A.; Hiebsch, R. R.; Huff, R. M.; Lachance, R. M.; Mischke, D. A.; Rapp, S. R.; Woerndle, R. S.; Ennis, M. D. Piperazinyl-glutamate-pyrimidines as potent $P2Y_{12}$ antagonists for inhibition of platelet aggregation. *Bioorg. Med. Chem. Lett.* **2009**, *19*, 6148−6156.

(50) Caroff, E.; Meyer, E.; Treiber, A.; Hilpert, K.; Riederer, M. A. Optimization of 2-phenyl-pyrimidine-4-carboxamides towards potent, orally bioavailable and selective $P2Y_{12}$ antagonists for inhibition of platelet aggregation. *Bioorg. Med. Chem. Lett.* **2014**, *24*, 4323−4331.

(51) Caroff, E.; Hubler, F.; Meyer, E.; Renneberg, D.; Gnerre, C.; Treiber, A.; Rey, M.; Hess, P.; Steiner, B.; Hilpert, K.; Riederer, M. A. 4-((*R*)-2-{[6-((*S*)-3-methoxypyrrolidin-1-yl)-2-phenylpyrimidine-4-carbonyl]amino}-3-phosphonopropionyl)piperazine-1-carboxylic acid butyl ester (ACT-246475) and Its prodrug (ACT-281959), a novel $P2Y_{12}$ receptor antagonist with a wider therapeutic window in the rat than clopidogrel. *J. Med. Chem.* **2015**, *58*, 9133−9153.

(52) Beavers, C. J.; Effoe, S. A.; Dobesh, P. P. Selatogrel: a novel subcutaneous $P2Y_{12}$ inhibitor. *J. Cardiovasc. Pharmacol.* **2022**, *79*, 161−167.

(53) Parlow, J. J.; Burney, M. W.; Case, B. L.; Girard, T. J.; Hall, K. A.; Harris, P. K.; Hiebsch, R. R.; Huff, R. M.; Lachance, R. M.; Mischke, D. A.; Rapp, S. R.; Woerndle, R. S.; Ennis, M. D. Piperazinyl glutamate pyridines as potent orally bioavailable $P2Y_{12}$ antagonists for inhibition of platelet aggregation. *J. Med. Chem.* **2010**, *53*, 2010−2037.

(54) Parlow, J. J.; Burney, M. W.; Case, B. L.; Girard, T. J.; Hall, K. A.; Harris, P. K.; Hiebsch, R. R.; Huff, R. M.; Lachance, R. M.; Mischke, D. A.; Rapp, S. R.; Woerndle, R. S.; Ennis, M. D. Part II: piperazinyl-glutamate-pyridines as potent orally bioavailable $P2Y_{12}$ antagonists for inhibition of platelet aggregation. *Bioorg. Med. Chem. Lett.* **2010**, *20*, 1388−1394.

(55) Zech, G.; Hessler, G.; Evers, A.; Weiss, T.; Florian, P.; Just, M.; Czech, J.; Czechtizky, W.; Gorlitzer, J.; Ruf, S.; Kohlmann, M.; Nazare, M. Identification of high-affinity $P2Y_{12}$ antagonists based on a phenylpyrazole glutamic acid piperazine backbone. *J. Med. Chem.* **2012**, *55*, 8615−8629.

(56) Nazare, M.; Zech, G.; Just, M.; Weiss, T.; Hessler, G.; Czech, J. Quinoline-carboxamide derivatives as $P2Y_{12}$ antagonists. United States Patent US-8669266-B2, March 11, **2014**.

(57) Bach, P.; Bostrom, J.; Brickmann, K.; van Giezen, J. J.; Groneberg, R. D.; Harvey, D. M.; O'Sullivan, M.; Zetterberg, F. Synthesis, structure-property relationships and pharmacokinetic evaluation of ethyl 6-aminonicotinate sulfonylureas as antagonists of the $P2Y_{12}$ receptor. *Eur. J. Med. Chem.* **2013**, *65*, 360−375.

(58) Bach, P.; Antonsson, T.; Bylund, R.; Björkman, J.; Österlund, K.; Giordanetto, F.; van Giezen, J.; Andersen, S. M.; Zachrisson, H.; Zetterberg, F. Lead optimization of ethyl 6-aminonicotinate acyl sulfonamides as antagonists of the $P2Y_{12}$ receptor. Separation of the antithrombotic effect and bleeding for candidate drug AZD1283. *J. Med. Chem.* **2013**, *56*, 7015−7024.

(59) Kortum, S. W.; Lachance, R. M.; Schweitzer, B. A.; Yalamanchili, G.; Rahman, H.; Ennis, M. D.; Huff, R. M.; TenBrink, R. E. Thienopyrimidine-based $P2Y_{12}$ platelet aggregation inhibitors. *Bioorg. Med. Chem. Lett.* **2009**, *19*, 5919−5923.

(60) Lee, C. S.; Lee, T. H.; Yoon, S. K.; Choi, J. S.; Jang, Y. J.; Kim, S. W.; Chang, H. K.; Park, M. J.; Kim, T. H.; Ahn, Y. H.; Park, H. D.; Park, H. J.; Lim, D. C.; Lee, J. Y.; Lee, S. H.; Park, W. S.; Oh, Y. S. Fused heterocyclic compound. Korean Patent, WO 2010/027236, March 11, **2010**.

(61) Ennis, M. D.; Kortum, S. W.; Tenbrink, R. E.; 4-Piperazinylthieno [2, 3-d] pyrimidine compounds as platelet aggregation inhibitors. U. S. Patent, WO 2006/103544, October 5, **2006**.

(62) Boldron, C.; Besse, A.; Bordes, M. F.; Tissandie, S.; Yvon, X.; Gau, B.; Badorc, A.; Rousseaux, T.; Barre, G.; Meneyrol, J.; Zech, G.; Nazare, M.; Fossey, V.; Pflieger, A. M.; Bonnet-Lignon, S.; Millet, L.; Briot, C.; Dol, F.; Herault, J. P.; Savi, P.; Lassalle, G.; Delesque, N.; Herbert, J. M.; Bono, F. *N*-[6-(4-butanoyl-5-methyl-1*H*-pyrazol-1-yl)pyridazin-3-yl]-5-chloro-1-[2-(4-methylpiperazin-1-yl)-2-oxoethyl]-1*H*-indole-3-carboxamide (SAR216471), a novel intravenous and oral, reversible, and directly acting $P2Y_{12}$ antagonist. *J. Med. Chem.* **2014**, *57*, 7293−7316.

(63) Badorc, A.; Boldron, C.; Delesque, N.; Fossey, V.; Lassalle, G.; Yvon, X.; Werner, A. Derivatves of *N*-[(1*H*-Pyrazol-1-yl) aryl]-1*H*-indole or 1*H*-indazole-3-carboxamide their preparation and their use as $P2Y_{12}$ antagonists. France Patent WO 2012/146318, November 1, **2012**.

(64) Pincemail, E.; Peyronneau, M.; Denis, C.; Bensalah, H.; Corbel, M.; Goutal, S.; Goislard, M.; Al-Hroub, H.; Al Musawi, H. A. M.; Théry, M.; Beuché, S.; Chauveau, F.; Van Camp, N.; Bemelmans, A.; Müller, C. E.; Kuhnast, B.; Winkeler, A.; Richard, M. Synthesis, labeling and biological evaluation of original $P2Y_{12}$ radioligands for PET imaging of neuroinflammation. *ACS Chem. Neurosci.* **2025**, *16*, 2639−2656.

(65) Houille, O.; Fretz, H.; Hilpert, K.; Riederer, M.; Giller, T.; Valdenaire, O. Pyrazolidinedione derivatives and their use as platelet aggregation inhibitors, Australian Patent AU2003249865A1, January 21, **2005**.

(66) Stéen, E. J. L.; van der Schatte Olivier, A.; van der Wildt, B.; Pereira, P.; Alkayal, K.; Gabella Carena, L. J.; Schuit, R. C.; Verlaan, M.; Beaino, W.; Zarzycka, B. A.; de Esch, I. J. P.; Windhorst, A. D. Exploration of fluorinated pyrazolidine-3,5-diones for positron emission tomography imaging of the $P2Y_{12}$ receptor in the central nervous system. *ChemMedChem* **2025**, *00*, 1−8.

(67) Malik, E. M.; Müller, C. E. Anthraquinones as pharmacological tools and drugs. *Med. Res. Rev.* **2016**, *36*, 705−748.

(68) Monks, T. J.; Hanzlik, R. P.; Cohen, G. M.; Ross, D.; Graham, D. G. Quinone chemistry and toxicity. *Toxicol. Appl. Pharmacol.* **1992**, *112*, 2−16.

(69) Gessler, N. N.; Egorova, A. S.; Belozerskaya, T. A. Fungal anthraquinones. *Appl. Biochem. Microbiol.* **2013**, *49*, 85−99.

(70) Pankewitz, F.; Zöllmer, A.; Gräser, Y.; Hilker, M. Anthraquinones as defensive compounds in eggs of Galerucini leaf beetles: biosynthesis by the beetles? *Arch. Insect. Biochem. Physiol.* **2007**, *66*, 98−108.

(71) Pearson, J. C.; Weaver, M. A.; Fleischer, J. C.; King, G. A. Copolymerizable methine and anthraquinone compounds and articles containing them. US 8,501,890 B2, August 6, **2013**.

(72) Caro, Y.; Anamale, L.; Fouillaud, M.; Laurent, P.; Petit, T.; Dufosse, L. Natural hydroxyanthraquinoid pigments as potent food grade colorants: an overview. *Nat. Products Bioprospect.* **2012**, *2*, 174−193.

(73) Considine, G. D.; Kulik, P. H. Dyes: Anthraquinone. In *Dyes: Anthraquinone.* In *Van Nostrand's Scientific Encyclopedia.* 10th ed.; Considine, G. D.; Kulik P. H., Eds.; John Wiley & Sons, Inc.: Hoboken, NJ; **2008**; pp 1613−1616.

(74) Shaw, D. W. Allergic contact dermatitis from carmine. *Dermatitis* **2009**, *20*, 292−295.

(75) DeSouza Gil, E.; DeOliveira, S. C. B.; DeOliveira-Brett, A. M. Hydroxyanthraquinones carminic acid and chrysazin anodic oxidation. *Electroanalysis* **2012**, *24*, 2079−2084.

(76) Kulick, M. B.; von Kügelgen, I. P2Y-receptors mediating an inhibition of the evoked entry of calcium through N-type calcium channels at neuronal processes. *J. Pharmacol. Exp. Ther.* **2002**, *303*, 520−526.

(77) Malik, E. M.; Müller, C. E. Synthetic access to novel anthraquinone derivatives, biological evaluation, and analysis of structure-activity relationships at P2Y receptors. *Rheinische Friedrich-Wilhelms-Universität Bonn* **2015**.

(78) Abourbeh, G.; Thézé, B.; Maroy, R.; Dubois, A.; Brulon, V.; Fontyn, Y.; Dollé, F.; Tavitian, B.; Boisgard, R. Imaging microglial/macrophage activation in spinal cords of experimental autoimmune encephalomyelitis rats by positron emission tomography using the mitochondrial 18 kDa translocator protein radioligand [^{18}F]DPA-714. *J. NeuroSci.* **2012**, *32*, 5728−5736.

(79) Hamelin, L.; Lagarde, J.; Dorothee, G.; Leroy, C.; Labit, M.; Comley, R. A.; Cruz de Souza, L.; Corne, H.; Dauphinot, L.; Bertoux, M.; Dubois, B.; Gervais, P.; Colliot, O.; Potier, M. C.; Bottlaender, M.; Sarazin, M.; Clinical IMABio3 team. Early and protective microglial activation in Alzheimer's disease: a prospective study using ^{18}F-DPA-714 PET imaging. *Brain* **2016**, *139*, 1252−1264.

(80) Hamelin, L.; Lagarde, J.; Dorothee, G.; Potier, M. C.; Corlier, F.; Corlier, F.; Kuhnast, B.; Caillé, F.; Dubois, B.; Fillon, L.; Chupin, M.; Bottlaender, M.; Sarazin, M. Distinct dynamic profiles of microglial activation are associated with progression of Alzheimer's disease. *Brain* **2018**, *141*, 1855−1870.

(81) Nguyen, D. L.; Wimberley, C.; Truillet, C.; Jego, B.; Caille, F.; Pottier, G.; Boisgard, R.; Buvat, I.; Bouilleret, V. Longitudinal positron emission tomography imaging of glial cell activation in a mouse model of mesial temporal lobe epilepsy: Toward identification of optimal treatment windows. *Epilepsia* **2018**, *59*, 1234−1244.

(82) Pike, V. W.; PET radiotracers: crossing the blood–brain barrier and surviving metabolism. *Trends Pharmacol. Sci*. **2009**, *30*, 431−440.

(83) El-Tayeb, A.; Griessmeier, K. J.; Müller, C. E. Synthesis and preliminary evaluation of [^{3}H] PSB-0413, a selective antagonist radioligand for platelet $P2Y_{12}$ receptors. *Bioorg. Med. Chem. Lett.* **2005**, *15*, 5450−5452.

(84) Ohlmann, P.; Lecchi, A.; El-Tayeb, A.; Müller, C. E.; Cattaneo, M.; Gachet, C. The platelet $P2Y_{12}$ receptor under normal and pathological conditions. Assessment with the radiolabeled selective antagonist [^{3}H]PSB-0413. *Purinergic Signal.* **2013,** *9*, 59−66.

(85) Van der Wildt, B.; Janssen, B.; Pekošak, A.; Stéen, E. J. L.; Schuit, R. C.; Kooijman, E. J. M.; Beaino, W.; Vugts, D. J.; Windhorst, A. D.; Svensson, P. Novel thienopyrimidine-based PET tracers for $P2Y_{12}$ receptor imaging in the brain. *ACS Chem. Neurosci*. **2021**, *12*, 4465−4474.

(86) Al-Hroub, H.; Al Musawi, H. A. M.; Abdelrahman, A.; Namasivayam, V.; Corbel, M.; Petit, F.; Aksyote, G.; Beau, F.; Jan, C.; Bemelmans, A.; Van Camp, N.; Peyronneau, M.; Winkeler, A.; Müller, C. E. Selective, non-nucleotidic radiotracer for $P2Y_{12}$ receptors: Design, synthesis, characterization, and imaging of brain slices. *J. Med. Chem.* **2025**, *68*, 11279−11298.

(87) Kopf, S.; Bourriquen, F.; Li, W.; Neumann, H.; Junge, K.; Beller, M. Recent developments for the deuterium and tritium labeling of organic molecules. *Chem. Rev*. **2022**, *122*, 6634−6718.

(88) Edelmann, M. R.; Erny, J.; Guba, W.; Hierl, M. Tritium Labeling of Neuromedin S by Conjugation with [^{3}H] N-Succinimidyl Propionate. *ACS Omega* **2023**, *8*, 2367−2376.

(89) Jackson, I. M.; Buccino, P. J.; Azevedo, E. C.; Carlson, M. L.; Luo, A. S. Z.; Deal, E. M.; Kalita, M.; Reyes, S. T.; Shao, X.; Beinat, C.; Nagy, S. C.; Chaney, A. M.; Anders, D. A.; Scott, P. J. H.; Smith, M.; Shen, B.; James, M. L. Radiosynthesis and initial preclinical evaluation of [^{11}C]AZD1283 as a potential $P2Y_{12}$R PET radiotracer. *Nucl. Med. Biol.* **2022,** *114−115*, 143−150.

(90) Steen, E. J. L.; Tousiaki, E. N.; Kingston, L.; van der Wildt, B.; Lénárt, N.; Beaino, W.; Verlaan, M.; Zarzycka, B.; Zinnhardt, B.; Dénes, Á.; Gobbi, L.; de Esch, I. J.; Elmore, C. S.; Windhorst, A. D.; Honer, M.; Leurs, R. Characterization of [^{3}H]AZ12464237 as a high affinity, non-nucleotide antagonist radioligand for the $P2Y_{12}$ receptor. *Biochem. Pharmacol.* **2025**, *237*, 116900.

(91) Villa, A.; Klein, B.; Janssen, B.; Pedragosa, J.; Pepe, G.; Zinnhardt, B.; Vugts, D. J.; Gelosa, P.; Sironi, L.; Beaino, W.; Damont, A.; Dollé, F.; Jego, B.; Winkeler, A.; Ory, D.; Solin, O.; Vercouillie, J.; Funke, U.; Laner-Plamberger, S.; Blomster, L. V.; Christophersen, P.; Vegeto, E.; Aigner, L.; Jacobs, A.; Planas, A. M.; Maggi, A.; Windhorst, A. D. Identification of new molecular targets for PET imaging of the microglial anti-inflammatory activation state. *Theranostics* **2018,** *8*, 5400−5418.

(92) Gao, C.; Jiang, J.; Tan, Y.; Chen, S. Microglia in neurodegenerative diseases: mechanism and potential therapeutic targets. *Signal Transduction Targeted Ther.* **2023**, *8*, 359.

(93) Guo, S.; Wang, H.; Yin, Y. Microglia polarization from M1 to M2 in neurodegenerative diseases. *Front. Aging Neurosci.* **2022**, *14*, No. 815347.

(94) Singh, D. Astrocytic and microglial cells as the modulators of neuroinflammation in Alzheimer's disease. *J. Neuroinflammation* **2022**, *19*, 206.

(95) Tahmasebi, F.; Barati, S. The role of microglial depletion approaches in pathological condition of CNS. *Cell. Mol. Neurobiol.* **2023**, *43*, 2459−2471.

(96) Wu, Z.; Tang, W.; Ibrahim, F. E. E. M.; Chen, X.; Yan, H.; Tao, C.; Wang, Z.; Guo, Y.; Fu, Y.; Wang, Q.; Ge, Y. Aβ induces neuroinflammation and microglial M1 polarization via cGAS-STINGIFITM3 signaling pathway in BV-2 Cells. *Neurochem. Res.* **2023**, *48*, 2881−2894.

(97) Joukal, M.; Vulchanova, L.; Dubový, P. Editorial: The brain barriers in diseases of the nervous system, *Front. Cell. Neurosci.* **2023**, *17*, 1−2.

(98) Abbott, N. J. Anatomy and physiology of the blood-brain barriers. In *drug delivery to the brain: physiological concepts, methodologies and approaches,* 2nd ed.; Springer International Publishing, **2022**; pp 3−25.

(99) Han, L. W.; Gao, C.; Mao, Q. An update on expression and function of P-gp/ABCB1 and BCRP/ABCG2 in the placenta and fetus, *Expert Opin. Drug Metab. Toxicol.* **2018**, *14*, 817−829.

(100) Wang, J.; Yang, Y.; Cai, C.; Teng, Q.; Cui, Q.; Lin, J.; Assaraf, Y. G.; Chen, Z. Multidrug resistance proteins (MRPs): Structure, function and the overcoming of cancer multidrug resistance, *Drug Resist. Updates* **2021**, *54*, 100743.

(101) Song, W.; Li, D.; Tao, L.; Luo, Q.; Chen, L. Solute carrier transporters: the metabolic gatekeepers of immune cells. *Acta Pharm. Sin. B.* **2020**, *10*, 61−78.

(102) Wager, T. T.; Hou, X.; Verhoest, P. R.; Villalobos, A. Moving beyond Rules: The development of a central nervous system multiparameter optimization (CNS MPO) approach to enable alignment of druglike properties, *ACS Chem. Neurosci.* **2010**, *1*, 435−449.

(103) Wager, T. T.; Hou, X.; Verhoest, P. R.; Villalobos, A. Central nervous system multiparameter optimization desirability: Application in drug discovery. *ACS Chem. Neurosci.* **2016**, *7*, 767−775.

(104) Bhattarai, S.; Pippel, J.; Meyer, A.; Freundlieb, M.; Schmies, C.; Abdelrahman, A.; Fiene, A.; Lee, S.; Zimmermann, H.; El-Tayeb, A.; Yegutkin, G. G.; Sträter, N.; Müller, C. E. X-Ray co-crystal structure guides the way to subnanomolar competitive ecto-5′-nucleotidase (CD73) inhibitors for cancer immunotherapy. *Adv. Ther.* **2019**, *2*, 1900075.

(105) Bhattarai, S.; Freundlieb, M.; Pippel, J.; Meyer, A.; Abdelrahman, A.; Fiene, A.; Lee, S.; Zimmermann, H.; Yegutkin, G. G.; Sträter, N.; El-Tayeb, A.; Müller, C. E. α,β-Methylene-ADP (AOPCP) derivatives and analogues: Development of potent and selective ecto-5′-nucleotidase (CD73) inhibitors. *J. Med. Chem.* **2015**, *58*, 6248−6263.

(106) Kundu, S.; Mandal, S.; Thirupathi, B. Kobayashi's aryne precursor for the one-step synthesis of anthraquinones and its application to the total synthesis of chrysophanol, danthron, and physcion. *J. Org. Chem.* **2025**, *90*, 2472−2478.

(107) Shaik, L.; Hari Haran, A. V. L. N. S. H.; Rao, R. M.; Murthy, Y. L. N. Synthesis and characterization of anthraquinone analog and studies on its bioassay. *Res. J. Chem. Environ.* **2022**, *26*, 24−29.

(108) Hashimoto, M.; Shimizu, Y.; Ogura, F.; Nakagawa, M. Optically active triptycenes. Vii. Synthesis, optical resolution and absolute configuration of 3-chloro and 4-chloro-7-substituted triptycenes. *Bull. Chem. Soc. Jpn.* **1974**, *47*, 1761−1766.

(109) Iijima, T.; Katoh, M.; Takedomi, K.; Yamamoto, Y.; Akatsuka, H.; Shirata, N.; Nishi, A.; Takakuwa, M.; Watanabe, Y.; Munakata, H.; Koyama, N.; Ikeda, T.; Iguchi, T.; Kato, H.; Kikkawa, K.; Kawaguchi, T. Discovery of apararenone (MT-3995) as a highly selective, potent, and novel nonsteroidal mineralocorticoid receptor antagonist. *J. Med. Chem.* **2022**, *65*, 8127−8143.

(110) Xie, Y.; Tummala, P.; Oakley, A. J.; Deora, G. S.; Nakano, Y.; Rooke, M.; Cuellar, M. E.; Strasser, J. M.; Dahlin, J. L.; Walters, M. A.; Casarotto, M. G.; Board, P. G.; Baell, J. B.

Development of benzenesulfonamide derivatives as potent glutathione transferase omega-1 inhibitors. *J. Med. Chem.* **2020**, *63*, 2894−2914.

(111) D'Ambrosio, K.; Vitale, R.-M.; Dogné, J.-M.; Masereel, B.; Innocenti, A.; Scozzafava, A.; De Simone, G.; Supuran, C. T. Carbonic anhydrase inhibitors: Bioreductive nitro-containing sulfonamides with selectivity for targeting the tumor associated isoforms IX and XII. *J. Med. Chem.* **2008**, *51*, 3230−3237.

(112) Hanson, J.; Reynaud, D.; Qiao, N.; Devel, P.; Moray, A.-L.; Renard, J.-F.; Kelley, L. P.; Winum, J.-Y.; Montero, J.-L.; Kinsella, B. T.; Pirotte, B.; Pace-Asciak, C. R.; Dogné, J.-M. Synthesis and pharmacological evaluation of novel nitrobenzenic thromboxane modulators as antiplatelet agents acting on both the alpha and beta isoforms of the human thromboxane receptor. *J. Med. Chem.* **2006**, *49*, 3701−3709.

(113) Pan, L.; Jiang, Y.; Liu, Z.; Liu, X.-H.; Liu, Z.; Wang, G.; Li, Z.-M.; Wang, D. Synthesis and evaluation of novel monosubstituted sulfonylurea derivatives as antituberculosis agents. *Eur. J. Med. Chem.* **2012**, *50*, 18−26.

(114) Giordanetto, F.; Bach, P.; Zetterberg, F.; Antonsson, T.; Bylund, R.; Johansson, J.; Sellén, M.; Brown, D.; Hidestål, L.; Berntsson, P.; Hovdal, D.; Zachrisson, H.; Björkman, J.; van Giezen, J. Optimization of ketone-based $P2Y_{12}$ receptor antagonists as antithrombotic agents: Pharmacodynamics and receptor kinetics considerations. *Bioorg. Med. Chem. Lett.* **2014**, *24*, 2963−2968.

(115) Kong, D.; Xue, T.; Guo, B.; Cheng, J.; Liu, S.; Wei, J.; Lu, Z.; Liu, H.; Gong, G.; Lan, T.; Hu, W.; Yang, Y. Optimization of $P2Y_{12}$ antagonist ethyl 6-(4-((benzylsulfonyl)carbamoyl)piperidin-1-yl)-5-cyano-2-methylnicotinate (AZD1283) led to the discovery of an oral antiplatelet agent with improved druglike properties. *J. Med. Chem.* **2019**, *62*, 3088−3106.

(116) Joseph, E.; Kunze, L. H.; Schaefer, R.; Palumbo, G.; Kugelmann, B.; Wagner, S.; Lammich, S.; Feederle, R.; Willem, M.; Werner, R. A.; Brendel, M.; Lindner, S. Design, synthesis and preclinical evaluation of a brain-permeable PET tracer for $P2Y_{12}$ receptor imaging in the brain. *J. Med. Chem.* **2025**, *68*, 15543−15562.

(117) Delesque-Touchard, N.; Pflieger, A. M.; Bonnet-Lignon, S.; Millet, L.; Salel, V.; Boldron, C.; Lassalle, G.; Herbert, J. M.; Savi, P.; Bono, F. SAR216471, an alternative to the use of currently available $P2Y_{12}$ receptor inhibitors? *Thromb. Res.* **2014**, *134*, 693−703.

(118) Lin, S.-S.; Tang, Y.; Illes, P.; Verkhratsky, A. The safeguarding microglia: Central role for $P2Y_{12}$ receptors. *Front. Pharmacol.* **2021**, *11*, No. 627760.

(119) Kobayashi, K.; Yamanaka, H.; Fukuoka, T.; Dai, Y.; Obata, K.; Noguchi, K. $P2Y_{12}$ receptor upregulation in activated microglia is a gateway of p38 signaling and neuropathic pain. *J. Neurosci.* **2008**, *28*, 2892.

(120) Chen, X.; Wang, Q.; Yang, J.; Zhang, L.; Liu, T.-T.; Liu, J.; Deng, B.-L.; Liu, J. Diagnostic and therapeutic value of $P2Y_{12}$R in epilepsy. *Front. Pharmacol.* **2023**, *14*, No. 1179028.

(121) Ferro, A.; Auguste, Y. S. S.; Cheadle, L. Microglia, cytokines, and neural activity: Unexpected interactions in brain development and function. *Front. Immunol.* **2021**, *12*, No. 703527.

(122) Warlo, E. M. K.; Arnesen, H.; Seljeflot, I. A brief review on resistance to $P2Y_{12}$ receptor antagonism in coronary artery disease. *Thromb. J.* **2019**, *17*, 11.

(123) Li, X.; Zhang, G.; Cao, X. The function and regulation of platelet $P2Y_{12}$ receptor. *Cardiovasc. Drugs Ther.* **2023**, *37*, 199−216.

(124) Cattaneo, M. The platelet $P2Y_{12}$ receptor for adenosine diphosphate: Congenital and drug-induced defects. *Blood* **2011**, *117*, 2102−2112.

(125) Aradi, D.; Kirtane, A.; Bonello, L.; Gurbel, P. A.; Tantry, U. S.; Huber, K.; Freynhofer, M. K.; ten Berg, J.; Janssen, P.; Angiolillo, D. J.; Siller-Matula, J. M.; Marcucci, R.; Patti, G.; Mangiacapra, F.; Valgimigli, M.; Morel, O.; Palmerini, T.; Price, M. J.; Cuisset, T.; Kastrati, A.; Stone, G. W.; Sibbing, D. Bleeding and stent thrombosis on $P2Y_{12}$- inhibitors: collaborative analysis on the role of platelet reactivity for risk stratification after percutaneous coronary intervention. *Eur. Heart J.* **2015**, *36*, 1762−1771.

(126) Lowry, O. H.; Rosebrough, N. J.; Farr, A. L.; Randall, R. J. Protein measurement with the folin phenol reagent. *J. Biol. Chem.* **1951**, *193*, 265−275.

(127) Arena A and Phillips J. Optimization of Caco-2 cell growth and differentiation for drug transport assay studies using a 96-well MultiScreen Caco-2 Assay System. Millipore protocol note PC1060EN00P, rev. 08/**2003**.

(128) Sevin, E.; Dehouck, L.; Fabulas-da Costa, A.; Cecchelli, R.; Dehouck, M. P.; Lundquist, S.; Culot, M. Accelerated Caco-2 cell permeability model for drug discovery. *J. Pharmacol. Toxicol. Methods* **2013**, *68*, 334−339.

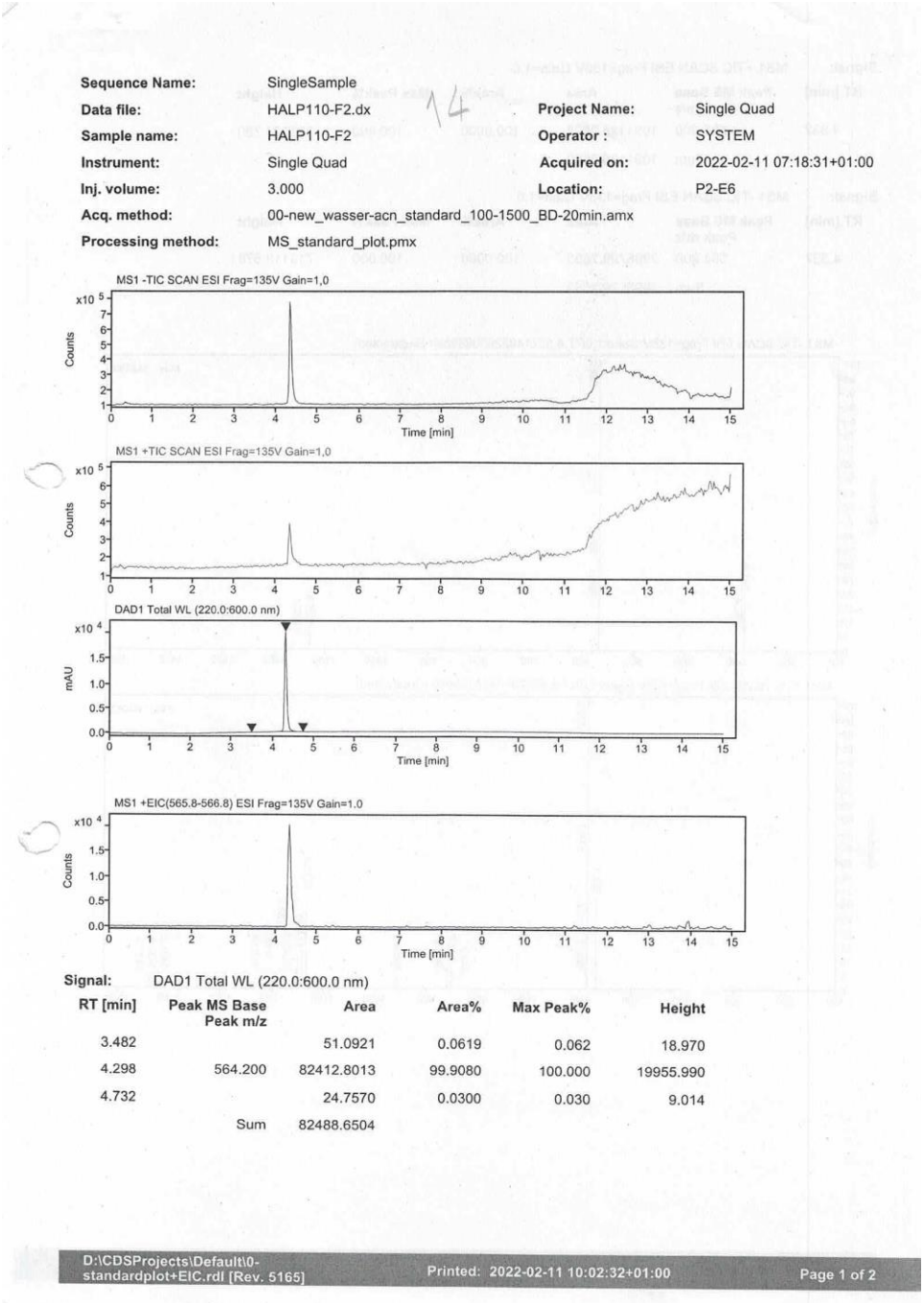
(129) Srinivasan, B.; Kolli, A. R.; Esch, M. B.; Abaci, H. E.; Shuler, M. L.; Hickman, J. J. TEER measurement techniques for in vitro barrier model systems. *SLAS Technol.* **2015**, *20*, 107−126.

7 Appendices

7.1 Appendix I: Synthesis of anthraquinone-based $P2Y_{12}$ receptor antagonists: Structure-activity relationships

Analytical data:

Sodium 1-amino-9,10-dioxo-4-((4-(phenylamino)-3-sulfonatophenyl)amino)-9,10-dihydroanthracene-2-sulfonate (**14**, **PSB-0739**)

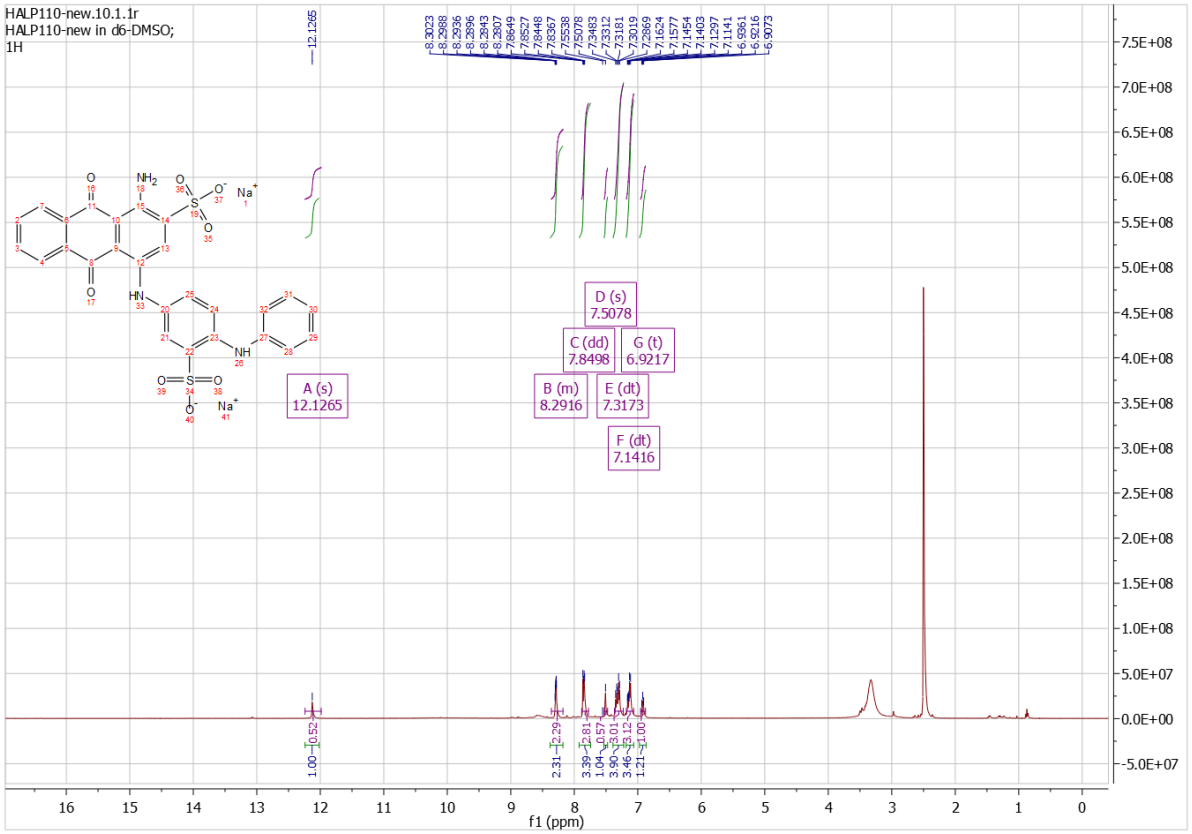


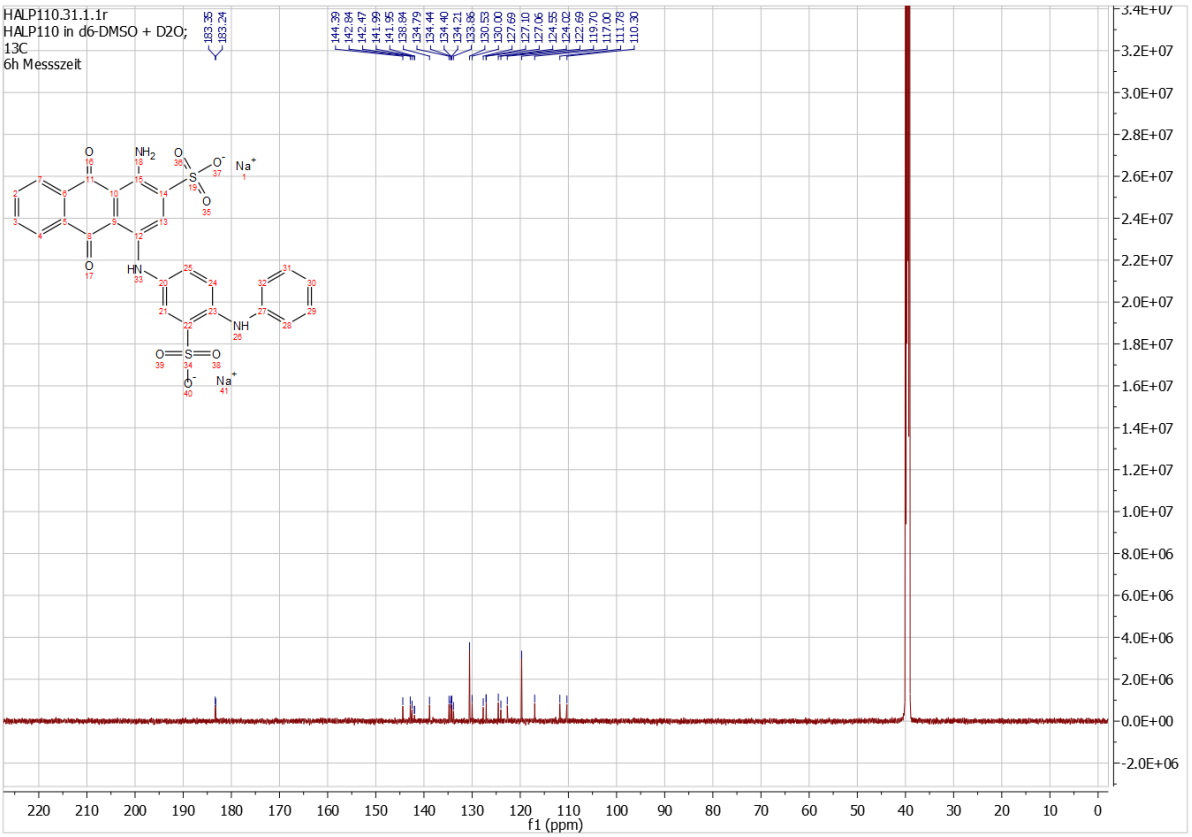
Sequence Name:	SingleSample		
Data file:	HALP110-F2.dx	**Project Name:**	Single Quad
Sample name:	HALP110-F2	**Operator :**	SYSTEM
Instrument:	Single Quad	**Acquired on:**	2022-02-11 07:18:31+01:00
Inj. volume:	3.000	**Location:**	P2-E6
Acq. method:	00-new_wasser-acn_standard_100-1500_BD-20min.amx		
Processing method:	MS_standard_plot.pmx		

Signal: DAD1 Total WL (220.0:600.0 nm)

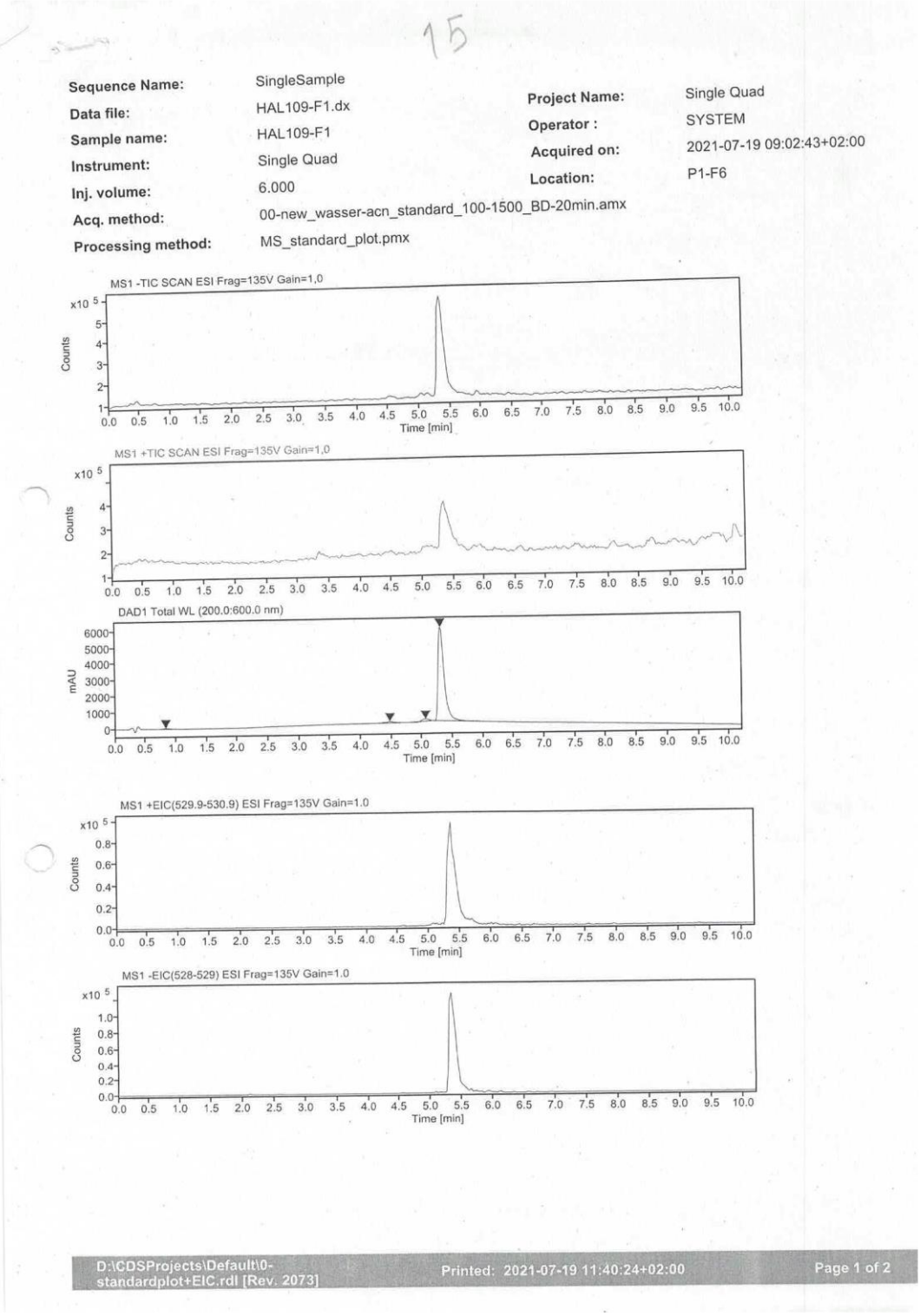
RT [min]	Peak MS Base Peak m/z	Area	Area%	Max Peak%	Height
3.482		51.0921	0.0619	0.062	18.970
4.298	564.200	82412.8013	99.9080	100.000	19955.990
4.732		24.7570	0.0300	0.030	9.014
	Sum	82488.6504			

D:\CDSProjects\Default\0-standardplot+EIC.rdl [Rev. 5165] Printed: 2022-02-11 10:02:32+01:00 Page 1 of 2


HALP110-new.10.1.1r
HALP110-new in d6-DMSO;
1H
A (s)
12.1265
B (m)
8.2916
C (dd)
7.8498
D (s)
7.5078
E (dt)
7.3173
F (dt)
7.1416
G (t)
6.9217
f1 (ppm)


HALP110.31.1.1r
HALP110 in d6-DMSO + D2O;
13C
6h Messszeit
f1 (ppm)

Sodium 5-((4-amino-3-carboxy-9,10-dioxo-9,10-dihydroanthracen-1-yl)amino)-2-(phenylamino)benzenesulfonate (**15**, **PSB-0702**)



Signal: DAD1 Total WL (200.0:600.0 nm)

RT [min]	Peak MS Base Peak m/z	Area	Area%	Max Peak%	Height
0.835		288.5829	0.6899	0.725	38.836
4.474		833.0257	1.9914	2.093	84.281
5.055		903.2770	2.1594	2.269	137.368
5.305		39805.3075	95.1593	100.000	5737.139
	Sum	41830.1931			

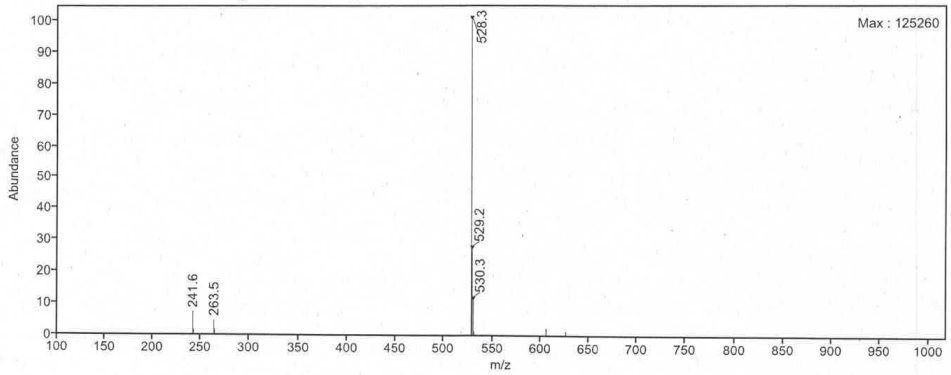
Signal: MS1 +TIC SCAN ESI Frag=135V Gain=1,0

RT [min]	Peak MS Base Peak m/z	Area	Area%	Max Peak%	Height
5.344	530.200	1584479.4867	100.0000	100.000	189041.372
	Sum	1584479.4867			

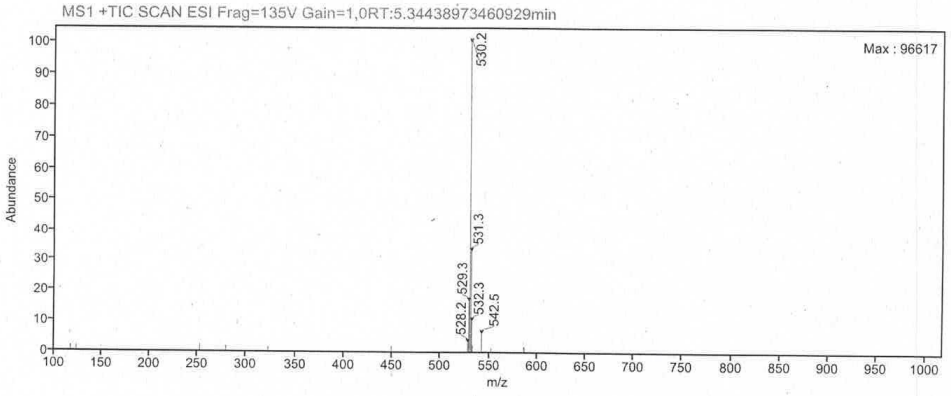
Signal: MS1 -TIC SCAN ESI Frag=135V Gain=1,0

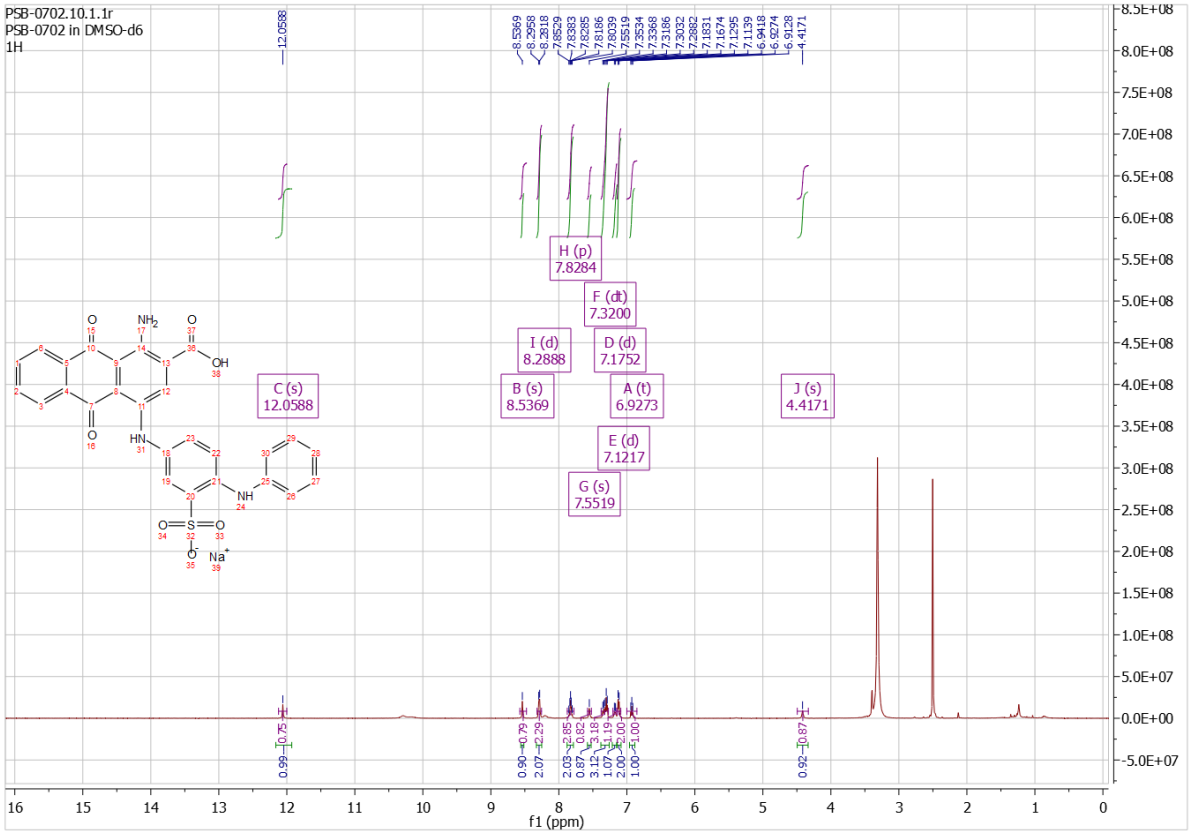
RT [min]	Peak MS Base Peak m/z	Area	Area%	Max Peak%	Height
5.339	528.300	3969655.5193	100.0000	100.000	468983.754
	Sum	3969655.5193			

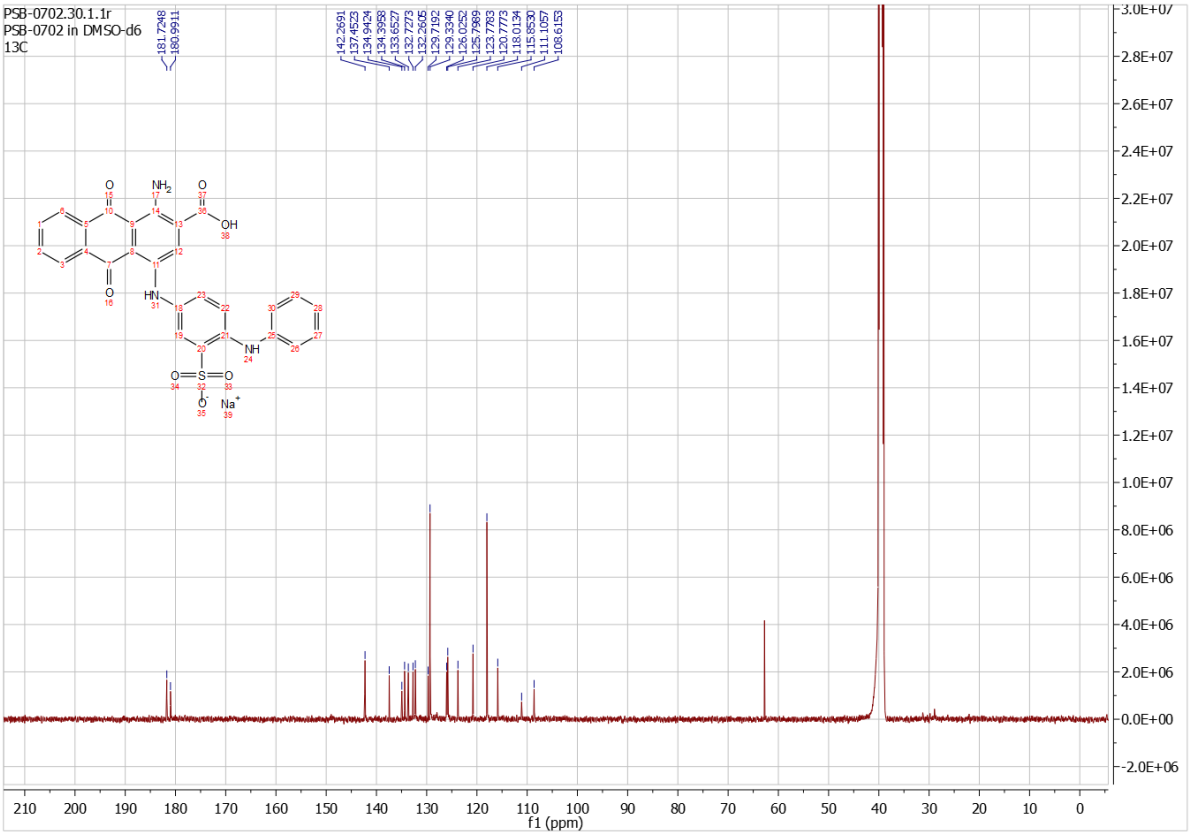
MS1 -TIC SCAN ESI Frag=135V Gain=1,0RT:5.33891857239251min



MS1 +TIC SCAN ESI Frag=135V Gain=1,0RT:5.34438973460929min



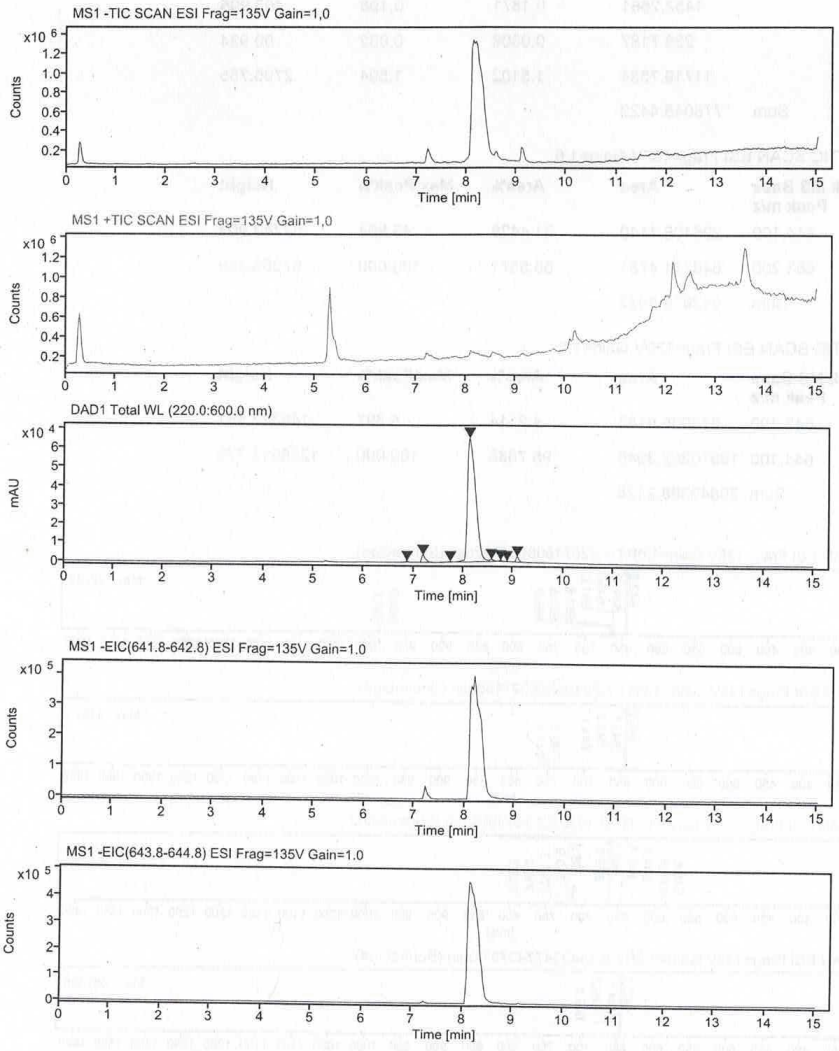

PSB-0702.10.1.1r
PSB-0702 in DMSO-d6
1H
C (s)
12.0588
H (p)
7.8284
F (dt)
7.3200
I (d)
8.2888
D (d)
7.1752
B (s)
8.5369
A (t)
6.9273
J (s)
4.4171
E (d)
7.1217
G (s)
7.5519
f1 (ppm)


PSB-0702.30.1.1r
PSB-0702 in DMSO-d6
13C
f1 (ppm)

Sodium 1-amino-4-((4-((4-bromophenyl)amino)-3-sulfonatophenyl)amino)- 9,10-dioxo-9,10-dihydroanthracene-2-sulfonate (**16**)

16

Sequence Name:	SingleSample		
Data file:	HALP174-F2-meoh.dx	**Project Name:**	Single Quad
Sample name:	HALP174-F2-meoh	**Operator :**	SYSTEM
Instrument:	Single Quad	**Acquired on:**	2022-03-18 08:56:22+01:00
Inj. volume:	3.000	**Location:**	P2-A5
Acq. method:	00-new_wasser-meoh_standard_100-1000_CD-20min.amx		
Processing method:	MS_standard_plot.pmx		



Signal: DAD1 Total WL (220.0:600.0 nm)

RT [min]	Peak MS Base Peak m/z	Area	Area%	Max Peak%	Height
6.869		2171.4560	0.2798	0.295	362.634
7.191	644.100	18995.3054	2.4477	2.584	3671.963
7.737		669.0571	0.0862	0.091	96.423
8.115	644.100	735231.0932	94.7407	100.000	64852.410
8.561		5567.7931	0.7175	0.757	1109.699
8.746		1452.2661	0.1871	0.198	405.995
8.874		238.7187	0.0308	0.032	90.934
9.084		11719.7534	1.5102	1.594	2795.755
	Sum	776045.4429			

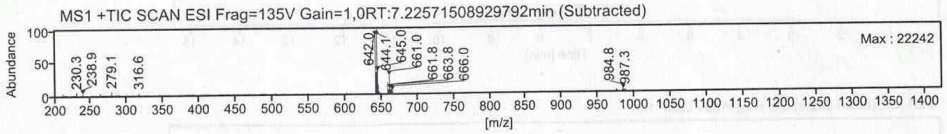
Signal: MS1 +TIC SCAN ESI Frag=135V Gain=1,0

RT [min]	Peak MS Base Peak m/z	Area	Area%	Max Peak%	Height
7.226	644.100	296405.4140	31.4429	45.864	57743.903
8.103	663.200	646271.4781	68.5571	100.000	67253.236
	Sum	942676.8922			

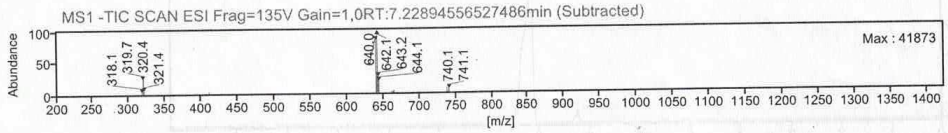
Signal: MS1 -TIC SCAN ESI Frag=135V Gain=1,0

RT [min]	Peak MS Base Peak m/z	Area	Area%	Max Peak%	Height
7.229	642.100	878005.8183	4.2114	4.397	149373.581
8.144	644.100	19970362.3945	95.7886	100.000	1255611.779
	Sum	20848368.2128			

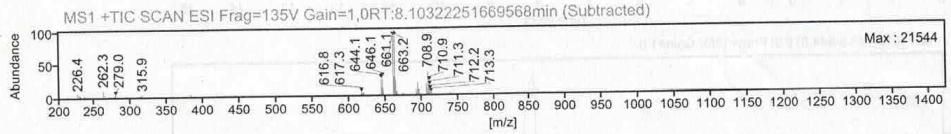
MS1 +TIC SCAN ESI Frag=135V Gain=1,0RT:7.22571508929792min (Subtracted)



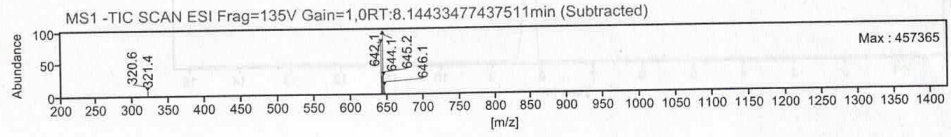
MS1 -TIC SCAN ESI Frag=135V Gain=1,0RT:7.22894556527486min (Subtracted)

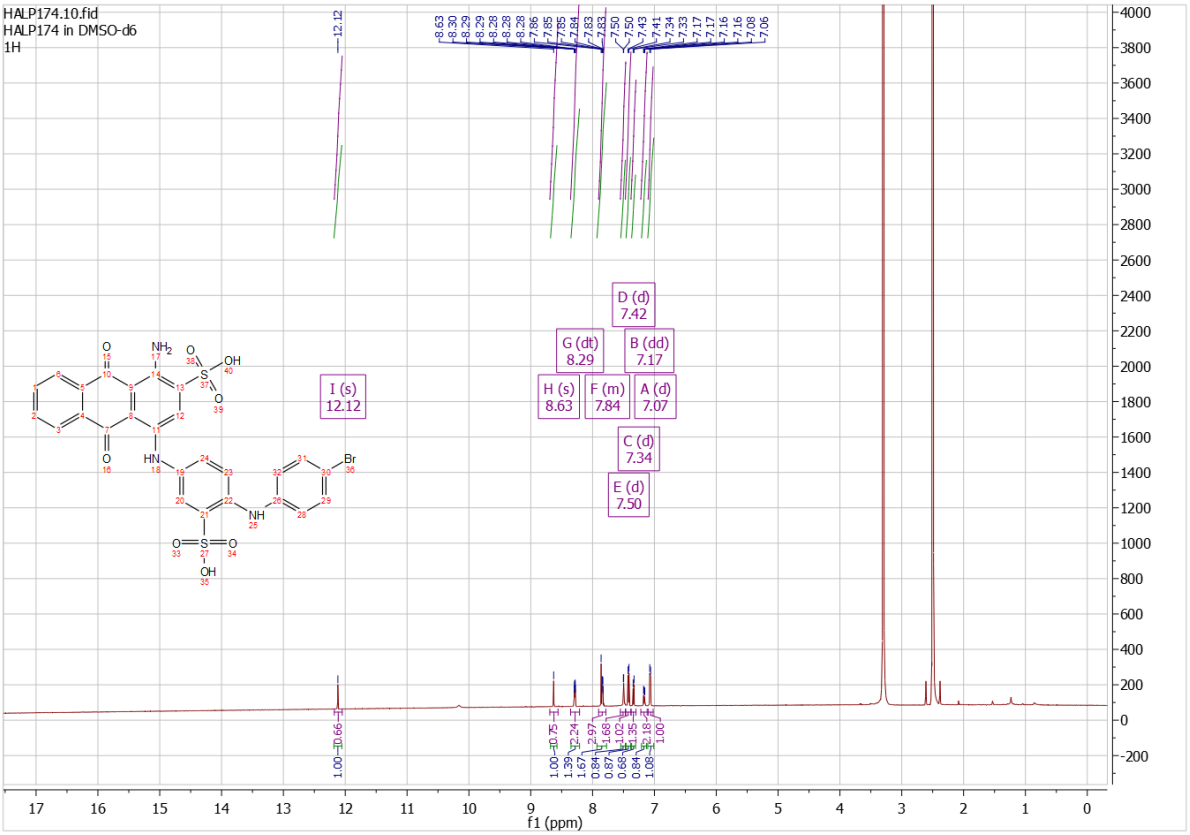


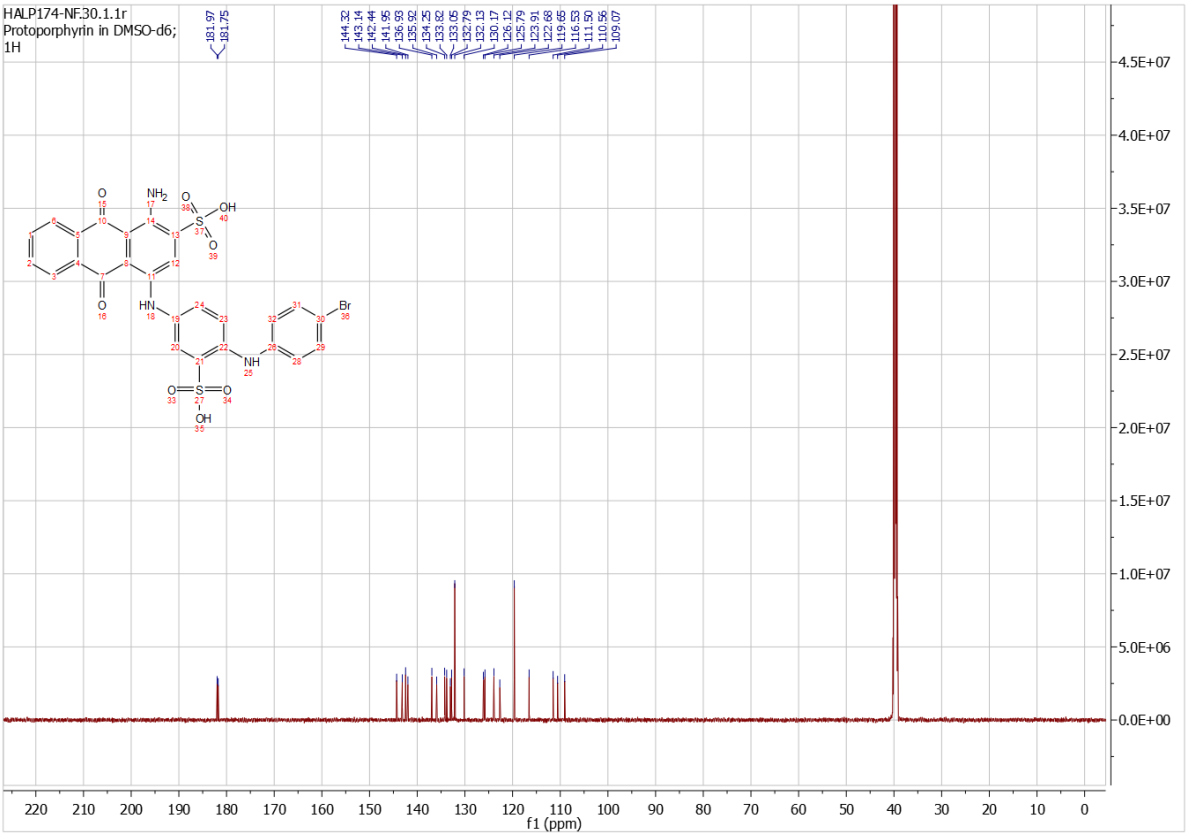
MS1 +TIC SCAN ESI Frag=135V Gain=1,0RT:8.10322251669568min (Subtracted)



MS1 -TIC SCAN ESI Frag=135V Gain=1,0RT:8.14433477437511min (Subtracted)



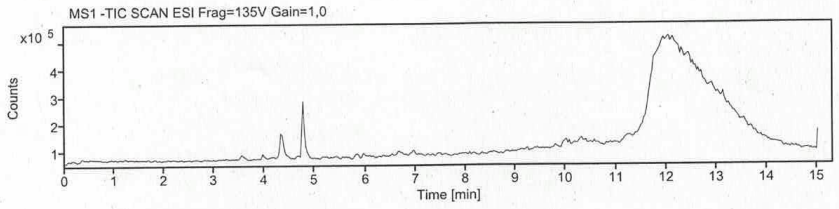

HALP174.10.fid
HALP174 in DMSO-d6
1H
I (s)
12.12
D (d)
7.42
G (dt)
8.29
B (dd)
7.17
H (s)
8.63
F (m)
7.84
A (d)
7.07
C (d)
7.34
E (d)
7.50
f1 (ppm)

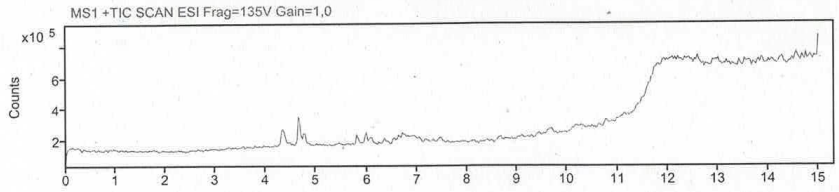

HALP174-NF.30.1.1r
Protoporphyrin in DMSO-d6;
1H
f1 (ppm)

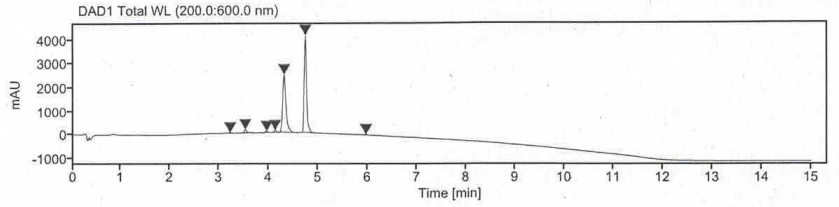
Sodium 5-((4-amino-3-carboxy-9,10-dioxo-9,10-dihydroanthracen-1-yl)amino)-2-((4-bromophenyl)amino)benzenesulfonate (**17**)

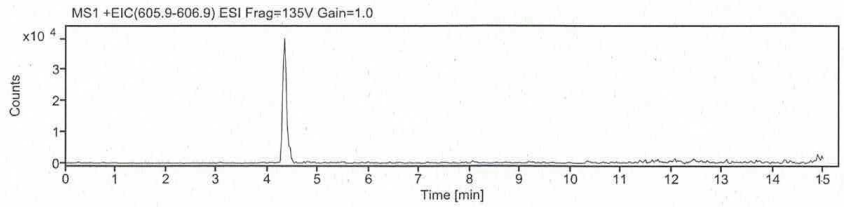
17

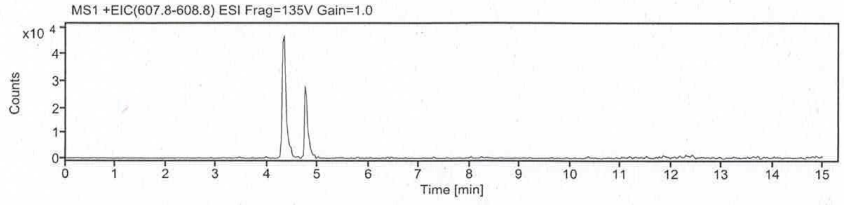
Sequence Name:	2021-06-11		
Data file:	HAL96-N.dx	**Project Name:**	Single Quad
Sample name:	HAL96-N	**Operator :**	SYSTEM
Instrument:	Single Quad	**Acquired on:**	2021-06-11 19:09:22+02:00
Inj. volume:	5.000	**Location:**	P2-B10
Acq. method:	00-new_wasser-acn_standard_100-1000_BD-20min.amx		
Processing method:	MS_standard_plot.pmx		











D:\CDSProjects\Default\0-standardplot+EIC.rdl [Rev. 1710] Printed: 2021-06-14 08:00:34+02:00 Page 1 of 3

Signal: DAD1 Total WL (200.0:600.0 nm)

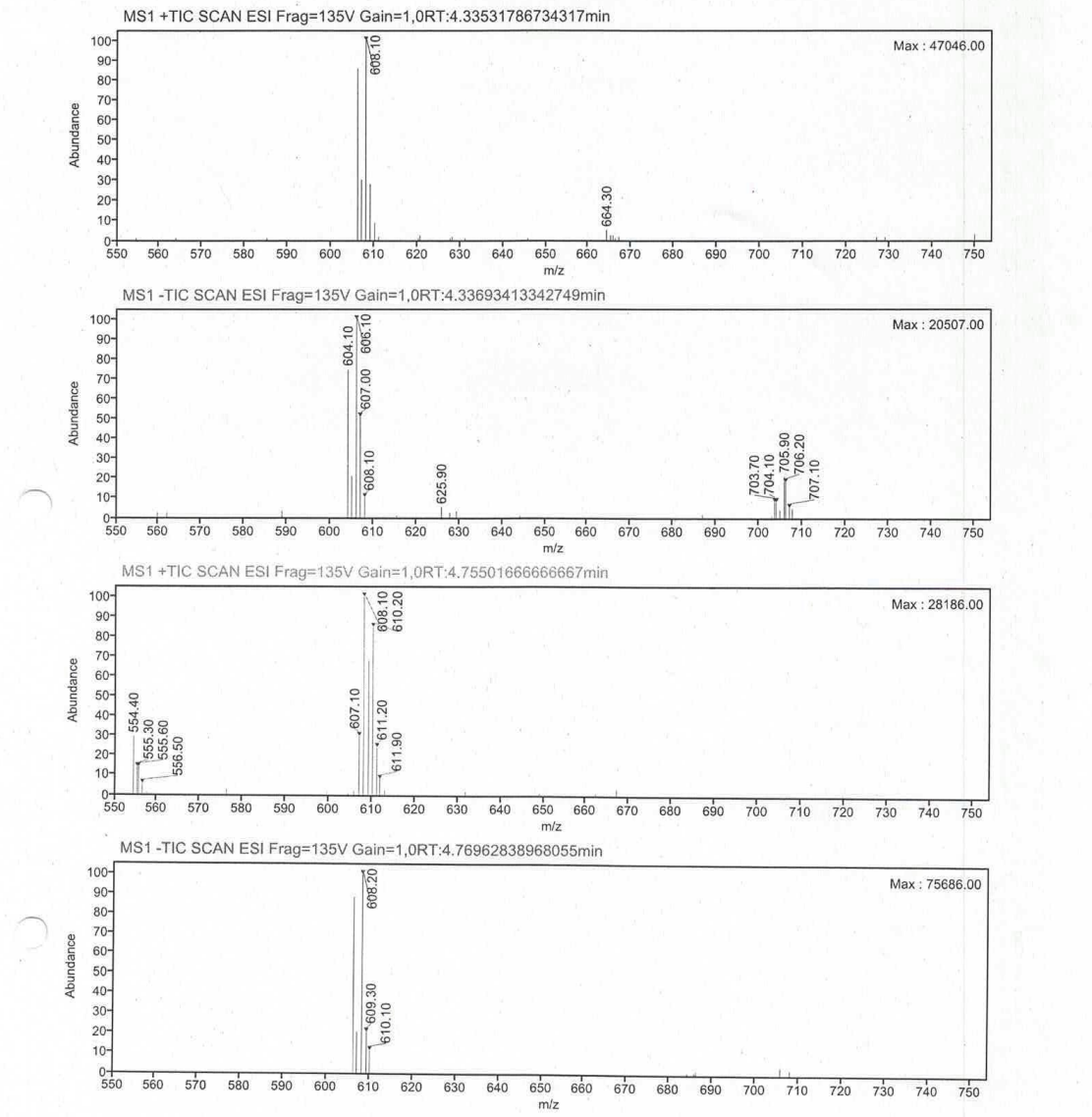
RT [min]	Peak MS Base Peak m/z	Area	Area%	Max Peak%	Height
3.214		57.3569	0.2220	0.430	18.587
3.521		465.2890	1.8012	3.485	140.406
3.949		196.0343	0.7589	1.468	66.851
4.120		212.9899	0.8245	1.595	83.964
4.301		11473.8973	44.4173	85.948	2453.468
4.734		13349.7507	51.6790	100.000	4109.977
5.954		76.7216	0.2970	0.575	22.610
	Sum	25832.0397			

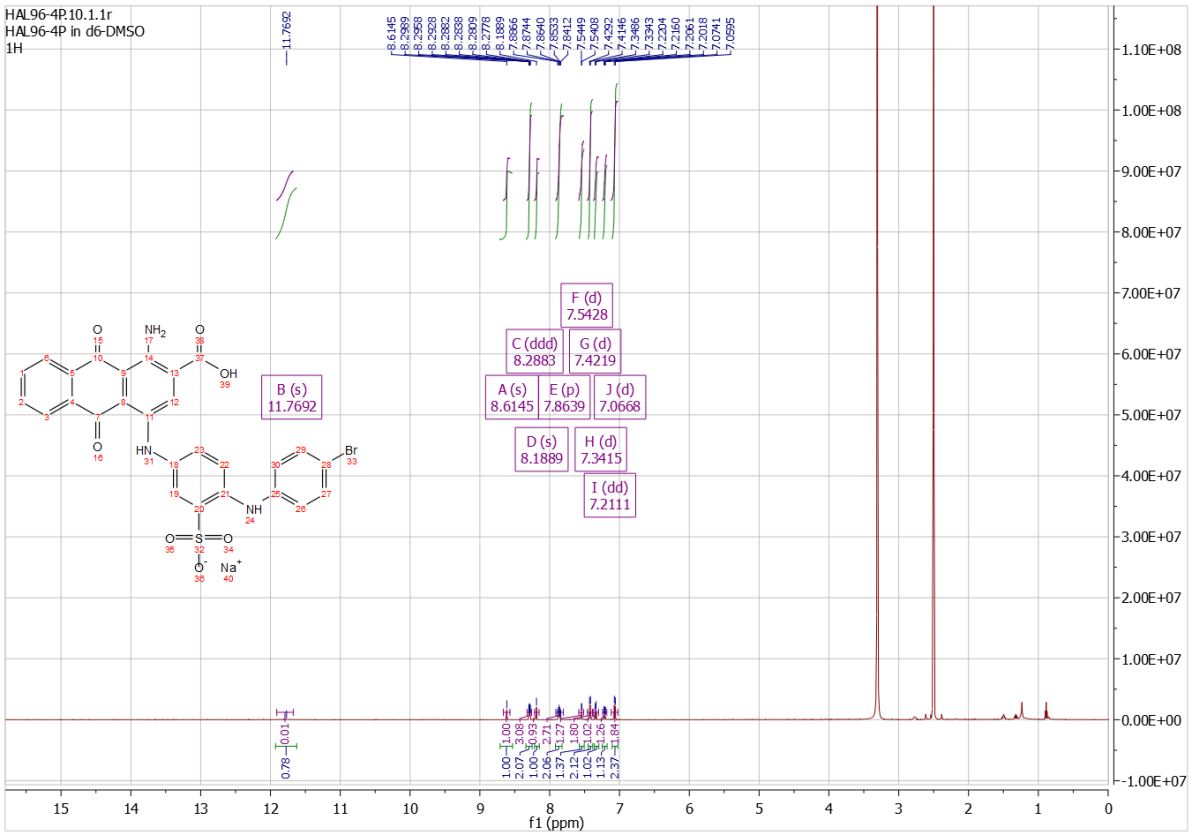
Signal: MS1 +TIC SCAN ESI Frag=135V Gain=1,0

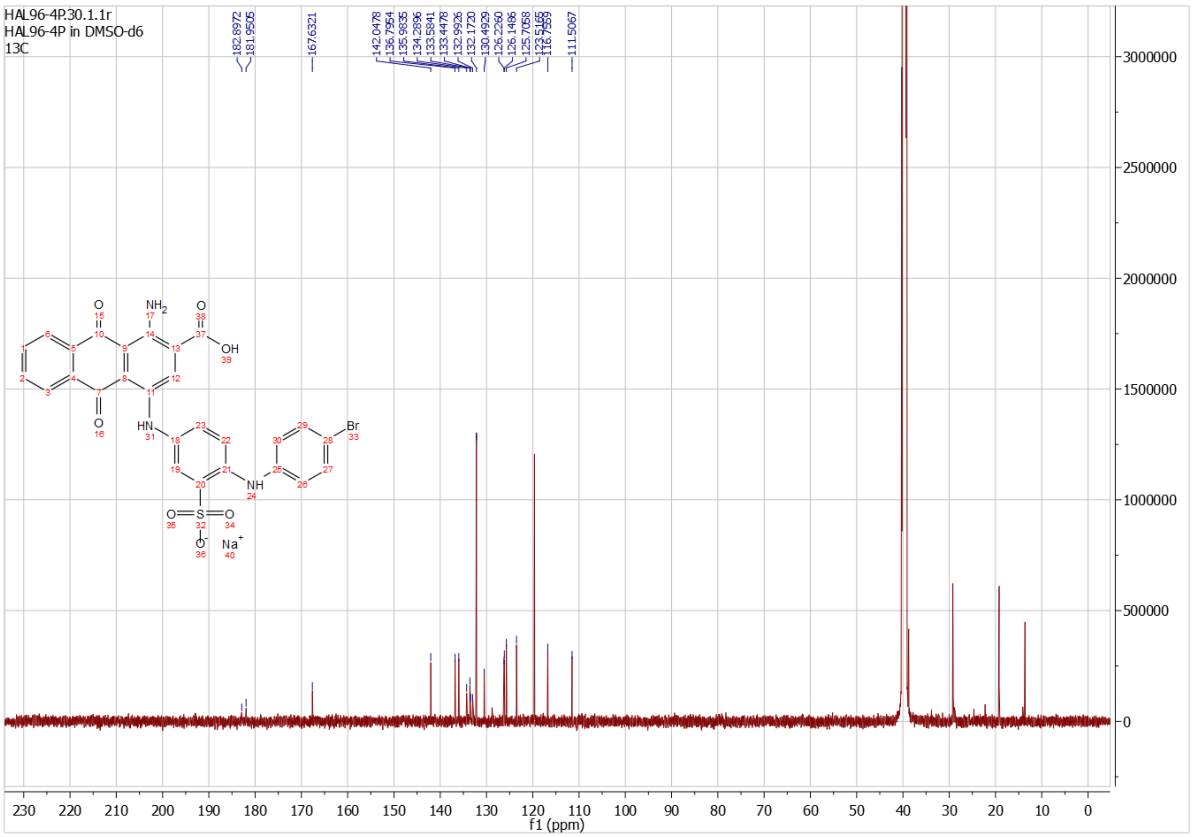
RT [min]	Peak MS Base Peak m/z	Area	Area%	Max Peak%	Height
4.335	608.100	498264.5817	80.3385	100.000	96616.620
4.755	608.100	121942.0392	19.6615	24.473	37235.545
	Sum	620206.6208			

Signal: MS1 -TIC SCAN ESI Frag=135V Gain=1,0

RT [min]	Peak MS Base Peak m/z	Area	Area%	Max Peak%	Height
4.337	606.100	363770.1873	32.7523	48.704	83752.544
4.770	608.200	746900.0460	67.2477	100.000	205856.733
	Sum	1110670.2332			


MS1 +TIC SCAN ESI Frag=135V Gain=1,0RT:4.33531786734317min
Max : 47046.00
608.10
664.30
MS1 -TIC SCAN ESI Frag=135V Gain=1,0RT:4.33693413342749min
Max : 20507.00
604.10
606.10
607.00
608.10
625.90
703.70
704.10
705.90
706.20
707.10
MS1 +TIC SCAN ESI Frag=135V Gain=1,0RT:4.75501666666667min
Max : 28186.00
554.40
555.30
555.60
556.50
607.10
608.10
610.20
611.20
611.90
MS1 -TIC SCAN ESI Frag=135V Gain=1,0RT:4.76962838968055min
Max : 75686.00
608.20
609.30
610.10
Abundance
m/z

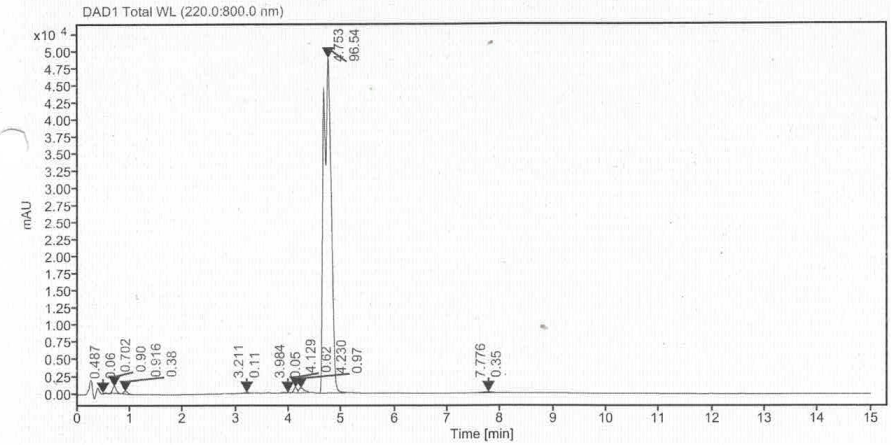

HAL96-4P.10.1.1r
HAL96-4P in d6-DMSO
1H
B (s)
11.7692
F (d)
7.5428
C (ddd)
8.2883
G (d)
7.4219
A (s)
8.6145
E (p)
7.8639
J (d)
7.0668
D (s)
8.1889
H (d)
7.3415
I (dd)
7.2111
f1 (ppm)

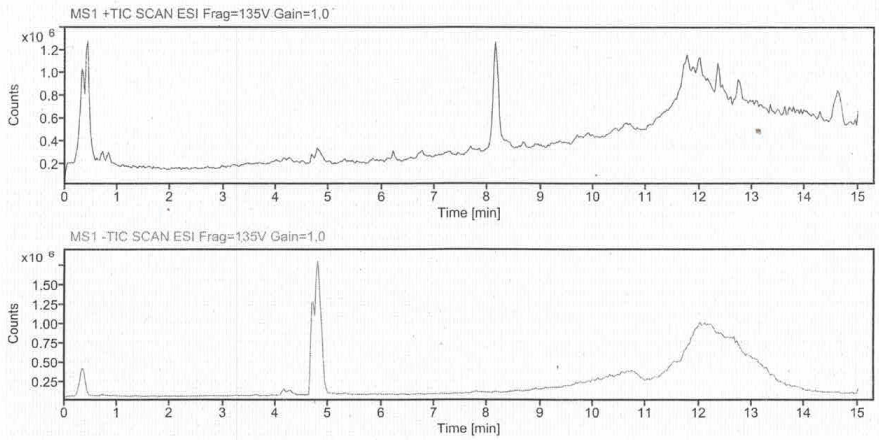

HAL96-4P.30.1.1r
HAL96-4P in DMSO-d6
13C
f1 (ppm)

Sodium 1-amino-4-bromo-6/7-chloro-9,10-dioxo-9,10-dihydroanthracene-2-sulfonate (**21**, 6-F1 & F2)

21 ✓

Sequence Name:	SingleSample		
Data file:	HAL25N.dx	**Project Name:**	Single Quad
Sample name:	HAL25N	**Operator :**	SYSTEM
Instrument:	Single Quad	**Acquired on:**	2020-09-14 07:09:32+02:00
Inj. volume:	3.000	**Location:**	P1-B2
Acq. method:	0_wasser-acn_standard_100-1000_AC-20min.amx		
Processing method:	MS_standard_plot.pmx		





Signal: DAD1 Total WL (220.0:800.0 nm)

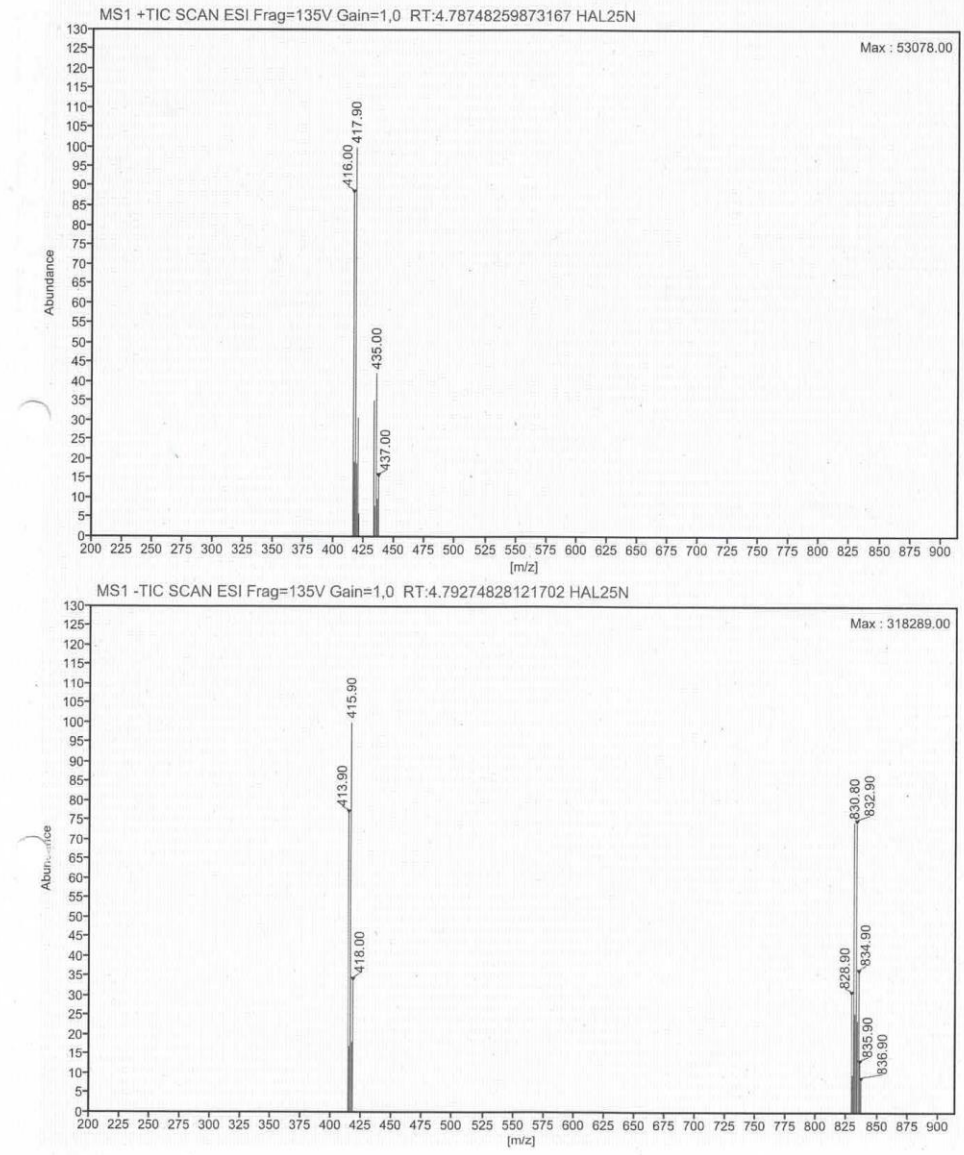
RT [min]	Peak MS Base Peak m/z	Type	Width [min]	Col0	Area	Height	Area%
0.487		MM n	0.1758		331.2834	62.6775	0.0639
0.702		MM m	0.1954		4681.1331	981.7292	0.9028
0.916		MM m	0.2345		1963.1130	367.3209	0.3786
3.211		MM m	0.2735		593.8902	135.6777	0.1145
3.984		MM m	0.2735		270.8829	53.8534	0.0522
4.129		MM m	0.1172		3223.6041	815.4794	0.6217
4.230		MM m	0.2735		5048.0768	693.2526	0.9735
4.753	417.900	MM m	0.6643		500615.0497	48903.8798	96.5439
7.776		MM m	0.4689		1809.1291	141.6129	0.3489
				Sum	518536.1624		

Signal: MS1 +TIC SCAN ESI Frag=135V Gain=1,0

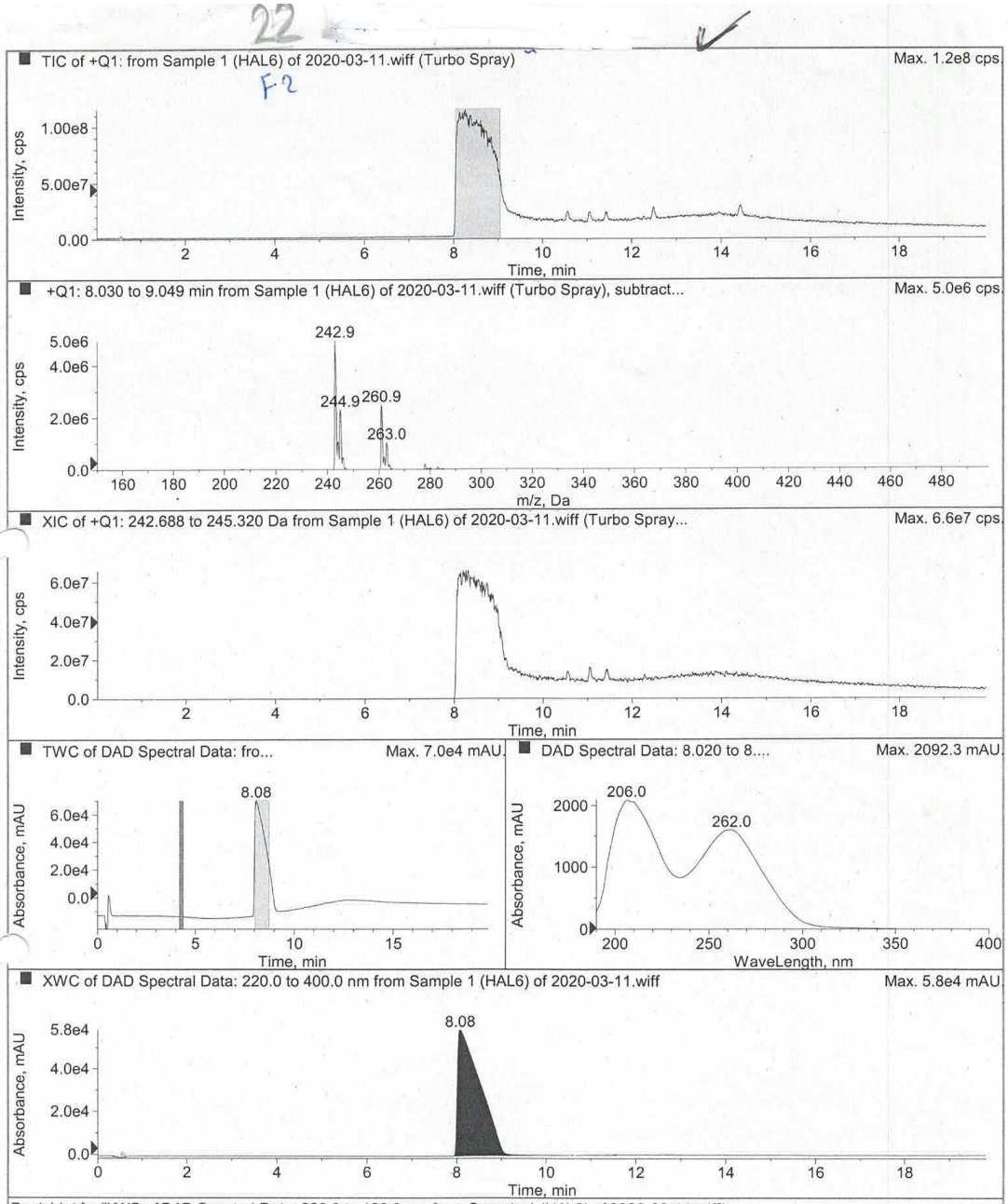
RT [min]	Peak MS Base Peak m/z	Type	Width [min]	Col0	Area	Height	Area%
4.787	417.900	MM m	0.3126		1086212.4481	127867.1995	100.0000
				Sum	1086212.4481		

Signal: MS1 -TIC SCAN ESI Frag=135V Gain=1,0

RT [min]	Peak MS Base Peak m/z	Type	Width [min]	Col0	Area	Height	Area%
4.793	415.900	MM m	0.3908		18569824.5015	1725745.5379	100.0000
				Sum	18569824.5015		


MS1 +TIC SCAN ESI Frag=135V Gain=1,0 RT:4.78748259873167 HAL25N
Max : 53078.00
Abundance
416.00
417.90
435.00
437.00
[m/z]
MS1 -TIC SCAN ESI Frag=135V Gain=1,0 RT:4.79274828121702 HAL25N
Max : 318289.00
415.90
413.90
418.00
830.80
832.90
826.90
834.90
835.90
836.90
[m/z]

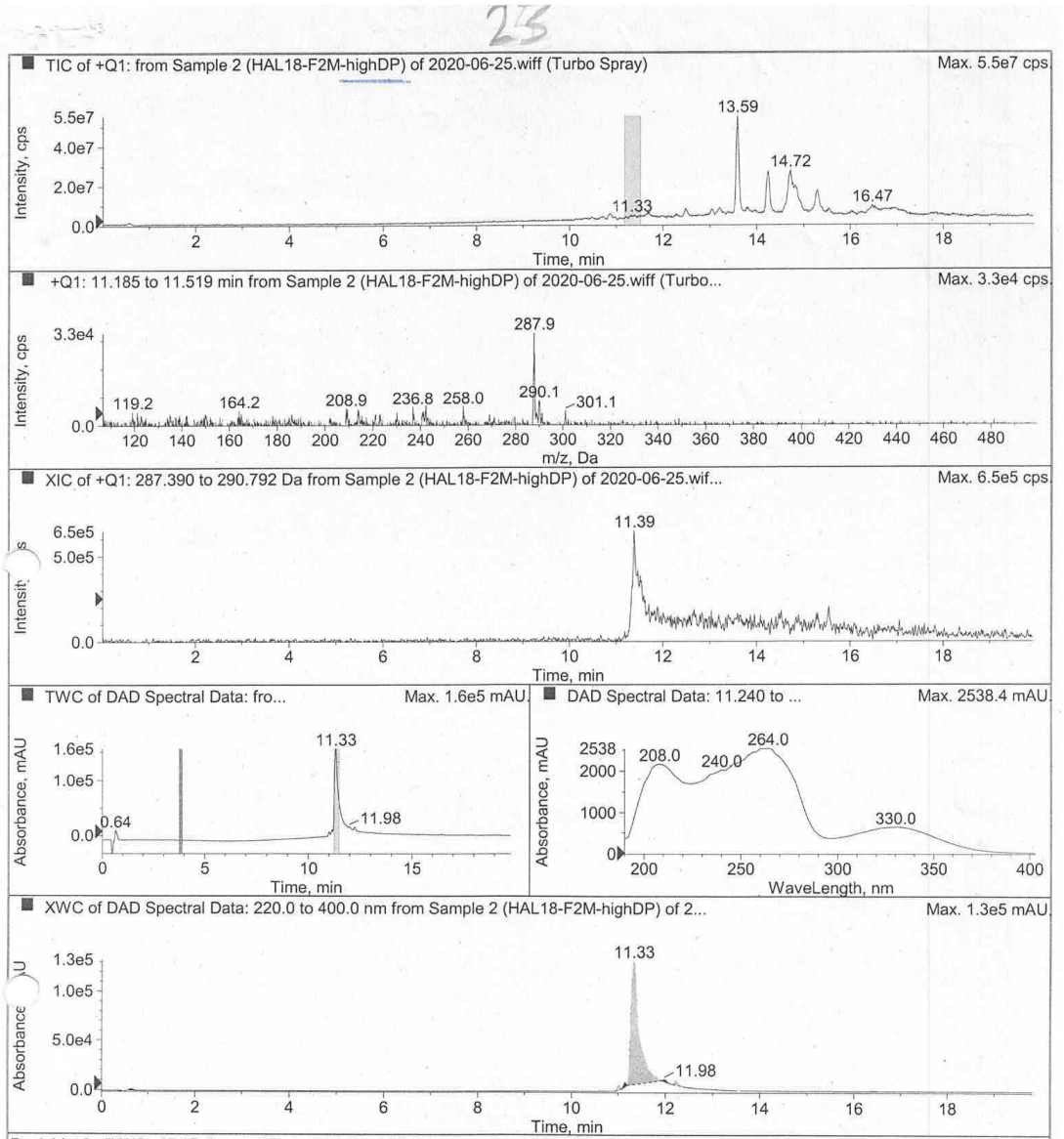
2-Chloroanthraquinone (**22**)



Peak List for "XWC of DAD Spectral Data: 220.0 to 400.0 nm from Sample 1 (HAL6) of 2020-03-11.wiff"

	Time (min)	Area (mAU x min)	% Area	Height (mAU)	% Height	Width (min)	Baseline Type
1	0.3567	1542.5527	0.0733	382.0052	0.6141	0.1133	Base to Base
2	0.5503	1.6900e4	0.8027	2415.3737	3.8827	0.2600	Base to Base
3	8.0763	2.0850e6	99.0257	5.8994e4	94.8319	2.1000	Base to Base
4	10.5475	1097.1596	0.0521	184.0221	0.2958	0.2667	Base to Base
5	11.5505	973.2597	0.0462	233.6253	0.3755	0.1800	Base to Base

6-/7-Chloro-1-nitroanthraquinone (**23-F1 and F2**)



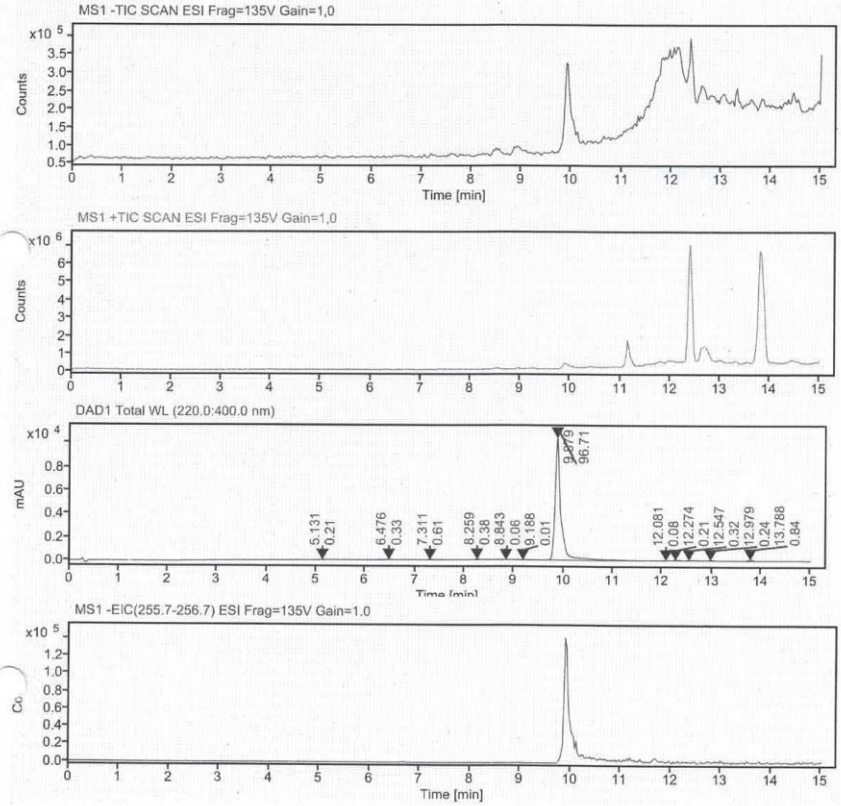
Peak List for "XWC of DAD Spectral Data: 220.0 to 400.0 nm from Sample 2 (HAL18-F2M-highDP) of 2020-06-25.wiff"

	Time (min)	Area (mAU x min)	% Area	Height (mAU)	% Height	Width (min)	Baseline Type
1	0.4060	2998.1873	0.1841	730.8014	0.5049	0.1200	Base to Base
2	0.5452	2251.8226	0.1383	634.8912	0.4386	0.1067	Base to Base
3	0.6311	9121.3236	0.5602	1467.0124	1.0135	0.2267	Base to Base
4	11.0078	1.9617e4	1.2048	4765.3118	3.2922	0.1533	Base to Base
5	11.1495	1.4613e4	0.8974	4328.8005	2.9906	0.1067	Base to Base
6	11.3314	1.5440e6	94.8259	1.2542e5	86.6478	0.7333	Base to Base
7	11.9834	1.0255e4	0.6298	2225.2761	1.5373	0.1600	Base to Base
8	12.2266	2.1772e4	1.3371	4502.0344	3.1103	0.2467	Base to Base
9	13.0713	1261.7287	0.0775	223.2547	0.1542	0.2133	Base to Base
10	13.5387	778.2063	0.0478	207.2042	0.1431	0.1400	Base to Base
11	16.4352	1580.0901	0.0970	242.3393	0.1674	0.3267	Base to Base

1-Nitro-6/7-chloro-9,10-dioxo-9,10-dihydroanthracene (**24**)

24

Sequence Name:	2020-10-09_LCMS_MeOH		
Data file:	2020-10-09 16-30-51+02-00.dx	**Project Name:**	Single Quad
Sample name:	HAL20new	**Operator :**	SYSTEM
Instrument:	Single Quad	**Acquired on:**	2020-10-09 16:31:48+02:00
Inj. volume:	3.000	**Location:**	P1-B1
Acq. method:	0_wasser-meoh_standard_100-1000_BD-20min.amx		
Processing method:	MS_standard_plot-new.pmx		



Signal: DAD1 Total WL (220.0:400.0 nm)

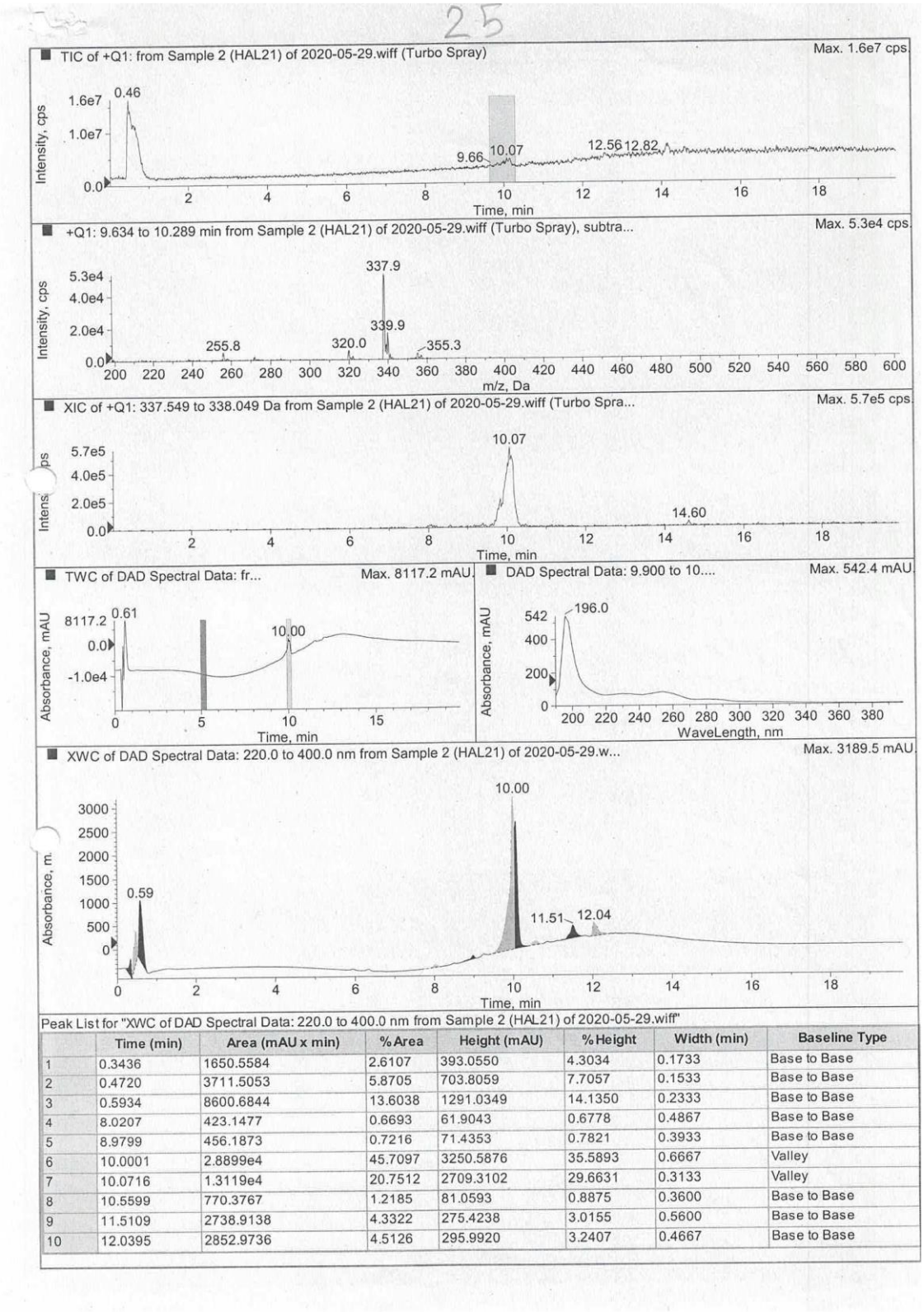
RT [min]	Name	Area	Area%	Max Peak%	Height	Type
5.131		183.8241	0.2088	0.216	31.761	MM m
6.476		293.6776	0.3336	0.345	37.847	MM m
7.311		532.9484	0.6054	0.626	34.387	MM m
8.259		335.7595	0.3814	0.394	53.449	MM m
8.843		49.1133	0.0558	0.058	11.486	MM m
9.188		9.0704	0.0103	0.011	7.463	MM n

RT [min]	Name	Area	Area%	Max Peak%	Height	Type
9.879		85144.8769	96.7136	100.000	10311.510	MM m
12.081		73.5330	0.0835	0.086	12.228	MM m
12.274		186.2395	0.2115	0.219	33.969	MM m
12.547		277.5717	0.3153	0.326	22.408	MM m
12.979		214.9044	0.2441	0.252	48.778	MM m
13.788		736.6783	0.8368	0.865	119.970	MM m
	Sum	88038.1971				

Signal: MS1 -TIC SCAN ESI Frag=135V Gain=1,0

RT [min]	Name	Area	Area%	Max Peak%	Height	Type
9.919		2086691.2302	100.0000	100.000	247970.176	MM m
	Sum	2086691.2302				

Sodium 1-amino-6/7-chloro-9,10-dioxo-9,10-dihydroanthracene-2-sulfonate (**25**)



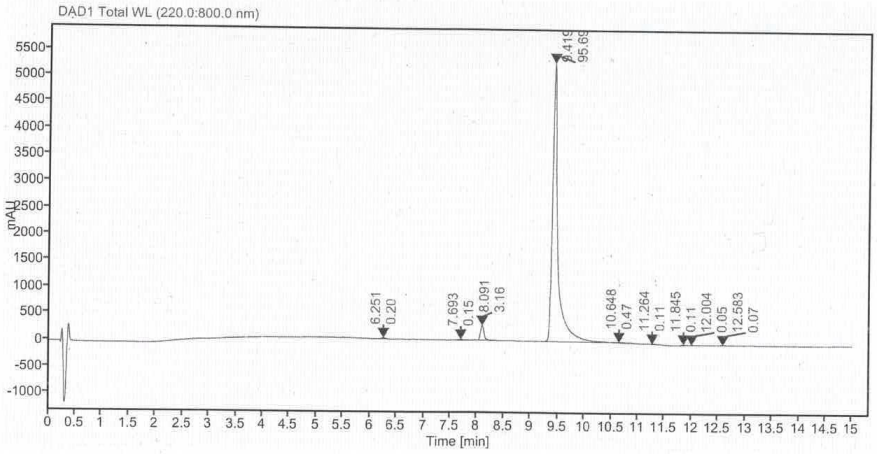
Peak List for "XWC of DAD Spectral Data: 220.0 to 400.0 nm from Sample 2 (HAL21) of 2020-05-29.wiff"

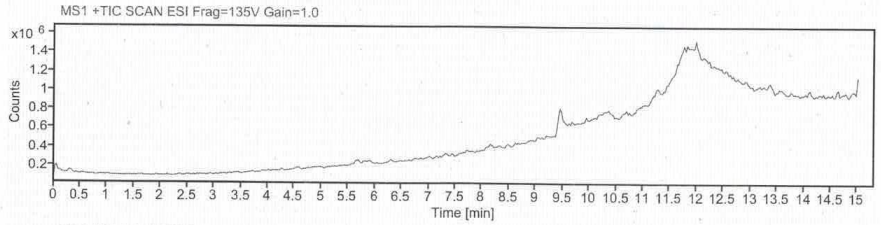
	Time (min)	Area (mAU x min)	% Area	Height (mAU)	% Height	Width (min)	Baseline Type
1	0.3436	1650.5584	2.6107	393.0550	4.3034	0.1733	Base to Base
2	0.4720	3711.5053	5.8705	703.8059	7.7057	0.1533	Base to Base
3	0.5934	8600.6844	13.6038	1291.0349	14.1350	0.2333	Base to Base
4	8.0207	423.1477	0.6693	61.9043	0.6778	0.4867	Base to Base
5	8.9799	456.1873	0.7216	71.4353	0.7821	0.3933	Base to Base
6	10.0001	2.8899e4	45.7097	3250.5876	35.5893	0.6667	Valley
7	10.0716	1.3119e4	20.7512	2709.3102	29.6631	0.3133	Valley
8	10.5599	770.3767	1.2185	81.0593	0.8875	0.3600	Base to Base
9	11.5109	2738.9138	4.3322	275.4238	3.0155	0.5600	Base to Base
10	12.0395	2852.9736	4.5126	295.9920	3.2407	0.4667	Base to Base

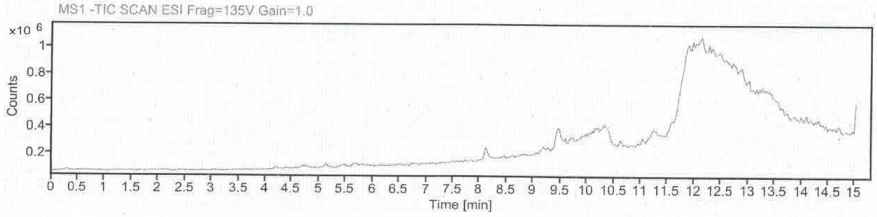
1-Amino-2,4-dibromo-6/7-chloroanthracene-9,10-dione (**26-F1/F2**)

26-F1

Sequence Name:	SingleSample		
Data file:	2020-06-18.dx	**Project Name:**	Single Quad
Sample name:	HAL23-F1	**Operator :**	SYSTEM
Instrument:	Single Quad	**Acquired on:**	2020-06-18 11:21:30+02:00
Inj. volume:	3.000	**Location:**	P2-B2
Acq. method:	0_wasser-acn_standard_100-1000_AC-20min.amx		
Processing method:	MS_standard_plot.pmx		







Signal: DAD1 Total WL (220.0:800.0 nm)

RT [min]	Peak MS Base Peak m/z	Type	Width [min]	Col0	Area	Height	Area%
6.251		MM m	0.0581		77.5709	20.5236	0.1950
7.693		MM m	0.0713		59.4891	12.5526	0.1496
8.091	544.000	MM m	0.0690		1257.6505	276.6351	3.1620
9.419		MM m	0.1043		38059.0640	5269.8569	95.6881
10.648		MM m	0.2353		186.4466	9.7394	0.4688
11.264		MM m	0.1644		44.7670	3.3396	0.1126
11.845		MM m	0.0671		43.0304	10.6679	0.1082
12.004		MM m	0.0782		19.7249	4.0954	0.0496
12.583		MM m	0.0865		26.3561	4.9180	0.0663
				Sum	39774.0995		

Signal: MS1 +TIC SCAN ESI Frag=135V Gain=1.0

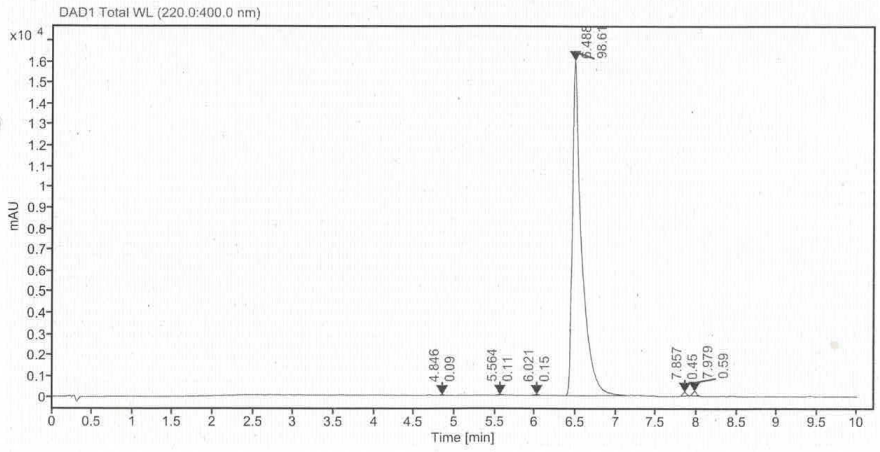
RT [min]	Peak MS Base Peak m/z	Type	Width [min]	Col0	Area	Height	Area%
8.156	546.300	MM m	0.1362		494339.6189	55938.7324	29.5581
9.450	416.000	MM m	0.0785		1178095.9042	250195.9738	70.4419
				Sum	1672435.5231		

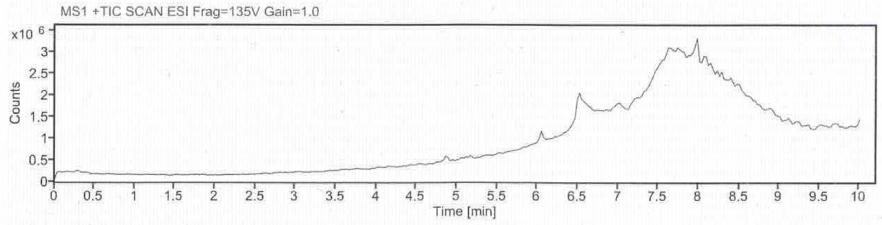
Signal: MS1 -TIC SCAN ESI Frag=135V Gain=1.0

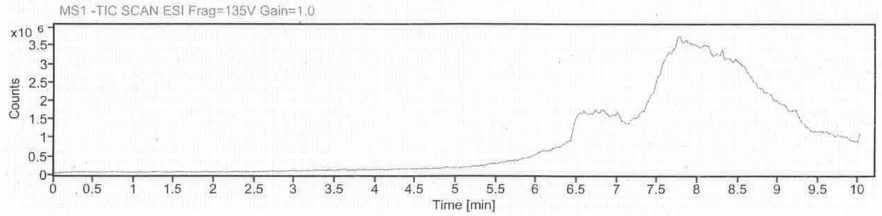
RT [min]	Peak MS Base Peak m/z	Type	Width [min]	Col0	Area	Height	Area%
8.118	544.000	MM m	0.0775		451725.8866	97153.2893	20.0067
9.468	391.500	MM m	0.1258		1806151.3843	208719.9166	79.9933
				Sum	2257877.2708		

26-F2

Sequence Name:	2020-06-22		
Data file:	2020-06-22 11-32-28+02-00.dx	**Project Name:**	Single Quad
Sample name:	HAL23-F2	**Operator :**	SYSTEM
Instrument:	Single Quad	**Acquired on:**	2020-06-22 11:33:25+02:00
Inj. volume:	3.000	**Location:**	P2-C1
Acq. method:	0_wasser-acn_standard_100-1000_AC_15min.amx		
Processing method:	*MS_standard_plot-new.pmx		







Signal: DAD1 Total WL (220.0:400.0 nm)

RT [min]	Peak MS Base Peak m/z	Type	Width [min]	Col0	Area	Height	Area%
4.846		MM m	0.0455		121.6155	42.3814	0.0928
5.564		MM m	0.0548		148.7379	42.4910	0.1135
6.021		MM m	0.0608		190.8870	47.6325	0.1456
6.488	852.900	MM m	0.1102		129247.3410	16009.2943	98.6076
7.857		MM m	0.0502		595.6363	192.0026	0.4544
7.979		MM m	0.0546		768.1403	232.3806	0.5860
				Sum	131072.3581		

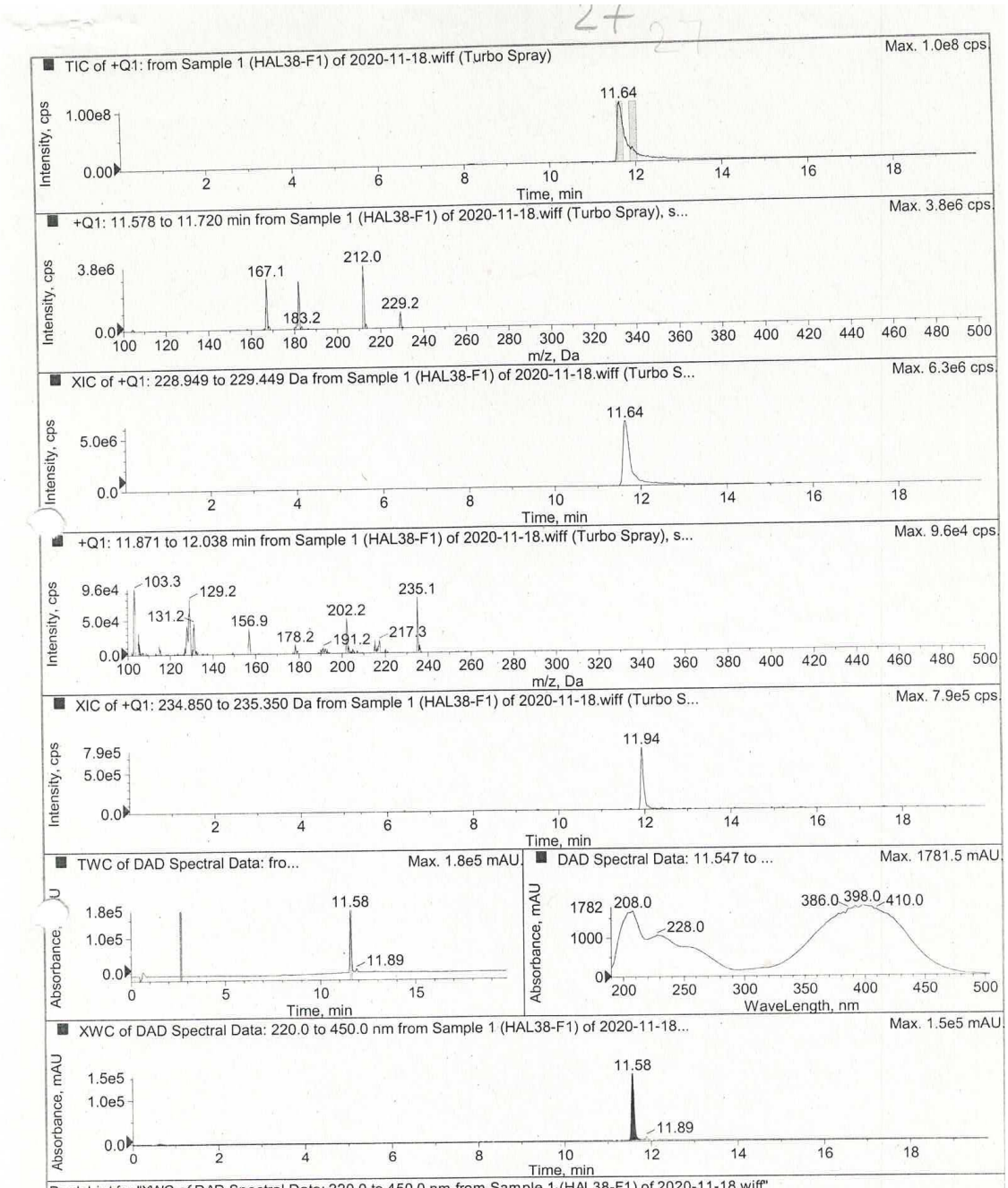
Signal: MS1 +TIC SCAN ESI Frag=135V Gain=1.0

RT [min]	Peak MS Base Peak m/z	Type	Width [min]	Col0	Area	Height	Area%
6.522	852.900	MM m	0.2259		20196359.6939	1125535.4389	100.0000
				Sum	20196359.6939		

Signal: MS1 -TIC SCAN ESI Frag=135V Gain=1.0

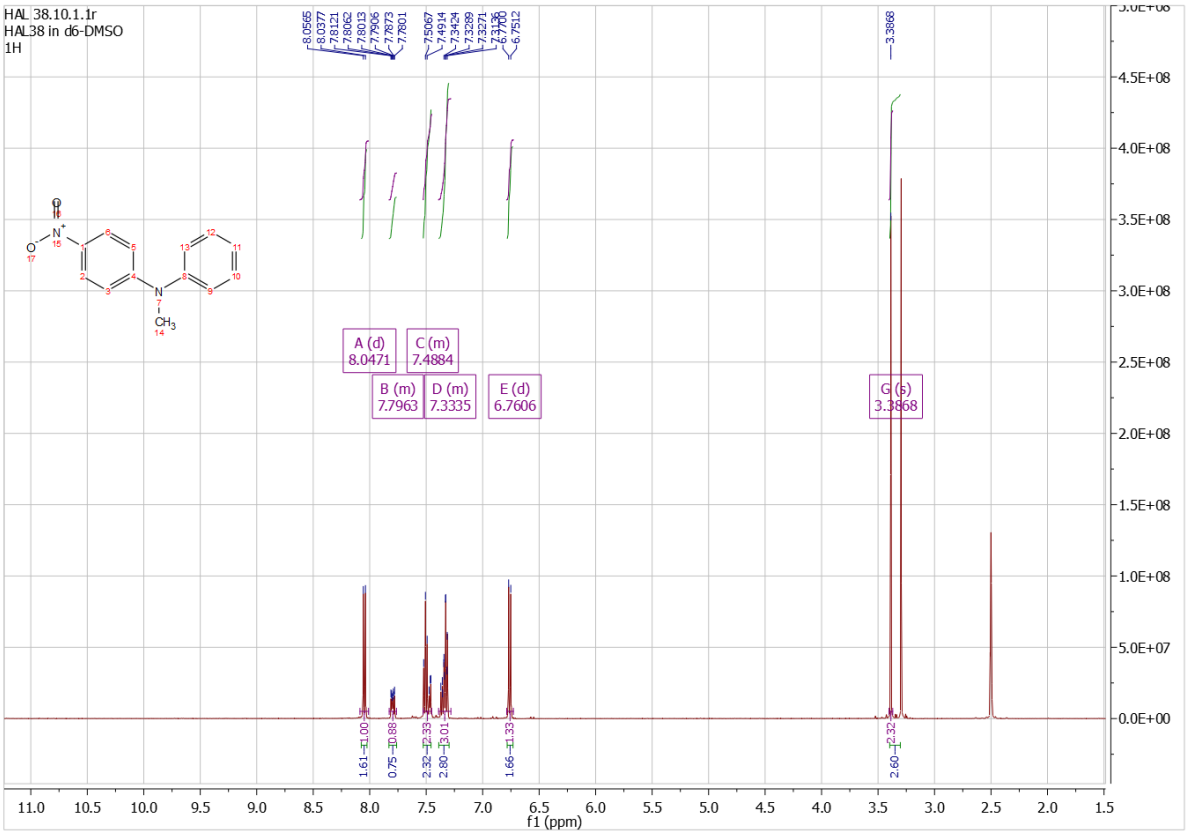
RT [min]	Peak MS Base Peak m/z	Type	Width [min]	Col0	Area	Height	Area%
6.823	391.300	MM m	0.5399		32394919.5782	909403.8114	100.0000
				Sum	32394919.5782		

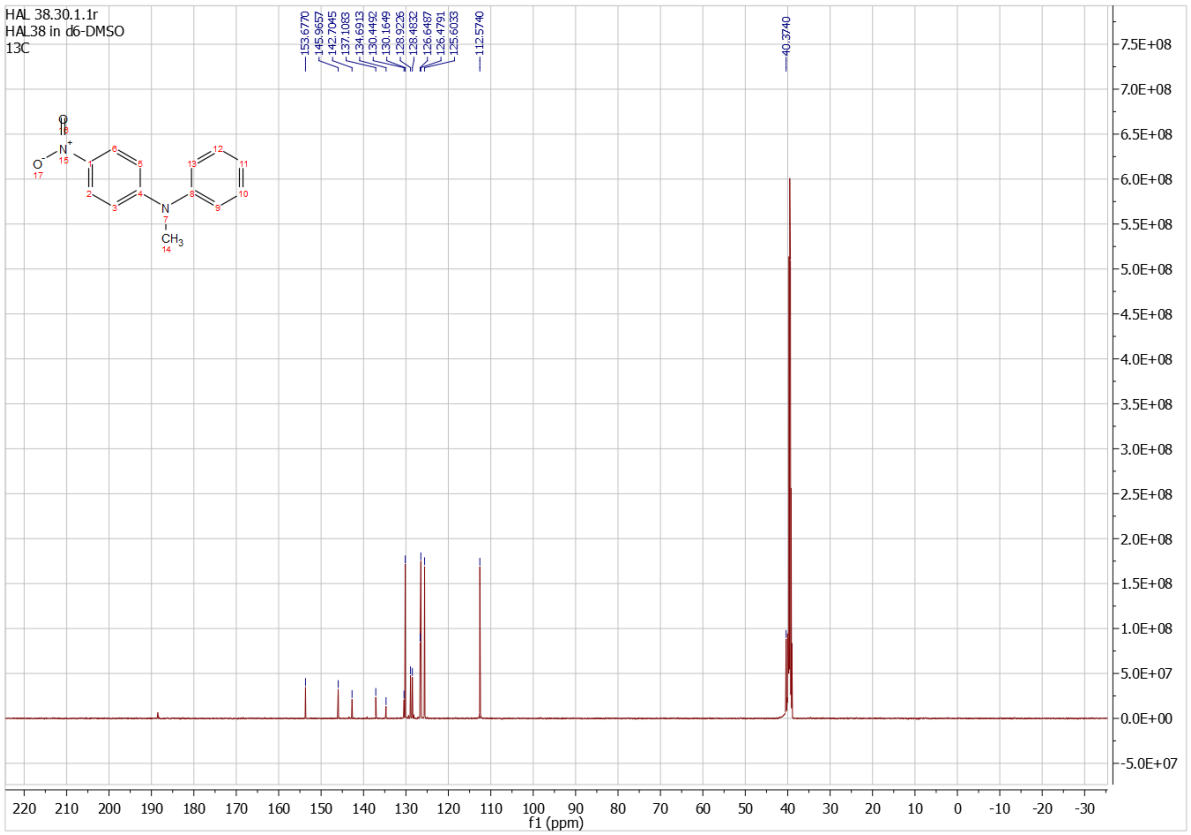
N-Methyl-4-nitro-*N*-phenylaniline (**27**)



Peak List for "XWC of DAD Spectral Data: 220.0 to 450.0 nm from Sample 1 (HAL38-F1) of 2020-11-18.wiff"

	Time (min)	Area (mAU x min)	% Area	Height (mAU)	% Height	Width (min)	Baseline Type
1	0.6277	2.7980e4	3.3853	2885.9791	1.7344	0.3733	Base to Base
2	8.1148	9917.3114	1.1999	1024.5767	0.6158	0.4667	Base to Base
3	10.6985	1632.9282	0.1976	288.7343	0.1735	0.2667	Base to Base
4	11.1431	2628.2178	0.3180	463.0959	0.2783	0.3000	Base to Base
5	11.5759	7.4670e5	90.3448	1.5326e5	92.1079	0.3533	Base to Base
6	11.8886	3.6507e4	4.4171	8180.7557	4.9165	0.3067	Base to Base
7	12.1967	1134.9230	0.1373	288.9558	0.1737	0.1533	Base to Base

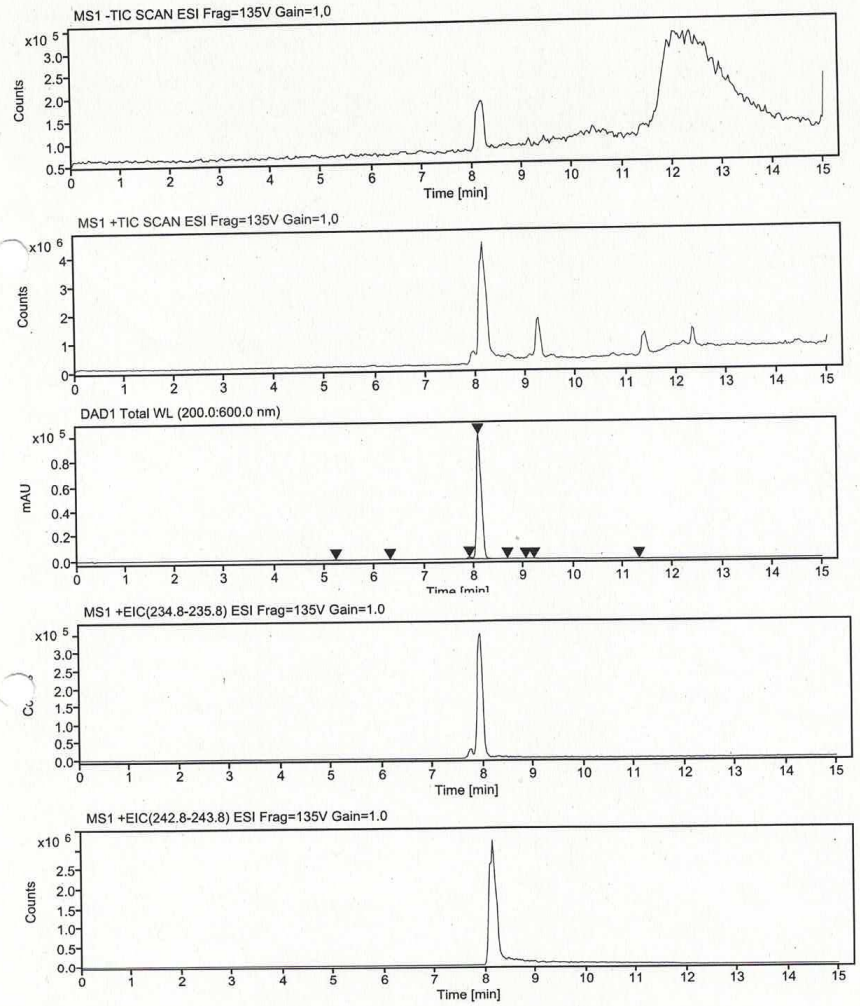

HAL 38.10.1.1r
HAL38 in d6-DMSO
1H
A (d) 8.0471
C (m) 7.4884
B (m) 7.7963
D (m) 7.3335
E (d) 6.7606
G (s) 3.3868
f1 (ppm)


HAL 38.30.1.1r
HAL38 in d6-DMSO
13C
f1 (ppm)

N-Ethyl-4-nitro-*N*-phenylaniline (**28**)

28

Sequence Name:	2020-11-26		
Data file:	2020-11-26 09-36-14+01-00.dx	**Project Name:**	Single Quad
Sample name:	HAL39	**Operator :**	SYSTEM
Instrument:	Single Quad	**Acquired on:**	2020-11-26 09:37:10+01:00
Inj. volume:	2.000	**Location:**	P1-C7
Acq. method:	0_wasser-acn_standard_100-1000_AC-20min.amx		
Processing method:	MS_standard_plot.pmx		



Signal: DAD1 Total WL (200.0:600.0 nm)

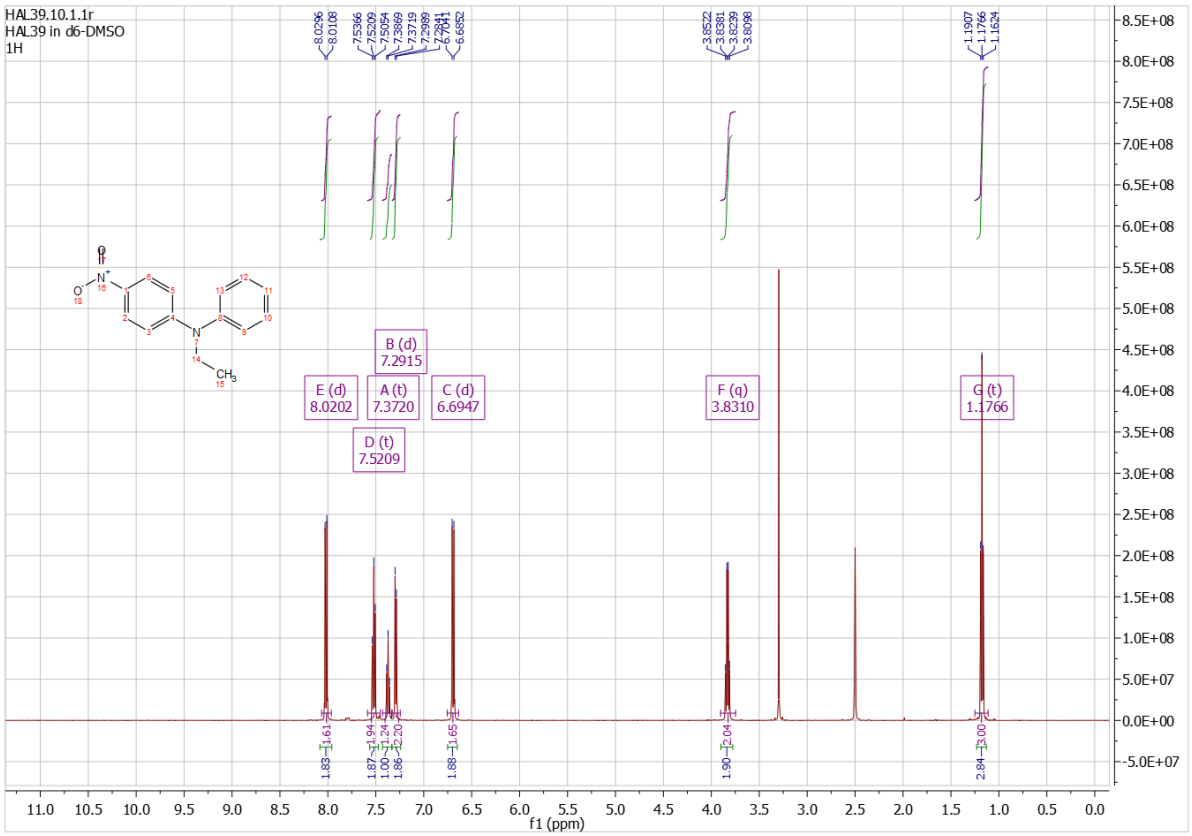
RT [min]	Name	Area	Area%	Max Peak%	Height	Type
5.226		1482.0190	0.2181	0.222	186.934	MM m
6.306		527.7450	0.0777	0.079	97.065	MM m
7.901		6700.5874	0.9862	1.002	1302.163	MM m
8.099		668434.1677	98.3767	100.000	100172.806	MM m
8.667		624.2315	0.0919	0.093	107.700	MM m
9.040		454.5050	0.0669	0.068	90.574	MM m
9.207		671.7276	0.0989	0.100	132.379	MM m
11.327		569.2592	0.0838	0.085	90.225	MM m
	Sum	679464.2425				

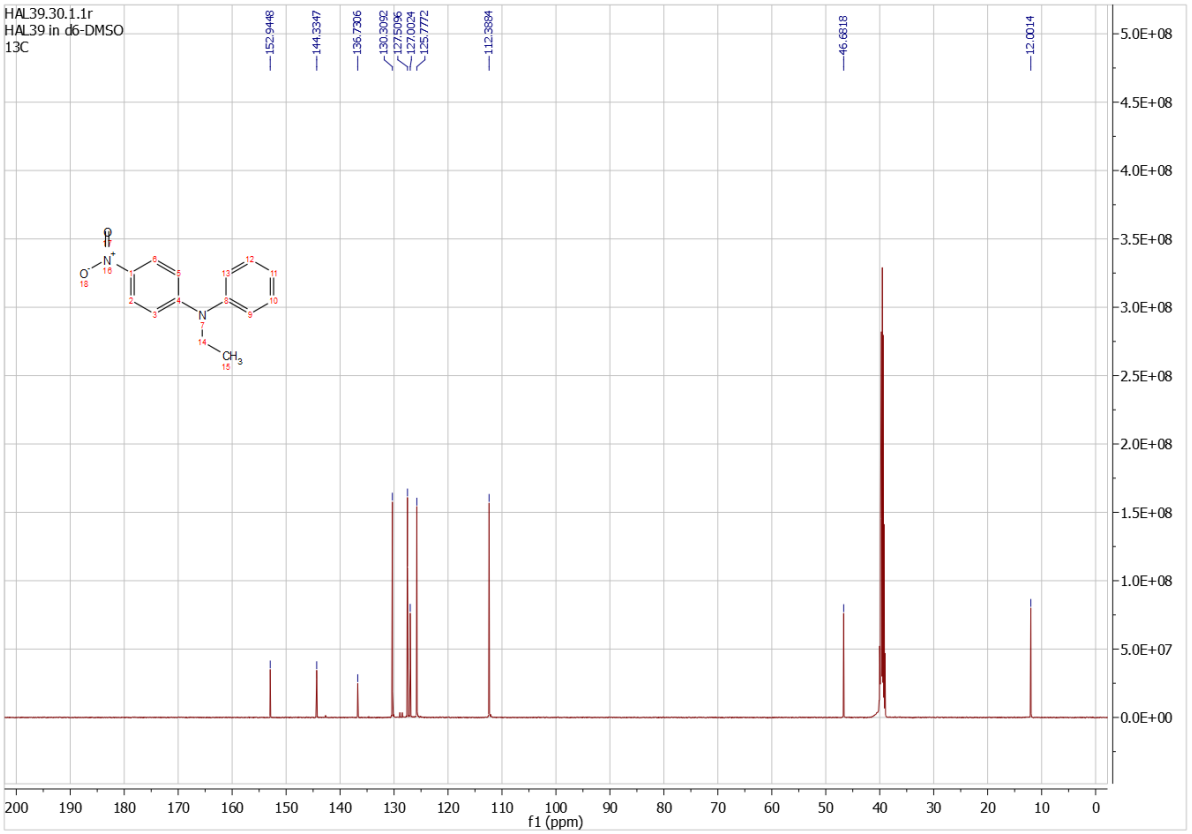
Signal: MS1 +TIC SCAN ESI Frag=135V Gain=1,0

RT [min]	Name	Area	Area%	Max Peak%	Height	Type
7.950		2472319.2187	6.4153	6.855	364423.802	MM m
8.151		36065577.6133	93.5847	100.000	3979181.033	MM m
	Sum	38537896.8320				

Signal: MS1 -TIC SCAN ESI Frag=135V Gain=1,0

RT [min]	Name	Area	Area%	Max Peak%	Height	Type
8.184		983457.1425	100.0000	100.000	96740.156	MM m
	Sum	983457.1425				

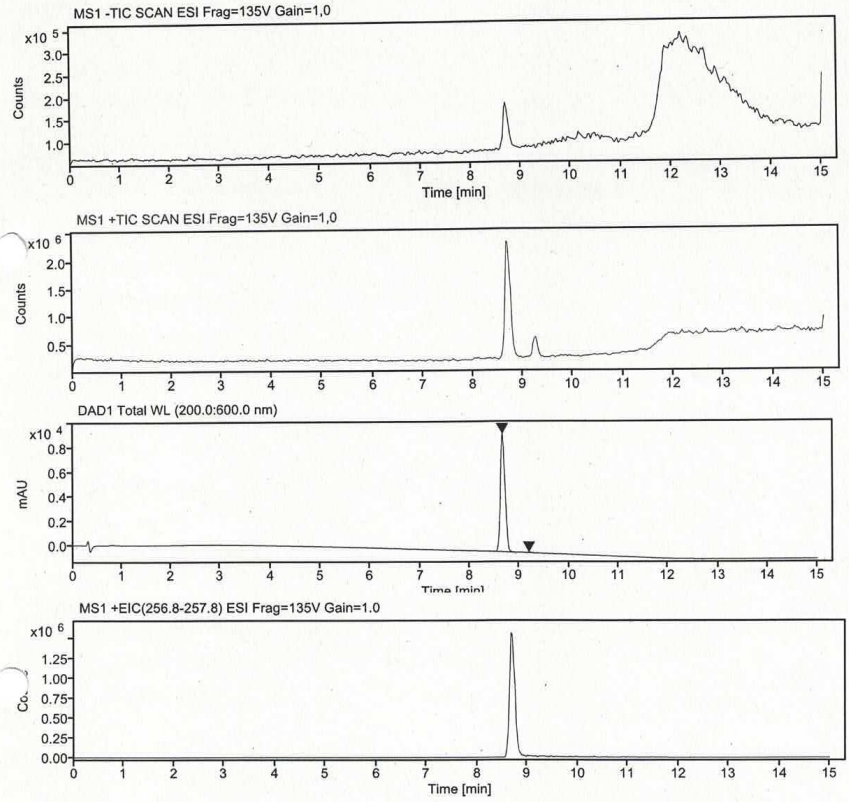

HAL39.10.1.1r
HAL39 in d6-DMSO
1H
B (d)
7.2915
E (d)
8.0202
A (t)
7.3720
C (d)
6.6947
D (t)
7.5209
F (q)
3.8310
G (t)
1.1766
f1 (ppm)


HAL39.30.1.1r
HAL39 in d6-DMSO
13C
f1 (ppm)

N-Propyl-4-nitro-*N*-phenylaniline (**29**)

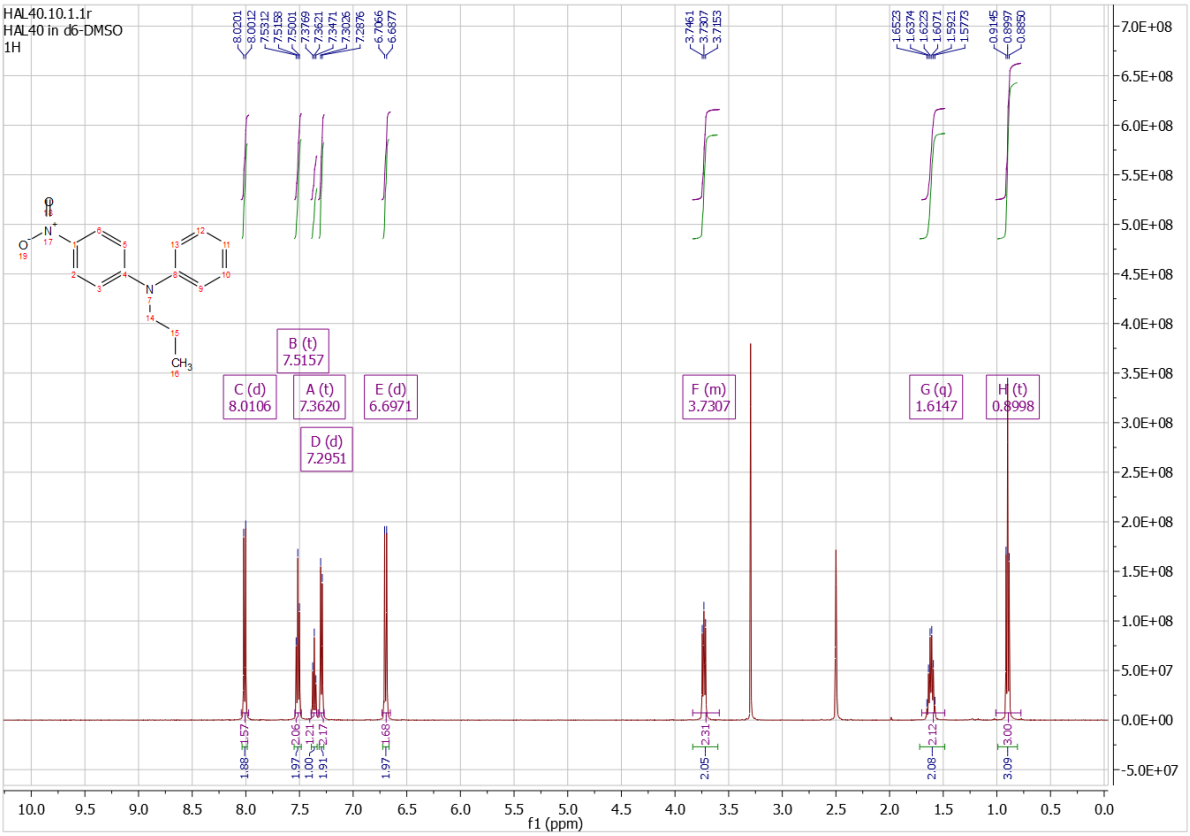
29

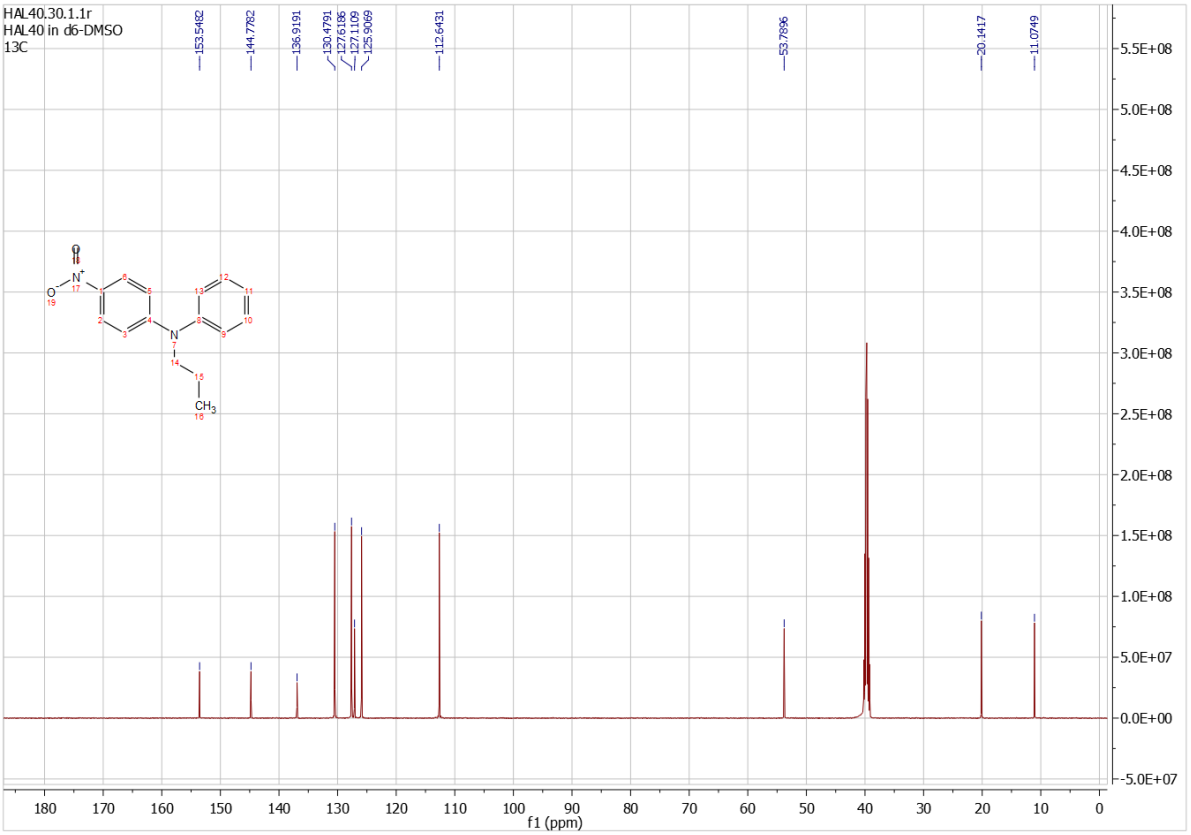
Sequence Name:	2020-11-26		
Data file:	2020-11-26 09-57-12+01-00.dx	**Project Name:**	Single Quad
Sample name:	HAL40	**Operator :**	SYSTEM
Instrument:	Single Quad	**Acquired on:**	2020-11-26 09:58:08+01:00
Inj. volume:	2.000	**Location:**	P1-C8
Acq. method:	0_wasser-acn_standard_100-1000_AC-20min.amx		
Processing method:	MS_standard_plot.pmx		



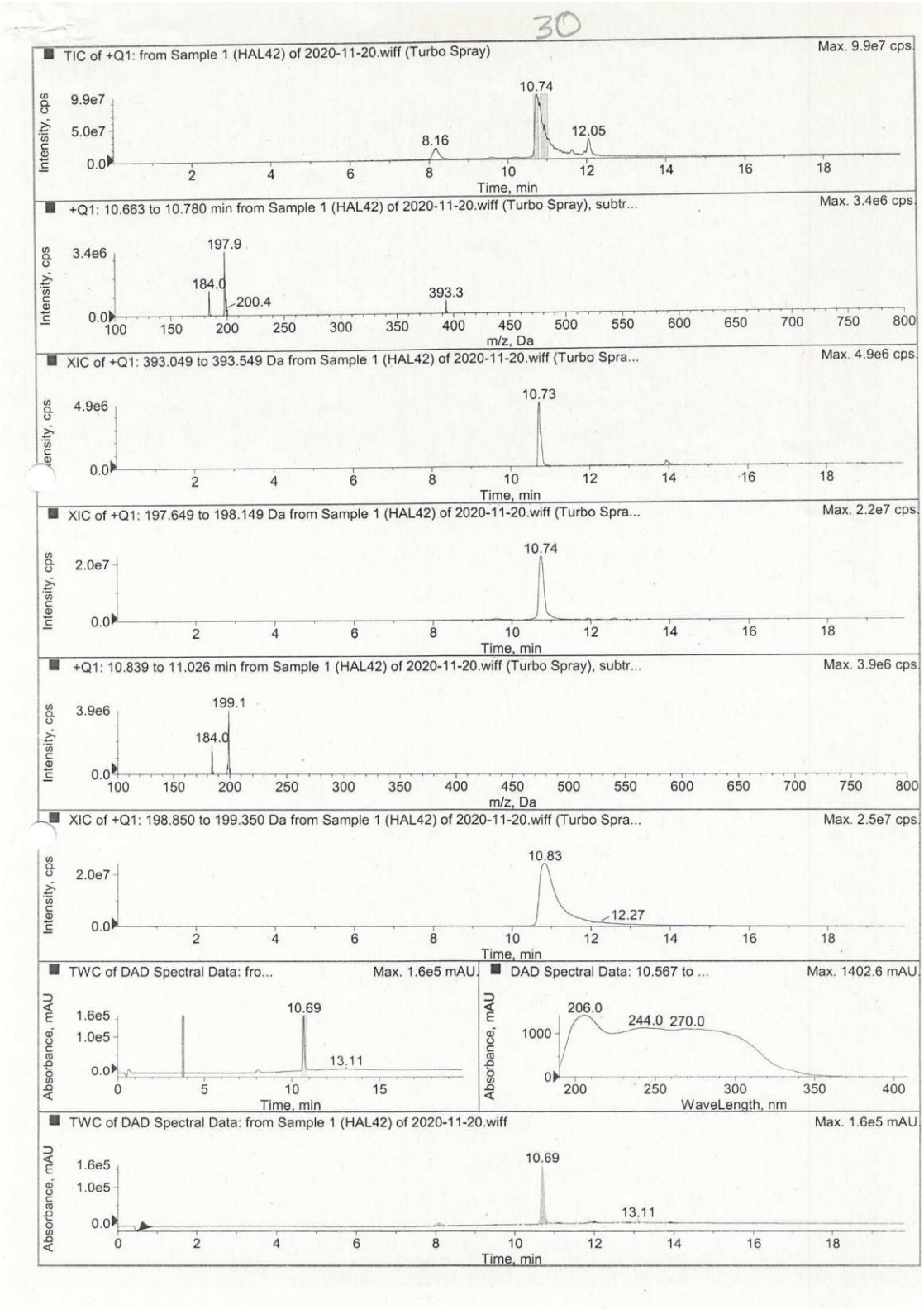
Signal: DAD1 Total WL (200.0:600.0 nm)

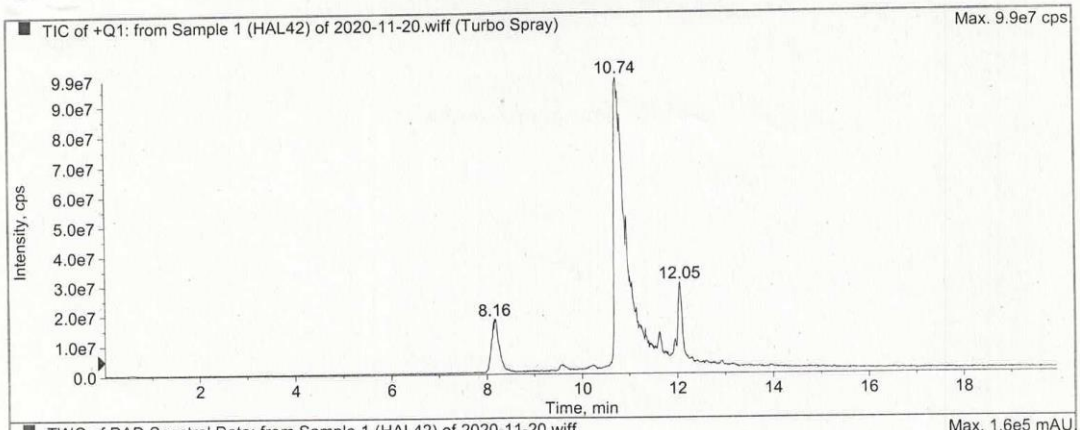
RT [min]	Name	Area	Area%	Max Peak%	Height	Type
8.659		64013.2869	99.8227	100.000	9646.004	MM m
9.199		113.7286	0.1773	0.178	24.758	MM m
	Sum	64127.0155				

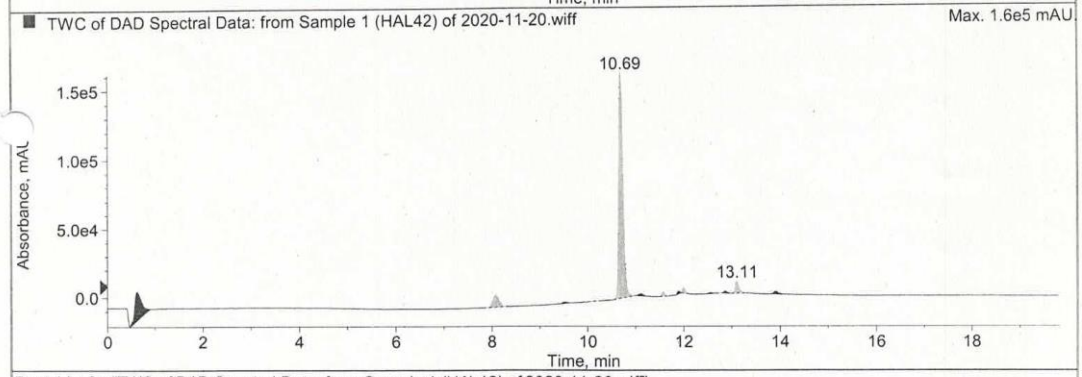

HAL40.10.1.1r
HAL40 in d6-DMSO
1H
B (t)
7.5157
C (d)
8.0106
A (t)
7.3620
E (d)
6.6971
D (d)
7.2951
F (m)
3.7307
G (q)
1.6147
H (t)
0.8998
f1 (ppm)


HAL40.30.1.1r
HAL40 in d6-DMSO
13C
153.5482
144.7762
136.9191
130.4791
127.6186
127.1109
125.9069
112.6431
53.7896
20.1417
11.0749
f1 (ppm)

N^1-Methyl-N^1-phenylbenzene-1,4-diamine (**30**)

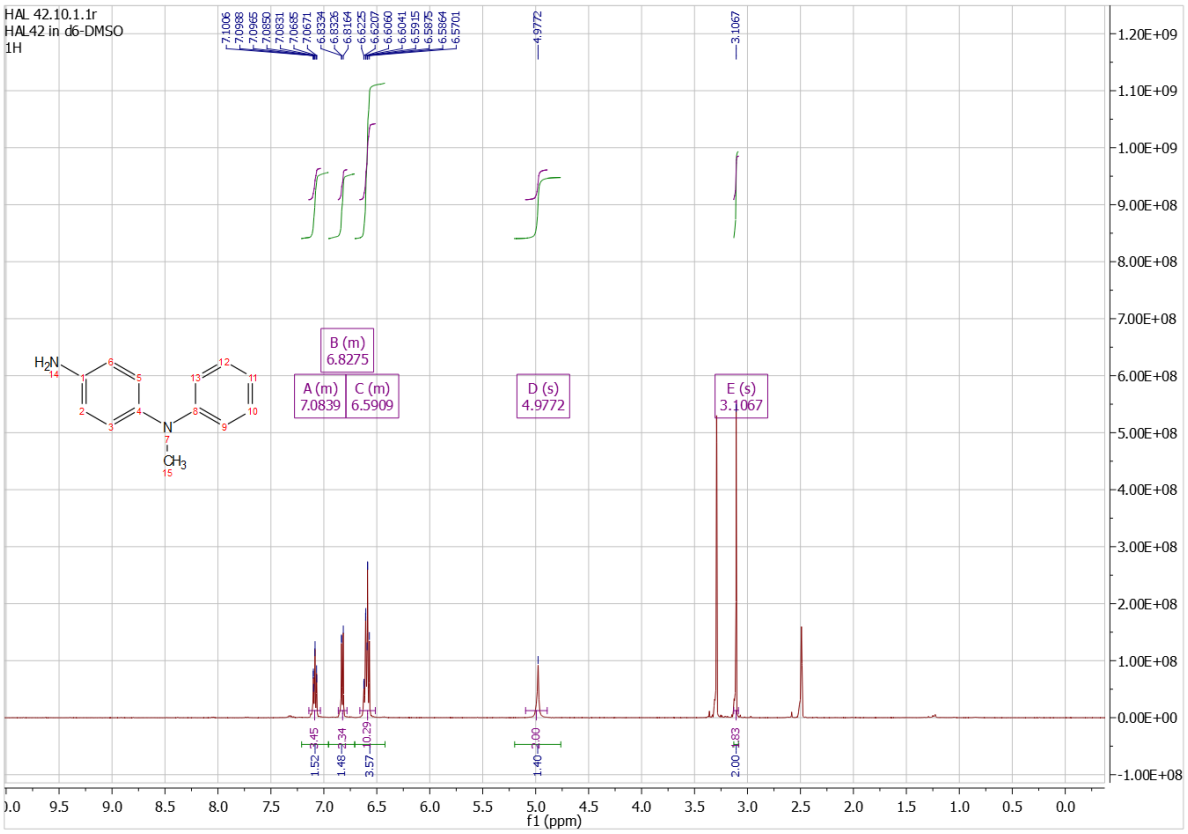


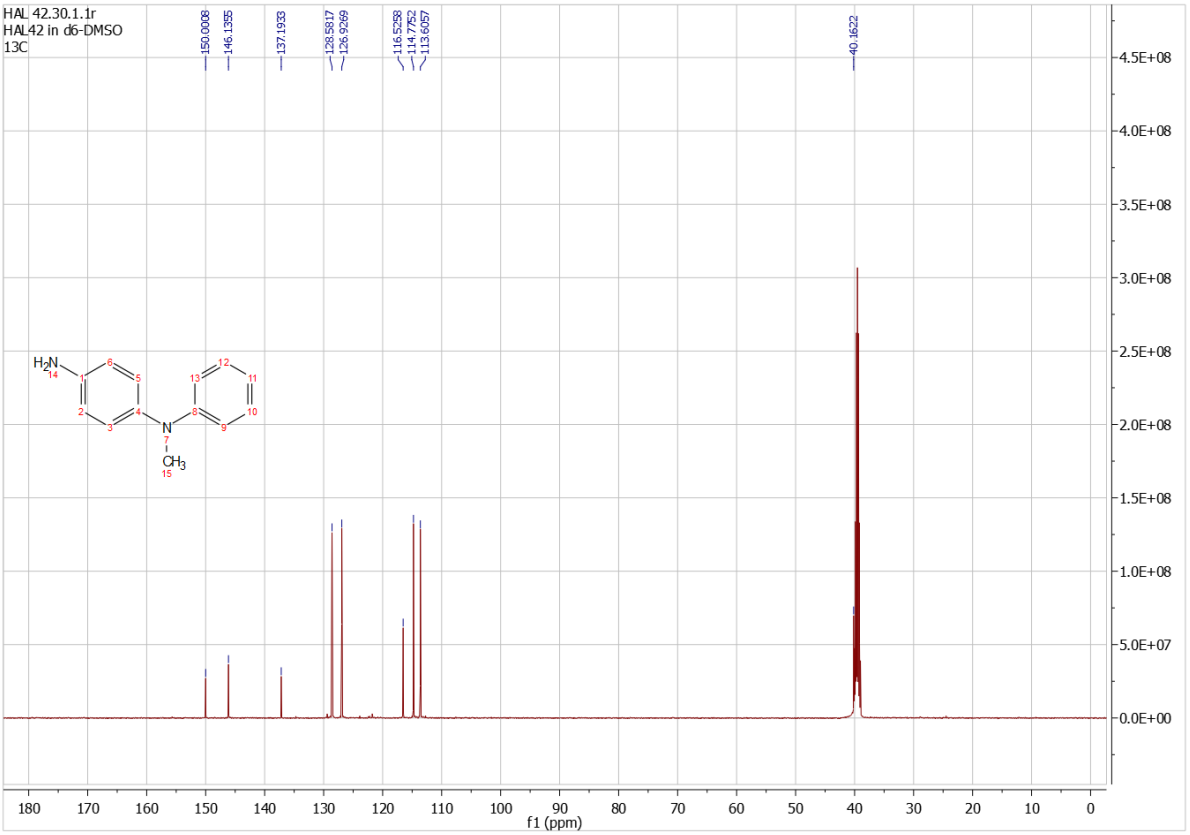




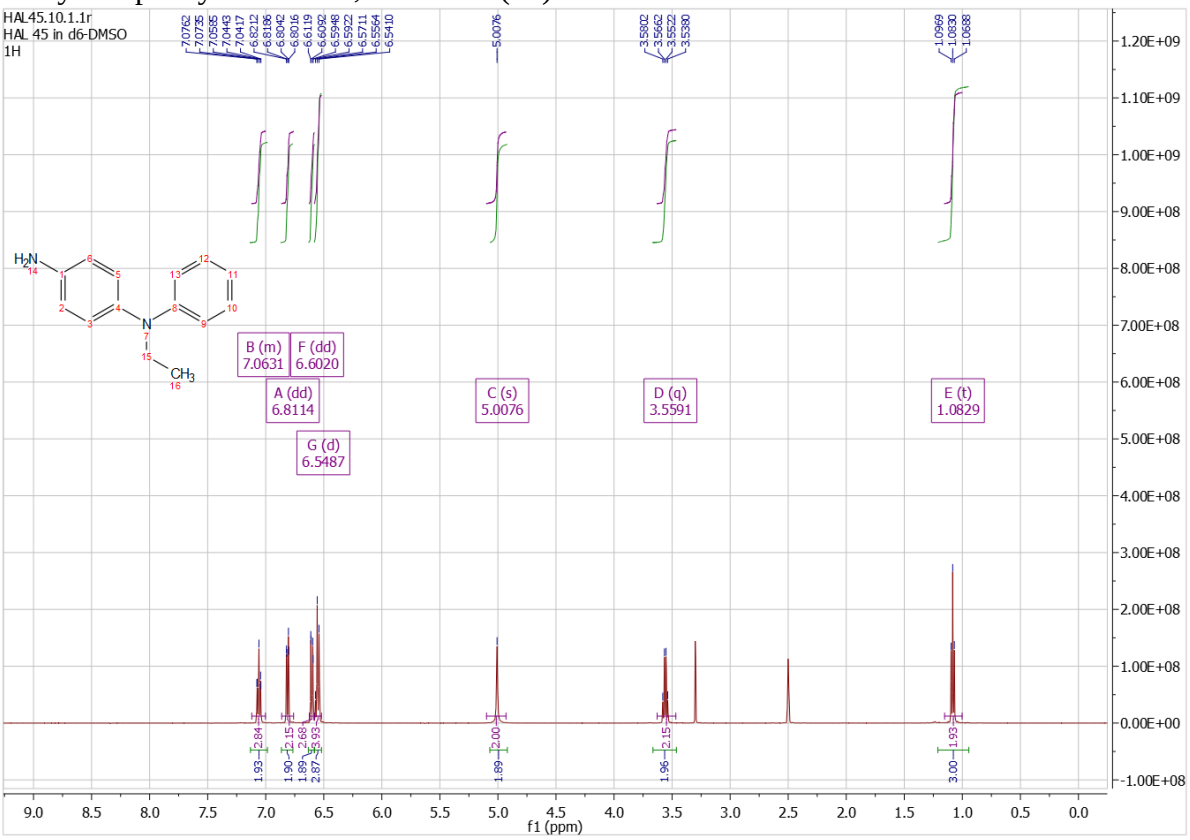
Peak List for "TWC of DAD Spectral Data: from Sample 1 (HAL42) of 2020-11-20.wiff"

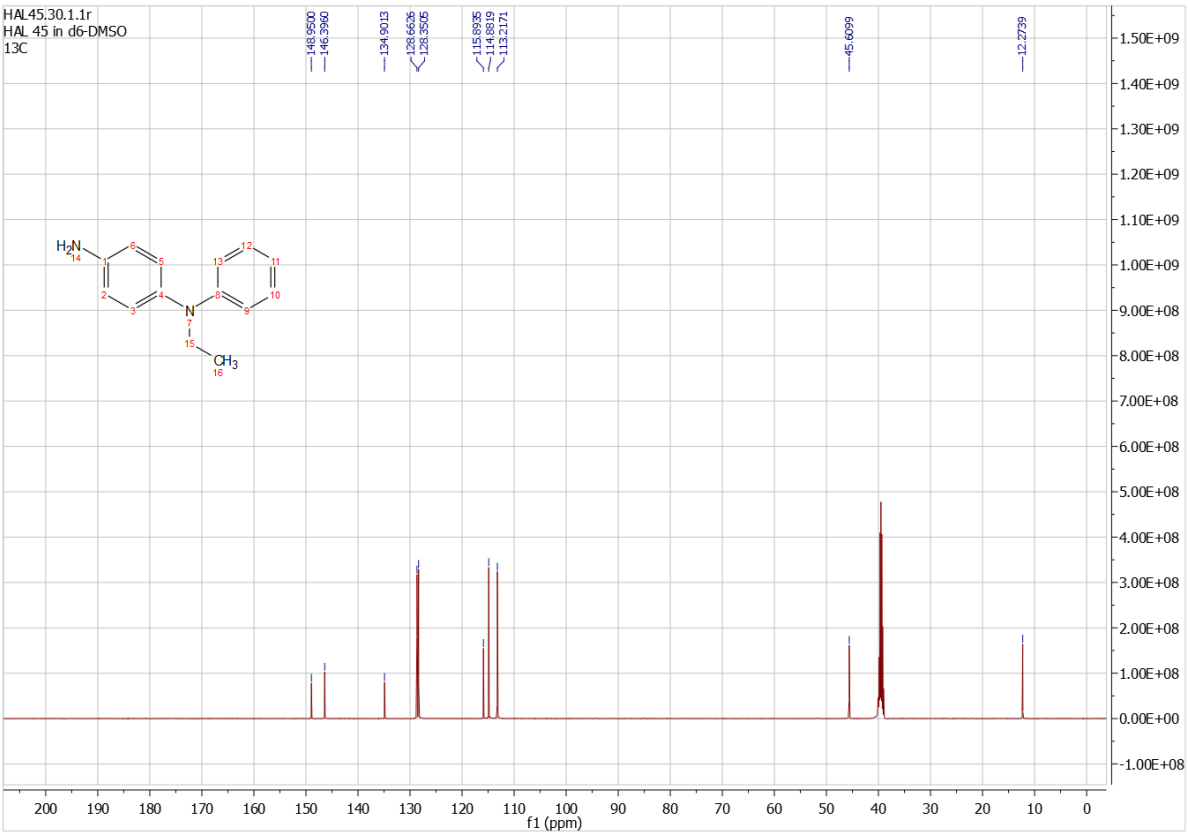
	Time (min)	Area (mAU x min)	%Area	Height (mAU)	%Height	Width (min)	Baseline Type
1	0.6245	2.1592e5	14.3186	2.0957e4	9.5632	0.4267	Base to Base
2	8.0796	8.5217e4	5.6511	8805.7034	4.0183	0.5000	Base to Base
3	9.5230	6760.6757	0.4483	998.1007	0.4555	0.2867	Base to Base
4	10.1937	1392.6981	0.0924	169.4852	0.0773	0.2333	Base to Base
5	10.4250	1075.7382	0.0713	204.7072	0.0934	0.1333	Base to Base
	10.6879	1.0754e6	71.3117	1.6270e5	74.2427	0.4333	Base to Base
7	11.1126	9419.4938	0.6246	1544.3090	0.7047	0.2067	Base to Base
8	11.5751	1.4999e4	0.9946	3312.9804	1.5118	0.1867	Base to Base
9	11.8965	6879.3342	0.4562	2135.3466	0.9744	0.1067	Base to Base
10	11.9988	1.7285e4	1.1462	4321.5495	1.9720	0.1733	Base to Base
11	12.5564	3283.8005	0.2178	633.1425	0.2889	0.2133	Base to Base
12	12.7181	2419.1098	0.1604	704.7528	0.3216	0.1267	Base to Base
13	12.8597	7493.3637	0.4969	1588.6515	0.7249	0.1933	Base to Base
14	13.1072	4.6562e4	3.0877	8790.7095	4.0114	0.3000	Base to Base
15	13.9090	1.3904e4	0.9220	2278.6431	1.0398	0.3200	Base to Base


HAL 42.10.1.1r
HAL42 in d6-DMSO
1H
B (m)
6.8275
A (m)
7.0839
C (m)
6.5909
D (s)
4.9772
E (s)
3.1067
f1 (ppm)

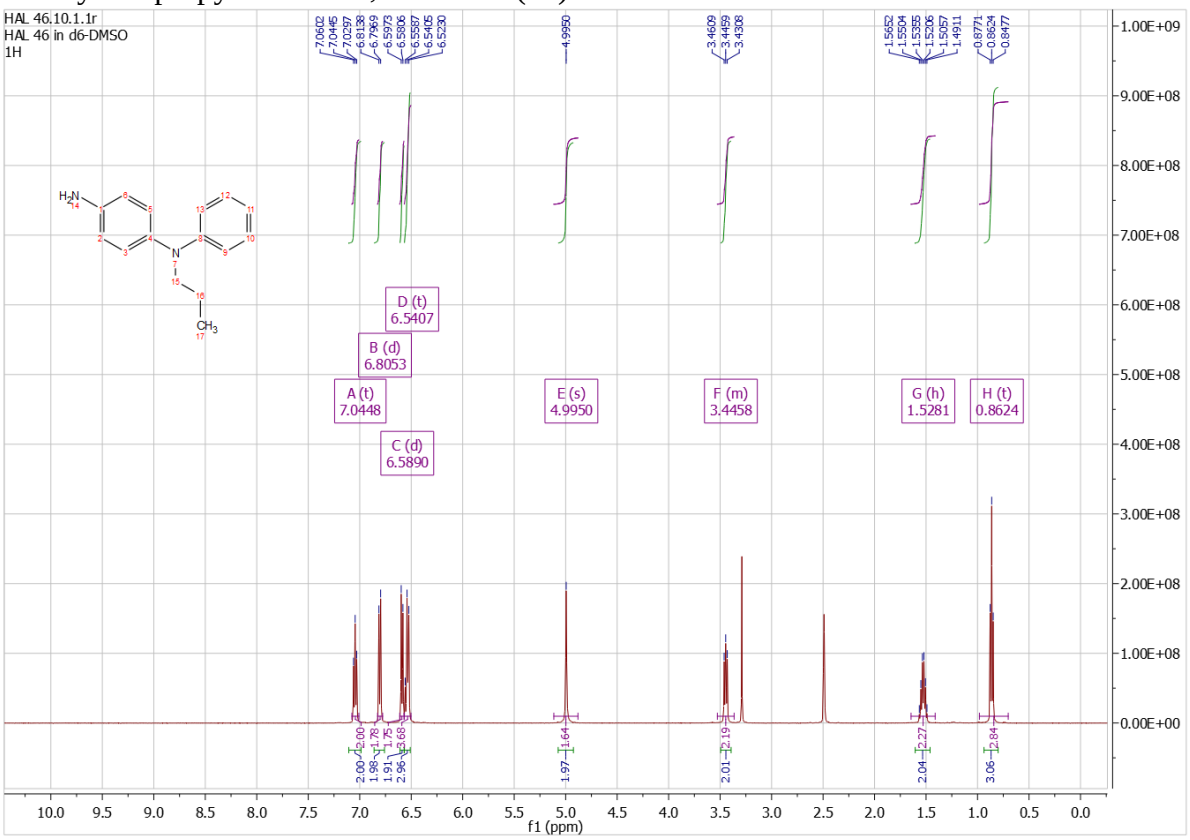

HAL 42.30.1.1r
HAL42 in d6-DMSO
13C
f1 (ppm)

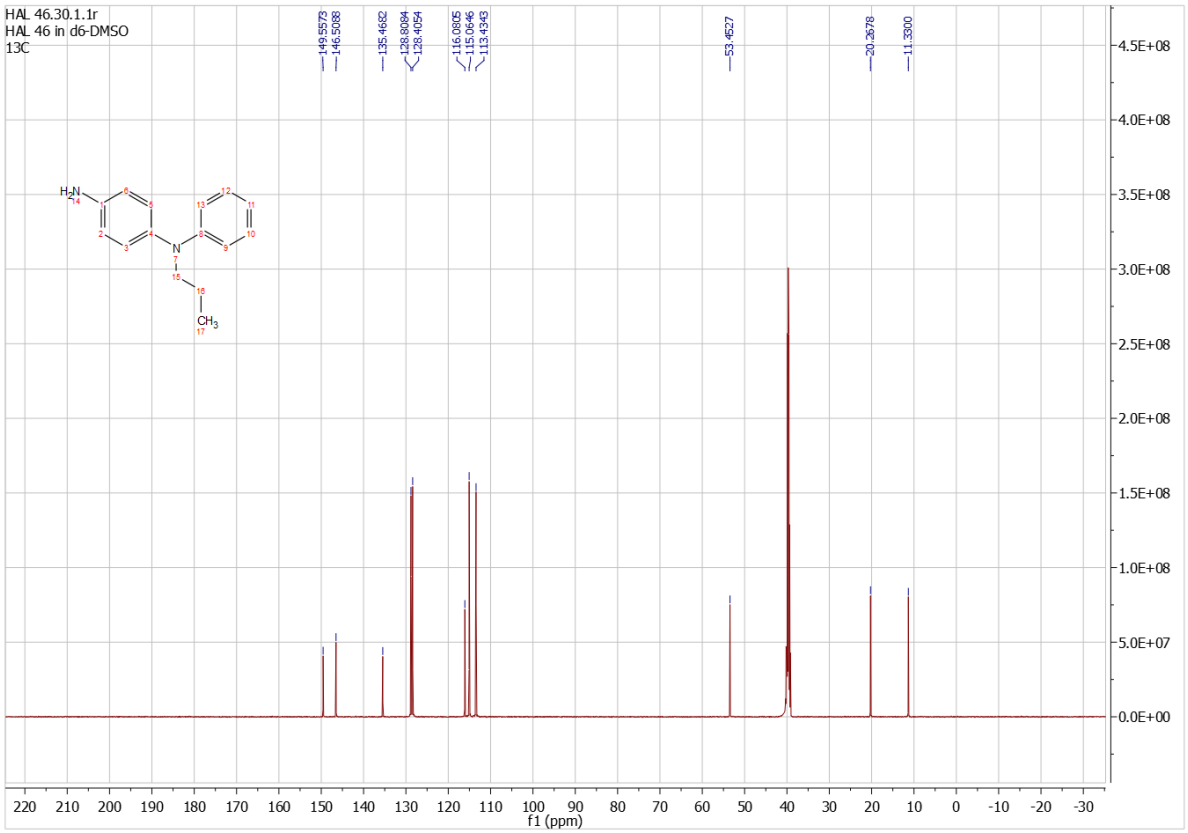
N^1-Ethyl-N^1-phenylbenzene-1,4-diamine (**31**)





N^1-Phenyl-N^1-propylbenzene-1,4-diamine (**32**)

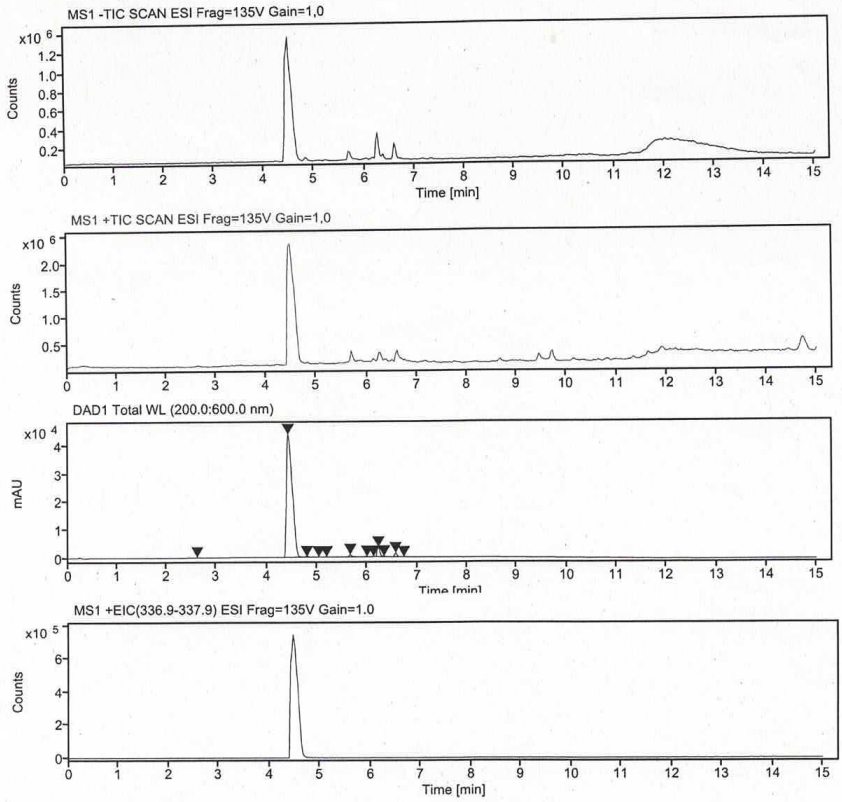




2-(Propyl(phenyl)amino)-5-nitrobenzenesulfonic acid (**34**)

34

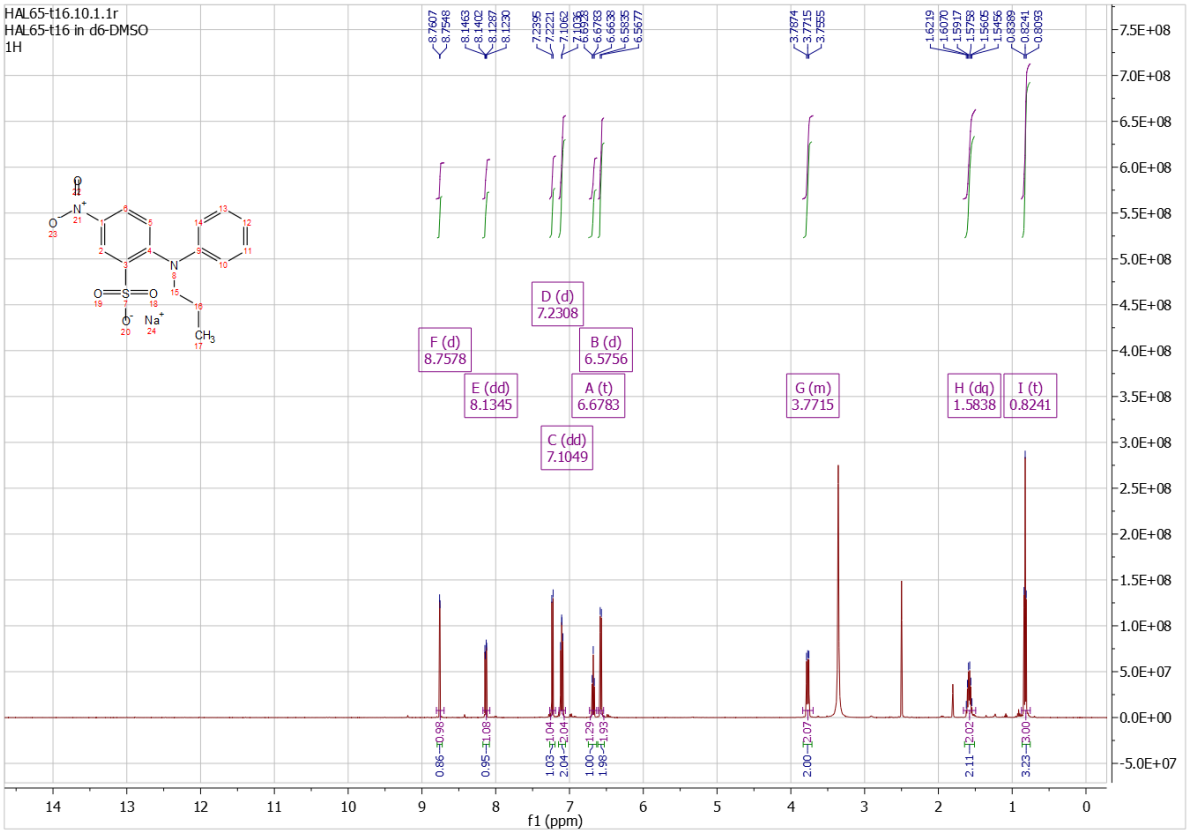
Sequence Name:	2021-04-11		
Data file:	2021-04-12 08-56-26+02-00-33.dx	**Project Name:**	Single Quad
Sample name:	HAL65-t16	**Operator :**	SYSTEM
Instrument:	Single Quad	**Acquired on:**	2021-04-12 08:57:22+02:00
Inj. volume:	2.000	**Location:**	P1-C8
Acq. method:	0_wasser-acn_standard_100-1000_AC-20min.amx		
Processing method:	MS_standard_plot.pmx		

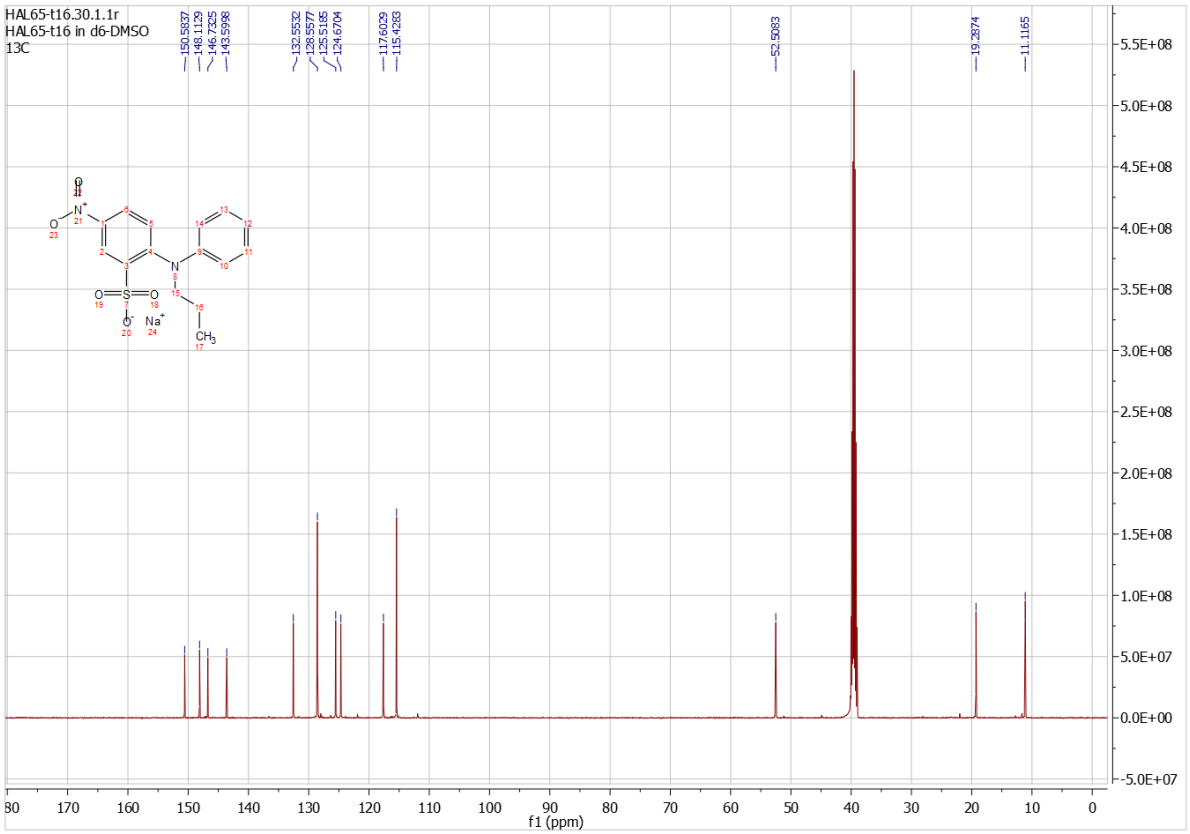


Signal: DAD1 Total WL (200.0:600.0 nm)

RT [min]	Peak MS Base Peak m/z	Area	Area%	Max Peak%	Height
2.616		290.1995	0.0778	0.083	48.845
4.428		350152.1029	93.9087	100.000	43859.633
4.799		558.6121	0.1498	0.160	166.334
5.036		219.9608	0.0590	0.063	64.402
5.190		177.3247	0.0476	0.051	68.973
5.663		3229.3013	0.8661	0.922	762.696
5.995		397.9606	0.1067	0.114	103.063

D:\CDSProjects\Default\Standard-Plot_MS+EIC.rdl [Rev. 582] Printed: 2021-04-12 12:45:38+02:00 Page 1 of 2

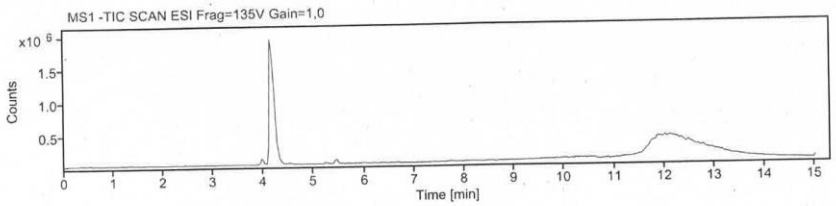

HAL65-t16.10.1.1r
HAL65-t16 in d6-DMSO
1H
D (d)
7.2308
F (d)
8.7578
B (d)
6.5756
E (dd)
8.1345
A (t)
6.6783
G (m)
3.7715
H (dq)
1.5838
I (t)
0.8241
C (dd)
7.1049
f1 (ppm)

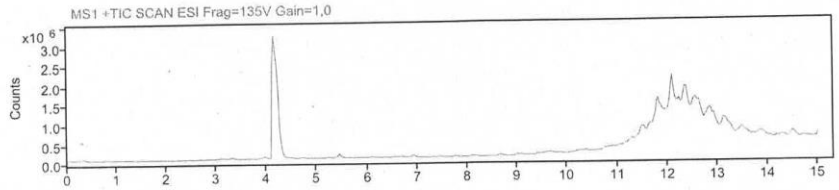

HAL65-t16.30.1.1r
HAL65-t16 in d6-DMSO
13C
f1 (ppm)

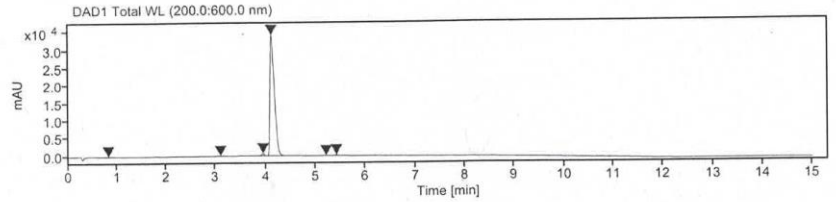
2-(Ethyl(phenyl)amino)-5-nitrobenzenesulfonic acid (**35**)

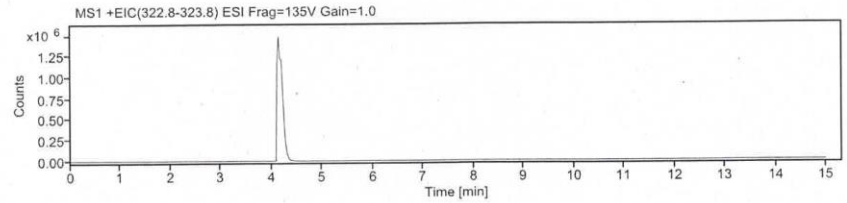
35

Sequence Name:	SingleSample		
Data file:	Single Quad-2021-06-26 02-09-23+02-00-10.dx	**Project Name:**	Single Quad
Sample name:	HAL71-N	**Operator :**	SYSTEM
Instrument:	Single Quad	**Acquired on:**	2021-06-26 02:10:22+02:00
Inj. volume:	4.000	**Location:**	P1-A9
Acq. method:	00-new_wasser-acn_standard_100-1000_BD-20min.amx		
Processing method:	MS_standard_plot.pmx		









Signal: DAD1 Total WL (200.0:600.0 nm)

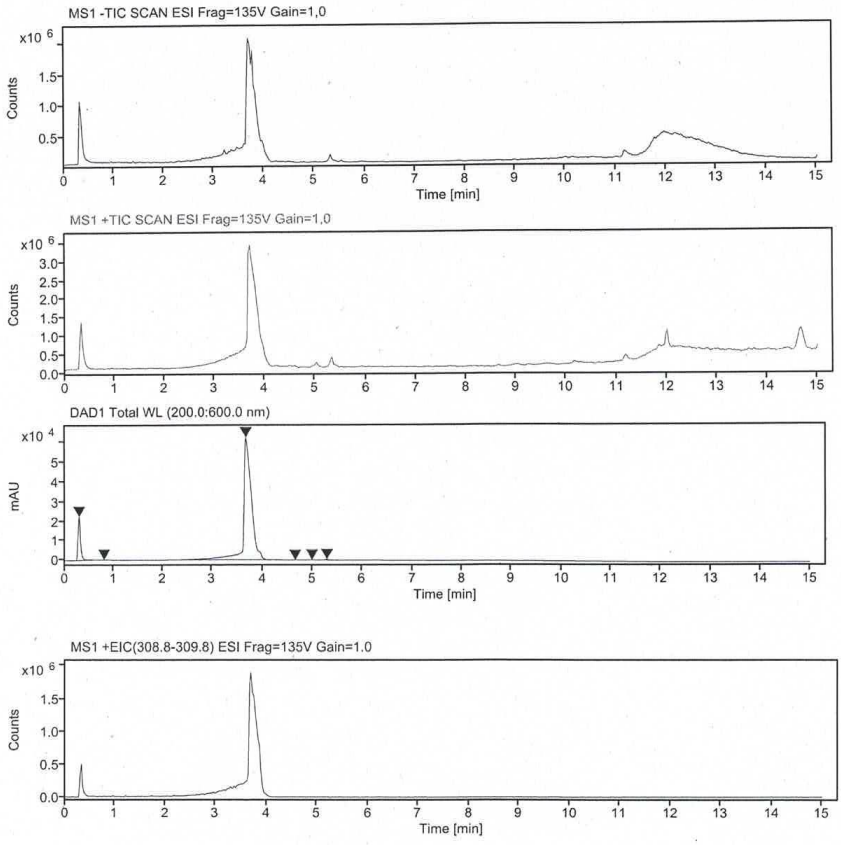
RT [min]	Peak MS Base Peak m/z	Area	Area%	Max Peak%	Height
0.832		402.8692	0.1866	0.190	55.463
3.097		574.3416	0.2661	0.271	66.615
3.944		2206.8318	1.0223	1.043	670.028
4.116		211683.6026	98.0627	100.000	34203.417
5.207		86.2567	0.0400	0.041	37.051
5.412		911.6269	0.4223	0.431	231.119
	Sum	215865.5289			

D:\CDSProjects\Default\0-standardplot+EIC.rdl [Rev. 1773] Printed: 2021-06-28 07:44:34+02:00 Page 1 of 2

2-(Methyl(phenyl)amino)-5-nitrobenzenesulfonic acid (**36**)

36

Sequence Name:	SingleSample		
Data file:	HAL70-NF1.dx	**Project Name:**	Single Quad
Sample name:	HAL70-NF1	**Operator :**	SYSTEM
Instrument:	Single Quad	**Acquired on:**	2021-07-01 07:02:30+02:00
Inj. volume:	8.000	**Location:**	P2-B2
Acq. method:	00-new_wasser-acn_standard_100-1000_BD-20min.amx		
Processing method:	MS_standard_plot.pmx		



Signal: DAD1 Total WL (200.0:600.0 nm)

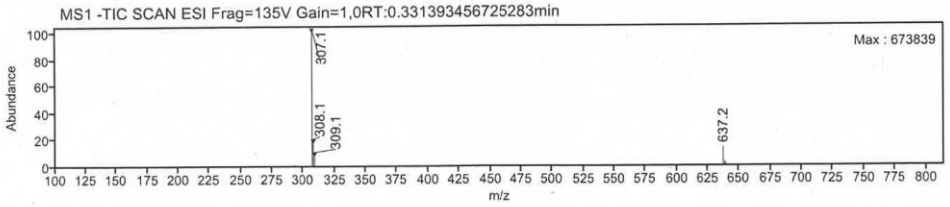
RT [min]	Peak MS Base Peak m/z	Area	Area%	Max Peak%	Height
0.302		79338.0866	10.2833	11.506	22383.739
0.814		378.1716	0.0490	0.055	79.620
3.667	307.000	689521.0616	89.3715	100.000	61947.830
4.649		105.4940	0.0137	0.015	7.913
4.992		244.9533	0.0317	0.036	88.081
5.288		1934.8578	0.2508	0.281	438.485
	Sum	771522.6248			

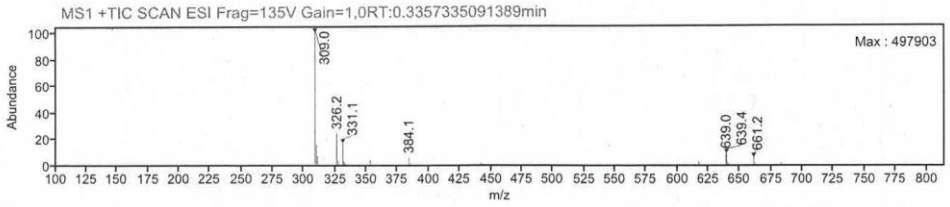
Signal: MS1 +TIC SCAN ESI Frag=135V Gain=1,0

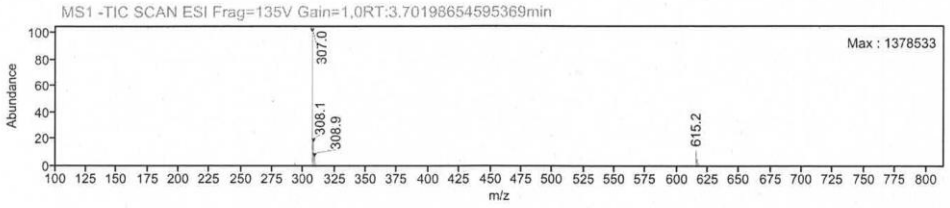
RT [min]	Peak MS Base Peak m/z	Area	Area%	Max Peak%	Height
0.336	309.000	5382524.4944	9.1835	10.112	1245754.747
3.703	309.100	53228507.3289	90.8165	100.000	3258881.545
	Sum	58611031.8233			

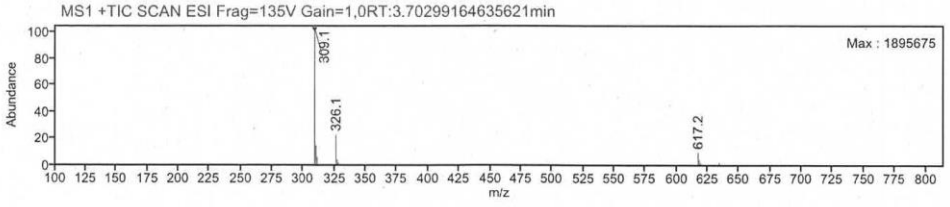
Signal: MS1 -TIC SCAN ESI Frag=135V Gain=1,0

RT [min]	Peak MS Base Peak m/z	Area	Area%	Max Peak%	Height
0.331	307.100	4347565.3982	12.4749	14.253	1068071.482
3.702	307.000	30503035.6123	87.5251	100.000	2049800.529
	Sum	34850601.0105			







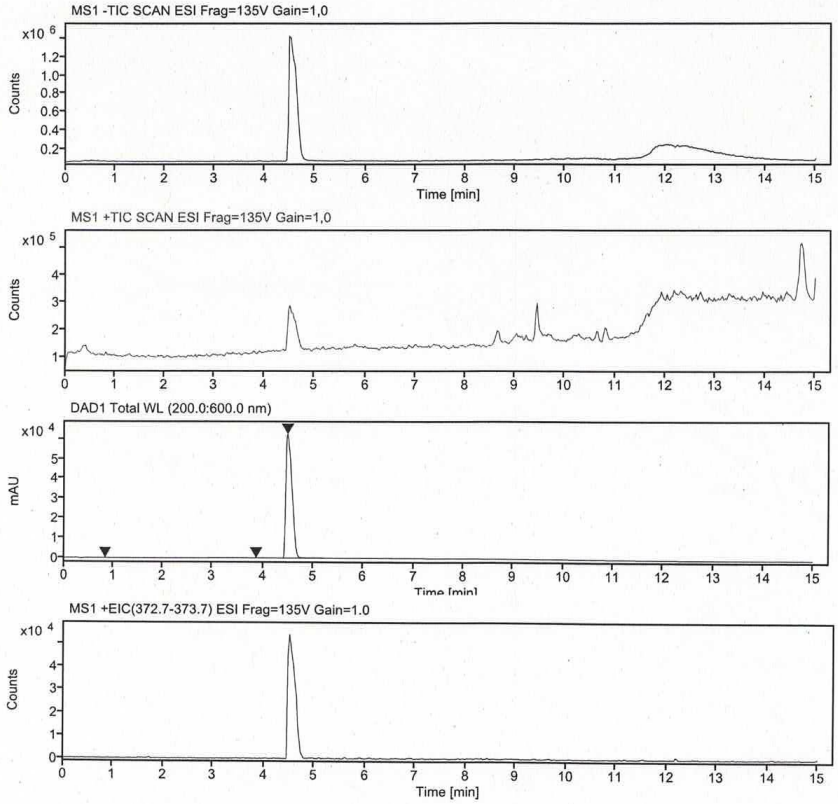


D:\CDSProjects\Default\0-standardplot+EIC.rdl [Rev. 1851] Printed: 2021-07-01 08:30:13+02:00 Page 2 of 2

2-((4-Bromophenyl)amino)-5-nitrobenzenesulfonic acid (**40**)

40 ✓

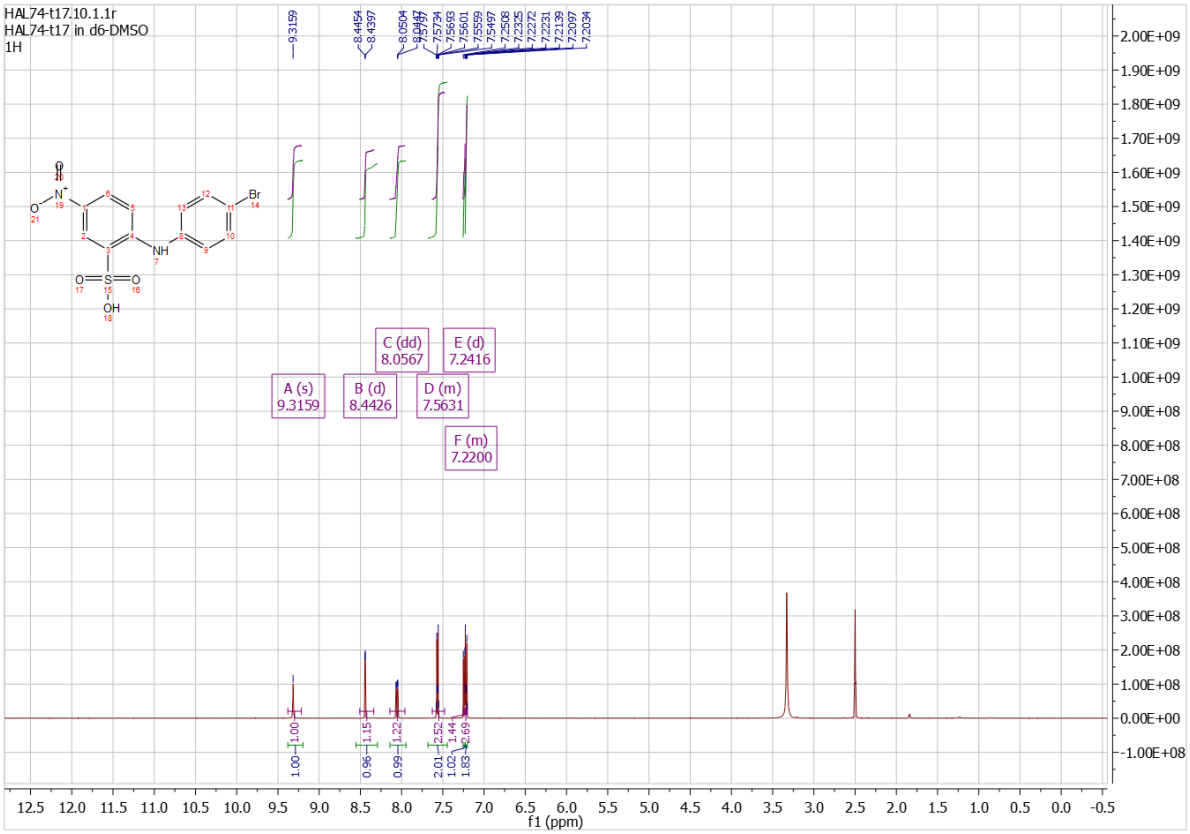
Sequence Name:	2021-04-11		
Data file:	2021-04-12 09-17-25+02-00-34.dx	**Project Name:**	Single Quad
Sample name:	HAL74-t17	**Operator :**	SYSTEM
Instrument:	Single Quad	**Acquired on:**	2021-04-12 09:18:18+02:00
Inj. volume:	2.000	**Location:**	P1-C9
Acq. method:	0_wasser-acn_standard_100-1000_AC-20min.amx		
Processing method:	MS_standard_plot.pmx		

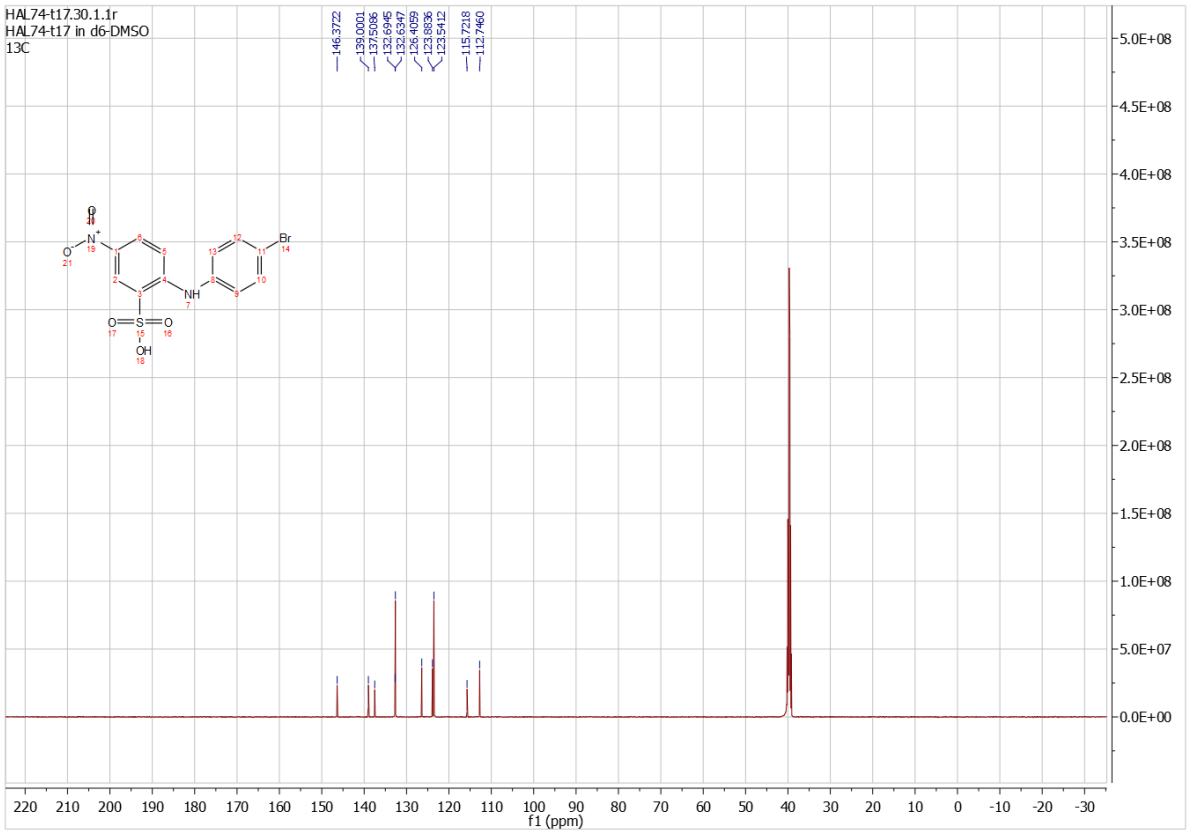


Signal: DAD1 Total WL (200.0:600.0 nm)

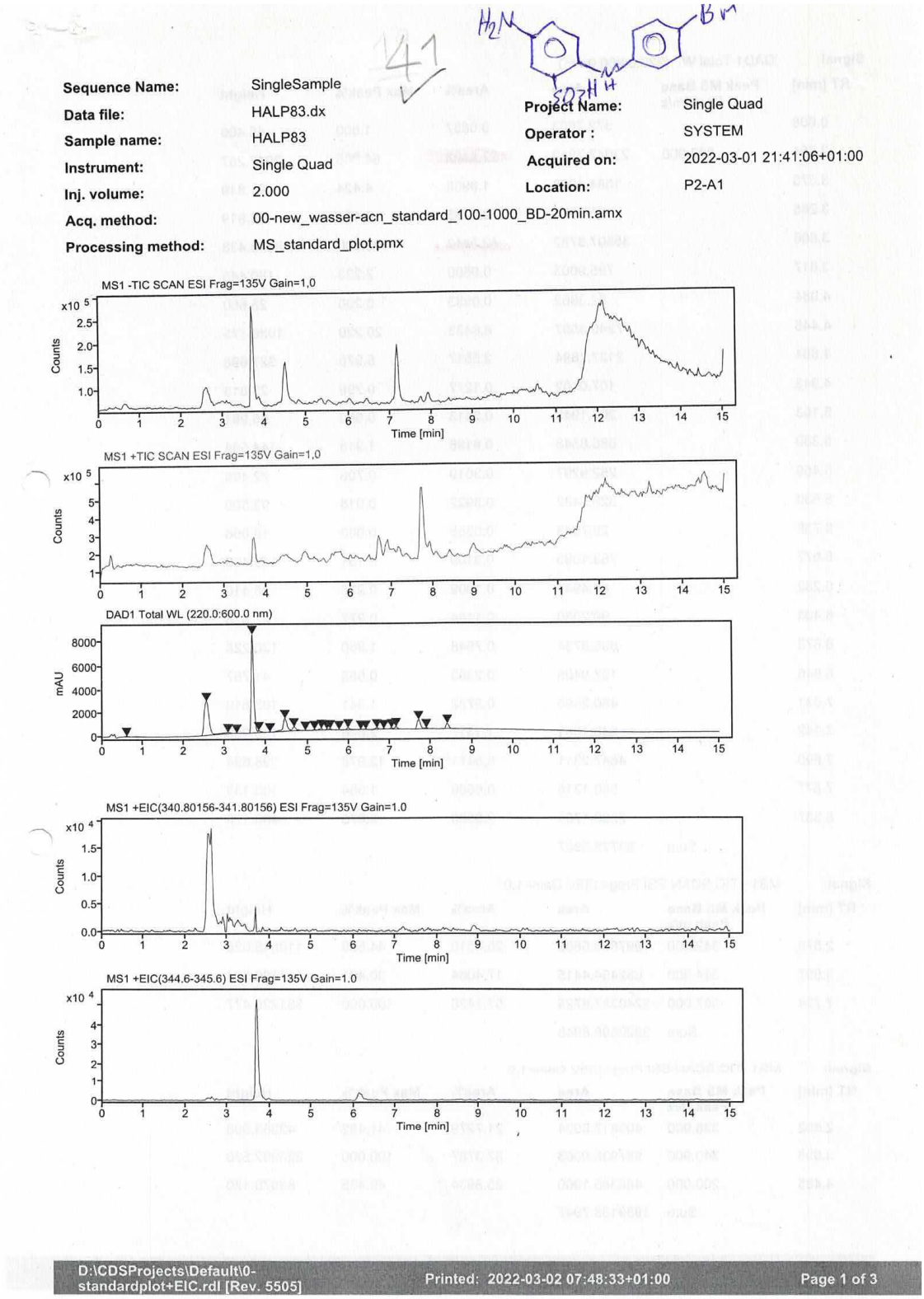
RT [min]	Peak MS Base Peak m/z	Area	Area%	Max Peak%	Height
0.837		231.2742	0.0441	0.044	32.984
3.863		154.8292	0.0295	0.030	53.638
4.482	375.000	524501.2541	99.9264	100.000	62278.502
	Sum	524887.3576			

D:\CDSProjects\Default\Standard-Plot_MS+EIC.rdl [Rev. 582] Printed: 2021-04-12 12:46:51+02:00 Page 1 of 2


HAL74-t17.10.1.1r
HAL74-t17 in d6-DMSO
1H
A (s)
9.3159
B (d)
8.4426
C (dd)
8.0567
D (m)
7.5631
E (d)
7.2416
F (m)
7.2200
f1 (ppm)


HAL74-t17.30.1.1r
HAL74-t17 in d6-DMSO
13C
f1 (ppm)

5-Amino-2-((4-bromophenyl)amino)benzenesulfonic acid (**41**)



Signal: DAD1 Total WL (220.0:600.0 nm)

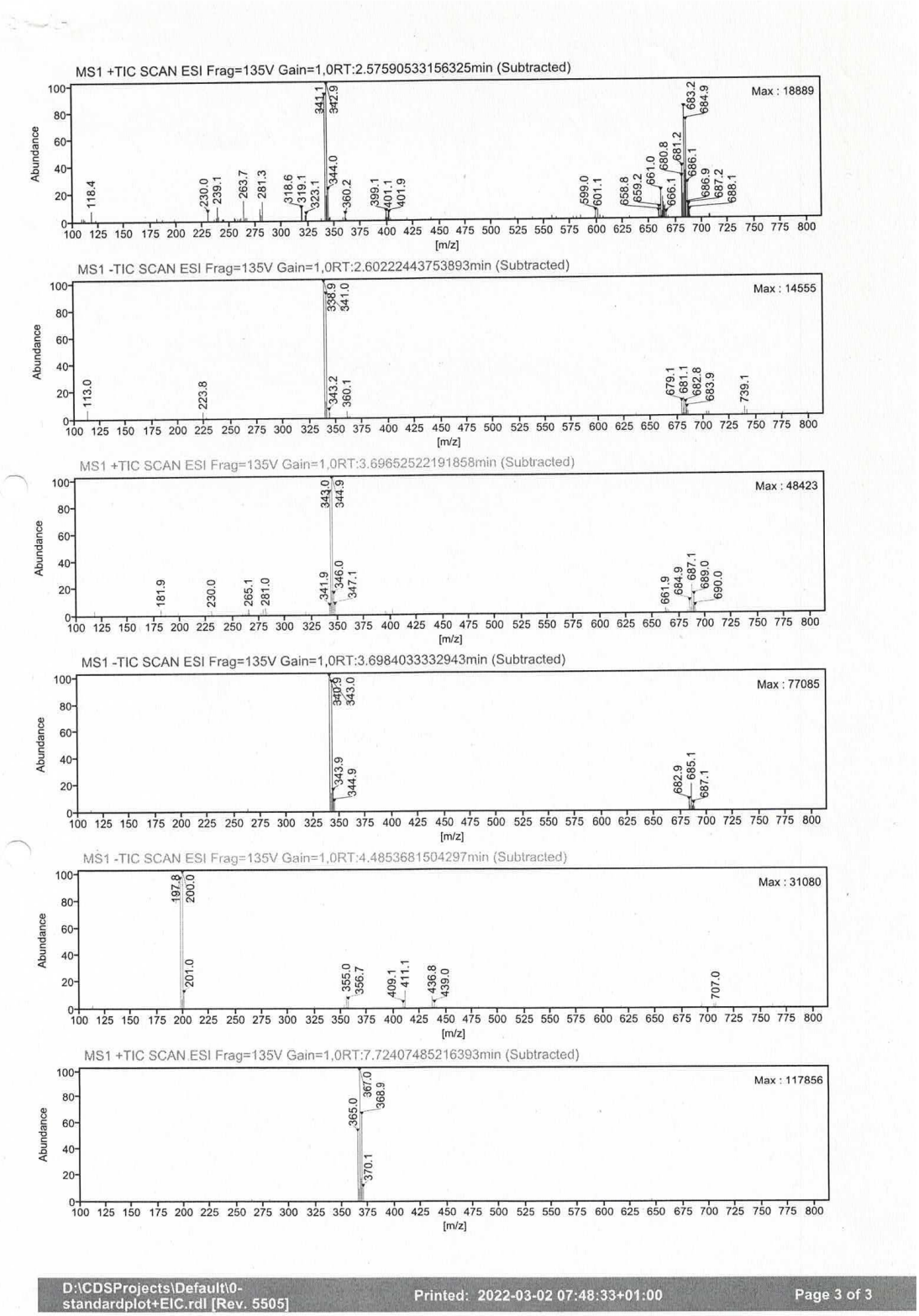
RT [min]	Peak MS Base Peak m/z	Area	Area%	Max Peak%	Height
0.608		572.7603	0.6837	1.600	45.466
2.551	342.900	23047.7249	27.5103	64.365	2947.257
3.076		1584.1068	1.8908	4.424	91.819
3.285		65.7375	0.0785	0.184	10.919
3.666		35807.8782	42.7412	100.000	8346.438
3.817		795.9003	0.9500	2.223	180.445
4.084		82.3862	0.0983	0.230	25.660
4.445		7240.3597	8.6423	20.220	1086.475
4.664		2137.7894	2.5517	5.970	327.698
4.943		107.0102	0.1277	0.299	23.813
5.163		202.1943	0.2413	0.565	65.981
5.330		686.8548	0.8198	1.918	144.564
5.459		252.9297	0.3019	0.706	72.486
5.539		328.5482	0.3922	0.918	93.509
5.756		29.7048	0.0355	0.083	18.056
5.977		763.1083	0.9109	2.131	159.436
6.282		84.4944	0.1009	0.236	25.410
6.403		99.2030	0.1184	0.277	27.975
6.672		665.8734	0.7948	1.860	120.225
6.846		197.9405	0.2363	0.553	41.757
7.031		480.2495	0.5732	1.341	103.819
7.142		948.1051	1.1317	2.648	199.953
7.690		4647.2311	5.5471	12.978	798.694
7.877		560.1315	0.6686	1.564	103.139
8.387		2390.1706	2.8530	6.675	450.196
	Sum	83778.3927			

Signal: MS1 +TIC SCAN ESI Frag=135V Gain=1,0

RT [min]	Peak MS Base Peak m/z	Area	Area%	Max Peak%	Height
2.576	342.900	997856.5808	25.4510	44.539	110945.026
3.697	344.900	682454.4415	17.4064	30.461	147386.534
7.724	367.000	2240387.8725	57.1426	100.000	381226.477
	Sum	3920698.8948			

Signal: MS1 -TIC SCAN ESI Frag=135V Gain=1,0

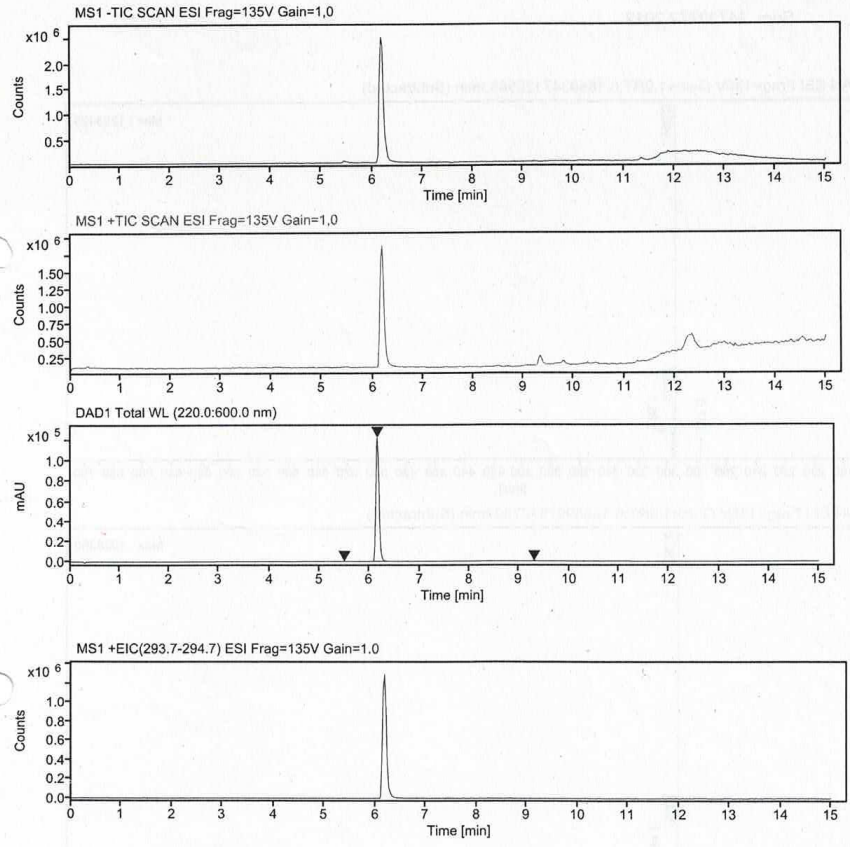
RT [min]	Peak MS Base Peak m/z	Area	Area%	Max Peak%	Height
2.602	338.900	409817.6924	21.7279	41.482	42363.006
3.698	340.900	987935.9063	52.3787	100.000	223392.530
4.485	200.000	488385.1960	25.8934	49.435	83970.120
	Sum	1886138.7947			


MS1 +TIC SCAN ESI Frag=135V Gain=1,0RT:2.57590533156325min (Subtracted)
Max : 18889
MS1 -TIC SCAN ESI Frag=135V Gain=1,0RT:2.60222443753893min (Subtracted)
Max : 14555
MS1 +TIC SCAN ESI Frag=135V Gain=1,0RT:3.69652522191858min (Subtracted)
Max : 48423
MS1 -TIC SCAN ESI Frag=135V Gain=1,0RT:3.6984033332943min (Subtracted)
Max : 77085
MS1 -TIC SCAN ESI Frag=135V Gain=1,0RT:4.4853681504297min (Subtracted)
Max : 31080
MS1 +TIC SCAN ESI Frag=135V Gain=1,0RT:7.72407485216393min (Subtracted)
Max : 117856
Abundance
[m/z]
D:\CDSProjects\Default\0-standardplot+EIC.rdl [Rev. 5505]
Printed: 2022-03-02 07:48:33+01:00
Page 3 of 3

5-Nitro-2-(phenylamino)benzenesulfonamide (**42**)

42

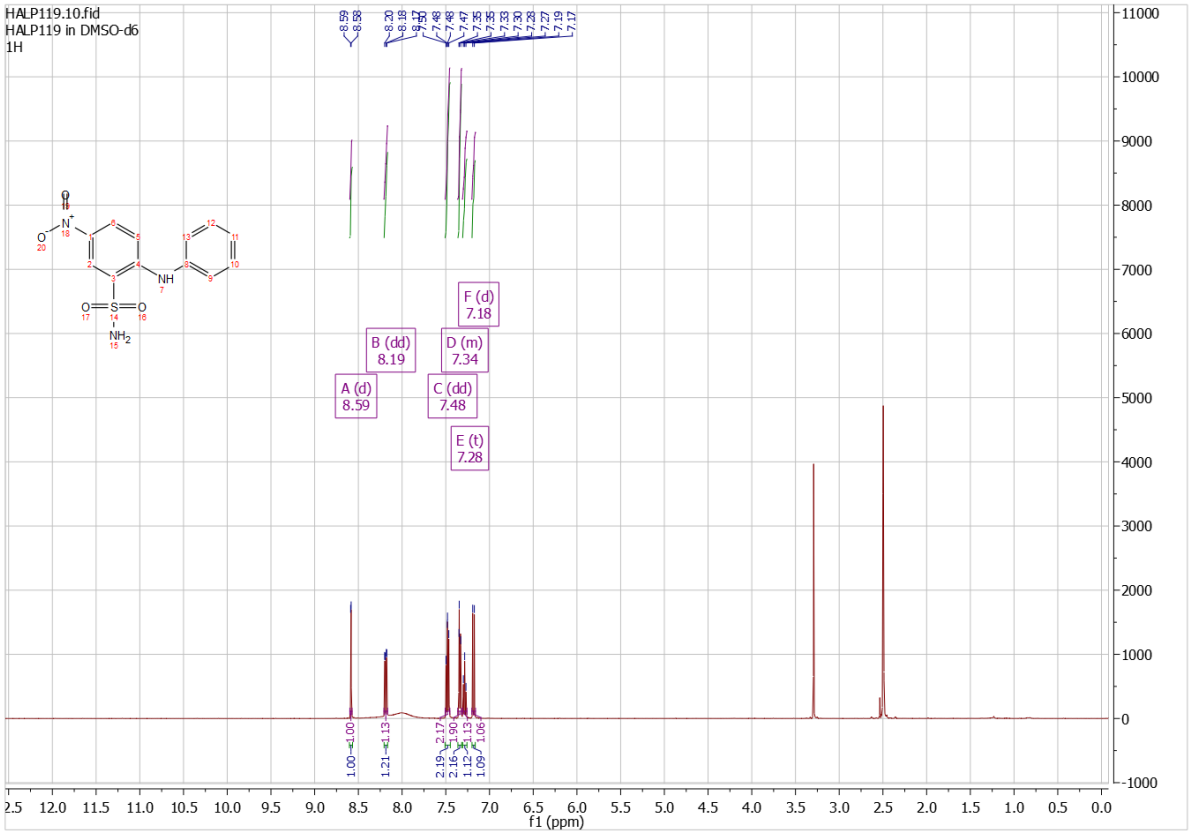
Sequence Name:	SingleSample		
Data file:	HALP119.dx	**Project Name:**	Single Quad
Sample name:	HALP119	**Operator :**	SYSTEM
Instrument:	Single Quad	**Acquired on:**	2022-02-22 07:04:38+01:00
Inj. volume:	4.000	**Location:**	P1-D2
Acq. method:	00-new_wasser-acn_standard_100-1000_BD-20min.amx		
Processing method:	MS_standard_plot.pmx		

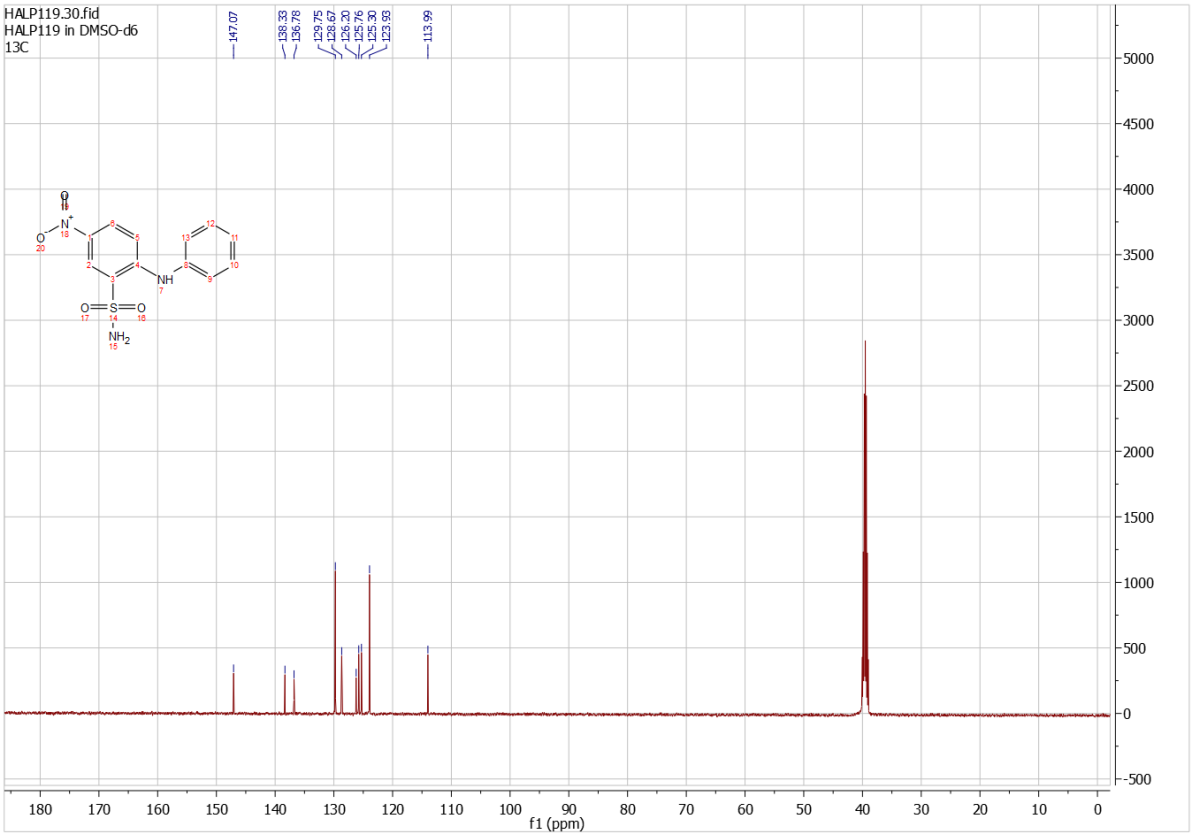


Signal: DAD1 Total WL (220.0:600.0 nm)

RT [min]	Peak MS Base Peak m/z	Area	Area%	Max Peak%	Height
5.495		559.7020	0.1049	0.105	82.830
6.157	294.000	531791.7667	99.6794	100.000	122514.917
9.306		1150.6394	0.2157	0.216	259.529
	Sum	533502.1082			

D:\CDSProjects\Default\0-standardplot+EIC.rdl [Rev. 5354] Printed: 2022-02-22 09:02:34+01:00 Page 1 of 2

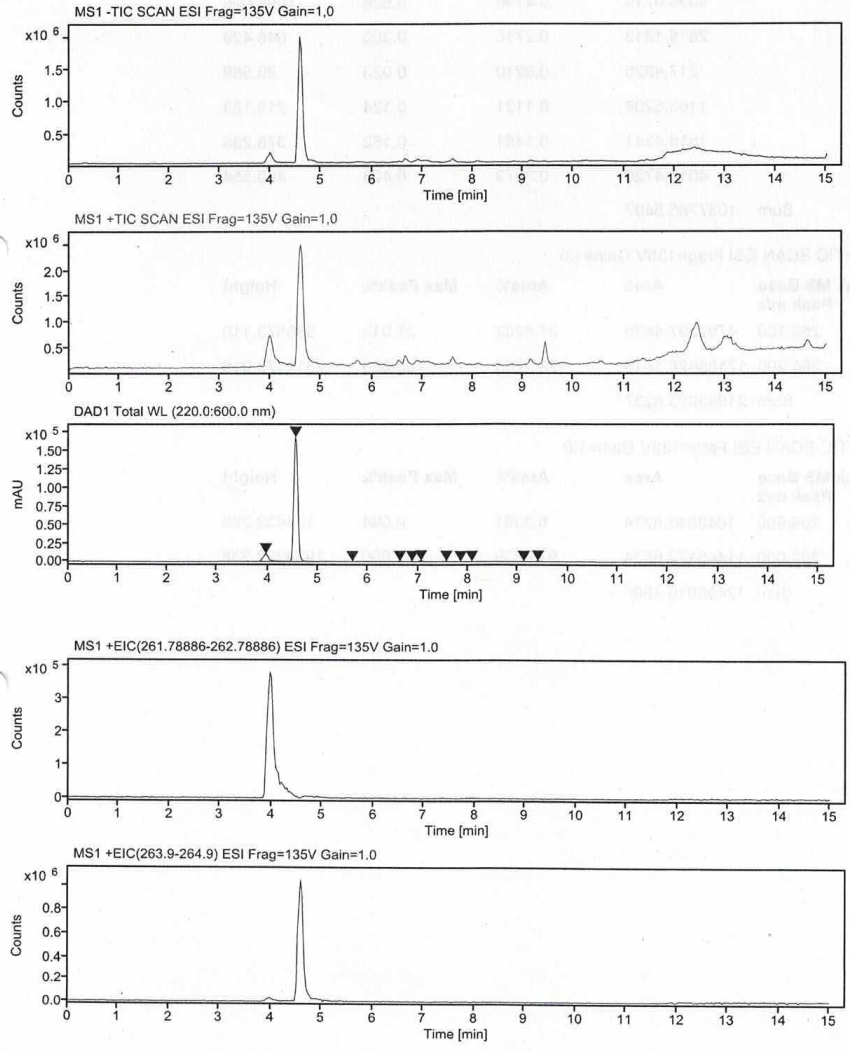

HALP119.10.fid
HALP119 in DMSO-d6
1H
A (d)
8.59
B (dd)
8.19
C (dd)
7.48
D (m)
7.34
E (t)
7.28
F (d)
7.18
f1 (ppm)

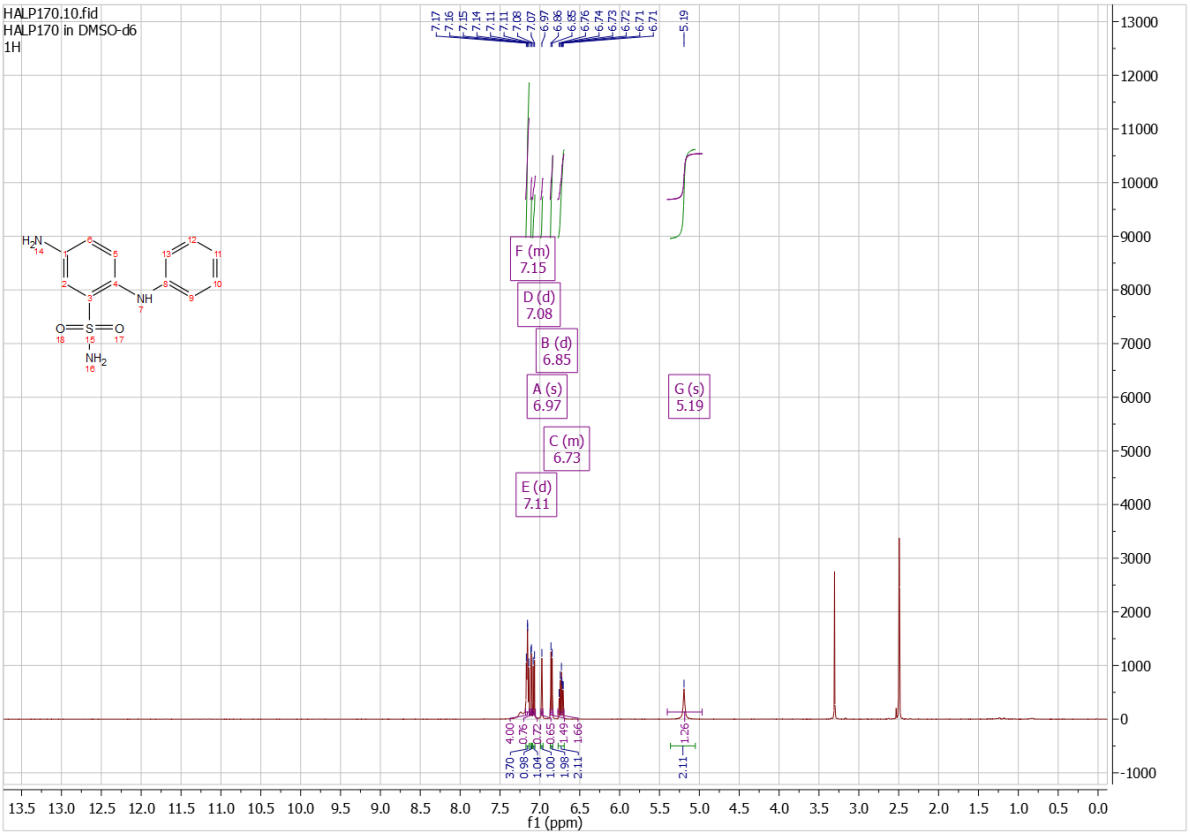

HALP119.30.fid
HALP119 in DMSO-d6
13C
f1 (ppm)

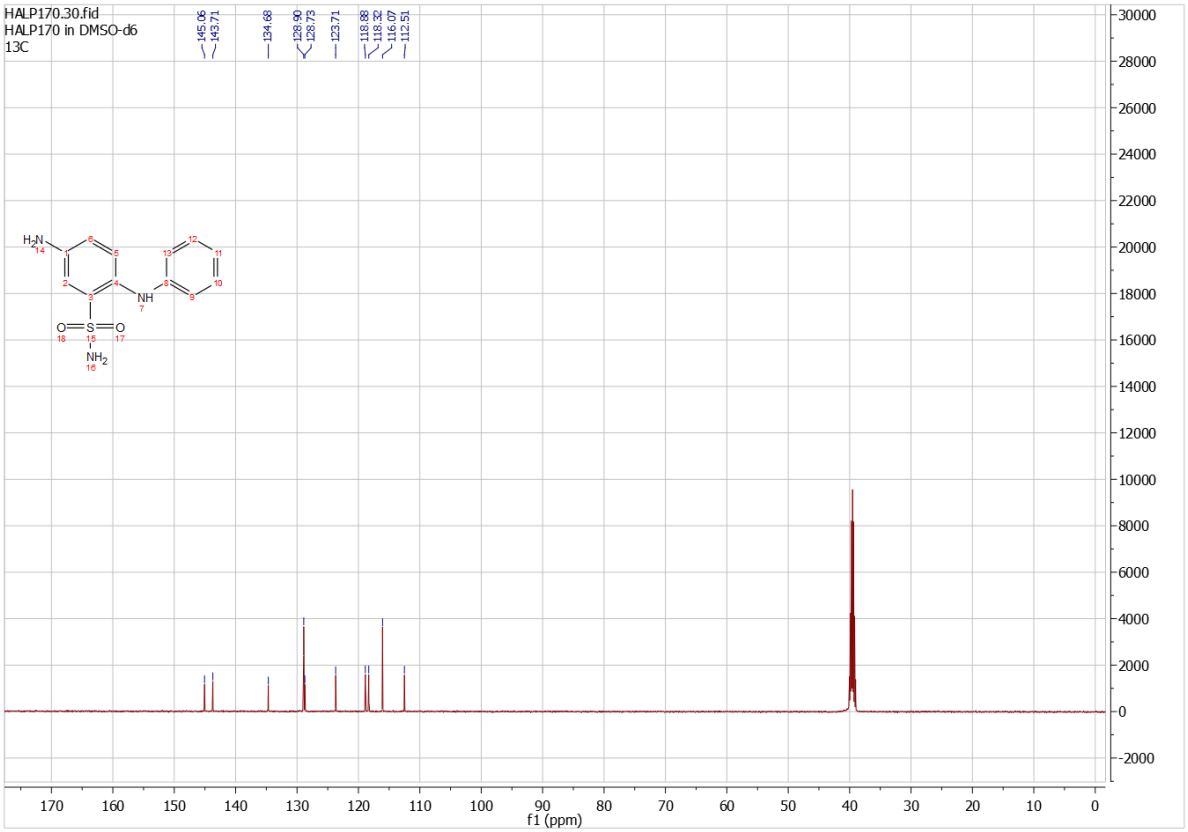
5-Amino-2-(phenylamino)benzenesulfonamide (**43**)

43

Sequence Name:	SingleSample		
Data file:	HALP170.dx	**Project Name:**	Single Quad
Sample name:	HALP170	**Operator :**	SYSTEM
Instrument:	Single Quad	**Acquired on:**	2022-03-01 22:23:03+01:00
Inj. volume:	6.000	**Location:**	P2-A3
Acq. method:	00-new_wasser-acn_standard_100-1000_BD-20min.amx		
Processing method:	MS_standard_plot.pmx		



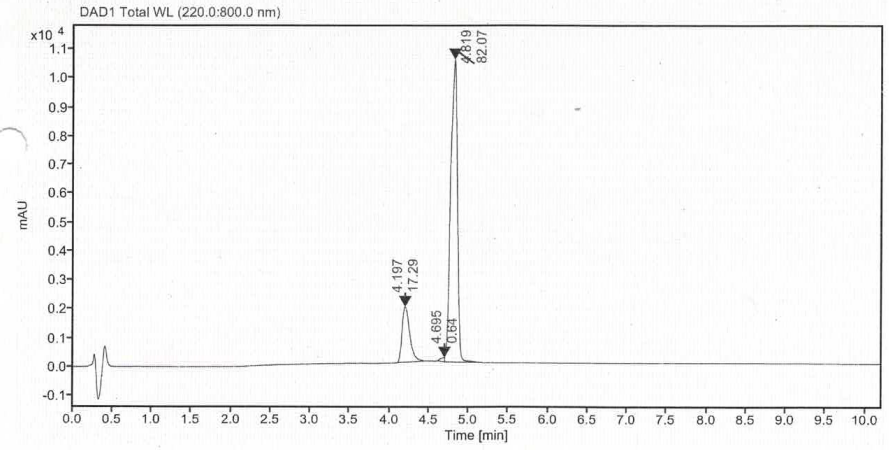

HALP170.10.fid
HALP170 in DMSO-d6
1H
F (m)
7.15
D (d)
7.08
B (d)
6.85
A (s)
6.97
G (s)
5.19
C (m)
6.73
E (d)
7.11
f1 (ppm)

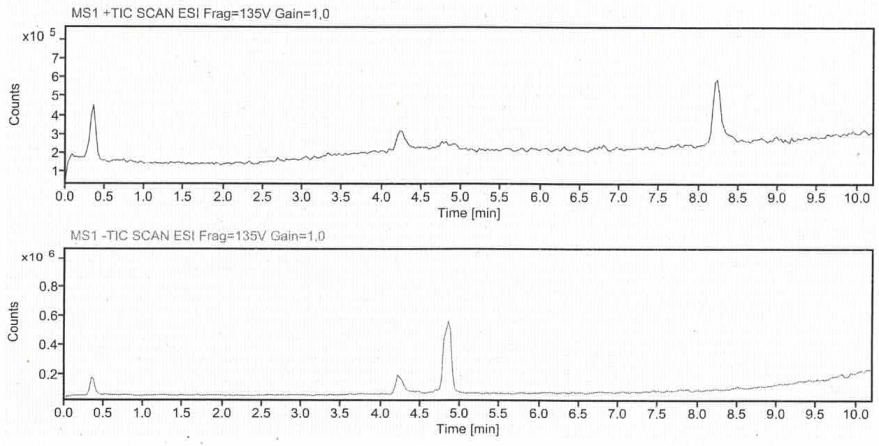

HALP170.30.fid
HALP170 in DMSO-d6
13C
f1 (ppm)

Sodium 1-amino-6-chloro-9,10-dioxo-4-((4-(phenylamino)-3-sulfonatophenyl)amino)-9,10-dihydroanthracene-2-sulfonate (**44**)

44

Sequence Name:	SingleSample		
Data file:	HAL30-F1N.dx	**Project Name:**	Single Quad
Sample name:	HAL30-F1N	**Operator :**	SYSTEM
Instrument:	Single Quad	**Acquired on:**	2020-09-07 07:20:22+02:00
Inj. volume:	5.000	**Location:**	P1-E4
Acq. method:	0_wasser-acn_standard_100-1000_AC-20min.amx		
Processing method:	MS_standard_plot.pmx		





Sequence Name:	SingleSample		
Data file:	HAL30-F1N.dx	**Project Name:**	Single Quad
Sample name:	HAL30-F1N	**Operator :**	SYSTEM
Instrument:	Single Quad	**Acquired on:**	2020-09-07 07:20:22+02:00
Inj. volume:	5.000	**Location:**	P1-E4
Acq. method:	0_wasser-acn_standard_100-1000_AC-20min.amx		
Processing method:	MS_standard_plot.pmx		

Signal: DAD1 Total WL (220.0:800.0 nm)

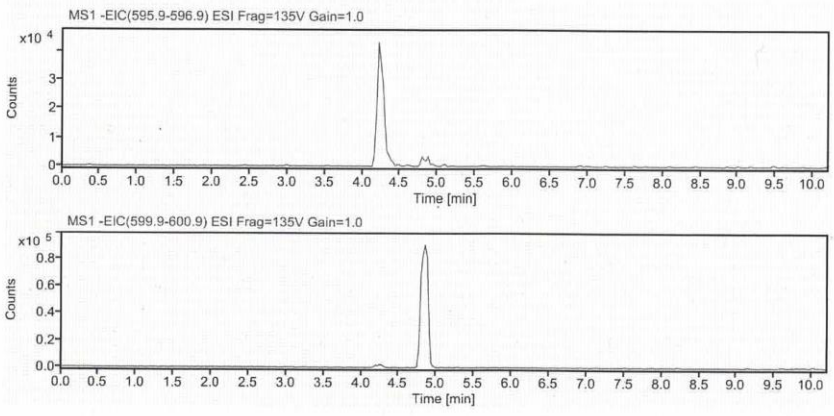
RT [min]	Name	Area	Area%	Max Peak%	Height	Type
4.197		12967.2177	17.2917	21.070	1930.707	MM m
4.695		481.5973	0.6422	0.783	156.309	MM m
4.819		61542.3163	82.0661	100.000	10470.745	MM m
	Sum	74991.1314				

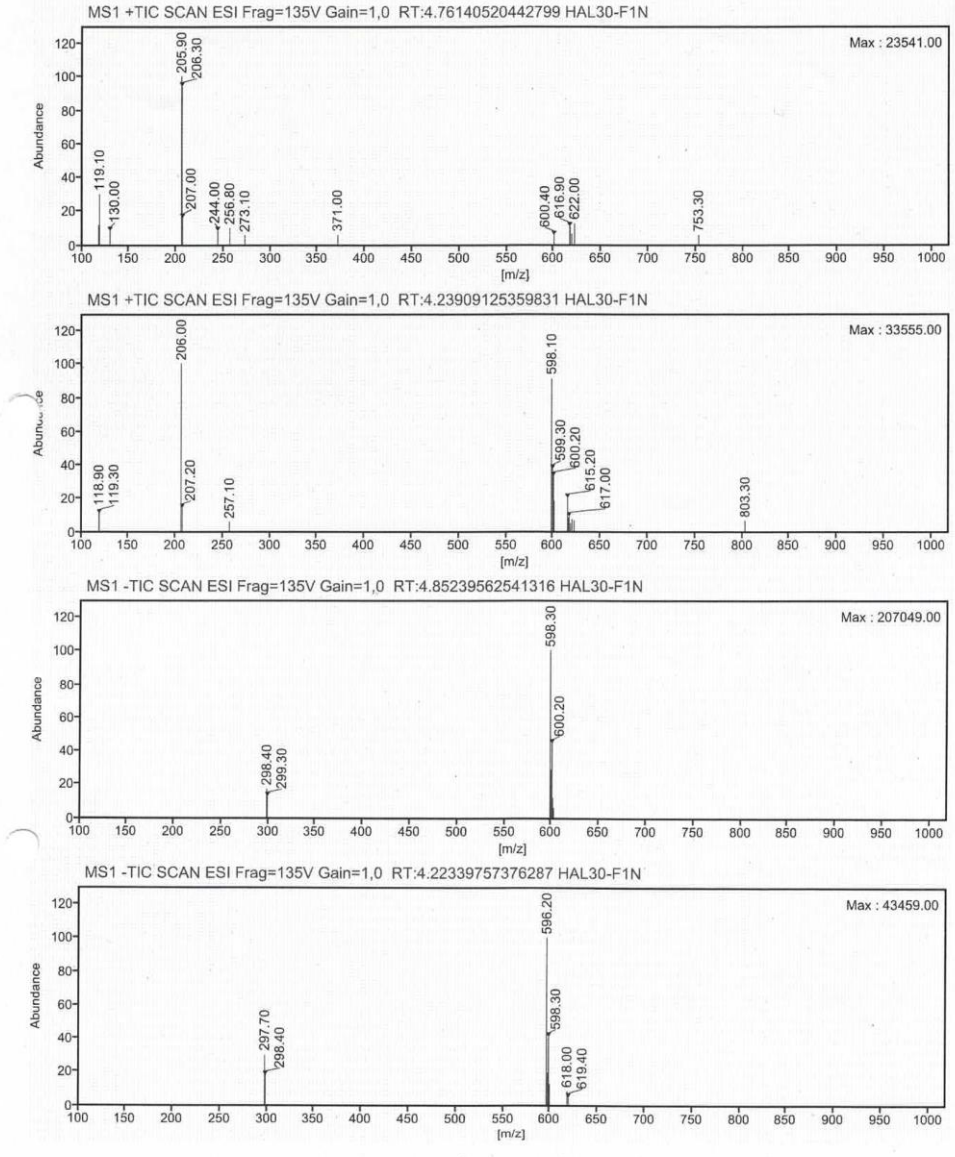
Signal: MS1 +TIC SCAN ESI Frag=135V Gain=1,0

RT [min]	Name	Area	Area%	Max Peak%	Height	Type
4.239		724741.9592	77.0536	100.000	99686.415	MM m
4.761		215826.2520	22.9464	29.780	30964.420	MM m
	Sum	940568.2112				

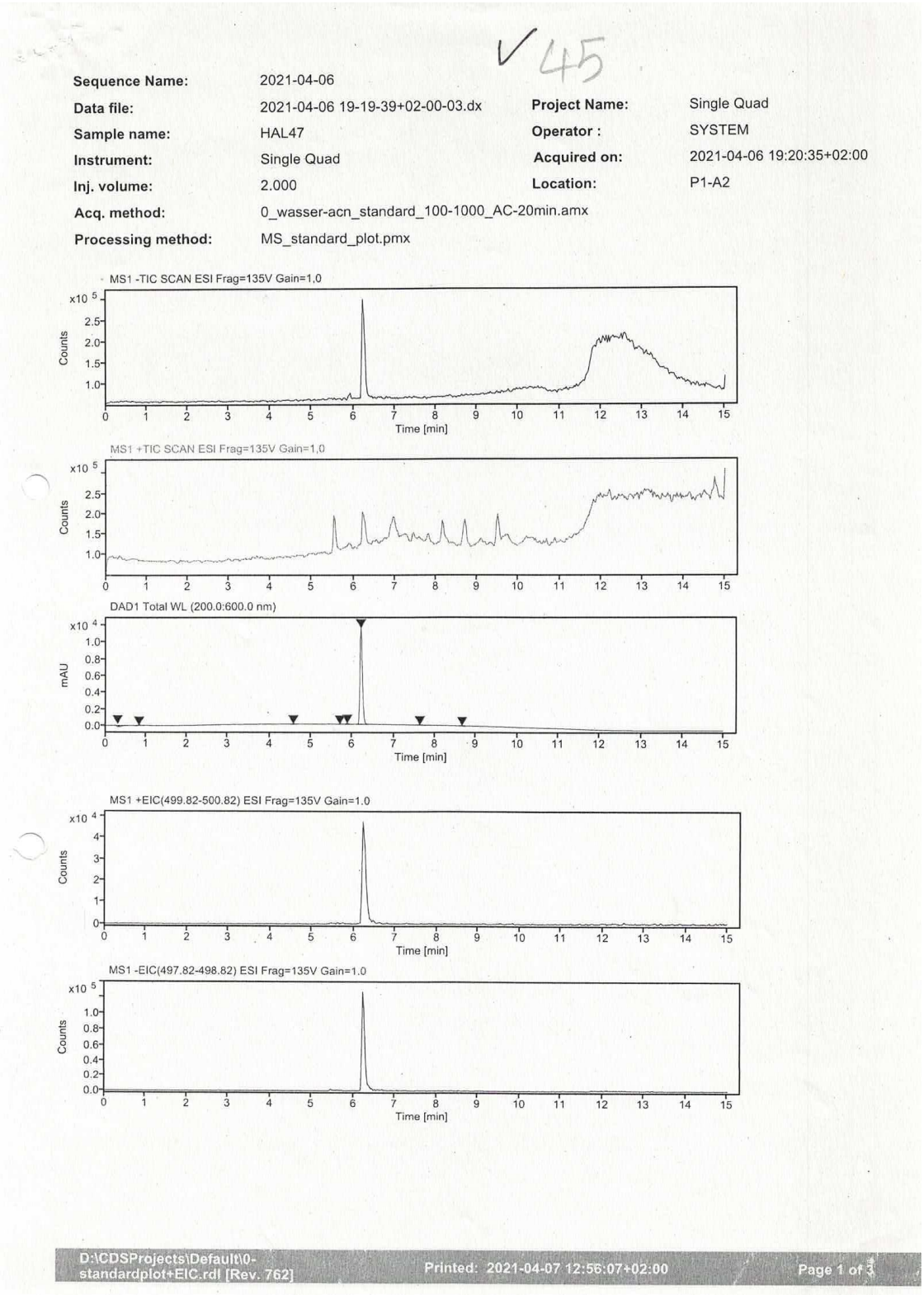
Signal: MS1 -TIC SCAN ESI Frag=135V Gain=1,0

RT [min]	Name	Area	Area%	Max Peak%	Height	Type
4.223		686820.9488	17.6350	21.411	119781.699	MM m
4.852		3207835.8688	82.3650	100.000	475192.382	MM m
	Sum	3894656.8177				




MS1 +TIC SCAN ESI Frag=135V Gain=1,0 RT:4.76140520442799 HAL30-F1N
Max : 23541.00
205.90
206.30
119.10
130.00
207.00
244.00
256.80
273.10
371.00
600.40
616.90
622.00
753.30
MS1 +TIC SCAN ESI Frag=135V Gain=1,0 RT:4.23909125359831 HAL30-F1N
Max : 33555.00
206.00
598.10
118.90
119.30
207.20
257.10
599.30
600.20
615.20
617.00
803.30
MS1 -TIC SCAN ESI Frag=135V Gain=1,0 RT:4.85239562541316 HAL30-F1N
Max : 207049.00
598.30
600.20
298.40
299.30
MS1 -TIC SCAN ESI Frag=135V Gain=1,0 RT:4.22339757376287 HAL30-F1N
Max : 43459.00
596.20
598.30
297.70
298.40
618.00
619.40
Abundance
[m/z]

Sodium 1-amino-4-((4-(methyl(phenyl)amino)phenyl)amino)-9,10-dioxo-9,10-dihydroanthracene-2-sulfonate (**45**)



Signal: DAD1 Total WL (200.0:600.0 nm)

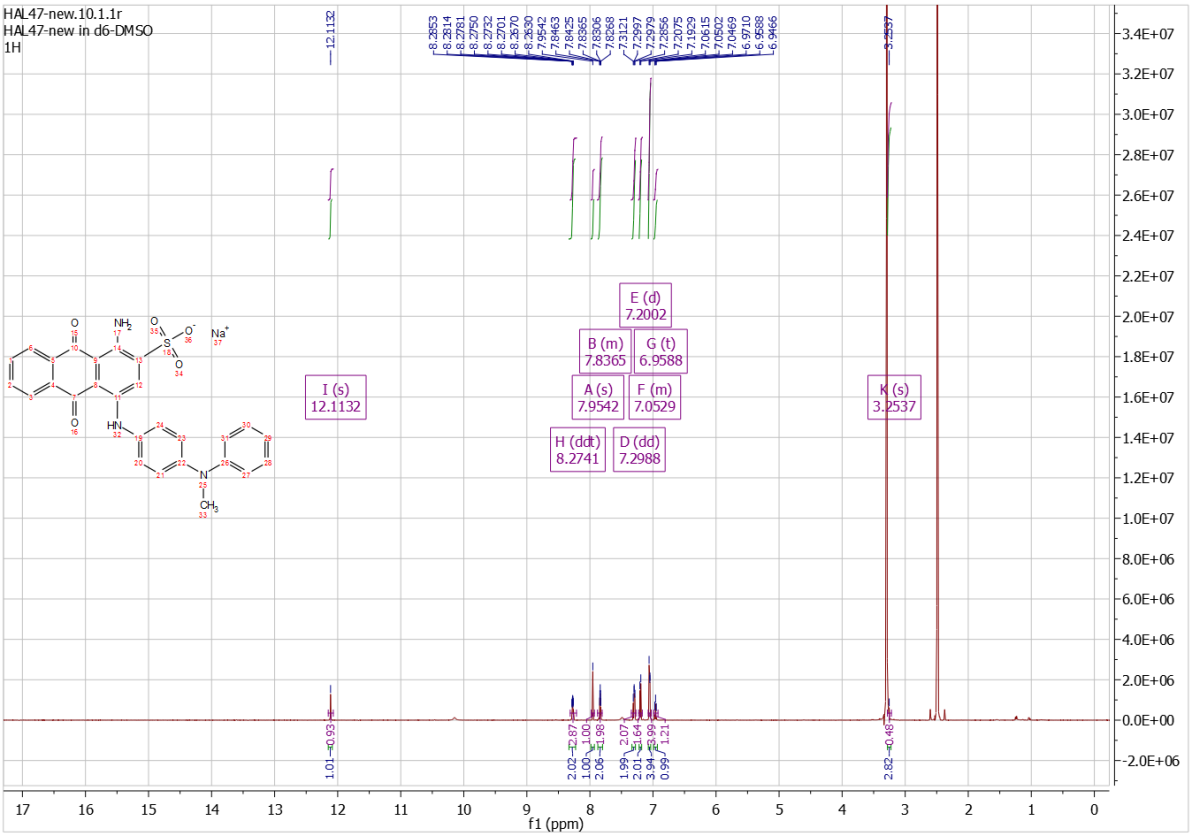
RT [min]	Peak MS Base Peak m/z	Area	Area%	Max Peak%	Height
0.303		1189.0975	2.3375	2.448	183.401
0.835		180.8013	0.3554	0.372	29.805
4.572		131.1009	0.2577	0.270	38.494
5.695		22.3870	0.0440	0.046	7.174
5.877		468.9705	0.9219	0.966	129.157
6.201		48565.1082	95.4701	100.000	11515.671
7.635		181.6403	0.3571	0.374	42.753
8.664		130.3450	0.2562	0.268	27.659
	Sum	50869.4508			

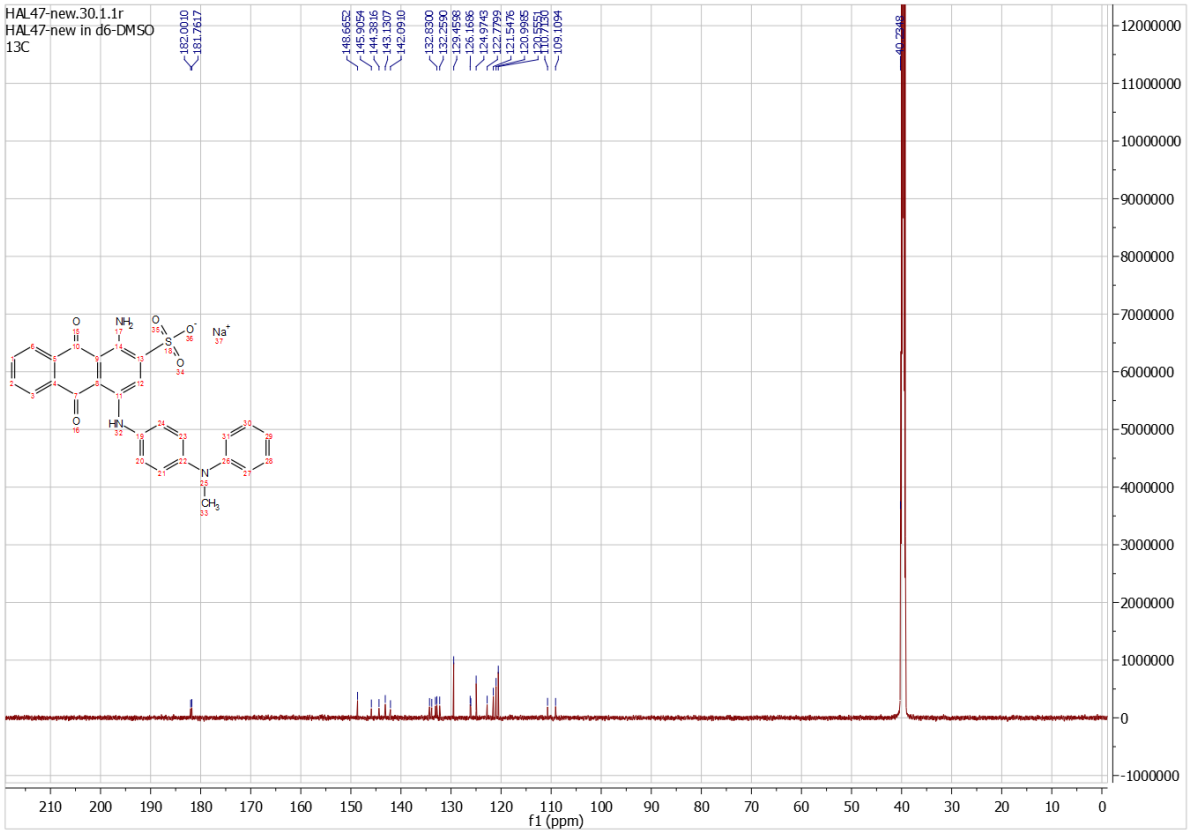
Signal: MS1 +TIC SCAN ESI Frag=135V Gain=1,0

RT [min]	Peak MS Base Peak m/z	Area	Area%	Max Peak%	Height
6.229	500.300	420081.1683	100.0000	100.000	85336.463
	Sum	420081.1683			

Signal: MS1 -TIC SCAN ESI Frag=135V Gain=1,0

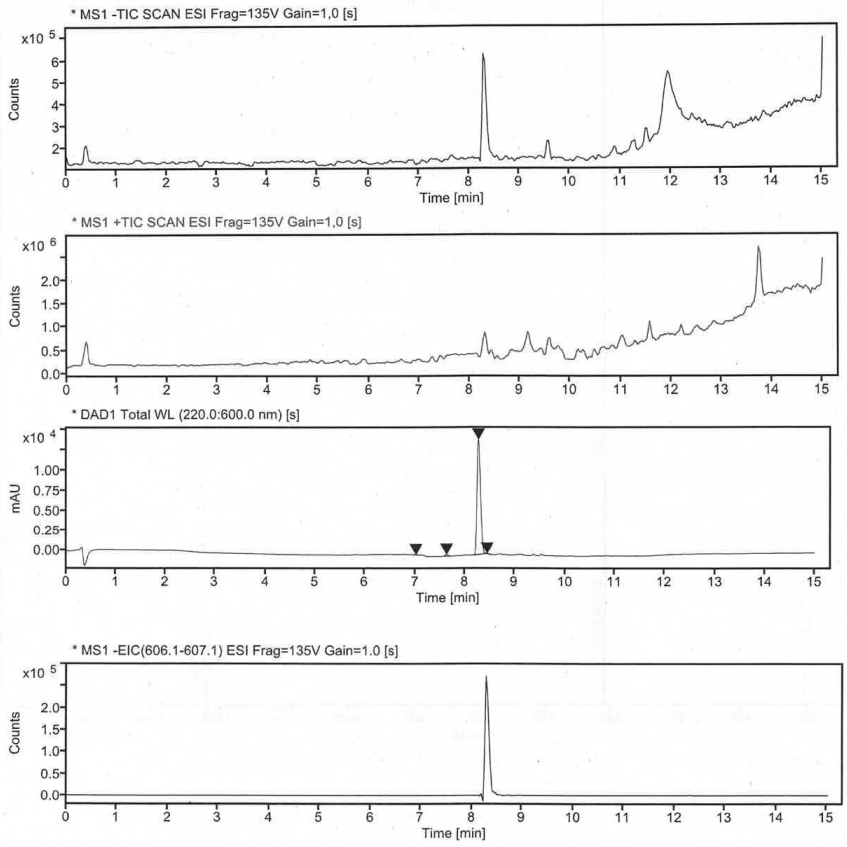
RT [min]	Peak MS Base Peak m/z	Area	Area%	Max Peak%	Height
6.239	498.200	1136701.4978	100.0000	100.000	233048.004
	Sum	1136701.4978			


HAL47-new.10.1.1r
HAL47-new in d6-DMSO
1H
I (s)
12.1132
E (d)
7.2002
B (m)
7.8365
G (t)
6.9588
A (s)
7.9542
F (m)
7.0529
H (ddt)
8.2741
D (dd)
7.2988
K (s)
3.2537
f1 (ppm)


HAL47-new.30.1.1r
HAL47-new in d6-DMSO
13C
f1 (ppm)

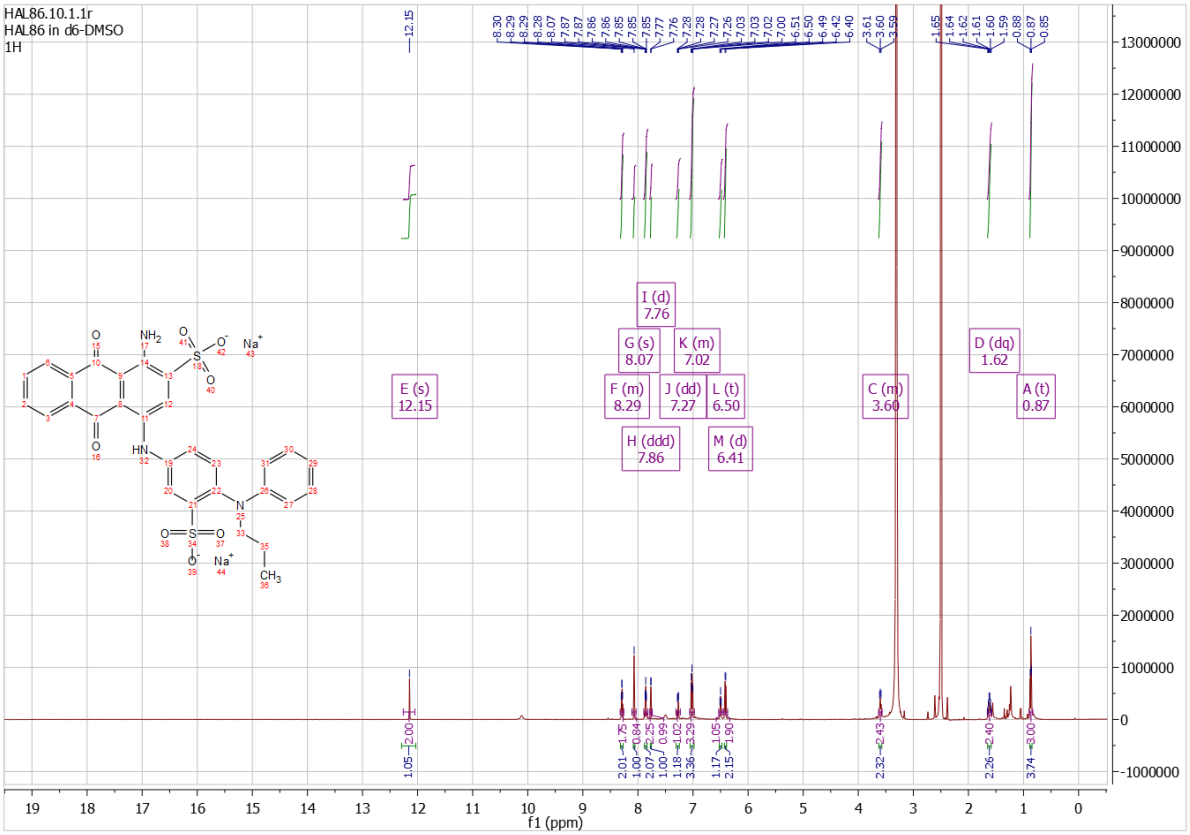
Sodium 1-amino-9,10-dioxo-4-((4-(phenyl(propyl)amino)-3-sulfonatophenyl)amino)-9,10-dihydroanthracene-2-sulfonate (**46**)

Sequence Name:	SingleSample		
Data file:	HALP86.dx	**Project Name:**	Single Quad
Sample name:	HALP86	**Operator :**	SYSTEM
Instrument:	Single Quad	**Acquired on:**	2025-05-27 17:54:32+02:00
Inj. volume:	8.000	**Location:**	P1-C5
Acq. method:	00-new_wasser-meoh_standard_100-1500_CD-20min.amx		
Processing method:	MS_standard_plot.pmx		



Signal: * DAD1 Total WL (220.0:600.0 nm) [s]

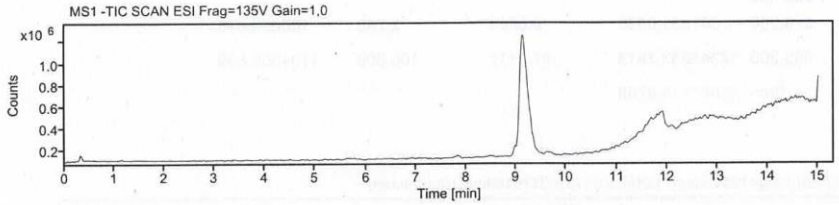
RT [min]	Peak MS Base Peak m/z	Area	Area%	Max Peak%	Height
7.021		171.3669	0.2460	0.250	44.408
7.633		866.2757	1.2434	1.265	235.671
8.269		68496.2763	98.3162	100.000	14235.157
8.444		135.4838	0.1945	0.198	46.217
	Sum	69669.4026			

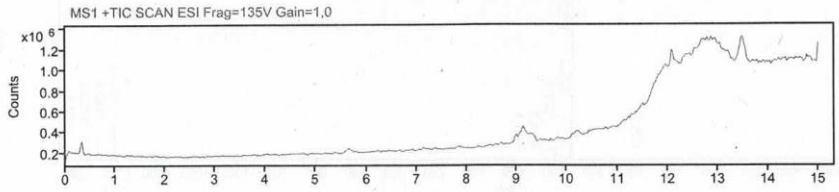

HAL86.10.1.1r
HAL86 in d6-DMSO
1H
E (s)
12.15
I (d)
7.76
G (s)
8.07
K (m)
7.02
F (m)
8.29
J (dd)
7.27
L (t)
6.50
H (ddd)
7.86
M (d)
6.41
C (m)
3.60
D (dq)
1.62
A (t)
0.87
f1 (ppm)

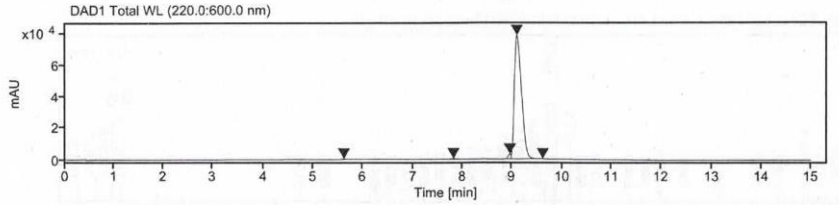
Sodium 1-amino-9,10-dioxo-4-((4-(phenylamino)-3-sulfamoylphenyl)amino)-9,10-dihydroanthracene-2-sulfonate (**47**)

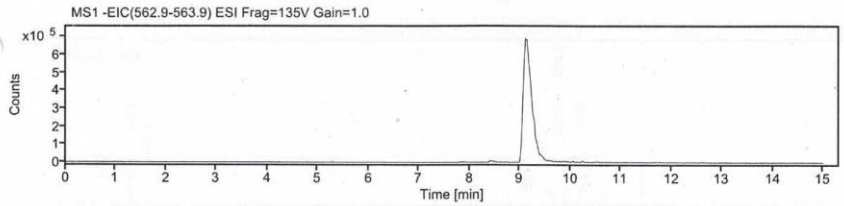
47V

Sequence Name:	SingleSample		
Data file:	HALP173-N_MeOH-neu.dx	**Project Name:**	Single Quad
Sample name:	HALP173-N_MeOH-neu	**Operator :**	SYSTEM
Instrument:	Single Quad	**Acquired on:**	2022-03-30 13:46:39+02:00
Inj. volume:	5.000	**Location:**	P1-C3
Acq. method:	00-new_wasser-meoh_standard_100-1500_CD-20min.amx		
Processing method:	MS_standard_plot.pmx		





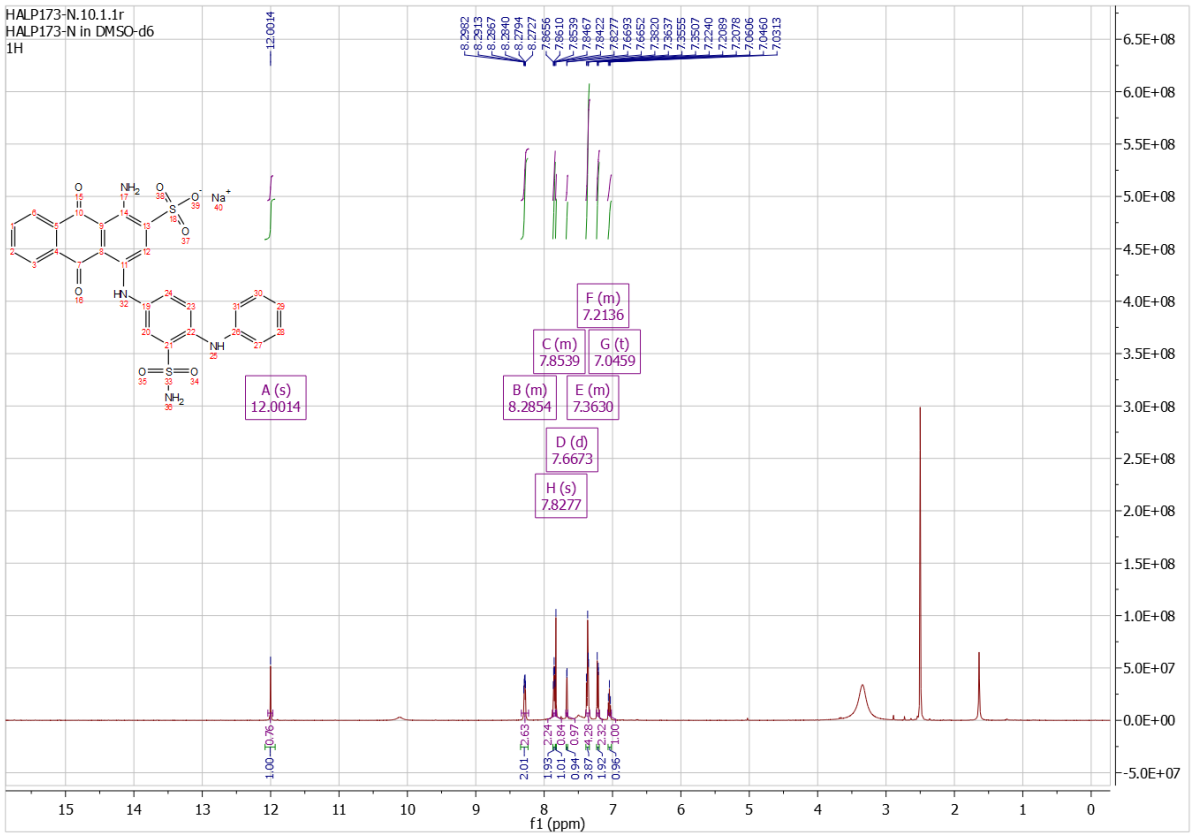


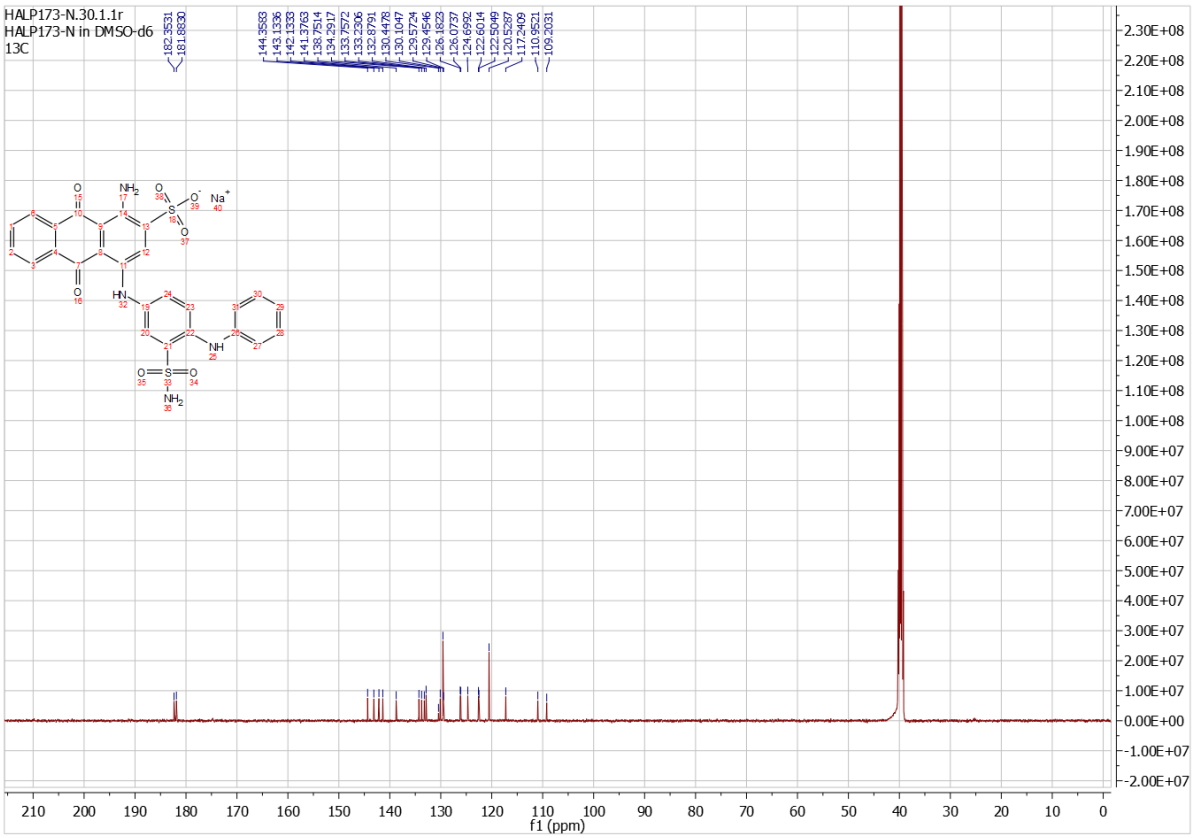


Signal: DAD1 Total WL (220.0:600.0 nm)

RT [min]	Peak MS Base Peak m/z	Area	Area%	Max Peak%	Height
5.615		1290.4048	0.1612	0.164	273.314
7.817		1591.8417	0.1989	0.203	317.921
8.957		11648.2959	1.4553	1.484	3040.439
9.097		785176.6113	98.1006	100.000	78370.508
9.617		672.2051	0.0840	0.086	131.466
	Sum	800379.3588			

D:\CDSProjects\Default\0-standardplot+EIC.rdl [Rev. 6152] Printed: 2022-03-30 14:14:12+02:00 Page 1 of 2

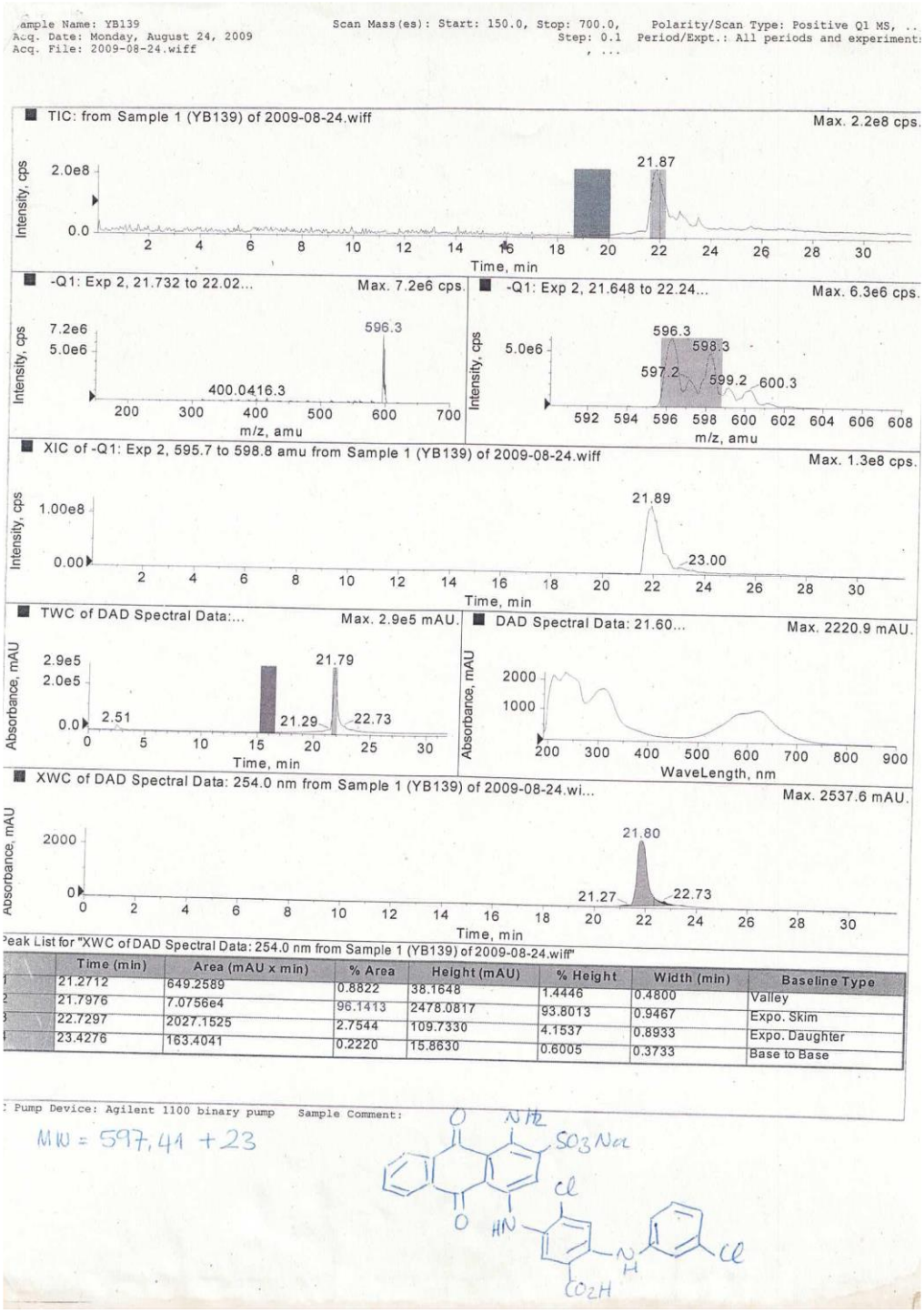

HALP173-N.10.1.1r
HALP173-N in DMSO-d6
1H
A (s)
12.0014
B (m)
8.2854
C (m)
7.8539
D (d)
7.6673
E (m)
7.3630
F (m)
7.2136
G (t)
7.0459
H (s)
7.8277
f1 (ppm)

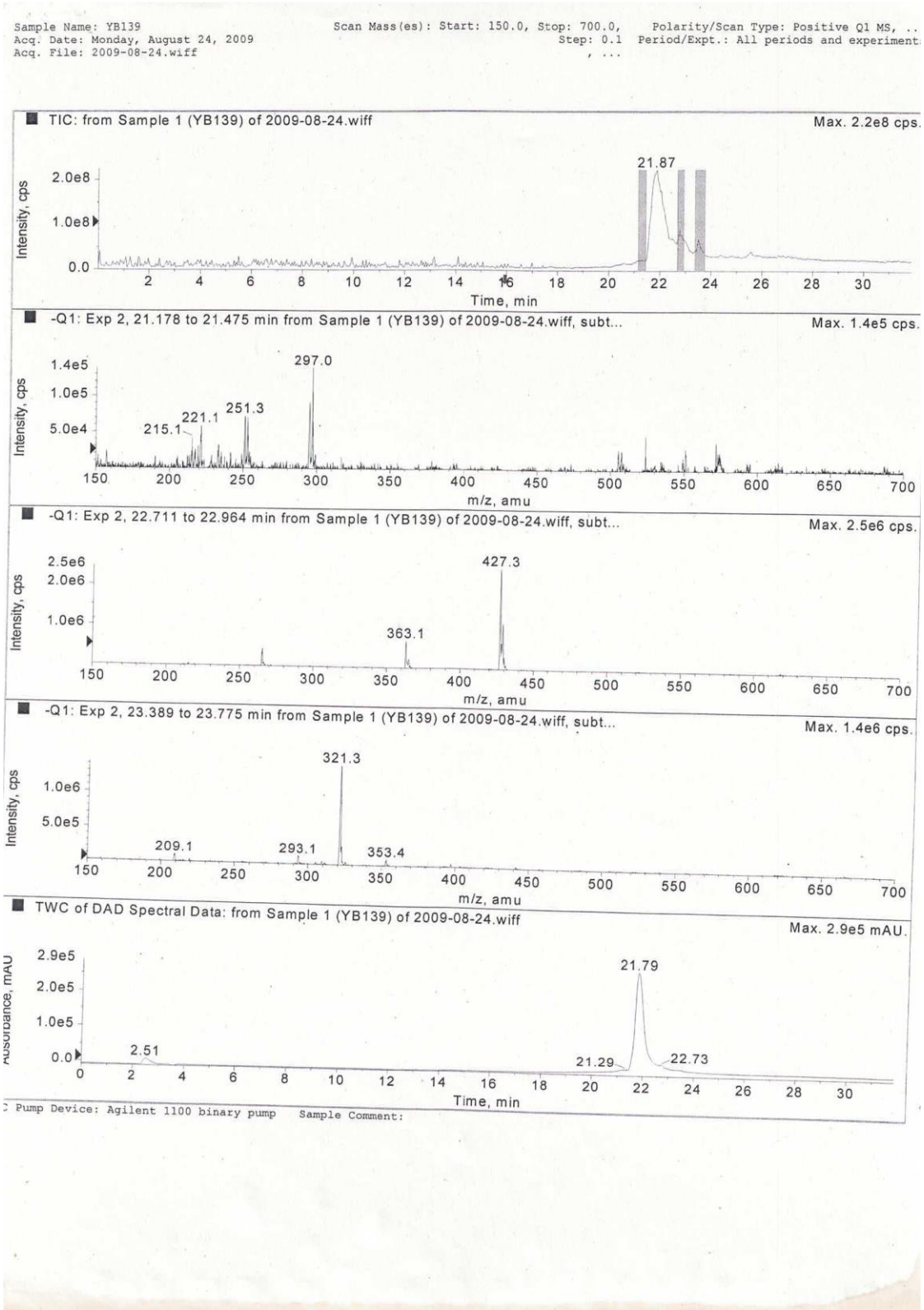

HALP173-N.30.1.1r
HALP173-N in DMSO-d6
13C
f1 (ppm)

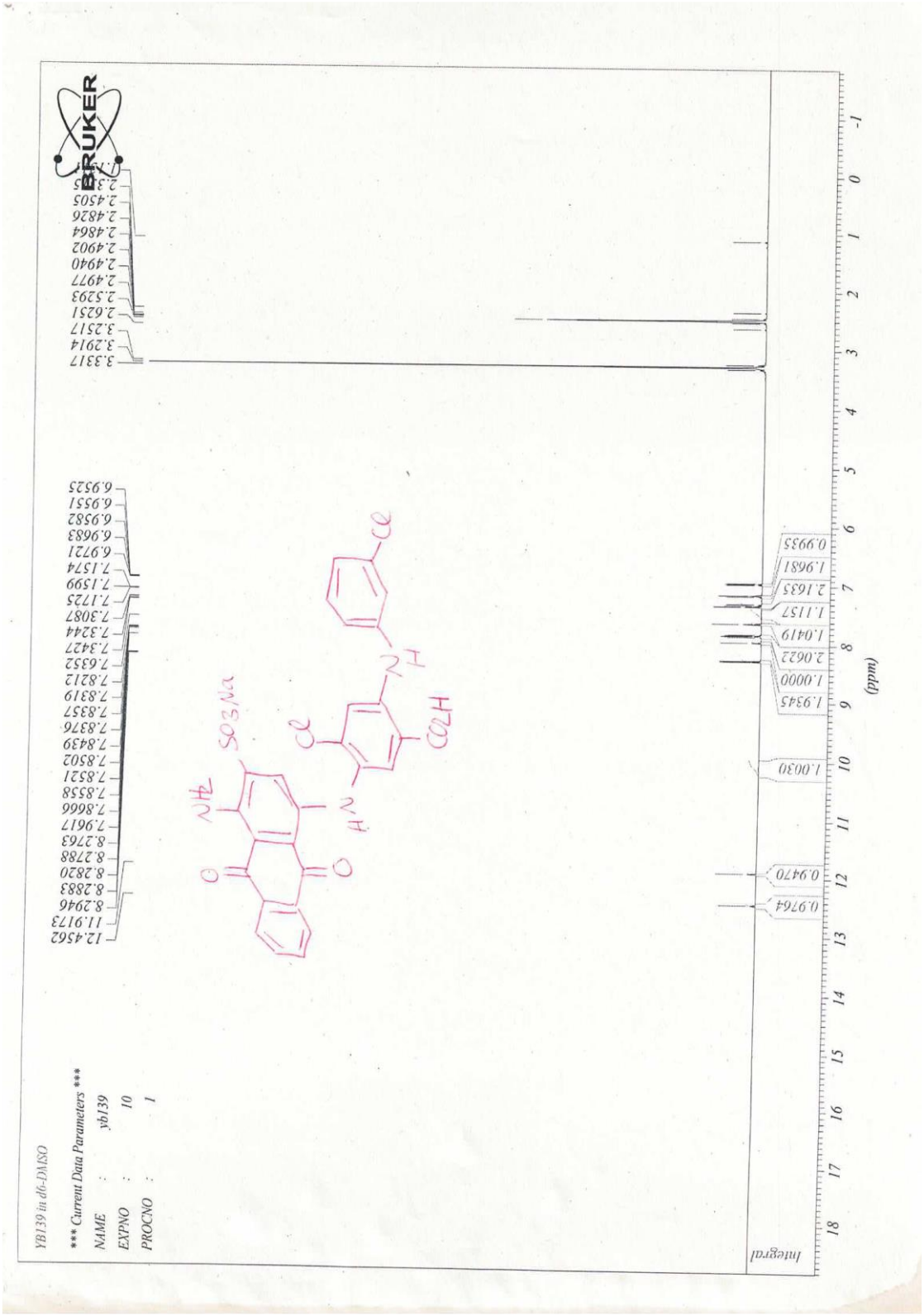
7.2 Appendix II: Systematic development of anthraquinone-derived $P2Y_{12}$ receptor antagonists as radioligand candidates (Manuscript I)

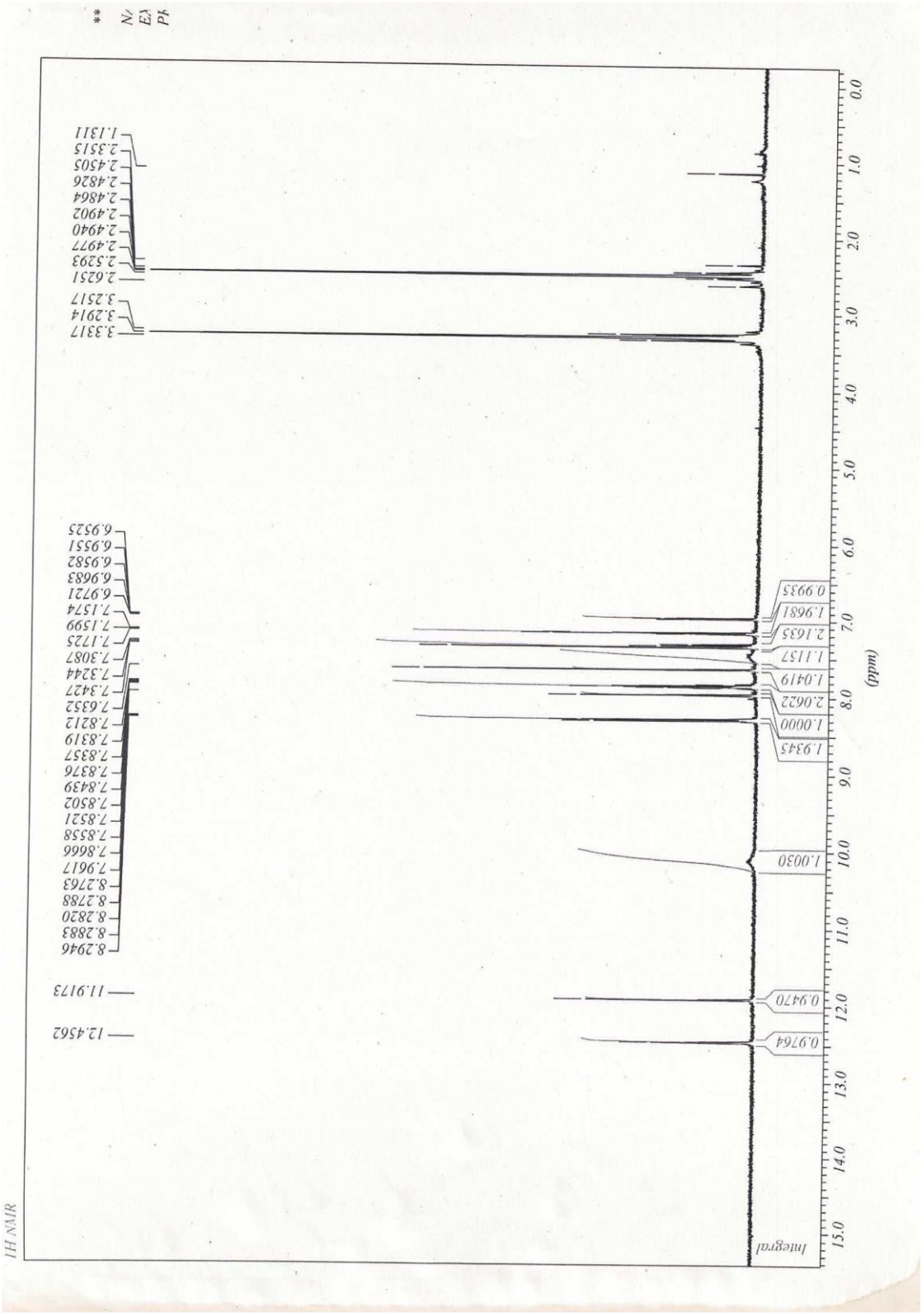
Analytical data:

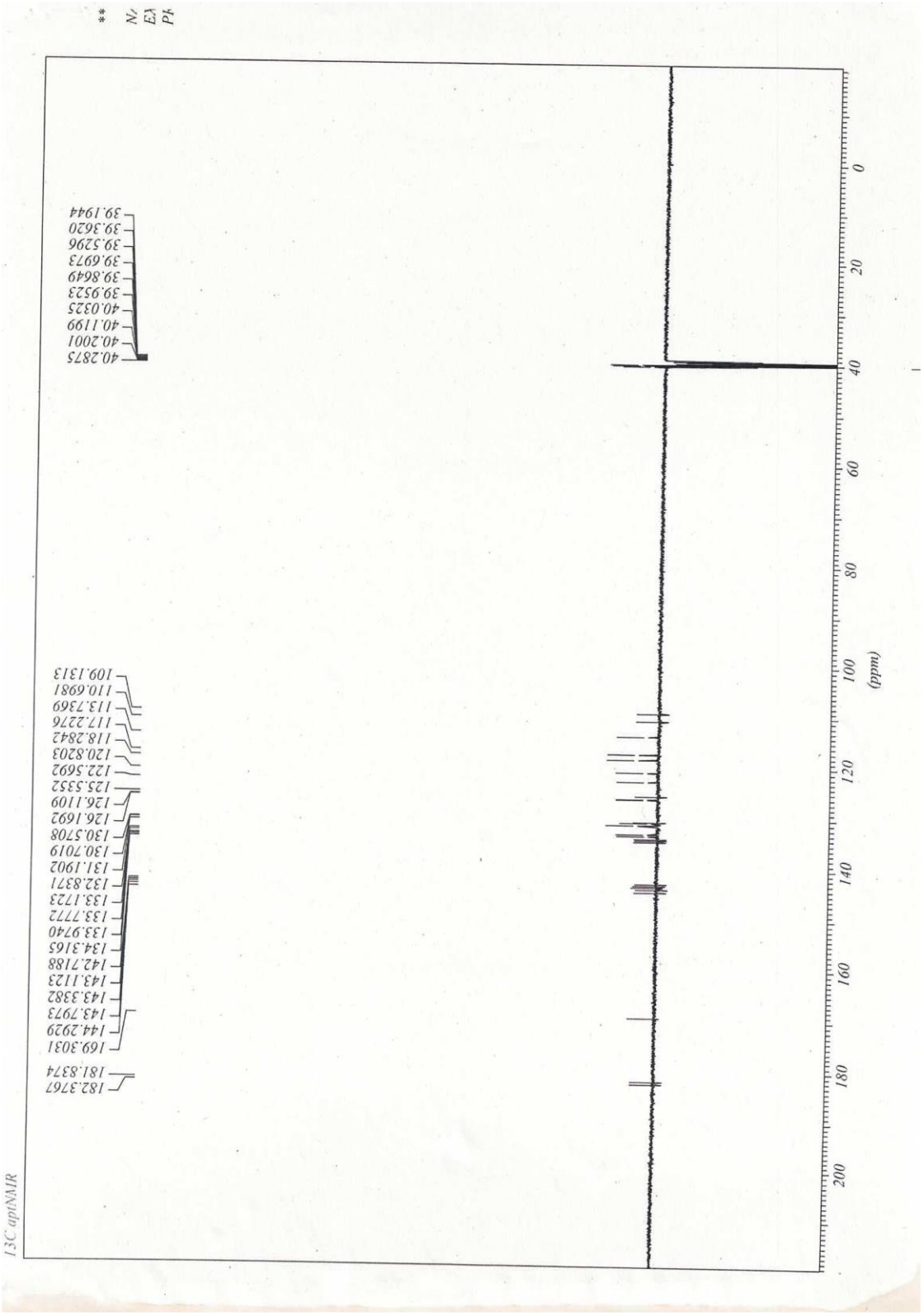
Sodium 1-amino-4-((5-carboxy-2-chloro-4-((3-chlorophenyl)amino)phenyl)amino)-9,10-dioxo-9,10-dihydroanthracene-2-sulfonate (**3**)




Sample Name: YB139
Acq. Date: Monday, August 24, 2009
Acq. File: 2009-08-24.wiff
Scan Mass(es): Start: 150.0, Stop: 700.0, Step: 0.1
Polarity/Scan Type: Positive Q1 MS, ..
Period/Expt.: All periods and experiment
TIC: from Sample 1 (YB139) of 2009-08-24.wiff
Max. 2.2e8 cps.
Intensity, cps
Time, min
21.87
-Q1: Exp 2, 21.178 to 21.475 min from Sample 1 (YB139) of 2009-08-24.wiff, subt...
Max. 1.4e5 cps.
297.0
251.3
221.1
215.1
m/z, amu
-Q1: Exp 2, 22.711 to 22.964 min from Sample 1 (YB139) of 2009-08-24.wiff, subt...
Max. 2.5e6 cps.
427.3
363.1
-Q1: Exp 2, 23.389 to 23.775 min from Sample 1 (YB139) of 2009-08-24.wiff, subt...
Max. 1.4e6 cps.
321.3
209.1
293.1
353.4
TWC of DAD Spectral Data: from Sample 1 (YB139) of 2009-08-24.wiff
Max. 2.9e5 mAU.
21.79
2.51
21.29
22.73
Pump Device: Agilent 1100 binary pump
Sample Comment:


YB139 in d6-DMSO
*** Current Data Parameters ***
NAME : yb139
EXPNO : 10
PROCNO : 1
BRUKER
integral
(ppm)
SO3Na
NH2
Cl
N
H
CO2H
O
O
H2N
Cl

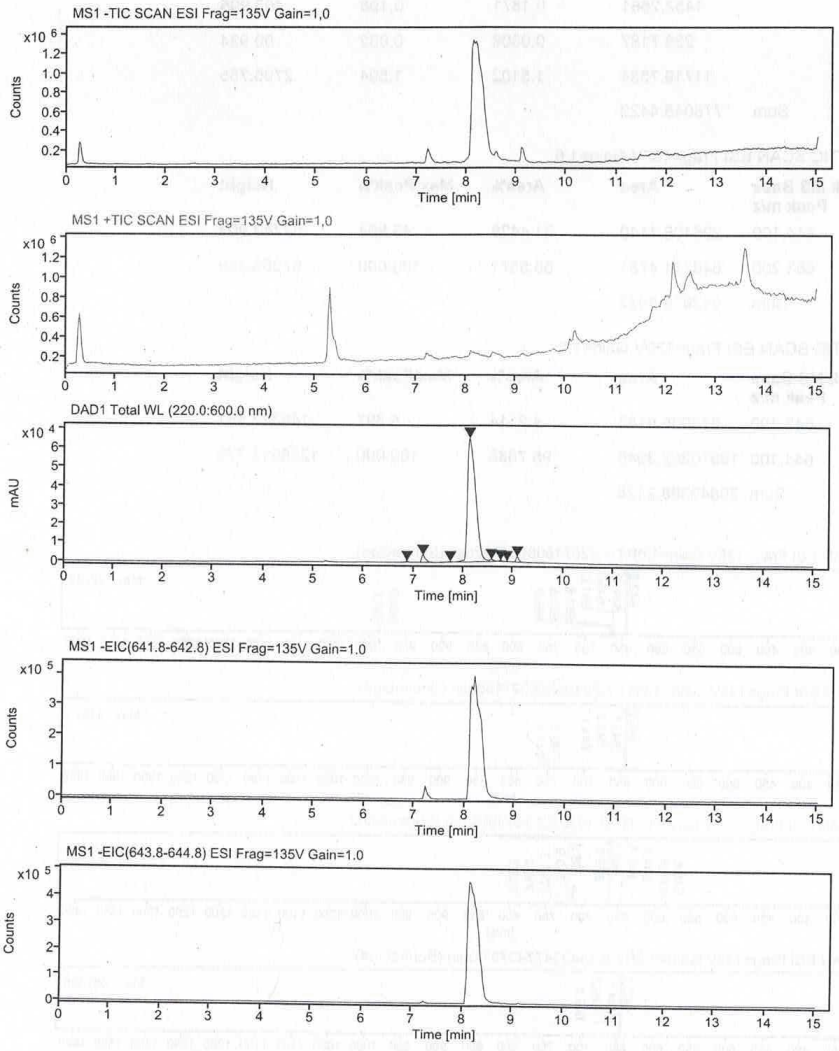

1H NMR
(ppm)
Integral
0.9764
0.9470
1.0030
1.9345
1.0000
2.0622
1.0419
1.1157
2.1635
1.9681
0.9935
11.9173
12.4562
8.2946
8.2883
8.2820
8.2788
8.2763
7.9617
7.8666
7.8558
7.8521
7.8502
7.8439
7.8376
7.8357
7.8319
7.8212
7.6352
7.3427
7.3244
7.3087
7.1725
7.1599
7.1574
6.9721
6.9683
6.9582
6.9551
6.9525
3.3317
3.2914
3.2517
2.6251
2.5293
2.4977
2.4940
2.4902
2.4864
2.4826
2.4505
2.3515
1.1311


13C aptNAIR
(ppm)
0
20
40
60
80
100
120
140
160
180
200
39.1944
39.3620
39.5296
39.6973
39.8649
39.9523
40.0325
40.1199
40.2001
40.2875
109.1313
110.6981
113.7369
117.2276
118.2842
120.8203
122.5692
125.3352
126.1109
126.1692
130.5708
130.7019
131.1902
132.8371
133.1723
133.7772
133.9740
134.3165
142.7188
143.1123
143.3382
143.7973
144.2929
169.3031
181.8374
182.3767

Sodium 1-amino-4-((4-((4-bromophenyl)amino)-3-sulfonatophenyl)amino)- 9,10-dioxo-9,10-dihydroanthracene-2-sulfonate (**5**)

16

Sequence Name:	SingleSample		
Data file:	HALP174-F2-meoh.dx	**Project Name:**	Single Quad
Sample name:	HALP174-F2-meoh	**Operator :**	SYSTEM
Instrument:	Single Quad	**Acquired on:**	2022-03-18 08:56:22+01:00
Inj. volume:	3.000	**Location:**	P2-A5
Acq. method:	00-new_wasser-meoh_standard_100-1000_CD-20min.amx		
Processing method:	MS_standard_plot.pmx		



Signal: DAD1 Total WL (220.0:600.0 nm)

RT [min]	Peak MS Base Peak m/z	Area	Area%	Max Peak%	Height
6.869		2171.4560	0.2798	0.295	362.634
7.191	644.100	18995.3054	2.4477	2.584	3671.963
7.737		669.0571	0.0862	0.091	96.423
8.115	644.100	735231.0932	94.7407	100.000	64852.410
8.561		5567.7931	0.7175	0.757	1109.699
8.746		1452.2661	0.1871	0.198	405.995
8.874		238.7187	0.0308	0.032	90.934
9.084		11719.7534	1.5102	1.594	2795.755
	Sum	776045.4429			

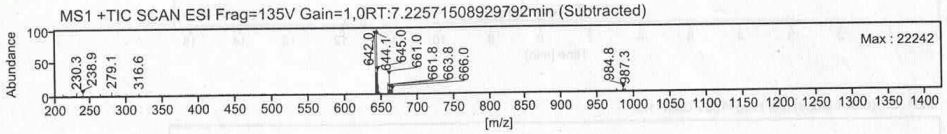
Signal: MS1 +TIC SCAN ESI Frag=135V Gain=1,0

RT [min]	Peak MS Base Peak m/z	Area	Area%	Max Peak%	Height
7.226	644.100	296405.4140	31.4429	45.864	57743.903
8.103	663.200	646271.4781	68.5571	100.000	67253.236
	Sum	942676.8922			

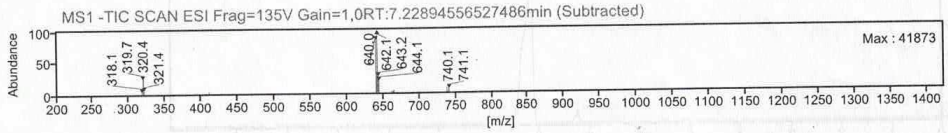
Signal: MS1 -TIC SCAN ESI Frag=135V Gain=1,0

RT [min]	Peak MS Base Peak m/z	Area	Area%	Max Peak%	Height
7.229	642.100	878005.8183	4.2114	4.397	149373.581
8.144	644.100	19970362.3945	95.7886	100.000	1255611.779
	Sum	20848368.2128			

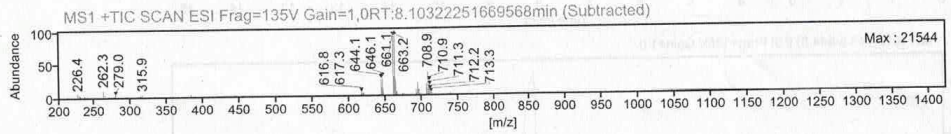
MS1 +TIC SCAN ESI Frag=135V Gain=1,0RT:7.22571508929792min (Subtracted)



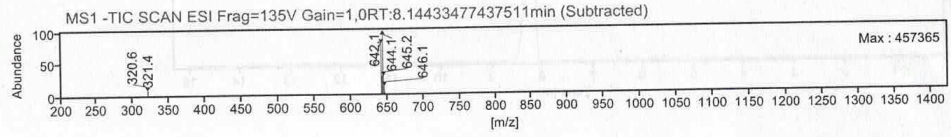
MS1 -TIC SCAN ESI Frag=135V Gain=1,0RT:7.22894556527486min (Subtracted)

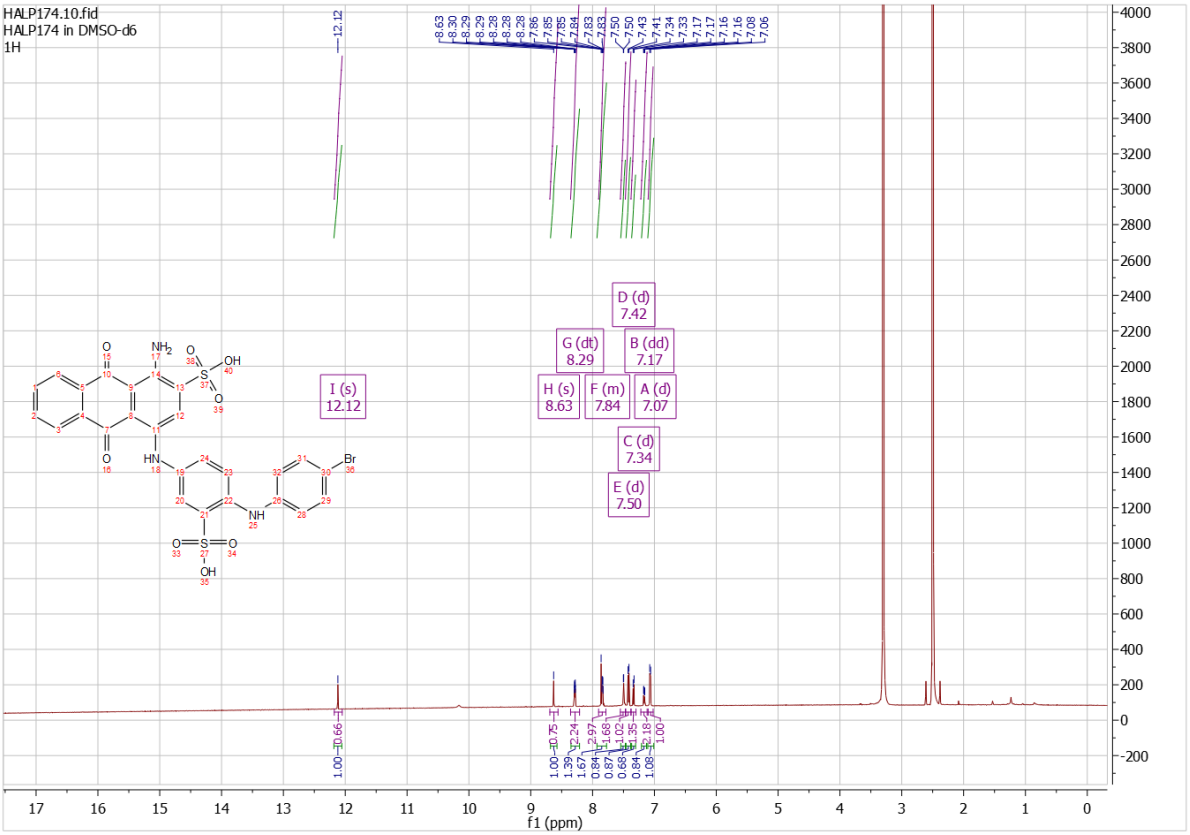


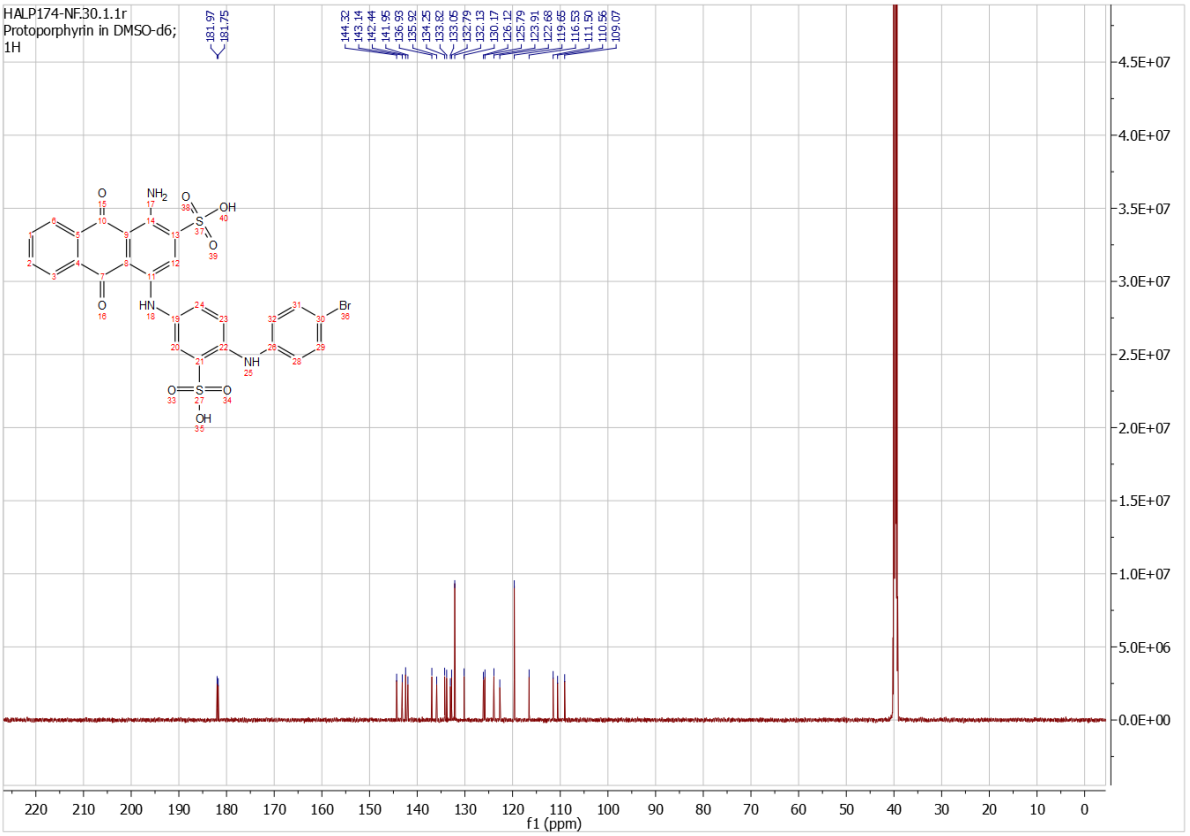
MS1 +TIC SCAN ESI Frag=135V Gain=1,0RT:8.10322251669568min (Subtracted)



MS1 -TIC SCAN ESI Frag=135V Gain=1,0RT:8.14433477437511min (Subtracted)



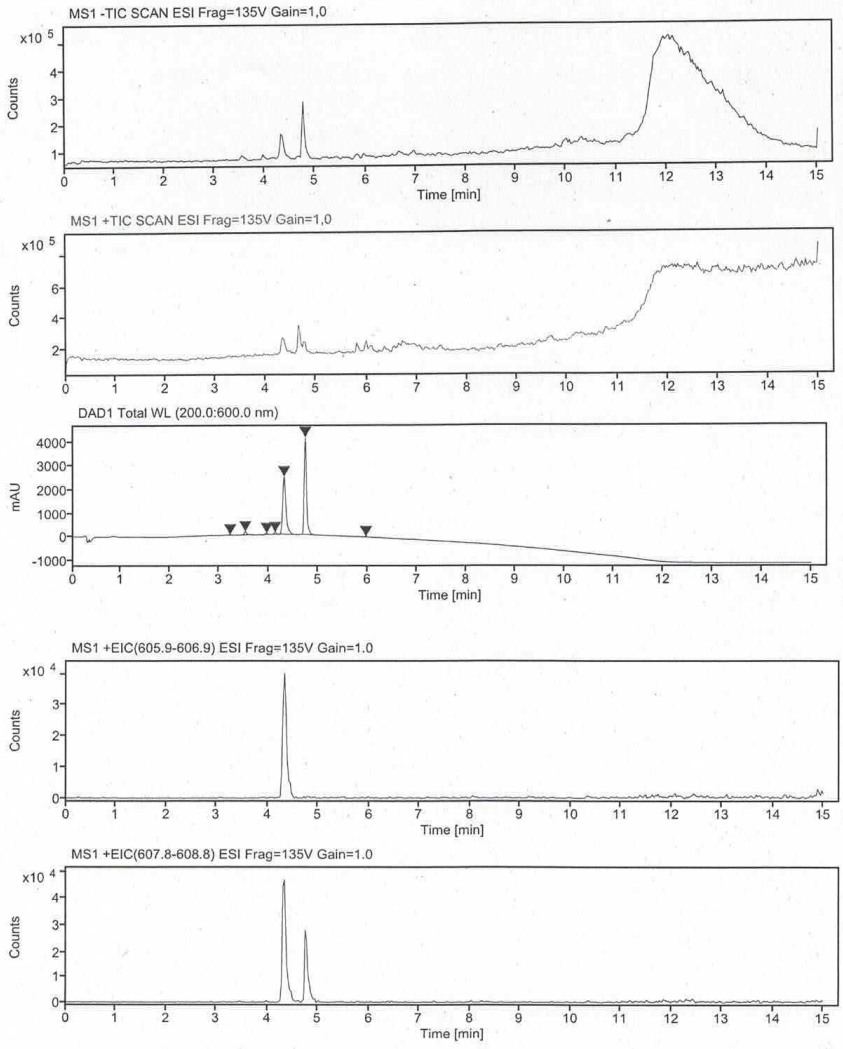

HALP174.10.fid
HALP174 in DMSO-d6
1H
I (s)
12.12
D (d)
7.42
G (dt)
8.29
B (dd)
7.17
H (s)
8.63
F (m)
7.84
A (d)
7.07
C (d)
7.34
E (d)
7.50
f1 (ppm)


HALP174-NF.30.1.1r
Protoporphyrin in DMSO-d6;
1H
f1 (ppm)

Sodium 5-((4-amino-3-carboxy-9,10-dioxo-9,10-dihydroanthracen-1-yl)amino)-2-((4-bromophenyl)amino)benzenesulfonate (**6**)

17

Sequence Name:	2021-06-11		
Data file:	HAL96-N.dx	**Project Name:**	Single Quad
Sample name:	HAL96-N	**Operator :**	SYSTEM
Instrument:	Single Quad	**Acquired on:**	2021-06-11 19:09:22+02:00
Inj. volume:	5.000	**Location:**	P2-B10
Acq. method:	00-new_wasser-acn_standard_100-1000_BD-20min.amx		
Processing method:	MS_standard_plot.pmx		



Signal: DAD1 Total WL (200.0:600.0 nm)

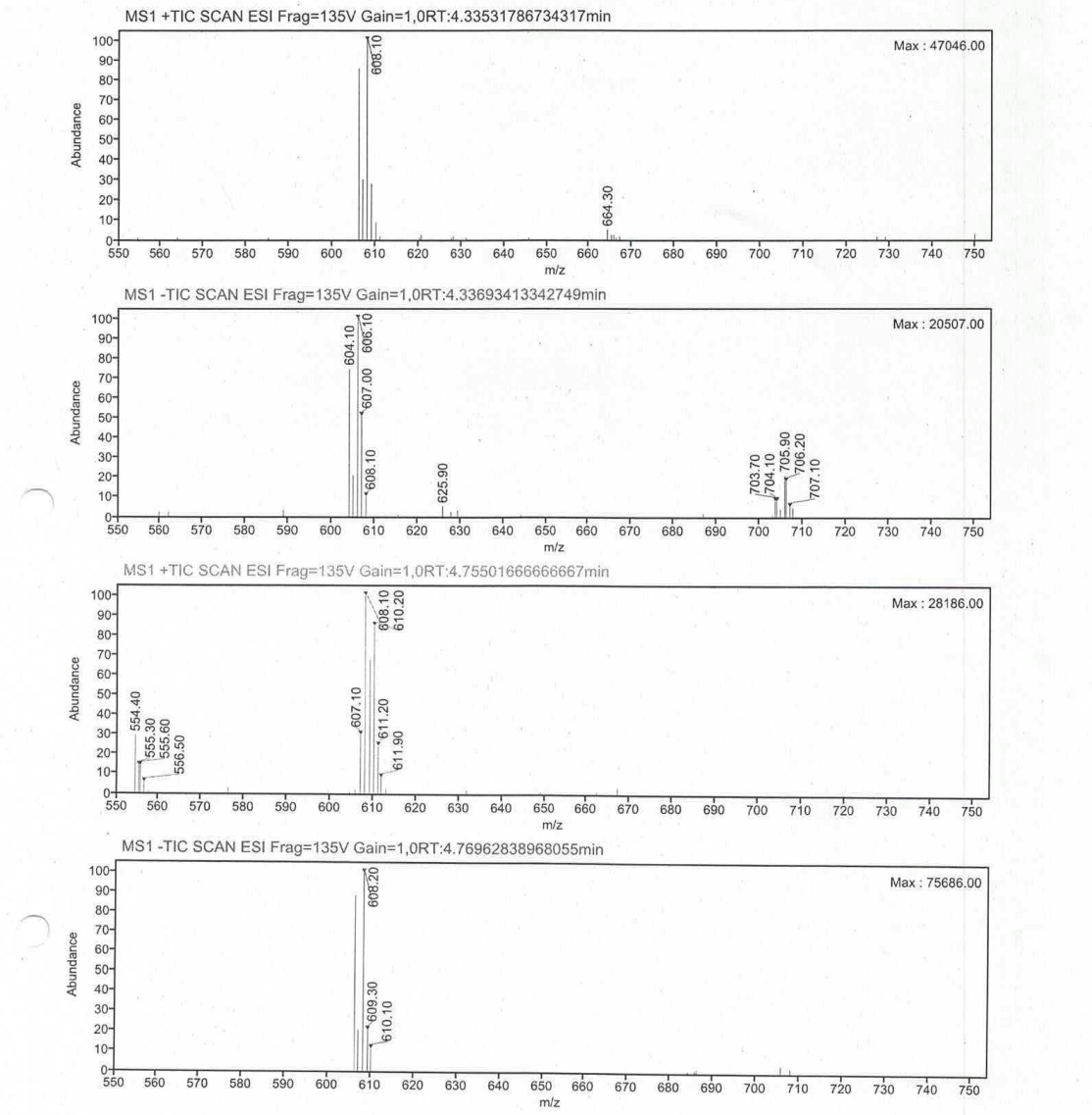
RT [min]	Peak MS Base Peak m/z	Area	Area%	Max Peak%	Height
3.214		57.3569	0.2220	0.430	18.587
3.521		465.2890	1.8012	3.485	140.406
3.949		196.0343	0.7589	1.468	66.851
4.120		212.9899	0.8245	1.595	83.964
4.301		11473.8973	44.4173	85.948	2453.468
4.734		13349.7507	51.6790	100.000	4109.977
5.954		76.7216	0.2970	0.575	22.610
	Sum	25832.0397			

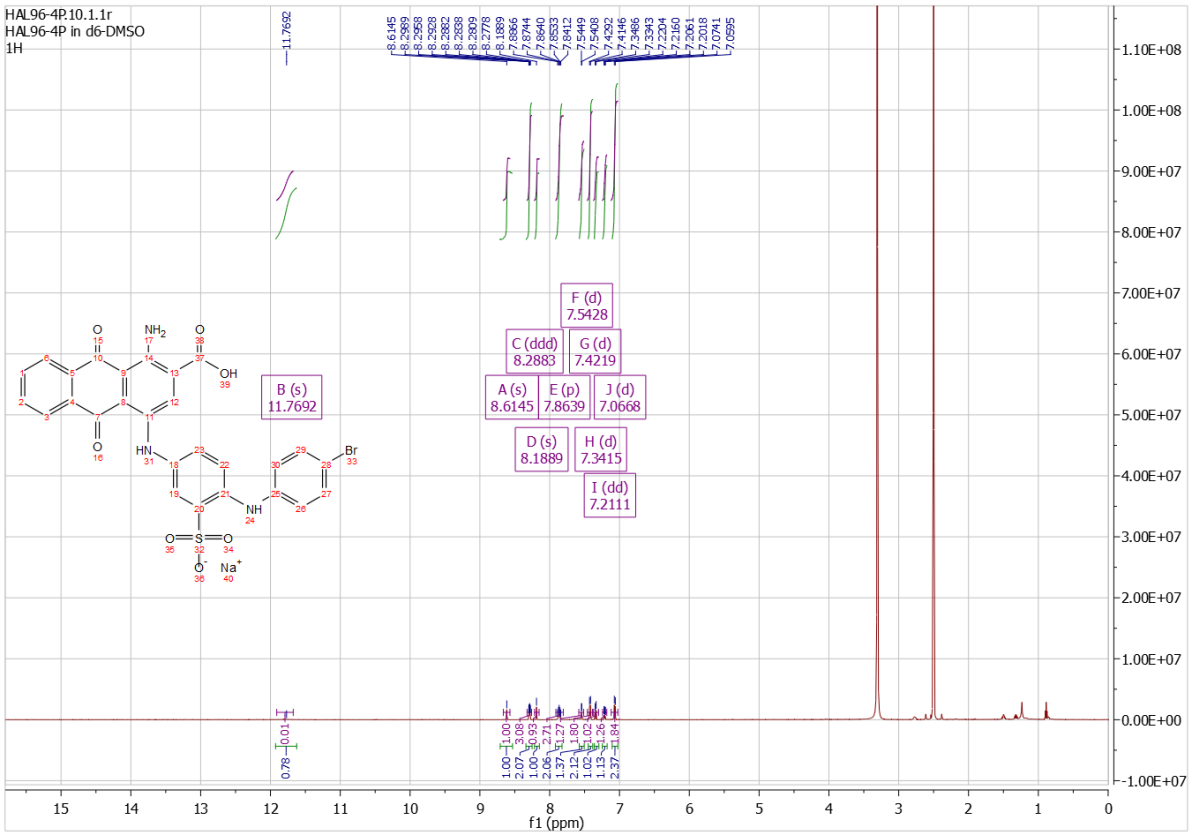
Signal: MS1 +TIC SCAN ESI Frag=135V Gain=1,0

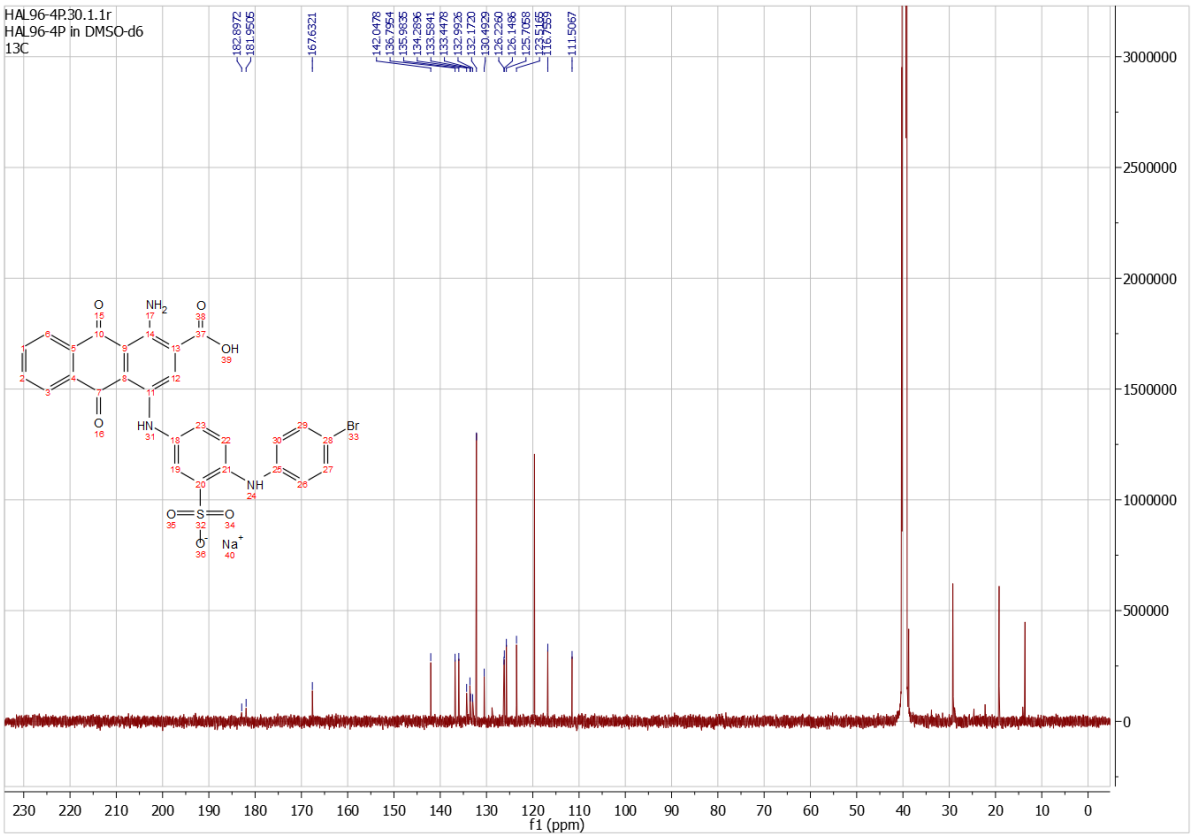
RT [min]	Peak MS Base Peak m/z	Area	Area%	Max Peak%	Height
4.335	608.100	498264.5817	80.3385	100.000	96616.620
4.755	608.100	121942.0392	19.6615	24.473	37235.545
	Sum	620206.6208			

Signal: MS1 -TIC SCAN ESI Frag=135V Gain=1,0

RT [min]	Peak MS Base Peak m/z	Area	Area%	Max Peak%	Height
4.337	606.100	363770.1873	32.7523	48.704	83752.544
4.770	608.200	746900.0460	67.2477	100.000	205856.733
	Sum	1110670.2332			

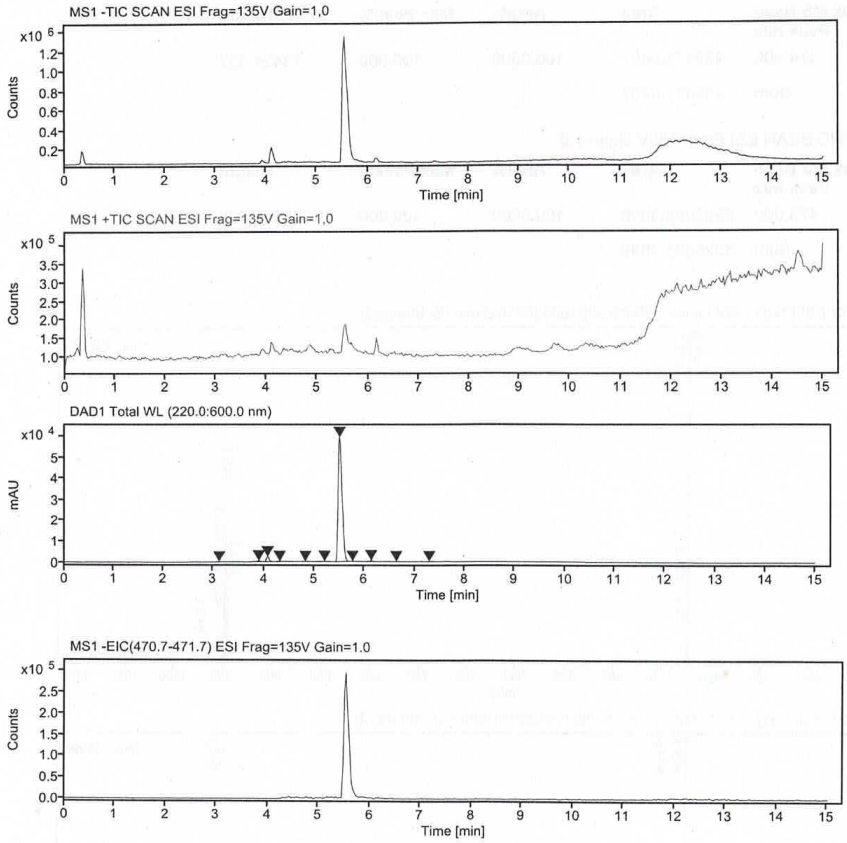

MS1 +TIC SCAN ESI Frag=135V Gain=1,0RT:4.33531786734317min
Max : 47046.00
608.10
664.30
MS1 -TIC SCAN ESI Frag=135V Gain=1,0RT:4.33693413342749min
Max : 20507.00
604.10
606.10
607.00
608.10
625.90
703.70
704.10
705.90
706.20
707.10
MS1 +TIC SCAN ESI Frag=135V Gain=1,0RT:4.75501666666667min
Max : 28186.00
554.40
555.30
555.60
556.50
607.10
608.10
610.20
611.20
611.90
MS1 -TIC SCAN ESI Frag=135V Gain=1,0RT:4.76962838968055min
Max : 75686.00
608.20
609.30
610.10
Abundance
m/z


HAL96-4P.10.1.1r
HAL96-4P in d6-DMSO
1H
B (s)
11.7692
F (d)
7.5428
C (ddd)
8.2883
G (d)
7.4219
A (s)
8.6145
E (p)
7.8639
J (d)
7.0668
D (s)
8.1889
H (d)
7.3415
I (dd)
7.2111
f1 (ppm)


HAL96-4P.30.1.1r
HAL96-4P in DMSO-d6
13C
f1 (ppm)

Sodium 1-amino-9,10-dioxo-4-((4-(phenylamino)-3-sulfonatophenyl)amino)-9,10-dihydroanthracene-2-sulfonate (**7**)

Sequence Name:	SingleSample		
Data file:	HALP124-F1.dx	**Project Name:**	Single Quad
Sample name:	HALP124-F1	**Operator :**	SYSTEM
Instrument:	Single Quad	**Acquired on:**	2022-03-08 17:11:33+01:00
Inj. volume:	5.000	**Location:**	P2-C2
Acq. method:	00-new_wasser-acn_standard_100-1000_BD-20min.amx		
Processing method:	MS_standard_plot.pmx		



Signal: DAD1 Total WL (220.0:600.0 nm)

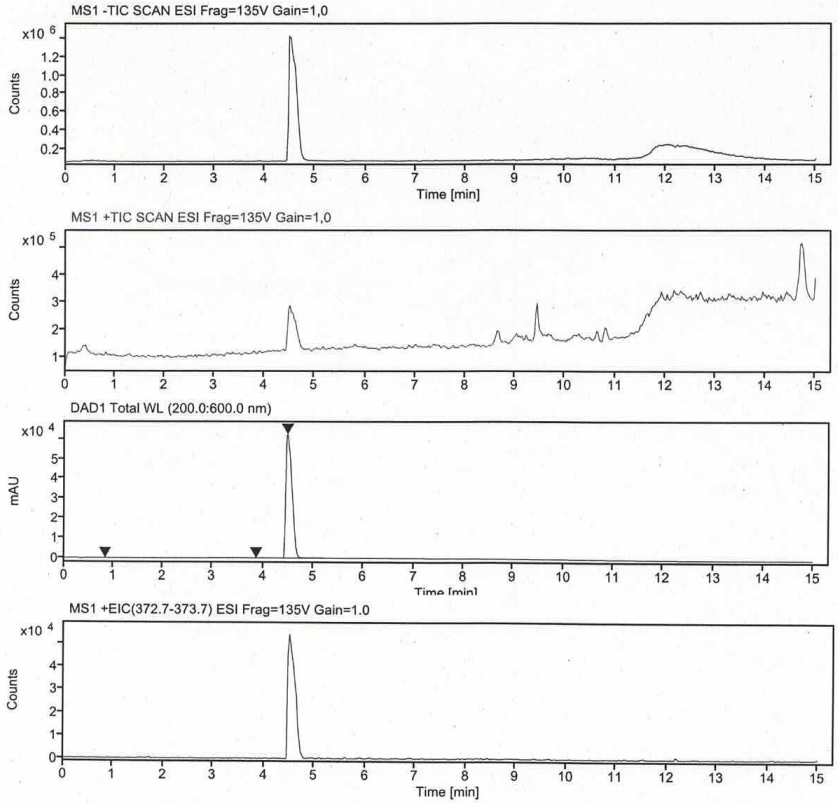
RT [min]	Peak MS Base Peak m/z	Area	Area%	Max Peak%	Height
3.113		364.9953	0.1060	0.111	86.463
3.897		1846.0277	0.5359	0.562	494.610
4.072		9026.0206	2.6203	2.748	2436.797
4.311		669.9456	0.1945	0.204	135.916
4.822		395.6497	0.1149	0.120	52.836
5.204		975.0710	0.2831	0.297	140.091
5.503		328450.9354	95.3492	100.000	59366.032

D:\CDSProjects\Default\0-standardplot+EIC.rdl [Rev. 5670] Printed: 2022-03-09 08:52:58+01:00 Page 1 of 2

2-((4-Bromophenyl)amino)-5-nitrobenzenesulfonic acid (**17**)

40 ✓

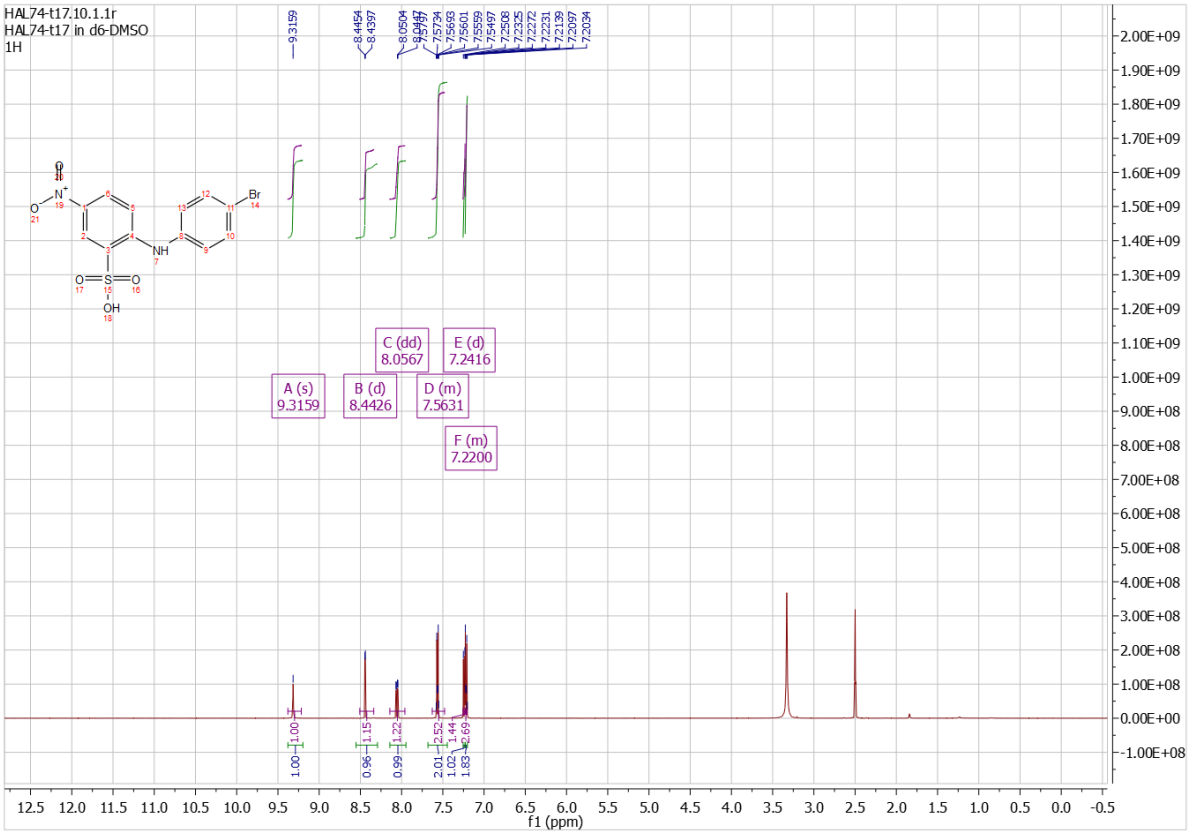
Sequence Name:	2021-04-11		
Data file:	2021-04-12 09-17-25+02-00-34.dx	**Project Name:**	Single Quad
Sample name:	HAL74-t17	**Operator :**	SYSTEM
Instrument:	Single Quad	**Acquired on:**	2021-04-12 09:18:18+02:00
Inj. volume:	2.000	**Location:**	P1-C9
Acq. method:	0_wasser-acn_standard_100-1000_AC-20min.amx		
Processing method:	MS_standard_plot.pmx		

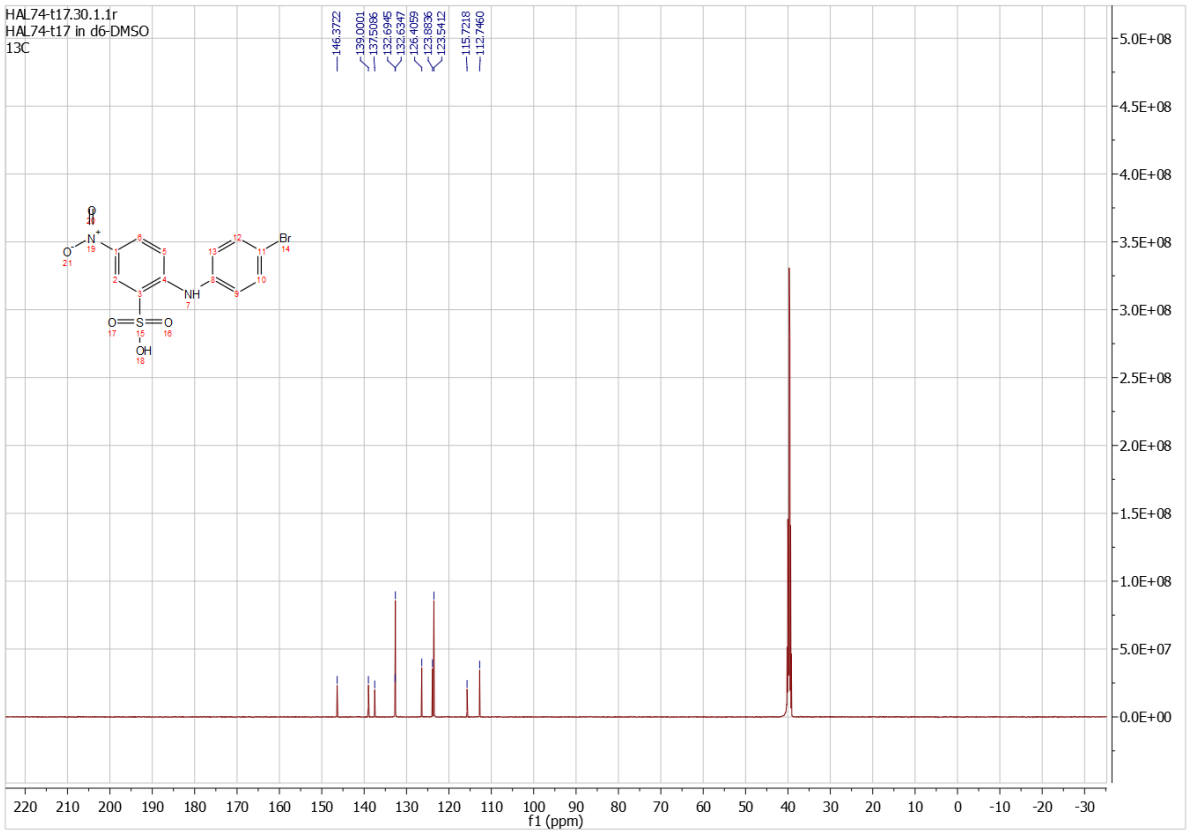


Signal: DAD1 Total WL (200.0:600.0 nm)

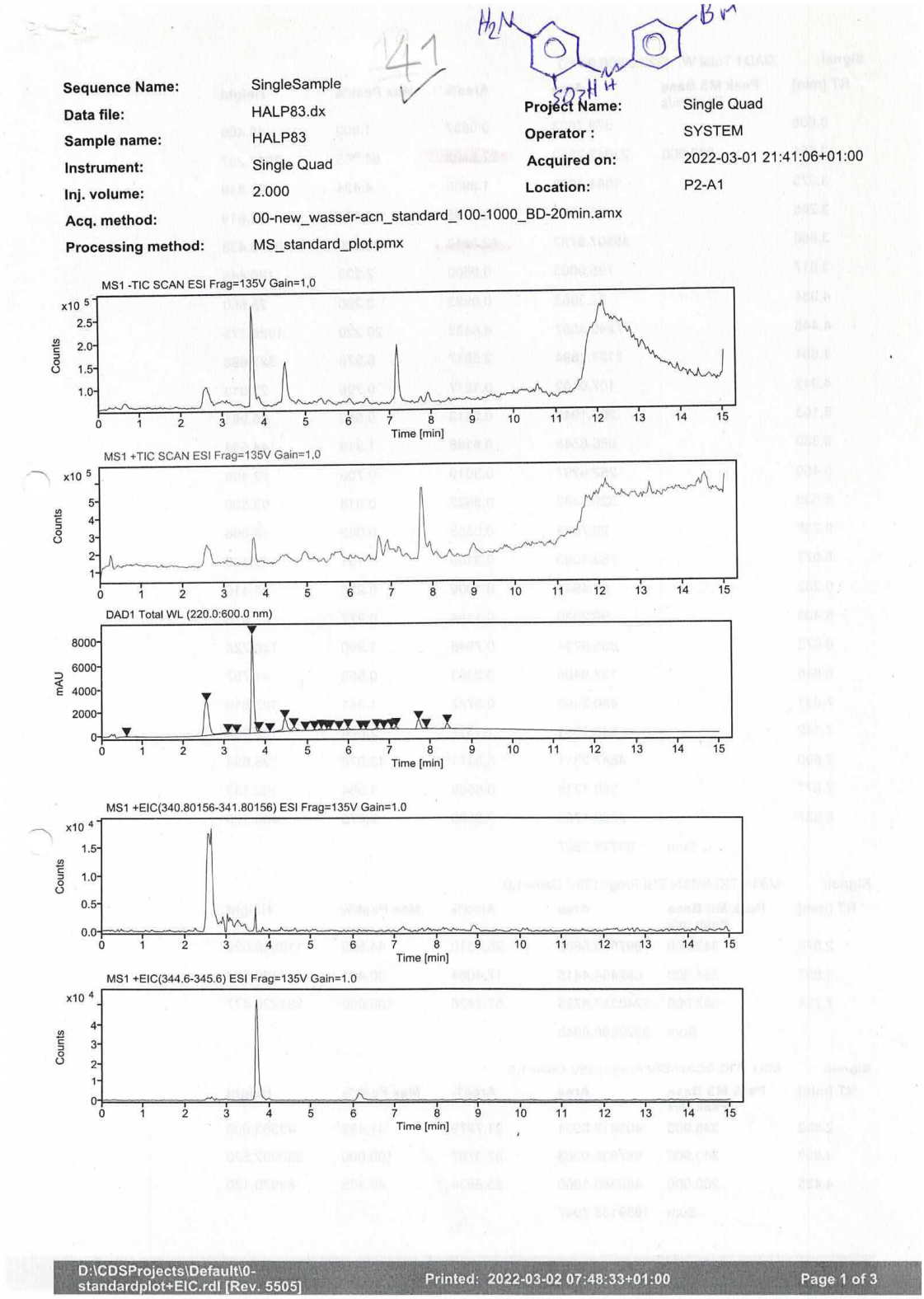
RT [min]	Peak MS Base Peak m/z	Area	Area%	Max Peak%	Height
0.837		231.2742	0.0441	0.044	32.984
3.863		154.8292	0.0295	0.030	53.638
4.482	375.000	524501.2541	99.9264	100.000	62278.502
	Sum	524887.3576			

D:\CDSProjects\Default\Standard-Plot_MS+EIC.rdl [Rev. 582] Printed: 2021-04-12 12:46:51+02:00 Page 1 of 2


HAL74-t17.10.1.1r
HAL74-t17 in d6-DMSO
1H
A (s)
9.3159
B (d)
8.4426
C (dd)
8.0567
D (m)
7.5631
E (d)
7.2416
F (m)
7.2200
f1 (ppm)


HAL74-t17.30.1.1r
HAL74-t17 in d6-DMSO
13C
f1 (ppm)

5-Amino-2-((4-bromophenyl)amino)benzenesulfonic acid (**41**)



Signal: DAD1 Total WL (220.0:600.0 nm)

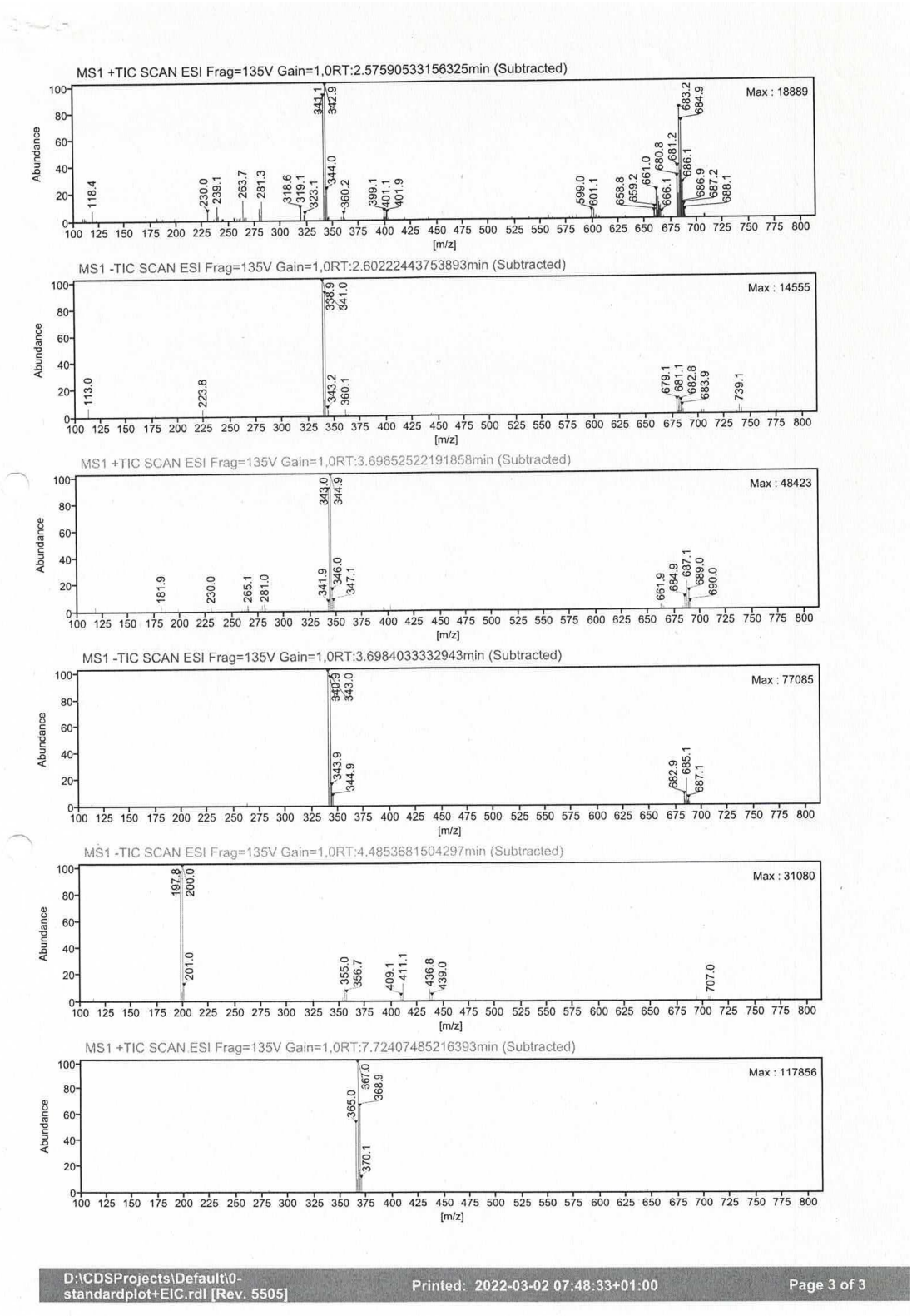
RT [min]	Peak MS Base Peak m/z	Area	Area%	Max Peak%	Height
0.608		572.7603	0.6837	1.600	45.466
2.551	342.900	23047.7249	27.5103	64.365	2947.257
3.076		1584.1068	1.8908	4.424	91.819
3.285		65.7375	0.0785	0.184	10.919
3.666		35807.8782	42.7412	100.000	8346.438
3.817		795.9003	0.9500	2.223	180.445
4.084		82.3862	0.0983	0.230	25.660
4.445		7240.3597	8.6423	20.220	1086.475
4.664		2137.7894	2.5517	5.970	327.698
4.943		107.0102	0.1277	0.299	23.813
5.163		202.1943	0.2413	0.565	65.981
5.330		686.8548	0.8198	1.918	144.564
5.459		252.9297	0.3019	0.706	72.486
5.539		328.5482	0.3922	0.918	93.509
5.756		29.7048	0.0355	0.083	18.056
5.977		763.1083	0.9109	2.131	159.436
6.282		84.4944	0.1009	0.236	25.410
6.403		99.2030	0.1184	0.277	27.975
6.672		665.8734	0.7948	1.860	120.225
6.846		197.9405	0.2363	0.553	41.757
7.031		480.2495	0.5732	1.341	103.819
7.142		948.1051	1.1317	2.648	199.953
7.690		4647.2311	5.5471	12.978	798.694
7.877		560.1315	0.6686	1.564	103.139
8.387		2390.1706	2.8530	6.675	450.196
	Sum	83778.3927			

Signal: MS1 +TIC SCAN ESI Frag=135V Gain=1,0

RT [min]	Peak MS Base Peak m/z	Area	Area%	Max Peak%	Height
2.576	342.900	997856.5808	25.4510	44.539	110945.026
3.697	344.900	682454.4415	17.4064	30.461	147386.534
7.724	367.000	2240387.8725	57.1426	100.000	381226.477
	Sum	3920698.8948			

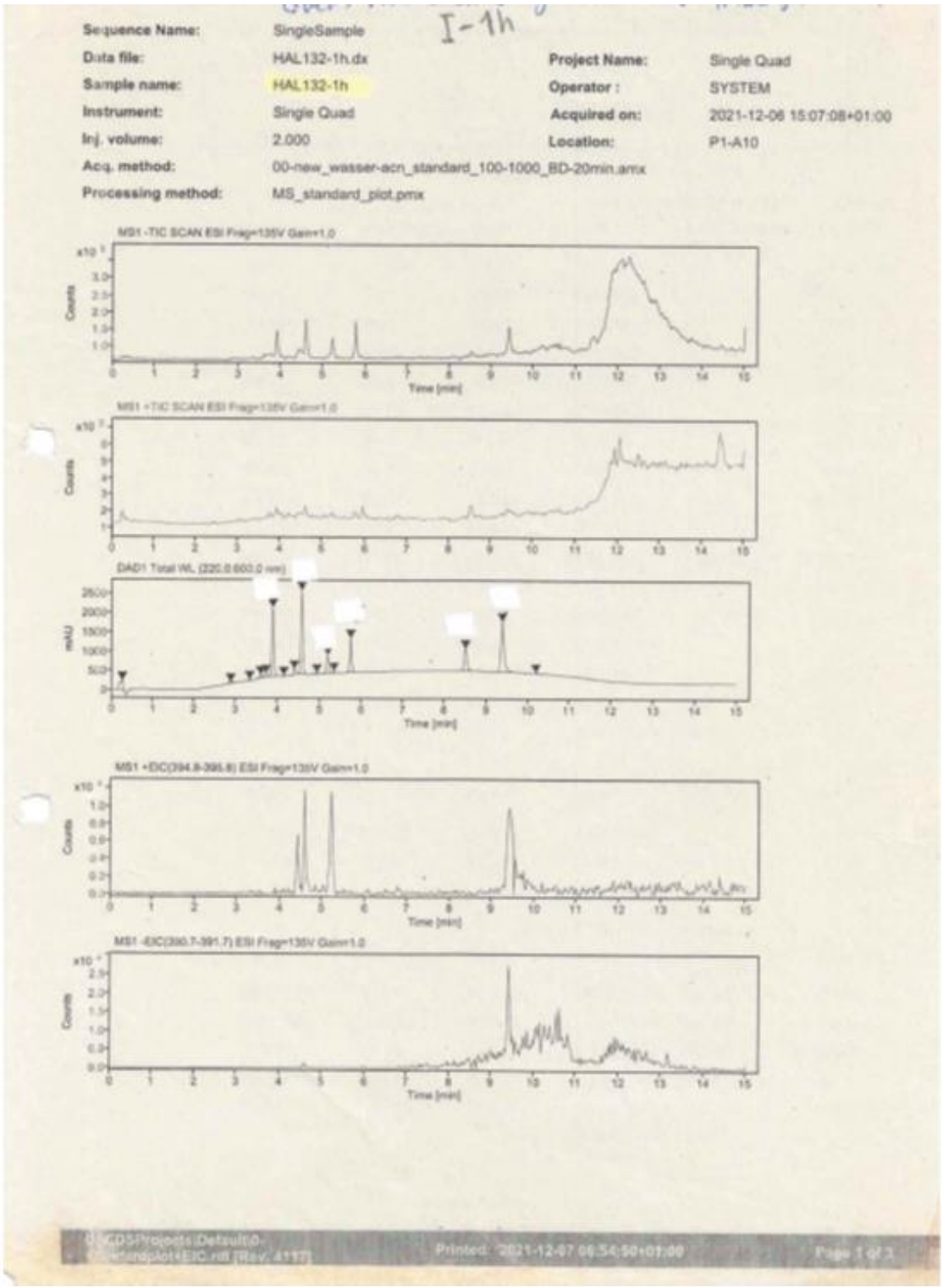
Signal: MS1 -TIC SCAN ESI Frag=135V Gain=1,0

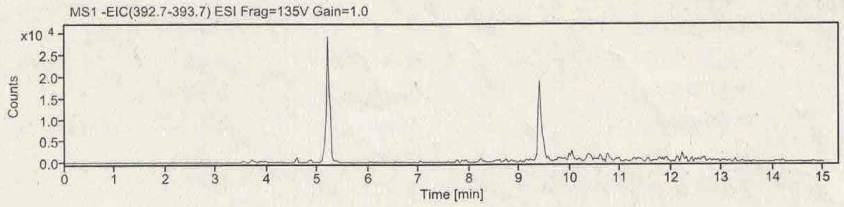
RT [min]	Peak MS Base Peak m/z	Area	Area%	Max Peak%	Height
2.602	338.900	409817.6924	21.7279	41.482	42363.006
3.698	340.900	987935.9063	52.3787	100.000	223392.530
4.485	200.000	488385.1960	25.8934	49.435	83970.120
	Sum	1886138.7947			


MS1 +TIC SCAN ESI Frag=135V Gain=1,0RT:2.57590533156325min (Subtracted)
Max : 18889
MS1 -TIC SCAN ESI Frag=135V Gain=1,0RT:2.60222443753893min (Subtracted)
Max : 14555
MS1 +TIC SCAN ESI Frag=135V Gain=1,0RT:3.69652522191858min (Subtracted)
Max : 48423
MS1 -TIC SCAN ESI Frag=135V Gain=1,0RT:3.6984033332943min (Subtracted)
Max : 77085
MS1 -TIC SCAN ESI Frag=135V Gain=1,0RT:4.4853681504297min (Subtracted)
Max : 31080
MS1 +TIC SCAN ESI Frag=135V Gain=1,0RT:7.72407485216393min (Subtracted)
Max : 117856
Abundance
[m/z]
D:\CDSProjects\Default\0-standardplot+EIC.rdl [Rev. 5505]
Printed: 2022-03-02 07:48:33+01:00
Page 3 of 3

LC/MS-Sheets of the trials I−XII.

Trial I





Signal: DAD1 Total WL (220.0:600.0 nm)

RT [min]	Peak MS Base Peak m/z	Area	Area%	Max Peak%	Height
0.262		1455.4390	4.7680	20.787	257.357
2.876		210.7403	0.6904	3.010	31.671
3.323		67.3249	0.2206	0.962	20.772
3.589		200.2376	0.6560	2.860	76.811
3.714		337.9349	1.1071	4.826	90.208
3.872		5630.6867	18.4462	80.418	1781.537
4.138		53.5643	0.1755	0.765	19.565
4.385		671.7095	2.2005	9.593	143.805
4.561		6969.0355	22.8307	99.532	2153.672
4.925		170.0393	0.5571	2.429	32.327
5.185	393.000	1695.7002	5.5551	24.218	476.280
5.335		123.1217	0.4033	1.758	39.606
5.733		3004.0454	9.8413	42.904	886.762
8.493		2896.6852	9.4896	41.371	579.756
9.382		7001.8127	22.9381	100.000	1295.607
10.188		36.7615	0.1204	0.525	13.451
	Sum	30524.8385			

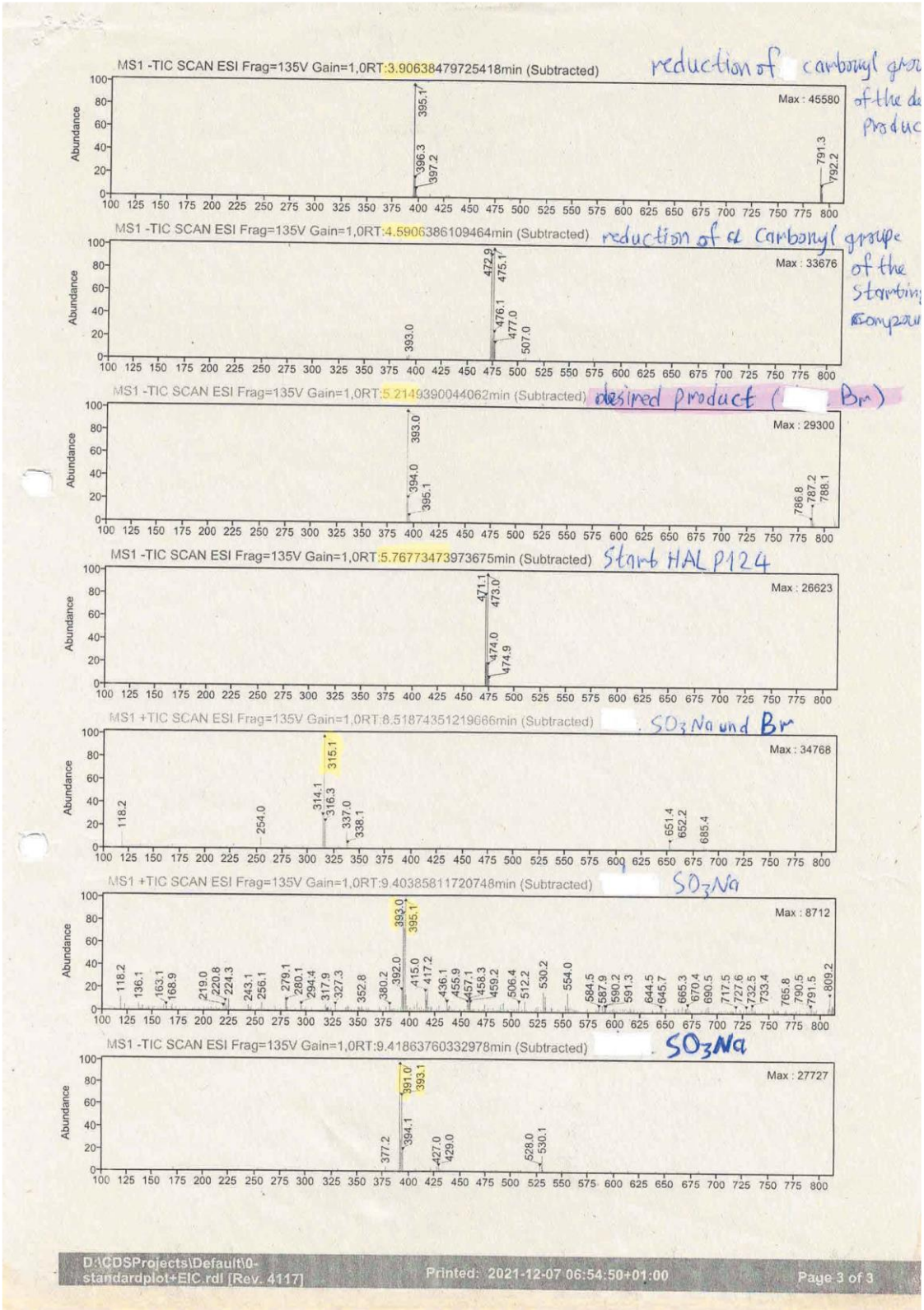
Signal: MS1 +TIC SCAN ESI Frag=135V Gain=1,0

RT [min]	Peak MS Base Peak m/z	Area	Area%	Max Peak%	Height
8.519	315.100	391092.9985	77.4256	100.000	76164.590
9.404	395.100	114027.7216	22.5744	29.156	28929.374
	Sum	505120.7202			

Signal: MS1 -TIC SCAN ESI Frag=135V Gain=1,0

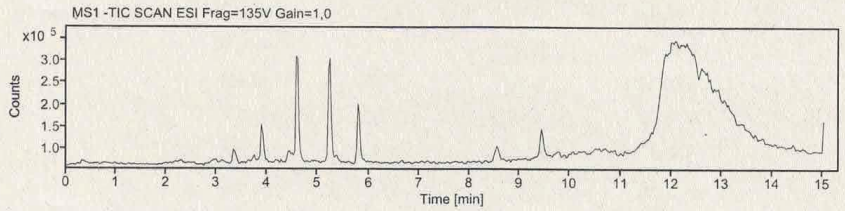
RT [min]	Peak MS Base Peak m/z	Area	Area%	Max Peak%	Height
3.906	395.100	270396.8254	16.2750	66.827	78407.200
4.591	475.100	404620.7301	24.3539	100.000	110423.369
5.215	393.000	233464.6218	14.0521	57.700	59356.175
5.768	473.000	350786.1444	21.1136	86.695	108348.596
9.419	391.000	402151.1367	24.2053	99.390	79672.165
	Sum	1661419.4585			

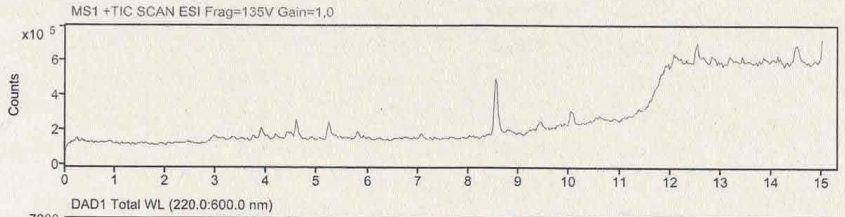
D:\CDSProjects\Default\0-standardplot+EIC.rdl [Rev. 4117] Printed: 2021-12-07 06:54:50+01:00 Page 2 of 3

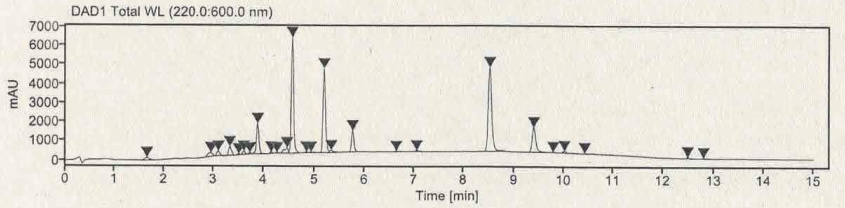

MS1 -TIC SCAN ESI Frag=135V Gain=1,0RT:3.90638479725418min (Subtracted)
reduction of carbonyl gro
of the de
Produc
Max : 45580
MS1 -TIC SCAN ESI Frag=135V Gain=1,0RT:4.59063861094 64min (Subtracted)
reduction of a Carbonyl groupe
of the
Max : 33676
MS1 -TIC SCAN ESI Frag=135V Gain=1,0RT:5.2149390044062min (Subtracted)
desired product (Br)
Max : 29300
MS1 -TIC SCAN ESI Frag=135V Gain=1,0RT:5.767734739736 75min (Subtracted)
Start HAL P124
Max : 26623
MS1 +TIC SCAN ESI Frag=135V Gain=1,0RT:8.51874351219666min (Subtracted)
SO3Na und Br
Max : 34768
MS1 +TIC SCAN ESI Frag=135V Gain=1,0RT:9.40385811720748min (Subtracted)
SO3Na
Max : 8712
MS1 -TIC SCAN ESI Frag=135V Gain=1,0RT:9.41863760332978min (Subtracted)
SO3Na
Max : 27727
Abundance
m/z
D:\CDSProjects\Default\0-standardplot+EIC.rdl [Rev. 4117]
Printed: 2021-12-07 06:54:50+01:00
Page 3 of 3

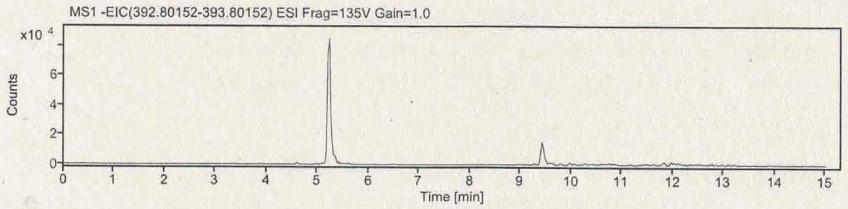
Sequence Name:	SingleSample		
Data file:	HALP132_2h.dx	**Project Name:**	Single Quad
Sample name:	HALP132_2h	**Operator :**	SYSTEM
Instrument:	Single Quad	**Acquired on:**	2021-12-07 10:26:20+01:00
Inj. volume:	4.000	**Location:**	P1-B9
Acq. method:	00-new_wasser-acn_standard_100-1000_BD-20min.amx		
Processing method:	MS_standard_plot.pmx		

I-2h









Signal: DAD1 Total WL (220.0:600.0 nm)

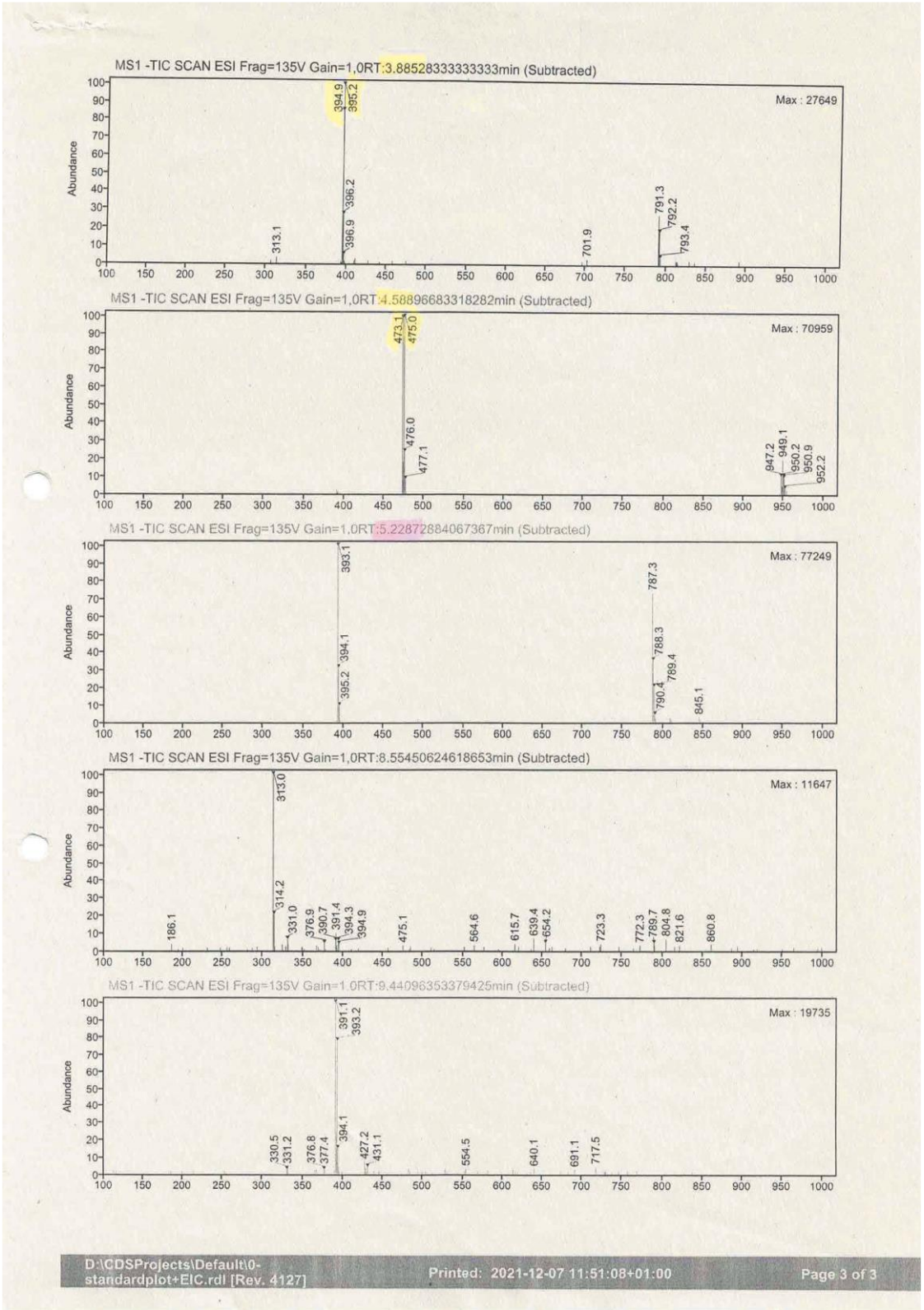
RT [min]	Peak MS Base Peak m/z	Area	Area%	Max Peak%	Height
1.660		878.8371	1.0393	3.914	131.389
2.944		1321.2521	1.5625	5.885	184.088
3.088		918.3352	1.0860	4.090	242.315
3.318		1791.7886	2.1189	7.980	447.148
3.497		124.2153	0.1469	0.553	35.841
3.597		491.8320	0.5816	2.191	159.318
3.716		170.7325	0.2019	0.760	61.559

D:\CDSProjects\Default\0-standardplot+EIC.rdl [Rev. 4127] Printed: 2021-12-07 11:51:08+01:00 Page 1 of 3

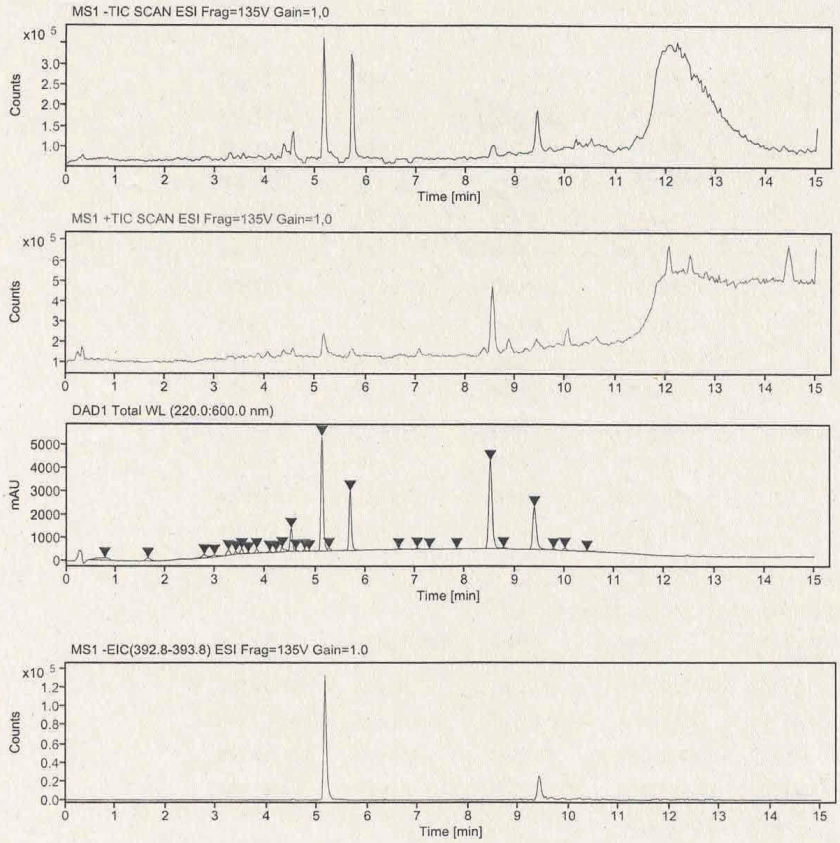
RT [min]	Peak MS Base Peak m/z	Area	Area%	Max Peak%	Height
3.871		5324.6995	6.2968	23.715	1583.025
4.137		222.8500	0.2635	0.993	76.004
4.253		73.7415	0.0872	0.328	26.650
4.451		1524.5600	1.8029	6.790	289.890
4.559		20990.1685	24.8222	93.486	6061.936
4.843		109.1412	0.1291	0.486	41.785
4.935		145.9932	0.1726	0.650	35.537
5.197		15549.1884	18.3879	69.253	4391.148
5.337		580.3060	0.6862	2.585	112.601
5.766		3853.5082	4.5570	17.163	1098.624
6.640		153.4213	0.1814	0.683	23.084
7.051		231.1682	0.2734	1.030	45.852
8.515		22452.8529	26.5519	100.000	4392.955
9.404		6719.4826	7.9462	29.927	1289.728
9.791		33.2174	0.0393	0.148	14.008
10.018		441.7575	0.5224	1.967	90.194
10.422		203.5181	0.2407	0.906	10.575
12.482		198.5058	0.2347	0.884	46.753
12.803		56.9875	0.0674	0.254	13.822
	Sum	84562.0609			

Signal: MS1 -TIC SCAN ESI Frag=135V Gain=1,0

RT [min]	Peak MS Base Peak m/z	Area	Area%	Max Peak%	Height
3.885	395.200	256638.3114	10.5209	27.949	74418.029
4.589	473.100	850552.8406	34.8686	92.629	251675.233
5.229	393.100	918240.9512	37.6434	100.000	236967.865
8.555	313.000	125879.7399	5.1605	13.709	25775.004
9.441	391.100	287999.5203	11.8066	31.364	61710.476
	Sum	2439311.3634			


MS1 -TIC SCAN ESI Frag=135V Gain=1,0RT:3.88528333333333min (Subtracted)
Max : 27649
Abundance
394.9
395.2
396.2
313.1
396.9
701.9
791.3
792.2
793.4
MS1 -TIC SCAN ESI Frag=135V Gain=1,0RT:4.58896683318282min (Subtracted)
Max : 70959
473.1
475.0
476.0
477.1
947.2
949.1
950.2
950.9
952.2
MS1 -TIC SCAN ESI Frag=135V Gain=1,0RT:5.22872884067367min (Subtracted)
Max : 77249
393.1
394.1
395.2
787.3
788.3
789.4
790.4
845.1
MS1 -TIC SCAN ESI Frag=135V Gain=1,0RT:8.55450624618653min (Subtracted)
Max : 11647
313.0
314.2
331.0
376.9
390.7
391.4
394.3
394.9
186.1
475.1
564.6
615.7
639.4
654.2
723.3
772.3
789.7
804.8
821.6
860.8
MS1 -TIC SCAN ESI Frag=135V Gain=1,0RT:9.44096353379425min (Subtracted)
Max : 19735
391.1
393.2
394.1
330.5
331.2
376.8
377.4
427.2
431.1
554.5
640.1
691.1
717.5
D:\CDSProjects\Default\0-standardplot+EIC.rdl [Rev. 4127]
Printed: 2021-12-07 11:51:08+01:00
Page 3 of 3

Sequence Name:	SingleSample		
Data file:	HALP132-2hF1.dx I-55h	**Project Name:**	Single Quad
Sample name:	HALP132-2hF1	**Operator :**	SYSTEM
Instrument:	Single Quad	**Acquired on:**	2021-12-08 14:52:25+01:00
Inj. volume:	4.000	**Location:**	P1-E1
Acq. method:	00-new_wasser-acn_standard_100-1000_BD-20min.amx		
Processing method:	MS_standard_plot.pmx		



Signal: DAD1 Total WL (220.0:600.0 nm)

RT [min]	Peak MS Base Peak m/z	Area	Area%	Max Peak%	Height
0.788		1730.9244	2.4935	9.112	105.646
1.653		882.3753	1.2711	4.645	128.063
2.784		1102.2698	1.5879	5.803	148.254
2.984		677.7945	0.9764	3.568	92.944
3.264		988.8167	1.4245	5.205	212.004
3.407		379.5131	0.5467	1.998	122.515
3.526		697.7951	1.0052	3.673	221.704

D:\CDSProjects\Default\0-standardplot+EIC.rdl [Rev. 4149] Printed: 2021-12-09 07:07:44+01:00 Page 1 of 3

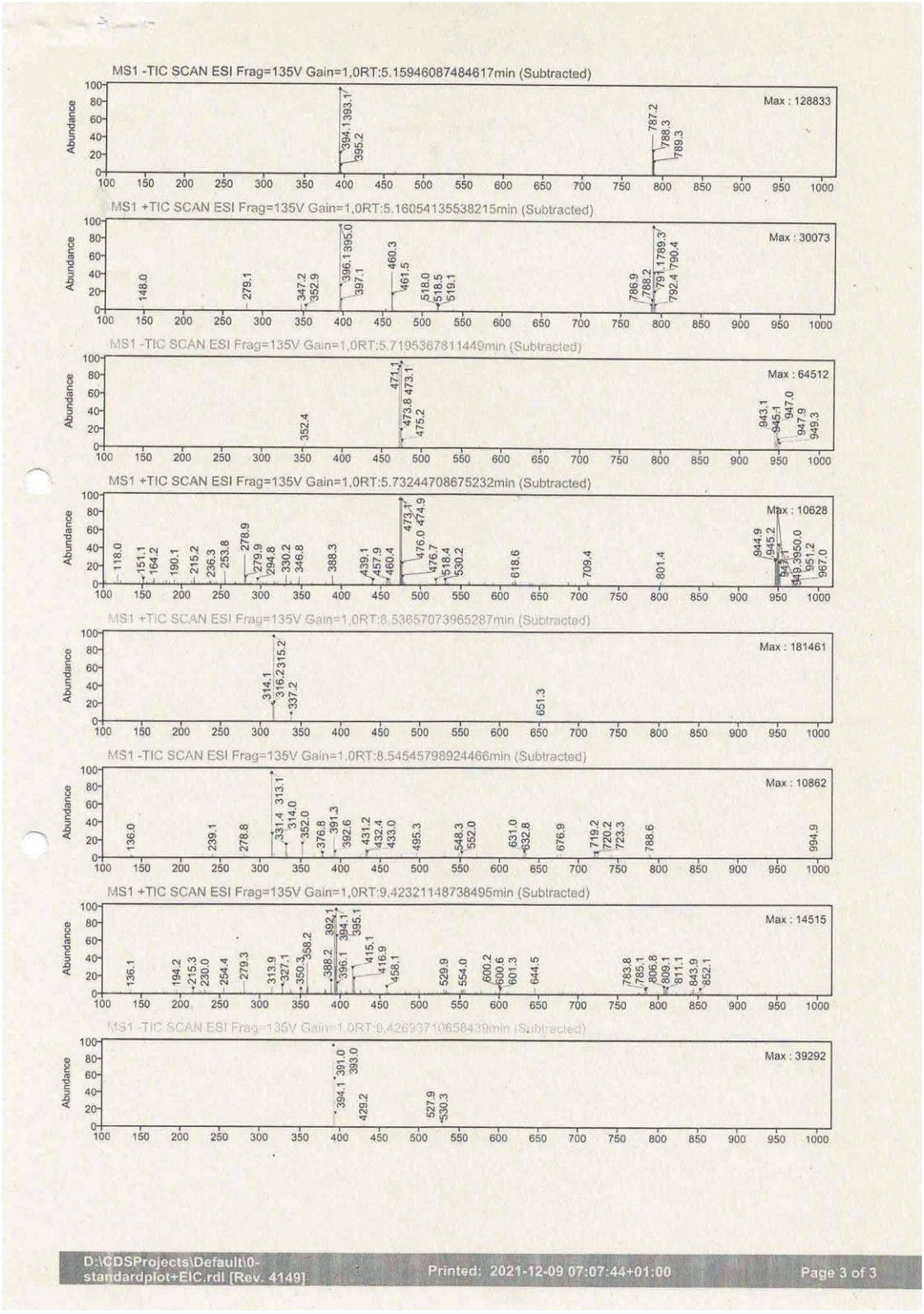
RT [min]	Peak MS Base Peak m/z	Area	Area%	Max Peak%	Height
3.658		121.2018	0.1746	0.638	38.436
3.823		743.7921	1.0715	3.916	197.154
4.079		300.9364	0.4335	1.584	77.817
4.206		137.1086	0.1975	0.722	53.602
4.329		964.5316	1.3895	5.078	193.828
4.509		3246.0055	4.6761	17.088	1000.377
4.603		165.3053	0.2381	0.870	63.897
4.781		237.6586	0.3424	1.251	79.543
4.873		87.9506	0.1267	0.463	30.052
5.126		17053.0342	24.5662	89.772	4967.381
5.267		432.4104	0.6229	2.276	111.695
5.690		8879.6502	12.7918	46.745	2563.159
6.662		212.8015	0.3066	1.120	35.334
7.034		211.6584	0.3049	1.114	48.150
7.281		131.6513	0.1897	0.693	22.252
7.826		118.0726	0.1701	0.622	13.796
8.502		18995.9231	27.3651	100.000	3798.460
8.770		288.6841	0.4159	1.520	47.558
9.392	394.100	9664.3197	13.9222	50.876	1855.118
9.774		238.8986	0.3442	1.258	52.587
10.002		454.1193	0.6542	2.391	103.865
10.446		271.3610	0.3909	1.429	21.976
	Sum	69416.5639			

Signal: MS1 +TIC SCAN ESI Frag=135V Gain=1,0

RT [min]	Peak MS Base Peak m/z	Area	Area%	Max Peak%	Height
5.161	789.300	468620.3350	17.1668	27.917	102598.290
5.732	473.100	192132.8601	7.0383	11.446	34207.490
8.537	315.200	1678596.4598	61.4915	100.000	324757.235
9.423	394.100	390451.5933	14.3033	23.261	54397.561
	Sum	2729801.2482			

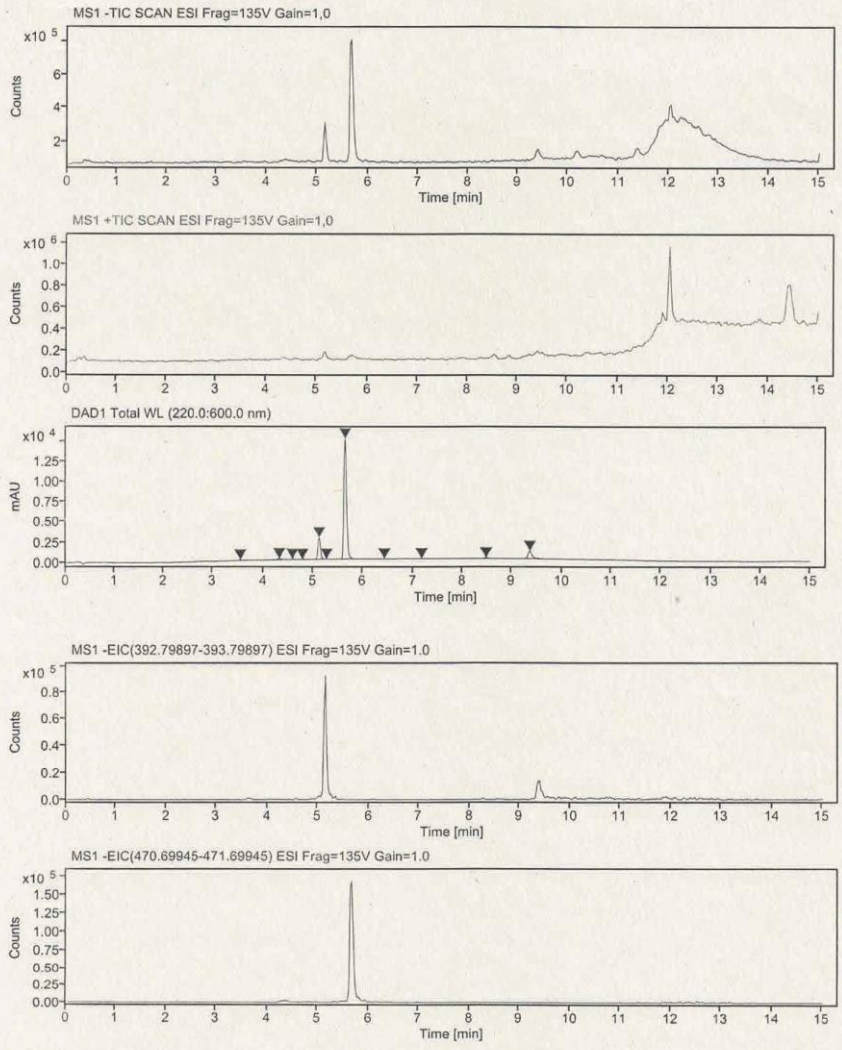
Signal: MS1 -TIC SCAN ESI Frag=135V Gain=1,0

RT [min]	Peak MS Base Peak m/z	Area	Area%	Max Peak%	Height
5.159	393.100	992442.4190	38.2160	100.000	285155.230
5.720	473.100	935586.7560	36.0267	94.271	268983.938
8.545	313.100	154711.9362	5.9575	15.589	25484.808
9.427	391.000	514186.4001	19.7998	51.810	101256.886
	Sum	2596927.5113			


MS1 -TIC SCAN ESI Frag=135V Gain=1,0RT:5.15946087484617min (Subtracted)
Max : 128833
MS1 +TIC SCAN ESI Frag=135V Gain=1,0RT:5.16054135538215min (Subtracted)
Max : 30073
MS1 -TIC SCAN ESI Frag=135V Gain=1,0RT:5.7195367811449min (Subtracted)
Max : 64512
MS1 +TIC SCAN ESI Frag=135V Gain=1,0RT:5.73244708675232min (Subtracted)
Max : 10628
MS1 +TIC SCAN ESI Frag=135V Gain=1,0RT:8.53657073965287min (Subtracted)
Max : 181461
MS1 -TIC SCAN ESI Frag=135V Gain=1,0RT:8.54545798924466min (Subtracted)
Max : 10862
MS1 +TIC SCAN ESI Frag=135V Gain=1,0RT:9.42321148738495min (Subtracted)
Max : 14515
MS1 -TIC SCAN ESI Frag=135V Gain=1,0RT:9.42693710658439min (Subtracted)
Max : 39292
Abundance
D:\CDSProjects\Default\0-standardplot+EIC.rdl [Rev. 4149]
Printed: 2021-12-09 07:07:44+01:00
Page 3 of 3

Trial II

Sequence Name:	2021-12-09_stabilityHALP134 II-1h		
Data file:	HALP134-1h.dx	**Project Name:**	Single Quad
Sample name:	HALP134-1h	**Operator :**	SYSTEM
Instrument:	Single Quad	**Acquired on:**	2021-12-09 15:15:50+01:00
Inj. volume:	4.000	**Location:**	P2-B3
Acq. method:	00-new_wasser-acn_standard_100-1000_BD-20min.amx		
Processing method:	MS_standard_plot.pmx		



D:\CDSProjects\Default\0-standardplot+EIC.rdl [Rev. 4192] Printed: 2021-12-13 07:37:36+01:00 Page 1 of 2

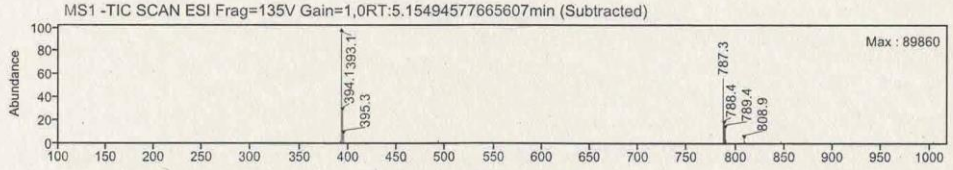
Signal: DAD1 Total WL (220.0:600.0 nm)

RT [min]	Peak MS Base Peak m/z	Area	Area%	Max Peak%	Height
3.545		419.9879	0.5593	0.713	73.823
4.319		687.5013	0.9156	1.167	136.493
4.584		115.0616	0.1532	0.195	24.547
4.787		65.1413	0.0868	0.111	16.615
5.121		8943.7718	11.9112	15.184	2614.224
5.268		10.0864	0.0134	0.017	8.426
5.640	471.000	58903.3993	78.4467	100.000	14850.097
6.426		24.5532	0.0327	0.042	7.329
7.179		59.6095	0.0794	0.101	14.158
8.477		491.6081	0.6547	0.835	86.998
9.365	391.100	5366.4128	7.1469	9.111	906.103
	Sum	75087.1333			

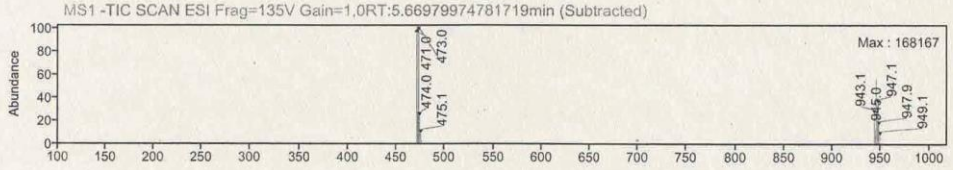
Signal: MS1 -TIC SCAN ESI Frag=135V Gain=1,0

RT [min]	Peak MS Base Peak m/z	Area	Area%	Max Peak%	Height
5.155	393.100	841757.4531	16.8509	21.984	230901.812
5.670	471.000	3829029.3111	76.6522	100.000	759026.507
9.401	391.100	324543.5803	6.4969	8.476	58450.598
	Sum	4995330.3445			

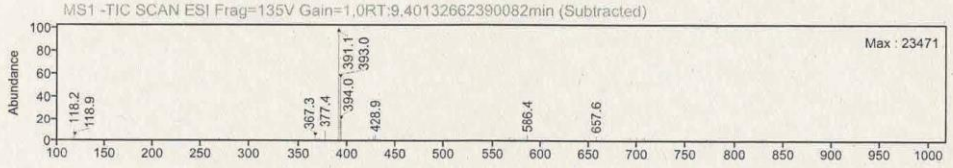
MS1 -TIC SCAN ESI Frag=135V Gain=1,0RT:5.15494577665607min (Subtracted)



MS1 -TIC SCAN ESI Frag=135V Gain=1,0RT:5.66979974781719min (Subtracted)



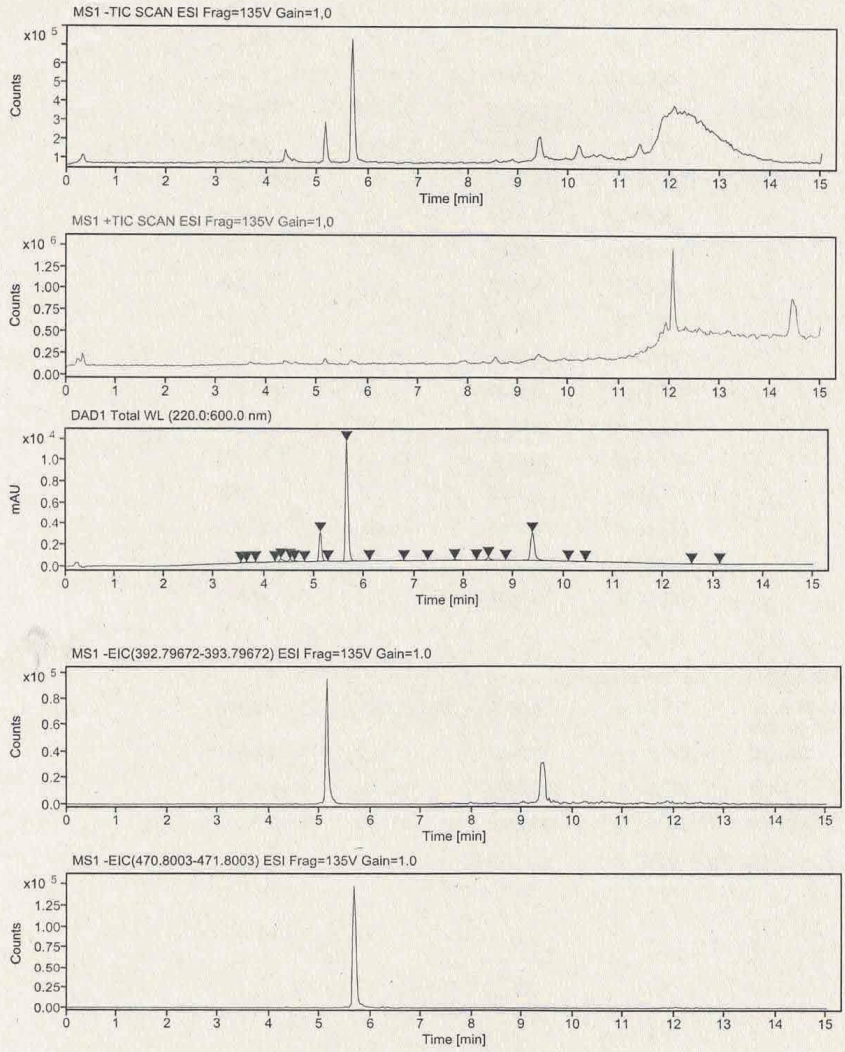
MS1 -TIC SCAN ESI Frag=135V Gain=1,0RT:9.40132662390082min (Subtracted)



D:\CDSProjects\Default\0-standardplot+EIC.rdl [Rev. 4192] Printed: 2021-12-13 07:37:36+01:00 Page 2 of 2

II-2h

Sequence Name:	2021-12-09_stabilityHALP134		
Data file:	HALP134-2h.dx	**Project Name:**	Single Quad
Sample name:	HALP134-2h	**Operator :**	SYSTEM
Instrument:	Single Quad	**Acquired on:**	2021-12-09 15:36:47+01:00
Inj. volume:	8.000	**Location:**	P2-B4
Acq. method:	00-new_wasser-acn_standard_100-1000_BD-20min.amx		
Processing method:	MS_standard_plot.pmx		



Signal: DAD1 Total WL (220.0:600.0 nm)

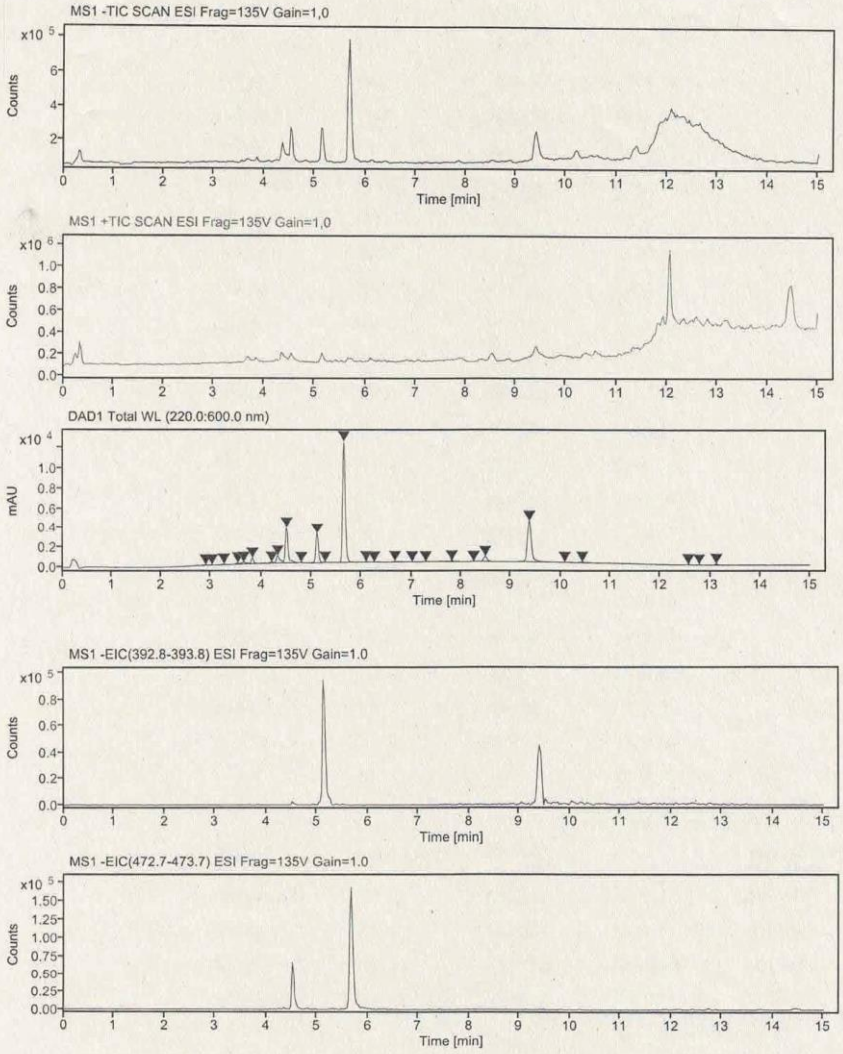
RT [min]	Peak MS Base Peak m/z	Area	Area%	Max Peak%	Height
3.533		73.6376	0.0986	0.167	46.273
3.645		61.6350	0.0825	0.140	35.967
3.822		85.5882	0.1146	0.194	41.724
4.210		131.4442	0.1760	0.298	35.636
4.328		1453.3053	1.9457	3.293	283.528
4.511		830.0681	1.1113	1.881	231.703
4.601		532.5465	0.7130	1.207	96.295
4.804		29.6681	0.0397	0.067	12.179
5.118	393.100	9163.0081	12.2678	20.763	2685.883
5.267		63.2119	0.0846	0.143	22.567
5.646	473.000	44130.5073	59.0835	100.000	11309.301
6.094		98.3558	0.1317	0.223	25.291
6.794		246.9221	0.3306	0.560	23.156
7.269		54.2853	0.0727	0.123	8.149
7.813		646.3379	0.8653	1.465	54.235
8.245		67.1041	0.0898	0.152	13.926
8.488		1398.3140	1.8721	3.169	263.161
8.841		64.4053	0.0862	0.146	12.867
9.378		14971.7563	20.0447	33.926	2603.776
10.096		121.3534	0.1625	0.275	14.320
10.441		273.4348	0.3661	0.620	35.240
12.566		72.9325	0.0976	0.165	20.262
13.133		122.0022	0.1633	0.276	27.117
	Sum	74691.8241			

Signal: MS1 -TIC SCAN ESI Frag=135V Gain=1,0

RT [min]	Peak MS Base Peak m/z	Area	Area%	Max Peak%	Height
5.152	393.100	755613.5207	19.0887	27.672	211759.631
5.681	473.000	2730558.8263	68.9809	100.000	634407.491
9.409	391.200	472253.9179	11.9303	17.295	114579.118
	Sum	3958426.2648			

II-3h

Sequence Name:	2021-12-09_stabilityHALP134		
Data file:	HALP134-3h.dx	**Project Name:**	Single Quad
Sample name:	HALP134-3h	**Operator :**	SYSTEM
Instrument:	Single Quad	**Acquired on:**	2021-12-09 15:57:44+01:00
Inj. volume:	8.000	**Location:**	P2-B5
Acq. method:	00-new_wasser-acn_standard_100-1000_BD-20min.amx		
Processing method:	MS_standard_plot.pmx		



Signal: DAD1 Total WL (220.0:600.0 nm)

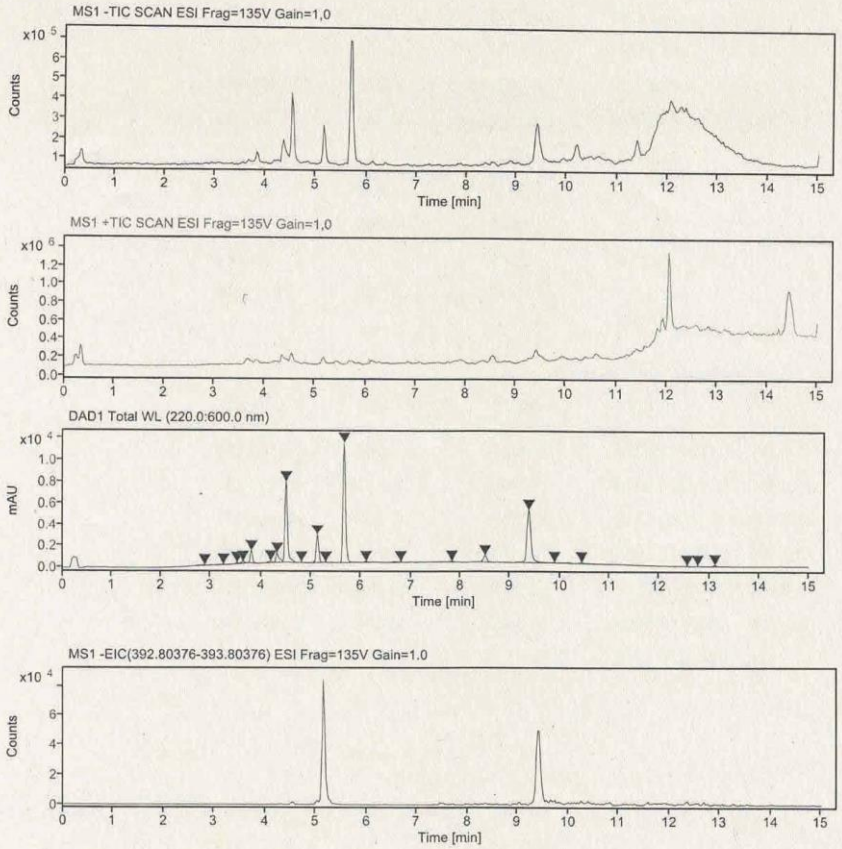
RT [min]	Peak MS Base Peak m/z	Area	Area%	Max Peak%	Height
2.893		56.7697	0.0518	0.121	18.273
3.019		100.6936	0.0918	0.214	27.553
3.257		410.2071	0.3740	0.871	64.818
3.532		505.1322	0.4606	1.072	138.036
3.649		1205.4852	1.0991	2.559	191.236
3.823		2068.3617	1.8859	4.390	567.868
4.204		695.1061	0.6338	1.475	117.968
4.324		3490.4593	3.1825	7.409	735.904
4.501		13699.2230	12.4906	29.079	3598.704
4.799		86.6057	0.0790	0.184	32.070
5.114		10541.7386	9.6117	22.377	2942.874
5.274		110.3006	0.1006	0.234	45.986
5.646		47109.9521	42.9537	100.000	12120.705
6.090		186.7880	0.1703	0.396	51.943
6.250		49.4018	0.0450	0.105	9.102
6.672		480.5674	0.4382	1.020	47.781
7.016		86.5130	0.0789	0.184	16.696
7.289		54.8273	0.0500	0.116	7.883
7.812		1006.8443	0.9180	2.137	80.697
8.252		46.6500	0.0425	0.099	14.251
8.485		2652.4701	2.4185	5.630	514.403
9.376	391.000	23791.8508	21.6928	50.503	4197.510
10.086		77.9639	0.0711	0.165	7.216
10.439		642.1824	0.5855	1.363	74.809
12.560		82.5282	0.0752	0.175	21.985
12.782		97.0172	0.0885	0.206	23.374
13.127		340.5198	0.3105	0.723	77.743
	Sum	109676.1590			

Signal: MS1 -TIC SCAN ESI Frag=135V Gain=1,0

RT [min]	Peak MS Base Peak m/z	Area	Area%	Max Peak%	Height
4.520	473.000	641025.1073	11.5663	20.126	188224.933
5.141	393.100	823971.1954	14.8673	25.870	213940.275
5.680	473.100	3184999.8217	57.4686	100.000	703397.688
9.405	391.000	892161.8984	16.0977	28.011	152932.714
	Sum	5542158.0228			

II- 4h

Sequence Name:	2021-12-09_stabilityHALP134		
Data file:	HALP134-4h.dx	**Project Name:**	Single Quad
Sample name:	HALP134-4h	**Operator :**	SYSTEM
Instrument:	Single Quad	**Acquired on:**	2021-12-09 16:18:42+01:00
Inj. volume:	8.000	**Location:**	P2-B6
Acq. method:	00-new_wasser-acn_standard_100-1000_BD-20min.amx		
Processing method:	MS_standard_plot.pmx		



Signal: DAD1 Total WL (220.0:600.0 nm)

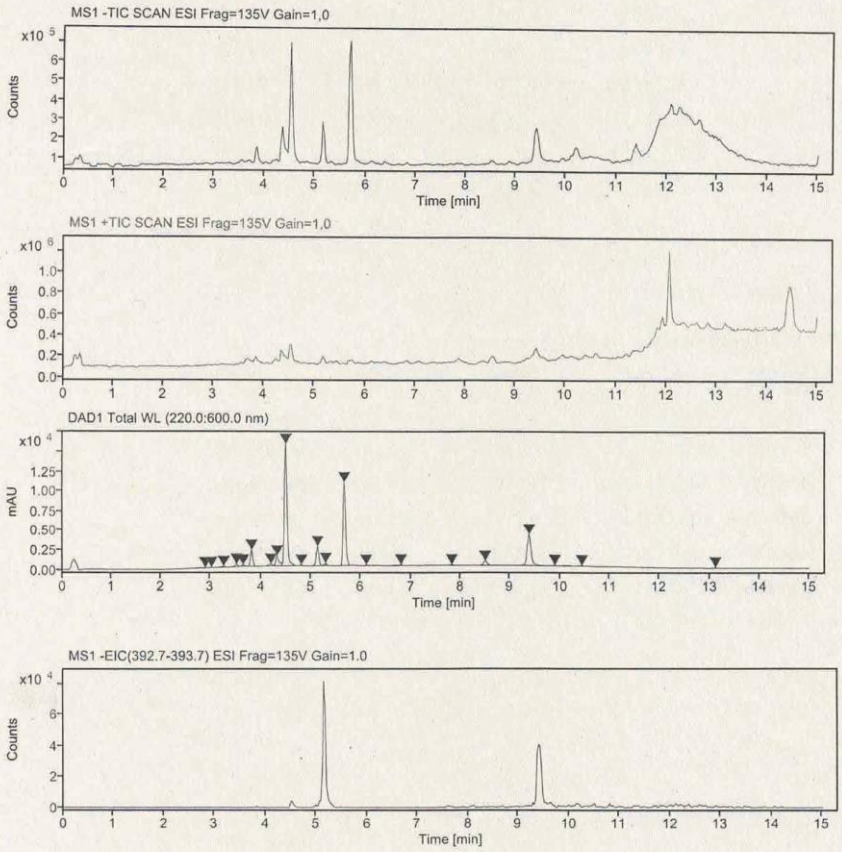
RT [min]	Peak MS Base Peak m/z	Area	Area%	Max Peak%	Height
2.879		271.5842	0.2219	0.650	40.083
3.249		370.7549	0.3030	0.888	32.755
3.519		472.7076	0.3863	1.132	115.638
3.639		769.1807	0.6286	1.841	187.838
3.808		3569.8320	2.9173	8.546	1106.074
4.191		719.8011	0.5882	1.723	157.428
4.319		3857.7596	3.1526	9.235	816.113

RT [min]	Peak MS Base Peak m/z	Area	Area%	Max Peak%	Height
4.498		27079.5468	22.1297	64.827	7478.196
4.809		162.3030	0.1326	0.389	48.082
5.129		8835.8169	7.2207	21.152	2512.758
5.291		88.8845	0.0726	0.213	34.179
5.661		41772.2622	34.1367	100.000	11022.090
6.099		563.1391	0.4602	1.348	79.889
6.802		710.5206	0.5806	1.701	66.909
7.825		943.5921	0.7711	2.259	85.759
8.494		2891.6570	2.3631	6.922	569.213
9.382	391.000	27376.5818	22.3724	65.538	4889.105
9.897		395.8734	0.3235	0.948	33.172
10.442		785.0425	0.6415	1.879	91.105
12.556		108.5152	0.0887	0.260	28.718
12.774		78.0309	0.0638	0.187	22.921
13.121		544.2151	0.4447	1.303	108.995
	Sum	122367.6013			

Signal: MS1 -TIC SCAN ESI Frag=135V Gain=1,0

RT [min]	Peak MS Base Peak m/z	Area	Area%	Max Peak%	Height
3.836	395.100	178489.6318	2.6694	6.287	52121.156
4.355	489.100	430358.9519	6.4363	15.158	96499.197
4.521	475.000	1210780.1316	18.1079	42.647	340246.927
5.161	393.100	697592.7926	10.4329	24.571	193831.626
5.680	473.000	2839091.2309	42.4602	100.000	611768.421
9.414	391.000	1330163.7858	19.8933	46.852	191986.156
	Sum	6686476.5247			

Sequence Name:	2021-12-09_stabilityHALP134 II-5h		
Data file:	HALP134-5h.dx	**Project Name:**	Single Quad
Sample name:	HALP134-5h	**Operator :**	SYSTEM
Instrument:	Single Quad	**Acquired on:**	2021-12-09 16:39:42+01:00
Inj. volume:	8.000	**Location:**	P2-B7
Acq. method:	00-new_wasser-acn_standard_100-1000_BD-20min.amx		
Processing method:	MS_standard_plot.pmx		



Signal: DAD1 Total WL (220.0:600.0 nm)

RT [min]	Peak MS Base Peak m/z	Area	Area%	Max Peak%	Height
2.889		229.7886	0.1529	0.401	27.145
3.017		85.0512	0.0566	0.148	25.227
3.259		563.8480	0.3751	0.983	88.556
3.513		1056.3098	0.7027	1.842	298.077
3.645		550.4388	0.3662	0.960	135.961
3.813		6834.8973	4.5468	11.916	2035.107
4.196		1305.1975	0.8683	2.276	230.939

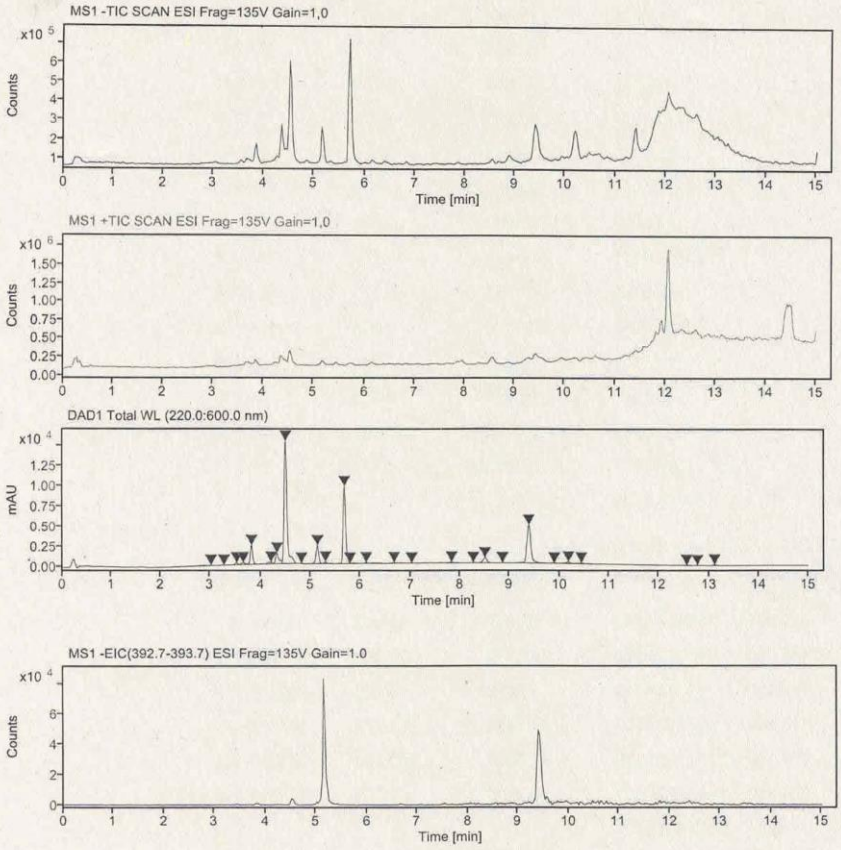
RT [min]	Peak MS Base Peak m/z	Area	Area%	Max Peak%	Height
4.321		5665.7349	3.7690	9.878	1258.097
4.491		57356.8021	38.1556	100.000	15546.911
4.808		229.6365	0.1528	0.400	67.803
5.132		8640.4901	5.7479	15.064	2415.908
5.293		771.5971	0.5133	1.345	263.023
5.665		39611.8159	26.3511	69.062	10575.497
6.103		251.9380	0.1676	0.439	60.965
6.805		581.8965	0.3871	1.015	91.918
7.825		392.2481	0.2609	0.684	69.857
8.497		2812.3103	1.8708	4.903	533.480
9.384		22101.7913	14.7028	38.534	3949.434
9.901		679.1221	0.4518	1.184	56.398
10.444		276.7878	0.1841	0.483	55.099
13.126		325.6268	0.2166	0.568	66.115
	Sum	150323.3288			

Signal: MS1 -TIC SCAN ESI Frag=135V Gain=1,0

RT [min]	Peak MS Base Peak m/z	Area	Area%	Max Peak%	Height
3.847	395.100	248357.1237	3.1839	8.519	76622.178
4.355	491.000	659230.6970	8.4511	22.614	163009.237
4.523	475.000	2180244.2329	27.9501	74.789	595771.176
5.162	393.100	742239.2201	9.5153	25.461	216483.346
5.699	473.000	2915197.1440	37.3719	100.000	644579.729
9.413	391.300	1055230.4103	13.5277	36.198	165838.327
	Sum	7800498.8280			

II-6h

Sequence Name:	2021-12-09_stabilityHALP134		
Data file:	HALP134-6h.dx	**Project Name:**	Single Quad
Sample name:	HALP134-6h	**Operator :**	SYSTEM
Instrument:	Single Quad	**Acquired on:**	2021-12-09 17:00:40+01:00
Inj. volume:	8.000	**Location:**	P2-B8
Acq. method:	00-new_wasser-acn_standard_100-1000_BD-20min.amx		
Processing method:	MS_standard_plot.pmx		



Signal: DAD1 Total WL (220.0:600.0 nm)

RT [min]	Peak MS Base Peak m/z	Area	Area%	Max Peak%	Height
3.012		1016.5869	0.6430	1.733	62.744
3.269		165.8860	0.1049	0.283	35.828
3.524		1024.9568	0.6483	1.747	262.308
3.651		1535.7326	0.9714	2.618	255.705
3.818		8135.1873	5.1457	13.869	2354.479
4.205		1466.5757	0.9276	2.500	198.803
4.324		6006.7480	3.7994	10.240	1303.669

D:\CDSProjects\Default\0-standardplot+EIC.rdl [Rev. 4194] Printed: 2021-12-13 07:40:10+01:00 Page 1 of 3

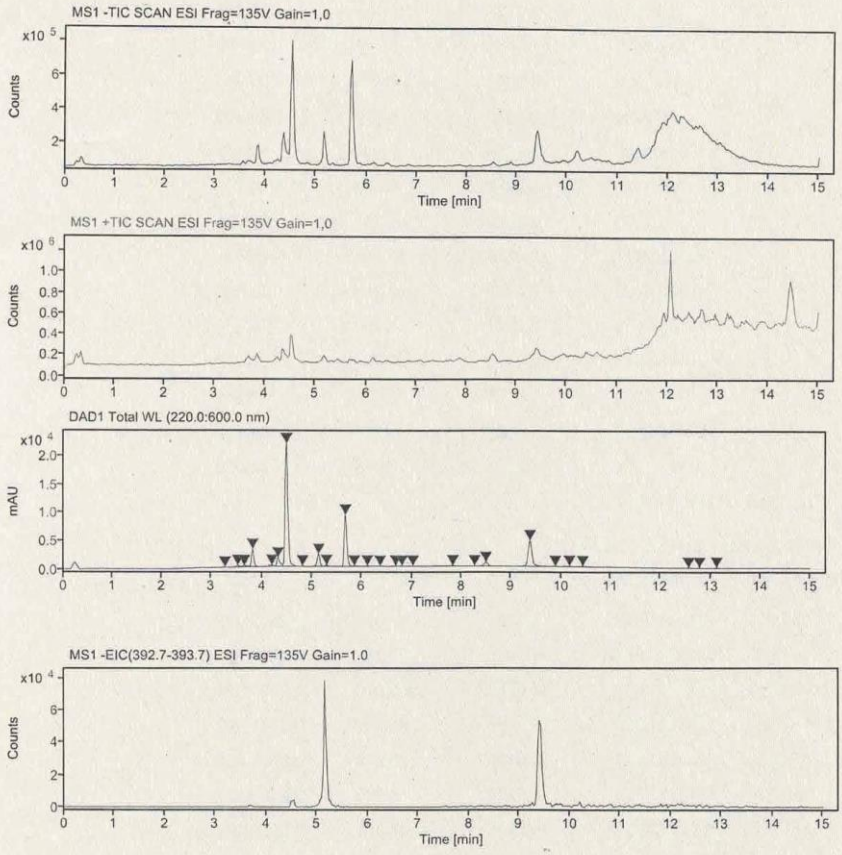
RT [min]	Peak MS Base Peak m/z	Area	Area%	Max Peak%	Height
4.493		58657.1034	37.1022	100.000	15110.459
4.816		113.0813	0.0715	0.193	54.035
5.135		8098.3093	5.1224	13.806	2199.054
5.297		803.4937	0.5082	1.370	206.648
5.675		35582.5214	22.5069	60.662	9523.919
5.789		350.8035	0.2219	0.598	55.974
6.111		664.0787	0.4200	1.132	85.813
6.671		627.8055	0.3971	1.070	63.947
7.028		88.0586	0.0557	0.150	23.586
7.829		1073.4697	0.6790	1.830	93.339
8.263		105.5664	0.0668	0.180	27.703
8.501		3298.2854	2.0863	5.623	630.685
8.858		165.2092	0.1045	0.282	38.174
9.389		26500.6015	16.7623	45.179	4748.946
9.900		160.0996	0.1013	0.273	31.258
10.183		977.0010	0.6180	1.666	177.164
10.446		732.2285	0.4632	1.248	88.909
12.555		149.4847	0.0946	0.255	41.032
12.775		112.0077	0.0708	0.191	25.290
13.120		485.2572	0.3069	0.827	97.178
	Sum	158096.1395			

Signal: MS1 -TIC SCAN ESI Frag=135V Gain=1,0

RT [min]	Peak MS Base Peak m/z	Area	Area%	Max Peak%	Height
3.852	395.100	328567.5449	5.9257	11.897	94836.477
4.357	489.100	616120.6522	11.1118	22.309	171705.829
4.603	472.900	89005.4118	1.6052	3.223	30356.139
5.163	393.100	628910.5897	11.3424	22.772	187985.470
5.709	473.100	2761752.9130	49.8083	100.000	649206.904
9.416	391.000	1120409.5661	20.2066	40.569	173789.318
	Sum	5544766.6776			

II-7h

Sequence Name:	2021-12-09_stabilityHALP134		
Data file:	HALP134-7h.dx	**Project Name:**	Single Quad
Sample name:	HALP134-7h	**Operator :**	SYSTEM
Instrument:	Single Quad	**Acquired on:**	2021-12-09 17:21:38+01:00
Inj. volume:	8.000	**Location:**	P2-B9
Acq. method:	00-new_wasser-acn_standard_100-1000_BD-20min.amx		
Processing method:	MS_standard_plot.pmx		



Signal: DAD1 Total WL (220.0:600.0 nm)

RT [min]	Peak MS Base Peak m/z	Area	Area%	Max Peak%	Height
3.265		427.4701	0.2361	0.518	75.687
3.518		1689.8616	0.9334	2.048	339.604
3.649		1629.2692	0.8999	1.975	267.294
3.815		10325.5979	5.7035	12.514	3069.887
4.195		1315.9112	0.7269	1.595	228.632
4.321		6454.3388	3.5651	7.822	1526.541
4.486		82513.9999	45.5777	100.000	21737.763

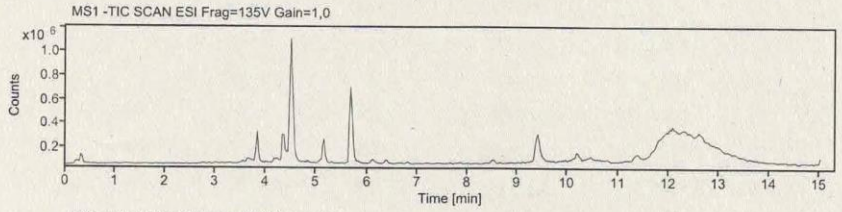
RT [min]	Peak MS Base Peak m/z	Area	Area%	Max Peak%	Height
4.811		314.2651	0.1736	0.381	80.089
5.132	393.100	8015.4589	4.4274	9.714	2151.575
5.291		648.5237	0.3582	0.786	207.351
5.668		34416.2155	19.0103	41.710	9171.763
5.845		376.7991	0.2081	0.457	68.260
6.107		424.1303	0.2343	0.514	81.751
6.363		136.1581	0.0752	0.165	31.481
6.673		187.1575	0.1034	0.227	38.386
6.807		159.2353	0.0880	0.193	53.640
7.024		100.6269	0.0556	0.122	24.460
7.822		816.5330	0.4510	0.990	76.267
8.262		69.1754	0.0382	0.084	15.799
8.490	313.100	3551.2126	1.9616	4.304	657.623
9.382		25200.9477	13.9201	30.541	4478.961
9.893		233.1598	0.1288	0.283	45.546
10.176		548.0119	0.3027	0.664	78.313
10.441		873.5113	0.4825	1.059	91.243
12.561		101.5295	0.0561	0.123	18.839
12.783		99.9157	0.0552	0.121	24.529
13.128		411.1936	0.2271	0.498	83.092
	Sum	181040.2097			

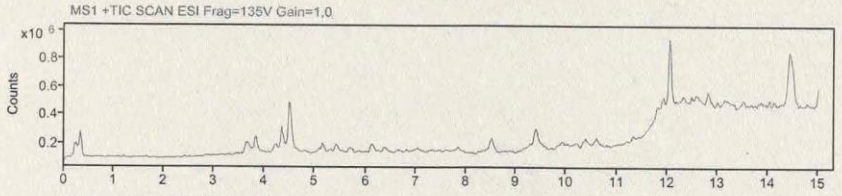
Signal: MS1 -TIC SCAN ESI Frag=135V Gain=1,0

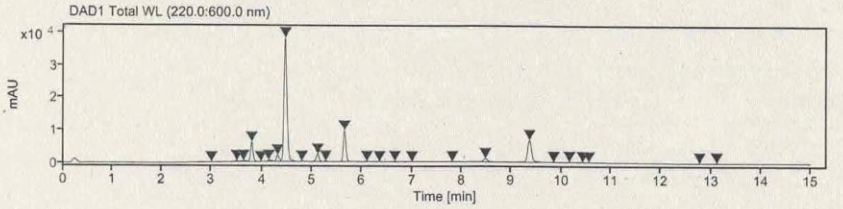
RT [min]	Peak MS Base Peak m/z	Area	Area%	Max Peak%	Height
3.845	395.100	428643.3449	4.9326	14.826	116973.213
4.355	491.000	639829.1284	7.3627	22.131	170654.721
4.521	475.100	2891086.7001	33.2688	100.000	708281.521
5.161	393.100	726112.8034	8.3556	25.116	199441.292
5.702	473.000	2609898.8705	30.0330	90.274	620272.065
8.527	313.100	134160.1002	1.5438	4.640	22183.089
9.413	391.100	1260360.4370	14.5034	43.595	186506.301
	Sum	8690091.3845			

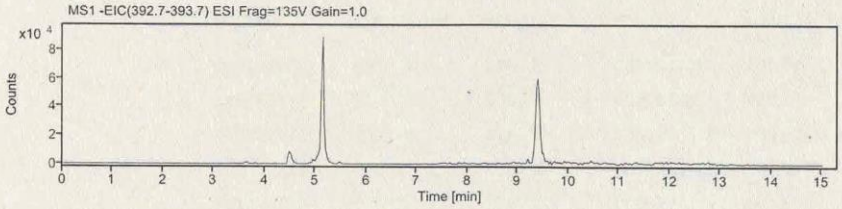
II-8h

Sequence Name:	2021-12-09_stabilityHALP134		
Data file:	HALP134-8h.dx	**Project Name:**	Single Quad
Sample name:	HALP134-8h	**Operator :**	SYSTEM
Instrument:	Single Quad	**Acquired on:**	2021-12-09 17:42:38+01:00
Inj. volume:	8.000	**Location:**	P2-B10
Acq. method:	00-new_wasser-acn_standard_100-1000_BD-20min.amx		
Processing method:	MS_standard_plot.pmx		









Signal: DAD1 Total WL (220.0:600.0 nm)

RT [min]	Peak MS Base Peak m/z	Area	Area%	Max Peak%	Height
2.998		520.9486	0.1804	0.327	29.529
3.502		1588.2794	0.5500	0.997	339.498
3.633		2375.6128	0.8227	1.490	392.308
3.798		21343.2849	7.3914	13.391	6056.157
3.976		122.5356	0.0424	0.077	33.133
4.135		1994.2909	0.6906	1.251	379.130
4.311		7838.4476	2.7145	4.918	1965.969

RT [min]	Peak MS Base Peak m/z	Area	Area%	Max Peak%	Height
4.461		159384.4716	55.1962	100.000	38151.399
4.798		294.0413	0.1018	0.184	107.431
5.115		9055.5326	3.1360	5.682	2335.075
5.274		547.5411	0.1896	0.344	178.801
5.648		35491.6975	12.2911	22.268	9518.492
6.093		511.8925	0.1773	0.321	126.012
6.346		218.2765	0.0756	0.137	59.971
6.657		802.0555	0.2778	0.503	91.004
7.003		294.9179	0.1021	0.185	47.865
7.810		802.9718	0.2781	0.504	75.835
8.476	315.100	5623.1386	1.9473	3.528	1043.851
9.368	391.100	36982.7283	12.8074	23.203	6716.548
9.851		303.4912	0.1051	0.190	51.659
10.167		683.3476	0.2366	0.429	138.902
10.431		808.4938	0.2800	0.507	113.874
10.559		152.0409	0.0527	0.095	51.166
12.777		140.0236	0.0485	0.088	45.020
13.122		879.8093	0.3047	0.552	174.787
	Sum	288759.8714			

Signal: MS1 +TIC SCAN ESI Frag=135V Gain=1,0

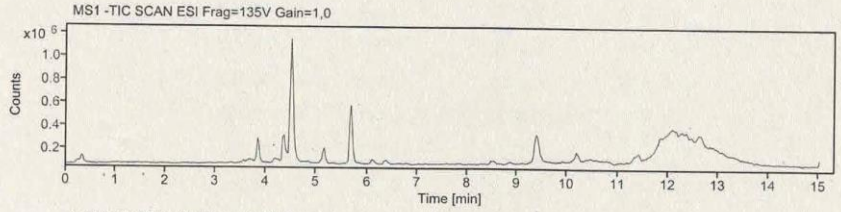
RT [min]	Peak MS Base Peak m/z	Area	Area%	Max Peak%	Height
8.509	315.100	554715.9587	100.0000	100.000	91380.605
	Sum	554715.9587			

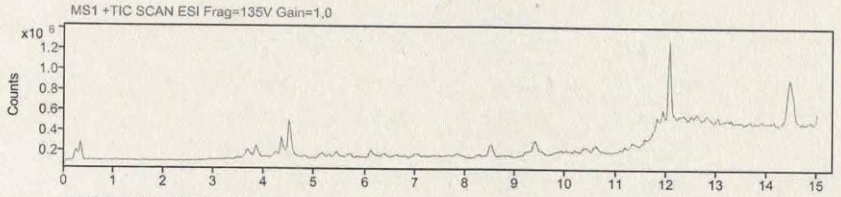
Signal: MS1 -TIC SCAN ESI Frag=135V Gain=1,0

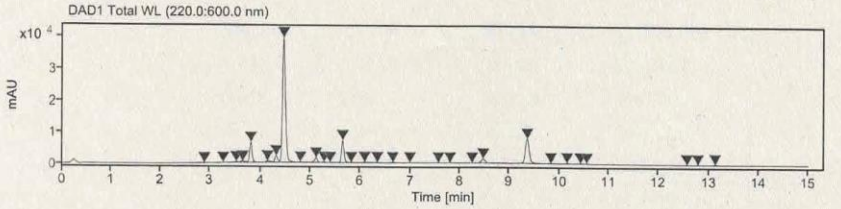
RT [min]	Peak MS Base Peak m/z	Area	Area%	Max Peak%	Height
3.830	395.100	697931.4687	6.2361	14.669	238579.894
4.327	491.000	823805.1339	7.3608	17.315	212720.563
4.493	475.000	4757786.6411	42.5115	100.000	1038023.878
5.148	393.100	636121.6269	5.6838	13.370	183779.740
5.682	473.100	2712357.8939	24.2353	57.009	628154.794
8.515	313.300	137827.3569	1.2315	2.897	27134.094
9.406	391.100	1425946.1597	12.7410	29.971	221369.995
	Sum	11191776.2811			

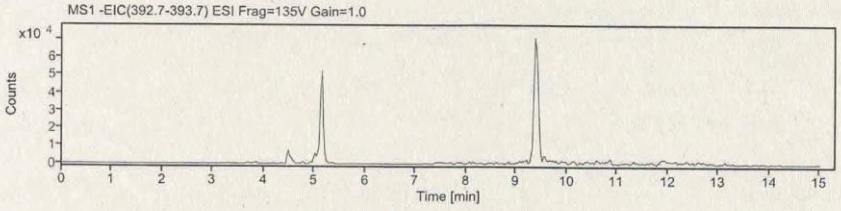
II-92

Sequence Name:	2021-12-09_stabilityHALP134		
Data file:	HALP134-9h.dx	**Project Name:**	Single Quad
Sample name:	HALP134-9h	**Operator :**	SYSTEM
Instrument:	Single Quad	**Acquired on:**	2021-12-09 18:03:36+01:00
Inj. volume:	8.000	**Location:**	P2-B11
Acq. method:	00-new_wasser-acn_standard_100-1000_BD-20min.amx		
Processing method:	MS_standard_plot.pmx		









Signal: DAD1 Total WL (220.0:600.0 nm)

RT [min]	Peak MS Base Peak m/z	Area	Area%	Max Peak%	Height
2.883		589.1457	0.2002	0.358	45.735
3.256		372.9420	0.1267	0.227	58.757
3.517		1786.6632	0.6072	1.085	305.169
3.644		2796.6537	0.9505	1.699	470.794
3.807		23058.7074	7.8367	14.004	6432.223
4.138		2512.0131	0.8537	1.526	452.693
4.310		8487.8128	2.8846	5.155	2150.390

D:\CDSProjects\Default\0-standardplot+EIC.rdl [Rev. 4194] Printed: 2021-12-13 07:41:22+01:00 Page 1 of 3

RT [min]	Peak MS Base Peak m/z	Area	Area%	Max Peak%	Height
4.459		164654.2866	55.9589	100.000	39234.071
4.797		243.4954	0.0828	0.148	100.032
5.113		6320.4777	2.1481	3.839	1453.482
5.269		533.0225	0.1812	0.324	175.848
5.392		9.2919	0.0032	0.006	20.963
5.643		25545.8376	8.6819	15.515	6973.593
5.815		151.1637	0.0514	0.092	37.423
6.083		890.3318	0.3026	0.541	183.315
6.336		284.1605	0.0966	0.173	80.852
6.647		1056.1968	0.3590	0.641	123.895
6.996		450.3505	0.1531	0.274	65.402
7.567		329.1412	0.1119	0.200	35.914
7.801		343.8207	0.1168	0.209	79.654
8.244		111.7231	0.0380	0.068	27.866
8.469		6897.7038	2.3442	4.189	1291.544
9.360	391.100	42649.2842	14.4947	25.902	7712.487
9.835		348.1328	0.1183	0.211	67.987
10.162		885.7617	0.3010	0.538	176.413
10.429		1057.7182	0.3595	0.642	141.438
10.559		274.4470	0.0933	0.167	74.494
12.565		196.7982	0.0669	0.120	36.176
12.788		260.3636	0.0885	0.158	66.342
13.134		1143.8571	0.3887	0.695	231.271
	Sum	294241.3043			

Signal: MS1 +TIC SCAN ESI Frag=135V Gain=1,0

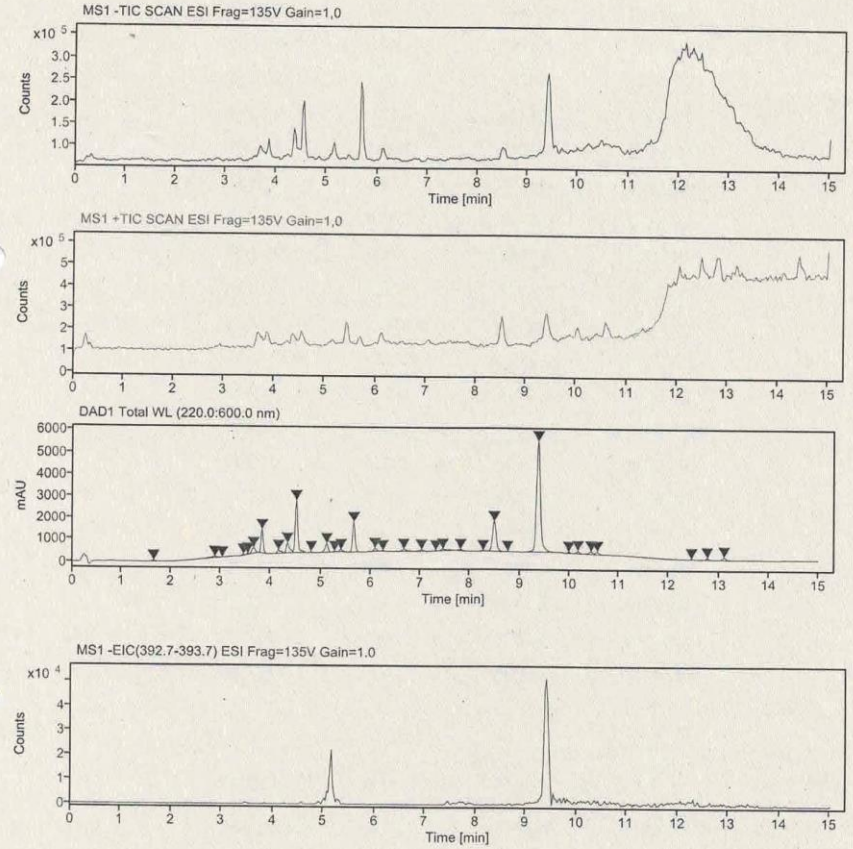
RT [min]	Peak MS Base Peak m/z	Area	Area%	Max Peak%	Height
8.506	315.200	646498.5518	100.0000	100.000	116936.051
	Sum	646498.5518			

Signal: MS1 -TIC SCAN ESI Frag=135V Gain=1,0

RT [min]	Peak MS Base Peak m/z	Area	Area%	Max Peak%	Height
3.838	395.100	684940.1991	6.3625	14.249	210940.684
4.345	489.000	897580.2581	8.3377	18.673	225461.778
4.494	473.100	4806810.1938	44.6511	100.000	1049030.339
5.148	393.000	567105.1663	5.2679	11.798	138186.333
5.678	471.100	2097820.6324	19.4869	43.643	502066.681
8.500	313.100	162011.8812	1.5049	3.370	25814.317
9.389	391.100	1549006.0802	14.3889	32.225	237119.189
	Sum	10765274.4110			

II - 24h

Sequence Name:	2021-12-09_stabilityHALP134		
Data file:	HALP134-24h.dx	**Project Name:**	Single Quad
Sample name:	HALP134-24h	**Operator :**	SYSTEM
Instrument:	Single Quad	**Acquired on:**	2021-12-09 18:24:35+01:00
Inj. volume:	4.000	**Location:**	P2-C1
Acq. method:	00-new_wasser-acn_standard_100-1000_BD-20min.amx		
Processing method:	MS_standard_plot.pmx		



Signal: DAD1 Total WL (220.0:600.0 nm)

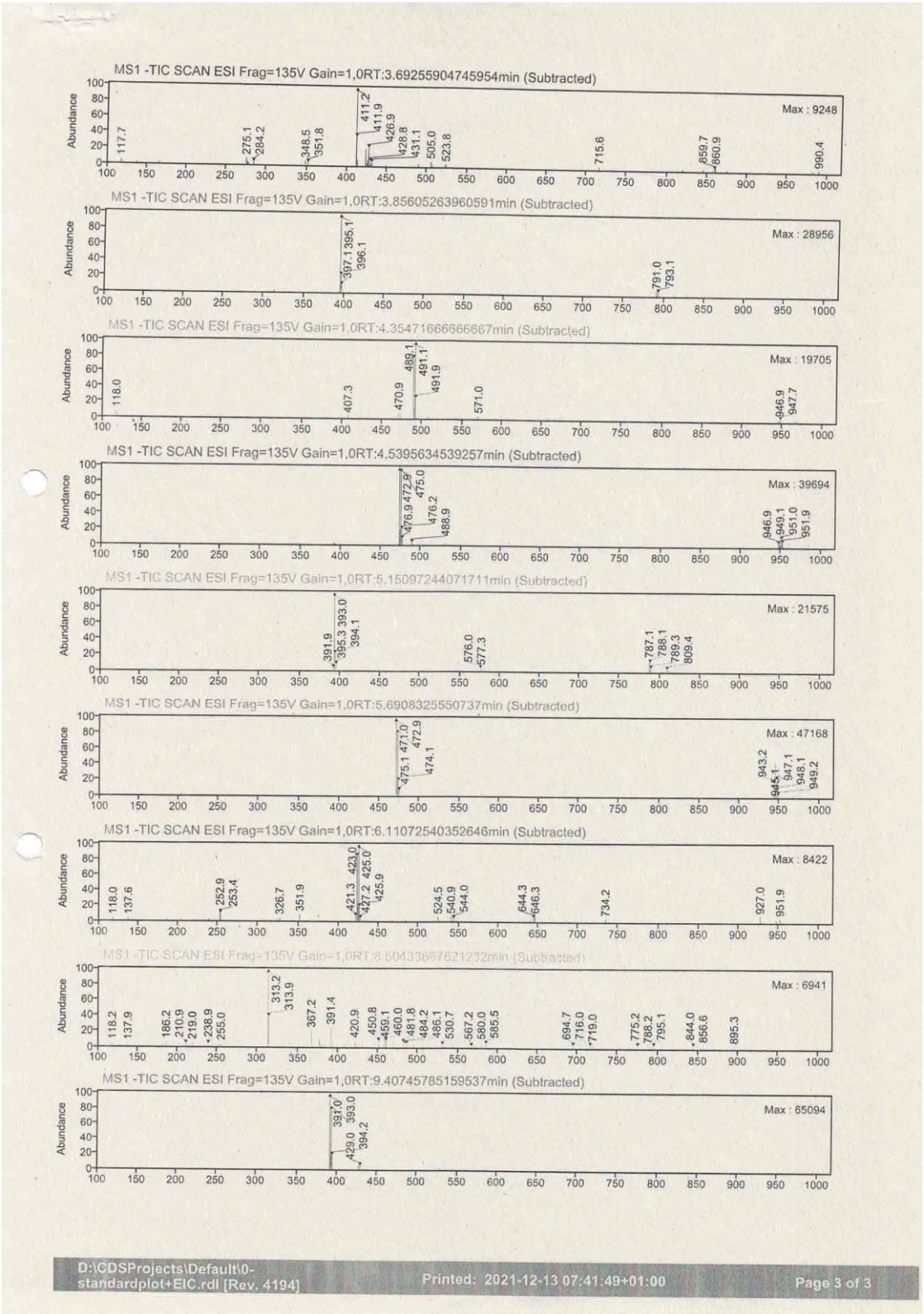
RT [min]	Peak MS Base Peak m/z	Area	Area%	Max Peak%	Height
1.653		248.3944	0.3877	0.893	37.601
2.886		480.2470	0.7496	1.726	59.946
3.033		6.0178	0.0094	0.022	5.627
3.454		120.3986	0.1879	0.433	47.522
3.541		115.6100	0.1804	0.415	50.676
3.656		1206.2889	1.8828	4.335	246.974
3.825		3398.1780	5.3038	12.212	1065.390

D:\CDSProjects\Default\0-standardplot+EIC.rdl [Rev. 4194] Printed: 2021-12-13 07:41:49+01:00 Page 1 of 3

RT [min]	Peak MS Base Peak m/z	Area	Area%	Max Peak%	Height
4.151		660.7244	1.0312	2.374	136.501
4.330		1932.1628	3.0157	6.943	428.339
4.507		8427.4176	13.1534	30.285	2387.006
4.807		120.1998	0.1876	0.432	34.978
5.118		1587.0690	2.4771	5.703	386.375
5.274		34.1710	0.0533	0.123	14.185
5.400		380.8069	0.5944	1.368	90.170
5.658		4866.6029	7.5957	17.489	1364.464
6.084		567.4731	0.8857	2.039	127.119
6.238		76.5033	0.1194	0.275	24.948
6.660		593.7666	0.9267	2.134	88.680
7.020		349.4468	0.5454	1.256	62.481
7.305		30.5692	0.0477	0.110	9.460
7.448		567.1920	0.8853	2.038	66.314
7.805		259.2780	0.4047	0.932	52.108
8.259		134.8245	0.2104	0.485	28.861
8.482		7212.2114	11.2567	25.918	1371.363
8.754		54.3561	0.0848	0.195	10.698
9.374		27826.9796	43.4319	100.000	5042.615
9.988		176.7548	0.2759	0.635	41.761
10.171		452.8803	0.7068	1.627	98.246
10.436		701.7311	1.0953	2.522	118.104
10.563		550.9834	0.8600	1.980	114.348
12.449		90.3774	0.1411	0.325	18.959
12.768		289.7399	0.4522	1.041	69.375
13.109		550.9987	0.8600	1.980	114.282
	Sum	64070.3553			

Signal: MS1 -TIC SCAN ESI Frag=135V Gain=1,0

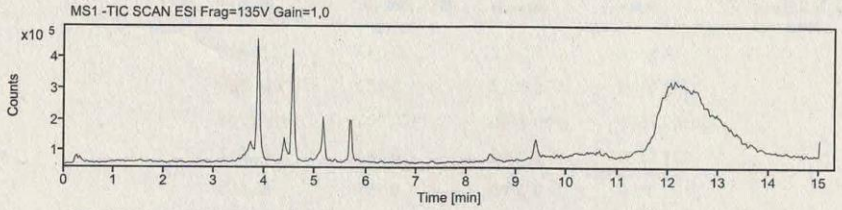
RT [min]	Peak MS Base Peak m/z	Area	Area%	Max Peak%	Height
3.693	411.200	146729.6910	4.5022	13.715	26392.634
3.856	395.100	146776.2802	4.5036	13.720	40664.900
4.355	491.100	232943.2430	7.1476	21.774	59005.432
4.540	472.900	540729.0693	16.5916	50.543	129854.489
5.151	393.000	170721.4887	5.2384	15.958	38218.376
5.691	471.000	687535.6205	21.0962	64.266	186596.951
6.111	425.000	117062.2559	3.5919	10.942	25225.020
8.504	313.200	146724.5865	4.5021	13.715	24699.025
9.407	391.000	1069834.0694	32.8265	100.000	174480.562
	Sum	3259056.3045			

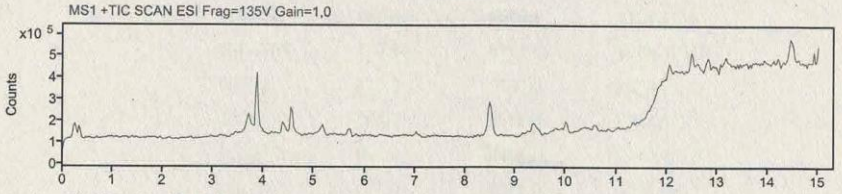

MS1 -TIC SCAN ESI Frag=135V Gain=1,0RT:3.69255904745954min (Subtracted)
Max : 9248
MS1 -TIC SCAN ESI Frag=135V Gain=1,0RT:3.85605263960591min (Subtracted)
Max : 28956
MS1 -TIC SCAN ESI Frag=135V Gain=1,0RT:4.35471666666667min (Subtracted)
Max : 19705
MS1 -TIC SCAN ESI Frag=135V Gain=1,0RT:4.5395634539257min (Subtracted)
Max : 39694
MS1 -TIC SCAN ESI Frag=135V Gain=1,0RT:5.15097244071711min (Subtracted)
Max : 21575
MS1 -TIC SCAN ESI Frag=135V Gain=1,0RT:5.6908325550737min (Subtracted)
Max : 47168
MS1 -TIC SCAN ESI Frag=135V Gain=1,0RT:6.11072540352646min (Subtracted)
Max : 8422
MS1 -TIC SCAN ESI Frag=135V Gain=1,0RT:8.50433667621232min (Subtracted)
Max : 6941
MS1 -TIC SCAN ESI Frag=135V Gain=1,0RT:9.40745785159537min (Subtracted)
Max : 65094
Abundance
D:\CDSProjects\Default\0-standardplot+EIC.rdl [Rev. 4194]
Printed: 2021-12-13 07:41:49+01:00
Page 3 of 3

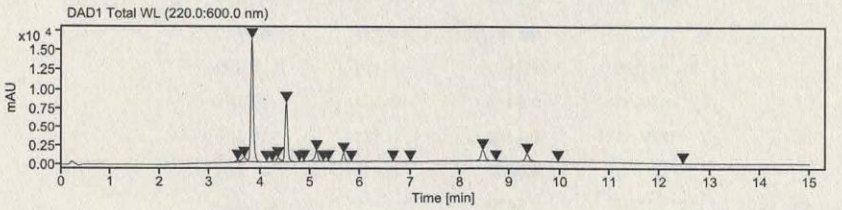
Trial III

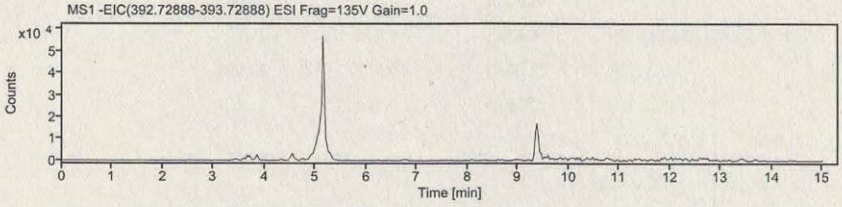
III-1h

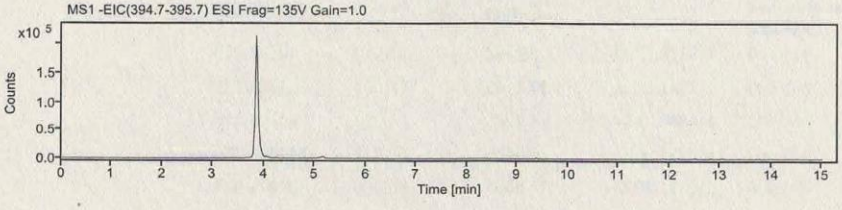
Sequence Name:	SingleSample		
Data file:	HALP137-1h.dx	**Project Name:**	Single Quad
Sample name:	HALP137-1h	**Operator :**	SYSTEM
Instrument:	Single Quad	**Acquired on:**	2021-12-14 00:49:49+01:00
Inj. volume:	8.000	**Location:**	P1-A8
Acq. method:	00-new_wasser-acn_standard_100-1000_BD-20min.amx		
Processing method:	MS_standard_plot.pmx		



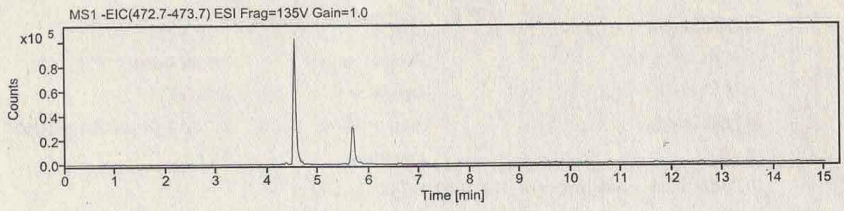








D:\CDSProjects\Default\0-standardplot+EIC.rdl [Rev. 4251] Printed: 2021-12-14 10:22:20+01:00 Page 1 of 3

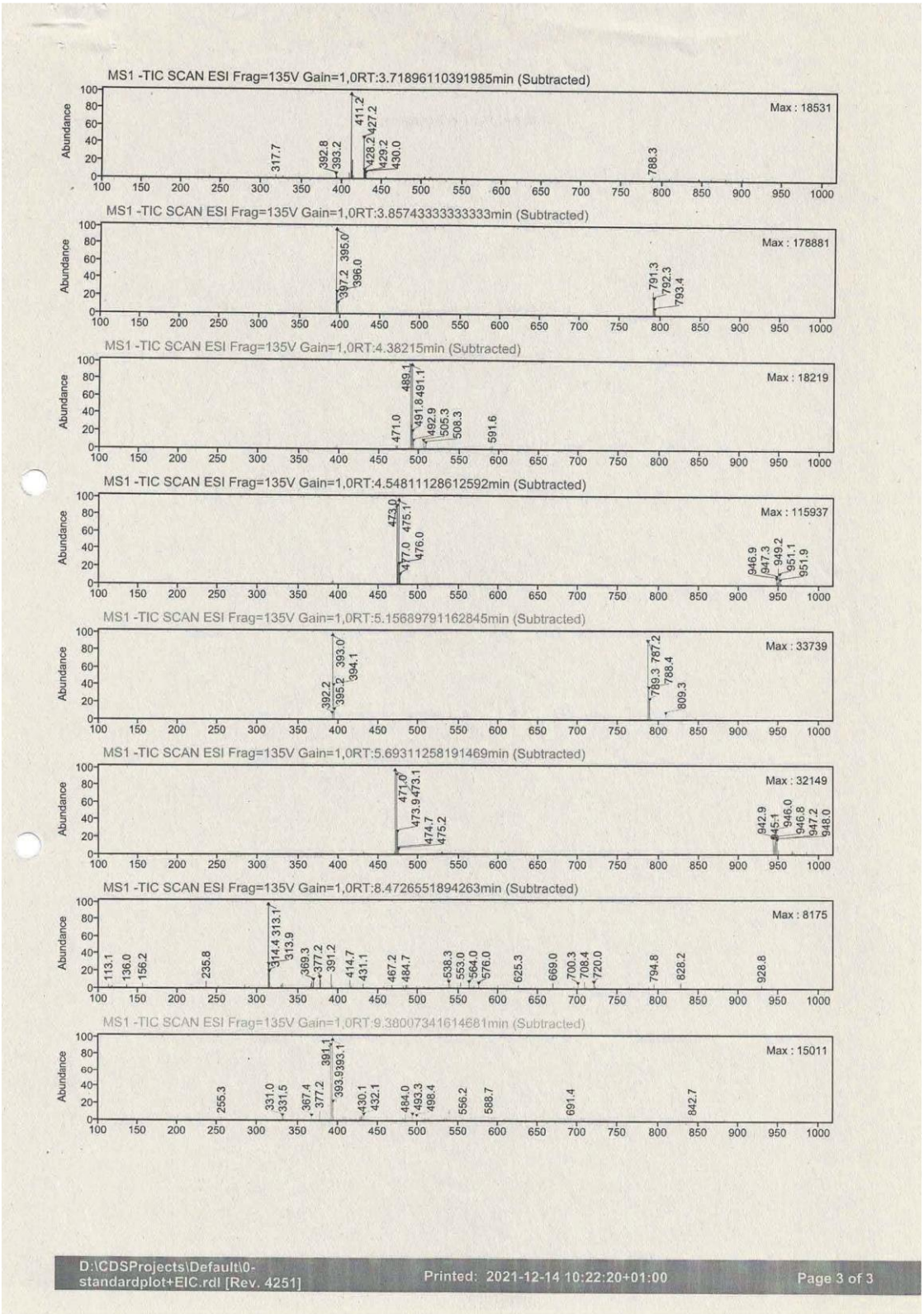


Signal: DAD1 Total WL (220.0:600.0 nm)

RT [min]	Peak MS Base Peak m/z	Area	Area%	Max Peak%	Height
3.551		1216.8589	1.0372	2.059	220.507
3.679		3352.0146	2.8572	5.672	564.569
3.834		59102.7598	50.3785	100.000	16175.798
4.124		121.7370	0.1038	0.206	40.617
4.236		92.0579	0.0785	0.156	33.190
4.350		2294.7360	1.9560	3.883	503.391
4.514		27207.9852	23.1918	46.035	7879.805
4.777		9.1356	0.0078	0.015	11.011
4.872		256.1505	0.2183	0.433	99.780
5.123		5789.8560	4.9352	9.796	1369.535
5.255		69.3507	0.0591	0.117	25.893
5.358		257.3528	0.2194	0.435	83.720
5.661		3802.4004	3.2411	6.434	1070.200
5.815		55.7530	0.0475	0.094	23.998
6.648		132.9154	0.1133	0.225	18.529
6.999		77.8469	0.0664	0.132	21.065
8.452	313.100	8073.7362	6.8820	13.661	1426.224
8.716		37.5571	0.0320	0.064	8.423
9.346	391.100	5206.9552	4.4383	8.810	921.826
9.965		99.4373	0.0848	0.168	23.028
12.463		60.8878	0.0519	0.103	13.401
	Sum	117317.4843			

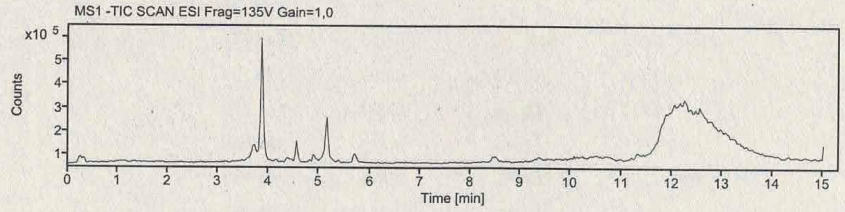
Signal: MS1 -TIC SCAN ESI Frag=135V Gain=1,0

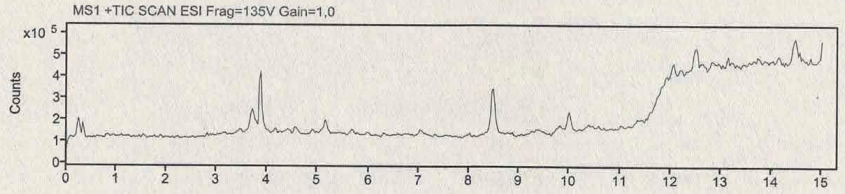
RT [min]	Peak MS Base Peak m/z	Area	Area%	Max Peak%	Height
3.719	411.200	229275.8199	5.1392	15.519	40837.686
3.857	395.000	1477346.3150	33.1145	100.000	371866.287
4.382	491.100	219880.7954	4.9286	14.883	60302.324
4.548	475.100	1185054.9027	26.5628	80.215	341409.370
5.157	393.000	516891.8322	11.5861	34.988	136575.886
5.693	471.000	519681.7138	11.6486	35.177	142557.690
8.473	313.100	141177.1186	3.1645	9.556	21588.569
9.380	391.100	172016.7586	3.8557	11.644	49915.447
	Sum	4461325.2562			

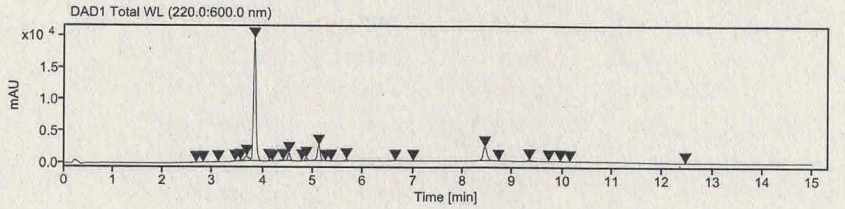

MS1 -TIC SCAN ESI Frag=135V Gain=1,0RT:3.71896110391985min (Subtracted)
Max : 18531
MS1 -TIC SCAN ESI Frag=135V Gain=1,0RT:3.85743333333333min (Subtracted)
Max : 178881
MS1 -TIC SCAN ESI Frag=135V Gain=1,0RT:4.38215min (Subtracted)
Max : 18219
MS1 -TIC SCAN ESI Frag=135V Gain=1,0RT:4.54811128612592min (Subtracted)
Max : 115937
MS1 -TIC SCAN ESI Frag=135V Gain=1,0RT:5.15689791162845min (Subtracted)
Max : 33739
MS1 -TIC SCAN ESI Frag=135V Gain=1,0RT:5.69311258191469min (Subtracted)
Max : 32149
MS1 -TIC SCAN ESI Frag=135V Gain=1,0RT:8.4726551894263min (Subtracted)
Max : 8175
MS1 -TIC SCAN ESI Frag=135V Gain=1,0RT:9.38007341614681min (Subtracted)
Max : 15011
Abundance
D:\CDSProjects\Default\0-standardplot+EIC.rdl [Rev. 4251]
Printed: 2021-12-14 10:22:20+01:00
Page 3 of 3

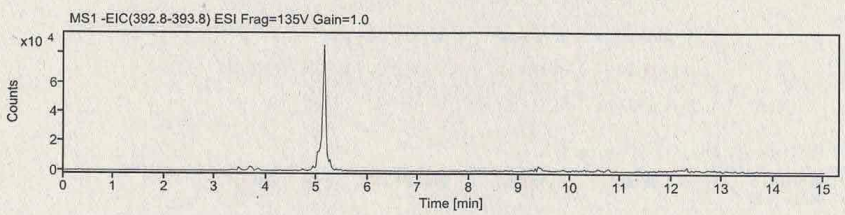
III- 2h

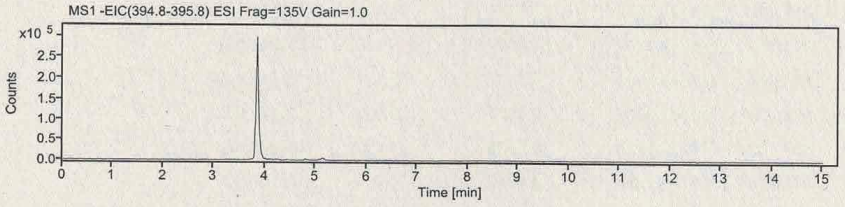
Sequence Name:	SingleSample		
Data file:	HALP137-2h.dx	**Project Name:**	Single Quad
Sample name:	HALP137-2h	**Operator :**	SYSTEM
Instrument:	Single Quad	**Acquired on:**	2021-12-14 01:10:51+01:00
Inj. volume:	8.000	**Location:**	P1-A9
Acq. method:	00-new_wasser-acn_standard_100-1000_BD-20min.amx		
Processing method:	MS_standard_plot.pmx		











Signal: DAD1 Total WL (220.0:600.0 nm)

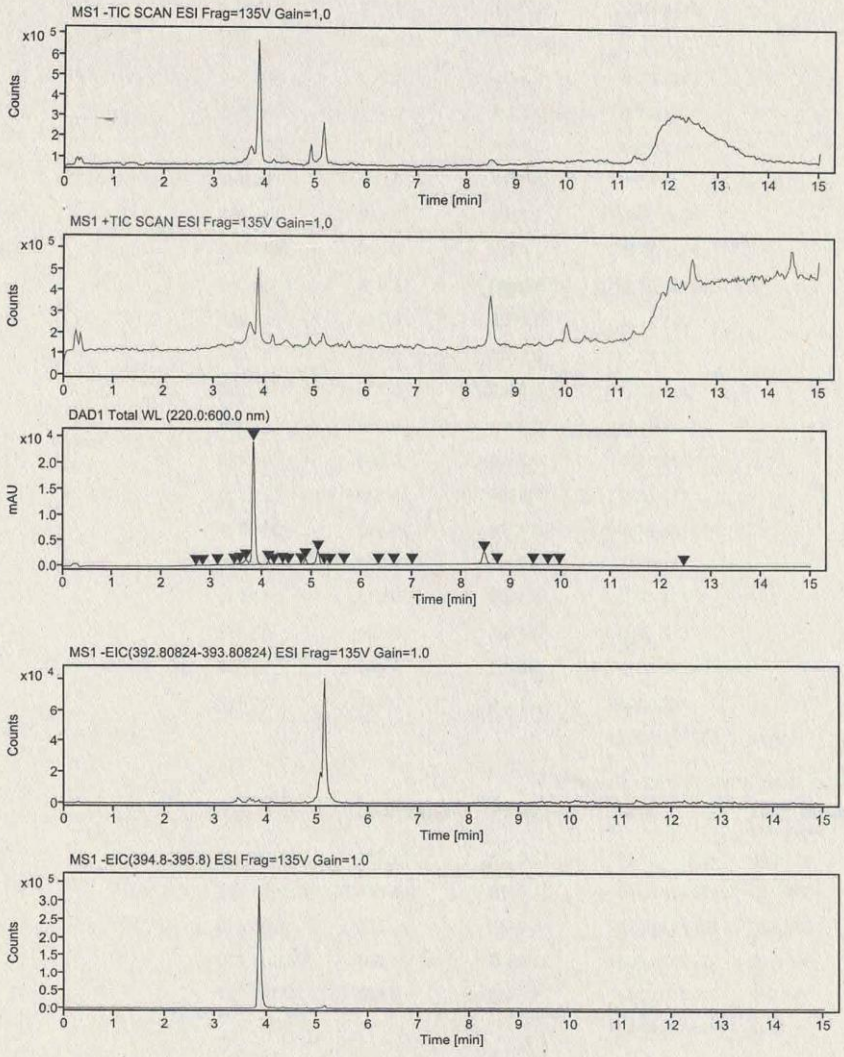
RT [min]	Peak MS Base Peak m/z	Area	Area%	Max Peak%	Height
2.666		108.9764	0.1032	0.157	21.568
2.809		64.6201	0.0612	0.093	15.109
3.112		403.0741	0.3816	0.581	60.825
3.448		142.9012	0.1353	0.206	45.324
3.553		639.6425	0.6056	0.922	175.632
3.678		4438.6168	4.2027	6.398	765.581
3.830		69377.0674	65.6893	100.000	19215.141
4.123		524.3543	0.4965	0.756	174.191
4.187		1.5736	0.0015	0.002	7.479
4.402		617.2004	0.5844	0.890	105.863
4.516		3642.2285	3.4486	5.250	1171.812
4.775		189.4099	0.1793	0.273	76.467
4.865		1328.2822	1.2577	1.915	439.059
5.115		9236.4768	8.7455	13.313	2371.796
5.243		5.1908	0.0049	0.007	17.849
5.355		195.6895	0.1853	0.282	67.599
5.664		1019.5884	0.9654	1.470	284.040
6.638		286.6540	0.2714	0.413	42.593
7.003		89.5478	0.0848	0.129	22.974
8.442		11416.9556	10.8101	16.456	2074.600
8.716		39.2781	0.0372	0.057	10.730
9.338		1248.0422	1.1817	1.799	187.201
9.726		136.6435	0.1294	0.197	25.137
9.959		289.8002	0.2744	0.418	62.297
10.150		32.4117	0.0307	0.047	7.276
12.459		139.7839	0.1324	0.201	33.790
	Sum	105614.0100			

Signal: MS1 -TIC SCAN ESI Frag=135V Gain=1,0

RT [min]	Peak MS Base Peak m/z	Area	Area%	Max Peak%	Height
3.710	411.200	295123.2557	7.8834	14.463	63381.190
3.861	395.100	2040482.1757	54.5057	100.000	525942.053
4.548	475.000	267583.8130	7.1477	13.114	87415.142
4.879	378.200	80027.0805	2.1377	3.922	25477.851
5.150	393.100	736752.7726	19.6803	36.107	182396.468
5.701	473.200	164781.7253	4.4017	8.076	35189.000
8.497	313.000	158862.0050	4.2435	7.786	21599.376
	Sum	3743612.8279			

III-4h

Sequence Name:	SingleSample		
Data file:	HALP137-4h.dx	**Project Name:**	Single Quad
Sample name:	HALP137-4h	**Operator :**	SYSTEM
Instrument:	Single Quad	**Acquired on:**	2021-12-14 01:53:02+01:00
Inj. volume:	8.000	**Location:**	P1-A11
Acq. method:	00-new_wasser-acn_standard_100-1000_BD-20min.amx		
Processing method:	MS_standard_plot.pmx		



D:\CDSProjects\Default\0-standardplot+EIC.rdl [Rev. 4251] Printed: 2021-12-14 10:27:31+01:00 Page 1 of 3

Signal: DAD1 Total WL (220.0:600.0 nm)

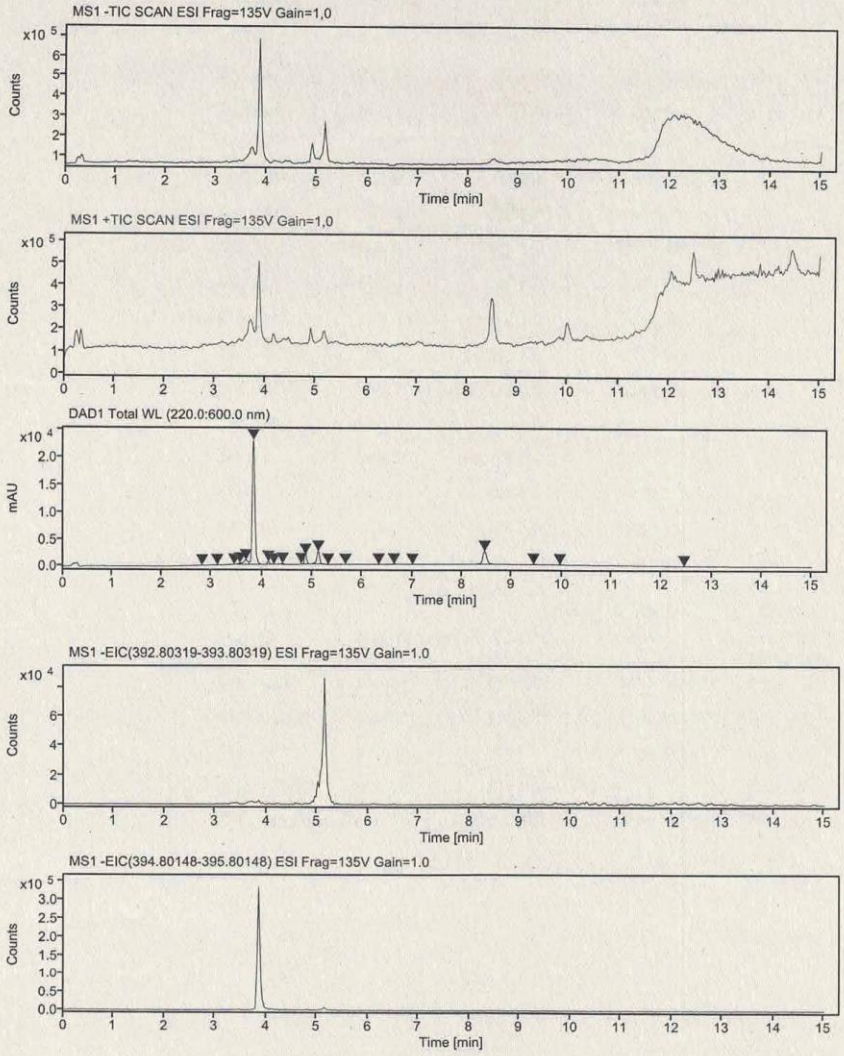
RT [min]	Peak MS Base Peak m/z	Area	Area%	Max Peak%	Height
2.683		212.0526	0.1602	0.234	44.790
2.820		67.6582	0.0511	0.075	22.448
3.119		733.2724	0.5539	0.809	102.119
3.453		455.9916	0.3444	0.503	104.379
3.560		1150.2667	0.8689	1.270	304.655
3.684		5634.4352	4.2561	6.219	935.552
3.832		90597.4540	68.4352	100.000	24036.825
4.127		1763.4656	1.3321	1.946	575.164
4.235		69.6825	0.0526	0.077	35.346
4.410		912.6301	0.6894	1.007	202.807
4.523		36.7253	0.0277	0.041	25.427
4.780		379.8642	0.2869	0.419	130.857
4.868		3841.3943	2.9017	4.240	1095.795
5.118		10943.6178	8.2666	12.079	2630.085
5.242		223.6105	0.1689	0.247	64.935
5.354		28.2223	0.0213	0.031	18.247
5.639		335.2781	0.2533	0.370	83.226
6.323		78.1991	0.0591	0.086	15.621
6.630		514.9678	0.3890	0.568	67.423
7.005		117.2692	0.0886	0.129	24.525
8.449		13102.3763	9.8972	14.462	2338.225
8.713		37.6214	0.0284	0.042	10.175
9.437		464.4865	0.3509	0.513	84.245
9.734		172.7996	0.1305	0.191	33.353
9.965		368.4812	0.2783	0.407	79.576
12.454		142.4265	0.1076	0.157	38.305
	Sum	132384.2492			

Signal: MS1 -TIC SCAN ESI Frag=135V Gain=1,0

RT [min]	Peak MS Base Peak m/z	Area	Area%	Max Peak%	Height
3.719	411.000	495318.3174	12.5125	21.781	74124.955
3.864	395.100	2274126.6343	57.4479	100.000	603676.225
4.902	378.000	239283.8328	6.0447	10.522	89286.638
5.152	393.100	779592.4995	19.6937	34.281	196398.493
8.489	313.000	170270.0313	4.3013	7.487	23123.197
	Sum	3958591.3153			

111-5h

Sequence Name:	SingleSample		
Data file:	HALP137-5h.dx	**Project Name:**	Single Quad
Sample name:	HALP137-5h	**Operator :**	SYSTEM
Instrument:	Single Quad	**Acquired on:**	2021-12-14 02:14:07+01:00
Inj. volume:	8.000	**Location:**	P1-B1
Acq. method:	00-new_wasser-acn_standard_100-1000_BD-20min.amx		
Processing method:	MS_standard_plot.pmx		



Signal: DAD1 Total WL (220.0:600.0 nm)

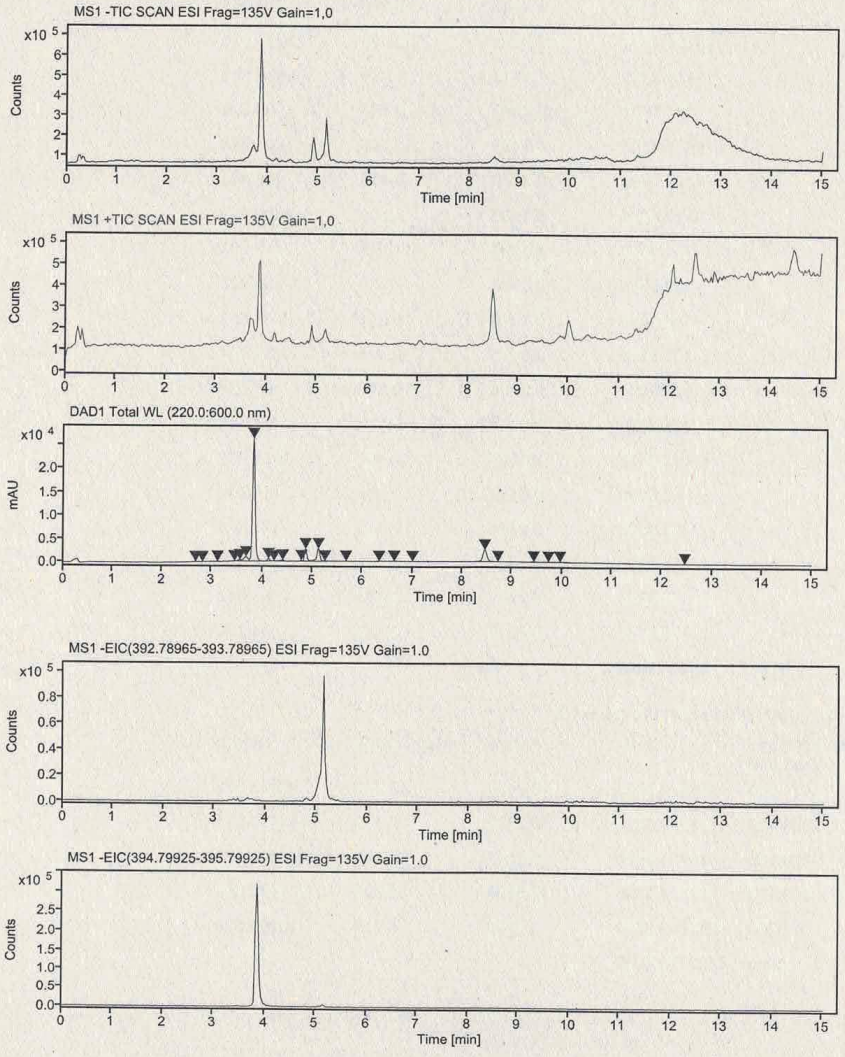
RT [min]	Peak MS Base Peak m/z	Area	Area%	Max Peak%	Height
2.809		262.1969	0.2109	0.308	16.771
3.111		535.9495	0.4311	0.630	84.774
3.448		24.4946	0.0197	0.029	27.345
3.557		798.6388	0.6424	0.939	236.952
3.681	411.200	4970.9090	3.9985	5.844	816.936
3.831		85062.6607	68.4228	100.000	22785.367
4.125		1671.5158	1.3445	1.965	539.561
4.232		97.6136	0.0785	0.115	42.478
4.406		966.5673	0.7775	1.136	197.630
4.780		81.6619	0.0657	0.096	74.041
4.868		5659.4114	4.5523	6.653	1758.222
5.123		9063.1261	7.2902	10.655	2315.189
5.319		62.5502	0.0503	0.074	22.923
5.663		93.4523	0.0752	0.110	34.158
6.327		82.7584	0.0666	0.097	18.819
6.631		482.5233	0.3881	0.567	64.885
7.007		83.5905	0.0672	0.098	20.960
8.455		13111.3243	10.5465	15.414	2344.867
9.441		421.5224	0.3391	0.496	77.031
9.968		625.0747	0.5028	0.735	81.499
12.453		161.5611	0.1300	0.190	41.080
	Sum	124319.1028			

Signal: MS1 -TIC SCAN ESI Frag=135V Gain=1,0

RT [min]	Peak MS Base Peak m/z	Area	Area%	Max Peak%	Height
3.712	411.200	333186.4789	8.3639	14.647	59204.107
3.862	395.100	2274728.2873	57.1023	100.000	611200.956
4.901	757.300	388122.0332	9.7430	17.062	98204.976
5.155	393.100	803803.9514	20.1778	35.336	206546.459
8.515	313.300	183763.9939	4.6130	8.079	22931.798
	Sum	3983604.7447			

III-6h

Sequence Name:	SingleSample		
Data file:	HALP137-6h.dx	**Project Name:**	Single Quad
Sample name:	HALP137-6h	**Operator :**	SYSTEM
Instrument:	Single Quad	**Acquired on:**	2021-12-14 02:35:13+01:00
Inj. volume:	8.000	**Location:**	P1-B2
Acq. method:	00-new_wasser-acn_standard_100-1000_BD-20min.amx		
Processing method:	MS_standard_plot.pmx		



Signal: DAD1 Total WL (220.0:600.0 nm)

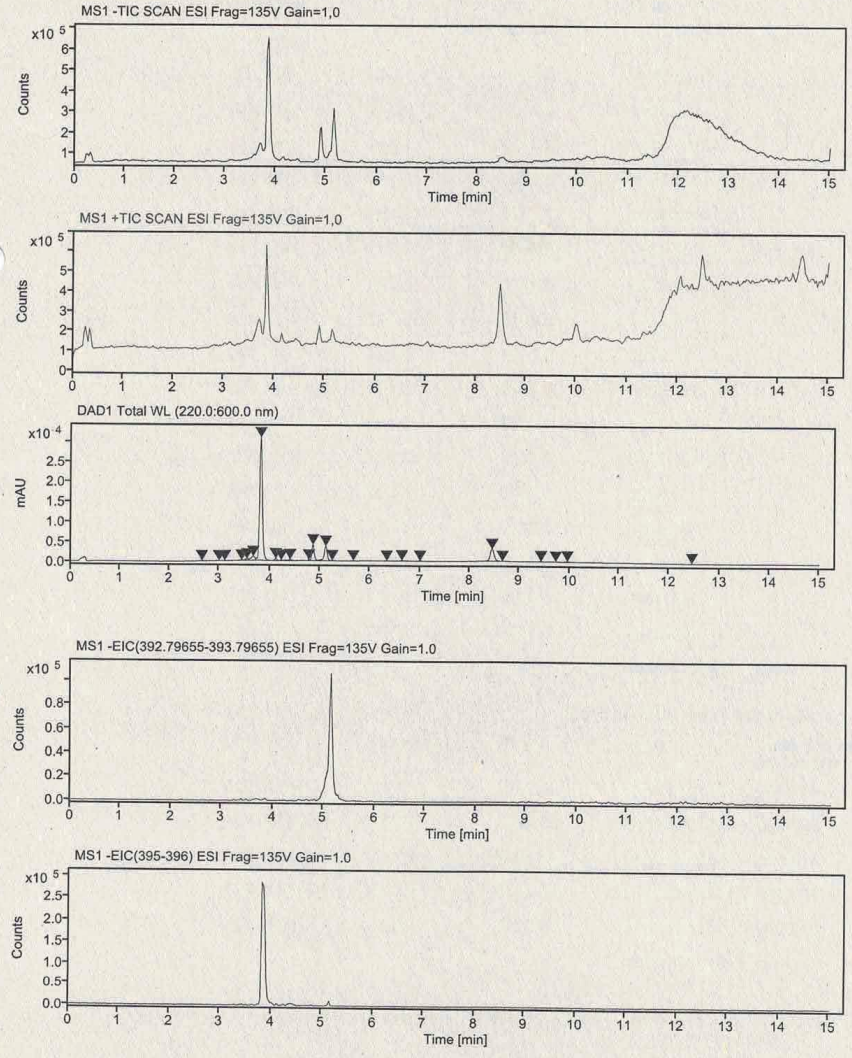
RT [min]	Peak MS Base Peak m/z	Area	Area%	Max Peak%	Height
2.671		347.2145	0.2362	0.354	70.499
2.813		98.0913	0.0667	0.100	25.117
3.114		689.9421	0.4694	0.703	84.085
3.450		270.8595	0.1843	0.276	70.034
3.554		1120.2680	0.7622	1.141	286.717
3.679		5494.3016	3.7380	5.596	917.063
3.827		98184.6452	66.7993	100.000	25928.576
4.124		1678.2395	1.1418	1.709	538.862
4.232		141.1632	0.0960	0.144	56.974
4.406		1086.4093	0.7391	1.106	227.615
4.780		407.0803	0.2770	0.415	148.544
4.867		9327.6664	6.3460	9.500	2665.424
5.123		11781.1000	8.0152	11.999	2717.083
5.251		372.6536	0.2535	0.380	93.200
5.671		148.3998	0.1010	0.151	41.889
6.331		101.8856	0.0693	0.104	22.764
6.632		507.9064	0.3456	0.517	67.539
7.004		125.4539	0.0854	0.128	24.322
8.452		13845.5466	9.4197	14.102	2452.612
8.718		60.6230	0.0412	0.062	11.992
9.440		402.8597	0.2741	0.410	76.578
9.736		197.8098	0.1346	0.201	34.252
9.967		415.7894	0.2829	0.423	85.818
12.460		178.6765	0.1216	0.182	44.789
	Sum	146984.5849			

Signal: MS1 -TIC SCAN ESI Frag=135V Gain=1,0

RT [min]	Peak MS Base Peak m/z	Area	Area%	Max Peak%	Height
3.716	411.000	488672.5023	10.9490	19.230	70943.988
3.861	395.100	2541248.1621	56.9379	100.000	604498.214
4.904	378.100	436711.8979	9.7847	17.185	116543.973
5.155	393.100	782814.4905	17.5393	30.804	211476.695
8.495	313.200	213742.9504	4.7890	8.411	29995.558
	Sum	4463190.0032			

111-7h

Sequence Name:	SingleSample		
Data file:	HALP137-7h.dx	**Project Name:**	Single Quad
Sample name:	HALP137-7h	**Operator :**	SYSTEM
Instrument:	Single Quad	**Acquired on:**	2021-12-14 02:56:16+01:00
Inj. volume:	8.000	**Location:**	P1-B3
Acq. method:	00-new_wasser-acn_standard_100-1000_BD-20min.amx		
Processing method:	MS_standard_plot.pmx		



Signal: DAD1 Total WL (220.0:600.0 nm)

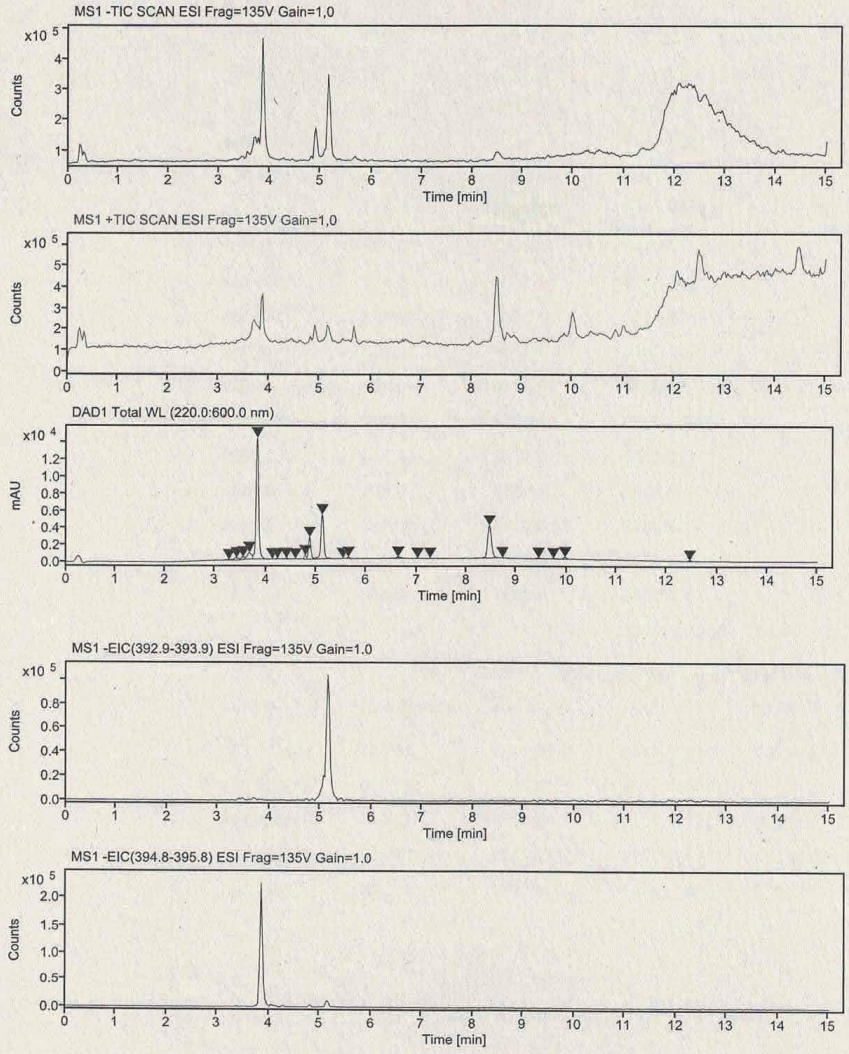
RT [min]	Peak MS Base Peak m/z	Area	Area%	Max Peak%	Height
2.650		856.9637	0.4718	0.714	103.818
2.995		94.8074	0.0522	0.079	28.144
3.107		173.9186	0.0958	0.145	46.864
3.443		476.1898	0.2622	0.397	85.375
3.546		1786.6891	0.9837	1.490	378.542
3.673		5674.8903	3.1245	4.731	1021.642
3.818		119943.5792	66.0379	100.000	30787.616
4.120		1615.7670	0.8896	1.347	505.150
4.228		472.3747	0.2601	0.394	124.213
4.403		1656.4879	0.9120	1.381	288.179
4.778		469.2627	0.2584	0.391	178.217
4.863		14043.9434	7.7322	11.709	4038.412
5.119	393.100	15002.9382	8.2602	12.508	3658.530
5.246		286.7925	0.1579	0.239	87.838
5.666		176.1713	0.0970	0.147	54.718
6.334		29.2255	0.0161	0.024	19.779
6.635		539.8025	0.2972	0.450	81.355
7.005		127.7433	0.0703	0.107	25.115
8.449		16585.2073	9.1314	13.828	3005.373
8.658		2.3820	0.0013	0.002	6.546
9.438		566.6085	0.3120	0.472	103.865
9.733		237.5690	0.1308	0.198	42.758
9.965		548.3641	0.3019	0.457	117.357
12.456		260.6485	0.1435	0.217	62.883
	Sum	181628.3266			

Signal: MS1 -TIC SCAN ESI Frag=135V Gain=1,0

RT [min]	Peak MS Base Peak m/z	Area	Area%	Max Peak%	Height
3.701	411.100	245970.2572	5.2624	9.492	54593.205
3.857	395.300	2591363.4353	55.4411	100.000	568739.781
4.896	378.100	527878.0360	11.2937	20.371	162527.299
5.153	393.100	1120905.5178	23.9813	43.255	244213.973
8.514	313.000	187968.8165	4.0215	7.254	22672.820
	Sum	4674086.0628			

111-55h

Sequence Name:	SingleSample		
Data file:	HALP137-55h.dx	**Project Name:**	Single Quad
Sample name:	HALP137-55h	**Operator :**	SYSTEM
Instrument:	Single Quad	**Acquired on:**	2021-12-14 03:17:20+01:00
Inj. volume:	8.000	**Location:**	P1-B4
Acq. method:	00-new_wasser-acn_standard_100-1000_BD-20min.amx		
Processing method:	MS_standard_plot.pmx		

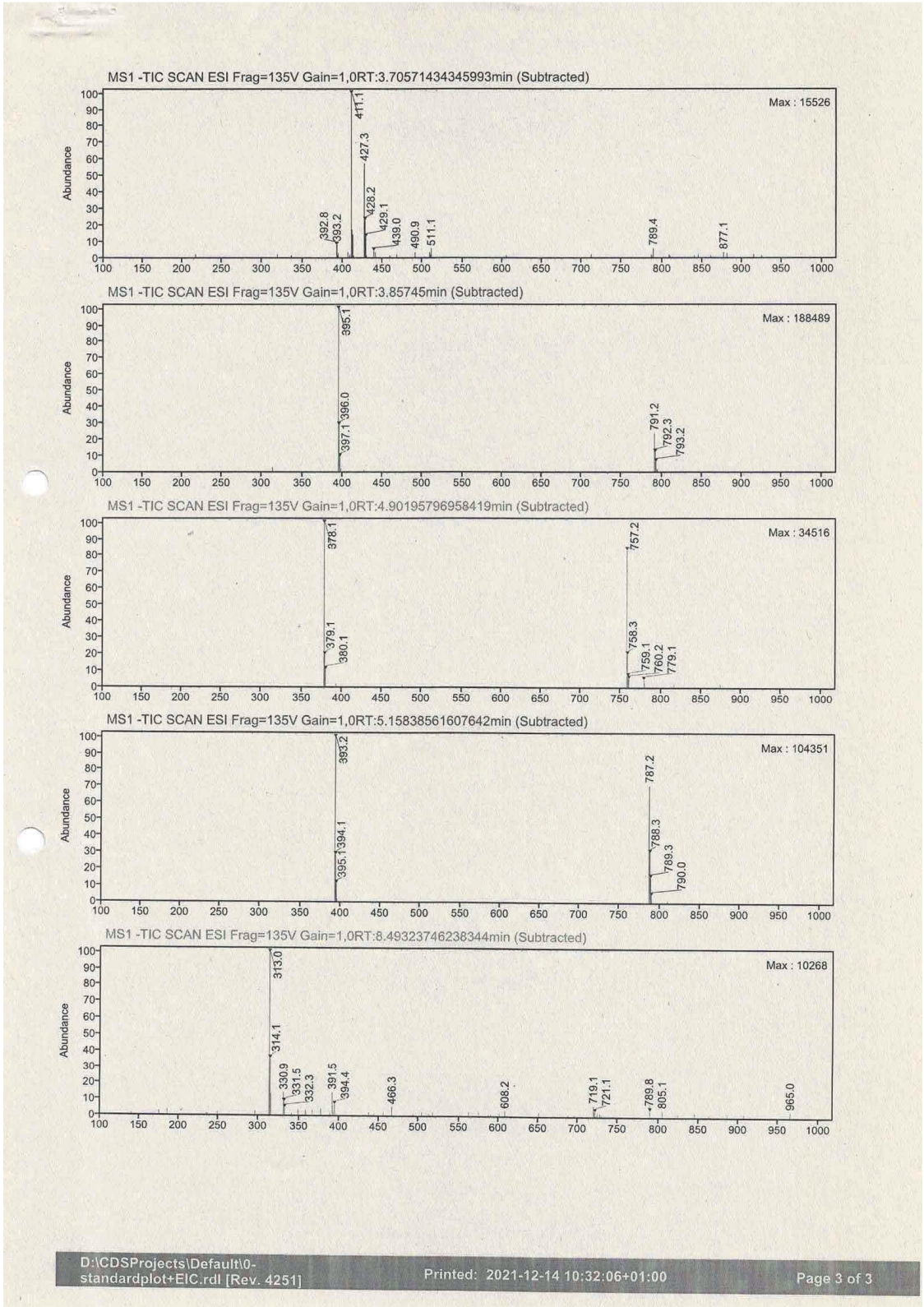


Signal: DAD1 Total WL (220.0:600.0 nm)

RT [min]	Peak MS Base Peak m/z	Area	Area%	Max Peak%	Height
3.274		782.1765	0.6749	1.506	92.861
3.425		1706.7910	1.4727	3.286	266.820
3.552		1515.1584	1.3073	2.917	310.772
3.676		4570.2675	3.9434	8.800	770.454
3.831		51934.7727	44.8108	100.000	14075.838
4.127		21.5389	0.0186	0.041	14.490
4.229		155.2282	0.1339	0.299	55.109
4.405		406.4041	0.3507	0.783	79.488
4.583		117.3328	0.1012	0.226	20.983
4.783		1324.0939	1.1425	2.550	420.390
4.871		8899.4334	7.6787	17.136	2534.698
5.123		20329.1330	17.5405	39.144	5203.379
5.530		17.5650	0.0152	0.034	21.922
5.641		546.3999	0.4714	1.052	154.868
6.629		1092.1241	0.9423	2.103	147.163
7.023		81.8844	0.0707	0.158	18.088
7.274		83.6871	0.0722	0.161	10.522
8.459		20080.1935	17.3258	38.664	3760.403
8.721		178.6737	0.1542	0.344	25.752
9.446		444.1390	0.3832	0.855	82.649
9.741		266.0872	0.2296	0.512	48.181
9.973		900.7968	0.7772	1.734	195.089
12.460		444.0446	0.3831	0.855	105.441
	Sum	115897.9257			

Signal: MS1 -TIC SCAN ESI Frag=135V Gain=1,0

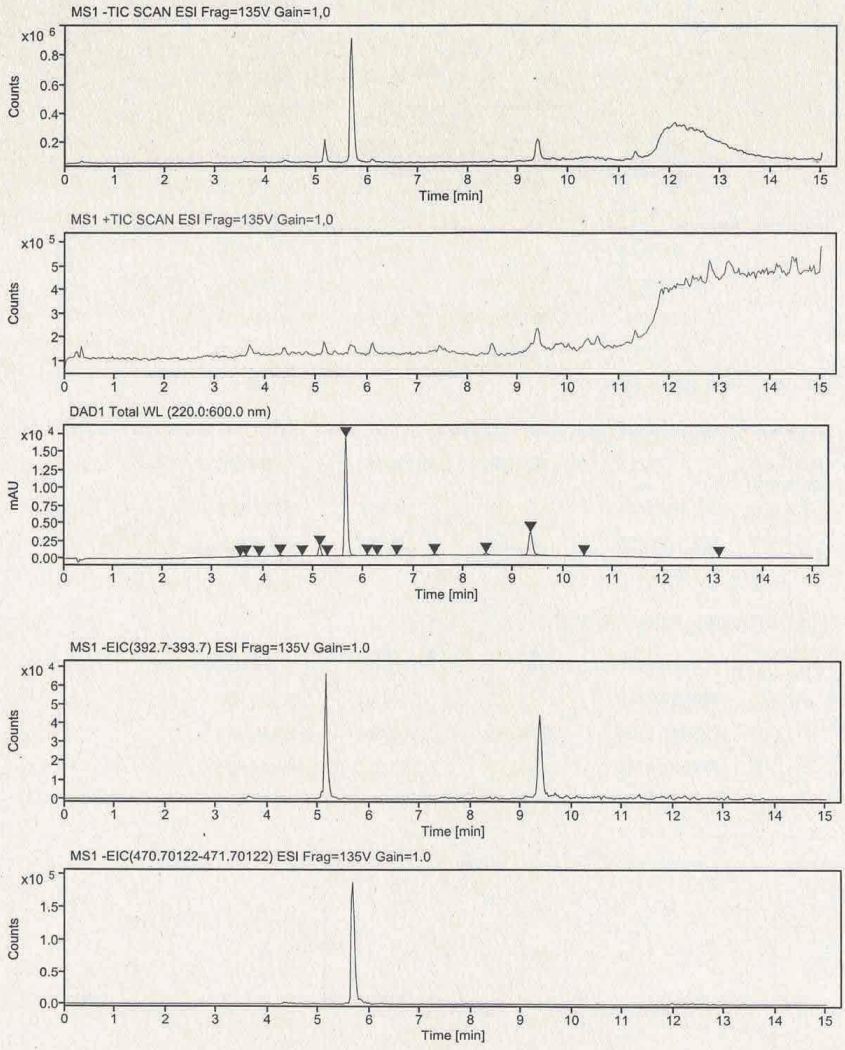
RT [min]	Peak MS Base Peak m/z	Area	Area%	Max Peak%	Height
3.706	411.100	504630.1440	14.1899	36.047	62908.033
3.857	395.100	1399940.1121	39.3655	100.000	388228.859
4.902	757.200	335187.2338	9.4253	23.943	94333.169
5.158	393.200	1171496.3726	32.9418	83.682	277254.852
8.493	313.000	145003.9547	4.0774	10.358	22089.341
	Sum	3556257.8173			


MS1 -TIC SCAN ESI Frag=135V Gain=1,0RT:3.70571434345993min (Subtracted)
Max : 15526
Abundance
411.1
427.3
428.2
429.1
392.8
393.2
439.0
490.9
511.1
789.4
877.1
MS1 -TIC SCAN ESI Frag=135V Gain=1,0RT:3.85745min (Subtracted)
Max : 188489
Abundance
395.1
396.0
397.1
791.2
792.3
793.2
MS1 -TIC SCAN ESI Frag=135V Gain=1,0RT:4.90195796958419min (Subtracted)
Max : 34516
Abundance
378.1
757.2
379.1
380.1
758.3
759.1
760.2
779.1
MS1 -TIC SCAN ESI Frag=135V Gain=1,0RT:5.15838561607642min (Subtracted)
Max : 104351
Abundance
393.2
787.2
394.1
395.1
788.3
789.3
790.0
MS1 -TIC SCAN ESI Frag=135V Gain=1,0RT:8.49323746238344min (Subtracted)
Max : 10268
Abundance
313.0
314.1
330.9
331.5
332.3
391.5
394.4
466.3
608.2
719.1
721.1
789.8
805.1
965.0
D:\CDSProjects\Default\0-standardplot+EIC.rdl [Rev. 4251]
Printed: 2021-12-14 10:32:06+01:00
Page 3 of 3

Trial IV

IV-2h

Sequence Name:	SingleSample		
Data file:	HALS138-2h.dx	**Project Name:**	Single Quad
Sample name:	HALS138-2h	**Operator :**	SYSTEM
Instrument:	Single Quad	**Acquired on:**	2021-12-14 12:09:44+01:00
Inj. volume:	8.000	**Location:**	P1-D4
Acq. method:	00-new_wasser-acn_standard_100-1000_BD-20min.amx		
Processing method:	MS_standard_plot.pmx		



D:\CDSProjects\Default\0-standardplot+EIC.rdl [Rev. 4268] Printed: 2021-12-15 07:16:20+01:00 Page 1 of 3

Signal: DAD1 Total WL (220.0:600.0 nm)

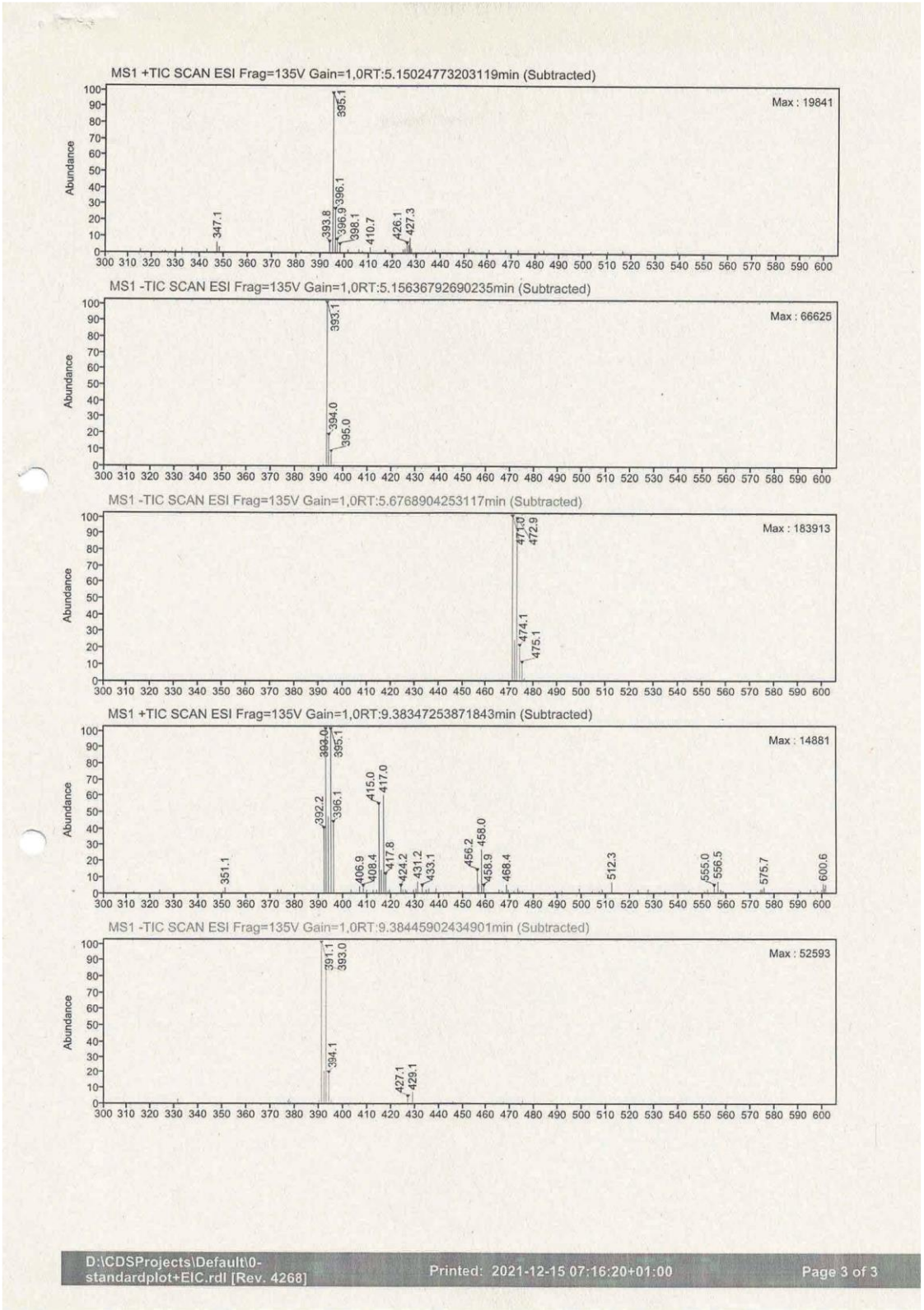
RT [min]	Peak MS Base Peak m/z	Area	Area%	Max Peak%	Height
3.542		224.4205	0.2284	0.328	64.708
3.652		491.7695	0.5004	0.718	98.213
3.917		102.2707	0.1041	0.149	24.742
4.336		668.7478	0.6805	0.976	153.947
4.775		325.0703	0.3308	0.475	44.294
5.124		4673.5954	4.7560	6.824	1356.193
5.272		19.7648	0.0201	0.029	15.575
5.643		68484.9218	69.6924	100.000	16512.604
6.069		356.8349	0.3631	0.521	75.976
6.267		82.8409	0.0843	0.121	13.682
6.662		180.2720	0.1835	0.263	19.928
7.417		1464.6203	1.4904	2.139	126.305
8.451		1301.0264	1.3240	1.900	250.315
9.347		18947.4827	19.2816	27.667	3229.303
10.418		511.7330	0.5208	0.747	71.766
13.116		432.0426	0.4397	0.631	89.227
	Sum	98267.4136			

Signal: MS1 +TIC SCAN ESI Frag=135V Gain=1,0

RT [min]	Peak MS Base Peak m/z	Area	Area%	Max Peak%	Height
5.150	395.100	223306.4414	23.6539	30.982	55187.085
9.383	395.100	720751.5456	76.3461	100.000	97078.951
	Sum	944057.9870			

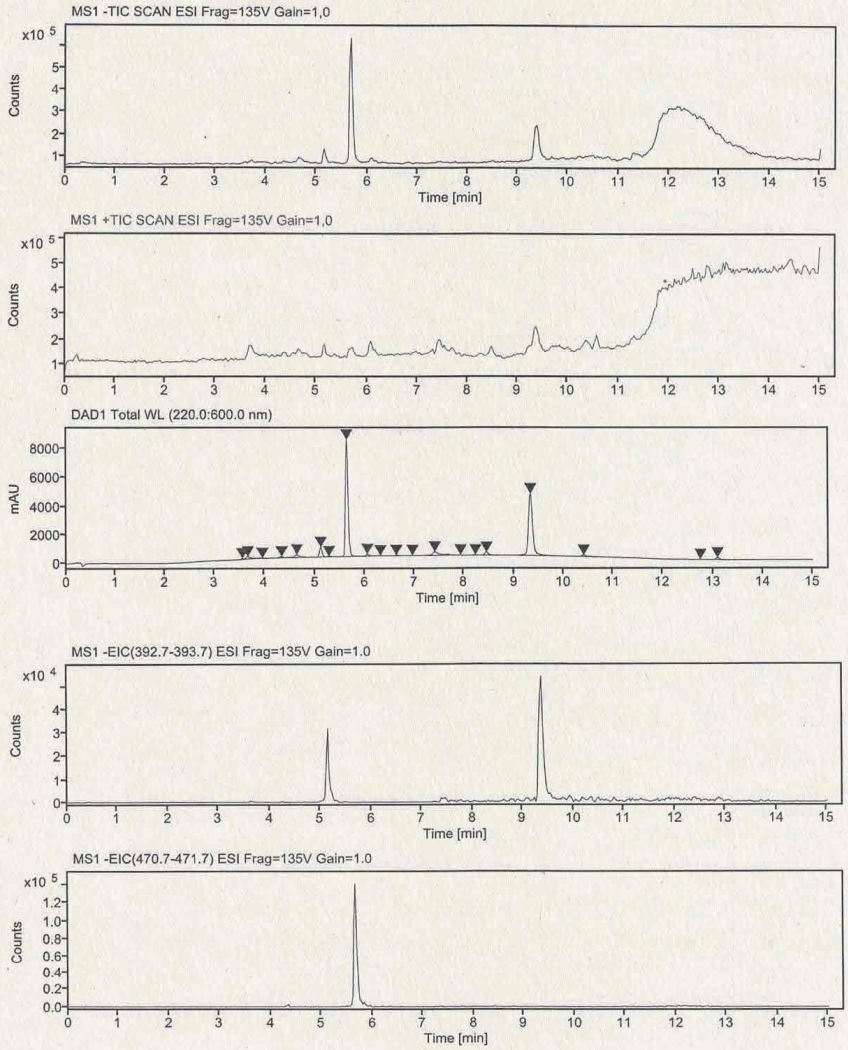
Signal: MS1 -TIC SCAN ESI Frag=135V Gain=1,0

RT [min]	Peak MS Base Peak m/z	Area	Area%	Max Peak%	Height
5.156	393.100	506962.8556	9.1829	12.255	153305.308
5.677	471.000	4136687.9465	74.9303	100.000	839116.840
9.384	391.100	877062.7103	15.8868	21.202	144067.985
	Sum	5520713.5124			


MS1 +TIC SCAN ESI Frag=135V Gain=1,0RT:5.15024773203119min (Subtracted)
Max : 19841
MS1 -TIC SCAN ESI Frag=135V Gain=1,0RT:5.15636792690235min (Subtracted)
Max : 66625
MS1 -TIC SCAN ESI Frag=135V Gain=1,0RT:5.6768904253117min (Subtracted)
Max : 183913
MS1 +TIC SCAN ESI Frag=135V Gain=1,0RT:9.38347253871843min (Subtracted)
Max : 14881
MS1 -TIC SCAN ESI Frag=135V Gain=1,0RT:9.38445902434901min (Subtracted)
Max : 52593
Abundance
D:\CDSProjects\Default\0-standardplot+EIC.rdl [Rev. 4268]
Printed: 2021-12-15 07:16:20+01:00
Page 3 of 3

IV-4h

Sequence Name:	SingleSample		
Data file:	HALS138-4h.dx	**Project Name:**	Single Quad
Sample name:	HALS138-4h	**Operator :**	SYSTEM
Instrument:	Single Quad	**Acquired on:**	2021-12-14 12:30:48+01:00
Inj. volume:	4.000	**Location:**	P1-D5
Acq. method:	00-new_wasser-acn_standard_100-1000_BD-20min.amx		
Processing method:	MS_standard_plot.pmx		



Signal: DAD1 Total WL (220.0:600.0 nm)

RT [min]	Peak MS Base Peak m/z	Area	Area%	Max Peak%	Height
3.554		225.0783	0.3304	0.731	58.004
3.663		1000.1964	1.4684	3.248	162.536
3.952		163.6492	0.2403	0.531	21.372
4.334		363.7235	0.5340	1.181	82.258
4.641		1285.8125	1.8877	4.176	170.633
5.119		2335.6882	3.4290	7.585	676.291
5.282		142.5105	0.2092	0.463	20.481
5.641	471.000	30793.7912	45.2085	100.000	8111.386
6.052		617.2322	0.9062	2.004	122.027
6.313		73.3266	0.1077	0.238	12.163
6.635		212.4745	0.3119	0.690	26.678
6.961		85.2166	0.1251	0.277	13.757
7.409		2862.1131	4.2019	9.294	249.923
7.928		51.4231	0.0755	0.167	12.963
8.225		84.2002	0.1236	0.273	18.130
8.447		1082.8841	1.5898	3.517	204.417
9.339		25293.5359	37.1335	82.138	4322.432
10.409		722.3560	1.0605	2.346	102.507
12.752		50.8662	0.0747	0.165	13.206
13.095		669.0010	0.9822	2.173	134.979
	Sum	68115.0794			

Signal: MS1 +TIC SCAN ESI Frag=135V Gain=1,0

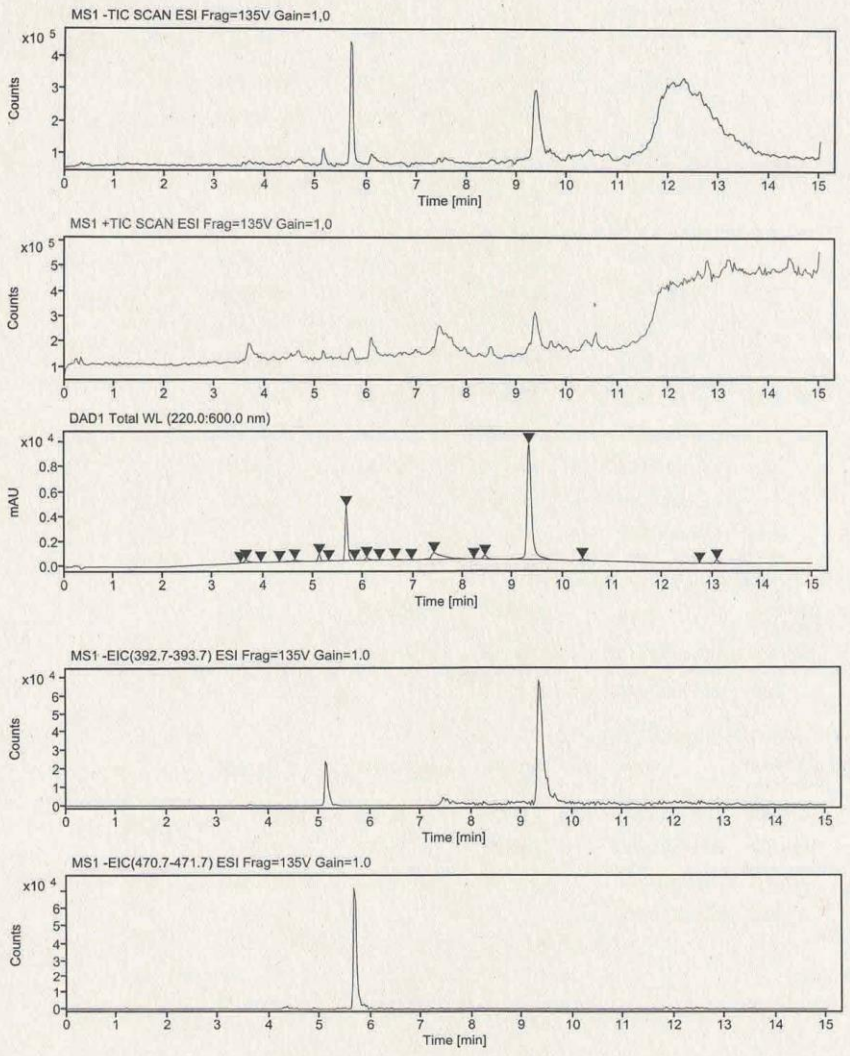
RT [min]	Peak MS Base Peak m/z	Area	Area%	Max Peak%	Height
7.445	394.100	368934.8996	31.7991	46.626	51540.646
9.366	395.000	791268.7679	68.2009	100.000	103007.164
	Sum	1160203.6675			

Signal: MS1 -TIC SCAN ESI Frag=135V Gain=1,0

RT [min]	Peak MS Base Peak m/z	Area	Area%	Max Peak%	Height
5.153	393.100	328063.3775	7.9676	12.372	66996.681
5.675	471.000	2651748.2466	64.4027	100.000	577416.916
9.373	391.000	1137638.2889	27.6297	42.901	157472.702
	Sum	4117449.9130			

IV-6h

Sequence Name:	SingleSample		
Data file:	HALS138-6h.dx	**Project Name:**	Single Quad
Sample name:	HALS138-6h	**Operator :**	SYSTEM
Instrument:	Single Quad	**Acquired on:**	2021-12-14 12:51:52+01:00
Inj. volume:	4.000	**Location:**	P1-D6
Acq. method:	00-new_wasser-acn_standard_100-1000_BD-20min.amx		
Processing method:	MS_standard_plot.pmx		



Signal: DAD1 Total WL (220.0:600.0 nm)

RT [min]	Peak MS Base Peak m/z	Area	Area%	Max Peak%	Height
3.545		104.4461	0.1106	0.176	40.087
3.658		1248.6604	1.3220	2.104	205.077
3.951		110.2776	0.1168	0.186	15.114
4.322		81.1310	0.0859	0.137	22.691
4.630		1095.4013	1.1597	1.846	124.626
5.120		1753.5456	1.8565	2.955	512.304
5.307		176.6673	0.1870	0.298	24.397
5.662		15985.2173	16.9236	26.937	4346.162
5.826		31.9721	0.0338	0.054	11.780
6.066		1133.6569	1.2002	1.910	218.218
6.320		88.5672	0.0938	0.149	18.559
6.635		404.3062	0.4280	0.681	50.429
6.964		89.0533	0.0943	0.150	17.032
7.419		8610.7171	9.1162	14.510	535.253
8.216		117.7780	0.1247	0.198	25.254
8.441		1456.5016	1.5420	2.454	278.596
9.335	393.000	59341.9598	62.8255	100.000	9279.188
10.402		1162.4291	1.2307	1.959	157.728
12.752		115.8096	0.1226	0.195	26.081
13.095		1347.1092	1.4262	2.270	269.405
	Sum	94455.2067			

Signal: MS1 +TIC SCAN ESI Frag=135V Gain=1,0

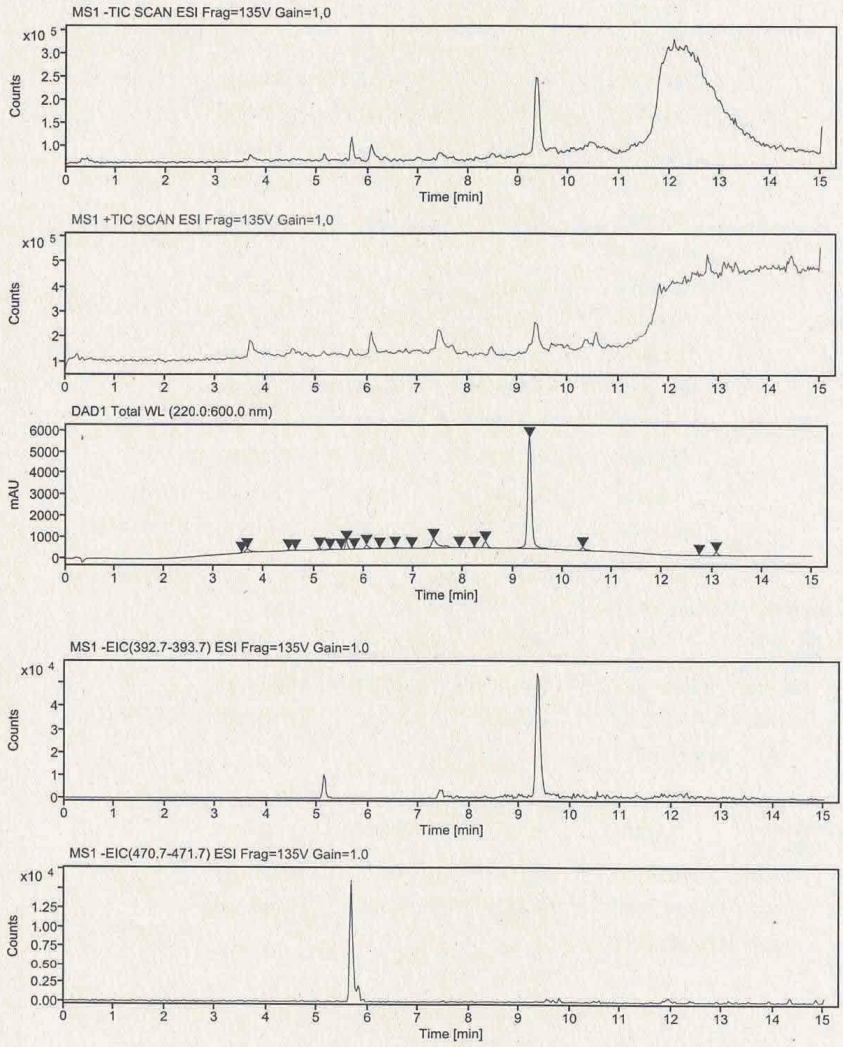
RT [min]	Peak MS Base Peak m/z	Area	Area%	Max Peak%	Height
9.366	393.000	1084160.7815	100.0000	100.000	141852.583
	Sum	1084160.7815			

Signal: MS1 -TIC SCAN ESI Frag=135V Gain=1,0

RT [min]	Peak MS Base Peak m/z	Area	Area%	Max Peak%	Height
5.146	393.100	242705.2168	6.8324	14.045	52605.364
5.693	473.100	1581450.6994	44.5196	91.514	408917.472
9.368	391.000	1728098.1061	48.6479	100.000	202233.544
	Sum	3552254.0222			

IV-8h

Sequence Name:	SingleSample		
Data file:	HALO138-8h.dx	**Project Name:**	Single Quad
Sample name:	HALO138-8h	**Operator :**	SYSTEM
Instrument:	Single Quad	**Acquired on:**	2021-12-14 13:12:53+01:00
Inj. volume:	4.000	**Location:**	P1-D7
Acq. method:	00-new_wasser-acn_standard_100-1000_BD-20min.amx		
Processing method:	MS_standard_plot.pmx		



D:\CDSProjects\Default\0-standardplot+EIC.rdl [Rev. 4268] Printed: 2021-12-15 07:15:32+01:00 Page 1 of 3

Signal: DAD1 Total WL (220.0:600.0 nm)

RT [min]	Peak MS Base Peak m/z	Area	Area%	Max Peak%	Height
3.550		52.4289	0.1264	0.179	22.458
3.662		1158.6850	2.7923	3.954	161.075
4.486		124.5299	0.3001	0.425	33.952
4.621		89.4975	0.2157	0.305	14.243
5.111		302.7462	0.7296	1.033	89.442
5.316		188.0368	0.4532	0.642	24.148
5.539		12.9986	0.0313	0.044	4.857
5.648		1285.4780	3.0979	4.387	371.448
5.803		64.8944	0.1564	0.221	20.665
6.047		852.9001	2.0554	2.911	166.021
6.311		82.4063	0.1986	0.281	18.185
6.623		383.6658	0.9246	1.309	46.078
6.960		114.3676	0.2756	0.390	17.440
7.399		4147.5691	9.9953	14.155	396.614
7.918		82.8901	0.1998	0.283	19.450
8.217		97.1587	0.2341	0.332	21.790
8.439		1451.8953	3.4990	4.955	276.014
9.330	395.100	29301.7236	70.6151	100.000	5161.129
10.402		902.7834	2.1756	3.081	126.074
12.742		70.7240	0.1704	0.241	17.505
13.084		727.6293	1.7535	2.483	149.275
	Sum	41495.0086			

Signal: MS1 +TIC SCAN ESI Frag=135V Gain=1,0

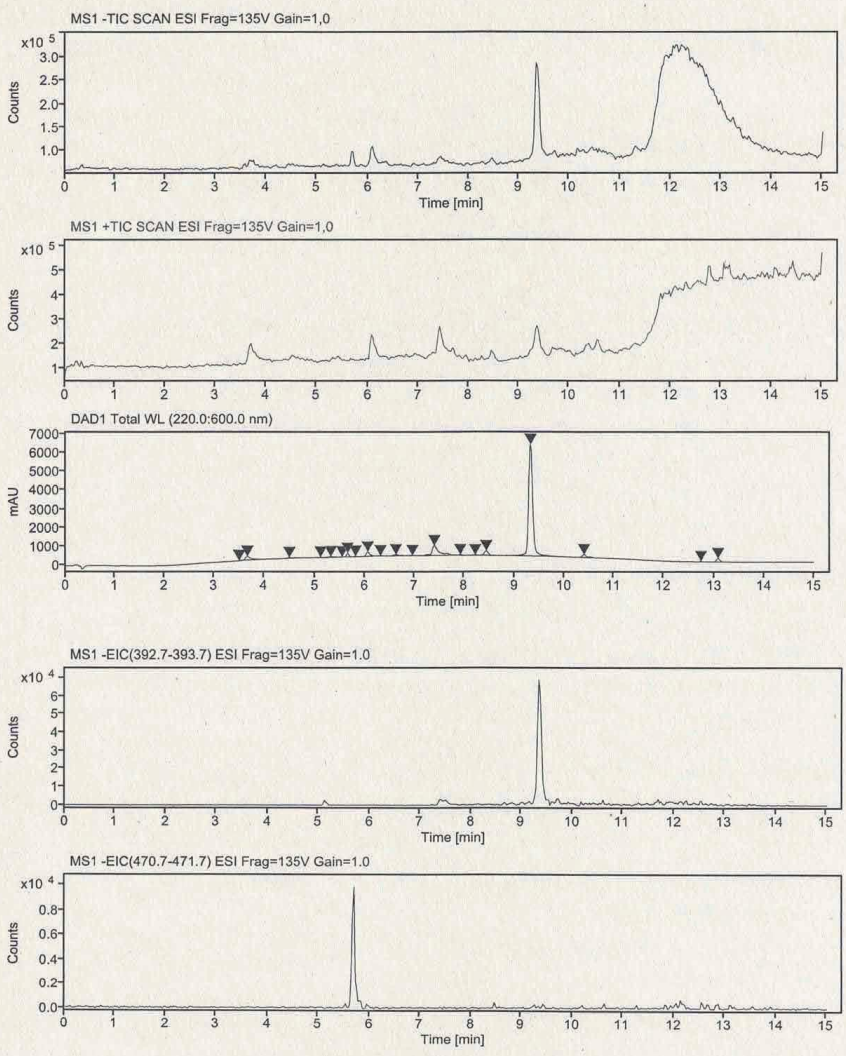
RT [min]	Peak MS Base Peak m/z	Area	Area%	Max Peak%	Height
7.419	392.100	542029.1295	38.3028	62.082	75867.282
9.351	395.100	873088.6282	61.6972	100.000	111160.796
	Sum	1415117.7576			

Signal: MS1 -TIC SCAN ESI Frag=135V Gain=1,0

RT [min]	Peak MS Base Peak m/z	Area	Area%	Max Peak%	Height
5.679	473.000	185308.3346	14.0973	16.411	48786.056
9.366	391.100	1129183.1907	85.9027	100.000	164037.239
	Sum	1314491.5253			

IV-10h

Sequence Name:	SingleSample		
Data file:	HALS138-10h.dx	**Project Name:**	Single Quad
Sample name:	HALS138-10h	**Operator :**	SYSTEM
Instrument:	Single Quad	**Acquired on:**	2021-12-14 13:33:56+01:00
Inj. volume:	4.000	**Location:**	P1-D8
Acq. method:	00-new_wasser-acn_standard_100-1000_BD-20min.amx		
Processing method:	MS_standard_plot.pmx		



Signal: DAD1 Total WL (220.0:600.0 nm)

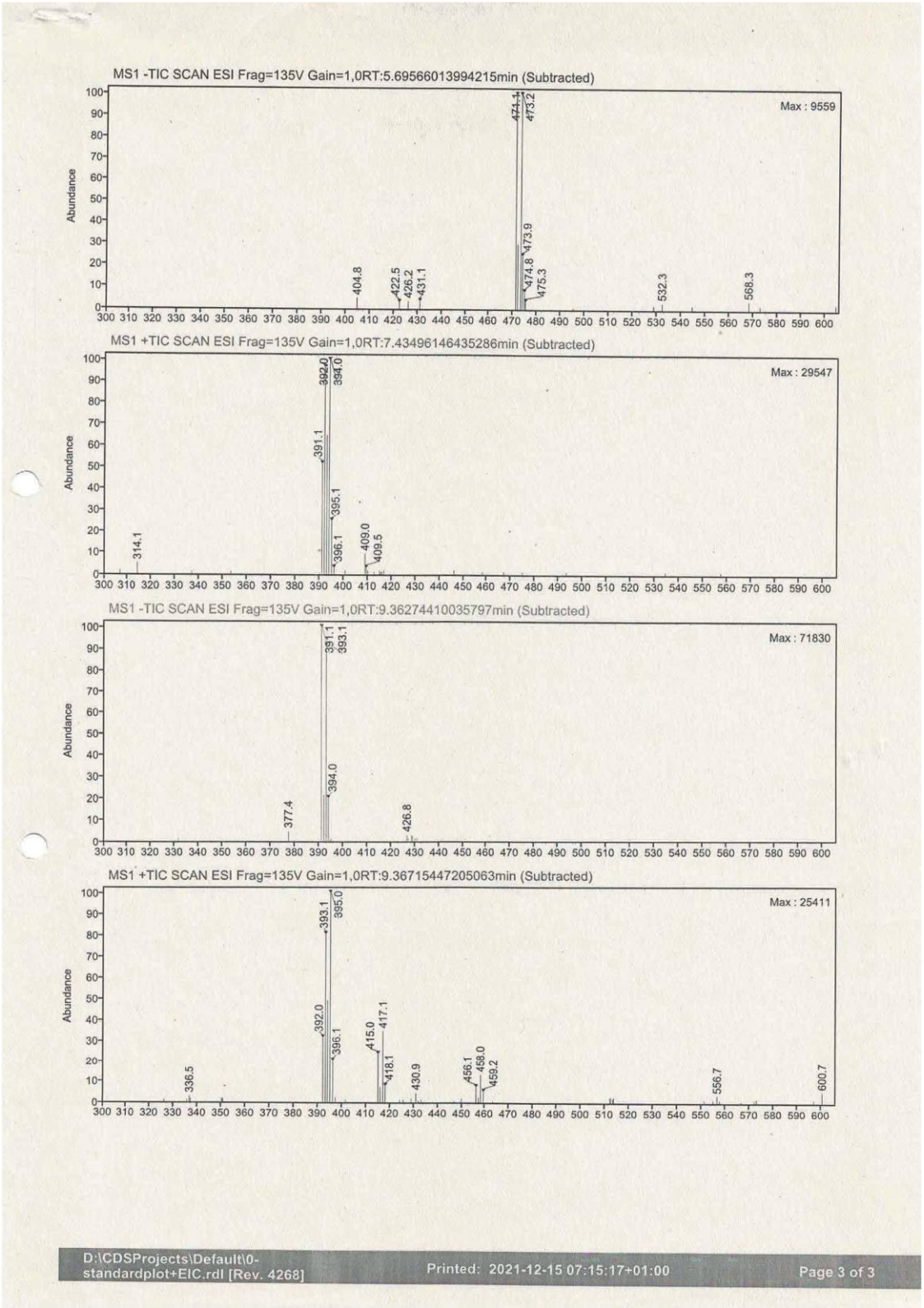
RT [min]	Peak MS Base Peak m/z	Area	Area%	Max Peak%	Height
3.495		3.4317	0.0074	0.010	9.620
3.659		1367.5481	2.9312	4.073	190.953
4.491		318.0536	0.6817	0.947	41.739
5.118		52.6010	0.1127	0.157	16.244
5.320		238.1126	0.5104	0.709	29.068
5.546		13.2003	0.0283	0.039	4.917
5.658	471.100	629.6929	1.3497	1.875	185.311
5.815		69.7464	0.1495	0.208	24.815
6.057		1179.2772	2.5276	3.512	231.735
6.313		50.2800	0.1078	0.150	13.944
6.624		431.6883	0.9253	1.286	54.595
6.956		126.3089	0.2707	0.376	19.959
7.396		5042.0510	10.8070	15.015	515.828
7.915		119.3139	0.2557	0.355	28.192
8.213		129.8113	0.2782	0.387	26.946
8.434		1282.6128	2.7491	3.820	242.030
9.330		33579.7513	71.9738	100.000	5905.294
10.401		1031.8464	2.2116	3.073	150.537
12.742		75.9532	0.1628	0.226	17.946
13.084		914.2237	1.9595	2.723	185.575
	Sum	46655.5047			

Signal: MS1 +TIC SCAN ESI Frag=135V Gain=1,0

RT [min]	Peak MS Base Peak m/z	Area	Area%	Max Peak%	Height
7.435	394.000	530171.8447	48.4514	93.992	100423.226
9.367	393.100	564062.2668	51.5486	100.000	94697.170
	Sum	1094234.1115			

Signal: MS1 -TIC SCAN ESI Frag=135V Gain=1,0

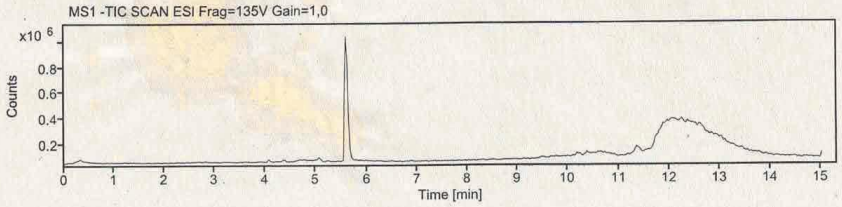
RT [min]	Peak MS Base Peak m/z	Area	Area%	Max Peak%	Height
5.696	471.100	119141.1838	9.3279	10.288	32395.057
9.363	391.100	1158114.3194	90.6721	100.000	196548.449
	Sum	1277255.5032			

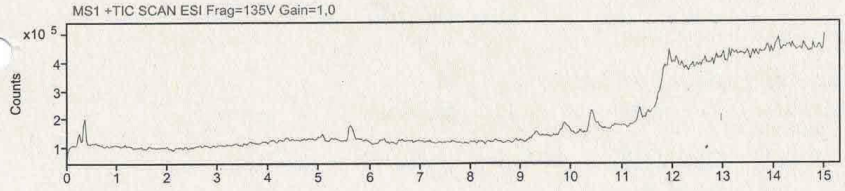

MS1 -TIC SCAN ESI Frag=135V Gain=1,0RT:5.69566013994215min (Subtracted)
Max : 9559
Abundance
MS1 +TIC SCAN ESI Frag=135V Gain=1,0RT:7.43496146435286min (Subtracted)
Max : 29547
Abundance
MS1 -TIC SCAN ESI Frag=135V Gain=1,0RT:9.36274410035797min (Subtracted)
Max : 71830
Abundance
MS1 +TIC SCAN ESI Frag=135V Gain=1,0RT:9.36715447205063min (Subtracted)
Max : 25411
Abundance
D:\CDSProjects\Default\0-standardplot+EIC.rdl [Rev. 4268]
Printed: 2021-12-15 07:15:17+01:00
Page 3 of 3

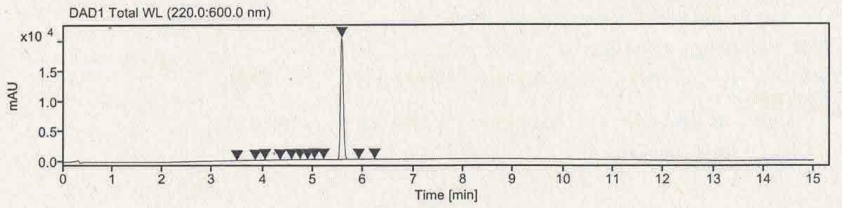
Trial V

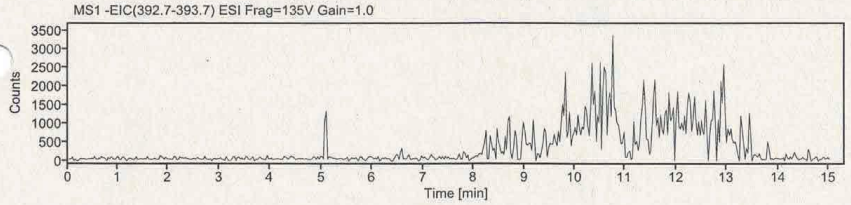
V-1h

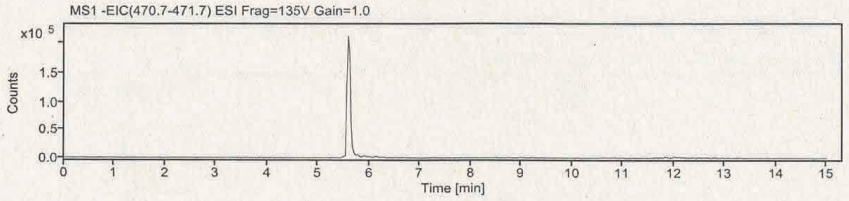
Sequence Name:	SingleSample		
Data file:	HALP141-1h.dx	**Project Name:**	Single Quad
Sample name:	HALP141-1h	**Operator :**	SYSTEM
Instrument:	Single Quad	**Acquired on:**	2021-12-17 11:02:07+01:00
Inj. volume:	5.000	**Location:**	P2-E1
Acq. method:	00-new_wasser-acn_standard_100-1000_BD-20min.amx		
Processing method:	MS_standard_plot.pmx		











D:\CDSProjects\Default\0-standardplot+EIC.rdl [Rev. 4346] Printed: 2021-12-20 07:37:16+01:00 Page 1 of 2

Signal: DAD1 Total WL (220.0:600.0 nm)

RT [min]	Peak MS Base Peak m/z	Area	Area%	Max Peak%	Height
3.486		140.7561	0.1771	0.181	22.421
3.847		50.7325	0.0638	0.065	12.859
4.040		356.5286	0.4485	0.459	110.610
4.341		184.2003	0.2317	0.237	39.461
4.565		139.7798	0.1759	0.180	34.998
4.741		122.7913	0.1545	0.158	42.304
4.889		32.2948	0.0406	0.042	7.625
5.026		447.3941	0.5628	0.576	111.839
5.208		260.7813	0.3281	0.336	69.868
5.567		77610.5350	97.6387	100.000	20161.488
5.906		70.6199	0.0888	0.091	20.263
6.222		71.0223	0.0894	0.092	18.646
	Sum	79487.4360			

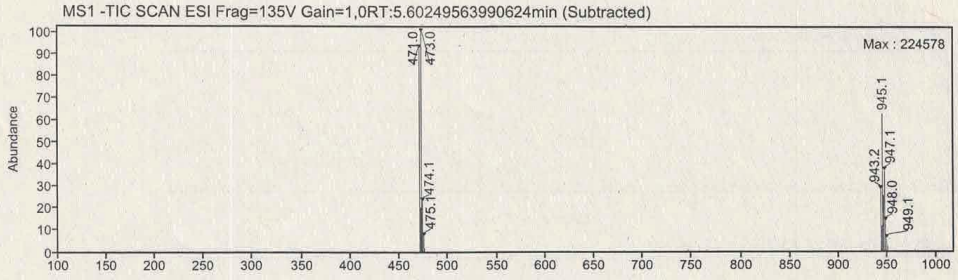
Signal: MS1 +TIC SCAN ESI Frag=135V Gain=1,0

RT [min]	Peak MS Base Peak m/z	Area	Area%	Max Peak%	Height
5.610	473.000	318620.9522	100.0000	100.000	51321.975
	Sum	318620.9522			

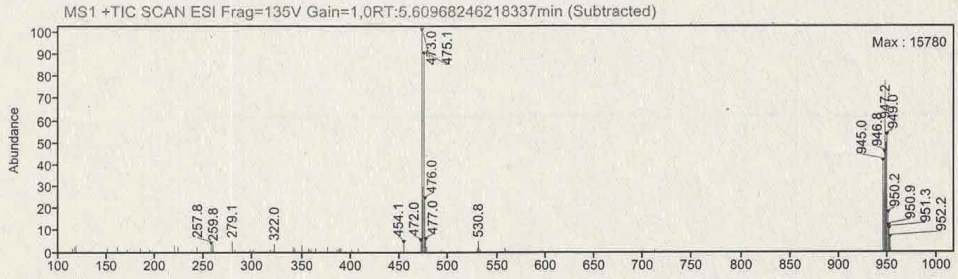
Signal: MS1 -TIC SCAN ESI Frag=135V Gain=1,0

RT [min]	Peak MS Base Peak m/z	Area	Area%	Max Peak%	Height
5.602	473.000	4342820.1351	100.0000	100.000	972473.962
	Sum	4342820.1351			

MS1 -TIC SCAN ESI Frag=135V Gain=1,0RT:5.60249563990624min (Subtracted)

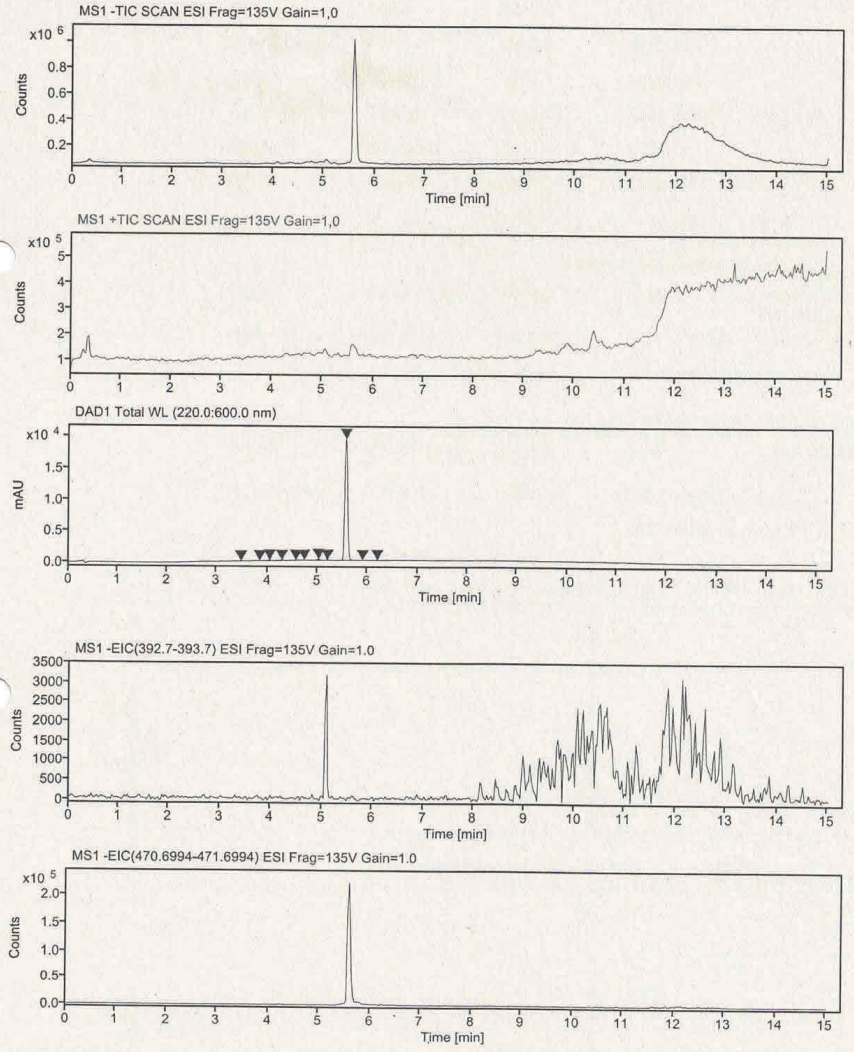


MS1 +TIC SCAN ESI Frag=135V Gain=1,0RT:5.60968246218337min (Subtracted)



V-2h

Sequence Name:	SingleSample		
Data file:	HALP141-2h.dx	**Project Name:**	Single Quad
Sample name:	HALP141-2h	**Operator :**	SYSTEM
Instrument:	Single Quad	**Acquired on:**	2021-12-17 11:23:08+01:00
Inj. volume:	5.000	**Location:**	P2-E2
Acq. method:	00-new_wasser-acn_standard_100-1000_BD-20min.amx		
Processing method:	MS_standard_plot.pmx		



Signal: DAD1 Total WL (220.0:600.0 nm)

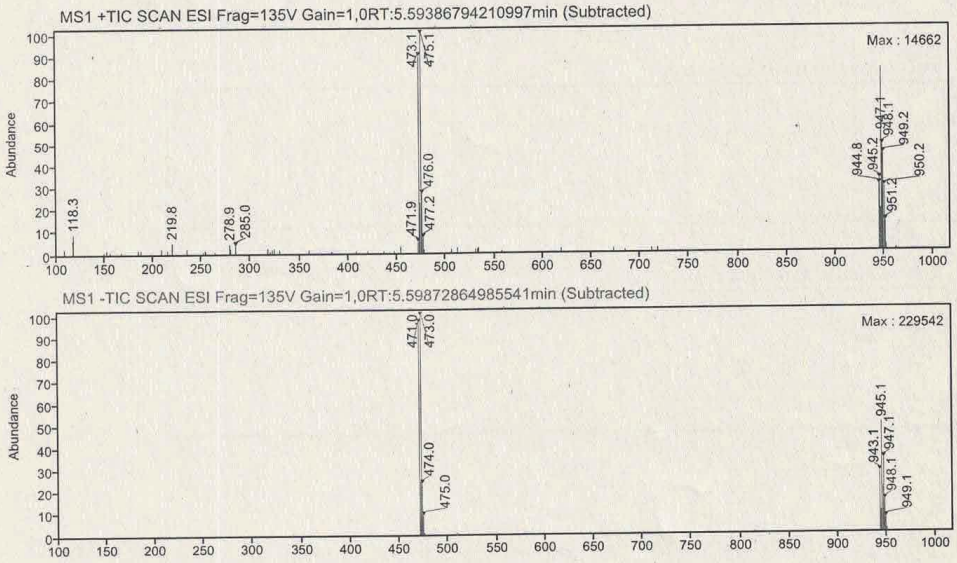
RT [min]	Peak MS Base Peak m/z	Area	Area%	Max Peak%	Height
3.478		57.0422	0.0758	0.078	17.362
3.849		52.5948	0.0699	0.072	13.521
4.044		309.4413	0.4114	0.422	102.271
4.288		308.2167	0.4098	0.420	54.239
4.567		158.5652	0.2108	0.216	34.875
4.732		37.4805	0.0498	0.051	37.382
5.021		615.3876	0.8181	0.839	150.402
5.198		293.0334	0.3896	0.400	75.185
5.563	475.100	73315.2587	97.4712	100.000	19145.182
5.899		5.7419	0.0076	0.008	3.127
6.194		64.6088	0.0859	0.088	17.892
	Sum	75217.3711			

Signal: MS1 +TIC SCAN ESI Frag=135V Gain=1,0

RT [min]	Peak MS Base Peak m/z	Area	Area%	Max Peak%	Height
5.594	475.100	286510.3453	100.0000	100.000	41671.668
	Sum	286510.3453			

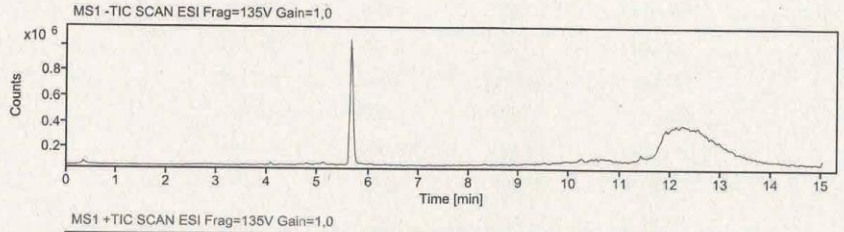
Signal: MS1 -TIC SCAN ESI Frag=135V Gain=1,0

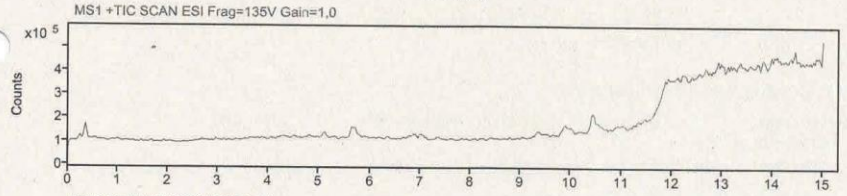
RT [min]	Peak MS Base Peak m/z	Area	Area%	Max Peak%	Height
5.599	473.000	4180999.0760	100.0000	100.000	945420.501
	Sum	4180999.0760			

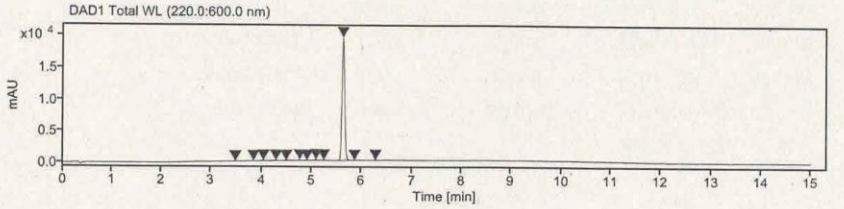


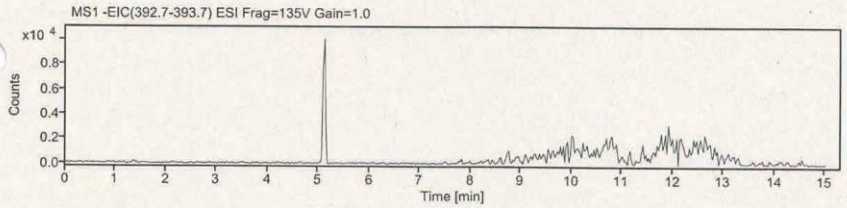
V-3h

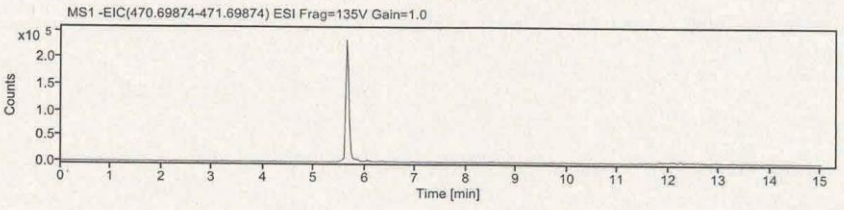
Sequence Name:	SingleSample		
Data file:	HALP141-3h.dx	**Project Name:**	Single Quad
Sample name:	HALP141-3h	**Operator :**	SYSTEM
Instrument:	Single Quad	**Acquired on:**	2021-12-17 11:44:10+01:00
Inj. volume:	5.000	**Location:**	P2-E3
Acq. method:	00-new_wasser-acn_standard_100-1000_BD-20min.amx		
Processing method:	MS_standard_plot.pmx		











Signal: DAD1 Total WL (220.0:600.0 nm)

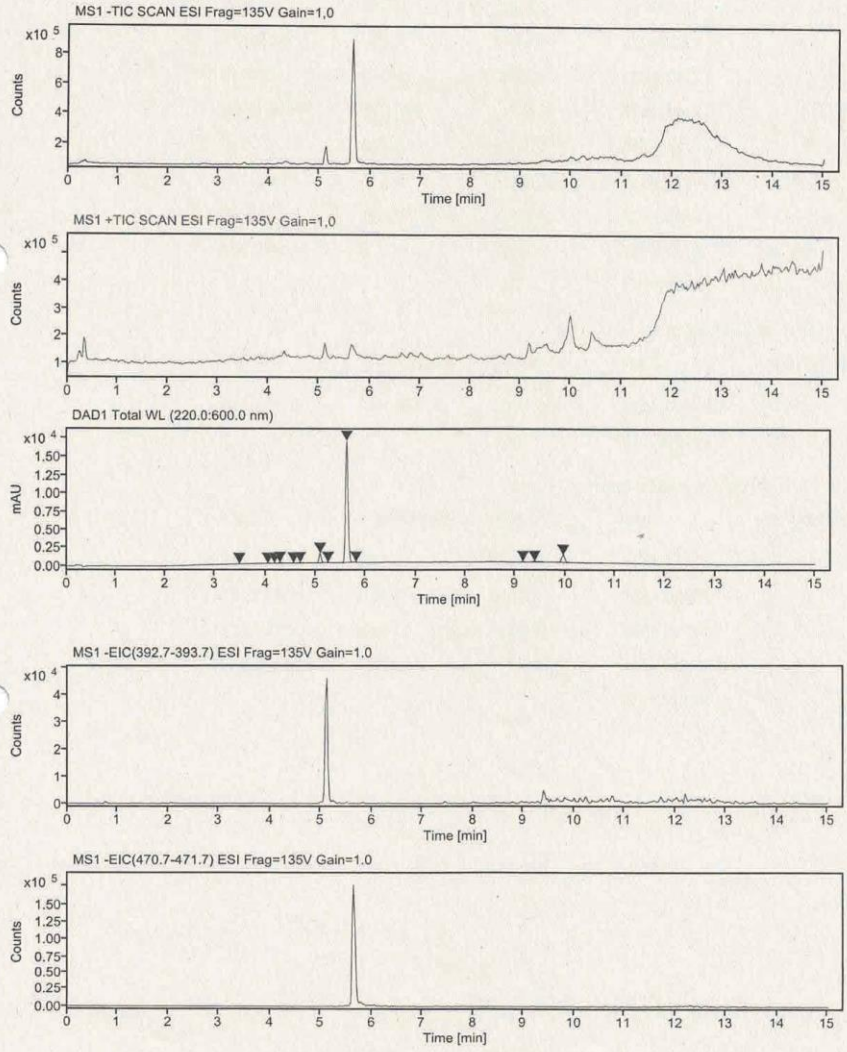
RT [min]	Peak MS Base Peak m/z	Area	Area%	Max Peak%	Height
3.478		64.4588	0.0846	0.087	19.590
3.838		57.2002	0.0751	0.077	11.882
4.036		272.5493	0.3579	0.367	89.621
4.285	474.200	309.1082	0.4059	0.416	59.552
4.488		121.3220	0.1593	0.163	18.127
4.755		162.3143	0.2132	0.218	50.111
4.906		90.6534	0.1190	0.122	24.141
5.085		479.0357	0.6291	0.645	118.165
5.241		249.1647	0.3272	0.335	66.071
5.623		74305.3334	97.5780	100.000	19174.456
5.853		6.9613	0.0091	0.009	2.553
6.272		31.5990	0.0415	0.043	10.194
	Sum	76149.7003			

Signal: MS1 -TIC SCAN ESI Frag=135V Gain=1,0

RT [min]	Peak MS Base Peak m/z	Area	Area%	Max Peak%	Height
4.067	381.800	66470.1123	1.4650	1.536	19843.695
4.275	474.200	20163.7606	0.4444	0.466	4046.140
5.109	392.800	103771.1425	2.2871	2.397	20200.343
5.290	474.100	18287.6664	0.4031	0.422	4598.469
5.657	471.000	4328505.1866	95.4004	100.000	981892.962
	Sum	4537197.8684			

V-4h

Sequence Name:	SingleSample		
Data file:	HALP141-4h.dx	**Project Name:**	Single Quad
Sample name:	HALP141-4h	**Operator :**	SYSTEM
Instrument:	Single Quad	**Acquired on:**	2021-12-17 12:05:09+01:00
Inj. volume:	5.000	**Location:**	P2-E4
Acq. method:	00-new_wasser-acn_standard_100-1000_BD-20min.amx		
Processing method:	MS_standard_plot.pmx		



Signal: DAD1 Total WL (220.0:600.0 nm)

RT [min]	Peak MS Base Peak m/z	Area	Area%	Max Peak%	Height
3.477		193.6174	0.2649	0.316	64.797
4.043		78.4500	0.1073	0.128	13.921
4.175		89.3025	0.1222	0.146	24.601
4.282		444.8884	0.6087	0.725	108.475
4.554		53.2024	0.0728	0.087	24.218
4.686		316.6943	0.4333	0.516	58.439
5.088		4088.4316	5.5937	6.665	1279.325
5.244		213.5927	0.2922	0.348	63.315
5.617		61345.3327	83.9316	100.000	16651.000
5.802		115.0246	0.1574	0.188	37.319
9.155		378.8869	0.5184	0.618	85.156
9.388		1239.7837	1.6962	2.021	138.920
9.964	479.100	4532.4897	6.2013	7.388	966.383
	Sum	73089.6971			

Signal: MS1 +TIC SCAN ESI Frag=135V Gain=1,0

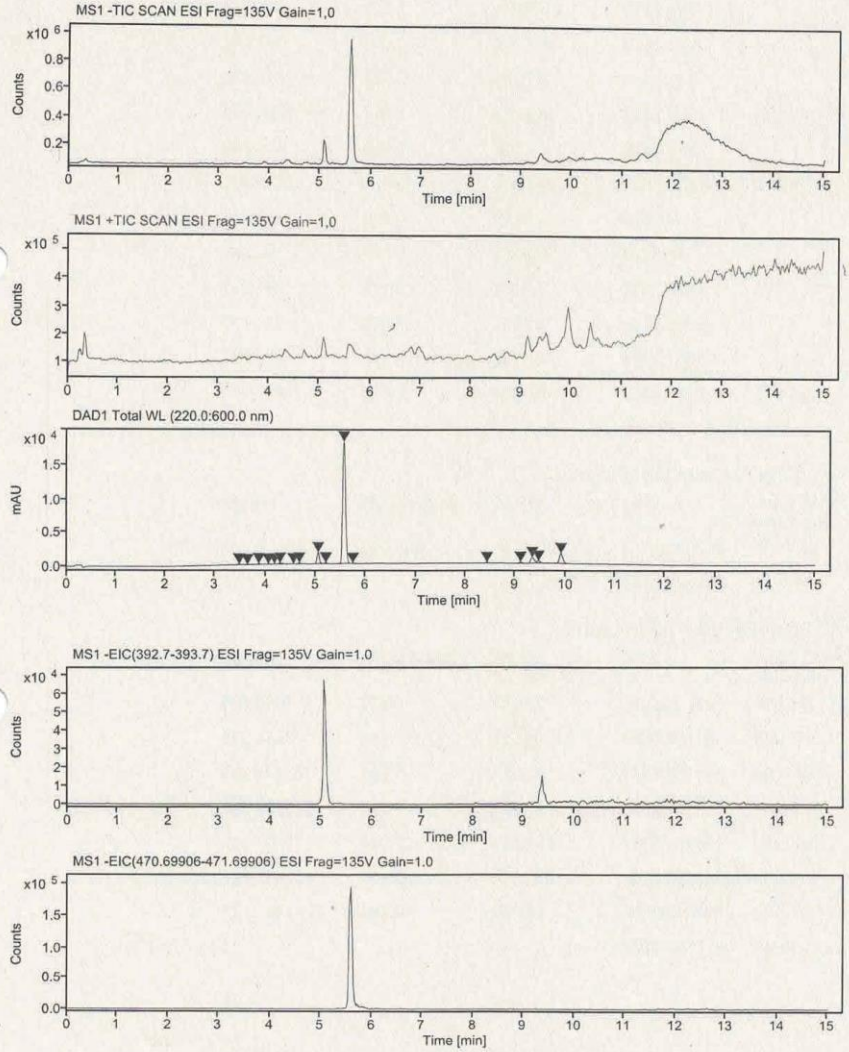
RT [min]	Peak MS Base Peak m/z	Area	Area%	Max Peak%	Height
9.998	479.100	865120.1578	100.0000	100.000	120873.953
	Sum	865120.1578			

Signal: MS1 -TIC SCAN ESI Frag=135V Gain=1,0

RT [min]	Peak MS Base Peak m/z	Area	Area%	Max Peak%	Height
3.504	301.800	37211.1471	0.8927	1.008	11610.612
4.320	488.900	65630.9988	1.5745	1.779	12971.277
5.121	393.200	375556.1875	9.0098	10.178	120707.877
5.652	473.000	3689893.9722	88.5229	100.000	830406.801
	Sum	4168292.3056			

V-5h

Sequence Name:	SingleSample		
Data file:	HALP141-5h.dx	**Project Name:**	Single Quad
Sample name:	HALP141-5h	**Operator :**	SYSTEM
Instrument:	Single Quad	**Acquired on:**	2021-12-17 12:26:08+01:00
Inj. volume:	5.000	**Location:**	P2-E5
Acq. method:	00-new_wasser-acn_standard_100-1000_BD-20min.amx		
Processing method:	MS_standard_plot.pmx		



Signal: DAD1 Total WL (220.0:600.0 nm)

RT [min]	Peak MS Base Peak m/z	Area	Area%	Max Peak%	Height
3.475		413.5658	0.4508	0.587	119.984
3.639		34.6599	0.0378	0.049	10.105
3.866		439.0299	0.4785	0.623	122.636
4.055		43.9784	0.0479	0.062	19.408
4.174		90.6873	0.0988	0.129	34.211
4.286		789.1237	0.8601	1.121	136.190
4.550		92.0437	0.1003	0.131	30.472
4.670		648.7144	0.7071	0.921	121.255
5.049	393.100	5356.7662	5.8388	7.607	1628.263
5.201		368.4528	0.4016	0.523	110.299
5.561	473.000	70420.3953	76.7566	100.000	17930.606
5.740		53.1620	0.0579	0.075	19.556
8.428		280.1329	0.3053	0.398	65.259
9.107		686.2882	0.7480	0.975	151.831
9.345		3996.1700	4.3557	5.675	810.738
9.472		1367.1455	1.4902	1.941	276.526
9.921	481.000	6664.7502	7.2644	9.464	1430.751
	Sum	91745.0661			

Signal: MS1 +TIC SCAN ESI Frag=135V Gain=1,0

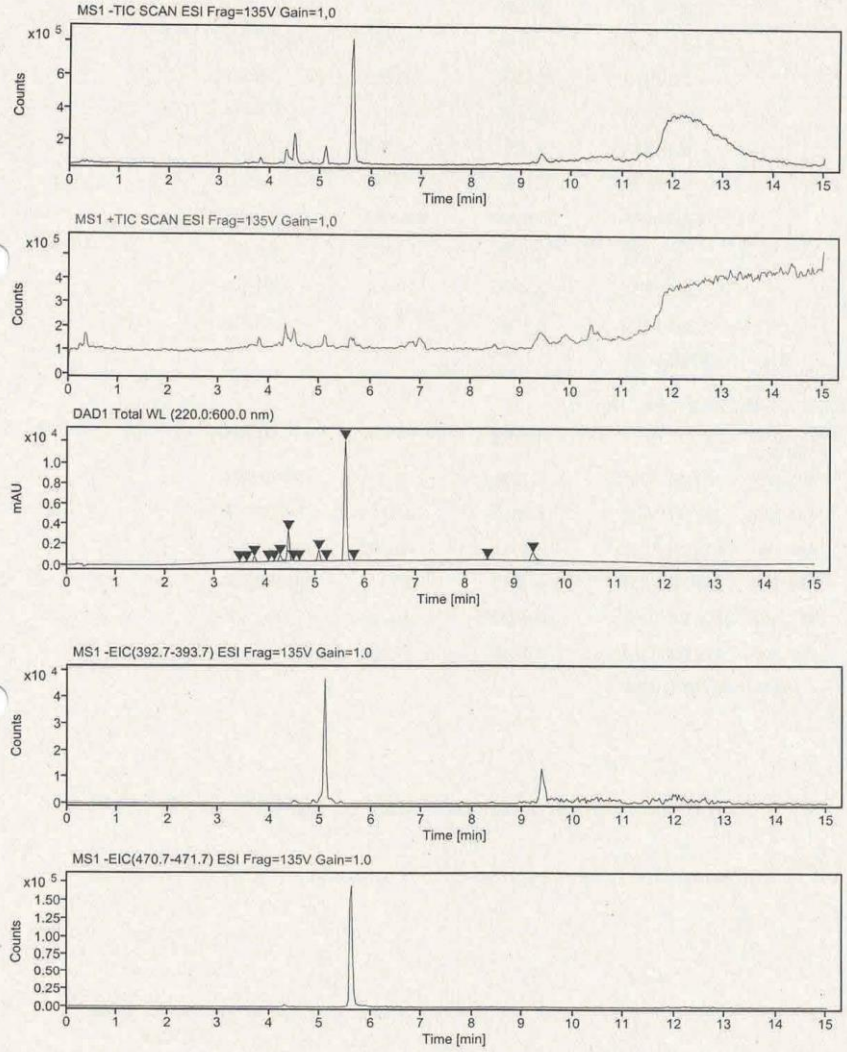
RT [min]	Peak MS Base Peak m/z	Area	Area%	Max Peak%	Height
9.946	481.000	800326.4738	100.0000	100.000	129470.748
	Sum	800326.4738			

Signal: MS1 -TIC SCAN ESI Frag=135V Gain=1,0

RT [min]	Peak MS Base Peak m/z	Area	Area%	Max Peak%	Height
3.514	301.900	30550.3526	0.5487	0.719	7959.485
3.893	317.900	58760.7863	1.0554	1.383	17484.335
4.336	489.000	140134.3329	2.5170	3.298	23759.934
4.729	488.900	61526.8815	1.1051	1.448	10888.529
5.081	393.100	638316.6012	11.4648	15.023	179002.922
5.595	473.000	4249053.8164	76.3174	100.000	889947.220
9.384	391.100	389262.5563	6.9916	9.161	61487.171
	Sum	5567605.3272			

Sequence Name:	SingleSample		
Data file:	HALP141-7h.dx	**Project Name:**	Single Quad
Sample name:	HALP141-7h	**Operator :**	SYSTEM
Instrument:	Single Quad	**Acquired on:**	2021-12-17 12:47:04+01:00
Inj. volume:	5.000	**Location:**	P2-E6
Acq. method:	00-new_wasser-acn_standard_100-1000_BD-20min.amx		
Processing method:	MS_standard_plot.pmx		

V-7h



Signal: DAD1 Total WL (220.0:600.0 nm)

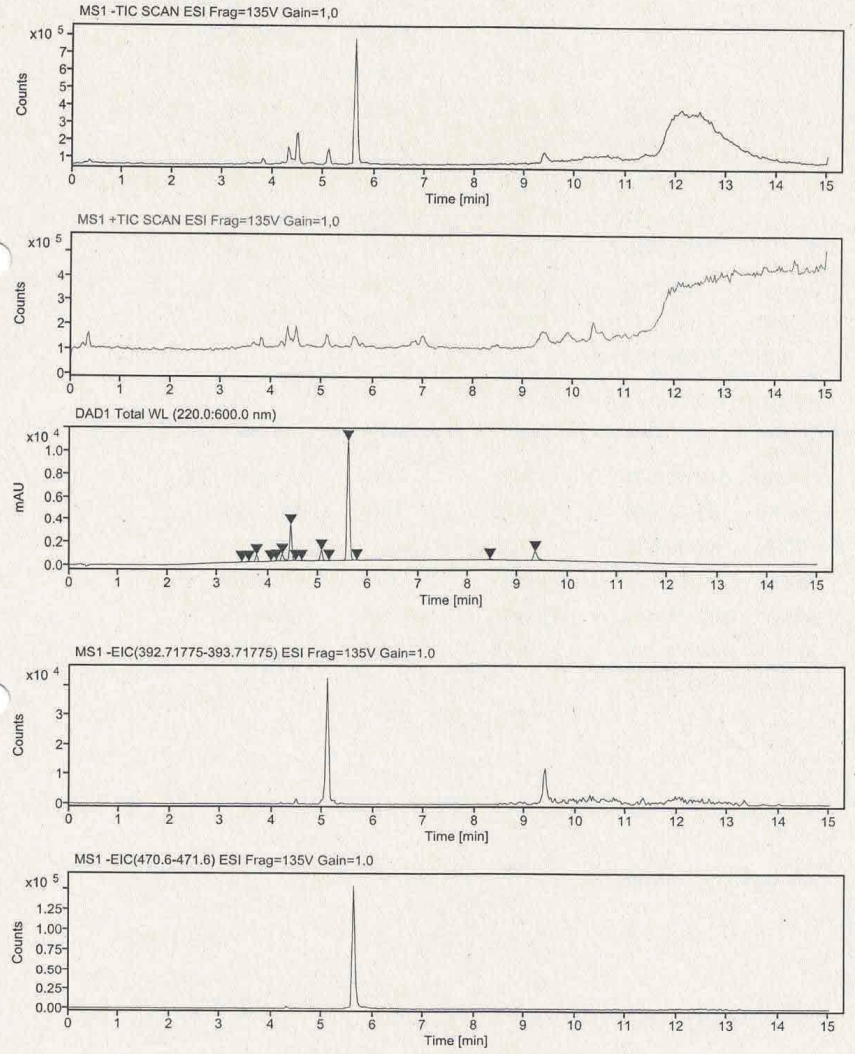
RT [min]	Peak MS Base Peak m/z	Area	Area%	Max Peak%	Height
3.478		157.2781	0.2426	0.369	52.155
3.619		176.0884	0.2716	0.413	41.925
3.775		1622.5766	2.5031	3.804	530.762
4.055		62.1842	0.0959	0.146	19.904
4.165		239.3986	0.3693	0.561	75.607
4.283		2271.6415	3.5043	5.326	577.693
4.449		9237.2100	14.2498	21.656	2946.427
4.547		22.3315	0.0344	0.052	8.901
4.666		187.9980	0.2900	0.441	37.864
5.061		3493.5294	5.3893	8.190	1012.532
5.209		84.3172	0.1301	0.198	24.132
5.585		42654.9808	65.8016	100.000	11708.810
5.756		52.8370	0.0815	0.124	21.471
8.441		315.7177	0.4870	0.740	63.017
9.360		4245.5296	6.5494	9.953	749.622
	Sum	64823.6188			

Signal: MS1 -TIC SCAN ESI Frag=135V Gain=1,0

RT [min]	Peak MS Base Peak m/z	Area	Area%	Max Peak%	Height
3.804	395.000	95190.7861	1.9336	3.065	37161.006
4.316	491.200	397944.6743	8.0833	12.813	85596.550
4.465	473.100	629218.7537	12.7811	20.260	172474.992
5.097	393.100	344007.7831	6.9877	11.077	106852.469
5.619	471.000	3105716.6768	63.0855	100.000	761736.356
9.390	391.100	350946.8286	7.1287	11.300	54012.734
	Sum	4923025.5026			

V-8h

Sequence Name:	SingleSample		
Data file:	HALP141-8h.dx	**Project Name:**	Single Quad
Sample name:	HALP141-8h	**Operator :**	SYSTEM
Instrument:	Single Quad	**Acquired on:**	2021-12-17 13:08:03+01:00
Inj. volume:	5.000	**Location:**	P2-E7
Acq. method:	00-new_wasser-acn_standard_100-1000_BD-20min.amx		
Processing method:	MS_standard_plot.pmx		



Signal: DAD1 Total WL (220.0:600.0 nm)

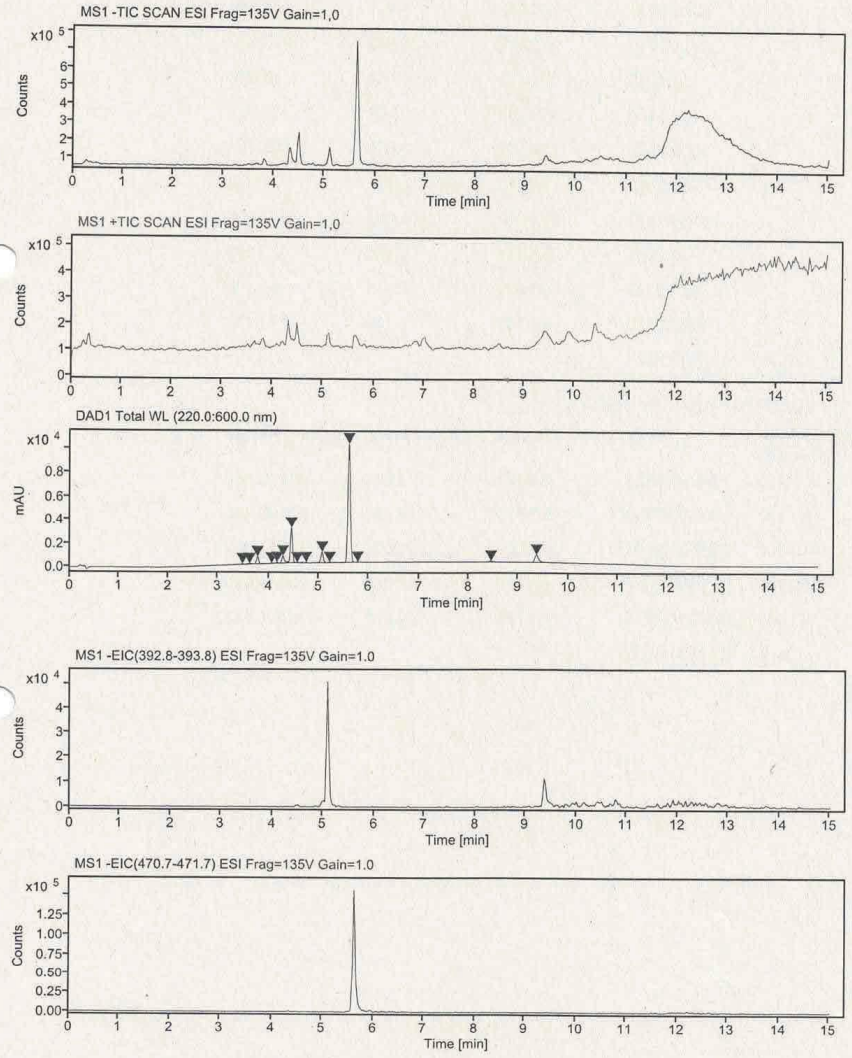
RT [min]	Peak MS Base Peak m/z	Area	Area%	Max Peak%	Height
3.474		167.9013	0.2822	0.448	48.899
3.613		180.6719	0.3036	0.482	43.987
3.771		1749.5850	2.9402	4.664	581.839
4.052		44.9759	0.0756	0.120	18.298
4.160		187.8915	0.3158	0.501	70.681
4.279		2237.5388	3.7602	5.965	577.796
4.448		9850.7341	16.5541	26.259	3141.662
4.545		13.5809	0.0228	0.036	5.655
4.664		201.7675	0.3391	0.538	44.066
5.064		3023.8230	5.0815	8.061	898.853
5.212		69.5450	0.1169	0.185	21.363
5.595		37513.7189	63.0416	100.000	10517.696
5.766		42.7895	0.0719	0.114	18.409
8.440		346.1741	0.5817	0.923	64.342
9.354	391.200	3875.6221	6.5130	10.331	735.340
	Sum	59506.3198			

Signal: MS1 -TIC SCAN ESI Frag=135V Gain=1,0

RT [min]	Peak MS Base Peak m/z	Area	Area%	Max Peak%	Height
3.804	395.100	80399.7925	1.8455	2.828	28368.410
4.308	489.000	229501.0406	5.2680	8.072	83831.776
4.480	473.000	569114.5468	13.0635	20.017	177505.166
5.097	393.000	294099.1388	6.7508	10.344	84677.630
5.628	473.100	2843178.5882	65.2627	100.000	719928.495
9.390	391.200	340218.9459	7.8094	11.966	54857.193
	Sum	4356512.0527			

V-24h

Sequence Name:	SingleSample		
Data file:	HALP141-24h.dx	**Project Name:**	Single Quad
Sample name:	HALP141-24h	**Operator :**	SYSTEM
Instrument:	Single Quad	**Acquired on:**	2021-12-17 13:29:03+01:00
Inj. volume:	5.000	**Location:**	P2-E8
Acq. method:	00-new_wasser-acn_standard_100-1000_BD-20min.amx		
Processing method:	MS_standard_plot.pmx		

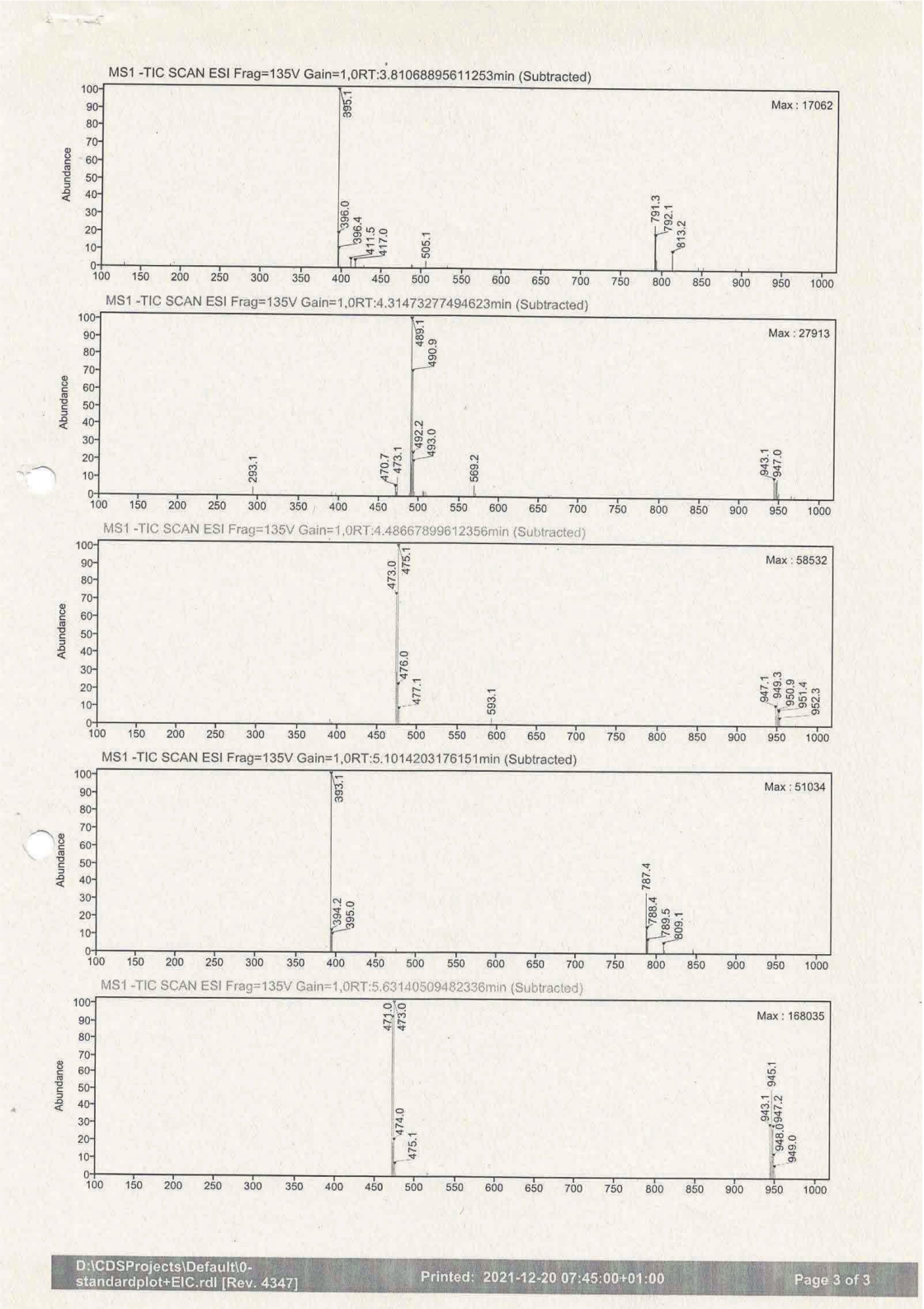


Signal: DAD1 Total WL (220.0:600.0 nm)

RT [min]	Peak MS Base Peak m/z	Area	Area%	Max Peak%	Height
3.482		101.5627	0.1833	0.292	36.429
3.621		212.6789	0.3838	0.611	49.424
3.779		1734.8994	3.1311	4.987	597.148
4.058		56.1277	0.1013	0.161	33.350
4.166		214.9491	0.3879	0.618	74.655
4.283		2226.6722	4.0187	6.401	588.269
4.452		9017.9175	16.2755	25.922	2930.082
4.566		53.4593	0.0965	0.154	19.146
4.746		167.4100	0.3021	0.481	27.571
5.068		3006.7858	5.4266	8.643	893.752
5.217		87.2838	0.1575	0.251	27.718
5.600		34788.4877	62.7860	100.000	9967.606
5.774		69.6951	0.1258	0.200	23.669
8.451		327.2317	0.5906	0.941	61.908
9.369		3342.9160	6.0333	9.609	618.431
	Sum	55408.0771			

Signal: MS1 -TIC SCAN ESI Frag=135V Gain=1,0

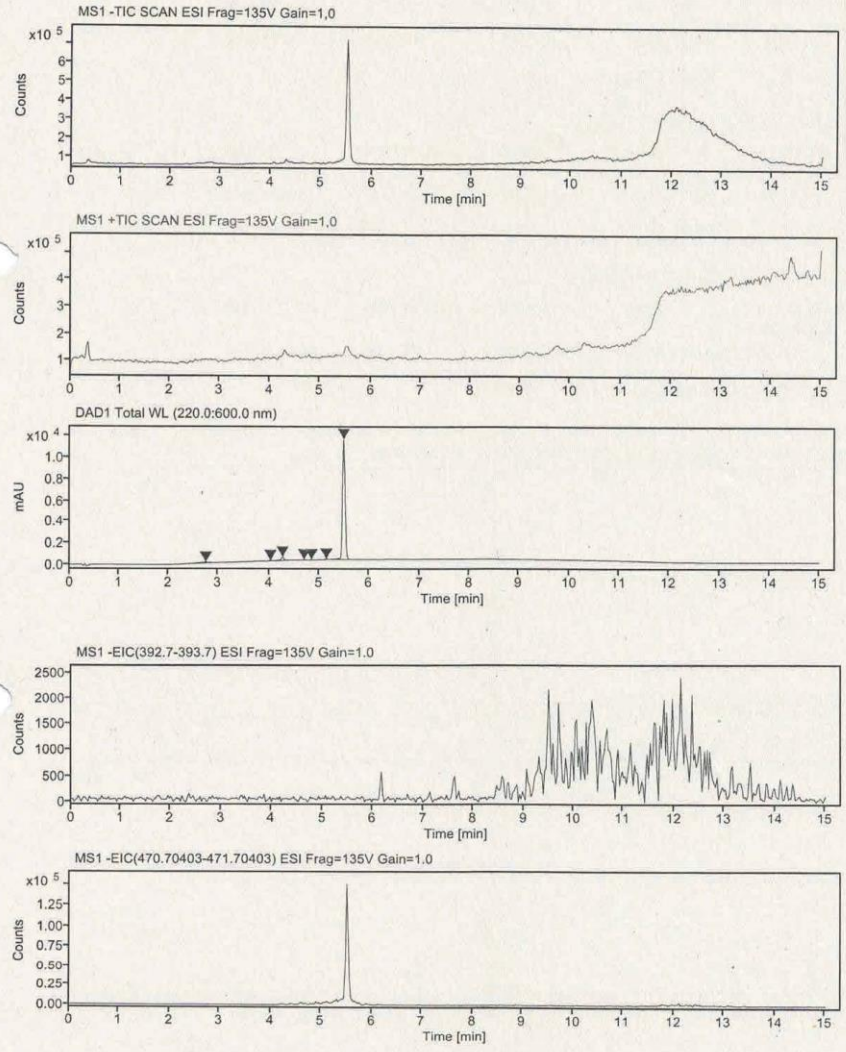
RT [min]	Peak MS Base Peak m/z	Area	Area%	Max Peak%	Height
3.811	395.100	96703.9607	2.5133	3.764	33368.841
4.315	489.100	331566.3638	8.6174	12.905	90269.410
4.487	475.100	539623.5691	14.0248	21.002	172743.082
5.101	393.100	310387.0880	8.0670	12.080	95530.639
5.631	473.000	2569356.4215	66.7775	100.000	693497.147
	Sum	3847637.4032			


MS1 -TIC SCAN ESI Frag=135V Gain=1,0RT:3.81068895611253min (Subtracted)
Max : 17062
Abundance
395.1
396.0
396.4
411.5
417.0
505.1
791.3
792.1
813.2
MS1 -TIC SCAN ESI Frag=135V Gain=1,0RT:4.31473277494623min (Subtracted)
Max : 27913
Abundance
489.1
490.9
492.2
493.0
293.1
470.7
473.1
569.2
943.1
947.0
MS1 -TIC SCAN ESI Frag=135V Gain=1,0RT:4.48667899612356min (Subtracted)
Max : 58532
Abundance
473.0
475.1
476.0
477.1
593.1
947.1
949.3
950.9
951.4
952.3
MS1 -TIC SCAN ESI Frag=135V Gain=1,0RT:5.1014203176151min (Subtracted)
Max : 51034
Abundance
393.1
394.2
395.0
787.4
788.4
789.5
809.1
MS1 -TIC SCAN ESI Frag=135V Gain=1,0RT:5.63140509482336min (Subtracted)
Max : 168035
Abundance
471.0
473.0
474.0
475.1
943.1
945.1
947.2
948.0
949.0
D:\CDSProjects\Default\0-standardplot+EIC.rdl [Rev. 4347]
Printed: 2021-12-20 07:45:00+01:00
Page 3 of 3

Trial VI

VI - 10min

Sequence Name:	SingleSample		
Data file:	HALP149_10min.dx	**Project Name:**	Single Quad
Sample name:	HALP149_10min	**Operator :**	SYSTEM
Instrument:	Single Quad	**Acquired on:**	2021-12-27 14:43:13+01:00
Inj. volume:	5.000	**Location:**	P1-B8
Acq. method:	00-new_wasser-acn_standard_100-1000_BD-20min.amx		
Processing method:	MS_standard_plot.pmx		



D:\CDSProjects\Default\0-standardplot+EIC.rdl [Rev. 4405] Printed: 2021-12-28 07:27:12+01:00 Page 1 of 2

Signal: DAD1 Total WL (220.0:600.0 nm)

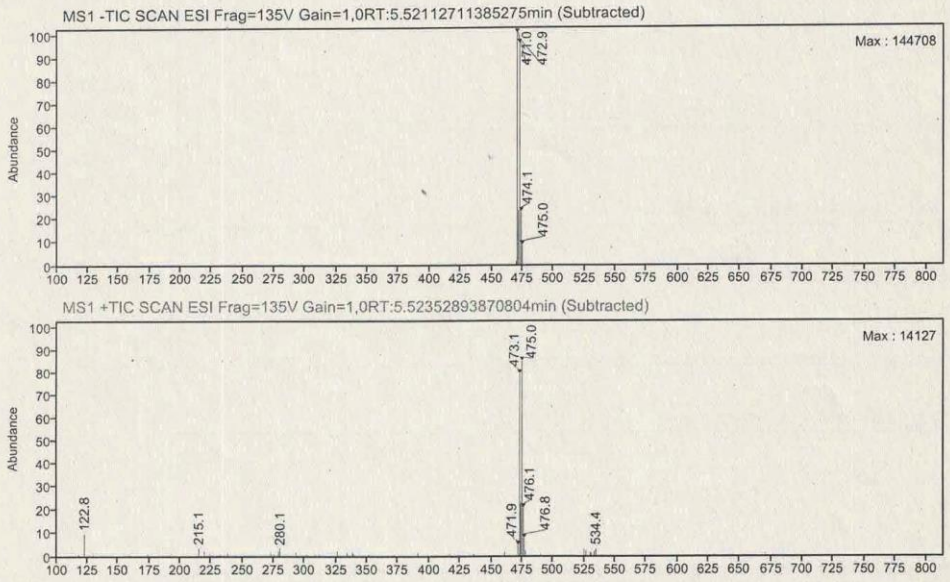
RT [min]	Peak MS Base Peak m/z	Area	Area%	Max Peak%	Height
2.745		1336.1457	3.0590	3.290	73.534
4.030		142.6510	0.3266	0.351	51.747
4.269		1367.5410	3.1309	3.367	310.076
4.698		71.4873	0.1637	0.176	17.158
4.851		20.8133	0.0476	0.051	14.242
5.145		128.3458	0.2938	0.316	38.858
5.490	471.000	40612.4802	92.9784	100.000	11241.818
	Sum	43679.4643			

Signal: MS1 +TIC SCAN ESI Frag=135V Gain=1,0

RT [min]	Peak MS Base Peak m/z	Area	Area%	Max Peak%	Height
5.524	947.000	240598.1099	100.0000	100.000	35405.840
	Sum	240598.1099			

Signal: MS1 -TIC SCAN ESI Frag=135V Gain=1,0

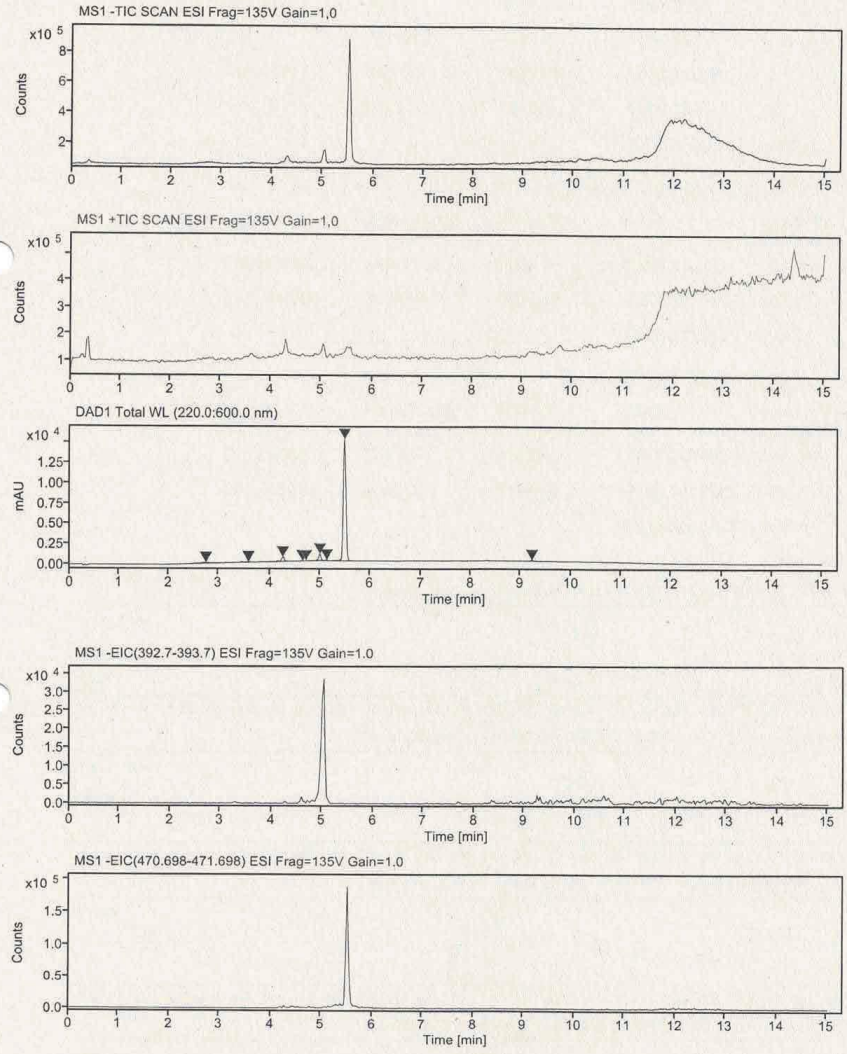
RT [min]	Peak MS Base Peak m/z	Area	Area%	Max Peak%	Height
5.521	471.000	2353117.3597	100.0000	100.000	652178.729
	Sum	2353117.3597			



D:\CDSProjects\Default\0-standardplot+EIC.rdl [Rev. 4405] Printed: 2021-12-28 07:27:12+01:00 Page 2 of 2

VI-1h

Sequence Name:	SingleSample		
Data file:	HALP149_1h.dx	**Project Name:**	Single Quad
Sample name:	HALP149_1h	**Operator :**	SYSTEM
Instrument:	Single Quad	**Acquired on:**	2021-12-27 15:04:14+01:00
Inj. volume:	5.000	**Location:**	P1-B9
Acq. method:	00-new_wasser-acn_standard_100-1000_BD-20min.amx		
Processing method:	MS_standard_plot.pmx		



Signal: DAD1 Total WL (220.0:600.0 nm)

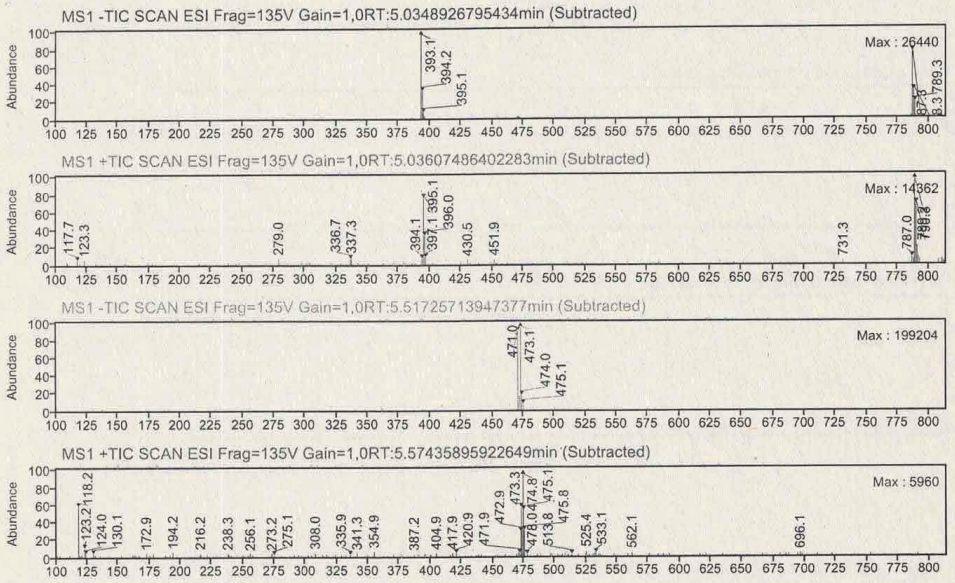
RT [min]	Peak MS Base Peak m/z	Area	Area%	Max Peak%	Height
2.740		1395.5594	2.2507	2.554	77.301
3.582		451.6277	0.7284	0.827	46.210
4.262		2270.8046	3.6623	4.156	523.553
4.651		41.6741	0.0672	0.076	11.281
4.722		3.7275	0.0060	0.007	12.939
5.000		2678.3409	4.3196	4.902	774.774
5.134		71.7487	0.1157	0.131	53.272
5.485		54637.8590	88.1191	100.000	14965.527
9.230		453.2174	0.7309	0.829	81.892
	Sum	62004.5592			

Signal: MS1 +TIC SCAN ESI Frag=135V Gain=1,0

RT [min]	Peak MS Base Peak m/z	Area	Area%	Max Peak%	Height
5.036	789.200	172036.2553	44.9441	81.633	45805.595
5.574	475.100	210742.3723	55.0559	100.000	32201.562
	Sum	382778.6276			

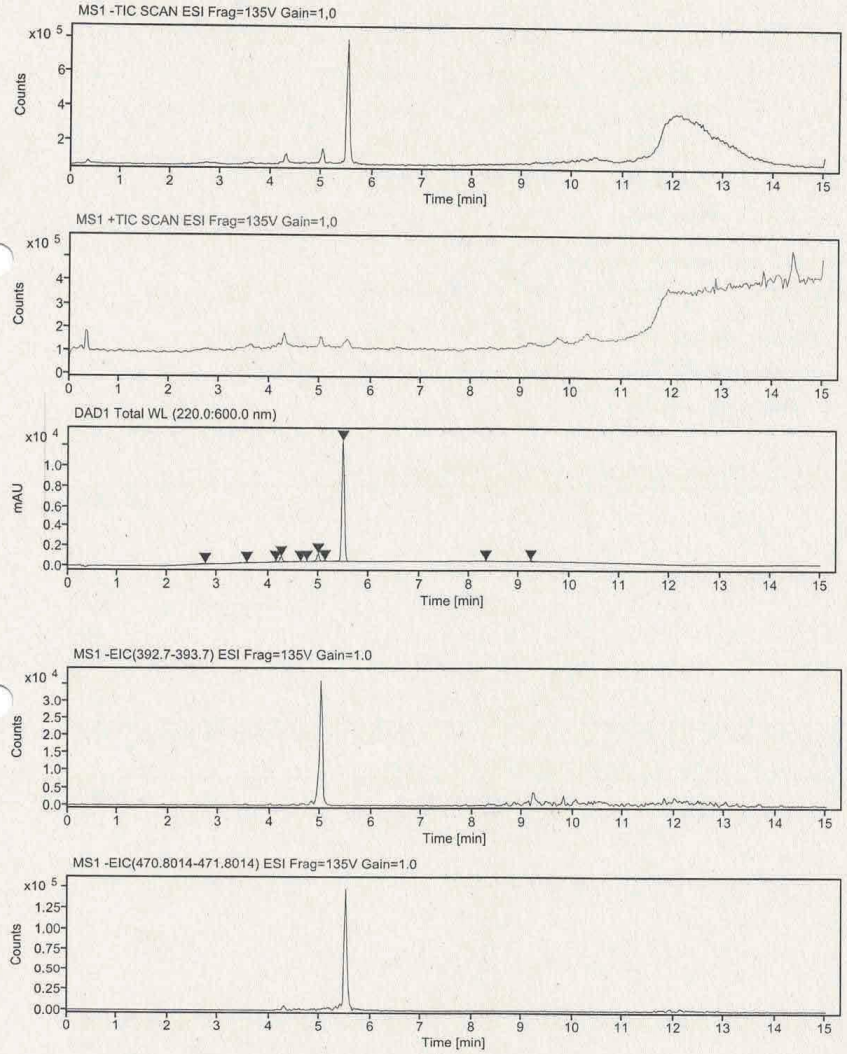
Signal: MS1 -TIC SCAN ESI Frag=135V Gain=1,0

RT [min]	Peak MS Base Peak m/z	Area	Area%	Max Peak%	Height
5.035	393.100	305591.1691	9.4588	10.447	88058.660
5.517	473.100	2925157.8040	90.5412	100.000	795470.186
	Sum	3230748.9730			



VI-2h

Sequence Name:	SingleSample		
Data file:	HALP149_2h.dx	**Project Name:**	Single Quad
Sample name:	HALP149_2h	**Operator :**	SYSTEM
Instrument:	Single Quad	**Acquired on:**	2021-12-27 15:25:15+01:00
Inj. volume:	5.000	**Location:**	P1-B10
Acq. method:	00-new_wasser-acn_standard_100-1000_BD-20min.amx		
Processing method:	MS_standard_plot.pmx		

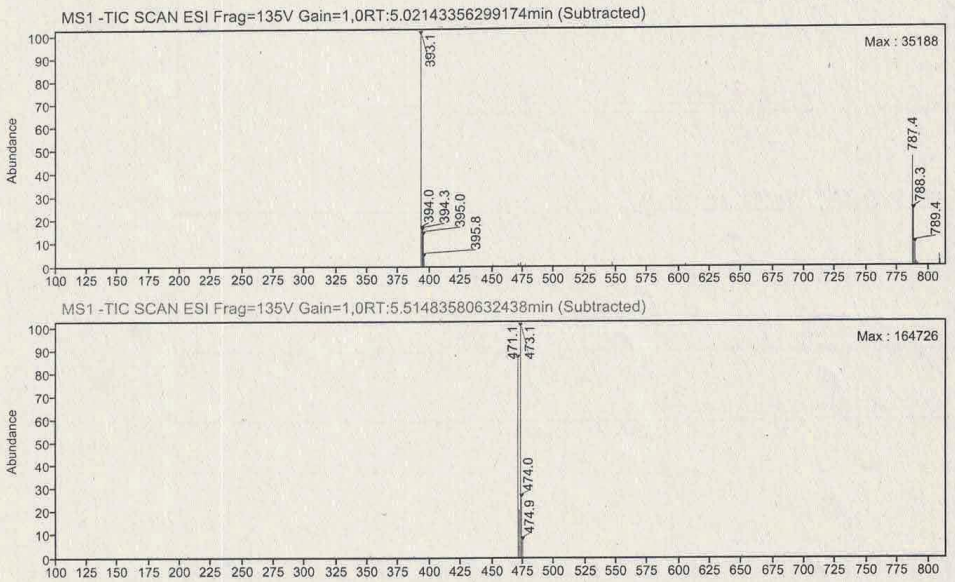


Signal: DAD1 Total WL (220.0:600.0 nm)

RT [min]	Peak MS Base Peak m/z	Area	Area%	Max Peak%	Height
2.754		796.9603	1.5477	1.825	53.850
3.577		525.6973	1.0209	1.204	63.666
4.149		628.5912	1.2207	1.439	100.593
4.256		2179.6051	4.2327	4.991	553.572
4.638		146.0801	0.2837	0.334	23.929
4.763		68.5316	0.1331	0.157	32.246
4.993	393.100	2600.8138	5.0507	5.955	734.099
5.125		127.8592	0.2483	0.293	60.808
5.481		43672.8847	84.8106	100.000	12089.285
8.332		167.1582	0.3246	0.383	29.247
9.235		580.3959	1.1271	1.329	104.277
	Sum	51494.5774			

Signal: MS1 -TIC SCAN ESI Frag=135V Gain=1,0

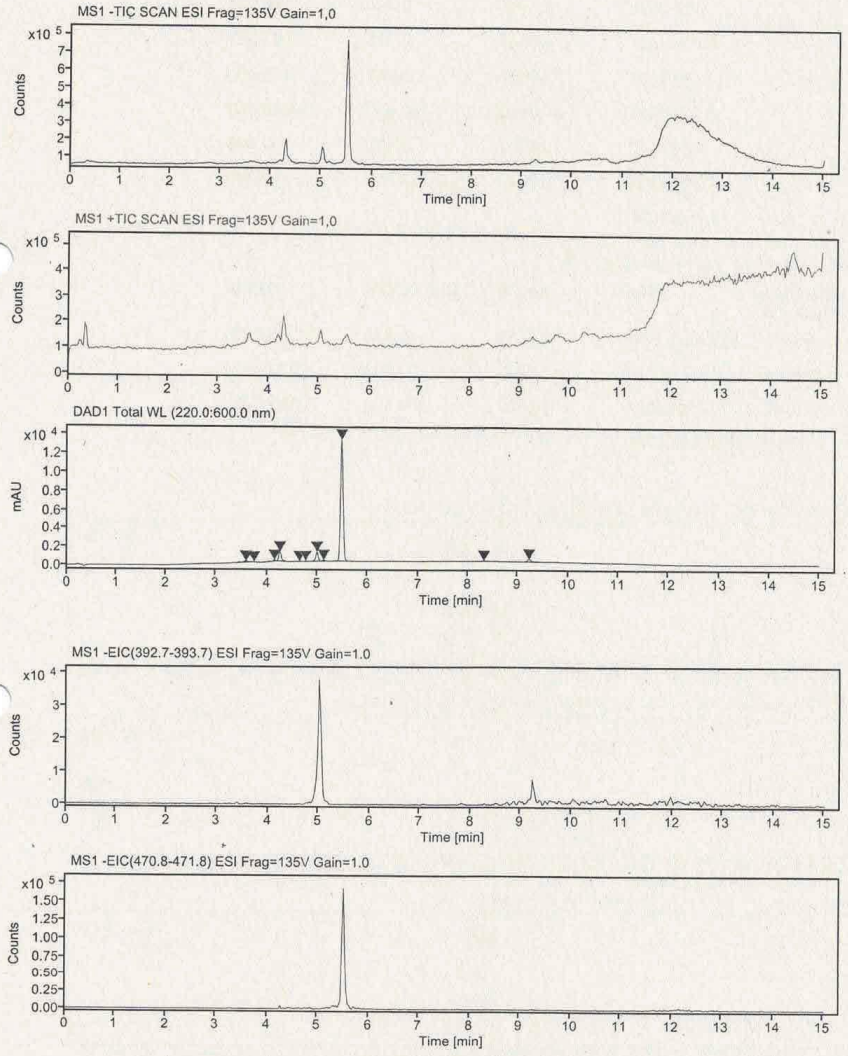
RT [min]	Peak MS Base Peak m/z	Area	Area%	Max Peak%	Height
5.021	393.100	301585.0964	10.1379	11.282	84187.069
5.515	473.100	2673237.7086	89.8621	100.000	707813.291
	Sum	2974822.8050			



D:\CDSProjects\Default\0-standardplot+EIC.rdl [Rev. 4405] Printed: 2021-12-28 07:27:46+01:00 Page 2 of 2

VI-4h

Sequence Name:	SingleSample		
Data file:	HALP149_4h.dx	**Project Name:**	Single Quad
Sample name:	HALP149_4h	**Operator :**	SYSTEM
Instrument:	Single Quad	**Acquired on:**	2021-12-27 15:46:19+01:00
Inj. volume:	5.000	**Location:**	P1-B11
Acq. method:	00-new_wasser-acn_standard_100-1000_BD-20min.amx		
Processing method:	MS_standard_plot.pmx		

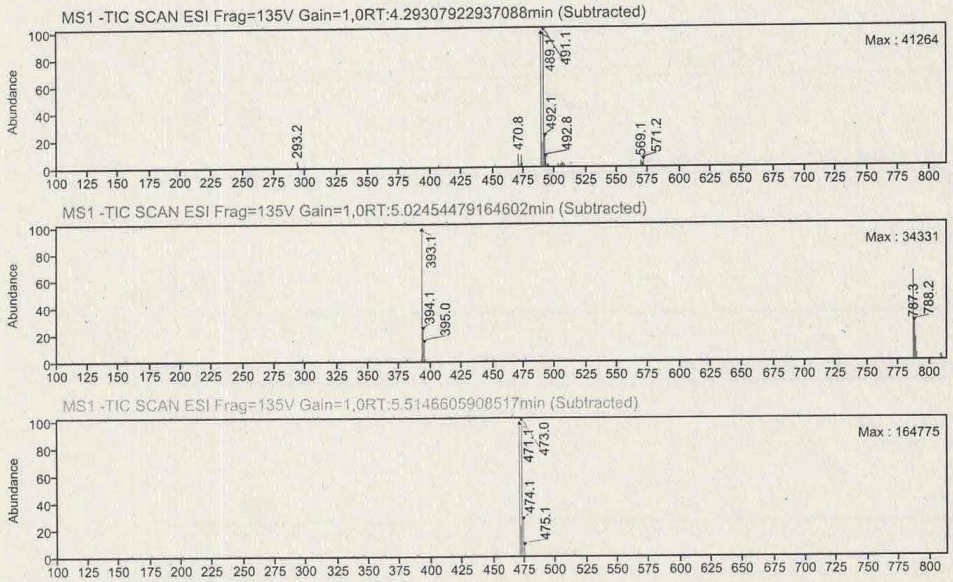


Signal: DAD1 Total WL (220.0:600.0 nm)

RT [min]	Peak MS Base Peak m/z	Area	Area%	Max Peak%	Height
3.585		869.6987	1.5117	1.854	138.753
3.745		80.0622	0.1392	0.171	38.837
4.146		449.3127	0.7810	0.958	130.709
4.257		3636.2844	6.3207	7.752	1033.408
4.641		106.0145	0.1843	0.226	32.416
4.764		97.0529	0.1687	0.207	49.011
4.994		3430.1097	5.9623	7.312	992.228
5.127		348.4697	0.6057	0.743	115.403
5.479		46910.3055	81.5409	100.000	13016.483
8.318		285.6129	0.4965	0.609	52.626
9.224		1316.8306	2.2890	2.807	252.189
	Sum	57529.7536			

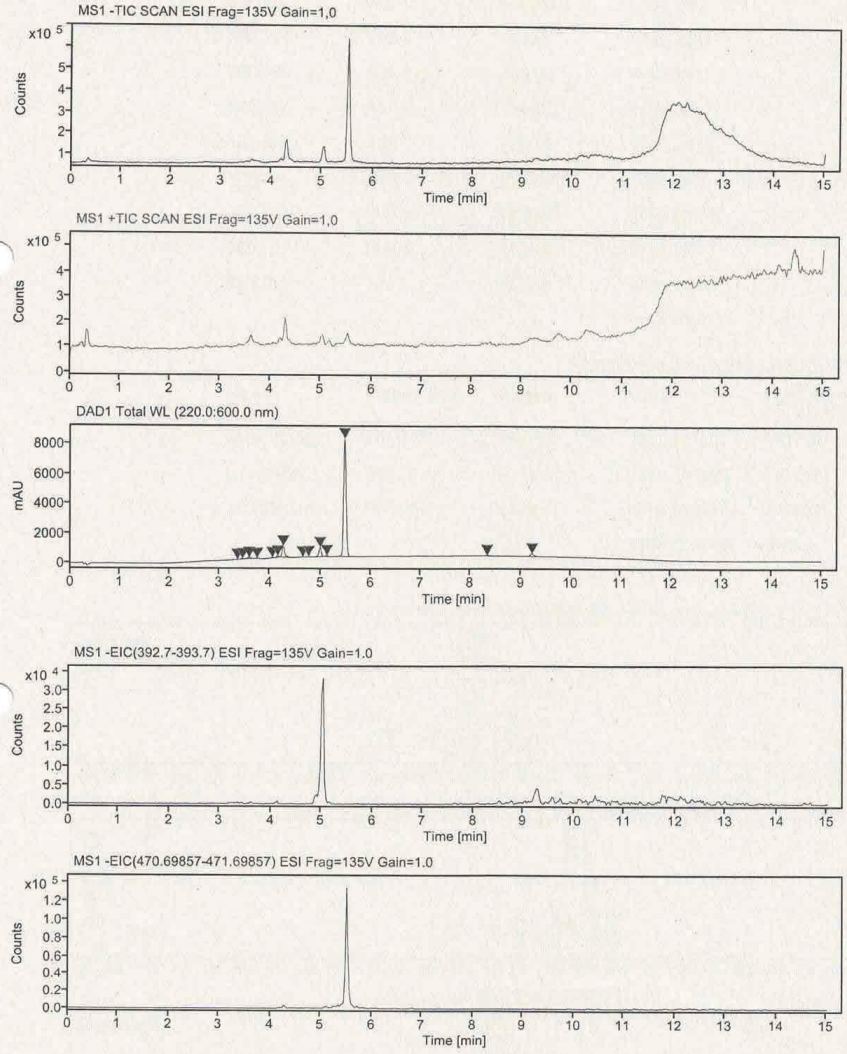
Signal: MS1 -TIC SCAN ESI Frag=135V Gain=1,0

RT [min]	Peak MS Base Peak m/z	Area	Area%	Max Peak%	Height
4.293	489.100	445363.1485	12.4511	15.838	130854.816
5.025	393.100	319527.5576	8.9331	11.363	92297.579
5.515	473.000	2812019.4391	78.6159	100.000	703850.767
	Sum	3576910.1451			



VI-5h

Sequence Name:	SingleSample		
Data file:	HALP149_5h.dx	**Project Name:**	Single Quad
Sample name:	HALP149_5h	**Operator :**	SYSTEM
Instrument:	Single Quad	**Acquired on:**	2021-12-27 16:07:21+01:00
Inj. volume:	5.000	**Location:**	P1-C1
Acq. method:	00-new_wasser-acn_standard_100-1000_BD-20min.amx		
Processing method:	MS_standard_plot.pmx		

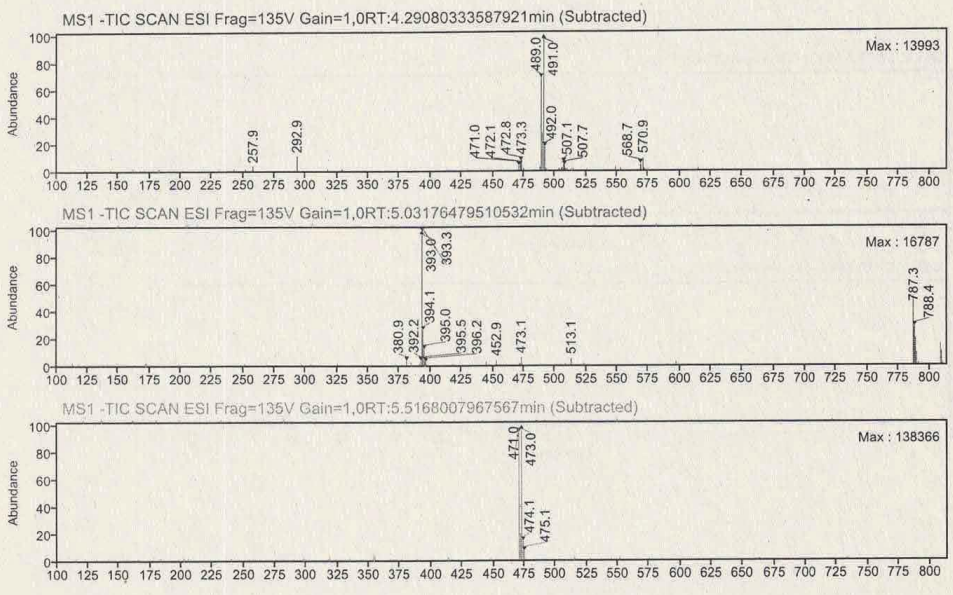


Signal: DAD1 Total WL (220.0:600.0 nm)

RT [min]	Peak MS Base Peak m/z	Area	Area%	Max Peak%	Height
3.357		40.5628	0.1184	0.149	12.017
3.457		82.0011	0.2394	0.302	34.309
3.587		376.4370	1.0988	1.386	87.609
3.743		50.1121	0.1463	0.184	20.939
4.042		68.8763	0.2010	0.254	32.483
4.149		305.9414	0.8930	1.126	99.316
4.260		2606.8957	7.6092	9.595	738.589
4.646		54.8146	0.1600	0.202	21.301
4.768		50.8020	0.1483	0.187	28.023
4.996		2066.9087	6.0331	7.607	598.537
5.129		242.5557	0.7080	0.893	81.297
5.484		27169.5845	79.3050	100.000	7853.953
8.326		228.1874	0.6661	0.840	41.490
9.230		915.9272	2.6735	3.371	179.745
	Sum	34259.6064			

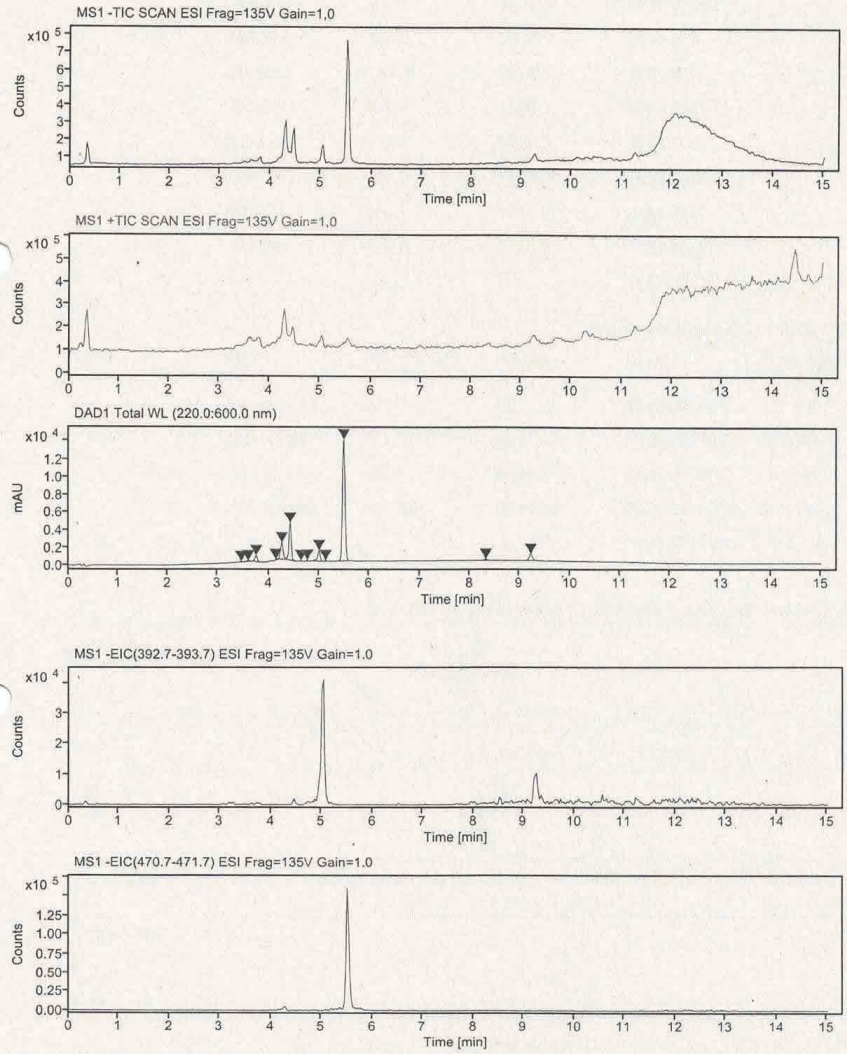
Signal: MS1 -TIC SCAN ESI Frag=135V Gain=1,0

RT [min]	Peak MS Base Peak m/z	Area	Area%	Max Peak%	Height
4.291	491.000	277187.7469	10.7421	13.779	90495.684
5.032	393.000	291515.8780	11.2974	14.491	75308.199
5.517	473.000	2011674.4458	77.9605	100.000	572878.393
	Sum	2580378.0707			



VI-6h

Sequence Name:	SingleSample		
Data file:	HALP149_6h.dx	**Project Name:**	Single Quad
Sample name:	HALP149_6h	**Operator :**	SYSTEM
Instrument:	Single Quad	**Acquired on:**	2021-12-27 16:28:23+01:00
Inj. volume:	10.000	**Location:**	P1-C2
Acq. method:	00-new_wasser-acn_standard_100-1000_BD-20min.amx		
Processing method:	MS_standard_plot.pmx		

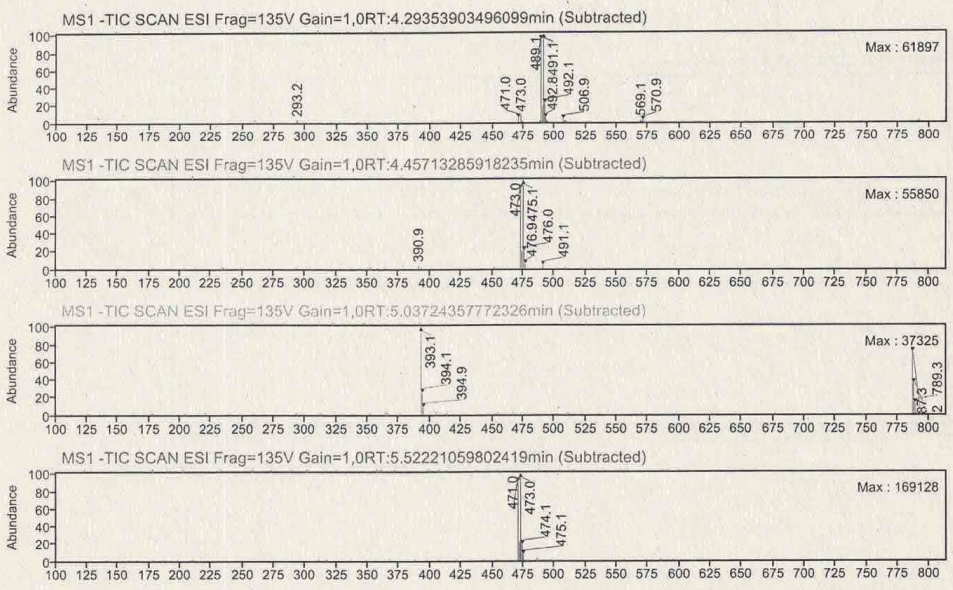


Signal: DAD1 Total WL (220.0:600.0 nm)

RT [min]	Peak MS Base Peak m/z	Area	Area%	Max Peak%	Height
3.457		130.7880	0.1608	0.266	48.536
3.592		308.1356	0.3789	0.626	81.725
3.756		2384.9296	2.9324	4.843	680.483
4.138		95.4510	0.1174	0.194	61.739
4.260		7073.0001	8.6966	14.362	1842.941
4.425		13411.9183	16.4907	27.233	4203.490
4.639		179.9258	0.2212	0.365	46.642
4.770		220.0524	0.2706	0.447	95.348
5.002		4296.4434	5.2827	8.724	1160.250
5.132		203.2333	0.2499	0.413	64.528
5.489		49248.7792	60.5541	100.000	13705.675
8.324		513.7883	0.6317	1.043	115.023
9.227		3263.7617	4.0130	6.627	698.934
	Sum	81330.2067			

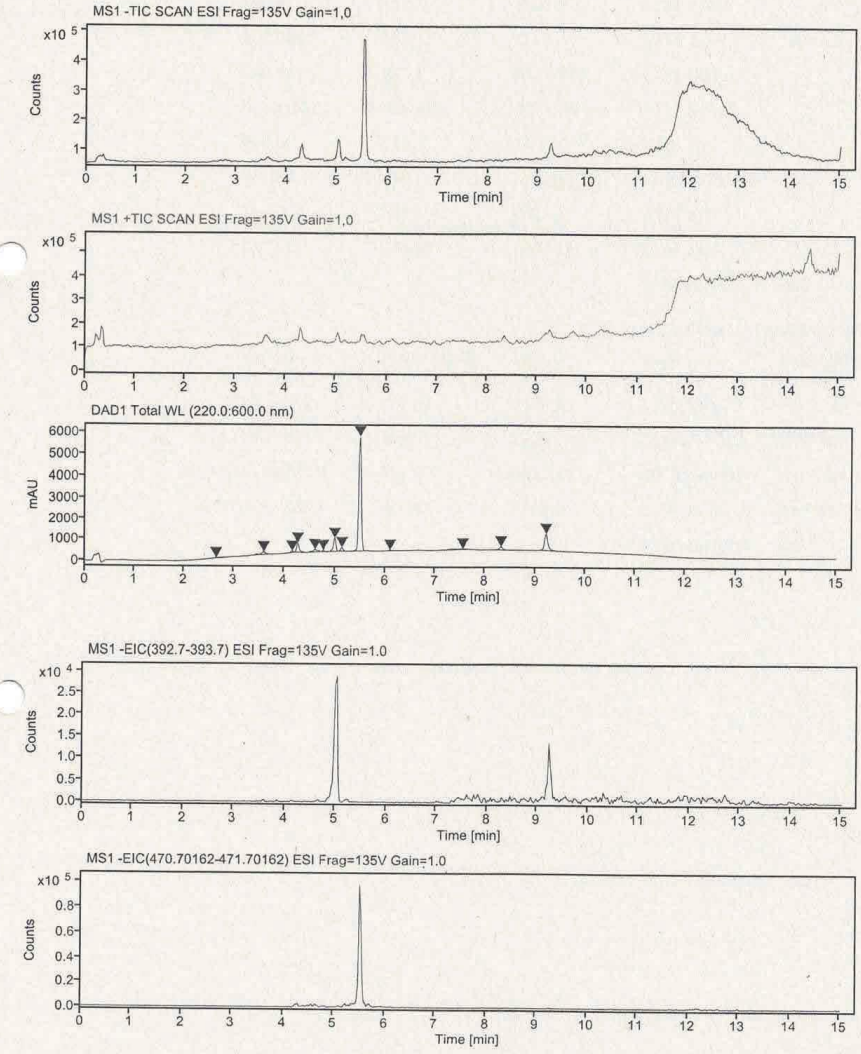
Signal: MS1 -TIC SCAN ESI Frag=135V Gain=1,0

RT [min]	Peak MS Base Peak m/z	Area	Area%	Max Peak%	Height
4.294	489.100	705100.7332	16.0538	25.785	200525.465
4.457	475.100	621948.3690	14.1606	22.745	183204.905
5.037	393.100	330565.3978	7.5264	12.089	99321.812
5.522	473.000	2734493.1508	62.2592	100.000	704746.578
	Sum	4392107.6507			



Sequence Name:	SingleSample		
Data file:	HALP149-24h.dx	**Project Name:**	Single Quad
Sample name:	HALP149-24h	**Operator :**	SYSTEM
Instrument:	Single Quad	**Acquired on:**	2021-12-27 21:22:41+01:00
Inj. volume:	5.000	**Location:**	P1-D4
Acq. method:	00-new_wasser-acn_standard_100-1000_BD-20min.amx		
Processing method:	MS_standard_plot.pmx		

VI-24h

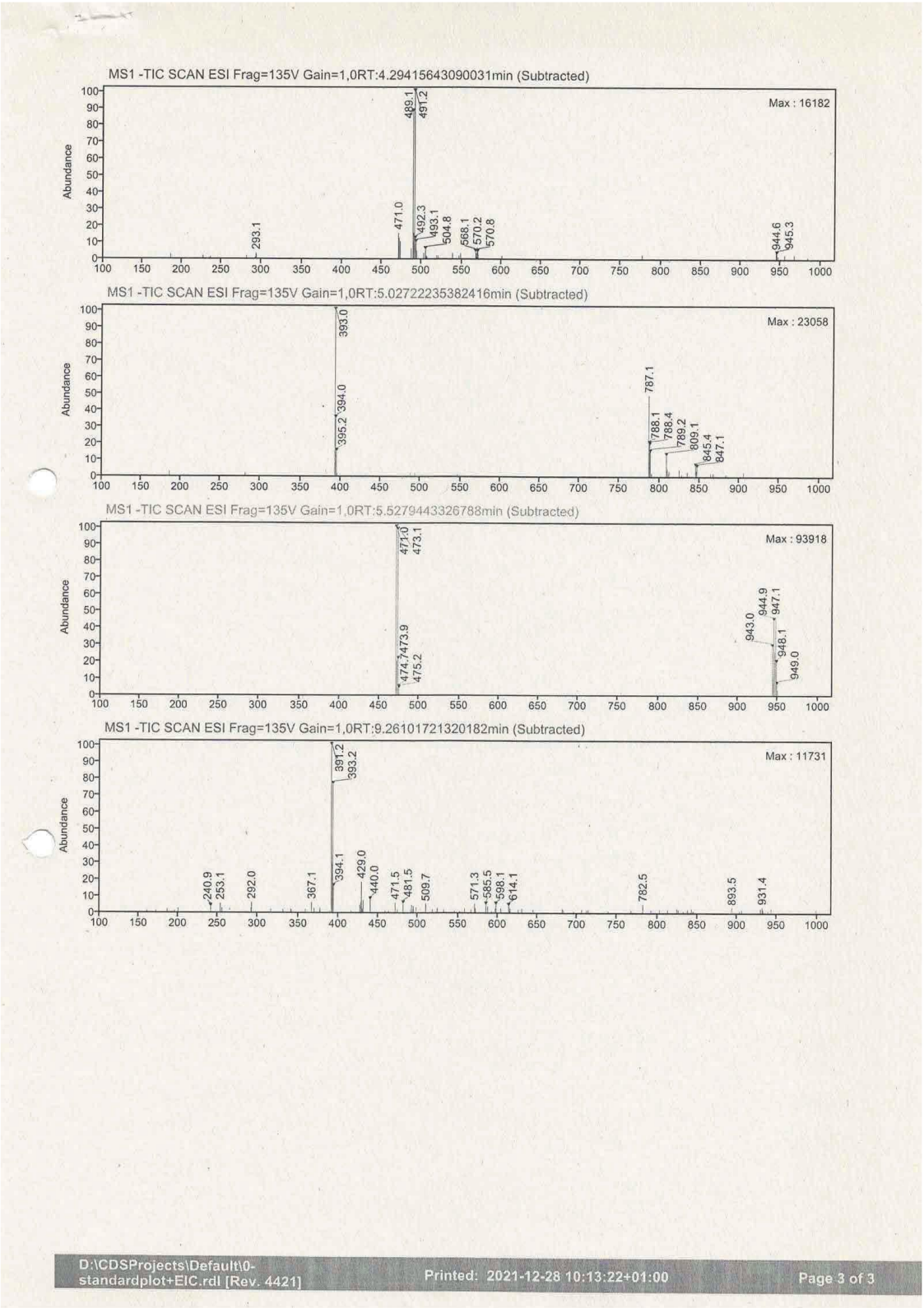


Signal: DAD1 Total WL (220.0:600.0 nm)

RT [min]	Peak MS Base Peak m/z	Area	Area%	Max Peak%	Height
2.644		235.5009	0.7906	1.294	17.790
3.590		876.1310	2.9414	4.812	127.633
4.150		154.8809	0.5200	0.851	57.238
4.261		1547.0224	5.1937	8.497	412.586
4.603		684.2183	2.2971	3.758	104.370
4.771		104.4615	0.3507	0.574	53.887
5.000	393.000	2181.9160	7.3252	11.984	600.503
5.140		550.1513	1.8470	3.022	159.649
5.494		18206.2711	61.1228	100.000	5292.515
6.096		168.1125	0.5644	0.923	30.039
7.550		699.6949	2.3490	3.843	35.586
8.315		636.9785	2.1385	3.499	136.827
9.220		3741.0422	12.5596	20.548	750.459
	Sum	29786.3816			

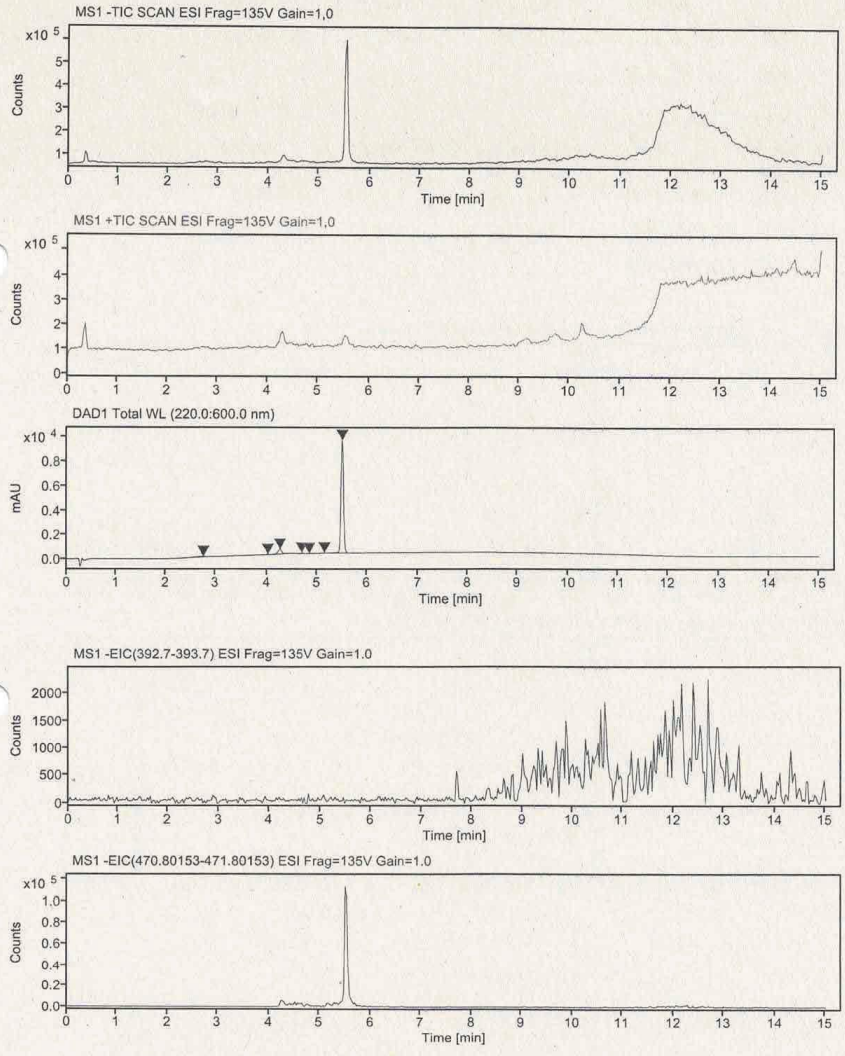
Signal: MS1 -TIC SCAN ESI Frag=135V Gain=1,0

RT [min]	Peak MS Base Peak m/z	Area	Area%	Max Peak%	Height
4.294	491.200	173584.0555	7.5598	10.511	49704.351
5.027	393.000	258725.6426	11.2679	15.666	71157.265
5.528	471.000	1651466.6736	71.9236	100.000	442559.819
9.261	391.200	212363.7828	9.2487	12.859	47931.130
	Sum	2296140.1545			


MS1 -TIC SCAN ESI Frag=135V Gain=1,0RT:4.29415643090031min (Subtracted)
Max : 16182
Abundance
489.1
491.2
471.0
293.1
492.3
493.1
504.8
568.1
570.2
570.8
944.6
945.3
MS1 -TIC SCAN ESI Frag=135V Gain=1,0RT:5.02722235382416min (Subtracted)
Max : 23058
Abundance
393.0
394.0
395.2
787.1
788.1
788.4
789.2
809.1
845.4
847.1
MS1 -TIC SCAN ESI Frag=135V Gain=1,0RT:5.5279443326788min (Subtracted)
Max : 93918
Abundance
471.0
473.1
474.7
473.9
475.2
943.0
944.9
947.1
948.1
949.0
MS1 -TIC SCAN ESI Frag=135V Gain=1,0RT:9.26101721320182min (Subtracted)
Max : 11731
Abundance
391.2
393.2
394.1
429.0
440.0
471.5
481.5
509.7
571.3
585.5
598.1
614.1
240.9
253.1
292.0
367.1
782.5
893.5
931.4
D:\CDSProjects\Default\0-standardplot+EIC.rdl [Rev. 4421]
Printed: 2021-12-28 10:13:22+01:00
Page 3 of 3

Trial VII

Sequence Name:	SingleSample VII-10min		
Data file:	HALP154-10min.dx	**Project Name:**	Single Quad
Sample name:	HALP154-10min	**Operator :**	SYSTEM
Instrument:	Single Quad	**Acquired on:**	2021-12-27 21:43:48+01:00
Inj. volume:	10,000	**Location:**	P1-D5
Acq. method:	00-new_wasser-acn_standard_100-1000_BD-20min.amx		
Processing method:	MS_standard_plot.pmx		



D:\CDSProjects\Default\0-standardplot+EIC.rdl [Rev. 4422] Printed: 2021-12-28 10:28:21+01:00 Page 1 of 2

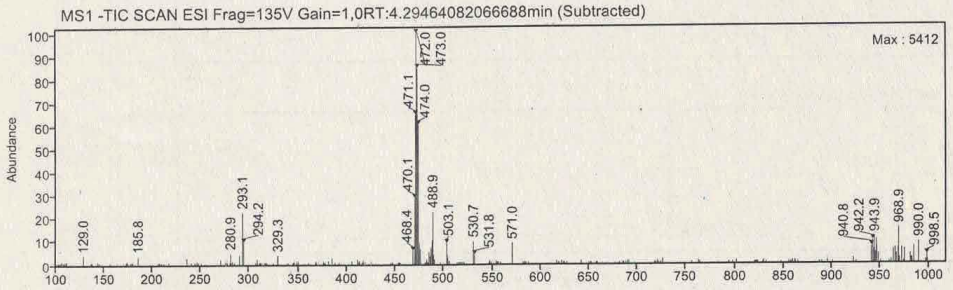
Signal: DAD1 Total WL (220.0:600.0 nm)

RT [min]	Peak MS Base Peak m/z	Area	Area%	Max Peak%	Height
2.749		538.7276	1.5439	1.682	42.439
4.026		67.7499	0.1942	0.212	29.606
4.264	473.000	2044.0511	5.8579	6.382	386.350
4.698		105.4218	0.3021	0.329	24.488
4.848		15.9707	0.0458	0.050	10.576
5.148		95.1049	0.2726	0.297	25.970
5.500	473.000	32026.8069	91.7836	100.000	9199.352
	Sum	34893.8329			

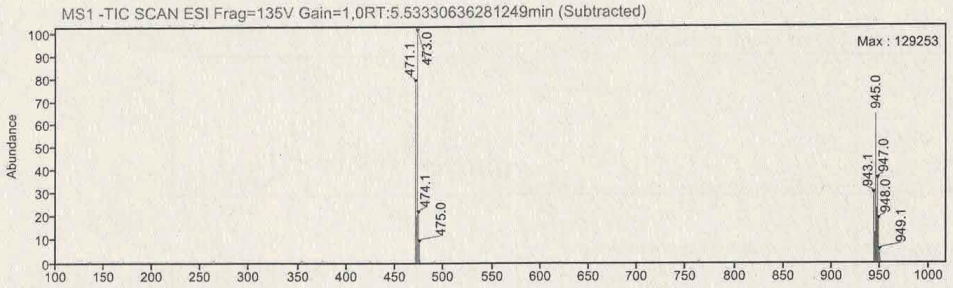
Signal: MS1 -TIC SCAN ESI Frag=135V Gain=1,0

RT [min]	Peak MS Base Peak m/z	Area	Area%	Max Peak%	Height
4.295	473.000	155699.2541	6.2706	6.690	27719.837
5.533	473.000	2327305.9470	93.7294	100.000	552001.039
	Sum	2483005.2011			

MS1 -TIC SCAN ESI Frag=135V Gain=1,0RT:4.29464082066688min (Subtracted)



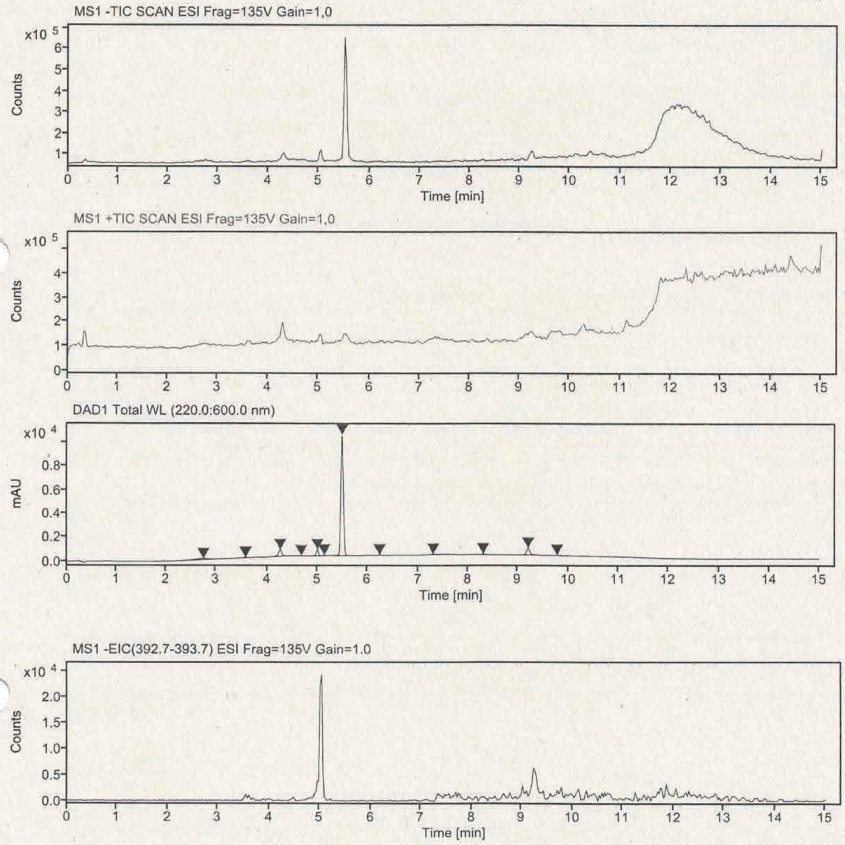
MS1 -TIC SCAN ESI Frag=135V Gain=1,0RT:5.53330636281249min (Subtracted)



D:\CDSProjects\Default\0-standardplot+EIC.rdl [Rev. 4422] Printed: 2021-12-28 10:28:21+01:00 Page 2 of 2

VII-2h

Sequence Name:	SingleSample		
Data file:	HALP154-2h.dx	**Project Name:**	Single Quad
Sample name:	HALP154-2h	**Operator :**	SYSTEM
Instrument:	Single Quad	**Acquired on:**	2021-12-27 22:04:53+01:00
Inj. volume:	5.000	**Location:**	P1-D6
Acq. method:	00-new_wasser-acn_standard_100-1000_BD-20min.amx		
Processing method:	MS_standard_plot.pmx		



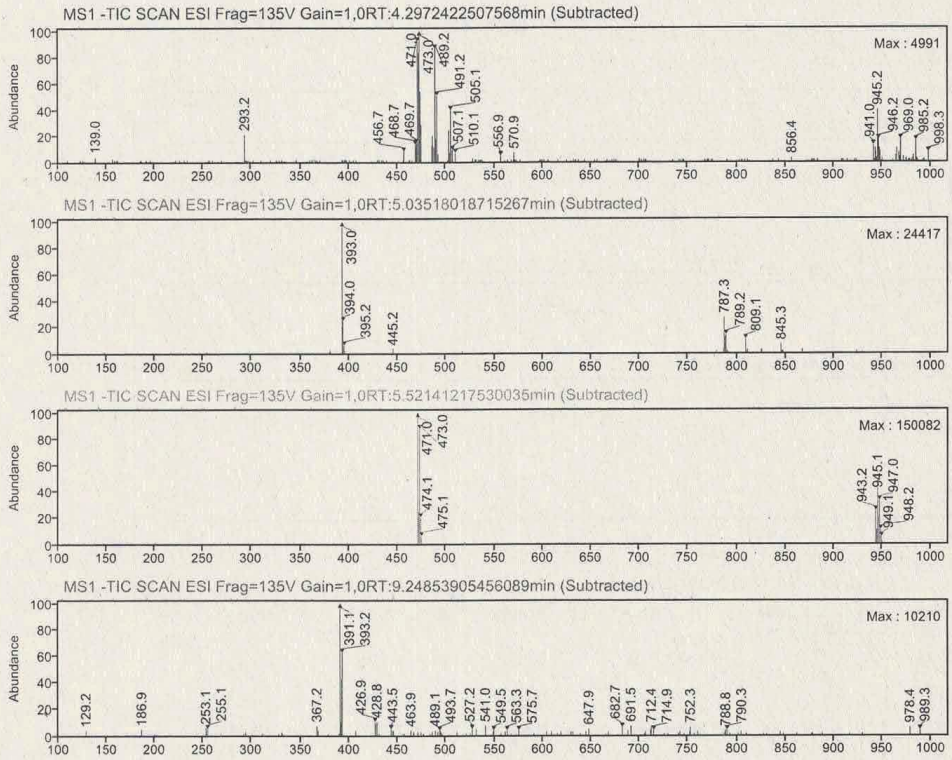
Signal: DAD1 Total WL (220.0:600.0 nm)

RT [min]	Peak MS Base Peak m/z	Area	Area%	Max Peak%	Height
2.744		1573.4022	3.4554	4.494	83.854
3.576		335.7408	0.7373	0.959	52.065
4.261	473.000	2663.3648	5.8492	7.607	562.354
4.680		95.9130	0.2106	0.274	21.121
5.002	393.000	1671.9919	3.6720	4.776	509.848
5.138		131.7293	0.2893	0.376	42.877
5.489	471.000	35009.8371	76.8871	100.000	10166.085

RT [min]	Peak MS Base Peak m/z	Area	Area%	Max Peak%	Height
6.233		130.4995	0.2866	0.373	34.482
7.305		816.0027	1.7921	2.331	47.797
8.302		253.0039	0.5556	0.723	58.936
9.206		2757.8382	6.0566	7.877	560.114
9.781		94.7610	0.2081	0.271	24.577
	Sum	45534.0845			

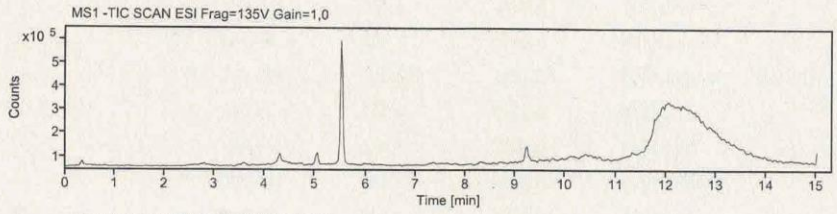
Signal: MS1 -TIC SCAN ESI Frag=135V Gain=1,0

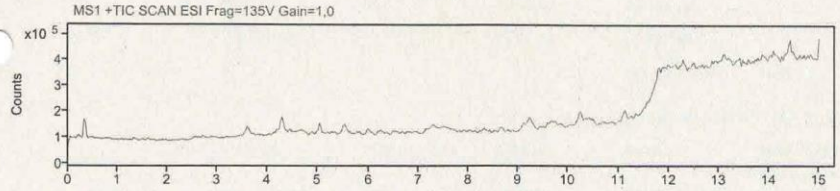
RT [min]	Peak MS Base Peak m/z	Area	Area%	Max Peak%	Height
4.297	473.000	182100.2793	6.1573	7.544	35531.963
5.035	393.000	191220.2023	6.4657	7.922	54417.383
5.521	471.000	2413896.0658	81.6204	100.000	605633.622
9.249	391.100	170250.2788	5.7566	7.053	36245.623
	Sum	2957466.8262			

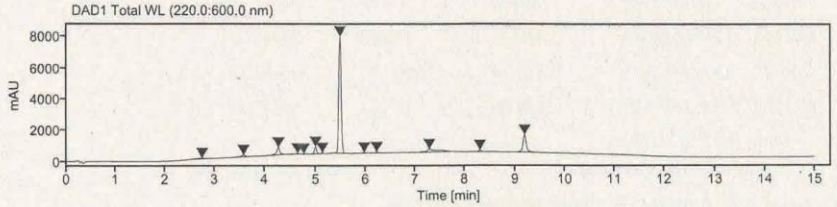


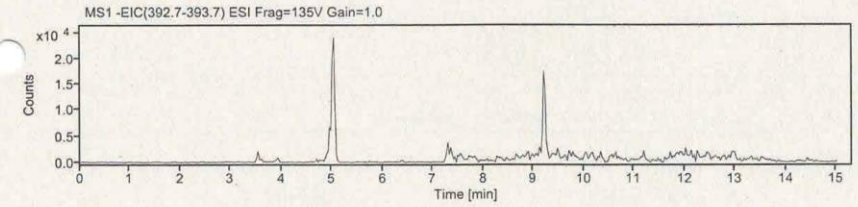
VII-4h

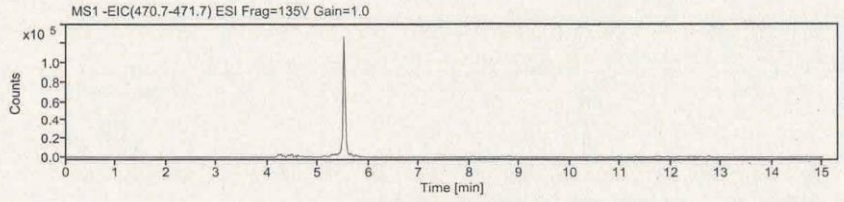
Sequence Name:	SingleSample		
Data file:	HALP154-4h.dx	**Project Name:**	Single Quad
Sample name:	HALP154-4h	**Operator :**	SYSTEM
Instrument:	Single Quad	**Acquired on:**	2021-12-27 22:25:56+01:00
Inj. volume:	5.000	**Location:**	P1-D7
Acq. method:	00-new_wasser-acn_standard_100-1000_BD-20min.amx		
Processing method:	MS_standard_plot.pmx		









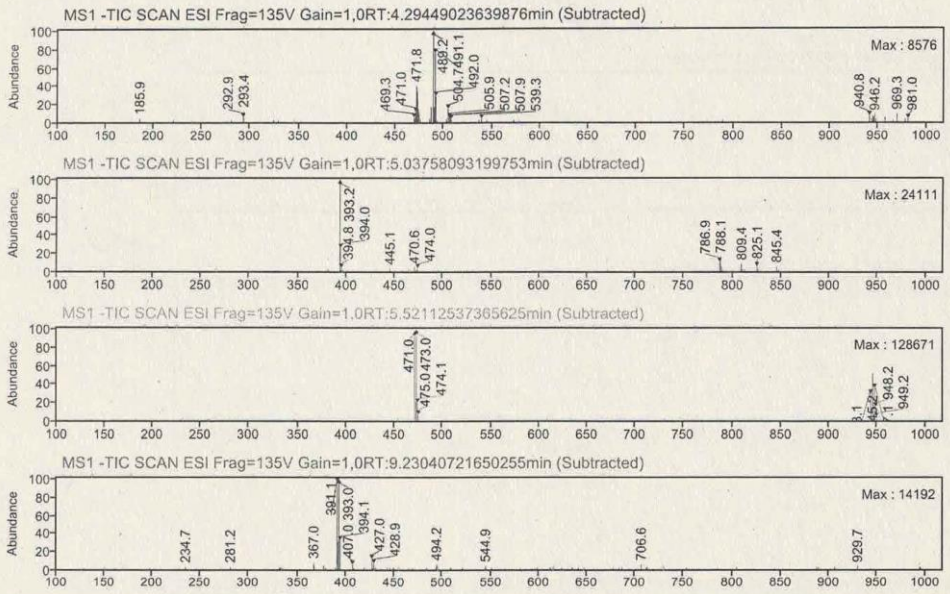


Signal: DAD1 Total WL (220.0:600.0 nm)

RT [min]	Peak MS Base Peak m/z	Area	Area%	Max Peak%	Height
2.745		524.8153	1.3655	2.163	38.473
3.566		613.4854	1.5962	2.529	103.815
4.259		2104.6919	5.4762	8.675	440.379
4.640		176.0494	0.4581	0.726	21.172
4.767		4.3982	0.0114	0.018	8.398
5.003		1403.3953	3.6515	5.785	438.862
5.137		111.6000	0.2904	0.460	36.206
5.490	473.000	24260.7803	63.1239	100.000	7463.608
5.972		124.5248	0.3240	0.513	25.343
6.221		157.4875	0.4098	0.649	41.461
7.277		3180.1352	8.2744	13.108	175.506
8.291		344.6189	0.8967	1.420	83.668
9.194		5427.6079	14.1220	22.372	1098.689
	Sum	38433.5901			

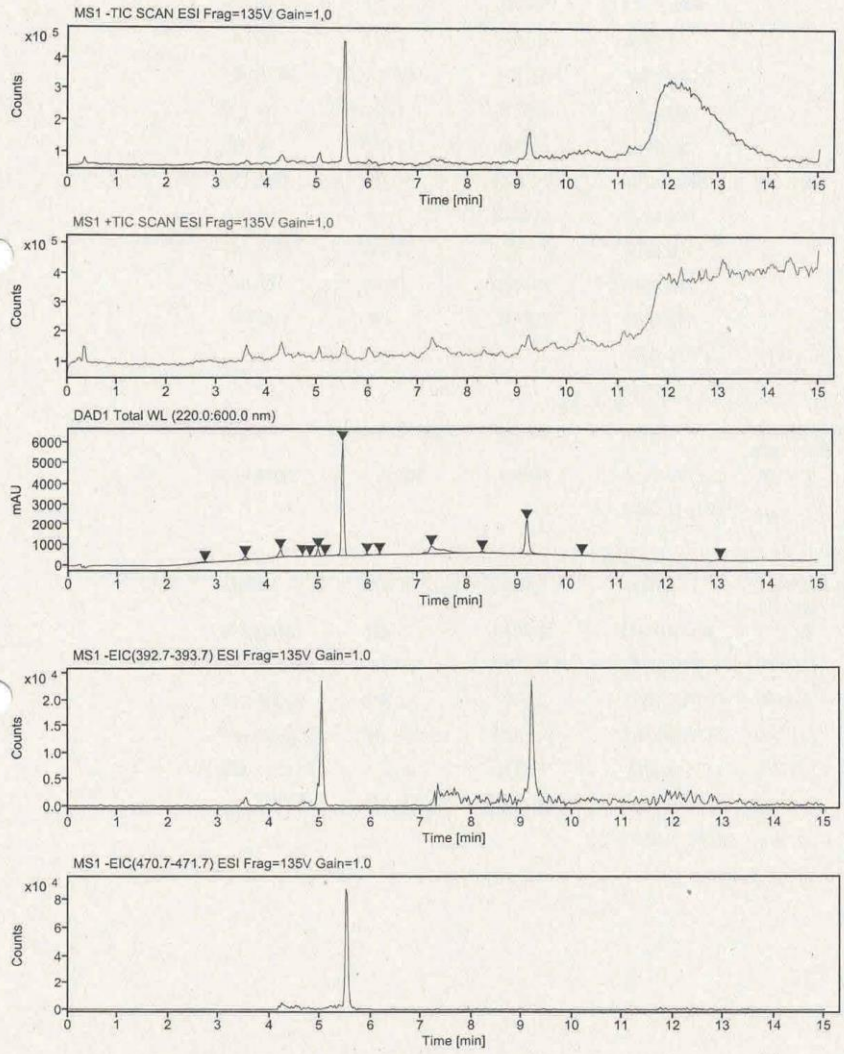
Signal: MS1 -TIC SCAN ESI Frag=135V Gain=1,0

RT [min]	Peak MS Base Peak m/z	Area	Area%	Max Peak%	Height
4.294	489.200	118367.8719	4.8452	6.226	34047.122
5.038	393.200	215168.9301	8.8076	11.318	52307.524
5.521	473.000	1901081.5878	77.8176	100.000	545493.324
9.230	391.100	208377.7707	8.5296	10.961	55970.335
	Sum	2442996.1605			



VII-6h

Sequence Name:	SingleSample		
Data file:	HALP154-6h.dx	**Project Name:**	Single Quad
Sample name:	HALP154-6h	**Operator :**	SYSTEM
Instrument:	Single Quad	**Acquired on:**	2021-12-27 22:46:58+01:00
Inj. volume:	5.000	**Location:**	P1-D8
Acq. method:	00-new_wasser-acn_standard_100-1000_BD-20min.amx		
Processing method:	MS_standard_plot.pmx		



Signal: DAD1 Total WL (220.0:600.0 nm)

RT [min]	Peak MS Base Peak m/z	Area	Area%	Max Peak%	Height
2.755		481.4999	1.2848	2.644	32.791
3.552		823.4970	2.1974	4.521	139.141
4.253		1657.7949	4.4236	9.102	343.962
4.693		205.3425	0.5479	1.127	31.526
4.844		36.6659	0.0978	0.201	11.181
5.006		1096.1170	2.9248	6.018	344.276
5.143		57.1676	0.1525	0.314	20.765
5.495		18213.3321	48.5994	100.000	5578.151
5.981		300.5376	0.8019	1.650	61.318
6.228		192.9693	0.5149	1.059	49.668
7.271	394.100	5791.1784	15.4528	31.796	349.415
8.289		361.6009	0.9649	1.985	87.993
9.191		7910.4732	21.1078	43.432	1659.949
10.291		156.4605	0.4175	0.859	35.677
13.057		191.8204	0.5118	1.053	43.565
	Sum	37476.4573			

Signal: MS1 +TIC SCAN ESI Frag=135V Gain=1,0

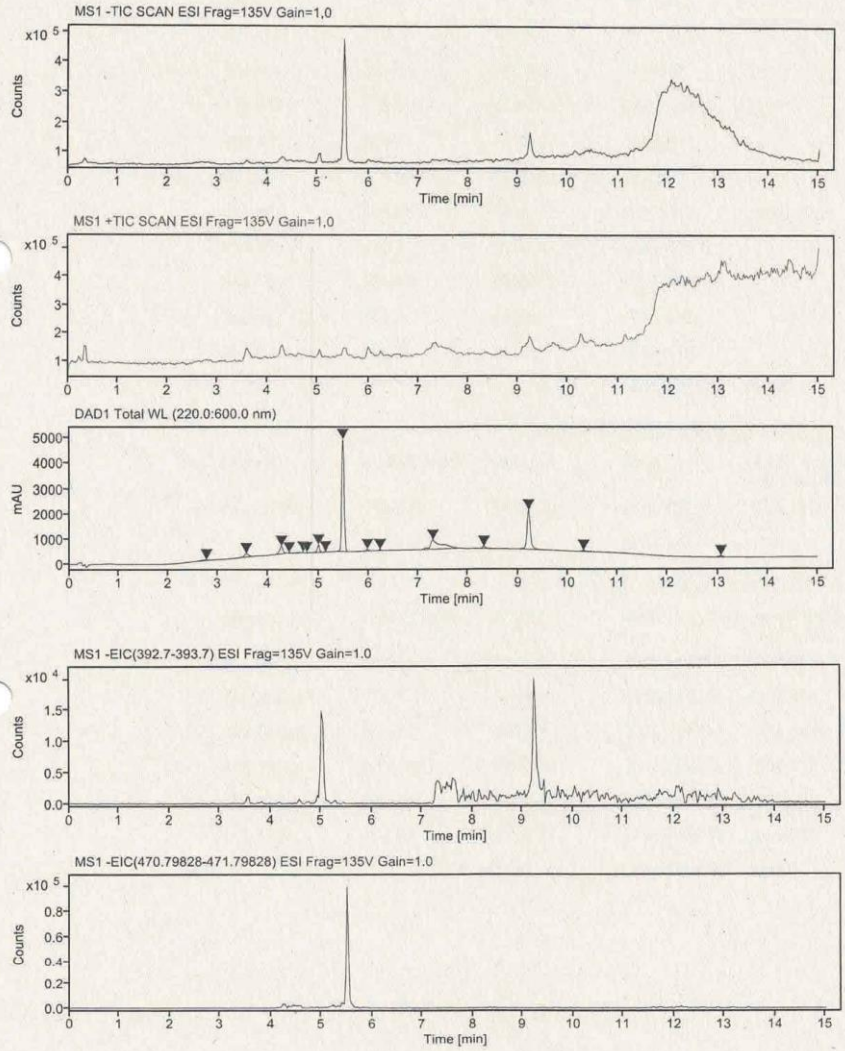
RT [min]	Peak MS Base Peak m/z	Area	Area%	Max Peak%	Height
7.289	394.100	678752.9424	100.0000	100.000	54978.869
	Sum	678752.9424			

Signal: MS1 -TIC SCAN ESI Frag=135V Gain=1,0

RT [min]	Peak MS Base Peak m/z	Area	Area%	Max Peak%	Height
3.587	423.300	53864.2400	2.1692	3.525	9883.245
4.289	472.000	109049.8704	4.3916	7.137	21744.318
5.039	393.100	100509.2563	4.0477	6.578	30995.046
5.514	471.000	1527935.2802	61.5327	100.000	382006.400
7.328	391.100	233712.9590	9.4120	15.296	14711.950
9.232	391.100	458055.9552	18.4467	29.979	87800.855
	Sum	2483127.5611			

VII-7h

Sequence Name:	SingleSample		
Data file:	HALP154-7h.dx	**Project Name:**	Single Quad
Sample name:	HALP154-7h	**Operator :**	SYSTEM
Instrument:	Single Quad	**Acquired on:**	2021-12-27 23:08:02+01:00
Inj. volume:	5.000	**Location:**	P1-D9
Acq. method:	00-new_wasser-acn_standard_100-1000_BD-20min.amx		
Processing method:	MS_standard_plot.pmx		



Signal: DAD1 Total WL (220.0:600.0 nm)

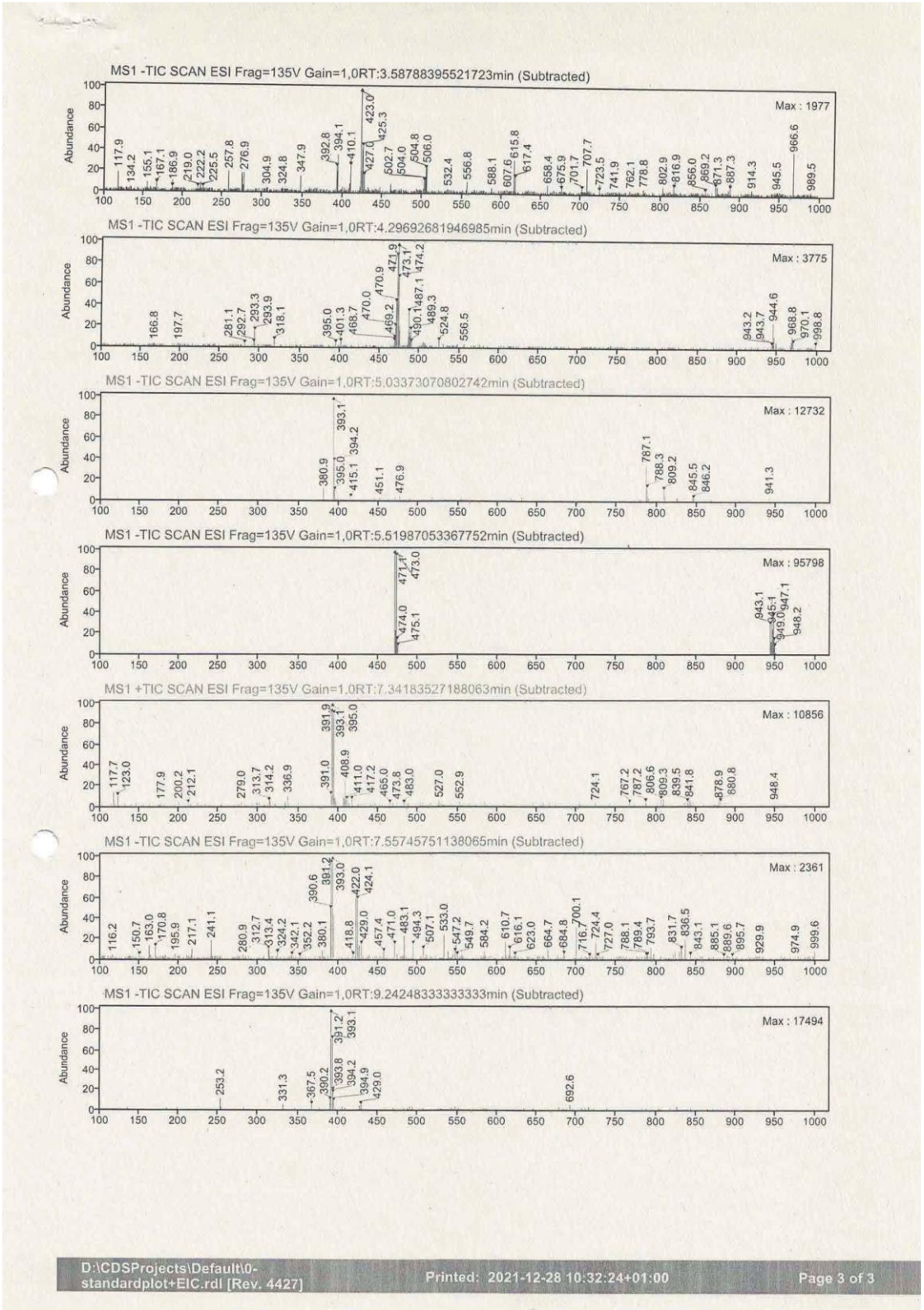
RT [min]	Peak MS Base Peak m/z	Area	Area%	Max Peak%	Height
2.770		411.2183	1.2631	2.868	27.223
3.560	423.000	830.9219	2.5523	5.795	134.803
4.256		1267.0410	3.8918	8.836	280.518
4.408		32.0063	0.0983	0.223	12.404
4.688		208.8497	0.6415	1.456	29.690
4.766		20.3050	0.0624	0.142	7.599
5.000		921.3347	2.8300	6.425	286.994
5.137		66.5607	0.2044	0.464	19.327
5.487		14339.3975	44.0449	100.000	4416.371
5.973		119.5267	0.3671	0.834	50.684
6.225		68.5837	0.2107	0.478	33.763
7.287	391.900	5613.5760	17.2427	39.148	354.546
8.310		289.4542	0.8891	2.019	75.074
9.216		7809.8110	23.9886	54.464	1587.946
10.315		280.2701	0.8609	1.955	39.992
13.067		277.4326	0.8522	1.935	49.228
	Sum	32556.2894			

Signal: MS1 +TIC SCAN ESI Frag=135V Gain=1,0

RT [min]	Peak MS Base Peak m/z	Area	Area%	Max Peak%	Height
7.342	391.900	811353.0824	100.0000	100.000	43878.421
	Sum	811353.0824			

Signal: MS1 -TIC SCAN ESI Frag=135V Gain=1,0

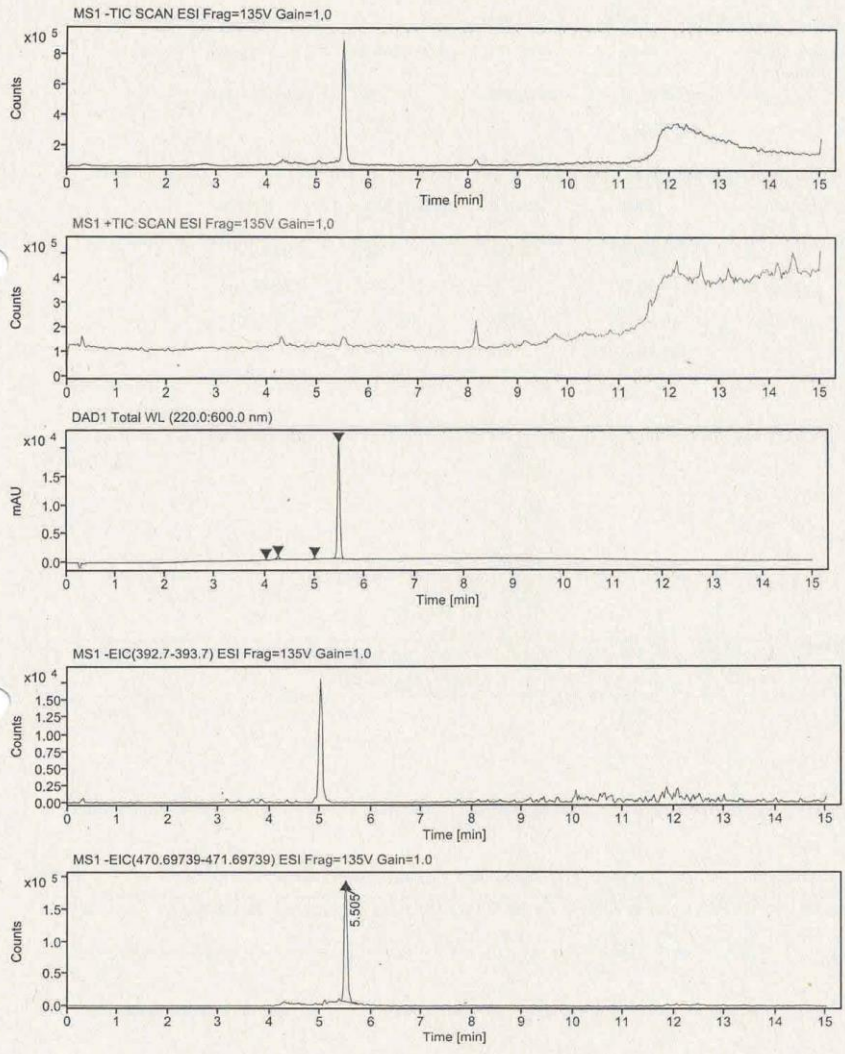
RT [min]	Peak MS Base Peak m/z	Area	Area%	Max Peak%	Height
3.588	423.000	41344.0237	2.0817	3.125	9709.773
4.297	473.100	101024.0728	5.0867	7.637	15648.341
5.034	393.100	145567.1305	7.3295	11.004	34680.430
5.520	471.100	1322896.9132	66.6094	100.000	410727.359
7.557	393.000	139637.8346	7.0309	10.555	9916.433
9.242	391.200	235582.6042	11.8619	17.808	69824.312
	Sum	1986052.5789			


MS1 -TIC SCAN ESI Frag=135V Gain=1,0RT:3.58788395521723min (Subtracted)
Max : 1977
MS1 -TIC SCAN ESI Frag=135V Gain=1,0RT:4.29692681946985min (Subtracted)
Max : 3775
MS1 -TIC SCAN ESI Frag=135V Gain=1,0RT:5.03373070802742min (Subtracted)
Max : 12732
MS1 -TIC SCAN ESI Frag=135V Gain=1,0RT:5.51987053367752min (Subtracted)
Max : 95798
MS1 +TIC SCAN ESI Frag=135V Gain=1,0RT:7.34183527188063min (Subtracted)
Max : 10856
MS1 -TIC SCAN ESI Frag=135V Gain=1,0RT:7.55745751138065min (Subtracted)
Max : 2361
MS1 -TIC SCAN ESI Frag=135V Gain=1,0RT:9.24248333333333min (Subtracted)
Max : 17494
Abundance
D:\CDSProjects\Default\0-standardplot+EIC.rdl [Rev. 4427]
Printed: 2021-12-28 10:32:24+01:00
Page 3 of 3

Trial VIII

VIII – 15min

Sequence Name:	SingleSample		
Data file:	HALP160-15min.dx	**Project Name:**	Single Quad
Sample name:	HALP160-15min	**Operator :**	SYSTEM
Instrument:	Single Quad	**Acquired on:**	2022-01-03 08:23:30+01:00
Inj. volume:	5.000	**Location:**	P2-A5
Acq. method:	00-new_wasser-acn_standard_100-1000_BD-20min.amx		
Processing method:	MS_standard_plot.pmx		



D:\CDSProjects\Default\0-standardplot+EIC.rdl [Rev. 4449] Printed: 2022-01-03 12:20:04+01:00 Page 1 of 2

Signal: DAD1 Total WL (220.0:600.0 nm)

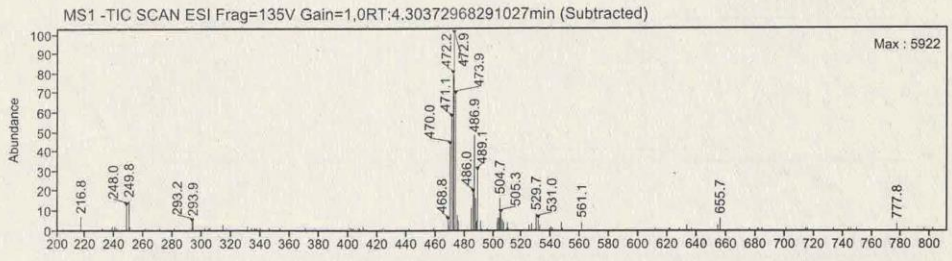
RT [min]	Peak MS Base Peak m/z	Area	Area%	Max Peak%	Height
4.021		190.7596	0.2519	0.261	57.470
4.260		1722.1154	2.2737	2.357	465.928
4.997		775.2207	1.0235	1.061	246.871
5.475		73053.0877	96.4509	100.000	20311.494
	Sum	75741.1834			

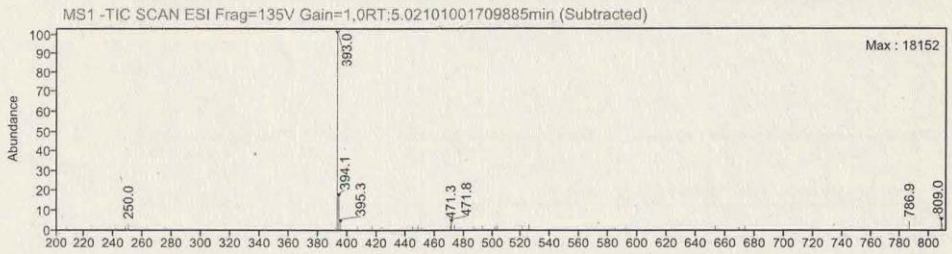
Signal: MS1 -EIC(470.69739-471.69739) ESI Frag=135V Gain=1.0

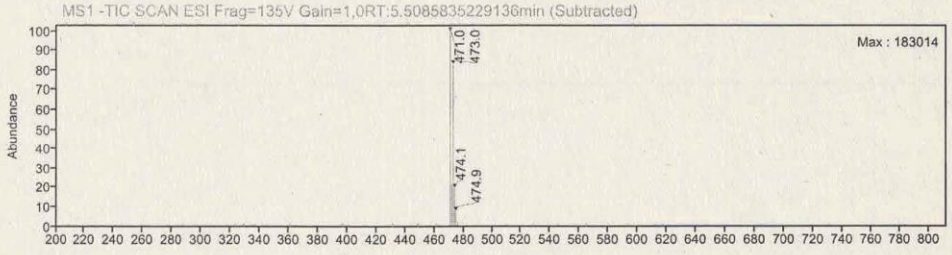
RT [min]	Peak MS Base Peak m/z	Area	Area%	Max Peak%	Height
5.505	471.000	821367.0807	100.0000	100.000	188443.556
	Sum	821367.0807			

Signal: MS1 -TIC SCAN ESI Frag=135V Gain=1,0

RT [min]	Peak MS Base Peak m/z	Area	Area%	Max Peak%	Height
4.304	472.900	61462.9827	1.6588	1.721	19105.711
5.021	393.000	73113.9222	1.9732	2.048	19385.016
5.509	471.000	3570714.9867	96.3680	100.000	818518.043
	Sum	3705291.8916			

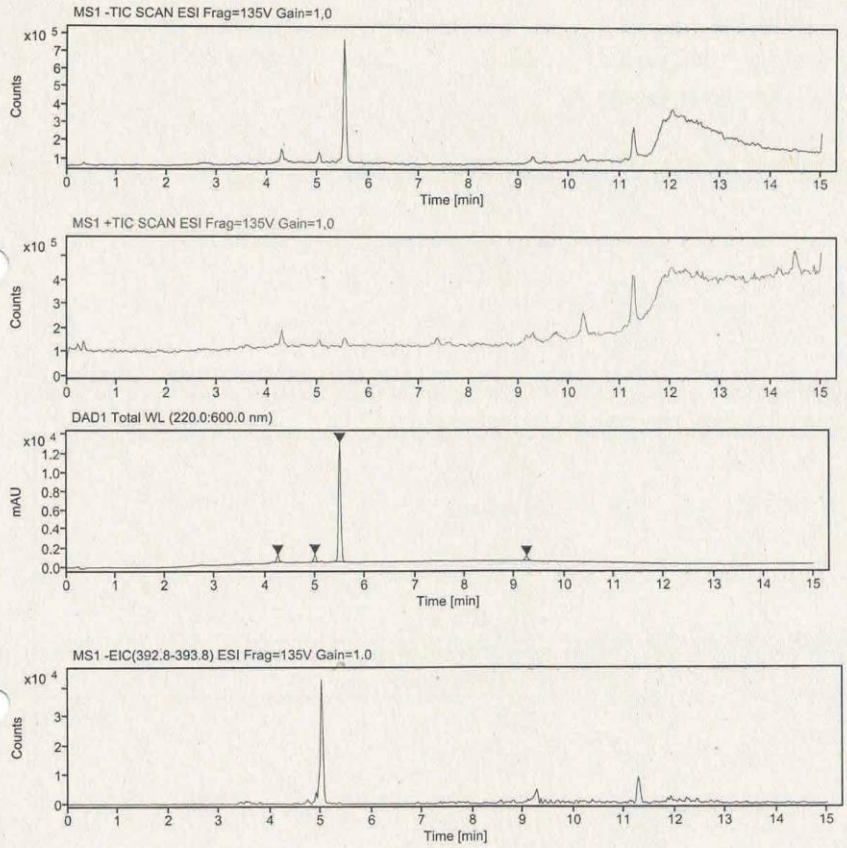






VIII-1h

Sequence Name:	SingleSample		
Data file:	HALP160-1h.dx	**Project Name:**	Single Quad
Sample name:	HALP160-1h	**Operator :**	SYSTEM
Instrument:	Single Quad	**Acquired on:**	2022-01-03 08:44:30+01:00
Inj. volume:	5.000	**Location:**	P2-A6
Acq. method:	00-new_wasser-acn_standard_100-1000_BD-20min.amx		
Processing method:	MS_standard_plot.pmx		



Signal: DAD1 Total WL (220.0:600.0 nm)

RT [min]	Peak MS Base Peak m/z	Area	Area%	Max Peak%	Height
4.249		2325.0842	4.7225	5.427	685.124
4.994		2325.5780	4.7235	5.429	754.071
5.488		42839.2980	87.0118	100.000	12534.434
9.247		1743.9153	3.5421	4.071	424.659
	Sum	49233.8755			

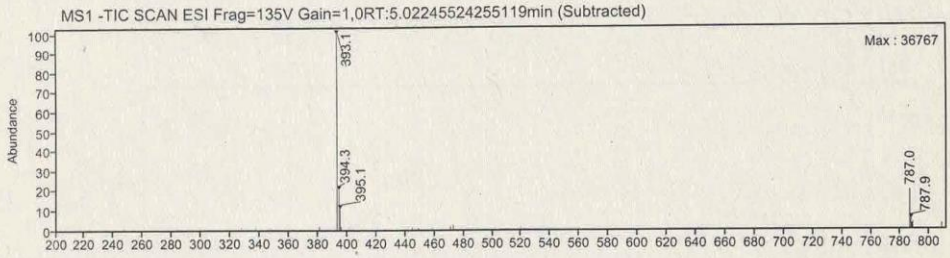
Signal: DAD1A,Sig=254,4 Ref=360,100

RT [min]	Peak MS Base Peak m/z	Area	Area%	Max Peak%	Height
5.488		632.6454	100.0000	100.000	186.425
	Sum	632.6454			

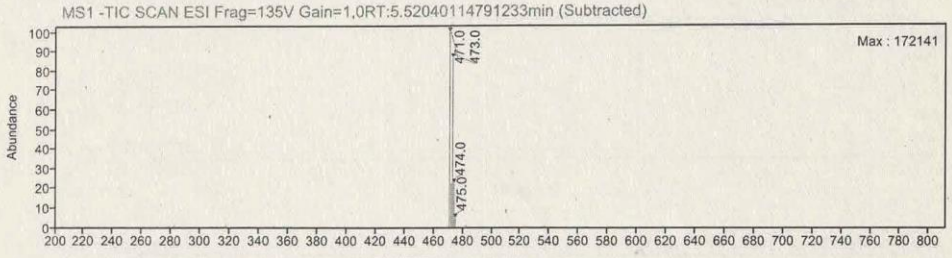
Signal: MS1 -TIC SCAN ESI Frag=135V Gain=1,0

RT [min]	Peak MS Base Peak m/z	Area	Area%	Max Peak%	Height
5.022	393.100	192013.4897	7.1730	8.130	57957.804
5.520	471.000	2361921.1143	88.2338	100.000	691697.289
9.277	391.100	122955.3389	4.5932	5.206	31391.634
	Sum	2676889.9428			

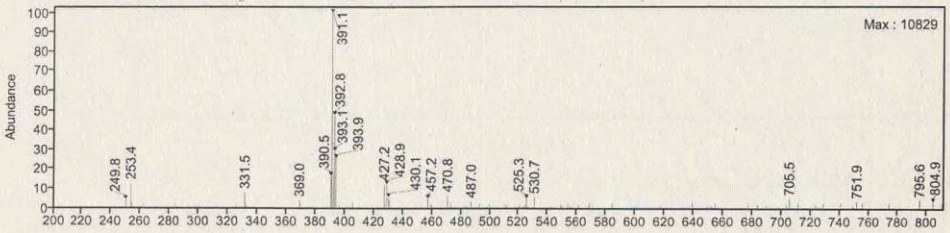
MS1 -TIC SCAN ESI Frag=135V Gain=1,0RT:5.02245524255119min (Subtracted)



MS1 -TIC SCAN ESI Frag=135V Gain=1,0RT:5.52040114791233min (Subtracted)

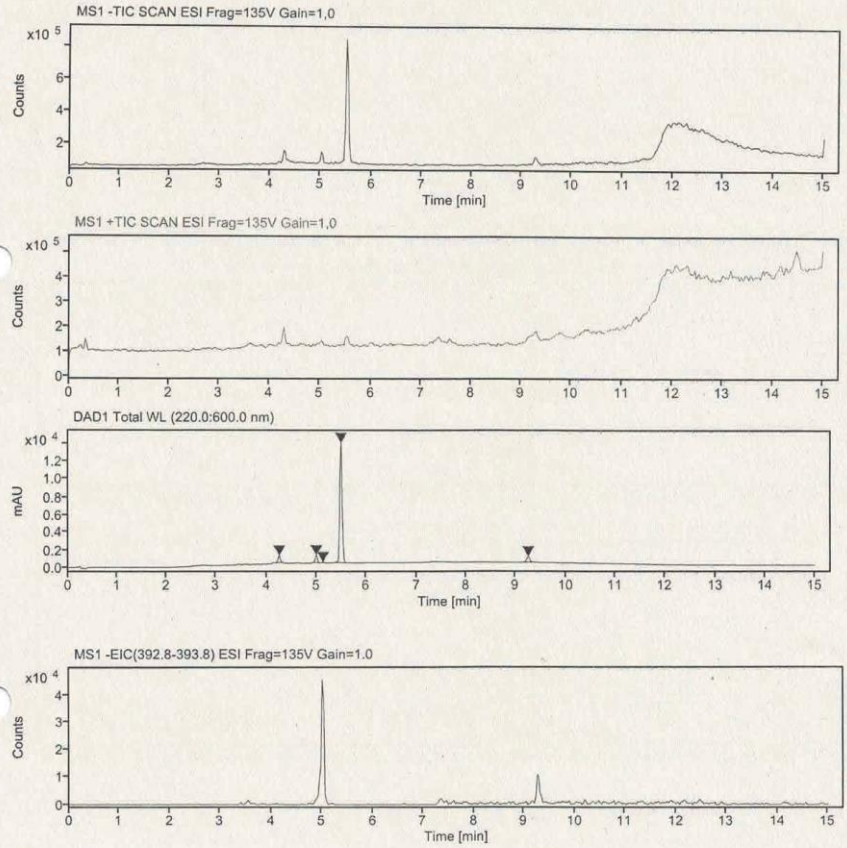


MS1 -TIC SCAN ESI Frag=135V Gain=1,0RT:9.27722449445695min (Subtracted)



VIII-2h

Sequence Name:	SingleSample		
Data file:	HALP160-2h.dx	**Project Name:**	Single Quad
Sample name:	HALP160-2h	**Operator :**	SYSTEM
Instrument:	Single Quad	**Acquired on:**	2022-01-03 09:05:30+01:00
Inj. volume:	5.000	**Location:**	P2-A7
Acq. method:	00-new_wasser-acn_standard_100-1000_BD-20min.amx		
Processing method:	MS_standard_plot.pmx		



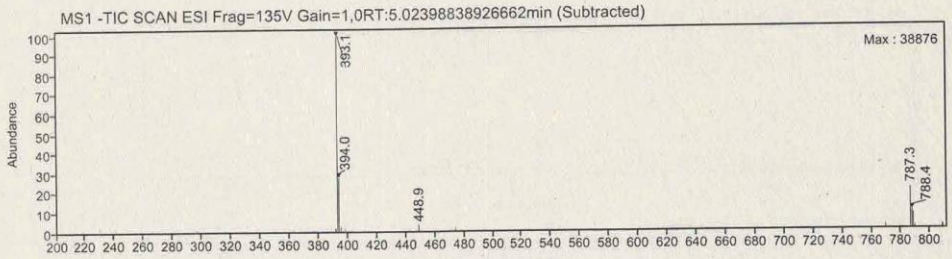
Signal: DAD1 Total WL (220.0:600.0 nm)

RT [min]	Peak MS Base Peak m/z	Area	Area%	Max Peak%	Height
4.249		2351.5986	4.3118	5.038	740.733
4.994		2554.2143	4.6833	5.472	834.355
5.127		152.7772	0.2801	0.327	61.133
5.487		46680.2102	85.5914	100.000	13504.106
9.254		2799.6613	5.1334	5.998	624.950
	Sum	54538.4615			

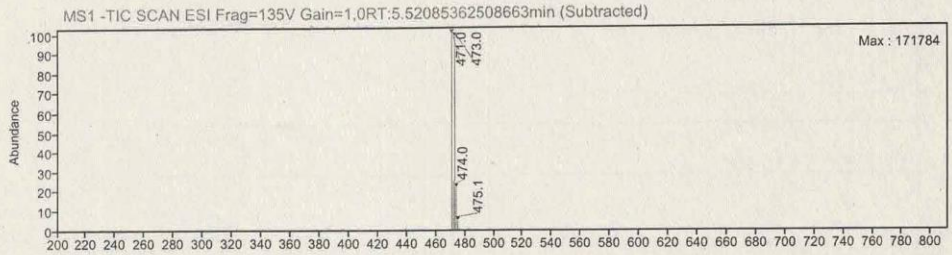
Signal: MS1 -TIC SCAN ESI Frag=135V Gain=1,0

RT [min]	Peak MS Base Peak m/z	Area	Area%	Max Peak%	Height
5.024	393.100	214266.9713	6.7326	7.721	68592.774
5.521	471.000	2775014.4126	87.1948	100.000	778947.343
9.284	393.100	193263.7676	6.0726	6.964	43397.370
	Sum	3182545.1515			

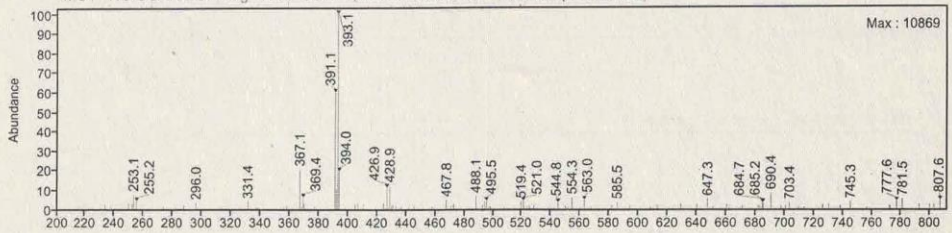
MS1 -TIC SCAN ESI Frag=135V Gain=1,0RT:5.02398838926662min (Subtracted)



MS1 -TIC SCAN ESI Frag=135V Gain=1,0RT:5.52085362508663min (Subtracted)

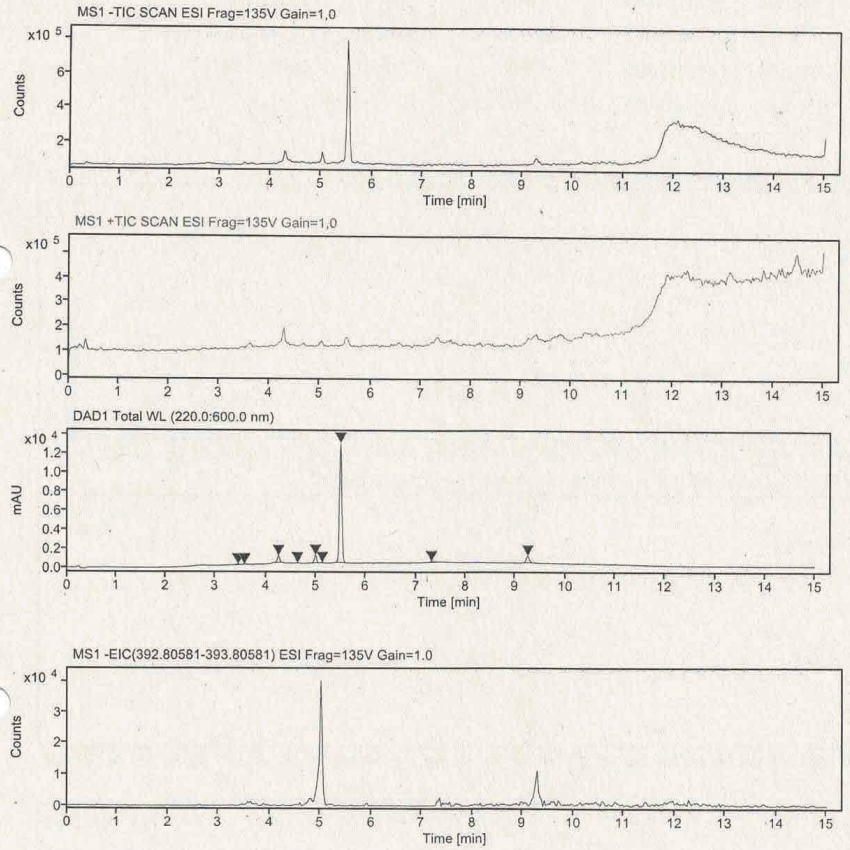


MS1 -TIC SCAN ESI Frag=135V Gain=1,0RT:9.28350517524406min (Subtracted)



VIII-3h

Sequence Name:	SingleSample		
Data file:	HALP160-3h.dx	**Project Name:**	Single Quad
Sample name:	HALP160-3h	**Operator :**	SYSTEM
Instrument:	Single Quad	**Acquired on:**	2022-01-03 09:26:31+01:00
Inj. volume:	5.000	**Location:**	P2-A8
Acq. method:	00-new_wasser-acn_standard_100-1000_BD-20min.amx		
Processing method:	MS_standard_plot.pmx		



Signal: DAD1 Total WL (220.0:600.0 nm)

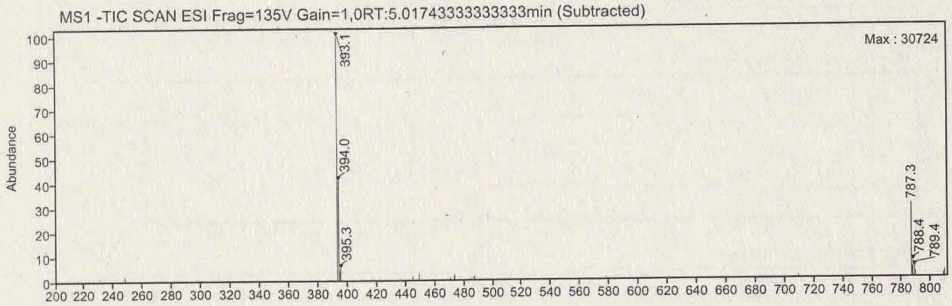
RT [min]	Peak MS Base Peak m/z	Area	Area%	Max Peak%	Height
3.445		200.2325	0.3825	0.464	67.013
3.572		114.9357	0.2195	0.266	36.782
4.248		2279.6722	4.3544	5.282	711.540
4.626		45.3860	0.0867	0.105	22.269
4.991		2554.9983	4.8802	5.920	805.615
5.125		176.5197	0.3372	0.409	64.915
5.488		43158.5007	82.4361	100.000	12614.158

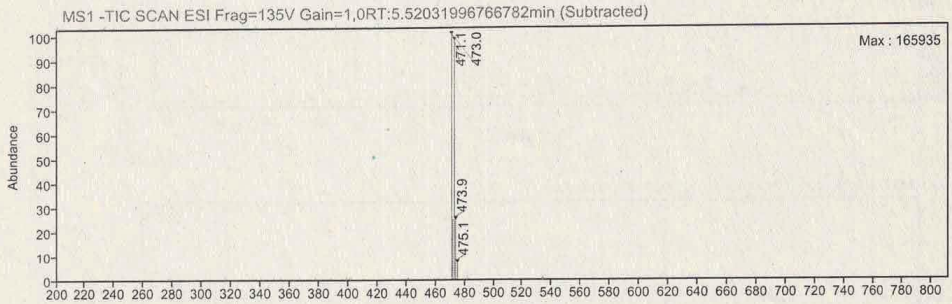
D:\CDSProjects\Default\0-standardplot+EIC.rdl [Rev. 4450] Printed: 2022-01-03 12:30:39+01:00 Page 1 of 2

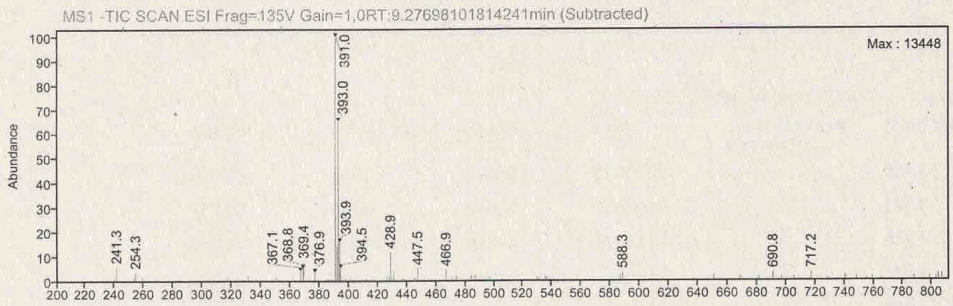
RT [min]	Peak MS Base Peak m/z	Area	Area%	Max Peak%	Height
7.314		636.8369	1.2164	1.476	94.542
9.251		3186.7928	6.0870	7.384	714.173
	Sum	52353.8748			

Signal: MS1 -TIC SCAN ESI Frag=135V Gain=1,0

RT [min]	Peak MS Base Peak m/z	Area	Area%	Max Peak%	Height
5.017	393.100	192213.1623	6.8714	7.652	66502.575
5.520	471.100	2511803.3417	89.7935	100.000	726670.006
9.277	391.000	93293.3982	3.3351	3.714	28076.687
	Sum	2797309.9021			

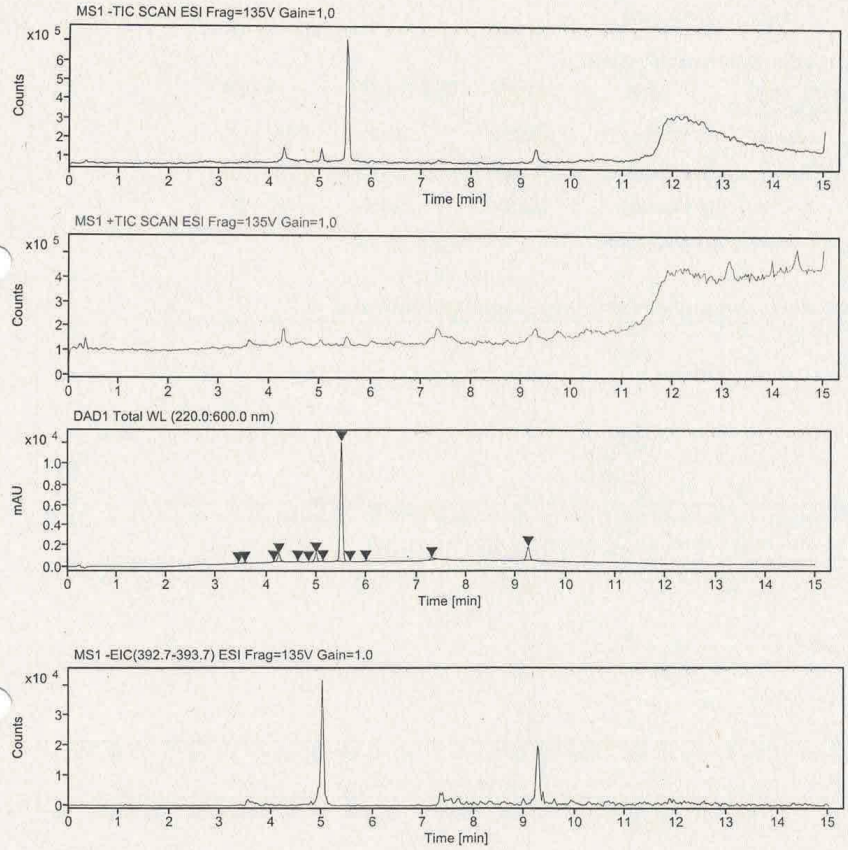






VIII-4h

Sequence Name:	SingleSample		
Data file:	HALP160-4h.dx	**Project Name:**	Single Quad
Sample name:	HALP160-4h	**Operator :**	SYSTEM
Instrument:	Single Quad	**Acquired on:**	2022-01-03 09:47:32+01:00
Inj. volume:	5.000	**Location:**	P2-A9
Acq. method:	00-new_wasser-acn_standard_100-1000_BD-20min.amx		
Processing method:	MS_standard_plot.pmx		



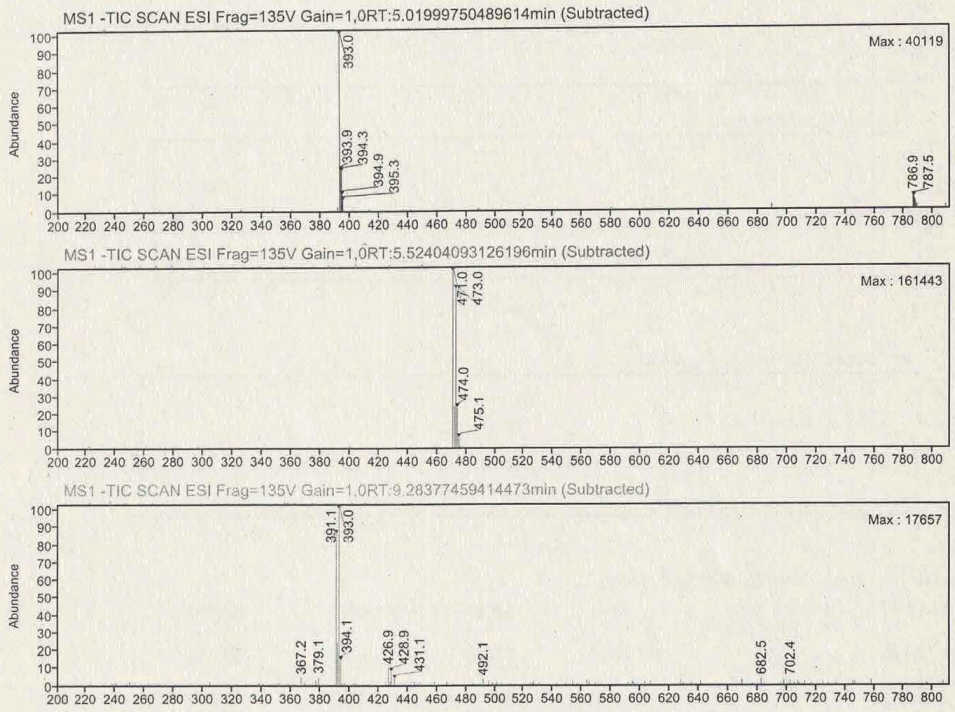
Signal: DAD1 Total WL (220.0:600.0 nm)

RT [min]	Peak MS Base Peak m/z	Area	Area%	Max Peak%	Height
3.440		207.8633	0.3889	0.519	69.719
3.568		382.6019	0.7158	0.956	91.939
4.141		174.9589	0.3273	0.437	65.304
4.245		2541.4017	4.7546	6.348	721.445
4.620		160.3234	0.2999	0.400	58.301
4.838		14.7624	0.0276	0.037	6.949
4.990		2750.0964	5.1450	6.869	836.594

RT [min]	Peak MS Base Peak m/z	Area	Area%	Max Peak%	Height
5.126		212.6205	0.3978	0.531	72.688
5.492	471.000	40037.7789	74.9051	100.000	11664.414
5.665		14.9769	0.0280	0.037	13.427
5.982		68.2218	0.1276	0.170	23.346
7.307		1159.3644	2.1690	2.896	211.611
9.247		5726.3454	10.7132	14.302	1304.157
	Sum	53451.3158			

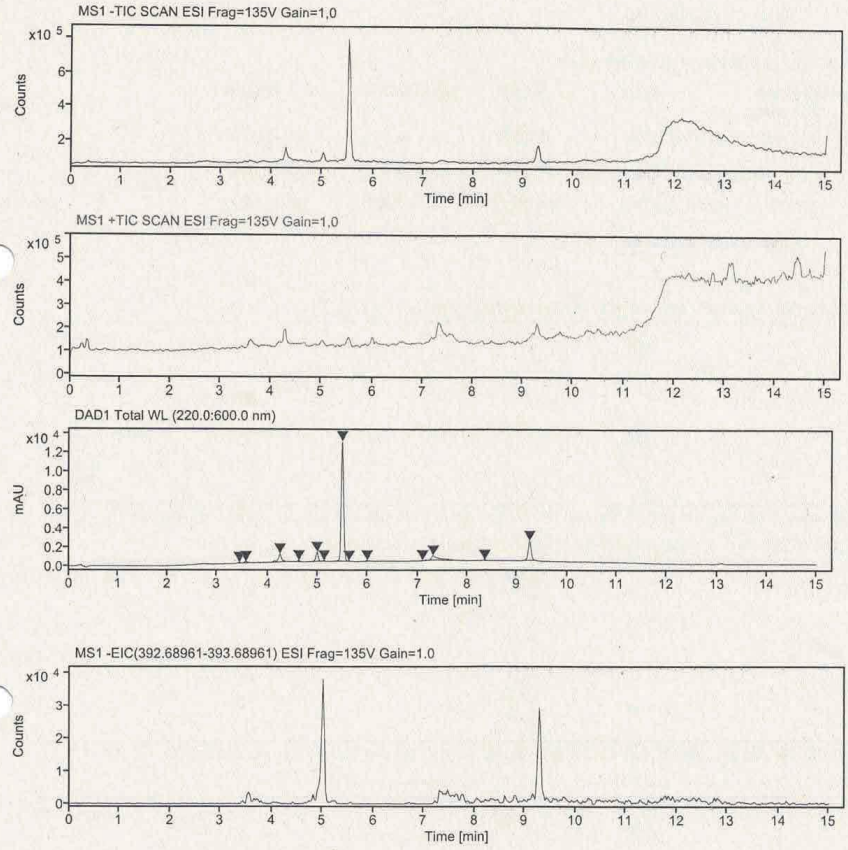
Signal: MS1 -TIC SCAN ESI Frag=135V Gain=1,0

RT [min]	Peak MS Base Peak m/z	Area	Area%	Max Peak%	Height
5.020	393.000	179797.2657	6.0714	7.131	65822.580
5.524	471.000	2521389.2866	85.1427	100.000	670029.925
9.284	391.100	260183.1650	8.7859	10.319	60264.043
	Sum	2961369.7174			



VIII-5h

Sequence Name:	SingleSample		
Data file:	HALP160-5h.dx	**Project Name:**	Single Quad
Sample name:	HALP160-5h	**Operator :**	SYSTEM
Instrument:	Single Quad	**Acquired on:**	2022-01-03 10:08:32+01:00
Inj. volume:	5.000	**Location:**	P2-A10
Acq. method:	00-new_wasser-acn_standard_100-1000_BD-20min.amx		
Processing method:	MS_standard_plot.pmx		



Signal: DAD1 Total WL (220.0:600.0 nm)

RT [min]	Peak MS Base Peak m/z	Area	Area%	Max Peak%	Height
3.435		284.0551	0.4319	0.645	90.487
3.566		678.3179	1.0315	1.540	142.127
4.242		3772.5263	5.7366	8.567	836.641
4.620		338.9259	0.5154	0.770	95.103
4.988		3041.2522	4.6246	6.906	942.833
5.125		114.6128	0.1743	0.260	64.360
5.490		44036.1346	66.9627	100.000	12703.899

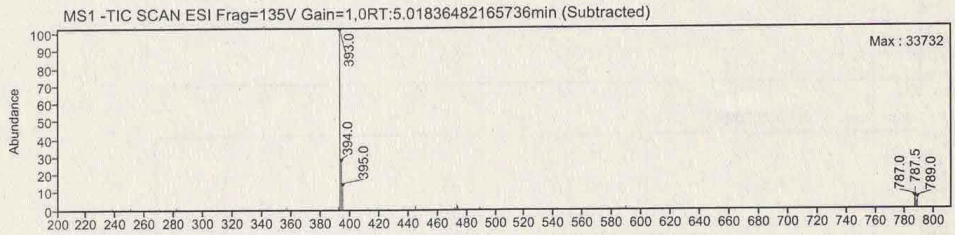
D:\CDSProjects\Default\0-standardplot+EIC.rdl [Rev. 4451] Printed: 2022-01-03 12:32:56+01:00 Page 1 of 2

RT [min]	Peak MS Base Peak m/z	Area	Area%	Max Peak%	Height
5.622		2.5678	0.0039	0.006	14.779
5.985		277.8459	0.4225	0.631	61.825
7.099		99.2600	0.1509	0.225	22.515
7.311		4493.7017	6.8333	10.205	441.617
8.347		124.0269	0.1886	0.282	38.954
9.255		8498.9161	12.9237	19.300	1995.321
	Sum	65762.1432			

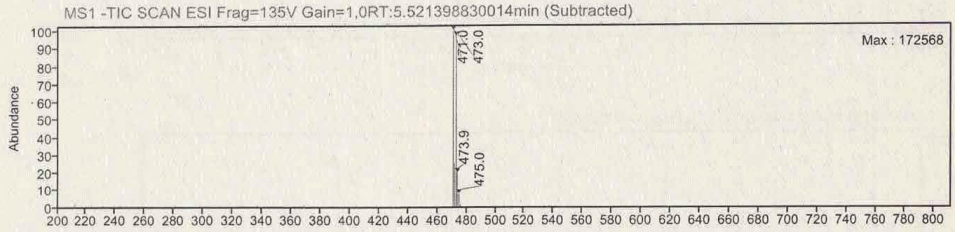
Signal: MS1 -TIC SCAN ESI Frag=135V Gain=1,0

RT [min]	Peak MS Base Peak m/z	Area	Area%	Max Peak%	Height
5.018	393.000	173947.6376	5.3893	6.693	51384.586
5.521	473.000	2598794.4847	80.5174	100.000	733476.822
9.292	391.300	454878.2477	14.0933	17.503	95514.299
	Sum	3227620.3699			

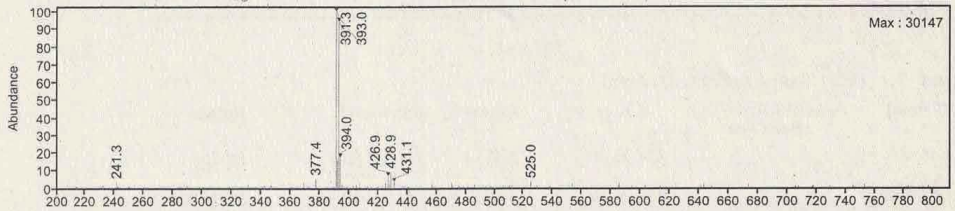
MS1 -TIC SCAN ESI Frag=135V Gain=1,0RT:5.01836482165736min (Subtracted)



MS1 -TIC SCAN ESI Frag=135V Gain=1,0RT:5.521398830014min (Subtracted)

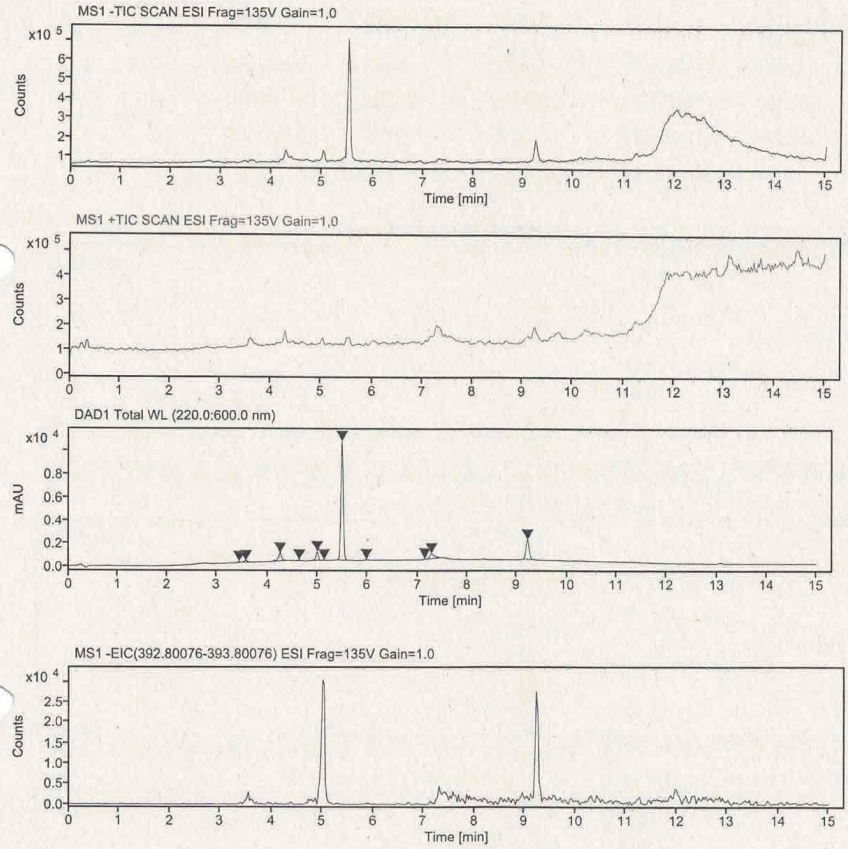


MS1 -TIC SCAN ESI Frag=135V Gain=1,0RT:9.29187632257362min (Subtracted)



VIII-6h

Sequence Name:	SingleSample		
Data file:	HALP160-6h.dx	**Project Name:**	Single Quad
Sample name:	HALP160-6h	**Operator :**	SYSTEM
Instrument:	Single Quad	**Acquired on:**	2022-01-03 10:29:32+01:00
Inj. volume:	5.000	**Location:**	P2-A11
Acq. method:	00-new_wasser-acn_standard_100-1000_BD-20min.amx		
Processing method:	MS_standard_plot.pmx		



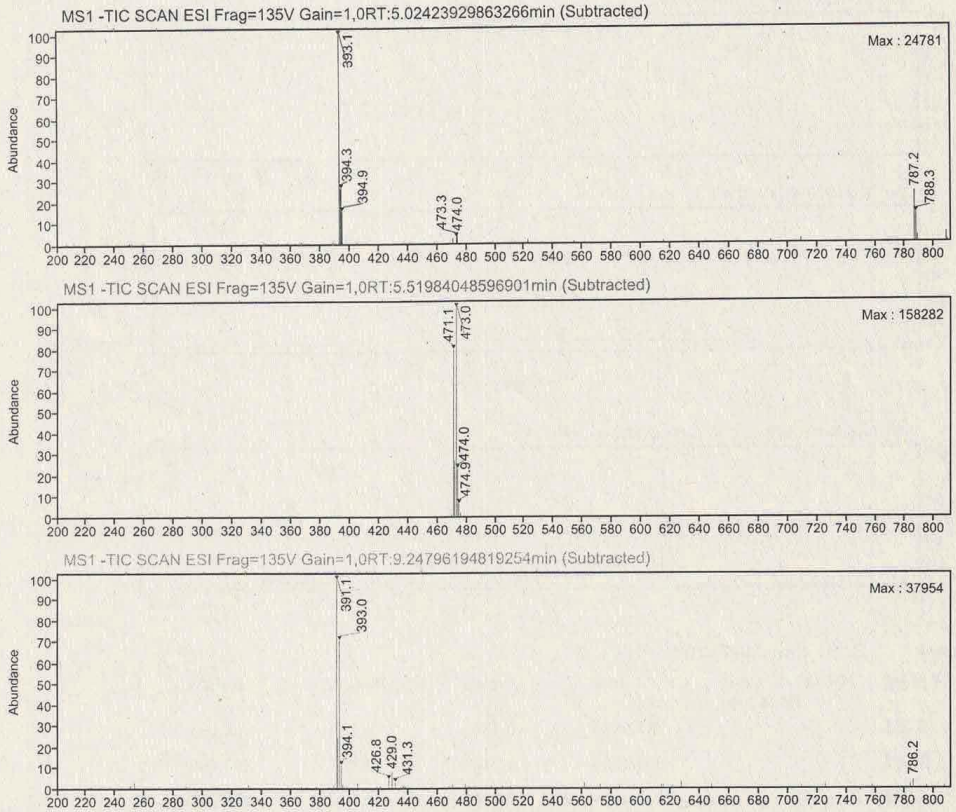
Signal: DAD1 Total WL (220.0:600.0 nm)

RT [min]	Peak MS Base Peak m/z	Area	Area%	Max Peak%	Height
3.438		187.9133	0.3584	0.533	65.001
3.567		639.1246	1.2190	1.811	136.463
4.249		3133.3524	5.9761	8.880	671.577
4.630		191.4814	0.3652	0.543	61.152
4.994		2495.7478	4.7601	7.073	761.816
5.129		127.9717	0.2441	0.363	49.556
5.486	473.000	35286.8033	67.3014	100.000	10263.028

RT [min]	Peak MS Base Peak m/z	Area	Area%	Max Peak%	Height
5.975		117.9012	0.2249	0.334	36.828
7.146		102.0190	0.1946	0.289	29.496
7.282		2835.0943	5.4073	8.034	412.330
9.216		7313.5715	13.9490	20.726	1655.001
	Sum	52430.9804			

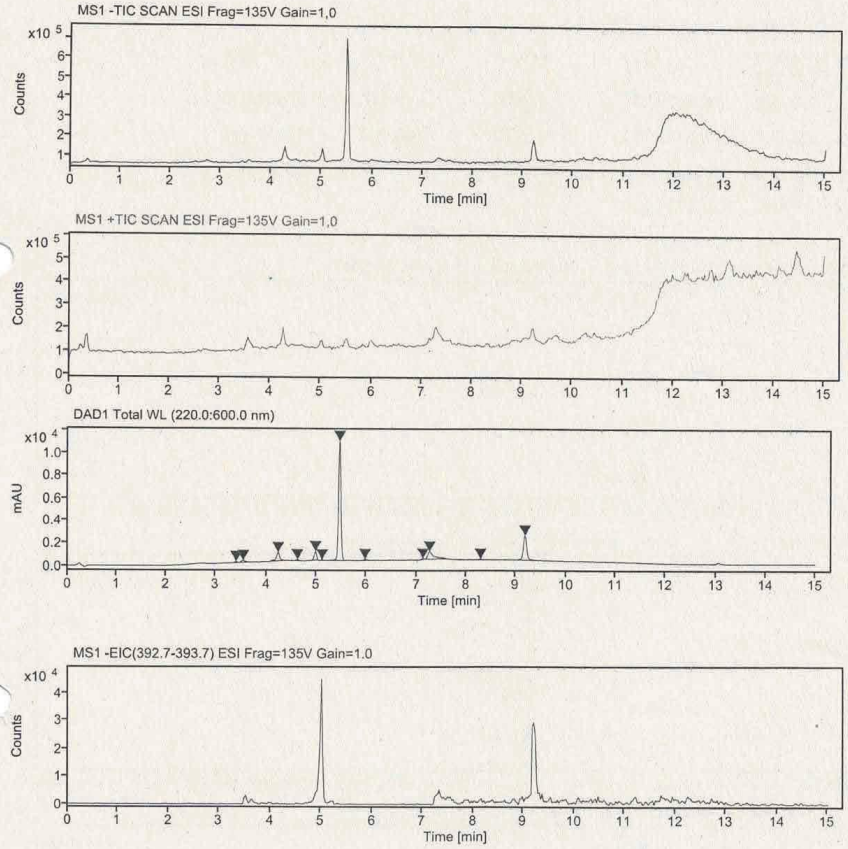
Signal: MS1 -TIC SCAN ESI Frag=135V Gain=1,0

RT [min]	Peak MS Base Peak m/z	Area	Area%	Max Peak%	Height
5.024	393.100	164527.3002	5.4811	7.022	50262.263
5.520	473.000	2343088.0879	78.0581	100.000	637103.107
9.248	391.100	494106.6907	16.4608	21.088	110043.440
	Sum	3001722.0787			



VIII-7h

Sequence Name:	SingleSample		
Data file:	HALP160-7h.dx	**Project Name:**	Single Quad
Sample name:	HALP160-7h	**Operator :**	SYSTEM
Instrument:	Single Quad	**Acquired on:**	2022-01-03 10:50:31+01:00
Inj. volume:	5.000	**Location:**	P2-B1
Acq. method:	00-new_wasser-acn_standard_100-1000_BD-20min.amx		
Processing method:	MS_standard_plot.pmx		



Signal: DAD1 Total WL (220.0:600.0 nm)

RT [min]	Peak MS Base Peak m/z	Area	Area%	Max Peak%	Height
3.401		298.7031	0.5000	0.827	88.241
3.539		885.0996	1.4815	2.452	168.912
4.234		3392.8255	5.6789	9.399	737.467
4.617		293.3085	0.4909	0.813	82.934
4.983	393.000	2286.8171	3.8277	6.335	745.043
5.115		156.0600	0.2612	0.432	54.468
5.461	473.000	36098.2364	60.4209	100.000	10556.870

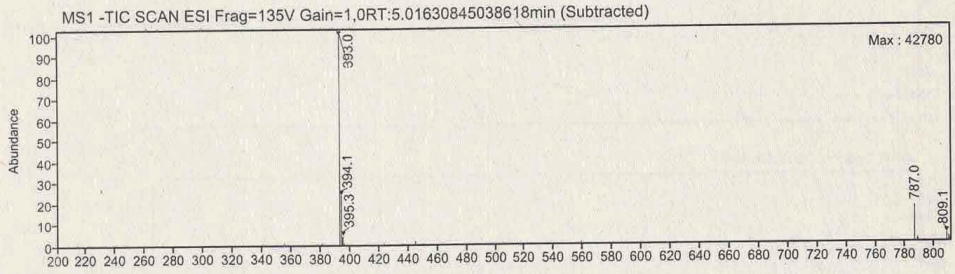
D:\CDSProjects\Default\0-standardplot+EIC.rdl [Rev. 4452] Printed: 2022-01-03 12:38:25+01:00 Page 1 of 2

RT [min]	Peak MS Base Peak m/z	Area	Area%	Max Peak%	Height
5.970		402.4567	0.6736	1.115	85.217
7.130		119.1349	0.1994	0.330	40.185
7.266		5603.2325	9.3786	15.522	623.367
8.287		186.2927	0.3118	0.516	48.607
9.187	391.100	10022.4251	16.7755	27.764	2131.934
	Sum	59744.5921			

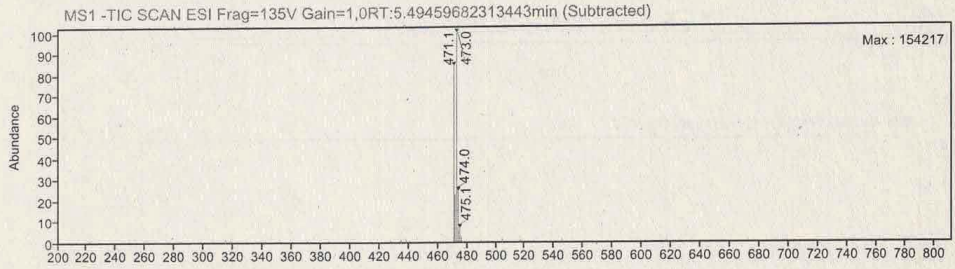
Signal: MS1 -TIC SCAN ESI Frag=135V Gain=1,0

RT [min]	Peak MS Base Peak m/z	Area	Area%	Max Peak%	Height
5.016	393.000	248657.5832	8.2450	10.817	67638.610
5.495	473.000	2298818.9795	76.2243	100.000	642557.442
9.216	391.100	468386.4009	15.5308	20.375	103888.310
	Sum	3015862.9636			

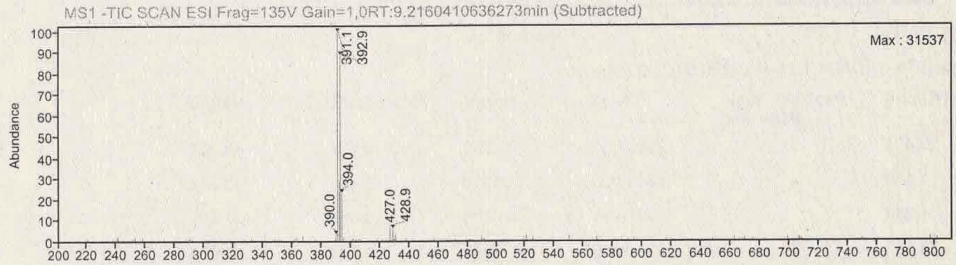
MS1 -TIC SCAN ESI Frag=135V Gain=1,0RT:5.01630845038618min (Subtracted)



MS1 -TIC SCAN ESI Frag=135V Gain=1,0RT:5.49459682313443min (Subtracted)

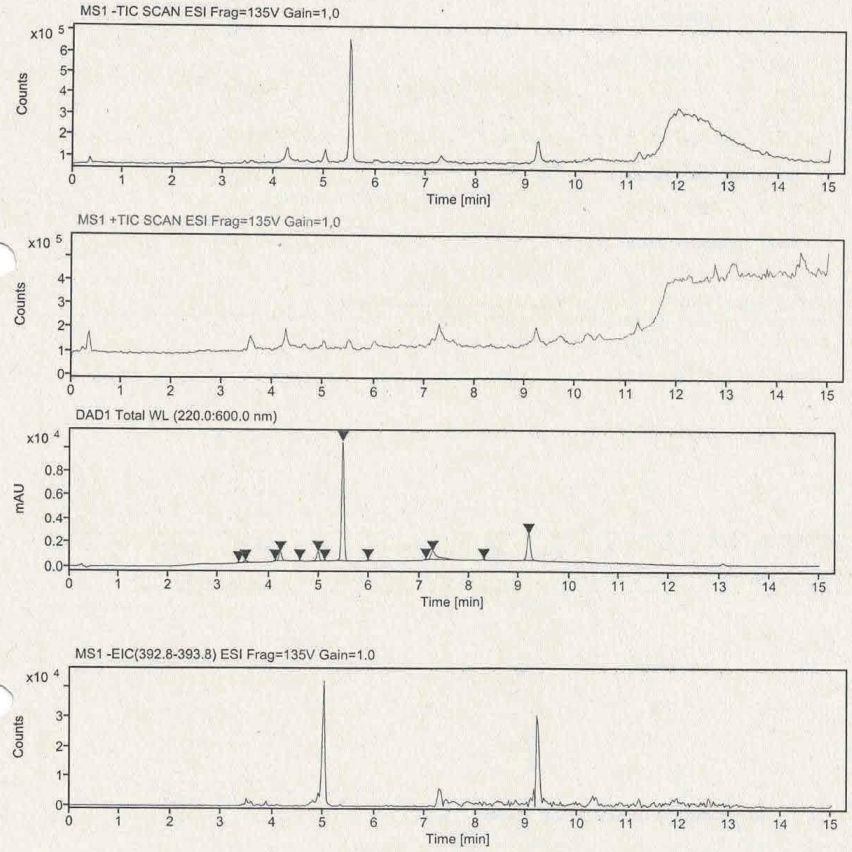


MS1 -TIC SCAN ESI Frag=135V Gain=1,0RT:9.2160410636273min (Subtracted)



VIII-8h

Sequence Name:	SingleSample		
Data file:	HALP160-8h.dx	**Project Name:**	Single Quad
Sample name:	HALP160-8h	**Operator :**	SYSTEM
Instrument:	Single Quad	**Acquired on:**	2022-01-03 11:11:31+01:00
Inj. volume:	5.000	**Location:**	P2-B2
Acq. method:	00-new_wasser-acn_standard_100-1000_BD-20min.amx		
Processing method:	MS_standard_plot.pmx		



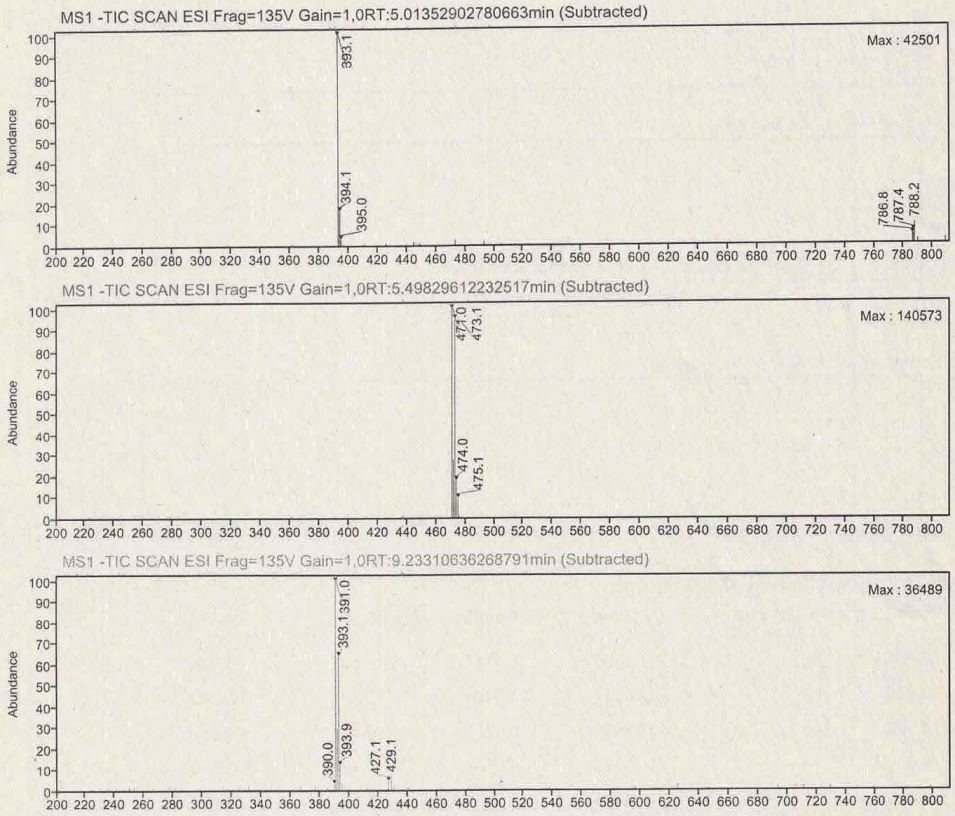
Signal: DAD1 Total WL (220.0:600.0 nm)

RT [min]	Peak MS Base Peak m/z	Area	Area%	Max Peak%	Height
3.401		241.4356	0.4117	0.692	78.326
3.535		789.9567	1.3469	2.264	156.446
4.122		139.9996	0.2387	0.401	49.061
4.228		2720.5147	4.6387	7.797	729.500
4.611		230.4944	0.3930	0.661	67.807
4.979		2577.8993	4.3955	7.388	765.786
5.112		168.1826	0.2868	0.482	60.332

RT [min]	Peak MS Base Peak m/z	Area	Area%	Max Peak%	Height
5.467		34893.8098	59.4969	100.000	10076.035
5.973		399.2847	0.6808	1.144	91.861
7.132		152.9691	0.2608	0.438	49.094
7.267		6170.0856	10.5205	17.682	662.958
8.293		187.2185	0.3192	0.537	48.951
9.197		9976.3117	17.0104	28.590	2172.657
	Sum	58648.1623			

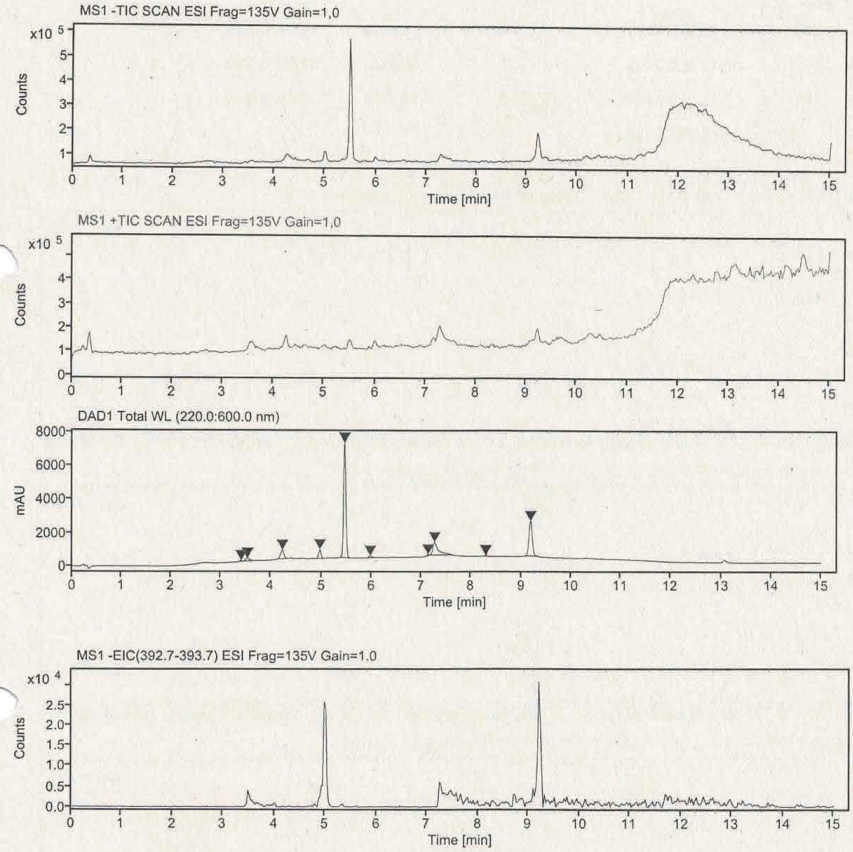
Signal: MS1 -TIC SCAN ESI Frag=135V Gain=1,0

RT [min]	Peak MS Base Peak m/z	Area	Area%	Max Peak%	Height
5.014	393.100	217547.9675	7.3419	9.558	59358.476
5.498	471.000	2276065.4650	76.8140	100.000	624046.072
9.233	391.000	469474.8056	15.8441	20.627	97294.881
	Sum	2963088.2381			



VIII-12h

Sequence Name:	SingleSample		
Data file:	HALP160-12h.dx	**Project Name:**	Single Quad
Sample name:	HALP160-12h	**Operator :**	SYSTEM
Instrument:	Single Quad	**Acquired on:**	2022-01-03 11:32:29+01:00
Inj. volume:	5.000	**Location:**	P2-B3
Acq. method:	00-new_wasser-acn_standard_100-1000_BD-20min.amx		
Processing method:	MS_standard_plot.pmx		



Signal: DAD1 Total WL (220.0:600.0 nm)

RT [min]	Peak MS Base Peak m/z	Area	Area%	Max Peak%	Height
3.405		142.0848	0.3211	0.617	48.820
3.529		883.7645	1.9975	3.837	162.286
4.221		2389.6690	5.4011	10.376	513.278
4.972		1695.5866	3.8323	7.362	511.575
5.463		23031.3436	52.0552	100.000	6820.691
5.974		411.9939	0.9312	1.789	93.188
7.132		194.0594	0.4386	0.843	55.395

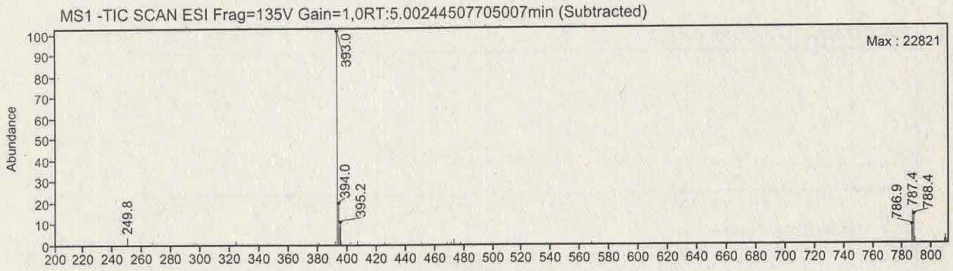
D:\CDSProjects\Default\0-standardplot+EIC.rdl [Rev. 4452] Printed: 2022-01-03 12:40:55+01:00 Page 1 of 2

RT [min]	Peak MS Base Peak m/z	Area	Area%	Max Peak%	Height
7.263		5951.0742	13.4506	25.839	740.249
8.287		104.5079	0.2362	0.454	34.164
9.192	391.100	9439.9788	21.3361	40.988	2098.423
	Sum	44244.0628			

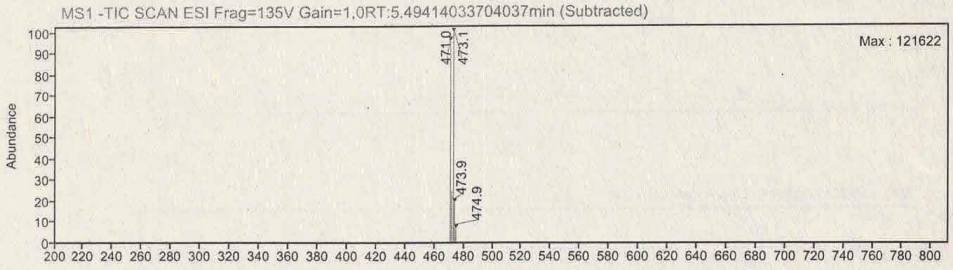
Signal: MS1 -TIC SCAN ESI Frag=135V Gain=1,0

RT [min]	Peak MS Base Peak m/z	Area	Area%	Max Peak%	Height
5.002	393.000	148247.6421	6.3373	8.663	41825.584
5.494	473.100	1711267.5991	73.1538	100.000	510805.750
9.222	391.100	479757.7754	20.5088	28.035	107180.396
	Sum	2339273.0166			

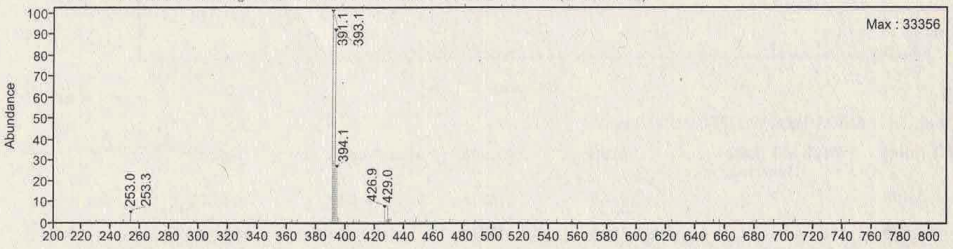
MS1 -TIC SCAN ESI Frag=135V Gain=1,0RT:5.00244507705007min (Subtracted)



MS1 -TIC SCAN ESI Frag=135V Gain=1,0RT:5.49414033704037min (Subtracted)



MS1 -TIC SCAN ESI Frag=135V Gain=1,0RT:9.22246164121551min (Subtracted)

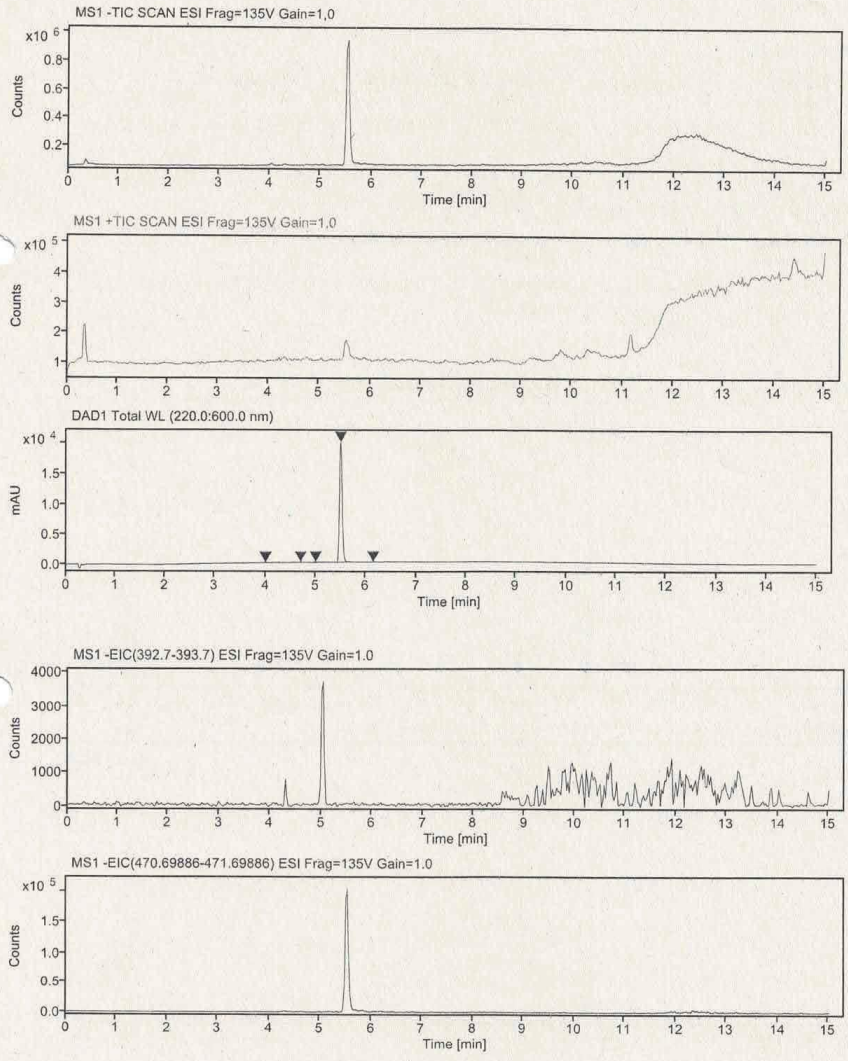


D:\CDSProjects\Default\0-standardplot+EIC.rdl [Rev. 4452] Printed: 2022-01-03 12:40:55+01:00 Page 2 of 2

Trial IX

VIII-7h

Sequence Name:	SingleSample		
Data file:	HALP164-7h.dx	**Project Name:**	Single Quad
Sample name:	HALP164-7h	**Operator :**	SYSTEM
Instrument:	Single Quad	**Acquired on:**	2022-01-17 18:16:19+01:00
Inj. volume:	8.000	**Location:**	P1-A4
Acq. method:	00-new_wasser-acn_standard_100-1000_BD-20min.amx		
Processing method:	MS_standard_plot.pmx		



Signal: DAD1 Total WL (220.0:600.0 nm)

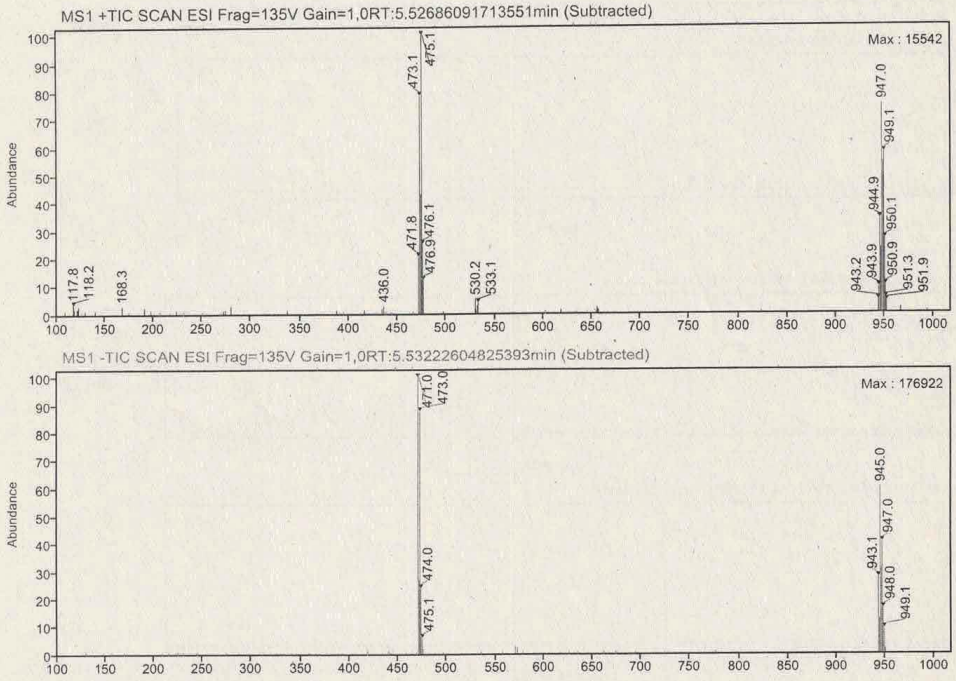
RT [min]	Peak MS Base Peak m/z	Area	Area%	Max Peak%	Height
4.002		106.1957	0.1363	0.137	66.608
4.699		134.8971	0.1731	0.174	37.725
5.001		113.5813	0.1458	0.147	42.017
5.496		77523.3924	99.5062	100.000	19833.976
6.142		30.0142	0.0385	0.039	9.268
	Sum	77908.0807			

Signal: MS1 +TIC SCAN ESI Frag=135V Gain=1,0

RT [min]	Peak MS Base Peak m/z	Area	Area%	Max Peak%	Height
5.527	475.100	342831.7839	100.0000	100.000	61526.561
	Sum	342831.7839			

Signal: MS1 -TIC SCAN ESI Frag=135V Gain=1,0

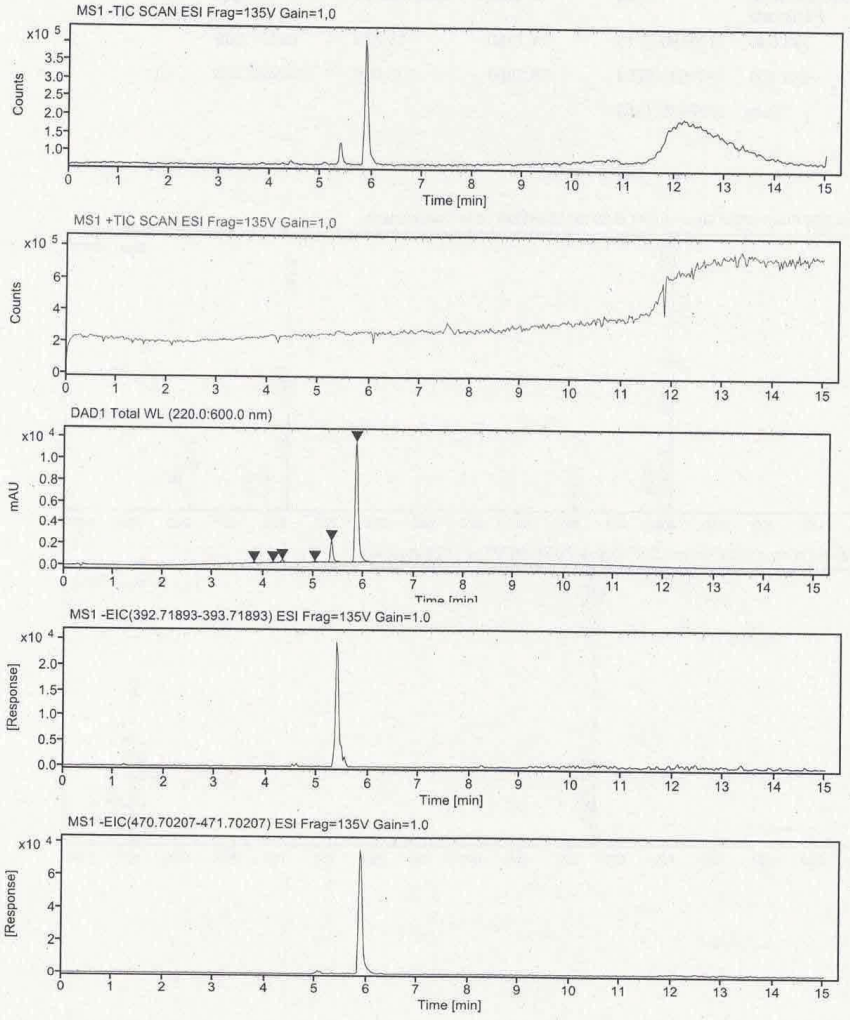
RT [min]	Peak MS Base Peak m/z	Area	Area%	Max Peak%	Height
5.532	471.000	3739875.5903	100.0000	100.000	870847.987
	Sum	3739875.5903			



Trial X

X-20min

Sequence Name:	SingleSample		
Data file:	HALP228-20min.dx	**Project Name:**	Single Quad
Sample name:	HALP228-20min	**Operator :**	SYSTEM
Instrument:	Single Quad	**Acquired on:**	2022-09-15 09:27:49+02:00
Inj. volume:	5.000	**Location:**	P2-D9
Acq. method:	00-new_wasser-acn_standard_100-1000_BD-20min.amx		
Processing method:	MS_standard_plot.pmx		



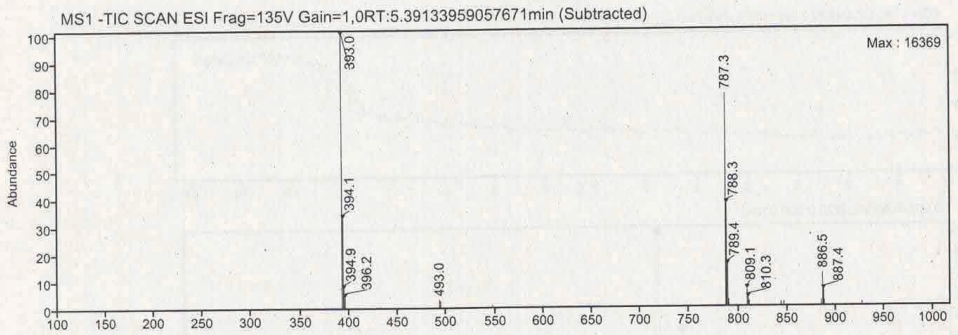
Signal: DAD1 Total WL (220.0:600.0 nm)

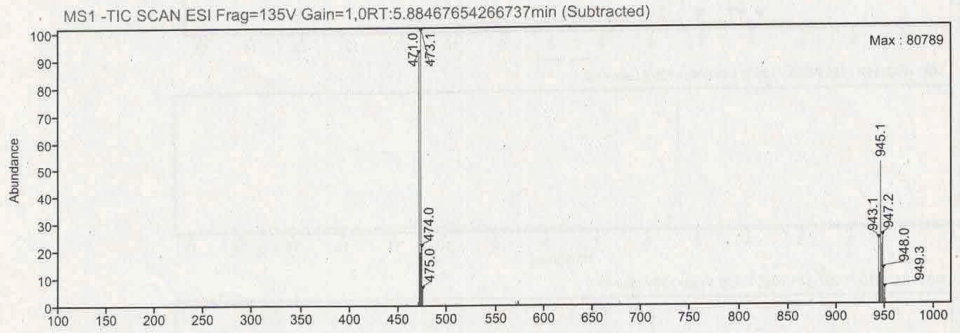
RT [min]	Peak MS Base Peak m/z	Area	Area%	Max Peak%	Height
3.817		265.9017	0.4423	0.524	81.217
4.194		198.9082	0.3309	0.392	59.850
4.376		935.7222	1.5566	1.845	265.310

RT [min]	Peak MS Base Peak m/z	Area	Area%	Max Peak%	Height
5.029		388.3874	0.6461	0.766	66.299
5.359		7618.8316	12.6743	15.026	1982.791
5.852		50704.7296	84.3498	100.000	11303.361
	Sum	60112.4807			

Signal: MS1 -TIC SCAN ESI Frag=135V Gain=1,0

RT [min]	Peak MS Base Peak m/z	Area	Area%	Max Peak%	Height
5.391	393.000	225799.7715	11.7150	13.270	60127.039
5.885	473.100	1701639.9754	88.2850	100.000	360793.778
	Sum	1927439.7469			

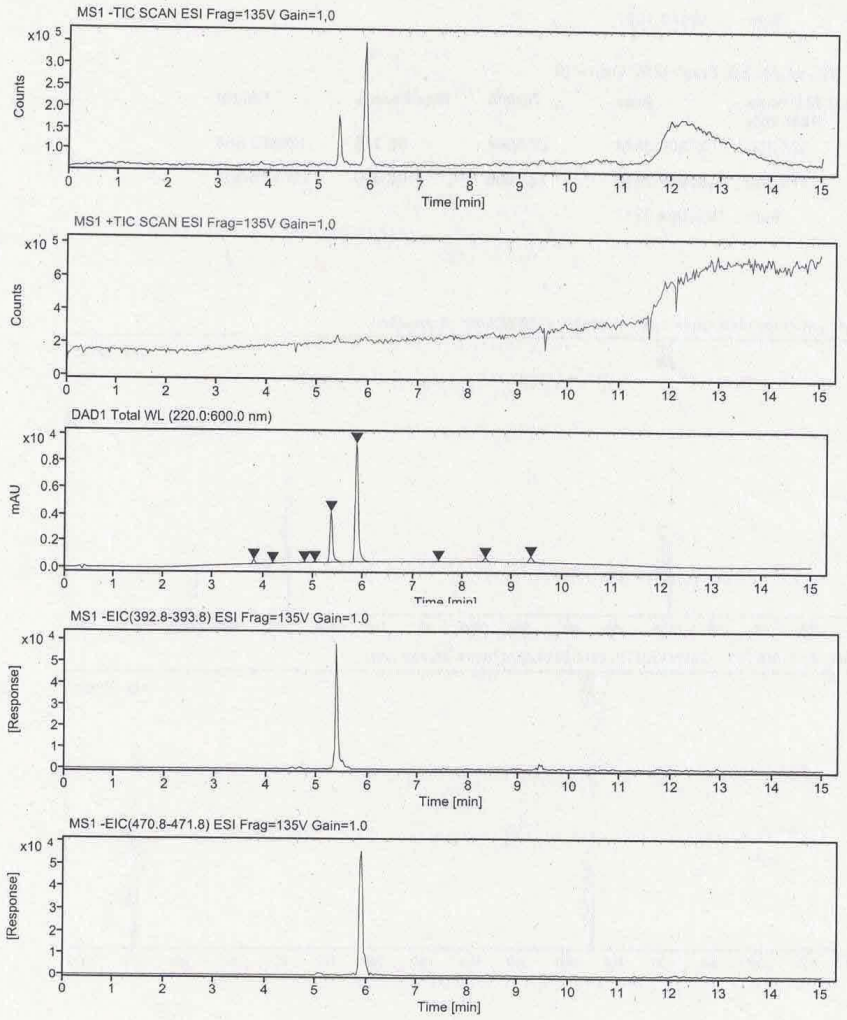




D:\CDSProjects\Default\00-standardplot+EIC.rdl [Rev. 2208] Printed: 2022-09-15 11:09:22+02:00 Page 2 of 2

X-2h

Sequence Name:	SingleSample		
Data file:	HALP228-2h.dx	**Project Name:**	Single Quad
Sample name:	HALP228-2h	**Operator :**	SYSTEM
Instrument:	Single Quad	**Acquired on:**	2022-09-15 10:09:51+02:00
Inj. volume:	5.000	**Location:**	P2-D11
Acq. method:	00-new_wasser-acn_standard_100-1000_BD-20min.amx		
Processing method:	MS_standard_plot.pmx		



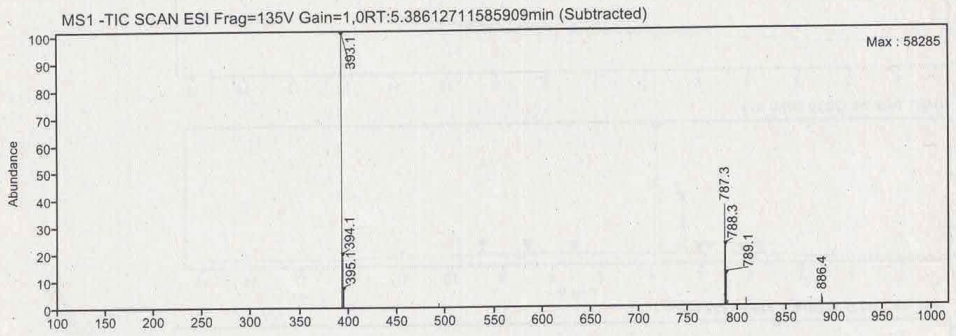
Signal: DAD1 Total WL (220.0:600.0 nm)

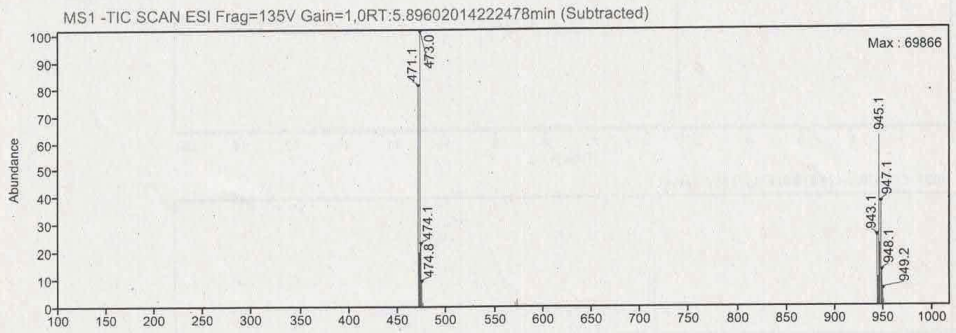
RT [min]	Peak MS Base Peak m/z	Area	Area%	Max Peak%	Height
3.811		1232.8909	2.0739	3.199	331.909
4.187		185.6748	0.3123	0.482	47.776
4.823		196.7529	0.3310	0.511	59.813

	RT [min]	Peak MS Base Peak m/z	Area	Area%	Max Peak%	Height
	5.030		349.9434	0.5887	0.908	62.279
A	5.354	393.100	15220.3017	25.6027	39.497	3873.285
S	5.860		38534.9543	64.8212	100.000	8916.739
	7.512		233.2695	0.3924	0.605	43.144
D	8.453		1371.1773	2.3065	3.558	257.349
E	9.376		2123.1378	3.5714	5.510	389.512
		Sum	59448.1027			

Signal: MS1 -TIC SCAN ESI Frag=135V Gain=1,0

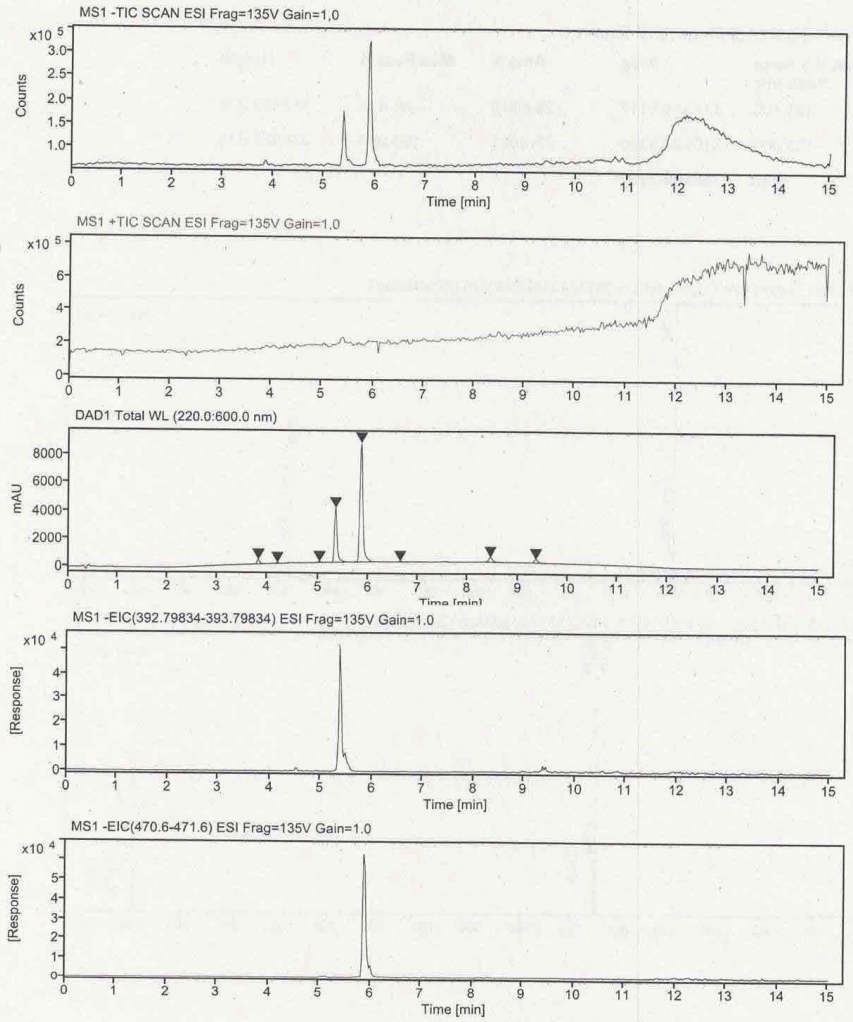
RT [min]	Peak MS Base Peak m/z	Area	Area%	Max Peak%	Height
5.386	393.100	527906.2594	27.5964	38.115	125653.956
5.896	473.000	1385047.7618	72.4036	100.000	291476.901
	Sum	1912954.0212			





X-3h

Sequence Name:	SingleSample		
Data file:	HALP228-3h.dx	**Project Name:**	Single Quad
Sample name:	HALP228-3h	**Operator :**	SYSTEM
Instrument:	Single Quad	**Acquired on:**	2022-09-15 10:30:54+02:00
Inj. volume:	5.000	**Location:**	P2-E1
Acq. method:	00-new_wasser-acn_standard_100-1000_BD-20min.amx		
Processing method:	MS_standard_plot.pmx		



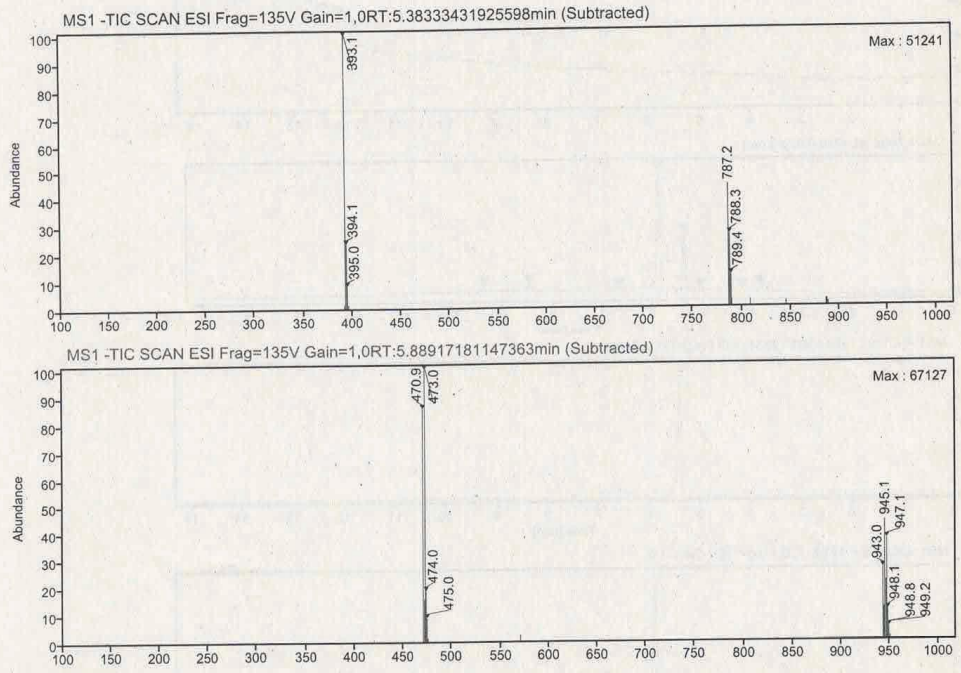
Signal: DAD1 Total WL (220.0:600.0 nm)

RT [min]	Peak MS Base Peak m/z	Area	Area%	Max Peak%	Height
3.815		1164.0588	2.0882	3.257	316.310
4.191		151.4662	0.2717	0.424	48.015
5.032		253.4018	0.4546	0.709	59.408

	RT [min]	Peak MS Base Peak m/z	Area	Area%	Max Peak%	Height
A	5.351		15032.1369	26.9657	42.064	3860.374
S	5.855	473.000	35736.4678	64.1067	100.000	8418.228
	6.641		170.3555	0.3056	0.477	27.264
D	8.448		1872.7959	3.3596	5.241	334.289
E	9.364		1364.6452	2.4480	3.819	249.164
		Sum	55745.3283			

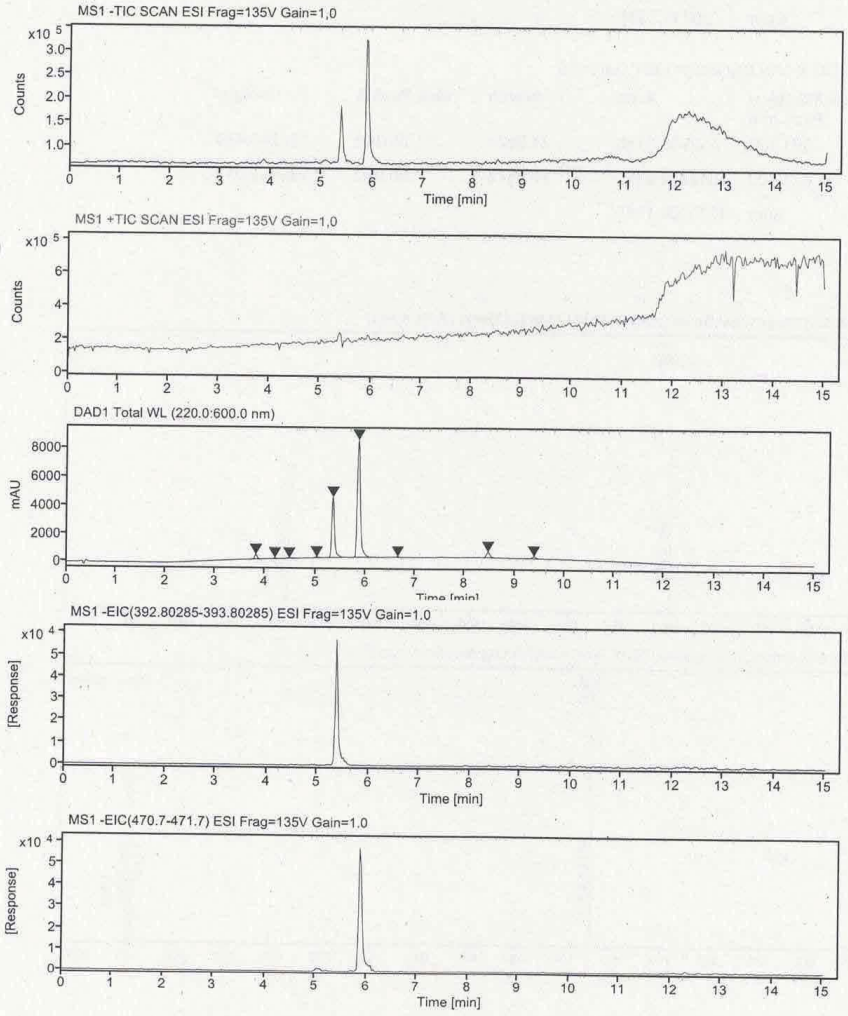
Signal: MS1 -TIC SCAN ESI Frag=135V Gain=1,0

RT [min]	Peak MS Base Peak m/z	Area	Area%	Max Peak%	Height
5.383	393.100	477314.7117	26.6919	36.411	117952.238
5.889	473.000	1310924.5335	73.3081	100.000	276572.839
	Sum	1788239.2452			



x-4h

Sequence Name:	SingleSample		
Data file:	HALP228-4h.dx	**Project Name:**	Single Quad
Sample name:	HALP228-4h	**Operator :**	SYSTEM
Instrument:	Single Quad	**Acquired on:**	2022-09-15 10:51:56+02:00
Inj. volume:	5.000	**Location:**	P2-E2
Acq. method:	00-new_wasser-acn_standard_100-1000_BD-20min.amx		
Processing method:	MS_standard_plot.pmx		



Signal: DAD1 Total WL (220.0:600.0 nm)

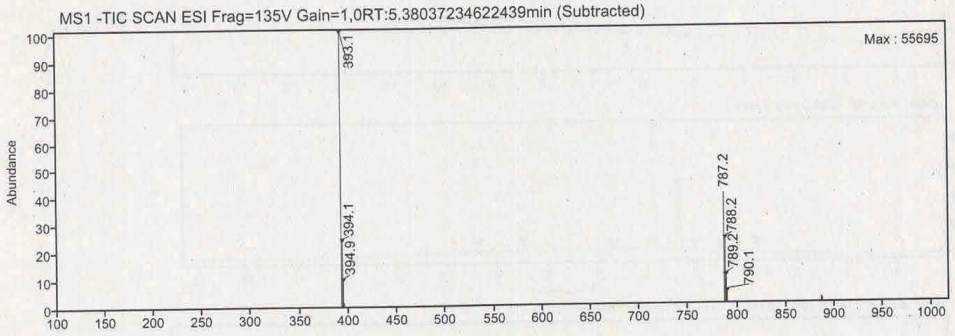
RT [min]	Peak MS Base Peak m/z	Area	Area%	Max Peak%	Height
B 3.810		1193.2340	2.1040	3.405	324.302
4.186		146.7463	0.2588	0.419	45.908
4.474		235.0027	0.4144	0.671	28.204

RT [min]	Peak MS Base Peak m/z	Area	Area%	Max Peak%	Height
5.025		396.9639	0.7000	1.133	72.052
5.347		16616.0339	29.2992	47.410	4258.371
5.856		35047.3413	61.7993	100.000	8237.099
6.646		201.7432	0.3557	0.576	40.300
8.460		2110.3650	3.7212	6.021	393.589
9.387		764.1585	1.3474	2.180	149.413
	Sum	56711.5888			

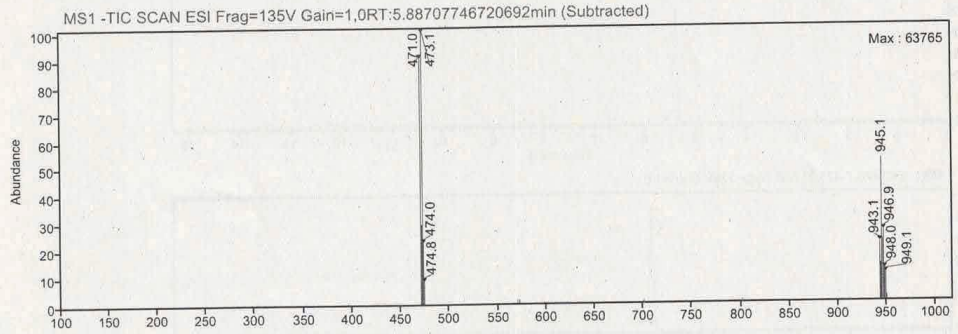
Signal: MS1 -TIC SCAN ESI Frag=135V Gain=1,0

RT [min]	Peak MS Base Peak m/z	Area	Area%	Max Peak%	Height
5.380	393.100	432931.3150	24.9528	33.249	118268.470
5.887	473.100	1302072.8165	75.0472	100.000	289452.019
	Sum	1735004.1315			

MS1 -TIC SCAN ESI Frag=135V Gain=1,0RT:5.38037234622439min (Subtracted)

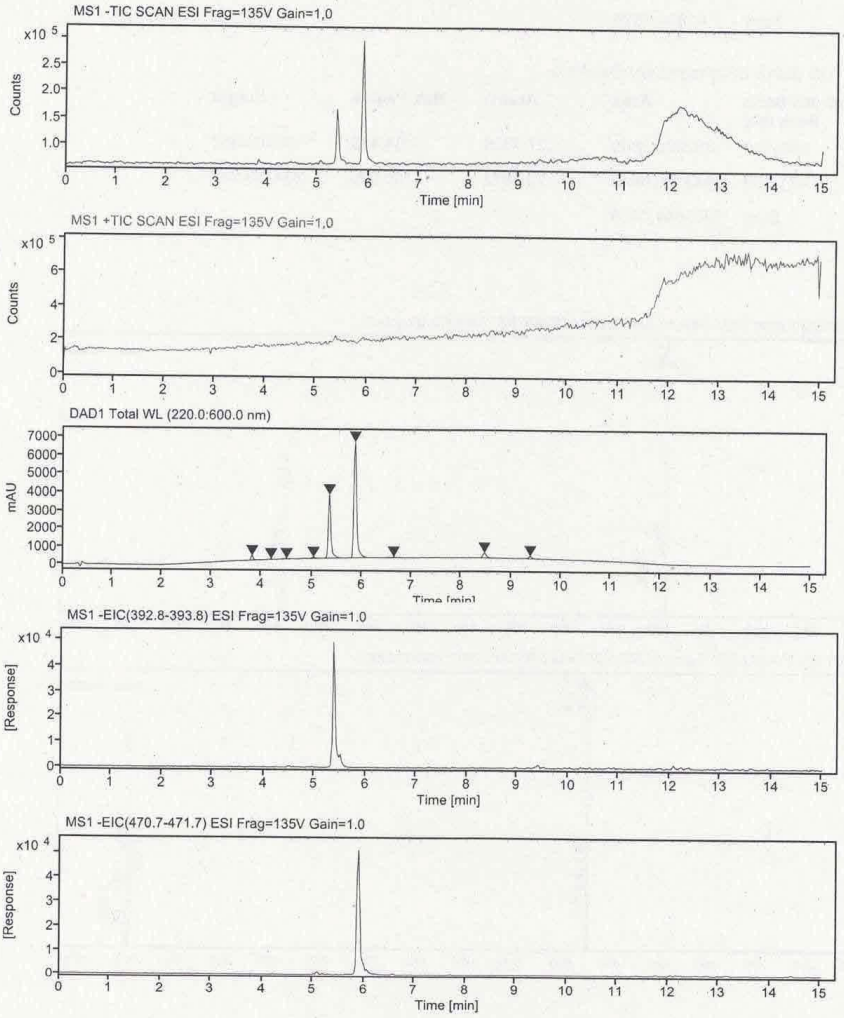


MS1 -TIC SCAN ESI Frag=135V Gain=1,0RT:5.88707746720692min (Subtracted)



x-5h

Sequence Name:	SingleSample		
Data file:	HALP228-5h.dx	**Project Name:**	Single Quad
Sample name:	HALP228-5h	**Operator :**	SYSTEM
Instrument:	Single Quad	**Acquired on:**	2022-09-15 11:12:58+02:00
Inj. volume:	5.000	**Location:**	P2-E3
Acq. method:	00-new_wasser-acn_standard_100-1000_BD-20min.amx		
Processing method:	MS_standard_plot.pmx		



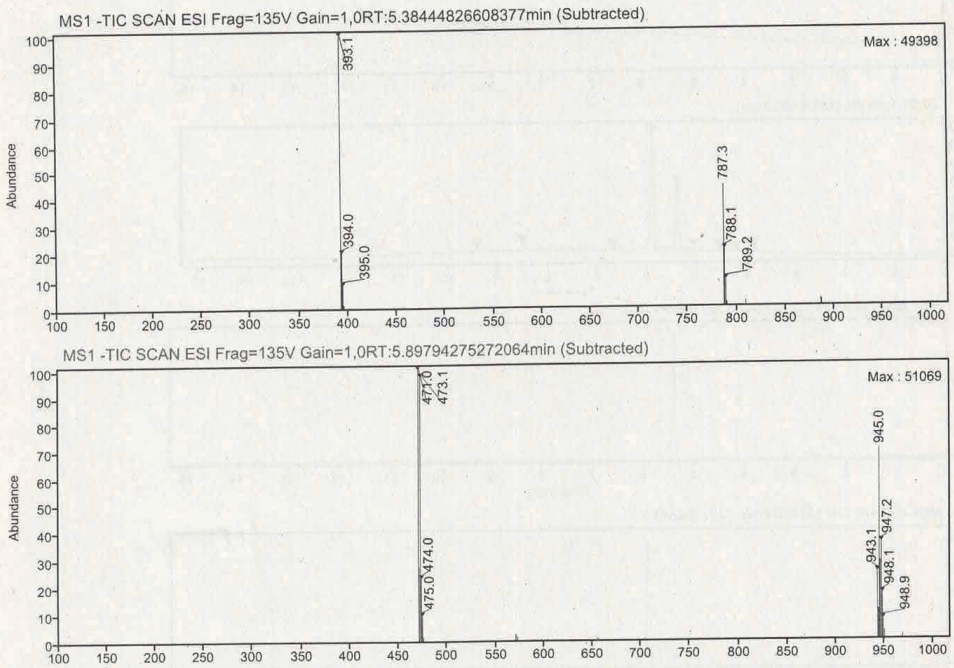
Signal: DAD1 Total WL (220.0:600.0 nm)

RT [min]	Peak MS Base Peak m/z	Area	Area%	Max Peak%	Height
B 3.811		808.4133	1.9296	3.191	245.206
4.188		121.3470	0.2896	0.479	37.194
4.495		205.6339	0.4908	0.812	22.442

RT [min]	Peak MS Base Peak m/z	Area	Area%	Max Peak%	Height
5.036		324.4960	0.7746	1.281	59.614
5.353		13048.9720	31.1470	51.501	3524.531
5.862		25337.2315	60.4783	100.000	6398.571
6.640		114.0098	0.2721	0.450	25.119
8.463		1310.8518	3.1289	5.174	266.401
9.390		623.8023	1.4890	2.462	122.859
	Sum	41894.7576			

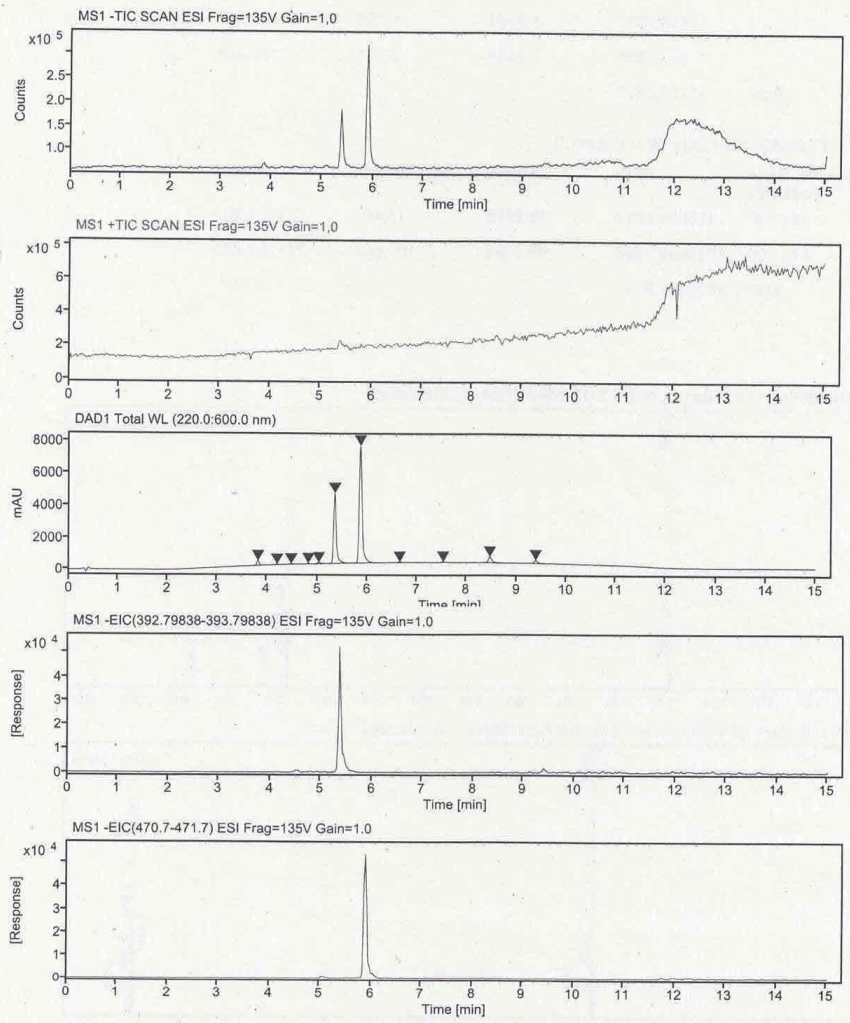
Signal: MS1 -TIC SCAN ESI Frag=135V Gain=1,0

RT [min]	Peak MS Base Peak m/z	Area	Area%	Max Peak%	Height
5.384	393.100	362488.3809	27.7628	38.433	105700.852
5.898	471.000	943175.6619	72.2372	100.000	234733.935
	Sum	1305664.0428			



x-6h

Sequence Name:	SingleSample		
Data file:	HALP228-6h.dx	**Project Name:**	Single Quad
Sample name:	HALP228-6h	**Operator :**	SYSTEM
Instrument:	Single Quad	**Acquired on:**	2022-09-15 11:33:59+02:00
Inj. volume:	5.000	**Location:**	P2-E4
Acq. method:	00-new_wasser-acn_standard_100-1000_BD-20min.amx		
Processing method:	MS_standard_plot.pmx		



Signal: DAD1 Total WL (220.0:600.0 nm)

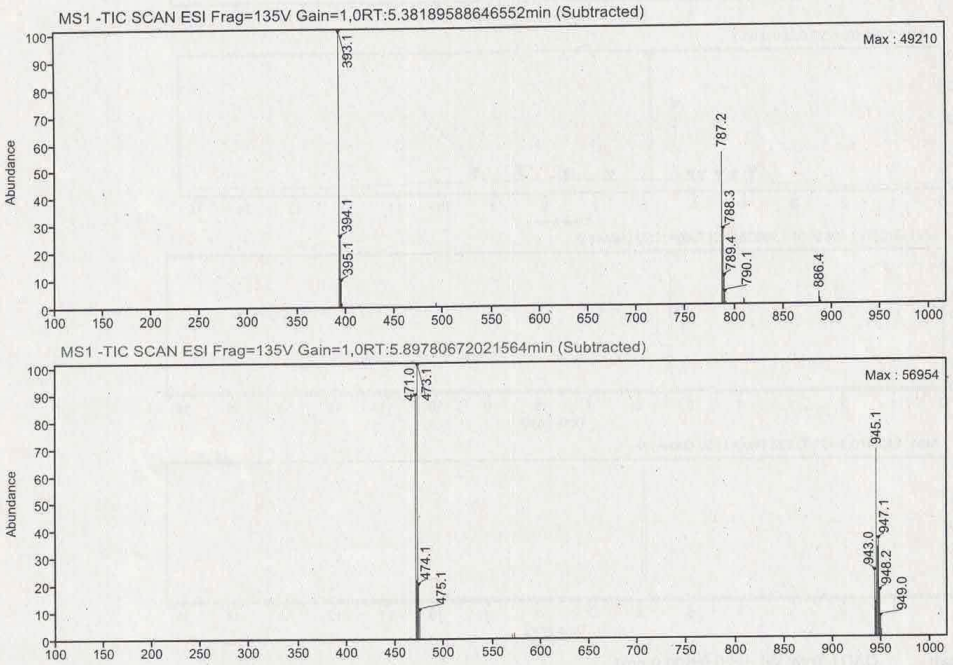
RT [min]	Peak MS Base Peak m/z	Area	Area%	Max Peak%	Height
3.816		1025.6562	2.0039	3.453	295.765
4.192		100.7082	0.1968	0.339	37.094
4.475		145.7526	0.2848	0.491	23.779

D:\CDSProjects\Default\00-standardplot+EIC.rdl [Rev. 2208] Printed: 2022-09-15 12:15:19+02:00 Page 1 of 2

RT [min]	Peak MS Base Peak m/z	Area	Area%	Max Peak%	Height
4.822		93.0849	0.1819	0.313	35.052
5.030		338.2394	0.6608	1.139	66.985
5.348		16706.5733	32.6408	56.242	4365.608
5.860		29704.7652	58.0363	100.000	7236.161
6.649		172.8716	0.3378	0.582	35.675
7.524		133.5078	0.2608	0.449	30.204
8.463		1818.7027	3.5533	6.123	361.215
9.390		943.1958	1.8428	3.175	186.205
	Sum	51183.0577			

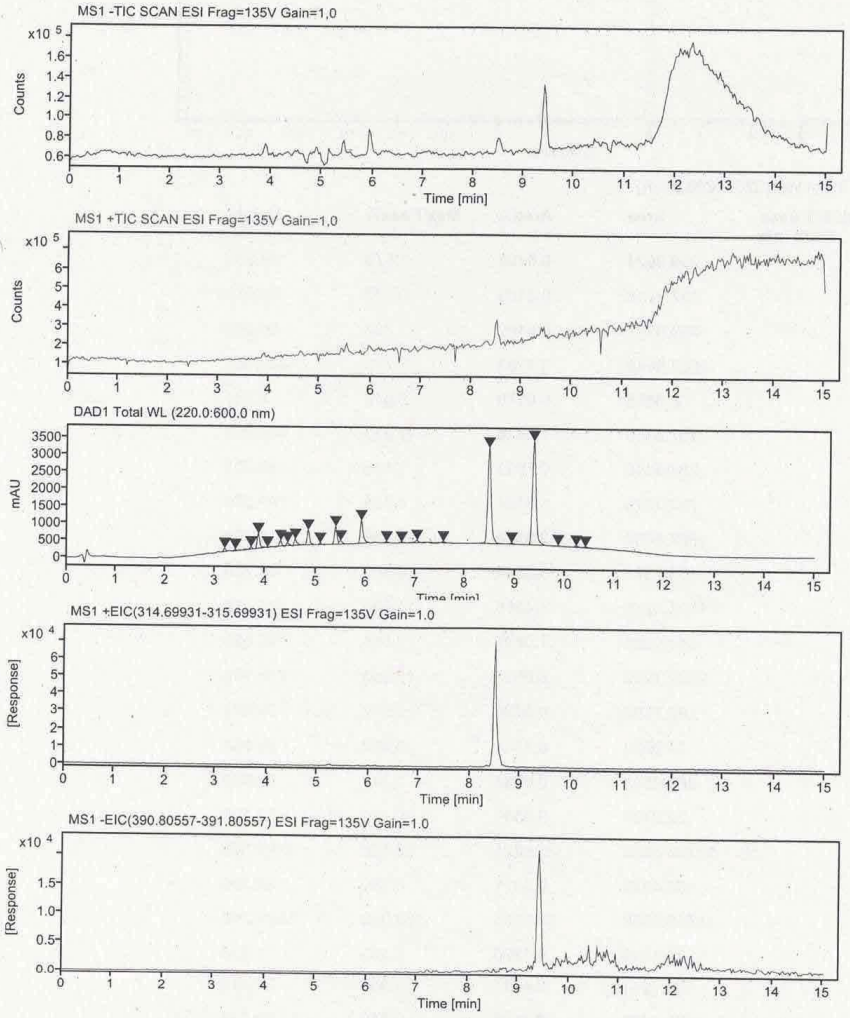
Signal: MS1 -TIC SCAN ESI Frag=135V Gain=1,0

RT [min]	Peak MS Base Peak m/z	Area	Area%	Max Peak%	Height
5.382	393.100	456699.0867	30.2975	43.467	122495.863
5.898	473.100	1050682.7323	69.7025	100.000	254103.925
	Sum	1507381.8190			

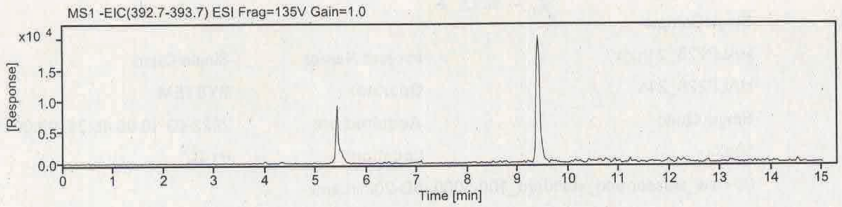


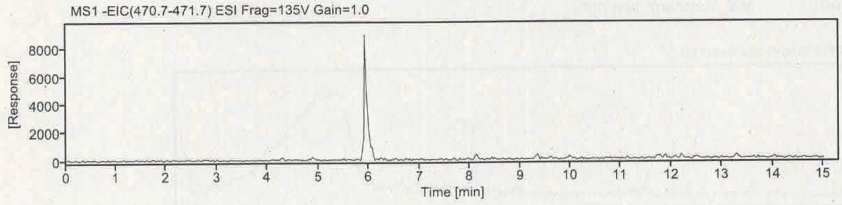
x-242

Sequence Name:	SingleSample		
Data file:	HALP228_24h.dx	**Project Name:**	Single Quad
Sample name:	HALP228_24h	**Operator :**	SYSTEM
Instrument:	Single Quad	**Acquired on:**	2022-09-16 06:45:31+02:00
Inj. volume:	10.000	**Location:**	P1-B7
Acq. method:	00-new_wasser-acn_standard_100-1000_BD-20min.amx		
Processing method:	MS_standard_plot.pmx		



D:\CDSProjects\Default\00-standardplot+EIC.rdl [Rev. 2178] Printed: 2022-09-16 07:36:28+02:00 Page 1 of 4





Signal: DAD1 Total WL (220.0:600.0 nm)

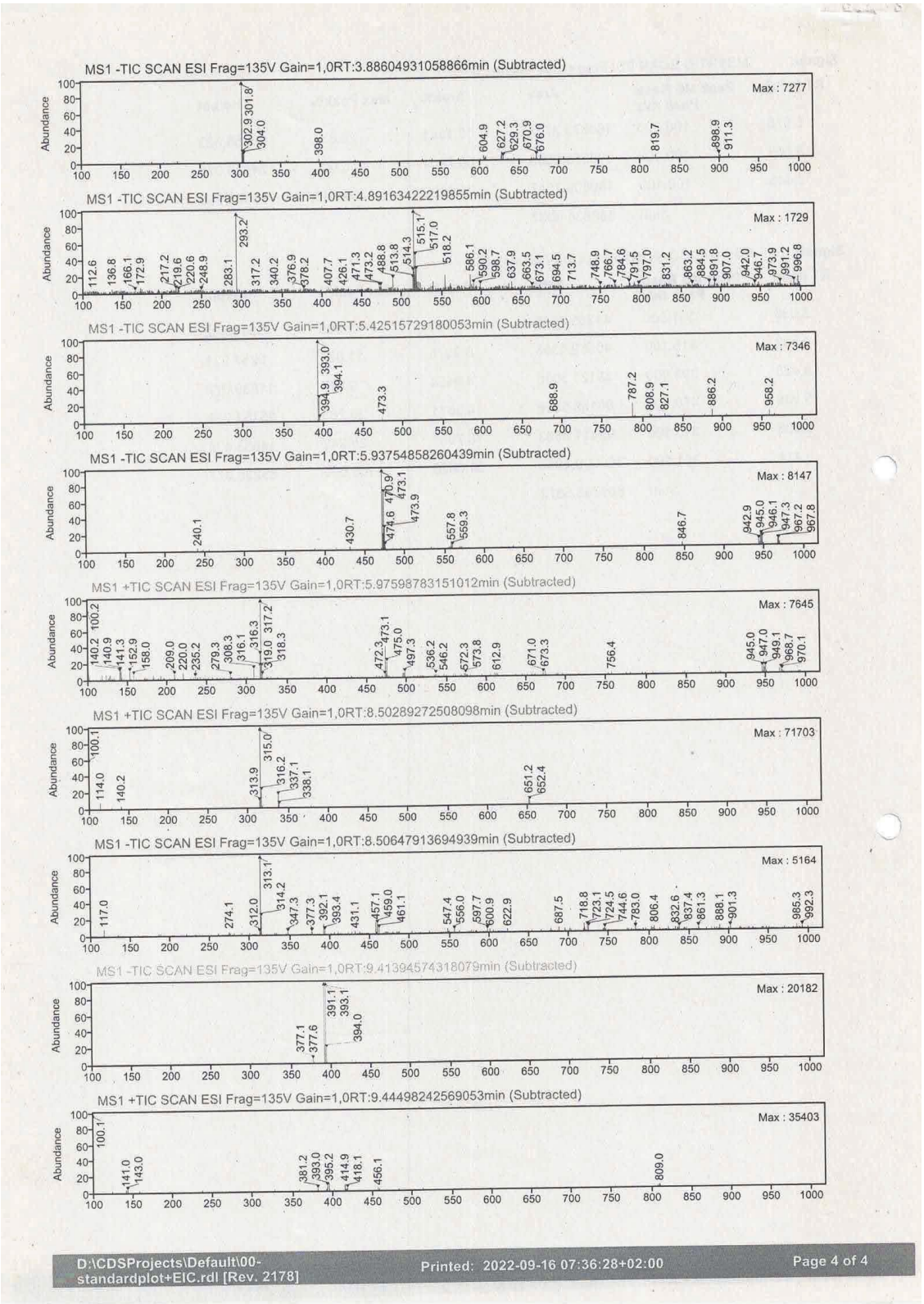
RT [min]	Peak MS Base Peak m/z	Area	Area%	Max Peak%	Height
3.190		259.9621	0.6423	1.676	88.830
3.402		127.2216	0.3143	0.820	33.575
3.713		209.9362	0.5187	1.354	60.096
3.856		1506.8649	3.7233	9.716	431.451
4.038		6.8878	0.0170	0.044	6.381
4.299		437.8409	1.0818	2.823	166.063
4.435		284.5440	0.7031	1.835	89.003
4.592		732.7018	1.8104	4.724	181.576
4.852		1607.6797	3.9724	10.366	434.304
5.089		103.1371	0.2548	0.665	44.230
5.397		1803.6276	4.4565	11.630	518.470
5.500		441.0384	1.0897	2.844	97.026
5.911		2692.7922	6.6535	17.363	665.316
6.414		150.7795	0.3726	0.972	34.577
6.722		74.8029	0.1848	0.482	20.884
7.029		269.8548	0.6668	1.740	68.664
7.556		22.2728	0.0550	0.144	32.565
8.471		13728.8709	33.9221	88.524	2797.585
8.933		136.4325	0.3371	0.880	29.530
9.375		15508.5659	38.3195	100.000	3028.280
9.866		76.4949	0.1890	0.493	21.518
10.228		163.7944	0.4047	1.056	37.310
10.413		125.6083	0.3104	0.810	22.523
	Sum	40471.7111			

Signal: MS1 +TIC SCAN ESI Frag=135V Gain=1,0

RT [min]	Peak MS Base Peak m/z	Area	Area%	Max Peak%	Height
5.976	100.200	160673.3727	18.1381	29.834	35756.323
8.503	100.100	538555.8063	60.7964	100.000	124023.076
9.445	100.100	186605.7547	21.0655	34.649	46826.759
	Sum	885834.9337			

Signal: MS1 -TIC SCAN ESI Frag=135V Gain=1,0

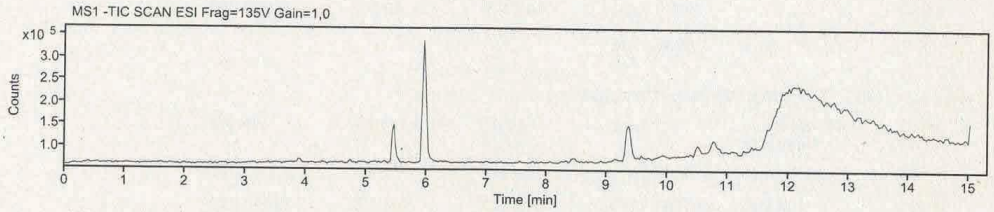
RT [min]	Peak MS Base Peak m/z	Area	Area%	Max Peak%	Height
3.886	301.800	41385.7965	6.1793	11.305	10513.342
4.892	515.100	40569.4356	6.0575	11.082	9257.921
5.425	393.000	33121.3915	4.9454	9.047	11539.077
5.938	470.900	96155.5816	14.3571	26.265	25152.268
8.506	313.100	92411.8863	13.7981	25.242	14633.638
9.414	391.100	366099.4957	54.6626	100.000	65235.077
	Sum	669743.5872			

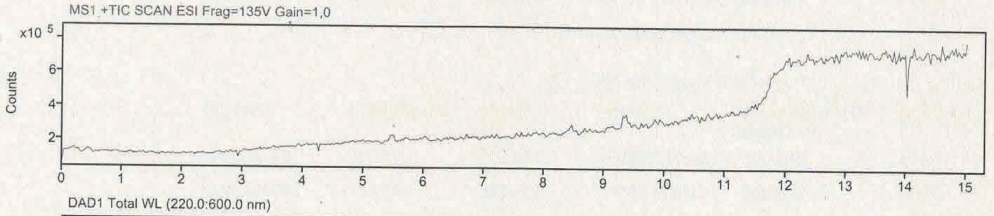

MS1 -TIC SCAN ESI Frag=135V Gain=1,0RT:3.88604931058866min (Subtracted)
Max : 7277
MS1 -TIC SCAN ESI Frag=135V Gain=1,0RT:4.89163422219855min (Subtracted)
Max : 1729
MS1 -TIC SCAN ESI Frag=135V Gain=1,0RT:5.42515729180053min (Subtracted)
Max : 7346
MS1 -TIC SCAN ESI Frag=135V Gain=1,0RT:5.93754858260439min (Subtracted)
Max : 8147
MS1 +TIC SCAN ESI Frag=135V Gain=1,0RT:5.97598783151012min (Subtracted)
Max : 7645
MS1 +TIC SCAN ESI Frag=135V Gain=1,0RT:8.50289272508098min (Subtracted)
Max : 71703
MS1 -TIC SCAN ESI Frag=135V Gain=1,0RT:8.50647913694939min (Subtracted)
Max : 5164
MS1 -TIC SCAN ESI Frag=135V Gain=1,0RT:9.41394574318079min (Subtracted)
Max : 20182
MS1 +TIC SCAN ESI Frag=135V Gain=1,0RT:9.44498242569053min (Subtracted)
Max : 35403
Abundance
D:\CDSProjects\Default\00-standardplot+EIC.rdl [Rev. 2178]
Printed: 2022-09-16 07:36:28+02:00
Page 4 of 4

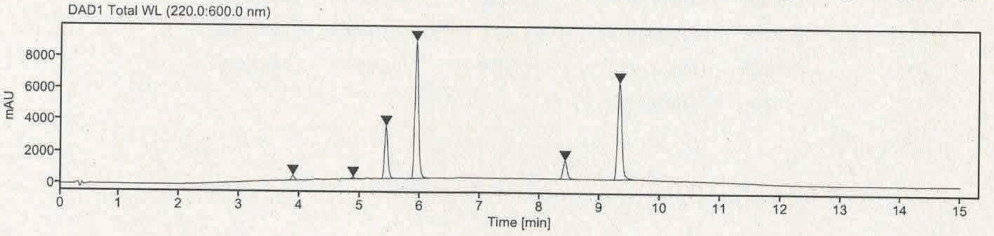
Trial XI

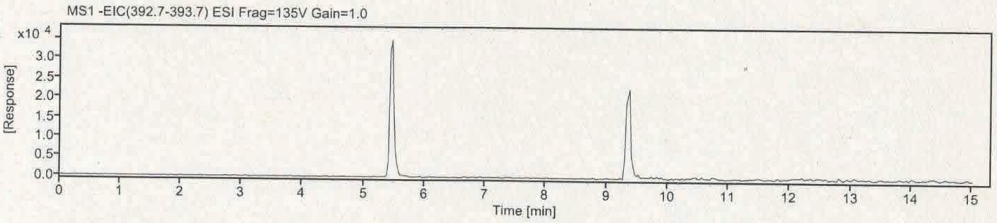
XI-2h

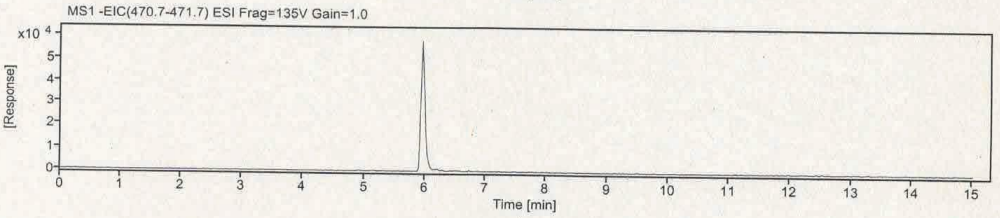
Sequence Name:	SingleSample		
Data file:	HALP228-R2h.dx	**Project Name:**	Single Quad
Sample name:	HALP228-R2h	**Operator :**	SYSTEM
Instrument:	Single Quad	**Acquired on:**	2022-09-28 14:14:30+02:00
Inj. volume:	6.000	**Location:**	P1-E9
Acq. method:	00-new_wasser-acn_standard_100-1000_BD-20min.amx		
Processing method:	MS_standard_plot.pmx		











D:\CDSProjects\Default\00-standardplot+EIC.rdl [Rev. 2415] Printed: 2022-09-29 07:36:47+02:00 Page 1 of 3

Signal: DAD1 Total WL (220.0:600.0 nm)

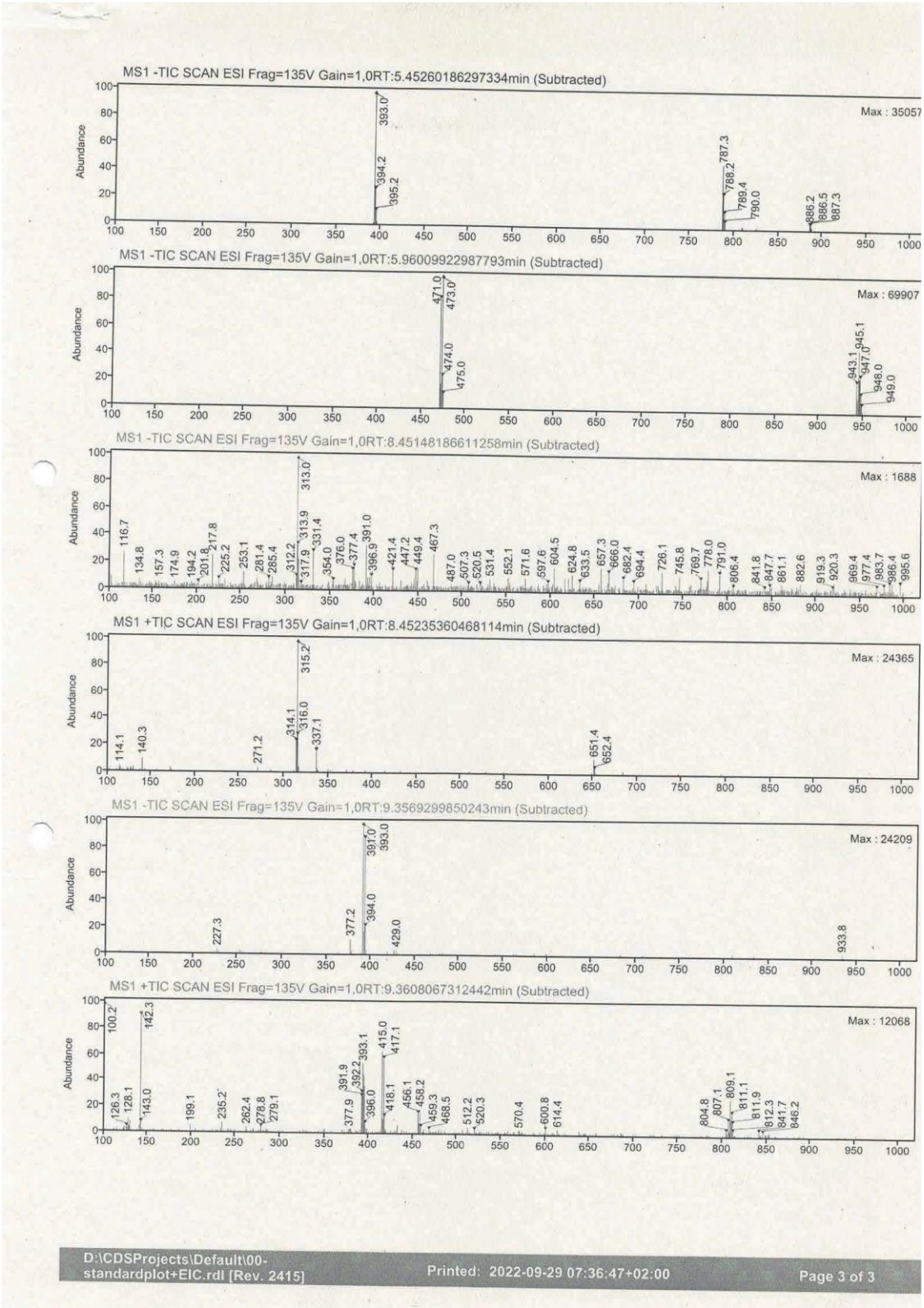
RT [min]	Peak MS Base Peak m/z	Area	Area%	Max Peak%	Height
3.877		1100.5472	1.2852	3.009	285.120
4.876		315.4347	0.3684	0.862	87.009
5.420		12736.6322	14.8733	34.822	3263.620
5.926		36576.8938	42.7130	100.000	8576.933
8.413		5349.8444	6.2473	14.626	1108.186
9.321		29554.8263	34.5129	80.802	6007.026
	Sum	85634.1785			

Signal: MS1 +TIC SCAN ESI Frag=135V Gain=1,0

RT [min]	Peak MS Base Peak m/z	Area	Area%	Max Peak%	Height
8.452	100.100	278183.6280	41.7715	71.737	52939.151
9.361	100.200	387781.1373	58.2285	100.000	72348.001
	Sum	665964.7653			

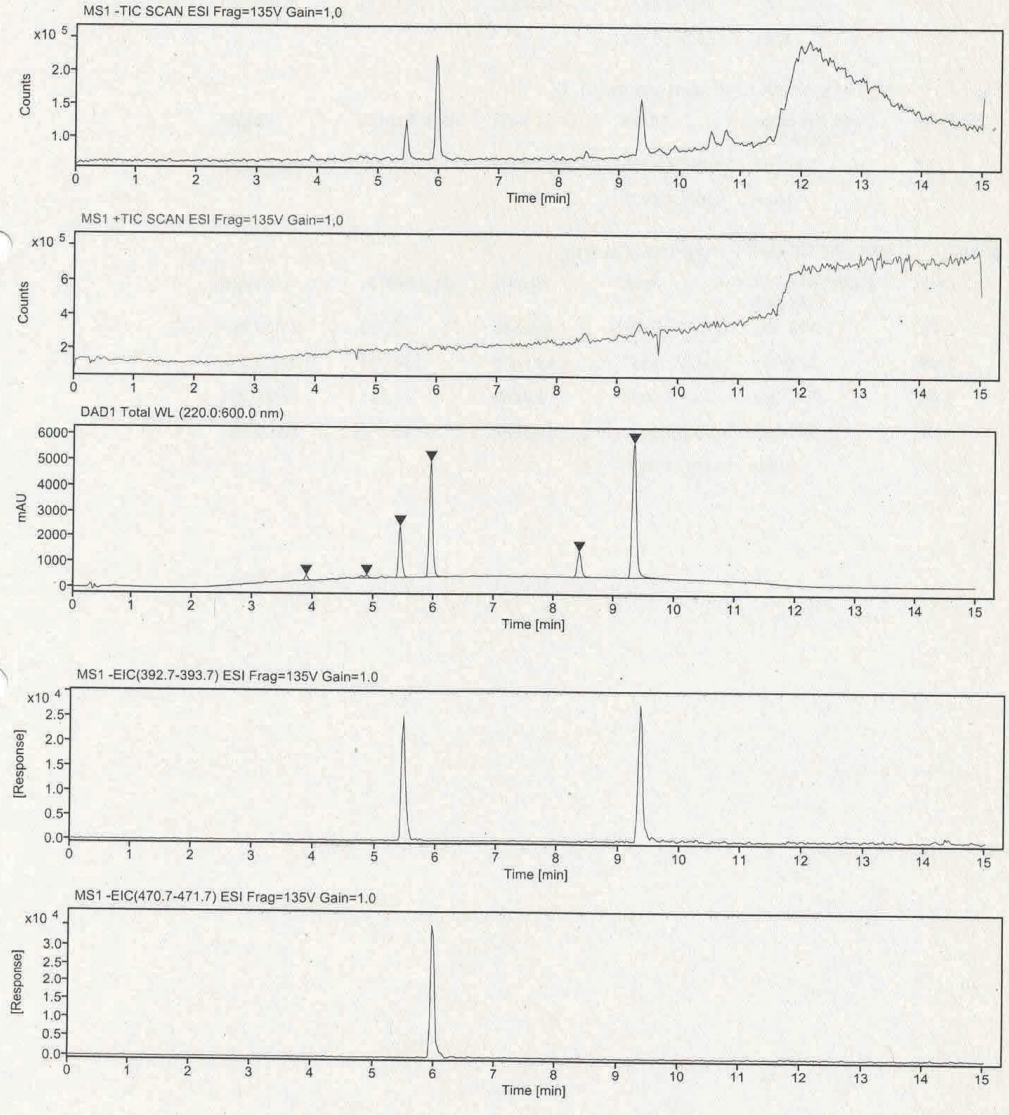
Signal: MS1 -TIC SCAN ESI Frag=135V Gain=1,0

RT [min]	Peak MS Base Peak m/z	Area	Area%	Max Peak%	Height
5.453	393.000	341937.9990	17.5908	30.049	84190.820
5.960	473.000	1137919.8054	58.5395	100.000	269957.088
8.451	313.000	19514.6129	1.0039	1.715	6114.964
9.357	391.000	444478.4162	22.8659	39.061	74570.664
	Sum	1943850.8335			


MS1 -TIC SCAN ESI Frag=135V Gain=1,0RT:5.45260186297334min (Subtracted)
Max : 35057
MS1 -TIC SCAN ESI Frag=135V Gain=1,0RT:5.96009922987793min (Subtracted)
Max : 69907
MS1 -TIC SCAN ESI Frag=135V Gain=1,0RT:8.45148186611258min (Subtracted)
Max : 1688
MS1 +TIC SCAN ESI Frag=135V Gain=1,0RT:8.45235360468114min (Subtracted)
Max : 24365
MS1 -TIC SCAN ESI Frag=135V Gain=1,0RT:9.3569299850243min (Subtracted)
Max : 24209
MS1 +TIC SCAN ESI Frag=135V Gain=1,0RT:9.3608067312442min (Subtracted)
Max : 12068
Abundance
D:\CDSProjects\Default\00-standardplot+EIC.rdl [Rev. 2415]
Printed: 2022-09-29 07:36:47+02:00
Page 3 of 3

X1 - 4h

Sequence Name:	SingleSample		
Data file:	HALP228-R4h.dx	**Project Name:**	Single Quad
Sample name:	HALP228-R4h	**Operator :**	SYSTEM
Instrument:	Single Quad	**Acquired on:**	2022-09-28 14:35:34+02:00
Inj. volume:	6.000	**Location:**	P1-E10
Acq. method:	00-new_wasser-acn_standard_100-1000_BD-20min.amx		
Processing method:	MS_standard_plot.pmx		



Signal: DAD1 Total WL (220.0:600.0 nm)

RT [min]	Peak MS Base Peak m/z	Area	Area%	Max Peak%	Height
3.876		752.0582	1.2687	2.831	200.611
4.876		850.8182	1.4353	3.202	111.327
5.425		7811.9045	13.1783	29.402	2020.481
5.936		18476.2111	31.1684	69.540	4540.629
8.413	313.300	4818.3959	8.1284	18.135	994.777
9.323	391.000	26569.2472	44.8209	100.000	5283.058
	Sum	59278.6351			

Signal: MS1 +TIC SCAN ESI Frag=135V Gain=1,0

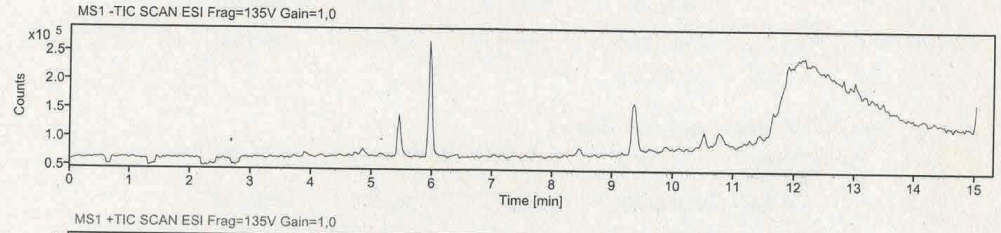
RT [min]	Peak MS Base Peak m/z	Area	Area%	Max Peak%	Height
8.452	100.100	310704.4708	100.0000	100.000	51554.828
	Sum	310704.4708			

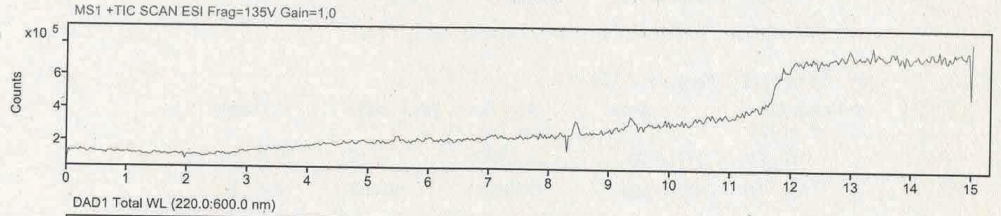
Signal: MS1 -TIC SCAN ESI Frag=135V Gain=1,0

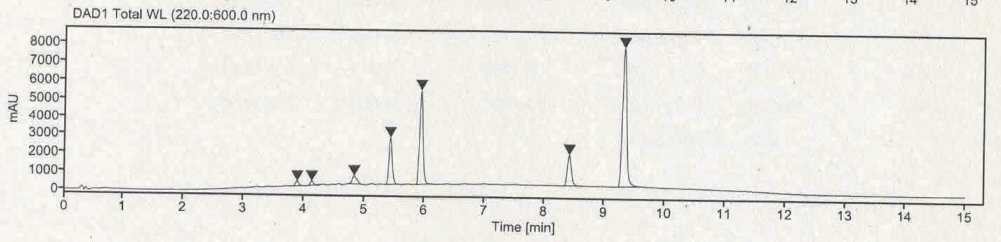
RT [min]	Peak MS Base Peak m/z	Area	Area%	Max Peak%	Height
5.460	393.100	225121.6162	16.5888	33.903	57853.867
5.968	471.100	664026.1941	48.9308	100.000	166413.485
8.449	313.300	28316.4080	2.0866	4.264	9771.214
9.357	391.000	439606.8637	32.3938	66.203	81942.921
	Sum	1357071.0820			

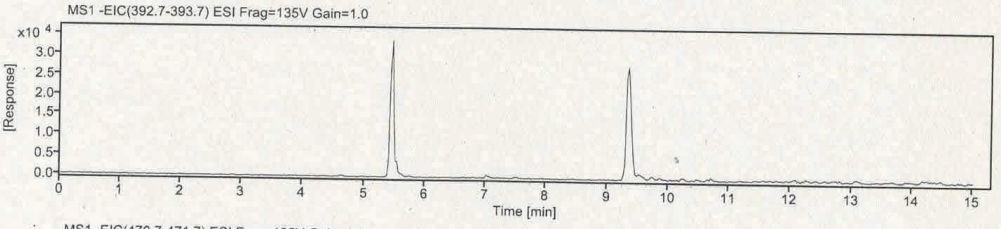
X1-6h

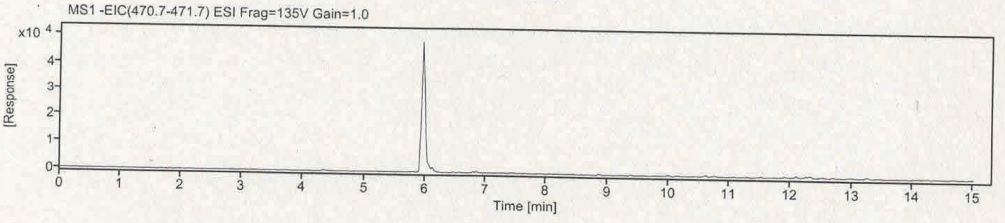
Sequence Name:	SingleSample		
Data file:	HALP228-R6h.dx	**Project Name:**	Single Quad
Sample name:	HALP228-R6h	**Operator :**	SYSTEM
Instrument:	Single Quad	**Acquired on:**	2022-09-28 14:56:36+02:00
Inj. volume:	6.000	**Location:**	P1-E11
Acq. method:	00-new_wasser-acn_standard_100-1000_BD-20min.amx		
Processing method:	MS_standard_plot.pmx		











D:\CDSProjects\Default\00-standardplot+EIC.rdl [Rev. 2415] Printed: 2022-09-29 07:37:07+02:00 Page 1 of 3

Signal: DAD1 Total WL (220.0:600.0 nm)

RT [min]	Peak MS Base Peak m/z	Area	Area%	Max Peak%	Height
3.879		1020.4592	1.2817	2.758	271.274
4.122		614.5904	0.7719	1.661	232.518
4.823		2378.8183	2.9877	6.429	452.121
5.421		9761.0799	12.2595	26.380	2534.669
5.932	471.000	20824.6362	26.1548	56.279	5147.095
8.409		8018.7061	10.0711	21.671	1672.697
9.321	393.000	37002.3922	46.4733	100.000	7570.529
	Sum	79620.6824			

Signal: MS1 +TIC SCAN ESI Frag=135V Gain=1,0

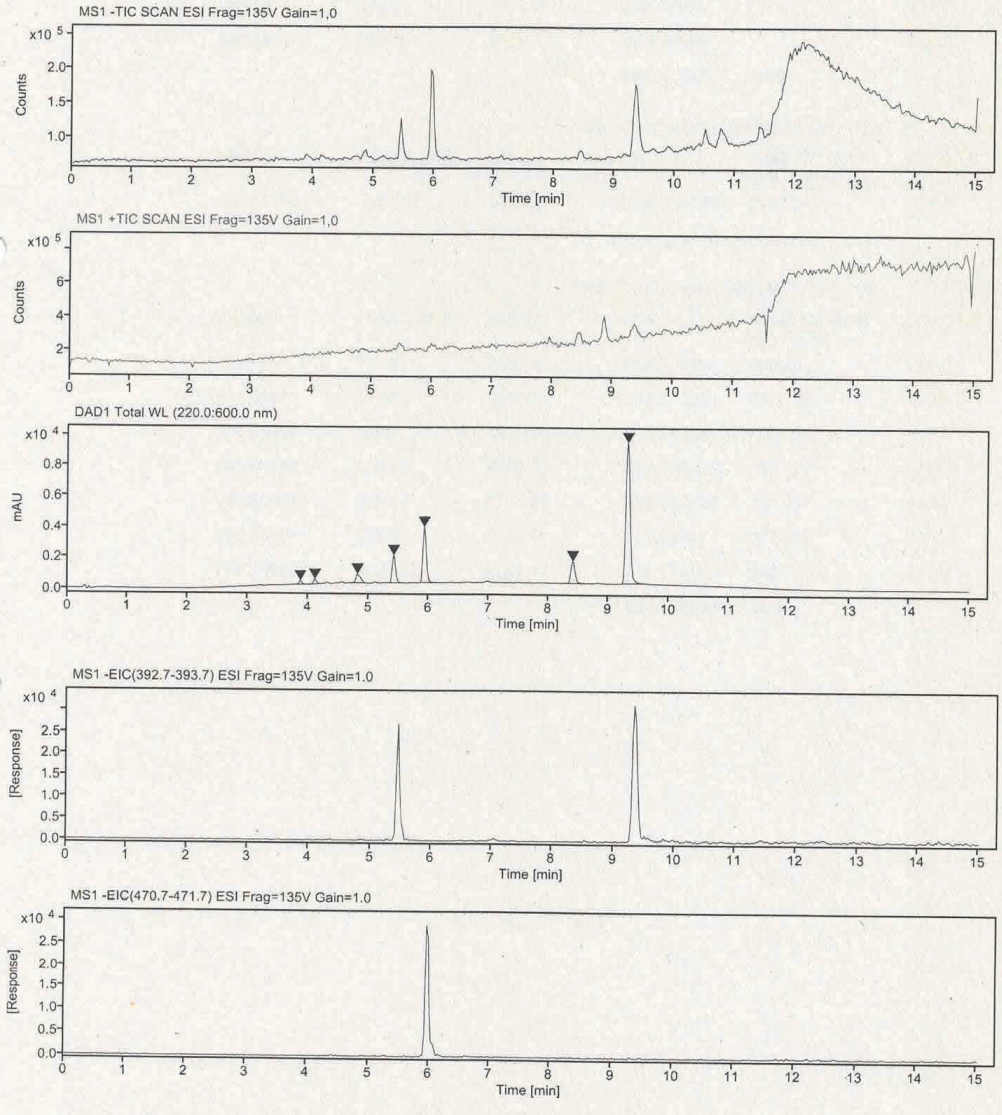
RT [min]	Peak MS Base Peak m/z	Area	Area%	Max Peak%	Height
8.438	100.200	423586.6394	100.0000	100.000	82168.696
	Sum	423586.6394			

Signal: MS1 -TIC SCAN ESI Frag=135V Gain=1,0

RT [min]	Peak MS Base Peak m/z	Area	Area%	Max Peak%	Height
4.851	475.000	39378.1641	2.3742	5.113	10047.147
5.456	393.100	297607.4801	17.9433	38.646	72508.362
5.964	471.000	770095.8943	46.4306	100.000	205014.914
8.446	313.100	49373.8798	2.9768	6.411	11246.419
9.349	393.000	502141.0626	30.2751	65.205	83418.189
	Sum	1658596.4810			

X1 - 72

Sequence Name:	SingleSample		
Data file:	HALP228-R7h.dx	**Project Name:**	Single Quad
Sample name:	HALP228-R7h	**Operator :**	SYSTEM
Instrument:	Single Quad	**Acquired on:**	2022-09-28 15:17:40+02:00
Inj. volume:	6.000	**Location:**	P1-F7
Acq. method:	00-new_wasser-acn_standard_100-1000_BD-20min.amx		
Processing method:	MS_standard_plot.pmx		



Signal: DAD1 Total WL (220.0:600.0 nm)

RT [min]	Peak MS Base Peak m/z	Area	Area%	Max Peak%	Height
3.877	301.900	883.2141	1.1300	1.962	223.945
4.120	395.100	1078.5606	1.3800	2.396	306.799
4.825		3149.1938	4.0292	6.996	571.678
5.423	393.100	6876.6461	8.7983	15.277	1756.838
5.935		14275.1855	18.2643	31.713	3561.612
8.411		6881.9966	8.8051	15.288	1407.672
9.324		45014.3028	57.5932	100.000	9124.986
	Sum	78159.0995			

Signal: MS1 +TIC SCAN ESI Frag=135V Gain=1,0

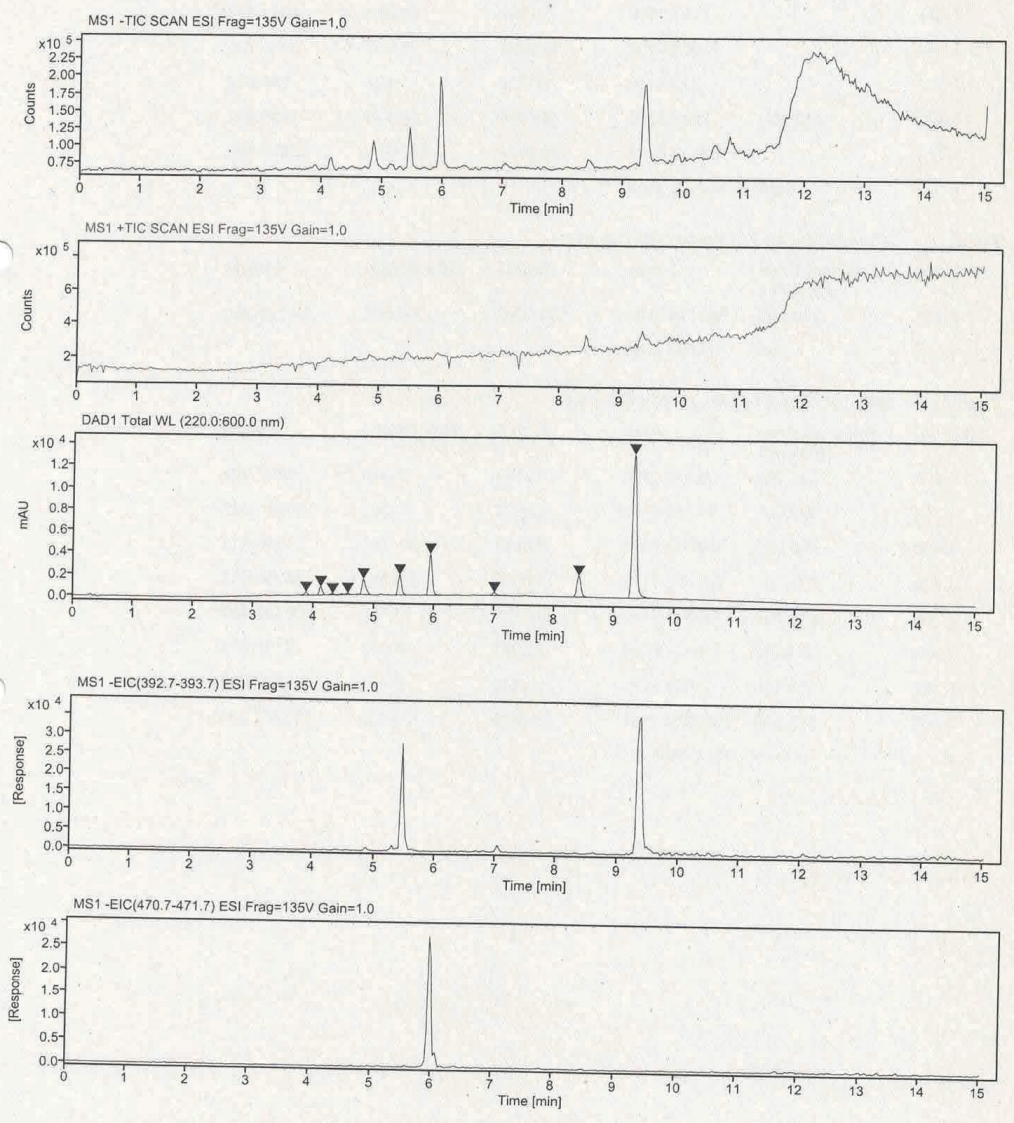
RT [min]	Peak MS Base Peak m/z	Area	Area%	Max Peak%	Height
8.446	100.100	357410.0045	100.0000	100.000	66517.061
	Sum	357410.0045			

Signal: MS1 -TIC SCAN ESI Frag=135V Gain=1,0

RT [min]	Peak MS Base Peak m/z	Area	Area%	Max Peak%	Height
3.899	301.900	46980.9250	3.0038	7.777	8464.150
4.143	395.100	39542.8151	2.5282	6.546	7476.346
4.871	473.000	58394.6388	3.7335	9.667	12992.113
5.458	393.100	227361.3365	14.5366	37.638	59196.353
5.968	473.100	543020.6505	34.7186	89.892	140928.697
8.446	313.100	44685.3322	2.8570	7.397	10612.939
9.361	391.000	604077.8312	38.6223	100.000	103265.162
	Sum	1564063.5293			

XI-8h

Sequence Name:	SingleSample		
Data file:	HALP228-R8h.dx	**Project Name:**	Single Quad
Sample name:	HALP228-R8h	**Operator :**	SYSTEM
Instrument:	Single Quad	**Acquired on:**	2022-09-28 15:38:44+02:00
Inj. volume:	6.000	**Location:**	P1-F8
Acq. method:	00-new_wasser-acn_standard_100-1000_BD-20min.amx		
Processing method:	MS_standard_plot.pmx		



Signal: DAD1 Total WL (220.0:600.0 nm)

RT [min]	Peak MS Base Peak m/z	Area	Area%	Max Peak%	Height
3.874	302.000	982.1478	0.9163	1.538	262.574
4.120		2746.9972	2.5630	4.303	772.253
4.317		394.2474	0.3678	0.618	113.585
4.565		542.1147	0.5058	0.849	120.645
4.825		6208.8913	5.7929	9.726	1413.049
5.424		7213.4560	6.7302	11.299	1841.879
5.935		15004.6406	13.9994	23.503	3756.702
7.000		1215.2116	1.1338	1.904	245.825
8.409	313.100	9032.5920	8.4274	14.149	1906.417
9.327		63840.6195	59.5634	100.000	13056.562
	Sum	107180.9181			

Signal: MS1 +TIC SCAN ESI Frag=135V Gain=1,0

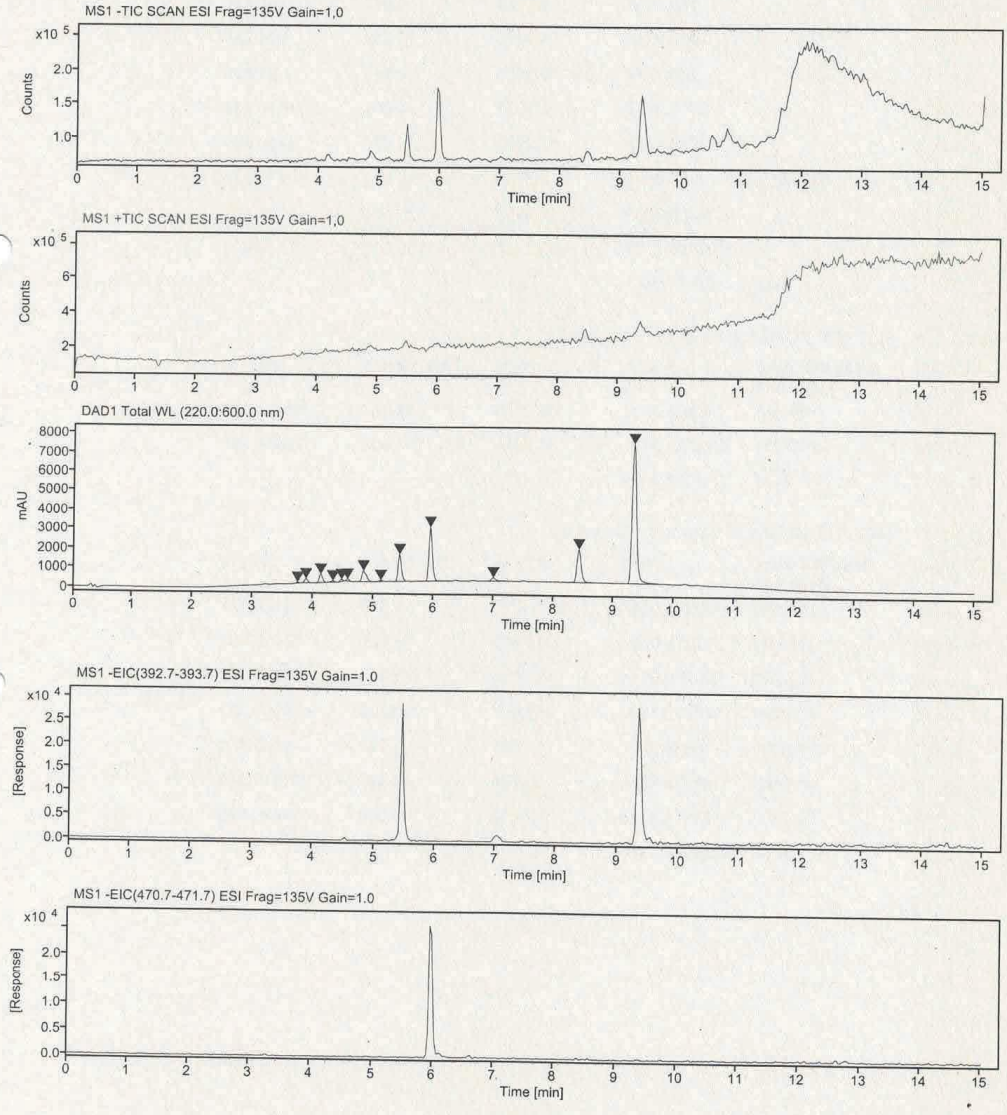
RT [min]	Peak MS Base Peak m/z	Area	Area%	Max Peak%	Height
8.434	100.200	393796.8786	100.0000	100.000	94139.294
	Sum	393796.8786			

Signal: MS1 -TIC SCAN ESI Frag=135V Gain=1,0

RT [min]	Peak MS Base Peak m/z	Area	Area%	Max Peak%	Height
3.894	302.000	23000.9350	1.3130	3.329	5817.369
4.153	395.000	71779.4758	4.0976	10.388	18511.017
4.859	475.000	150603.3831	8.5973	21.796	37553.311
5.460	393.100	209339.3143	11.9503	30.297	58036.487
5.966	473.000	509372.1137	29.0779	73.720	138433.239
7.039	393.000	38644.5366	2.2061	5.593	7137.853
8.425	313.100	58052.6281	3.3140	8.402	12566.692
9.368	391.100	690957.7640	39.4439	100.000	118237.234
	Sum	1751750.1507			

XI-9h

Sequence Name:	SingleSample		
Data file:	HALP228-R9h.dx	**Project Name:**	Single Quad
Sample name:	HALP228-R9h	**Operator :**	SYSTEM
Instrument:	Single Quad	**Acquired on:**	2022-09-28 15:59:46+02:00
Inj. volume:	6.000	**Location:**	P1-F9
Acq. method:	00-new_wasser-acn_standard_100-1000_BD-20min.amx		
Processing method:	MS_standard_plot.pmx		



Signal: DAD1 Total WL (220.0:600.0 nm)

RT [min]	Peak MS Base Peak m/z	Area	Area%	Max Peak%	Height
3.733		145.7566	0.2100	0.394	48.217
3.872		741.7855	1.0685	2.005	203.834
4.119		1545.6109	2.2264	4.178	433.876
4.317		262.4123	0.3780	0.709	68.222
4.463		298.6798	0.4302	0.807	100.115
4.562		350.2067	0.5045	0.947	107.840
4.825		2907.2289	4.1878	7.859	548.988
5.111		238.4874	0.3435	0.645	64.520
5.421		5419.9399	7.8073	14.651	1374.134
5.936		11265.8999	16.2283	30.454	2760.699
6.987	393.000	951.3944	1.3705	2.572	175.146
8.414		8300.6053	11.9569	22.438	1675.423
9.328		36993.2775	53.2881	100.000	7178.802
	Sum	69421.2851			

Signal: MS1 +TIC SCAN ESI Frag=135V Gain=1,0

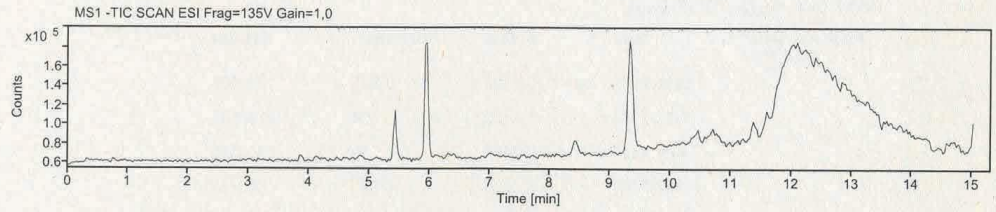
RT [min]	Peak MS Base Peak m/z	Area	Area%	Max Peak%	Height
8.446	100.200	258560.0021	45.3155	82.867	63421.096
9.364	100.200	312017.9171	54.6845	100.000	62984.832
	Sum	570577.9192			

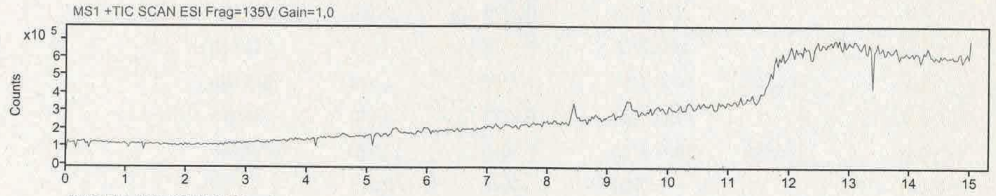
Signal: MS1 -TIC SCAN ESI Frag=135V Gain=1,0

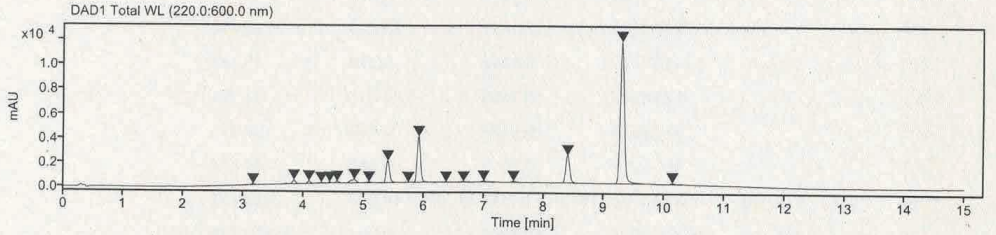
RT [min]	Peak MS Base Peak m/z	Area	Area%	Max Peak%	Height
4.153	395.100	40248.0447	3.1235	8.535	9123.172
4.859	475.000	61475.0367	4.7708	13.036	13453.955
5.459	393.200	203200.6614	15.7695	43.090	53972.903
5.957	473.100	428703.7520	33.2697	90.909	102962.580
7.010	393.000	15336.6967	1.1902	3.252	4825.625
8.452	313.100	68033.8315	5.2798	14.427	13470.379
9.358	393.100	471572.6958	36.5966	100.000	84520.870
	Sum	1288570.7187			

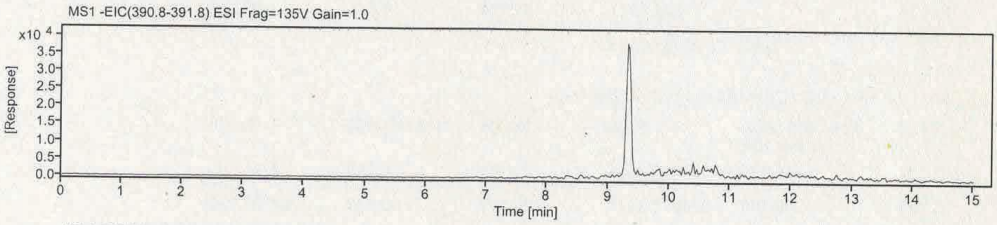
X1-24h

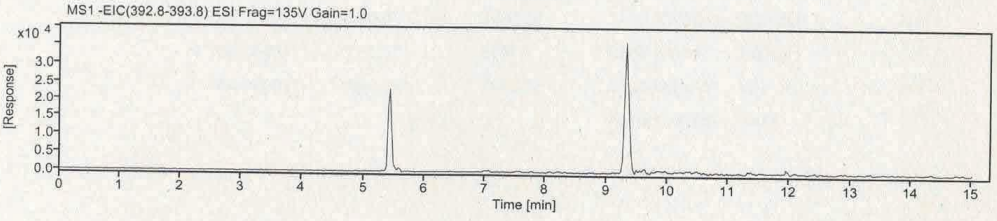
Sequence Name:	SingleSample		
Data file:	HALP228-24h.dx	**Project Name:**	Single Quad
Sample name:	HALP228-24h	**Operator :**	SYSTEM
Instrument:	Single Quad	**Acquired on:**	2022-09-29 14:44:28+02:00
Inj. volume:	5.000	**Location:**	P2-B11
Acq. method:	00-new_wasser-acn_standard_100-1000_BD-20min.amx		
Processing method:	*MS_standard_plot.pmx		



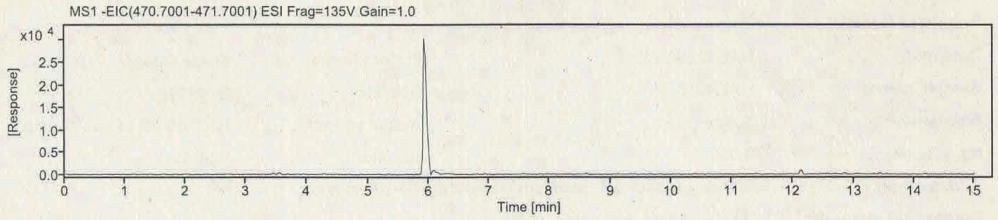








D:\CDSProjects\Default\00-standardplot+EIC.rdl [Rev. 2432] Printed: 2022-10-04 07:25:13+02:00 Page 1 of 3

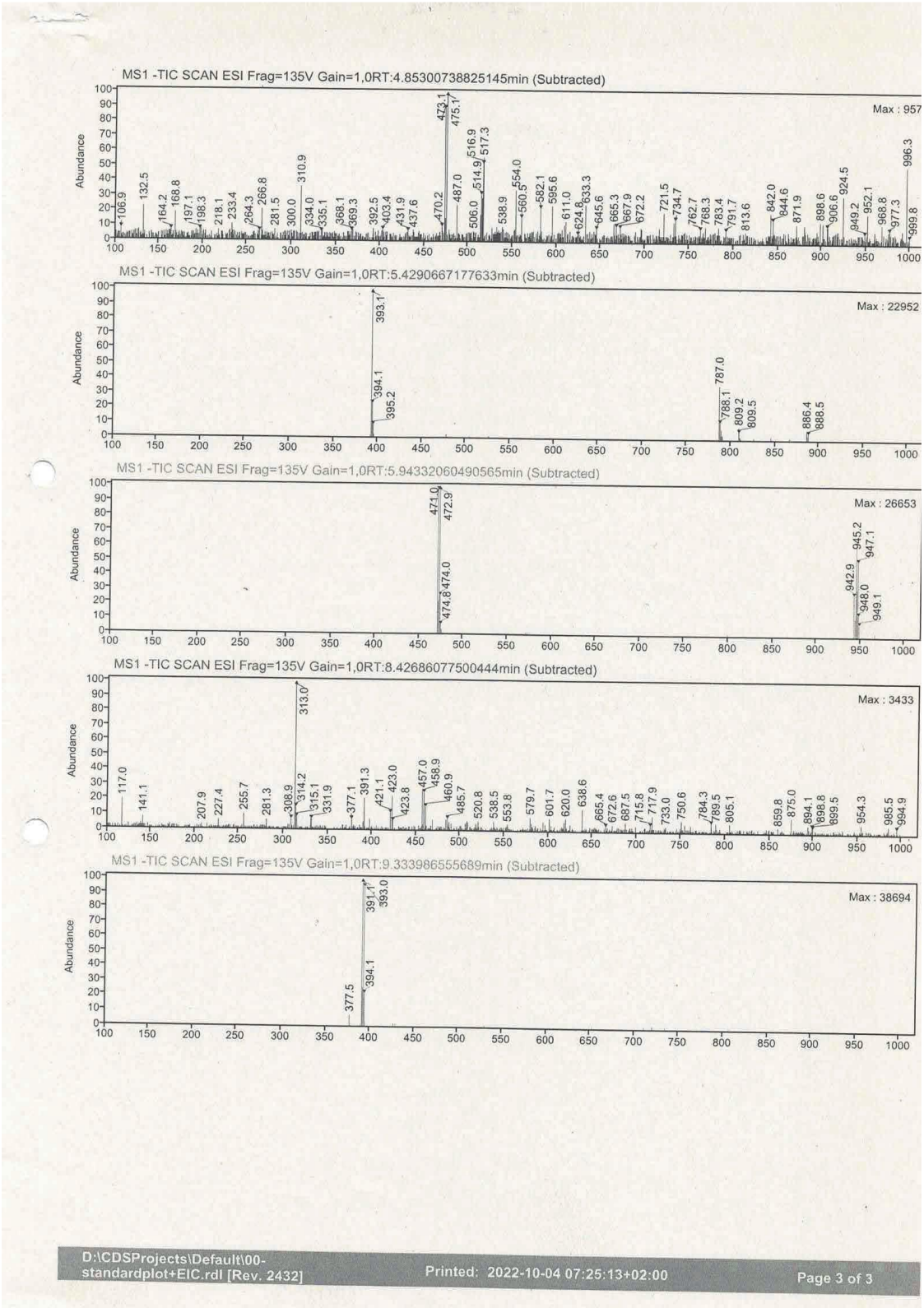


Signal: DAD1 Total WL (220.0:600.0 nm)

RT [min]	Peak MS Base Peak m/z	Area	Area%	Max Peak%	Height
3.169		216.9276	0.2320	0.395	59.806
3.843		1321.4150	1.4135	2.404	308.804
4.094		691.4246	0.7396	1.258	211.775
4.297		192.5794	0.2060	0.350	60.583
4.435		226.8011	0.2426	0.413	67.571
4.560		452.2488	0.4838	0.823	135.160
4.845	475.100	1655.1854	1.7705	3.012	273.905
5.086		259.6581	0.2777	0.472	70.923
5.396	393.100	6884.9155	7.3646	12.528	1793.498
5.743		7.0530	0.0075	0.013	9.183
5.912		14647.6895	15.6681	26.653	3744.455
6.370		116.3733	0.1245	0.212	23.133
6.661		188.6878	0.2018	0.343	37.194
6.995		576.2604	0.6164	1.049	95.221
7.497		366.4207	0.3919	0.667	84.574
8.397	313.000	10416.1351	11.1418	18.953	2263.872
9.300	391.100	54957.6225	58.7862	100.000	11502.870
10.138		309.8217	0.3314	0.564	95.645
	Sum	93487.2195			

Signal: MS1 -TIC SCAN ESI Frag=135V Gain=1,0

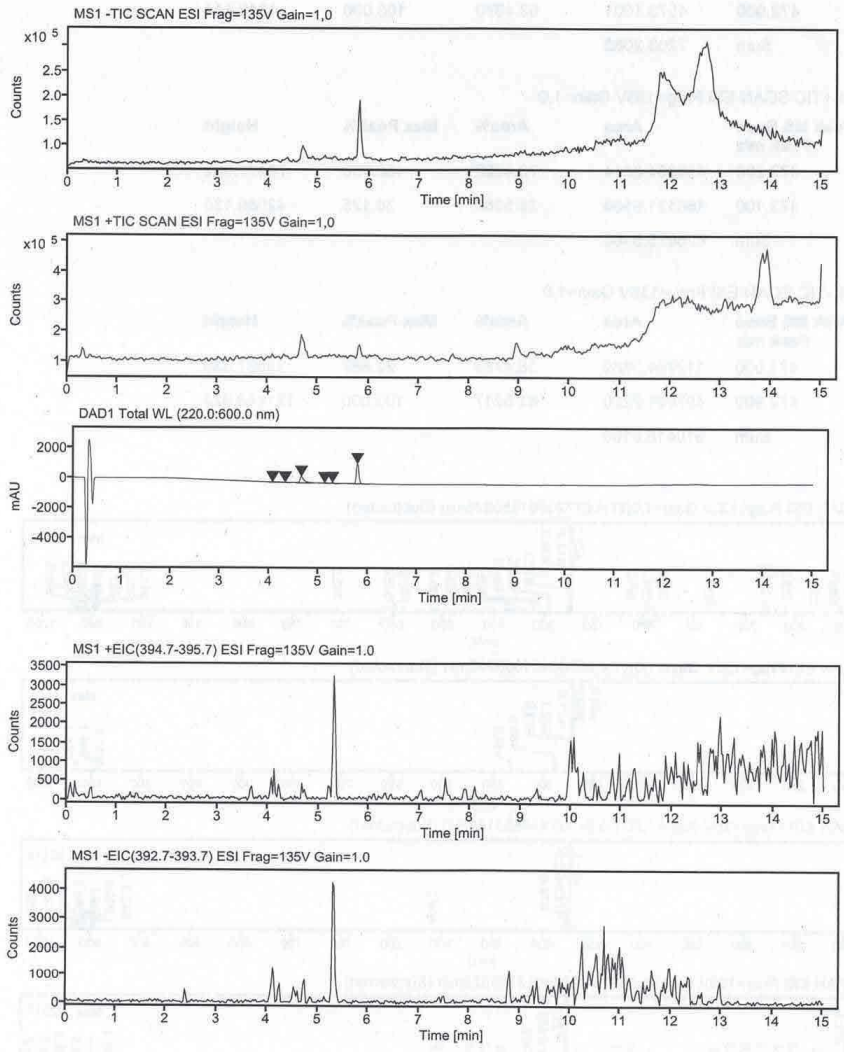
RT [min]	Peak MS Base Peak m/z	Area	Area%	Max Peak%	Height
4.853	475.100	37206.3334	2.4181	5.519	4746.243
5.429	393.100	206473.3411	13.4191	30.628	52398.090
5.943	472.900	506028.1447	32.8878	75.064	127450.111
8.427	313.000	114811.6660	7.4618	17.031	15953.507
9.334	391.100	674132.3302	43.8132	100.000	115656.331
	Sum	1538651.8154			


MS1 -TIC SCAN ESI Frag=135V Gain=1,0RT:4.85300738825145min (Subtracted)
Max : 957
MS1 -TIC SCAN ESI Frag=135V Gain=1,0RT:5.4290667177633min (Subtracted)
Max : 22952
MS1 -TIC SCAN ESI Frag=135V Gain=1,0RT:5.94332060490565min (Subtracted)
Max : 26653
MS1 -TIC SCAN ESI Frag=135V Gain=1,0RT:8.42686077500444min (Subtracted)
Max : 3433
MS1 -TIC SCAN ESI Frag=135V Gain=1,0RT:9.333986555689min (Subtracted)
Max : 38694
Abundance
D:\CDSProjects\Default\00-standardplot+EIC.rdl [Rev. 2432]
Printed: 2022-10-04 07:25:13+02:00
Page 3 of 3

Trial XII

XII-1h

Sequence Name:	SingleSample		
Data file:	HALP400_1h.dx	**Project Name:**	Single Quad
Sample name:	HALP400_1h	**Operator :**	SYSTEM
Instrument:	Single Quad	**Acquired on:**	2024-03-19 08:08:00+01:00
Inj. volume:	5.000	**Location:**	P1-D4
Acq. method:	00-new_wasser-acn_standard_100-1000_BD-20min.amx		
Processing method:	MS_standard_plot.pmx		



Signal: DAD1 Total WL (220.0:600.0 nm)

RT [min]	Peak MS Base Peak m/z	Area	Area%	Max Peak%	Height
4.057		70.9771	0.9854	1.552	13.325
4.311		67.4700	0.9367	1.475	22.712
4.644		2235.4470	31.0340	48.883	426.199
5.113		105.7860	1.4686	2.313	17.647
5.272		150.4280	2.0883	3.289	55.900
5.777	472.900	4573.1001	63.4870	100.000	1342.444
	Sum	7203.2082			

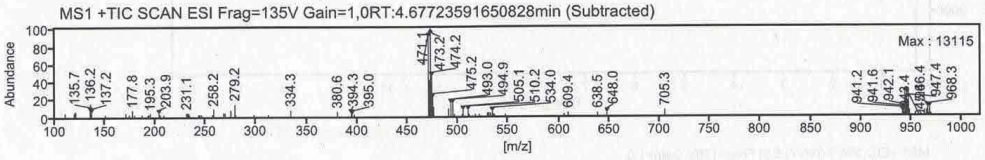
Signal: MS1 +TIC SCAN ESI Frag=135V Gain=1,0

RT [min]	Peak MS Base Peak m/z	Area	Area%	Max Peak%	Height
4.677	473.200	459854.0014	73.4620	100.000	76477.962
5.823	473.100	166121.6166	26.5380	36.125	42089.130
	Sum	625975.6180			

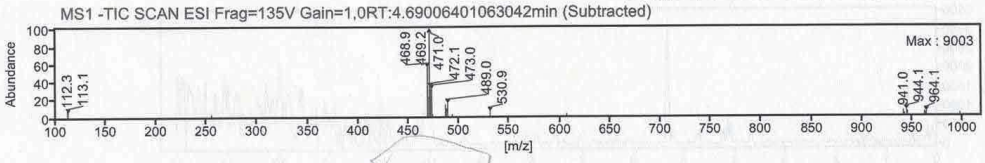
Signal: MS1 -TIC SCAN ESI Frag=135V Gain=1,0

RT [min]	Peak MS Base Peak m/z	Area	Area%	Max Peak%	Height
4.690	471.000	112794.3880	18.4783	22.667	26637.638
5.813	472.900	497621.2220	81.5217	100.000	121448.924
	Sum	610415.6100			

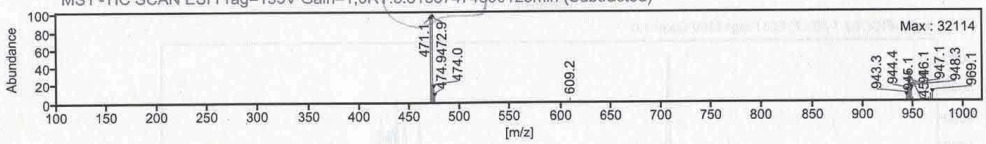
MS1 +TIC SCAN ESI Frag=135V Gain=1,0RT:4.67723591650828min (Subtracted)



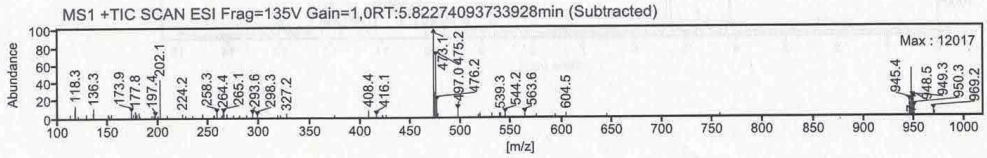
MS1 -TIC SCAN ESI Frag=135V Gain=1,0RT:4.69006401063042min (Subtracted)



MS1 -TIC SCAN ESI Frag=135V Gain=1,0RT:5.81337474890128min (Subtracted)

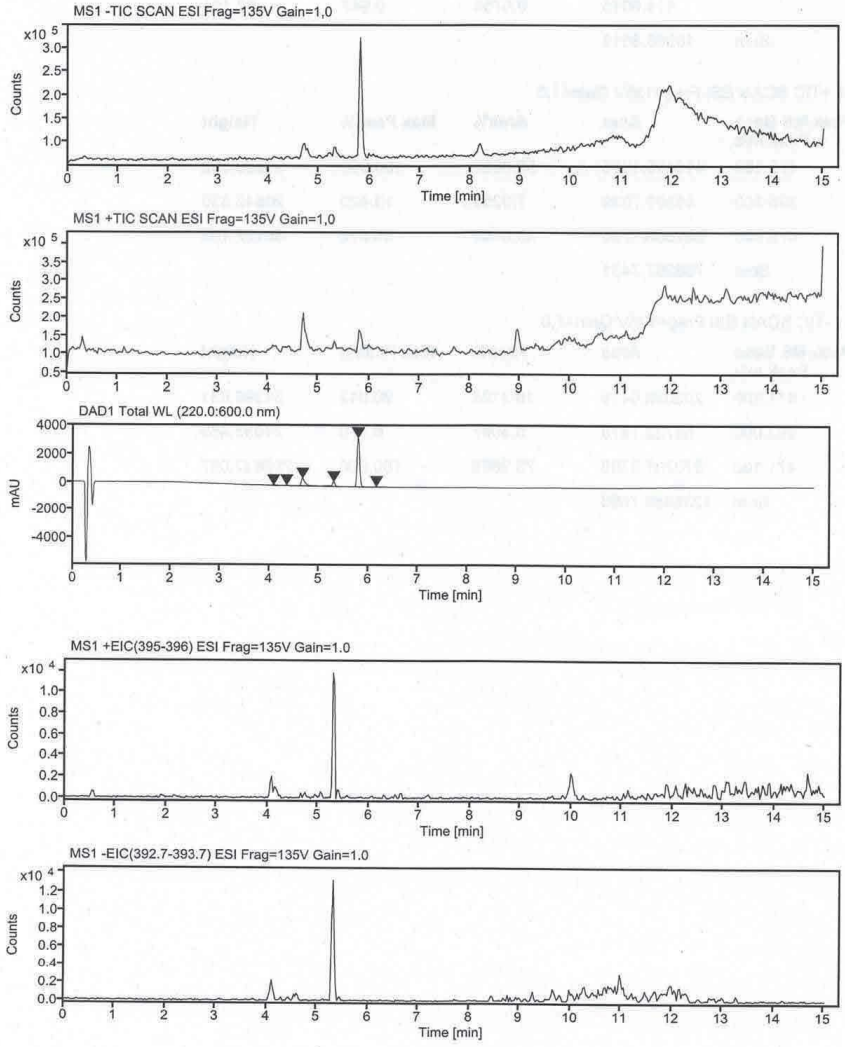


MS1 +TIC SCAN ESI Frag=135V Gain=1,0RT:5.82274093733928min (Subtracted)



D:\CDSProjects\Default\0-standardplot+EIC.rdl [Rev. 8034] Printed: 2024-03-19 09:35:13+01:00 Page 2 of 2

Sequence Name:	SingleSample		
Data file:	HALP400_2.5h.dx	**Project Name:**	Single Quad
Sample name:	HALP400_2.5h	**Operator :**	SYSTEM
Instrument:	Single Quad	**Acquired on:**	2024-03-19 09:39:28+01:00
Inj. volume:	5.000	**Location:**	P1-D8
Acq. method:	00-new_wasser-acn_standard_100-1000_BD-20min.amx		
Processing method:	MS_standard_plot.pmx		



D:\CDSProjects\Default\0-standardplot+EIC.rdl [Rev. 8040] Printed: 2024-03-19 10:07:04+01:00 Page 1 of 3

Signal: DAD1 Total WL (220.0:600.0 nm)

RT [min]	Peak MS Base Peak m/z	Area	Area%	Max Peak%	Height
4.068		199.8413	1.1778	1.651	40.068
4.332		168.1052	0.9908	1.389	50.900
4.659		2934.5120	17.2956	24.244	557.124
5.285		1445.6544	8.5205	11.943	342.275
5.779		12104.1368	71.3399	100.000	3487.228
6.146		114.6015	0.6754	0.947	37.199
	Sum	16966.8513			

Signal: MS1 +TIC SCAN ESI Frag=135V Gain=1,0

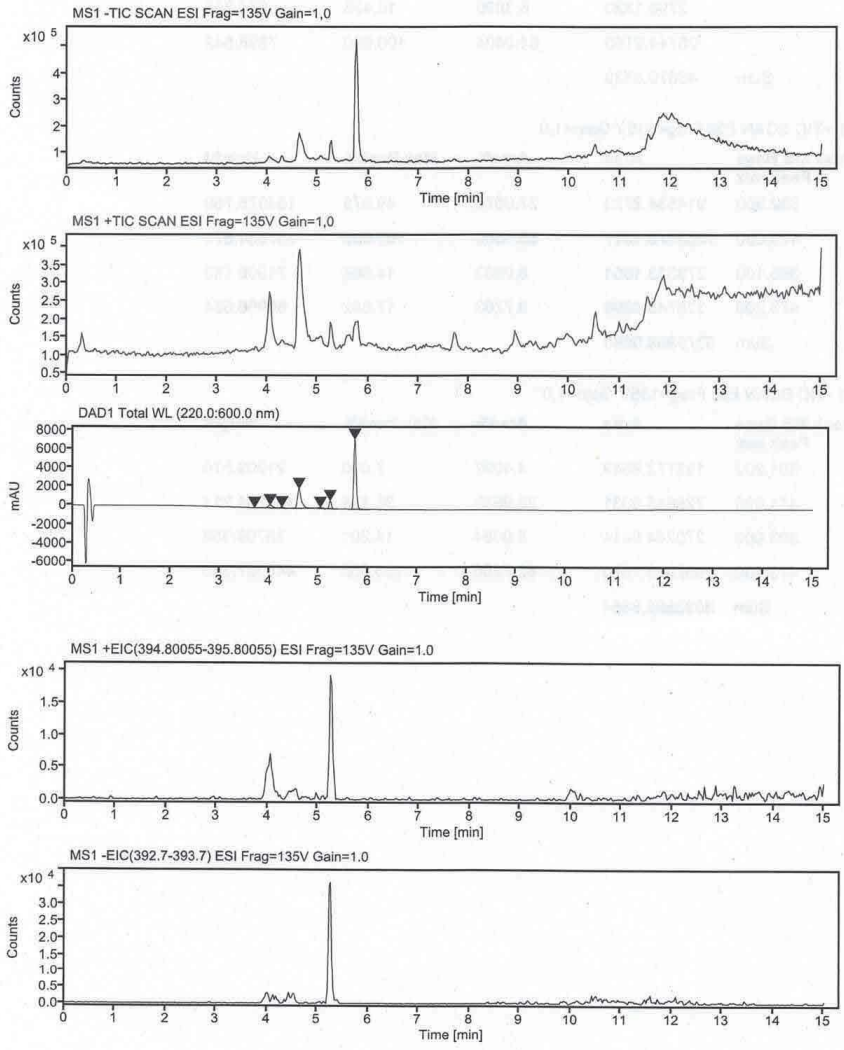
RT [min]	Peak MS Base Peak m/z	Area	Area%	Max Peak%	Height
4.700	473.100	416495.1996	59.0557	100.000	91220.552
5.313	395.300	55893.7639	7.9253	13.420	20545.336
5.815	475.300	232868.7796	33.0190	55.912	56127.103
	Sum	705257.7431			

Signal: MS1 -TIC SCAN ESI Frag=135V Gain=1,0

RT [min]	Peak MS Base Peak m/z	Area	Area%	Max Peak%	Height
4.703	471.200	202028.6419	16.3125	20.812	31396.631
5.308	393.000	65722.7479	5.3067	6.770	21053.469
5.817	471.100	970737.3799	78.3808	100.000	252832.037
	Sum	1238488.7696			

X11-4h

Sequence Name:	SingleSample		
Data file:	HALP400_4h.dx	**Project Name:**	Single Quad
Sample name:	HALP400_4h	**Operator :**	SYSTEM
Instrument:	Single Quad	**Acquired on:**	2024-03-19 11:24:58+01:00
Inj. volume:	6.000	**Location:**	P1-E1
Acq. method:	00-new_wasser-acn_standard_100-1000_BD-20min.amx		
Processing method:	MS_standard_plot.pmx		



Signal: DAD1 Total WL (220.0:600.0 nm)

RT [min]	Peak MS Base Peak m/z	Area	Area%	Max Peak%	Height
3.694		47.6714	0.1092	0.178	15.066
4.007	391.200	1978.0068	4.5294	7.396	337.383
4.245		388.4292	0.8894	1.452	124.103
4.594		11210.7943	25.6711	41.919	2064.514
5.026		511.6037	1.1715	1.913	86.558
5.225		2790.1320	6.3890	10.433	867.249
5.724		26744.2165	61.2404	100.000	7398.542
	Sum	43670.8539			

Signal: MS1 +TIC SCAN ESI Frag=135V Gain=1,0

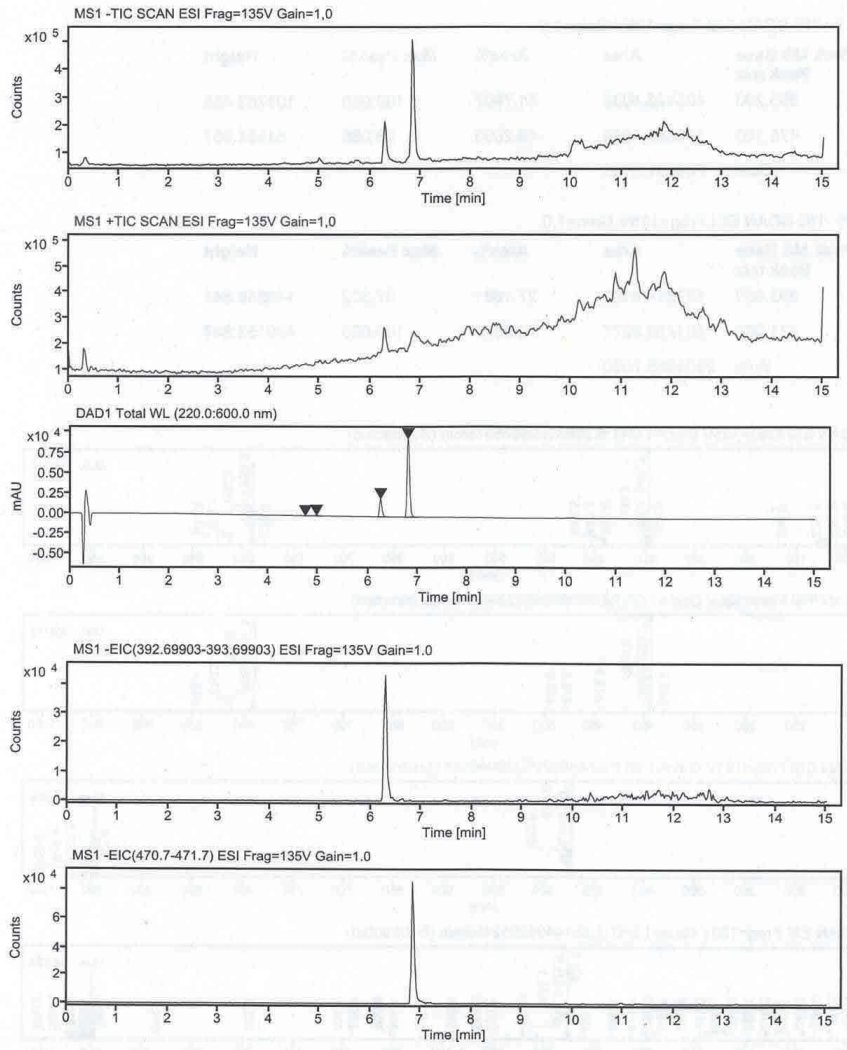
RT [min]	Peak MS Base Peak m/z	Area	Area%	Max Peak%	Height
4.044	392.900	914534.2723	27.0575	49.079	154075.769
4.638	473.000	1863376.1317	55.1300	100.000	257634.871
5.260	395.100	273313.1651	8.0863	14.668	71306.153
5.791	473.200	328745.4998	9.7263	17.642	60966.554
	Sum	3379969.0688			

Signal: MS1 -TIC SCAN ESI Frag=135V Gain=1,0

RT [min]	Peak MS Base Peak m/z	Area	Area%	Max Peak%	Height
4.030	391.200	133772.9549	4.4097	7.030	21209.570
4.633	471.000	726645.9331	23.9533	38.186	101864.214
5.259	393.000	270244.8414	8.9084	14.201	75709.358
5.760	473.100	1902933.1370	62.7286	100.000	445387.383
	Sum	3033596.8664			

XII-75h

Sequence Name:	SingleSample		
Data file:	HALP400_7.5h.dx	**Project Name:**	Single Quad
Sample name:	HALP400_7.5h	**Operator :**	SYSTEM
Instrument:	Single Quad	**Acquired on:**	2024-03-20 06:30:26+01:00
Inj. volume:	6.000	**Location:**	P2-C2
Acq. method:	00-new_wasser-acn_standard_100-1000_BD-20min.amx		
Processing method:	MS_standard_plot.pmx		



Signal: DAD1 Total WL (220.0:600.0 nm)

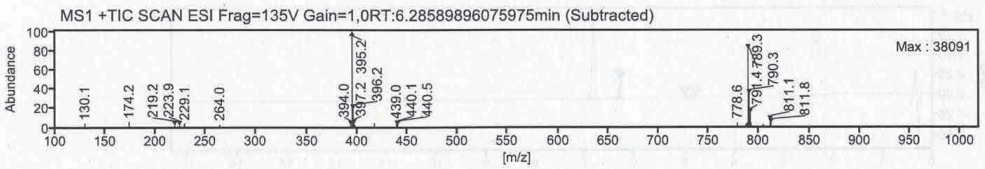
RT [min]	Peak MS Base Peak m/z	Area	Area%	Max Peak%	Height
4.744		67.1042	0.1504	0.184	20.074
4.968		340.9777	0.7642	0.937	103.230
6.256		7829.6414	17.5479	21.521	2248.573
6.814		36380.9557	81.5375	100.000	9670.496
	Sum	44618.6790			

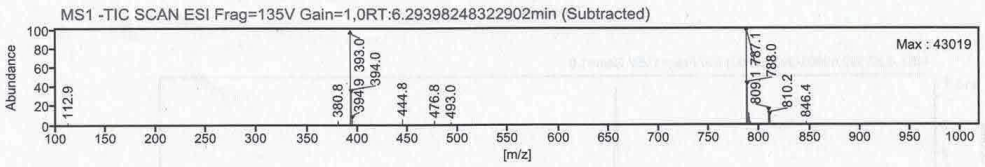
Signal: MS1 +TIC SCAN ESI Frag=135V Gain=1,0

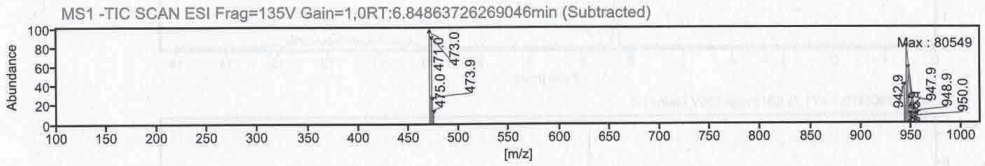
RT [min]	Peak MS Base Peak m/z	Area	Area%	Max Peak%	Height
6.286	395.200	406495.4039	51.7907	100.000	101763.458
6.881	475.100	378386.4065	48.2093	93.085	51581.907
	Sum	784881.8104			

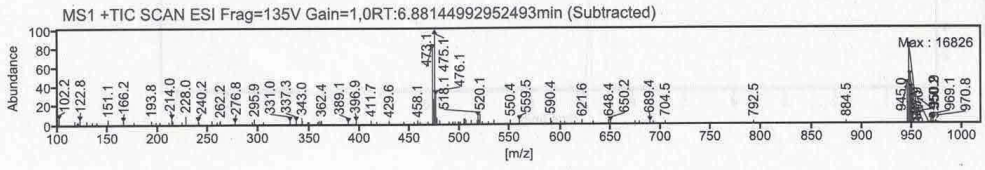
Signal: MS1 -TIC SCAN ESI Frag=135V Gain=1,0

RT [min]	Peak MS Base Peak m/z	Area	Area%	Max Peak%	Height
6.294	393.000	627217.4102	27.1681	37.302	146556.846
6.849	471.000	1681438.3277	72.8319	100.000	429153.847
	Sum	2308655.7380			





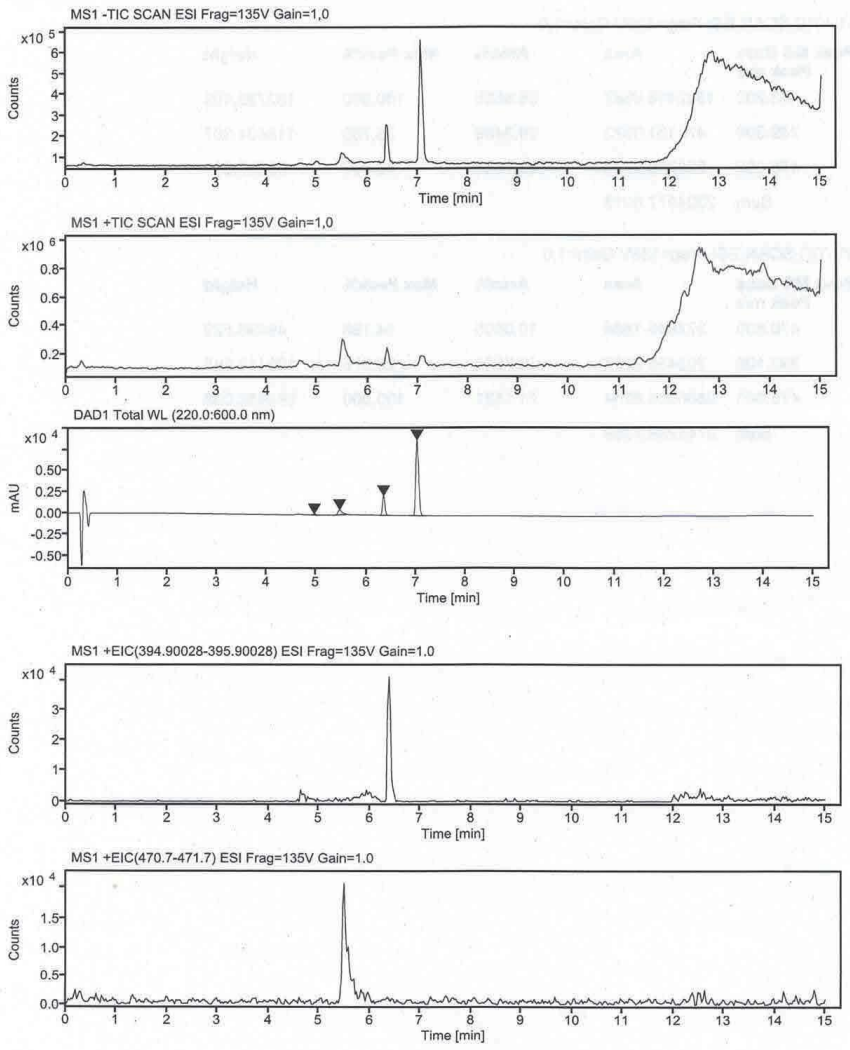




D:\CDSProjects\Default\0-standardplot+EIC.rdl [Rev. 8073] Printed: 2024-03-20 07:48:38+01:00 Page 2 of 2

XII - 9h

Sequence Name:	SingleSample		
Data file:	HALP400_9h.dx	**Project Name:**	Single Quad
Sample name:	HALP400_9h	**Operator :**	SYSTEM
Instrument:	Single Quad	**Acquired on:**	2024-03-20 06:51:28+01:00
Inj. volume:	6.000	**Location:**	P2-C3
Acq. method:	00-new_wasser-acn_standard_100-1000_BD-20min.amx		
Processing method:	MS_standard_plot.pmx		



Signal: DAD1 Total WL (220.0:600.0 nm)

RT [min]	Peak MS Base Peak m/z	Area	Area%	Max Peak%	Height
4.961		420.5874	0.8751	1.167	120.103
5.469		3534.3654	7.3537	9.810	580.247
6.352		8080.5137	16.8126	22.429	2289.852
7.029		36026.8815	74.9586	100.000	8890.536
	Sum	48062.3480			

Signal: MS1 +TIC SCAN ESI Frag=135V Gain=1,0

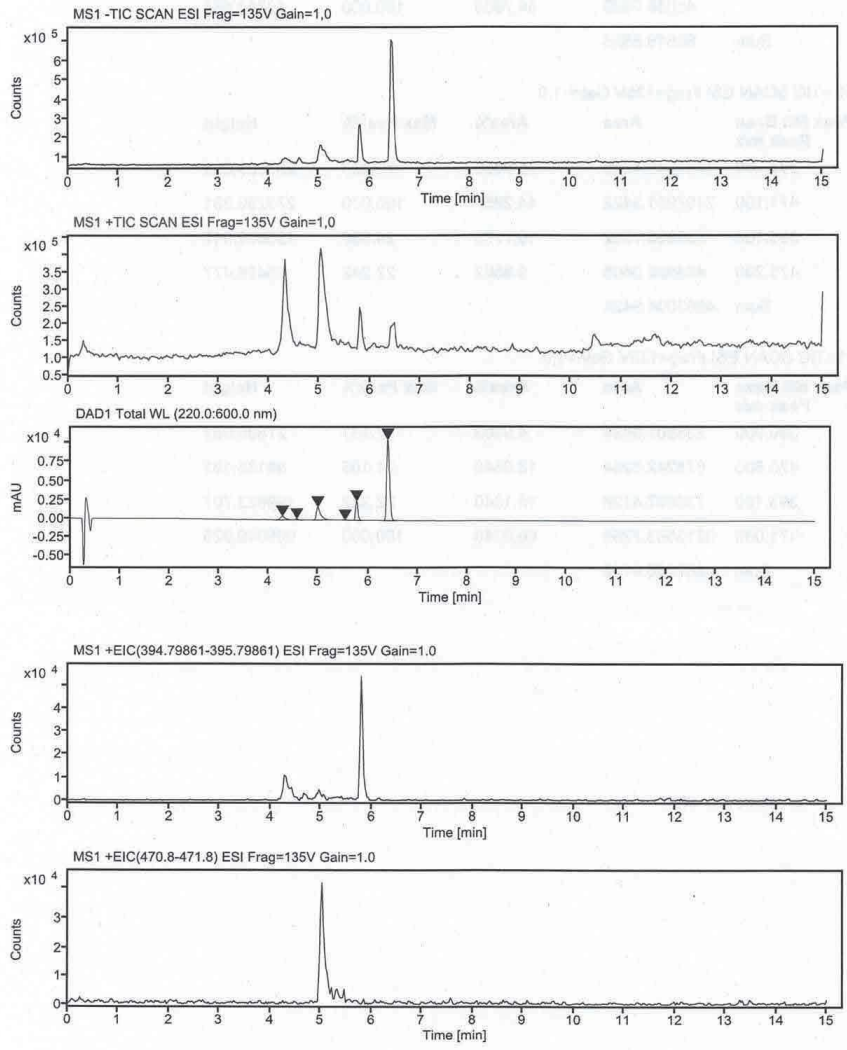
RT [min]	Peak MS Base Peak m/z	Area	Area%	Max Peak%	Height
5.509	473.200	1322116.9667	56.8658	100.000	182728.499
6.386	789.300	473131.3573	20.3499	35.786	118404.307
7.084	475.000	529729.2773	22.7843	40.067	68237.591
	Sum	2324977.6013			

Signal: MS1 -TIC SCAN ESI Frag=135V Gain=1,0

RT [min]	Peak MS Base Peak m/z	Area	Area%	Max Peak%	Height
5.497	470.800	377846.1888	10.0805	14.168	49496.529
6.384	393.100	703455.9227	18.7674	26.376	196413.665
7.064	473.000	2666986.6254	71.1521	100.000	584464.093
	Sum	3748288.7369			

XII-11h

Sequence Name:	SingleSample		
Data file:	HALP400_11h.dx	**Project Name:**	Single Quad
Sample name:	HALP400_11h	**Operator :**	SYSTEM
Instrument:	Single Quad	**Acquired on:**	2024-03-20 07:12:32+01:00
Inj. volume:	6.000	**Location:**	P2-C4
Acq. method:	00-new_wasser-acn_standard_100-1000_BD-20min.amx		
Processing method:	MS_standard_plot.pmx		



Signal: DAD1 Total WL (220.0:600.0 nm)

RT [min]	Peak MS Base Peak m/z	Area	Area%	Max Peak%	Height
4.280	393.200	3635.6246	5.2296	8.072	544.555
4.572		634.3608	0.9125	1.408	185.252
4.996	470.800	10898.5058	15.6769	24.198	1750.594
5.542		207.9161	0.2991	0.462	40.274
5.775		9104.3632	13.0961	20.214	2624.757
6.403		45038.7820	64.7858	100.000	10748.566
	Sum	69519.5526			

Signal: MS1 +TIC SCAN ESI Frag=135V Gain=1,0

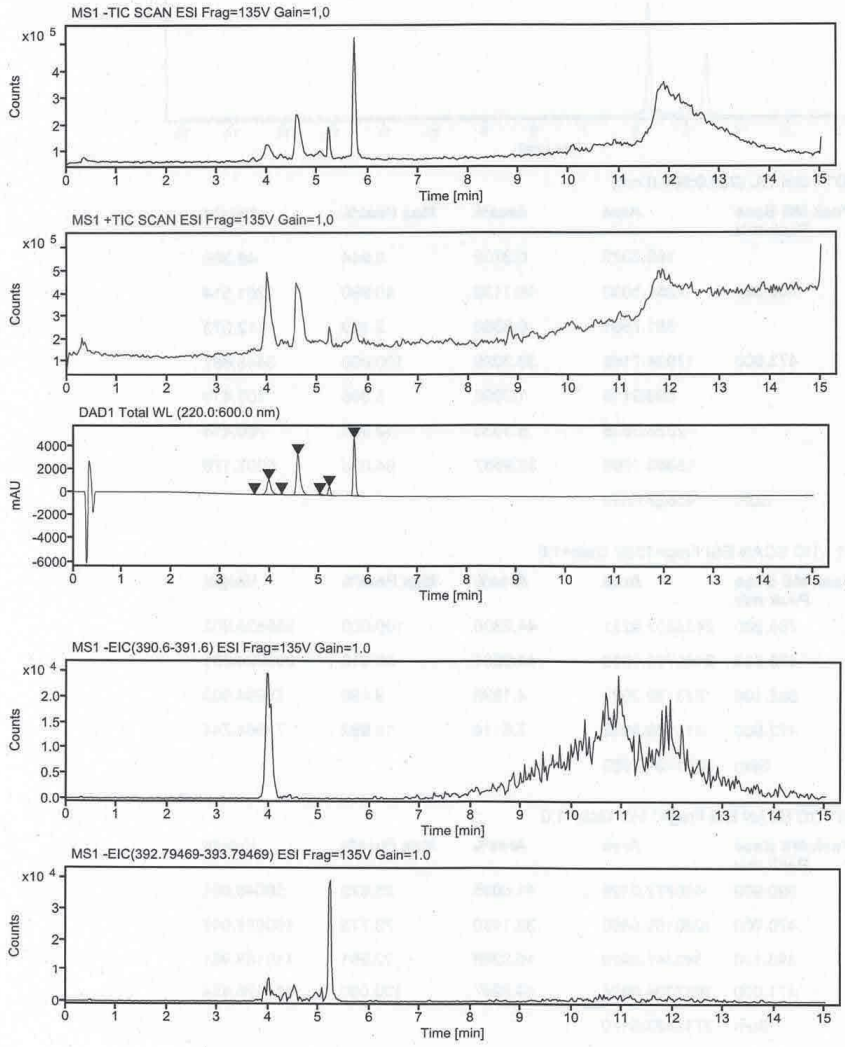
RT [min]	Peak MS Base Peak m/z	Area	Area%	Max Peak%	Height
4.316	393.200	1741348.4845	35.0866	79.228	257096.863
5.032	471.100	2197901.3422	44.2857	100.000	273290.331
5.813	395.100	534888.7552	10.7775	24.336	125802.917
6.485	475.200	488866.3605	9.8502	22.242	75456.477
	Sum	4963004.9424			

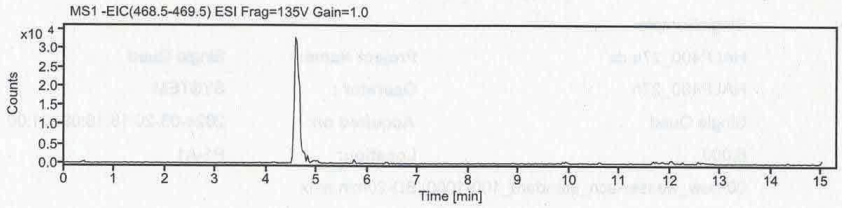
Signal: MS1 -TIC SCAN ESI Frag=135V Gain=1,0

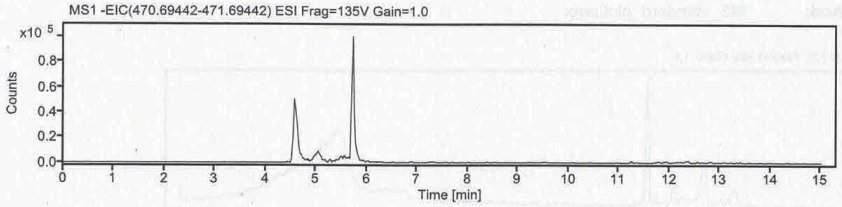
RT [min]	Peak MS Base Peak m/z	Area	Area%	Max Peak%	Height
4.327	390.900	238801.9494	4.9063	7.431	27880.051
5.031	470.800	678242.3264	13.9349	21.105	88135.183
5.806	393.100	736607.4126	15.1340	22.922	199823.707
6.439	471.000	3213583.7258	66.0248	100.000	669949.926
	Sum	4867235.4142			

XII-27h

Sequence Name:	SingleSample		
Data file:	HALP400_27h.dx	**Project Name:**	Single Quad
Sample name:	HALP400_27h	**Operator :**	SYSTEM
Instrument:	Single Quad	**Acquired on:**	2024-03-20 18:18:08+01:00
Inj. volume:	6.000	**Location:**	P1-A1
Acq. method:	00-new_wasser-acn_standard_100-1000_BD-20min.amx		
Processing method:	MS_standard_plot.pmx		







Signal: DAD1 Total WL (220.0:600.0 nm)

RT [min]	Peak MS Base Peak m/z	Area	Area%	Max Peak%	Height
3.677		169.2379	0.3709	0.944	46.399
3.964	786.200	7351.5053	16.1133	40.990	1261.514
4.223		381.7581	0.8368	2.129	112.073
4.557	473.000	17934.7165	39.3099	100.000	3448.687
5.002		592.9116	1.2996	3.306	105.419
5.192		2328.5638	5.1038	12.984	760.414
5.697		16865.1708	36.9657	94.036	4967.170
	Sum	45623.8639			

Signal: MS1 +TIC SCAN ESI Frag=135V Gain=1,0

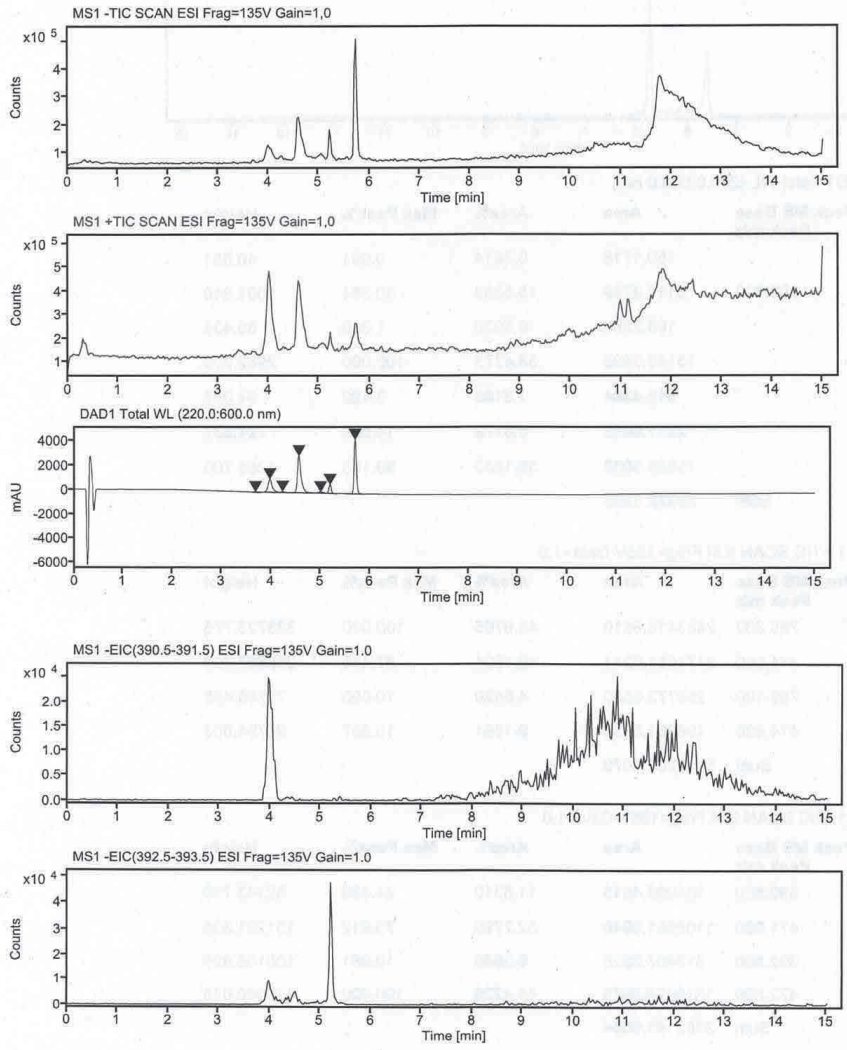
RT [min]	Peak MS Base Peak m/z	Area	Area%	Max Peak%	Height
3.990	786.200	2455302.0231	44.2306	100.000	339820.802
4.574	473.000	2445724.0838	44.0581	99.610	295294.231
5.224	395.100	233139.2521	4.1998	9.495	75954.900
5.727	472.900	416969.3933	7.5114	16.982	78664.744
	Sum	5551134.7523			

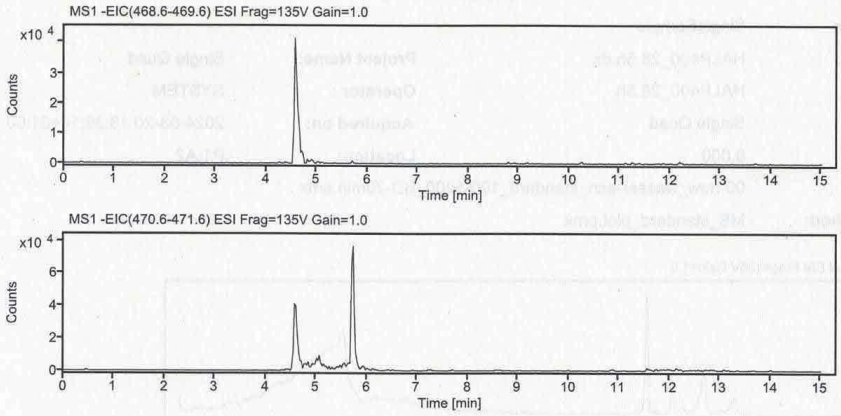
Signal: MS1 -TIC SCAN ESI Frag=135V Gain=1,0

RT [min]	Peak MS Base Peak m/z	Area	Area%	Max Peak%	Height
4.002	390.900	430772.0128	11.6035	25.829	50040.951
4.589	470.700	1230409.5498	33.1430	73.775	160856.947
5.210	393.100	383447.2920	10.3288	22.991	110168.981
5.732	471.000	1667794.6624	44.9247	100.000	441128.454
	Sum	3712423.5170			

X11-285h

Sequence Name:	SingleSample		
Data file:	HALP400_28.5h.dx	**Project Name:**	Single Quad
Sample name:	HALP400_28.5h	**Operator :**	SYSTEM
Instrument:	Single Quad	**Acquired on:**	2024-03-20 18:39:14+01:00
Inj. volume:	6.000	**Location:**	P1-A2
Acq. method:	00-new_wasser-acn_standard_100-1000_BD-20min.amx		
Processing method:	MS_standard_plot.pmx		





Signal: DAD1 Total WL (220.0:600.0 nm)

RT [min]	Peak MS Base Peak m/z	Area	Area%	Max Peak%	Height
3.676		150.1718	0.3814	0.991	40.551
3.965	390.800	6117.9789	15.5388	40.384	1091.840
4.223		198.2395	0.5035	1.309	89.434
4.556		15149.3405	38.4773	100.000	2982.209
4.994		518.4384	1.3168	3.422	94.097
5.183		2211.6013	5.6172	14.599	721.837
5.693		15026.3888	38.1650	99.188	4385.700
	Sum	39372.1593			

Signal: MS1 +TIC SCAN ESI Frag=135V Gain=1,0

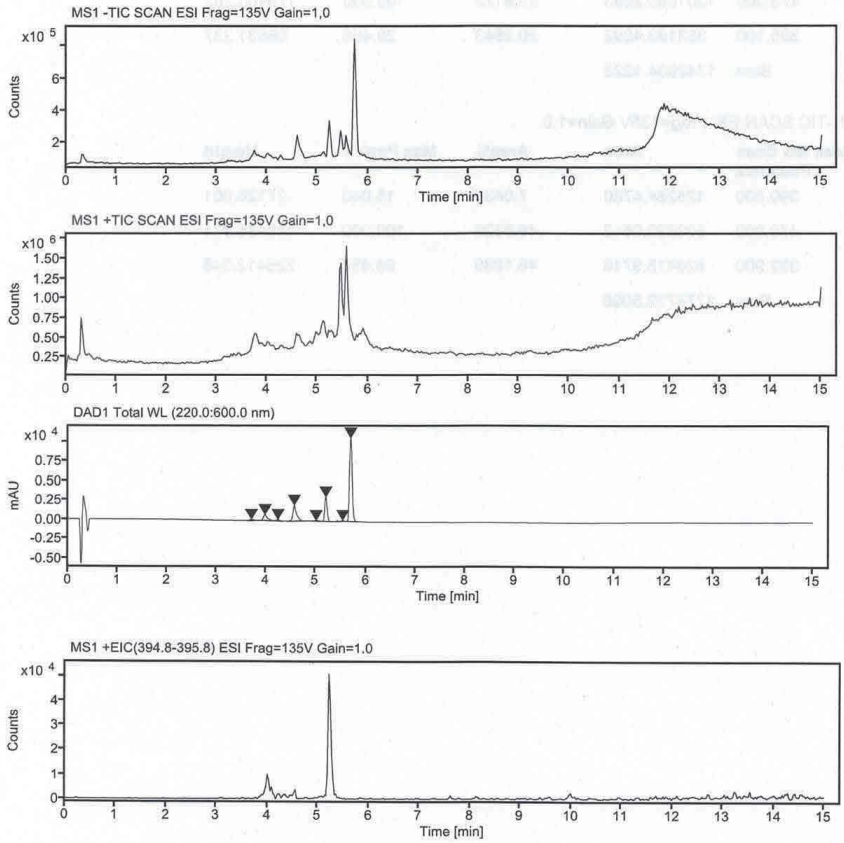
RT [min]	Peak MS Base Peak m/z	Area	Area%	Max Peak%	Height
4.005	785.300	2483416.6510	45.9705	100.000	333723.775
4.597	471.000	2171651.0211	40.1994	87.446	280667.309
5.224	789.100	250772.5520	4.6420	10.098	78785.435
5.733	474.800	496361.8838	9.1881	19.987	96794.803
	Sum	5402202.1079			

Signal: MS1 -TIC SCAN ESI Frag=135V Gain=1,0

RT [min]	Peak MS Base Peak m/z	Area	Area%	Max Peak%	Height
3.994	390.800	389993.4615	11.5310	24.839	52143.710
4.592	471.000	1108661.9949	32.7799	70.612	151201.336
5.210	392.800	313407.3325	9.2665	19.961	100196.829
5.729	472.800	1570078.8675	46.4226	100.000	427060.618
	Sum	3382141.6564			

X11-31.5h

Sequence Name:	SingleSample		
Data file:	HALP400-31.5h.dx	**Project Name:**	Single Quad
Sample name:	HALP400-31.5h	**Operator :**	SYSTEM
Instrument:	Single Quad	**Acquired on:**	2024-03-21 20:22:44+01:00
Inj. volume:	6.000	**Location:**	P1-D8
Acq. method:	00-new_wasser-acn_standard_100-1000_BD-20min.amx		
Processing method:	MS_standard_plot.pmx		



Signal: DAD1 Total WL (220.0:600.0 nm)

RT [min]	Peak MS Base Peak m/z	Area	Area%	Max Peak%	Height
3.706		611.9783	0.9054	1.555	128.782
3.978		4133.1490	6.1146	10.503	743.190
4.238		602.0265	0.8906	1.530	172.283
4.567		11279.7686	16.6874	28.663	2050.038
5.011		487.5508	0.7213	1.239	87.629
5.203		10480.7866	15.5053	26.633	3185.210
5.543		646.2126	0.9560	1.642	120.440

RT [min]	Peak MS Base Peak m/z	Area	Area%	Max Peak%	Height
5.702		39353.1919	58.2194	100.000	10731.233
	Sum	67594.6643			

Signal: MS1 +TIC SCAN ESI Frag=135V Gain=1,0

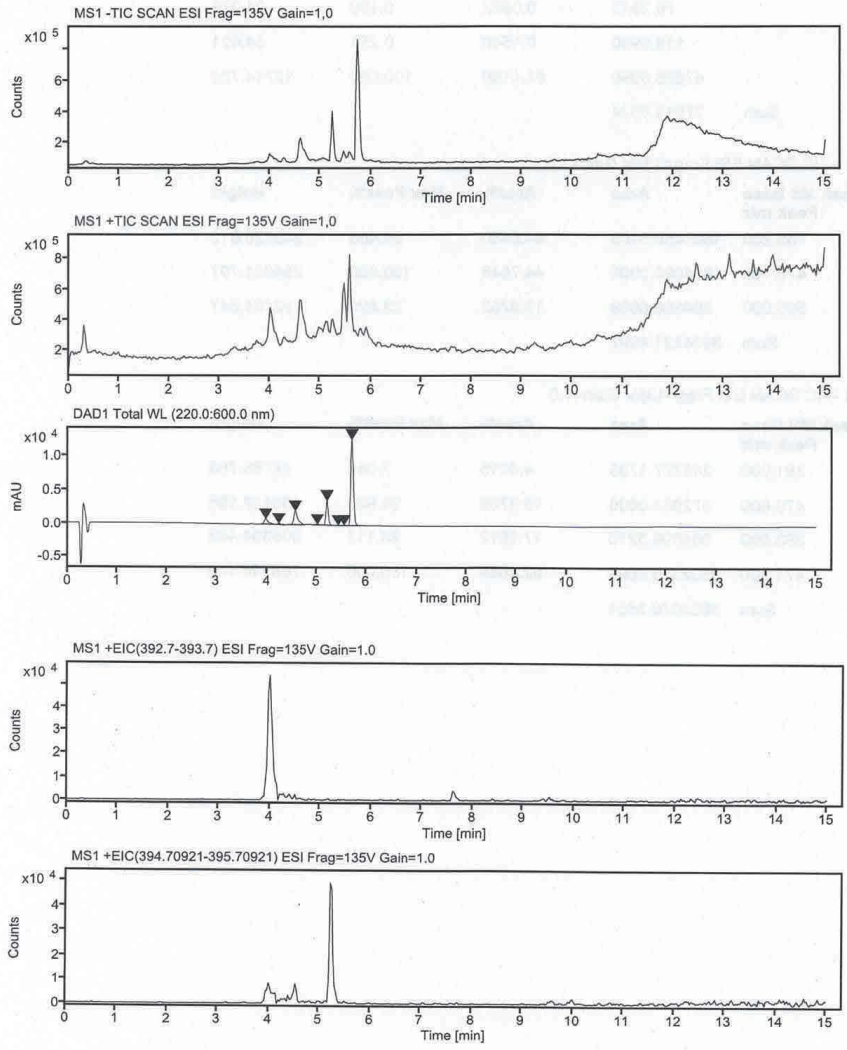
RT [min]	Peak MS Base Peak m/z	Area	Area%	Max Peak%	Height
4.017	393.200	188645.5049	10.8234	15.706	54582.524
4.596	473.000	1201095.2083	68.9123	100.000	179480.262
5.225	395.100	353193.4092	20.2643	29.406	66531.237
	Sum	1742934.1223			

Signal: MS1 -TIC SCAN ESI Frag=135V Gain=1,0

RT [min]	Peak MS Base Peak m/z	Area	Area%	Max Peak%	Height
4.009	390.800	125284.4780	7.0435	15.040	27126.801
4.605	470.800	833022.0512	46.8326	100.000	148486.971
5.239	392.900	820415.9716	46.1239	98.487	225412.548
	Sum	1778722.5008			

XII-33,5h

Sequence Name:	SingleSample		
Data file:	HALP400-33.5h.dx	**Project Name:**	Single Quad
Sample name:	HALP400-33.5h	**Operator :**	SYSTEM
Instrument:	Single Quad	**Acquired on:**	2024-03-21 20:43:48+01:00
Inj. volume:	6.000	**Location:**	P1-D9
Acq. method:	00-new_wasser-acn_standard_100-1000_BD-20min.amx		
Processing method:	MS_standard_plot.pmx		



Signal: DAD1 Total WL (220.0:600.0 nm)

RT [min]	Peak MS Base Peak m/z	Area	Area%	Max Peak%	Height
3.976		4737.1981	6.0999	9.932	852.889
4.237		549.9082	0.7081	1.153	179.973
4.565		11710.3616	15.0790	24.552	2127.176
5.012		486.1905	0.6261	1.019	98.337
5.204		12284.7359	15.8186	25.757	3713.479
5.428		76.2542	0.0982	0.160	24.279
5.546		119.5950	0.1540	0.251	34.621
5.701		47695.6090	61.4160	100.000	12714.738
	Sum	77659.8524			

Signal: MS1 +TIC SCAN ESI Frag=135V Gain=1,0

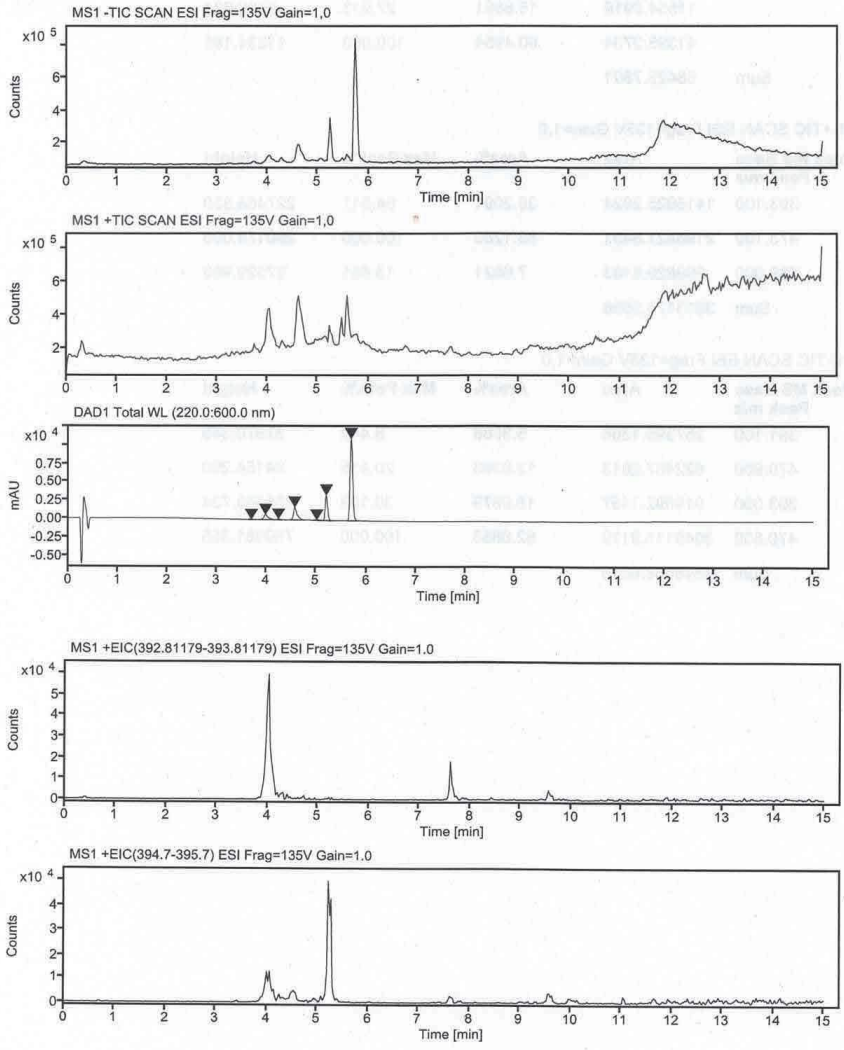
RT [min]	Peak MS Base Peak m/z	Area	Area%	Max Peak%	Height
4.013	785.200	1605456.5103	44.5450	99.465	243726.510
4.603	473.100	1614098.3006	44.7848	100.000	254051.797
5.242	395.000	384566.6889	10.6702	23.825	92754.547
	Sum	3604121.4997			

Signal: MS1 -TIC SCAN ESI Frag=135V Gain=1,0

RT [min]	Peak MS Base Peak m/z	Area	Area%	Max Peak%	Height
4.000	391.000	246777.1735	4.4015	7.046	44785.783
4.600	470.600	872984.0606	15.5705	24.926	135182.598
5.239	393.000	984598.3215	17.5612	28.113	305394.483
5.739	471.000	3502310.8095	62.4669	100.000	768744.405
	Sum	5606670.3651			

XII - 36h

Sequence Name:	SingleSample		
Data file:	HALP400-36h.dx	**Project Name:**	Single Quad
Sample name:	HALP400-36h	**Operator :**	SYSTEM
Instrument:	Single Quad	**Acquired on:**	2024-03-21 21:04:51+01:00
Inj. volume:	6.000	**Location:**	P1-D10
Acq. method:	00-new_wasser-acn_standard_100-1000_BD-20min.amx		
Processing method:	MS_standard_plot.pmx		



Signal: DAD1 Total WL (220.0:600.0 nm)

RT [min]	Peak MS Base Peak m/z	Area	Area%	Max Peak%	Height
3.695		258.7543	0.3782	0.625	70.044
3.978		4569.0537	6.6776	11.038	766.790
4.238		496.0991	0.7250	1.199	152.542
4.568		9750.5982	14.2503	23.556	1789.618
5.012		401.9098	0.5874	0.971	82.644
5.203		11554.0916	16.8861	27.913	3496.624
5.703		41393.2734	60.4954	100.000	11234.185
	Sum	68423.7801			

Signal: MS1 +TIC SCAN ESI Frag=135V Gain=1,0

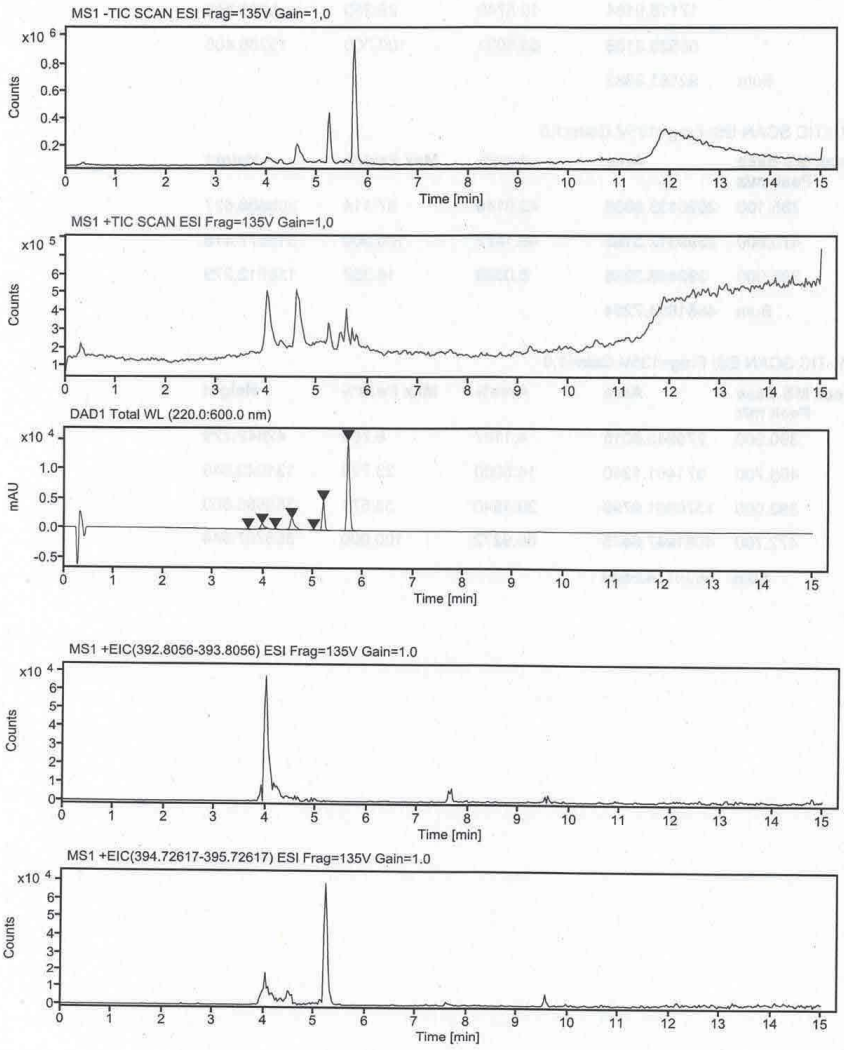
RT [min]	Peak MS Base Peak m/z	Area	Area%	Max Peak%	Height
4.025	393.100	1416925.2924	36.2091	64.511	227465.830
4.614	473.100	2196421.8491	56.1289	100.000	290179.005
5.225	789.000	299829.8183	7.6621	13.651	87529.966
	Sum	3913176.9598			

Signal: MS1 -TIC SCAN ESI Frag=135V Gain=1,0

RT [min]	Peak MS Base Peak m/z	Area	Area%	Max Peak%	Height
4.031	391.100	257395.1366	5.3086	8.442	37870.345
4.612	470.900	622487.2813	12.8383	20.415	94154.250
5.239	393.000	919692.3457	18.9679	30.163	266963.734
5.736	470.800	3049113.9179	62.8853	100.000	750981.355
	Sum	4848688.6815			

X11-51.5h

Sequence Name:	SingleSample		
Data file:	HALP400-51.5h.dx	**Project Name:**	Single Quad
Sample name:	HALP400-51.5h	**Operator :**	SYSTEM
Instrument:	Single Quad	**Acquired on:**	2024-03-21 21:25:54+01:00
Inj. volume:	6.000	**Location:**	P1-D11
Acq. method:	00-new_wasser-acn_standard_100-1000_BD-20min.amx		
Processing method:	MS_standard_plot.pmx		



Signal: DAD1 Total WL (220.0:600.0 nm)

RT [min]	Peak MS Base Peak m/z	Area	Area%	Max Peak%	Height
3.694		295.1815	0.3203	0.504	91.150
3.975		4071.3352	4.4176	6.957	847.680
4.236		449.7583	0.4880	0.768	156.946
4.564		11331.5353	12.2953	19.362	2017.493
5.010		369.2938	0.4007	0.631	83.730
5.201		17118.9184	18.5749	29.250	5096.542
5.694		58525.3158	63.5031	100.000	15286.400
	Sum	92161.3382			

Signal: MS1 +TIC SCAN ESI Frag=135V Gain=1,0

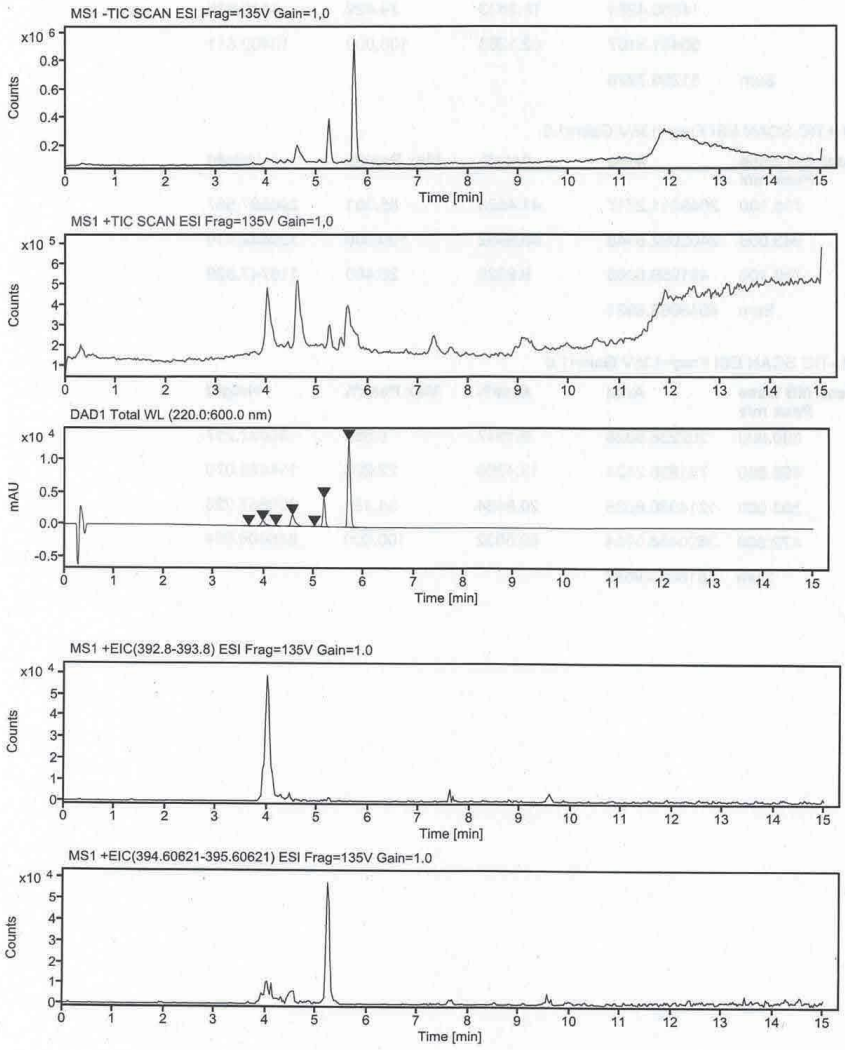
RT [min]	Peak MS Base Peak m/z	Area	Area%	Max Peak%	Height
4.014	785.100	2090133.8036	42.8140	87.114	305686.627
4.597	470.800	2399312.5182	49.1472	100.000	315077.418
5.225	395.000	392448.3986	8.0389	16.357	110512.279
	Sum	4881894.7204			

Signal: MS1 -TIC SCAN ESI Frag=135V Gain=1,0

RT [min]	Peak MS Base Peak m/z	Area	Area%	Max Peak%	Height
4.003	390.900	275943.8015	4.1187	6.760	42642.729
4.603	468.700	971461.1240	14.5000	23.799	131043.645
5.233	393.000	1370361.9799	20.4540	33.571	359886.803
5.731	472.700	4081947.6475	60.9272	100.000	885767.944
	Sum	6699714.5529			

XII-54h

Sequence Name:	SingleSample		
Data file:	HALP400-54h.dx	**Project Name:**	Single Quad
Sample name:	HALP400-54h	**Operator :**	SYSTEM
Instrument:	Single Quad	**Acquired on:**	2024-03-21 21:46:57+01:00
Inj. volume:	6.000	**Location:**	P1-E3
Acq. method:	00-new_wasser-acn_standard_100-1000_BD-20min.amx		
Processing method:	MS_standard_plot.pmx		



Signal: DAD1 Total WL (220.0:600.0 nm)

RT [min]	Peak MS Base Peak m/z	Area	Area%	Max Peak%	Height
3.694		309.1187	0.3804	0.612	87.203
3.975		4685.2718	5.7660	9.281	818.283
4.236		455.0897	0.5601	0.901	153.270
4.565		10112.8691	12.4456	20.033	1812.322
5.011		356.1993	0.4384	0.706	78.796
5.201		14856.4284	18.2833	29.429	4442.825
5.698		50481.8107	62.1263	100.000	13402.611
	Sum	81256.7876			

Signal: MS1 +TIC SCAN ESI Frag=135V Gain=1,0

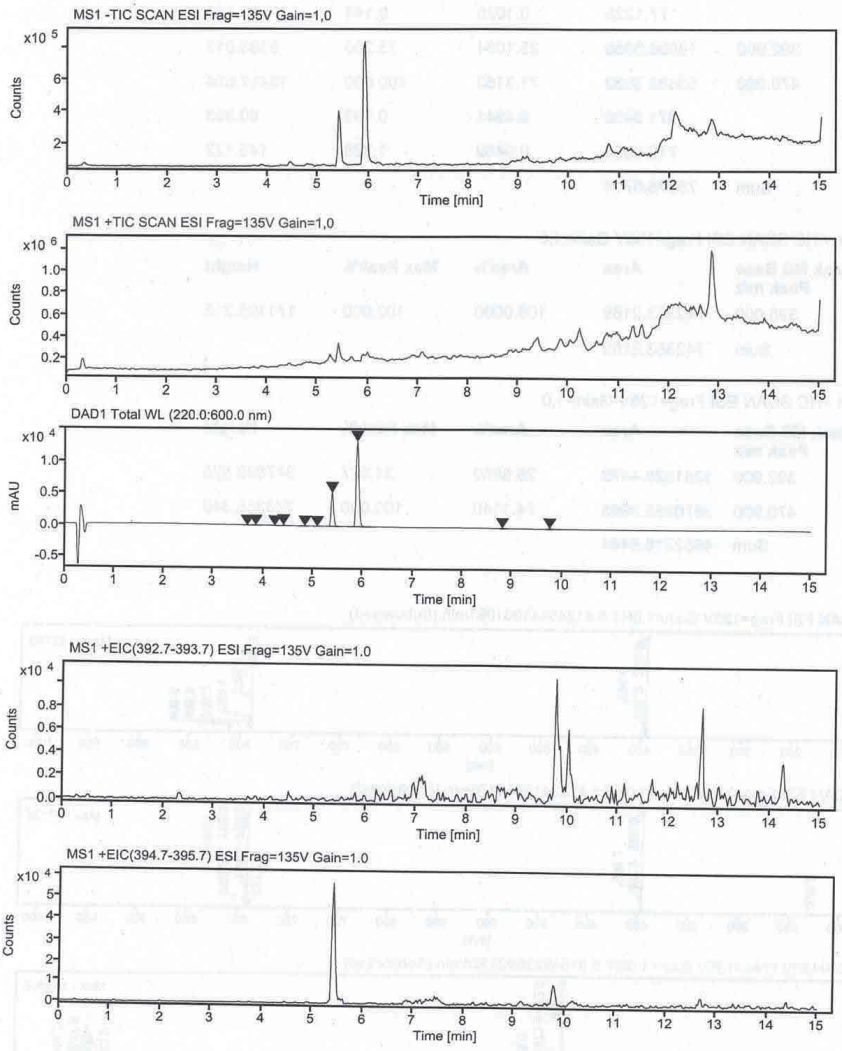
RT [min]	Peak MS Base Peak m/z	Area	Area%	Max Peak%	Height
4.013	785.100	2049011.2717	41.4523	85.301	296597.567
4.605	943.000	2402092.8148	48.5952	100.000	329842.416
5.242	789.100	491959.6065	9.9525	20.480	116747.829
	Sum	4943063.6931			

Signal: MS1 -TIC SCAN ESI Frag=135V Gain=1,0

RT [min]	Peak MS Base Peak m/z	Area	Area%	Max Peak%	Height
4.005	390.800	302258.5828	5.1947	8.586	39037.217
4.606	468.800	781838.2124	13.4368	22.208	114428.070
5.236	393.000	1214080.8036	20.8654	34.486	309857.226
5.734	472.900	3520458.3704	60.5032	100.000	846606.664
	Sum	5818635.9692			

XII-59h

Sequence Name:	SingleSample		
Data file:	2024-03-22 06-32-19+01-00.dx	**Project Name:**	Single Quad
Sample name:	HALP400_59h	**Operator :**	SYSTEM
Instrument:	Single Quad	**Acquired on:**	2024-03-22 06:33:36+01:00
Inj. volume:	6.000	**Location:**	P2-A1
Acq. method:	00-new_wasser-acn_standard_100-1000_BD-20min.amx		
Processing method:	MS_standard_plot.pmx		



Signal: DAD1 Total WL (220.0:600.0 nm)

RT [min]	Peak MS Base Peak m/z	Area	Area%	Max Peak%	Height
3.675		97.3102	0.1293	0.181	30.064
3.848		284.9634	0.3786	0.531	74.319
4.226		127.6004	0.1695	0.238	28.273
4.402		716.0985	0.9513	1.334	213.603
4.837		307.2626	0.4082	0.572	76.470
5.084		77.1225	0.1025	0.144	23.480
5.381	392.900	18896.5856	25.1034	35.200	5393.013
5.883	470.900	53683.3832	71.3163	100.000	13417.694
8.808		371.9400	0.4941	0.693	80.993
9.757		712.8050	0.9469	1.328	145.122
	Sum	75275.0714			

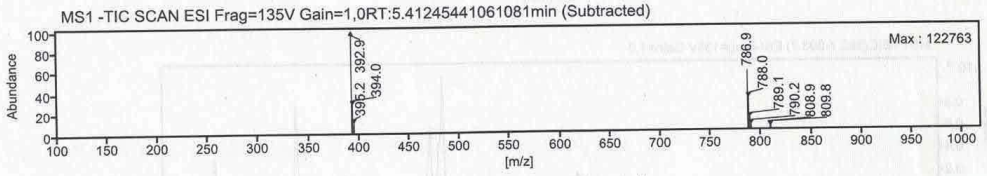
Signal: MS1 +TIC SCAN ESI Frag=135V Gain=1,0

RT [min]	Peak MS Base Peak m/z	Area	Area%	Max Peak%	Height
5.418	395.000	742353.2169	100.0000	100.000	171195.213
	Sum	742353.2169			

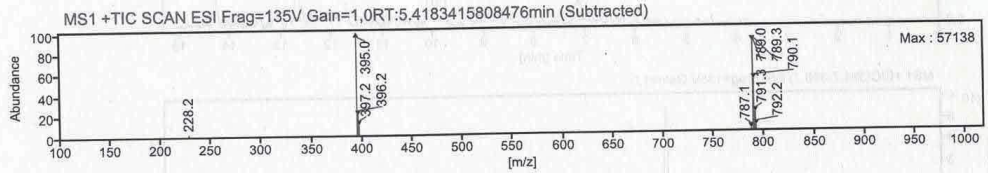
Signal: MS1 -TIC SCAN ESI Frag=135V Gain=1,0

RT [min]	Peak MS Base Peak m/z	Area	Area%	Max Peak%	Height
5.412	392.900	1281928.4478	25.8860	34.927	347899.828
5.919	470.900	3670288.3985	74.1140	100.000	773355.340
	Sum	4952216.8464			

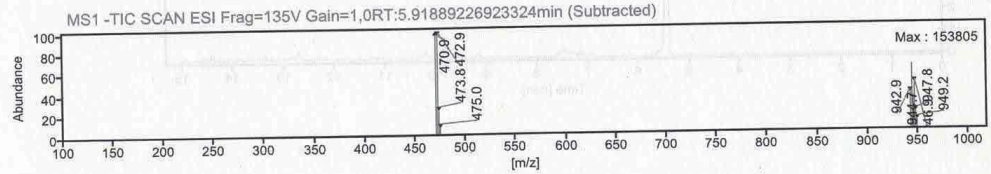
MS1 -TIC SCAN ESI Frag=135V Gain=1,0RT:5.41245441061081min (Subtracted)



MS1 +TIC SCAN ESI Frag=135V Gain=1,0RT:5.4183415808476min (Subtracted)

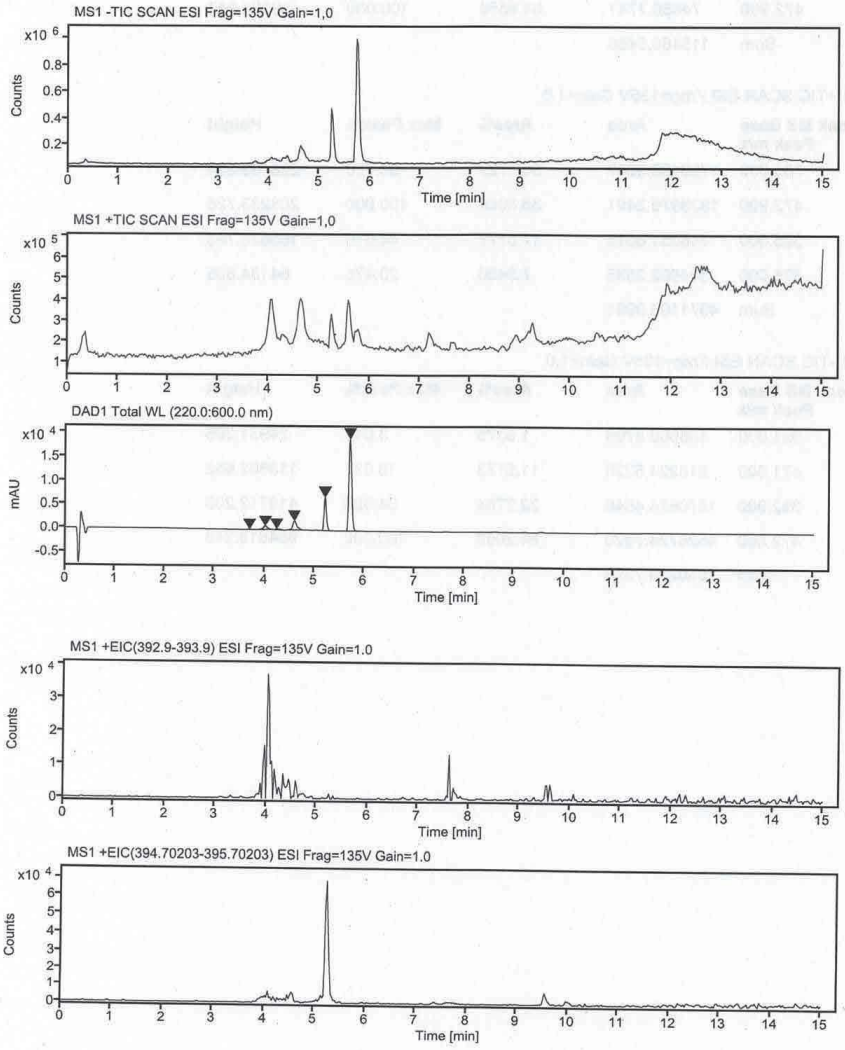


MS1 -TIC SCAN ESI Frag=135V Gain=1,0RT:5.91889226923324min (Subtracted)



X11-76h

Sequence Name:	SingleSample		
Data file:	HALP400_76h.dx	**Project Name:**	Single Quad
Sample name:	HALP400_76h	**Operator :**	SYSTEM
Instrument:	Single Quad	**Acquired on:**	2024-03-22 16:01:07+01:00
Inj. volume:	8.000	**Location:**	P2-C6
Acq. method:	00-new_wasser-acn_standard_100-1000_BD-20min.amx		
Processing method:	MS_standard_plot.pmx		



Signal: DAD1 Total WL (220.0:600.0 nm)

RT [min]	Peak MS Base Peak m/z	Area	Area%	Max Peak%	Height
3.703		395.5834	0.3426	0.528	104.074
4.017		4265.5104	3.6942	5.696	746.322
4.245		807.1664	0.6990	1.078	183.841
4.598		11249.5791	9.7427	15.022	1945.946
5.216	392.900	23861.9323	20.6657	31.864	6978.632
5.713	472.900	74886.7741	64.8558	100.000	19063.247
	Sum	115466.5456			

Signal: MS1 +TIC SCAN ESI Frag=135V Gain=1,0

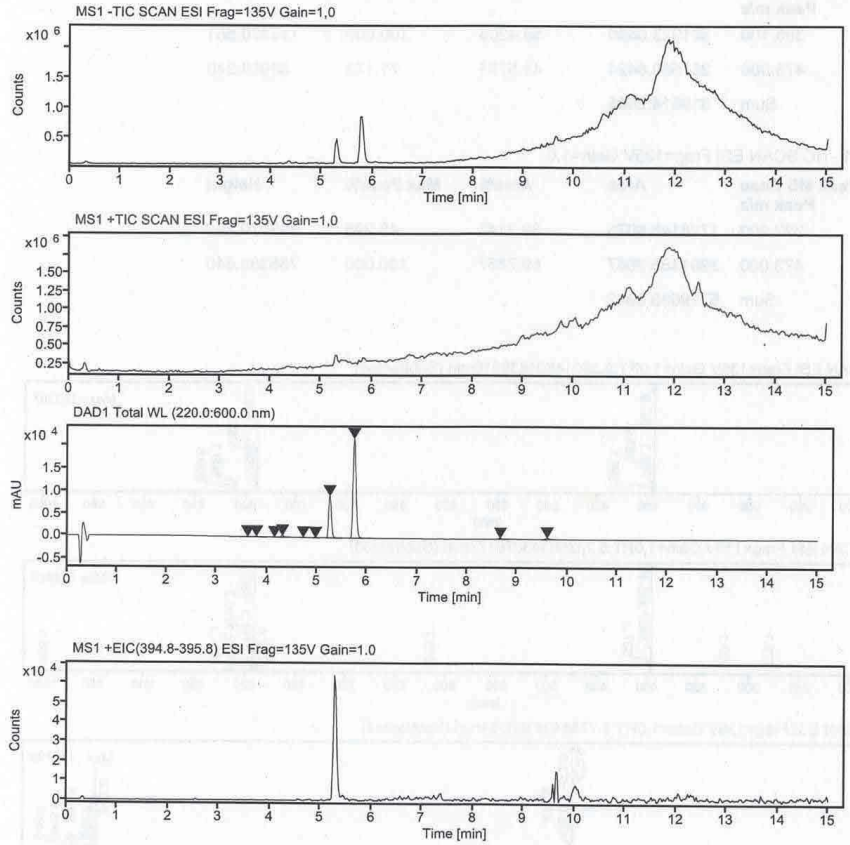
RT [min]	Peak MS Base Peak m/z	Area	Area%	Max Peak%	Height
4.051	785.300	1798193.6947	36.1729	93.220	228433.394
4.644	472.900	1928976.2491	38.8038	100.000	208233.726
5.251	395.000	848951.8019	17.0777	44.010	165638.793
5.775	475.000	394982.2535	7.9456	20.476	64134.805
	Sum	4971103.9991			

Signal: MS1 -TIC SCAN ESI Frag=135V Gain=1,0

RT [min]	Peak MS Base Peak m/z	Area	Area%	Max Peak%	Height
4.048	391.000	136600.9706	1.9375	3.018	24931.286
4.633	471.000	816224.5226	11.5773	18.031	113602.652
5.247	392.900	1570674.4546	22.2784	34.698	419712.203
5.747	472.900	4526724.7920	64.2068	100.000	984813.248
	Sum	7050224.7398			

X11 - 82

Sequence Name:	SingleSample		
Data file:	2024-03-25 06-18-20+01-00.dx	**Project Name:**	Single Quad
Sample name:	HALP400_82h	**Operator :**	SYSTEM
Instrument:	Single Quad	**Acquired on:**	2024-03-25 06:19:38+01:00
Inj. volume:	6.000	**Location:**	P2-C8
Acq. method:	00-new_wasser-acn_standard_100-1000_BD-20min.amx		
Processing method:	MS_standard_plot.pmx		



Signal: DAD1 Total WL (220.0:600.0 nm)

RT [min]	Peak MS Base Peak m/z	Area	Area%	Max Peak%	Height
3.616		223.3650	0.1709	0.243	85.375
3.791		354.1151	0.2709	0.385	135.018
4.149		194.2112	0.1486	0.211	43.661
4.308		1410.0174	1.0789	1.534	428.123
4.728		268.6276	0.2055	0.292	87.138
4.973		140.6372	0.1076	0.153	41.933
5.256		33794.4779	25.8574	36.756	9303.631

D:\CDSProjects\Default\0-standardplot+EIC.rdl [Rev. 8164] Printed: 2024-03-25 06:48:07+01:00 Page 1 of 2

RT [min]	Peak MS Base Peak m/z	Area	Area%	Max Peak%	Height
5.743		91943.2191	70.3492	100.000	21969.749
8.667		880.3874	0.6736	0.958	186.159
9.602		1486.5022	1.1374	1.617	325.955
	Sum	130695.5602			

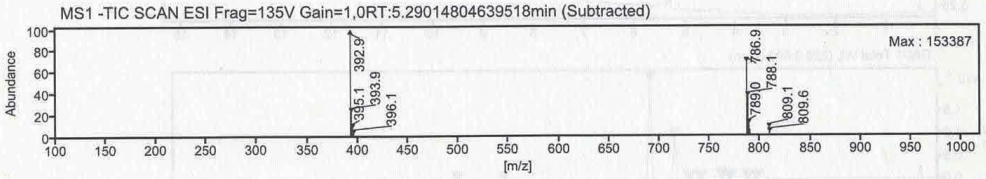
Signal: MS1 +TIC SCAN ESI Frag=135V Gain=1,0

RT [min]	Peak MS Base Peak m/z	Area	Area%	Max Peak%	Height
5.294	395.100	361923.6480	58.4205	100.000	116370.881
5.840	475.000	257590.6424	41.5795	71.173	58956.240
	Sum	619514.2905			

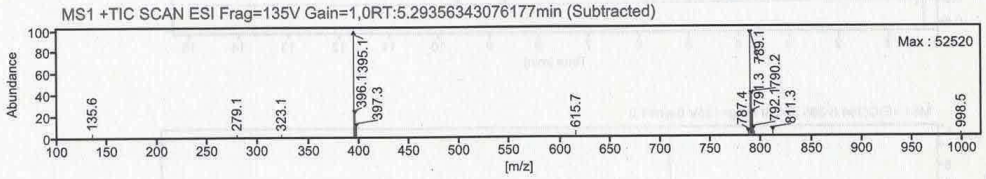
Signal: MS1 -TIC SCAN ESI Frag=135V Gain=1,0

RT [min]	Peak MS Base Peak m/z	Area	Area%	Max Peak%	Height
5.290	392.900	1728148.6075	30.2143	43.296	403070.262
5.779	473.000	3991485.2867	69.7857	100.000	765383.640
	Sum	5719633.8942			

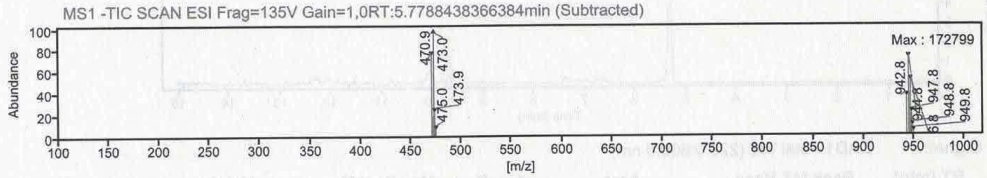
MS1 -TIC SCAN ESI Frag=135V Gain=1,0RT:5.29014804639518min (Subtracted)



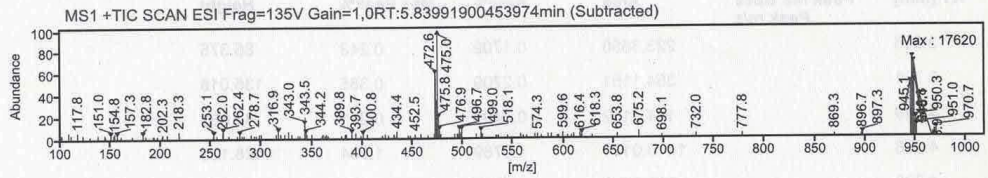
MS1 +TIC SCAN ESI Frag=135V Gain=1,0RT:5.29356343076177min (Subtracted)



MS1 -TIC SCAN ESI Frag=135V Gain=1,0RT:5.7788438366384min (Subtracted)



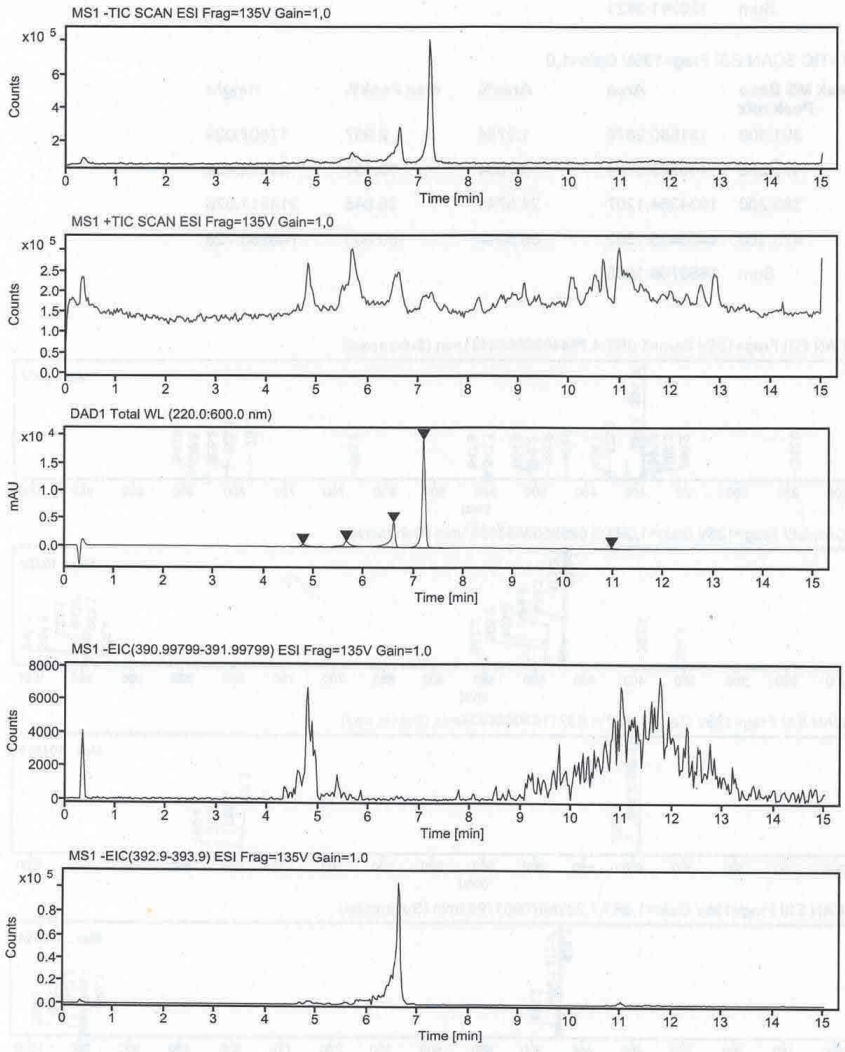
MS1 +TIC SCAN ESI Frag=135V Gain=1,0RT:5.83991900453974min (Subtracted)



D:\CDSProjects\Default\0-standardplot+EIC.rdl [Rev. 8164] Printed: 2024-03-25 06:48:07+01:00 Page 2 of 2

XII-5d 9h

Sequence Name:	SingleSample		
Data file:	HALP400-5d&9h.dx	**Project Name:**	Single Quad
Sample name:	HALP400-5d&9h	**Operator :**	SYSTEM
Instrument:	Single Quad	**Acquired on:**	2024-03-26 22:25:04+01:00
Inj. volume:	8.000	**Location:**	P2-A1
Acq. method:	00-new_wasser-acn_standard_100-1000_BD-20min.amx		
Processing method:	MS_standard_plot.pmx		



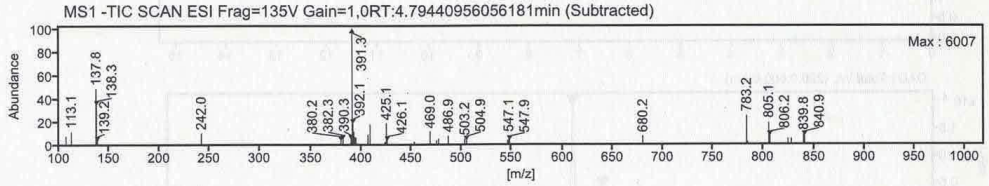
Signal: DAD1 Total WL (220.0:600.0 nm)

RT [min]	Peak MS Base Peak m/z	Area	Area%	Max Peak%	Height
4.785	391.300	3362.6652	2.5819	3.780	381.464
5.652	471.200	9165.5113	7.0373	10.304	997.514
6.597	393.200	28128.5294	21.5972	31.622	4500.336
7.199	473.100	88952.8872	68.2985	100.000	19577.541
10.969		631.7690	0.4851	0.710	177.808
	Sum	130241.3621			

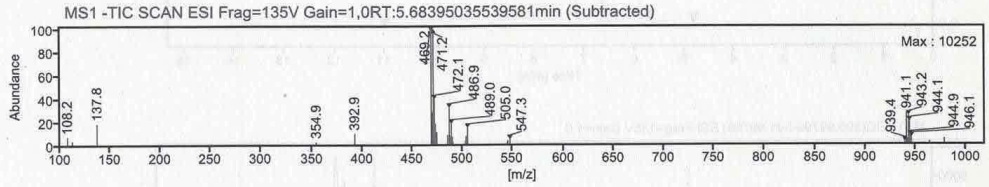
Signal: MS1 -TIC SCAN ESI Frag=135V Gain=1,0

RT [min]	Peak MS Base Peak m/z	Area	Area%	Max Peak%	Height
4.794	391.300	131580.2876	1.9784	2.967	17807.029
5.684	471.200	449348.6121	6.7564	10.131	44874.459
6.632	393.200	1634354.1207	24.5741	36.848	214611.676
7.233	473.100	4435425.1332	66.6910	100.000	746255.726
	Sum	6650708.1535			

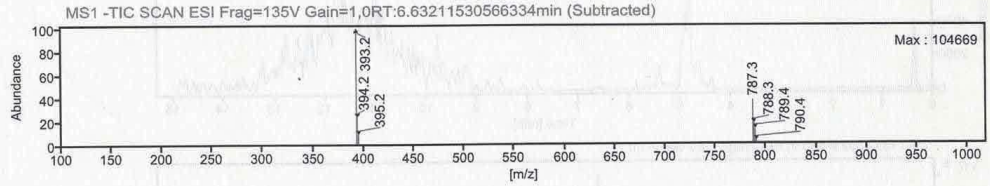
MS1 -TIC SCAN ESI Frag=135V Gain=1,0RT:4.79440956056181min (Subtracted)



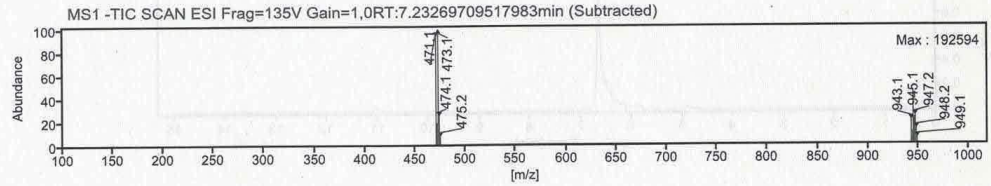
MS1 -TIC SCAN ESI Frag=135V Gain=1,0RT:5.68395035539581min (Subtracted)



MS1 -TIC SCAN ESI Frag=135V Gain=1,0RT:6.63211530566334min (Subtracted)

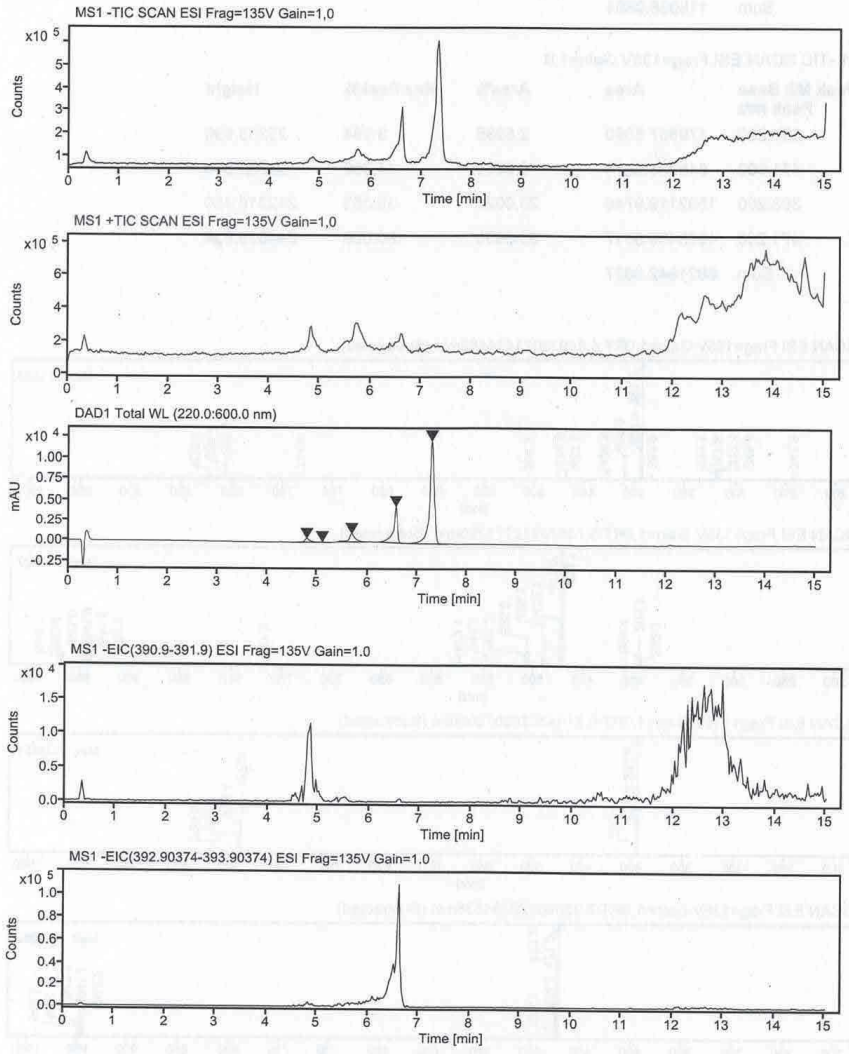


MS1 -TIC SCAN ESI Frag=135V Gain=1,0RT:7.23269709517983min (Subtracted)



X11-6d 5h

Sequence Name:	SingleSample		
Data file:	HALP400-6d&5h.dx	**Project Name:**	Single Quad
Sample name:	HALP400-6d&5h	**Operator :**	SYSTEM
Instrument:	Single Quad	**Acquired on:**	2024-03-26 22:46:05+01:00
Inj. volume:	8.000	**Location:**	P2-A2
Acq. method:	00-new_wasser-acn_standard_100-1000_BD-20min.amx		
Processing method:	MS_standard_plot.pmx		



D:\CDSProjects\Default\0-standardplot+EIC.rdl [Rev. 8227] Printed: 2024-03-27 08:16:30+01:00 Page 1 of 2

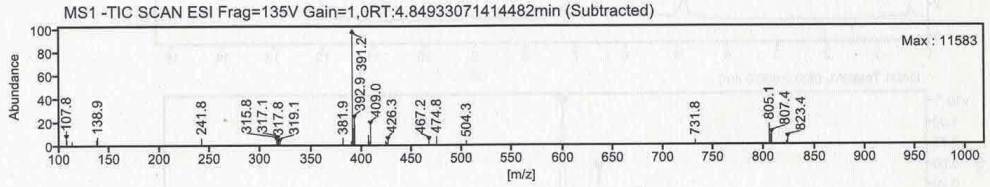
Signal: DAD1 Total WL (220.0:600.0 nm)

RT [min]	Peak MS Base Peak m/z	Area	Area%	Max Peak%	Height
4.791		3133.3085	2.6545	3.862	455.833
5.100		66.5589	0.0564	0.082	58.564
5.690	471.000	8716.0296	7.3841	10.743	1006.291
6.577	393.200	24986.5452	21.1682	30.796	4429.917
7.300	471.200	81135.6182	68.7368	100.000	12407.242
	Sum	118038.0604			

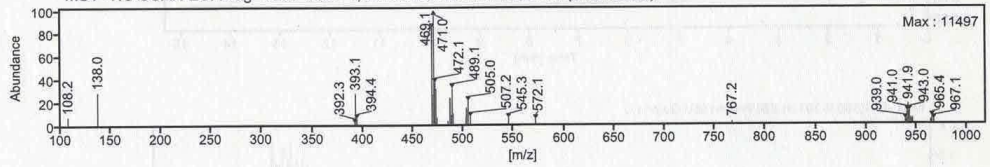
Signal: MS1 -TIC SCAN ESI Frag=135V Gain=1,0

RT [min]	Peak MS Base Peak m/z	Area	Area%	Max Peak%	Height
4.849	391.200	179857.5390	2.5985	3.994	25203.996
5.739	471.000	646233.9874	9.3364	14.350	52233.368
6.614	393.200	1592119.9746	23.0021	35.353	242316.450
7.331	471.200	4503430.8617	65.0630	100.000	544328.694
	Sum	6921642.3627			

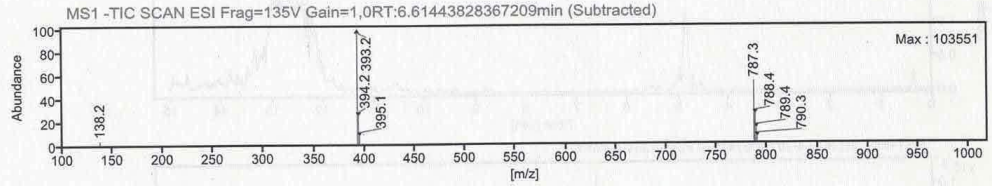
MS1 -TIC SCAN ESI Frag=135V Gain=1,0RT:4.84933071414482min (Subtracted)



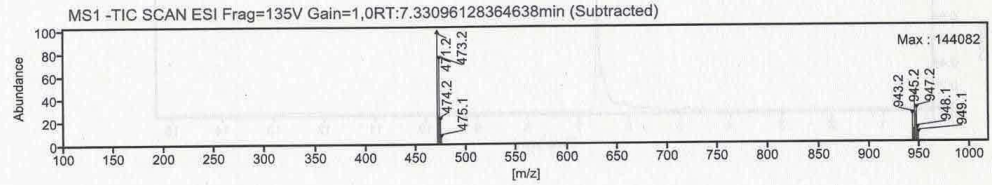
MS1 -TIC SCAN ESI Frag=135V Gain=1,0RT:5.73878932171295min (Subtracted)



MS1 -TIC SCAN ESI Frag=135V Gain=1,0RT:6.61443828367209min (Subtracted)

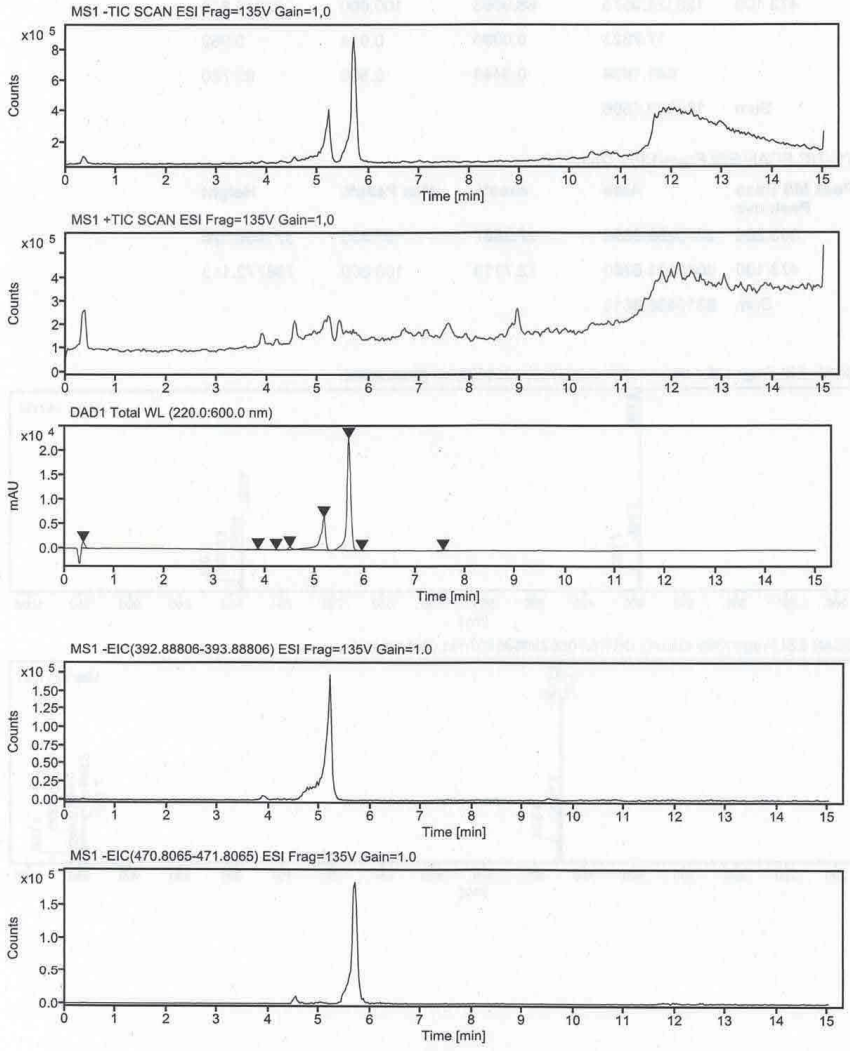


MS1 -TIC SCAN ESI Frag=135V Gain=1,0RT:7.33096128364638min (Subtracted)



X11 - 7d 3h

Sequence Name:	SingleSample		
Data file:	HALP400_7d3h.dx	**Project Name:**	Single Quad
Sample name:	HALP400_7d3h	**Operator :**	SYSTEM
Instrument:	Single Quad	**Acquired on:**	2024-04-03 22:17:50+02:00
Inj. volume:	8.000	**Location:**	P1-C10
Acq. method:	00-new_wasser-acn_standard_100-1000_BD-20min.amx		
Processing method:	MS_standard_plot.pmx		



D:\CDSProjects\Default\0-standardplot+EIC.rdl [Rev. 8304] Printed: 2024-04-04 07:44:00+02:00 Page 1 of 2

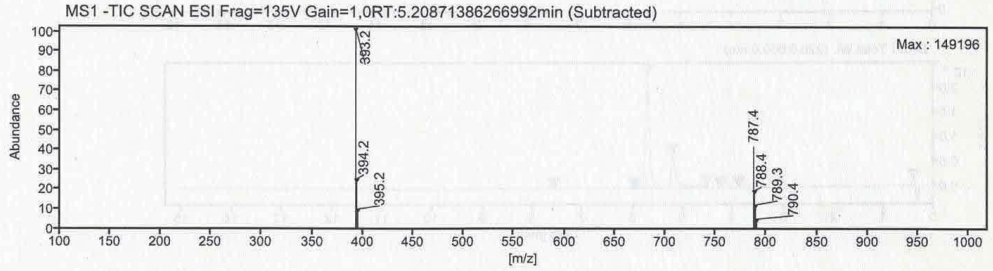
Signal: DAD1 Total WL (220.0:600.0 nm)

RT [min]	Peak MS Base Peak m/z	Area	Area%	Max Peak%	Height
0.381		4534.2618	2.4386	3.539	1246.498
3.861		665.3571	0.3578	0.519	154.437
4.221		244.3432	0.1314	0.191	71.963
4.495		2075.1353	1.1160	1.620	496.904
5.176	393.200	49637.5299	26.6955	38.742	6786.421
5.672	473.100	128124.0575	68.9063	100.000	22912.814
5.933		17.7823	0.0096	0.014	0.952
7.558		641.1834	0.3448	0.500	93.780
	Sum	185939.6506			

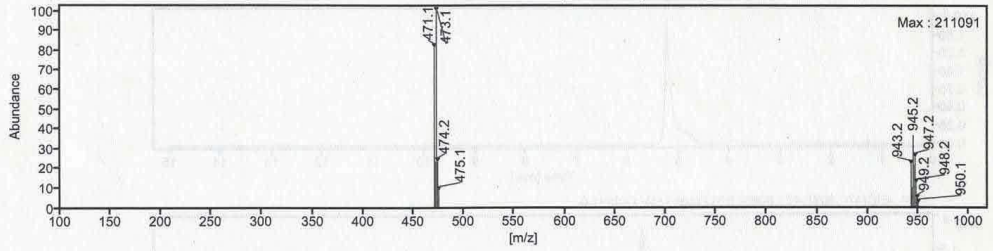
Signal: MS1 -TIC SCAN ESI Frag=135V Gain=1,0

RT [min]	Peak MS Base Peak m/z	Area	Area%	Max Peak%	Height
5.209	393.200	2270266.9855	27.2887	37.530	321956.576
5.707	473.100	6049171.6760	72.7113	100.000	798772.113
	Sum	8319438.6615			

MS1 -TIC SCAN ESI Frag=135V Gain=1,0RT:5.20871386266992min (Subtracted)



MS1 -TIC SCAN ESI Frag=135V Gain=1,0RT:5.7065299836407min (Subtracted)



7.3 Appendix III: Selective, non-nucleotidic radiotracer for P2Y$_{12}$ receptors: Design, synthesis, characterization, and imaging of brain slices (Publication I)

Journal of Medicinal Chemistry

pubs.acs.org/jmc Article

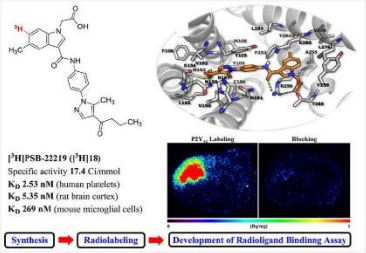
Selective, Non-nucleotidic Radiotracer for P2Y$_{12}$ Receptors: Design, Synthesis, Characterization, and Imaging of Brain Slices

Haneen Al-Hroub,[†] Hashem Ali M. Al Musawi,[†] Aliaa Abdelrahman, Vigneshwaran Namasivayam, Margot Corbel, Fanny Petit, Gunes Aksiyote, Fabrice Beau, Caroline Jan, Alexis-Pierre Bemelmans, Nadja Van Camp, Marie-Anne Peyronneau, Alexandra Winkeler, and Christa E. Müller*

Cite This: J. Med. Chem. 2025, 68, 11279−11298 Read Online

ACCESS | Metrics & More | Article Recommendations | Supporting Information

ABSTRACT: The G protein-coupled, ADP-activated P2Y$_{12}$ receptor (P2Y$_{12}$R) expressed by microglial cells is involved in neuroinflammation constituting a promising biomarker. Here, we designed and characterized a potent and selective non-nucleotidic P2Y$_{12}$-antagonist radioligand, [^{3}H]PSB-22219 ([^{3}H]**18**). The unlabeled compound was stable in rat liver microsomes and selective versus other ADP-activated receptors. [^{3}H]**18** displayed high-affinity binding to membrane preparations recombinantly expressing the human P2Y$_{12}$R (K_D = 4.57 nM), showing very low nonspecific binding. Radioligand binding assays were established and employed to characterize P2Y$_{12}$Rs natively expressed in human platelet (K_D = 2.53 nM), rat brain cortex (K_D = 5.35 nM), and mouse microglial cell preparations (K_D = 269 nM), with microglia showing extraordinarily high P2Y$_{12}$R expression. Autoradiography studies allowed the visualization of human P2Y$_{12}$R overexpression in the brain of a humanized rat model. The new radioligand is expected to become a useful pharmacological tool that will contribute to the development of therapeutics and radiodiagnostics targeting brain P2Y$_{12}$Rs.



Downloaded via BONN LIBRARIES on September 29, 2025 at 15:13:38 (UTC).
See https://pubs.acs.org/sharingguidelines for options on how to legitimately share published articles.

INTRODUCTION

The P2Y$_{12}$ receptor (P2Y$_{12}$R) is a member of the P2Y receptor family,[1−4] a group of G protein-coupled receptors (GPCR) that are activated by extracellular nucleotides, including ATP, ADP, UTP, and UDP nucleotide sugars and dinucleotides.[2,5−7] The primary endogenous agonist for the P2Y$_{12}$R is ADP (**1**), shown in Figure 1, which, upon binding to the receptor, triggers the activation of G$_i$ proteins,[8] that leads to a reduction in intracellular cAMP levels, thereby controlling various cellular functions.[3,4] The understanding of P2Y$_{12}$R activation and inhibition has been significantly enhanced by insights gained from its crystal structures.[9−11] These elucidated how different ligands interact with the receptor, namely, the full agonist 2-methylthioadenosine diphosphate (2-MeSADP, **2**), the partial agonist 2-methylthioadenosine triphosphate (2-MeSATP, **3**), and the non-nucleotidic antagonist ethyl 6-(4-[(benzylsulfonyl)carbamoyl]piperidin-1-yl)-5-cyano-2-methyl-nicotinate (AZD1283, **4**). Various scaffolds have been developed as P2Y$_{12}$R antagonists, including the irreversibly acting thienotetrahydropyridines (e.g., ticlopidine (**5**), clopidogrel (**6**), and prasugrel (**7**)), which are allosteric antagonist prodrugs,[1,12,13] and several reversible competitive antagonists, e.g., adenine nucleotide analogs (e.g., cangrelor (**8**) and ticagrelor (**9**)), anthraquinone derivatives (e.g., PSB-0739 (**10**) and PSB-0702 (**11**)) and a variety of nitrogen-containing heterocyclic compounds (e.g., **4** and compounds shown in Figure 2).[4,14−17] The uncharged nucleoside analog ticagrelor was previously claimed to act as a noncompetitive antagonist versus ADP and as a competitive antagonist versus 2-MeSADP,[18] but this might be due to a misinterpretation. ADP and its metabolites can interact with many other proteins, while 2-MeSADP is metabolically more stable and more selective. In fact, both ADP and 2-MeSADP are structurally similar and are generally believed to bind to the same site, the orthosteric site, on P2Y$_{12}$ receptors.[10]

The P2Y$_{12}$R is predominantly expressed on platelets inducing aggregation and in the brain, particularly on microglial cells, which are involved in inflammatory and neurodegenerative diseases.[19,20] The receptor has become a major drug target for preventing stroke and heart infarction.[21−24] In recent years, evidence has been accumulating that it may serve as a biomarker for detecting brain inflammation and as a novel therapeutic for neuroinflammatory diseases.[19,21−25] Microglial cells are specialized glial cells located throughout the brain and spinal cord, serving as the central nervous system's primary immune

Received: January 21, 2025
Revised: April 23, 2025
Accepted: April 25, 2025
Published: May 14, 2025



ACS Publications © 2025 American Chemical Society

https://doi.org/10.1021/acs.jmedchem.5c00213
J. Med. Chem. 2025, 68, 11279−11298

Journal of Medicinal Chemistry pubs.acs.org/jmc Article

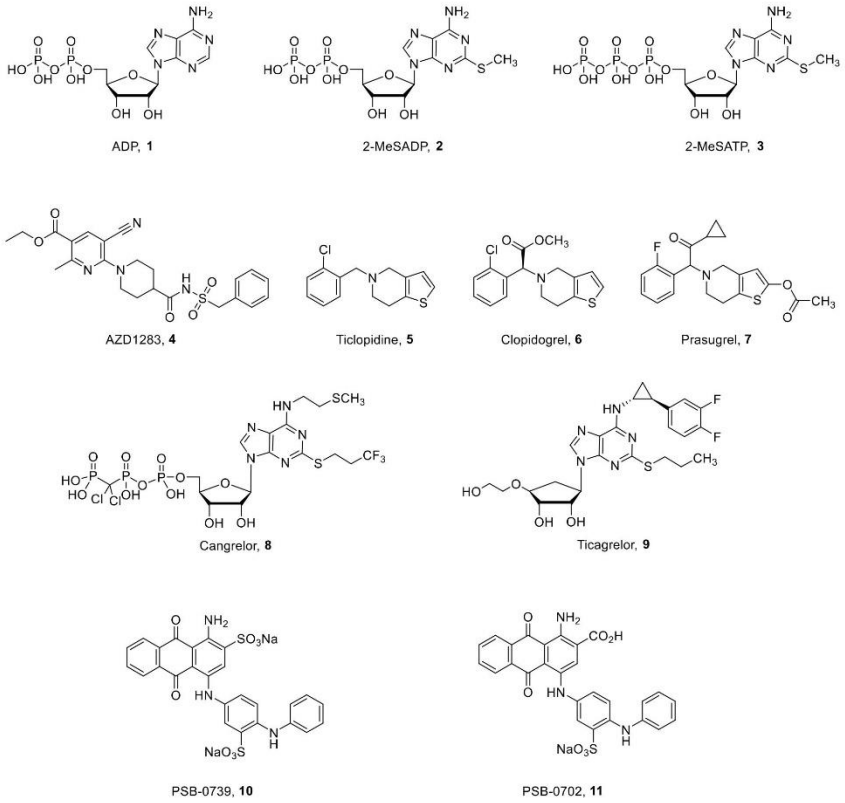


Figure 1. Selection of reported $P2Y_{12}R$ agonists (**1** and **2**), partial agonist (**3**), antagonists (**4** and **8**–**11**), and antagonist prodrugs (**5**–**7**).

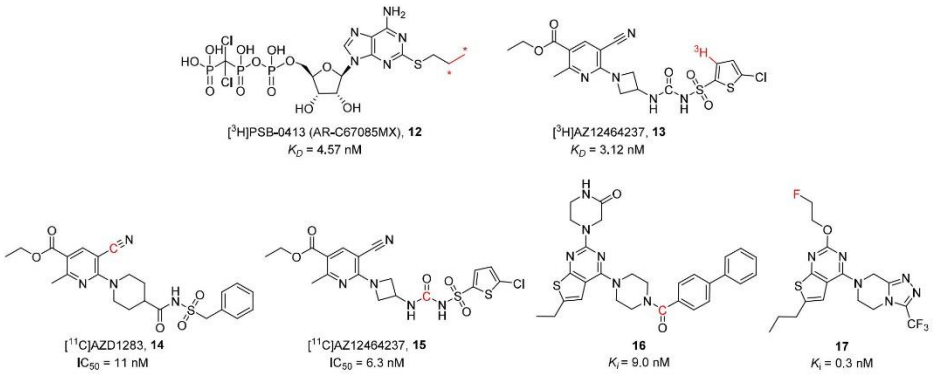
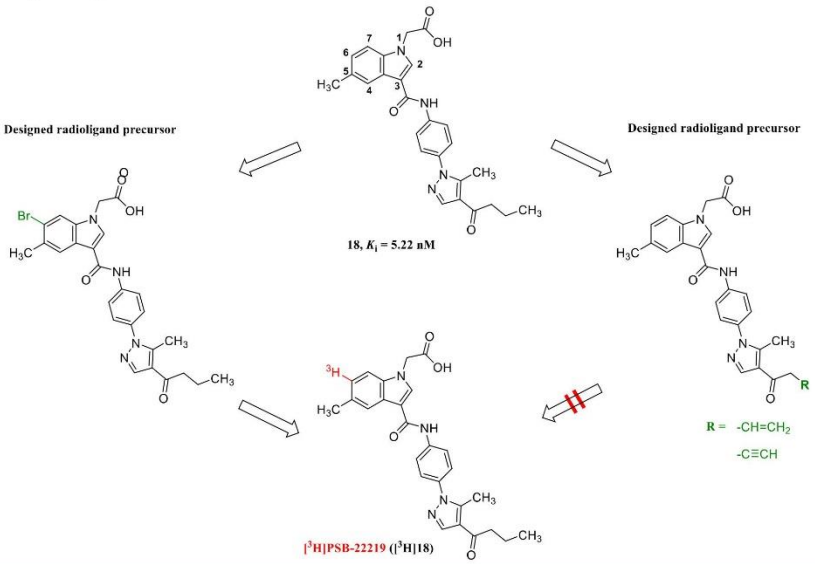


Figure 2. Structures of radioligands developed for $P2Y_{12}Rs$; red asterisks represent the tritiated position, and a red-colored atom designates a radioactive isotope (^{3}H, ^{11}C, and ^{18}F).[63–66,68]

https://doi.org/10.1021/acs.jmedchem.5c00213
J. Med. Chem. 2025, 68, 11279–11298

Scheme 1. Structure of the Unlabeled Potent and Selective $P2Y_{12}R$ Antagonist 18,[70,71] Its Designed Radioligand Precursors, and the Resulting Radioligand [^{3}H]18



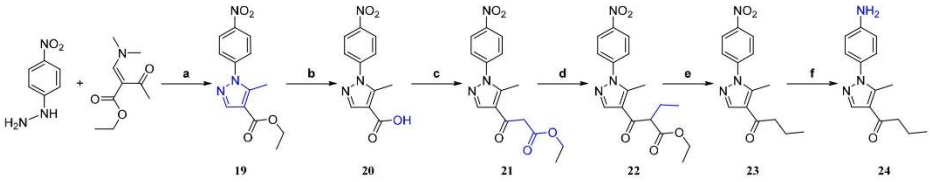
defense.[25−28] Their functions include surveying the CNS environment for disturbances, engulfing and digesting cellular debris and pathogens, regulating inflammatory responses, and supporting neuronal functions through development and regulation of synaptic plasticity.[29−32] Microglia exhibit different activation states, adapting their behavior to meet the needs of their environment. In their resting state, they display a ramified morphology and continuously monitor their surroundings.[33−36] Upon detecting damage or pathogens, they become activated, adopting an amoeboid shape; they can differentiate into either proinflammatory or anti-inflammatory states.[34,37−39] In the proinflammatory state, they produce cytokines that can lead to neurotoxicity, while in the anti-inflammatory state, they facilitate tissue repair and regeneration, supporting the resolution of inflammation.[34,37,40−42] The $P2Y_{12}R$ expressed on microglia is integral to their functions. This receptor enables microglia to migrate toward ATP/ADP signals emitted from injured or diseased cells, facilitating their role in chemotaxis.[3,19,43] Furthermore, through $P2Y_{12}R$ activation, microglia can modulate the release of various cytokines, thereby playing a significant role in CNS inflammation.[44,45] Given the pivotal role of $P2Y_{12}Rs$ for microglial functions and their impact on neuroinflammatory and neurodegenerative diseases such as Alzheimer's disease (AD), Parkinson's disease (PD), multiple sclerosis (MS), and epilepsy, they have become a focal point of research.[19,29,36,44] Targeting the $P2Y_{12}$ receptor to regulate microglial activity offers a promising therapeutic approach for controlling excessive inflammation. Furthermore, experimental evidence for $P2Y_{12}R$ downregulation in neurodegenerative diseases, in particular in Alzheimer's disease, tauopathy, and multiple sclerosis, both in animal models and in humans[46−51] has been described, suggesting the $P2Y_{12}R$ as a target of choice for in vivo imaging of patients. $P2Y_{12}R$ imaging may be useful for early diagnosis of neurodegenerative processes long before symptoms can be observed and for monitoring changes of expression levels and effects of therapeutic interventions.[19,29,52−55]

Therefore, the development of a potent and selective $P2Y_{12}R$ radioligand has become of high interest since it will provide a better understanding of the microglial $P2Y_{12}Rs$' roles in the brain, e.g., by imaging techniques such as autoradiography, positron emission tomography (PET), or the establishment of crucial methods needed in the drug development process such as radioligand binding assays.[56−62] ^{11}C- and ^{18}F-labeled $P2Y_{12}R$ antagonists have recently been reported (compounds **13**−**17** (Figure 2)).[63−66] Tritium-based $P2Y_{12}R$ antagonist radioligands serve as optimal candidates for radioligand binding assays.[67] A [^{3}H]-labeled $P2Y_{12}R$ antagonist radioligand has previously been developed by our group **12** (Figure 2).[68] Compound **12** is a nucleotide derivative (an ATP analog) showing high polarity, associated with difficulties in its synthesis and purification, limited selectivity since it can also bind to other adenine nucleotide-binding proteins, and low metabolic stability, which limits its applications in complex systems.[68,69] ^{11}C and ^{18}F-labeled $P2Y_{12}R$ antagonists were developed to serve as PET-tracers; however, they did not show brain uptake. The nicotinic acid ethyl ester derivatives **13**−**15** (Figure 2) were found to be metabolically instable.

In this study, we present the design and synthesis of a selective $P2Y_{12}R$ radiotracer, [^{3}H]PSB-22219 ([^{3}H]**18**), along with its characterization at $P2Y_{12}Rs$ of different species and in various cell lines and tissues. In addition, we explored its application in autoradiography studies and for diagnostic purposes and found it to display outstanding properties.

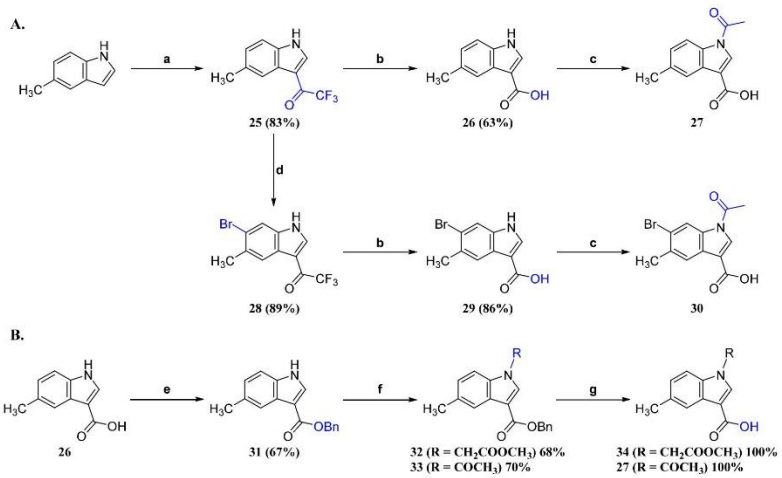
https://doi.org/10.1021/acs.jmedchem.5c00213
J. Med. Chem. 2025, 68, 11279−11298

Scheme 2. Synthesis of Aniline Derivative 24[a]



[a](a) EtOH, 80 °C, 3 h (77%); (b) aq. KOH, THF:EtOH (1:1), 100 °C, 2 h (98%); (c) carbonyldiimidazole (CDI), THF, 25 °C, 16 h; anhydrous $MgCl_2$, ethyl potassium malonate, 55 °C, 6 h (91%); (d) NaH, THF, 0 °C, 30 min; CH_3CH_2I, 25 °C, 24 h (83%); (e) aq. HCl 37%, 105 °C, 2 h (96%); (f) $SnCl_2{\cdot}2H_2O$, EtOH, 80 °C, 2 h (67%) or Pd/C, H_2 gas (1 atm), MeOH, 25 °C, 16 h (97%).

Scheme 3. Synthesis of Key Carboxylic Acid Intermediates (A) 27 and 30, and (B) 34[a]



[a](A) Classical pathway: (a) $(CF_3CO)_2O$, Et_2O, −5 °C, 2 h (83%); (b) KOH, H_2O, 105 °C, 4 h (63, 86%); (c) Et_3N, 4-dimethylaminopyridine (4-DMAP), CH_2Cl_2, 0 °C; acetyl chloride, 25 °C, 3 h; (d) Br_2, CH_3CO_2H, 10 °C; 25 °C, 5 h (89%). (B) Optimized pathway: (e) $(CF_3CO)_2O$, CH_2Cl_2, 0 °C; 25 °C, 1 h; acetyl chloride, 25 °C, 3 h; BnOH, 2 h (67%); (f) K_2CO_3, dimethylformamide (DMF), methyl 2-bromoacetate, 25 °C, 24 h (68%)/NaH, DMF, 0 °C, 30 min; acetyl chloride, 25 °C, 24 h (70%); (g) Pd/C (10%), MeOH, H_2 (35 psi = 241.3 kPa), 25 °C, 2 h (100%).

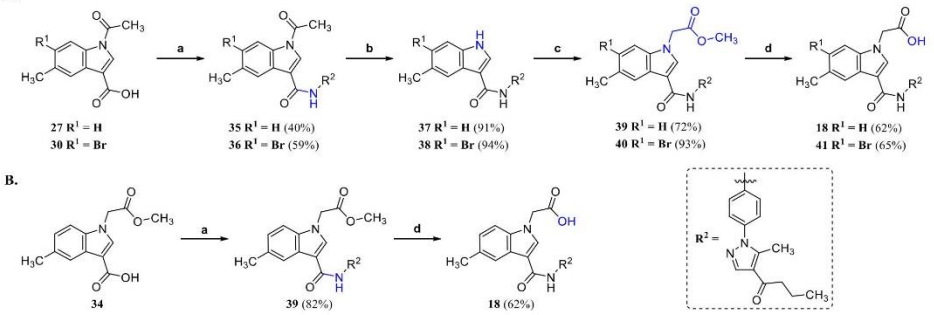
RESULTS AND DISCUSSION

Radioligand Design, Synthesis, and Radiolabeling. *Design.* A systematic comprehensive data analysis among the reported $P2Y_{12}R$ antagonists led to the identification of the pyrazolyl-phenyl-indole series of compounds[70,71] as a promising scaffold for the development of potent and selective $P2Y_{12}R$ antagonist radioligand candidates. Figure S1 provides a general structure−activity relationship (SAR) analysis derived from the data analysis[70,71] among this scaffold. The unlabeled ligand **18** (Scheme 1) was subsequently selected as the most promising structure for the development of a $P2Y_{12}R$ antagonist radioligand. Different tritiation strategies have been taken into consideration, including catalytic hydrogenation of precursors with a triple or double bond or a halogenated aromatic system suitable for catalytic dehalogenation reaction. Selective bromination at position 6 of the indole led to the formation of the selected precursor, while the introduction of a double or triple bond into the butanone residue attached to the pyrazole moiety was found to be synthetically challenging (see Scheme S1 in the Supporting Information).

Synthesis. Convergent synthesis of the unlabeled ligand **18** and its radioligand precursor **41** was performed, requiring the preparation of **24** (Scheme 2) and the three key indole carboxylic acid derivatives **27**, **30**, and **34** (Scheme 3). Coupling of the aniline **24** with a carboxylic acid (**27**, **30**, and **34**), followed by the subsequent steps shown in Scheme 4, yielded the final compounds. The reported eight-step synthesis of aniline **24**[71] could be reduced to six steps. Condensation of the commercially available 4-nitrophenylhydrazine with ethyl (*E*)-2-((dimethylamino)methylene)-3-oxobutanoate provided the pyrazole ethyl ester derivative **19**. Ester hydrolysis using aqueous potassium hydroxide in a 1:1 mixture of tetrahydrofuran (THF) and ethanol under reflux produced carboxylic acid **20**. To improve yields, the subsequent step to the *β*-keto ester **21** was modified, avoiding the formation of the magnesium bis(3-ethoxy-3-oxopropanoate) complex, by directly utilizing anhydrous

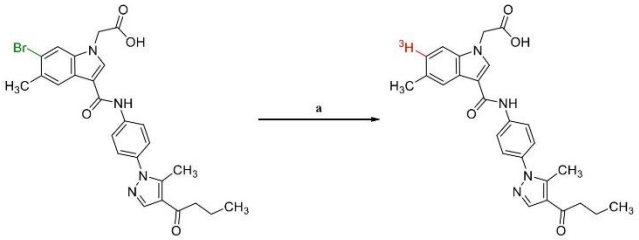
https://doi.org/10.1021/acs.jmedchem.5c00213
J. Med. Chem. 2025, 68, 11279−11298

Scheme 4. (A,B) Synthesis of the Potent and Selective $P2Y_{12}R$ Antagonist 18 (Unlabeled Ligand) and Its Radioligand Precursor 41[71a]



[a]Amide coupling and final steps: (a) **24**, 4-DMAP, EDC·HCl, CH_2Cl_2, 0 °C, 25 °C, 24 h (40–82%); (b) K_2CO_3, MeOH, 25 °C, 4 h (91, 94%); (c) K_2CO_3, DMF, methyl 2-bromoacetate, 25 °C, 24 h (72, 93%); (d) aq. 2N NaOH, MeOH, 25 °C, 24 h (62, 65%).

Scheme 5. Synthesis of [^{3}H]18 through Catalytic Dehalogenative Tritiation of 41[a]



[a]Tritium gas (515 mbar, 51.5 kPa), *N*,*N*-diisopropylethylamine (DIPEA), Lindlar's catalyst, dimethylformamide (DMF), 25 °C, 24 h.

magnesium chloride and potassium malonate, after **20** had been treated with carbonyldiimidazole (CDI) in THF. This modification provided a 91% yield of **21**, a significant improvement over the reported method (67%).[71] **22** and **23** were synthesized as reported, using alkylation of the active methylene with ethyl iodide followed by acidic decarboxylation with concentrated HCl.[71] The nitrophenyl derivative **23** was subsequently reduced to the corresponding aniline **24** using two alternative methods: $SnCl_2{\cdot}2H_2O$ in refluxing ethanol (yielding 67%) or Pd/C in methanol under H_2 at atmospheric pressure overnight (yielding 97%) (Scheme 2).

For the synthesis of the carboxylic acid intermediates **27**, **30**, and **34** (Scheme 3), 5-methyl-1*H*-indole was treated with 2,2,2-trifluoroacetic anhydride in diethyl ether to yield **25**, followed by selective bromination with Br_2 in acetic acid to obtain **28**. Basic hydrolysis of **25** and **28** yielded carboxylic acids **26** and **29**. The indolyl-nitrogen atom in both acids was subsequently protected with acetyl chloride using triethylamine and 4-dimethylamino-pyridine (4-DMAP) in dichloromethane to yield the crude intermediates **27** and **30** (Scheme 3).[71] Due to the high polarity and instability of the acetyl group, purification of these intermediates was challenging. An alternative pathway was developed to optimize the synthesis of **27**. This route involved benzyl protection of **26** using trifluoroacetic anhydride and benzyl alcohol to form the novel benzyl ester **31**, followed by *N*-alkylation reactions using either methyl 2-bromoacetate and potassium carbonate, or acetyl chloride and sodium hydride, yielding the new compounds **32** (68%) and **33** (70%), respectively. Deprotection of the esters on Pd/C in methanol with H_2 (35 psi, 241.3 kPa) afforded the key intermediates **27** and **34** (Scheme 3). It should be noted that the optimized synthetic pathway could not be applied to the preparation of **30** due to the risk of dehalogenation during the Pd/C-mediated deprotection of the benzyl ester. Therefore, **30** was synthesized according to the classical procedure (see Scheme 3).

Amide coupling of the carboxylic acid **27** or **30** and the aniline **24** in the presence of 1-(3-(dimethylamino)propyl)-3-ethyl-carbodiimide hydrochloride (EDC·HCl) and 4-DMAP in CH_2Cl_2 yielded **35** and **36**. Deacetylation with potassium carbonate (K_2CO_3) in methanol produced **37** and **38**, which were further alkylated with methyl 2-bromoacetate in DMF in the presence of K_2CO_3 to form the esters **39** and **40**. Direct amide coupling of carboxylic acid **34** and aniline **24** leading to **39** facilitated the synthesis by avoiding two steps, deacetylation and *N*-alkylation. This optimized approach not only reduced the overall synthesis time but also minimized the handling and

https://doi.org/10.1021/acs.jmedchem.5c00213
J. Med. Chem. 2025, 68, 11279−11298

purification requirements, thereby increasing the overall efficiency of the synthesis. Finally, hydrolysis of the esters **39** and **40** yielded the target compounds **18** and **41** (Scheme 4).

Radiolabeling. Tritiation of the bromo-substituted precursor **41** was performed by Pd-catalyzed dehalogenative hydrogenation with tritium gas (515 mbar, 51.5 kPa) using Lindlar's catalyst in DMF in the presence of DIPEA at room temperature for 24 h to form [^{3}H]**18** (Scheme 5). The radioligand was subsequently purified by an HPLC system coupled to serial UV and radio detectors yielding [^{3}H]**18** with a high radiochemical purity (>99%). For details, see the Supporting Information.

Biological Studies. For initial characterization, recombinant cell preparations were employed to investigate $P2Y_{12}R$ binding, namely, Chinese hamster ovary (CHO) cells and 1321N1 human astrocytoma cells stably expressing the human $P2Y_{12}R$ (CHO-h$P2Y_{12}$ and astrocytoma-h$P2Y_{12}$). The CHO-h$P2Y_{12}$ cell line was additionally used to perform β-arrestin recruitment assays,[74,73,72] providing insights into $P2Y_{12}R$-mediated signaling. In addition, we examined cell membrane preparations that natively express $P2Y_{12}Rs$, human blood platelets, rat brain cortex tissues, and mouse BV-2 microglial cells, thereby capturing physiologically relevant contexts of $P2Y_{12}R$ expression and binding across different biological systems.

Establishment of a Radioligand Binding Assay. In preliminary experiments, we examined numerous parameters, including diverse filter types, incubation and washing buffers, protein amounts, and radioligand concentrations, with the goal to achieve optimal specific binding and low nonspecific binding and to avoid radioligand depletion. At first, we encountered high filter binding of the radioligand. Subsequent improvement of the assay conditions was achieved by adding a solubilizing agent into the washing buffer (0.1% of Tween 20). Three different sources of human $P2Y_{12}Rs$ were studied for [^{3}H]**18** binding: recombinant cell membrane preparations of CHO and 1321N1 astrocytoma cell lines stably transfected with the human $P2Y_{12}$ (CHO-h$P2Y_{12}$ and astrocytoma-h$P2Y_{12}$) and cell membrane preparations of human blood platelets that show a high native expression of $P2Y_{12}Rs$.[4,75,76] Specific binding of [^{3}H]**18** (2 nM) to human $P2Y_{12}R$-expressing membrane preparations was detected in the three membrane preparations, while only insignificant binding to nontransfected CHO and 1321N1 astrocytoma membrane preparations was observed (Figure 3). Since CHO-h$P2Y_{12}$ cell membranes displayed the highest level of specific binding combined with a low nonspecific binding of 10% of total binding, they were used in further experiments. The optimized conditions for the radioligand binding assay were established as follows: binding was determined using a membrane preparation of CHO cells expressing human $P2Y_{12}Rs$ (5 μg of protein per vial). It was carried out with 2 nM [^{3}H]**18** in 50 mM Tris-HCl buffer at pH 7.4 and incubated for 1 h at 18 °C in a final volume of 500 μL. Separation of bound from unbound radioligand was performed by filtration through GF/B glass fiber filters and subsequent washing with ice-cold 50 mM Tris-HCl buffer supplemented with 0.1% Tween 20, pH 7.4. In the radioligand characterization study, nonspecific binding was determined either in the presence of 10 μM unlabeled ligand **18** or 1 μM $P2Y_{12}$-selective anthraquinone-derived antagonist **10**.[14] Both of the structurally diverse competitors yielded similar results, showing very low nonspecific binding.

Binding Kinetics. As a next step, kinetic studies using CHO-h$P2Y_{12}$ cell membranes (5 μg of protein) were performed at 25 °C employing 2 nM [^{3}H]**18** in 50 mM Tris-HCl buffer, pH 7.4. A very fast association behavior with a half-life of 1.6 ± 0.4 min and an association rate (K_{on}) of 0.0982 ± 0.0289 nM^{-1} min^{-1} was observed (Figure 4A, association). A steady state was attained within less than 10 min and remained stable for more than 20 min. The addition of a high concentration (10 μM) of a nonradioactive ligand led to a rapid displacement of the radiotracer from the binding site, with a dissociation half-life of 1.8 ± 0.1 min and an exponential decay constant (K_{off}) of 0.381 ± 0.023 min^{-1} (see Figure 4A, dissociation). A kinetic K_D value of 4.02 ± 0.84 nM was determined. A fast dissociation rate constant could be problematic since it may be difficult to perform radioligand binding experiments as the radioligand might dissociate from the receptor during filter washing. To overcome this issue, the binding kinetics were further evaluated at a lower incubation temperature (18 °C), at which [^{3}H]**18** displayed slower kinetics, as expected (Figure 4B). Lowering the temperature resulted in a 2-fold increase in both the association half-life (3.4 ± 0.3 min) and the dissociation half-life (4.3 ± 0.3 min), resulting in decreased K_{on} (0.0510 ± 0.0040 nM^{-1} min^{-1}) and K_{off} values (0.162 ± 0.009 min^{-1}). The kinetically derived K_D value was not affected by the temperature being virtually identical at both temperatures (for results, see Table 1).

Upon fitting of specific binding of dissociation data on a logarithmic plot versus time, the resulting graphs were found to be linear with absolute values of their slopes close to the dissociation rates (K_{off} = −slope) determined at both temperatures. This indicates that the system follows the law of mass action with a single affinity state. The goodness of fitting (r^2) at both temperatures (25 and 18 °C) was close to unity, which denotes that the regression predictions perfectly fit the data. This proves that the assay performed at room temperature of 25 °C is reliable, giving the same results as those determined at a lower temperature of 18 °C.

Saturation Binding. To assess the expression level of the human $P2Y_{12}$ receptor in CHO-h$P2Y_{12}$ membrane preparations and to determine the apparent dissociation constant (K_D value), saturation experiments were conducted at both 25 °C (Figure 5A) and 18 °C (Figure 5B) using a range of different concentrations of [^{3}H]**18**. Binding was saturable, and the Scatchard plot was linear, indicating that only one class of high-

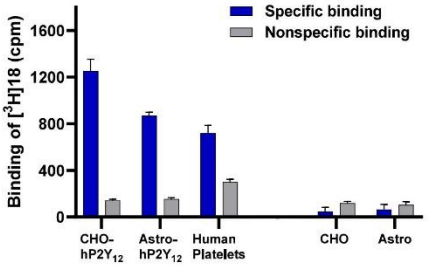


Figure 3. Specific binding of [^{3}H]**18** (2 nM) to membranes of human $P2Y_{12}$ expressed in CHO-h$P2Y_{12}$ (5 μg of protein/vial), 1321N1 astrocytoma-h$P2Y_{12}$ (5 μg of protein/vial), and native human platelets (100 μg of protein/vial) and to membranes of nontransfected CHO (5 μg of protein/vial) and 1321N1 astrocytoma (5 μg of protein/vial) cells performed at 18 °C. Nonspecific binding was determined in the presence of 1 μM **10**. Values represent means ± SEM of three independent experiments, each performed in duplicate.

https://doi.org/10.1021/acs.jmedchem.5c00213
J. Med. Chem. 2025, 68, 11279−11298

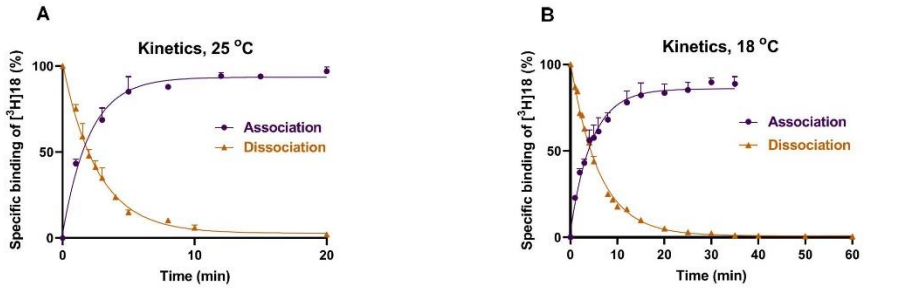


Figure 4. Kinetics of [^{3}H]**18** binding (2 nM) to 5 μg of protein/vial membranes of CHO cells recombinantly expressing the human P2Y$_{12}$R in 50 mM Tris-HCl buffer, pH 7.4, (A) at 25 °C and (B) at 18 °C. Dissociation was achieved by the addition of 10 μM **18** after 1 h of preincubation.

Table 1. Saturation Binding and Kinetic Parameters for [^{3}H]-18 Binding to Membrane Preparations of Human P2Y$_{12}$Rs Expressed in CHO Cells, Determined at 25 and 18 °C[a]

	Incubation temperature	
	25 °C	18 °C
Saturation binding		
K_D (nM)	4.57 ± 0.17	4.57 ± 0.29
B_{max} (pmol/mg of protein)	7.89 ± 0.21	7.39 ± 1.62
Association		
half-life (min)	1.6 ± 0.4	3.4 ± 0.3
K_{on} (nM^{-1} min^{-1})	0.0982 ± 0.0289	0.0510 ± 0.0040
K_{obs} (min^{-1})	0.447 ± 0.097	0.207 ± 0.015
Dissociation		
half-life (min)	1.8 ± 0.1	4.3 ± 0.3
K_{off} (min^{-1})	0.381 ± 0.023	0.162 ± 0.009
residence time (min)	2.7 ± 0.2	6.2 ± 0.4
K_D [K_{off}/K_{on}] (nM)	4.02 ± 0.84	4.24 ± 0.32

[a] K_D: equilibrium dissociation constant; B_{max}: maximum number of binding sites; K_{on}: association rate constant; K_{obs}: apparent association rate constant; K_{off}: dissociation rate constant.

affinity binding sites is present. The following values were calculated: at 25 °C, K_D = 4.57 ± 0.17 nM, and B_{max} = 7.89 ± 0.21 pmol/mg protein; at 18 °C, K_D = 4.57 ± 0.29 nM, and B_{max} = 7.39 ± 1.62 pmol/mg protein. There was no statistically significant difference between the apparent K_D and B_{max} values obtained at both temperatures. Nonspecific binding was very low, even at high radioligand concentrations (see Figure 5).

Competition Binding Assays. As a next step, we conducted homologous competition binding experiments to assess the concentration-dependent inhibition of unlabeled **18** versus [^{3}H]**18** at 25 and 18 °C (Figure 6A). The determined K_D values (K_D = 5.74 ± 0.94 nM at 25 °C; K_D = 5.22 ± 0.47 nM at 18 °C) were virtually identical to the K_D values obtained in saturation binding and kinetic studies (K_D saturation = 4.57 ± 0.17 and K_D kinetic studies = 4.02 ± 0.84 nM at 25 °C; K_D saturation = 4.57 ± 0.29 and K_D kinetic studies = 4.24 ± 0.32 nM at 18 °C).

Subsequently, several P2Y$_{12}$R ligands, including agonists and antagonists, were examined by competition binding assays versus the new antagonist radioligand. All of the compounds displayed full concentration-dependent inhibition (see Figure 6B). In general, pK_i values of ligands determined in the new radioligand binding assays correlated quite well with pEC$_{50}$/pIC$_{50}$ values determined in functional β-arrestin recruitment assays, although they were somewhat lower (about one order of magnitude) for most of the investigated antagonists. This may be explained by compound binding to serum albumin present in the β-arrestin assay medium, but not in the buffer used for binding studies (see Figure 6C and Table S1 in the Supporting Information). In contrast, ADP (**1**) displayed somewhat lower affinity in the binding assay as compared to the potency determined in the functional assay. This may be due to its metabolic instability. Incubation times, temperature, and the receptor preparations in the two assays differ: compounds were incubated for 1 h at 18 °C in the radioligand binding assay using membrane preparations, while incubation was performed for 3.5 h at 37 °C in the β-arrestin assay using intact cells of the same cell line. These variations in assay conditions may have affected the determined results leading to moderate variations.

Analysis of Structure–Activity Relationships (SARs) Based on Competition Binding Assays. Using the newly established radioligand, competition binding assays were performed to determine the affinities of the resynthesized unlabeled final compound **18**, its brominated derivative **41** used as radioligand precursor, and the intermediate compounds **35**, **37**, and **39** (see Figure 7). The determined K_i values were consistent with the SAR analysis based on functional biological data (see Figure S1 of the Supporting Information).[70,71] The acetic acid moiety attached to the indole nitrogen atom (R^1) in compound **18** was superior to all other investigated modifications (K_i 5.22 ± 0.47 nM). However, the negative charge of **18** was not essential since the methyl ester **39**, the unsubstituted **37**, and the acetyl derivative **35** still showed K_i values below 100 nM. It should be noted that the value for the ester **39** might be overestimated since partial hydrolysis may have occurred during the incubation period by esterases likely present in the employed cell membrane preparations. The results show that a keto function directly attached to the indole *N*-atom (in **35**) is unfavorable. The unsubstituted indole **37** is even somewhat more potent, while the compounds having a keto group attached to the indole nitrogen via a methylene linker are more potent. The bromine atom at the 6-position of the indole ring (R^2) in compound **41** was tolerated but slightly reduced the affinity compared to **18**, despite its increased lipophilicity. This indicates either limited space or unfavorable electrostatic interactions of the bromine atom with the receptor binding site.

https://doi.org/10.1021/acs.jmedchem.5c00213
J. Med. Chem. 2025, 68, 11279−11298

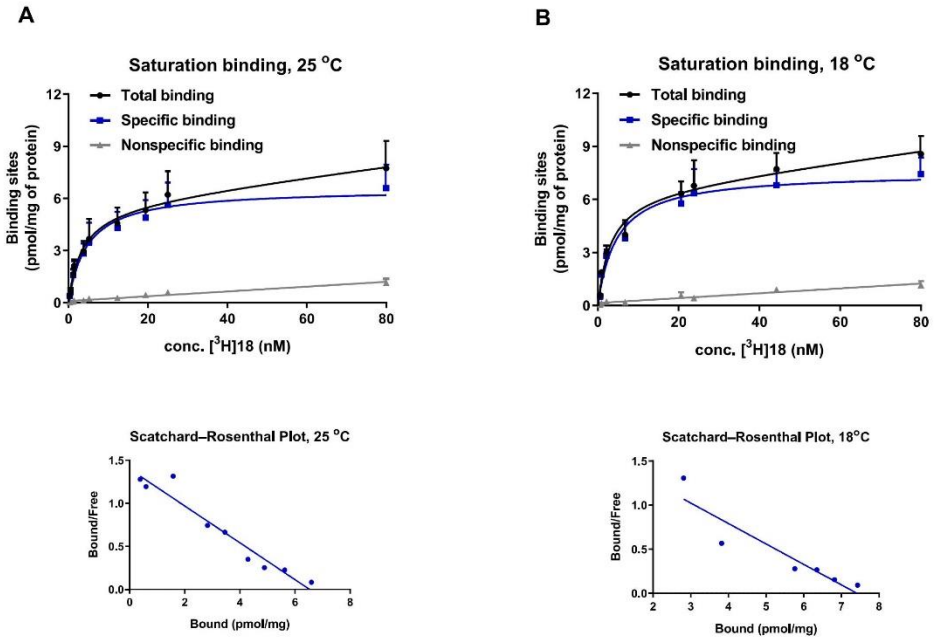


Figure 5. Saturation binding experiments of [^{3}H]**18** conducted with CHO-hP2Y$_{12}$ membrane preparation along with the corresponding Scatchard/Rosenthal plots (below). The radioligand (0.3–80 nM) was incubated with 5 μg of protein for 60 min (A) at 25 °C and (B) at 18 °C. Nonspecific binding was determined in the presence of 10 μM **18**. K_D and B_{max} values are collected in Table 1. Data represent means ± SEM from a minimum of three independent experiments, each conducted in duplicate.

Metabolic Stability. Compound **18** was further assessed for its metabolic stability using rat liver microsomes. Metabolic profiling of the unlabeled P2Y$_{12}$R ligand was performed through liquid chromatography–mass spectrometry (LC-MS) after incubation with rat liver microsomes in the presence of an NADPH-generating system. After 60 min of incubation, minimal degradation was observed, with 98.9% of the compound remaining intact. LC-MS and MS^2 analysis identified three primary metabolites, which were formed as a result of hydroxylation of **18** (see MS chromatogram and fragmentation table provided in Analytical Data S1).

Functional Characterization of the Unlabeled Ligand. The P2Y$_{12}$ inhibitory potency and mode of antagonism of the unlabeled compound **18** were assessed using a β-arrestin recruitment assay (Figure 8). To determine whether **18** acts as a competitive or allosteric antagonist on the P2Y$_{12}$ receptor, concentration–response curves of the agonist **2** were generated following preincubation with various fixed concentrations of the antagonist, utilizing a β-arrestin recruitment assay (Figure 8A). A noticeable parallel shift of the **2** agonist curve toward higher **2** agonist concentrations, along with an increased EC$_{50}$ value for **2**, was observed with increasing concentrations of the antagonist **18**, while the upper plateaus of the curves remained constant. The corresponding Schild plot displayed a linear curve with a slope close to unity (Figure 8B). The EC$_{50}$ values and maximum receptor activation are shown in Table S2. These data confirm that the mode of action of the antagonist **18** is indeed competitive as previously suggested using a radioligand binding assay.[77]

Docking Studies. To elucidate the binding mode of **18** and its interactions with the P2Y$_{12}$R, the compound was docked into the receptor's binding pocket (Figure 9A). The planar indole core plays a crucial role by forming arene-hydrogen interactions with Arg256 and Lys280, ensuring the precise alignment of **18** within the receptor's binding site (Figure 9B,C). The carboxylate at the indole-*N*1 substituent (acetic acid residue) likely establishes electrostatic interactions with Arg256 and potentially withThr260, which is located at a distance of 3.1 Å in the docked pose. Additionally, a water molecule near this region may play a role in enabling a water-mediated interaction as supported by structural flexibility and previous SAR findings.[71] The hydrophobic methyl group at the 5-position of the indole aligns with SAR insights, interacting with a subpocket formed by Phe252, Ala255, Val279, and Thr283. Similarly, the phenyl substituent at another key position is proposed to engage in π-stacking interactions with Tyr105, further stabilizing the ligand–receptor complex. This observation reinforces SAR findings that favor phenyl-based substitutions for high potency and receptor affinity. The carbonyl group of the amide may form a robust hydrogen bond with Arg256, significantly enhancing stabilization within the active site. Additionally, the carbonyl linker probably interacts with Asn159, further reinforcing

https://doi.org/10.1021/acs.jmedchem.5c00213
J. Med. Chem. 2025, 68, 11279–11298

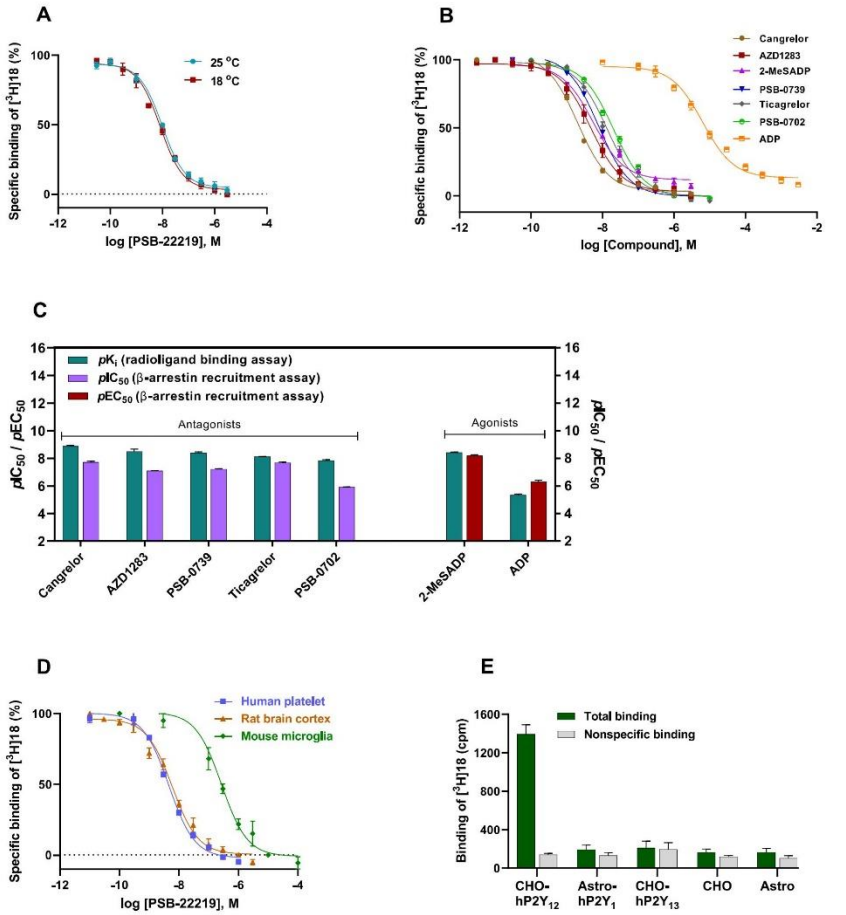


Figure 6. (A) Homologous competition was conducted at both 25 and 18 °C using 2 nM [^{3}H]**18** at human CHO-hP2Y$_{12}$ (5 μg of protein) for 60 min. The calculated K_D value was 5.74 ± 0.94 nM at 25 °C and 5.22 ± 0.47 nM at 18 °C. (B) Heterologous competition binding experiments were carried out with serial dilutions of each competitor that were incubated with 2 nM [^{3}H]**18** and membrane preparations of CHO-hP2Y$_{12}$ (5 μg of protein) for 60 min at 18 °C; calculated K_i values are shown in Table S1. (C) pK_i values of selected ligands were determined in the new optimized radioligand binding assay (curves in graph B) and compared to the pIC$_{50}$ or pEC$_{50}$ values obtained in β-arrestin recruitment assays. (D) Homologous competition was performed at 18 °C using 2 nM [^{3}H]**18** on human platelet (100 μg of protein) and rat brain cortex (250 μg of protein) membrane preparations or 15 nM [^{3}H]**18** on mouse microglial membrane preparations (2 μg of protein) for 60 min. K_D values were determined as follows: 2.53 ± 0.43 nM at human P2Y$_{12}$-platelets, 5.35 ± 0.62 nM at the rat P2Y$_{12}$-brain cortex, and 269 ± 23 nM at mouse P2Y$_{12}$-microglia. (E) Binding of [^{3}H]**18** (2 nM) at 18 °C to P2Y$_{12}$ receptors in CHO-hP2Y$_{12}$ (5 μg/vial), 1321N1 astrocytoma-hP2Y$_1$ (5 μg/vial), CHO-hP2Y$_{13}$ (5 μg/vial), nontransfected CHO (5 μg/vial), and 1321N1 astrocytoma (5 μg/vial) cells. In all radioligand binding experiments (A–B and D–E), nonspecific binding was assessed in the presence of 1 μM **10**, except for the rat brain cortex and mouse microglia where it was assessed in the presence of 1 μM **18** as well as 10 μM **10**. Data are presented as means ± SEM from at least three independent experiments, each conducted in duplicate.

binding stability, while the propyl chain extends into a hydrophobic groove defined by Tyr105, Phe106, Tyr109, Met152, Leu155, and Cys194, maximizing hydrophobic interactions and contributing to the overall stability and high affinity of **18** for the P2Y$_{12}$R, according to the model. Overall, the docking pose of **18** demonstrates a well-balanced network of hydrophobic interactions, hydrogen bonds, and π–π stacking interactions within the P2Y$_{12}$R (Figure 9). These findings emphasize the critical role of specific structural substitutions in enhancing the binding affinity and receptor blocking activity of

https://doi.org/10.1021/acs.jmedchem.5c00213
J. Med. Chem. 2025, 68, 11279−11298

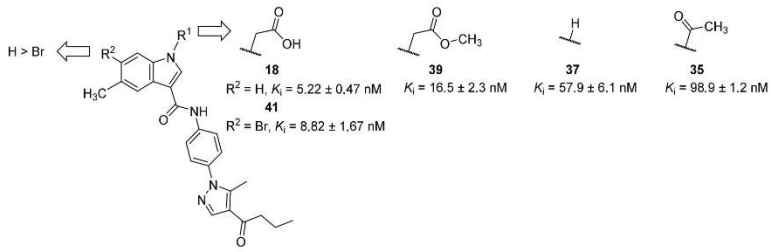


Figure 7. K_i values of **18**, its analogs, and derivatives determined in competition binding studies using the new radioligand. Data are presented as means ± SEM from at least three independent experiments, each conducted in duplicate.

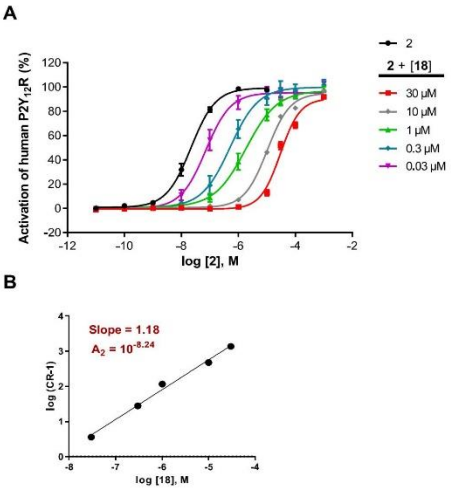


Figure 8. Characterization of **18**. (A) Concentration–response curves of the $P2Y_{12}R$ agonist **2** at the human $P2Y_{12}R$ following preincubation with different concentrations of antagonist **18**, determined in β-arrestin assays. Data points represent mean values ± SEM of three separate experiments performed in duplicates. Where no error bar is apparent, the SEM is too low to be visible. (B) Respective Schild plot: slope = 1.18 and $pA_2 = pK_B = 8.24$, corresponding to 5.25 nM, were calculated. The EC_{50} values and maximum receptor activation are shown in Table S2. CR: concentration ratio of the antagonist **18**.

18. In addition, it provides information for future structural optimization.

Native Tissues. To determine the broad utility of the radioligand for the detection of natively expressed $P2Y_{12}Rs$ of different species, we conducted studies on human platelet, rat cortical, and mouse microglial membrane preparations (see Figure 6D). Competition binding studies on human platelet and rat cortical membranes showed similar binding characteristics to those obtained with membranes recombinantly expressing human $P2Y_{12}R$ in CHO cells. The radioligand exhibited a binding affinity (K_D) of 2.53 ± 0.43 nM at human $P2Y_{12}R$ in platelets and of 5.35 ± 0.62 nM at rat $P2Y_{12}R$ natively expressed in the brain cortex. Homologous competition binding experiments performed on human platelets indicated the presence of a single class of high-affinity binding sites (B_{max} = 1.13 ± 0.26 pmol/mg protein), which was similar to the number of binding sites observed in rat brain cortical membranes (B_{max} = 1.22 ± 0.19 pmol/mg protein). This high similarity between human and rat $P2Y_{12}Rs$ can be explained by the high conservation of the $P2Y_{12}R$ protein sequences of both species. A sequence identity of 86.4% was calculated by alignment of human and rat $P2Y_{12}R$ protein sequences (see Figure S2 in the Supporting Information). The binding capacity in mouse microglial membranes was significantly higher, as indicated by a B_{max} value of 14.8 ± 2.02 pmol/mg of protein. The notably higher B_{max} value in mouse microglial cell membranes compared to human platelet and rat cortical membranes suggests a much greater density of $P2Y_{12}Rs$ in microglial cells supporting its prominent role in these key immune cells in the brain.[8,78] Surprisingly, a significantly higher K_D value was observed for $P2Y_{12}R$, as determined in mouse microglial cell membranes (269 ± 23 nM), compared to human and rat $P2Y_{12}Rs$. Despite the high sequence identities (see Figure S2) between these species (human–rat: 86.4%, human–mouse: 86.8%, and rat–mouse: 94.8%) with a conserved binding site, the binding affinities reveal notable interspecies differences. This discrepancy in affinity may be caused by subtle differences of the ligand binding domain induced by amino acid residues in the vicinity of the binding pocket, which may influence receptor conformation, ligand–receptor interaction, or receptor–ligand complex stability. Moreover, post-translational modifications such as glycosylation[79] or phosphorylation, or the presence of allosteric modulators such as lipids that can differ among species, may modulate receptor–ligand interactions.

In addition to the $P2Y_{12}$ receptor, there are two G protein-coupled ADP-activated receptors, namely $P2Y_1R$ and $P2Y_{13}R$. The binding affinity of the $P2Y_{12}R$ radioligand [^{3}H]**18** was therefore investigated at the human $P2Y_1R$ expressed in 1321N1 astrocytoma cells and the human $P2Y_{13}R$ expressed in CHO cells. [^{3}H]**18** (2 nM) showed a high selectivity for the $P2Y_{12}R$ versus the other purinergic ADP receptors (Figure 6E). Both human $P2Y_1R$ and $P2Y_{13}R$ displayed negligible binding affinity. Our results are in agreement with a previous study, in which a structurally related $P2Y_{12}R$ antagonist had not shown any antagonistic activity at $P2Y_1R$ and $P2Y_{13}R$.[77]

Autoradiography Study. Finally, the newly developed radioligand [^{3}H]**18** was studied in brain sections. Since the $P2Y_{12}R$ is a promising biomarker for microglial cells, which play a crucial role in neuroinflammation, our ultimate goal is to develop a radioligand that selectively binds to the human $P2Y_{12}R$ and can be used for imaging. On the way to clinical

https://doi.org/10.1021/acs.jmedchem.5c00213
J. Med. Chem. 2025, 68, 11279–11298

Journal of Medicinal Chemistry pubs.acs.org/jmc Article

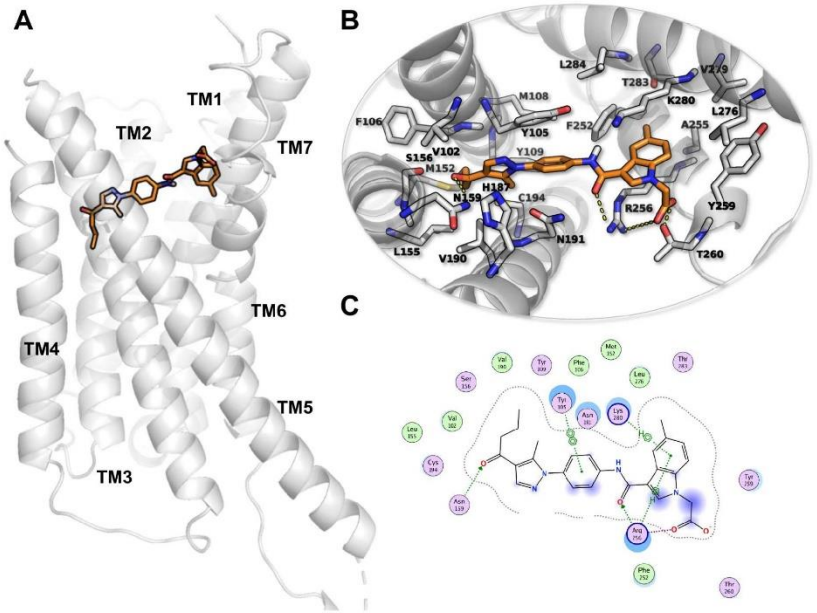


Figure 9. Putative binding pose of **18** to the hP2Y$_{12}$ receptor. (A) Overall docking pose of **18** within the P2Y$_{12}$R. The receptor is depicted in a cartoon representation, with the seven transmembrane helices (TM1−TM7) labeled. The ligand **18** is shown in orange stick representation, positioned within the receptor's binding pocket. (B) Close-up view of the binding interactions between **18** and the P2Y$_{12}$R. Key residues involved in ligand binding are displayed in stick representation and labeled. Hydrogen bonds and other interactions between **18** and the receptor are illustrated with dashed yellow lines, highlighting the key residues that stabilize the ligand within the binding pocket. (C) 2D interaction diagram of **18** with the P2Y$_{12}$R.

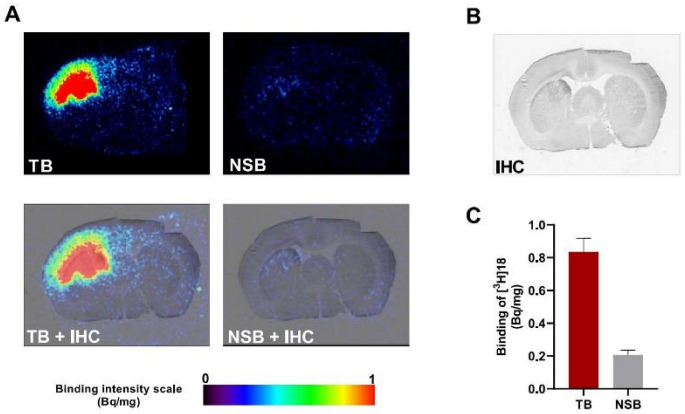


Figure 10. (A) Autoradiography images of brain sections obtained from the AAV-CAG-h*P2ry12* rat model (top). Slices were incubated with 2 nM [^{3}H]**18** for total binding (TB) or in the presence of 1 μM **4** for nonspecific binding (NSB) at room temperature for 1 h. The same autoradiographs superposed to immunohistochemistry (IHC) images from adjacent brain slices (bottom). Human P2Y$_{12}$ receptor expression was detected by immunostaining with a specific primary antibody against P2Y$_{12}$R (dark color in the left unilateral part of brain slices), which matches with the autoradiographic signal (red color). (B) Immunohistochemical image of P2Y$_{12}$R labeling on a brain slice from the AAV-CAG-h*P2ry12* rat model. (C) Radioligand binding values obtained by analysis of autoradiography images.

https://doi.org/10.1021/acs.jmedchem.5c00213
J. Med. Chem. 2025, 68, 11279−11298

radiotracers, extensive screening and investigations are conducted in animal models. Thus, a humanized rat model overexpressing the human $P2Y_{12}$ receptor was created by gene transfer to the central nervous system.[80] Animal models that specifically express a receptor by viral vector induction are efficient tools to evaluate specific and off-target binding of radioligands both by in vivo PET imaging and by in vitro autoradiography. Such models have previously been used for the evaluation of other purinergic receptor ligands such as the $P2Y_6R$.[81] Briefly, the humanized $hP2Y_{12}R$ model was obtained by creation of an adeno-associated virus (AAV) vector carrying the cDNA for human *P2ry12* (Figure S3 in the Supporting Information). To verify the expression of the human $P2Y_{12}R$ protein, HEK293T cells were transfected with the AAV shuttle plasmid, and a Western blot analysis was conducted using a specific anti-$P2Y_{12}R$ antibody. As reported by Savi et al.,[82] a band at 250 kDa was detected, indicating the tetrameric form of the $hP2Y_{12}R$ (Figure S4). Following the unilateral stereotactic injection of AAV-CAG-h*P2ry12* into the rat striatum of Sprague−Dawley rats (Figure S5A), $P2Y_{12}R$ expression was confirmed unilaterally at the site of injection, mainly in neurons due to vector tropism. Additionally, in the ipsilateral striatum, a moderate reactive astrogliosis was observed by $GFAP^+$ astrocytes. However, Iba1 immunolabeling did not show any significant microglial reactivity (Figure S5B).

An autoradiographic study was conducted on brain sections from the AAV-CAG-h*P2ry12* rat model, incubated with [^{3}H]**18** (Figure 10). Significant [^{3}H]**18** ligand binding ($p < 0.01$), indicated by the red color, was observed on the injected side. Adjacent brain sections, immunostained with specific primary antibody against $P2Y_{12}R$, revealed expression of the $hP2Y_{12}R$ in the corresponding striatal region. Addition of a high concentration of the $P2Y_{12}$-selective antagonist 4[83] (1 μM) displaced [^{3}H]**18** (Figure 10A). Nonspecific binding (0.206 ± 0.030 Bq/mg) accounted for only 24.7% of total binding (0.835 ± 0.083 Bq/mg) as shown in Figure 10C.

In summary, the new radioligand was proven to selectively bind to $hP2Y_{12}Rs$ in the brain in the employed model. As a next step, more relevant animal models will have to be studied, e.g., measuring microglial $P2Y_{12}R$ expression, which are difficult to transduce. Based on the present results, the new radioligand can be expected to be suitable for application in animal models and human brain slices affected by neurodegenerative diseases, where it is crucial to comprehend the dynamics of $P2Y_{12}R$ expression during disease progression. Additionally, these results will support the development of future preclinical and clinical imaging studies, eventually contributing to the development of new therapeutic strategies.

CONCLUSIONS

In the present study, we designed and synthesized a new radioligand and developed binding assays for labeling the purinergic $P2Y_{12}R$. The competitive and reversible radiotracer [^{3}H]**18** was characterized at various recombinant and natively expressed $hP2Y_{12}Rs$ of human, rat, and mouse, showing high affinity and minimal nonspecific binding. The metabolic profile of **18** was assessed in rat liver microsomes, and it showed high metabolic stability. Additionally, we performed docking studies of the unlabeled antagonist **18** and predicted the binding mode and interactions with the amino acids in the binding site including Tyr105, Asn159, Lys280, Tr260, and Arg256. High selectivity of the radioligand was confirmed versus closely related ADP-activated receptors. It enabled $P2Y_{12}R$ detection in an autoradiography study on brain sections of a humanized rat model. Compared to previously reported radiotracers for $P2Y_{12}Rs$ (see Figure 2), [^{3}H]PSB-22219 ([^{3}H]**18**) is a balanced radioligand that combines several advantages: Its affinity (K_i 4.57 nM, human $P2Y_{12}R$) is similar to that of the published radiotracers **12**−**17** (Figure 2) with a K_i value in the low nanomolar range; only **17** is even more potent (K_i 0.30 nM). However, compared to the highly lipophilic **17** (clogD 4.67, calculated by Instant JChem 5.3.4), compound **18** is significantly less lipophilic (clogD 1.17) and therefore shows an extremely low degree of nonspecific binding (<10% under the applied conditions), which makes it ideal for biological applications. Moreover, **18** has a lower molecular weight and a lower polar surface area than most of the radioligands described so far (**12**−**16**). Importantly, it exhibits high metabolic stability and high selectivity, showing no off-target binding. The only drawback is its expected low brain penetration, which will require chemical modification to turn it into a diagnostic for brain imaging. This could be achieved by replacement of the negatively charged carboxylate function, e.g., by amide formation or its replacement by a ketone. For in vitro and ex vivo studies, the new radioligand [^{3}H]PSB-22219 features a combination of ideal properties. It represents a valuable tool for further characterization of $P2Y_{12}R$ antagonists. Moreover, it constitutes a significant advancement toward PET tracer development targeting the purinergic $P2Y_{12}R$, thereby opening up new avenues for exploring the role of this receptor in inflammatory brain diseases associated with microglial activation, such as neuropathic pain and neurodegenerative disorders.

EXPERIMENTAL SECTION

Chemistry. *General Methods.* All commercially available reagents were used as purchased (BLDpharm, Acros, Alfa Aesar, Sigma-Aldrich, abcr, or TCI). Solvents were used without additional purification or drying. Thin-layer chromatography (TLC) using aluminum sheets with silica gel 60 F254 were utilized to monitor the reactions (Merck). Column chromatography was performed with silica gel of 0.060−0.200 mm, pore diameter ca. 6 nm. All synthesized compounds were finally dried in vacuum at 8−12 Pa (0.08−0.12 mbar) using a sliding vane rotary vacuum pump (Vacuubrand GmbH). ^{1}H and ^{13}C NMR data were collected on a Bruker Avance 500 MHz NMR spectrometer at 500 MHz (^{1}H) or 126 MHz (^{13}C), respectively. If indicated, NMR data were collected on a Bruker Ascend 600 MHz NMR spectrometer at 600 MHz (^{1}H) or 151 MHz (^{13}C). DMSO-d_6 was employed as a solvent at 303 K. Chemical shifts are reported in parts per million (ppm) relative to the deuterated solvent: DMSO, δ ^{1}H: 2.49 ppm; ^{13}C: 39.7 ppm. Coupling constants J are given in Hertz, and spin multiplicities are given as s (singlet), d (doublet), dd (doublet of doublet), t (triplet), q (quartet), sext (sextet), m (multiplet), and br (broad). The purities of all isolated products were determined by an HPLC 1260 Infinity II (Agilent) using an EC 50/2 Nucleodur C18 Gravity 3 μm column (Macherey-Nagel), coupled to a UV/vis diode array detector, and a mass spectrometer (Infinity Lab LC MSD system, Agilent, with an EC 50/2 Nucleodur C18 Gravity 3 μm column, Machery-Nagel). All compounds are >95% pure by HPLC/UV. The column temperature was 40 degrees. The compounds were dissolved at a concentration of 1.0 mg/mL in water, methanol, or acetonitrile. Then, 2 μL of the sample solution was injected to a flow of 0.5 mL/min. Elution started with a gradient of water containing 2 mM ammonium acetate/acetonitrile from 90:10 to 0:100 for 10 min, and then, it was flushed with 100% acetonitrile for an additional 5 min. Positive total ion scans were observed from 100−1000 m/z (or more if necessary). UV absorption was detected from 190 to 600 nm using a diode array detector (DAD). The purity of all compounds was determined at 220−600 nm. The radiolabeling procedure along with the synthesis of the final compounds and the optimized reaction conditions for the intermediates are detailed

https://doi.org/10.1021/acs.jmedchem.5c00213
J. Med. Chem. 2025, 68, 11279−11298

below. Comprehensive synthesis procedures for all reported intermediates, as well as the analytical characterization of all compounds, are provided in the Supporting Information (SI).

*Radiolabeling and Purification Protocol of the Radioligand [^{3}H]-**18**.* The brominated precursor **41** (1.72 mg, 3.20 μmol), 50 μL (37.26 mg, 0.29 mmol) of *N*,*N*-diisopropylethylamine (DIPEA), and Lindlar's catalyst (32.53 mg, 0.31 mmol) were suspended in DMF (0.3 mL). The suspension was degassed three times applying high vacuum and stirred under an atmosphere of tritium gas (515 mbar (51.5 kPa), 6.2 Ci) overnight at room temperature. At the end of the reaction, a pressure of 445 mbar (44.5 kPa) at room temperature was measured. The solvent was removed in vacuo, and labile tritium was exchanged by adding 0.3 mL of methanol, stirring the solution, and removing the solvent again in vacuo. This process was repeated twice. Finally, the well-dried solid was extracted with 5 mL of EtOH, and the suspension was filtered through a 0.2 μm nylon membrane (PA-20/25), obtaining a clear solution. The radiochemical purity of the crude material was determined to be approximately 66% determined by HPLC (Waters Sunfire C18, 5 μm, 4.6 × 250 mm), eluted with a gradient of solvents (A: water + 0.05% TFA; B: acetonitrile + 0.05% TFA), starting with 20% B, then for 10–14.5 min with 95% B, and finally with 20% B for 15 min. Detection was performed with a UV detector at a wavelength of 254 nm. The flow rate was 1.0 mL/min, and the column temperature was 30 °C. The product had a retention time of 10.35 min. For purification of the radioligand, the following HPLC conditions were found to be suitable: Waters Sunfire C18, 10 × 250 mm; solvent A: water + 0.1% TFA; B: acetonitrile + 0.1% TFA; 60% B isocratic; 4.7 mL/min; 25 °C. The target compound was eluted at 6.1–6.6 min. The desired product was eluted with 5 mL of ethanol. The extracted product showed a radiochemical purity of >99%, and the specific activity was determined to be 17.4 Ci/mmol (determined by LC-MS).

*Synthesis of 2-(3-((4-(4-Butyryl-5-methyl-1H-pyrazol-1-yl)-phenyl)carbamoyl)-5-methyl-1H-indol-1-yl)acetic Acid (**18**).* In a sealed tube, aqueous 2 N NaOH (1.6 mL, 2.3 mmol) was added to a solution of **39** (1.0 g, 2.1 mmol) in MeOH (10 mL). The reaction mixture was stirred at room temperature overnight. Then, it was concentrated under vacuum and neutralized via aqueous 1 N HCl. The precipitate was filtered off, washed with water, and dried under high vacuum to afford the unlabeled ligand **18** as a white powder (0.34 g, 62%).[71] ^{1}H NMR, DMSO-d_6 (600 MHz): δ 10.02 (s, 1H), 8.23 (d, J = 5.3 Hz, 2H), 8.02 (s, 1H), 7.96 (d, J = 8.7 Hz, 2H), 7.48 (d, J = 8.7 Hz, 2H), 7.39 (d, J = 8.4 Hz, 1H), 7.08 (d, J = 8.3 Hz, 1H), 5.12 (s, 2H), 2.81 (t, J = 7.2 Hz, 2H), 2.52 (s, 3H), 2.43 (s, 3H), 1.64 (sext, J = 7.3 Hz, 2H), 0.94 (t, J = 7.4 Hz, 3H); ^{13}C NMR, DMSO-d_6 (151 MHz): δ 195.35, 169.81, 162.92, 142.00, 141.32, 139.99, 135.14, 132.71, 132.55, 129.80, 126.70, 125.56, 123.84, 120.77, 120.10, 119.60, 110.01, 109.50, 47.41, 41.83, 21.10, 17.26, 13.55, 11.78. mp = 201–202 °C (lit. 201 °C). LC-MS (m/z): positive mode 459.3 $[M + H]^{1+}$; purity by HPLC-UV (254 nm)-ESI-MS: 99.8%.

*Synthesis of Ethyl 3-(5-methyl-1-(4-nitrophenyl)-1H-pyrazol-4-yl)-3-oxopropanoate (**21**).* In a 250 mL round-bottom flask, compound **20** (2.0 g, 8.10 mmol) was dissolved in THF (150 mL) and treated with 1,1′-carbonyldiimidazole (1.97 g, 12.14 mmol). The mixture was stirred at room temperature for 16 h, followed by the addition of anhydrous $MgCl_2$ (3.08 g, 32.40 mmol) and potassium malonate (5.52 g, 32.40 mmol). The mixture was stirred at 55 °C for 6 h. After concentration under reduced pressure, the residue was extracted with EtOAc (100 mL), washed with aqueous 1 N NaOH and brine, dried over $MgSO_4$, and evaporated to dryness to yield **21** as a brown powder (2.34 g, 91%). ^{1}H NMR, DMSO-d_6 (500 MHz): δ 8.41 (d, J = 9.1 Hz, 2H), 8.37 (s, 1H), 7.89 (d, J = 9.1 Hz, 2H), 4.13 (q, J = 7.1 Hz, 2H), 4.02 (s, 2H), 2.62 (s, 3H), 1.21 (t, J = 7.1 Hz, 3H); ^{13}C NMR, DMSO-d_6 (126 MHz): δ 188.09, 167.39, 146.74, 143.92, 143.22, 143.00, 125.97, 124.73, 120.68, 60.53, 47.47, 13.99, 12.06; mp 108–109 °C. LC-MS (m/z): positive mode 318.2 $[M + H]^{1+}$; purity by HPLC (220–600 nm)-ESI-MS: 94.0%.

*Synthesis of Benzyl 5-Methyl-1H-indole-3-carboxylate (**31**).* In a 250 mL round-bottom flask, 2,2,2-trifluoroacetic anhydride (6.0 g, 28.5 mmol, 4.0 mL) in DCM (30 mL) was added dropwise to a stirred suspension of **26** (5.0 g, 28.5 mmol) in DCM (350 mL) at 0 °C. The reaction mixture was stirred at 25 °C for 1 h. A color change to pink was observed; then, benzyl alcohol (3.1 g, 28.5 mmol, 3.0 mL) was added. After stirring for a further 2 h, TLC analysis confirmed the formation of the desired product. The reaction mixture was quenched with satd. aq. Na_2CO_3 solution (50 mL) and then washed with water and brine. The organic phase was dried over $MgSO_4$ and evaporated under reduced pressure to afford the crude product, which was subjected to column chromatography (silica gel chromatography, eluent: petrol ether/EtOAc 8:2) to afford the novel compound **31** as a brown powder (5.1 g, 67%). ^{1}H NMR, DMSO-d_6 (600 MHz): δ 11.83 (s, 1H), 8.06 (s, 1H), 7.80 (s, 1H), 7.47 (d, J = 7.4 Hz, 2H), 7.42–7.31 (m, 4H), 7.04–7.00 (m, 1H), 5.33 (s, 2H), 2.39 (s, 3H); ^{13}C NMR, DMSO-d_6 (151 MHz): δ 164.26, 137.25, 134.87, 132.72, 130.18, 128.55, 127.89, 127.81, 126.09, 124.04, 120.18, 112.16, 105.81, 64.49, 21.46; mp 165–167 °C. LC-MS (m/z): positive mode 266.1 $[M + H]^{1+}$; purity by HPLC (220–600 nm)-ESI-MS: 98.0%.

*Synthesis of Benzyl 1-(2-Methoxy-2-oxoethyl)-5-methyl-1H-indole-3-carboxylate (**32**).* In a 100 mL round-bottom flask, K_2CO_3 (1.04 g, 7.6 mmol) and methyl 2-bromoacetate (1.16 g, 7.6 mmol, 0.73 mL) were added to a solution of **31** (1.0 g, 3.8 mmol) in DMF (10 mL), and the mixture was stirred at 25 °C for 24 h. TLC analysis indicated the formation of the product. The reaction mixture was then quenched via water (25 mL) and extracted with EtOAc (3 × 25 mL). The organic phase was dried over $MgSO_4$, evaporated under reduced pressure, and then purified by column chromatography (silica gel chromatography, eluent: petrol ether/EtOAc 8:2) to afford the new compound **32** as a white powder (0.87 g, 68%). ^{1}H NMR, DMSO-d_6 (600 MHz): δ 8.13 (s, 1H), 7.83 (s, 1H), 7.48 (d, J = 7.4 Hz, 2H), 7.44–7.37 (m, 3H), 7.34 (t, J = 7.3 Hz, 1H), 7.08 (dd, J = 8.4, 1.3 Hz, 1H), 5.33 (s, 2H), 5.22 (s, 2H), 3.68 (s, 3H), 2.41 (s, 3H); ^{13}C NMR, DMSO-d_6 (151 MHz): δ 168.82, 163.71, 136.89, 136.47, 135.33, 130.71, 128.44, 127.82, 126.17, 124.17, 120.20, 110.59, 105.52, 64.61, 52.22, 47.20, 21.20; mp = 95–97 °C. LC-MS (m/z): positive mode 338.9 $[M + H]^{1+}$; purity by HPLC-UV (254 nm)-ESI-MS: 99.9%.

*Synthesis of Benzyl 1-Acetyl-5-methyl-1H-indole-3-carboxylate (**33**).* In a 100 mL round-bottom flask, **31** (1.0 g, 3.8 mmol) was added to a mixture of sodium hydride (NaH, 0.36 g, 15.2 mmol) in DMF (10 mL), and the mixture was stirred for 30 min at 0 °C. Then, acetyl chloride (0.59 g, 7.6 mmol, 0.54 mL) was added dropwise, and the reaction mixture was stirred at 25 °C for 24 h. After completion of the reaction, the mixture was poured into water (25 mL) and extracted with EtOAc (3 × 25 mL). The organic layer was dried over $MgSO_4$ and evaporated under reduced pressure. The crude product was purified by column chromatography (silica gel chromatography, eluent: petroleum ether/EtOAc 8:2) to afford the new compound **33** as a white-yellowish powder (0.82 g, 70%). ^{1}H NMR, DMSO-d_6 (500 MHz): δ 8.46 (s, 1H), 8.23 (d, J = 8.5 Hz, 1H), 7.87 (s, 1H), 7.51 (d, J = 7.3 Hz, 2H), 7.42 (t, J = 7.4 Hz, 2H), 7.36 (t, J = 7.3 Hz, 1H), 7.25–7.20 (m, 2H), 5.40 (s, 2H), 2.73 (s, 3H), 2.41 (s, 3H); ^{13}C NMR, DMSO-d_6 (126 MHz): δ 170.09, 163.19, 136.36, 133.62, 133.46, 128.47, 128.02, 127.95, 127.16, 126.71, 120.63, 115.72, 111.23, 65.39, 23.67, 21.09. mp 133–135 °C. LC-MS (m/z): positive mode 308.0 $[M + H]^{1+}$; purity by HPLC-UV (254 nm)-ESI-MS: 99.0%.

*Synthesis of 1-(2-Methoxy-2-oxoethyl)-5-methyl-1H-indole-3-carboxylic Acid (**34**).* In a 25 mL hydrogenation flask, benzyl ester **32** (0.8 g, 23.7 mmol) was dissolved in MeOH (14 mL); then, Pd/C (10%, 0.08 g) was added under an argon atmosphere with stirring. The mixture was then evacuated three times and flushed with H_2 gas (241.3 kPa) at 25 °C for 2 h. After TLC analysis, the reaction mixture was filtered over Celite, washed with methanol, and evaporated under reduced pressure to obtain the desired key intermediate **34** as a pale-brown powder (0.585 g, 100%). ^{1}H NMR, DMSO-d_6 (600 MHz): δ 11.97 (s, 1H), 7.99 (s, 1H), 7.82 (s, 1H), 7.36 (d, J = 8.4 Hz, 1H), 7.09–6.97 (m, 1H), 5.20 (s, 2H), 3.68 (s, 3H), 2.41 (s, 3H). ^{13}C NMR, DMSO-d_6 (151 MHz): δ 168.93, 165.56, 136.15, 135.34, 130.30, 126.49, 123.89, 120.43, 110.34, 106.74, 52.20, 47.15, 21.16; mp 220–222 °C. LC-MS (m/z): positive mode 248.0 $[M + H]^{1+}$; purity by HPLC-UV (254 nm)-ESI-MS: 99.7%.

*Synthesis of 1-Acetyl-5-methyl-1H-indole-3-carboxylic Acid (**27**).* Following the same procedure as for **34**, starting with **33** (0.565 g, 1.84

https://doi.org/10.1021/acs.jmedchem.5c00213
J. Med. Chem. 2025, 68, 11279–11298

mmol), **27** was synthesized as a pale-brown powder (0.4 g, 100%). ^{1}H NMR (600 MHz, DMSO-d_6): δ 8.37 (s, 1H), 8.22 (d, J = 8.5 Hz, 1H), 7.89 (s, 1H), 7.21 (dd, J = 8.5, 1.5 Hz, 1H), 2.71 (s, 3H), 2.42 (s, 3H); ^{13}C NMR (151 MHz, DMSO): δ 170.04, 165.02, 133.59, 133.40, 133.13, 127.66, 126.49, 120.87, 115.63, 112.65, 23.65, 21.08. mp 238−240 °C. LC-MS (m/z): positive mode 218.0 $[M + H]^{1+}$; purity by HPLC-UV (254 nm)-ESI-MS: 99.0%.

*Synthesis of Methyl 2-(3-((4-(4-Butyryl-5-methyl-1H-pyrazol-1-yl)phenyl)carbamoyl)-5-methyl-1H-indol-1-yl)acetate (**39**).* In a sealed tube, 1-(1-(4-aminophenyl)-5-methyl-1*H*-pyrazol-4-yl)butan-1-one (**24**) (0.76 g, 3.1 mmol), 4-dimethylaminopyridine (DMAP) (0.48 g, 3.9 mmol), and 1-ethyl-3-(3′-dimethylaminopropyl)-carbodiimide hydrochloride (EDC·HCl) (0.44 g, 2.9 mmol) were added to a solution of **34** (0.58 g, 2.3 mmol) in DCM (30 mL) at 0 °C. The reaction mixture was stirred at RT overnight. The mixture was then washed sequentially with 1 N HCl, water, and brine. The organic layer was dried over $MgSO_4$ and evaporated under reduced pressure, and the residue was purified by silica gel column chromatography (DCM, followed by DCM/EtOAc, 8/2 v/v) to afford **39** as a white-yellowish powder (0.91 g, 82%). ^{1}H NMR, DMSO-d_6 (600 MHz): δ 10.05 (s, 1H), 8.24 (s, 1H), 8.22 (s, 1H), 8.02 (s, 1H), 7.96 (d, J = 8.8 Hz, 2H), 7.48 (d, J = 8.8 Hz, 2H), 7.39 (d, J = 8.4 Hz, 1H), 7.08 (d, J = 8.4 Hz, 1H), 5.26 (s, 2H), 3.71 (s, 3H), 2.81 (t, J = 7.2 Hz, 2H), 2.52 (s, 3H), 2.43 (s, 3H), 1.64 (sext, J = 7.3 Hz, 2H), 0.94 (t, J = 7.4 Hz, 3H); ^{13}C NMR, DMSO-d_6 (151 MHz): δ 195.61, 169.16, 163.13, 142.26, 141.59, 140.22, 135.37, 132.86, 130.22, 126.96, 125.83, 124.23, 121.08, 120.37, 119.89, 110.30, 110.08, 52.41, 47.50, 42.10, 21.36, 17.53, 13.82, 12.05. mp 210−212 °C (lit. mp 211 °C). LC-MS (m/z): positive mode 473.3 $[M + H]^{1+}$; purity by HPLC-UV (254 nm)-ESI-MS: 98.0%.

*Synthesis of 2-(6-Bromo-3-((4-(4-butyryl-5-methyl-1H-pyrazol-1-yl)phenyl)carbamoyl)-5-methyl-1H-indol-1-yl)acetic Acid (**41**).* Following the same procedure as for **18**, starting with **40** (95.0 mg, 0.17 mmol), **41** was obtained as a white-yellowish powder (60.0 mg, 65%).[71] ^{1}H NMR, DMSO-d_6 (600 MHz): δ 13.17 (br, 1H), 10.09 (s, 1H), 8.26 (s, 1H), 8.23 (s, 1H), 8.17 (s, 1H), 7.94 (d, J = 8.9 Hz, 2H), 7.86 (s, 1H), 7.48 (d, J = 8.8 Hz, 2H), 5.16 (s, 2H), 2.81 (t, J = 7.2 Hz, 2H), 2.52 (s, 3H), 2.46 (s, 3H), 1.64 (sext, J = 7.3 Hz, 2H), 0.94 (t, J = 7.4 Hz, 3H). ^{13}C NMR, DMSO-d_6 (151 MHz): δ 195.48, 169.83, 162.66, 142.13, 141.47, 139.93, 136.34, 133.65, 132.83, 129.22, 126.26, 125.71, 122.47, 120.24, 119.80, 118.56, 114.07, 109.73, 62.76, 47.70, 41.97, 22.79, 17.39, 13.68, 11.91. mp 232−234 °C (no mp reported in the literature). LC-MS (m/z): positive mode 537.9 $[M + H]^{1+}$; purity by HPLC-UV (254 nm)-ESI-MS: 95.0%.

clogD Value Calculation. The clogD value, representing the logarithm of the distribution coefficient between a lipophilic phase and an aqueous phase at pH 7.4, was calculated using the program Instant JChem 5.3.4. (https://chemaxon.com/instant-jchem).

Biology. *Cell Culture.* The recombinant Chinese hamster ovary (CHO) cell line expressing the human $P2Y_{12}R$ (CHO-h$P2Y_{12}R$ cells) with a β-galactosidase fragment and β-arrestin containing the complementary fragment of the enzyme for performing β-arrestin recruitment assays (Pathhunter, DiscoverX) was created as previously described.[74] This cell line was used for β-arrestin recruitment assays as well as for radioligand binding assays. CHO-h$P2Y_{12}R$ recombinant cells were cultured at 37 °C, 5% CO_2 in Ham's F12 Nutrient Mix medium (F12, no. 11765054, Thermo Fisher Scientific, MA, USA), supplemented with 10% fetal bovine serum (FBS, no. P30-1502, PAN Biotech, Germany), penicillin 100 U/mL + streptomycin 100 μg/mL (no. P06-07100, PAN Biotech, Germany), 300 μg/mL hygromycin (np. P06-08020, PAN Biotech, Germany), and 800 μg/mL G418 (no. P06-07100, PAN Biotech, Germany). After cells reached 80−90% confluency, the medium was discarded and the cell monolayer was rinsed with phosphate-buffered saline (PBS; 137 mM NaCl, 2.7 mM KCl, 4.3 mM Na_2HPO_4, and 1.47 mM KH_2PO_4). Subsequently, trypsin-ethylenediaminetetraacetic acid (EDTA) solution (0.05%/0.6 mM) was added to detach the cells from the cell culture flask, and they were split into new cell culture flasks at a ratio of 1:10. The cell line underwent regular PCR analysis to detect potential mycoplasma contamination. The h$P2Y_{12}R$ and the h$P2Y_1R$ were stably expressed in 1321N1 astrocytoma (1321N1 astrocytoma-$P2Y_{12}R$ and 1321N1 astrocytoma-$P2Y_1R$),[84,85] while the h$P2Y_{13}R$ receptor was expressed in CHOs (CHO-$P2Y_{13}R$)[74] as previously described.

Membrane Preparation of Recombinant CHO Cells. Once the CHO-β-arrestin-h$P2Y_{12}R$ cells reached a confluence of ∼90%, the content of one 175 cm^2 flask was passed into 20 sterile 150 mm dishes and incubated at 37 °C and 5% CO_2 for 4 days. After the cells had grown into a monolayer of ∼90% confluence again, the medium was decanted, and dishes were rinsed with 5 mL of PBS and frozen at −20 °C. Frozen cells were scraped off the dishes with 1 mL of ice-cold buffer (25 mM Tris-HCl, 1 mM EDTA, and 0.32 M saccharose, pH 7.4) using a rubber cell scraper. This step was repeated to ensure that all cells were collected from each dish. Once the content of all dishes was unified in a beaker, the cell suspension was treated with an UltraTurrax (IKA Labortechnik, Staufen, Germany) twice for 30 s each at level 4. To remove nuclei, other larger organelles, and cell debris, the homogenate was centrifuged at 1000g for 10 min (4 °C). The pellet (P1) was discarded, and the supernatant (S1) was collected and centrifuged at 48,000g for 1 h (4 °C). Then, the supernatant (S2) was decanted, and the obtained pellet (P2) was resuspended in 25 mL of 50 mM Tris-HCl, pH 7.4 washing buffer and centrifuged for at 48,000g for 30 min (4 °C). After two more washing steps, the pellet was resuspended in 0.1 mL per dish of 50 mM Tris-HCl, pH 7.4 buffer, and crude membrane solutions were aliquoted and stored at −80 °C until use. All steps should be carried out swiftly at a temperature of 4 °C to avoid receptor internalization. Membrane preparations of the following human receptor-transfected cells were obtained: 1321N1 astrocytoma-$P2Y_{12}R$, 1321N1 astrocytoma-$P2Y_1R$, and CHO-$P2Y_{13}R$. As controls, membrane preparations of non-transfected cells, 1321N1 astrocytoma cells and CHO cells, were obtained. Moreover, membranes of mouse microglial cells (BV-2, no. 305156, Cytion Company, Germany) were prepared. All membrane preparations were obtained according to the same method as described from human recombinant CHO-β-arrestin-h$P2Y_{12}R$ cells.

Human Platelet Membrane Preparations Natively Expressing $P2Y_{12}R$. Outdated apheresis-purified human thrombocyte-plasma concentrates were obtained from the blood bank, University of Bonn, in accordance with ethical guidelines, and generously provided by Prof. Dr. Gerd Bendas from the Pharmaceutical Institute, University of Bonn. These concentrates were then stored in sterile infusion bags at 22 °C, with gentle agitation. The suspension was poured carefully from the infusion bags into centrifuge tubes and centrifuged at 1000g for 10 min (4 °C). The discarded pellet contains residual components, including remnants of red blood cells. The supernatant (platelet rich plasma) was moved to clean centrifuge tubes and subjected to centrifugation at 48,000g for 60 min (4 °C). Subsequently, the formed pellet was resuspended in buffer 1 (50 mM Tris-HCl, 5 mM EDTA, and 150 mM NaCl, pH 7.4), homogenized with an UltraTurrax (IKA Labortechnik, Staufen, Germany) twice for 30 s each at level 4, and centrifuged at 48,000g for 60 min (4 °C). Once more, the supernatant was discarded, and the pellet was reconstituted in buffer 2 (5 mM Tris-HCl and 5 mM EDTA, pH 7.4) and centrifuged again at the same settings. The last fraction of pellet was resuspended in an appropriate volume of buffer 3 (50 mM Tris-HCl, pH 7.4). The protein suspension was subsequently aliquoted into 2 mL Eppendorf tubes and frozen at −80 °C until needed.

Rat Brain Cortex Membrane Preparation Natively Expressing $P2Y_{12}R$. Rat brains were defrosted in 0.32 M saccharose solution and dissected to obtain the cortex. Rat cortex membrane preparations were prepared (P2), according to the methods described above for CHO cells recombinantly expressing human $P2Y_{12}R$.

Determination of Protein Concentration. The Lowry method[86] was employed to determine the protein concentration. This involved dissolving 2% (w/v) $NaHCO_3$ in NaOH and mixing this solution in a 50:1 ratio with an aqueous solution containing 0.5% (w/v) Cu_2SO_4 and 1% (w/v) sodium tartrate. Subsequently, 1 mL of the resulting mixture was added to 200 μL of the sample solution (diluted 1:20 in Tris buffer) in 50 mM Tris-HCl buffer at pH 7.4. After a 20 min incubation at room temperature, 100 μL of Folin phenol reagent solution (containing 18 mL of the Folin reagent in 90 mL of distilled water) was added to the mixture, followed by thorough vortexing. Following an additional 30 min incubation at room temperature, the absorption was measured

https://doi.org/10.1021/acs.jmedchem.5c00213
J. Med. Chem. 2025, 68, 11279−11298

photometrically at wavelengths of 750 and 500 nm (using a DU 530 spectrophotometer, Beckman Coulter, Krefeld, Germany). Calibration was performed using bovine serum albumin (BSA), serving as a standard reference, with the calibration curve ranging from 0.1 to 0.5 mg BSA/mL.

Binding Assay Development and Optimization. Various incubation buffers including 25 mM Tris-HCl, 50 mM Tris-HCl, and 25 mM *N*-2-hydroxyethylpiperazine-*N*-2-ethanesulfonic acid (HEPES) were tested, along with the addition of different ions (NaCl, $MgCl_2$, and EDTA), all at a physiological blood pH value of 7.4, in an effort to optimize conditions for the high specific binding of [^{3}H]**18**. Additionally, 0.1% Tween 20 and 0.1% bovine serum albumin (BSA) were separately or jointly added to the washing buffer consisting of 50 mM Tris-HCl, aiming to decrease nonspecific filter binding of the radioligand. Optimized conditions were identified, which resulted in low nonspecific binding and avoided depletion of the radioligand. Various competitors, such as **1**, **2**, and **18** at different concentrations, were assessed to determine their effects on nonspecific binding. The following optimized parameters were applied consistently across all experiments (unless specified otherwise): a protein amount of 5 μg per vial and a final concentration of 2 nM of the radioligand [^{3}H]**18** were utilized. Incubation was performed in 50 mM Tris-HCl buffer, pH 7.4, for 1 h at 18 °C (final volume 500 μL). Nonspecific binding was assessed in the presence of 1 μM **10**. Binding assays were conducted in polypropylene test tubes (cat. no. 55.535, Sarstedt, Nümbrecht, Germany). The bound radioligand was separated from the unbound radioligand by filtration through GF/B glass fiber filters using a Brandel cell harvester (model M-48, Brandel, MD, USA). Samples were washed three times with 3 mL each of ice-cold 50 mM Tris-HCl containing 0.1% Tween 20 at pH 7.4. The filters were then punched out and transferred into scintillation vials, where they were incubated with 2.5 mL of scintillation cocktail (ProSafe FC+, Triskem) for 9 h. Radioactivity was subsequently quantified using a Hidex 600 SL automatic TDCR liquid scintillation counter (with a counting efficiency of 53−55%).

Competition Binding Assays. The experiments were conducted in 50 mM Tris-HCl buffer, pH 7.4. The final assay volume of 500 μL consisted of 5 μL of test compound solution (different concentrations prepared by serial dilutions), 100 μL of [^{3}H]**18** in buffer at a final concentration of 2 nM, and 100 μL of CHO-human $P2Y_{12}R$ membrane preparation (5 μg of protein). Nonspecific binding was determined in the presence of 1 μM compound **10**. The incubation was initiated by the addition of the membrane preparation and lasted for 1 h at 18 °C under the above-mentioned conditions. Each experiment was independently repeated three times, each in duplicate. pIC_{50} and pK_i values were computed using equations for one-site homologous or one-site-fit K_i models as provided in GraphPad Prism software version 8.4.2 (GraphPad Software, Inc., San Diego, CA, USA).

Binding Kinetic Studies. Association experiments were performed initially by incubation of 5 μg of protein/vial of CHO-$P2Y_{12}R$ membrane preparations with 2 nM [^{3}H]**18** solution at 25 °C for different periods of time ranging from 1 to 60 min until binding equilibrium was reached. Nonspecific binding was determined in the presence of 5 μL of **18** (final concentration 10 μM) in DMSO. Since the association was too fast to monitor, the association study was repeated at lower temperatures and the mixture was incubated at 18 °C in a water bath upon gentle shaking. The subsequent assay procedure was the same as described above. For data analysis, raw data (in cpm) obtained from kinetic binding experiments were utilized. Nonspecific binding was subtracted, and the data were then normalized to express the percentage of specific binding at time 0 (set as 100%), with 0 cpm corresponding to 0%. The association half-life was determined using the "one phase association" equation, which is implemented in GraphPad Prism version 8.4.2 (GraphPad, San Diego, CA, USA): $Y = Y_{max}{}^* [1 - \exp(-k_{obs} \times X)]$, with $t_{1/2} = \ln(2)/k_{obs}$ (Y, specific binding; Y_{max}, maximum specific binding; X, time (min); k_{obs}, observed association rate).

In dissociation experiments, a mixture of 300 μL of assay buffer, 100 μL of CHO-$P2Y_{12}R$ cell membrane suspension (5 μg), and 100 μL of radioligand solution (2 nM) was preincubated for 60 min at 18 °C to achieve equilibrium. Dissociation was triggered at specified time intervals ranging from 1 to 60 min by adding 5 μL of **18** in DMSO (10 μM). All the remaining procedures and conditions were as described above in the "Binding Assay Development and Optimization" part. Specific binding was computed and normalized following the procedure outlined earlier for association. For the calculation of the dissociation rate (K_{off}) and the dissociation half-life ($t_{1/2}$), the "one phase exponential decay" equation ($Y = (Y_0 - NS) \times \exp(-k_{off} \times X) + NS$), implemented in GraphPad Prism, was employed.

Saturation Binding. Increasing concentrations of [^{3}H]**18** (0.3−80 nM) were incubated with membrane preparations (5 μg of protein) derived from recombinant CHO-$P2Y_{12}R$ cell membranes for 1 h at 25 °C and 18 °C. Nonspecific binding was determined using 10 μM unlabeled ligand **18** in DMSO for all radioligand concentrations. All other conditions and procedures were as described above. Specific binding (in cpm) was determined by subtracting nonspecific binding from total binding. Both total and specific bindings were fitted using GraphPad Prism version 8.4.2 (GraphPad, San Diego, CA) with the equations "one site−total" ($Y = (B_{max} \times X)/(K_D + X) + NS \times X$) and "one site−specific" ($Y = (B_{max} \times X)/(K_D + X)$), respectively. Nonspecific binding was fitted as a linear function.

Assay Validation. In addition to the displacement of the radiotracer by the cold ligand **18**, competitive inhibitors of $P2Y_{12}R$ with diverse scaffolds were tested using the developed method. The determined pK_i values using the new radioligand binding assay were compared with pIC_{50} or pEC_{50} values from the β-arrestin recruitment assay.

*[^{3}H]**18** Specificity and Selectivity.* Membrane preparations from recombinant cell lines expressing human ADP-activated P2Y receptor subtypes ($P2Y_1R$ or $P2Y_{13}R$) were examined for [^{3}H]**18** radioligand binding selectivity using the developed method. Therefore, binding of 2 nM [^{3}H]**18** to protein preparations from 1321N1 astrocytoma-$P2Y_1$ (5 μg) and CHO-$P2Y_{13}$ (5 μg) was determined. In addition, the respective nontransfected cell lines, 1321N1 astrocytoma and CHO (using two different protein amounts, 5 and 100 μg), were investigated. All other conditions and procedures were as described above in the "Binding Assay Development and Optimization" section.

Radioligand Binding to Cells and Tissues Natively Expressing $P2Y_{12}$ Receptors. Homologous competition binding curves were determined in 50 mM Tris-HCl buffer, pH 7.4. The final assay volume of 400 μL contained 4 μL of the test compound (prepared using serial dilutions), 100 μL of [^{3}H]**18** in buffer at a final concentration of 2 nM (for the human platelet and rat brain cortex), and 15 nM (for mouse microglia). A suspension (100 μL) of membrane preparation (100 μg of protein for human platelet membranes, 250 μg of protein for rat brain cortical membranes, and 2 μg of protein for mouse microglial cell membranes) was used to initiate the experiment. Nonspecific binding was determined in the presence of 1 μM **10** for human platelet membranes, 1 μM **18** for rat brain cortex membranes, and 10 μM **10** for mouse microglial membranes. The incubation was initiated by the addition of membrane preparation and lasted for 1 h at 18 °C under the above-mentioned conditions. Each experiment was independently repeated three times, each in duplicate. pIC_{50} and pK_i values were computed using equations for one-site homologous or one-site-fit K_i models as provided in GraphPad Prism software version 8.4.2 (GraphPad Software, Inc., San Diego, CA, USA).

The alignment of $P2Y_{12}R$ protein sequences from human, rat, and mouse species was conducted using Clustal Omega tool, and the results are included in the Supporting Information (Figure S2).

$P2Y_{12}$ Receptor β-Arrestin Recruitment Assays. $P2Y_{12}R$-induced β-arrestin recruitment assays were performed as previously reported.[72−74] CHO-β-arrestin-h$P2Y_{12}R$ cells were cultured in F12 medium (Gibco−Life Technologies) supplemented with 10% FCS, 1% penicillin−streptomycin, hygromycin B (300 μg/mL), and G418 (800 μg/mL). One day before the assay, cells were detached from the flask using dissociation buffer (2 mM EDTA and 10 mM glucose in PBS) and seeded into white 96-well plates (Thermo Scientific, Waltham, MA) at a density of 30,000 cells per well in 90 μL of Optimem medium supplemented with 2% FCS, 100 units/mL penicillin G, 100 μg/mL streptomycin, hygromycin B (300 μg/mL), and G418 (800 μg/mL). Test compounds (prepared as 10 mM stock solutions in dimethyl

https://doi.org/10.1021/acs.jmedchem.5c00213
J. Med. Chem. 2025, 68, 11279−11298

sulfoxide (DMSO)) were diluted in Optimem medium without supplements, and 5 μL of the diluted compounds was added to each well. The final concentration of DMSO was 1%. Following a 60 min incubation at 37 °C, 5 μL of agonist **2** was added at a concentration corresponding to its EC_{80} value, and the mixture was incubated for 90 min at 37 °C. A detection reagent (50 μL per well, DiscoverX, Fremont, CA) was added, and the plate was further incubated for 60 min at room temperature. Luminescence was then measured using a Berthold Tech Mithras plate reader. Three to four independent experiments were conducted, each in duplicate. GraphPad Prism version 8.4.2 (GraphPad, San Diego, CA) was employed for data analysis.

Studies on Rats. Procedures were in accordance with the recommendations of the European Community (council directive 2010/63/EU) and the French National Committee (Decree 2013-118) for the care and use of laboratory animals. The experimental protocols were validated by a local ethics committee for animal use and approved by the French government (nos. APAFIS#38612-2022092015556744 v2 and APAFIS#28255-2020112314343452 v1).

Overexpression of Human $P2Y_{12}$ Receptors in a Rat Model. Two male Sprague−Dawley rats were stereotactically injected in the left striatum (reference to bregma: AP +0.5 mm, L +3 mm, V −4.5 mm) under isoflurane anesthesia with 4 μL of AAV-CAG-h*P2ry12* (5.0×10^9 Vg/μL). One month after surgery, animals were euthanized under anesthesia (Vetergesic, dose: 0.05 mg/kg, ketamine 75 mg/kg + xylazine 5 mg/kg) by exsanguinations with PBS before brain extraction.

Cryosectioning and Autoradiography. Brains were snap-frozen at −40 °C, cut into 20 μm-thick coronal sections with a CM3050S cryostat (CryoStar NX70, Thermo Fisher Diagnostics GmbH, Henningsdorf, Germany), and stored at −80 °C. Prior to autoradiography, brain slices were placed at room temperature for 45 min and hydrated in 100 mM Tris-HCl buffer (pH = 7.4) for 15 min. Pairs of adjacent slices were then incubated for 1 h at room temperature with 2 nM [^{3}H]**18** or with 2 nM [^{3}H]**18** in the presence of 1 μM **4** to evaluate total and nonspecific binding. After incubation, slices were rinsed three times for 5 min in ice-cold Tris-HCl buffer, washed in ice-cold distilled water, and dried for 24 h. A high-performance autoradiography imager (β-imager 2000, Biospace Lab, Paris, France) allowing real-time radioactive imaging through direct β-particle counting and absolute radioactivity quantification (detection threshold of 0.001 cpm/mm^2 for ^{3}H) was used to measure radioactivity in dried tissue sections. A calibration curve was constructed using duplicate standards spotted with known concentrations (from 0.001 to 0.1 nCi in 10 mg) to convert the grayscale intensity of the autoradiography images into activity per mg. Autoradiography images were segmented using PMOD 3.8 software in order to measure total and nonspecific binding, from which specific binding was calculated.

Immunohistochemistry. A third series of adjacent slices was used for immunohistochemistry using an antibody against $hP2Y_{12}R$ to validate $hP2Y_{12}R$ expression in the injected striatum. Slide-mounted tissues were postfixated for 1 h with 4% paraformaldehyde (PFA). Tissues were washed with 0.1 M phosphate-buffered saline (PBS) three times (3 × 10 min) and pretreated for 20 min with 0.3% hydrogen peroxide (1:100; Sigma-Aldrich; 31642-1L-M) to quench endogenous peroxidases. Slides were rinsed three times (3 × 10 min) with PBS and immersed in blocking serum solution (4.5% normal goat serum with 0.2% Triton X-100 in 1× PBS) for 30 min. Slide-mounted tissues were then washed three times and were incubated for 48 h at 4 °C with a primary antibody (1:1000; Anaspec; 55043A) diluted in blocking serum solution (3% normal goat serum with 0.2% Triton X-100 in 1× PBS). After three rinses, slides were incubated for 1 h with a secondary antibody (1:1000; Vector Laboratories; BA1000) diluted in 0.2% Triton X-100 in 1× PBS. To get rid of the excess, slides were rinsed three times and incubated with an avidin−biotin complex (ABC) (1:250 solution A; 1:250 solution B; Vector Laboratories; PK-6100) in 0.2% Triton X-100 in 1× PBS for 1 h. Slides were washed three times in PBS, before visualization by the addition of 3,3′-diaminobenzidine tetrachloride dihydrate (DAB) (Vector Laboratories; SK-4100). Before coverslipping, slide-mounted tissues were consecutively dehydrated in 50% ethanol for 1 min, 70% ethanol for 1 min, 95% ethanol for 1 min twice, 100% ethanol for 1 min twice, and xylene for 3 min twice. The images were taken via an Epson scanner to have a macroscopic look onto the injection site.

*Metabolic Stability. In Vitro Metabolism of the $P2Y_{12}$ Receptor Antagonist **18**.* Rat liver microsomes (RLM), fully characterized for their protein content, P450 concentration, and catalytic activities, were obtained from Corning (France) and stored at −80 °C prior to use. Stock solutions (10 mM) of the $P2Y_{12}R$ antagonist **18** were prepared in DMSO. The incubation mixtures containing 1 mg of microsomal proteins (RLM), an NADPH-generating system (10 mM glucose-6-phosphate, 1.3 mM $NADP^+$, and 2 IU/assay of glucose-6-phosphate dehydrogenase), the $P2Y_{12}R$ antagonist at a final concentration of 100 μM, and 0.1 M aqueous potassium phosphate buffer, pH 7.4 in a final volume of 1 mL, were preincubated for 2 min at 37 °C. The reaction was started by the addition of the NADPH-generating system (200 μL) and conducted in a water bath at 37 °C for 60 min. The reaction was stopped by the addition of an equal volume of acetonitrile (1 mL). The mixtures were centrifuged at 4 °C for 5 min at 10,000*g*. The resulting supernatants were analyzed by LC/MS as described below. In control assays, the mixtures were incubated without the NADPH-generating system or without microsomes to confirm the stability of the ligand under the experimental conditions. The percentage of each metabolite was determined as a percentage of the total peak area (UV detection).

*Identification of Metabolites of **18** by LC-MS.* The main metabolites of the $P2Y_{12}R$ antagonist **18** generated in rat liver microsomes were identified by LC-MS and MS^2 analyses. All incubation mixtures containing liver microsomes were deproteinated with an equal volume of acetonitrile and filtered (Vecta Spin Micro, 0.2 μm, Whatman, France) prior to extract analysis by LC-MS-MS. The main oxidative metabolites generated by P450 oxidation in microsomal incubates were characterized by LC-MS in the positive mode using an Ion Trap LTQ Velos Pro ion mass spectrometer equipped with an electrospray source (Thermo Fisher Scientific, France). An Ultimate 3000 UPLC system interfaced with the LTQ consisted of LC pumps (HPG3400RS series no. 8041829), PDA (DAD3000 series no. 8041519), and an autosampler (WPS3000TRS series no. 8043592). Pressurized nitrogen was used as sheath gas with a flow rate of 25 units (arbitrary units for sheath gas pressure as defined by the manufacturer). The source voltage for electrospray ionization was 4 kV; the source temperature was 250 °C; the capillary voltage was 40 V, and the capillary temperature was 350 °C. The parent ligand and its metabolites were separated on a reverse-phase UPLC Atlantis C18, 1.8 μm, 2.1 × 100 mm column (Waters, France). The mobile phase consisted of (A) water containing 0.05% formic acid and (B) acetonitrile containing 0.05% formic acid. A linear gradient from 20 to 100% of B in 20 min was applied to the column at a flow rate of 300 μL/min. The full-scan MS acquisition mode was set up to detect ions in the range of m/z 50−600. The MS was set up in the MS-MS mode for acquiring, isolating with a mass width of 1−3 amu (Cl), and dissociating the ions m/z = 459 (**18**) and its main metabolites by collision-induced dissociation and in the ion trap using helium as the collision gas with an energy of 35%. Data acquisition and processing were performed with Xcalibur software (version 2.2) with the assistance of Mass Frontier software (version 7.0) for proposed fragmentation mechanisms (Thermo Fisher Scientific, France).

Molecular Docking Studies. The X-ray crystal structure of the human $P2Y_{12}R$ in complex with the cocrystallized ligand **4** (PDB ID 4NTJ)[11] was selected for molecular docking studies using AutoDock4.2. The structure of the $P2Y_{12}R$ was prepared for docking using the Protein Preparation Wizard, and protonation states were assigned using the Protonate 3D tool implemented in Molecular Operating Environment (MOE 2021).[87] AutoDockTools was utilized to assign atomic partial charges and to compute the three-dimensional energy scoring grid for a box of 60 × 60 × 60 points with a grid spacing of 0.375 Å centered based on the cocrystallized ligand **4**.[88] The docking calculations for **18** were performed using the flexible docking approach in AutoDock4.2.[89] Fifty independent docking runs were conducted using the varCPSO-ls algorithm from PSO@Autodock implemented in AutoDock4.2,[89,90] with termination criteria set at 50,000 evaluation steps. The cognitive coefficient (c1) and social coefficient (c2) parameters of the algorithm were set at 6.05, and the swarm size was

https://doi.org/10.1021/acs.jmedchem.5c00213
J. Med. Chem. 2025, 68, 11279−11298

fixed at 60 individual particles. Default values were retained for all other algorithm parameters. The docking poses obtained for **18** were ranked based on their docking scores. The top-ranked pose was selected as the putative binding pose after thorough visual inspection, with emphasis on the predicted interaction network, including hydrogen bonds, hydrophobic interactions, and π-stacking interactions within the $P2Y_{12}R$ binding pocket.

■ ASSOCIATED CONTENT

Supporting Information

The Supporting Information is available free of charge at https://pubs.acs.org/doi/10.1021/acs.jmedchem.5c00213.

$P2Y_{12}$**−18** complex (PDB)

Molecular formula strings and biological data of final compounds (CSV)

List of compounds with SMILES structures (CSV)

General SARs of pyrazolylbenzamidoindoles as $P2Y_{12}$ receptor antagonists (Figure S1); failed attempts to synthesize the key intermediate compound (Scheme S1); affinities of compounds at human $P2Y_{12}$ receptors determined in [^{3}H]**18** radioligand binding as compared to data from β-arrestin recruitment assays (Table S1); sequence alignment of $P2Y_{12}$ receptor orthologs (Figure S2); plasmid for AAV-CAG-h*P2ry12* expression in 293T cells (Figure S3); Western blot of human $P2Y_{12}$ receptors (Figure S4); AAV-CAG-h*P2ry12* expression in the rat brain (Figure S5); EC_{50} values and maximal receptor activation (Schild analysis) (Table S2); identification of **18** and its metabolites (Analytical Data S1); synthesis of the intermediate compounds (page S11); characterization of the [^{3}H]**18** radioligand and all other compounds (Analytical Data S2) (PDF)

■ AUTHOR INFORMATION

Corresponding Author

Christa E. Müller − *PharmaCenter Bonn, Pharmaceutical Institute, Department of Pharmaceutical & Medicinal Chemistry, University of Bonn, Bonn 53121, Germany;* orcid.org/0000-0002-0013-6624; Phone: +49-228-73-2301; Email: christa.mueller@uni-bonn.de; Fax: +49-228-73-2567

Authors

Haneen Al-Hroub − *PharmaCenter Bonn, Pharmaceutical Institute, Department of Pharmaceutical & Medicinal Chemistry, University of Bonn, Bonn 53121, Germany;* orcid.org/0000-0002-2033-0344

Hashem Ali M. Al Musawi − *PharmaCenter Bonn, Pharmaceutical Institute, Department of Pharmaceutical & Medicinal Chemistry, University of Bonn, Bonn 53121, Germany;* orcid.org/0000-0003-0664-4942

Aliaa Abdelrahman − *PharmaCenter Bonn, Pharmaceutical Institute, Department of Pharmaceutical & Medicinal Chemistry, University of Bonn, Bonn 53121, Germany*

Vigneshwaran Namasivayam − *PharmaCenter Bonn, Pharmaceutical Institute, Department of Pharmaceutical & Medicinal Chemistry, University of Bonn, Bonn 53121, Germany;* orcid.org/0000-0003-3031-3377

Margot Corbel − *Laboratoire des Maladies Neurodégénératives, CEA, CNRS, MIRCen, Université Paris-Saclay, Fontenay-aux-Roses 92265, France;* orcid.org/0000-0001-7297-2448

Fanny Petit − *Laboratoire des Maladies Neurodégénératives, CEA, CNRS, MIRCen, Université Paris-Saclay, Fontenay-aux-Roses 92265, France*

Gunes Aksiyote − *Laboratoire des Maladies Neurodégénératives, CEA, CNRS, MIRCen, Université Paris-Saclay, Fontenay-aux-Roses 92265, France*

Fabrice Beau − *Laboratoire des Maladies Neurodégénératives, CEA, CNRS, MIRCen, Université Paris-Saclay, Fontenay-aux-Roses 92265, France*

Caroline Jan − *Laboratoire des Maladies Neurodégénératives, CEA, CNRS, MIRCen, Université Paris-Saclay, Fontenay-aux-Roses 92265, France*

Alexis-Pierre Bemelmans − *Laboratoire des Maladies Neurodégénératives, CEA, CNRS, MIRCen, Université Paris-Saclay, Fontenay-aux-Roses 92265, France;* orcid.org/0000-0001-7605-5225

Nadja Van Camp − *Laboratoire des Maladies Neurodégénératives, CEA, CNRS, MIRCen, Université Paris-Saclay, Fontenay-aux-Roses 92265, France*

Marie-Anne Peyronneau − *Laboratoire d'Imagerie Biomédicale Multimodale (BioMaps), CEA, CNRS, Inserm, Université Paris-Saclay, Orsay 91401, France;* orcid.org/0000-0003-1520-4666

Alexandra Winkeler − *Laboratoire d'Imagerie Biomédicale Multimodale (BioMaps), CEA, CNRS, Inserm, Université Paris-Saclay, Orsay 91401, France;* orcid.org/0000-0003-3397-2570

Complete contact information is available at: https://pubs.acs.org/10.1021/acs.jmedchem.5c00213

Author Contributions

[†]H.A.-H. and H.A.M.A.M. contributed equally. All authors contributed to the study and the manuscript.

Notes

The authors declare no competing financial interest.

■ ACKNOWLEDGMENTS

We thank Marion Schneider and Rasha Abu Shamleh for their assistance with LC-MS and NMR analyses. We also thank Katharina Sylvester and Christiane Bous for laboratory organization, and Christin Vielmuth for managing our in-house compound library. This study was supported by the Deutsche Forschungsgemeinschaft (DFG) and the Agence Nationale de la Recherche (ANR); MU 1665/12-1, project 1291 number 471773752 and ANR-21-CE18-0067-01, project 'PURImaging'. H.A.M.A.M. is grateful for a PhD scholarship from the Saudi Ministry of Education, Saudi Arabia.

■ ABBREVIATIONS

AAV-CAG, adeno-associated viral-cmv enhancer chicken beta actin promoter rabbit beta globin intron; ABC, avidin−biotin complex; AD, Alzheimer's disease; ADP, adenosine 5′-diphosphate; ATP, adenosine 5′-triphosphate; BBB, blood−brain barrier; BSA, bovine serum albumin; cAMP, 3′,5′-cyclic adenosine monophosphate; cDNA, complementary deoxyribonucleic acid; CHO, Chinese hamster ovary; CNS, central nervous system; DAB, diaminobenzidine; DAD, diode array detector; 4-DMAP, 4-dimethylaminopyridine; DMF, dimethylformamide; DMSO, dimethyl sulfoxide; EDC·HCl, 1-ethyl-3-(3′-dimethylaminopropyl)carbodiimide hydrochloride; EDTA, ethylenediaminetetraacetic acid; ESI-MS, electrospray ionization-mass spectrometry; FBS, fetal bovine serum; G6P, glucose-

6-phosphate; G6PDH, glucose-6-phosphate dehydrogenase; GFAP, glial fibrillary acidic protein; GPCR, G protein-coupled receptor; HEPES, *N*-2-hydroxyethylpiperazine-*N*-2-ethanesulfonic acid; HPLC, high-performance liquid chromatography; Iba1, ionized calcium-binding adapter molecule 1; LC-MS, liquid chromatography—mass spectrometry; 2-MeSADP, 2-methylthioadenosine diphosphate; 2-MeSATP, 2-methylthioadenosine triphosphate; mp, melting point; MS, multiple sclerosis; NADP, nicotinamide adenine dinucleotide phosphate; NMR, nuclear magnetic resonance; NSB, nonspecific binding; PBS, phosphate-buffered saline; PD, Parkinson's disease; PET, positron emission tomography; PFA, paraformaldehyde; PSB, Pharmaceutical Sciences Bonn; RT, retention time; SAR, structure—activity relationship; SB, specific binding; TB, total binding; TFAA, trifluoroacetic anhydride; TLC, thin-layer chromatography; UDP, uridine 5′-diphosphate; UTP, uridine 5′-triphosphate

REFERENCES

(1) Wang, L.; Wang, J.; Xu, J.; Qin, W.; Wang, Y.; Luo, S.; Wang, G. The role and molecular mechanism of $P2Y_{12}$ receptors in the pathogenesis of atherosclerotic cardiovascular diseases. *Appl. Sci.* **2021**, *11*, 9078.

(2) von Kügelgen, I. Pharmacological characterization of P2Y receptor subtypes – an update. *Purinergic Signalling* **2024**, *20*, 99–108.

(3) Entsie, P.; Kang, Y.; Amoafo, E. B.; Schöneberg, T.; Liverani, E. The signaling pathway of the ADP receptor $P2Y_{12}$ in the immune system: Recent discoveries and new challenges. *Int. J. Mol. Sci.* **2023**, *24*, 6709.

(4) Baqi, Y.; Müller, C. E. Antithrombotic $P2Y_{12}$ receptor antagonists: recent developments in drug discovery. *Drug Discovery Today* **2019**, *24*, 325–333.

(5) Erb, L.; Weisman, G. A. Coupling of P2Y receptors to G proteins and other signaling pathways. *Wiley Interdiscip. Rev. Membr. Transp. Signal.* **2012**, *1*, 789–803.

(6) Guo, X.; Li, Q.; Pi, S.; Xia, Y.; Mao, L. G protein-coupled purinergic P2Y receptor oligomerization: Pharmacological changes and dynamic regulation. *Biochem. Pharmacol.* **2021**, *192*, No. 114689.

(7) Jacobson, K. A.; Delicado, E. G.; Gachet, C.; Kennedy, C.; von Kügelgen, I.; Li, B.; Miras-Portugal, M. T.; Novak, I.; Schöneberg, T.; Perez-Sen, R.; Thor, D.; Wu, B.; Yang, Z.; Müller, C. E. Update of P2Y receptor pharmacology: IUPHAR review 27. *Br. J. Pharmacol.* **2020**, *177*, 2413–2433.

(8) Sasaki, Y.; Hoshi, M.; Akazawa, C.; Nakamura, Y.; Tsuzuki, H.; Inoue, K.; Kohsaka, S. Selective expression of Gi/o-coupled ATP receptor $P2Y_{12}$ in microglia in rat brain. *Glia* **2003**, *44*, 242–250.

(9) Paoletta, S.; Sabbadin, D.; von Kügelgen, I.; Hinz, S.; Katritch, V.; Hoffmann, K.; Abdelrahman, A.; Straßburger, J.; Baqi, Y.; Zhao, Q.; Stevens, R. C.; Moro, S.; Müller, C. E.; Jacobson, K. A. Modeling ligand recognition at the $P2Y_{12}$ receptor in light of X-ray structural information. *J. Comput.-Aided Mol. Des.* **2015**, *29*, 737–756.

(10) Zhang, J.; Zhang, K.; Gao, Z.-G.; Paoletta, S.; Zhang, D.; Han, G. W.; Li, T.; Ma, L.; Zhang, W.; Müller, C. E.; Yang, H.; Jiang, H.; Cherezov, V.; Katritch, V.; Jacobson, K. A.; Stevens, R. C.; Wu, B.; Zhao, Q. Agonist-bound structure of the human $P2Y_{12}$ receptor. *Nature* **2014**, *509*, 119–122.

(11) Zhang, K.; Zhang, J.; Gao, Z.-G.; Zhang, D.; Zhu, L.; Han, G. W.; Moss, S. M.; Paoletta, S.; Kiselev, E.; Lu, W.; Fenalti, G.; Zhang, W.; Müller, C. E.; Yang, H.; Jiang, H.; Cherezov, V.; Katritch, V.; Jacobson, K. A.; Stevens, R. C.; Wu, B.; Zhao, Q. Structure of the human $P2Y_{12}$ receptor in complex with an antithrombotic drug. *Nature* **2014**, *509*, 115–118.

(12) Savi, P.; Pereillo, J. M.; Uzabiaga, M. F.; Combalbert, J.; Picard, C.; Maffrand, J. P.; Pascal, M.; Herbert, J. M. Identification and biological activity of the active metabolite of clopidogrel. *Thromb. Haemost.* **2000**, *84*, 891–896.

(13) Wallentin, L. $P2Y(_{12})$ inhibitors: differences in properties and mechanisms of action and potential consequences for clinical use. *Eur. Heart J.* **2009**, *30*, 1964–1977.

(14) Baqi, Y.; Atzler, K.; Köse, M.; Glänzel, M.; Müller, C. E. High-affinity, non-nucleotide-derived competitive antagonists of platelet $P2Y_{12}$ receptors. *J. Med.* **2009**, *52*, 3784–3793.

(15) Springthorpe, B.; Bailey, A.; Barton, P.; Birkinshaw, T. N.; Bonnert, R. V.; Brown, R. C.; Chapman, D.; Dixon, J.; Guile, S. D.; Humphries, R. G.; Hunt, S. F.; Ince, F.; Ingall, A. H.; Kirk, I. P.; Leeson, P. D.; Leff, P.; Lewis, R. J.; Martin, B. P.; McGinnity, D. F.; Mortimore, M. P.; Paine, S. W.; Pairaudeau, G.; Patel, A.; Rigby, A. J.; Riley, R. J.; Teobald, B. J.; Tomlinson, W.; Webborn, P. J.; Willis, P. A. From ATP to AZD6140: The discovery of an orally active reversible $P2Y_{12}$ receptor antagonist for the prevention of thrombosis. *Bioorg. Med. Chem. Lett.* **2007**, *17*, 6013–6018.

(16) Jacobson, K. A.; Ivanov, A. A.; de Castro, S.; Harden, T. K.; Ko, H. Development of selective agonists and antagonists of P2Y receptors. *Purinergic Signalling* **2009**, *5*, 75–89.

(17) Kerru, N.; Gummidi, L.; Maddila, S.; Gangu, K. K.; Jonnalagadda, S. B. A Review on recent advances in nitrogen-containing molecules and their biological applications. *Molecules* **2020**, *25*, 1909.

(18) van Giezen, J. J. J.; Nilsson, L.; Berntsson, P.; Wissing, B.-M.; Giordanetto, F.; Tomlinson, W.; Greasley, P. J. Ticagrelor binds to human P2Y(12) independently from ADP but antagonizes ADP-induced receptor signaling and platelet aggregation. *J. Thromb. Haemost.* **2009**, *7*, 1556–1565.

(19) Lin, S.-S.; Tang, Y.; Illes, P.; Verkhratsky, A. The safeguarding microglia: Central role for $P2Y_{12}$ receptors. *Front. Pharmacol.* **2021**, *11*, No. 627760.

(20) Li, F.; Xu, D.; Hou, K.; Gou, X.; Li, Y. The role of $P2Y_{12}$ receptor inhibition in ischemic stroke on microglia, platelets and vascular smooth muscle cells. *J. Thromb. Thrombolysis* **2020**, *50*, 874–885.

(21) Warlo, E. M. K.; Arnesen, H.; Seljeflot, I. A brief review on resistance to $P2Y_{12}$ receptor antagonism in coronary artery disease. *Thromb. J.* **2019**, *17*, 11.

(22) Li, X.; Zhang, G.; Cao, X. The function and regulation of platelet $P2Y_{12}$ receptor. *Cardiovasc. Drugs Ther.* **2023**, *37*, 199–216.

(23) Cattaneo, M. The platelet $P2Y_{12}$ receptor for adenosine diphosphate: Congenital and drug-induced defects. *Blood* **2011**, *117*, 2102–2112.

(24) Aradi, D.; Kirtane, A.; Bonello, L.; Gurbel, P. A.; Tantry, U. S.; Huber, K.; Freynhofer, M. K.; ten Berg, J.; Janssen, P.; Angiolillo, D. J.; Siller-Matula, J. M.; Marcucci, R.; Patti, G.; Mangiacapra, F.; Valgimigli, M.; Morel, O.; Palmerini, T.; Price, M. J.; Cuisset, T.; Kastrati, A.; Stone, G. W.; Sibbing, D. Bleeding and stent thrombosis on $P2Y_{12}$-inhibitors: collaborative analysis on the role of platelet reactivity for risk stratification after percutaneous coronary intervention. *Eur. Heart J.* **2015**, *36*, 1762–1771.

(25) Gómez Morillas, A.; Besson, V. C.; Lerouet, D. Microglia and neuroinflammation: What place for $P2RY_{12}$? *Int. J. Mol. Sci.* **2021**, *22*, 1636.

(26) Bachiller, S.; Jiménez-Ferrer, I.; Paulus, A.; Yang, Y.; Swanberg, M.; Deierborg, T.; Boza-Serrano, A. Microglia in neurological diseases: A road map to brain-disease dependent-inflammatory response. *Front. Cell. Neurosci.* **2018**, *12*, 488.

(27) von Bernhardi, R.; Eugenín-von Bernhardi, J.; Flores, B.; Eugenín León, J. Glial cells and integrity of the nervous system. In *Glial cells in health and disease of the CNS*; von Bernhardi, R., Ed.; Springer International Publishing: Cham, pp 1–24.

(28) Qin, J.; Ma, Z.; Chen, X.; Shu, S. Microglia activation in central nervous system disorders: A review of recent mechanistic investigations and development efforts. *Front. Neurol.* **2023**, *14*, No. 1103416.

(29) Illes, P.; Rubini, P.; Ulrich, H.; Zhao, Y.; Tang, Y. Regulation of microglial functions by purinergic mechanisms in the healthy and diseased CNS. *Cells* **2020**, *9*, 1108.

(30) Kitaoka, S. Microglia regulate neuronal and behavioural functions under physiological and pathological conditions. *J. Biochem* **2023**, *173*, 153–157.

https://doi.org/10.1021/acs.jmedchem.5c00213
J. Med. Chem. 2025, 68, 11279–11298

(31) Soares, N. L.; Vieira, H. L. A. Microglia at the centre of brain research: Accomplishments and challenges for the future. *Neurochem. Res.* **2022**, *47*, 218−233.
(32) Wake, H.; Moorhouse, A. J.; Nabekura, J. Functions of microglia in the central nervous system − beyond the immune response. *Neuron Glia Biol.* **2011**, *7*, 47−53.
(33) Eggen, B. J. L.; Raj, D.; Hanisch, U.-K.; Boddeke, H. W. G. M. Microglial phenotype and adaptation. *J. Neuroimmune Pharmacol.* **2013**, *8*, 807−823.
(34) Gao, C.; Jiang, J.; Tan, Y.; Chen, S. Microglia in neurodegenerative diseases: mechanism and potential therapeutic targets. *Signal Transduction Targeted Ther.* **2023**, *8*, 359.
(35) Vidal-Itriago, A.; Radford, R. A. W.; Aramideh, J. A.; Maurel, C.; Scherer, N. M.; Don, E. K.; Lee, A.; Chung, R. S.; Graeber, M. B.; Morsch, M. Microglia morphophysiological diversity and its implications for the CNS. *Front. Immunol.* **2022**, *13*, No. 997786.
(36) Woodburn, S. C.; Bollinger, J. L.; Wohleb, E. S. The semantics of microglia activation: Neuroinflammation, homeostasis, and stress. *J. Neuroinflammation* **2021**, *18*, 258.
(37) Guo, S.; Wang, H.; Yin, Y. Microglia polarization from M1 to M2 in neurodegenerative diseases. *Front. Aging Neurosci.* **2022**, *14*, No. 815347.
(38) Darwish, S. F.; Elbadry, A. M. M.; Elbokhomy, A. S.; Salama, G. A.; Salama, R. M. The dual face of microglia (M1/M2) as a potential target in the protective effect of nutraceuticals against neurodegenerative diseases. *Front. Aging* **2023**, *4*, No. 1231706.
(39) Dey, R.; Bishayi, B. Microglial inflammatory responses to SARS-CoV-2 infection: A comprehensive review. *Cell. Mol. Neurobiol.* **2024**, *44*, 2.
(40) Singh, D. Astrocytic and microglial cells as the modulators of neuroinflammation in Alzheimer's disease. *J. Neuroinflammation* **2022**, *19*, 206.
(41) Tahmasebi, F.; Barati, S. The role of microglial depletion approaches in pathological condition of CNS. *Cell. Mol. Neurobiol.* **2023**, *43*, 2459−2471.
(42) Wu, Z.; Tang, W.; Ibrahim, F. E. E. M.; Chen, X.; Yan, H.; Tao, C.; Wang, Z.; Guo, Y.; Fu, Y.; Wang, Q.; Ge, Y. Aβ induces neuroinflammation and microglial M1 polarization via cGAS-STING-IFITM3 signaling pathway in BV-2 Cells. *Neurochem. Res.* **2023**, *48*, 2881−2894.
(43) Kobayashi, K.; Yamanaka, H.; Fukuoka, T.; Dai, Y.; Obata, K.; Noguchi, K. $P2Y_{12}$ receptor upregulation in activated microglia is a gateway of p38 signaling and neuropathic pain. *J. Neurosci.* **2008**, *28*, 2892.
(44) Chen, X.; Wang, Q.; Yang, J.; Zhang, L.; Liu, T.-T.; Liu, J.; Deng, B.-L.; Liu, J. Diagnostic and therapeutic value of $P2Y_{12}R$ in epilepsy. *Front. Pharmacol.* **2023**, *14*, No. 1179028.
(45) Ferro, A.; Auguste, Y. S. S.; Cheadle, L. Microglia, cytokines, and neural activity: Unexpected interactions in brain development and function. *Front. Immunol.* **2021**, *12*, No. 703527.
(46) Kenkhuis, B.; Somarakis, A.; Kleindouwel, L. R. T.; van Roon-Mom, W. M. C.; Höllt, T.; van der Weerd, L. Co-expression patterns of microglia markers Iba1, TMEM119 and $P2RY_{12}$ in Alzheimer's disease. *Neurobiol. Dis.* **2022**, *167*, No. 105684.
(47) Maeda, J.; Minamihisamatsu, T.; Shimojo, M.; Zhou, X.; Ono, M.; Matsuba, Y.; Ji, B.; Ishii, H.; Ogawa, M.; Akatsu, H.; Kaneda, D.; Hashizume, Y.; Robinson, J. L.; Lee, V. M.-Y.; Saito, T.; Saido, T. C.; Trojanowski, J. Q.; Zhang, M.-R.; Suhara, T.; Higuchi, M.; Sahara, N. Distinct microglial response against Alzheimer's amyloid and tau pathologies characterized by $P2Y_{12}$ receptor. *Brain Commun.* **2021**, *3*, No. fcab011.
(48) Beaino, W.; Janssen, B.; Kooij, G.; van der Pol, S. M. A.; van Het Hof, B.; van Horssen, J.; Windhorst, A. D.; de Vries, H. E. Purinergic receptors $P2Y_{12}R$ and P2X7R: potential targets for PET imaging of microglia phenotypes in multiple sclerosis. *J. Neuroinflammation* **2017**, *14*, 259.
(49) Keren-Shaul, H.; Spinrad, A.; Weiner, A.; Matcovitch-Natan, O.; Dvir-Szternfeld, R.; Ulland, T. K.; David, E.; Baruch, K.; Lara-Astaiso, D.; Toth, B.; Itzkovitz, S.; Colonna, M.; Schwartz, M.; Amit, I. A unique microglia type associated with restricting development of Alzheimer's disease. *Cell* **2017**, *169*, 1276−1290.
(50) Zrzavy, T.; Hametner, S.; Wimmer, I.; Butovsky, O.; Weiner, H. L.; Lassmann, H. Loss of 'homeostatic' microglia and patterns of their activation in active multiple sclerosis. *Brain* **2017**, *140*, 1900−1913.
(51) Sanchez-Mejias, E.; Navarro, V.; Jimenez, S.; Sanchez-Mico, M.; Sanchez-Varo, R.; Nuñez-Diaz, C.; Trujillo-Estrada, L.; Davila, J. C.; Vizuete, M.; Gutierrez, A.; Vitorica, J. Soluble phospho-tau from Alzheimer's disease hippocampus drives microglial degeneration. *Acta Neuropathol.* **2016**, *132*, 897−916.
(52) Luo, E. Y.; Sugimura, R. R. Taming microglia: the promise of engineered microglia in treating neurological diseases. *J. Neuroinflammation* **2024**, *21*, 19.
(53) Zhang, L.; Wang, Y.; Liu, T.; Mao, Y.; Peng, B. Novel microglia-based therapeutic approaches to neurodegenerative disorders. *Neurosci. Bull.* **2023**, *39*, 491−502.
(54) Kwon, M.-S. Advanced therapeutic strategies targeting microglia: beyond neuroinflammation. *Arch. Pharmacal. Res.* **2022**, *45*, 618−630.
(55) Peng, J.; Liu, Y.; Umpierre, A. D.; Xie, M.; Tian, D. S.; Richardson, J. R.; Wu, L. J. Microglial $P2Y_{12}$ receptor regulates ventral hippocampal CA1 neuronal excitability and innate fear in mice. *Mol. Brain* **2019**, *12*, 71.
(56) Abourbeh, G.; Thézé, B.; Maroy, R.; Dubois, A.; Brulon, V.; Fontyn, Y.; Dollé, F.; Tavitian, B.; Boisgard, R. Imaging microglial/macrophage activation in spinal cords of experimental autoimmune encephalomyelitis rats by positron emission tomography using the mitochondrial 18 kDa translocator protein radioligand [^{18}F]DPA-714. *J. Neurosci.* **2012**, *32*, 5728.
(57) Hamelin, L.; Lagarde, J.; Dorothée, G.; Leroy, C.; Labit, M.; Comley, R. A.; de Souza, L. C.; Corne, H.; Dauphinot, L.; Bertoux, M.; Dubois, B.; Gervais, P.; Colliot, O.; Potier, M. C.; Bottlaender, M.; Sarazin, M. Early and protective microglial activation in Alzheimer's disease: A prospective study using ^{18}F-DPA-714 PET imaging. *Brain* **2016**, *139*, 1252−1264.
(58) Hamelin, L.; Lagarde, J.; Dorothée, G.; Potier, M. C.; Corlier, F.; Kuhnast, B.; Caillé, F.; Dubois, B.; Fillon, L.; Chupin, M.; Bottlaender, M.; Sarazin, M. Distinct dynamic profiles of microglial activation are associated with progression of Alzheimer's disease. *Brain* **2018**, *141*, 1855−1870.
(59) Mildner, A.; Huang, H.; Radke, J.; Stenzel, W.; Priller, J. $P2Y_{12}$ receptor is expressed on human microglia under physiological conditions throughout development and is sensitive to neuroinflammatory diseases. *Glia* **2017**, *65*, 375−387.
(60) Nguyen, D.-L.; Wimberley, C.; Truillet, C.; Jego, B.; Caillé, F.; Pottier, G.; Boisgard, R.; Buvat, I.; Bouilleret, V. Longitudinal positron emission tomography imaging of glial cell activation in a mouse model of mesial temporal lobe epilepsy: Toward identification of optimal treatment windows. *Epilepsia* **2018**, *59*, 1234−1244.
(61) Pike, V. W. PET radiotracers: crossing the blood−brain barrier and surviving metabolism. *Trends Pharmacol. Sci.* **2009**, *30*, 431−440.
(62) Uff, C. E. G.; Patel, K.; Yeung, C.; Yip, P. K. Advances in visualizing microglial cells in human central nervous system tissue. *Biomolecules* **2022**, *12*, 603.
(63) van der Wildt, B.; Janssen, B.; Pekošak, A.; Stéen, E. J. L.; Schuit, R. C.; Kooijman, E. J. M.; Beaino, W.; Vugts, D. J.; Windhorst, A. D. Novel thienopyrimidine-based PET tracers for $P2Y_{12}$ receptor imaging in the brain. *ACS Chem. Neurosci.* **2021**, *12*, 4465−4474.
(64) Jackson, I. M.; Buccino, P. J.; Azevedo, E. C.; Carlson, M. L.; Luo, A. S. Z.; Deal, E. M.; Kalita, M.; Reyes, S. T.; Shao, X.; Beinat, C.; Nagy, S. C.; Chaney, A. M.; Anders, D. A.; Scott, P. J. H.; Smith, M.; Shen, B.; James, M. L. Radiosynthesis and initial preclinical evaluation of [^{11}C]AZD1283 as a potential $P2Y_{12}R$ PET radiotracer. *Nucl. Med. Biol.* **2022**, *114*−*115*, 143−150.
(65) Steen, E. J. L.; Tousiaki, E.-N.; Kingston, L.; van der Wildt, B.; Lenart, N.; Beaino, W.; Verlaan, M.; Zarzycka, B.; Zinnhardt, B.; Denes, A.; Gobbi, L.; de Esch, I. J.P.; Elmore, C. S.; Windhorst, A. D.; Honer, M.; Leurs, R. Characterization of [^{3}H]AZ12464237 as a high affinity, non-nucleotide antagonist radioligand for the $P2Y_{12}$ receptor. *bioRxiv* **2025**.237116900

https://doi.org/10.1021/acs.jmedchem.5c00213
J. Med. Chem. 2025, 68, 11279−11298

(66) Villa, A.; Klein, B.; Janssen, B.; Pedragosa, J.; Pepe, G.; Zinnhardt, B.; Vugts, D. J.; Gelosa, P.; Sironi, L.; Beaino, W.; Damont, A.; Dollé, F.; Jego, B.; Winkeler, A.; Ory, D.; Solin, O.; Vercouillie, J.; Funke, U.; Laner-Plamberger, S.; Blomster, L. V.; Christophersen, P.; Vegeto, E.; Aigner, L.; Jacobs, A.; Planas, A. M.; Maggi, A.; Windhorst, A. D. Identification of new molecular targets for PET imaging of the microglial anti-inflammatory activation state. *Theranostics* **2018**, *8*, 5400−5418.
(67) Edelmann, M. R.; Erny, J.; Guba, W.; Hierl, M. Tritium labeling of neuromedin S by conjugation with [^{3}H]*N*-succinimidyl propionate. *ACS Omega* **2023**, *8*, 2367−2376.
(68) Ohlmann, P.; Lecchi, A.; El-Tayeb, A.; Müller, C. E.; Cattaneo, M.; Gachet, C. The platelet $P2Y_{12}$ receptor under normal and pathological conditions. Assessment with the radiolabeled selective antagonist [^{3}H]PSB-0413. *Purinergic Signal.* **2013**, *9*, 59−66.
(69) Shonberg, J.; Kling, R. C.; Gmeiner, P.; Löber, S. GPCR crystal structures: Medicinal chemistry in the pocket. *Bioorg. Med. Chem. Lett.* **2015**, *23*, 3880−3906.
(70) Badorc, A.; Boldron, C.; Delesque, N.; Fossey, V.; Lassalle, G.; Yvon, X. Derivatives of *N*-[(1*H*-Pyrazol-1-yl) aryl]-1*H*-indole or 1*H*-indazole-3-carboxamide their preparation and their use as $P2Y_{12}$ antagonists. France patent WO 2012/146318A l, 2012.
(71) Boldron, C.; Besse, A.; Bordes, M.-F.; Tissandié, S.; Yvon, X.; Gau, B.; Badorc, A.; Rousseaux, T.; Barré, G.; Meneyrol, J.; Zech, G.; Nazare, M.; Fossey, V.; Pflieger, A.-M.; Bonnet-Lignon, S.; Millet, L.; Briot, C.; Dol, F.; Hérault, J.-P.; Savi, P.; Lassalle, G.; Delesque, N.; Herbert, J.-M.; Bono, F. *N*-[6-(4-Butanoyl-5-methyl-1*H*-pyrazol-1-yl)pyridazin-3-yl]-5-chloro-1-[2-(4-methylpiperazin-1-yl)-2-oxoethyl]-1*H*-indole-3-carboxamide (SAR216471), a novel intravenous and oral, reversible, and directly acting $P2Y_{12}$ antagonist. *J. Med. Chem.* **2014**, *57*, 7293−7316.
(72) Schmies, C. C.; Rolshoven, G.; Idris, R. M.; Losenkova, K.; Renn, C.; Schäkel, L.; Al-Hroub, H.; Wang, Y.; Garofano, F.; Schmidt-Wolf, I. G. H.; Zimmermann, H.; Yegutkin, G. G.; Müller, C. E. Fluorescent probes for ecto-5′-nucleotidase (CD73). *ACS Med. Chem. Lett.* **2020**, *11*, 2253−2260.
(73) Bhattarai, S.; Pippel, J.; Meyer, A.; Freundlieb, M.; Schmies, C.; Abdelrahman, A.; Fiene, A.; Lee, S.-Y.; Zimmermann, H.; El-Tayeb, A.; Yegutkin, G. G.; Sträter, N.; Müller, C. E. X-Ray Co-Crystal Structure Guides the Way to Subnanomolar Competitive Ecto-5′-Nucleotidase (CD73) Inhibitors for Cancer Immunotherapy. *Advanced Therapeutics* **2019**, *2*, 1900075.
(74) Bhattarai, S.; Freundlieb, M.; Pippel, J.; Meyer, A.; Abdelrahman, A.; Fiene, A.; Lee, S.-Y.; Zimmermann, H.; Yegutkin, G. G.; Sträter, N.; El-Tayeb, A.; Müller, C. E. α,β-Methylene-ADP (AOPCP) derivatives and analogues: Development of potent and selective *ecto*-5′-nucleotidase (CD73) inhibitors. *J. Med. Chem.* **2015**, *58*, 6248−6263.
(75) Burnstock, G. Blood cells: an historical account of the roles of purinergic signalling. *Purinergic Signal.* **2015**, *11*, 411−434.
(76) Hollopeter, G.; Jantzen, H.-M.; Vincent, D.; Li, G.; England, L.; Ramakrishnan, V.; Yang, R.-B.; Nurden, P.; Nurden, A.; Julius, D.; Conley, P. B. Identification of the platelet ADP receptor targeted by antithrombotic drugs. *Nature* **2001**, *409*, 202−207.
(77) Delesque-Touchard, N.; Pflieger, A. M.; Bonnet-Lignon, S.; Millet, L.; Salel, V.; Boldron, C.; Lassalle, G.; Herbert, J. M.; Savi, P.; Bono, F. SAR216471, an alternative to the use of currently available $P2Y_{12}$ receptor inhibitors? *Thromb. Res.* **2014**, *134*, 693−703.
(78) Lou, N.; Takano, T.; Pei, Y.; Xavier, A. L.; Goldman, S. A.; Nedergaard, M. Purinergic receptor $P2RY_{12}$-dependent microglial closure of the injured blood−brain barrier. *Proc. Natl. Acad. Sci. U. S. A.* **2016**, *113*, 1074−1079.
(79) Zhong, X.; Kriz, R.; Seehra, J.; Kumar, R. N-linked glycosylation of platelet $P2Y_{12}$ ADP receptor is essential for signal transduction but not for ligand binding or cell surface expression. *FEBS Lett.* **2004**, *562*, 111−117.
(80) Kantor, B.; Bailey, R. M.; Wimberly, K.; Kalburgi, S. N.; Gray, S. J. Methods for gene transfer to the central nervous system. *Adv. Genet.* **2014**, *87*, 125−197.
(81) Janssen, B.; Vugts, D. J.; Wilkinson, S. M.; Ory, D.; Chalon, S.; Hoozemans, J. J. M.; Schuit, R. C.; Beaino, W.; Kooijman, E. J. M.; van den Hoek, J.; Chishty, M.; Doméné, A.; Van der Perren, A.; Villa, A.; Maggi, A.; Molenaar, G. T.; Funke, U.; Shevchenko, R. V.; Baekelandt, V.; Bormans, G.; Lammertsma, A. A.; Kassiou, M.; Windhorst, A. D. Identification of the allosteric P2X7 receptor antagonist [^{11}C]SMW139 as a PET tracer of microglial activation. *Sci. Rep.* **2018**, *8*, 6580.
(82) Savi, P.; Zachayus, J.-L.; Delesque-Touchard, N.; Labouret, C.; Hervé, C.; Uzabiaga, M.-F.; Pereillo, J.-M.; Culouscou, J.-M.; Bono, F.; Ferrara, P.; Herbert, J.-M. The active metabolite of clopidogrel disrupts $P2Y_{12}$ receptor oligomers and partitions them out of lipid rafts. *Proc. Natl. Acad. Sci. U. S. A.* **2006**, *103*, 11069−11074.
(83) Bach, P.; Antonsson, T.; Bylund, R.; Björkman, J.-A.; Österlund, K.; Giordanetto, F.; van Giezen, J. J. J.; Andersen, S. M.; Zachrisson, H.; Zetterberg, F. Lead optimization of ethyl 6-aminonicotinate acyl sulfonamides as antagonists of the $P2Y_{12}$ receptor. separation of the antithrombotic effect and bleeding for candidate drug AZD1283. *J. Med. Chem.* **2013**, *56*, 7015−7024.
(84) Attah, I. Y.; Neumann, A.; Al-Hroub, H.; Rafehi, M.; Baqi, Y.; Namasivayam, V.; Müller, C. E. Ligand binding and activation of UTP-activated G protein-coupled $P2Y_2$ and $P2Y_4$ receptors elucidated by mutagenesis, pharmacological and computational studies. *Biochim. Biophys. Acta Gen. Subj.* **2020**, *1864*, No. 129501.
(85) Neumann, A.; Attah, I.; Al-Hroub, H.; Namasivayam, V.; Müller, C. E. Discovery of $P2Y_2$ receptor antagonist scaffolds through virtual high-throughput screening. *J. Chem. Inf. Model.* **2022**, *62*, 1538−1549.
(86) Lowry, O. H.; Rosebrough, N. J.; Farr, A. L.; Randall, R. J. Protein measurement with the folin phenol reagent. *J. Biol. Chem.* **1951**, *193*, 265−275.
(87) Sherbrooke St., W. *Molecular operating environment (MOE)*; CCGU: Montreal, 2021.
(88) Sanner, M. F. Python: A programming language for software integration and development. *J. Mol. Graph. Model.* **1999**, *17*, 57−61.
(89) Morris, G. M.; Huey, R.; Lindstrom, W.; Sanner, M. F.; Belew, R. K.; Goodsell, D. S.; Olson, A. J. AutoDock4 and AutoDockTools4: Automated docking with selective receptor flexibility. *J. Comput. Chem.* **2009**, *30*, 2785−2791.
(90) Namasivayam, V.; Günther, R. Pso@autodock: A fast flexible molecular docking program based on Swarm intelligence. *Chem. Biol. Drug Des.* **2007**, *70*, 475−484.

https://doi.org/10.1021/acs.jmedchem.5c00213
J. Med. Chem. 2025, 68, 11279−11298

Supplementary Information

Selective, Non-nucleotidic Radiotracer for $P2Y_{12}$ Receptors: Design, Synthesis, Characterization, and Imaging of Brain Slices

Haneen Al-Hroub,[1‡] Hashem Ali M Al Musawi,[1‡] Aliaa Abdelrahman,[1] Vigneshwaran Namasivayam,[1] Margot Corbel,[2] Fanny Petit,[2] Gunes Aksyote,[2] Fabrice Beau,[2] Caroline Jan,[2] Alexis-Pierre Bemelmans,[2] Nadja Van Camp,[2] Marie-Anne Peyronneau,[2] Alexandra Winkeler[3] and Christa E. Müller[1*]

[1]PharmaCenter Bonn, Pharmaceutical Institute, Department of Pharmaceutical & Medicinal Chemistry, University of Bonn, An der Immenburg 4, 53121 Bonn, Germany

[2]Laboratoire des Maladies Neurodégénératives, CEA, CNRS, MIRCen, Université Paris-Saclay, 92265 Fontenay-aux-Roses, France

[3]Laboratoire d'Imagerie Biomédicale Multimodale (BioMaps), CEA, CNRS, Inserm, Université Paris-Saclay, Orsay, France

[‡]These authors contributed equally

***Corresponding Author**

Prof. Dr. Christa E. Müller

PharmaCenter Bonn

Pharmaceutical Institute

Pharmaceutical & Medicinal Chemistry

University of Bonn

An der Immenburg 4, 53121 Bonn, Germany

Phone: +49-228-73-2301

Fax: +49-228-73-2567

E-mail: christa.mueller@uni-bonn.de

Table of Contents

Scheme S1: Failed attempts to synthesize the key-intermediate **46** S3

Table S1: Affinities of compounds at human $P2Y_{12}$ receptors determined in [^{3}H]**18** radioligand binding as compared to the data from β-arrestin recruitment assays S4

Figure S1: Sequence alignment of $P2Y_{12}$ receptor orthologs. S5

Figure S2: Plasmid for AAV-CAG-h*P2ry12* expression in 293T cells S6

Figure S3: Western blot of human $P2Y_{12}$ receptors S7

Figure S4: AAV-CAG-h*P2ry12* expression in rat brain S8

Table S2: EC_{50} values and maximal receptor activation (Schild analysis) S9

Analytical data S1: Identification of **18** and its metabolites. S10

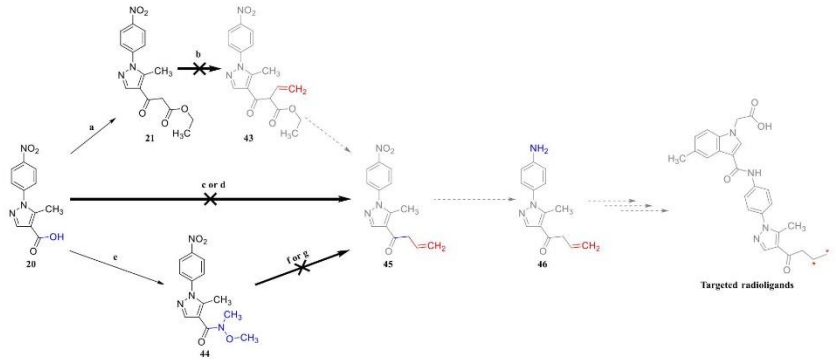
Synthesis of the intermediates S11

Analytical data S2: For [^{3}H]**18** radioligand and all compounds S19

References S77

Failed attempts to synthesize the key-intermediate 46

Different pathways were undertaken to prepare the key-intermediate **46** needed for the radioligand precursor. Unfortunately, none of these trials yielded the desired compound. The initial strategy involved treatment of **21** with vinyl iodide instead of ethyl iodide to produce the analog of **22** (**43**), which would serve as a precursor for **46**. Compound **20** was reacted with thionyl chloride ($SOCl_2$) under reflux overnight to obtain the acid chloride, which was subsequently utilized in two different reactions either with the commercially available Grignard reagent allylmagnesium chloride in diethyl ether (Et_2O) or with allyltrimethylsilane in the presence of aluminum trichloride ($AlCl_3$) as a Lewis acid in dichloromethane. Both reactions failed to produce the desired **45**, which would have subsequently been reduced using tin chloride to form **46**. Synthesis of the Weinreb amide **44** using *N*,*O*-dimethylhydroxylamine hydrochloride in the presence of pyridine as a base over 15 h was successful. Compound **44** was utilized in two Grignard reactions to achieve CC-bond formation. However, neither reaction resulted in the formation of the targeted **45** needed to produce **46**. These unsuccessful attempts prohibited the synthesis of a desired $P2Y_{12}R$ antagonist radioligand containing tritium atoms in the butanone residue.



Scheme S1: Synthesis of the radioligand key-intermediate **46** (failed attempts). **a** carbonyldiimidazole (CDI), THF, 25 °C, 16 h; anhydrous $MgCl_2$, ethyl potassium malonate, 55 °C, 6 h (91%); **b** NaH, THF, 0 °C, 30 min; CH_2CHI, 25 °C, 24 h; **c** 1.1. $SOCl_2$, 80 °C, 6 h; 1.2. CH_2CHCH_2MgCl, Et_2O, -78 to 25 °C, 4 h; aq. NH_4Cl; **d** 1.1. $SOCl_2$, 80 °C, 6 h; 1.2. $(CH_3)_3SiCH_2CHCH_2$, $AlCl_3$, CH_2Cl_2, 25 °C, 4 h; **e** 1.1. $SOCl_2$, 80 °C, 6 h; 1.2. $CH_3NHOCH_3 \cdot HCl$, NEt_3, CH_2Cl_2, 0 °C; 25 °C,15 h; **f** 1.1. CH_2CHCH_2MgCl, THF, -50 °C,30

min; 25 °C,24 h; 1.2. -30 °C, H_2O; **g** NaH, THF, -78 °C, 10 min; CH_2CHCH_2MgCl,-78 to 25 °C, 4 h; aq.NH_4Cl).

Table S1: Affinities of compounds at the human $P2Y_{12}R$ determined in [^{3}H]**18** radioligand binding as compared to data from β-arrestin recruitment assays.

Compound	**Human $P2Y_{12}$ receptor membrane preparation [^{3}H]18 binding assay K_i ± SEM (µM)** [a]	**Human $P2Y_{12}$ receptor β-arrestin assay IC_{50} [b] or EC_{50} ± SEM (µM)** [a]
PSB-22219	**0.00522** ± 0.00047	**0.0603** ± 0.0089
PSB-0739	**0.00431**± 0.00066	**0.0613** ± 0.0196
Cangrelor	**0.00137** ± 0.00022	**0.0195** ± 0.0029
AZD1283	**0.00376** ± 0.00118	**0.0810** ± 0.0047
Ticagrelor	**0.00779** ± 0.00049	**0.0214** ± 0.0029
PSB-0702	**0.0146** ± 0.0017	**1.21** ± 0.03
2-MeSADP	**0.00383** ± 0.00033	EC_{50} = **0.00546** ± 0.00979
ADP	**4.87** ± 0.95	EC_{50} = **0.509** ± 0. 109

[a] Data represent mean ± SEM of 3-4 independent experiments each in duplicates. [b] IC_{50} vs an EC_{80} concentration of the standard agonist 2-MeSADP (25 nM)

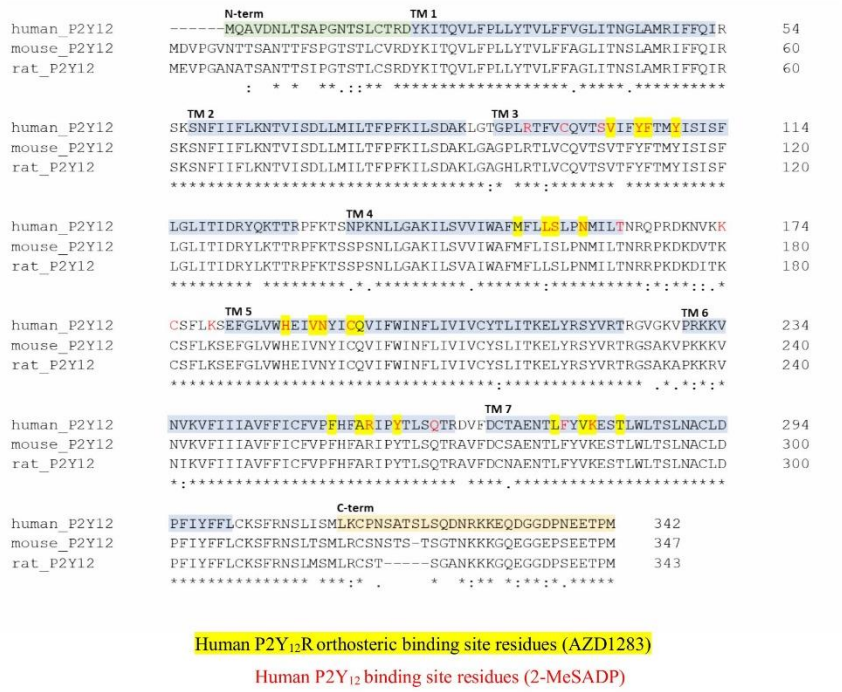


Figure S1: Sequence alignment of $P2Y_{12}$ receptor orthologs. $P2Y_{12}R$ protein sequences were exported from the Uniprot data base and aligned via the Clustal Omega tool. Percent of sequence identity: human-rat (86.4%), human-mouse (86.8%), rat-mouse (94.8%). The amino acid residues of the binding site are identical in all three species. Amino acid residues of the human $P2Y_{12}R$ binding site are highlighted in yellow (with the antagonist AZD1283), and colored in red (with the agonist 2-MeSADP), respectively. *Abbreviations*: N-term, N-terminus; TM, transmembrane; C-term, C-terminus

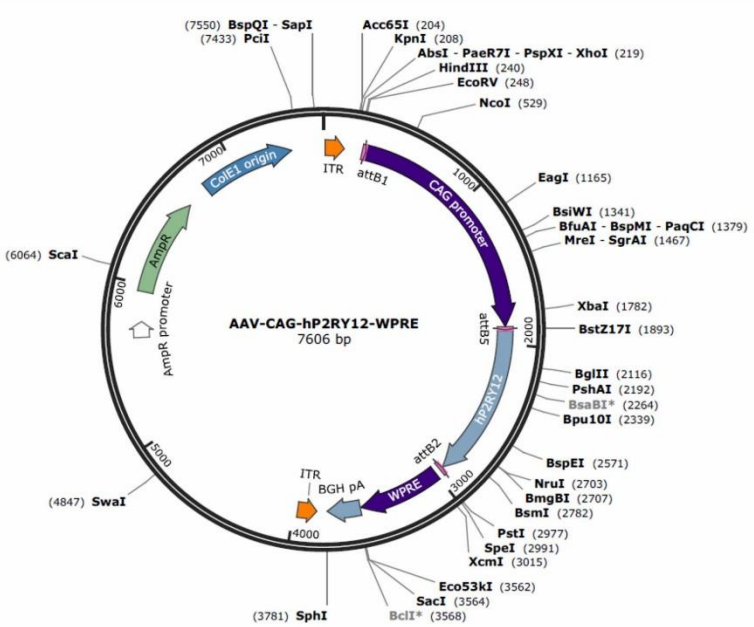


Figure S2: Plasmid for AAV-CAG-h*P2ry12* expression in 293T cells. The human *P2ry12* cDNA was placed under the transcriptional control of the ubiquitous CAG promoter and the woodchuck port-transcriptional regulatory element (WPRE) was added in the expression cassette to enhance transgene expression. *Abbreviations*: AAV, adeno-associated virus; pA, bovine growth hormone polyadenylation sequence.

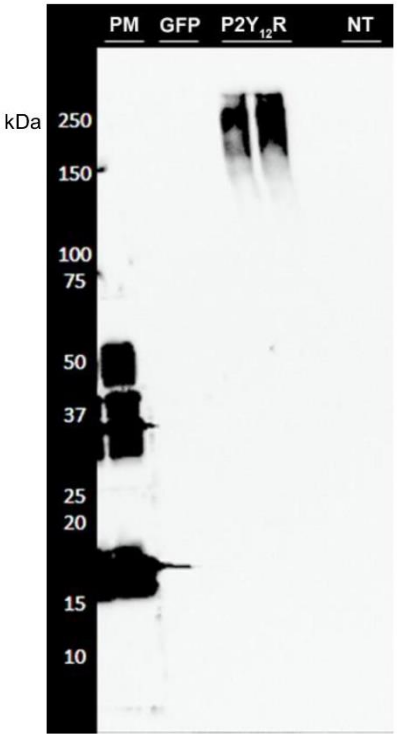


Figure S3: Western blot of hP2Y$_{12}$R. Functionality of the hP2Y$_{12}$R expression cassette was assessed by transient transfection in 293T cells with 5 ug of AAV-CAG-h*P2ry12* plasmid. Negative controls included GFP and non-transfected cells. Cells were harvested 48 h post-transfection and lyzed for Western blot analysis (Anaspec anti-P2Y$_{12}$R antibody diluted 1:500). In accordance with Savi et al. PNAS 2006,[1] a band was observed at 250 kDa, corresponding to the tetrameric hP2Y$_{12}$R. *Abbreviations*: PM, protein marker; GFP, cells transfected with a green fluorescent protein (GFP) plasmid; NT, non-transfected cells.

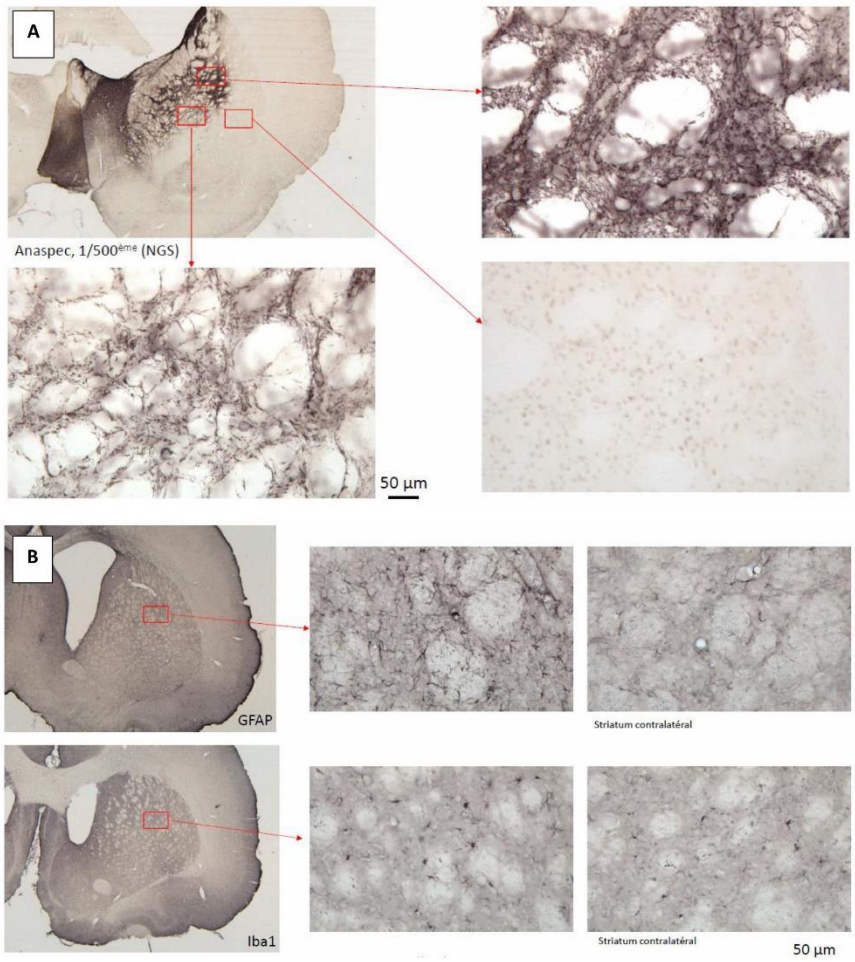


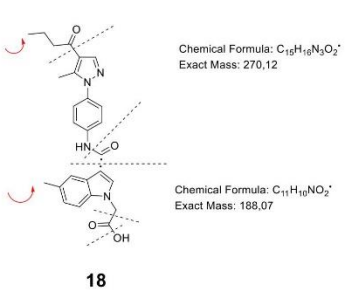
Figure S4: AAV-CAG-h*P2ry12* expression in rat brain. (**A**) Unilateral stereotaxic injection of AAV-CAG-h*P2ry12* in the rat striatum induced localized expression of $hP2Y_{12}R$. (**B**) GFAP staining indicated a moderate astrogliosis at the site of injection. However, no obvious microglial activation was evidenced by Iba1 immunolabeling. *Abbreviations*: GFAP, glial fibrillary acidic protein; Iba1, ionized calcium-binding adaptor molecule 1.

Table S2: EC_{50} values and maximal receptor activation for different concentration-response curves of the agonist 2-MeSADP following pre-incubation with different, fixed concentrations of the antagonist PSB-22219, determined using a β-arrestin assay.[a]

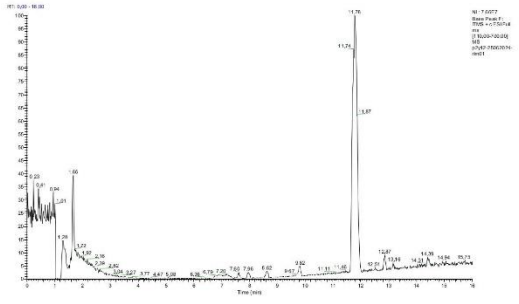
2-MeSADP + [PSB-22219] (µM)	EC_{50} of 2-MeSADP ± S.E.M (µM)[b], n = 3-4	Maximal receptor activation in the presence of 10 µM 2-MeSADP (%)
0	**0.0221** ± 0.0048	100
0.03	**0.1002** ± 0.0079 ^{ns}	95
0.3	**0.632** ± 0.171 ^{ns}	100
1	**2.58** ± 0.09 ^{ns}	97
10	**10.3** ± 0.7 ***	95
30	**30.0** ± 3 ****	90

[a] Data represent mean ± SEM of 3-4 independent experiments each in duplicates. [b] Results of one-way ANOVA with Dunnett's post-hoc test: ^{ns} not significant; * $p \leq 0.05$; ** $p \leq 0.01$; *** $p \leq 0.001$; **** $p \leq 0.0001$. Data were used for Schild plot analysis.

Analytical data S1: Identification of **18** and its metabolites.



18



The mass of the MS2 fragments of the molecular ions for **18** and its main metabolites (electrospray ionization *m/z* [M+H+])

Parent (18) ***Rt =11.78***	**Metabolite (1)** ***Rt=6.64*** **Hydroxylation**	**Metabolite (2)** ***Rt= 8.62*** **Hydroxylation**	**Metabolite (3)** ***Rt=12.87*** **Hydroxylation**
459	**475 (+16)**	**475 (+16)**	**475 (+16)**
441	**457**	**457**	**457**
413	**429**	**429**	**429**
389	389	389	**405**
270	**286**	**286**	270
216	216	216	**232**
200	200	200	
190	190	190	**206**
172	172	172	**188**

Rt: retention time (min)

Synthesis of the intermediates

Synthesis of ethyl 5-methyl-1-(4-nitrophenyl)-1*H*-pyrazole-4-carboxylate (19)

In a 500 mL round-bottom flask, 4-nitrophenylhydrazine hydrochloride (8.00 g, 52.24 mmol) was added to a solution of ethyl (*E*)-2-((dimethylamino)methylene)-3-oxobutanoate (9.68 g, 52.24 mmol) in ethanol (200 mL). The reaction mixture was refluxed for 3h. After completion, the solvent was concentrated in vacuo and poured into water (400 mL). The resulting precipitate was collected by filtration, washed with water and dried under ultra-high vacuum to yield **19** as a brown powder (11.10 g, 77%). ^{1}H NMR (500 MHz, DMSO-d_6) δ 8.40 (d, J = 9.0 Hz, 2H), 8.10 (s, 1H), 7.88 (d, J = 9.0 Hz, 2H), 4.27 (q, J = 7.1 Hz, 2H), 2.62 (s, 3H), 1.30 (t, J = 7.1 Hz, 3H); ^{13}C NMR (126 MHz, DMSO) δ 162.61, 146.57, 144.13, 143.34, 142.23, 125.78, 124.72, 113.27, 59.74, 14.20, 11.72. LC-MS (*m*/*z*): positive mode 276.1 $[M + H]^{1+}$; purity by HPLC WL (220-600 nm)-ESI-MS: 99.0%.

Synthesis of 5-methyl-1-(4-nitrophenyl)-1*H*-pyrazole-4-carboxylic acid (20)

In a 250 mL round-bottom flask, a solution of **19** (5.23 g, 18.99 mmol) in a solvent mixture of tetrahydrofuran and ethanol (THF/EtOH, 1:1, 100 mL) was treated with an aqueous solution of potassium hydroxide (KOH, 5.35 g, 94.95 mmol) in water (50 mL). The reaction mixture was refluxed for 2 h. After completion, the organic solvents were removed under reduced pressure, and the resulting aqueous phase was carefully neutralized by the slow addition of 6N HCl. The precipitate formed was collected by filtration, washed with water, and dried under ultra-high vacuum to yield **20** as a brown powder (4.60 g, 98%). ^{1}H NMR (500 MHz, DMSO-d_6) δ 12.55 (s, 1H), 8.38 (d, J = 9.0 Hz, 2H), 8.05 (s, 1H), 7.87 (d, J = 9.0 Hz, 2H), 2.61 (s, 3H); ^{13}C NMR (126 MHz, DMSO) δ 164.21, 146.49, 144.00, 143.52, 142.66, 125.69, 124.72, 114.10, 11.69; mp = 231 −232 °C. LC-MS (*m*/*z*): positive mode 248.0 $[M + H]^{1+}$; purity by HPLC WL (220-600 nm)-ESI-MS: 98.0%.

Synthesis of ethyl 3-(5-methyl-1-(4-nitrophenyl)-1*H*-pyrazol-4-yl)-3-oxopropanoate (21)

In a 250 mL round-bottom flask, **20** (1.10 g, 4.44 mmol) was dissolved in THF (77 mL) and treated with 1,1'-carbonyldiimidazole (0.94 g, 5.78 mmol). The mixture was stirred at room temperature for 20 h. Then, magnesium bis(3-ethoxy-3-oxopropanoate (1.53 g, 5.34 mmol) was added, and the mixture was stirred at 55 °C for an additional 20 h. After TLC analysis, EtOAc (100 mL) was added, and the mixture was washed with aqueous 2 N NaOH and brine. The organic layer was dried over $MgSO_4$, evaporated to dryness, and purified via silica gel

column chromatography (DCM, followed by DCM/MeOH, 95/5 v/v) to afford **21** as a brown powder (0.85 g, 60%). ^{1}H NMR, DMSO-d_6 (500 MHz) δ 8.41 (d, J = 9.1 Hz, 2H), 8.37 (s, 1H), 7.89 (d, J = 9.1 Hz, 2H), 4.13 (q, J = 7.1 Hz, 2H), 4.02 (s, 2H), 2.62 (s, 3H), 1.21 (t, J = 7.1 Hz, 3H); ^{13}C NMR, DMSO-d_6 (126 MHz) δ 188.09, 167.39, 146.74, 143.92, 143.22, 143.00, 125.97, 124.73, 120.68, 60.53, 47.47, 13.99, 12.06; mp = 108 −109 °C. LC-MS (*m*/*z*): positive mode 318.2 $[M + H]^{1+}$; purity by HPLC WL (220-600 nm)-ESI-MS: 94.0%.

Synthesis of ethyl 2-(5-methyl-1-(4-nitrophenyl)-1*H*-pyrazole-4-carbonyl)butanoate (22)

In a 100 mL round-bottom flask, **21** (3.0 g, 9.45 mmol) was dissolved in THF (40 mL) and cooled to 0 °C. Sodium hydride (NaH**,** 0.45 g, 18.90 mmol) was added in portions, and the mixture was stirred for 30 min. Iodoethane (2.21 g, 14.18 mmol, 1.13 mL) was added dropwise, and the mixture was stirred overnight at room temperature. After the reaction, water was added, and the organic phase was removed under reduced pressure. The residue was extracted with DCM (3×), washed with water, dried over $MgSO_4$, and evaporated to dryness. Purification via column chromatography (DCM, followed by DCM/MeOH, 95/5 v/v) yielded **22** as pale brown crystals (2.70 g, 83%). ^{1}H NMR (600 MHz, DMSO-d_6) δ 8.45 (s, 1H), 8.43 – 8.38 (m, 2H), 7.95 – 7.85 (m, 2H), 4.29 (t, J = 7.1 Hz, 1H), 4.11 (qd, J = 7.0, 2.5 Hz, 2H), 2.62 (s, 3H), 1.90 – 1.80 (m, 2H), 1.15 (t, J = 7.1 Hz, 3H), 0.92 (t, J = 7.4 Hz, 3H); ^{13}C NMR (151 MHz, DMSO) δ 190.73, 169.50, 146.78, 144.35, 143.02, 142.94, 126.04, 124.75, 120.69, 60.61, 56.81, 21.89, 13.96, 12.18, 11.63. LC-MS (*m*/*z*): positive mode 346.2 $[M + H]^{1+}$; purity by HPLC WL (220-600 nm)-ESI-MS: 97.0%.

Synthesis of 1-(5-methyl-1-(4-nitrophenyl)-1*H*-pyrazol-4-yl)butan-1-one (23)

In a 250 mL round-bottom flask, **22** (2.70 g, 7.82 mmol) was refluxed in aqueous 37% HCl (66 mL) at 105 °C for 2 h. After cooling to 0 °C, the mixture was neutralized using 40% NaOH (61 mL). The resulting mixture was extracted with EtOAc (3×), washed with water, dried over $MgSO_4$, and evaporated to dryness. The residue was purified via column chromatography (DCM, followed by DCM/EtOAc, 8/2 v/v) to yield **23** as bright brown crystals (2.05 g, 96%). ^{1}H NMR (500 MHz, DMSO-d_6) δ 8.41 – 8.38 (m, 2H), 8.36 (s, 1H), 7.89 – 7.85 (m, 2H), 2.83 (t, J = 7.2 Hz, 2H), 2.61 (s, 3H), 1.63 (sext, J = 7.3 Hz, 2H), 0.93 (t, J = 7.4 Hz, 3H); ^{13}C NMR (126 MHz, DMSO) δ 195.61, 146.61, 143.26, 143.00, 142.73, 125.88, 124.74, 121.20, 42.18, 17.27, 13.62, 12.08. LC-MS (*m*/*z*): positive mode 274.1 $[M + H]^{1+}$; purity by HPLC WL (220-600 nm)-ESI-MS: 98.0%.

Synthesis of 1-(1-(4-aminophenyl)-5-methyl-1*H*-pyrazol-4-yl)butan-1-one (24)

Method I: **Catalytic hydrogenation**. In a 250 mL round-bottom flask, **23** (1.0 g, 3.66 mmol) was dissolved in MeOH (100 mL), and Pd/C (10%, 0.10 g) was added. The mixture was stirred under a hydrogen atmosphere (balloon) at 25 °C for 16 h. After TLC confirmation, the mixture was filtered over celite, washed with methanol, and evaporated under reduced pressure to afford **24** as a pale brown powder (0.86 g, 97%).

Method II: $SnCl_2$ reduction. Alternatively, **23** (1.0 g, 3.66 mmol) was dissolved in EtOH (100 mL) and treated with Sn(II) chloride dihydrate (2.4 g, 18.30 mmol). The mixture was stirred at 80 °C for 1.5 h, cooled, and quenched with 20% sodium carbonate solution (200 mL). The resulting mixture was extracted with EtOAc and washed with 1 N NaOH. After drying over $MgSO_4$ and solvent removal, the residue was purified by column chromatography (DCM/EtOAc, 8/2 v/v) to afford **24** as a pale brown powder.^{1}H NMR, DMSO-d_6 (600 MHz) δ 8.12 (s, 1H), 7.07 (d, J = 8.7 Hz, 2H), 6.64 (d, J = 8.7 Hz, 2H), 5.43 (s, 2H, NH_2), 2.76 (t, J = 7.2 Hz, 2H), 2.40 (s, 3H), 1.60 (sext, J = 7.3 Hz, 2H), 0.91 (t, J = 7.4 Hz, 3H); ^{13}C NMR, DMSO-d_6 (151 MHz) δ 195.20, 149.04, 141.74, 140.72, 126.55, 126.17, 119.65, 113.25, 41.69, 17.28, 13.55, 11.70. mp = 120 −121 °C. LC-MS (m/z): positive mode 244.0 $[M + H]^{1+}$; purity by HPLC WL (220-600 nm)-ESI-MS: 97.0%.

Synthesis of 2,2,2-trifluoro-1-(5-methyl-1*H*-indol-3-yl)ethan-1-one (25)

In a 250 mL round-bottom flask, 5-methyl-1*H*-indole (5.0 g, 38.12 mmol) was dissolved in Et_2O (50 mL) and cooled to -5 °C. 2,2,2-Trifluoroacetic anhydride (8.0 g, 38.12 mmol, 5.30 mL) in Et_2O (16 mL) was added dropwise under stirring. The mixture was stirred at -5 °C for 2 h. The resulting precipitate was filtered, washed with Et_2O, and dried to afford **25** as a white powder (7.2 g, 83%). ^{1}H NMR (600 MHz, DMSO-d_6) δ 12.58 (s, 1H), 8.40 (dd, J = 3.3, 1.7 Hz, 1H), 7.99 (s, 1H), 7.47 (d, J = 8.3 Hz, 1H), 7.16 (d, J = 8.2 Hz, 1H), 2.43 (s, 3H); ^{13}C NMR (151 MHz, DMSO) δ 173.67, 173.45, 137.19, 134.77, 132.44, 125.90, 125.58, 120.68, 112.46, 108.34, 21.10. mp = 247-248 °C. LC-MS (m/z): positive mode 228.2 $[M + H]^{1+}$; purity by HPLC WL (220-600 nm)-ESI-MS: 99.8%.

Synthesis of 5-methyl-1*H*-indole-3-carboxylic acid (26)

Compound **25** (7.20 g, 31.69 mmol) was added to an aqueous solution of KOH (13.85 g, 247.19 mmol) in water (18 mL). The mixture was refluxed for 4 h. After cooling it down, the reaction

mixture was washed with Et_2O (30 mL). The aqueous phase was neutralized by slow addition of 6 N HCl to pH 2. The precipitate formed was filtered, washed with water and dried under ultra-high vacuum to afford the desired intermediate **26** as white powder (4.8 g, 86%). ^{1}H NMR (600 MHz, DMSO-d_6) δ 11.85 (s, 1H), 11.67 (s, 1H), 7.96 (s, 1H), 7.84 (s, 1H), 7.35 (d, J = 8.2 Hz, 1H), 7.00 (d, J = 8.2 Hz, 1H), 2.40 (s, 3H); ^{13}C NMR (151 MHz, DMSO) δ 166.08, 134.83, 132.24, 129.74, 126.35, 123.72, 120.33, 111.87, 106.92, 21.34. mp = 202 −203 °C. LC-MS (*m*/*z*): positive mode 176.0 $[M + H]^{1+}$; purity by HPLC WL (220-600 nm)-ESI-MS: 93.0%.

Synthesis of 1-acetyl-5-methyl-1*H*-indole-3-carboxylic acid (27*, alternative method)

A mixture of **26** (0.65 g, 3.71 mmol), Et_3N (0.83 g, 8.17 mmol, 1.14 mL), and 4-*N*,*N*-dimethylaminopyridine (0.09 g, 0.74 mmol) in DCM (14.0 mL) was cooled to 0 °C in a sealed tube and treated with acetyl chloride (0.29 g, 3.71 mmol, 0.26 mL). The reaction mixture was then allowed to stir at 25 °C for 3 h. TLC-control confirmed the consumption of **26**. Then, the mixture was washed with an aq. 1N HCl solution, water, and brine. The organic phase was dried over $MgSO_4$ and evaporated under reduced pressure to afford the crude product **27** (0.38 g crude product, purity 79%), which was used for next step without further purification. ^{1}H NMR (600 MHz, DMSO-d_6) δ 8.37 (s, 1H, 4-H), 8.22 (d, J = 8.5 Hz, 1H, 7-H), 7.89 (s, 1H, 2-H), 7.21 (dd, J = 8.5, 1.5 Hz, 1H, 6-H), 2.71 (s, 3H, 10-H), 2.42 (s, 3H, 8-H); ^{13}C NMR (151 MHz, DMSO) δ 170.04, 165.02, 133.59, 133.40, 133.13, 127.66, 126.49, 120.87, 115.63, 112.65, 23.65, 21.08. LC-MS (*m*/*z*): positive mode 218.1 $[M + H]^{1+}$.

Synthesis of 1-(6-bromo-5-methyl-1*H*-indol-3-yl)-2,2,2-trifluoroethan-1-one (28)

In a 250 round bottom flask, Br_2 (3.36 g, 21.14 mmol, 2.60 mL) was added dropwise to a solution of **25** (4.00 g, 17.60 mmol) in acetic acid (AcOH) (100 mL) at 10 °C. The mixture was allowed to stir at RT for 5 h, before removal of the solvent under reduced pressure. Then, the residue was suspended in Et_2O, and *n*-hexane was added. The formed precipitate was filtered, washed with *n*-hexane, and dried under ultra-high vacuum to afford **28** as white-yellowish powder (4.8 g, 89%). ^{1}H NMR (500 MHz, DMSO-d_6) δ 12.58 (s, 1H), 8.46 (s, 1H), 8.13 (s, 1H), 7.80 (s, 1H), 2.47 (s, 3H); ^{13}C NMR (126 MHz, DMSO) δ 173.63, 138.33, 138.29, 135.95, 131.82, 125.44, 122.36, 119.84, 116.16, 108.36, 22.83. mp = 271-272 °C. LC-MS (*m*/*z*): positive mode 308.0 $[M + H]^{1+}$; purity by HPLC WL (220-600 nm)-ESI-MS: 98.0%.

Synthesis of 6-bromo-5-methyl-1*H*-indole-3-carboxylic acid (29)

Following the same procedure as for **26**, starting with **28** (4.80 g, 15.69 mmol), **29** was synthesized as a white-yellowish powder (2.47 g, 62%). ^{1}H NMR (600 MHz, DMSO-d_6) δ 12.02 (s, 1H), 11.77 (s, 1H), 7.99 (d, J = 2.8 Hz, 1H), 7.96 (s, 1H), 7.68 (s, 1H), 2.43 (s, 3H); ^{13}C NMR (151 MHz, DMSO) δ 165.78, 135.94, 133.33, 129.12, 125.89, 122.02, 118.11, 115.46, 107.18, 22.96. LC-MS (*m*/*z*): positive mode 255.9 $[M + H]^{1+}$; purity by HPLC WL (220-600 nm)-ESI-MS: 95.0%.

Synthesis of 1-acetyl-6-bromo-5-methyl-1*H*-indole-3-carboxylic acid (30)

Following the same procedure as for **27***, starting with **29** (1.8 g, 7.08 mmol), **30** (0.92 g crude (purity =70%)) which was used for next step also without further purification. ^{1}H NMR (600 MHz, DMSO-d_6) δ 12.85 (s, 1H), 8.53 (s, 1H), 8.42 (s, 1H), 8.01 (s, 1H), 2.72 (s, 3H), 2.46 (s, 3H); ^{13}C NMR (151 MHz, DMSO) δ 170.19, 164.60, 134.24, 133.81, 132.93, 127.07, 122.35, 120.94, 119.05, 112.38, 23.56, 22.76. LC-MS (*m*/*z*): positive mode 297.9 $[M + H]^{1+}$; purity by HPLC WL (220-600 nm)-ESI-MS: 70.0%.

Synthesis of 1-acetyl-*N*-(4-(4-butyryl-5-methyl-1*H*-pyrazol-1-yl)phenyl)-5-methyl-1*H*-indole-3-carboxamide (35)

In a sealed tube, **24** (0.51 g, 2.10 mmol), 4-dimethylaminopyridine (DMAP) (0.32 g, 2.62 mmol), and 1-ethyl-3-(3'-dimethylaminopropyl)carbodiimide hydrochloride (EDC-HCl**)** (0.30 g, 1.92 mmol) were added to **27** (0.38 g, 1.75 mmol) in DCM (14 mL) at 0 °C. The reaction mixture was stirred at room temperature overnight. After washing with 1 N HCl, water, and brine, the organic layer was dried over $MgSO_4$ and evaporated under reduced pressure. Purification by column chromatography (DCM, then DCM/EtOAc, 8/2 v/v) yielded **35** as a pale brown powder (0.31 g, 40%). ^{1}H NMR (600 MHz, DMSO-d_6) δ 10.27 (s, 1H), 8.75 (s, 1H), 8.24 (d, J = 8.7 Hz, 2H), 8.06 (s, 1H), 7.95 (d, J = 8.8 Hz, 2H), 7.54 (d, J = 8.8 Hz, 2H), 7.23 (d, J = 8.5 Hz, 1H), 2.81 (t, J = 7.2 Hz, 2H), 2.74 (s, 3H), 2.53 (s, 3H), 2.44 (s, 3H), 1.64 (q, J = 7.3 Hz, 2H), 0.94 (t, J = 7.4 Hz, 3H); ^{13}C NMR (151 MHz, DMSO) δ 195.62, 169.83, 162.27, 142.30, 141.67, 139.43, 133.49, 133.43, 129.93, 128.44, 126.73, 125.95, 121.48, 120.43, 120.29, 115.60, 115.20, 42.12, 23.93, 21.26, 17.52, 13.82, 12.06. LC-MS (*m*/*z*): positive mode 443.3 $[M + H]^{1+}$; purity by HPLC UV (254 nm)-ESI-MS: 97.0%.

Synthesis of 1-acetyl-6-bromo-*N*-(4-(4-butyryl-5-methyl-1*H*-pyrazol-1-yl)phenyl)-5-methyl-1*H*-indole-3-carboxamide (36)

Following the same procedure as for **35**, starting with **30** (0.39 g, 1.30 mmol), **36** was synthesized as a white-yellowish powder (0.4 g, 59%). ^{1}H NMR (600 MHz, DMSO-d_6) δ 10.30 (s, 1H), 8.79 (s, 1H), 8.55 (s, 1H), 8.24 (s, 1H), 8.20 (s, 1H), 7.93 (d, J = 8.9 Hz, 2H), 7.54 (d, J = 8.8 Hz, 2H), 2.81 (t, J = 7.2 Hz, 2H), 2.74 (s, 3H), 2.53 (s, 3H), 2.47 (s, 3H), 1.63 (sext, J = 7.3 Hz, 2H), 0.94 (t, J = 7.4 Hz, 3H); ^{13}C NMR (151 MHz, DMSO) δ 195.61, 169.96, 161.85, 142.29, 141.69, 139.26, 134.15, 133.59, 132.96, 130.54, 127.88, 125.96, 123.00, 121.17, 120.44, 120.34, 119.02, 114.88, 42.12, 23.81, 22.96, 17.52, 13.82, 12.06. LC-MS (*m*/*z*): positive mode 523.2 $[M + H]^{1+}$; purity by HPLC UV (254 nm)-ESI-MS: 95.0%.

Synthesis of *N*-(4-(4-butyryl-5-methyl-1*H*-pyrazol-1-yl)phenyl)-5-methyl-1*H*-indole-3-carboxamide (37)

In a 100 mL round-bottom flask, **35** (0.20 g, 0.45 mmol) was reacted with potassium carbonate (K_2CO_3) **(**0.25 g, 1.81 mmol) in methanol (MeOH**)** (14 mL) at room temperature for 4 h. The solvent was removed under reduced pressure, and the residue was dissolved in EtOAc, washed with aqueous 1N HCl, water, and brine. The organic phase was dried over $MgSO_4$, and the solvent was evaporated. The residue was purified by column chromatography (DCM, followed by DCM/EtOAc, 8/2 v/v) to yield **37** as a pale brown powder (0.17 g, 94%). ^{1}H NMR (600 MHz, DMSO-d_6) δ 11.65 (s, 1H), 9.90 (s, 1H), 8.27 (d, J = 3.0 Hz, 1H), 8.23 (s, 1H), 8.01 (s, 1H), 7.96 (d, J = 8.8 Hz, 2H), 7.47 (d, J = 8.8 Hz, 2H), 7.37 (d, J = 8.3 Hz, 1H), 7.02 (d, J = 9.4 Hz, 1H), 2.81 (t, J = 7.2 Hz, 2H), 2.52 (s, 3H), 2.42 (s, 3H), 1.64 (q, J = 7.3 Hz), 0.94 (t, J = 7.4 Hz, 3H); ^{13}C NMR (151 MHz, DMSO) δ 195.47, 163.44, 142.12, 141.44, 140.20, 134.58, 132.60, 129.41, 128.97, 126.62, 125.67, 123.76, 120.71, 120.23, 119.70, 111.64, 109.77, 41.97, 21.35, 17.40, 13.69, 11.92. LC-MS (*m*/*z*): positive mode 401.3 $[M + H]^{1+}$; purity by HPLC UV (254 nm)-ESI-MS: 98.0%.

Synthesis of 6-bromo-*N*-(4-(4-butyryl-5-methyl-1*H*-pyrazol-1-yl)phenyl)-5-methyl-1*H*-indole-3-carboxamide (38)

Using the same procedure as for **37**, starting with **36** (0.37 g, 0.71 mmol), **38** was obtained as a white-yellowish powder (0.31 g, 91%). ^{1}H NMR (600 MHz, DMSO-d_6) δ 11.75 (s, 1H), 9.98 (s, 1H), 8.32 (d, J = 2.8 Hz, 1H), 8.23 (s, 1H), 8.16 (s, 1H), 7.94 (d, J = 8.8 Hz, 2H), 7.73 (s,

1H), 7.48 (d, *J* = 8.8 Hz, 2H), 2.81 (t, *J* = 7.2 Hz, 2H), 2.52 (s, 3H), 2.45 (s, 3H), 1.63 (sext, *J* = 7.3 Hz, 2H), 0.94 (t, *J* = 7.4 Hz, 3H); ^{13}C NMR (151 MHz, DMSO) δ 195.47, 163.02, 142.12, 141.46, 139.99, 135.59, 132.74, 129.89, 128.72, 126.12, 125.69, 122.34, 120.23, 119.76, 118.09, 115.14, 109.86, 59.71, 41.96, 22.87, 17.39, 13.68, 11.91. LC-MS (*m*/*z*): positive mode 481.1 $[M + H]^{1+}$; purity by HPLC UV (254 nm)-ESI-MS: 95.0%.

Synthesis of methyl 2-(3-((4-(4-butyryl-5-methyl-1*H*-pyrazol-1-yl)phenyl)carbamoyl)-5-methyl-1*H*-indol-1-yl)acetate (39)

In a sealed tube, **37** (0.14 g, 0.35 mmol), potassium carbonate (K_2CO_3) (54.1 mg, 0.39 mmol), and methyl bromoacetate (59.9 mg, 0.39 mmol, 37 µL) were added to DMF (5 mL). The reaction mixture was stirred at RT overnight. After quenching with water, the mixture was extracted with EtOAc (3×), washed with brine, dried over $MgSO_4$, and evaporated under reduced pressure. Purification by column chromatography (DCM, then DCM/EtOAc, 8/2 v/v) afforded **39** as a white-yellowish powder (0.12 g, 72%). ^{1}H NMR (600 MHz, DMSO-d_6) δ 10.05 (s, 1H), 8.23 (d, *J* = 7.9 Hz, 2H), 8.02 (s, 1H), 7.96 (d, *J* = 8.8 Hz, 2H), 7.48 (d, *J* = 8.8 Hz, 2H), 7.39 (d, *J* = 8.4 Hz, 1H), 7.08 (d, *J* = 8.4 Hz, 1H), 5.26 (s, 2H), 3.71 (s, 3H), 2.81 (t, *J* = 7.2 Hz, 2H), 2.52 (s, 3H), 2.43 (s, 3H), 1.64 (sext, *J* = 7.3 Hz, 2H), 0.94 (t, *J* = 7.4 Hz, 3H); ^{13}C NMR (151 MHz, DMSO) δ 195.61, 169.16, 163.13, 142.26, 141.59, 140.22, 135.37, 132.86, 130.22, 126.96, 125.83, 124.23, 121.08, 120.37, 119.89, 110.30, 110.08, 52.41, 47.50, 42.10, 21.36, 17.53, 13.82, 12.05. mp = 210-212 °C (literature mp = 210 °C).[71] LC-MS (*m*/*z*): positive mode 473.3 $[M + H]^{1+}$; purity by HPLC UV (254 nm)-ESI-MS: 98.0%.

Synthesis of methyl 2-(6-bromo-3-((4-(4-butyryl-5-methyl-1*H*-pyrazol-1-yl)phenyl)carbamoyl)-5-methyl-1*H*-indol-1-yl)acetate (40)

Following the same procedure as for **39**, starting with **38** (0.10 g, 0.21 mmol), **40** was obtained as a white-yellowish powder (0.108 g, 93%). ^{1}H NMR (600 MHz, DMSO-d_6) δ 10.11 (s, 1H), 8.24 (d, *J* = 5.4 Hz, 2H), 8.17 (s, 1H), 7.94 (d, *J* = 8.9 Hz, 2H), 7.89 (s, 1H), 7.48 (d, *J* = 8.8 Hz, 2H), 5.30 (s, 2H), 3.73 (s, 3H), 2.81 (t, *J* = 7.2 Hz, 2H), 2.52 (s, 3H), 2.46 (s, 3H), 1.64 (q, *J* = 7.3 Hz, 2H), 0.94 (t, *J* = 7.4 Hz, 3H); ^{13}C NMR (151 MHz, DMSO) δ 195.62, 169.09, 162.74, 142.27, 141.62, 140.02, 136.43, 133.64, 133.02, 129.54, 126.36, 125.86, 122.64, 120.38, 119.97, 118.85, 114.23, 110.19, 52.47, 47.55, 42.11, 22.94, 17.53, 13.82, 12.05. LC-MS (*m*/*z*): positive mode 553.3 $[M + H]^{1+}$; purity by HPLC UV (254 nm)-ESI-MS: 96.0%.

Synthesis of magnesium bis(3-ethoxy-3-oxopropanoate) (2:1) (42)

In a 500 mL round-bottom flask, an aqueous solution of magnesium chloride hexahydrate ($MgCl_2 \cdot 6H_2O$, 3.05 g, 14.98 mmol, 10 mL, 1.5 M) was added to an aqueous solution of ethyl potassium malonate (5.10 g, 29.96 mmol, 30 mL). The mixture was stirred at 25 °C for 30 min. Subsequently, isopropanol (200 mL) was added, and the resulting mixture was stirred for an additional 30 min. The mixture was then filtered, and the filtrate was concentrated under reduced pressure. The solid residue was dried under ultra-high vacuum to yield **42** as white crystals (5.30 g, 62%). ^{1}H NMR (500 MHz, DMSO-d_6) δ 4.03 (q, J = 7.1 Hz, 4H), 3.12 (s, 4H), 1.18 (t, J = 7.1 Hz, 6H); ^{13}C NMR (126 MHz, DMSO) δ 171.02, 168.96, 59.82, 44.17, 14.02; LC-MS (m/z): positive mode 287.1 $[M + H]^{1+}$; purity by HPLC WL (220-600 nm)-ESI-MS: 100.0%.

Synthesis of *N*-methoxy-*N*,5-dimethyl-1-(4-nitrophenyl)-1*H*-pyrazole-4-carboxamide (43)

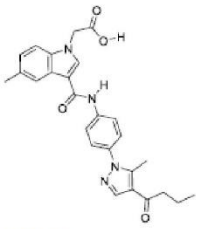
In a 100 mL round-bottom flask, **20** (3.00 g, 12.14 mmol) was refluxed in $SOCl_2$ (12 mL) for 6 h. The rest of thionyl chloride was removed under reduced pressure after mixing it with toluene (25 mL, 3x). Then the residue was dissolved in DCM (25 mL) and added dropwise to a solution of dimethylhydroxylamine hydrochloride (1.10 g, 12.14 mmol) in DCM (14 mL) and triethylamine (2.46 g, 24.27 mmol, 3.4 mL) at 0°C. The reaction mixture was stirred at 25 °C for 15 h. After completion, the mixture was quenched with saturated NH_4Cl (14 mL) and extracted 3x with DCM (15 mL). The combined organic layers were washed with brine and water, dried over $MgSO_4$, and filtered. The solvent was removed under reduced pressure to afford the crude compound **43**, which was purified by column chromatography (petroleum ether/EtOAc, 8/2 v/v) to afford **43** as a pale-yellow powder (2.65 g, 75%). LC-MS (m/z): positive mode 291.1 $[M + H]^{1+}$; purity by HPLC WL (220-600 nm)-ESI-MS: 99.0%.

Analytical data S2: For [^{3}H]**18** radioligand and all compounds

[^{3}H]2-(3-((4-(4-Butyryl-5-methyl-1*H*-pyrazol-1-yl)phenyl)carbamoyl)-5-methyl-1*H*-indol-1-yl)acetic acid ([^{3}H]PSB-22219)

Certificate of Analysis

RC TRITEC
Your Labeling Company.

Compound	**[^{3}H]PSB-22219**
Molecular formula (unlabeled)	$C_{26}H_{26}N_4O_4$
Molecular weight (unlabeled)	458.52 g/mol
Structure	
Lot number	22-1101-94
Date of analysis	October 20, 2022
Radiochemical purity	>99% (HPLC)
Specific activity	17.4 Ci/mmol (644 GBq/mmol) (determined by MS using an iterative residue correction method (^{13}C correction))
Concentration	1 mCi/ml (37 MBq/ml) in EtOH
Recommended storage cond.	store below –60 °C

Chromatographic data	
HPLC column	Waters Sunfire C18 (5 µm), 4.6 x 250 mm
Mobile phase	A: water + 0.05% TFA; B: MeCN + 0.05% TFA
Conditions	0 min 50% B; 10 min 95% B; 10 - 14.5 min 95% B; 15 min 50% B
Flow rate	1.0 ml/min
Sample	7.9 mCi/ml (2.99 GBq/ml) in EtOH
Injection	1.0 µl (7.9 µCi, 299 kBq)
UV detection	254 nm
Temperature	30 °C
Radio detector	Berthold LB 513
Cocktail	Quicksafe Flow 2+

RC TRITEC AG
Speicherstrasse 60a
CH-9053 Teufen
☎ +41 71 335 73 73
🖷 +41 71 335 73 74
labeling@rctritec.com
www.rctritec.com

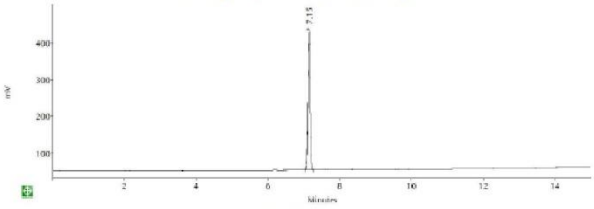
Certificate of Analysis

RC TRITEC
Your Labeling Company.

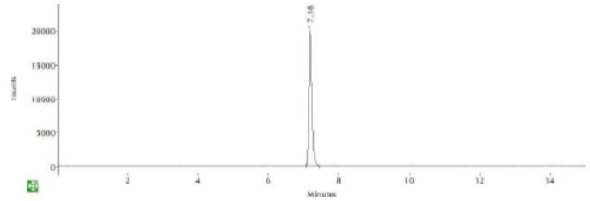
Flow rate	2.0 ml/min
Retention time	7.15 min (UV); 7.18 min (radio detector) The delay between UV and radio signal is due to the serial detection system.

Note: The mass spectrum is consistent with the proposed structure and a non-labeled reference; the HPLC retention time is consistent with a non-labeled reference. Actual position of labels not verified. For research and development use only, not for use in humans.

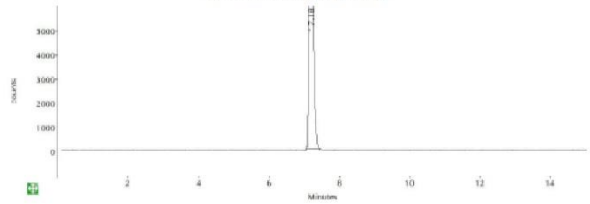
UV signal (reference, co-injected)



Radio detector



Radio detector (magnified)



RC TRITEC AG
Speicherstrasse 60a
CH-9053 Teufen

☎ +41 71 335 73 73
🖷 +41 71 335 73 74

labeling@rctritec.com
www.rctritec.com

S20

Certificate of Analysis

RC TRITEC
Your Labeling Company.

Results radio detector:

#	Peak name	Rt.	Area	% Area
1	**[^{3}H]PSB-22219**	**7.18**	**117731.50**	**100.00**
Sum			117731.50	100.00

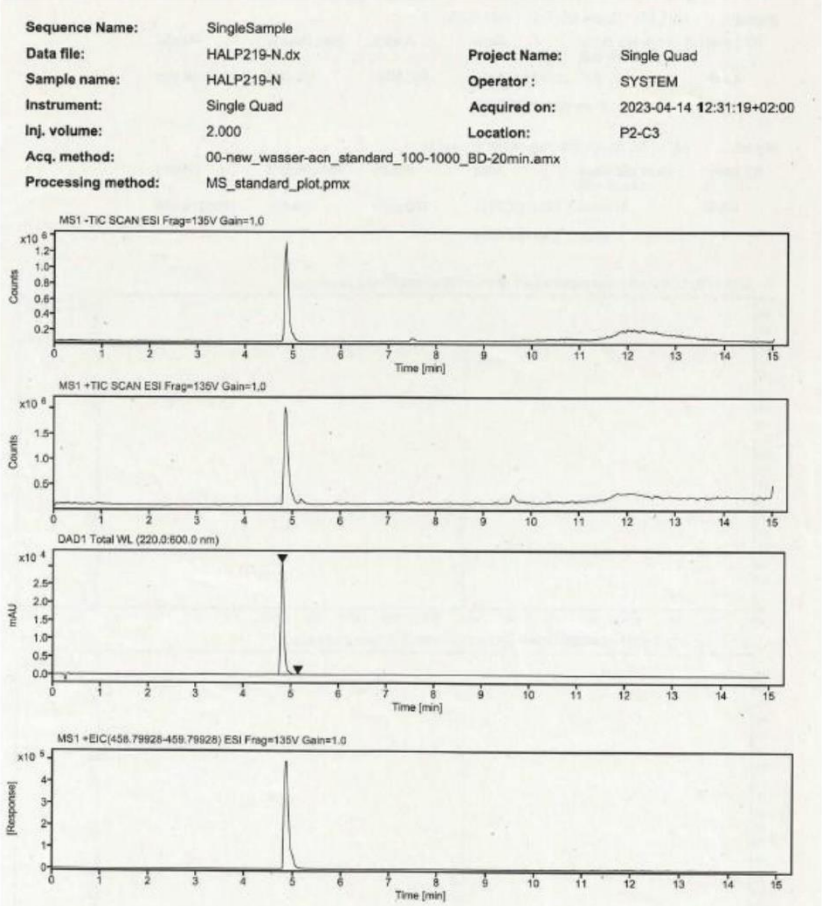
RC TRITEC LTD.

RC TRITEC AG
Speicherstrasse 60a
CH-9053 Teufen
☏ + 41 71 335 73 73
🖷 + 41 71 335 73 74
labeling@rctritec.com
www.rctritec.com

S21

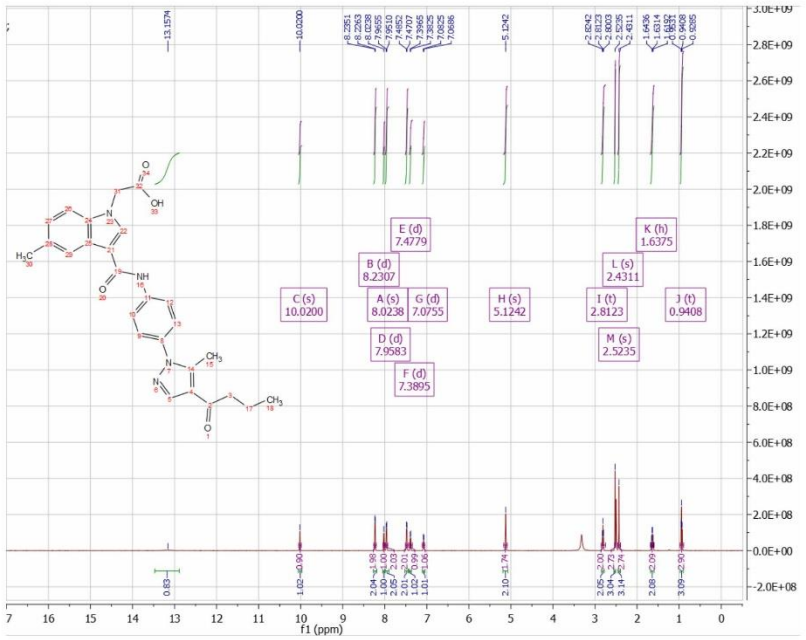
2-(3-((4-(4-Butyryl-5-methyl-1*H*-pyrazol-1-yl)phenyl)carbamoyl)-5-methyl-1*H*-indol-1-yl)acetic acid (18).[2] (Yield = 62%).

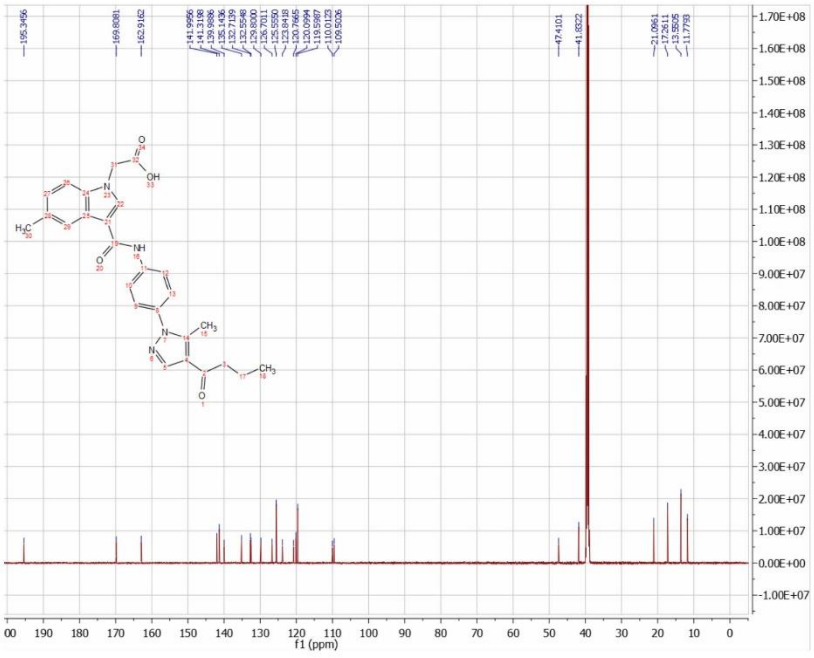
LC-MS (*m*/*z*): positive mode $[M + H]^{1+}$ (Rt) = 459.3 (4.81 min). purity by HPLC UV (254 nm)-ESI-MS: 99.8%, mp = 201-202 °C (Lit. 201 °C).



Signal: DAD1 Total WL (220.0:600.0 nm)

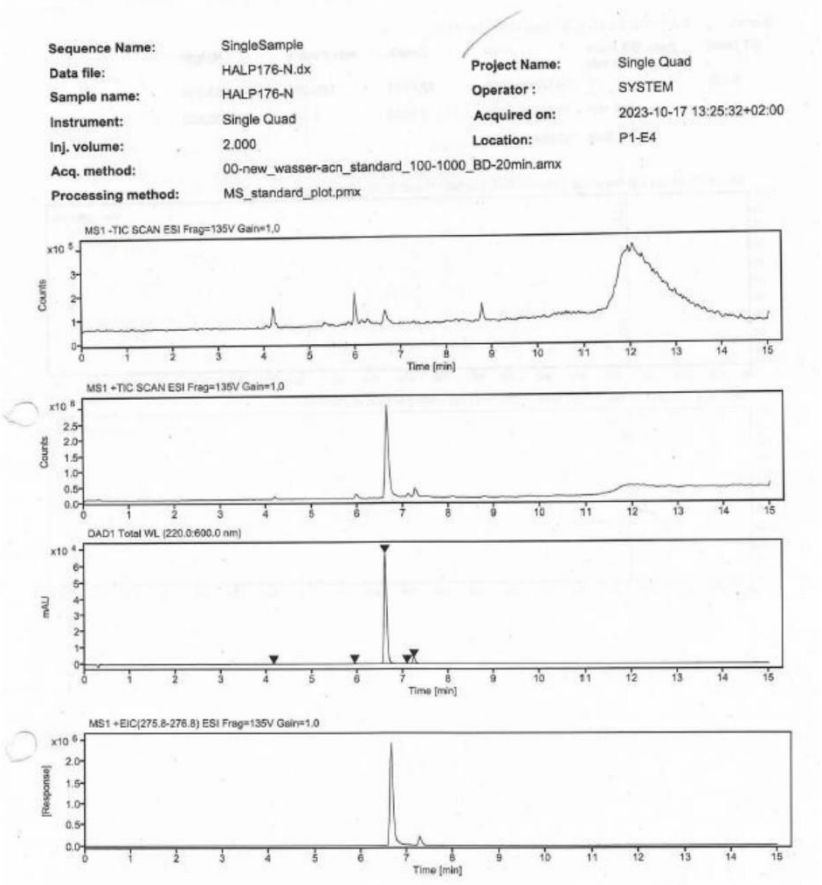
RT [min]	Peak MS Base Peak m/z	Area	Area%	Max Peak%	Height
4.809		144753.1706	99.8377	100.000	31048.309
5.146		235.3478	0.1623	0.163	73.356
	Sum	144988.5184			


E (d)
7.4779
B (d)
8.2307
K (h)
1.6375
L (s)
2.4311
C (s)
10.0200
A (s)
8.0238
G (d)
7.0755
H (s)
5.1242
I (t)
2.8123
J (t)
0.9408
D (d)
7.9583
M (s)
2.5235
F (d)
7.3895
f1 (ppm)


f1 (ppm)

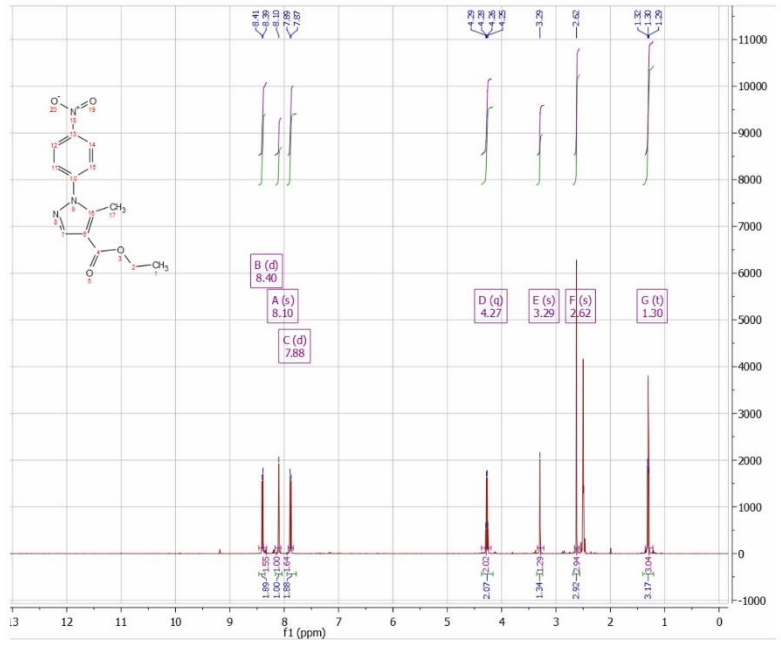
S23

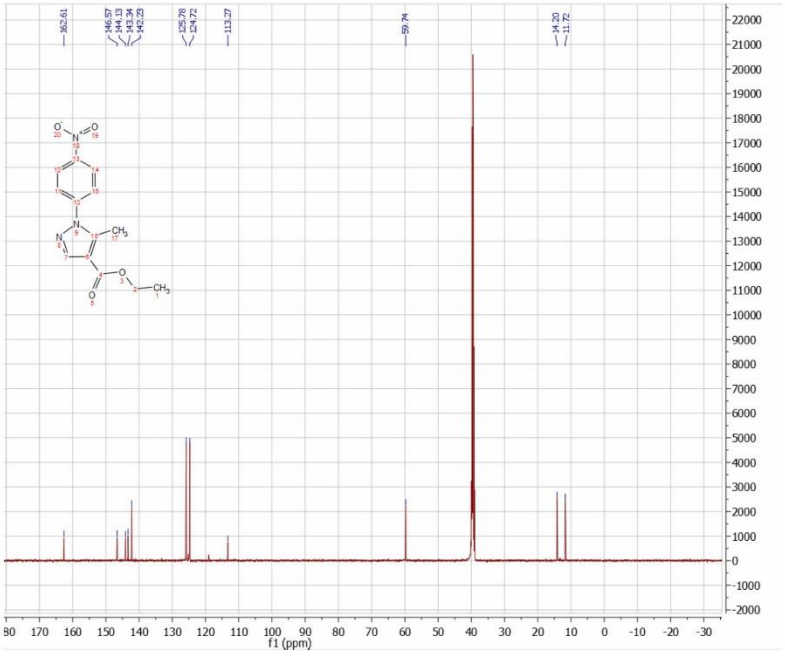
Ethyl 5-methyl-1-(4-nitrophenyl)-1*H*-pyrazole-4-carboxylate (19).[2] (Yield = 77%)
LC-MS (*m*/*z*): positive mode $[M + H]^{1+}$ (Rt) = 276.1 (6.62 min). purity by HPLC WL (220-600 nm)-ESI-MS: 99.0%.



Signal: DAD1 Total WL (220.0:600.0 nm)

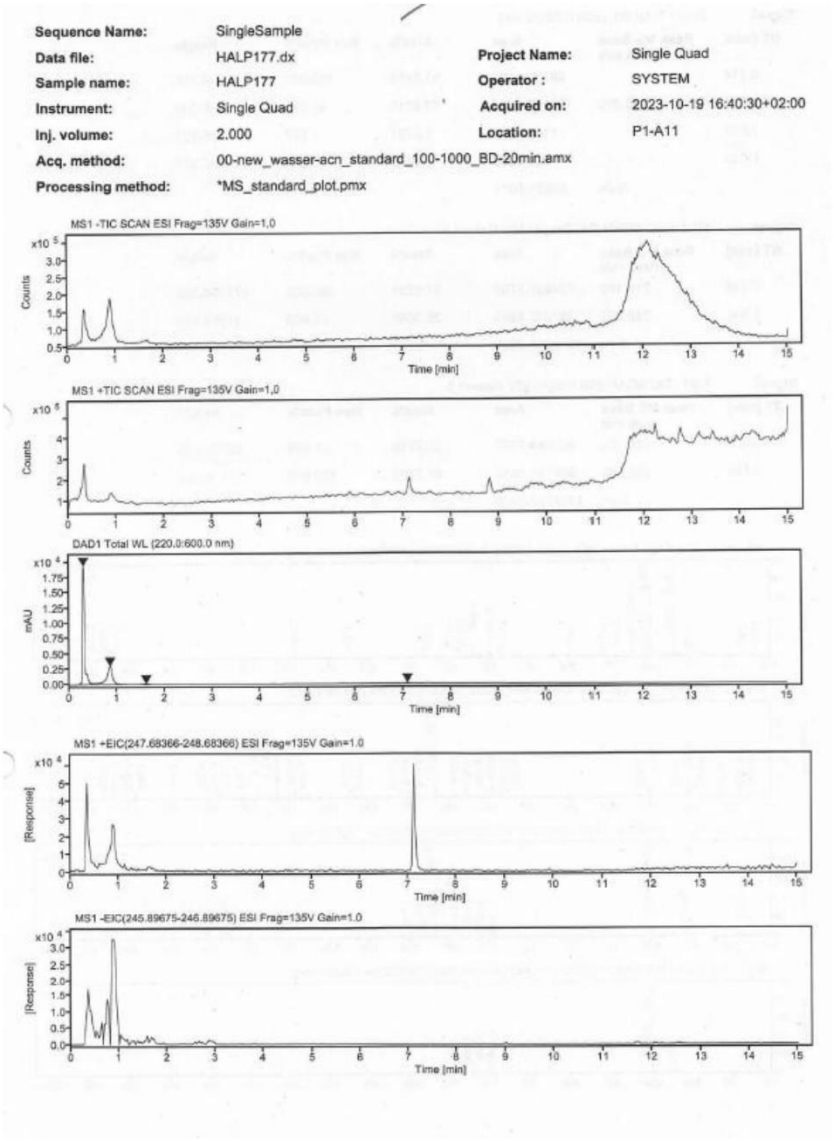
RT [min]	Peak MS Base Peak m/z	Area	Area%	Max Peak%	Height
4.166		844.0012	0.2953	0.313	241.691
5.946		1329.2231	0.4651	0.494	368.352
6.619		269281.9823	94.2147	100.000	67346.630
7.095		387.8134	0.1357	0.144	125.932
7.248		13974.3897	4.8893	5.190	3455.783
	Sum	285817.4098			


B (d)
8.40
A (s)
8.10
C (d)
7.88
D (q)
4.27
E (s)
3.29
F (s)
2.62
G (t)
1.30
f1 (ppm)


162.61
146.57
144.13
143.34
142.29
125.78
124.72
113.27
59.74
14.20
11.72
f1 (ppm)

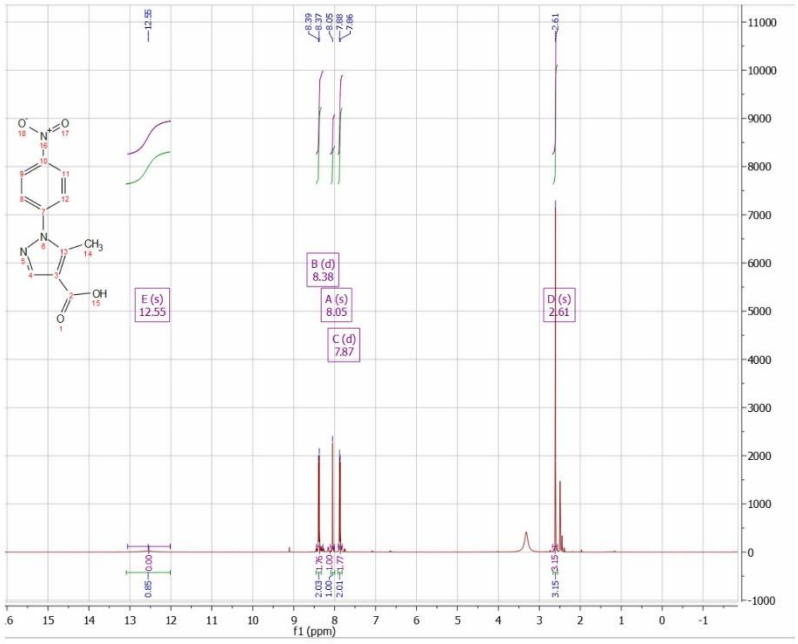
S25

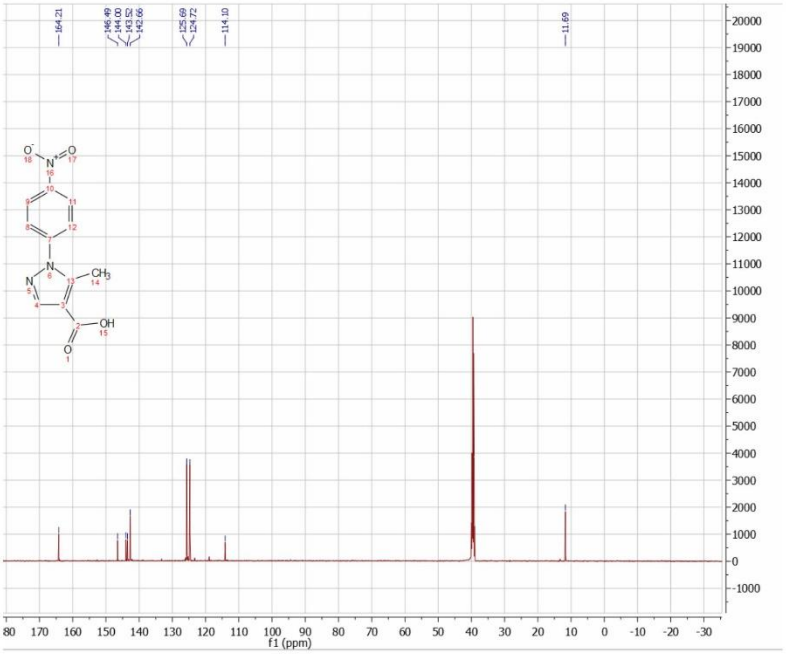
5-Methyl-1-(4-nitrophenyl)-1*H*-pyrazole-4-carboxylic acid (20).[2] (Yield = 98%)
LC-MS (*m*/*z*): positive mode $[M + H]^{1+}$ (Rt) = 248.0 (0.31 to 0.87 min).; purity by HPLC-(220-600 nm)-ESI-MS: 98.0%. mp = 231 −232 °C.



Signal: DAD1 Total WL (220.0:600.0 nm)

RT [min]	Peak MS Base Peak m/z	Area	Area%	Max Peak%	Height
0.314		58731.4154	67.8454	100.000	19434.700
0.868	246.200	26412.3524	30.5110	44.971	3018.045
1.624		1102.5836	1.2737	1.877	125.723
7.093		320.2502	0.3699	0.545	80.213
	Sum	86566.6016			

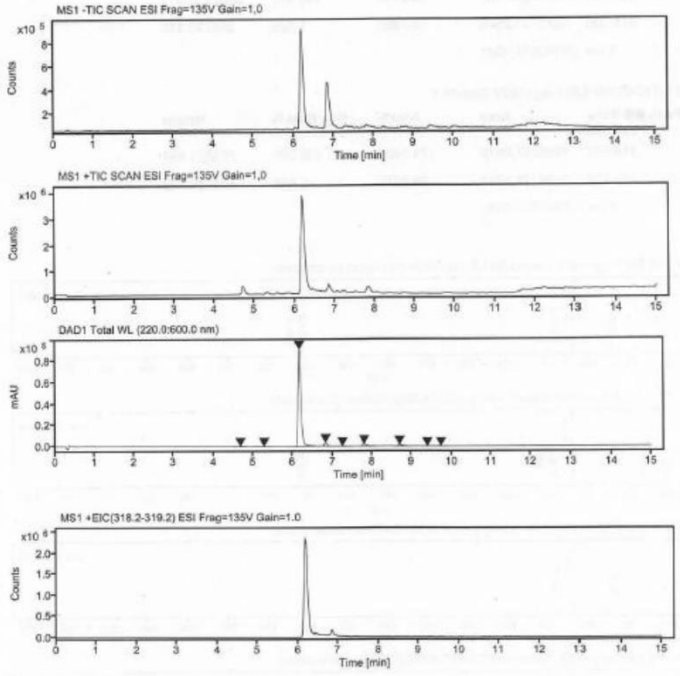




Ethyl 3-(5-methyl-1-(4-nitrophenyl)-1*H*-pyrazol-4-yl)-3-oxopropanoate (21).[2] (Yield 91%)

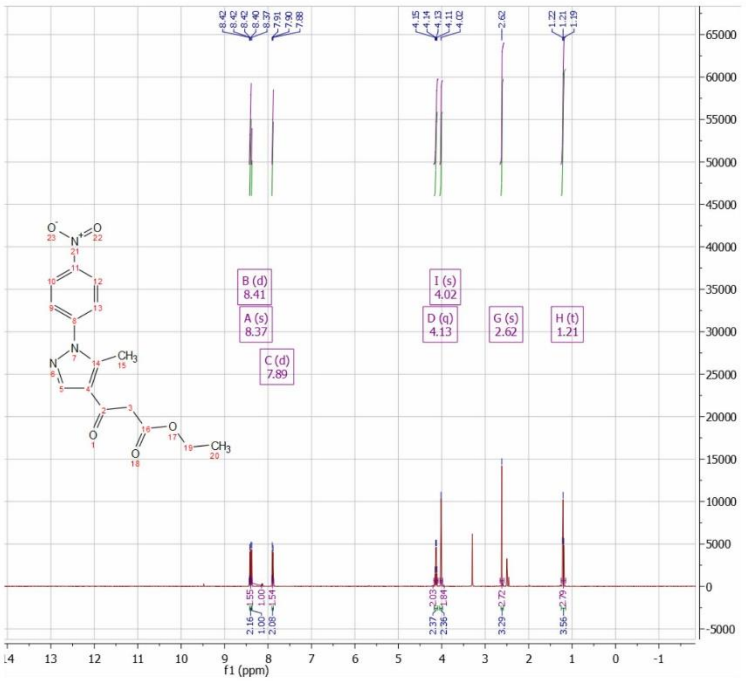
LC-MS (*m*/*z*): positive mode $[M + H]^{1+}$ (Rt) = 318.2 (6.17 min).; purity by HPLC-(220-600 nm)-ESI-MS: 94.0%. mp = 108-109 °C.

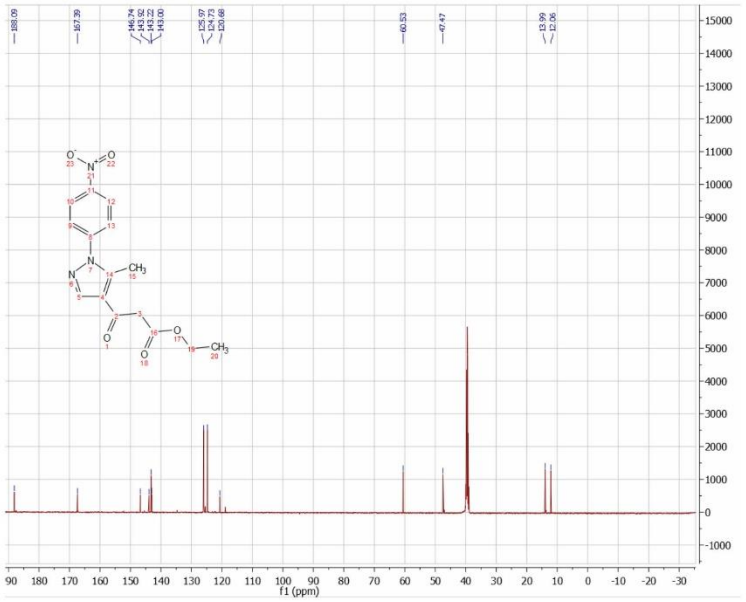
Sequence Name:	SingleSample		
Data file:	HALP179-F1.dx	**Project Name:**	Single Quad
Sample name:	HALP179-F1	**Operator :**	SYSTEM
Instrument:	Single Quad	**Acquired on:**	2024-11-20 15:20:11+01:00
Inj. volume:	3.000	**Location:**	P1-E5
Acq. method:	00-new_wasser-acn_standard_100-1000_BD-20min.amx		
Processing method:	MS_standard_plot.pmx		



Signal: DAD1 Total WL (220.0:600.0 nm)

RT [min]	Peak MS Base Peak m/z	Area	Area%	Max Peak%	Height
4.687		1610.0090	0.3088	0.339	319.788
5.281		1090.1928	0.2091	0.229	245.191
6.171		475070.7285	91.1078	100.000	91019.939
6.830	316.400	16554.5993	3.1748	3.485	3423.007
7.258		2165.0107	0.4152	0.456	312.359
7.801		12929.9049	2.4797	2.722	2334.643
8.898		9736.5135	1.8672	2.049	1474.260



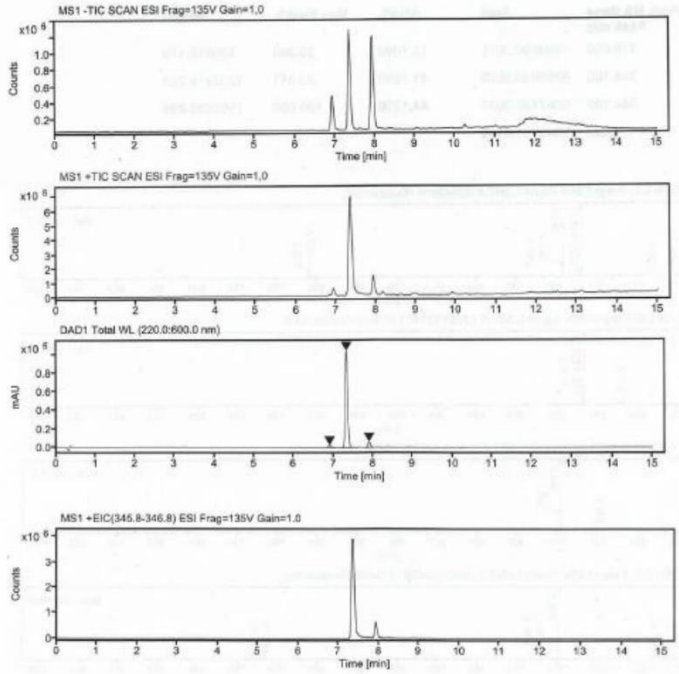


S30

Ethyl 2-(5-methyl-1-(4-nitrophenyl)-1*H*-pyrazole-4-carbonyl)butanoate (22).[2] (Yield 83%)

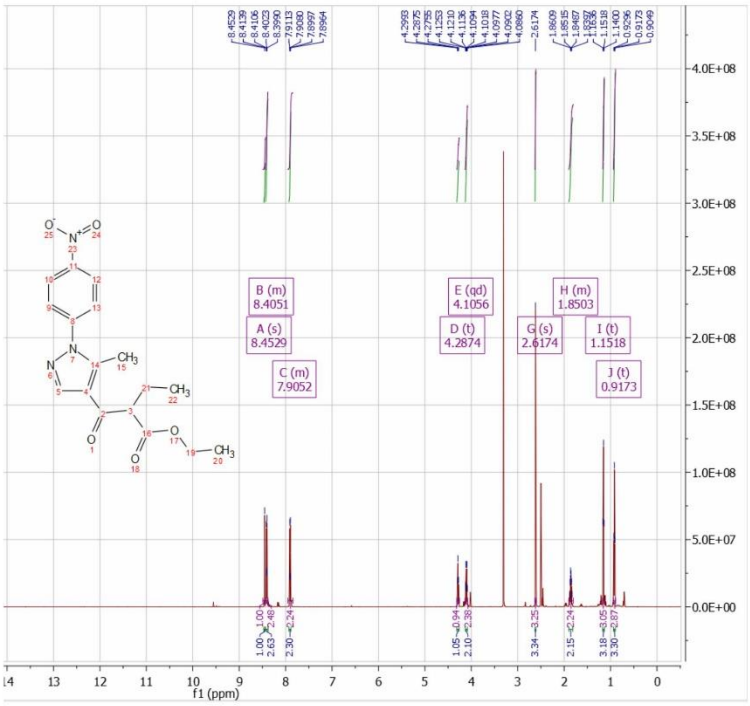
LC-MS (*m*/*z*): positive mode $[M + H]^{1+}$ (Rt) = 346.2 (7.34 min).; purity by HPLC-(220-600 nm)-ESI-MS: 97.0%.

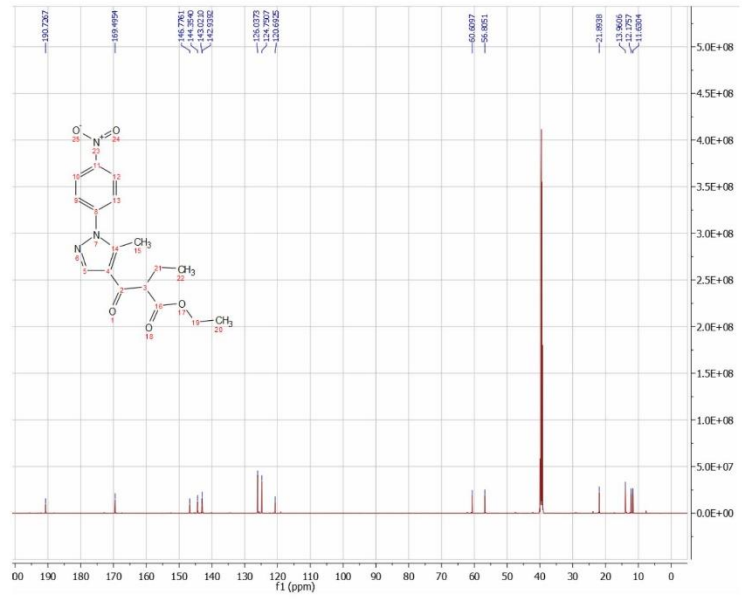
Sequence Name:	SingleSample		
Data file:	HALP201-F1.dx	**Project Name:**	Single Quad
Sample name:	HALP201-F1	**Operator :**	SYSTEM
Instrument:	Single Quad	**Acquired on:**	2024-03-04 18:23:05+01:00
Inj. volume:	3.000	**Location:**	P2-A5
Acq. method:	00-new_wasser-acn_standard_100-1000_BD-20min.amx		
Processing method:	MS_standard_plot.pmx		



Signal: DAD1 Total WL (220.0:600.0 nm)

RT [min]	Peak MS Base Peak m/z	Area	Area%	Max Peak%	Height
6.909		10646.3077	2.2705	2.464	2788.856
7.334		432090.5374	92.1496	100.000	104969.493
7.903		26164.5572	5.5800	6.055	6541.294
	Sum	468901.4023			


B (m)
8.4051
A (s)
8.4529
C (m)
7.9052
E (qd)
4.1056
D (t)
4.2874
G (s)
2.6174
H (m)
1.8503
I (t)
1.1518
J (t)
0.9173
f1 (ppm)

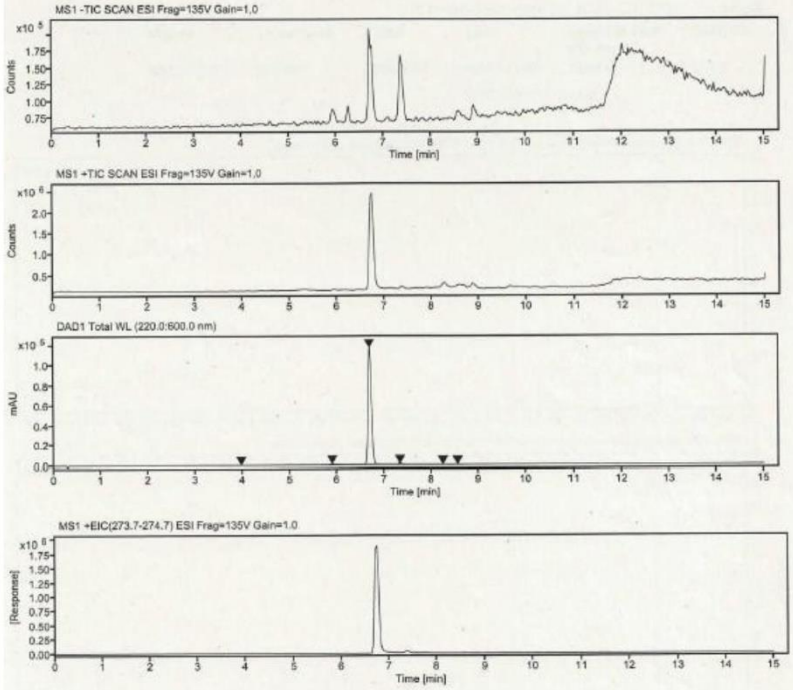

f1 (ppm)

S32

1-(5-Methyl-1-(4-nitrophenyl)-1*H*-pyrazol-4-yl)butan-1-one (23).[2] (Yield 96%)

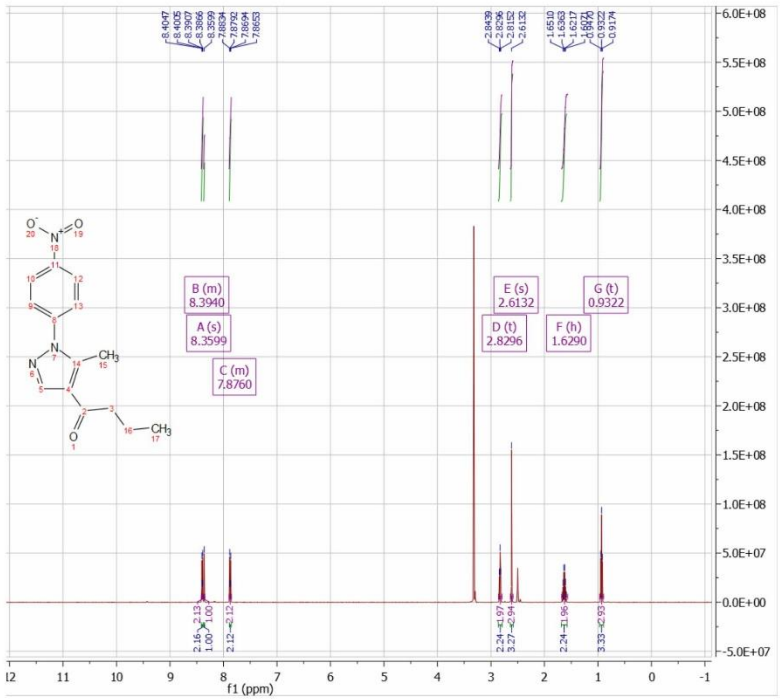
LC-MS (*m*/*z*): positive mode $[M + H]^{1+}$ (Rt) = 274.1 (6.70 min).; purity by HPLC-(220-600 nm)-ESI-MS: 98.0%.

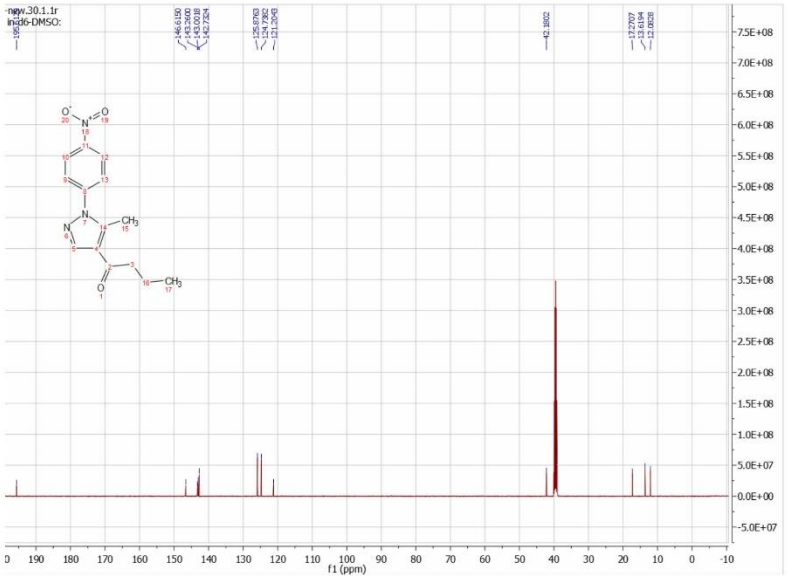
Sequence Name:	SingleSample		
Data file:	HALP206-F4.dx	**Project Name:**	Single Quad
Sample name:	HALP206-F4	**Operator :**	SYSTEM
Instrument:	Single Quad	**Acquired on:**	2023-05-11 07:39:45+02:00
Inj. volume:	2.000	**Location:**	P2-D9
Acq. method:	00-new_wasser-acn_standard_100-1000_BD-20min.amx		
Processing method:	MS_standard_plot.pmx		



Signal: DAD1 Total WL (220.0:600.0 nm)

RT [min]	Peak MS Base Peak m/z	Area	Area%	Max Peak%	Height
3.982		236.5594	0.0391	0.040	39.335
5.905		4089.0556	0.6755	0.687	735.167
6.697	271.800	595022.8471	98.2931	100.000	117264.204
7.341		4772.8358	0.7884	0.802	929.475
8.246		527.4588	0.0871	0.089	89.479
8.560		706.6835	0.1167	0.119	86.622

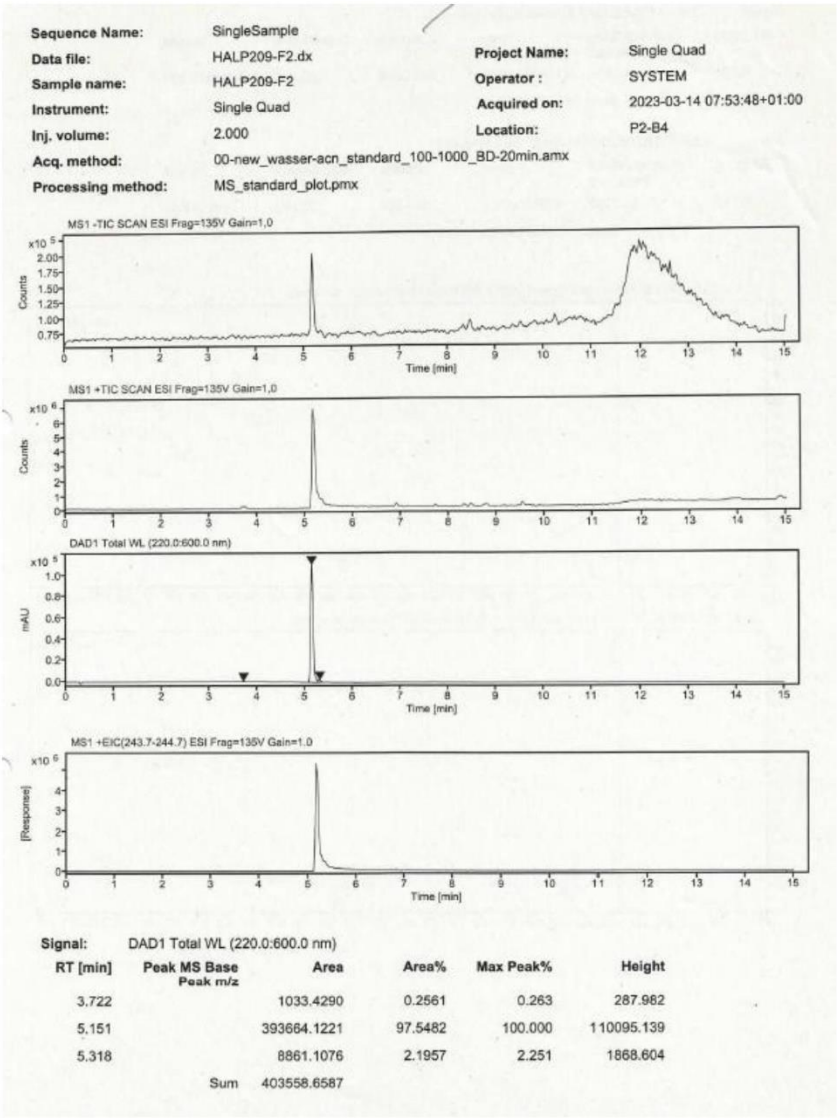

B (m)
8.3940
A (s)
8.3599
C (m)
7.8760
E (s)
2.6132
D (t)
2.8296
F (h)
1.6290
G (t)
0.9322
f1 (ppm)


f1 (ppm)

S34

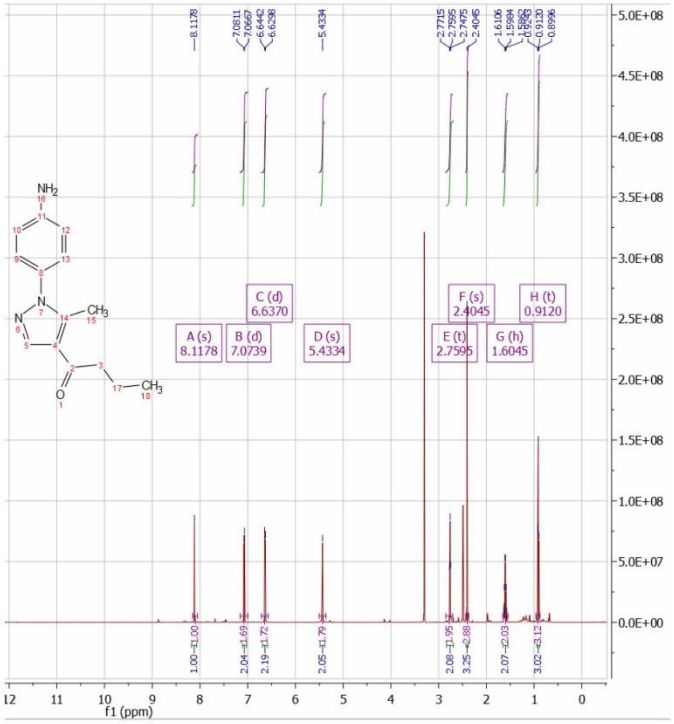
1-(1-(4-Aminophenyl)-5-methyl-1*H*-pyrazol-4-yl)butan-1-one (24).[2] (Yield 97%)

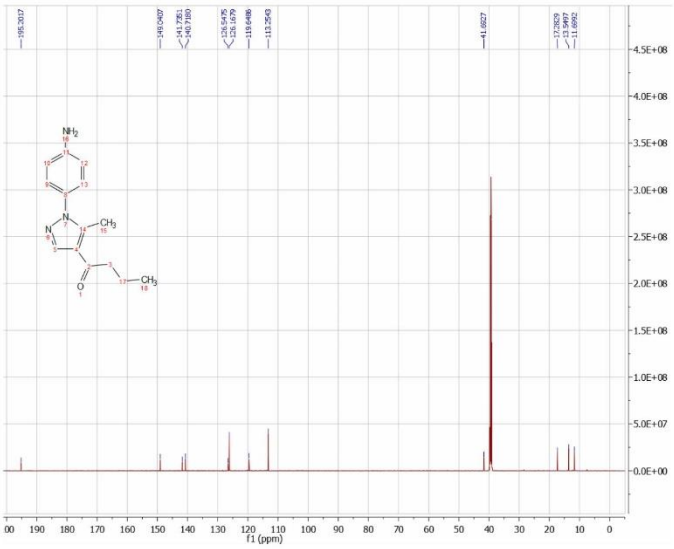
LC-MS (*m*/*z*): positive mode $[M + H]^{1+}$ (Rt) = 244.0 (5.15 min).; purity by HPLC-(220-600 nm)-ESI-MS: 97.0%. mp = 120 −121 °C.



Signal: DAD1 Total WL (220.0:600.0 nm)

RT [min]	Peak MS Base Peak m/z	Area	Area%	Max Peak%	Height
3.722		1033.4290	0.2561	0.263	287.982
5.151		393664.1221	97.5482	100.000	110095.139
5.318		8861.1076	2.1957	2.251	1868.604
	Sum	403558.6587			

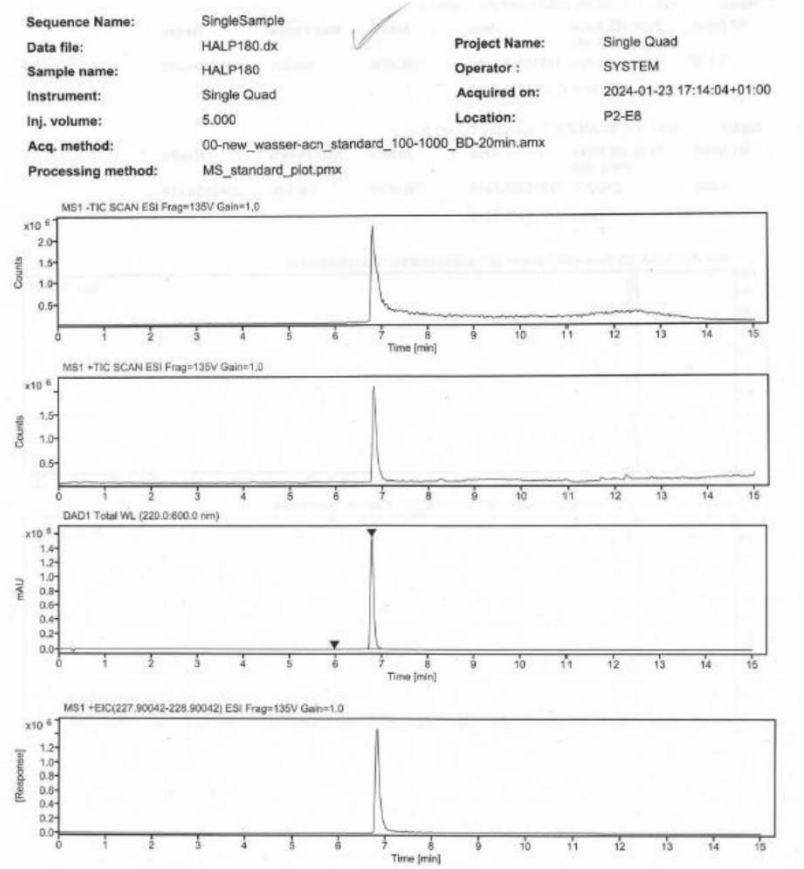

A (s)
8.1178
B (d)
7.0739
C (d)
6.6370
D (s)
5.4334
E (t)
2.7595
F (s)
2.4045
G (h)
1.6045
H (t)
0.9120
f1 (ppm)


f1 (ppm)

S36

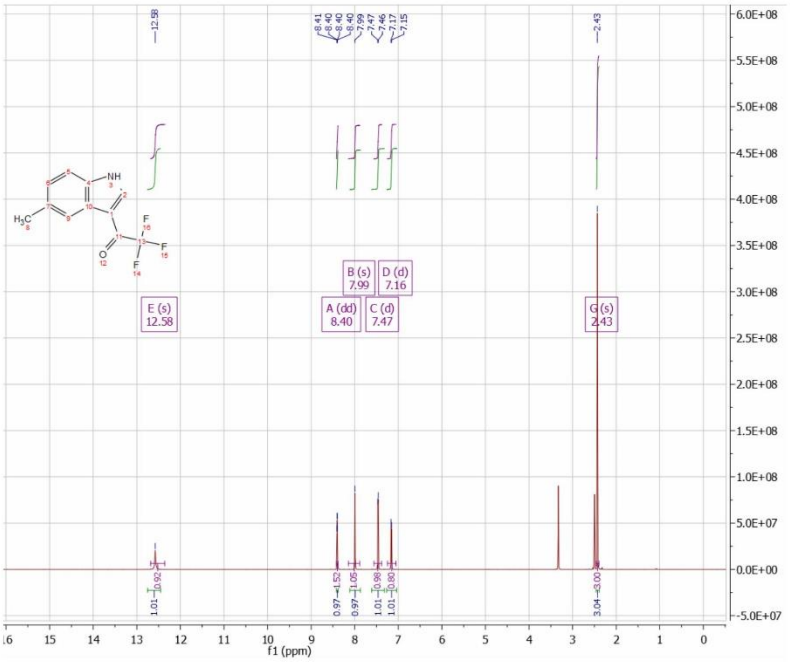
2,2,2-Trifluoro-1-(5-methyl-1*H*-indol-3-yl)ethan-1-one (25).[2] (Yield = 83%)

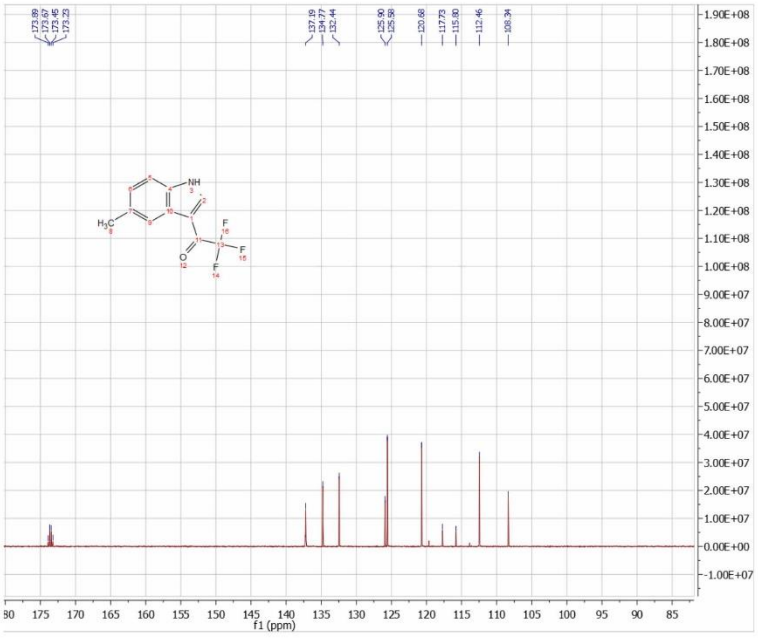
LC-MS (*m*/*z*): positive mode $[M + H]^{1+}$ (Rt) = 228.2 (6.78 min).; purity by HPLC-(220-600 nm)-ESI-MS: 99.8%. mp = 247-248 °C.



Signal: DAD1 Total WL (220.0:600.0 nm)

RT [min]	Peak MS Base Peak m/z	Area	Area%	Max Peak%	Height
5.976		1356.7771	0.1655	0.166	309.462
6.784		818685.2593	99.8345	100.000	155426.287
	Sum	820042.0364			

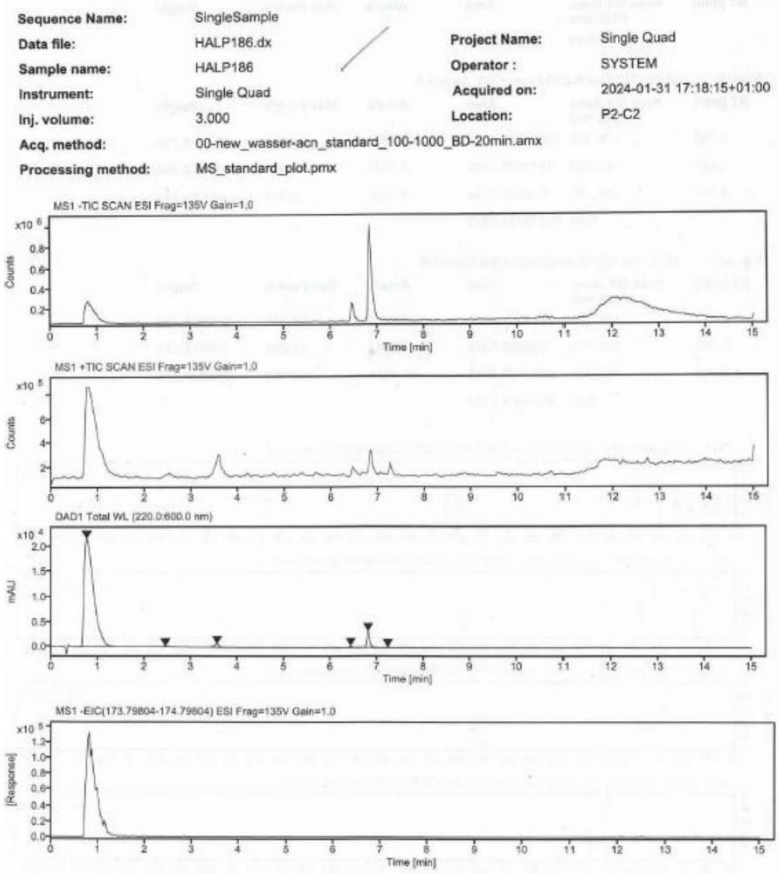

12.58
8.41
8.40
7.99
7.47
7.46
7.17
7.15
2.43
B (s) 7.99
D (d) 7.16
E (s) 12.58
A (dd) 8.40
C (d) 7.47
G (s) 2.43
f1 (ppm)


173.89
173.67
173.45
173.23
137.19
134.77
132.44
125.90
125.59
120.68
117.73
115.80
112.46
108.34
f1 (ppm)

S38

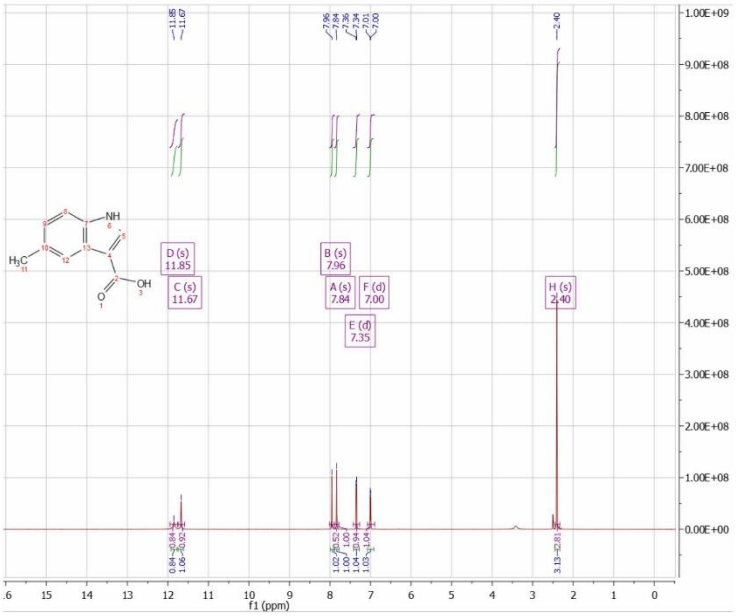
5-Methyl-1*H*-indole-3-carboxylic acid (26).[2] (Yield = 63%)

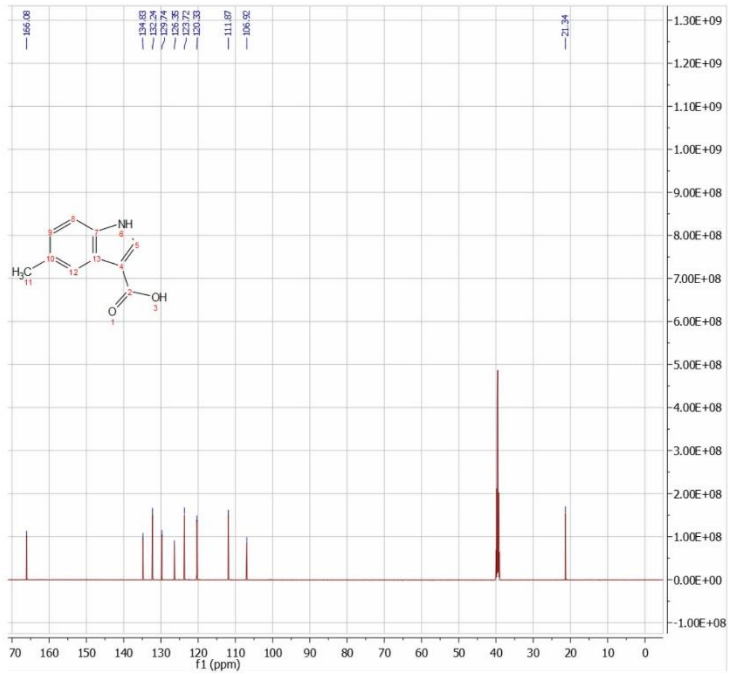
LC-MS (*m*/*z*): positive mode $[M + H]^{1+}$ (Rt) = 176.0 (0.78 min).; purity by HPLC-(220-600 nm)-ESI-MS: 93.0%. mp = 202-203 °C.



Signal: DAD1 Total WL (220.0:600.0 nm)

RT [min]	Peak MS Base Peak m/z	Area	Area%	Max Peak%	Height
0.776	176.100	295975.3522	93.3974	100.000	21414.393
2.465		1166.8049	0.3682	0.394	99.544
3.569	162.000	4559.4560	1.4388	1.540	648.488
6.439		1068.8528	0.3373	0.361	277.933
6.812		13863.3884	4.3747	4.684	3244.790
7.239		265.0439	0.0836	0.090	69.949

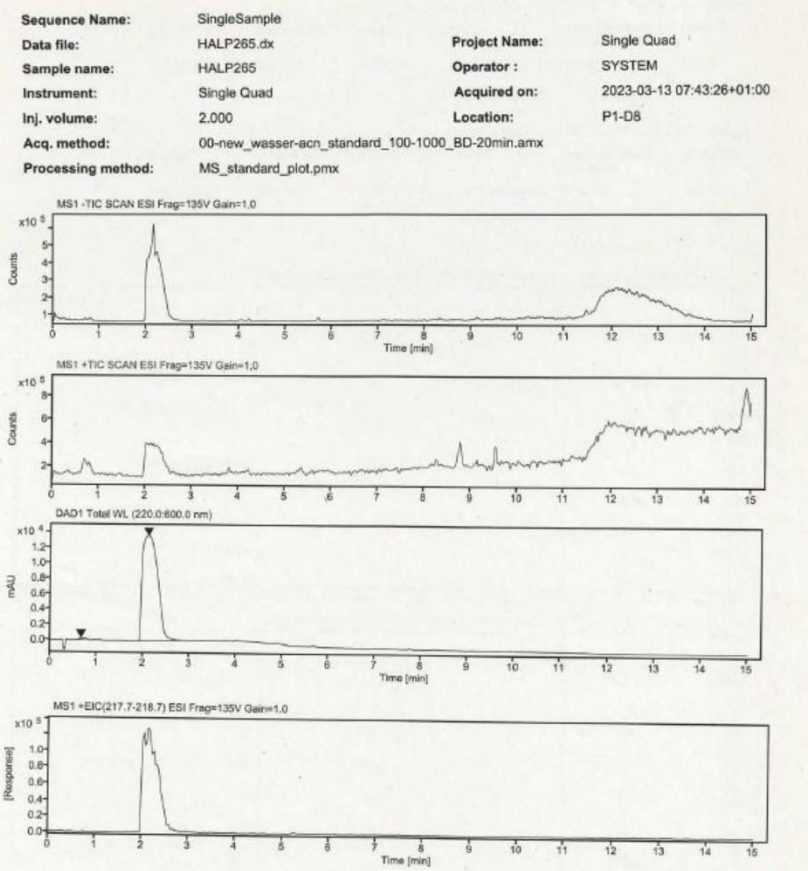




S40

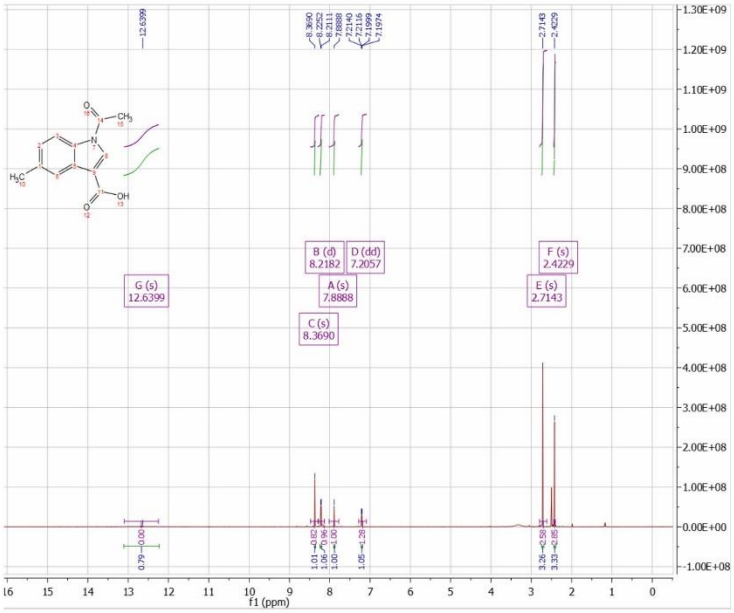
1-Acetyl-5-methyl-1*H*-indole-3-carboxylic acid (27).[2] (Yield 100%).

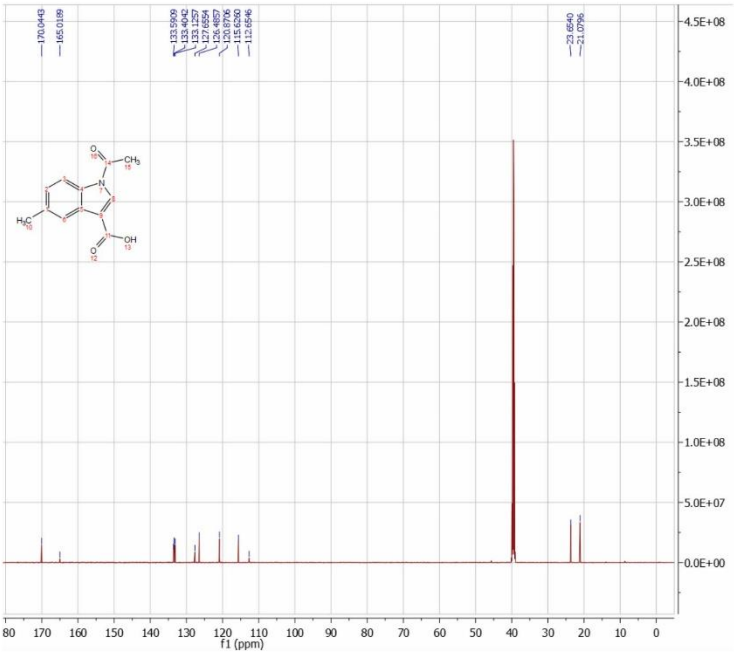
LC-MS (*m*/*z*): positive mode $[M + H]^{1+}$ (Rt) = 218.0 (2.12 min). purity by HPLC-UV(254 nm)-ESI-MS: 99.5%, mp = 238-240 °C.



Signal: DAD1 Total WL (220.0:600.0 nm)

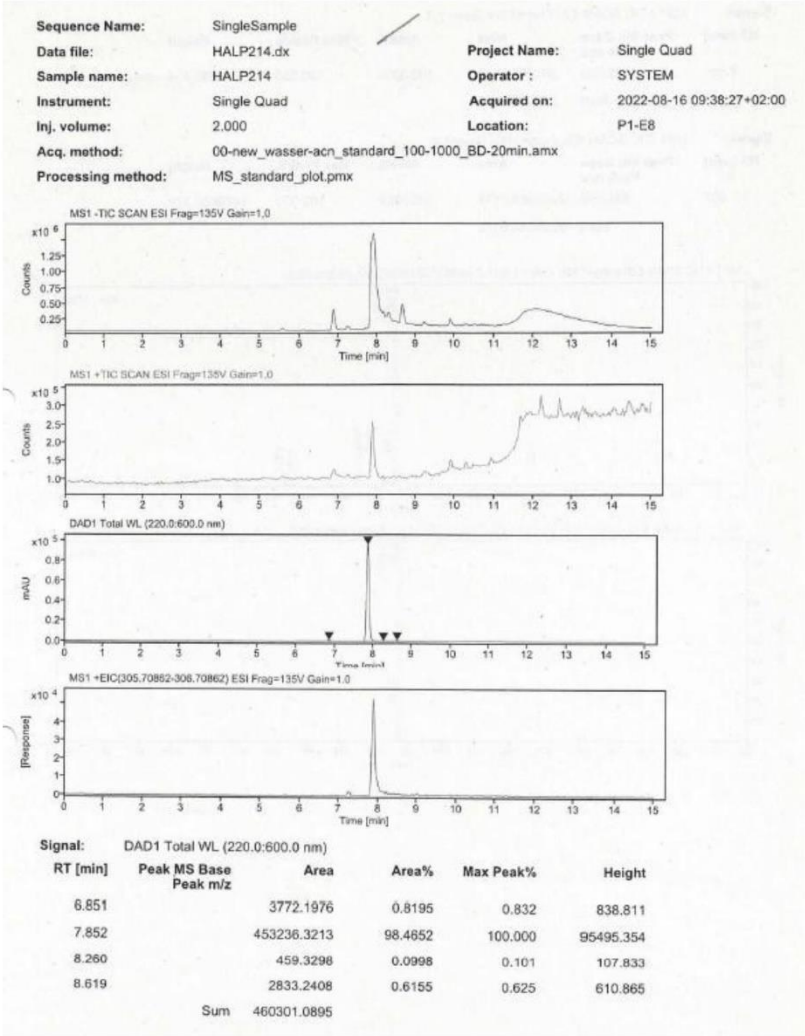
RT [min]	Peak MS Base Peak m/z	Area	Area%	Max Peak%	Height
0.678		1349.7074	0.4347	0.437	236.984
2.118	215.800	309129.4763	99.5653	100.000	13618.555
	Sum	310479.1837			


12.6399
8.3690
8.2552
8.2182
7.8888
7.2214
7.2057
7.1974
2.7148
2.4229
B (d) 8.2182
D (dd) 7.2057
F (s) 2.4229
G (s) 12.6399
A (s) 7.8888
E (s) 2.7143
C (s) 8.3690
f1 (ppm)


170.0443
165.0189
133.5909
133.4042
133.1257
129.6957
126.4657
120.8706
115.6260
112.6546
29.6640
21.0796
f1 (ppm)

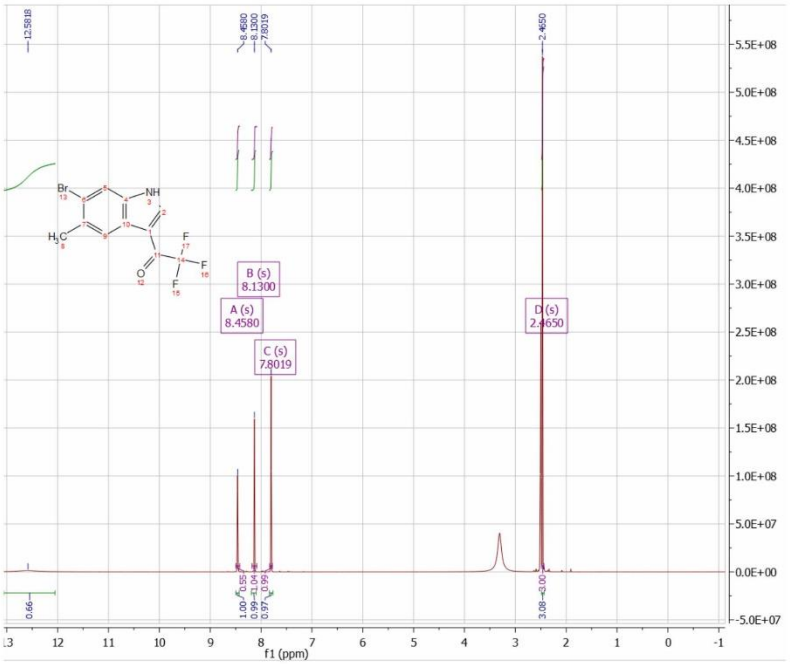
S42

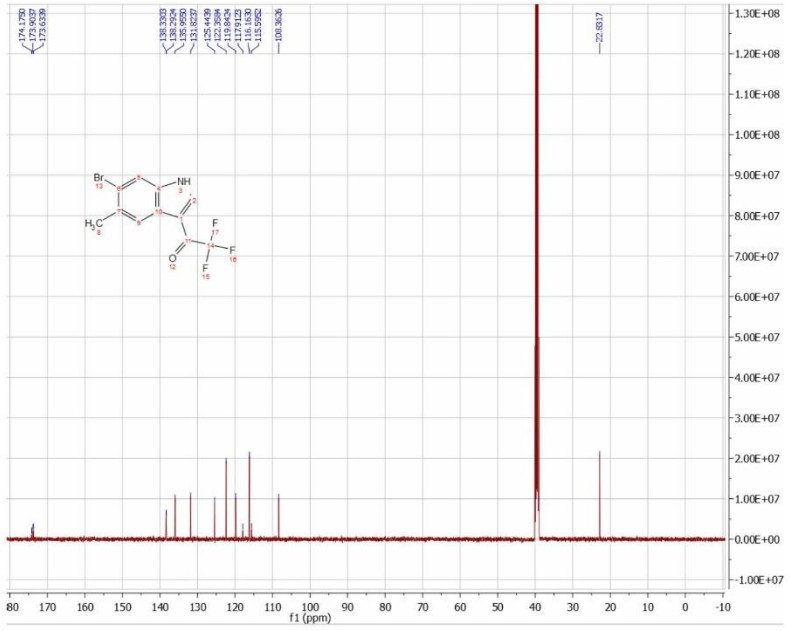
1-(6-Bromo-5-methyl-1*H*-indol-3-yl)-2,2,2-trifluoroethan-1-one (28).[2] (Yield = 89%) LC-MS (*m*/*z*): positive mode $[M + H]^{1+}$ (Rt) = 308.0 (7.85 min).; purity by HPLC-(220-600 nm)-ESI-MS: 98.0%. mp = 271-272 °C.



Signal: DAD1 Total WL (220.0:600.0 nm)

RT [min]	Peak MS Base Peak m/z	Area	Area%	Max Peak%	Height
6.851		3772.1976	0.8195	0.832	838.811
7.852		453236.3213	98.4652	100.000	95495.354
8.260		459.3298	0.0998	0.101	107.833
8.619		2833.2408	0.6155	0.625	610.865
	Sum	460301.0895			

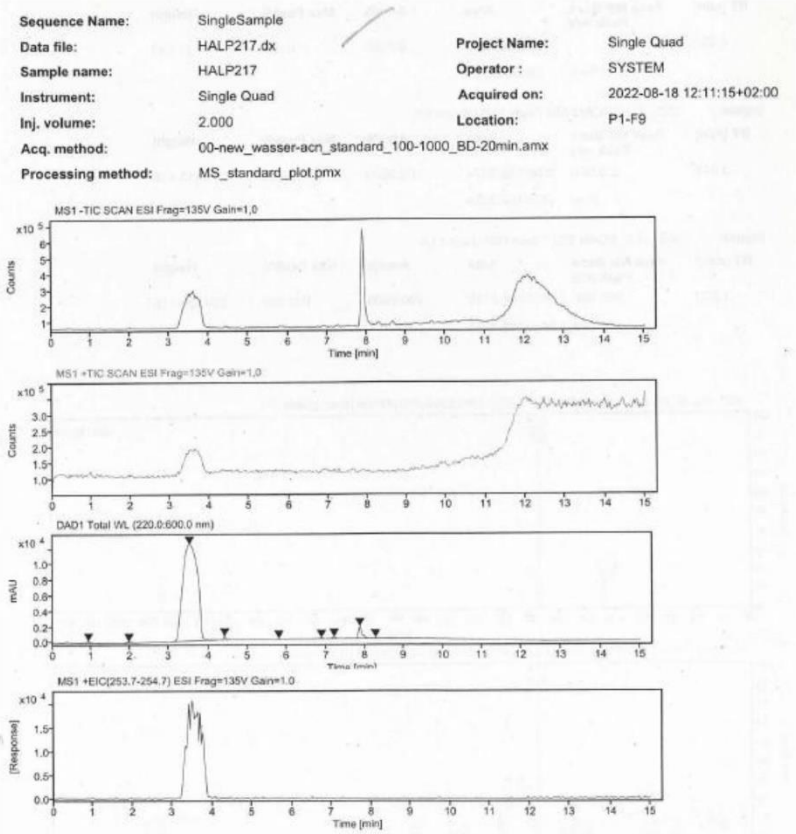

12.5818
8.4580
8.1300
7.8019
2.4650
B (s)
8.1300
A (s)
8.4580
C (s)
7.8019
D (s)
2.4650
f1 (ppm)


174.1797
173.9037
173.6339
138.3303
138.2054
135.9950
131.6237
125.4439
122.3984
119.8424
117.9123
116.1830
115.0952
108.3626
22.8817
f1 (ppm)

S44

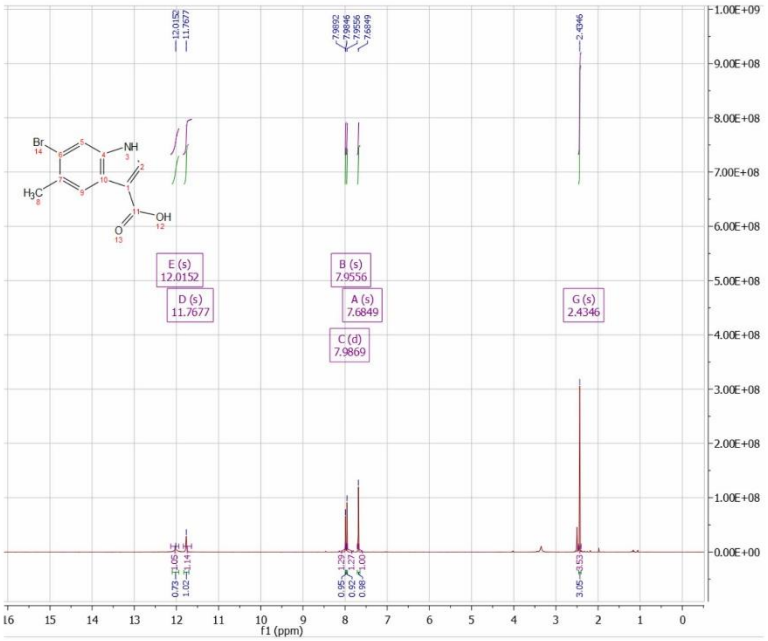
6-Bromo-5-methyl-1*H*-indole-3-carboxylic acid (29).[2] (Yield = 86%)

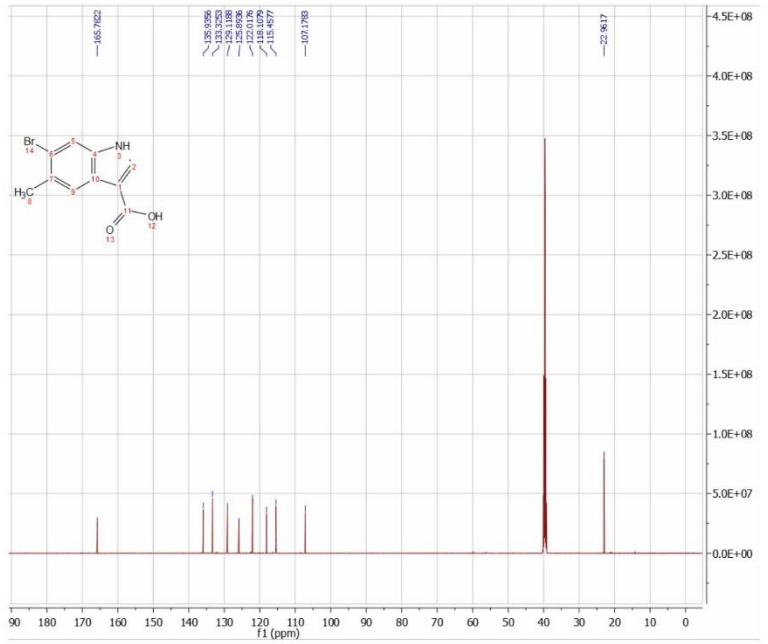
LC-MS (*m*/*z*): positive mode $[M + H]^{1+}$ (Rt) = 255.9 (3.53 min).; purity by HPLC-(220-600 nm)-ESI-MS: 95.0%.



Signal: DAD1 Total WL (220.0:600.0 nm)

RT [min]	Peak MS Base Peak m/z	Area	Area%	Max Peak%	Height
0.934		1367.7148	0.4068	0.426	189.107
1.973		1054.0323	0.3135	0.328	136.297
3.527	253.900	321174.7721	95.5245	100.000	12389.903
4.407		1987.9405	0.5913	0.619	415.026
5.788		224.0915	0.0666	0.070	44.190
6.882		272.3695	0.0810	0.085	57.893
7.204		841.9544	0.2504	0.262	183.204
7.865		9103.5130	2.7076	2.834	1509.513

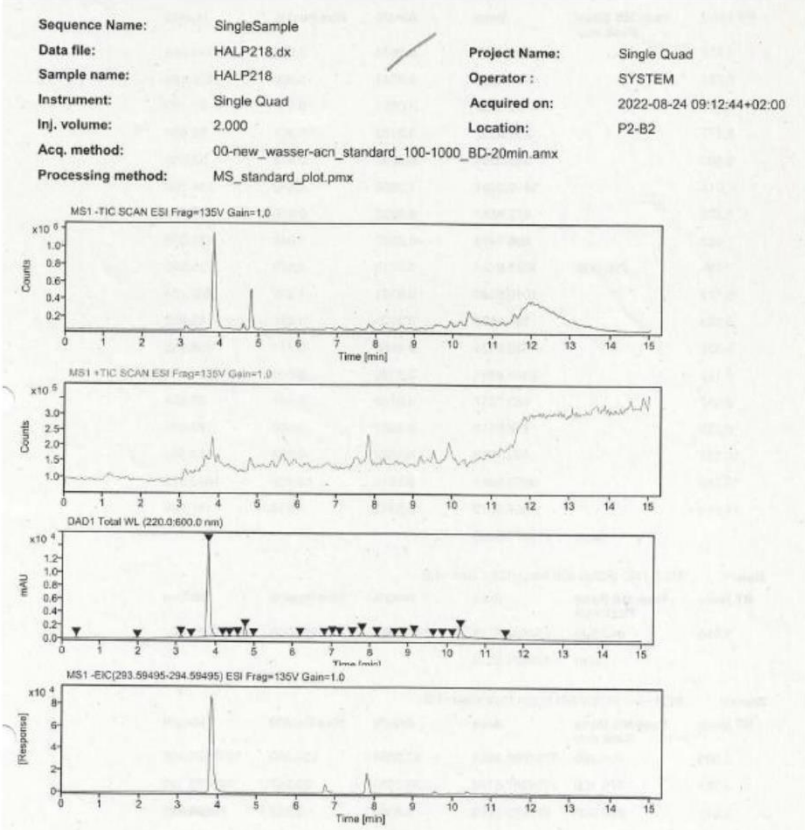

E (s)
12.0152
D (s)
11.7677
B (s)
7.9556
A (s)
7.6849
C (d)
7.9869
G (s)
2.4346
f1 (ppm)


f1 (ppm)

S46

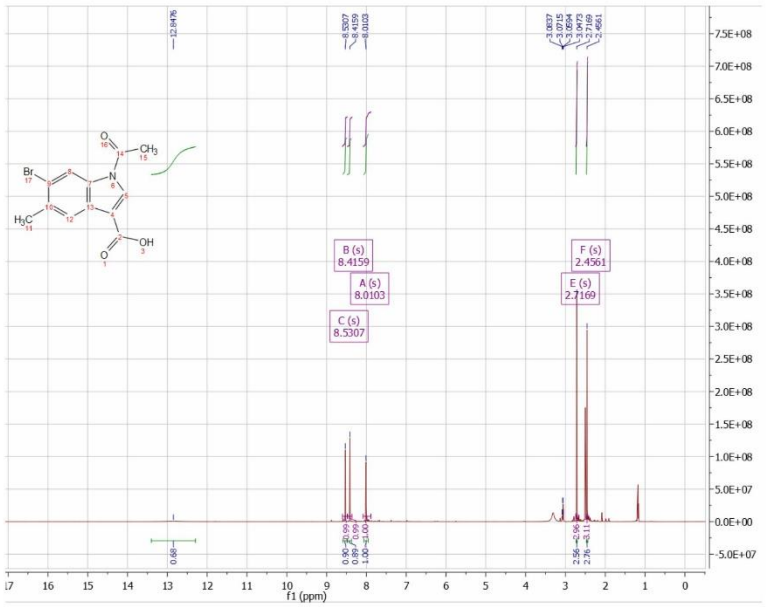
1-Acetyl-6-bromo-5-methyl-1*H*-indole-3-carboxylic acid (30)[2]

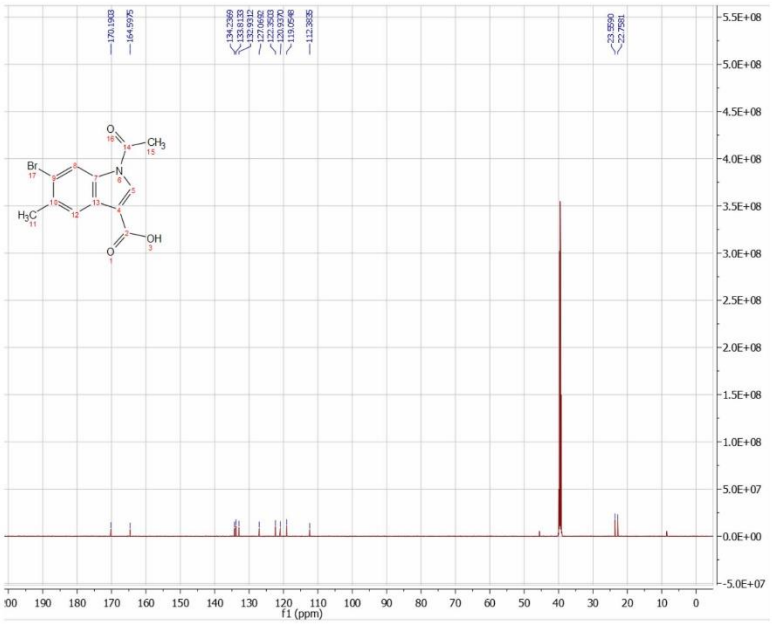
LC-MS (*m*/*z*): positive mode $[M + H]^{1+}$ (Rt) = 297.9 (3.80 min).; purity by HPLC-(220-600 nm)-ESI-MS: 70.0%.



Signal: DAD1 Total WL (220.0:600.0 nm)

RT [min]	Peak MS Base Peak m/z	Area	Area%	Max Peak%	Height
0.377		924.4960	0.8399	1.201	308.588
1.970		686.7178	0.6238	0.892	59.992
3.100		1582.9323	1.4380	2.057	380.604
3.364		167.9143	0.1525	0.218	43.792
3.795		76951.3357	69.9063	100.000	14353.550
4.173		328.4060	0.2983	0.427	101.456
4.350		623.7856	0.5667	0.811	133.859

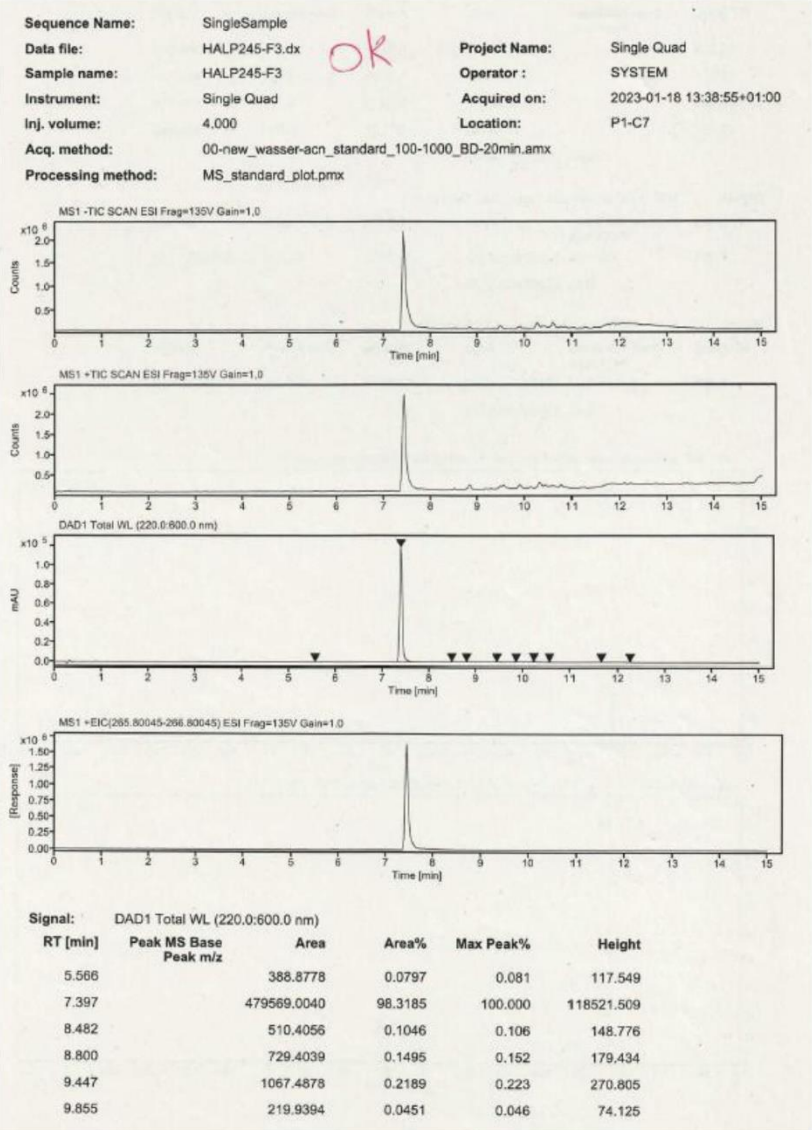




S48

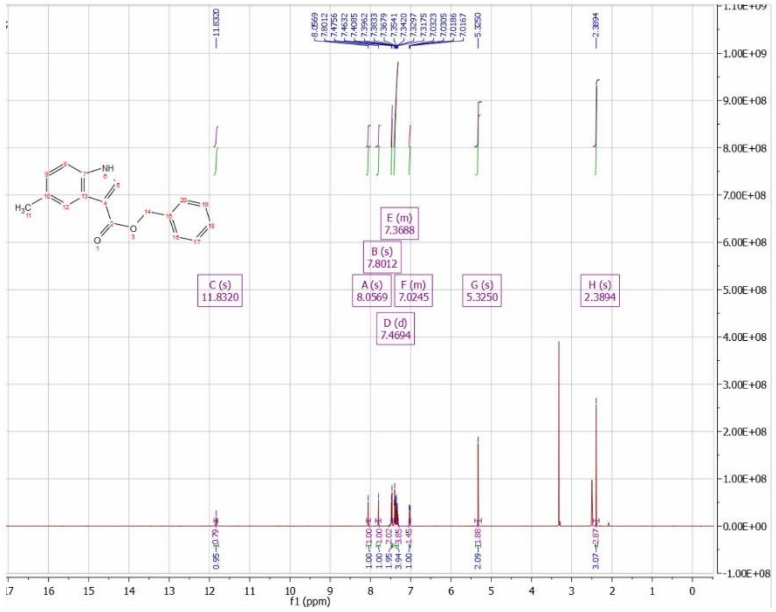
Benzyl 5-methyl-1*H*-indole-3-carboxylate (31) (Yield = 67%) (new compound)-

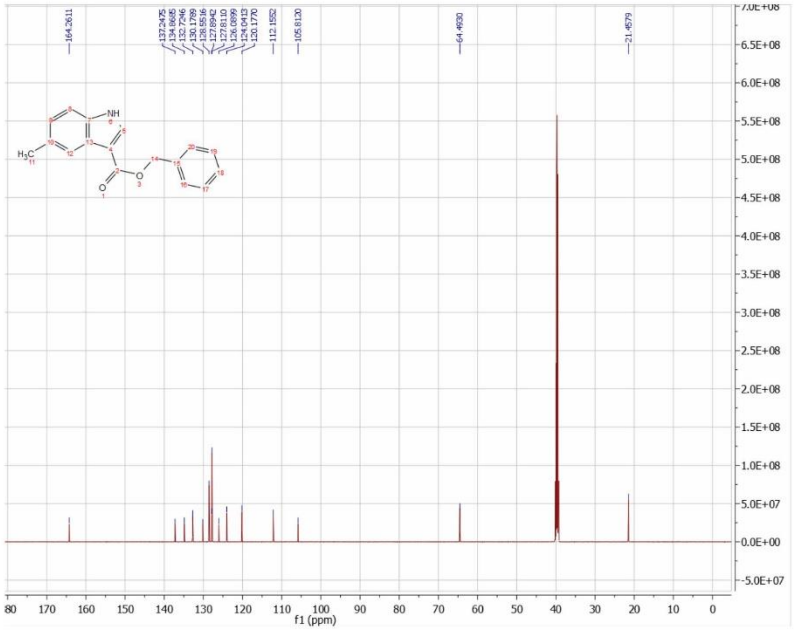
LC-MS (*m*/*z*): positive mode $[M + H]^{1+}$ (Rt) = 266.1 (7.40 min). purity by HPLC-UV(254 nm)-ESI-MS: 98.0%, mp = 165-167 °C.



Signal: DAD1 Total WL (220.0:600.0 nm)

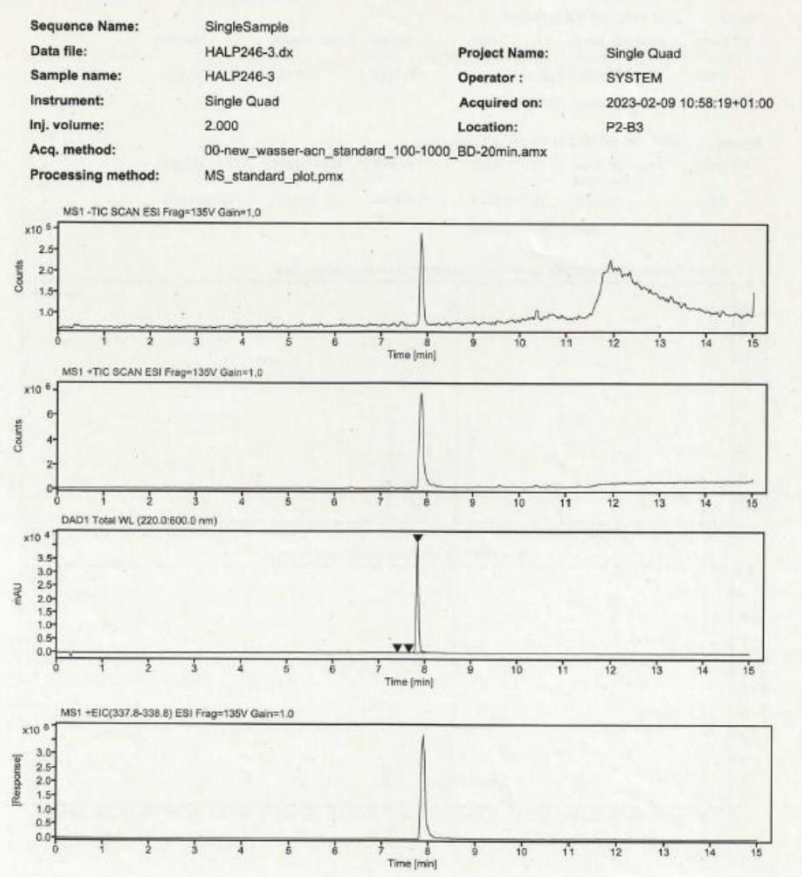
RT [min]	Peak MS Base Peak m/z	Area	Area%	Max Peak%	Height
5.566		388.8778	0.0797	0.081	117.549
7.397		479569.0040	98.3185	100.000	118521.509
8.482		510.4056	0.1046	0.106	148.776
8.800		729.4039	0.1495	0.152	179.434
9.447		1067.4878	0.2189	0.223	270.805
9.855		219.9394	0.0451	0.046	74.125


C (s)
11.8320
A (s)
8.0569
B (s)
7.8012
D (d)
7.4694
E (m)
7.3688
F (m)
7.0245
G (s)
5.3250
H (s)
2.3894
f1 (ppm)


164.2611
137.2425
134.8685
132.7246
131.3788
126.8536
124.0413
120.1770
112.1552
105.8130
64.4930
21.4579
f1 (ppm)

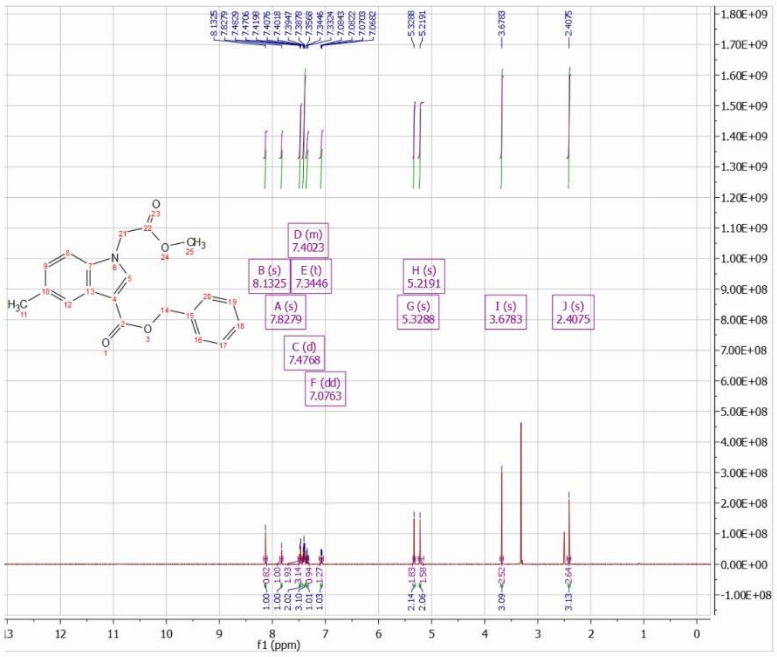
Benzyl 1-(2-methoxy-2-oxoethyl)-5-methyl-1*H*-indole-3-carboxylate (32) (Yield = 68%) (new compound).

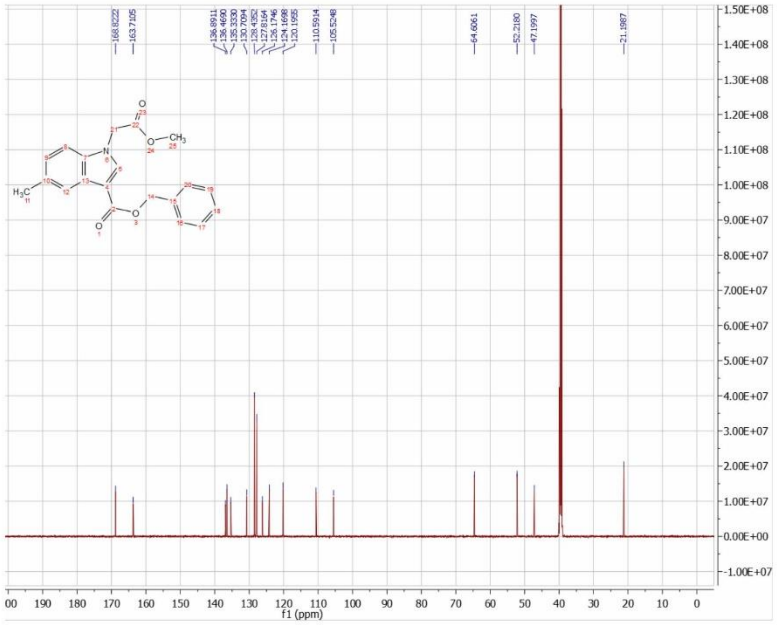
LC-MS (*m*/*z*): positive mode $[M + H]^{1+}$ (Rt) = 338.9 (7.83 min). purity by HPLC-UV-(254 nm)-ESI-MS: 99.9%, mp = 95-97 °C.



Signal: DAD1 Total WL (220.0:600.0 nm)

RT [min]	Peak MS Base Peak m/z	Area	Area%	Max Peak%	Height
7.401		23.0446	0.0157	0.016	7.763
7.650		116.7558	0.0793	0.079	36.573
7.833		147059.9383	99.9050	100.000	40985.553
	Sum	147199.7388			

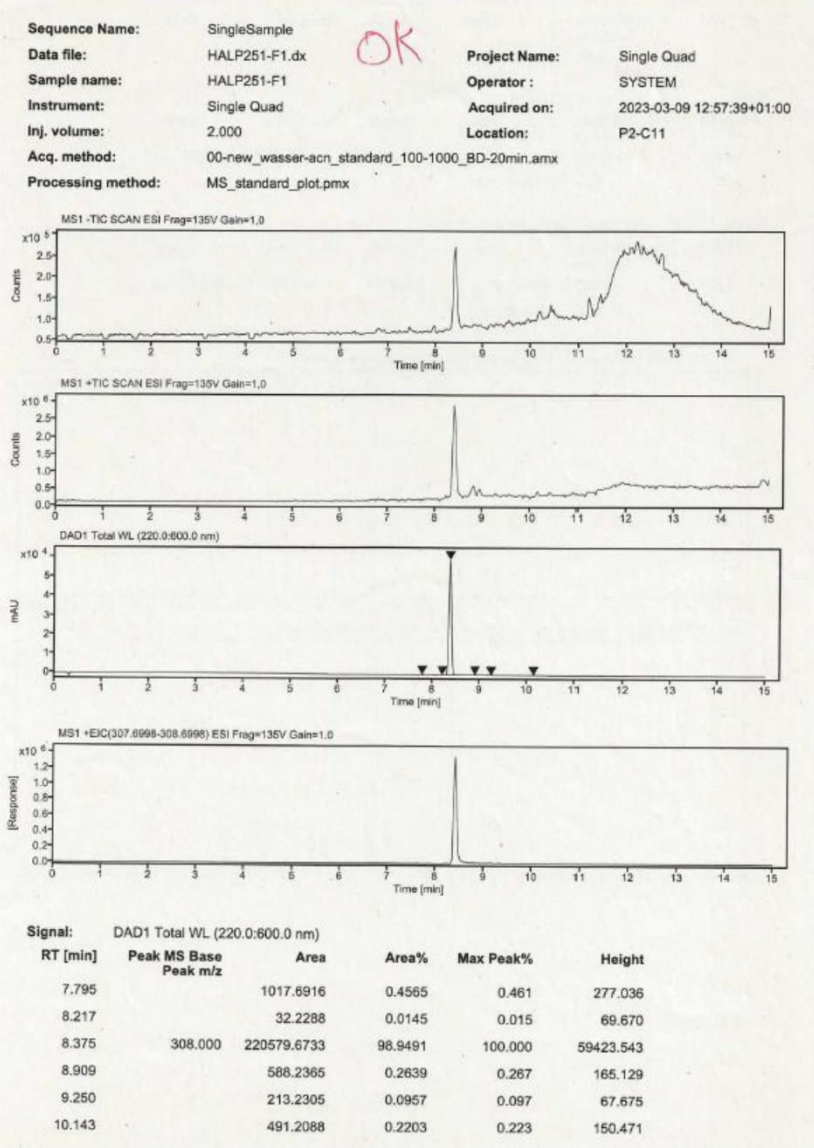

D (m)
7.4023
B (s)
8.1325
E (t)
7.3446
H (s)
5.2191
A (s)
7.8279
G (s)
5.3288
I (s)
3.6783
J (s)
2.4075
C (d)
7.4768
F (dd)
7.0763
f1 (ppm)


f1 (ppm)

S52

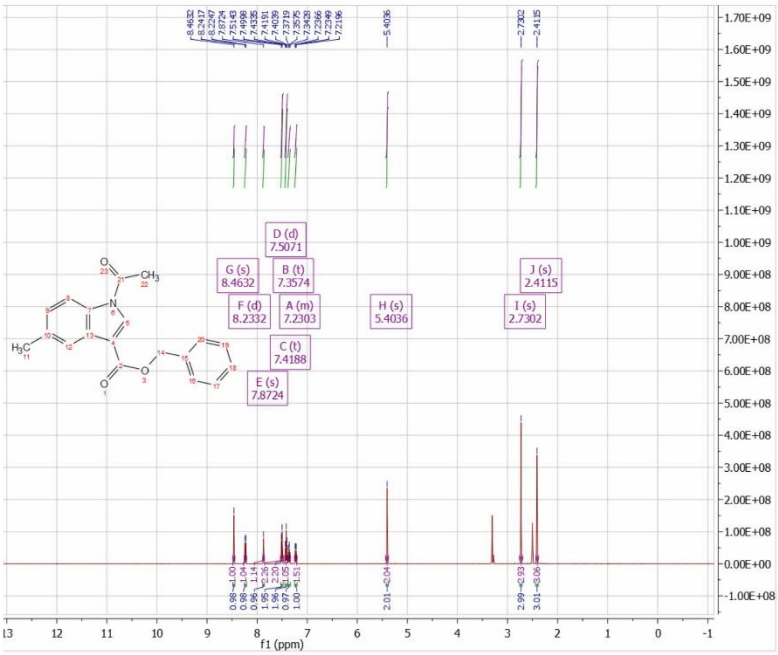
Benzyl 1-acetyl-5-methyl-1*H*-indole-3-carboxylate (33) (Yield = 70%) (new compound).

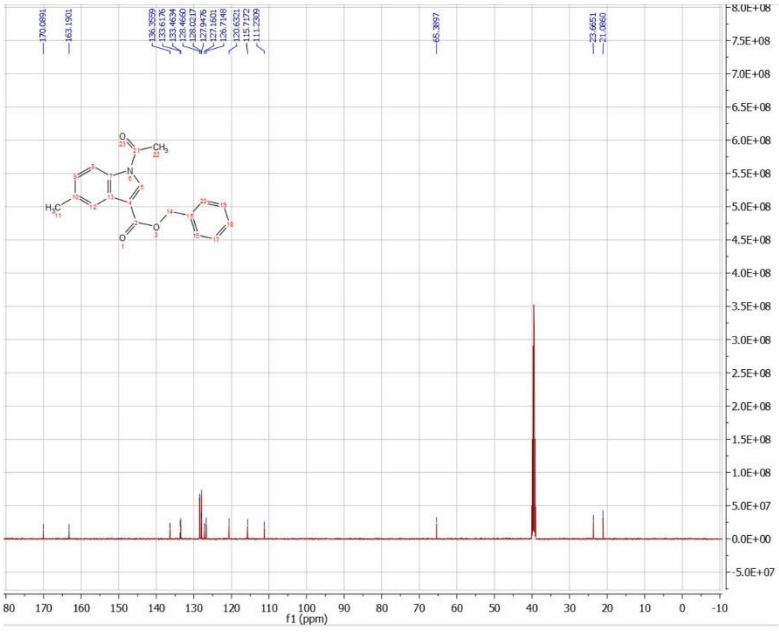
LC-MS (*m*/*z*): positive mode $[M + H]^{1+}$ (Rt) = 308.0 (8.38 min). Purity by HPLC-UV-(254 nm)-ESI-MS: 99.0%, mp = 133-135 °C.



Signal: DAD1 Total WL (220.0:600.0 nm)

RT [min]	Peak MS Base Peak m/z	Area	Area%	Max Peak%	Height
7.795		1017.6916	0.4565	0.461	277.036
8.217		32.2288	0.0145	0.015	69.670
8.375	308.000	220579.6733	98.9491	100.000	59423.543
8.909		588.2365	0.2639	0.267	165.129
9.250		213.2305	0.0957	0.097	67.675
10.143		491.2088	0.2203	0.223	150.471

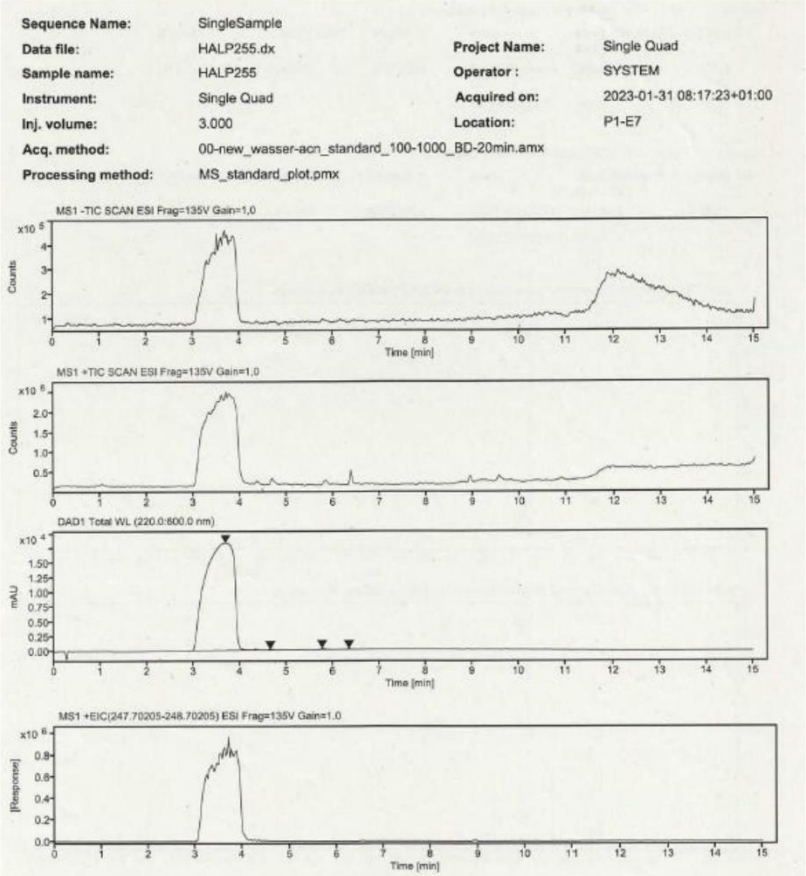

D (d)
7.5071
G (s)
8.4632
B (t)
7.3574
J (s)
2.4115
F (d)
8.2332
A (m)
7.2303
H (s)
5.4036
I (s)
2.7302
C (t)
7.4188
E (s)
7.8724
f1 (ppm)


f1 (ppm)

S54

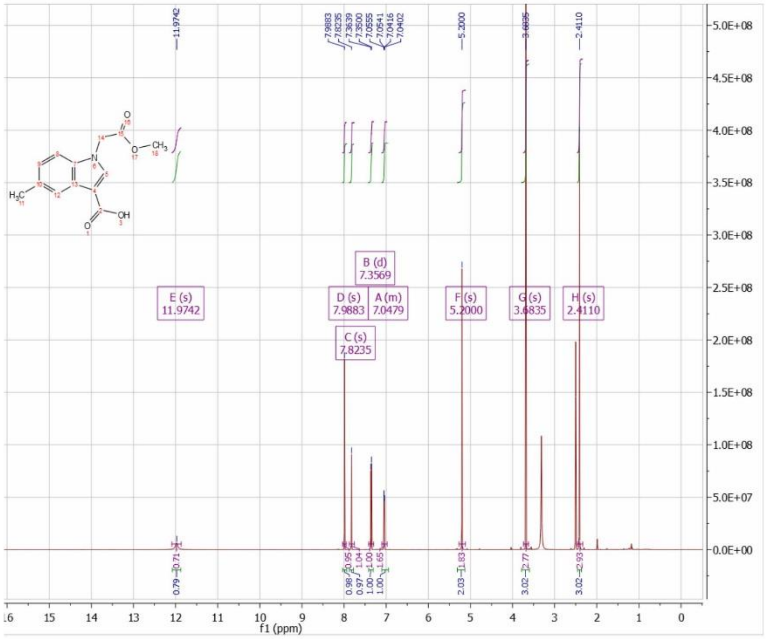
1-(2-Methoxy-2-oxoethyl)-5-methyl-1*H*-indole-3-carboxylic acid (34).[2] (Yield = 100%).

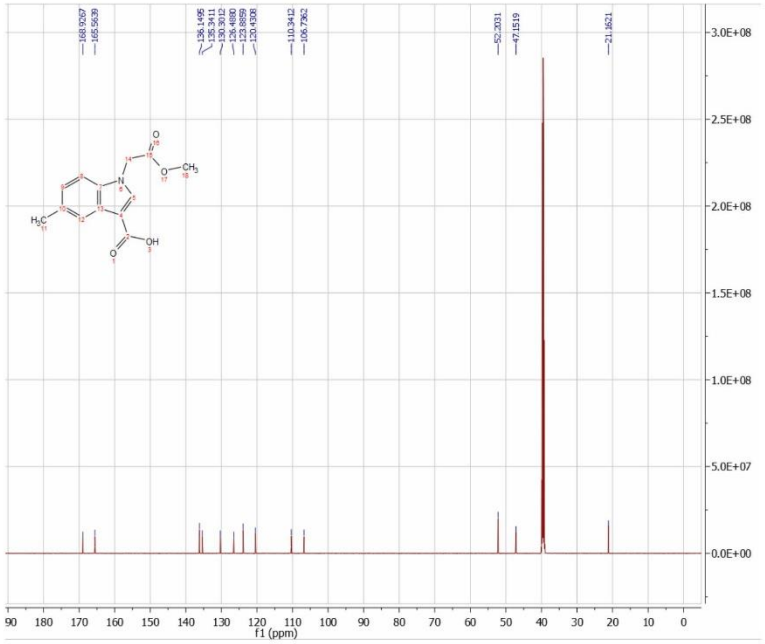
LC-MS (*m*/*z*): positive mode $[M + H]^{1+}$ (Rt) = 248.0 (3.70 min). purity by HPLC-UV-(254 nm)-ESI-MS: 99.7%, mp = 220-222 °C.



Signal: DAD1 Total WL (220.0:600.0 nm)

RT [min]	Peak MS Base Peak m/z	Area	Area%	Max Peak%	Height
3.704	248.000	773620.4375	99.7474	100.000	18230.686
4.660		525.1120	0.0677	0.068	109.565
5.776		989.6152	0.1276	0.128	194.689
6.353		444.5642	0.0573	0.057	137.224
	Sum	775579.7288			

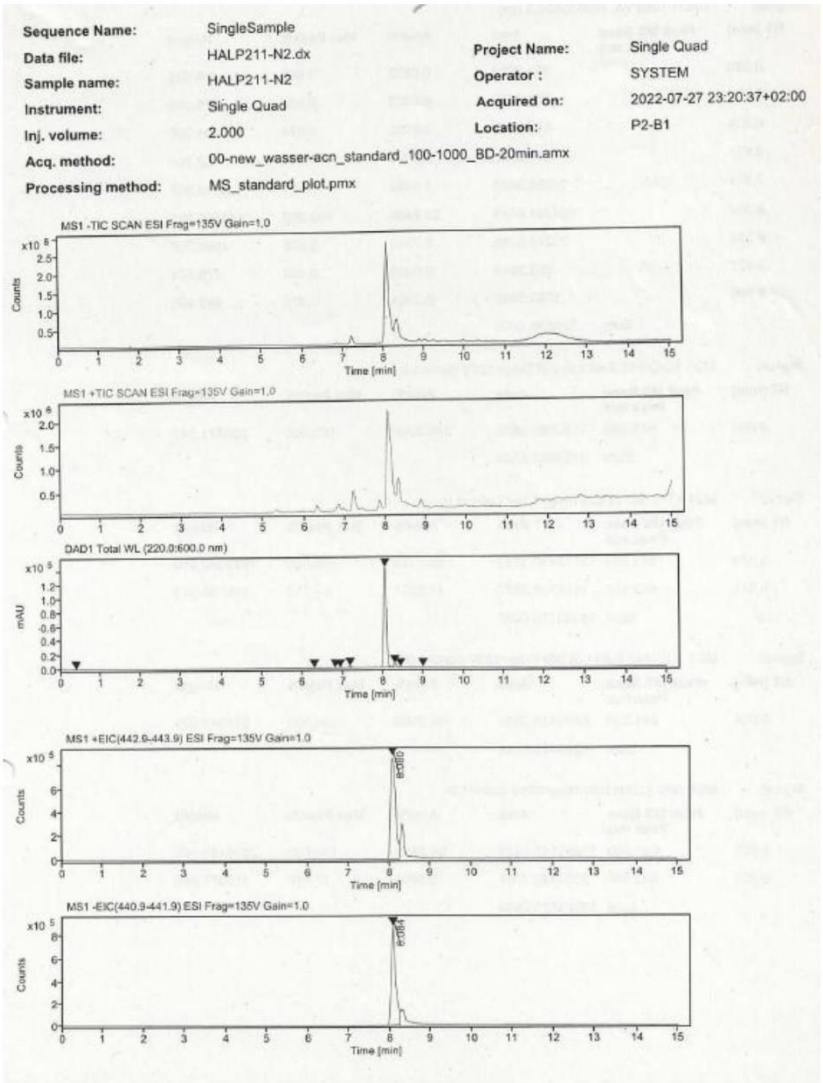

11.9742
7.9883
7.8235
7.3839
7.3569
7.0659
7.0541
7.0479
7.0402
5.2000
3.6835
2.4110
B (d)
7.3569
E (s)
11.9742
D (s)
7.9883
A (m)
7.0479
C (s)
7.8235
F (s)
5.2000
G (s)
3.6835
H (s)
2.4110
f1 (ppm)


168.9267
165.5639
136.1495
135.3411
130.3913
126.4680
123.8899
120.4308
110.3412
106.7362
52.2031
47.1519
21.1621
f1 (ppm)

S56

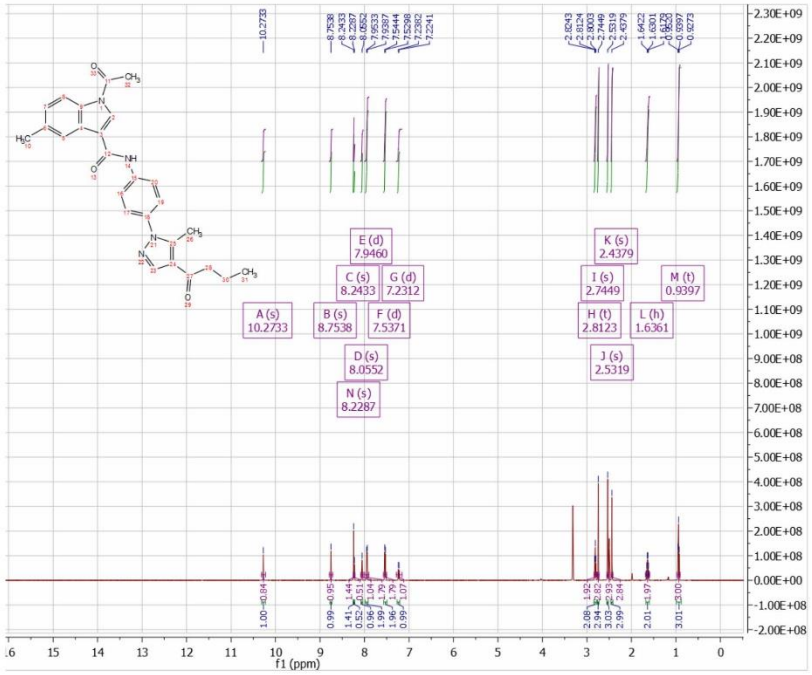
1-Acetyl-*N*-(4-(4-butyryl-5-methyl-1*H*-pyrazol-1-yl)phenyl)-5-methyl-1*H*-indole-3-carboxamide (35).[2] (Yield = 40%)

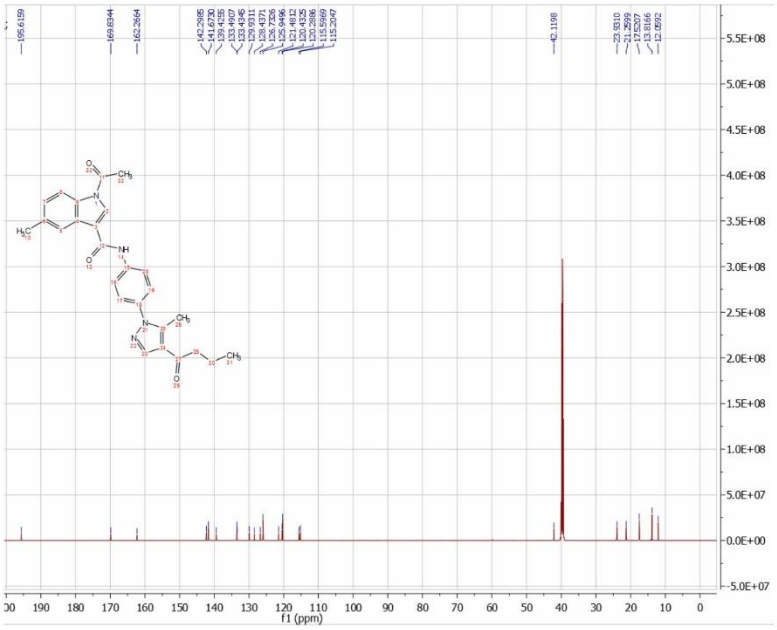
LC-MS (*m*/*z*): positive mode $[M + H]^{1+}$ (Rt) = 443.3 (8.05 min).; purity by HPLC-(220-600 nm)-ESI-MS: 97.0%.



Signal: DAD1 Total WL (220.0:600.0 nm)

RT [min]	Peak MS Base Peak m/z	Area	Area%	Max Peak%	Height
0.386		381.3221	0.0523	0.055	169.508
6.282		658.0169	0.0903	0.095	175.295
6.804		513.7240	0.0705	0.074	131.207
6.931		234.2735	0.0321	0.034	67.108
7.174		10556.9488	1.4484	1.521	2519.007
8.050		694261.6478	95.2496	100.000	143546.085
8.282		20274.5085	2.7816	2.920	4960.206
8.427		253.3649	0.0348	0.036	179.771
8.989		1752.5945	0.2404	0.252	485.996
	Sum	728886.4009			

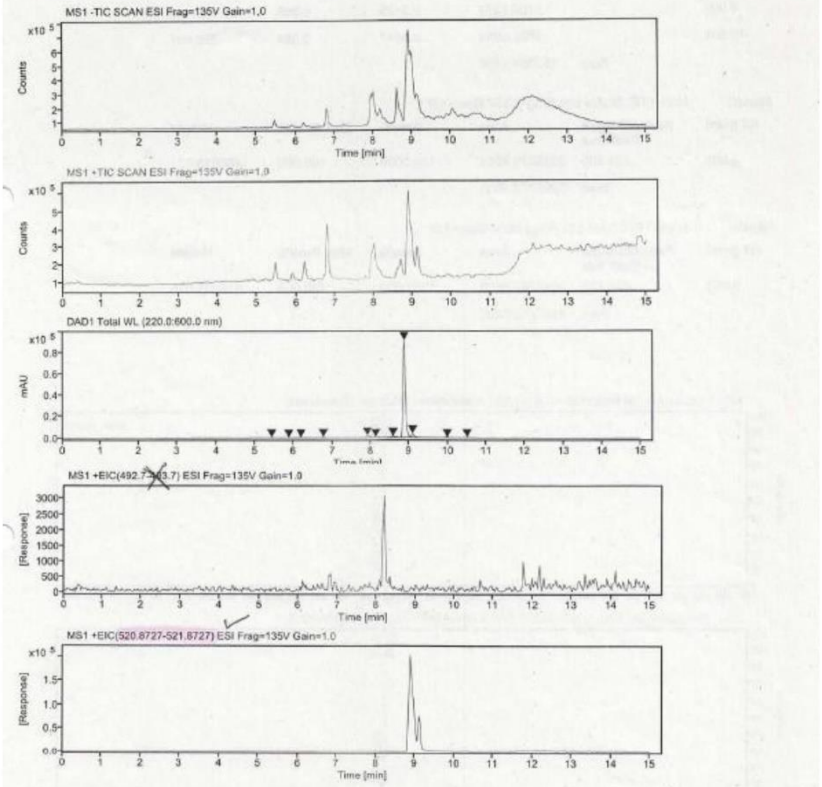




1-Acetyl-6-bromo-*N*-(4-(4-butyryl-5-methyl-1*H*-pyrazol-1-yl)phenyl)-5-methyl-1*H*-indole-3-carboxamide (36).[2] (Yield = 59%)

LC-MS (*m*/*z*): positive mode $[M + H]^{1+}$ (Rt) = 523.2 (8.90 min).; purity by HPLC-(220-600 nm)-ESI-MS: 95.0%.

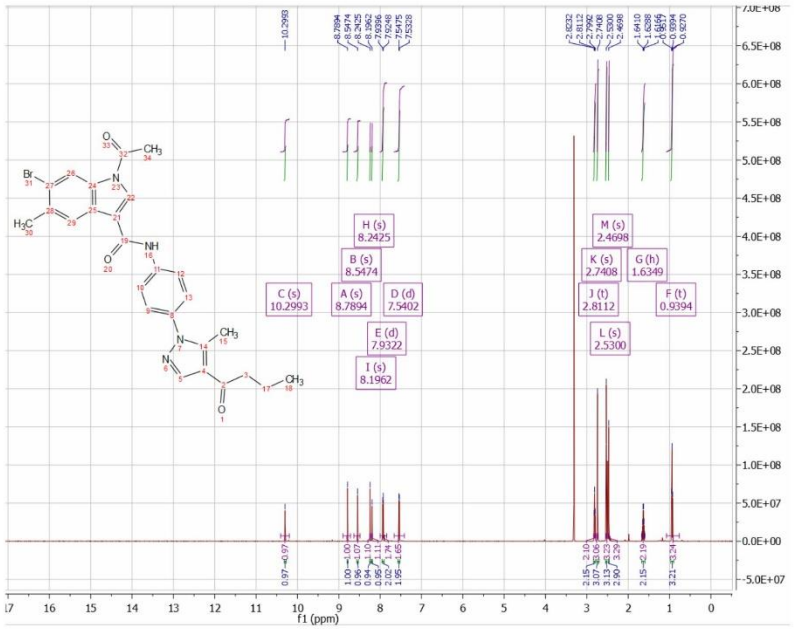
Sequence Name:	SingleSample		
Data file:	HALP220-F2.dx	**Project Name:**	Single Quad
Sample name:	HALP220-F2	**Operator :**	SYSTEM
Instrument:	Single Quad	**Acquired on:**	2022-09-07 08:29:50+02:00
Inj. volume:	2.000	**Location:**	P1-D11
Acq. method:	00-new_wasser-acn_standard_100-1000_BD-20min.amx		
Processing method:	MS_standard_plot.pmx		

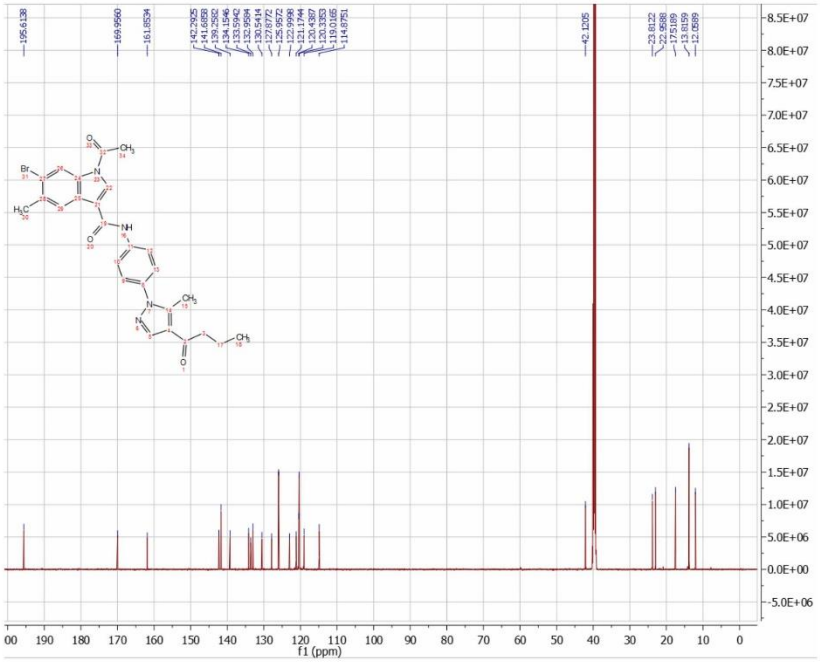


Signal: DAD1 Total WL (220.0:600.0 nm)

RT [min]	Peak MS Base Peak m/z	Area	Area%	Max Peak%	Height
5.432		1209.6615	0.2665	0.291	318.464
5.871		293.1048	0.0646	0.071	79.179
6.187		736.3860	0.1622	0.177	157.980

RT [min]	Peak MS Base Peak m/z	Area	Area%	Max Peak%	Height
6.765		1465.4360	0.3229	0.353	387.469
7.907		9866.2193	2.1738	2.376	1552.110
8.131		443.6171	0.0977	0.107	145.031
8.578		6053.0134	1.3337	1.458	1192.953
8.866		415300.1471	91.5039	100.000	90888.977
9.091		15796.0998	3.4804	3.804	3391.927
9.989		1100.7372	0.2425	0.265	198.449
10.504		1596.0944	0.3517	0.384	296.697
	Sum	453860.5166			

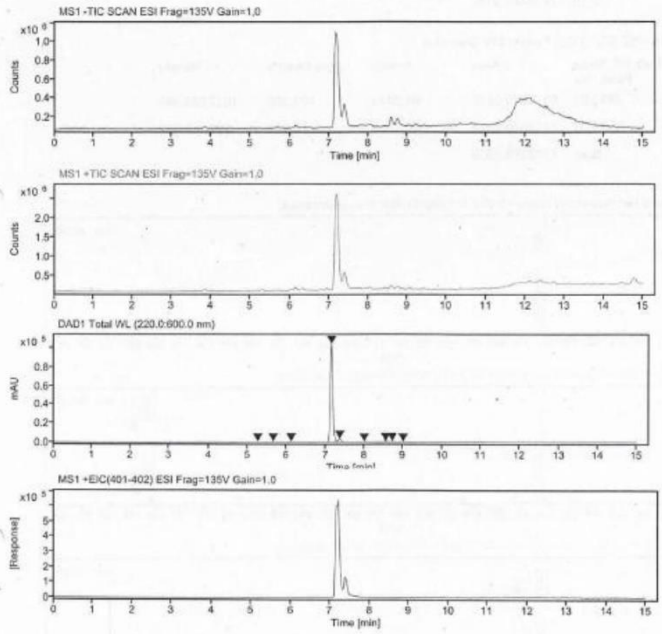




***N*-(4-(4-Butyryl-5-methyl-1*H*-pyrazol-1-yl)phenyl)-5-methyl-1*H*-indole-3-carboxamide (37)**.[2] (Yield = 94%)

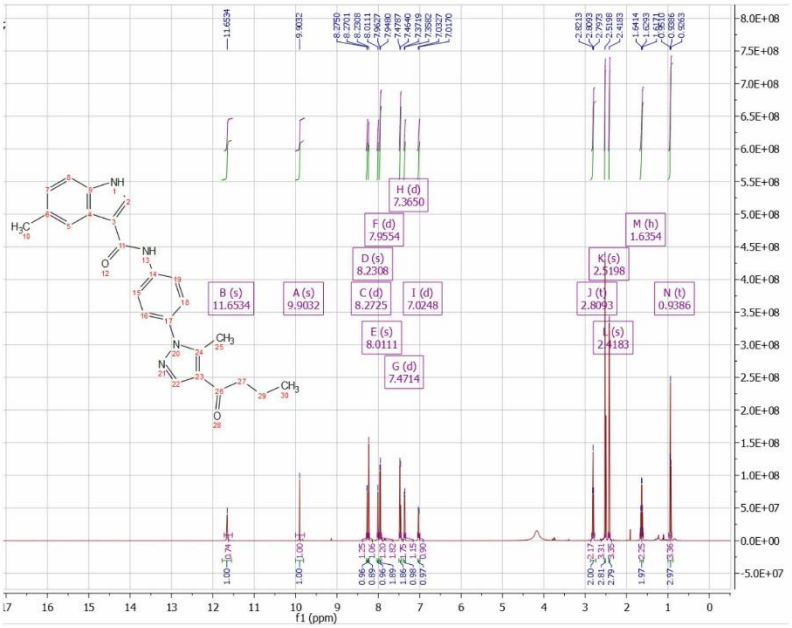
LC-MS (*m*/*z*): positive mode $[M + H]^{1+}$ (Rt) = 401.3 (7.20 min).; purity by HPLC-(220-600 nm)-ESI-MS: 98.0%.

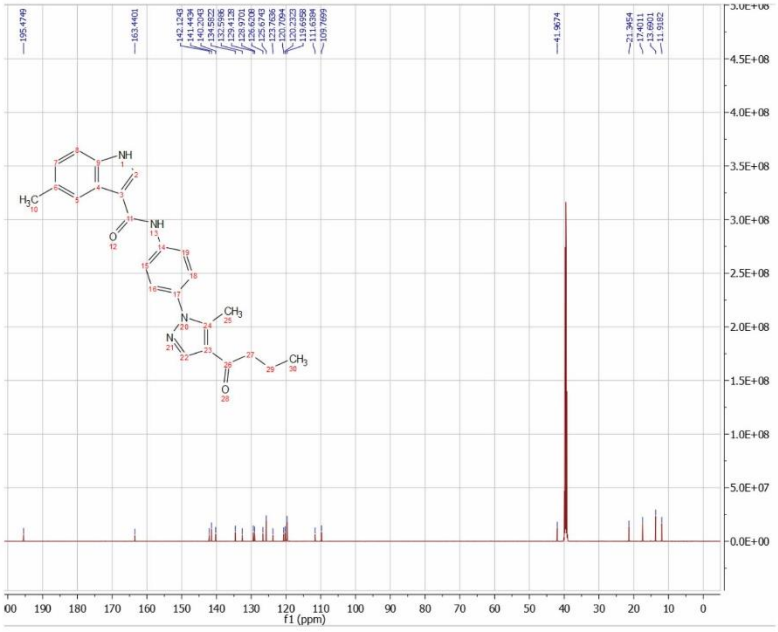
Sequence Name:	SingleSample		
Data file:	HALP213.dx	**Project Name:**	Single Quad
Sample name:	HALP213	**Operator :**	SYSTEM
Instrument:	Single Quad	**Acquired on:**	2022-08-16 09:59:30+02:00
Inj. volume:	2.000	**Location:**	P1-E9
Acq. method:	00-new_wasser-acn_standard_100-1000_BD-20min.amx		
Processing method:	MS_standard_plot.pmx		



Signal: DAD1 Total WL (220.0:600.0 nm)

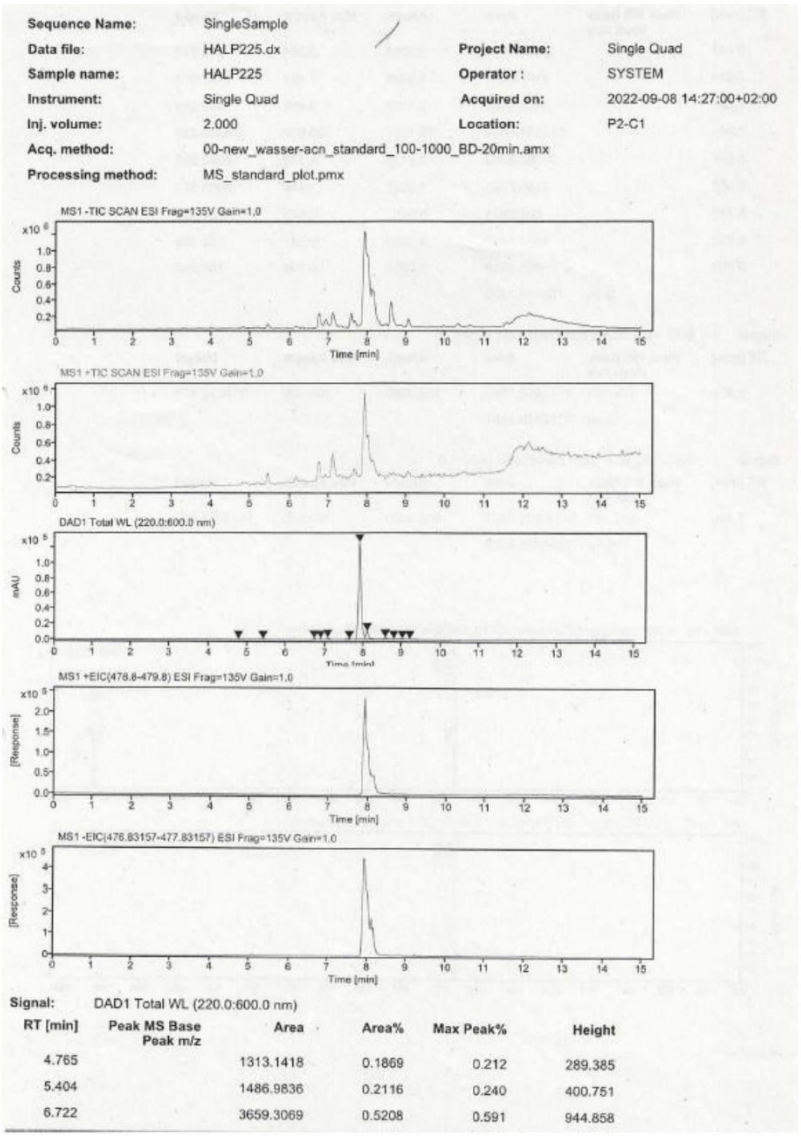
RT [min]	Peak MS Base Peak m/z	Area	Area%	Max Peak%	Height
5.262		261.1824	0.0525	0.055	68.463
5.655		804.2530	0.1615	0.169	168.914
6.120		1503.5673	0.3019	0.316	258.048
7.156	399.200	476114.5456	95.6129	100.000	104705.198
7.366		15105.7914	3.0335	3.173	2970.873
7.999		772.8154	0.1552	0.162	99.246
8.550		1719.9781	0.3454	0.361	426.914
8.720		1334.4321	0.2680	0.280	311.491
9.006		344.1781	0.0691	0.072	91.905


B (s)
11.6534
A (s)
9.9032
H (d)
7.3650
F (d)
7.9554
D (s)
8.2308
C (d)
8.2725
I (d)
7.0248
E (s)
8.0111
G (d)
7.4714
M (h)
1.6354
K (s)
2.5198
J (t)
2.8093
L (s)
2.4183
N (t)
0.9386
f1 (ppm)


f1 (ppm)

6-Bromo-*N*-(4-(4-butyryl-5-methyl-1*H*-pyrazol-1-yl)phenyl)-5-methyl-1*H*-indole-3-carboxamide (38).[2] (Yield = 91%)

LC-MS (*m*/*z*): positive mode $[M + H]^{1+}$ (Rt) = 481.1 (7.90 min).; purity by HPLC-(220-600 nm)-ESI-MS: 95.0%.

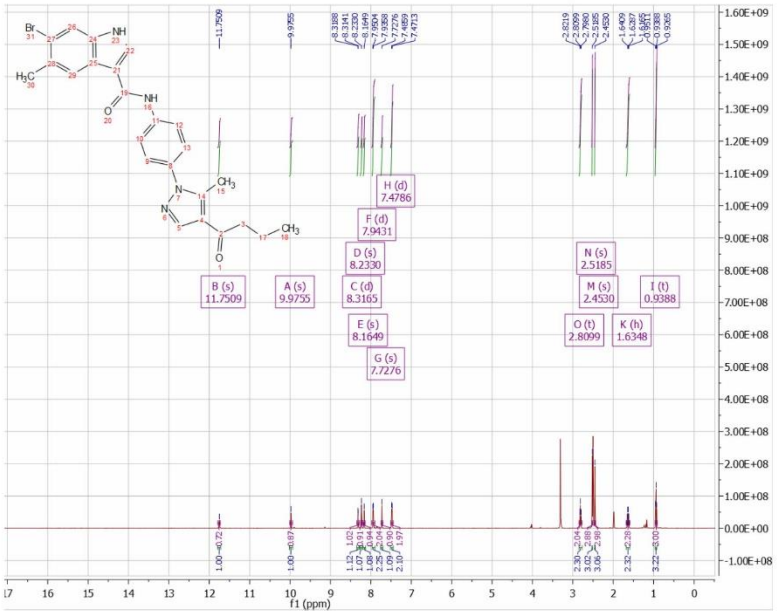


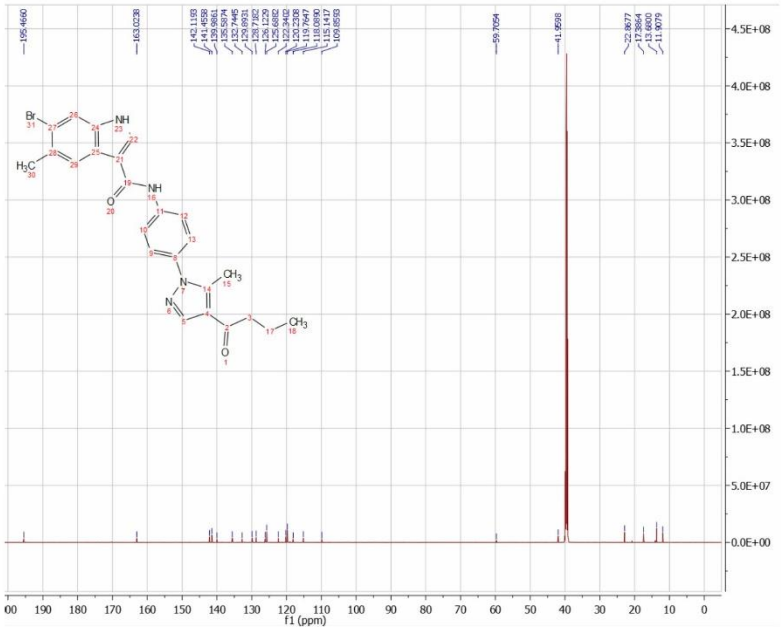
Signal: DAD1 Total WL (220.0:600.0 nm)

RT [min]	Peak MS Base Peak m/z	Area	Area%	Max Peak%	Height
4.765		1313.1418	0.1869	0.212	289.385
5.404		1486.9836	0.2116	0.240	400.751
6.722		3659.3069	0.5208	0.591	944.858

S65

RT [min]	Peak MS Base Peak m/z	Area	Area%	Max Peak%	Height
6.887		2312.7174	0.3292	0.374	616.710
7.077		9167.6051	1.3048	1.481	1992.014
7.636		3037.4408	0.4323	0.491	380.249
7.894		619184.6869	88.1277	100.000	126343.223
8.098		50682.2362	7.2135	8.185	10392.240
8.565		9152.7765	1.3027	1.478	2005.372
8.785		464.7121	0.0661	0.075	109.654
9.012		1469.9337	0.2092	0.237	352.386
9.203		668.1918	0.0951	0.108	165.042
	Sum	702599.7328			

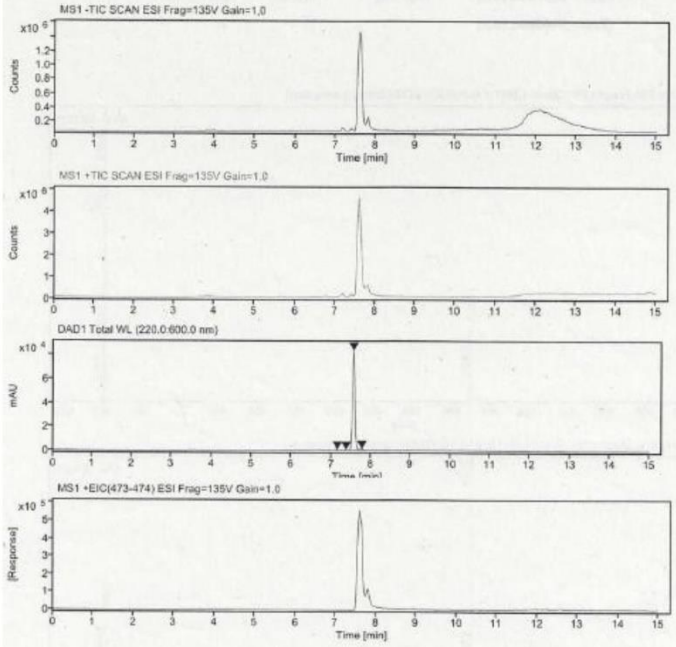




Methyl 2-(3-((4-(4-butyryl-5-methyl-1*H*-pyrazol-1-yl)phenyl)carbamoyl)-5-methyl-1*H*-indol-1-yl)acetate (39).[2] (Yield = 72% (*N*-alkylation), 82% (amide coupling))

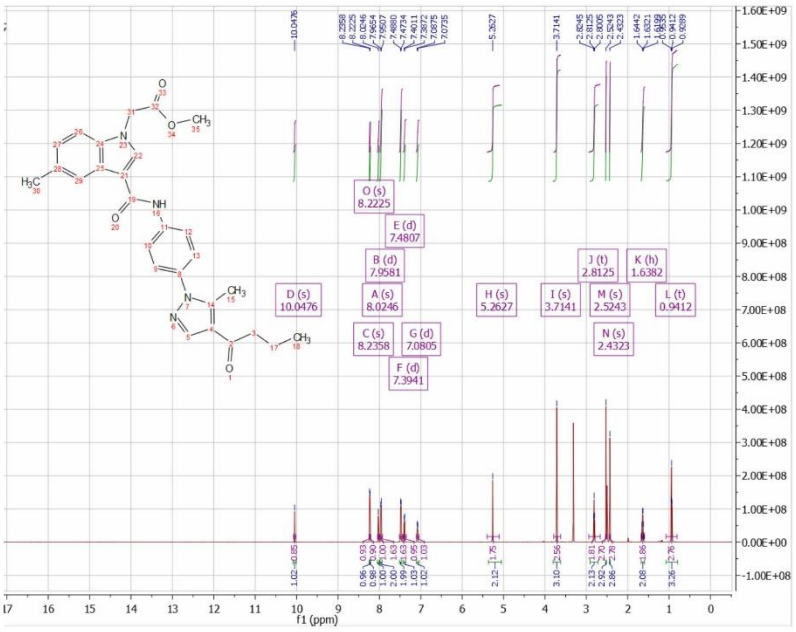
LC-MS (*m*/*z*): positive mode $[M + H]^{1+}$ (Rt) = 473.3 (7.57 min); purity by HPLC-(220-600 nm)-ESI-MS: 98.0%. mp = 210-212 °C. (Literature mp = 210 °C).[1]

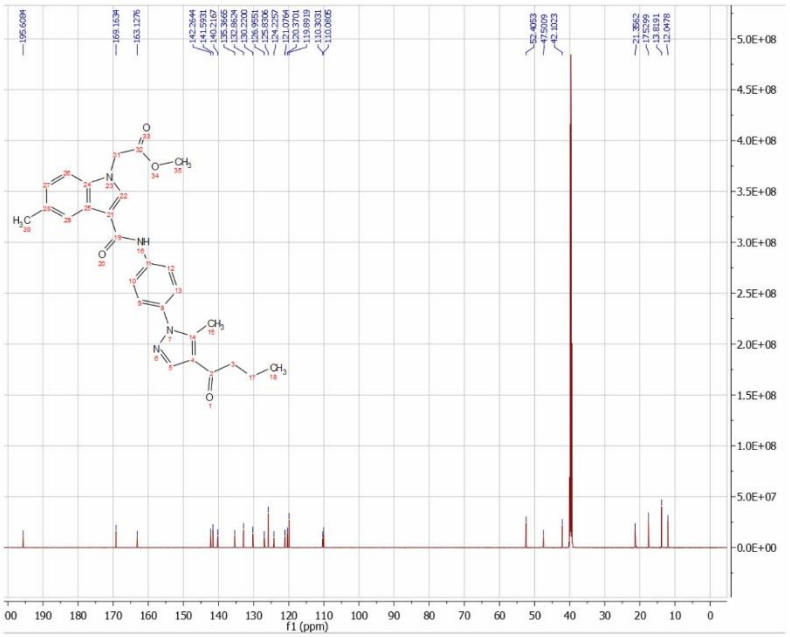
Sequence Name:	SingleSample		
Data file:	HALP216-F1.dx	**Project Name:**	Single Quad
Sample name:	HALP216-F1	**Operator :**	SYSTEM
Instrument:	Single Quad	**Acquired on:**	2022-08-24 09:33:42+02:00
Inj. volume:	2.000	**Location:**	P2-B3
Acq. method:	00-new_wasser-acn_standard_100-1000_BD-20min.amx		
Processing method:	MS_standard_plot.pmx		



Signal: DAD1 Total WL (220.0:600.0 nm)

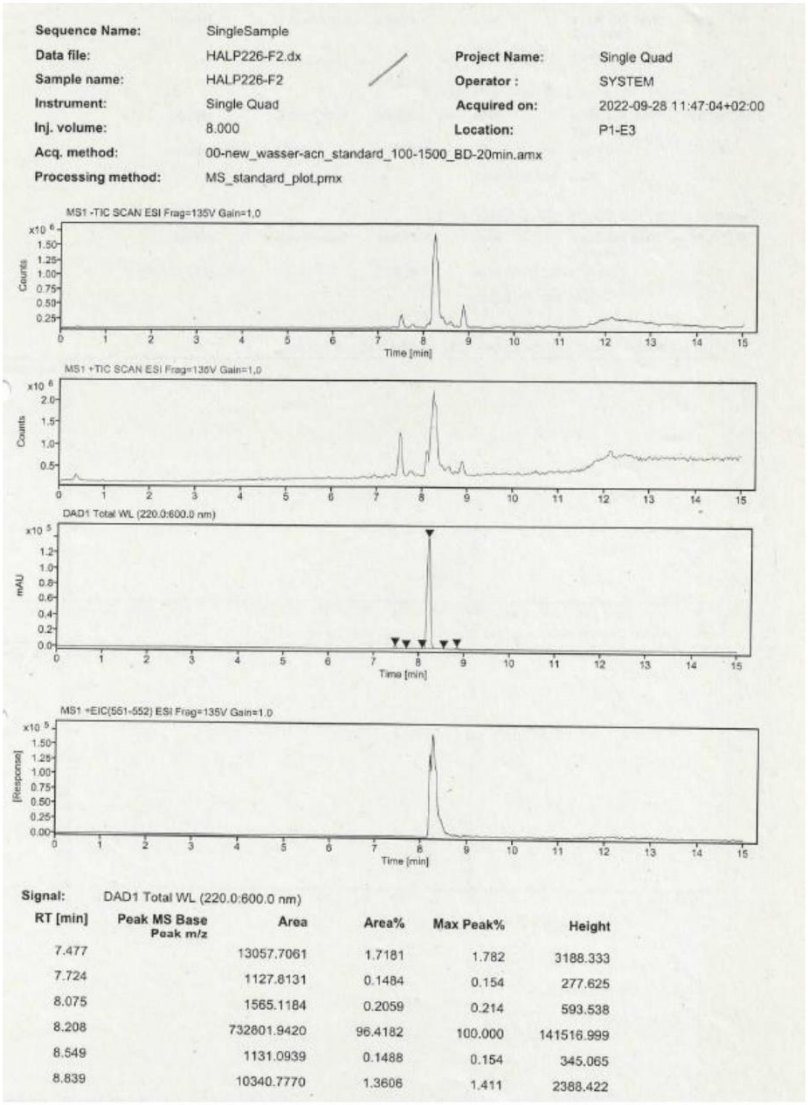
RT [min]	Peak MS Base Peak m/z	Area	Area%	Max Peak%	Height
7.158		1462.9333	0.3894	0.397	336.600
7.377		829.3100	0.2207	0.225	207.632
7.570		368645.2903	98.1188	100.000	82658.499
7.777		4775.5217	1.2711	1.295	940.645
	Sum	375713.0553			


O (s)
8.2225
E (d)
7.4807
B (d)
7.9581
A (s)
8.0246
D (s)
10.0476
H (s)
5.2627
I (s)
3.7141
J (t)
2.8125
K (h)
1.6382
M (s)
2.5243
L (t)
0.9412
N (s)
2.4323
C (s)
8.2358
G (d)
7.0805
F (d)
7.3941
f1 (ppm)


f1 (ppm)

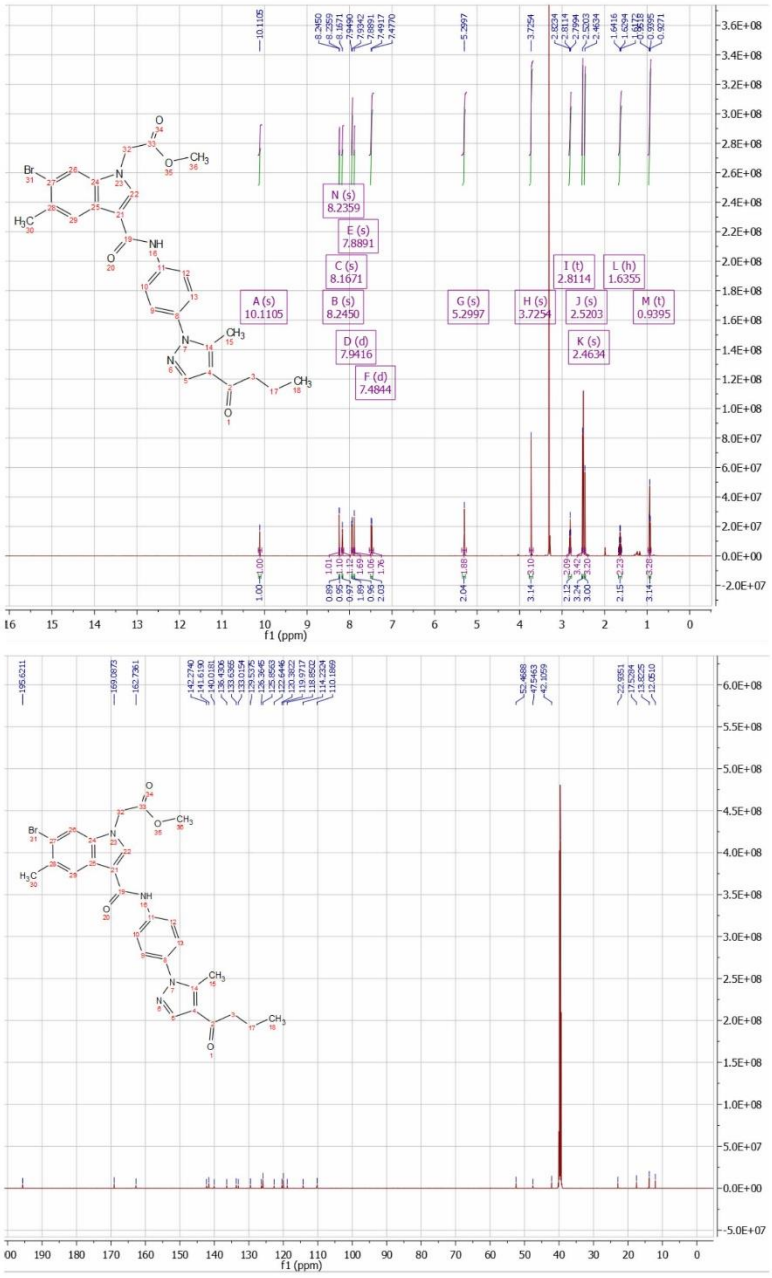
Methyl 2-(6-bromo-3-((4-(4-butyryl-5-methyl-1*H*-pyrazol-1-yl)phenyl)carbamoyl)-5-methyl-1*H*-indol-1-yl)acetate (40).[2] (Yield = 93%)

LC-MS (*m*/*z*): positive mode $[M + H]^{1+}$ (Rt) = 553.3 (8.21 min); purity by HPLC-(220-600 nm)-ESI-MS: 96.0%.



Signal: DAD1 Total WL (220.0:600.0 nm)

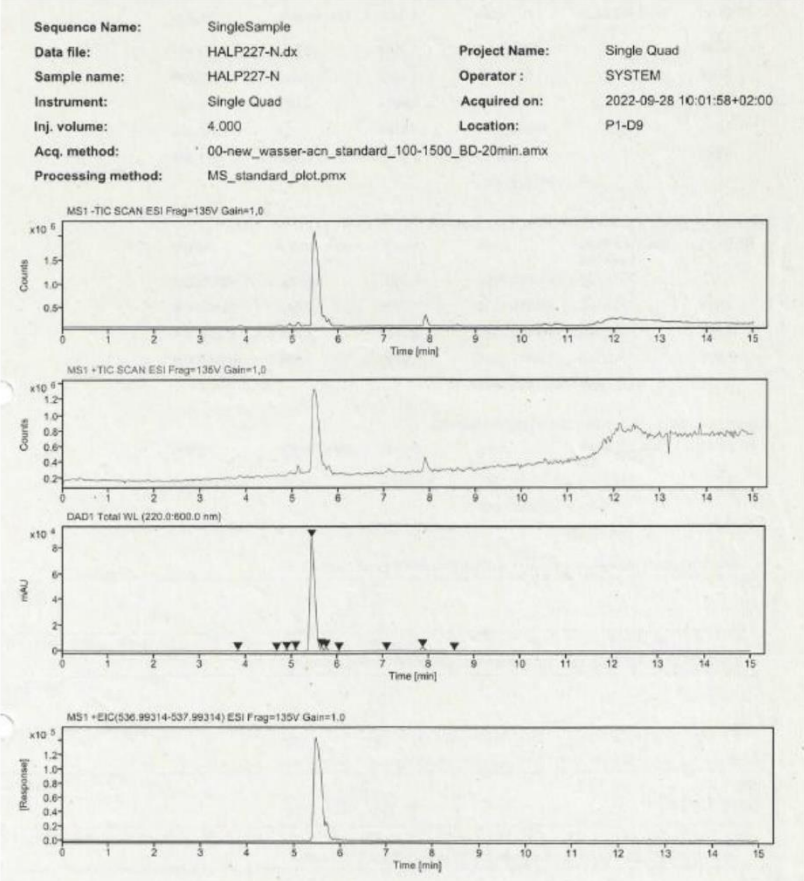
RT [min]	Peak MS Base Peak m/z	Area	Area%	Max Peak%	Height
7.477		13057.7061	1.7181	1.782	3188.333
7.724		1127.8131	0.1484	0.154	277.625
8.075		1565.1184	0.2059	0.214	593.538
8.208		732601.9420	96.4182	100.000	141516.999
8.549		1131.0939	0.1488	0.154	345.065
8.839		10340.7770	1.3606	1.411	2388.422


A (s) 10.1105
B (s) 8.2450
C (s) 8.1671
D (d) 7.9416
E (s) 7.8891
F (d) 7.4844
G (s) 5.2997
H (s) 3.7254
I (t) 2.8114
J (s) 2.5203
K (s) 2.4634
L (h) 1.6355
M (t) 0.9395
f1 (ppm)
f1 (ppm)

S71

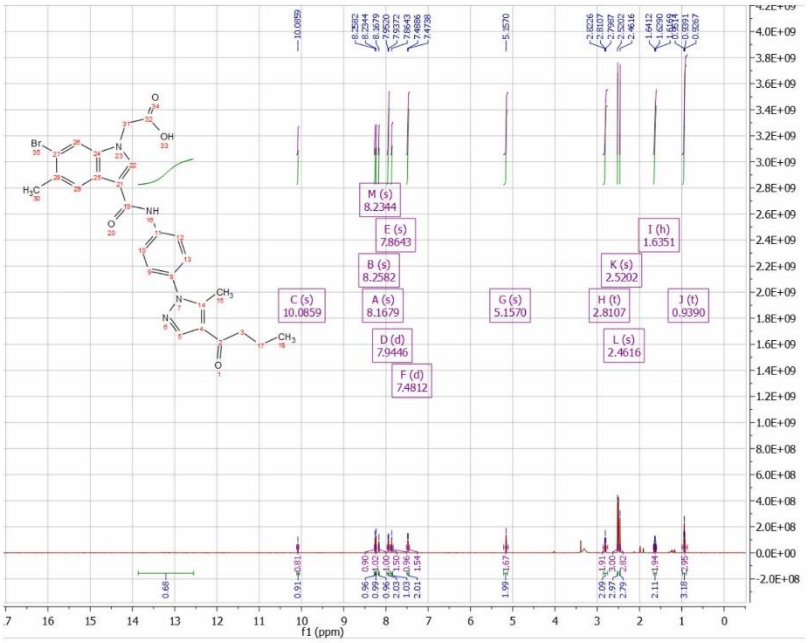
2-(6-Bromo-3-((4-(4-butyryl-5-methyl-1*H*-pyrazol-1-yl)phenyl)carbamoyl)-5-methyl-1*H*-indol-1-yl)acetic acid (41).[2] (Yield = 65%).

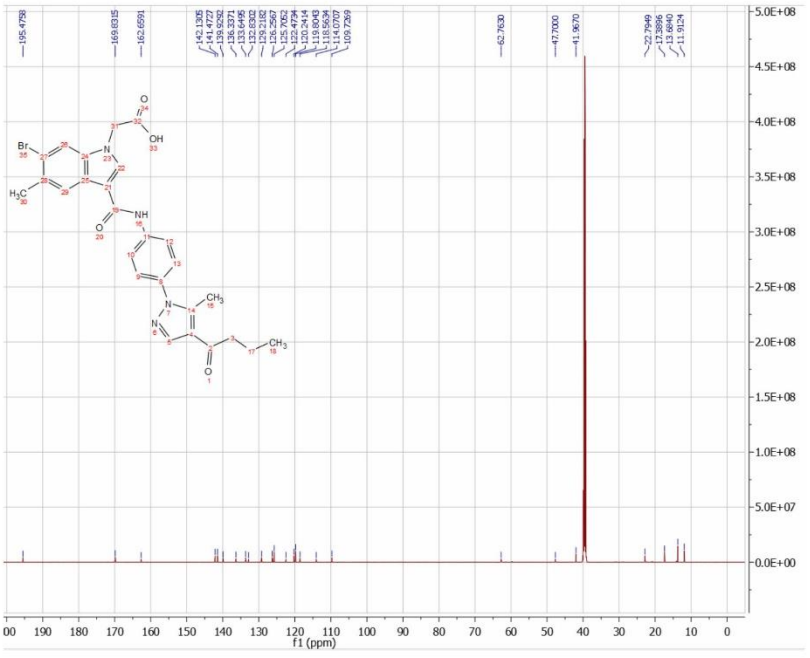
LC-MS (*m*/*z*): positive mode $[M + H]^{1+}$ (Rt) = 537.9 (5.44 min). purity by HPLC-UV(254 nm)-ESI-MS: 95.0%, mp = 232-234 °C.



Signal: DAD1 Total WL (220.0:600.0 nm)

RT [min]	Peak MS Base Peak m/z	Area	Area%	Max Peak%	Height
3.832		1916.3046	0.2749	0.293	486.977
4.677		1374.6819	0.1972	0.210	208.135
4.899		2393.9530	0.3435	0.366	759.989
5.094		4040.5955	0.5797	0.617	1032.125
5.438		654688.6454	93.9265	100.000	87327.206
5.659		10405.5751	1.4929	1.589	2945.669

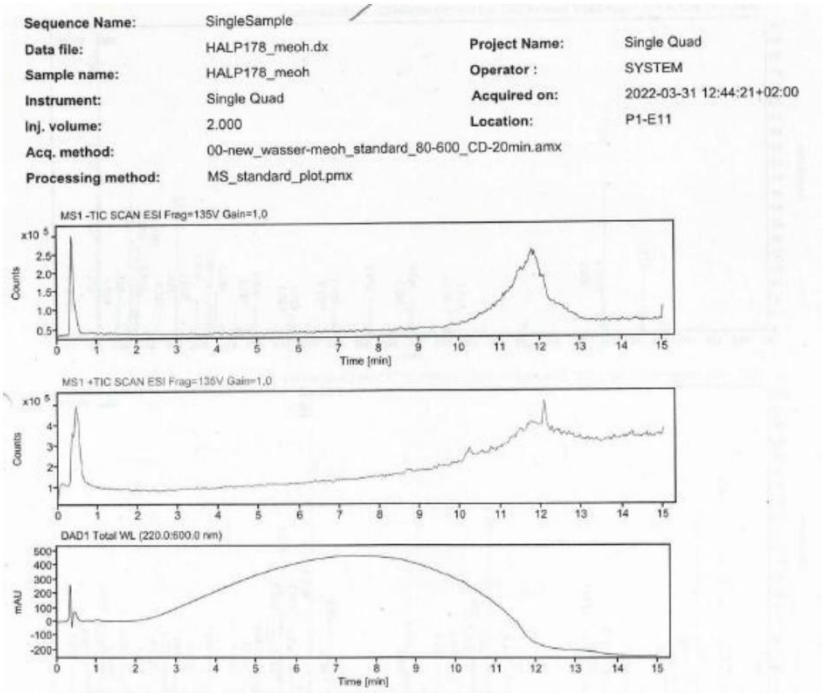

M (s)
8.2344
E (s)
7.8643
B (s)
8.2582
C (s)
10.0859
A (s)
8.1679
D (d)
7.9446
F (d)
7.4812
G (s)
5.1570
H (t)
2.8107
K (s)
2.5202
I (h)
1.6351
L (s)
2.4616
J (t)
0.9390
f1 (ppm)


f1 (ppm)

S73

Magnesium bis(3-ethoxy-3-oxopropanoate) (2:1) (42).[2] (Yield = 62%)

LC-MS (*m*/*z*): positive mode $[M + H]^{1+}$ (Rt) = 287.1 (0.47 min).; purity by HPLC-(220-600 nm)-ESI-MS: 100.0%.

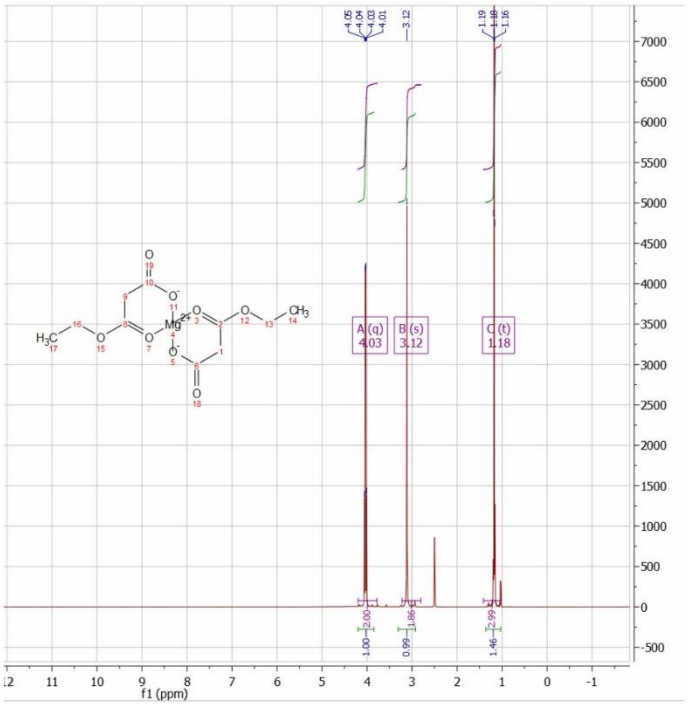


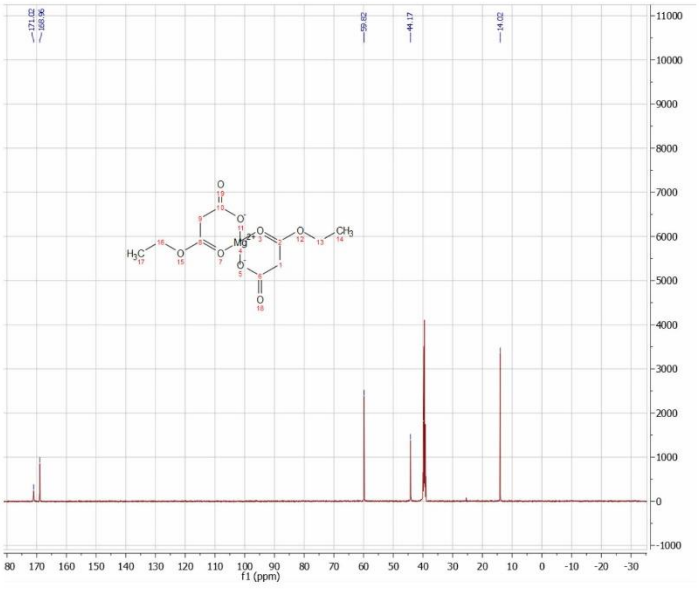
Signal: MS1 +TIC SCAN ESI Frag=135V Gain=1,0

RT [min]	Peak MS Base Peak m/z	Area	Area%	Max Peak%	Height
0.468	419.100	4967823.2016	100.0000	100.000	389892.504
	Sum	4967823.2016			

Signal: MS1 -TIC SCAN ESI Frag=135V Gain=1,0

RT [min]	Peak MS Base Peak m/z	Area	Area%	Max Peak%	Height
0.377	575.100	1679014.2791	100.0000	100.000	269721.900
	Sum	1679014.2791			

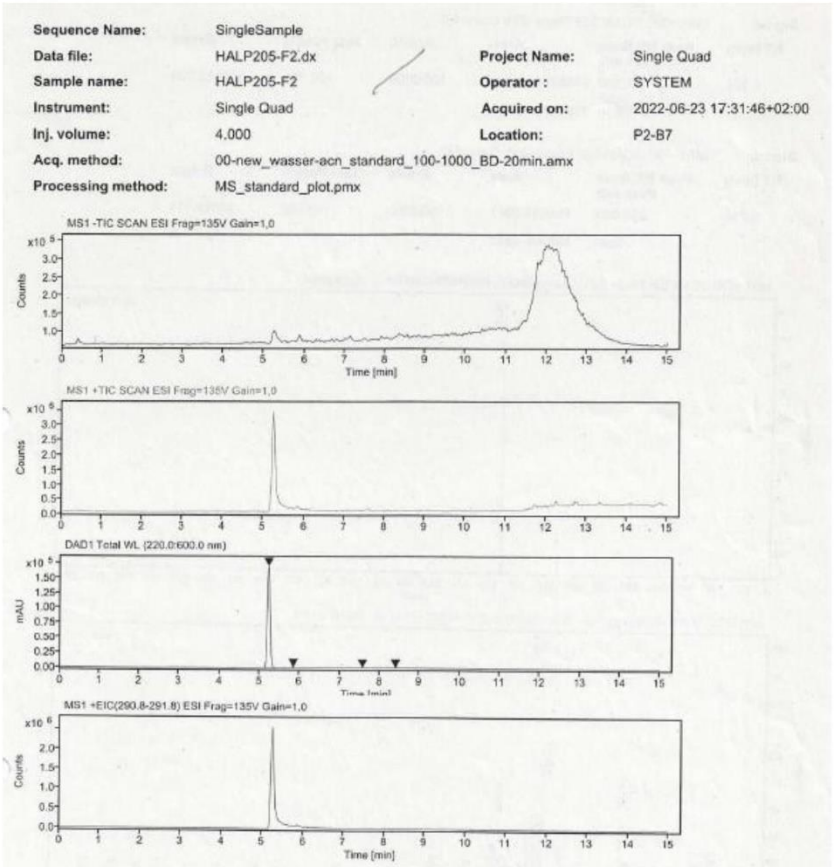




S75

***N*-Methoxy-*N*,5-dimethyl-1-(4-nitrophenyl)-1*H*-pyrazole-4-carboxamide (44)**. (Yield = 75%) (new compound).

LC-MS (*m*/*z*): positive mode $[M + H]^{1+}$ (Rt) = 291.1 (5.22 min). purity by HPLC-UV-(254 nm)-ESI-MS: 99.0%.



Signal: DAD1 Total WL (220.0:600.0 nm)

RT [min]	Peak MS Base Peak m/z	Area	Area%	Max Peak%	Height
5.222	291.100	844809.7474	99.5618	100.000	170580.778
5.838		3168.3666	0.3734	0.375	723.049
7.573		372.9969	0.0440	0.044	93.750
8.398		176.5904	0.0208	0.021	38.545
	Sum	848527.7013			

S76

References

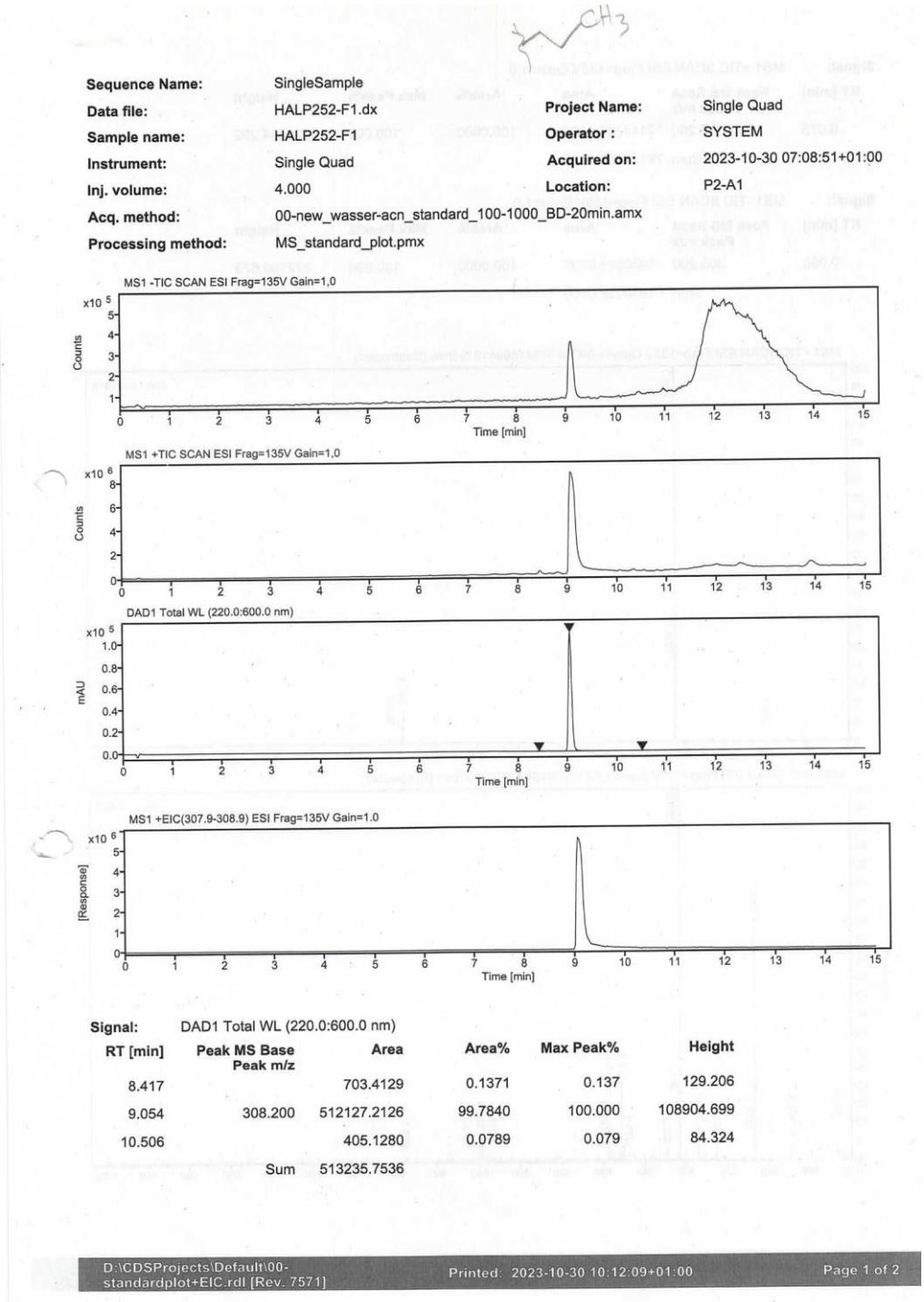
1. Savi P, Zachayus J-L, Delesque-Touchard N, et al. The active metabolite of clopidogrel disrupts $P2Y_{12}$ receptor oligomers and partitions them out of lipid rafts. *Proc. Natl. Acad. Sci.* **2006**,*103*, 11069-11074. doi:10.1073/pnas.0510446103

2. Boldron C, Besse A, Bordes M-F, et al. *N*-[6-(4-Butanoyl-5-methyl-1*H*-pyrazol-1-yl)pyridazin-3-yl]-5-chloro-1-[2-(4-methylpiperazin-1-yl)-2-oxoethyl]-1*H*-indole-3-carboxamide (SAR216471), a novel intravenous and oral, reversible, and directly acting $P2Y_{12}$ antagonist. *J. Med. Chem.* **2014**, *57*, 7293-7316. doi:10.1021/jm500588w

7.4 Appendix IV: Design, synthesis, and properties of brain-bermeable $P2Y_{12}$ receptor antagonists for neuroinflammation diseases (Manuscript III)

Analytical data:

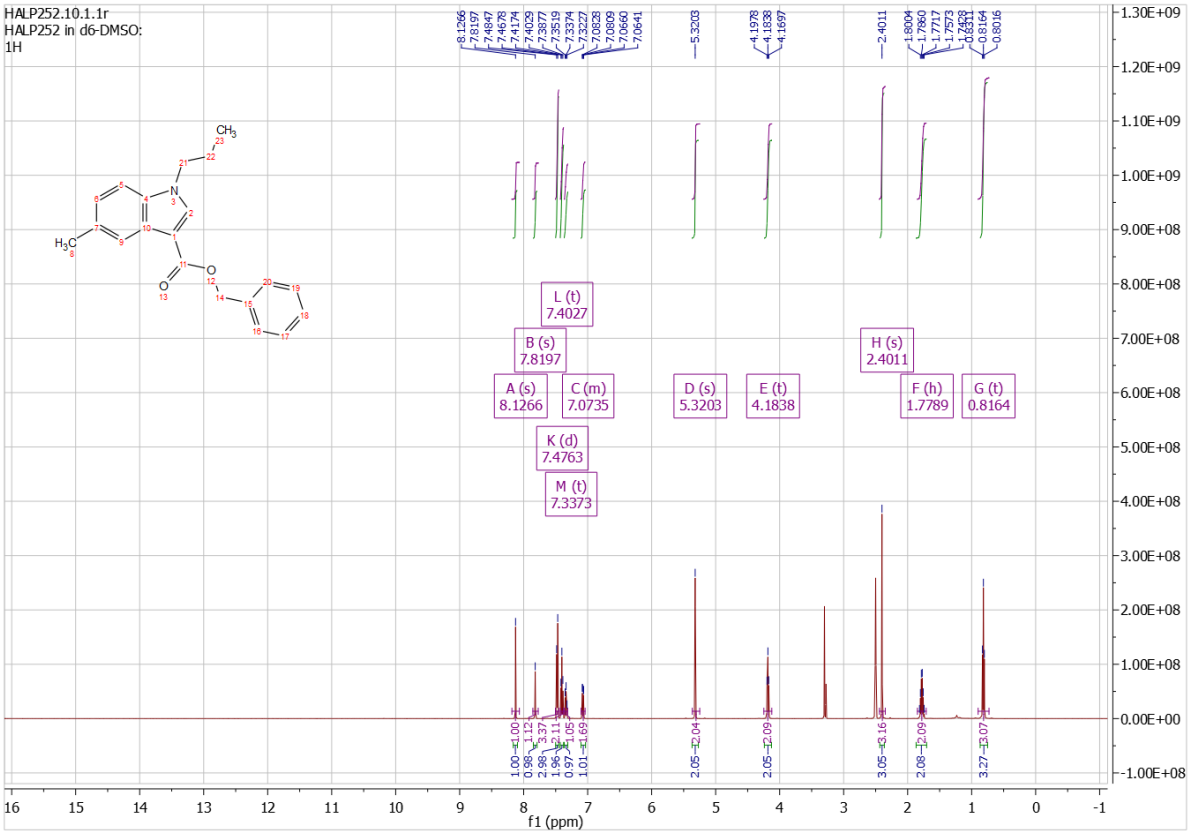
Benzyl 5-methyl-1-propyl-1*H*-indole-3-carboxylate (2a)

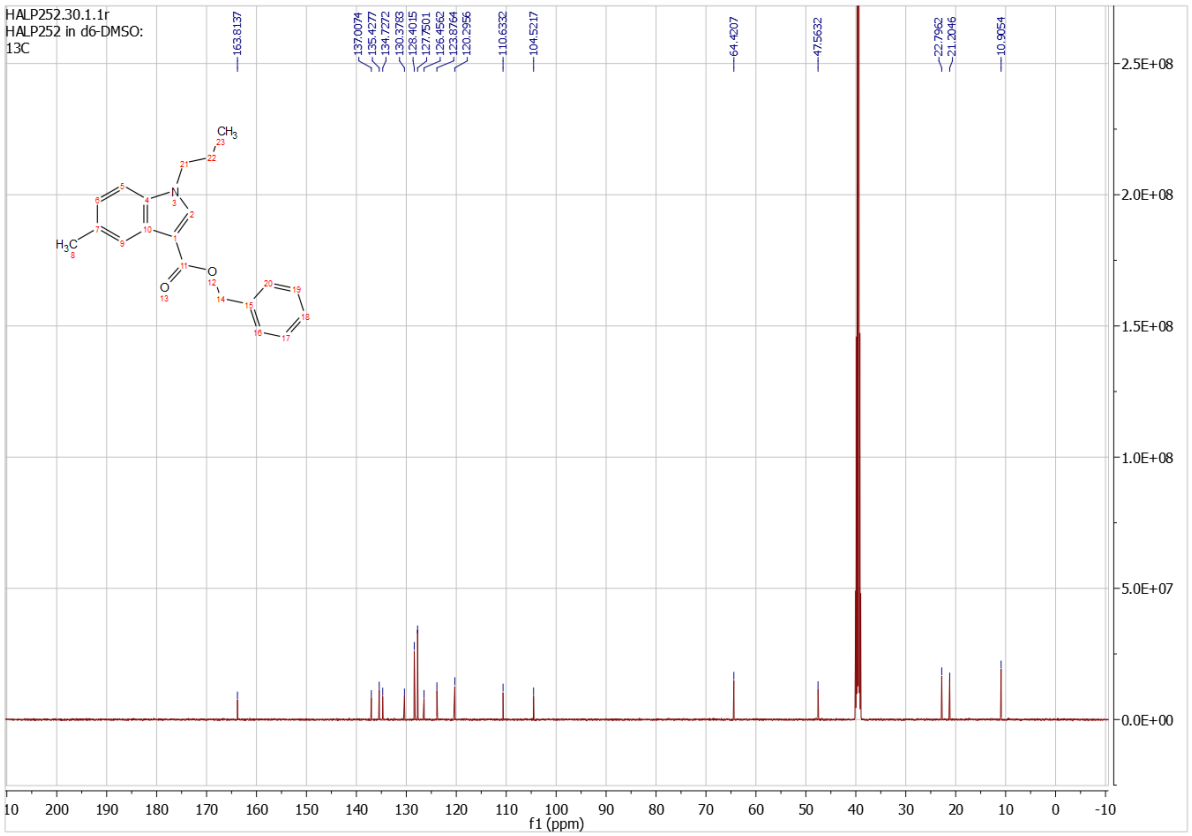


Signal: DAD1 Total WL (220.0:600.0 nm)

RT [min]	Peak MS Base Peak m/z	Area	Area%	Max Peak%	Height
8.417		703.4129	0.1371	0.137	129.206
9.054	308.200	512127.2126	99.7840	100.000	108904.699
10.506		405.1280	0.0789	0.079	84.324
	Sum	513235.7536			

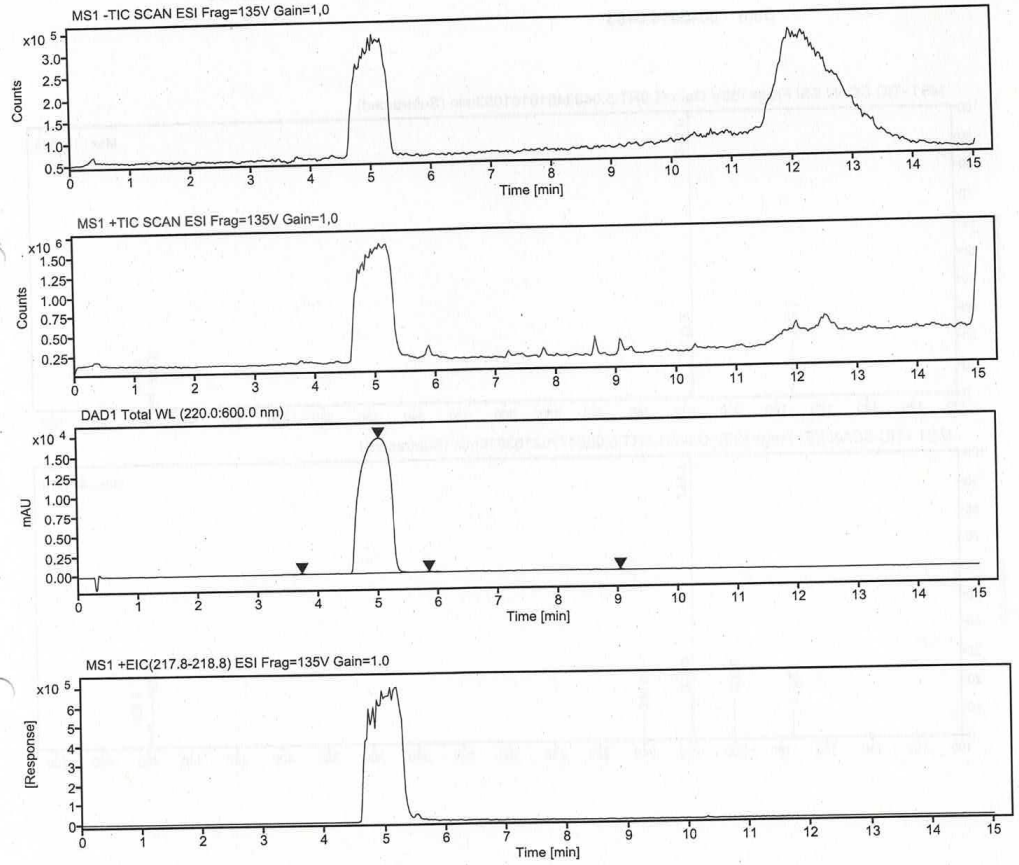
D:\CDSProjects\Default\00-standardplot+EIC.rdl [Rev. 7571] Printed: 2023-10-30 10:12:09+01:00 Page 1 of 2


HALP252.10.1.1r
HALP252 in d6-DMSO:
1H
L (t)
7.4027
B (s)
7.8197
H (s)
2.4011
A (s)
8.1266
C (m)
7.0735
D (s)
5.3203
E (t)
4.1838
F (h)
1.7789
G (t)
0.8164
K (d)
7.4763
M (t)
7.3373
f1 (ppm)


HALP252.30.1.1r
HALP252 in d6-DMSO:
13C
f1 (ppm)

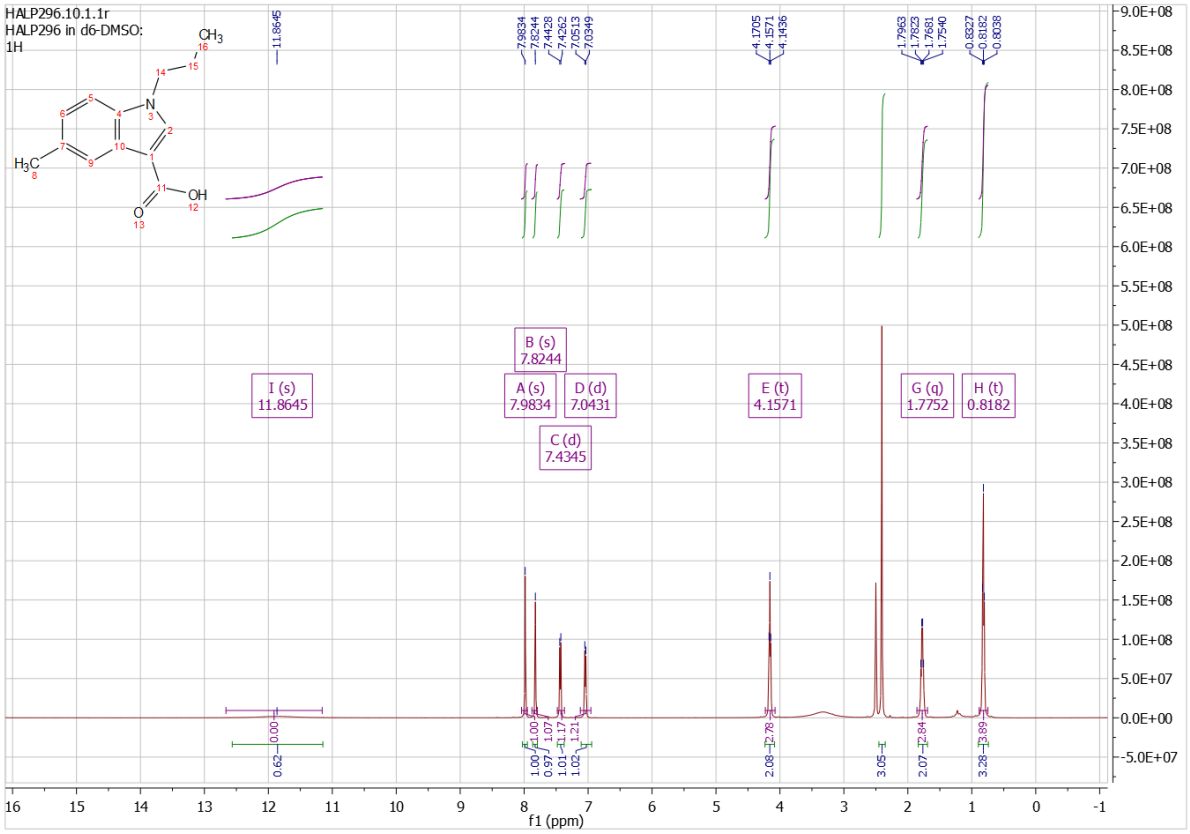
5-Methyl-1-propyl-1*H*-indole-3-carboxylic acid (2b)

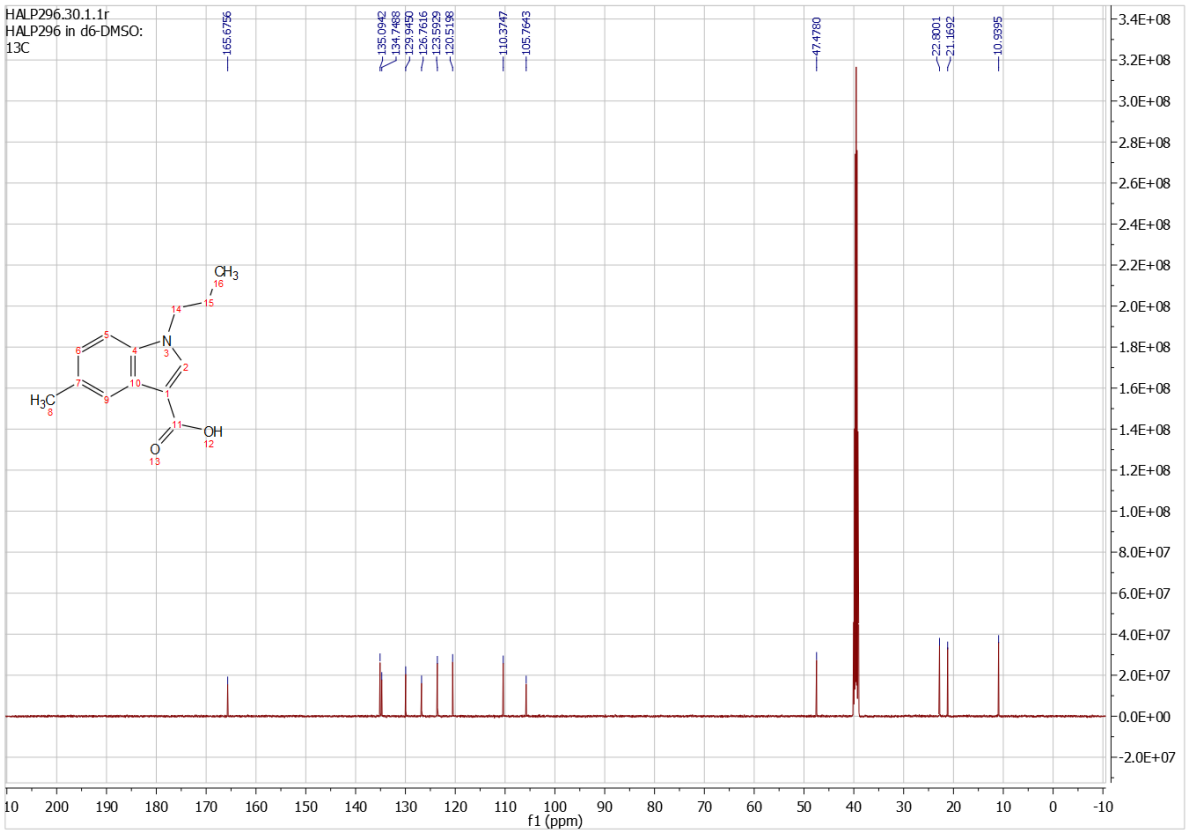
Sequence Name:	SingleSample		
Data file:	HALP296.dx	**Project Name:**	Single Quad
Sample name:	HALP296	**Operator :**	SYSTEM
Instrument:	Single Quad	**Acquired on:**	2023-11-02 13:55:09+01:00
Inj. volume:	5.000	**Location:**	P1-B10
Acq. method:	00-new_wasser-acn_standard_100-1000_BD-20min.amx		
Processing method:	MS_standard_plot.pmx		



Signal: DAD1 Total WL (220.0:600.0 nm)

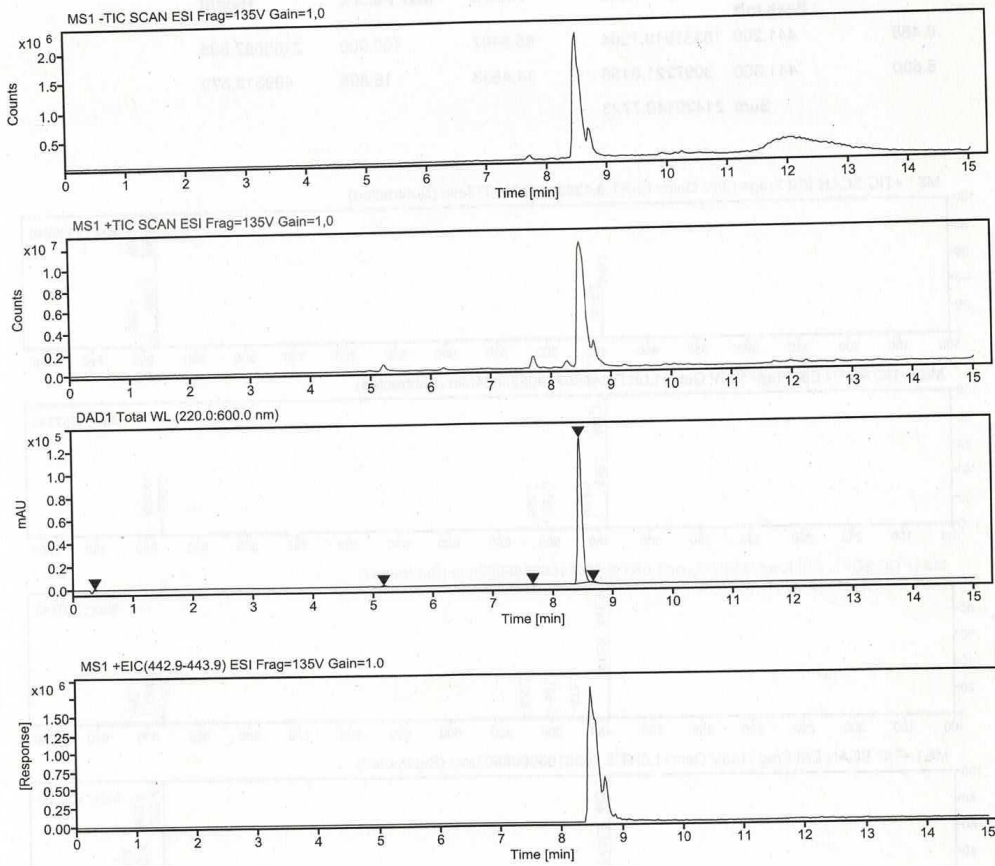
RT [min]	Peak MS Base Peak m/z	Area	Area%	Max Peak%	Height
3.736		335.5463	0.0581	0.058	101.418
5.032	216.100	575925.1332	99.7620	100.000	16918.829
5.850		666.9592	0.1155	0.116	91.908
9.041		371.6060	0.0644	0.065	89.091
	Sum	577299.2447			


HALP296.10.1.1r
HALP296 in d6-DMSO:
1H
11.8645
7.9834
7.8244
7.4428
7.4262
7.0513
7.0349
4.1705
4.1571
4.1436
1.7963
1.7823
1.7681
1.7540
0.8327
0.8182
0.8038
B (s)
7.8244
I (s)
11.8645
A (s)
7.9834
D (d)
7.0431
C (d)
7.4345
E (t)
4.1571
G (q)
1.7752
H (t)
0.8182
f1 (ppm)


HALP296.30.1.1r
HALP296 in d6-DMSO:
13C
165.6756
135.0942
134.7488
129.9450
126.7616
123.5929
120.5198
110.3747
105.7643
47.4780
22.8001
21.1692
10.9395
f1 (ppm)

_N_-(4-(4-Butyryl-5-methyl-1_H_-pyrazol-1-yl)phenyl)-5-methyl-1-propyl-1_H_-indole-3-carboxamide (2c)

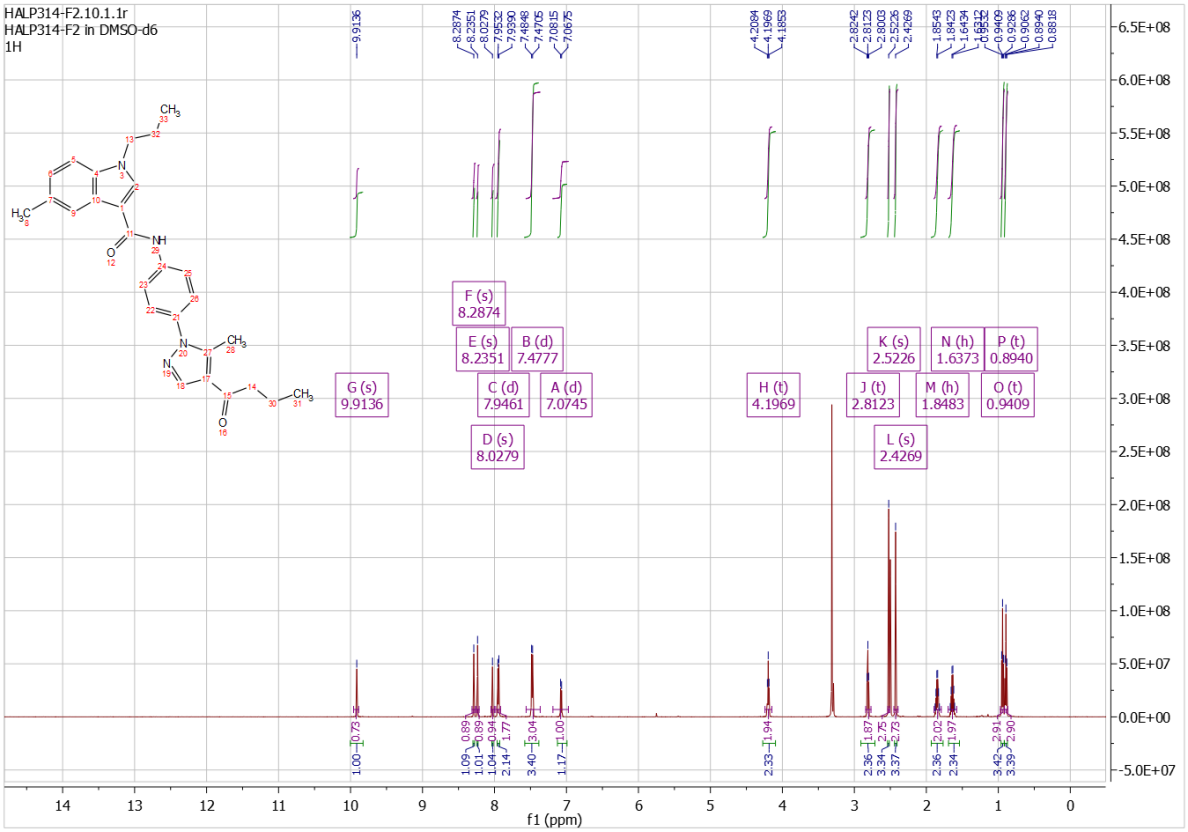
Sequence Name:	SingleSample		
Data file:	HALP314-F2.dx	**Project Name:**	Single Quad
Sample name:	HALP314-F2	**Operator :**	SYSTEM
Instrument:	Single Quad	**Acquired on:**	2024-01-08 22:21:07+01:00
Inj. volume:	4.000	**Location:**	P1-D6
Acq. method:	00-new_wasser-acn_standard_100-1000_BD-20min.amx		
Processing method:	MS_standard_plot.pmx		

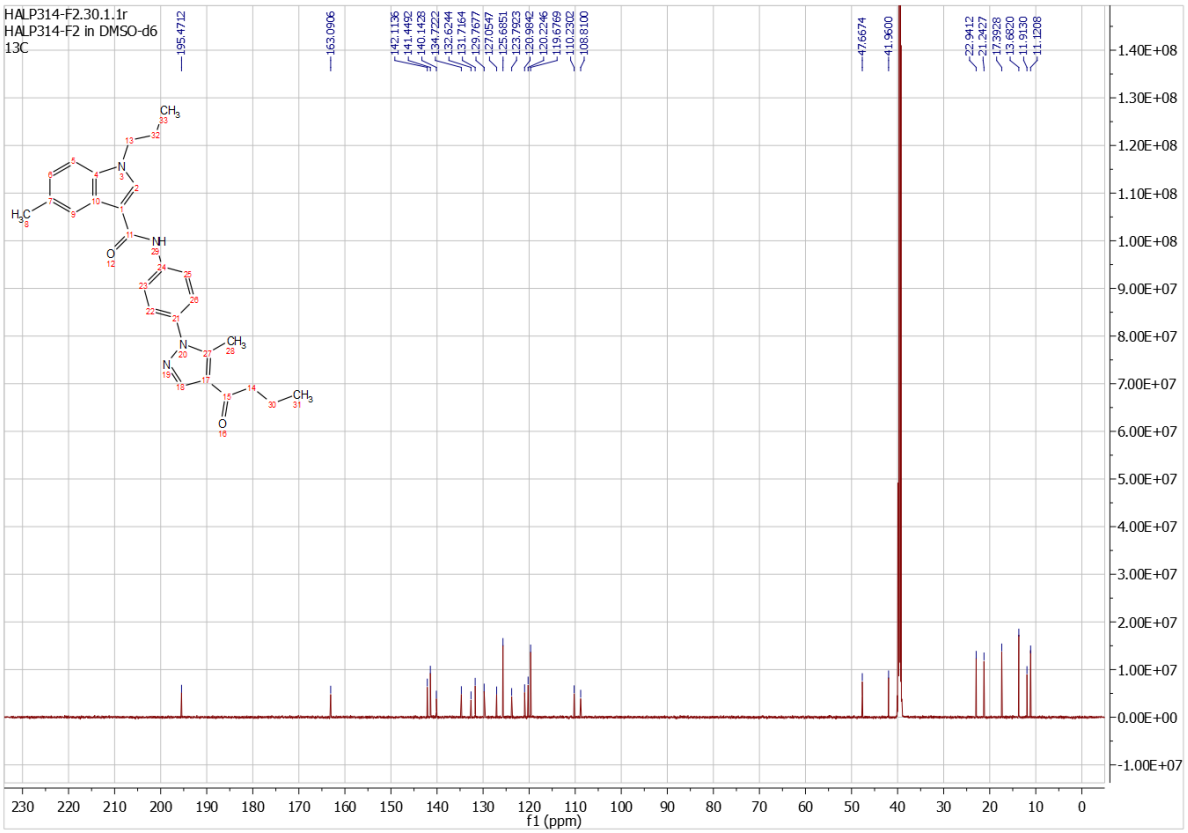


Signal: DAD1 Total WL (220.0:600.0 nm)

RT [min]	Peak MS Base Peak m/z	Area	Area%	Max Peak%	Height
0.369		2178.9920	0.3254	0.331	891.186
5.177		2676.7700	0.3998	0.406	720.825
7.661		1722.9513	0.2573	0.262	413.011
8.451		658581.4591	98.3616	100.000	127020.263
8.669		4391.2689	0.6559	0.667	1278.055
	Sum	669551.4412			

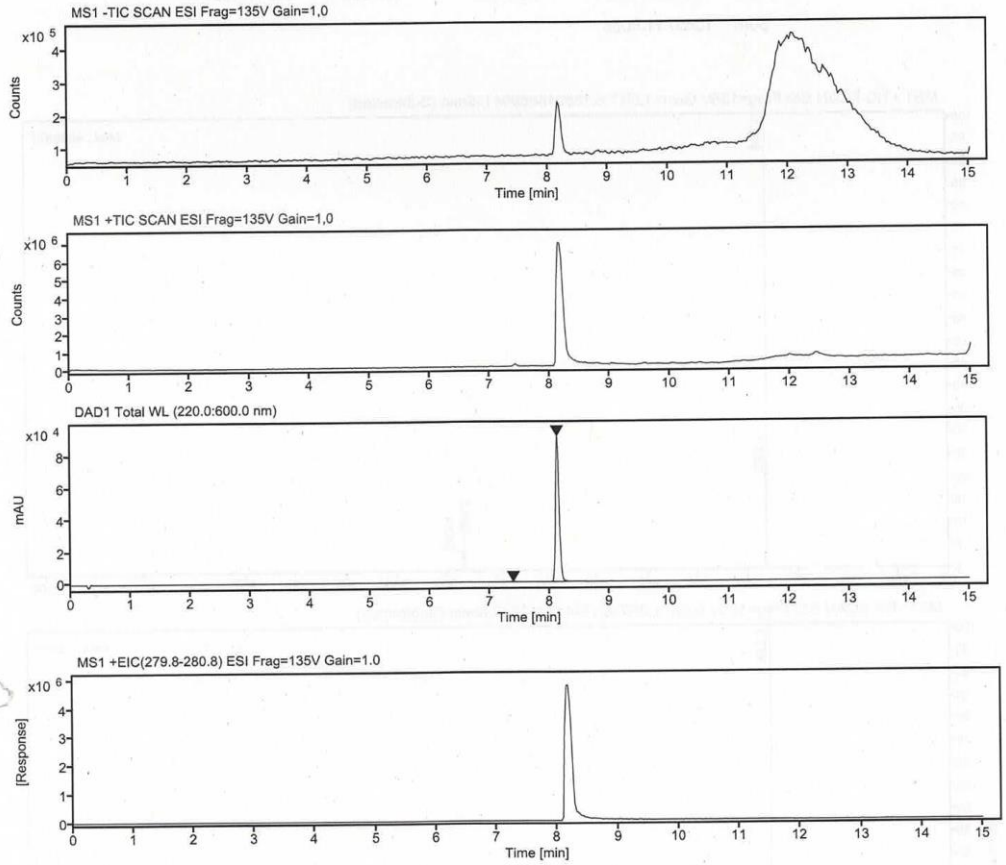
D:\CDSProjects\Default\00-standardplot+EIC.rdl [Rev. 8589] Printed: 2024-01-09 11:11:52+01:00 Page 1 of 2


HALP314-F2.10.1.1r
HALP314-F2 in DMSO-d6
1H
F (s) 8.2874
E (s) 8.2351
B (d) 7.4777
C (d) 7.9461
A (d) 7.0745
D (s) 8.0279
G (s) 9.9136
H (t) 4.1969
K (s) 2.5226
N (h) 1.6373
P (t) 0.8940
J (t) 2.8123
M (h) 1.8483
O (t) 0.9409
L (s) 2.4269
f1 (ppm)


HALP314-F2.30.1.1r
HALP314-F2 in DMSO-d6
13C
f1 (ppm)

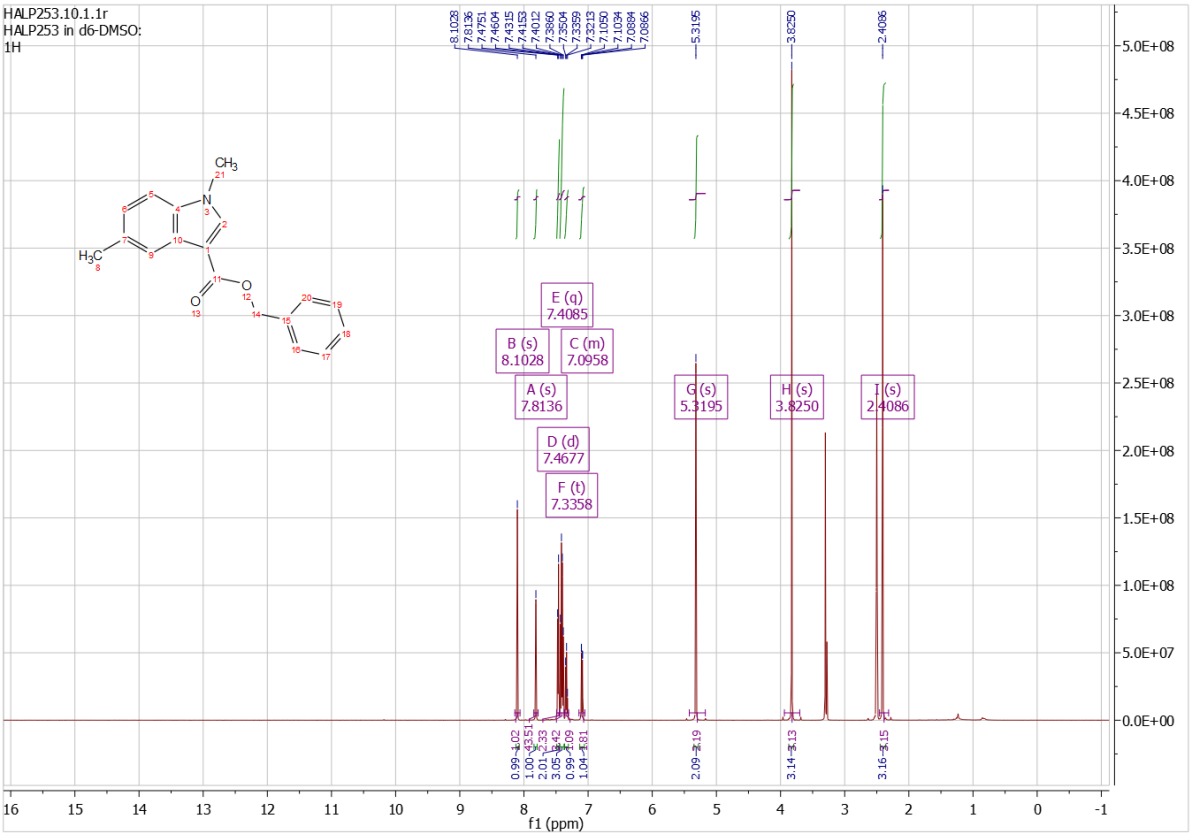
Benzyl 1,5-dimethyl-1*H*-indole-3-carboxylate (3a)

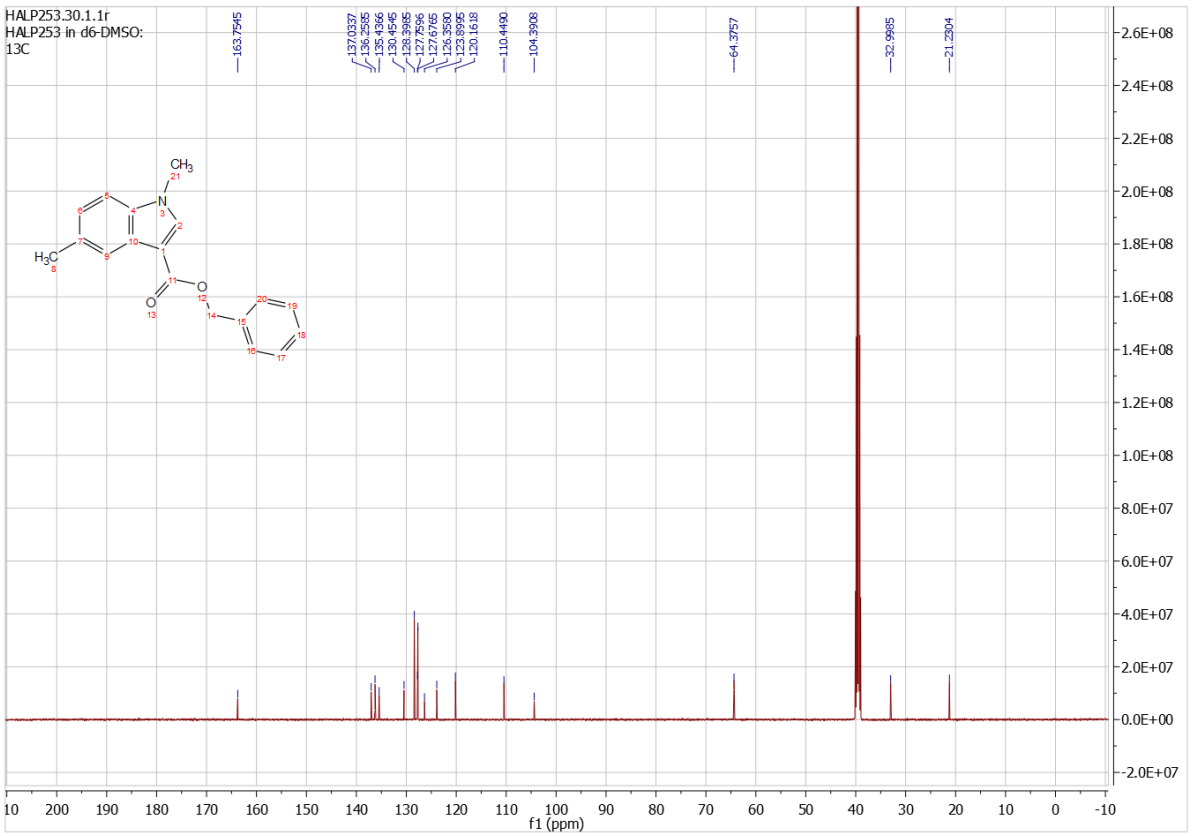
Sequence Name:	SingleSample		
Data file:	HALP253-F1.dx	**Project Name:**	Single Quad
Sample name:	HALP253-F1	**Operator :**	SYSTEM
Instrument:	Single Quad	**Acquired on:**	2023-10-30 07:30:00+01:00
Inj. volume:	2.000	**Location:**	P2-A2
Acq. method:	00-new_wasser-acn_standard_100-1000_BD-20min.amx		
Processing method:	MS_standard_plot.pmx		



Signal: DAD1 Total WL (220.0:600.0 nm)

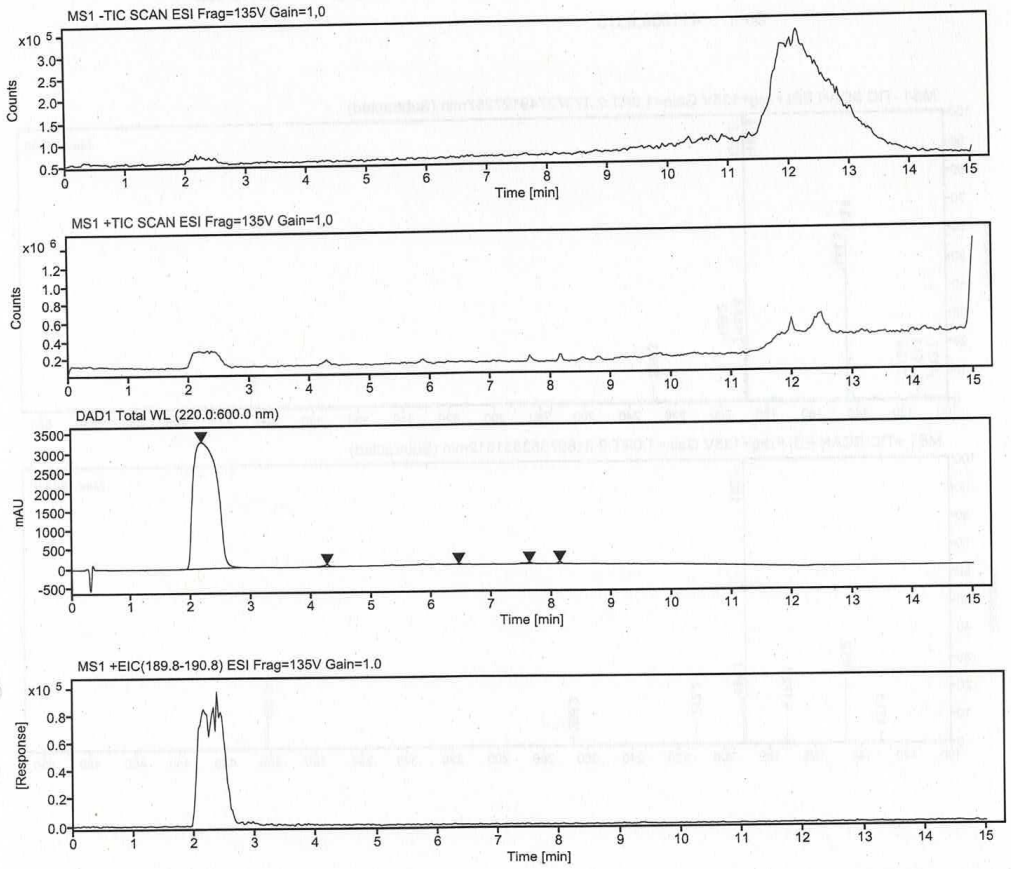
RT [min]	Peak MS Base Peak m/z	Area	Area%	Max Peak%	Height
7.400		376.1925	0.0971	0.097	104.884
8.138	280.100	387109.9802	99.9029	100.000	90349.482
	Sum	387486.1728			


HALP253.10.1.1r
HALP253 in d6-DMSO:
1H
E (q)
7.4085
B (s)
8.1028
C (m)
7.0958
A (s)
7.8136
D (d)
7.4677
F (t)
7.3358
G (s)
5.3195
H (s)
3.8250
I (s)
2.4086
f1 (ppm)


HALP253.30.1.1r
HALP253 in d6-DMSO:
13C
f1 (ppm)

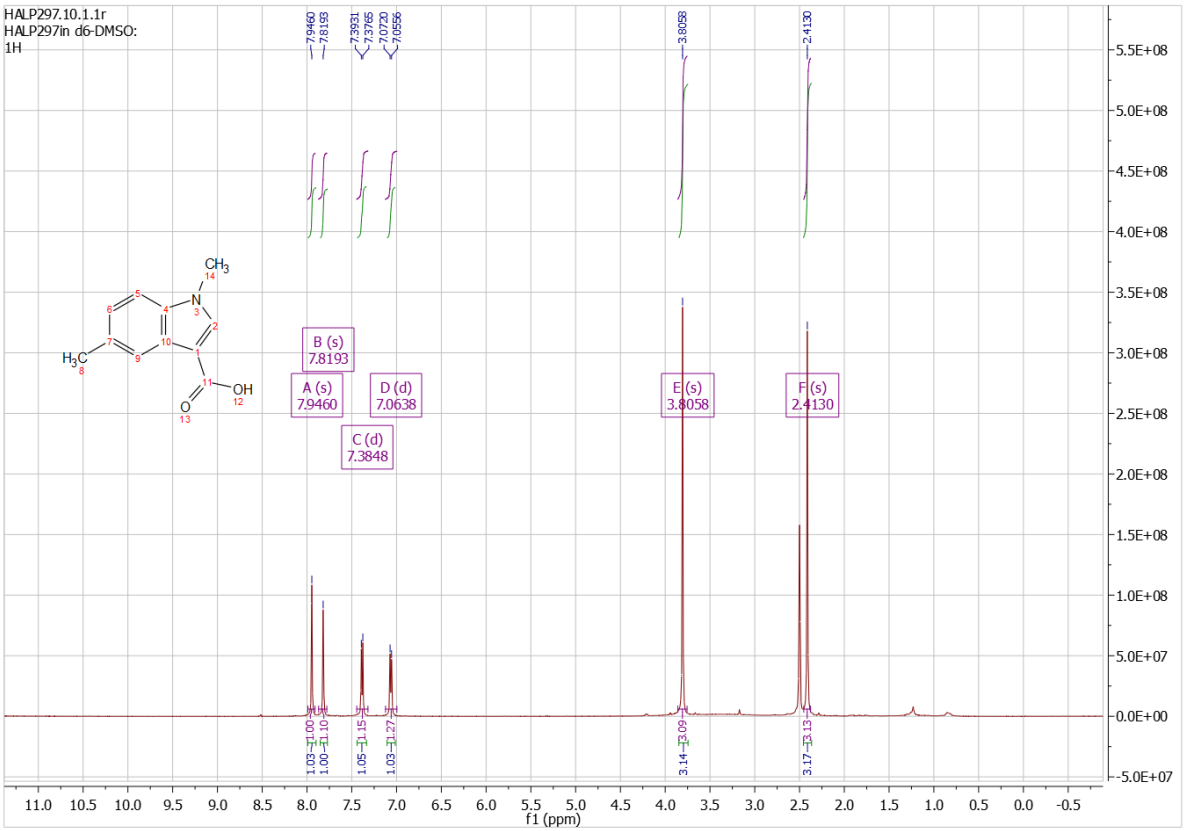
1,5-Dimethyl-1*H*-indole-3-carboxylic acid (3b)

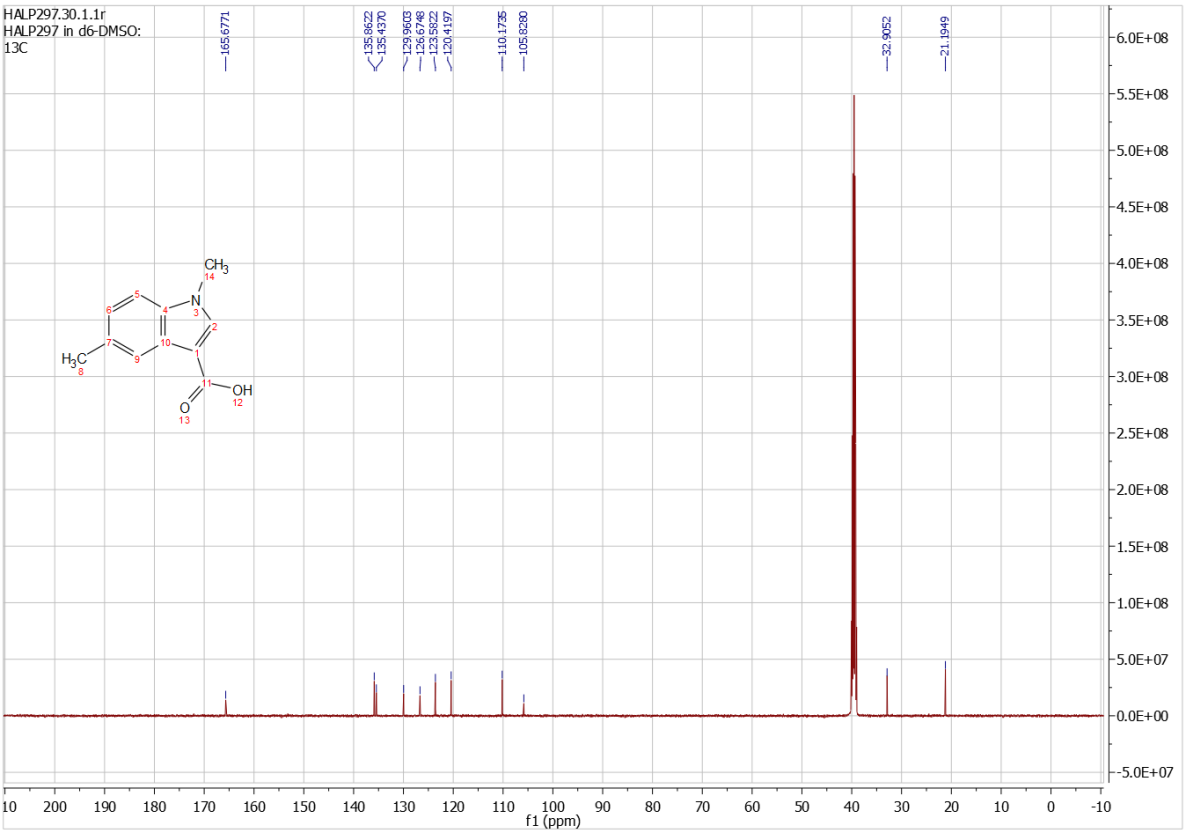
Sequence Name:	SingleSample		
Data file:	HALP297.dx	**Project Name:**	Single Quad
Sample name:	HALP297	**Operator :**	SYSTEM
Instrument:	Single Quad	**Acquired on:**	2023-11-02 14:16:10+01:00
Inj. volume:	2.000	**Location:**	P1-B11
Acq. method:	00-new_wasser-acn_standard_100-1000_BD-20min.amx		
Processing method:	MS_standard_plot.pmx		



Signal: DAD1 Total WL (220.0:600.0 nm)

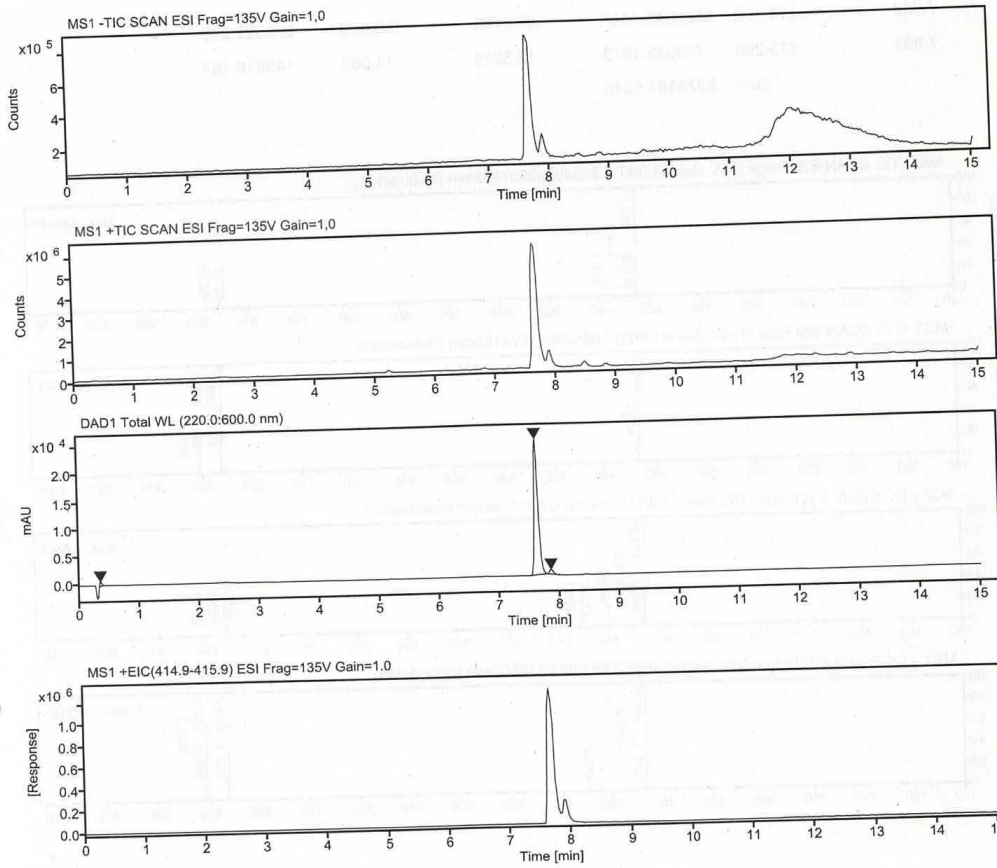
RT [min]	Peak MS Base Peak m/z	Area	Area%	Max Peak%	Height
2.180	190.100	88898.1942	98.9448	100.000	3272.886
4.257		458.0893	0.5099	0.515	54.843
6.447		82.1612	0.0914	0.092	21.271
7.626		212.7174	0.2368	0.239	31.852
8.130		195.0664	0.2171	0.219	52.722
	Sum	89846.2285			


HALP297.10.1.1r
HALP297in d6-DMSO:
1H
7.9460
7.8159
7.3931
7.3765
7.0720
7.0556
3.8058
2.4130
B (s)
7.8193
A (s)
7.9460
D (d)
7.0638
C (d)
7.3848
E (s)
3.8058
F (s)
2.4130
1.03
1.00
1.10
1.05
1.15
1.03
1.27
3.14
3.09
3.17
3.13
f1 (ppm)


HALP297.30.1.1r
HALP297 in d6-DMSO:
13C
165.6771
135.8622
135.4370
129.9603
126.6748
123.5822
120.4197
110.1735
105.8280
32.9052
21.1949
f1 (ppm)

_N_-(4-(4-Butyryl-5-methyl-1_H_-pyrazol-1-yl)phenyl)-1,5-dimethyl-1_H_-indole-3-carboxamide (3c)

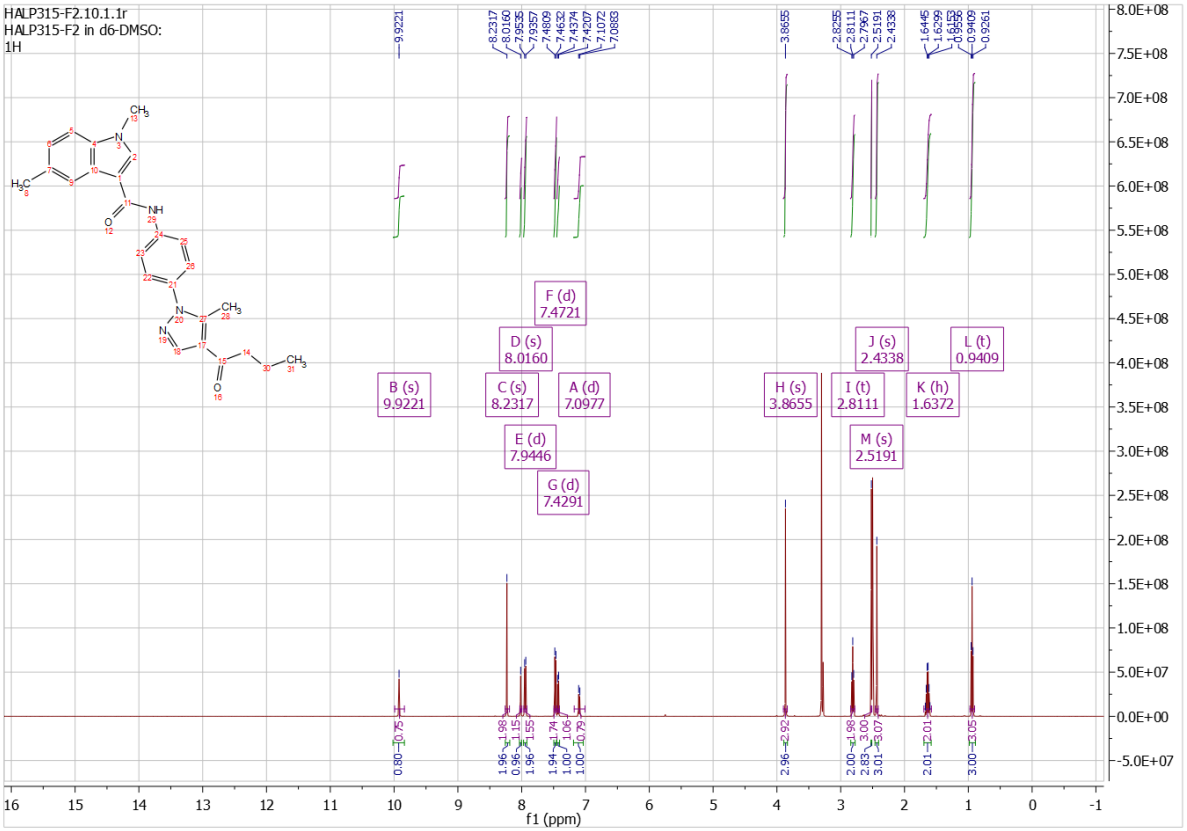
Sequence Name:	SingleSample		
Data file:	HALP315-F2.dx	**Project Name:**	Single Quad
Sample name:	HALP315-F2	**Operator :**	SYSTEM
Instrument:	Single Quad	**Acquired on:**	2024-01-04 14:12:24+01:00
Inj. volume:	3.000	**Location:**	P2-D8
Acq. method:	00-new_wasser-acn_standard_100-1000_BD-20min.amx		
Processing method:	MS_standard_plot.pmx		

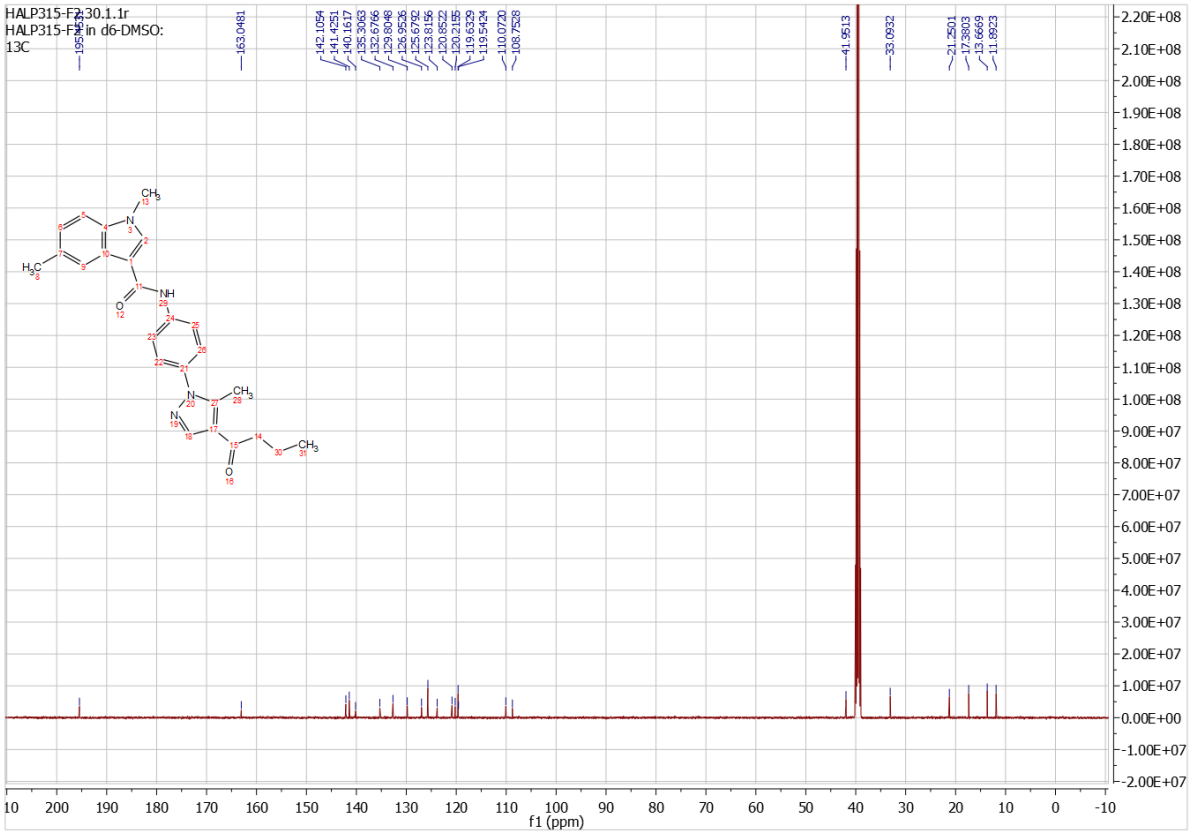


Signal: DAD1 Total WL (220.0:600.0 nm)

RT [min]	Peak MS Base Peak m/z	Area	Area%	Max Peak%	Height
0.366		1682.7865	1.3830	1.444	746.951
7.625	413.100	116559.5767	95.7965	100.000	24553.736
7.859		3431.8412	2.8205	2.944	814.116
	Sum	121674.2044			

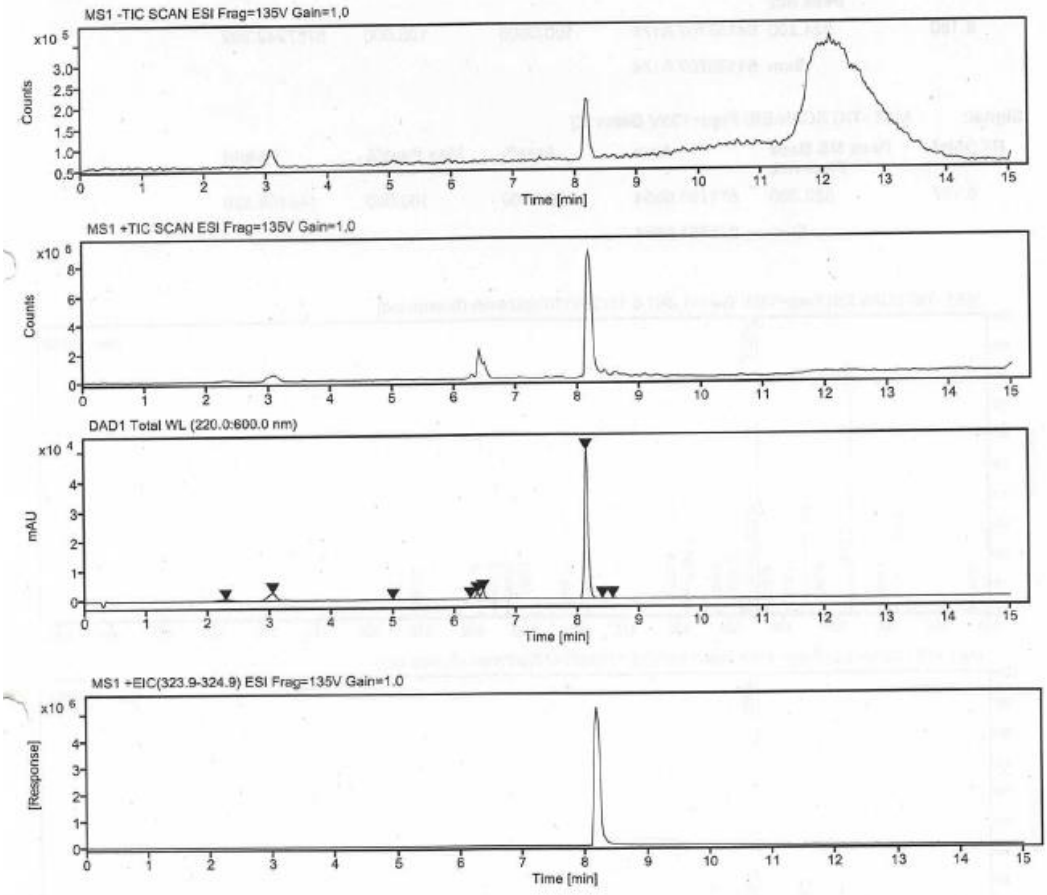
D:\CDSProjects\Default\00-standardplot+EIC.rdl [Rev. 8559] Printed: 2024-01-08 10:26:44+01:00 Page 1 of 2


HALP315-F2.10.1.1r
HALP315-F2 in d6-DMSO:
1H
B (s)
9.9221
C (s)
8.2317
D (s)
8.0160
E (d)
7.9446
F (d)
7.4721
G (d)
7.4291
A (d)
7.0977
H (s)
3.8655
I (t)
2.8111
J (s)
2.4338
M (s)
2.5191
K (h)
1.6372
L (t)
0.9409
f1 (ppm)


HALP315-F2.30.1.1r
HALP315-F2 in d6-DMSO:
13C
f1 (ppm)

Benzyl 1-(2-methoxyethyl)-5-methyl-1*H*-indole-3-carboxylate (4a)

Sequence Name:	SingleSample		
Data file:	HALP290.dx	**Project Name:**	Single Quad
Sample name:	HALP290	**Operator :**	SYSTEM
Instrument:	Single Quad	**Acquired on:**	2023-10-30 11:42:03+01:00
Inj. volume:	2.000	**Location:**	P2-B1
Acq. method:	00-new_wasser-acn_standard_100-1000_BD-20min.amx		
Processing method:	MS_standard_plot.pmx		



Signal: DAD1 Total WL (220.0:600.0 nm)

RT [min]	Peak MS Base Peak m/z	Area	Area%	Max Peak%	Height
2.295		5663.4711	2.1988	2.712	420.211
3.054		23177.0932	8.9984	11.097	2439.616
5.002		609.4686	0.2366	0.292	126.831
6.259		358.7061	0.1393	0.172	140.027
6.372		7598.3446	2.9500	3.638	1921.892
6.459		9929.4455	3.8551	4.754	2544.617

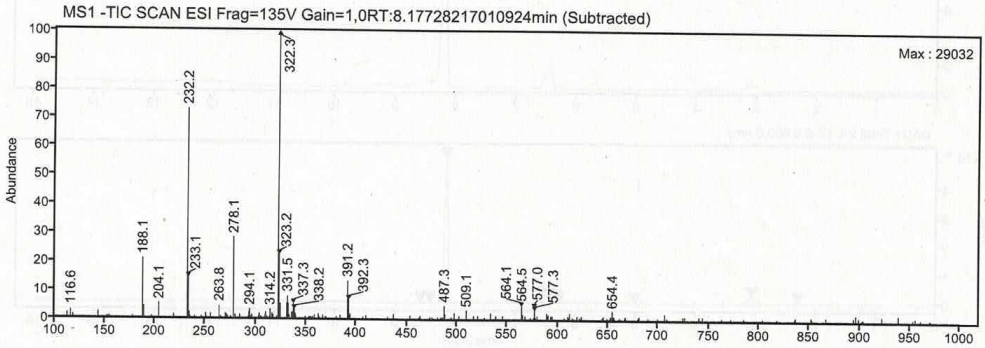
RT [min]	Peak MS Base Peak m/z	Area	Area%	Max Peak%	Height
8.142		208850.2191	81.0852	100.000	49763.473
8.401		480.6030	0.1866	0.230	139.136
8.569		901.5300	0.3500	0.432	166.945
	Sum	257568.8812			

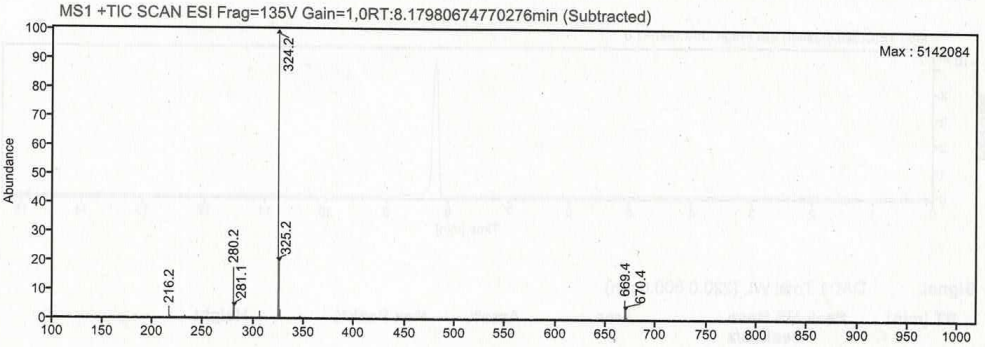
Signal: MS1 +TIC SCAN ESI Frag=135V Gain=1,0

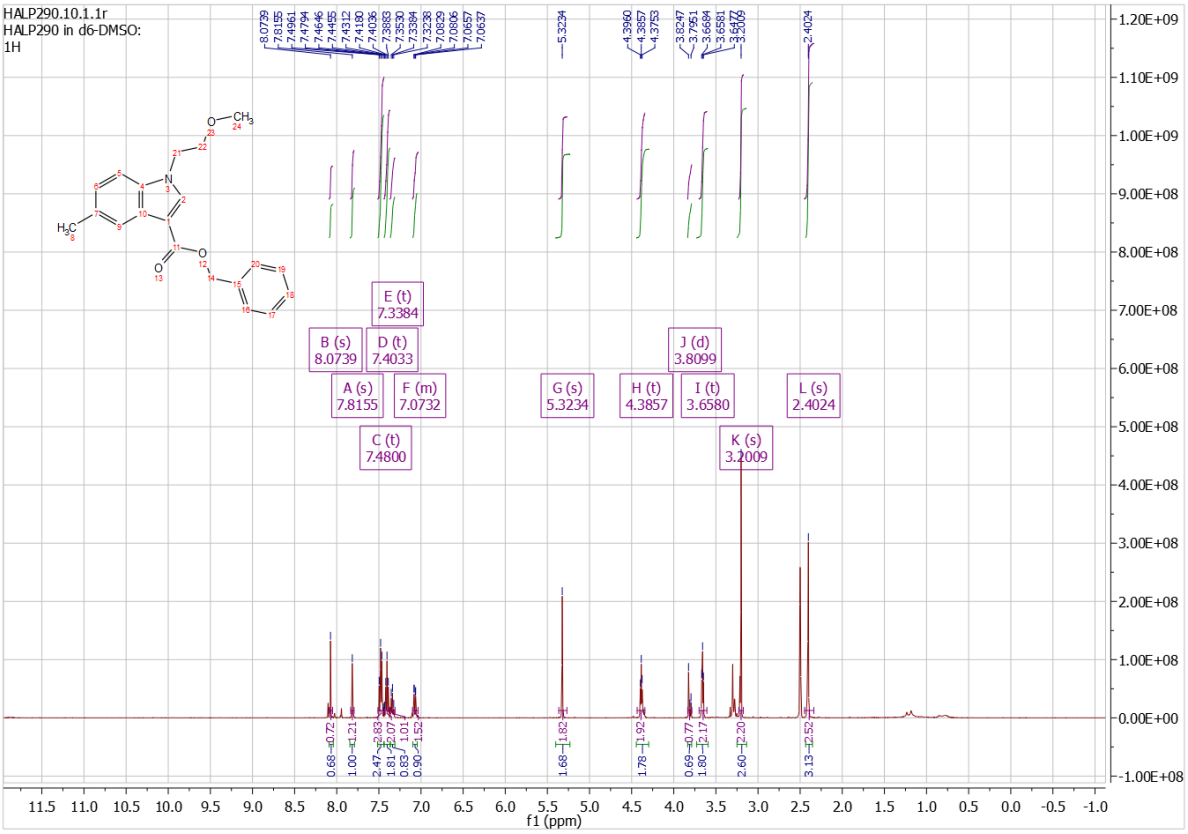
RT [min]	Peak MS Base Peak m/z	Area	Area%	Max Peak%	Height
8.180	324.200	64133707.6174	100.0000	100.000	8757242.382
	Sum	64133707.6174			

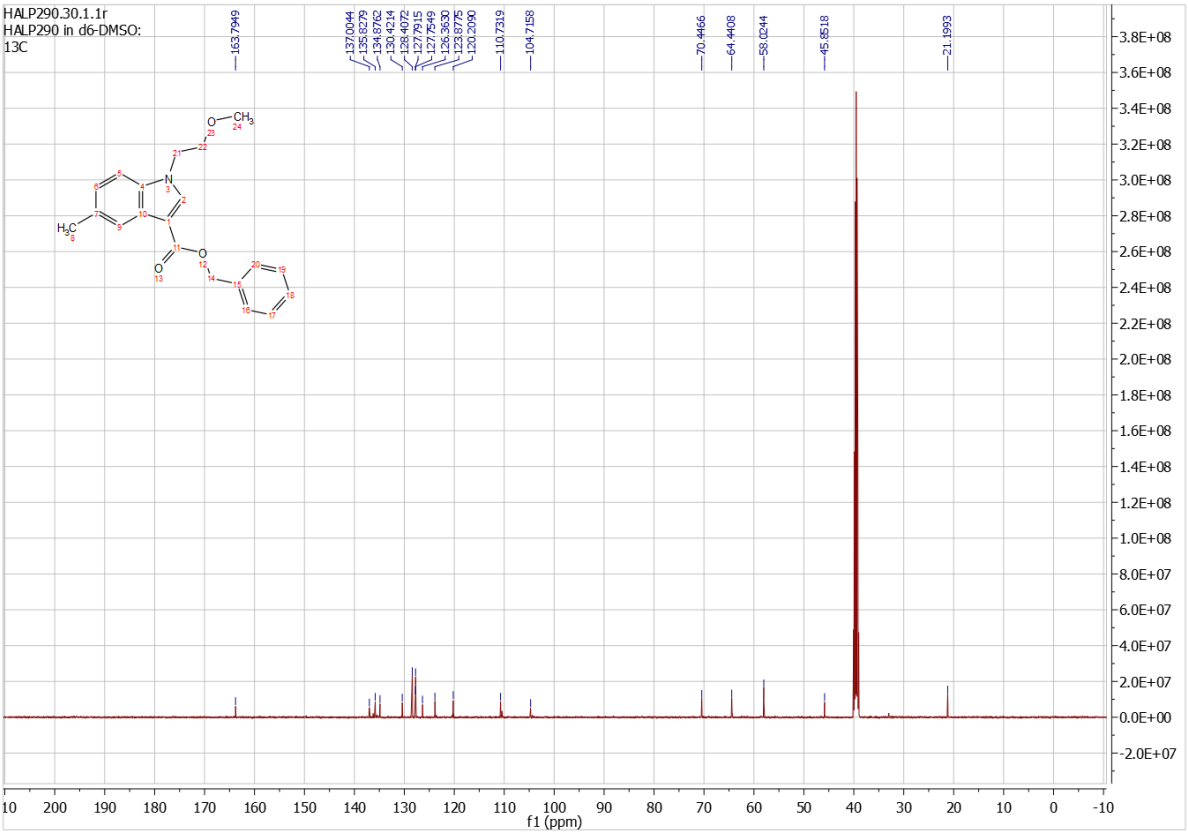
Signal: MS1 -TIC SCAN ESI Frag=135V Gain=1,0

RT [min]	Peak MS Base Peak m/z	Area	Area%	Max Peak%	Height
8.177	322.300	871751.6554	100.0000	100.000	146406.329
	Sum	871751.6554			



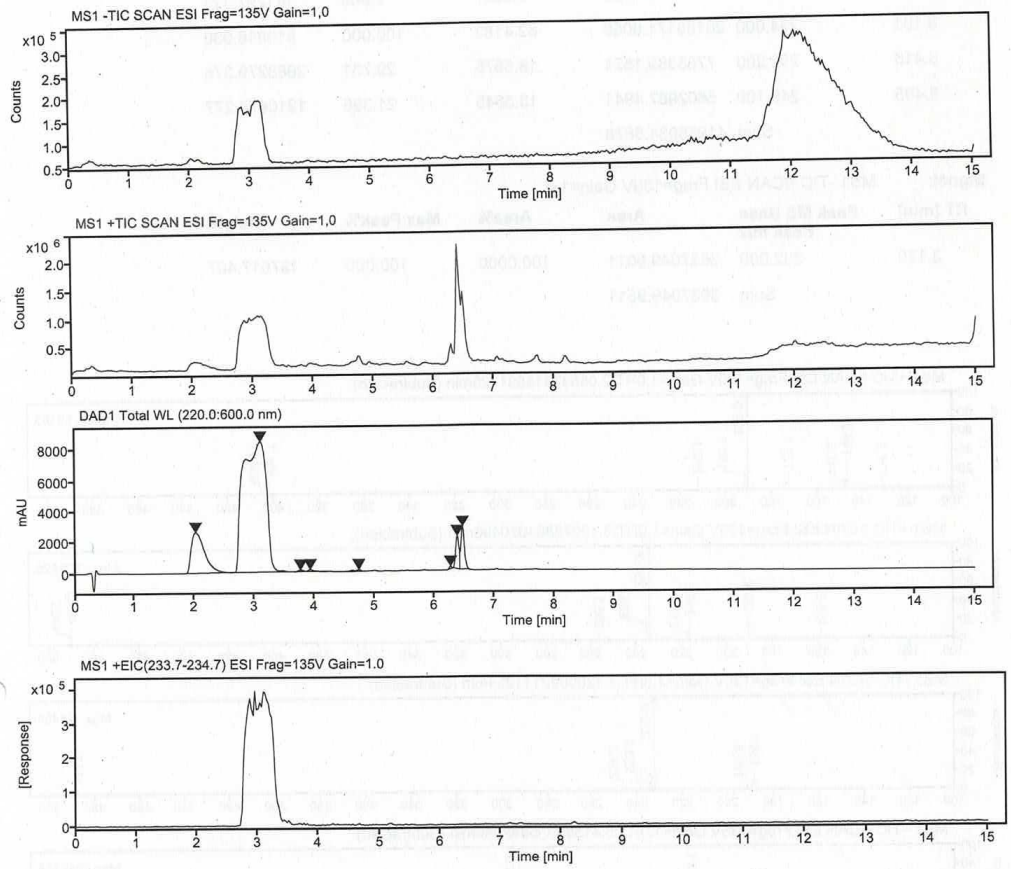



HALP290.10.1.1r
HALP290 in d6-DMSO:
1H
B (s) 8.0739
A (s) 7.8155
C (t) 7.4800
D (t) 7.4033
E (t) 7.3384
F (m) 7.0732
G (s) 5.3234
H (t) 4.3857
I (t) 3.6580
J (d) 3.8099
K (s) 3.2009
L (s) 2.4024
f1 (ppm)


HALP290.30.1.1r
HALP290 in d6-DMSO:
13C
f1 (ppm)

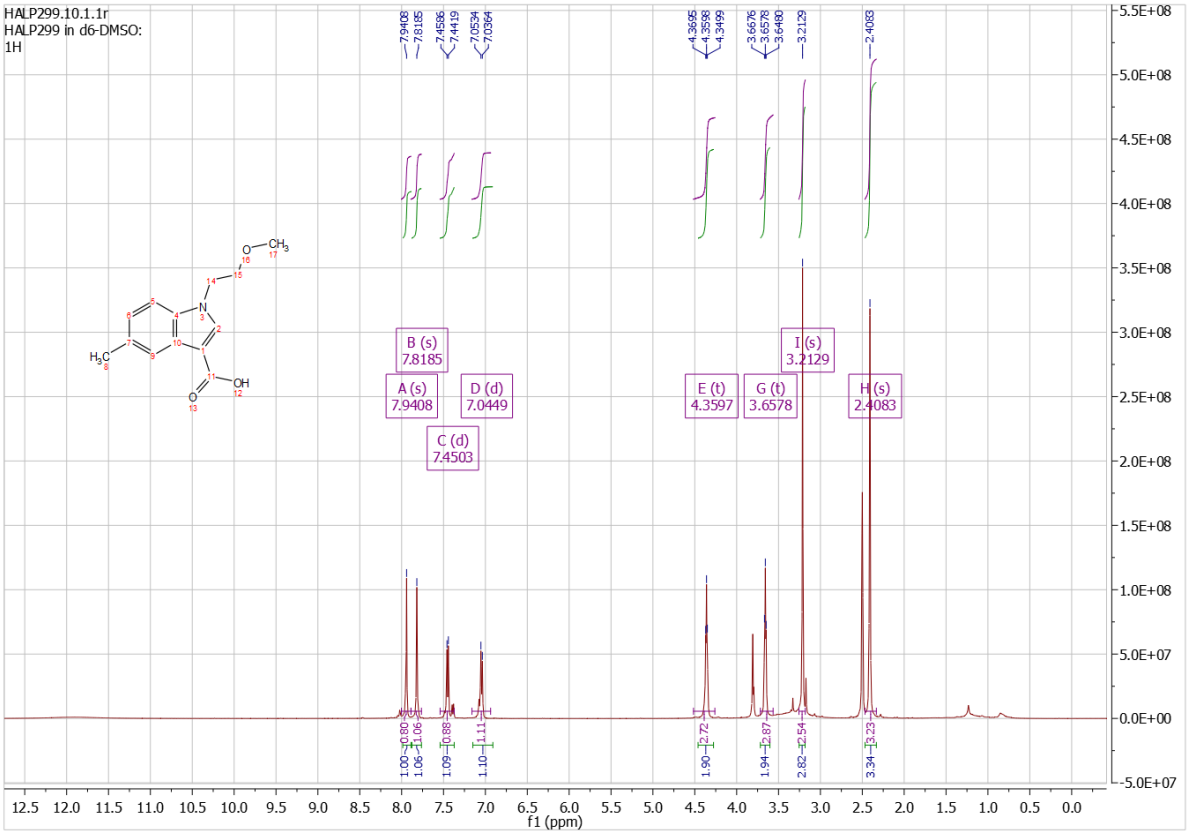
1-(2-Methoxyethyl)-5-methyl-1*H*-indole-3-carboxylic acid (4b)

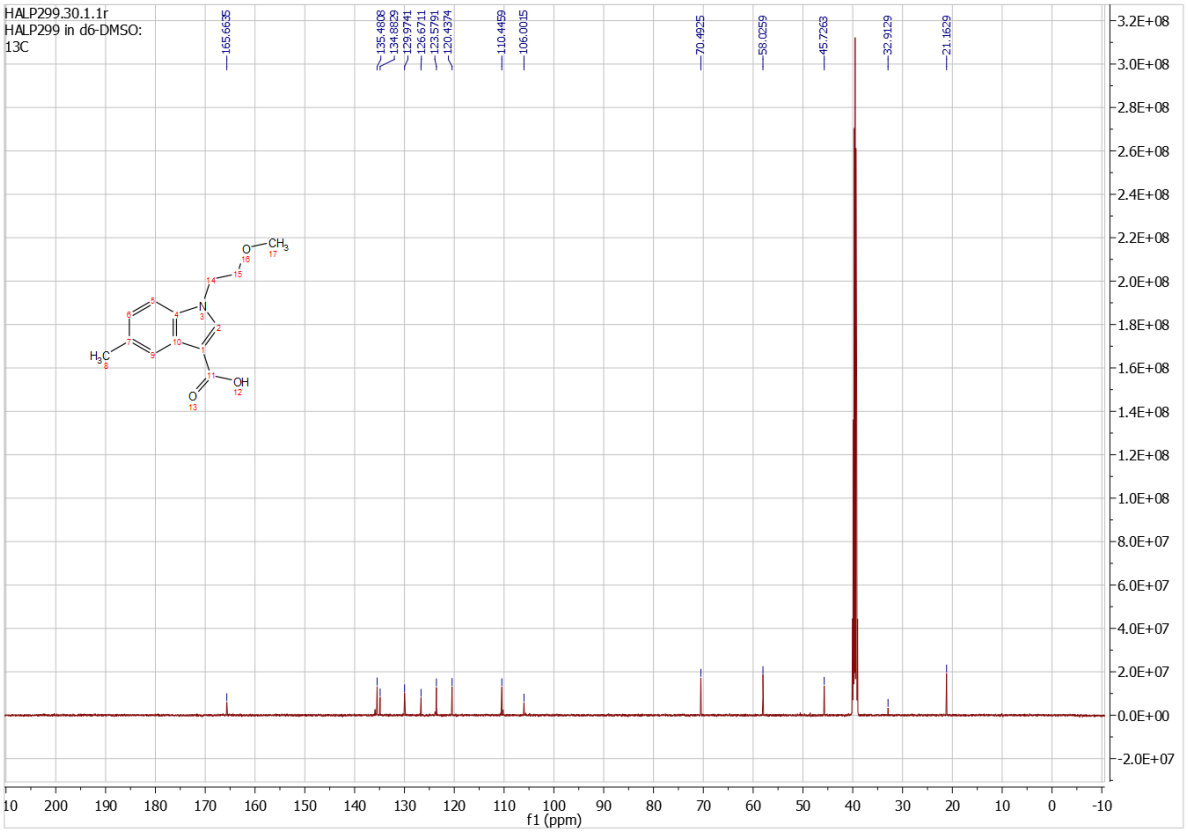
Sequence Name:	SingleSample		
Data file:	HALP299.dx	**Project Name:**	Single Quad
Sample name:	HALP299	**Operator :**	SYSTEM
Instrument:	Single Quad	**Acquired on:**	2023-11-02 14:37:10+01:00
Inj. volume:	4.000	**Location:**	P1-C1
Acq. method:	00-new_wasser-acn_standard_100-1000_BD-20min.amx		
Processing method:	MS_standard_plot.pmx		



Signal: DAD1 Total WL (220.0:600.0 nm)

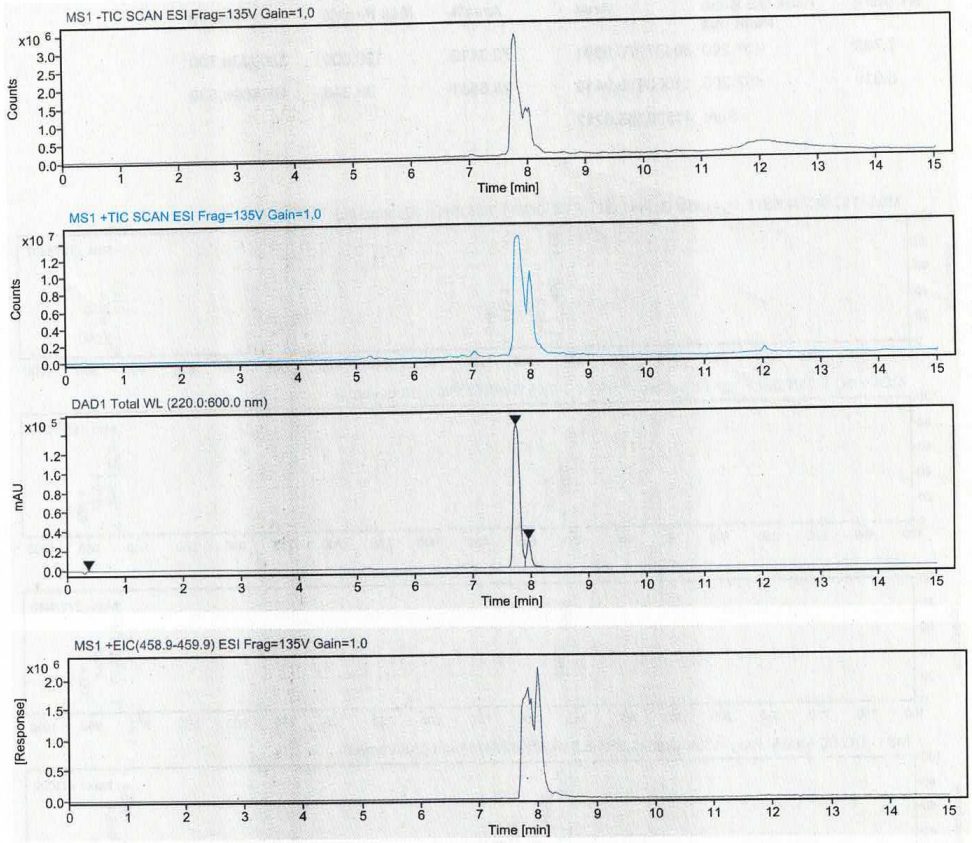
RT [min]	Peak MS Base Peak m/z	Area	Area%	Max Peak%	Height
2.025	190.000	39539.5111	13.9224	17.745	2604.055
3.105	232.000	222819.1845	78.4579	100.000	8415.152
3.766		409.7548	0.1443	0.184	99.153
3.928		543.4163	0.1913	0.244	113.963
4.735		832.7807	0.2932	0.374	102.819
6.266		398.4762	0.1403	0.179	153.918


HALP299.10.1.1r
HALP299 in d6-DMSO:
1H
B (s)
7.8185
A (s)
7.9408
D (d)
7.0449
C (d)
7.4503
I (s)
3.2129
E (t)
4.3597
G (t)
3.6578
H (s)
2.4083
f1 (ppm)


HALP299.30.1.1r
HALP299 in d6-DMSO:
13C
f1 (ppm)

_N_-(4-(4-Butyryl-5-methyl-1_H_-pyrazol-1-yl)phenyl)-1-(2-methoxyethyl)-5-methyl-1_H_-indole-3-carboxamide (4c)

Sequence Name:	SingleSample		
Data file:	HALP316-F3.dx	**Project Name:**	Single Quad
Sample name:	HALP316-F3	**Operator :**	SYSTEM
Instrument:	Single Quad	**Acquired on:**	2024-01-11 13:08:40+01:00
Inj. volume:	8.000	**Location:**	P1-B1
Acq. method:	00-new_wasser-acn_standard_100-1000_BD-20min.amx		
Processing method:	MS_standard_plot.pmx		



Signal: DAD1 Total WL (220.0:600.0 nm)

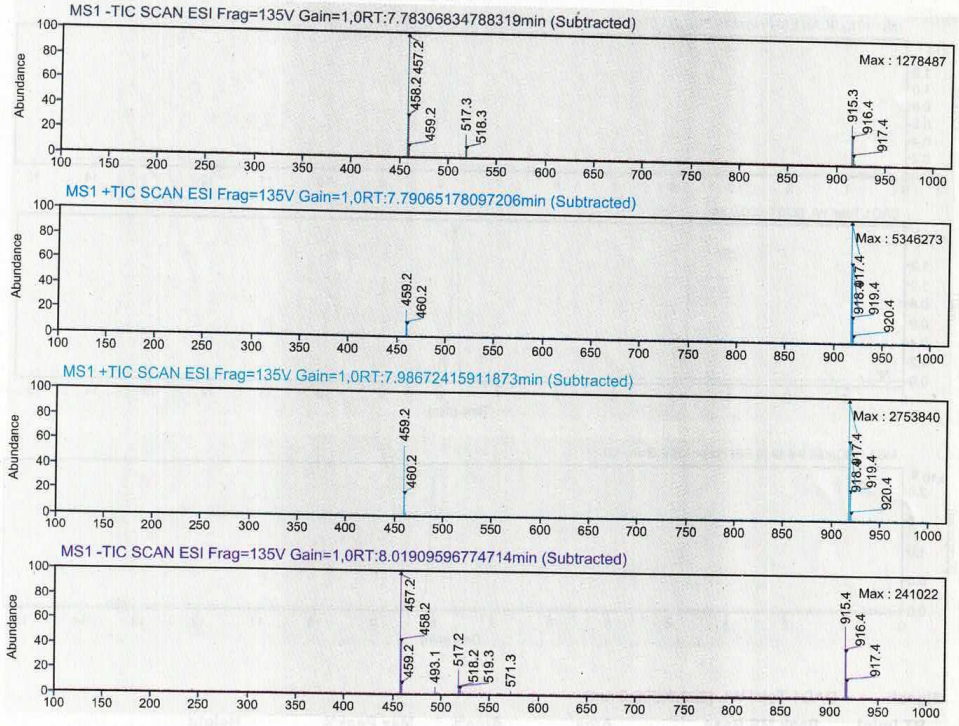
RT [min]	Peak MS Base Peak m/z	Area	Area%	Max Peak%	Height
0.370		2802.1503	0.2136	0.241	824.675
7.743	457.200	1160644.1636	88.4684	100.000	146609.277
7.953		148485.0097	11.3180	12.793	28120.596
	Sum	1311931.3236			

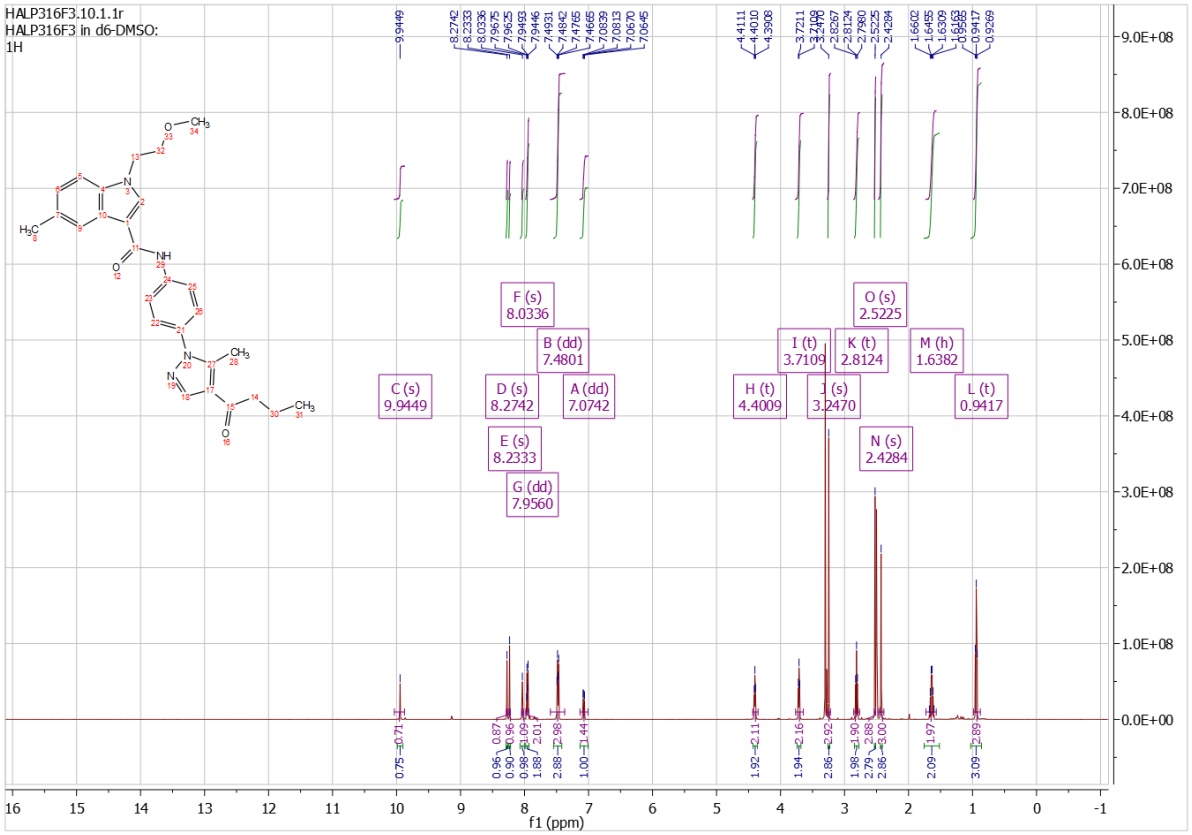
Signal: MS1 +TIC SCAN ESI Frag=135V Gain=1,0

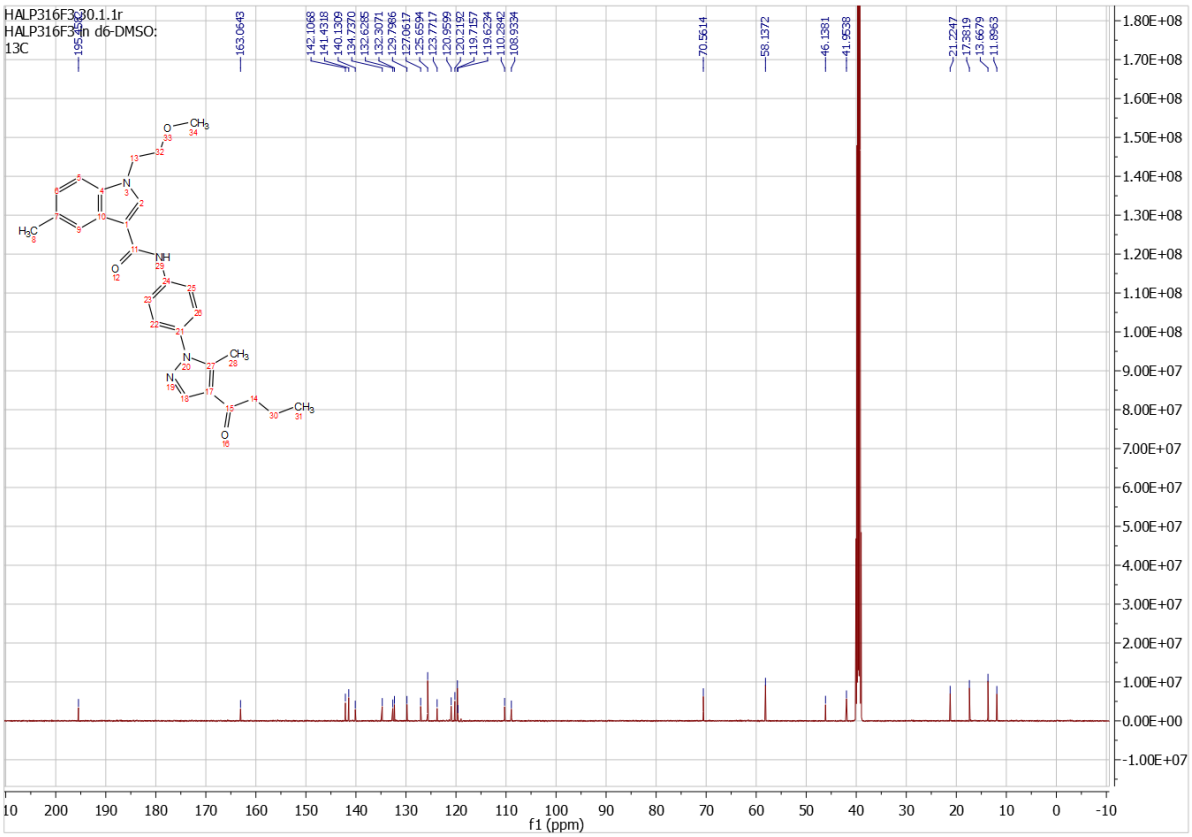
RT [min]	Peak MS Base Peak m/z	Area	Area%	Max Peak%	Height
7.791	917.400	152559757.3447	68.1407	100.000	14056121.667
7.987	917.400	71329449.8145	31.8593	46.755	9760055.678
	Sum	223889207.1592			

Signal: MS1 -TIC SCAN ESI Frag=135V Gain=1,0

RT [min]	Peak MS Base Peak m/z	Area	Area%	Max Peak%	Height
7.783	457.200	30437076.8801	73.3419	100.000	3300236.790
8.019	457.200	11063178.9410	26.6581	36.348	1268996.538
	Sum	41500255.8212			



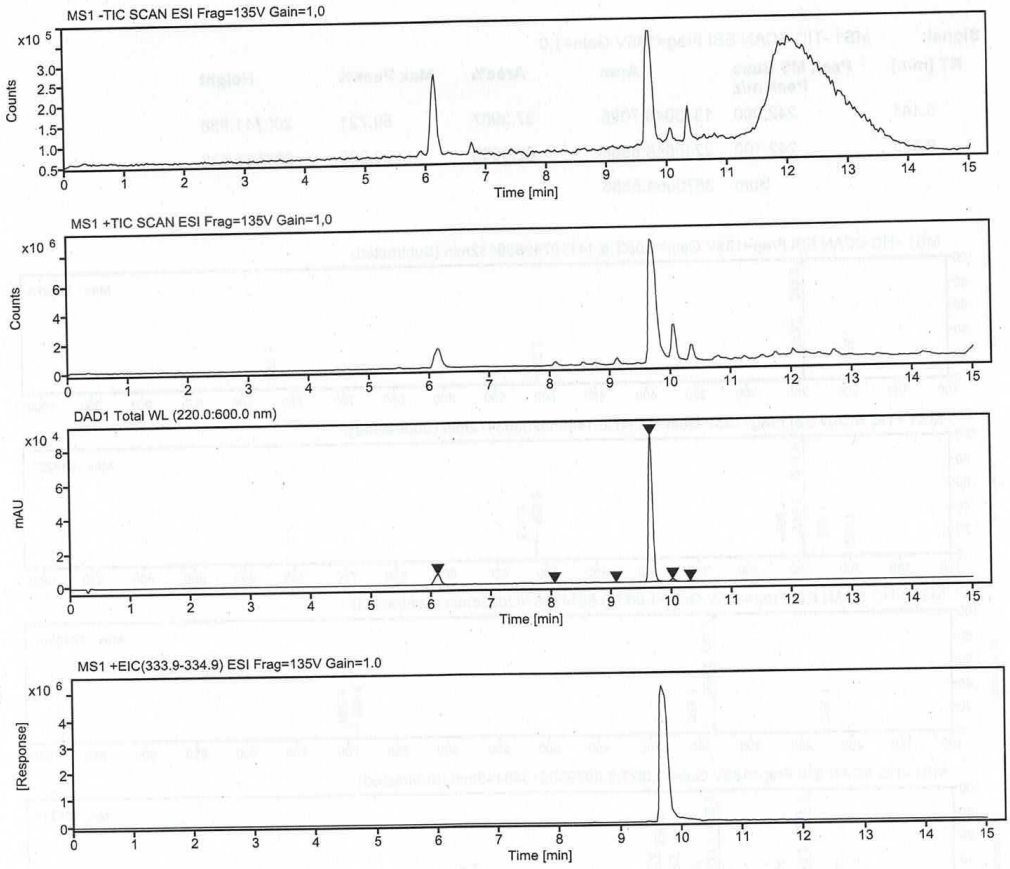

HALP316F3.10.1.1r
HALP316F3 in d6-DMSO:
1H
F (s)
8.0336
B (dd)
7.4801
C (s)
9.9449
D (s)
8.2742
A (dd)
7.0742
E (s)
8.2333
G (dd)
7.9560
O (s)
2.5225
I (t)
3.7109
K (t)
2.8124
M (h)
1.6382
H (t)
4.4009
J (s)
3.2470
L (t)
0.9417
N (s)
2.4284
f1 (ppm)


HALP316F3.30.1.1r
HALP316F3 in d6-DMSO:
13C
f1 (ppm)

Benzyl 1-(cyclobutylmethyl)-5-methyl-1*H*-indole-3-carboxylate (5a)

go for reduction

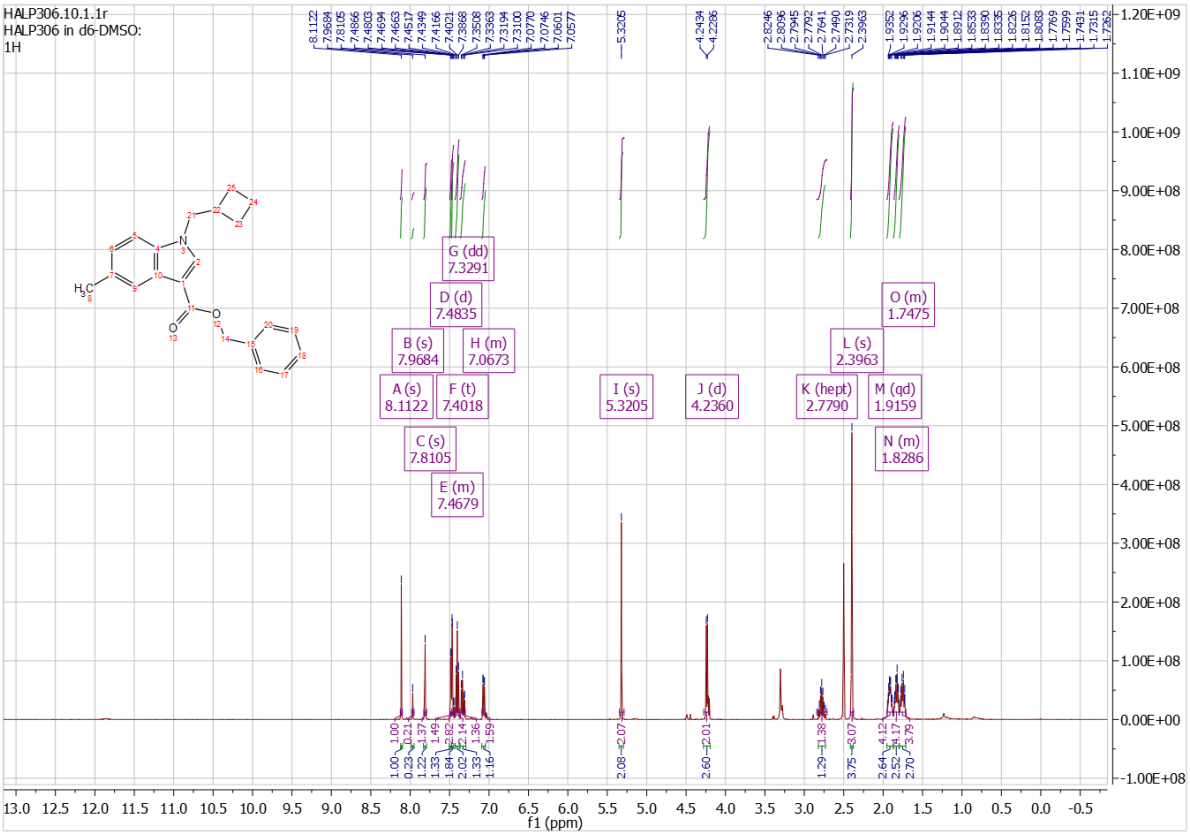
Sequence Name:	SingleSample		
Data file:	HALP306.dx	**Project Name:**	Single Quad
Sample name:	HALP306	**Operator :**	SYSTEM
Instrument:	Single Quad	**Acquired on:**	2023-11-07 17:49:31+01:00
Inj. volume:	4.000	**Location:**	P1-A10
Acq. method:	00-new_wasser-acn_standard_100-1000_BD-20min.amx		
Processing method:	MS_standard_plot.pmx		

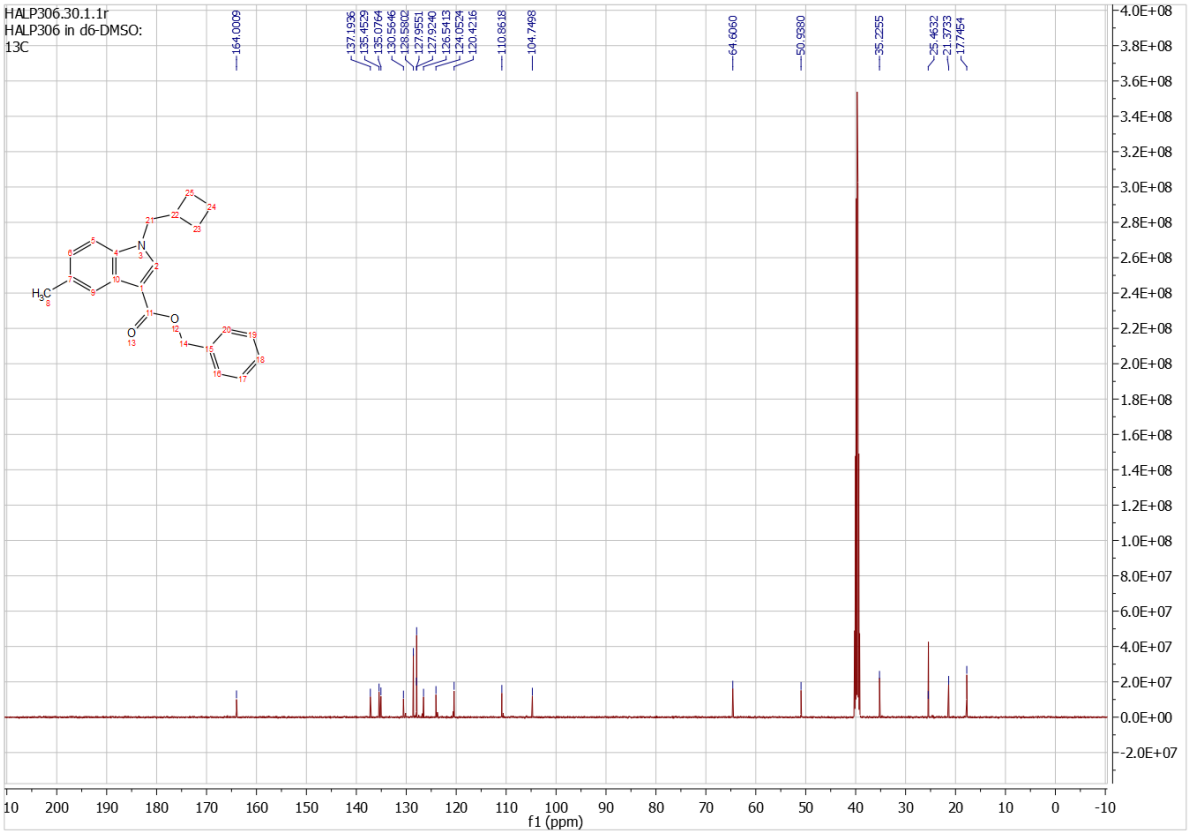


Signal: DAD1 Total WL (220.0:600.0 nm)

RT [min]	Peak MS Base Peak m/z	Area	Area%	Max Peak%	Height
6.114	242.000	41416.7733	9.0948	10.227	5779.660
8.056		735.0184	0.1614	0.181	88.524
9.081		430.7125	0.0946	0.106	112.008
9.657	334.200	404994.1561	88.9340	100.000	85407.928
10.015		6503.5515	1.4281	1.606	1547.459
10.313		1307.1043	0.2870	0.323	322.452

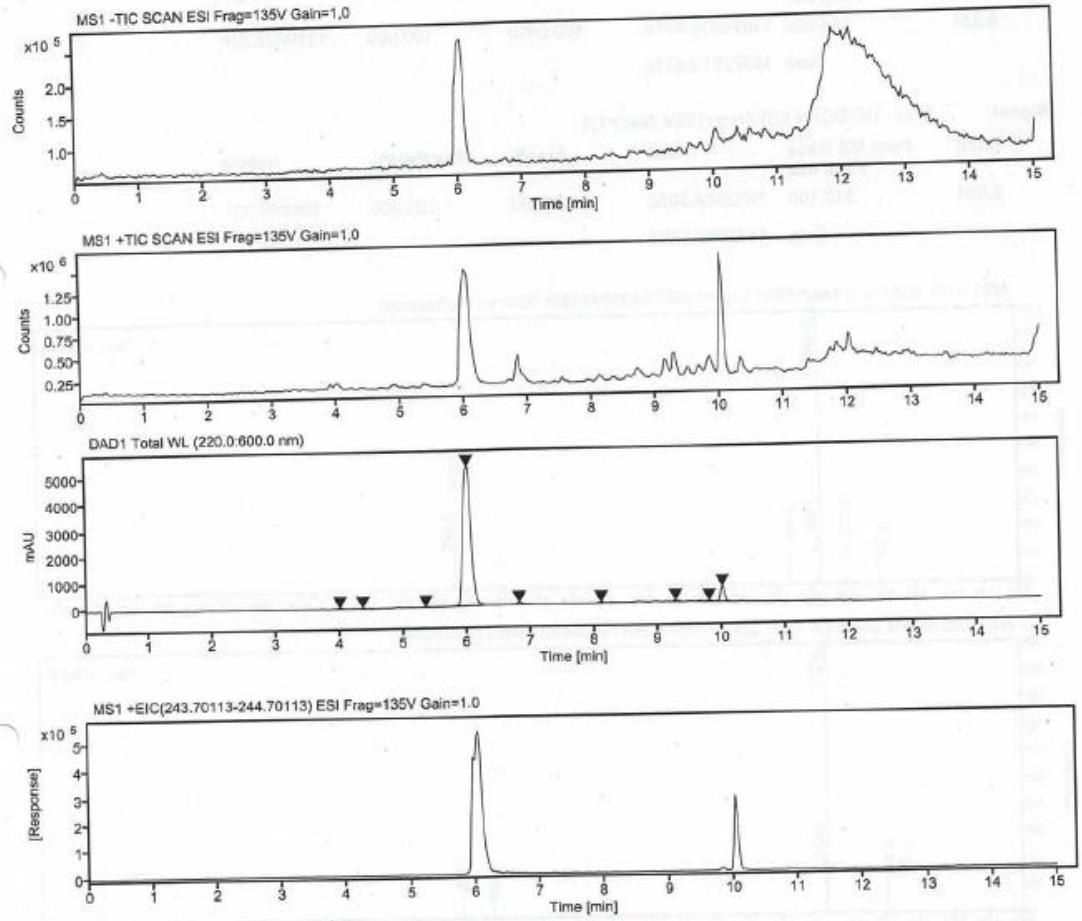
D:\CDSProjects\Default\00-standardplot+EIC.rdl [Rev. 7725] Printed: 2023-11-08 08:31:41+01:00 Page 1 of 2


HALP306.10.1.1r
HALP306 in d6-DMSO:
1H
G (dd)
7.3291
D (d)
7.4835
O (m)
1.7475
B (s)
7.9684
H (m)
7.0673
L (s)
2.3963
A (s)
8.1122
F (t)
7.4018
I (s)
5.3205
J (d)
4.2360
K (hept)
2.7790
M (qd)
1.9159
C (s)
7.8105
N (m)
1.8286
E (m)
7.4679
f1 (ppm)


HALP306.30.1.1r
HALP306 in d6-DMSO:
13C
f1 (ppm)

1-(Cyclobutylmethyl)-5-methyl-1*H*-indole-3-carboxylic acid (5b)

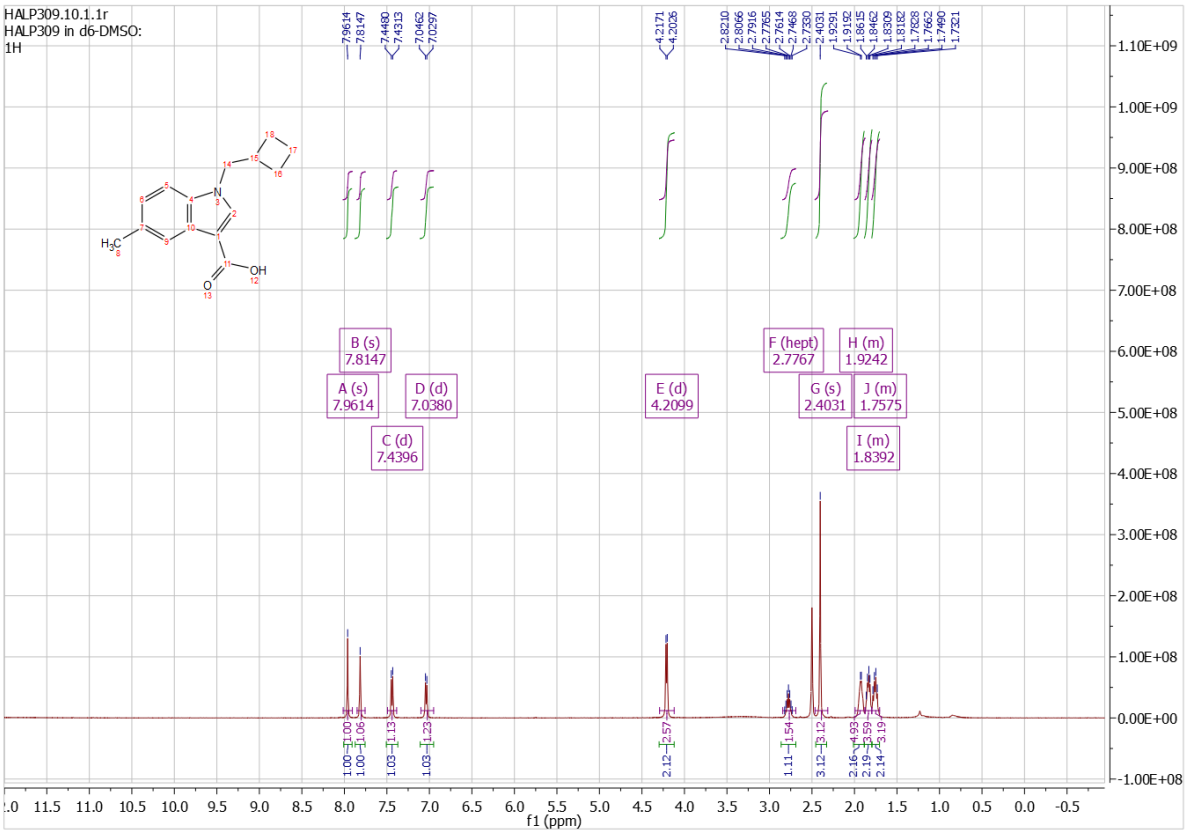
Sequence Name:	SingleSample		
Data file:	2023-11-14 16-32-02+01-00.dx	**Project Name:**	Single Quad
Sample name:	HALP309	**Operator :**	SYSTEM
Instrument:	Single Quad	**Acquired on:**	2023-11-14 16:33:01+01:00
Inj. volume:	2.000	**Location:**	P1-C6
Acq. method:	00-new_wasser-acn_standard_100-1000_BD-20min.amx		
Processing method:	MS_standard_plot.pmx		

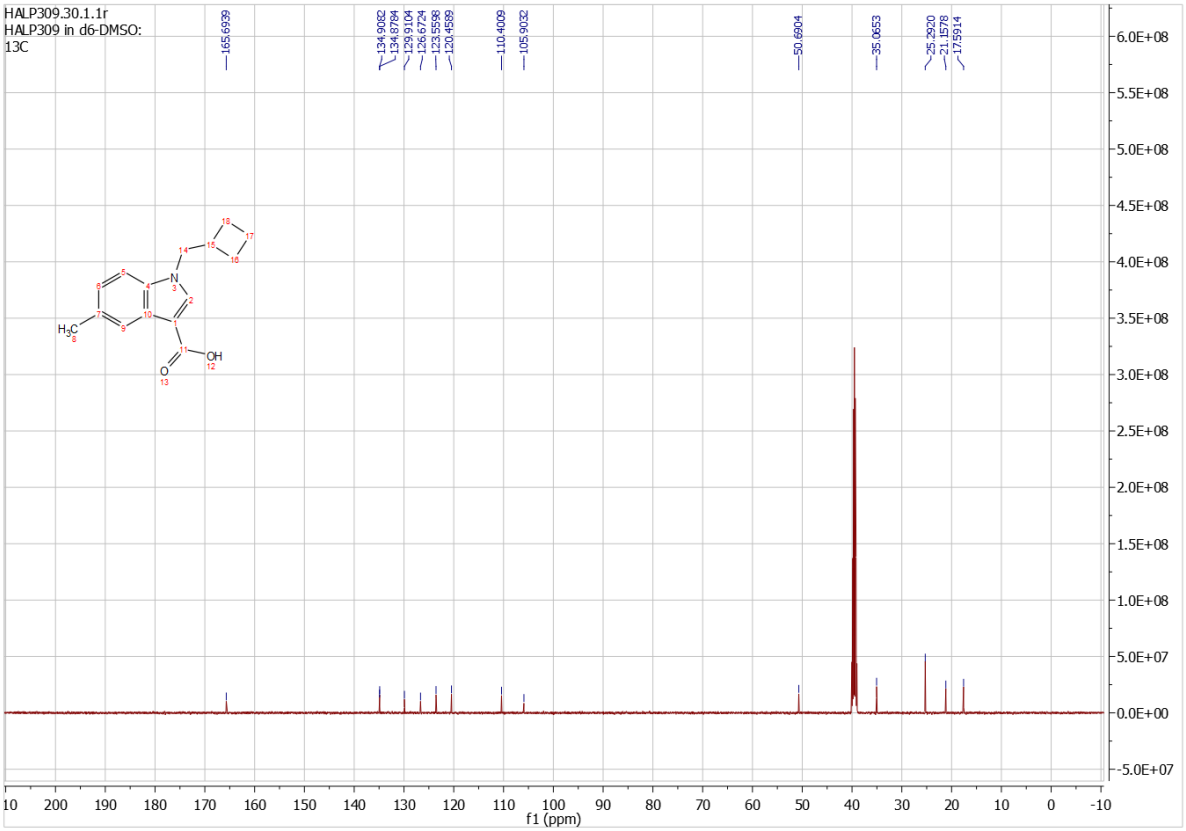


Signal: DAD1 Total WL (220.0:600.0 nm)

RT [min]	Peak MS Base Peak m/z	Area	Area%	Max Peak%	Height
3.998		167.7627	0.3282	0.358	35.048
4.356		136.0011	0.2661	0.290	30.395
5.346		48.3765	0.0946	0.103	19.422
6.012	244.000	46900.8184	91.7589	100.000	5302.353
6.812		642.1671	1.2564	1.369	85.640
8.101		110.1811	0.2156	0.235	31.336

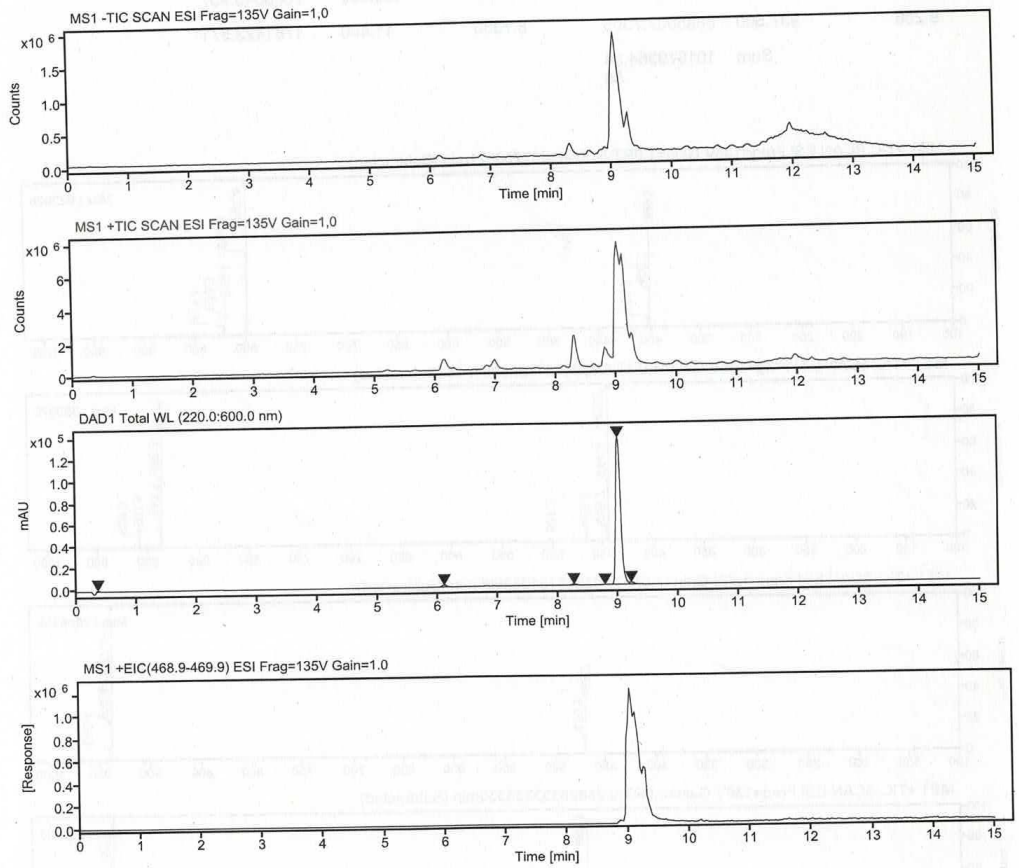
D:\CDSProjects\Default\00-standardplot+EIC.rdl [Rev. 7829] Printed: 2023-11-15 06:57:58+01:00 Page 1 of 2


HALP309.10.1.1r
HALP309 in d6-DMSO:
1H
B (s)
7.8147
A (s)
7.9614
D (d)
7.0380
C (d)
7.4396
E (d)
4.2099
F (hept)
2.7767
H (m)
1.9242
G (s)
2.4031
J (m)
1.7575
I (m)
1.8392
f1 (ppm)


HALP309.30.1.1r
HALP309 in d6-DMSO:
13C
f1 (ppm)

_N_-(4-(4-Butyryl-5-methyl-1_H_-pyrazol-1-yl)phenyl)-1-(cyclobutylmethyl)-5-methyl-1_H_-indole-3-carboxamide (5c)

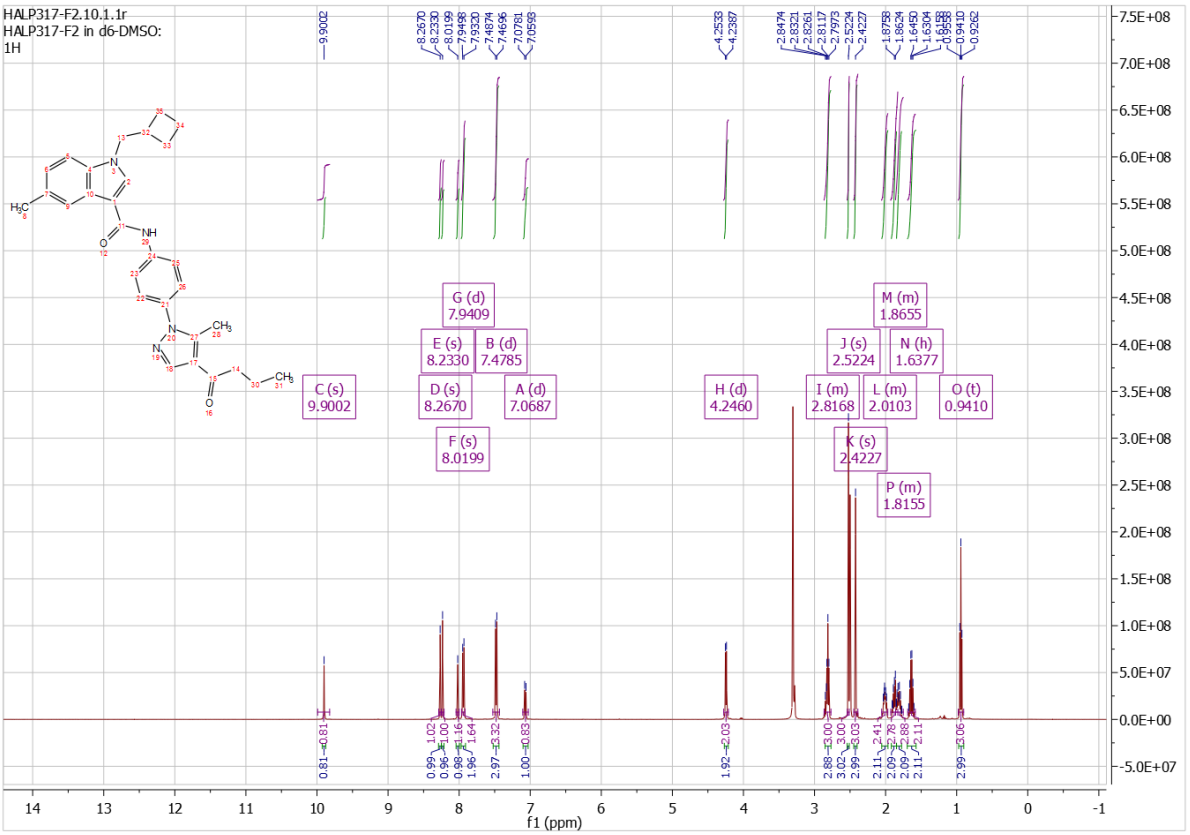
Sequence Name:	SingleSample		
Data file:	HALP317-F2.dx	**Project Name:**	Single Quad
Sample name:	HALP317-F2	**Operator :**	SYSTEM
Instrument:	Single Quad	**Acquired on:**	2024-01-09 00:06:22+01:00
Inj. volume:	6.000	**Location:**	P1-D11
Acq. method:	00-new_wasser-acn_standard_100-1000_BD-20min.amx		
Processing method:	MS_standard_plot.pmx		

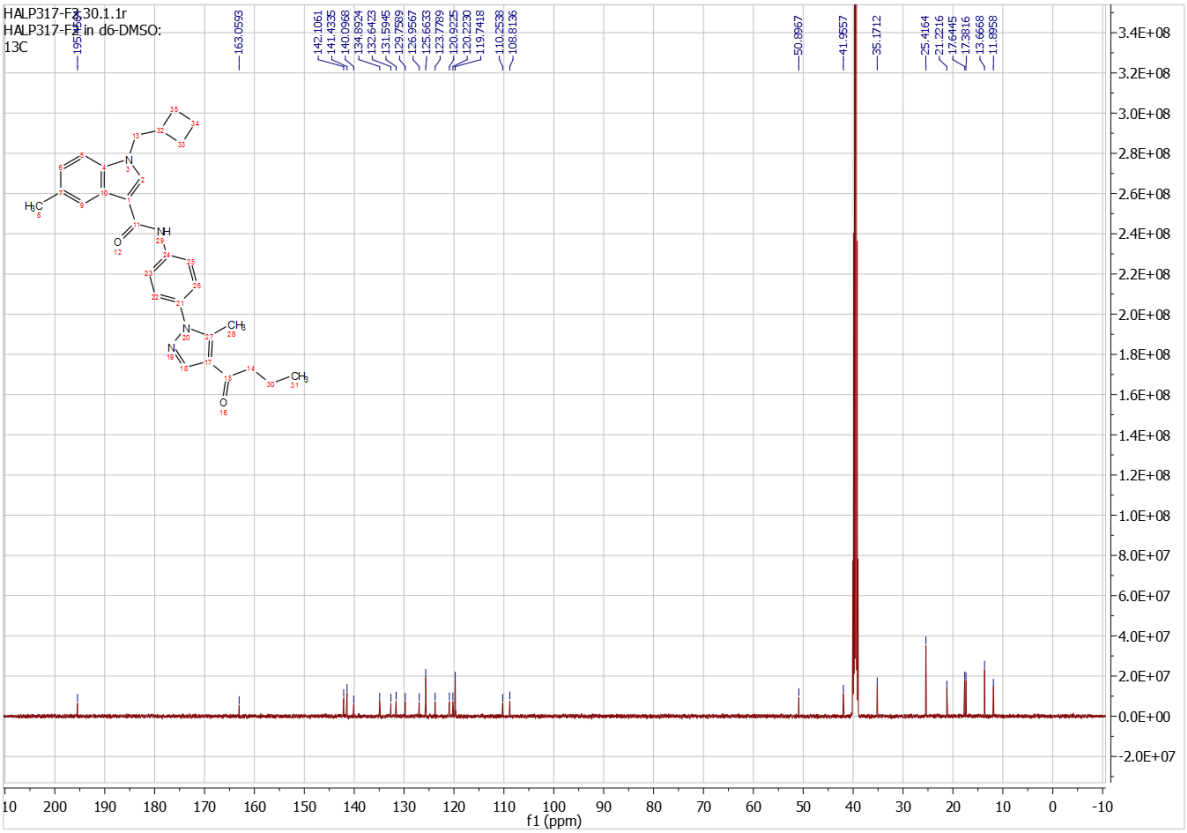


Signal: DAD1 Total WL (220.0:600.0 nm)

RT [min]	Peak MS Base Peak m/z	Area	Area%	Max Peak%	Height
0.375		1746.3456	0.2188	0.226	724.912
6.114		8257.2460	1.0344	1.068	1654.825
8.268		4524.3193	0.5668	0.585	1045.714
8.791		830.5086	0.1040	0.107	158.804
9.015	937.400	773509.2106	96.9014	100.000	135358.299
9.225		9376.1258	1.1746	1.212	1887.282

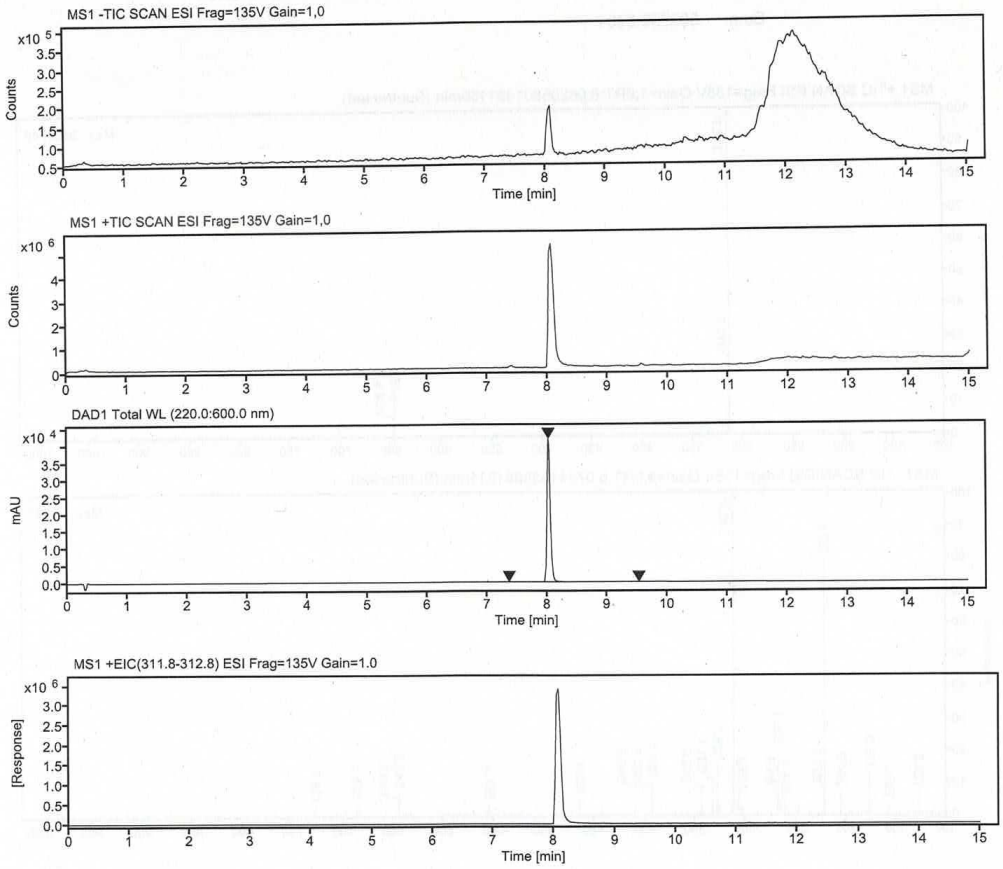
D:\CDSProjects\Default\00-standardplot+EIC.rdl [Rev. 8592] Printed: 2024-01-09 11:40:04+01:00 Page 1 of 2


HALP317-F2.10.1.1r
HALP317-F2 in d6-DMSO:
1H
G (d) 7.9409
E (s) 8.2330
B (d) 7.4785
D (s) 8.2670
A (d) 7.0687
F (s) 8.0199
C (s) 9.9002
M (m) 1.8655
J (s) 2.5224
N (h) 1.6377
H (d) 4.2460
I (m) 2.8168
L (m) 2.0103
O (t) 0.9410
K (s) 2.4227
P (m) 1.8155
f1 (ppm)


HALP317-F2.30.1.1r
HALP317-F2 in d6-DMSO:
13C
f1 (ppm)

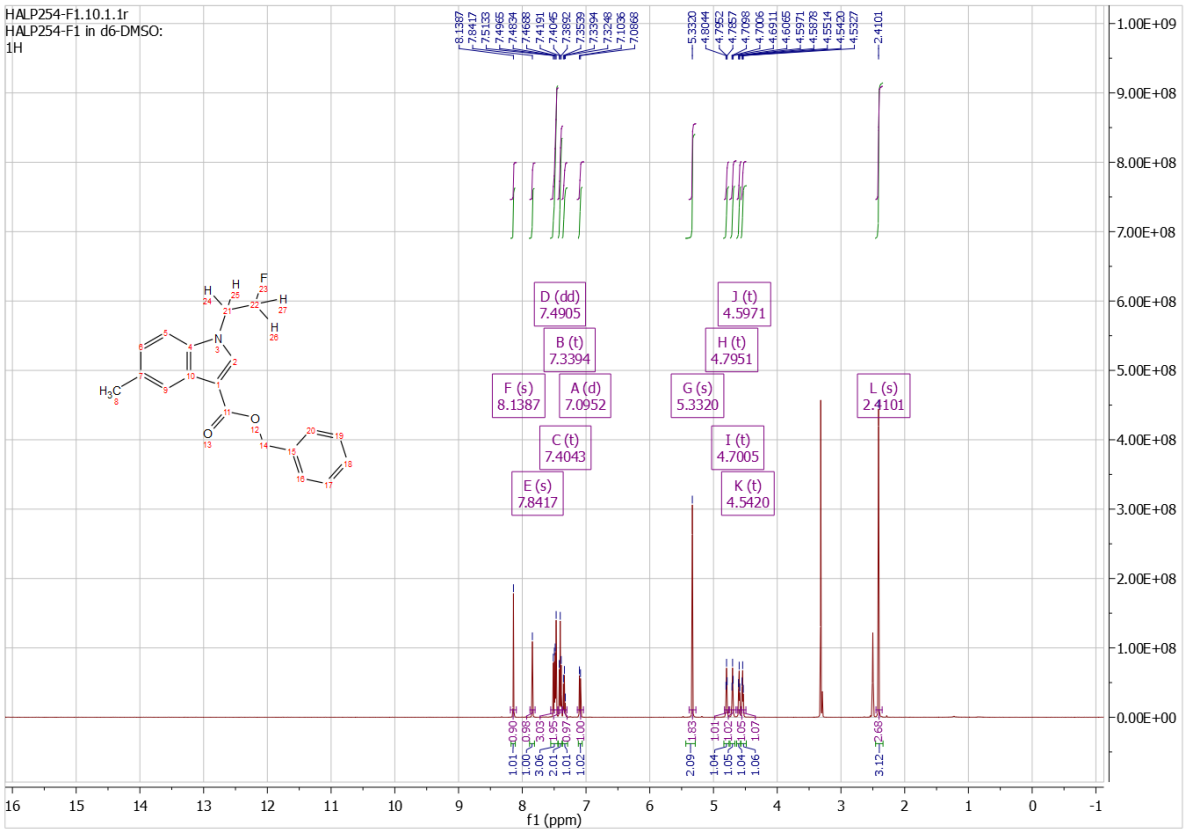
Benzyl 1-(2-fluoroethyl)-5-methyl-1*H*-indole-3-carboxylate (6a)

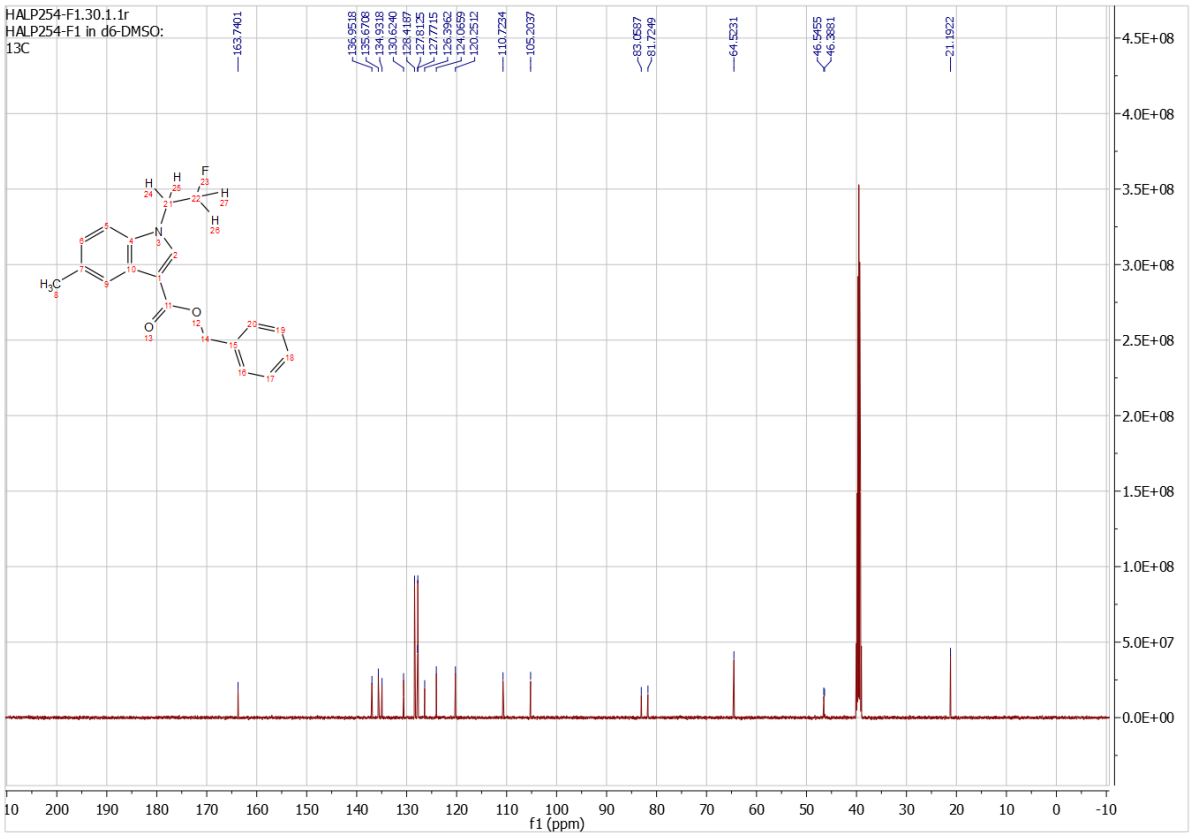
Sequence Name:	SingleSample		
Data file:	HALP254-F1.dx	**Project Name:**	Single Quad
Sample name:	HALP254-F1	**Operator :**	SYSTEM
Instrument:	Single Quad	**Acquired on:**	2023-10-26 11:48:34+02:00
Inj. volume:	2.000	**Location:**	P1-B3
Acq. method:	00-new_wasser-acn_standard_100-1000_BD-20min.amx		
Processing method:	MS_standard_plot.pmx		



Signal: DAD1 Total WL (220.0:600.0 nm)

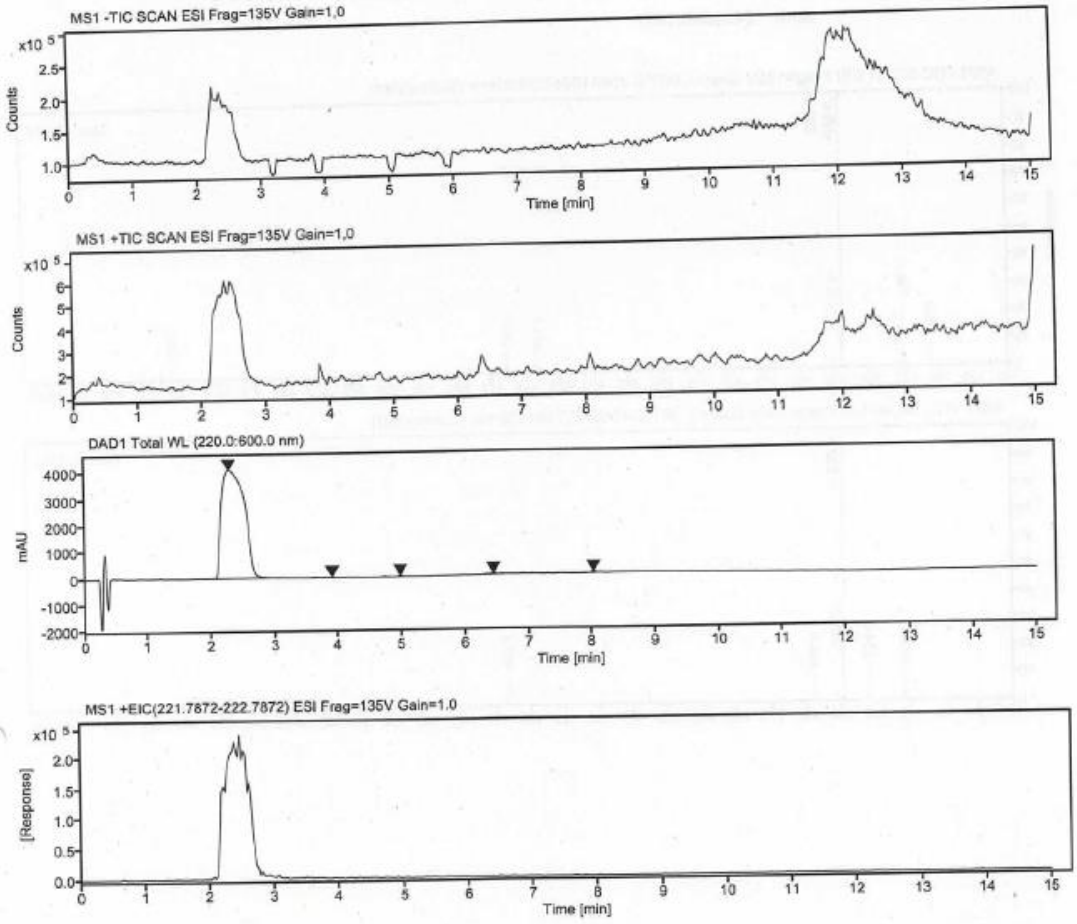
RT [min]	Peak MS Base Peak m/z	Area	Area%	Max Peak%	Height
7.373		191.0122	0.1162	0.116	27.220
8.031	312.100	164048.7818	99.8337	100.000	41893.127
9.532		82.3269	0.0501	0.050	23.028
	Sum	164322.1209			


HALP254-F1.10.1.1r
HALP254-F1 in d6-DMSO:
1H
D (dd)
7.4905
B (t)
7.3394
F (s)
8.1387
A (d)
7.0952
C (t)
7.4043
E (s)
7.8417
J (t)
4.5971
H (t)
4.7951
G (s)
5.3320
I (t)
4.7005
K (t)
4.5420
L (s)
2.4101
f1 (ppm)


HALP254-F1.30.1.1r
HALP254-F1 in d6-DMSO:
13C
f1 (ppm)

1-(2-Fluoroethyl)-5-methyl-1*H*-indole-3-carboxylic acid (6b)

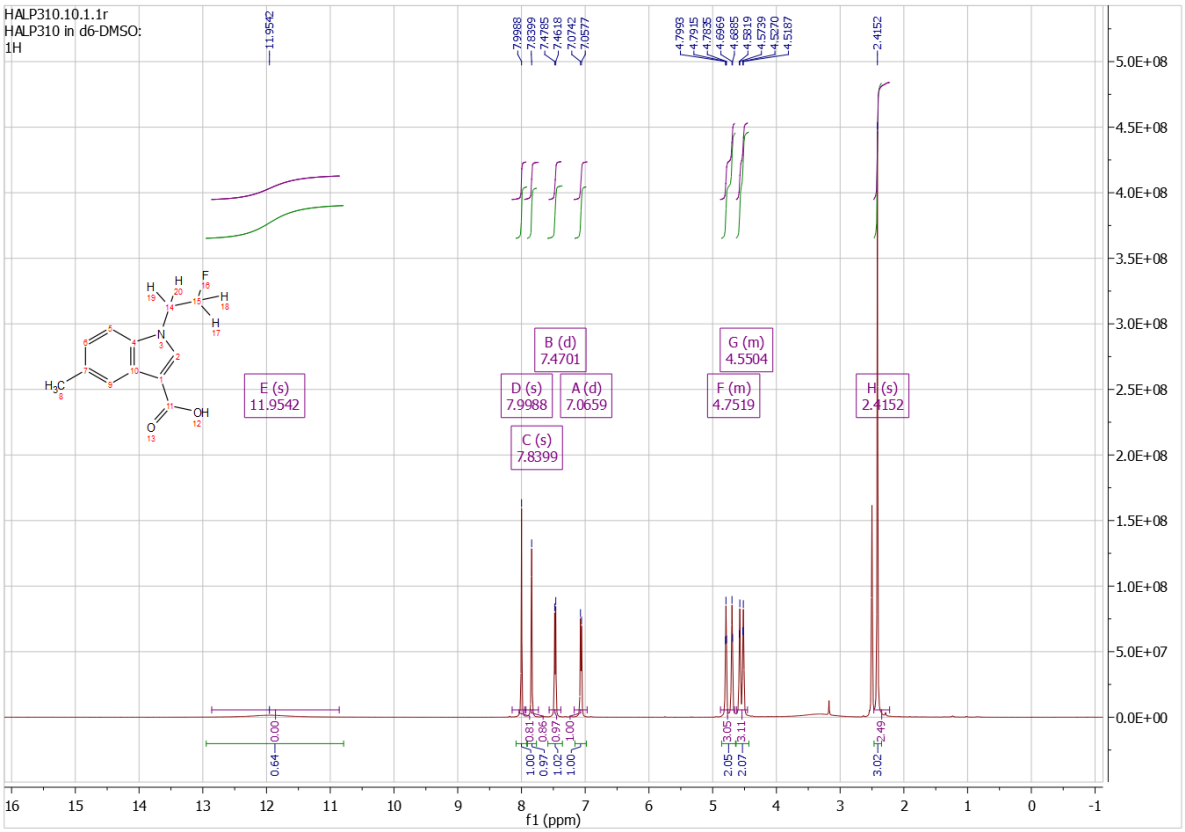
Sequence Name:	SingleSample		
Data file:	2023-11-14 16-53-03+01-00.dx	**Project Name:**	Single Quad
Sample name:	HALP310	**Operator :**	SYSTEM
Instrument:	Single Quad	**Acquired on:**	2023-11-14 16:54:03+01:00
Inj. volume:	4.000	**Location:**	P1-C7
Acq. method:	00-new_wasser-acn_standard_100-1500_BD-20min.amx		
Processing method:	MS_standard_plot.pmx		

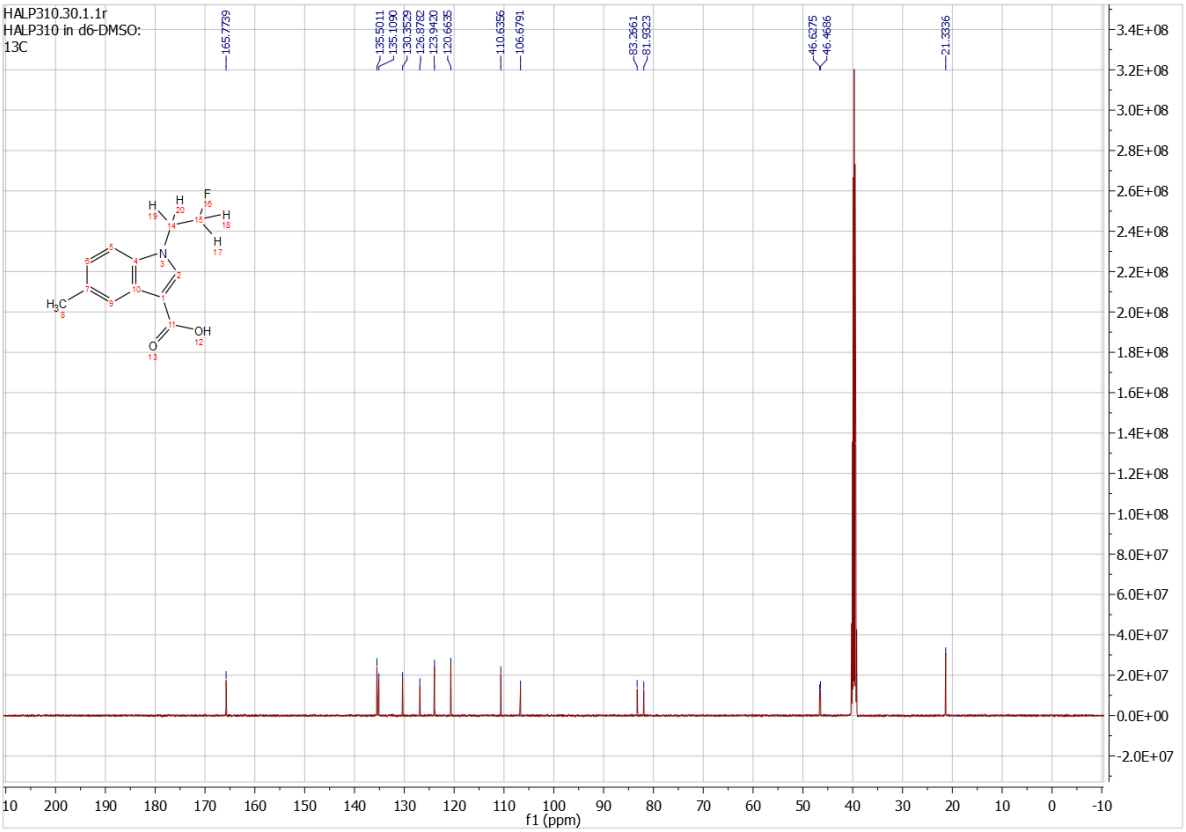


Signal: DAD1 Total WL (220.0:600.0 nm)

RT [min]	Peak MS Base Peak m/z	Area	Area%	Max Peak%	Height
2.295	219.900	101368.4094	99.1902	100.000	4086.343
3.910		43.0047	0.0421	0.042	9.799
4.981		285.0390	0.2789	0.281	27.935
6.449		319.0936	0.3122	0.315	34.176
8.028		180.4905	0.1766	0.178	45.130
	Sum	102196.0371			

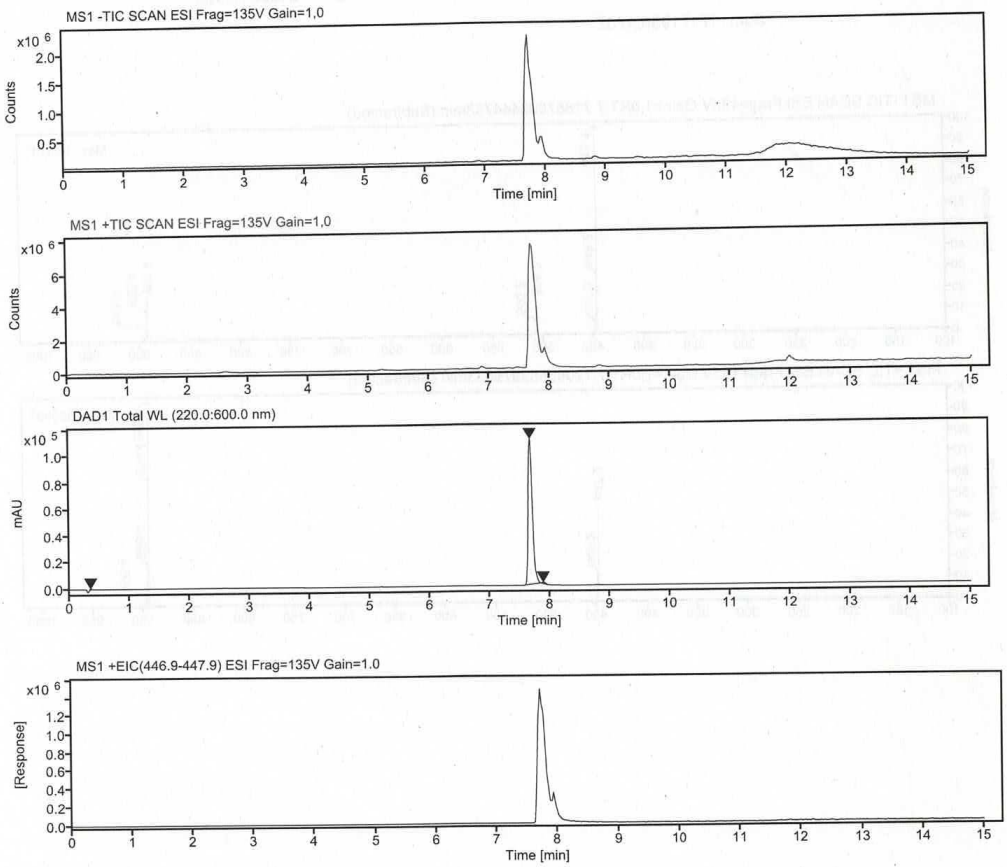
D:\CDSProjects\Default\00-standardplot+EIC.rdl [Rev. 7829] Printed: 2023-11-15 06:59:40+01:00 Page 1 of 2


HALP310.10.1.1r
HALP310 in d6-DMSO:
1H
E (s)
11.9542
B (d)
7.4701
D (s)
7.9988
A (d)
7.0659
C (s)
7.8399
G (m)
4.5504
F (m)
4.7519
H (s)
2.4152
f1 (ppm)


HALP310.30.1.1r
HALP310 in d6-DMSO:
13C
f1 (ppm)

N-(4-(4-Butyryl-5-methyl-1*H*-pyrazol-1-yl)phenyl)-1-(2-fluoroethyl)-5-methyl-1*H*-indole-3-carboxamide (6c)

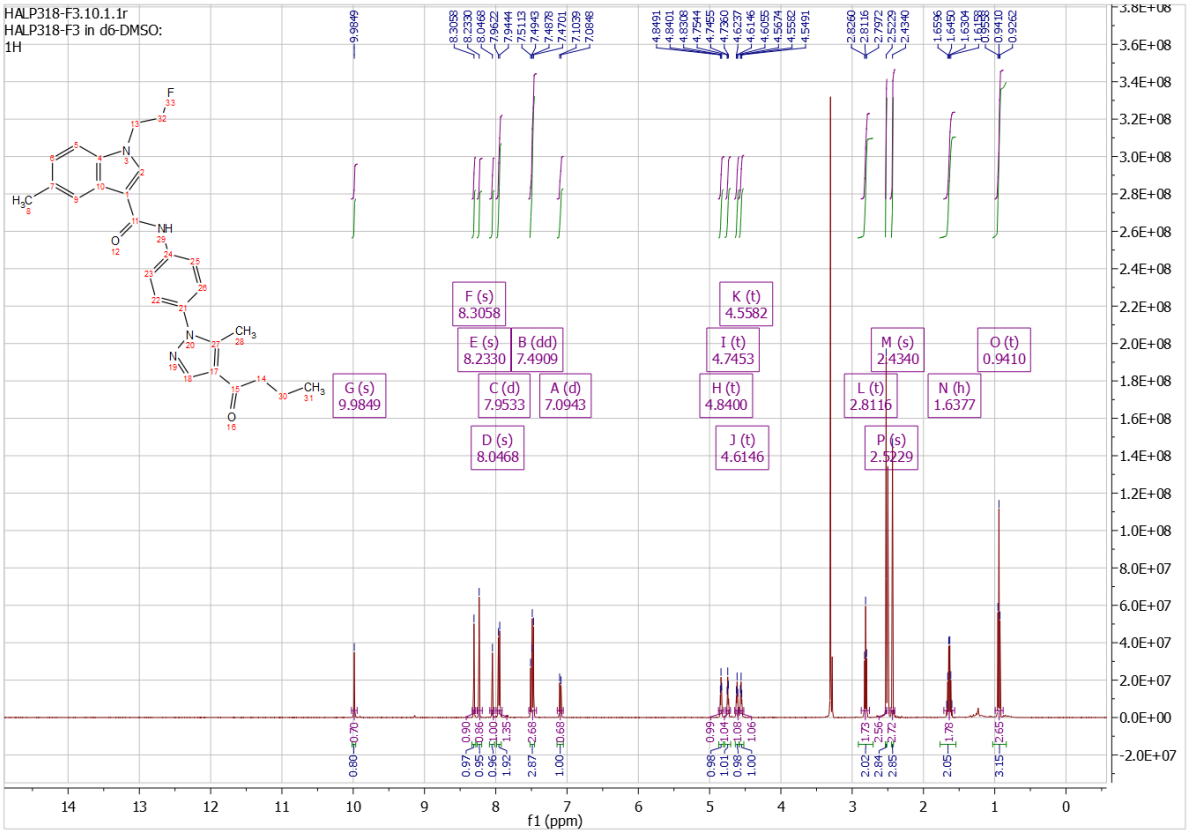
Sequence Name:	SingleSample		
Data file:	HALP318-F3.dx	**Project Name:**	Single Quad
Sample name:	HALP318-F3	**Operator :**	SYSTEM
Instrument:	Single Quad	**Acquired on:**	2023-12-28 18:31:30+01:00
Inj. volume:	2.000	**Location:**	P2-A1
Acq. method:	00-new_wasser-acn_standard_100-1000_BD-20min.amx		
Processing method:	MS_standard_plot.pmx		

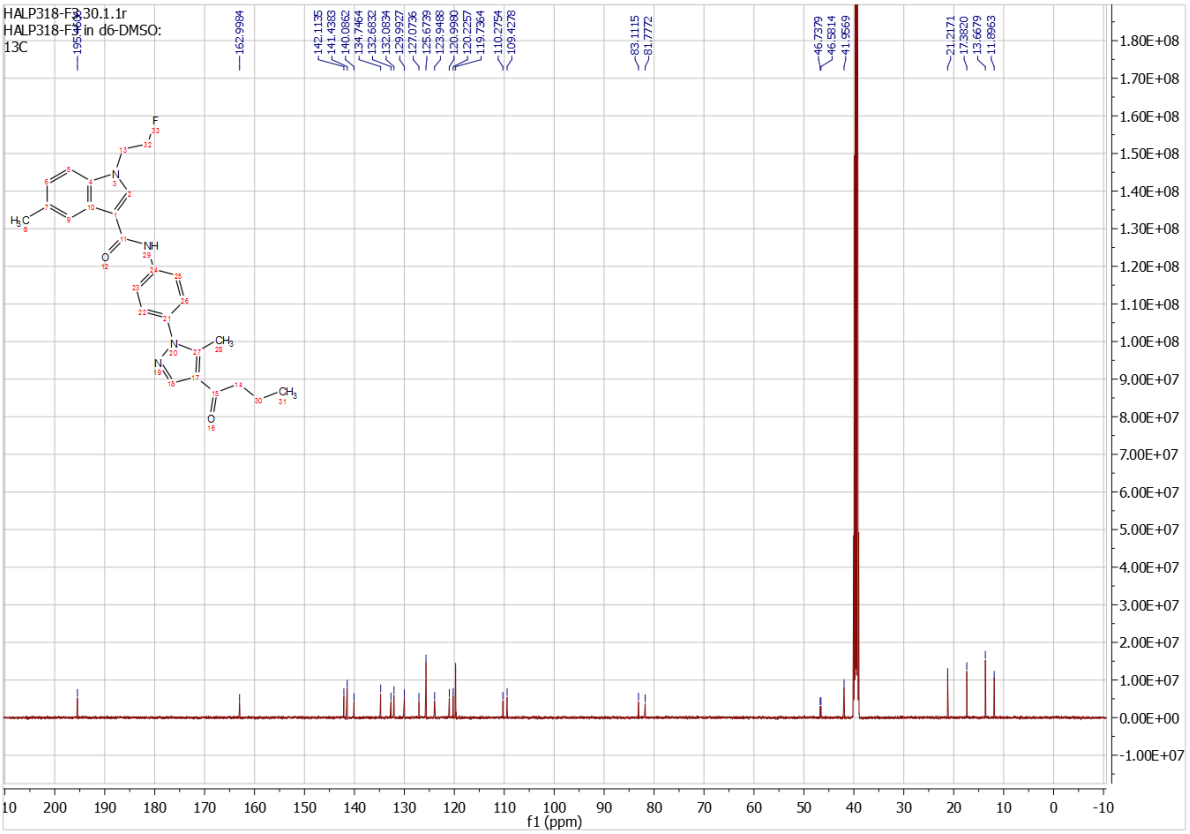


Signal: DAD1 Total WL (220.0:600.0 nm)

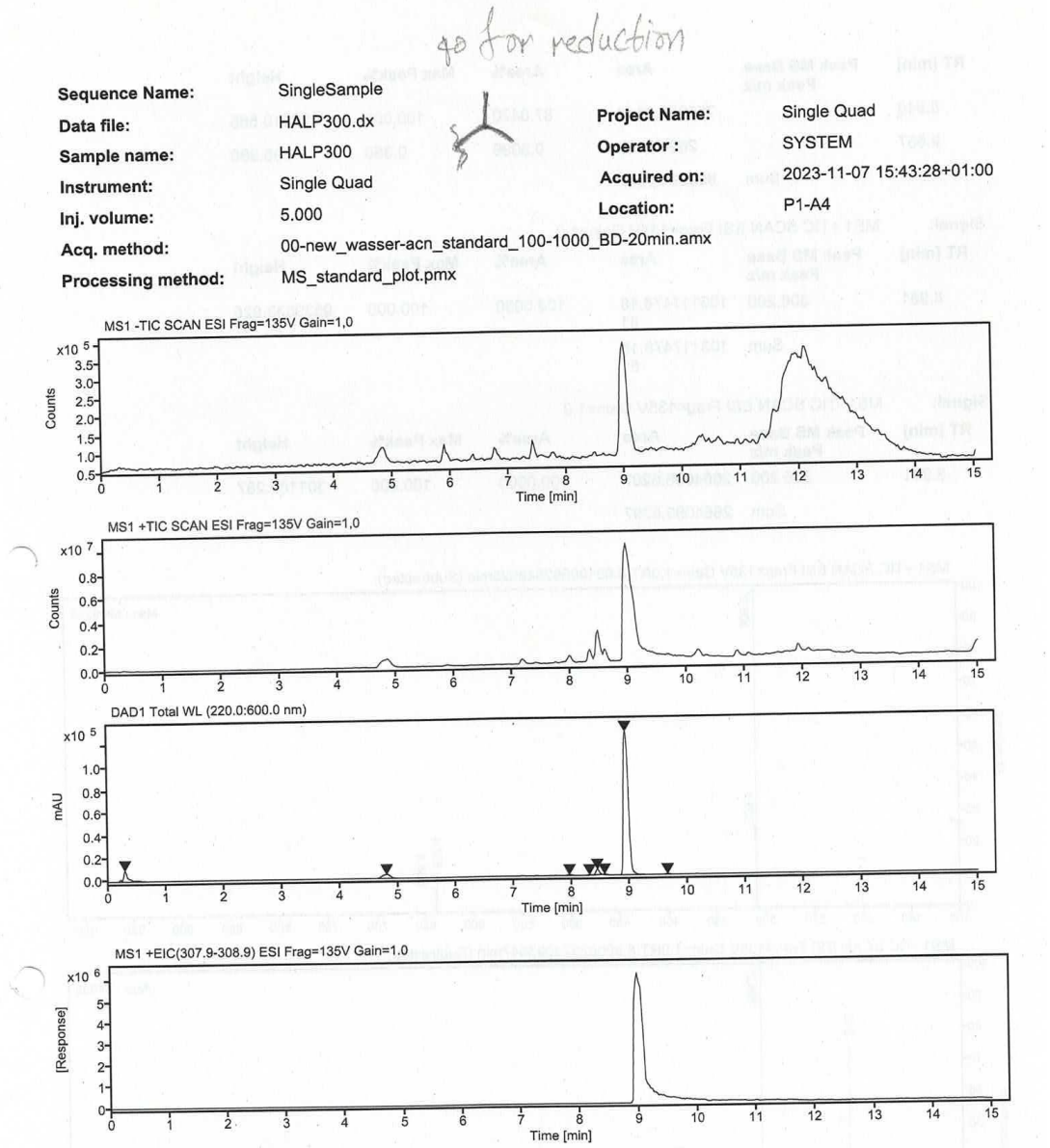
RT [min]	Peak MS Base Peak m/z	Area	Area%	Max Peak%	Height
0.366		1170.7839	0.2180	0.220	655.114
7.683	445.100	532357.8632	99.1358	100.000	109576.947
7.893		3470.1692	0.6462	0.652	991.193
	Sum	536998.8163			

D:\CDSProjects\Default\00-standardplot+EIC.rdl [Rev. 8517] Printed: 2024-01-02 12:43:50+01:00 Page 1 of 2


HALP318-F3.10.1.1r
HALP318-F3 in d6-DMSO:
1H
F (s) 8.3058
E (s) 8.2330
B (dd) 7.4909
C (d) 7.9533
A (d) 7.0943
D (s) 8.0468
G (s) 9.9849
K (t) 4.5582
I (t) 4.7453
H (t) 4.8400
J (t) 4.6146
M (s) 2.4340
L (t) 2.8116
P (s) 2.5229
O (t) 0.9410
N (h) 1.6377
f1 (ppm)


HALP318-F3.30.1.1r
HALP318-F3 in d6-DMSO:
13C
f1 (ppm)

Benzyl 1-isopropyl-5-methyl-1*H*-indole-3-carboxylate (7a)



Signal: DAD1 Total WL (220.0:600.0 nm)

RT [min]	Peak MS Base Peak m/z	Area	Area%	Max Peak%	Height
0.305		51097.2618	5.8760	6.750	9403.939
4.810		32517.3246	3.7394	4.296	3322.764
7.963		3423.8472	0.3937	0.452	762.747
8.307		1392.7059	0.1602	0.184	390.873
8.445		19856.7291	2.2834	2.623	4819.282
8.572		1655.8551	0.1904	0.219	501.089

D:\CDSProjects\Default\00-standardplot+EIC.rdl [Rev. 7723] Printed: 2023-11-08 08:22:20+01:00 Page 1 of 2

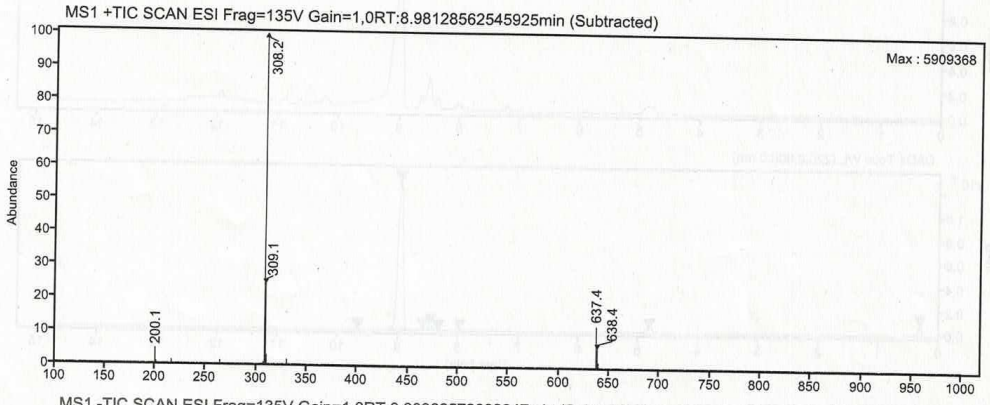
RT [min]	Peak MS Base Peak m/z	Area	Area%	Max Peak%	Height
8.946		756955.8148	87.0470	100.000	126010.565
9.657		2694.5168	0.3099	0.356	595.386
	Sum	869594.0552			

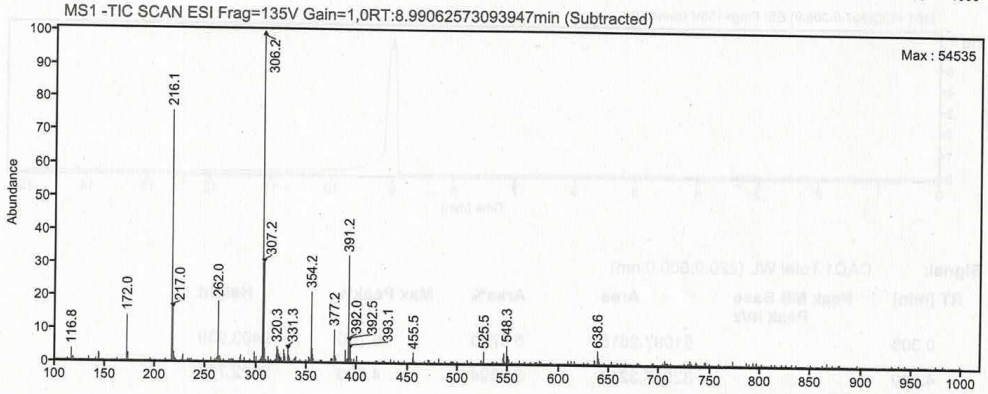
Signal: MS1 +TIC SCAN ESI Frag=135V Gain=1,0

RT [min]	Peak MS Base Peak m/z	Area	Area%	Max Peak%	Height
8.981	308.200	103117478.1861	100.0000	100.000	9539633.826
	Sum	103117478.1861			

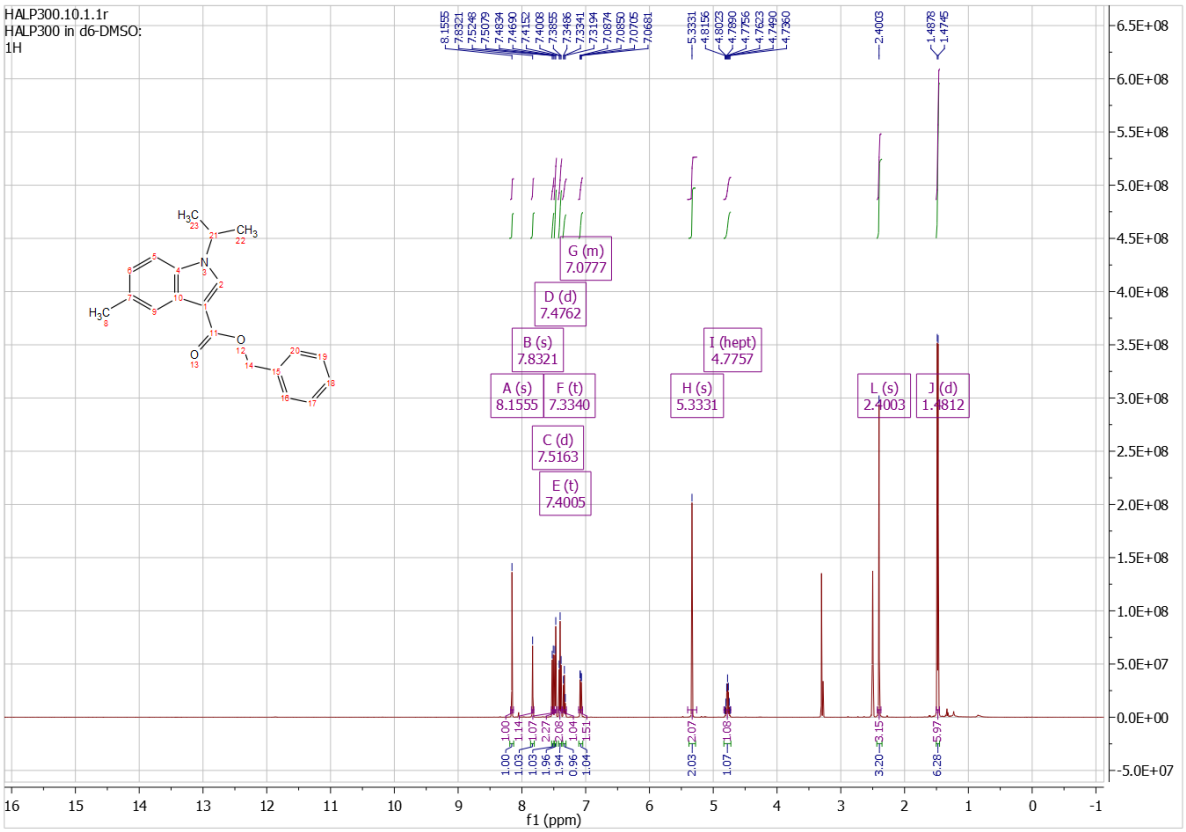
Signal: MS1 -TIC SCAN ESI Frag=135V Gain=1,0

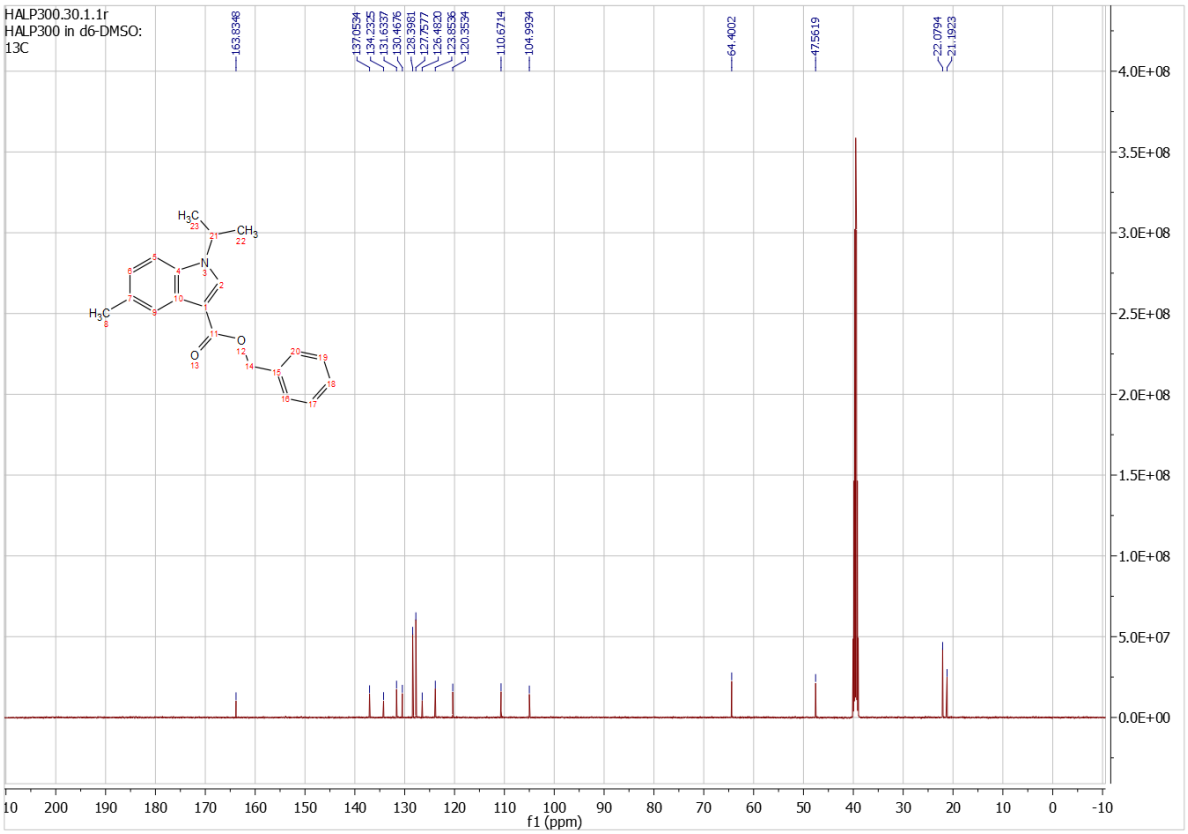
RT [min]	Peak MS Base Peak m/z	Area	Area%	Max Peak%	Height
8.991	306.200	2664098.6297	100.0000	100.000	301180.287
	Sum	2664098.6297			





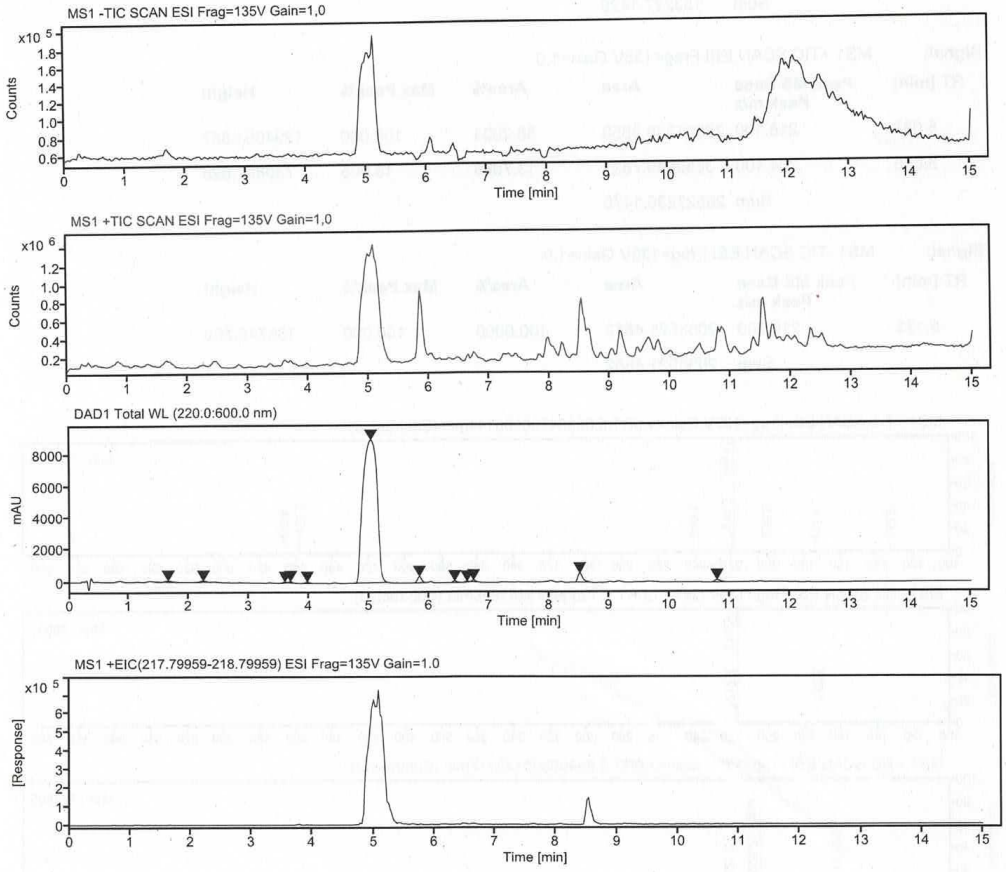
D:\CDSProjects\Default\00-standardplot+EIC.rdl [Rev. 7723] Printed: 2023-11-08 08:22:20+01:00 Page 2 of 2


HALP300.10.1.1r
HALP300 in d6-DMSO:
1H
G (m)
7.0777
D (d)
7.4762
B (s)
7.8321
I (hept)
4.7757
A (s)
8.1555
F (t)
7.3340
H (s)
5.3331
L (s)
2.4003
J (d)
1.4812
C (d)
7.5163
E (t)
7.4005
f1 (ppm)


HALP300.30.1.1r
HALP300 in d6-DMSO:
13C
f1 (ppm)

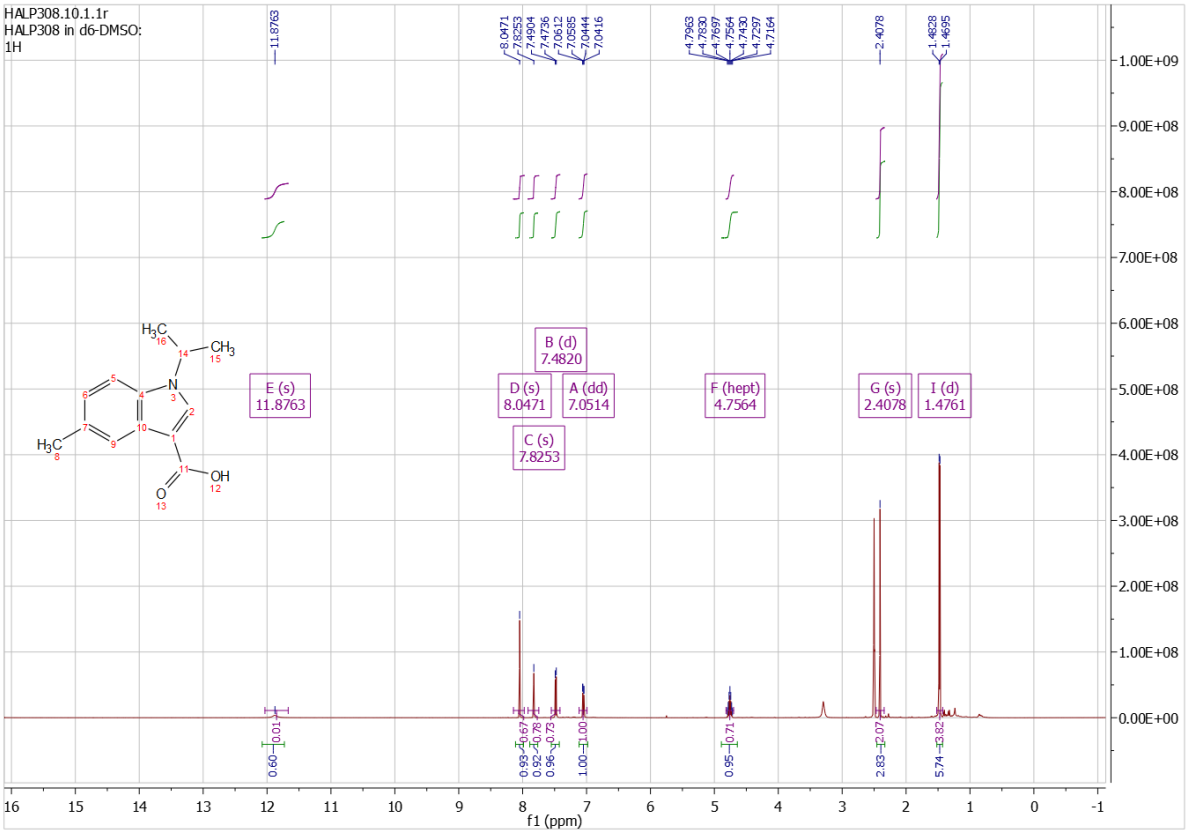
1-Isopropyl-5-methyl-1*H*-indole-3-carboxylic acid (7b)

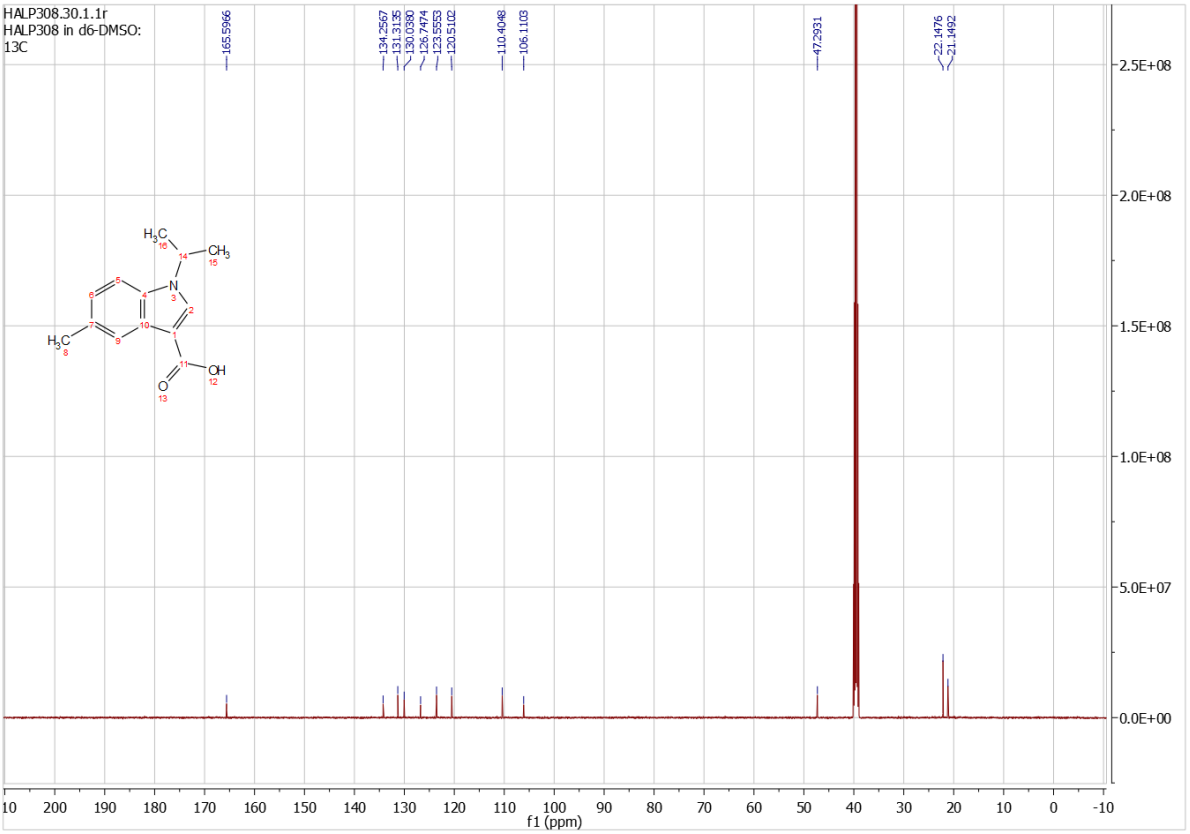
Sequence Name:	SingleSample		
Data file:	HALP308.dx	**Project Name:**	Single Quad
Sample name:	HALP308	**Operator :**	SYSTEM
Instrument:	Single Quad	**Acquired on:**	2023-12-12 12:51:25+01:00
Inj. volume:	2.000	**Location:**	P1-D4
Acq. method:	00-new_wasser-acn_standard_100-1000_BD-20min.amx		
Processing method:	MS_standard_plot.pmx		



Signal: DAD1 Total WL (220.0:600.0 nm)

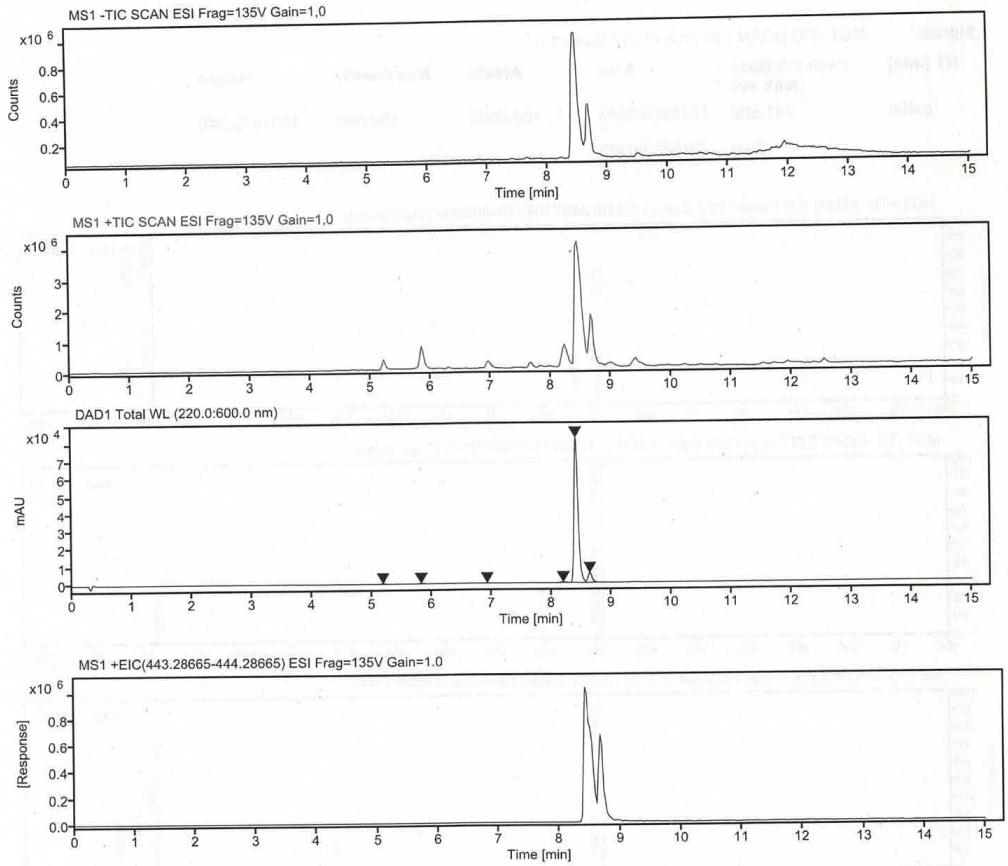
RT [min]	Peak MS Base Peak m/z	Area	Area%	Max Peak%	Height
1.649		379.6297	0.2478	0.262	62.211
2.238		487.3063	0.3180	0.336	71.833
3.596		138.4700	0.0904	0.095	39.223
3.687		219.6771	0.1434	0.151	76.108
3.964		313.5375	0.2046	0.216	63.859
5.029	218.100	145033.3428	94.6525	100.000	8927.195


HALP308.10.1.1r
HALP308 in d6-DMSO:
1H
E (s)
11.8763
B (d)
7.4820
D (s)
8.0471
A (dd)
7.0514
C (s)
7.8253
F (hept)
4.7564
G (s)
2.4078
I (d)
1.4761
f1 (ppm)


HALP308.30.1.1r
HALP308 in d6-DMSO:
13C
f1 (ppm)

N-(4-(4-Butyryl-5-methyl-1*H*-pyrazol-1-yl)phenyl)-1-isopropyl-5-methyl-1*H*-indole-3-carboxamide (7c)

Sequence Name:	SingleSample		
Data file:	HALP327-F1.dx	**Project Name:**	Single Quad
Sample name:	HALP327-F1	**Operator :**	SYSTEM
Instrument:	Single Quad	**Acquired on:**	2024-01-23 16:32:02+01:00
Inj. volume:	2.000	**Location:**	P2-E6
Acq. method:	00-new_wasser-acn_standard_100-1000_BD-20min.amx		
Processing method:	MS_standard_plot.pmx		



Signal: DAD1 Total WL (220.0:600.0 nm)

RT [min]	Peak MS Base Peak m/z	Area	Area%	Max Peak%	Height
5.196		1334.5106	0.3178	0.345	357.083
5.832		1595.0304	0.3799	0.413	372.947
6.932		640.6041	0.1526	0.166	135.961
8.200		2170.2573	0.5169	0.561	379.215
8.419		386557.2063	92.0678	100.000	82414.473
8.647		27563.7723	6.5650	7.131	5588.431

D:\CDSProjects\Default\00-standardplot+EIC.rdl [Rev. 8842] Printed: 2024-01-24 07:07:59+01:00 Page 1 of 2

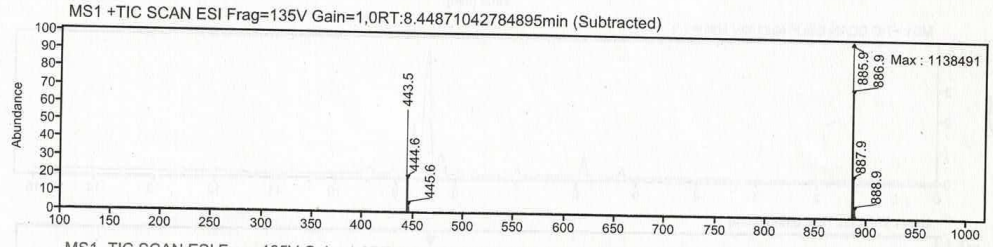
RT [min]	Peak MS Base Peak m/z	Area	Area%	Max Peak%	Height
	Sum	419861.3811			

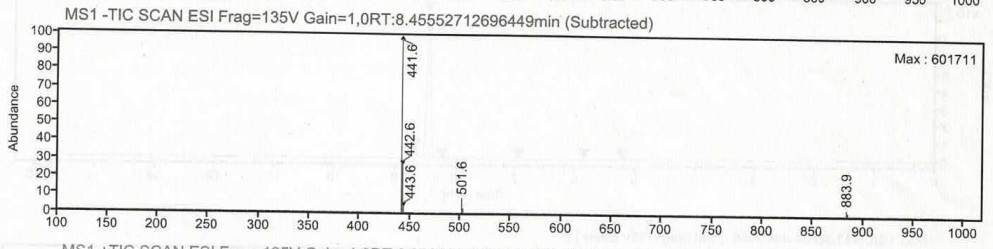
Signal: MS1 +TIC SCAN ESI Frag=135V Gain=1,0

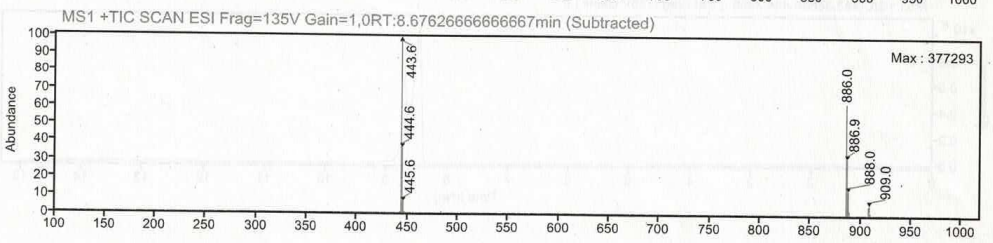
RT [min]	Peak MS Base Peak m/z	Area	Area%	Max Peak%	Height
8.449	885.900	28580258.0898	81.1167	100.000	3962022.030
8.676	443.600	6653254.4046	18.8833	23.279	1457546.220
	Sum	35233512.4944			

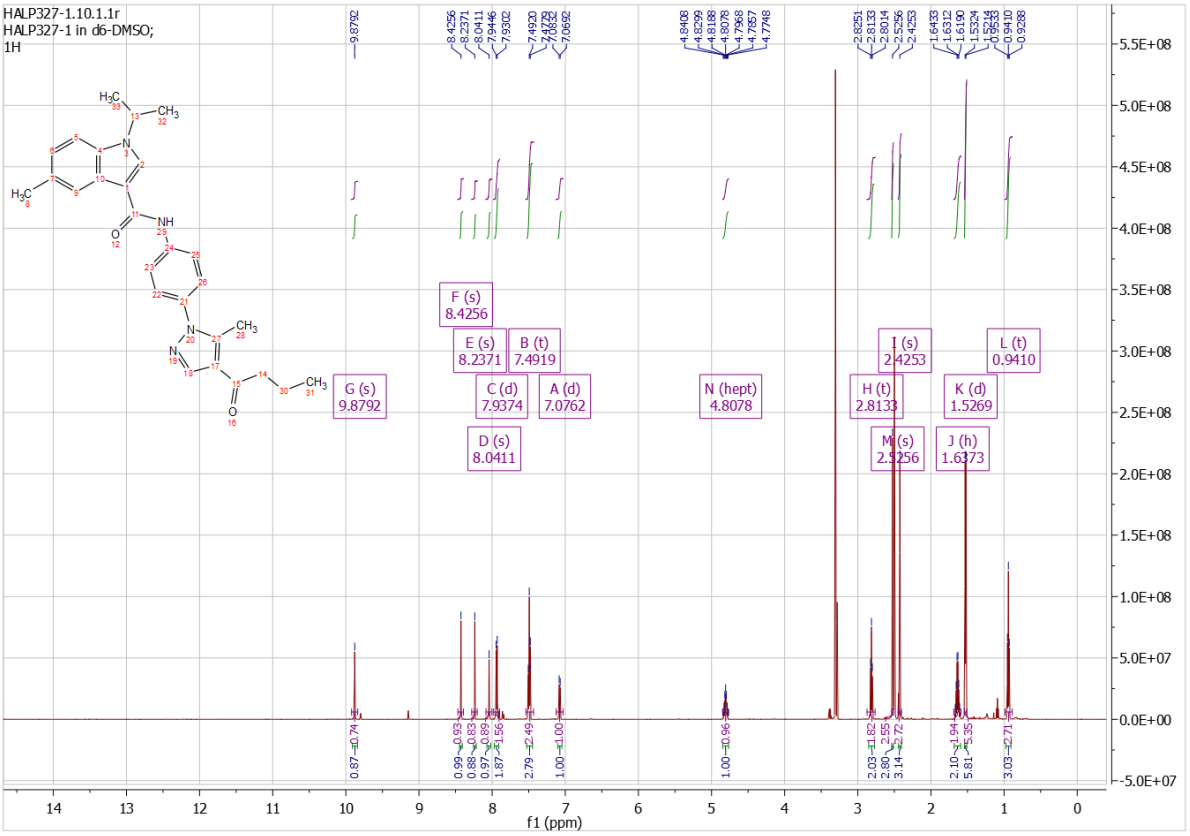
Signal: MS1 -TIC SCAN ESI Frag=135V Gain=1,0

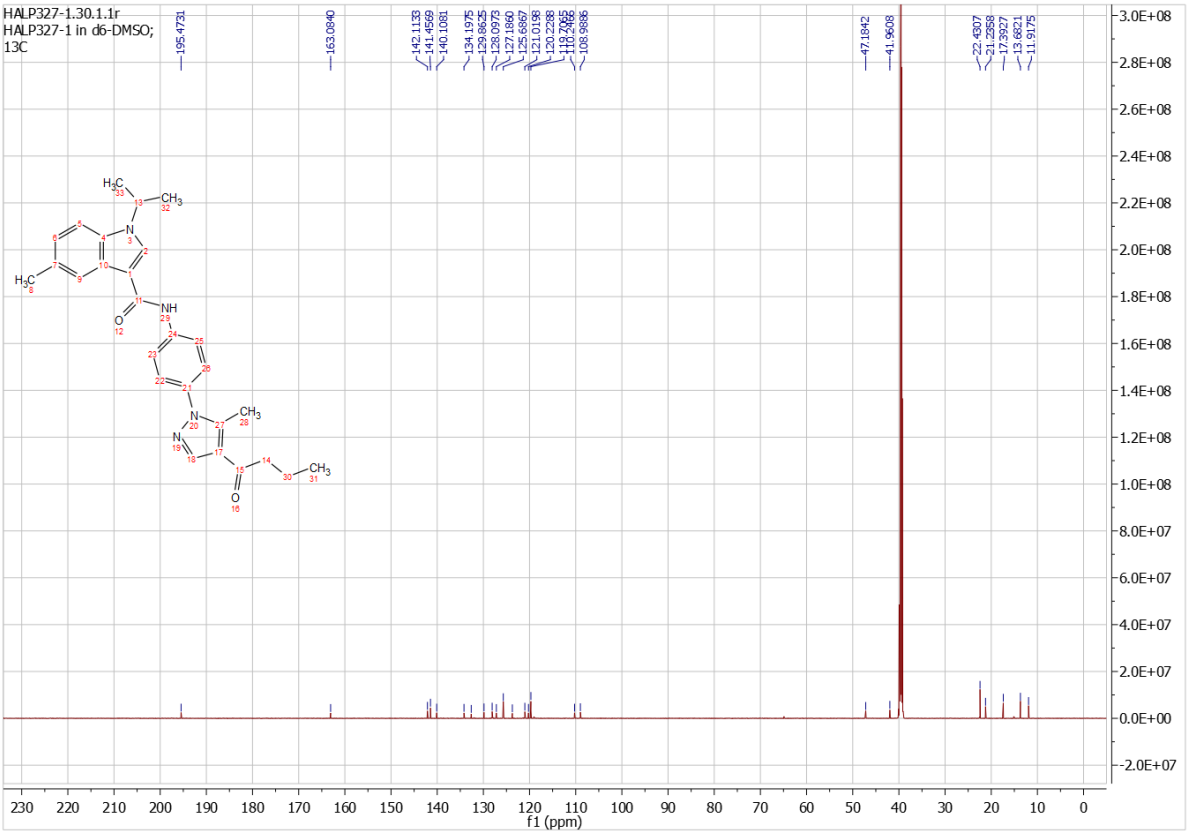
RT [min]	Peak MS Base Peak m/z	Area	Area%	Max Peak%	Height
8.456	441.600	7245353.0363	100.0000	100.000	1001678.946
	Sum	7245353.0363			





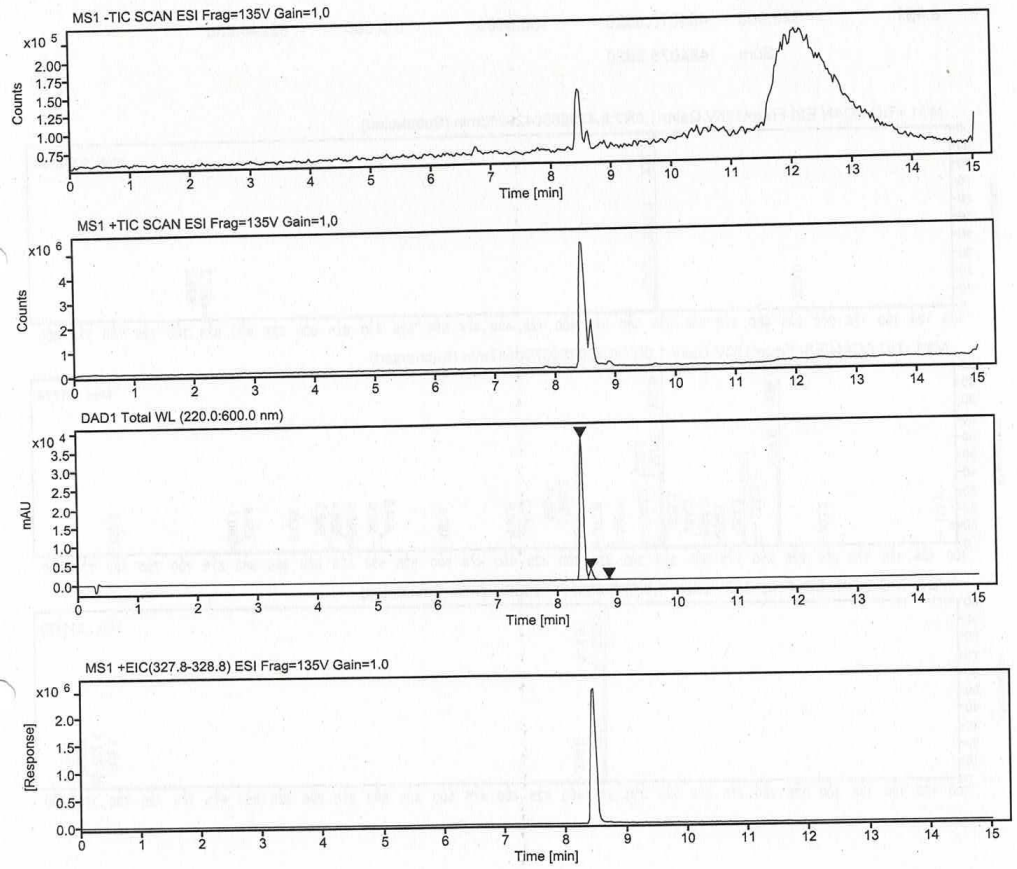



HALP327-1.10.1.1r
HALP327-1 in d6-DMSO;
1H
G (s)
9.8792
F (s)
8.4256
E (s)
8.2371
B (t)
7.4919
C (d)
7.9374
A (d)
7.0762
D (s)
8.0411
N (hept)
4.8078
H (t)
2.8133
I (s)
2.4253
M (s)
2.5256
K (d)
1.5269
J (h)
1.6373
L (t)
0.9410
f1 (ppm)


HALP327-1.30.1.1r
HALP327-1 in d6-DMSO;
13C
f1 (ppm)

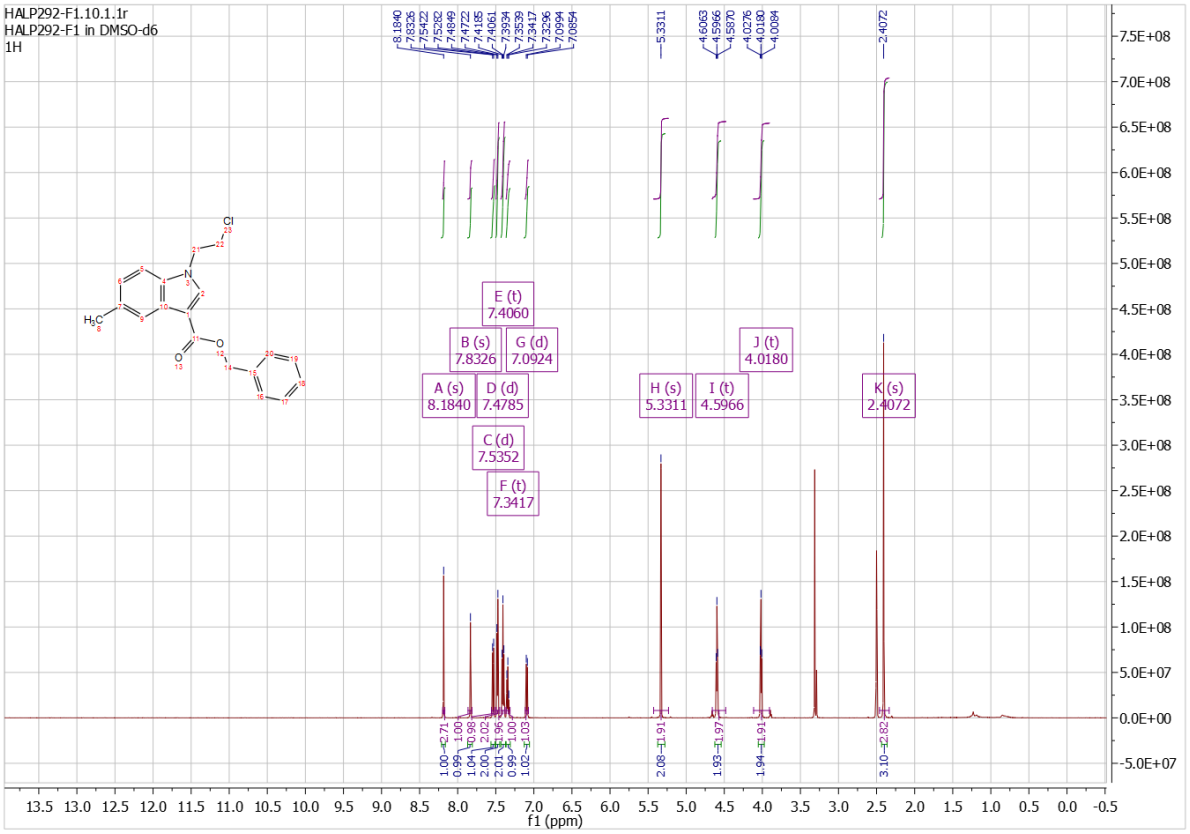
Benzyl 1-(2-chloroethyl)-5-methyl-1*H*-indole-3-carboxylate (8a)

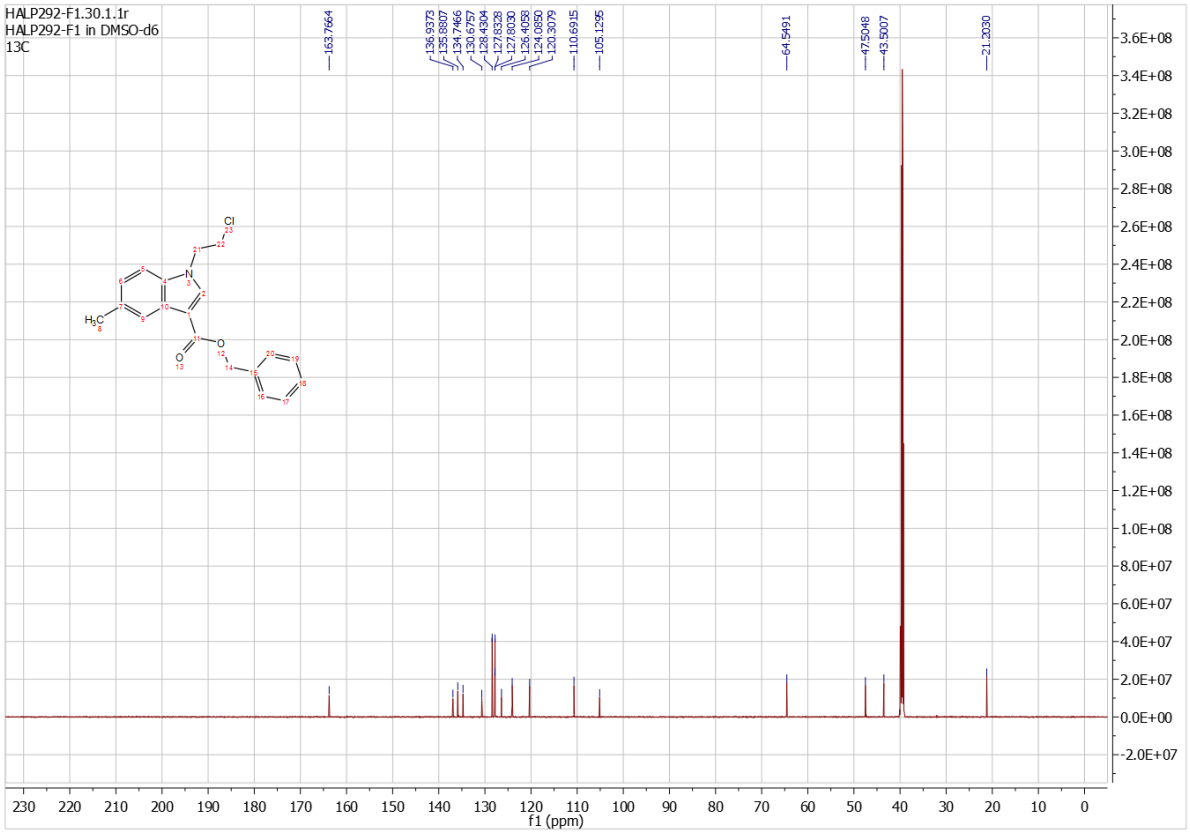
Sequence Name:	SingleSample		
Data file:	HALP292-F1.dx	**Project Name:**	Single Quad
Sample name:	HALP292-F1	**Operator :**	SYSTEM
Instrument:	Single Quad	**Acquired on:**	2023-11-16 15:05:12+01:00
Inj. volume:	2.000	**Location:**	P1-C2
Acq. method:	00-new_wasser-acn_standard_100-1000_BD-20min.amx		
Processing method:	MS_standard_plot.pmx		



Signal: DAD1 Total WL (220.0:600.0 nm)

RT [min]	Peak MS Base Peak m/z	Area	Area%	Max Peak%	Height
8.407		163753.7617	92.5915	100.000	37401.987
8.557		12039.0410	6.8072	7.352	2683.021
8.859		1063.3609	0.6013	0.649	247.414
	Sum	176856.1636			

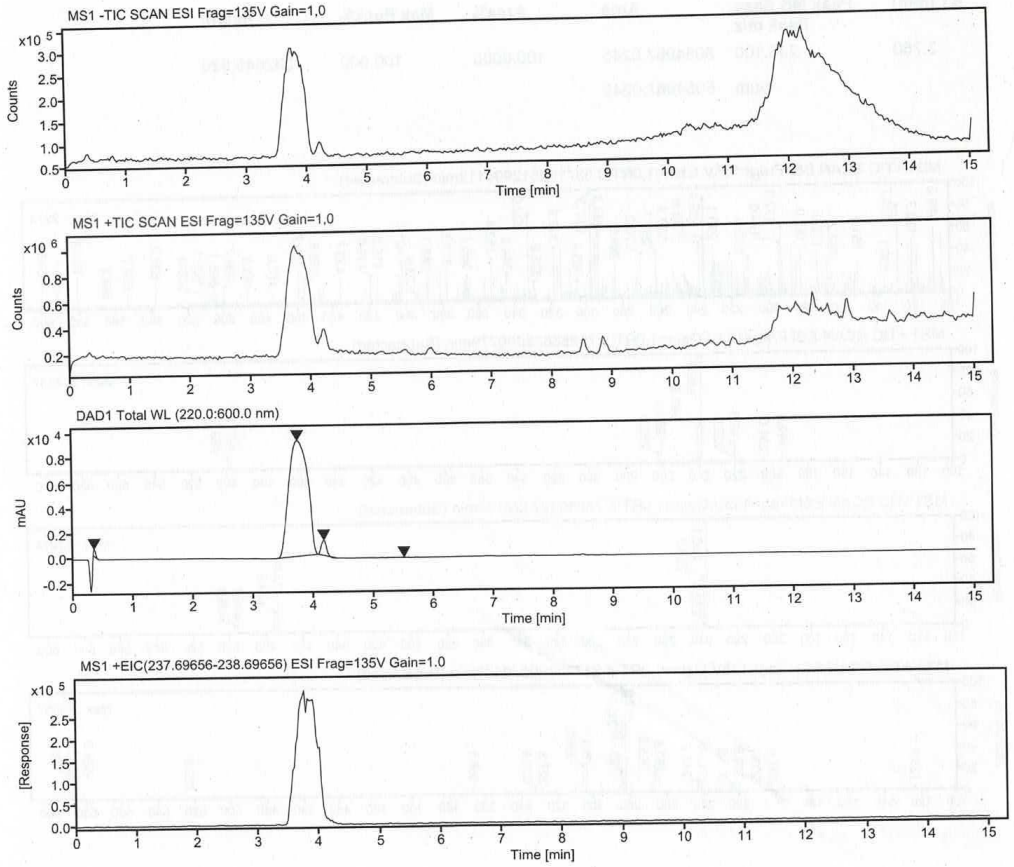

HALP292-F1.10.1.1r
HALP292-F1 in DMSO-d6
1H
E (t) 7.4060
B (s) 7.8326
G (d) 7.0924
J (t) 4.0180
A (s) 8.1840
D (d) 7.4785
H (s) 5.3311
I (t) 4.5966
K (s) 2.4072
C (d) 7.5352
F (t) 7.3417
f1 (ppm)


HALP292-F1.30.1.1r
HALP292-F1 in DMSO-d6
13C
f1 (ppm)

1-(2-Chloroethyl)-5-methyl-1*H*-indole-3-carboxylic acid (8b)

Sequence Name:	SingleSample		
Data file:	HALP321.dx	**Project Name:**	Single Quad
Sample name:	HALP321	**Operator :**	SYSTEM
Instrument:	Single Quad	**Acquired on:**	2024-01-04 13:30:25+01:00
Inj. volume:	5.000	**Location:**	P2-D6
Acq. method:	00-new_wasser-acn_standard_100-1000_BD-20min.amx		
Processing method:	MS_standard_plot.pmx		

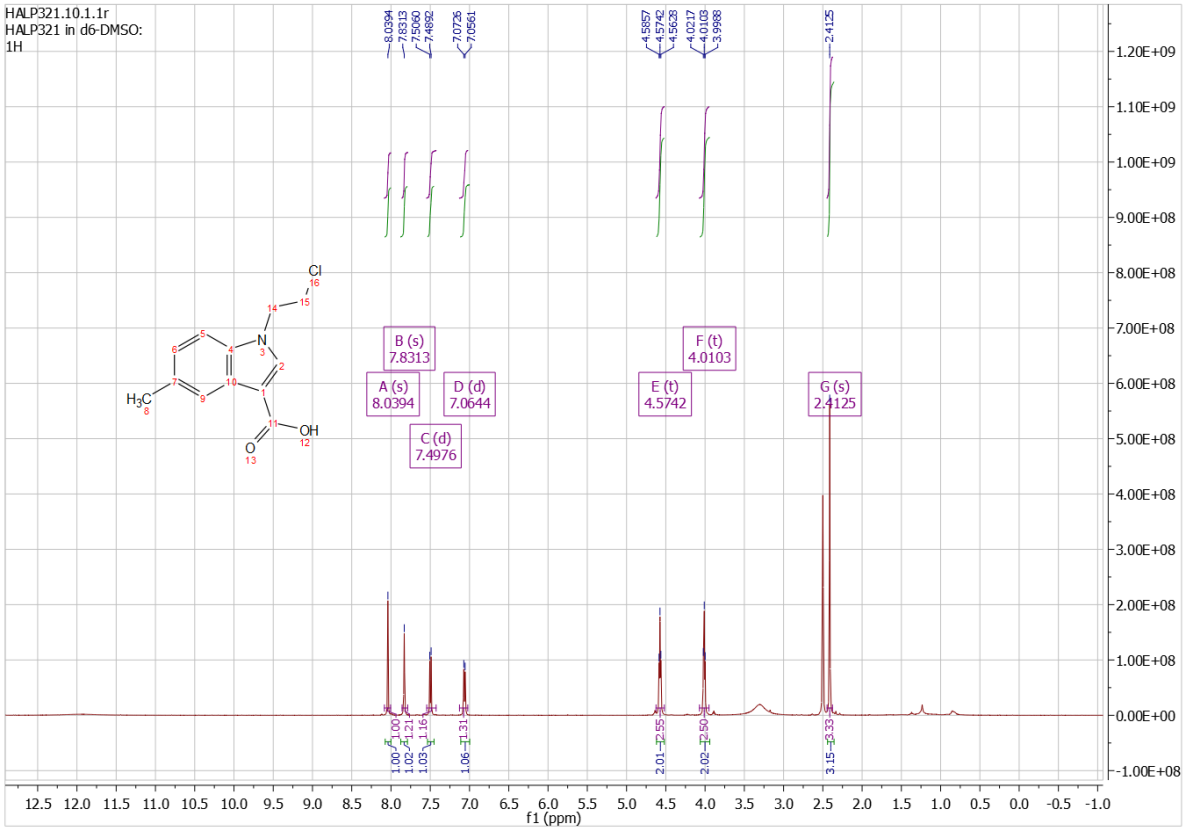
NMR

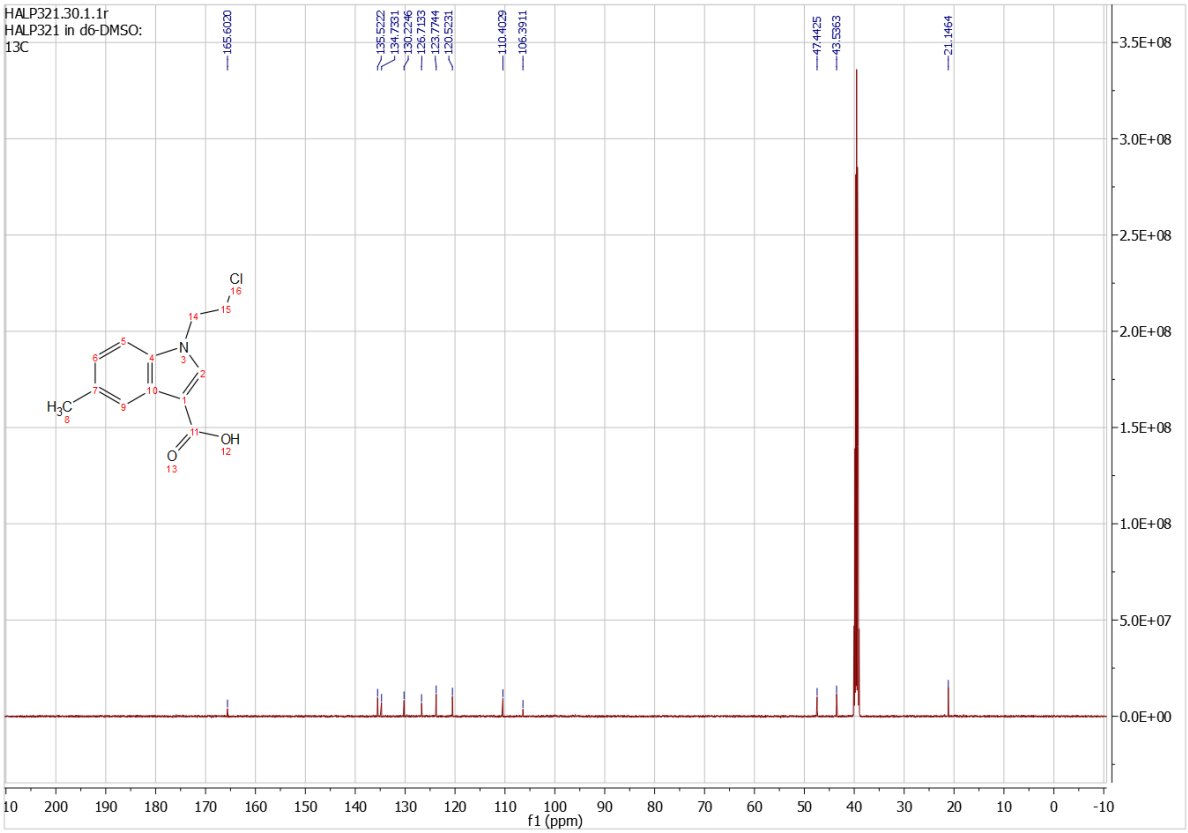


Signal: DAD1 Total WL (220.0:600.0 nm)

RT [min]	Peak MS Base Peak m/z	Area	Area%	Max Peak%	Height
0.367		1361.8567	0.6475	0.674	563.153
3.759	238.000	201979.5776	96.0356	100.000	9252.059
4.181		6929.9795	3.2950	3.431	1213.194
5.514		46.0760	0.0219	0.023	13.214
	Sum	210317.4899			

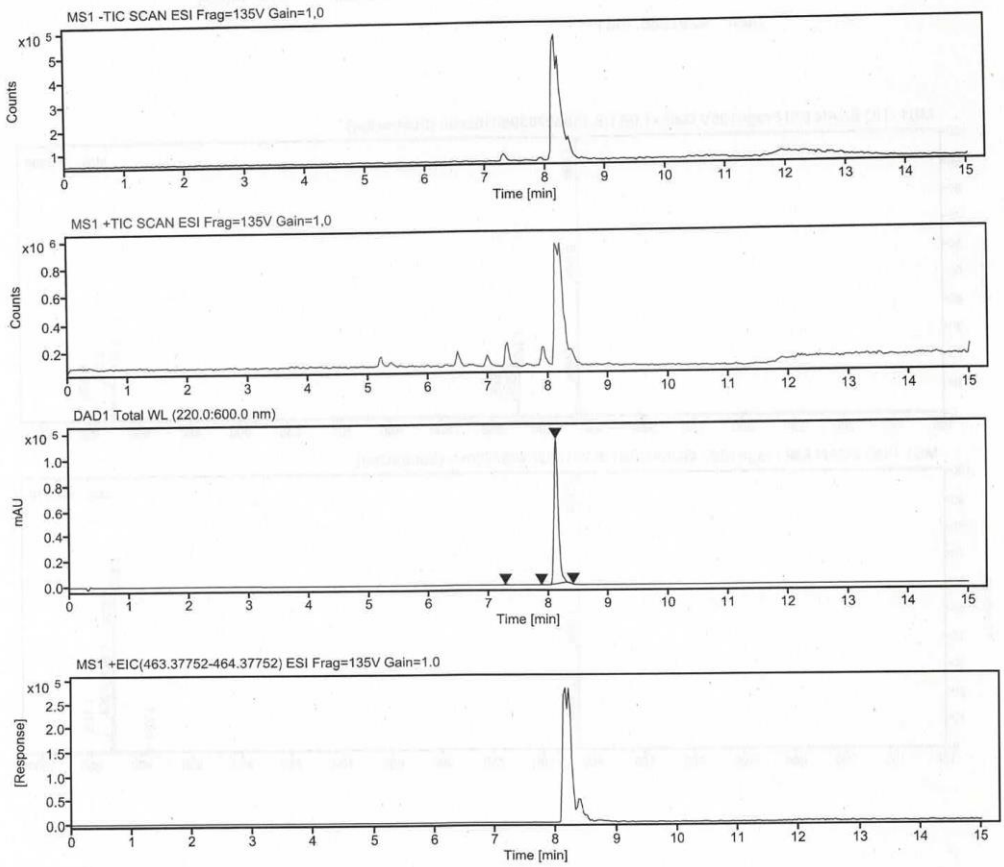
D:\CDSProjects\Default\00-standardplot+EIC.rdl [Rev. 8558] Printed: 2024-01-08 10:22:54+01:00 Page 1 of 2


HALP321.10.1.1r
HALP321 in d6-DMSO:
1H
B (s)
7.8313
A (s)
8.0394
D (d)
7.0644
C (d)
7.4976
F (t)
4.0103
E (t)
4.5742
G (s)
2.4125
f1 (ppm)


HALP321.30.1.1r
HALP321 in d6-DMSO:
13C
f1 (ppm)

_N_-(4-(4-Butyryl-5-methyl-1_H_-pyrazol-1-yl)phenyl)-1-(2-chloroethyl)-5-methyl-1_H_-indole-3-carboxamide (8c)

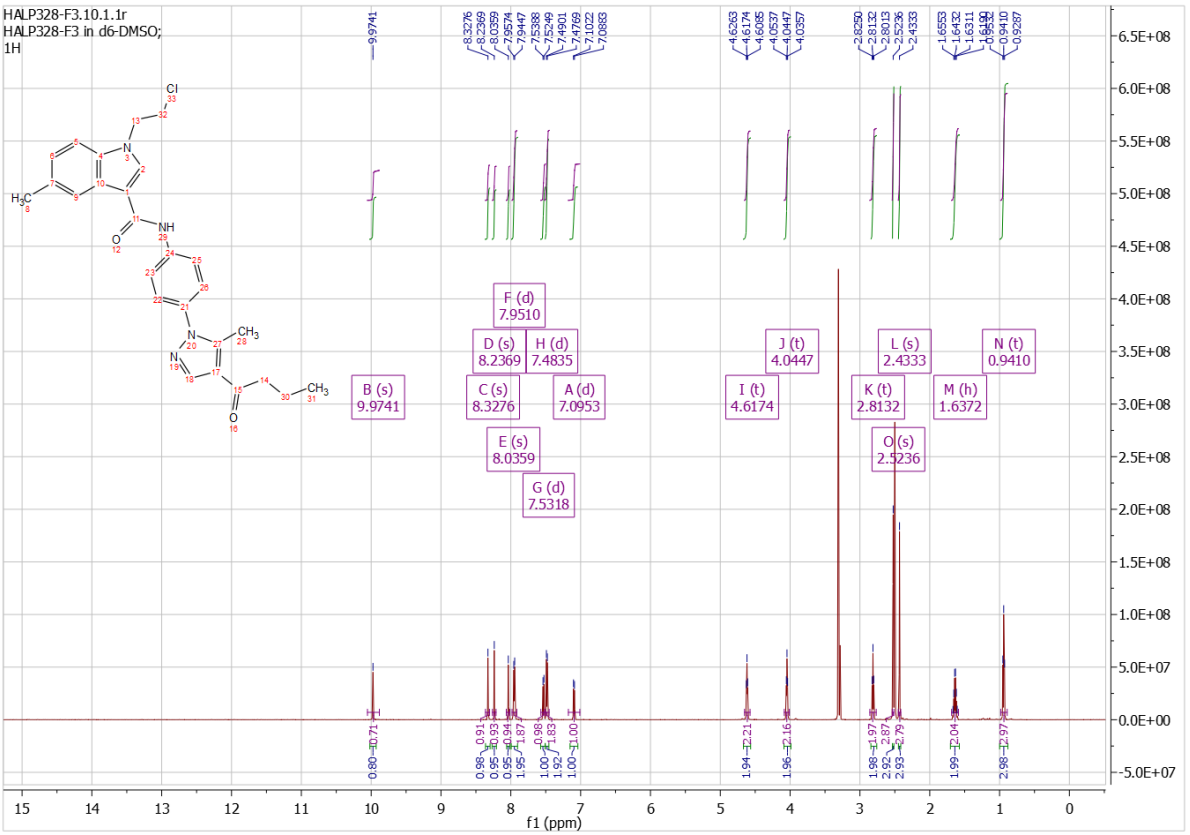
Sequence Name:	SingleSample		
Data file:	HALP328-F3.dx	**Project Name:**	Single Quad
Sample name:	HALP328-F3	**Operator :**	SYSTEM
Instrument:	Single Quad	**Acquired on:**	2024-01-17 20:25:25+01:00
Inj. volume:	2.000	**Location:**	P1-B11
Acq. method:	00-new_wasser-acn_standard_100-1000_BD-20min.amx		
Processing method:	*MS_standard_plot.pmx		

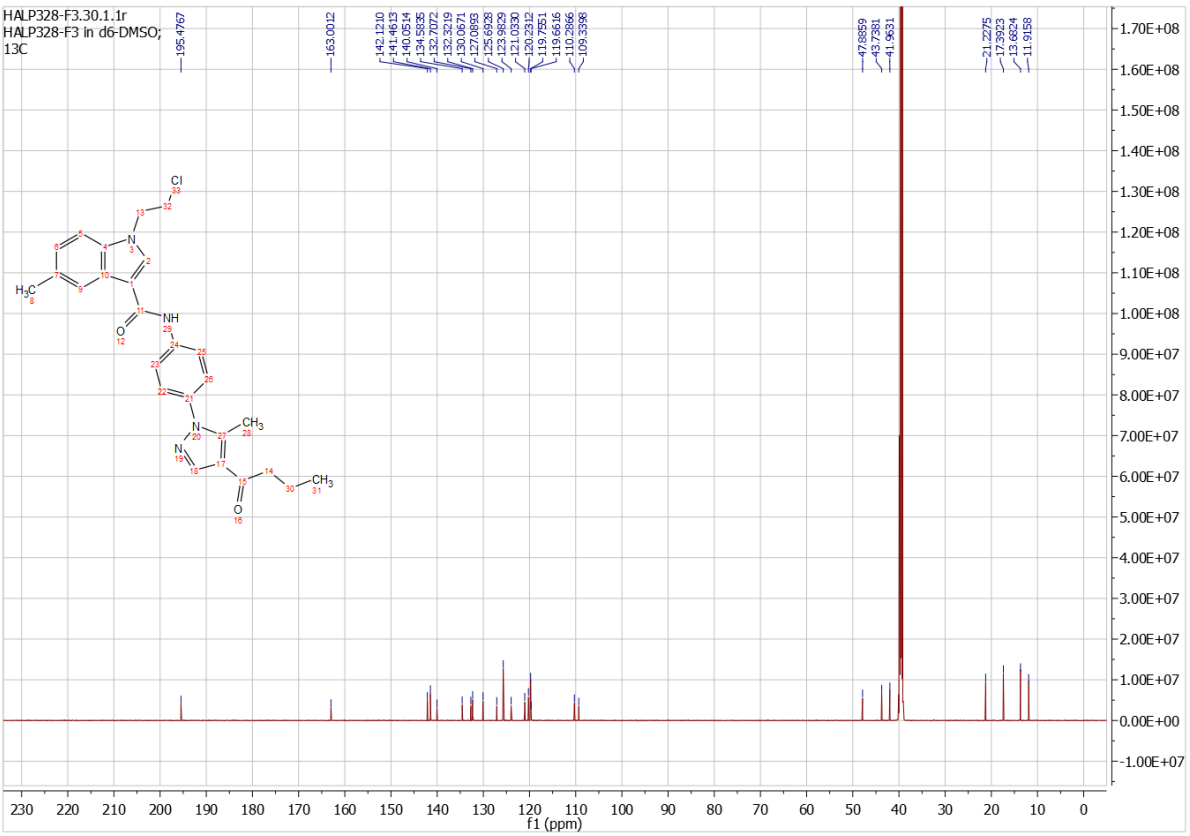


Signal: DAD1 Total WL (220.0:600.0 nm)

RT [min]	Peak MS Base Peak m/z	Area	Area%	Max Peak%	Height
7.283		1780.0785	0.3110	0.313	423.935
7.882		953.9503	0.1667	0.168	222.518
8.129	461.700	569429.0324	99.4987	100.000	114201.180
8.410		134.6956	0.0235	0.024	165.015
	Sum	572297.7567			

D:\CDSProjects\Default\00-standardplot+EIC.rdl [Rev. 8781] Printed: 2024-01-22 09:27:22+01:00 Page 1 of 2

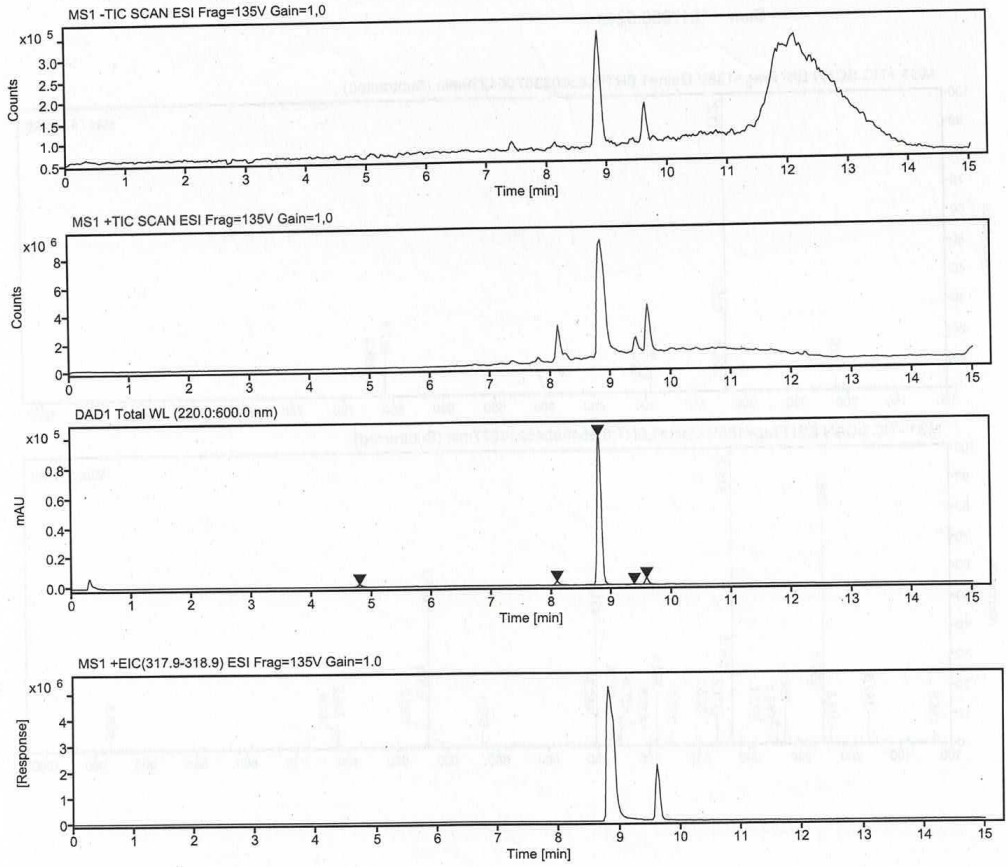

HALP328-F3.10.1.1r
HALP328-F3 in d6-DMSO;
1H
B (s)
9.9741
C (s)
8.3276
D (s)
8.2369
E (s)
8.0359
F (d)
7.9510
G (d)
7.5318
H (d)
7.4835
A (d)
7.0953
I (t)
4.6174
J (t)
4.0447
K (t)
2.8132
L (s)
2.4333
M (h)
1.6372
N (t)
0.9410
O (s)
2.5236
f1 (ppm)


HALP328-F3.30.1.1r
HALP328-F3 in d6-DMSO;
13C
f1 (ppm)

Benzyl 1-(but-2-yn-1-yl)-5-methyl-1*H*-indole-3-carboxylate (9a)

GO for reduction

Sequence Name:	SingleSample		
Data file:	HALP304.dx	**Project Name:**	Single Quad
Sample name:	HALP304	**Operator :**	SYSTEM
Instrument:	Single Quad	**Acquired on:**	2023-11-07 17:07:29+01:00
Inj. volume:	3.000	**Location:**	P1-A8
Acq. method:	00-new_wasser-acn_standard_100-1000_BD-20min.amx		
Processing method:	MS_standard_plot.pmx		



Signal: DAD1 Total WL (220.0:600.0 nm)

RT [min]	Peak MS Base Peak m/z	Area	Area%	Max Peak%	Height
4.804		7281.1143	1.3743	1.482	1350.943
8.094		11736.9122	2.2153	2.389	2369.105
8.802	318.200	491299.2593	92.7313	100.000	99098.354
9.381		1378.4194	0.2602	0.281	401.219
9.586		18113.8547	3.4189	3.687	4071.371
	Sum	529809.5598			

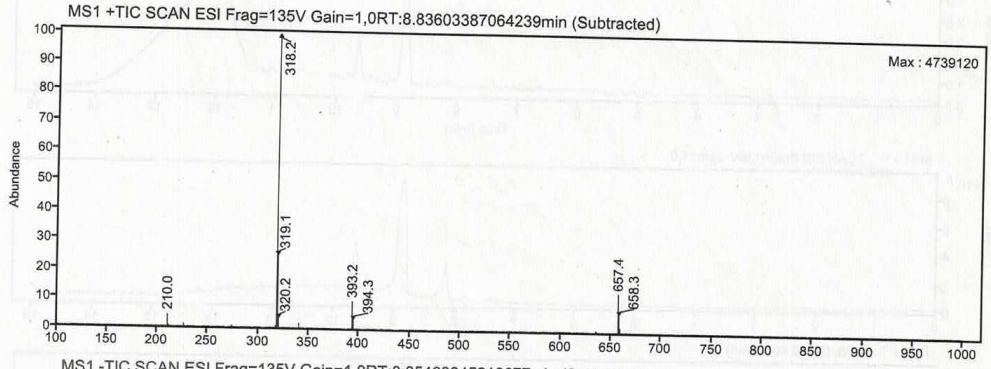
Signal: MS1 +TIC SCAN ESI Frag=135V Gain=1,0

RT [min]	Peak MS Base Peak m/z	Area	Area%	Max Peak%	Height
8.836	318.200	69904899.3218	100.0000	100.000	8055197.244
	Sum	69904899.3218			

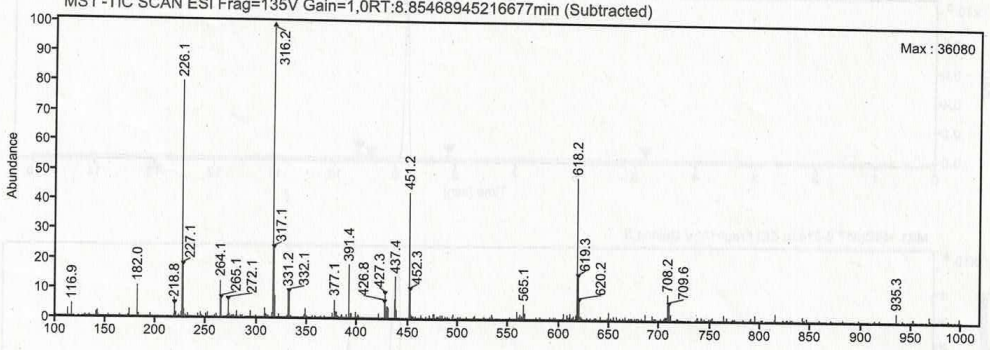
Signal: MS1 -TIC SCAN ESI Frag=135V Gain=1,0

RT [min]	Peak MS Base Peak m/z	Area	Area%	Max Peak%	Height
8.855	316.200	1817966.5213	100.0000	100.000	268200.811
	Sum	1817966.5213			

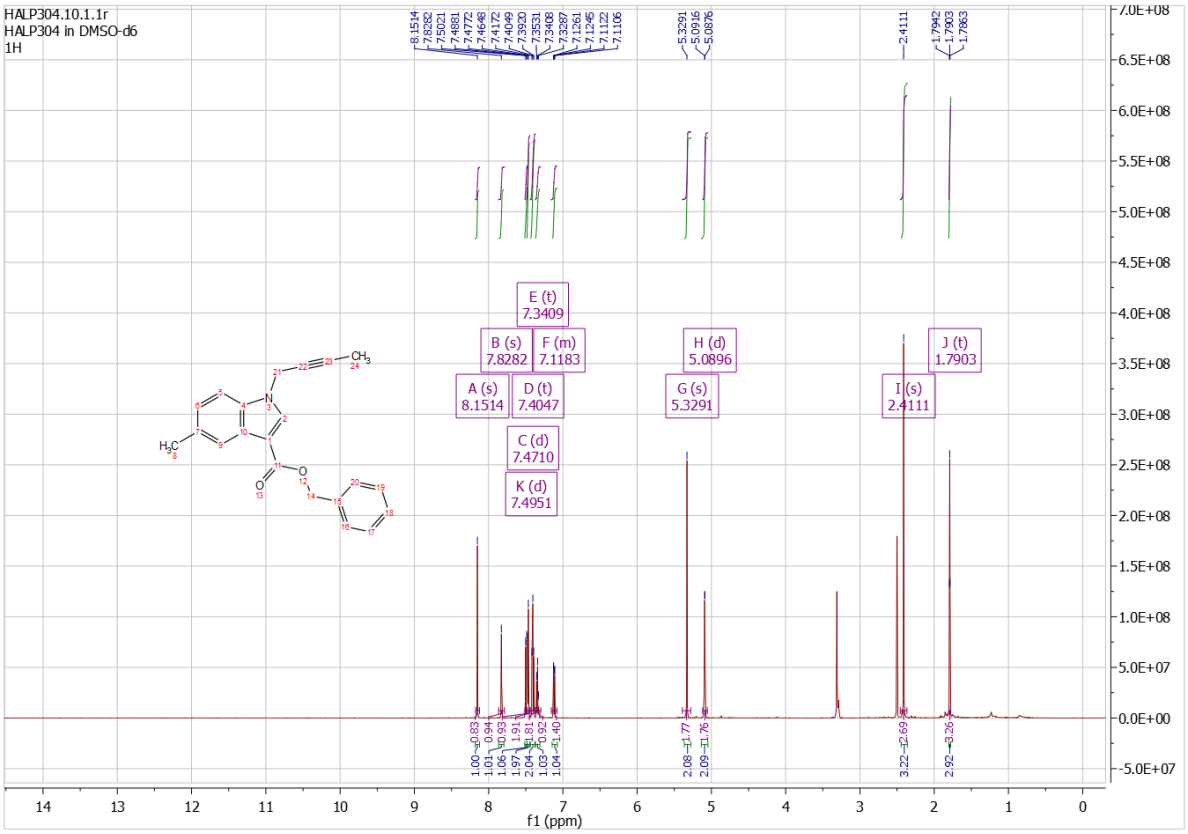
MS1 +TIC SCAN ESI Frag=135V Gain=1,0RT:8.83603387064239min (Subtracted)

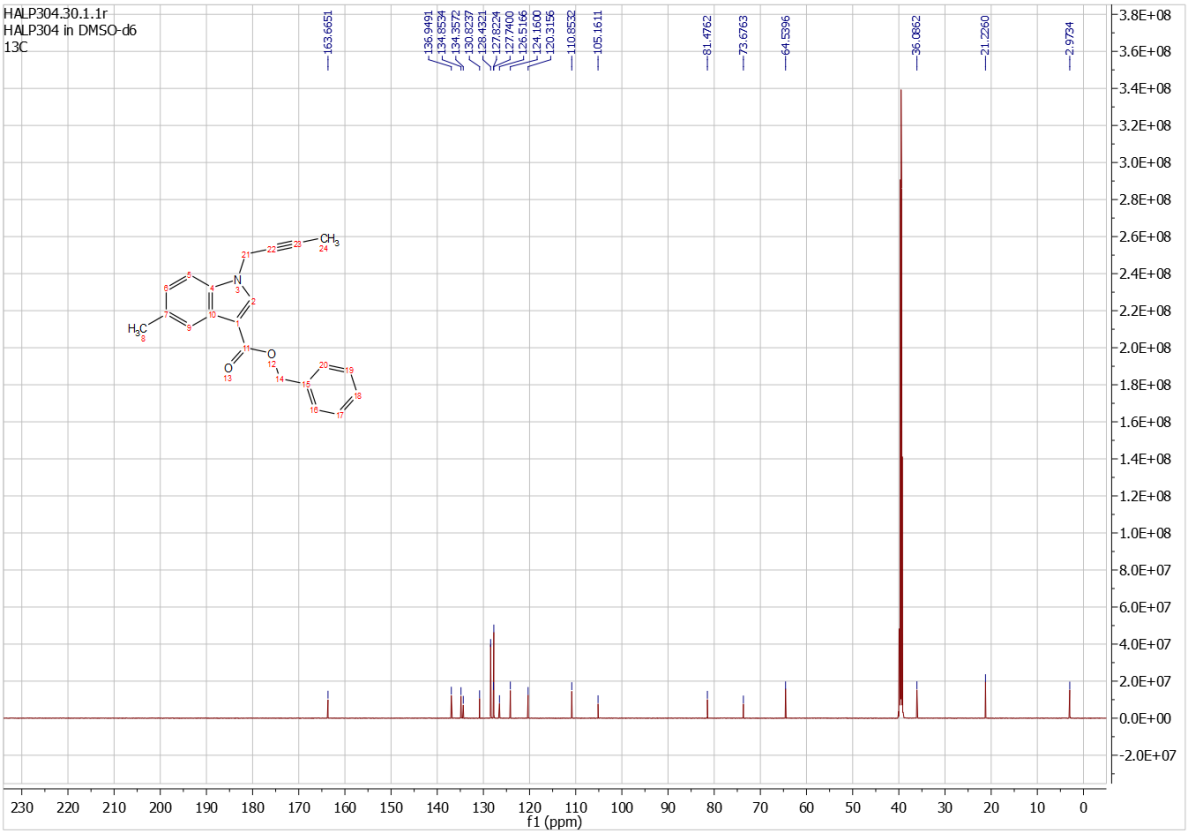


MS1 -TIC SCAN ESI Frag=135V Gain=1,0RT:8.85468945216677min (Subtracted)



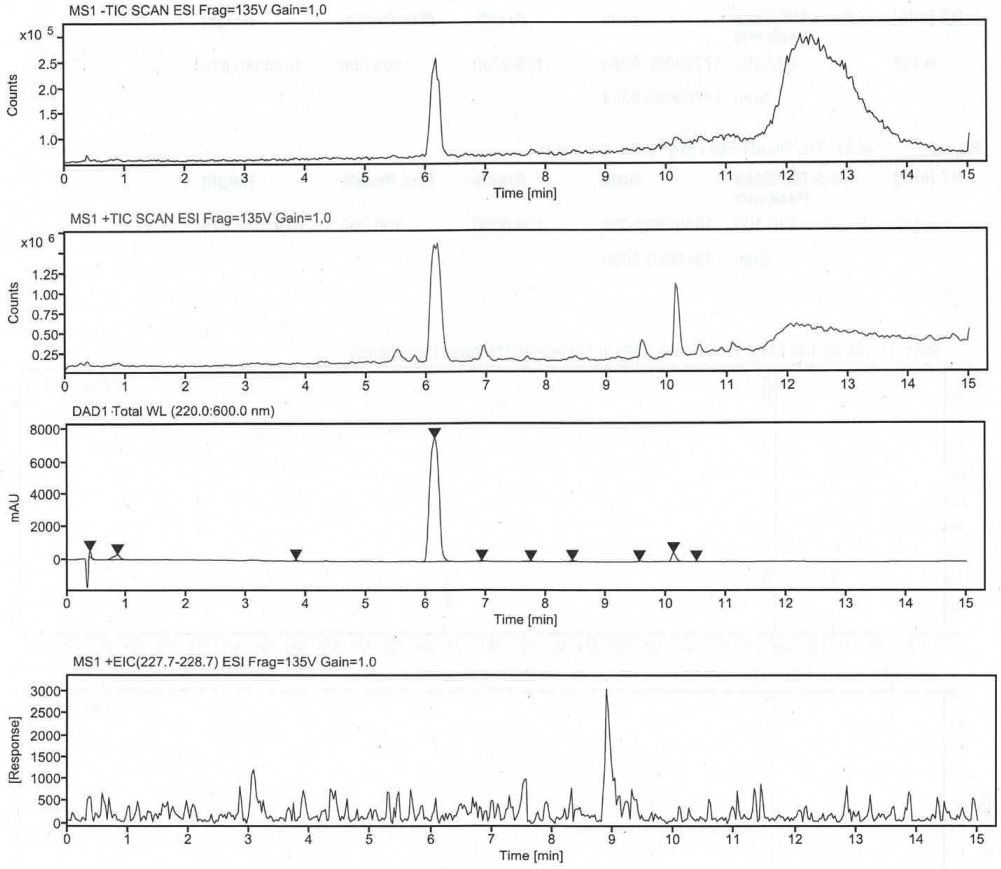
D:\CDSProjects\Default\00-standardplot+EIC.rdl [Rev. 7725] Printed: 2023-11-08 08:29:12+01:00 Page 2 of 2


HALP304.10.1.1r
HALP304 in DMSO-d6
1H
A (s) 8.1514
B (s) 7.8282
C (d) 7.4710
D (t) 7.4047
E (t) 7.3409
F (m) 7.1183
G (s) 5.3291
H (d) 5.0896
I (s) 2.4111
J (t) 1.7903
K (d) 7.4951
f1 (ppm)


HALP304.30.1.1r
HALP304 in DMSO-d6
13C
f1 (ppm)

1-Butyl-5-methyl-1*H*-indole-3-carboxylic acid (9b)

Sequence Name:	SingleSample		
Data file:	HALP323.dx	**Project Name:**	Single Quad
Sample name:	HALP323	**Operator :**	SYSTEM
Instrument:	Single Quad	**Acquired on:**	2024-01-16 00:25:15+01:00
Inj. volume:	3.000	**Location:**	P2-E1
Acq. method:	00-new_wasser-acn_standard_100-1000_BD-20min.amx		
Processing method:	MS_standard_plot.pmx		



Signal: DAD1 Total WL (220.0:600.0 nm)

RT [min]	Peak MS Base Peak m/z	Area	Area%	Max Peak%	Height
0.388		595.4211	0.6898	0.748	350.545
0.850		2251.8291	2.6087	2.829	288.959
3.823		250.5538	0.2903	0.315	67.396
6.142	230.100	79611.0314	92.2271	100.000	7491.573
6.922		229.0938	0.2654	0.288	51.448
7.744		250.6073	0.2903	0.315	33.379

D:\CDSProjects\Default\00-standardplot+EIC.rdl [Rev. 8743] Printed: 2024-01-17 14:58:59+01:00 Page 1 of 2

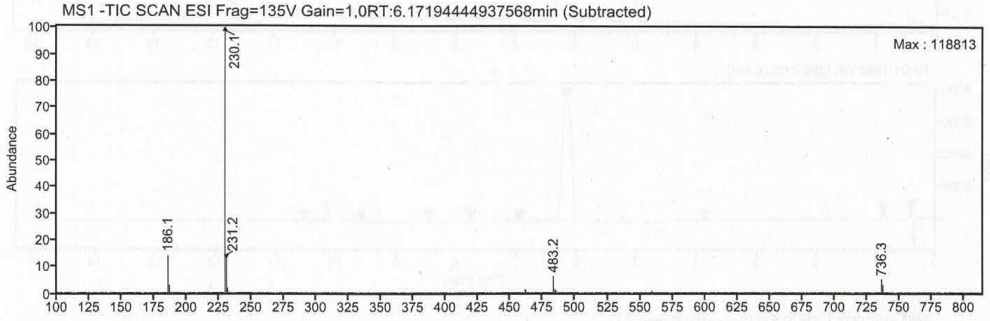
RT [min]	Peak MS Base Peak m/z	Area	Area%	Max Peak%	Height
8.434		342.2576	0.3965	0.430	64.498
9.555		29.0629	0.0337	0.037	12.726
10.121		2693.1660	3.1200	3.383	521.431
10.503		67.6223	0.0783	0.085	18.780
	Sum	86320.6452			

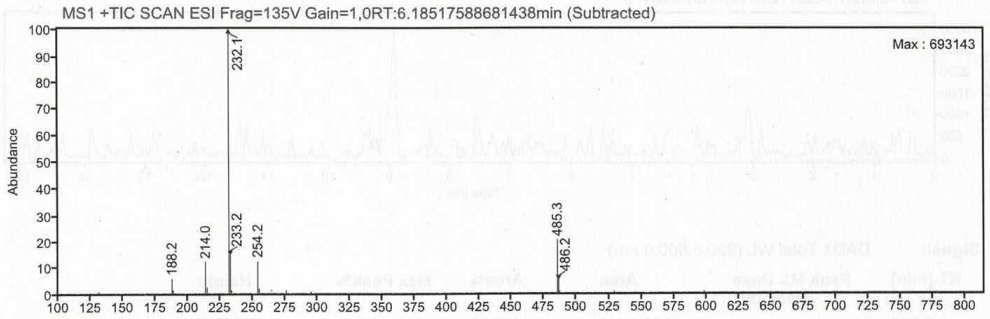
Signal: MS1 +TIC SCAN ESI Frag=135V Gain=1,0

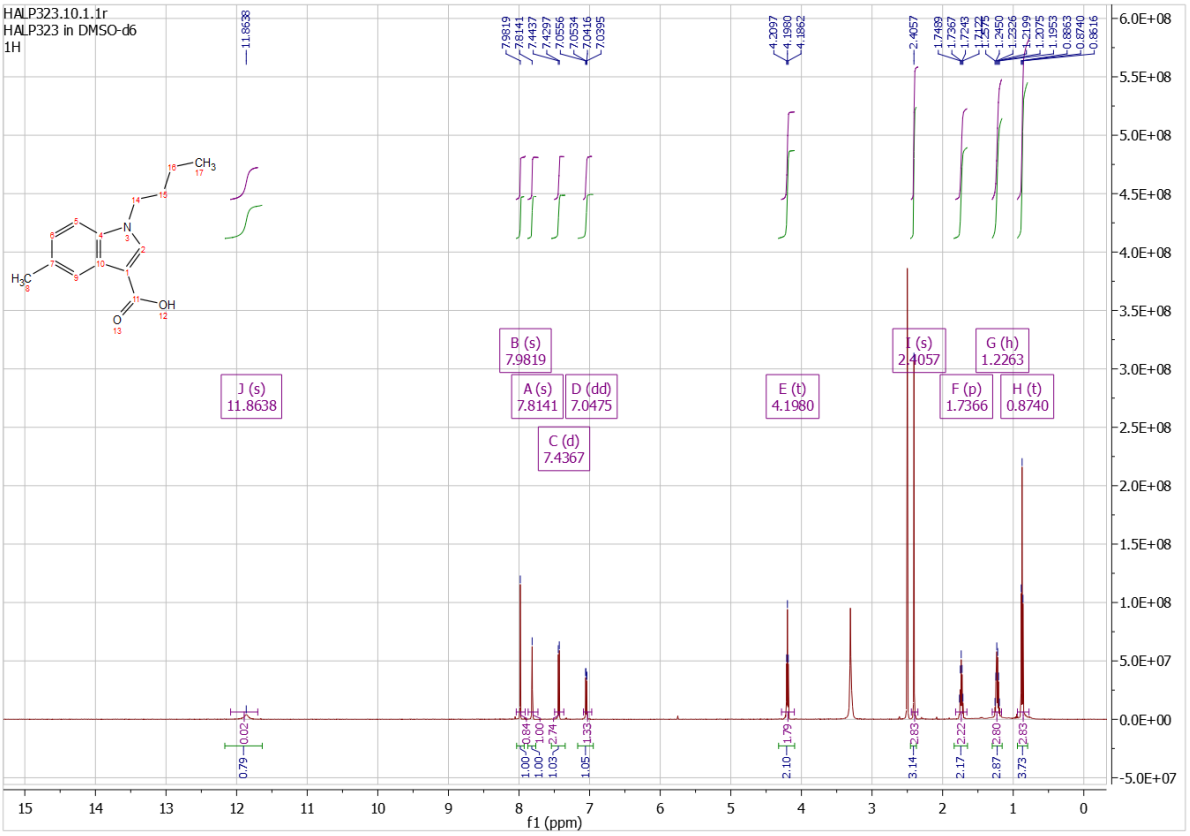
RT [min]	Peak MS Base Peak m/z	Area	Area%	Max Peak%	Height
6.185	232.100	17763090.9384	100.0000	100.000	1476840.874
	Sum	17763090.9384			

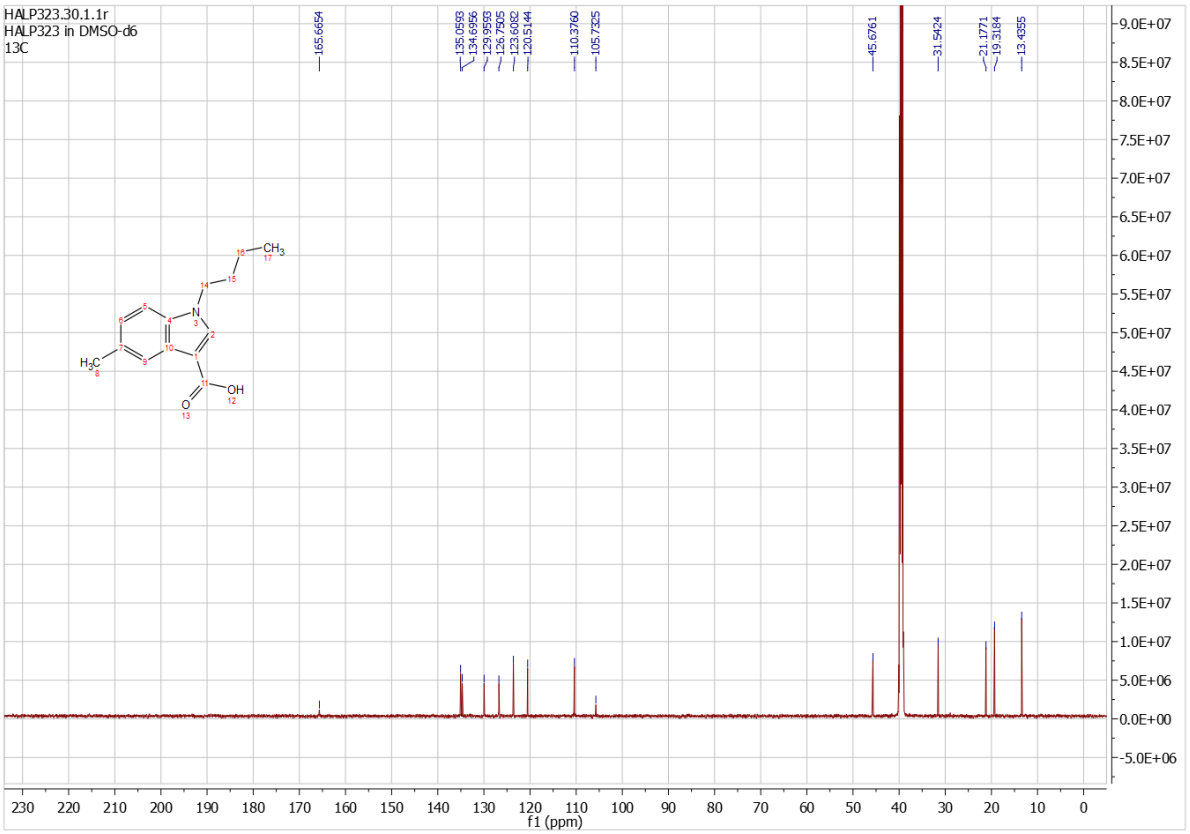
Signal: MS1 -TIC SCAN ESI Frag=135V Gain=1,0

RT [min]	Peak MS Base Peak m/z	Area	Area%	Max Peak%	Height
6.172	230.100	1845860.9020	100.0000	100.000	191017.075
	Sum	1845860.9020			



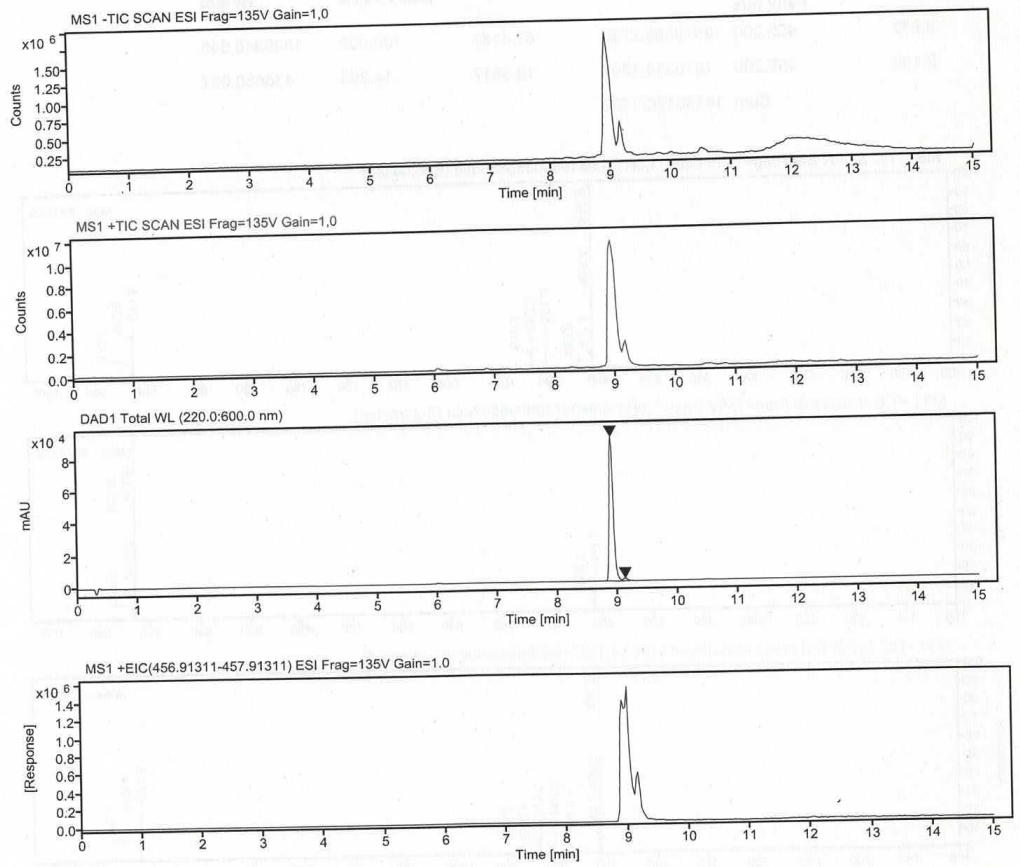



HALP323.10.1.1r
HALP323 in DMSO-d6
1H
J (s)
11.8638
B (s)
7.9819
A (s)
7.8141
D (dd)
7.0475
C (d)
7.4367
E (t)
4.1980
I (s)
2.4057
F (p)
1.7366
G (h)
1.2263
H (t)
0.8740
f1 (ppm)


HALP323.30.1.1r
HALP323 in DMSO-d6
13C
f1 (ppm)

1-Butyl-*N*-(4-(4-butyryl-5-methyl-1*H*-pyrazol-1-yl)phenyl)-5-methyl-1*H*-indole-3-carboxamide (9c)

Sequence Name:	SingleSample		
Data file:	HALP331-F3.dx	**Project Name:**	Single Quad
Sample name:	HALP331-F3	**Operator :**	SYSTEM
Instrument:	Single Quad	**Acquired on:**	2024-01-31 15:33:19+01:00
Inj. volume:	3.000	**Location:**	P2-B8
Acq. method:	00-new_wasser-acn_standard_100-1500_BD-20min.amx		
Processing method:	MS_standard_plot.pmx		



Signal: DAD1 Total WL (220.0:600.0 nm)

RT [min]	Peak MS Base Peak m/z	Area	Area%	Max Peak%	Height
8.905		419483.0055	97.9625	100.000	89917.664
9.128		8724.9267	2.0375	2.080	1726.570
	Sum	428207.9322			

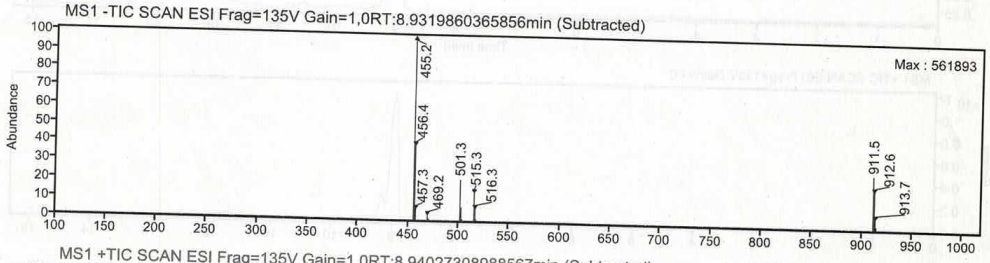
Signal: MS1 +TIC SCAN ESI Frag=135V Gain=1,0

RT [min]	Peak MS Base Peak m/z	Area	Area%	Max Peak%	Height
8.940	913.500	98967258.2220	89.8262	100.000	11145759.361
9.162	457.200	11209174.6326	10.1738	11.326	2201373.095
	Sum	110176432.8546			

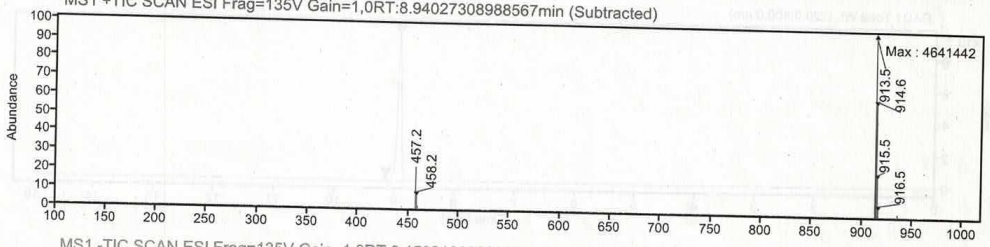
Signal: MS1 -TIC SCAN ESI Frag=135V Gain=1,0

RT [min]	Peak MS Base Peak m/z	Area	Area%	Max Peak%	Height
8.932	455.200	12619856.2720	87.4183	100.000	1649946.045
9.153	455.200	1816314.1382	12.5817	14.393	438650.067
	Sum	14436170.4102			

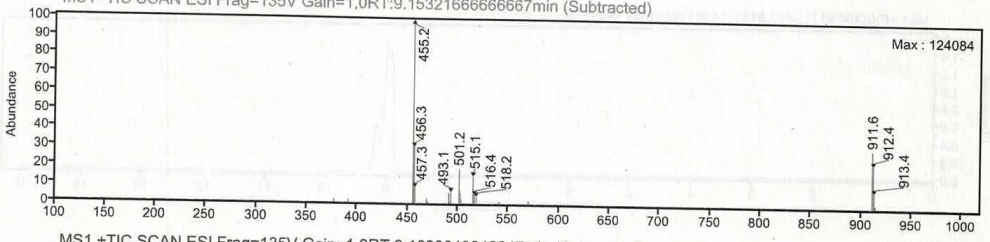
MS1 -TIC SCAN ESI Frag=135V Gain=1,0RT:8.9319860365856min (Subtracted)



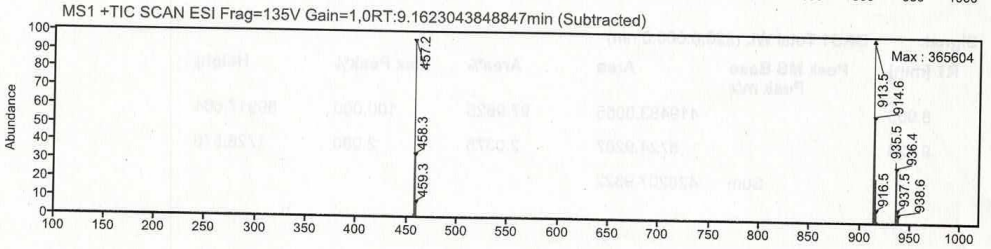
MS1 +TIC SCAN ESI Frag=135V Gain=1,0RT:8.94027308988567min (Subtracted)



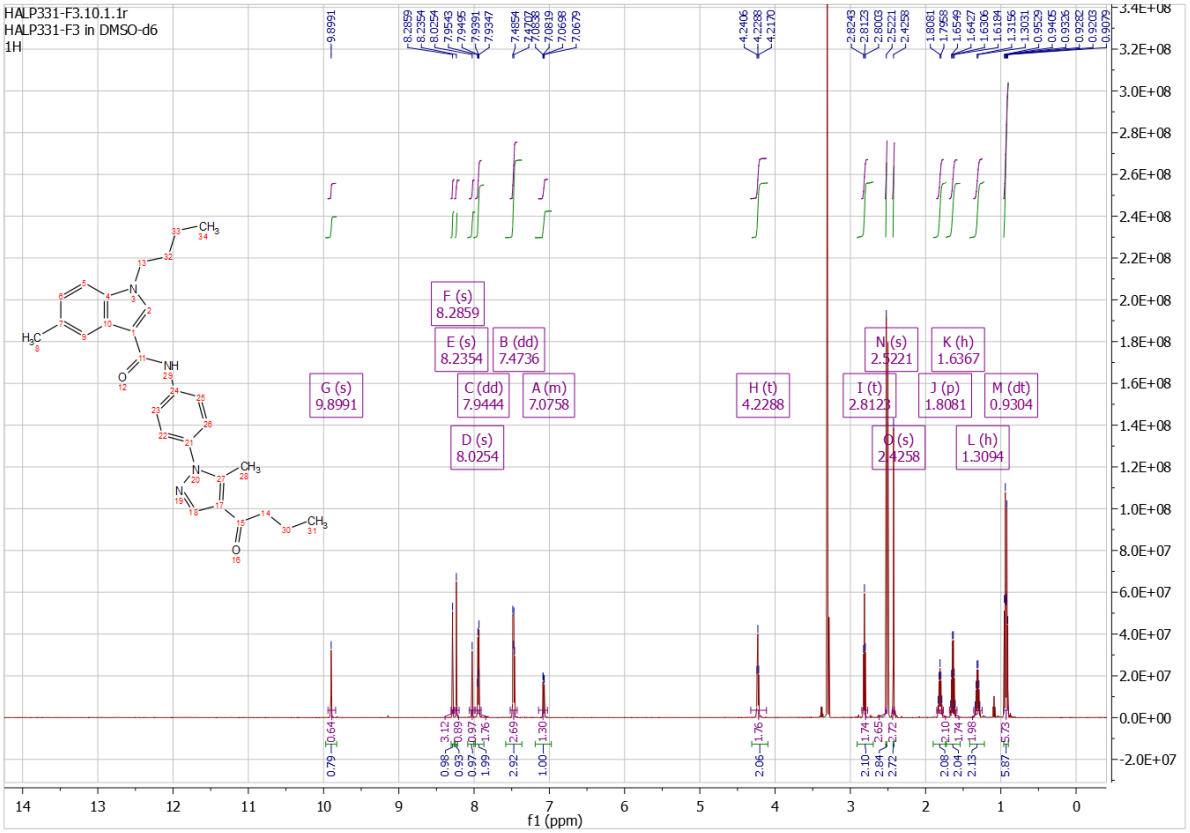
MS1 -TIC SCAN ESI Frag=135V Gain=1,0RT:9.15321666666667min (Subtracted)

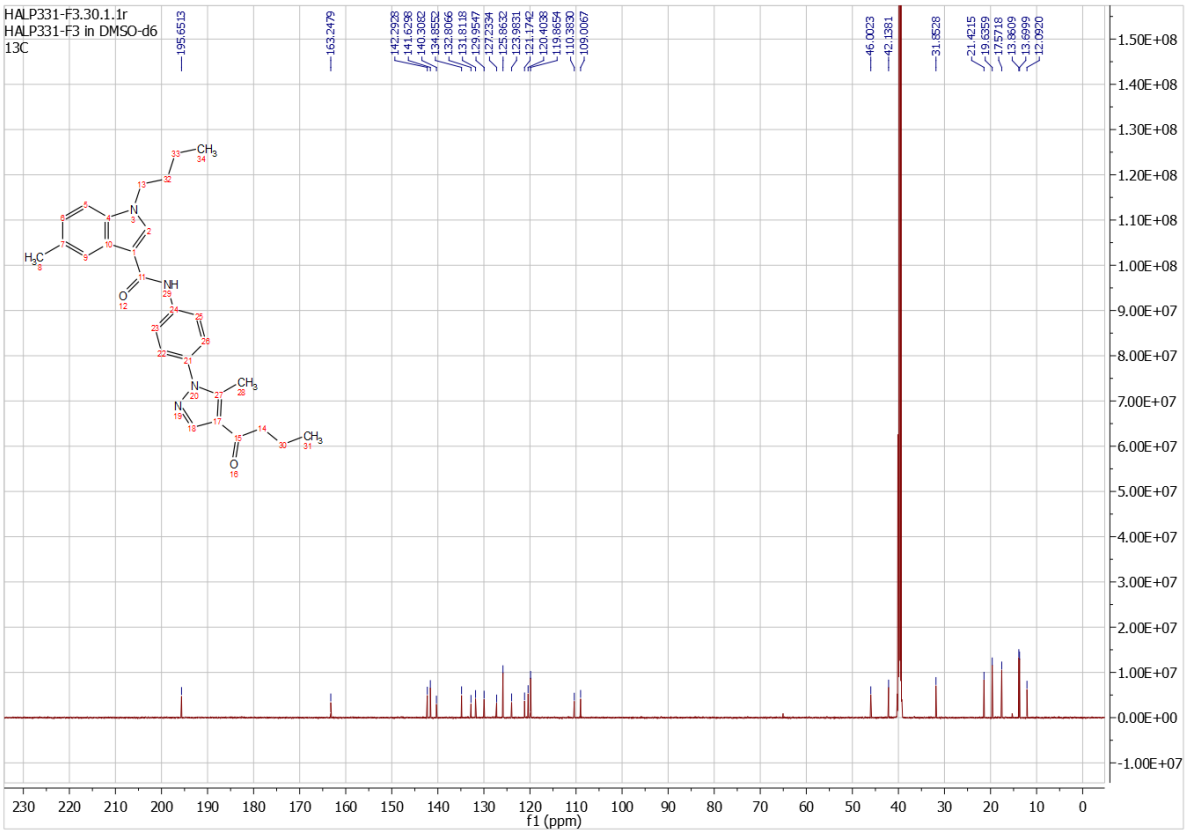


MS1 +TIC SCAN ESI Frag=135V Gain=1,0RT:9.1623043848847min (Subtracted)

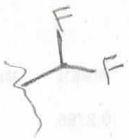


D:\CDSProjects\Default\00-standardplot+EIC.rdl [Rev. 8989] Printed: 2024-02-01 07:07:44+01:00 Page 2 of 2

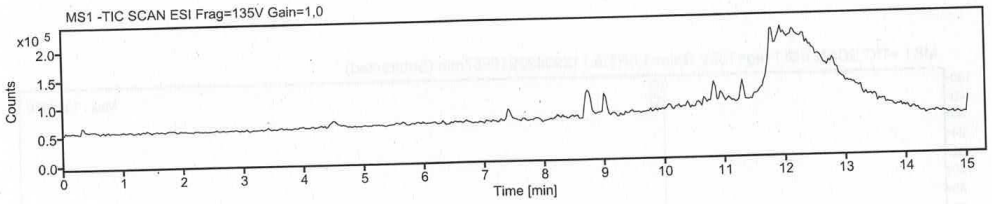

HALP331-F3.10.1.1r
HALP331-F3 in DMSO-d6
1H
F (s) 8.2859
E (s) 8.2354
B (dd) 7.4736
G (s) 9.8991
C (dd) 7.9444
A (m) 7.0758
D (s) 8.0254
H (t) 4.2288
N (s) 2.5221
K (h) 1.6367
I (t) 2.8123
J (p) 1.8081
M (dt) 0.9304
O (s) 2.4258
L (h) 1.3094
f1 (ppm)

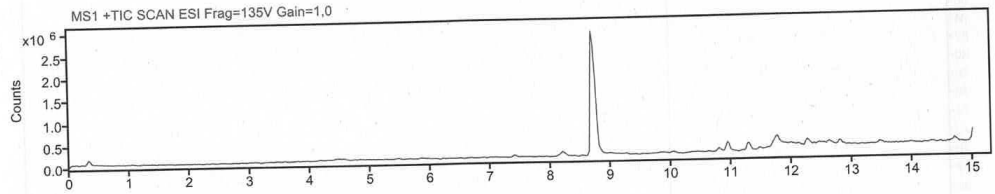

HALP331-F3.30.1.1r
HALP331-F3 in DMSO-d6
13C
f1 (ppm)

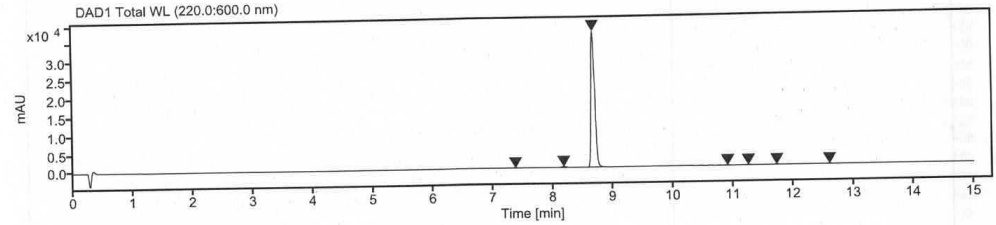
Benzyl 1-(difluoromethyl)-5-methyl-1*H*-indole-3-carboxylate (10a)

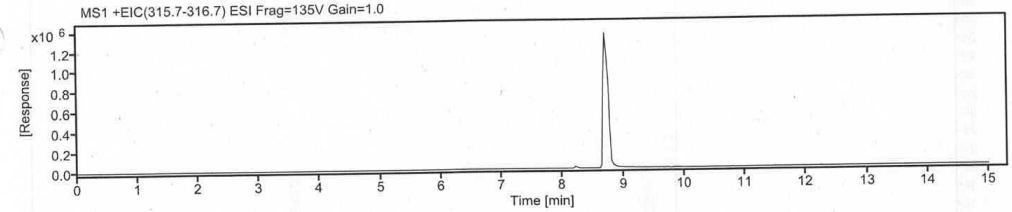


Sequence Name:	SingleSample		
Data file:	HALP294-F1.dx	**Project Name:**	Single Quad
Sample name:	HALP294-F1	**Operator :**	SYSTEM
Instrument:	Single Quad	**Acquired on:**	2023-11-29 10:20:28+01:00
Inj. volume:	5.000	**Location:**	P2-B1
Acq. method:	00-new_wasser-acn_standard_100-1000_BD-20min.amx		
Processing method:	MS_standard_plot.pmx		





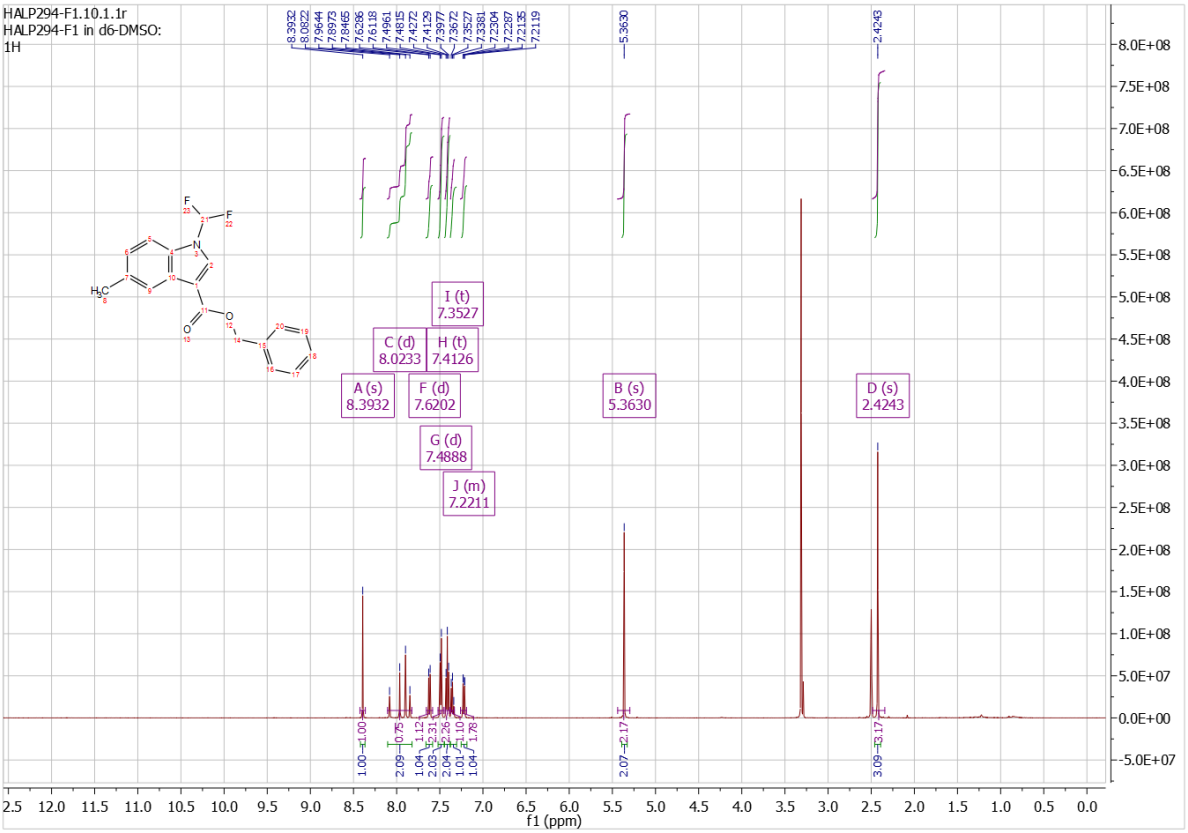


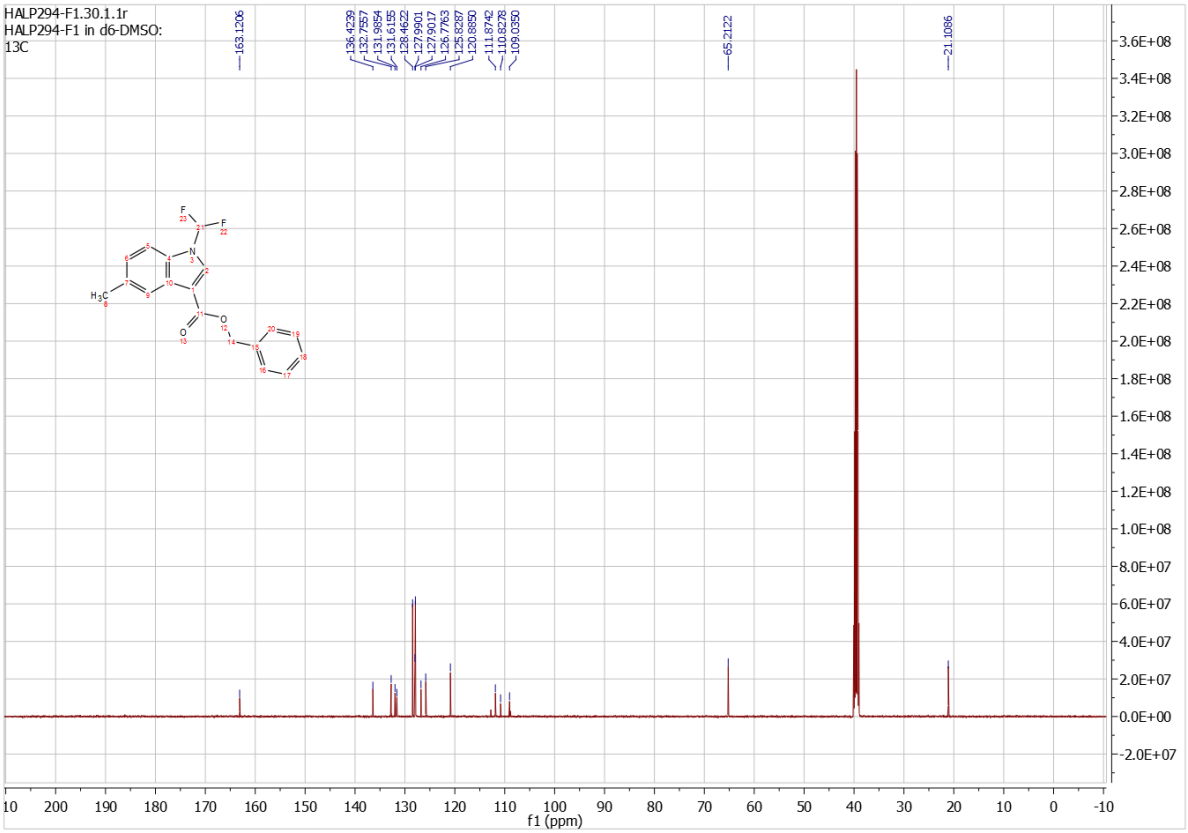


Signal: DAD1 Total WL (220.0:600.0 nm)

RT [min]	Peak MS Base Peak m/z	Area	Area%	Max Peak%	Height
7.381		282.5842	0.1753	0.178	66.223
8.182		1380.2807	0.8564	0.870	293.462
8.683		158577.9600	98.3885	100.000	37061.583
10.912		141.8616	0.0880	0.089	29.458
11.254		171.2728	0.1063	0.108	47.235
11.726		170.7681	0.1060	0.108	39.932

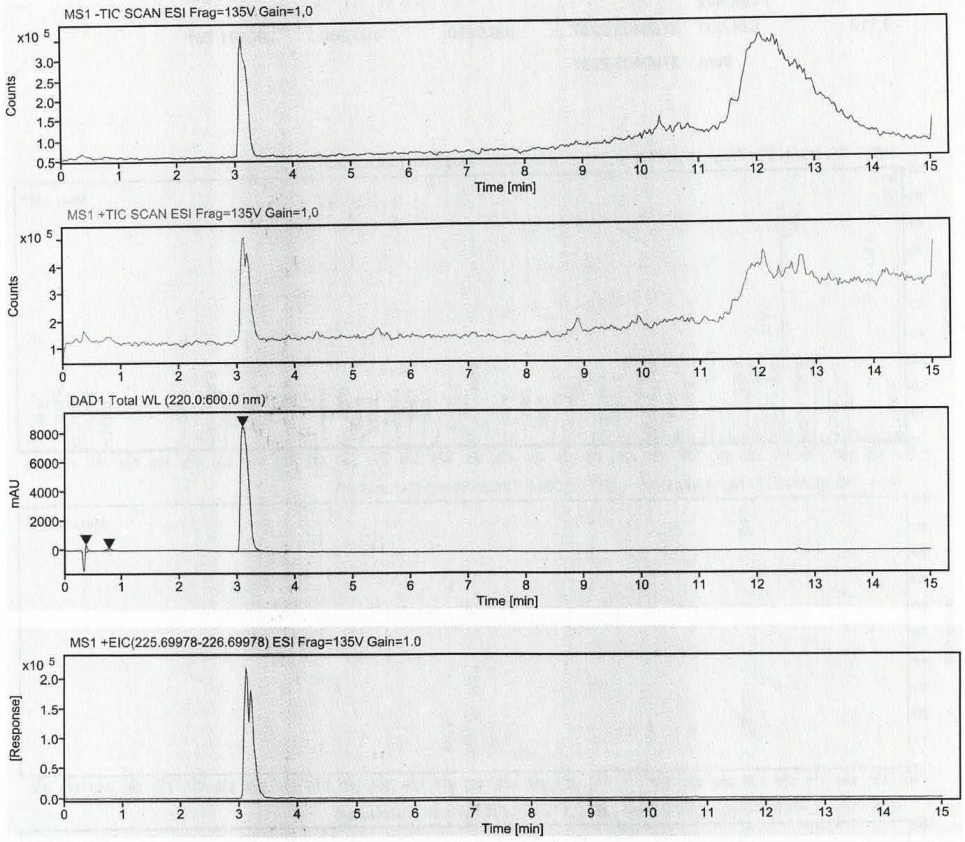
D:\CDSProjects\Default\00-standardplot+EIC.rdl [Rev. 8128] Printed: 2023-11-29 12:09:32+01:00 Page 1 of 2


HALP294-F1.10.1.1r
HALP294-F1 in d6-DMSO:
1H
A (s)
8.3932
C (d)
8.0233
F (d)
7.6202
G (d)
7.4888
I (t)
7.3527
H (t)
7.4126
J (m)
7.2211
B (s)
5.3630
D (s)
2.4243
f1 (ppm)


HALP294-F1.30.1.1r
HALP294-F1 in d6-DMSO:
13C
f1 (ppm)

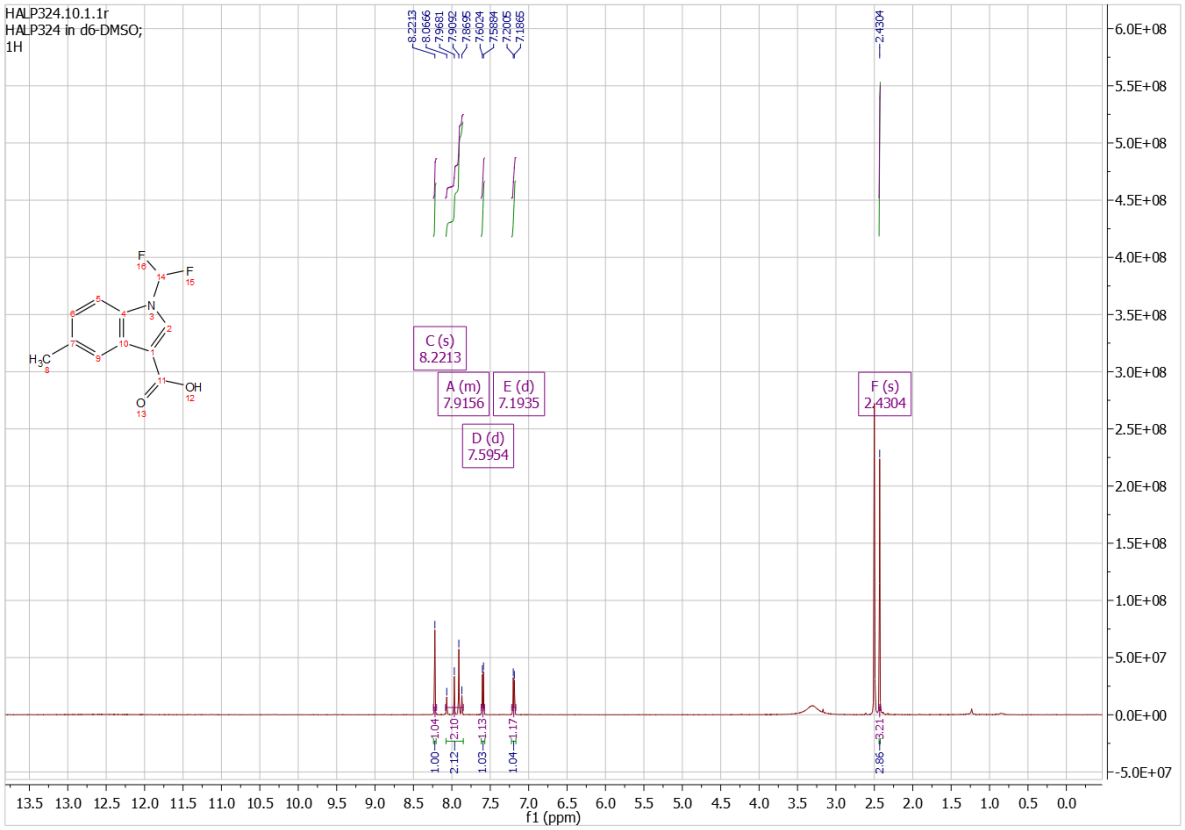
1-(Difluoromethyl)-5-methyl-1*H*-indole-3-carboxylic acid (10b)

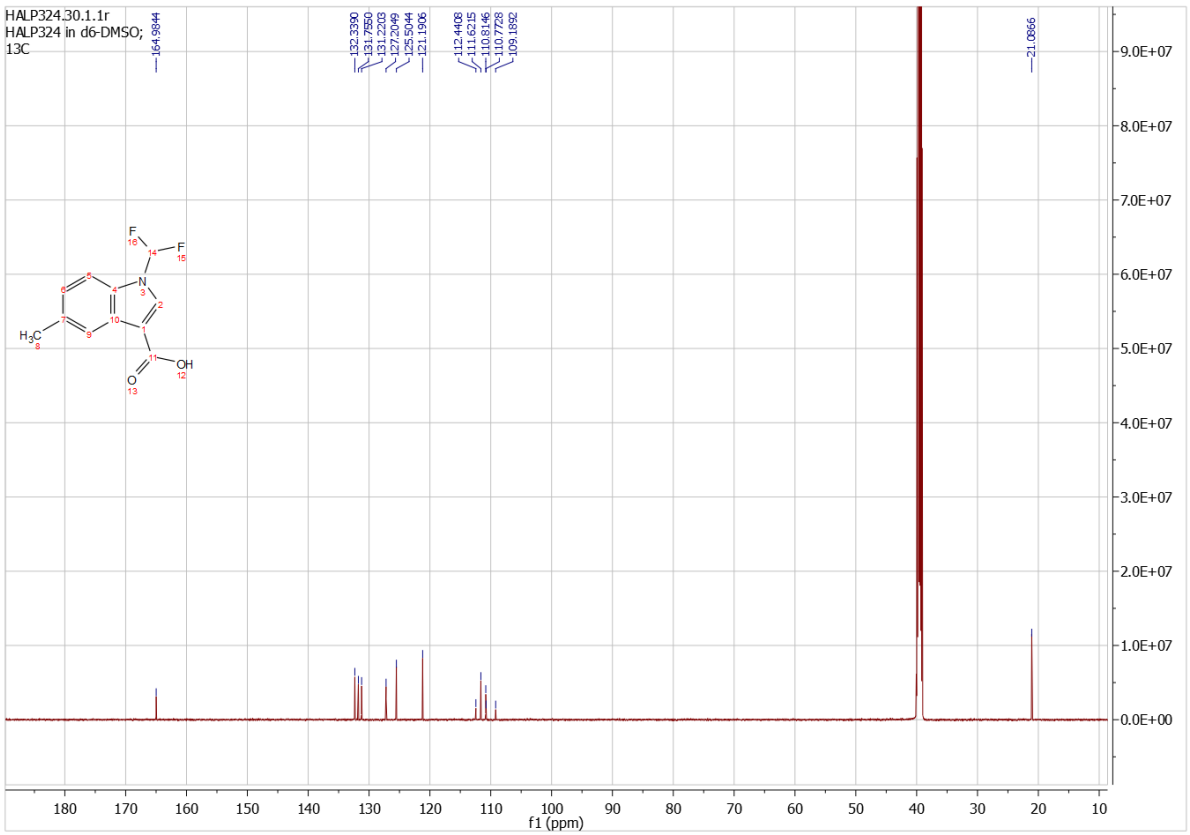
Sequence Name:	SingleSample		
Data file:	HALP324.dx	**Project Name:**	Single Quad
Sample name:	HALP324	**Operator :**	SYSTEM
Instrument:	Single Quad	**Acquired on:**	2024-01-11 13:50:46+01:00
Inj. volume:	2.000	**Location:**	P1-B3
Acq. method:	00-new_wasser-acn_standard_100-1000_BD-20min.amx		
Processing method:	MS_standard_plot.pmx		



Signal: DAD1 Total WL (220.0:600.0 nm)

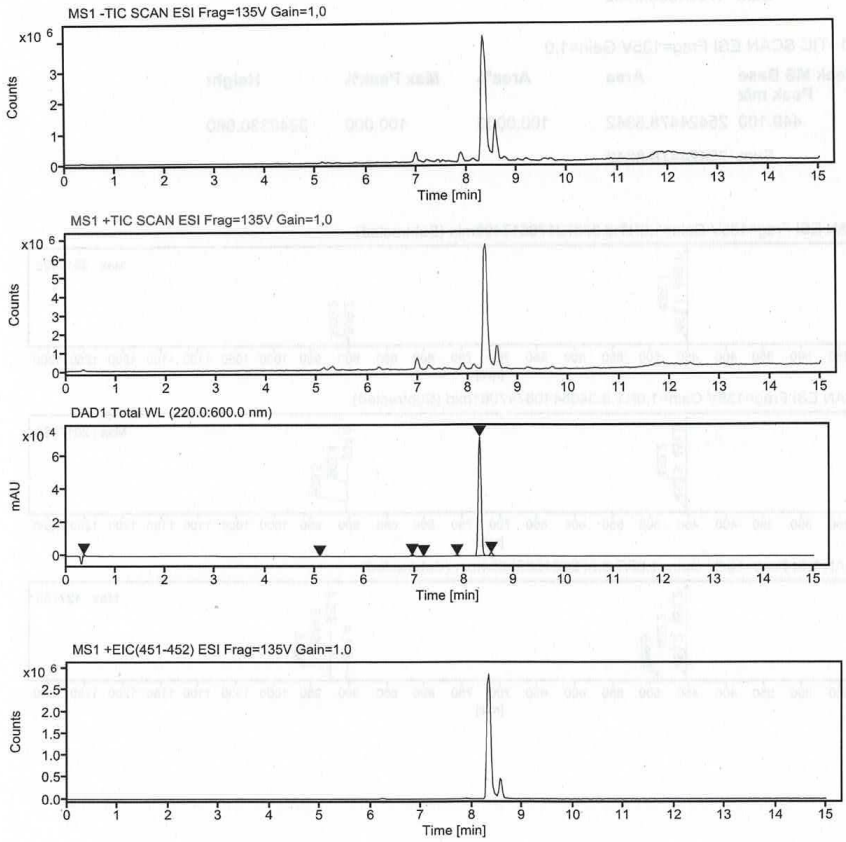
RT [min]	Peak MS Base Peak m/z	Area	Area%	Max Peak%	Height
0.370	198.100	960.1248	1.1524	1.177	496.873
0.769		788.7887	0.9467	0.967	133.753
3.083		81568.8894	97.9009	100.000	8582.081
	Sum	83317.8028			


HALP324.10.1.1r
HALP324 in d6-DMSO;
1H
8.2213
8.0666
7.9681
7.9092
7.8695
7.6024
7.5884
7.2005
7.1865
2.4304
C (s)
8.2213
A (m)
7.9156
E (d)
7.1935
D (d)
7.5954
F (s)
2.4304
1.00
1.04
2.12
2.10
1.03
1.13
1.04
1.17
2.86
3.21
f1 (ppm)


HALP324.30.1.1r
HALP324 in d6-DMSO;
13C
164.9844
132.3390
131.7850
131.2203
127.2049
125.5044
121.1906
112.4408
111.6215
110.8146
110.7728
109.1892
21.0866
f1 (ppm)

_N_-(4-(4-Butyryl-5-methyl-1_H_-pyrazol-1-yl)phenyl)-1-(difluoromethyl)-5-methyl-1_H_-indole-3-carboxamide (10c)

Sequence Name:	SingleSample		
Data file:	HALP333-F2.dx	**Project Name:**	Single Quad
Sample name:	HALP333-F2	**Operator :**	SYSTEM
Instrument:	Single Quad	**Acquired on:**	2024-03-13 11:37:52+01:00
Inj. volume:	5.000	**Location:**	P2-E7
Acq. method:	00-new_wasser-acn_standard_100-1000_BD-20min.amx		
Processing method:	MS_standard_plot.pmx		



Signal: DAD1 Total WL (220.0:600.0 nm)

RT [min]	Peak MS Base Peak m/z	Area	Area%	Max Peak%	Height
0.371		2917.9478	0.9491	1.001	1201.181
5.101		9.0088	0.0029	0.003	11.487
6.956		2301.2111	0.7485	0.789	738.298
7.185		823.9859	0.2680	0.283	224.051
7.855		2208.2676	0.7183	0.757	589.800
8.307		291632.3364	94.8552	100.000	72063.552
8.544		7557.4109	2.4581	2.591	1938.549

D:\CDSProjects\Default\0-standardplot+EIC.rdl [Rev. 7891] Printed: 2024-03-13 12:03:04+01:00 Page 1 of 2

RT [min]	Peak MS Base Peak m/z	Area	Area%	Max Peak%	Height
	Sum	307450.1685			

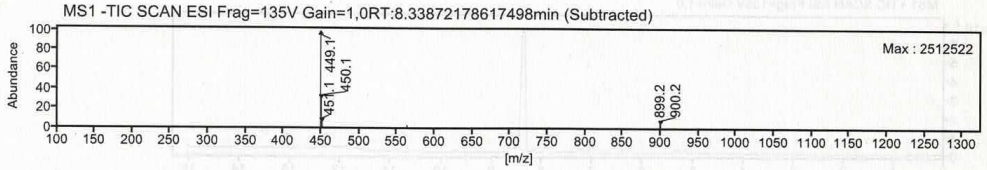
Signal: MS1 +TIC SCAN ESI Frag=135V Gain=1,0

RT [min]	Peak MS Base Peak m/z	Area	Area%	Max Peak%	Height
8.341	451.300	41316548.4947	87.8048	100.000	6588377.210
8.579	451.200	5738437.3615	12.1952	13.889	1274198.871
	Sum	47054985.8562			

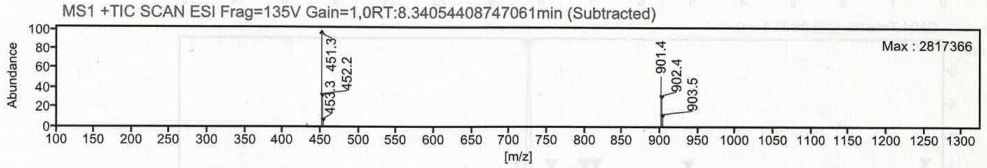
Signal: MS1 -TIC SCAN ESI Frag=135V Gain=1,0

RT [min]	Peak MS Base Peak m/z	Area	Area%	Max Peak%	Height
8.339	449.100	25424478.8342	100.0000	100.000	3940330.660
	Sum	25424478.8342			

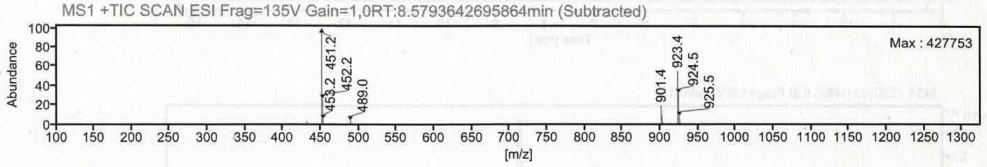
MS1 -TIC SCAN ESI Frag=135V Gain=1,0RT:8.33872178617498min (Subtracted)

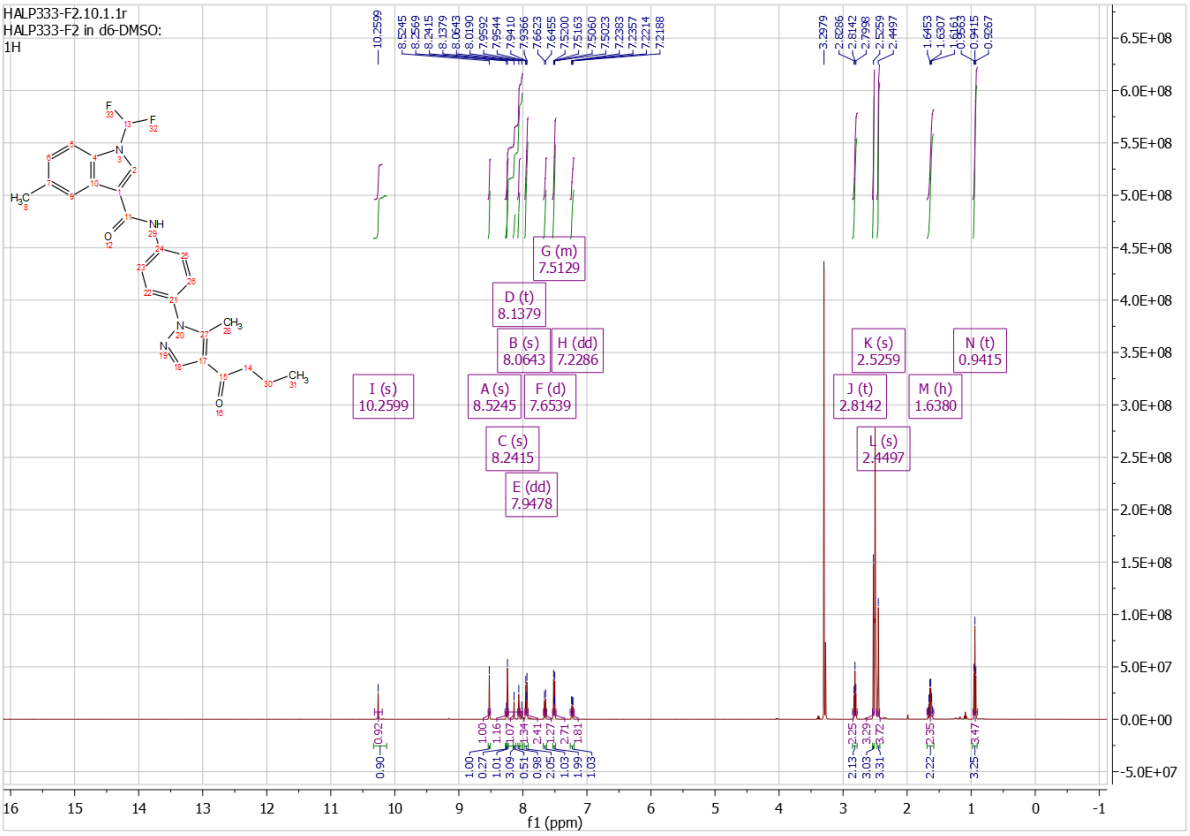


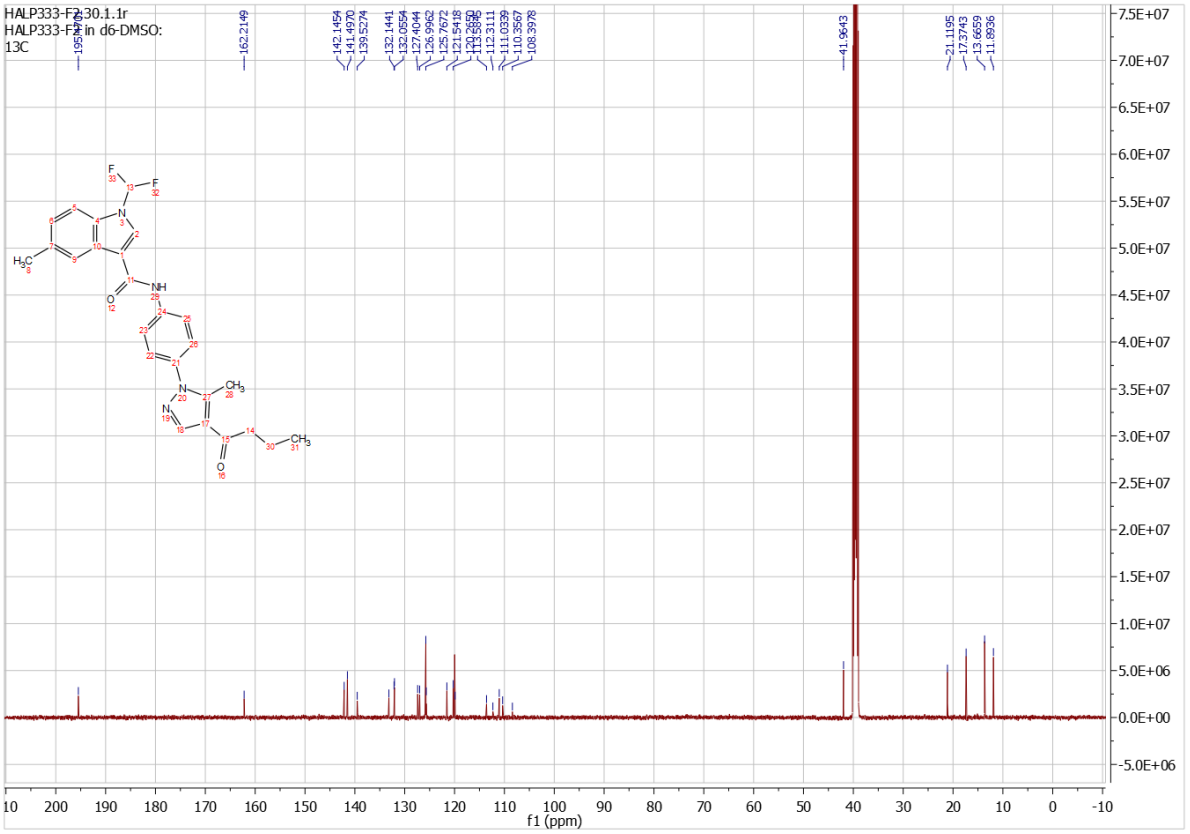
MS1 +TIC SCAN ESI Frag=135V Gain=1,0RT:8.34054408747061min (Subtracted)



MS1 +TIC SCAN ESI Frag=135V Gain=1,0RT:8.5793642695864min (Subtracted)

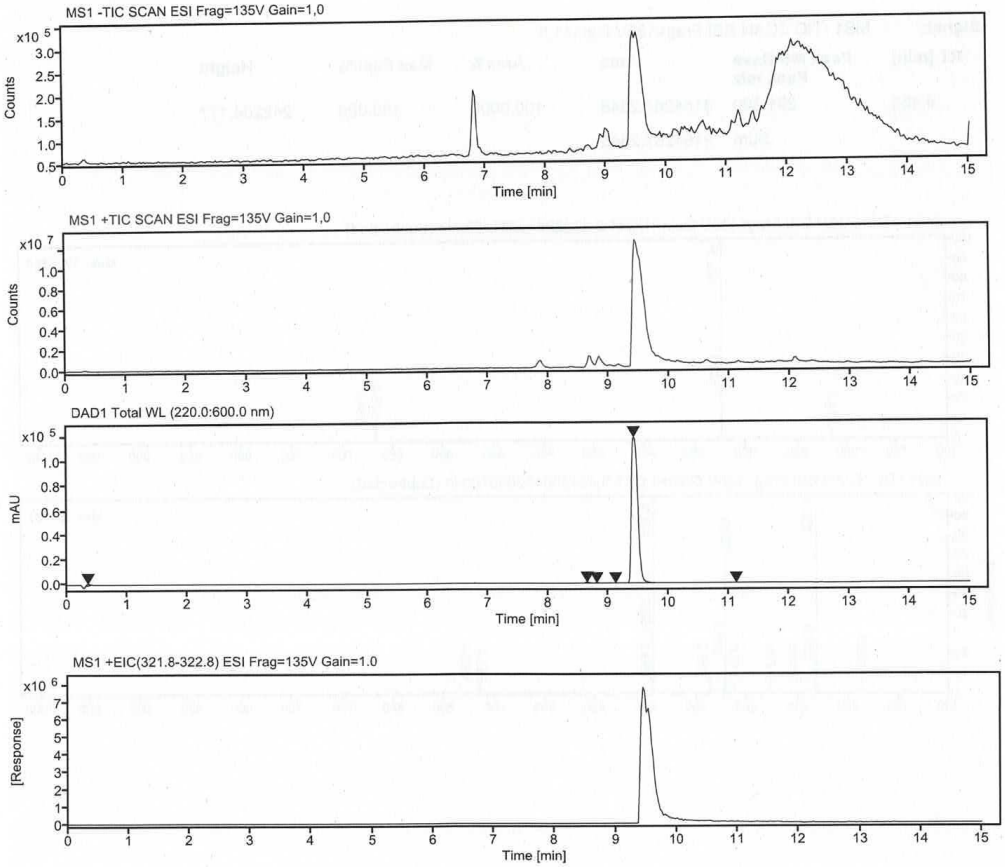



HALP333-F2.10.1.1r
HALP333-F2 in d6-DMSO:
1H
I (s)
10.2599
A (s)
8.5245
B (s)
8.0643
C (s)
8.2415
D (t)
8.1379
E (dd)
7.9478
F (d)
7.6539
G (m)
7.5129
H (dd)
7.2286
J (t)
2.8142
K (s)
2.5259
L (s)
2.4497
M (h)
1.6380
N (t)
0.9415
f1 (ppm)


HALP333-F2.30.1.1r
HALP333-F2 in d6-DMSO:
13C
162.2149
142.1454
141.4970
139.5274
132.1441
132.0554
127.4044
126.9952
125.7672
121.5418
120.2650
113.5886
112.3111
111.0339
110.3567
108.3978
41.9643
21.1195
17.3743
13.6659
11.8936
f1 (ppm)

(*R,S*)-Benzyl 1-(*sec*-butyl)-5-methyl-1*H*-indole-3-carboxylate (11a)

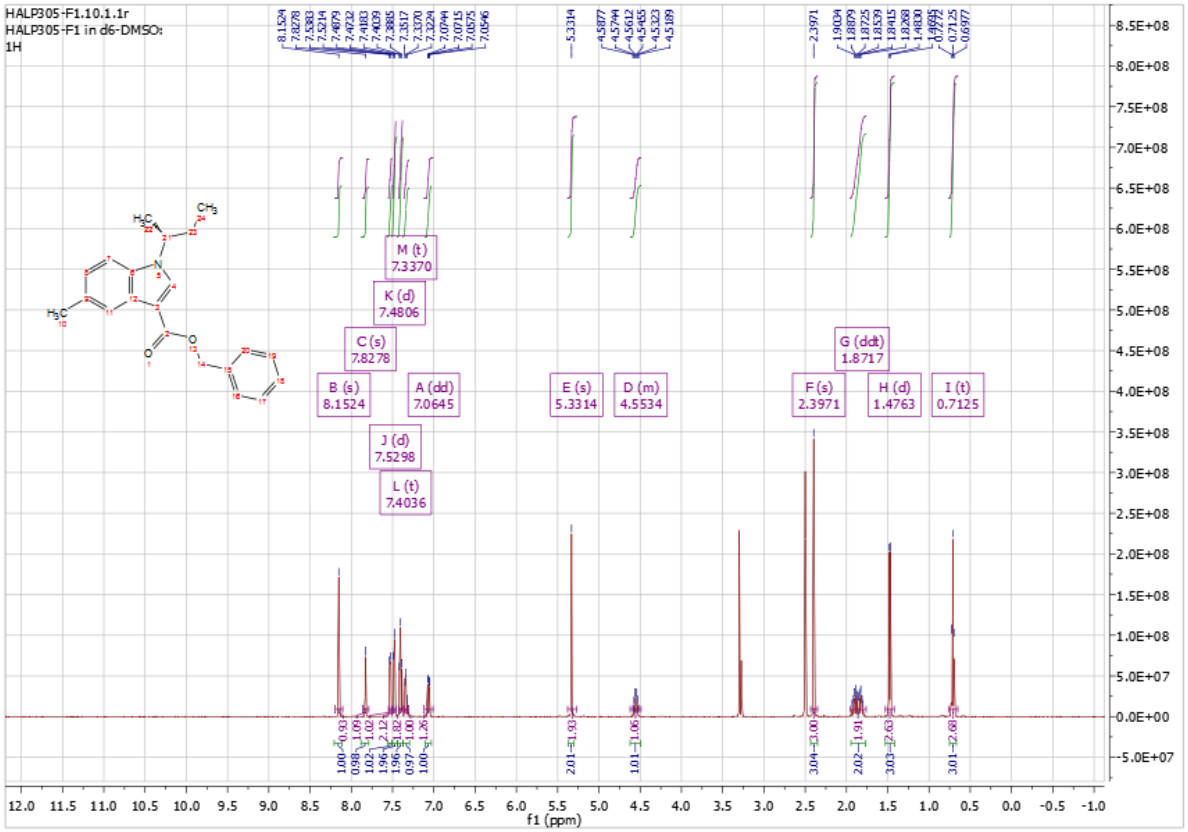
Sequence Name:	SingleSample		
Data file:	HALP305-F1.dx	**Project Name:**	Single Quad
Sample name:	HALP305-F1	**Operator :**	SYSTEM
Instrument:	Single Quad	**Acquired on:**	2024-01-04 15:36:30+01:00
Inj. volume:	8.000	**Location:**	P2-E1
Acq. method:	00-new_wasser-acn_standard_100-1000_BD-20min.amx		
Processing method:	MS_standard_plot.pmx		

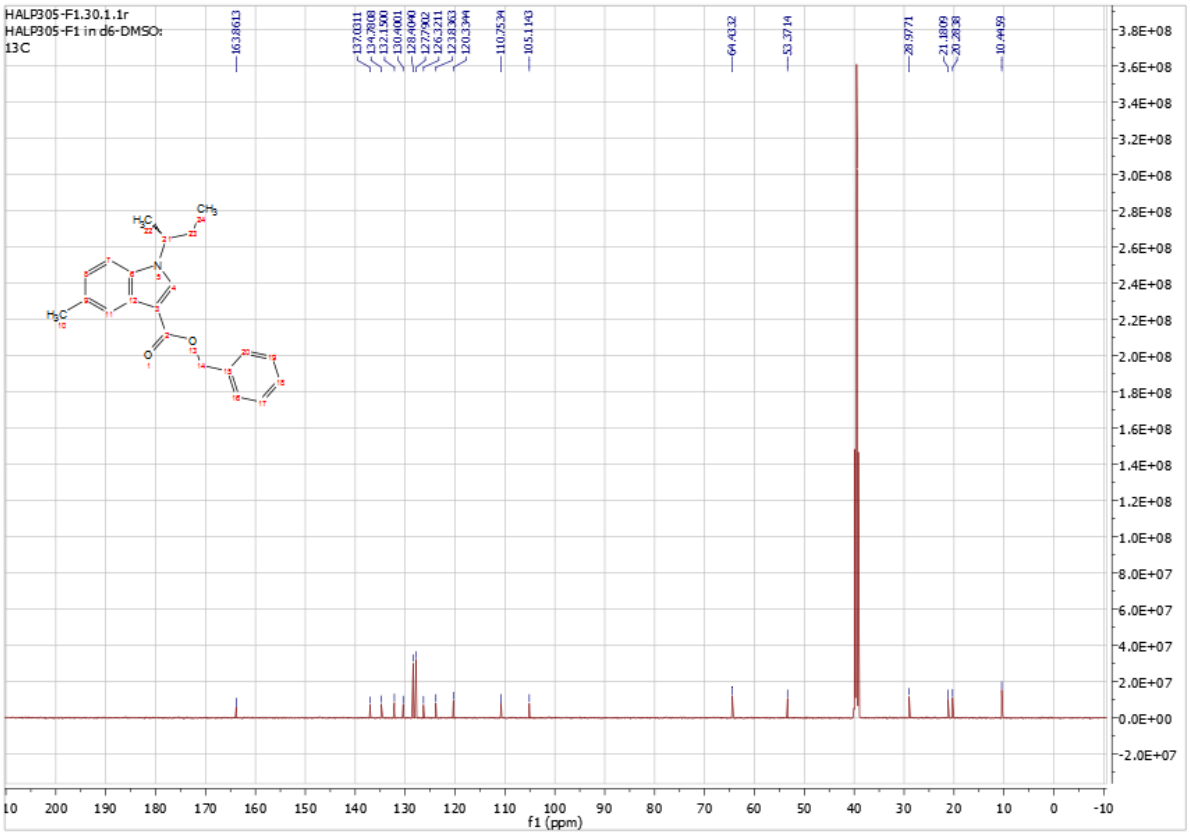


Signal: DAD1 Total WL (220.0:600.0 nm)

RT [min]	Peak MS Base Peak m/z	Area	Area%	Max Peak%	Height
0.365		4437.2269	0.5085	0.514	1205.455
8.656		3604.8421	0.4131	0.418	779.888
8.816		909.1440	0.1042	0.105	180.454
9.128		151.4515	0.0174	0.018	48.686
9.435	322.100	863397.9489	98.9393	100.000	118092.646
11.128		153.8442	0.0176	0.018	32.747

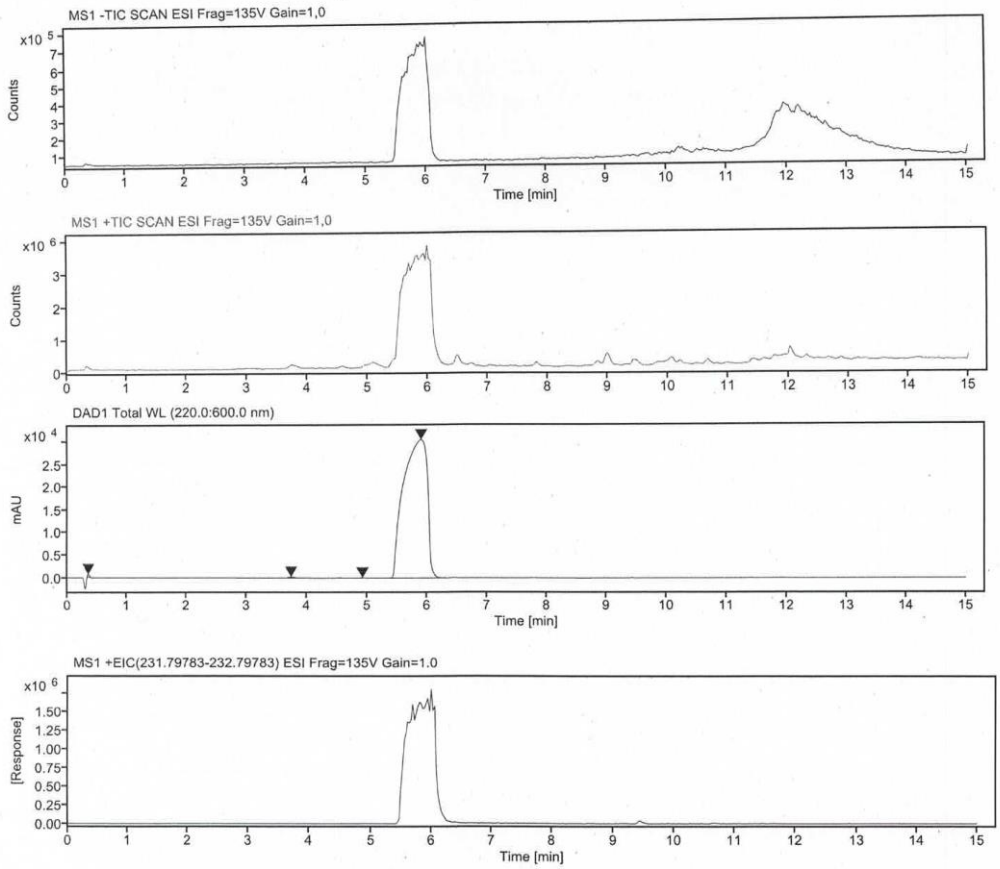
D:\CDSProjects\Default\00-standardplot+EIC.rdl [Rev. 8561] Printed: 2024-01-08 10:37:41+01:00 Page 1 of 2


HALP305-F1.10.1.1r
HALP305-F1 in d6-DMSO
1H
M (t)
7.3370
K (d)
7.4806
C (s)
7.8278
G (ddt)
1.8717
B (s)
8.1524
A (dd)
7.0645
E (s)
5.3314
D (m)
4.5534
F (s)
2.3971
H (d)
1.4763
I (t)
0.7125
J (d)
7.5298
L (t)
7.4036
f1 (ppm)


HALP305-F1.30.1.1r
HALP305-F1 in d6-DMSO
13C
f1 (ppm)

(*R,S*)-1-(*Sec*-butyl)-5-methyl-1*H*-indole-3-carboxylic acid (11b)

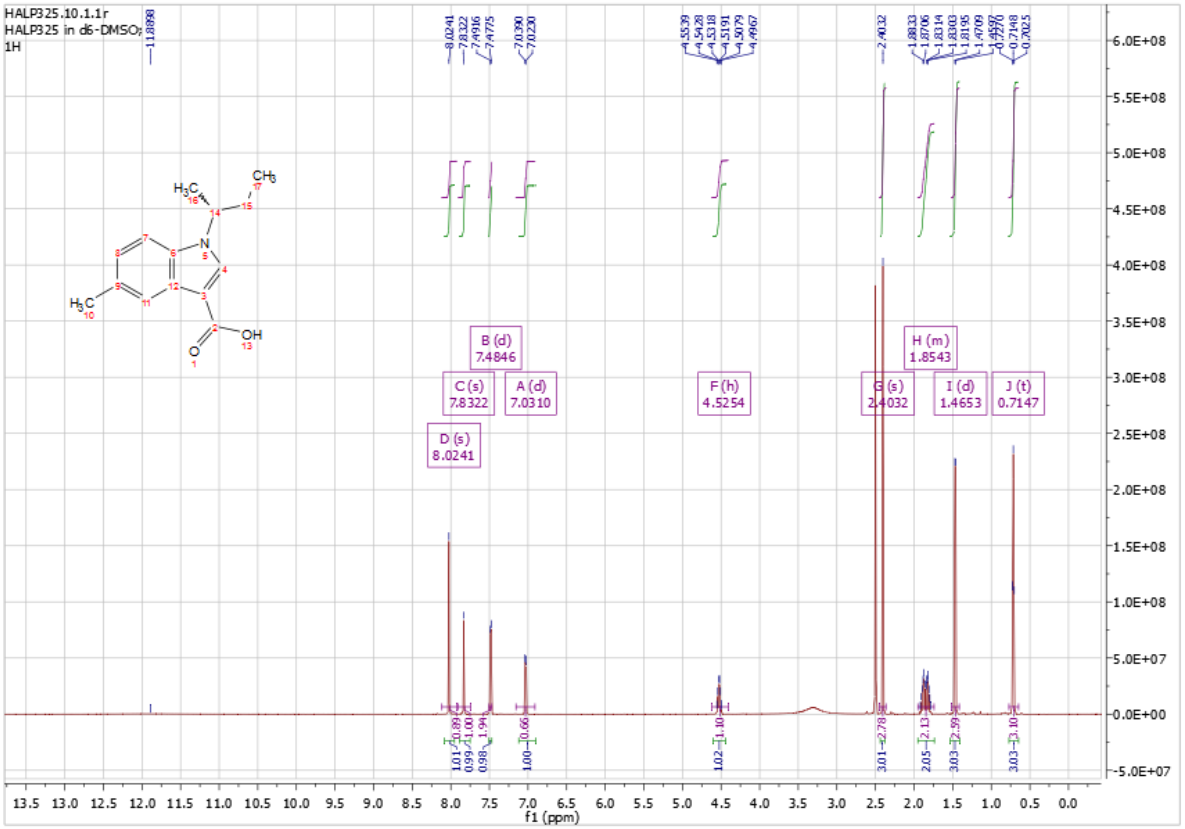
Sequence Name:	SingleSample		
Data file:	HALP325.dx	**Project Name:**	Single Quad
Sample name:	HALP325	**Operator :**	SYSTEM
Instrument:	Single Quad	**Acquired on:**	2024-01-11 19:48:41+01:00
Inj. volume:	4.000	**Location:**	P1-C9
Acq. method:	00-new_wasser-acn_standard_100-1000_BD-20min.amx		
Processing method:	MS_standard_plot.pmx		

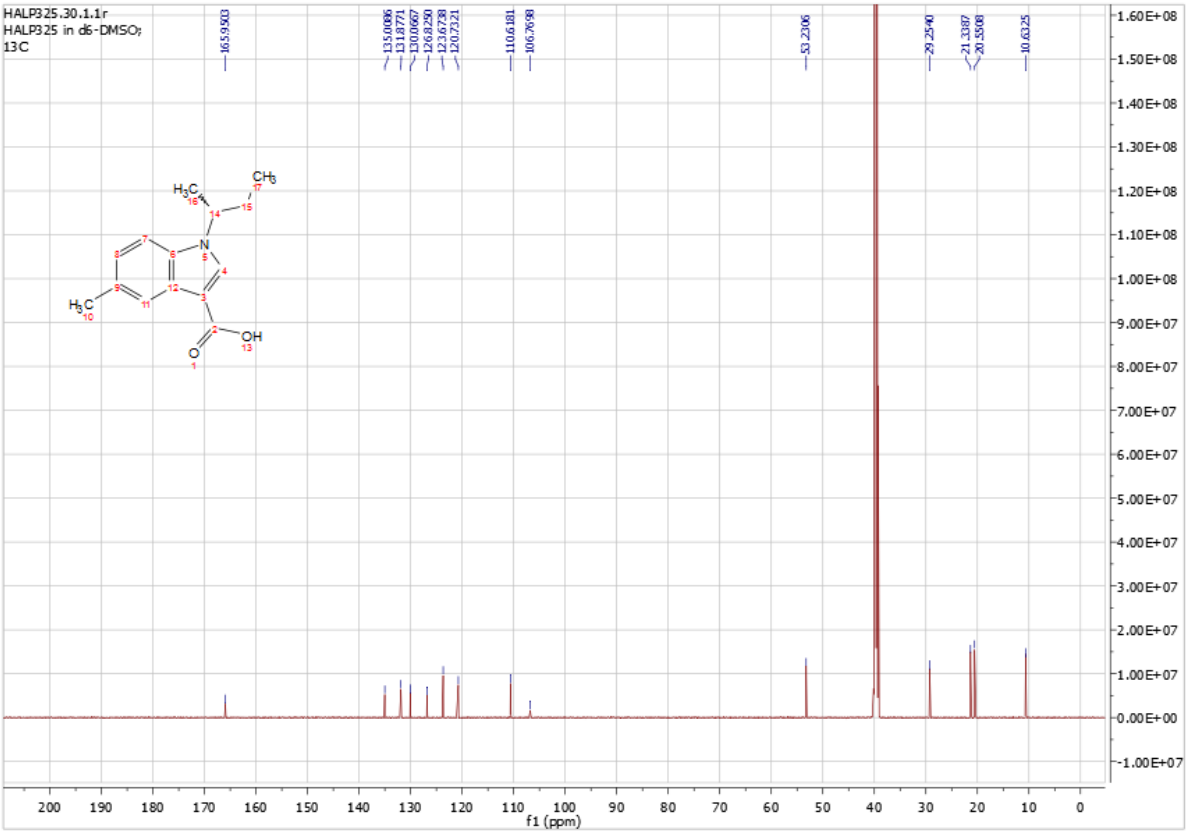


Signal: DAD1 Total WL (220.0:600.0 nm)

RT [min]	Peak MS Base Peak m/z	Area	Area%	Max Peak%	Height
0.366		1178.1413	0.1401	0.141	549.936
3.748		1764.4430	0.2099	0.211	233.495
4.929		118.9675	0.0142	0.014	39.564
5.908	232.100	837611.3739	99.6358	100.000	30405.205
	Sum	840672.9257			

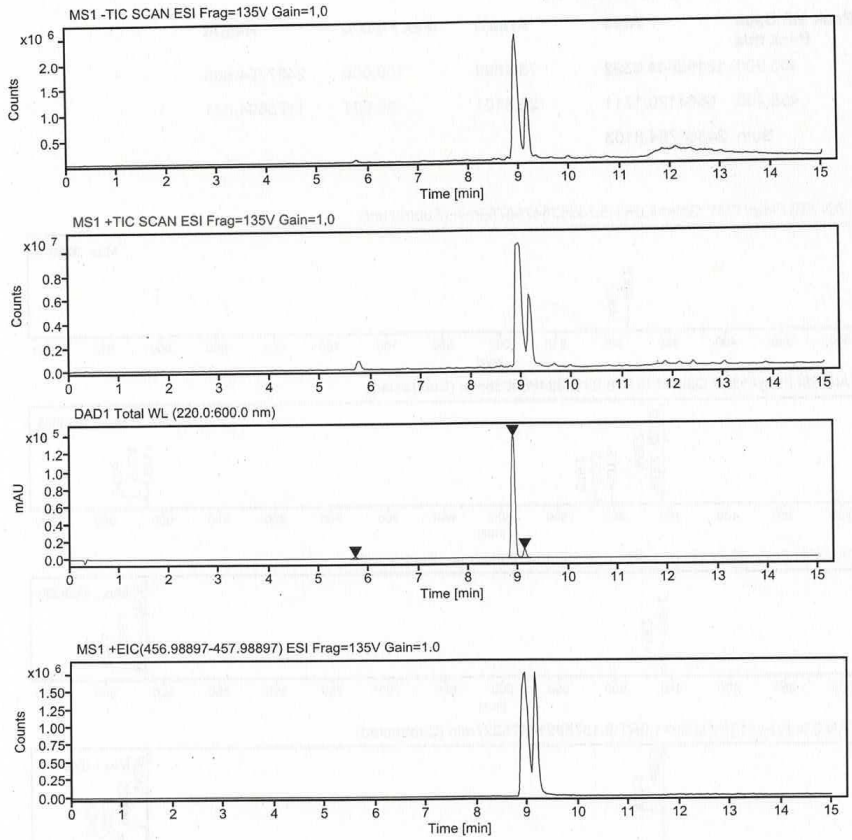
D:\CDSProjects\Default\00-standardplot+EIC.rdl [Rev. 8713] Printed: 2024-01-16 12:09:11+01:00 Page 1 of 2


HALP325.10.1.1r
HALP325 in d6-DMSO;
1H
B (d)
7.4846
C (s)
7.8322
A (d)
7.0310
D (s)
8.0241
F (h)
4.5254
G (s)
2.4032
H (m)
1.8543
I (d)
1.4653
J (t)
0.7147
f1 (ppm)


HALP325.30.1.1r
HALP325 in d6-DMSO;
13C
f1 (ppm)

(*R,S*)-1-(*Sec*-butyl)-*N*-(4-(4-butyryl-5-methyl-1*H*-pyrazol-1-yl)phenyl)-5-methyl-1*H*-indole-3-carboxamide (11c)

Sequence Name:	SingleSample		
Data file:	HALP334-F3.dx	**Project Name:**	Single Quad
Sample name:	HALP334-F3	**Operator :**	SYSTEM
Instrument:	Single Quad	**Acquired on:**	2024-02-18 12:05:17+01:00
Inj. volume:	4.000	**Location:**	P1-E5
Acq. method:	00-new_wasser-acn_standard_100-1000_BD-20min.amx		
Processing method:	MS_standard_plot.pmx		



Signal: DAD1 Total WL (220.0:600.0 nm)

RT [min]	Peak MS Base Peak m/z	Area	Area%	Max Peak%	Height
5.730	232.100	10291.9208	1.3208	1.415	1993.735
8.899		727398.9315	93.3522	100.000	138333.951
9.129		41507.7523	5.3270	5.706	9709.765
	Sum	779198.6046			

D:\CDSProjects\Default\0-standardplot+EIC.rdl [Rev. 7306] Printed: 2024-02-19 06:32:45+01:00 Page 1 of 2

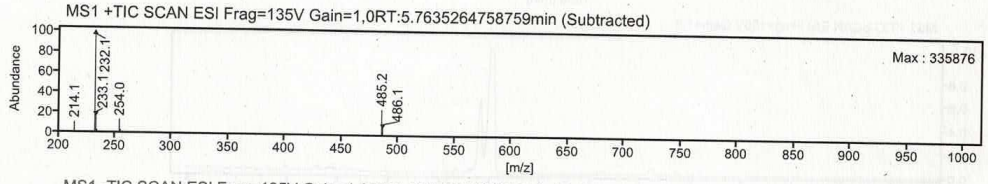
Signal: MS1 +TIC SCAN ESI Frag=135V Gain=1,0

RT [min]	Peak MS Base Peak m/z	Area	Area%	Max Peak%	Height
5.764	232.100	4063796.0984	3.0178	4.197	708418.902
8.946	913.500	96835778.6856	71.9110	100.000	10390664.513
9.158	913.500	33761071.3780	25.0712	34.864	6351968.297
	Sum	134660646.1620			

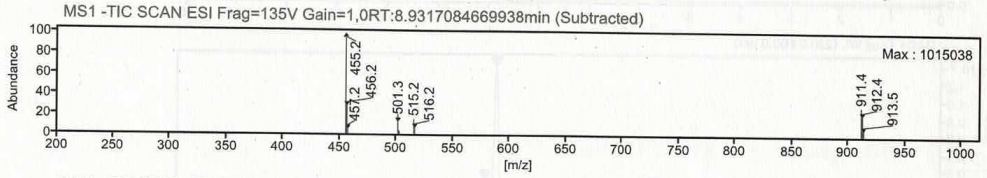
Signal: MS1 -TIC SCAN ESI Frag=135V Gain=1,0

RT [min]	Peak MS Base Peak m/z	Area	Area%	Max Peak%	Height
8.932	455.200	18192644.6392	73.1899	100.000	2437754.606
9.167	455.200	6664120.1711	26.8101	36.631	1173694.041
	Sum	24856764.8103			

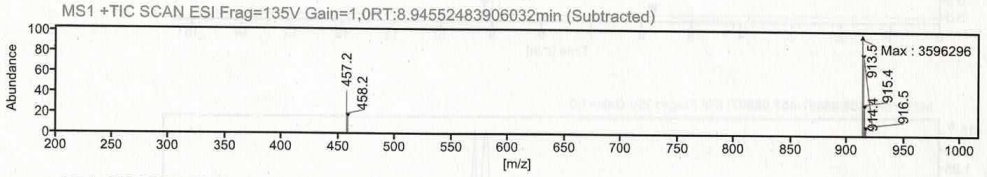
MS1 +TIC SCAN ESI Frag=135V Gain=1,0RT:5.7635264758759min (Subtracted)



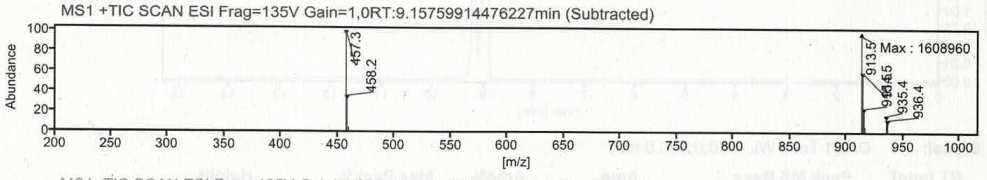
MS1 -TIC SCAN ESI Frag=135V Gain=1,0RT:8.9317084669938min (Subtracted)



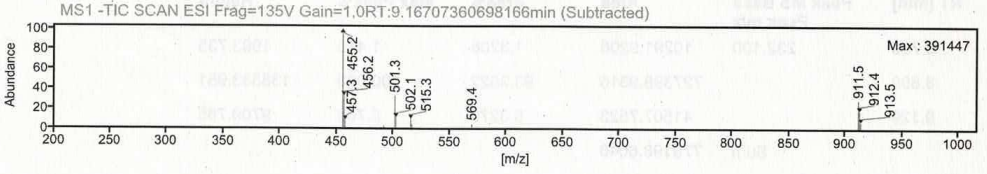
MS1 +TIC SCAN ESI Frag=135V Gain=1,0RT:8.94552483906032min (Subtracted)



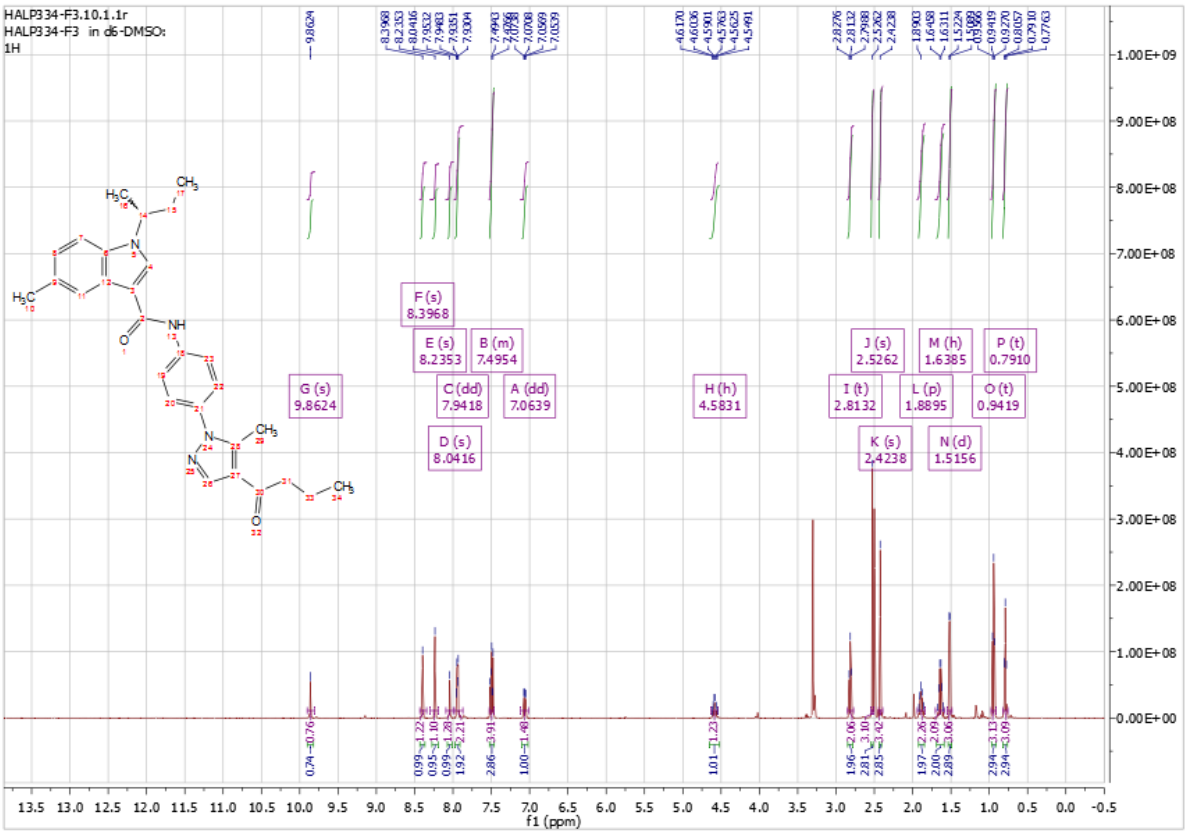
MS1 +TIC SCAN ESI Frag=135V Gain=1,0RT:9.15759914476227min (Subtracted)

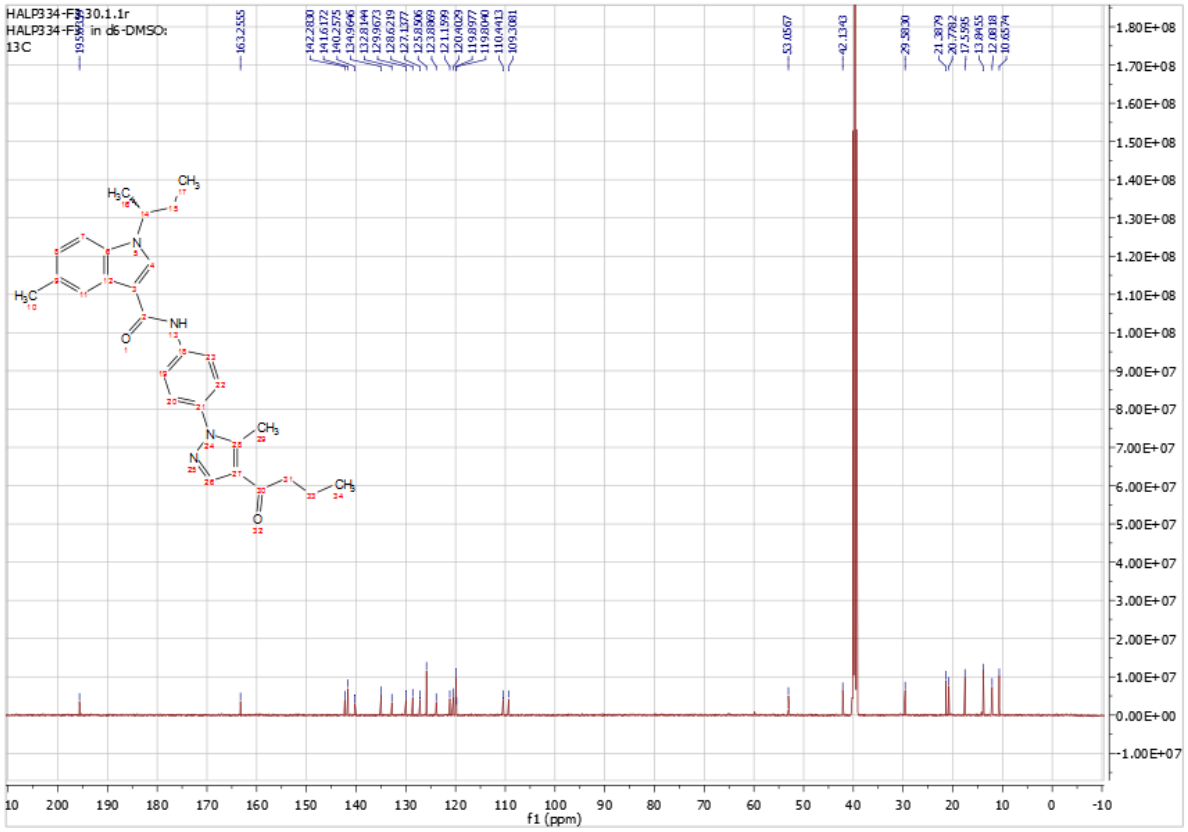


MS1 -TIC SCAN ESI Frag=135V Gain=1,0RT:9.16707360698166min (Subtracted)



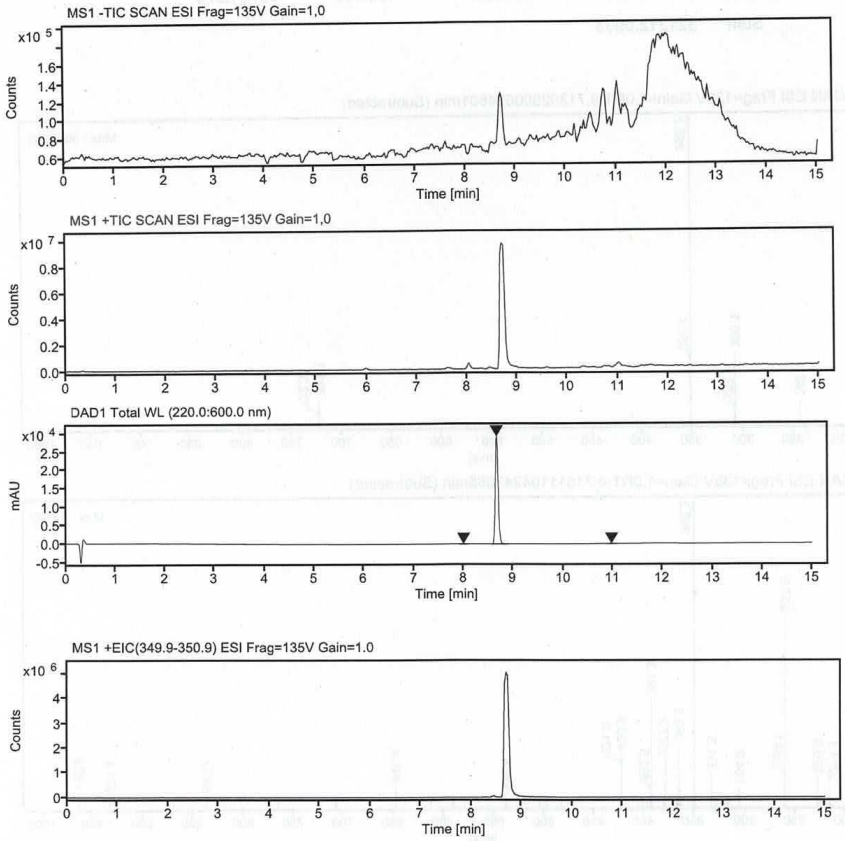
D:\CDSProjects\Default\0-standardplot+EIC.rdl [Rev. 7306] Printed: 2024-02-19 06:32:45+01:00 Page 2 of 2


HALP334-F3.10.1.1r
HALP334-F3 in d6-DMSO
1H
F (s) 8.3968
E (s) 8.2353
B (m) 7.4954
C (dd) 7.9418
A (dd) 7.0639
D (s) 8.0416
G (s) 9.8624
H (h) 4.5831
J (s) 2.5262
M (h) 1.6385
P (t) 0.7910
I (t) 2.8132
L (p) 1.8895
O (t) 0.9419
K (s) 2.4238
N (d) 1.5156
f1 (ppm)


HALP334-F3.30.1.1r
HALP334-F3 in d6-DMSO
13C
f1 (ppm)

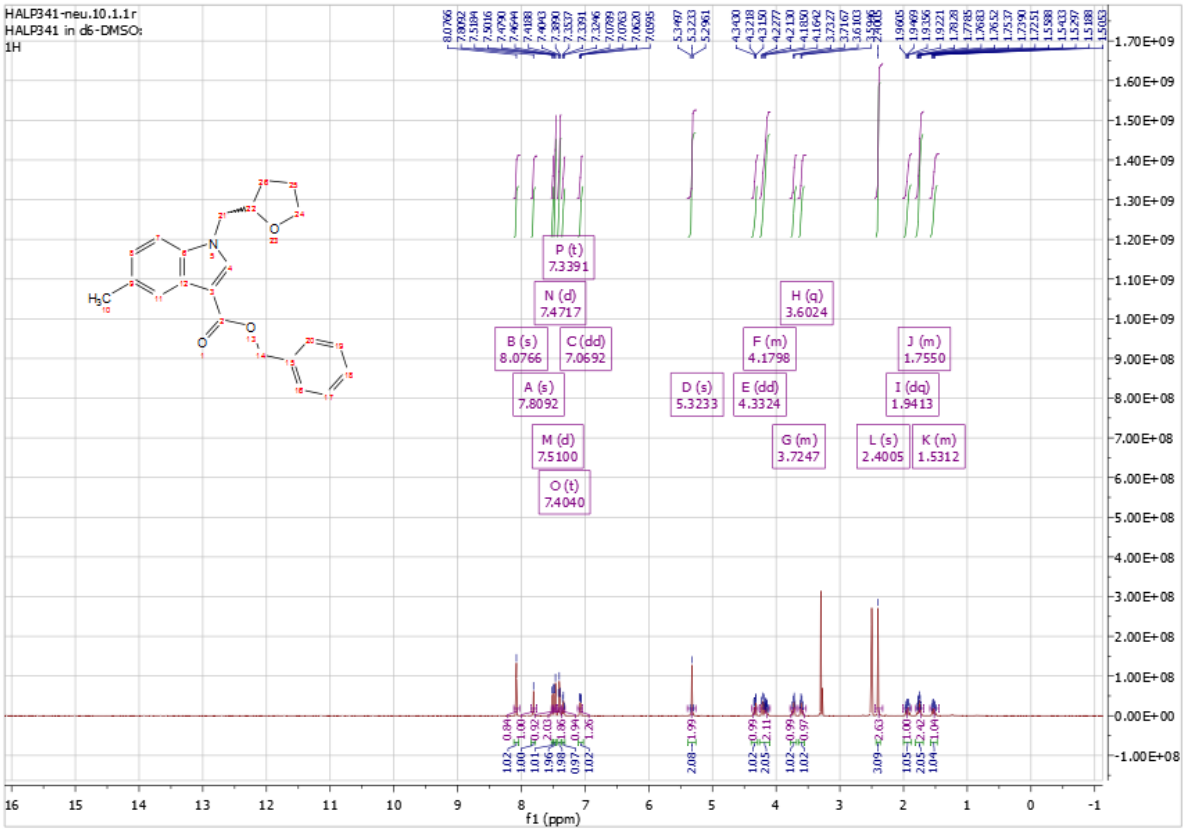
(*R*,*S*)-Benzyl 5-methyl-1-((tetrahydrofuran-2-yl)methyl)-1*H*-indole-3-carboxylate (12a)

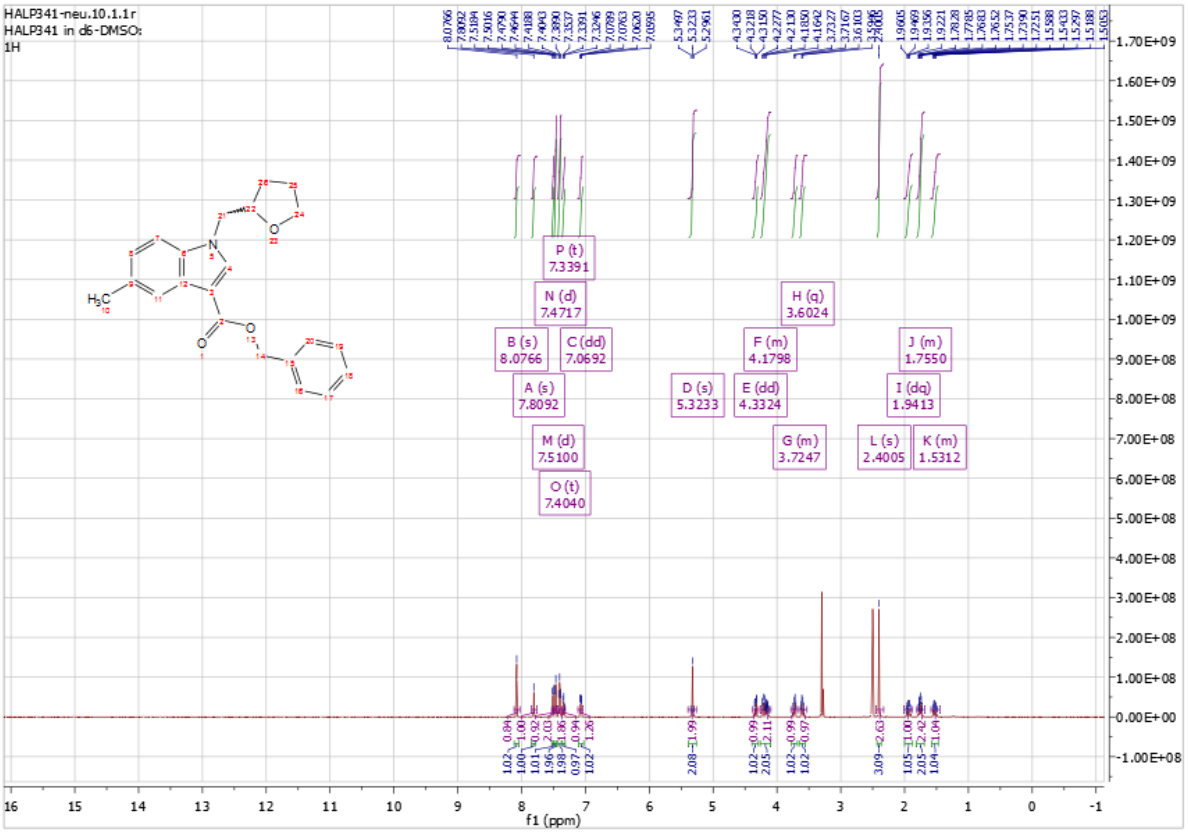
Sequence Name:	SingleSample		
Data file:	HALP341-F4.dx	**Project Name:**	Single Quad
Sample name:	HALP341-F4	**Operator :**	SYSTEM
Instrument:	Single Quad	**Acquired on:**	2024-03-04 21:53:08+01:00
Inj. volume:	5.000	**Location:**	P2-B4
Acq. method:	00-new_wasser-acn_standard_100-1000_BD-20min.amx		
Processing method:	MS_standard_plot.pmx		



Signal: DAD1 Total WL (220.0:600.0 nm)

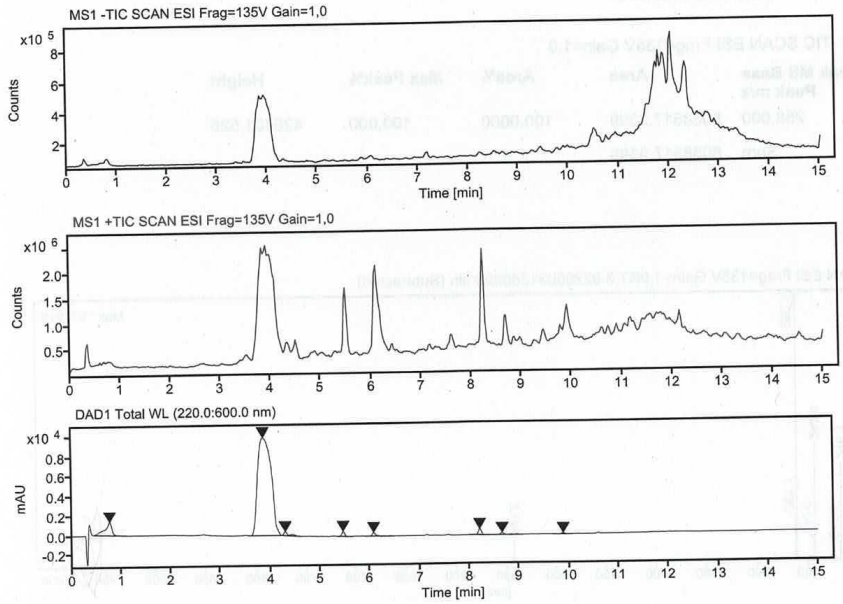
RT [min]	Peak MS Base Peak m/z	Area	Area%	Max Peak%	Height
8.003		393.6069	0.3232	0.325	97.782
8.675		120926.9532	99.3013	100.000	29362.560
10.983		457.2478	0.3755	0.378	89.687
	Sum	121777.8079			

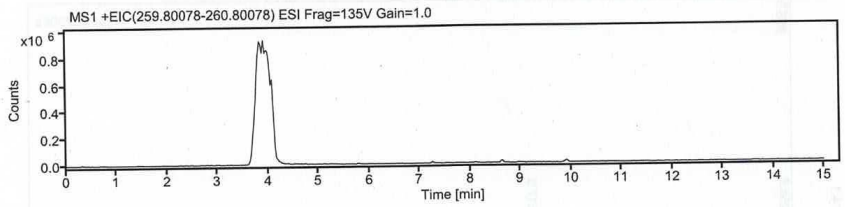

HALP341-neu.10.1.1r
HALP341 in d6-DMSO
1H
P (t)
7.3391
N (d)
7.4717
H (q)
3.6024
B (s)
8.0766
C (dd)
7.0692
F (m)
4.1798
J (m)
1.7550
A (s)
7.8092
D (s)
5.3233
E (dd)
4.3324
I (dq)
1.9413
M (d)
7.5100
G (m)
3.7247
L (s)
2.4005
K (m)
1.5312
O (t)
7.4040
f1 (ppm)


HALP341-neu.10.1.1r
HALP341 in d6-DMSO
1H
P (t)
7.3391
N (d)
7.4717
H (q)
3.6024
B (s)
8.0766
C (dd)
7.0692
F (m)
4.1798
J (m)
1.7550
A (s)
7.8092
D (s)
5.3233
E (dd)
4.3324
I (dq)
1.9413
M (d)
7.5100
G (m)
3.7247
L (s)
2.4005
K (m)
1.5312
O (t)
7.4040
f1 (ppm)

(*R,S*)-5-Methyl-1-((tetrahydrofuran-2-yl)methyl)-1*H*-indole-3-carboxylic acid (12b)

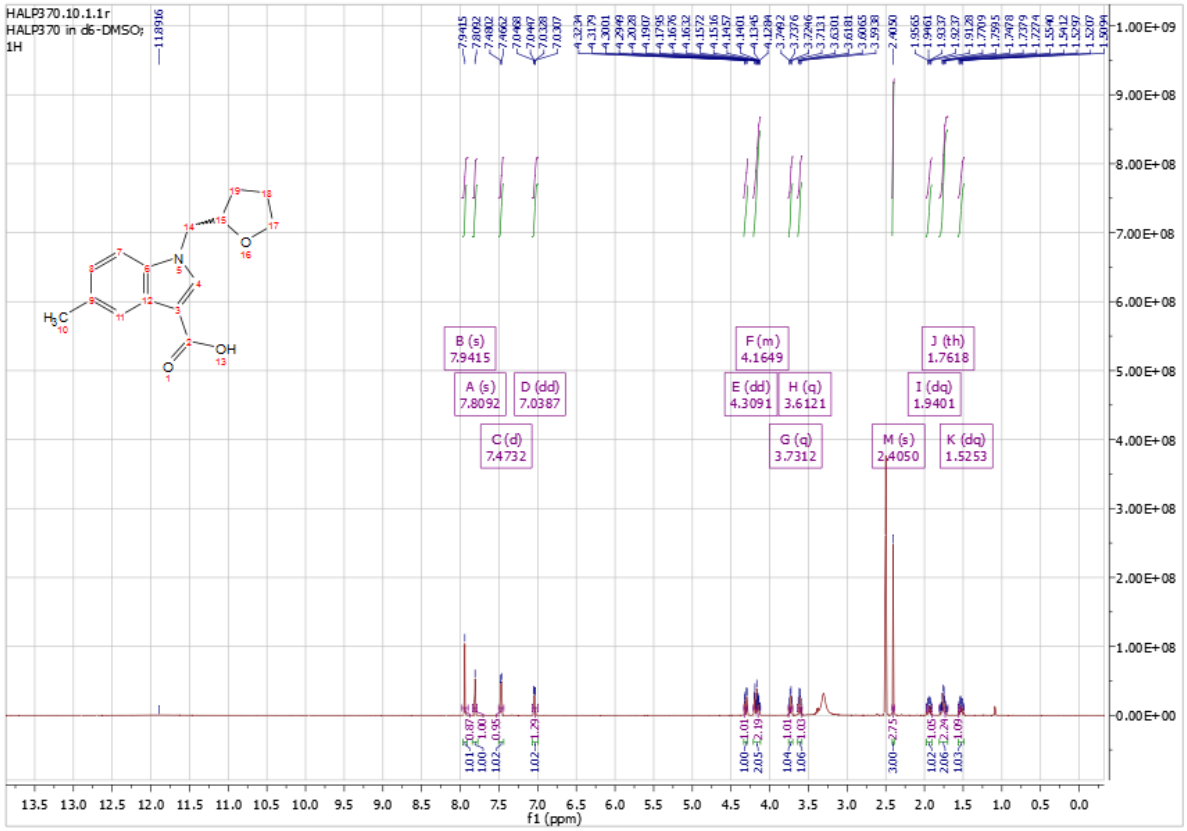
Sequence Name:	SingleSample		
Data file:	HALP370.dx	**Project Name:**	Single Quad
Sample name:	HALP370	**Operator :**	SYSTEM
Instrument:	Single Quad	**Acquired on:**	2024-03-11 15:17:23+01:00
Inj. volume:	4.000	**Location:**	P1-D7
Acq. method:	00-new_wasser-acn_standard_100-1000_BD-20min.amx		
Processing method:	MS_standard_plot.pmx		

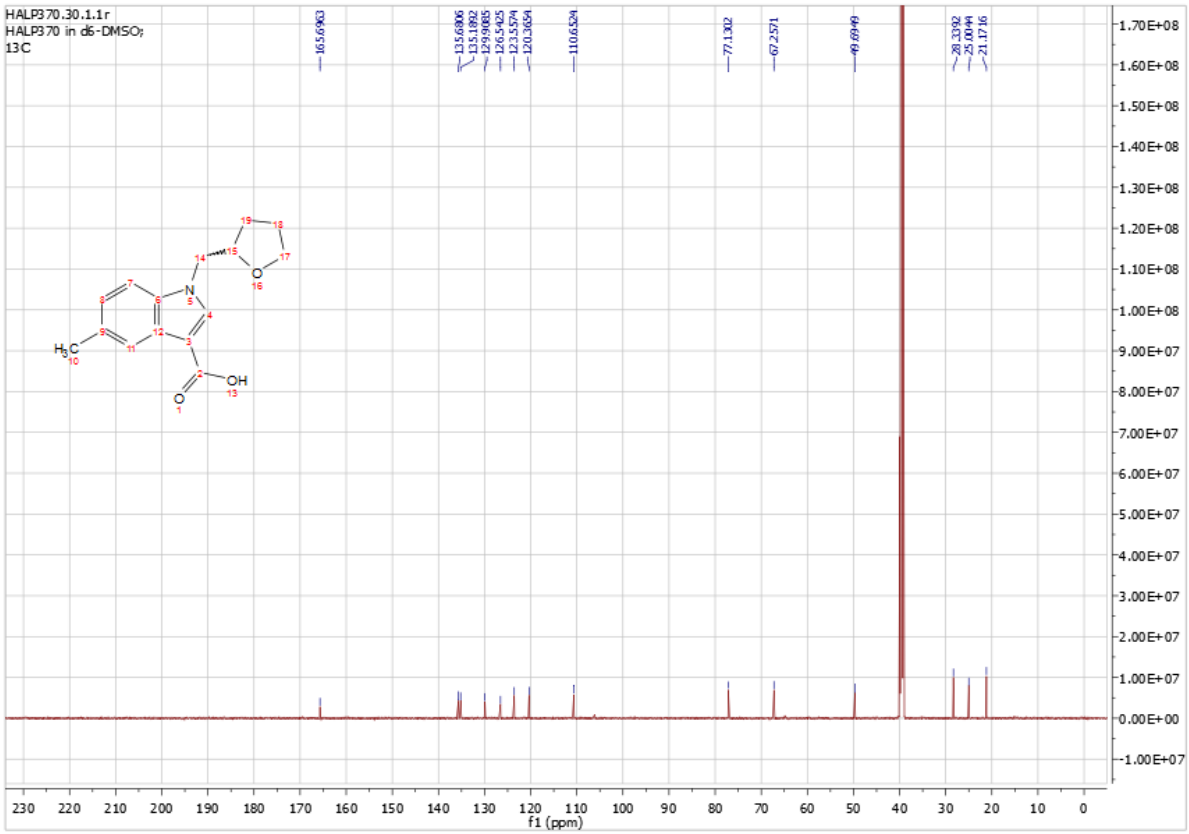




Signal: DAD1 Total WL (220.0:600.0 nm)

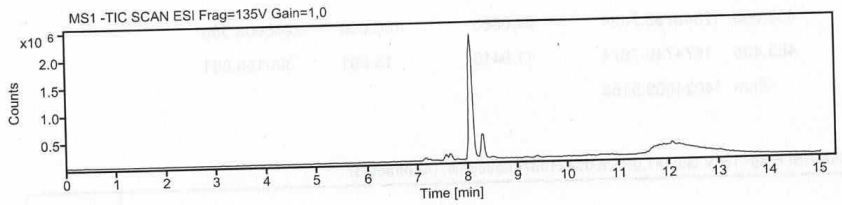
RT [min]	Peak MS Base Peak m/z	Area	Area%	Max Peak%	Height
0.777		13352.9142	6.3650	7.189	1340.029
3.868	260.100	185748.9761	88.5418	100.000	9910.439
4.298		2868.3315	1.3673	1.544	385.929
5.463		1871.0426	0.8919	1.007	485.155
6.073		1858.7060	0.8860	1.001	358.627
8.206		2516.0701	1.1993	1.355	594.624
8.661		1000.9934	0.4771	0.539	190.114

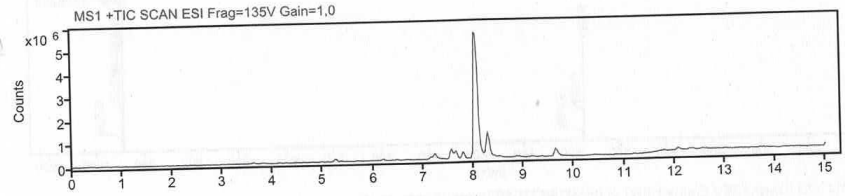

HALP370.10.1.1r
HALP370 in d6-DMSO;
1H
B (s)
7.9415
A (s)
7.8092
D (dd)
7.0387
C (d)
7.4732
F (m)
4.1649
E (dd)
4.3091
H (q)
3.6121
G (q)
3.7312
J (th)
1.7618
I (dq)
1.9401
M (s)
2.4050
K (dq)
1.5253
f1 (ppm)

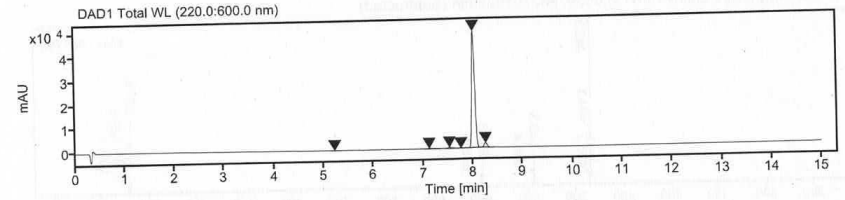

HALP370.30.1.1r
HALP370 in d6-DMSO;
13C
f1 (ppm)

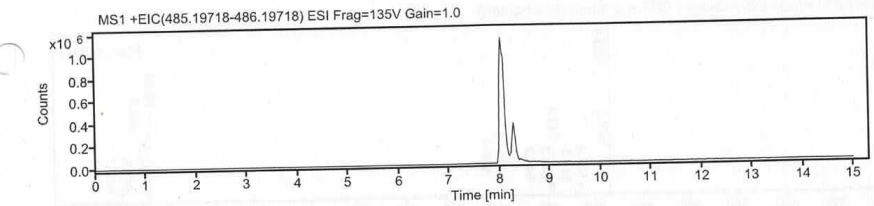
(*R,S*)-*N*-(4-(4-Butyryl-5-methyl-1*H*-pyrazol-1-yl)phenyl)-5-methyl-1-((tetrahydrofuran-2-yl)methyl)-1*H*-indole-3-carboxamide (12c)

Sequence Name:	SingleSample		
Data file:	HALP392-F2.dx	**Project Name:**	Single Quad
Sample name:	HALP392-F2	**Operator :**	SYSTEM
Instrument:	Single Quad	**Acquired on:**	2024-06-13 14:42:21+02:00
Inj. volume:	3.000	**Location:**	P1-F1
Acq. method:	00-new_wasser-acn_standard_100-1000_BD-20min.amx		
Processing method:	MS_standard_plot.pmx		









Signal: DAD1 Total WL (220.0:600.0 nm)

RT [min]	Peak MS Base Peak m/z	Area	Area%	Max Peak%	Height
5.225		235.5975	0.1088	0.116	76.993
7.126		1290.1426	0.5957	0.633	253.834
7.529		2548.7996	1.1768	1.251	516.706
7.761		414.1004	0.1912	0.203	106.211
8.022		203789.0924	94.0892	100.000	48973.879
8.254		8313.7525	3.8384	4.080	1945.268
	Sum	216591.4850			

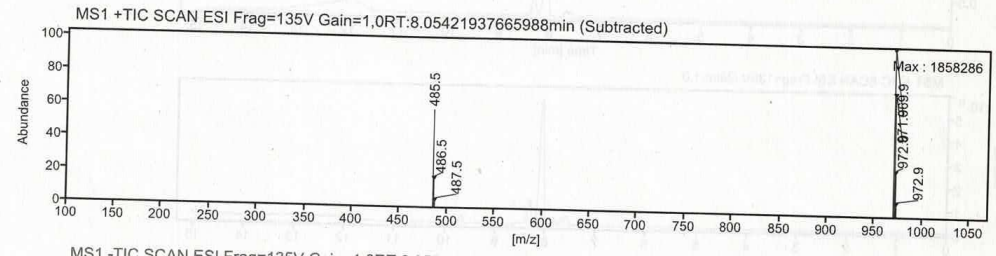
D:\CDSProjects\Default\0-standardplot+EIC.rdl [Rev. 9418] Printed: 2024-06-17 07:55:38+02:00 Page 1 of 2

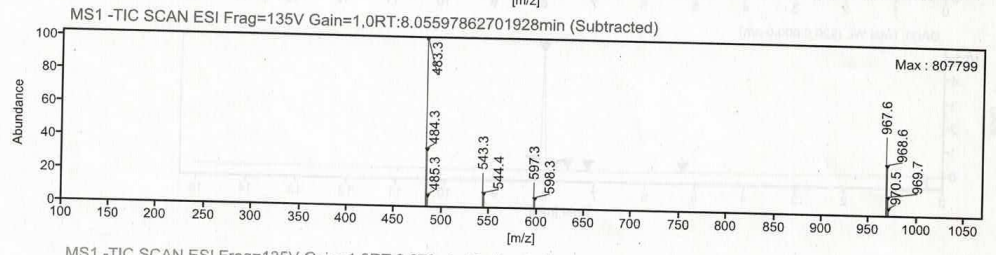
Signal: MS1 +TIC SCAN ESI Frag=135V Gain=1,0

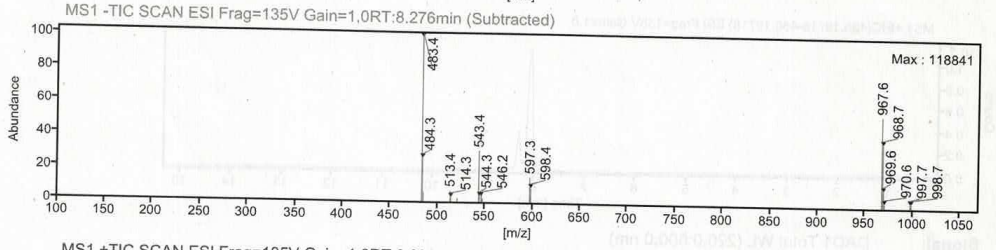
RT [min]	Peak MS Base Peak m/z	Area	Area%	Max Peak%	Height
8.054	969.900	33190179.6294	89.6183	100.000	5710325.951
8.291	485.500	3844882.4202	10.3817	11.584	921763.024
	Sum	37035062.0496			

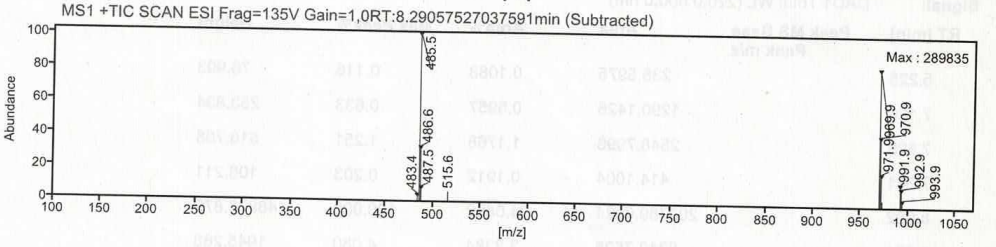
Signal: MS1 -TIC SCAN ESI Frag=135V Gain=1,0

RT [min]	Peak MS Base Peak m/z	Area	Area%	Max Peak%	Height
8.056	483.300	12349768.7484	88.0585	100.000	2245908.386
8.276	483.400	1674740.7674	11.9415	13.561	390155.881
	Sum	14024509.5158			

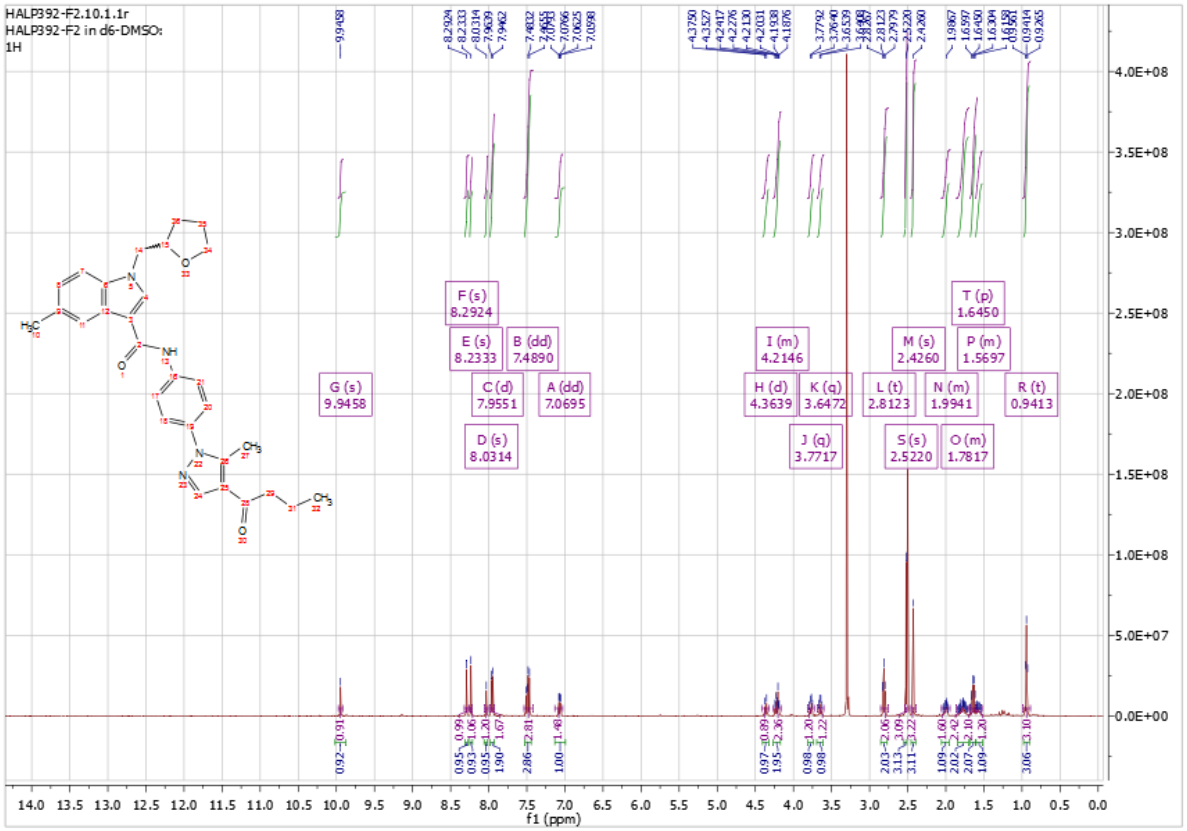


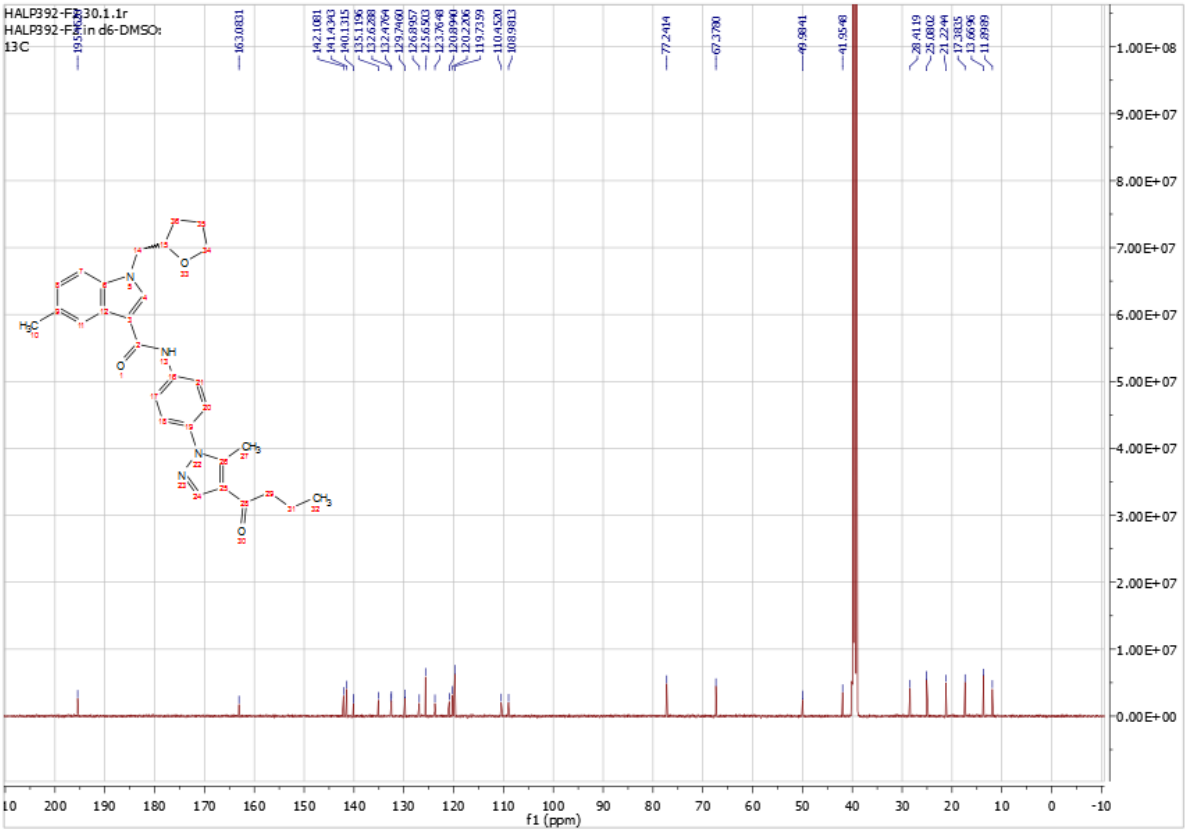






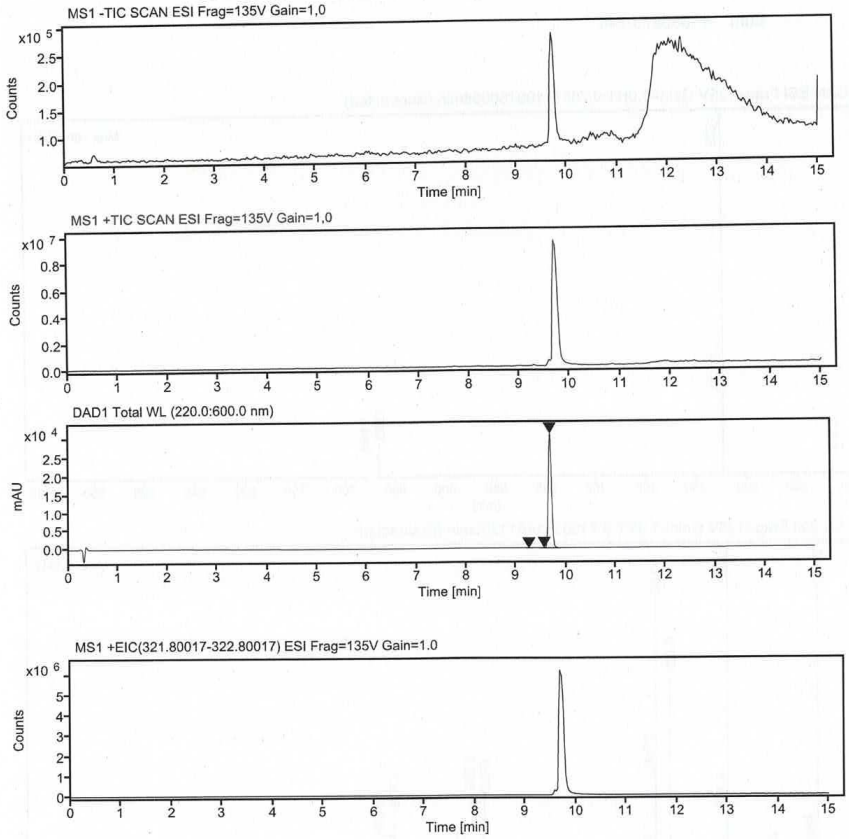
D:\CDSProjects\Default\0-standardplot+EIC.rdl [Rev. 9418] Printed: 2024-06-17 07:55:38+02:00 Page 2 of 2


HALP392-F2.10.1.1r
HALP392-F2 in d6-DMSO
1H
F (s) 8.2924
E (s) 8.2333
B (dd) 7.4890
C (d) 7.9551
A (dd) 7.0695
D (s) 8.0314
G (s) 9.9458
I (m) 4.2146
H (d) 4.3639
K (q) 3.6472
J (q) 3.7717
L (t) 2.8123
M (s) 2.4260
S (s) 2.5220
N (m) 1.9941
O (m) 1.7817
P (m) 1.5697
T (p) 1.6450
R (t) 0.9413
f1 (ppm)


HALP392-F2.30.1.1r
HALP392-F2 in d6-DMSO
13C
f1 (ppm)

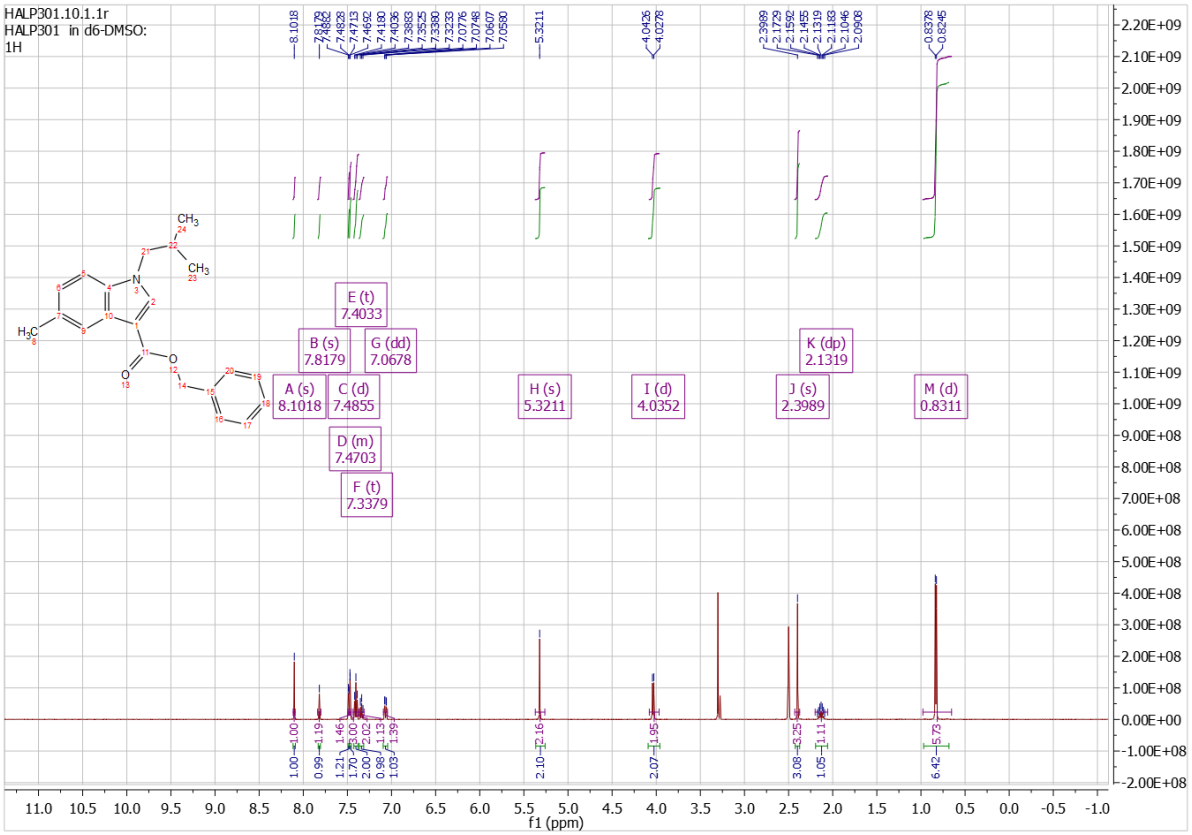
Benzyl 1-isobutyl-5-methyl-1*H*-indole-3-carboxylate (13a)

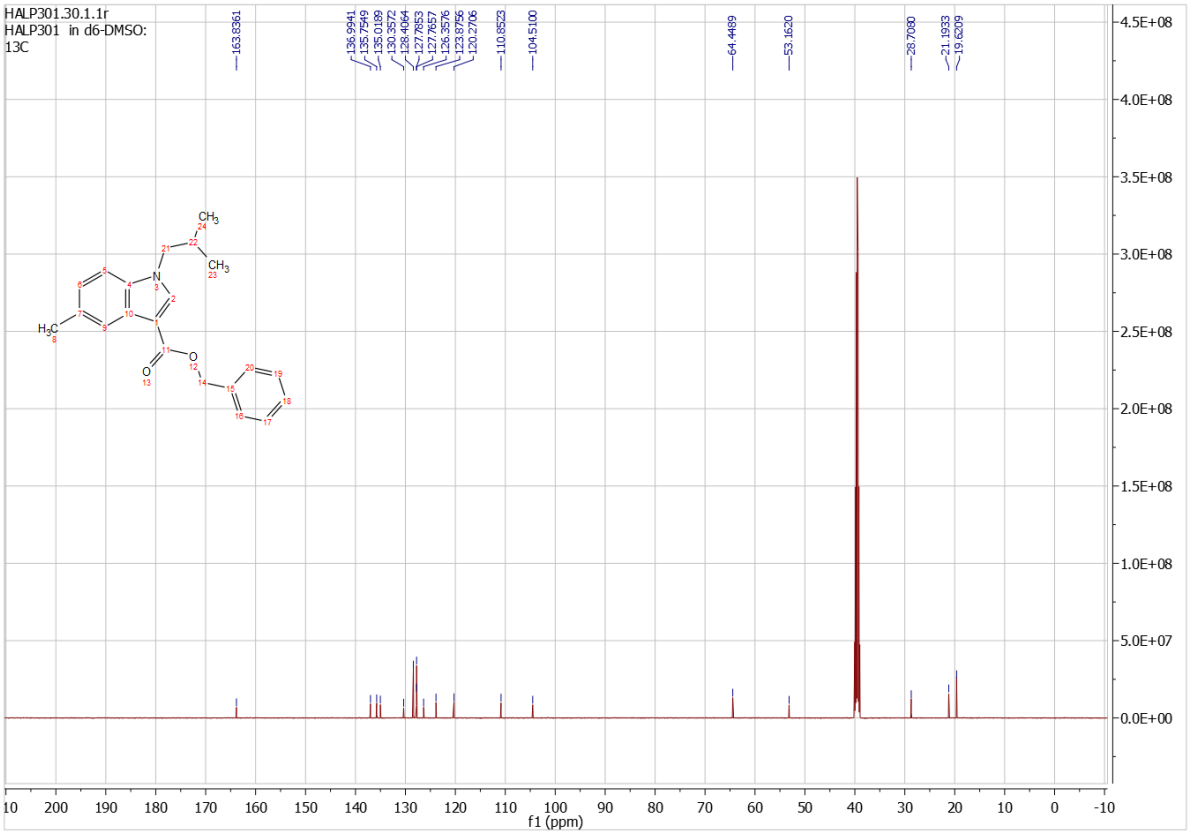
Sequence Name:	SingleSample		
Data file:	2024-02-17 19-14-10+01-00.dx	**Project Name:**	Single Quad
Sample name:	HALP301-F1	**Operator :**	SYSTEM
Instrument:	Single Quad	**Acquired on:**	2024-02-17 19:15:18+01:00
Inj. volume:	3.000	**Location:**	P1-A1
Acq. method:	00-new_wasser-acn_standard_100-1000_BD-20min.amx		
Processing method:	MS_standard_plot.pmx		



Signal: DAD1 Total WL (220.0:600.0 nm)

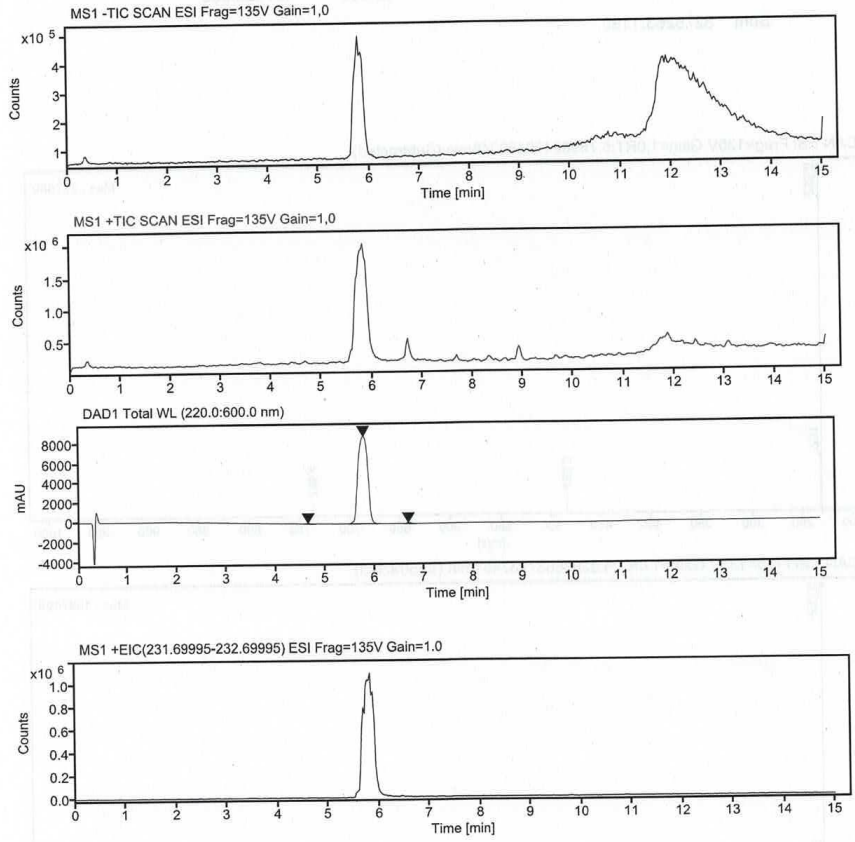
RT [min]	Peak MS Base Peak m/z	Area	Area%	Max Peak%	Height
9.258		90.9206	0.0653	0.066	24.093
9.566		449.6267	0.3228	0.324	135.543
9.684		138729.9788	99.6119	100.000	31040.966
	Sum	139270.5261			


HALP301.10.1.1r
HALP301 in d6-DMSO:
1H
A (s) 8.1018
B (s) 7.8179
C (d) 7.4855
D (m) 7.4703
E (t) 7.4033
F (t) 7.3379
G (dd) 7.0678
H (s) 5.3211
I (d) 4.0352
J (s) 2.3989
K (dp) 2.1319
M (d) 0.8311
f1 (ppm)


HALP301.30.1.1r
HALP301 in d6-DMSO:
13C
f1 (ppm)

1-Isobutyl-5-methyl-1*H*-indole-3-carboxylic acid (13b)

Sequence Name:	SingleSample		
Data file:	HALP369.dx	**Project Name:**	Single Quad
Sample name:	HALP369	**Operator :**	SYSTEM
Instrument:	Single Quad	**Acquired on:**	2024-03-11 14:14:10+01:00
Inj. volume:	4.000	**Location:**	P1-D4
Acq. method:	00-new_wasser-acn_standard_100-1000_BD-20min.amx		
Processing method:	MS_standard_plot.pmx		

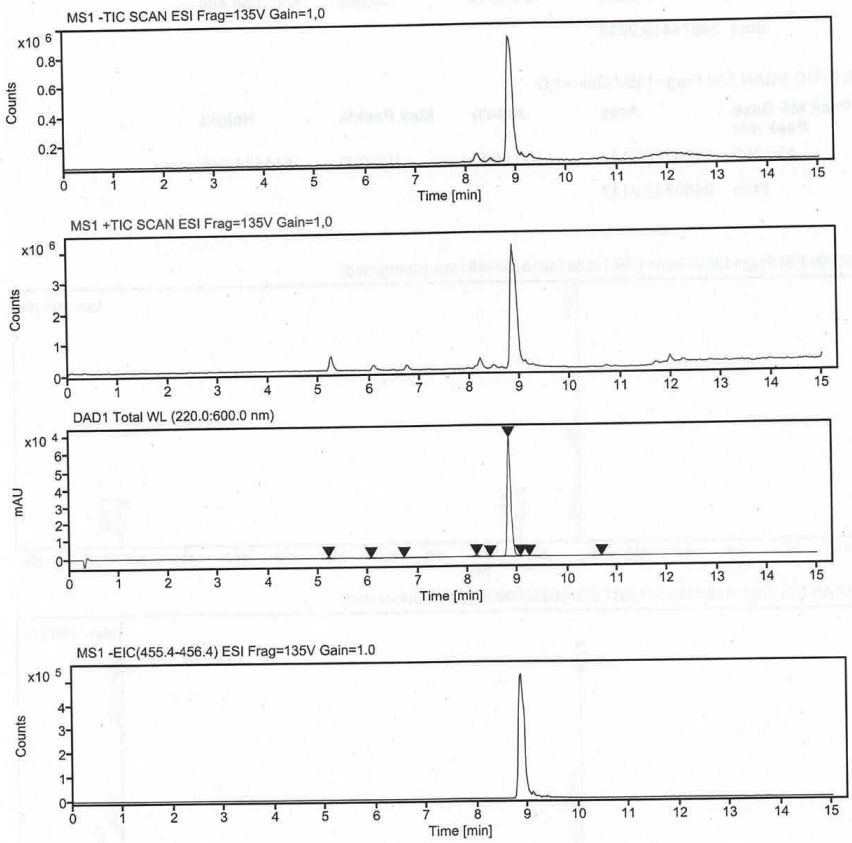


Signal: DAD1 Total WL (220.0:600.0 nm)

RT [min]	Peak MS Base Peak m/z	Area	Area%	Max Peak%	Height
4.650		136.3136	0.1122	0.113	25.401
5.774	230.000	120949.6929	99.5125	100.000	8836.191
6.678		456.2237	0.3754	0.377	80.996
	Sum	121542.2302			

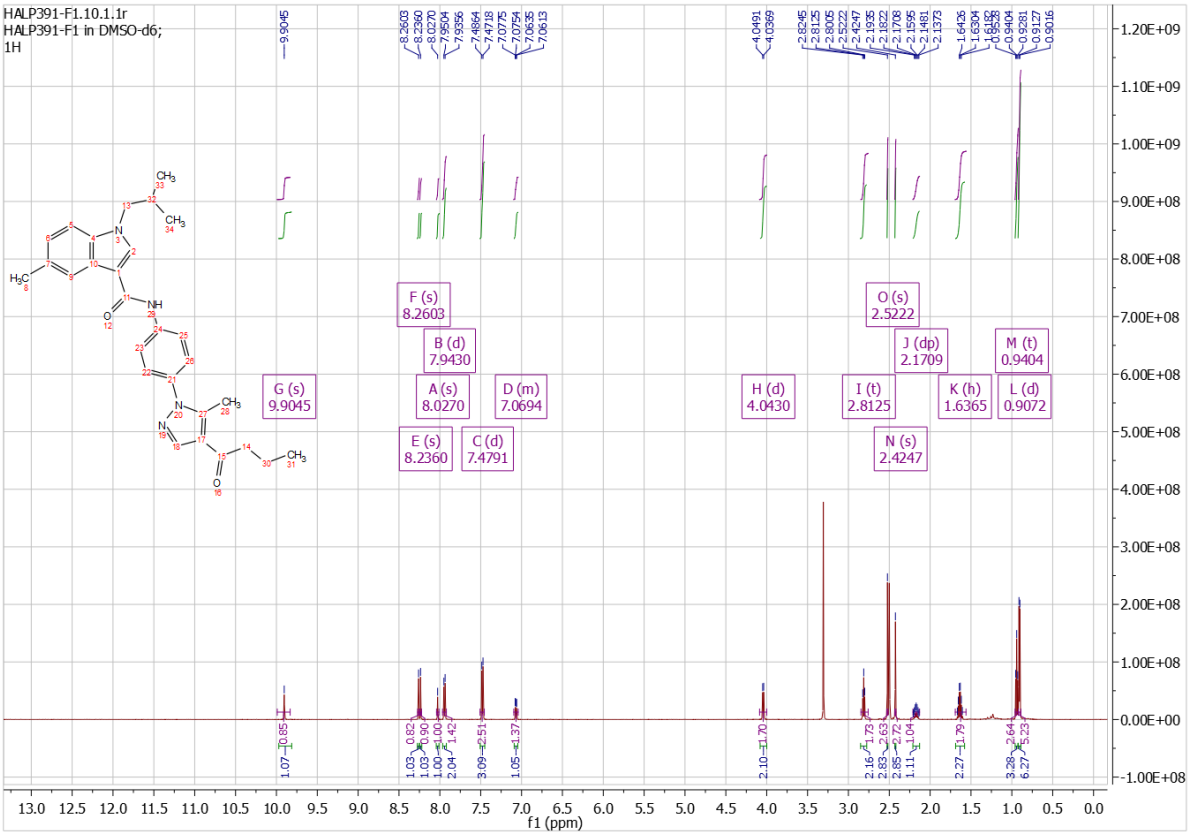
_N_-(4-(4-Butyryl-5-methyl-1_H_-pyrazol-1-yl)phenyl)-1-isobutyl-5-methyl-1_H_-indole-3-carboxamide (13c)

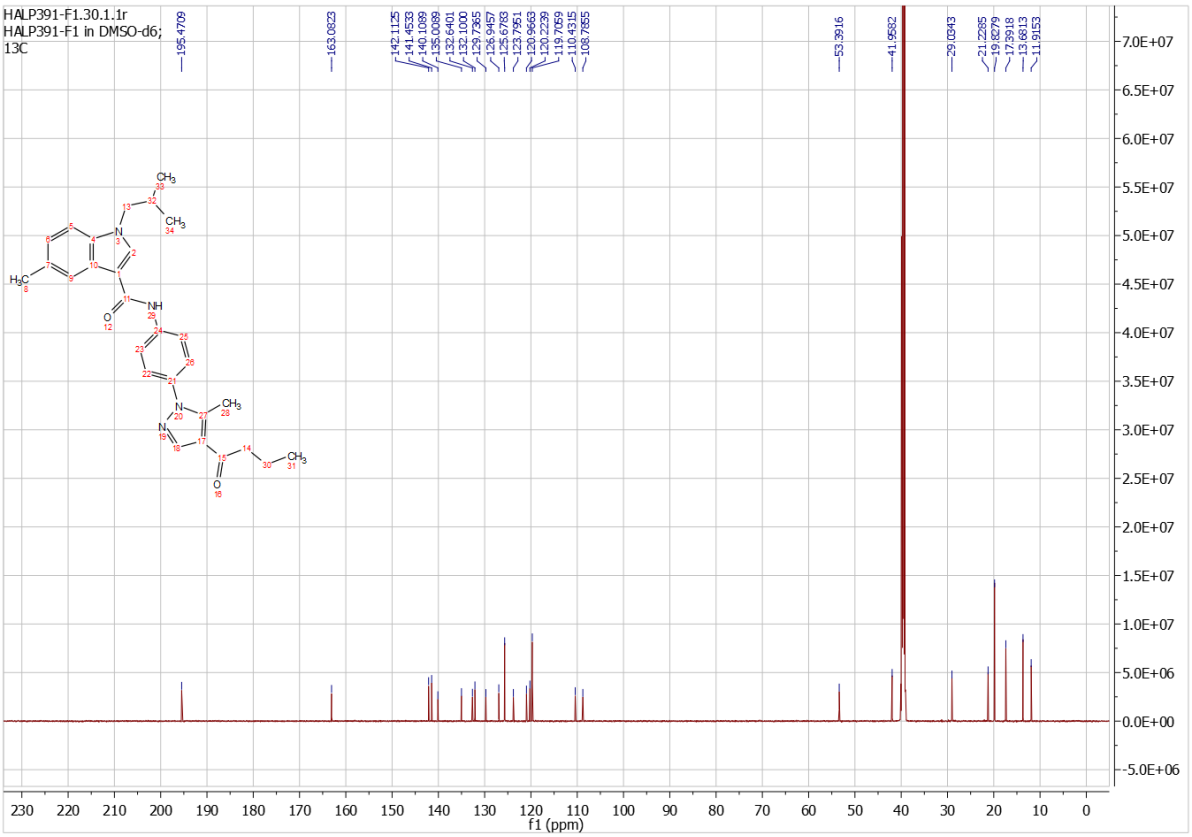
Sequence Name:	SingleSample		
Data file:	HALP391.dx	**Project Name:**	Single Quad
Sample name:	HALP391	**Operator :**	SYSTEM
Instrument:	Single Quad	**Acquired on:**	2024-11-20 16:02:10+01:00
Inj. volume:	4.000	**Location:**	P1-E7
Acq. method:	00-new_wasser-acn_standard_100-1000_BD-20min.amx		
Processing method:	MS_standard_plot.pmx		



Signal: DAD1 Total WL (220.0:600.0 nm)

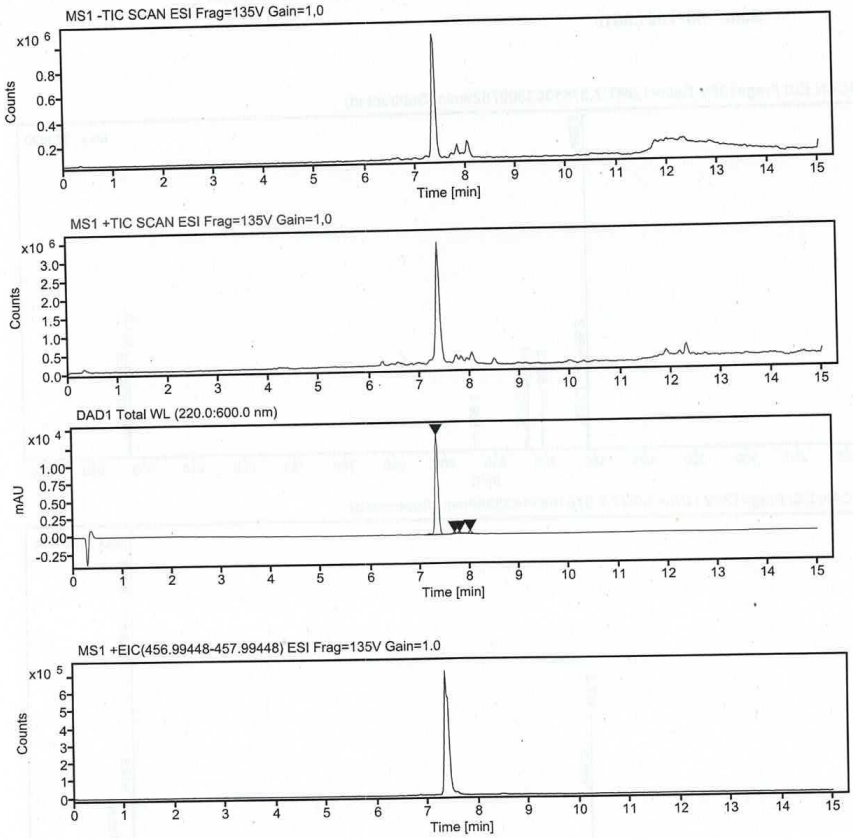
RT [min]	Peak MS Base Peak m/z	Area	Area%	Max Peak%	Height
5.210		3312.5586	0.9059	0.934	719.580
6.060		587.5480	0.1607	0.166	112.905
6.723		210.0081	0.0574	0.059	33.522
8.174		3852.4044	1.0536	1.086	735.027
8.451		771.4122	0.2110	0.217	148.198
8.838	455.700	354752.0779	97.0199	100.000	67931.842
9.063		1446.2553	0.3955	0.408	292.861


HALP391-F1.10.1.1r
HALP391-F1 in DMSO-d6;
1H
F (s)
8.2603
B (d)
7.9430
A (s)
8.0270
D (m)
7.0694
G (s)
9.9045
E (s)
8.2360
C (d)
7.4791
O (s)
2.5222
J (dp)
2.1709
M (t)
0.9404
H (d)
4.0430
I (t)
2.8125
K (h)
1.6365
L (d)
0.9072
N (s)
2.4247
f1 (ppm)


HALP391-F1.30.1.1r
HALP391-F1 in DMSO-d6;
13C
f1 (ppm)

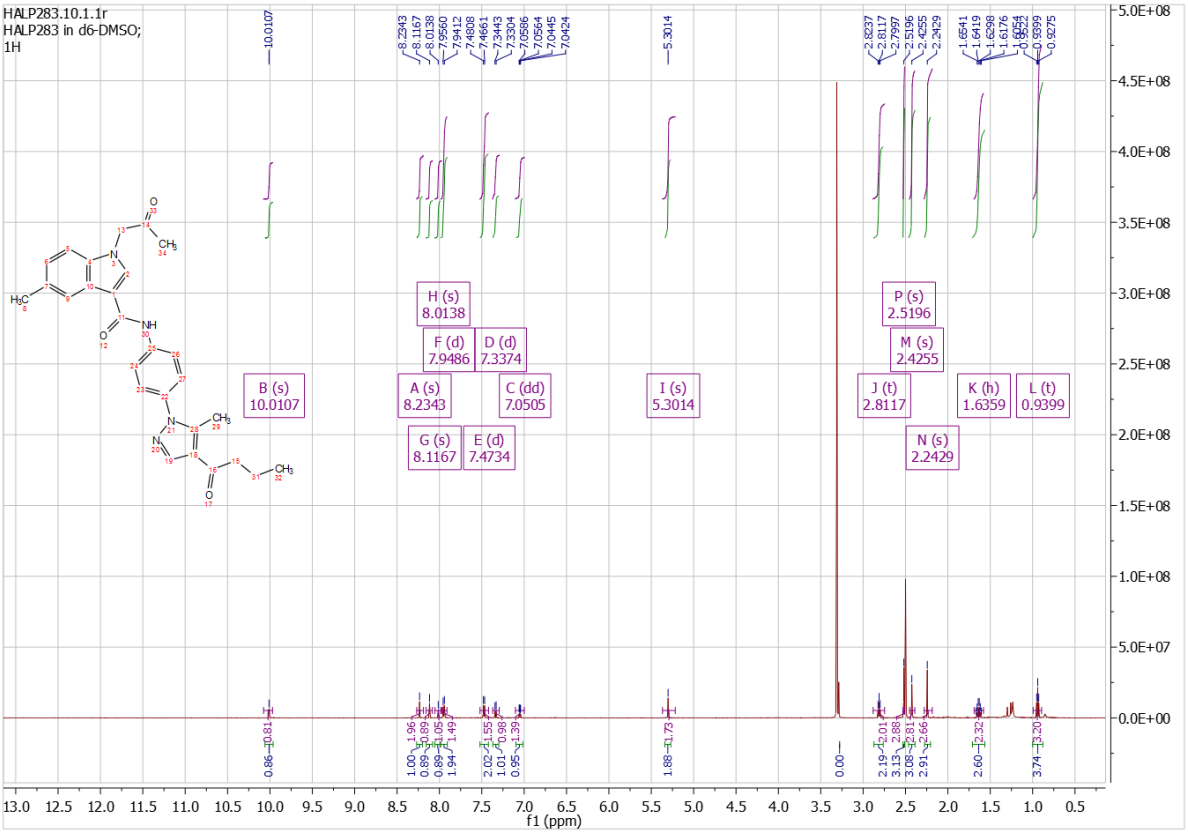
_N_-(4-(4-Butyryl-5-methyl-1_H_-pyrazol-1-yl)phenyl)-5-methyl-1-(2-oxopropyl)-1_H_-indole-3-carboxamide (17)

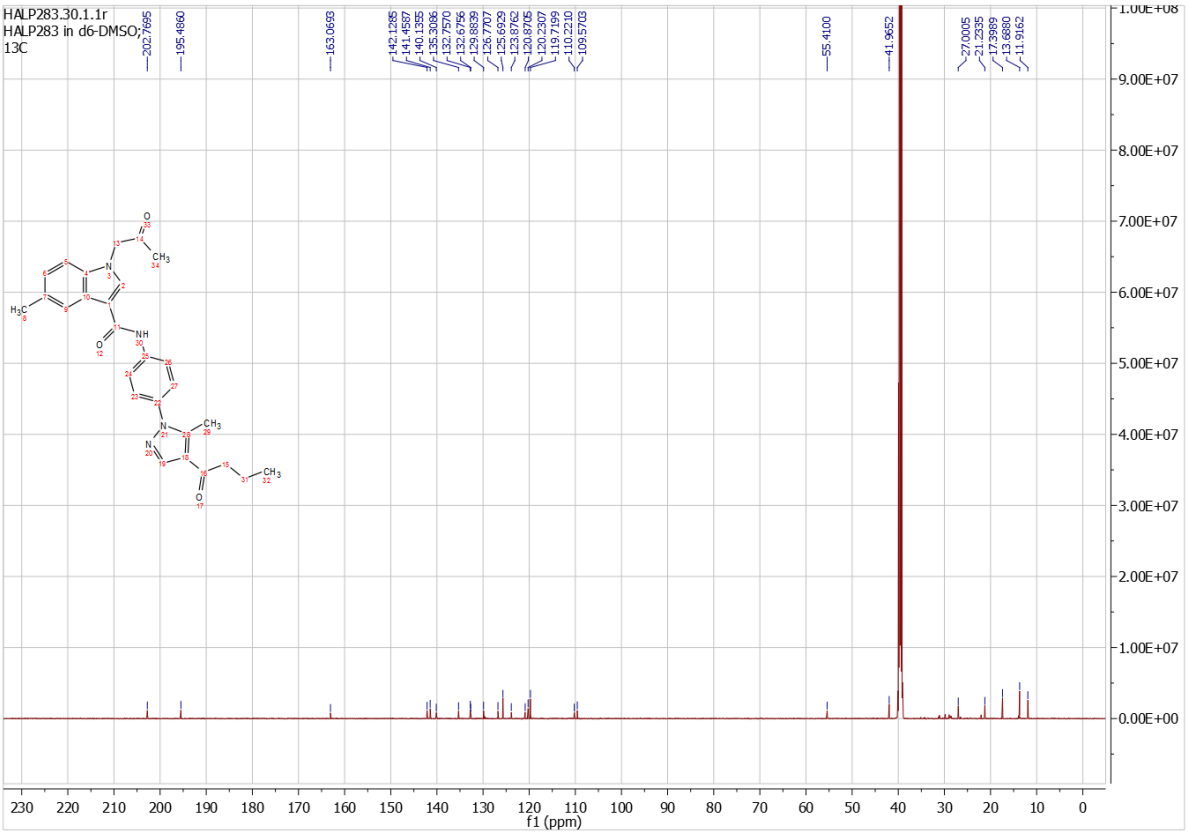
Sequence Name:	SingleSample		
Data file:	HALP283-F5.dx	**Project Name:**	Single Quad
Sample name:	HALP283-F5	**Operator :**	SYSTEM
Instrument:	Single Quad	**Acquired on:**	2024-02-26 01:29:29+01:00
Inj. volume:	8.000	**Location:**	P2-D5
Acq. method:	00-new_wasser-acn_standard_100-1000_BD-20min.amx		
Processing method:	MS_standard_plot.pmx		



Signal: DAD1 Total WL (220.0:600.0 nm)

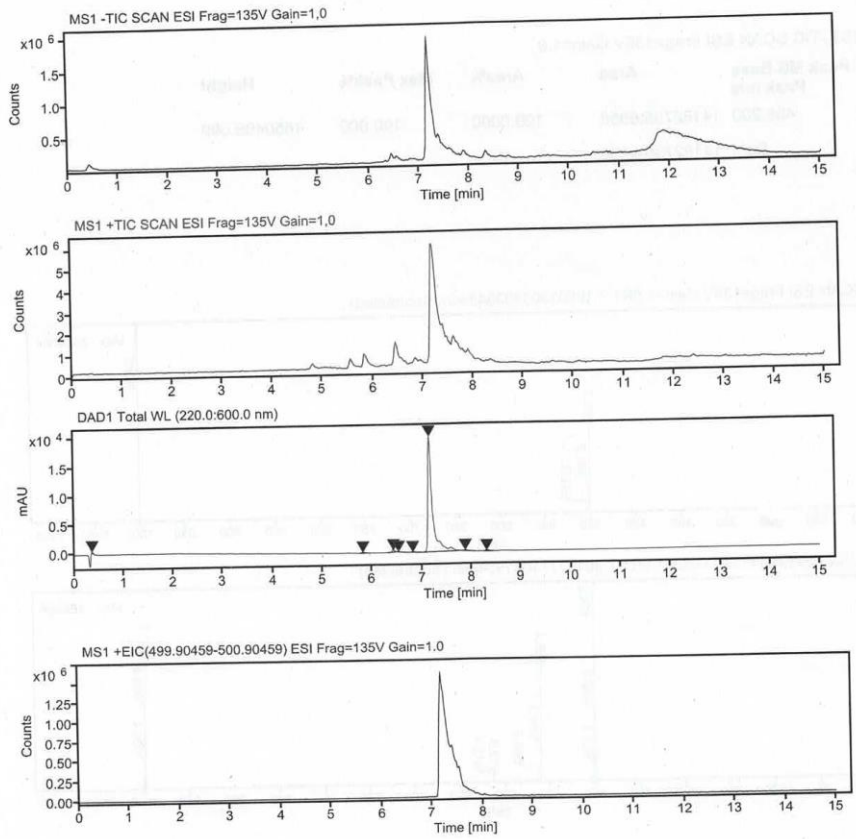
RT [min]	Peak MS Base Peak m/z	Area	Area%	Max Peak%	Height
7.342		60107.5109	96.2454	100.000	14071.703
7.693		521.4077	0.8349	0.867	221.345
7.794		490.2209	0.7850	0.816	221.898
8.007		1333.1802	2.1347	2.218	398.423
	Sum	62452.3196			


HALP283.10.1.1r
HALP283 in d6-DMSO;
1H
B (s)
10.0107
H (s)
8.0138
F (d)
7.9486
D (d)
7.3374
A (s)
8.2343
C (dd)
7.0505
G (s)
8.1167
E (d)
7.4734
I (s)
5.3014
P (s)
2.5196
M (s)
2.4255
J (t)
2.8117
K (h)
1.6359
L (t)
0.9399
N (s)
2.2429
f1 (ppm)


HALP283.30.1.1r
HALP283 in d6-DMSO;
13C
f1 (ppm)

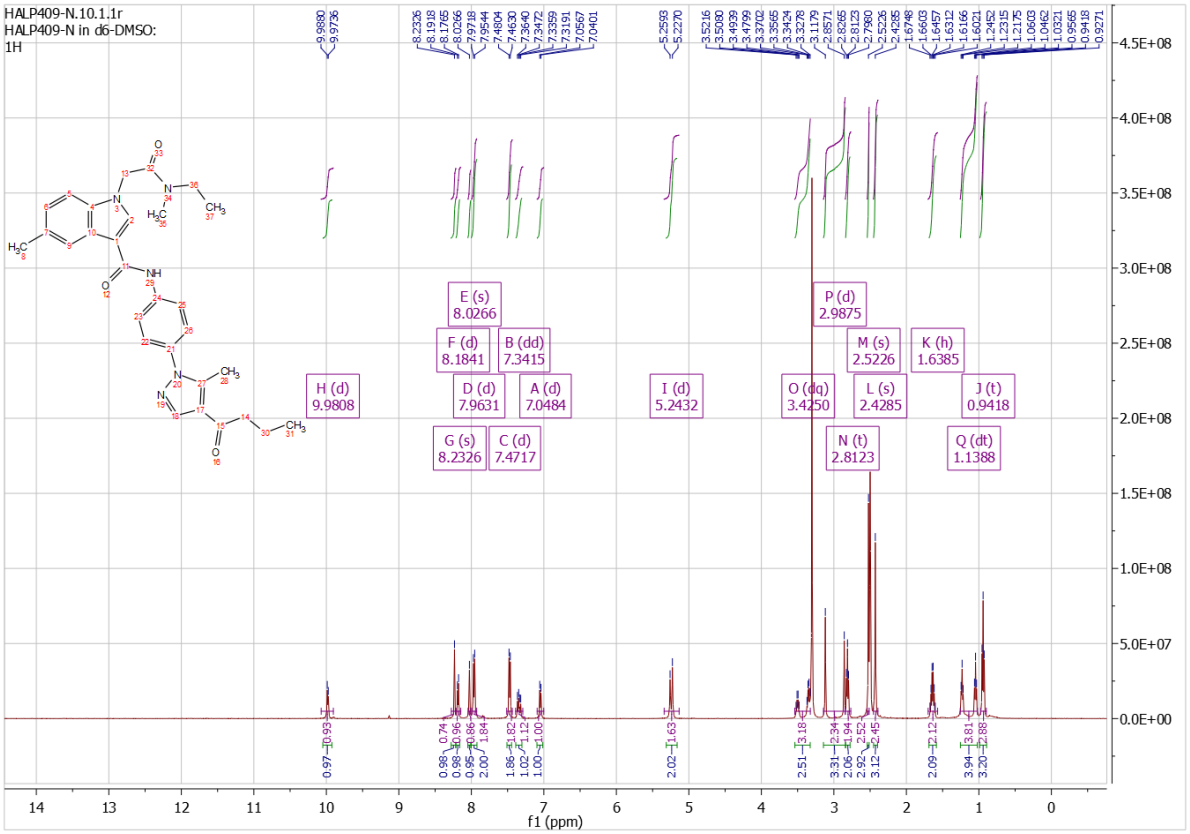
_N_-(4-(4-Butyryl-5-methyl-1_H_-pyrazol-1-yl)phenyl)-1-(2-(ethyl(methyl)amino)-2-oxoethyl)-5-methyl-1_H_-indole-3-carboxamide (18)

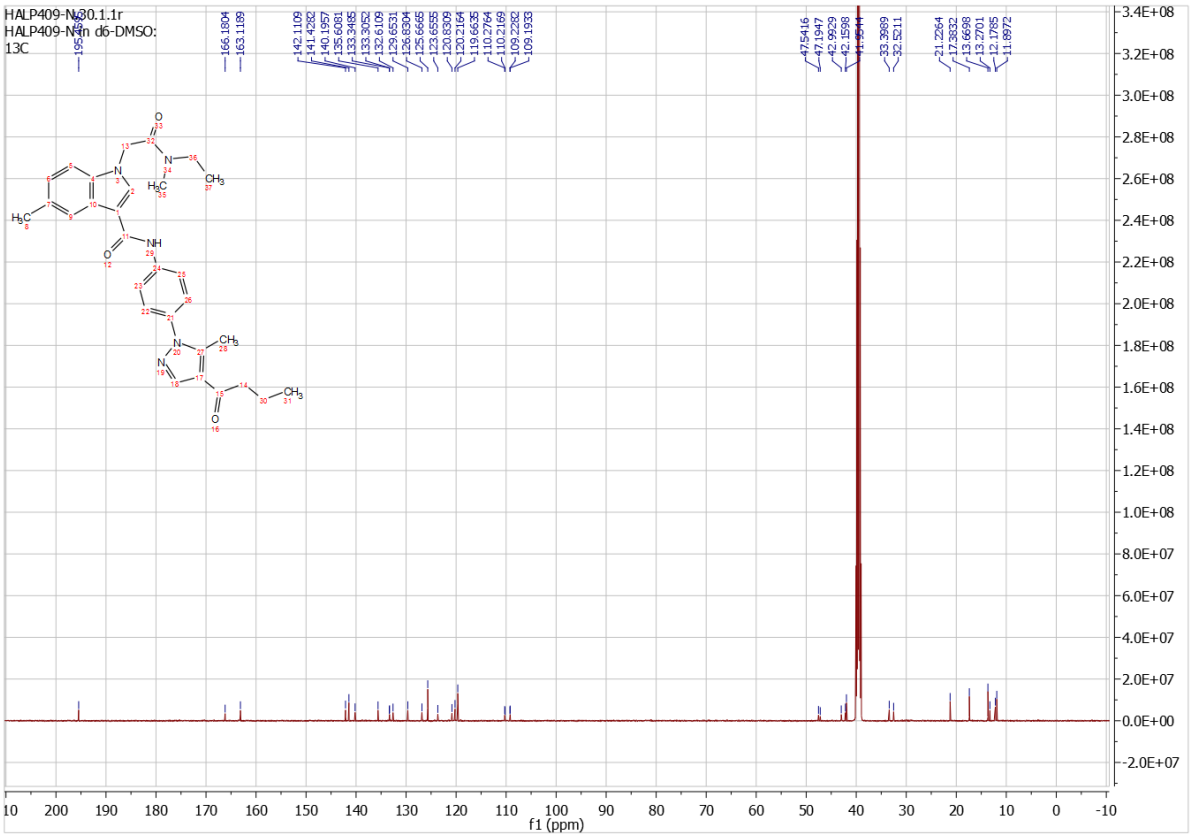
Sequence Name:	SingleSample		
Data file:	HALP409-new.dx	**Project Name:**	Single Quad
Sample name:	HALP409-new	**Operator :**	SYSTEM
Instrument:	Single Quad	**Acquired on:**	2024-09-12 10:02:40+02:00
Inj. volume:	2.000	**Location:**	P2-E1
Acq. method:	00-new_wasser-acn_standard_100-1000_BD-20min.amx		
Processing method:	MS_standard_plot.pmx		



Signal: DAD1 Total WL (220.0:600.0 nm)

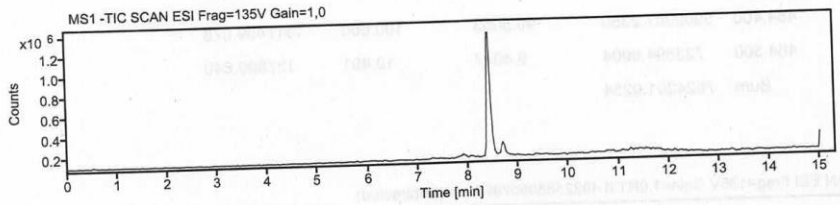
RT [min]	Peak MS Base Peak m/z	Area	Area%	Max Peak%	Height
0.374		353.9325	0.2716	0.281	275.235
5.814		845.3990	0.6487	0.671	179.131
6.429		1150.9793	0.8832	0.913	362.545
6.535		41.4709	0.0318	0.033	47.661
6.819		611.4913	0.4692	0.485	89.374
7.167		126053.7823	96.7233	100.000	19951.709
7.874		517.1916	0.3969	0.410	154.020

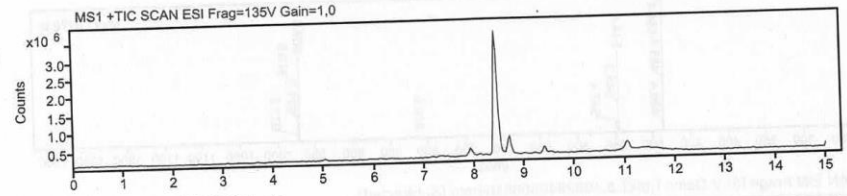

HALP409-N.10.1.1r
HALP409-N in d6-DMSO:
1H
H (d) 9.9808
E (s) 8.0266
F (d) 8.1841
B (dd) 7.3415
D (d) 7.9631
A (d) 7.0484
G (s) 8.2326
C (d) 7.4717
I (d) 5.2432
P (d) 2.9875
M (s) 2.5226
K (h) 1.6385
O (dq) 3.4250
L (s) 2.4285
J (t) 0.9418
N (t) 2.8123
Q (dt) 1.1388
f1 (ppm)

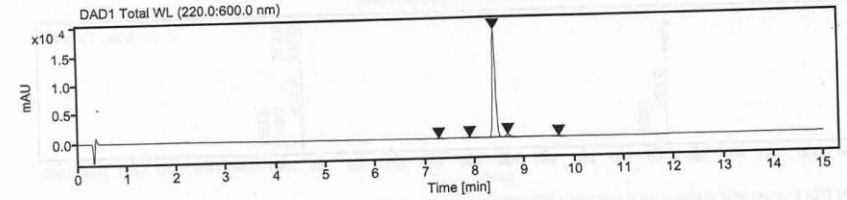

HALP409-N30.1.1r
HALP409-N in d6-DMSO:
13C
f1 (ppm)

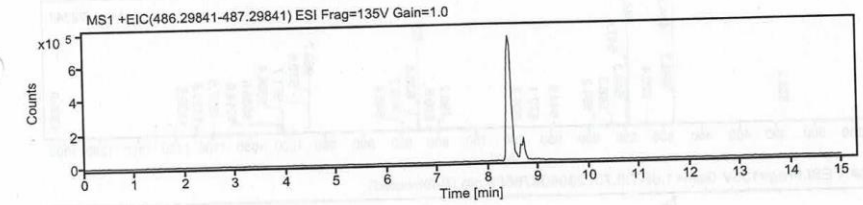
_N_-(4-(4-Butyryl-5-methyl-1_H_-pyrazol-1-yl)phenyl)-1-(2-(dimethylamino)-2-oxoethyl)-5-methyl-1_H_-indole-3-carboxamide (19)

Sequence Name:	SingleSample		
Data file:	HALP383-F1.dx	**Project Name:**	Single Quad
Sample name:	HALP383-F1	**Operator :**	SYSTEM
Instrument:	Single Quad	**Acquired on:**	2024-05-07 15:38:53+02:00
Inj. volume:	2.000	**Location:**	P2-B1
Acq. method:	00-new_wasser-acn_standard_100-1500_BD-20min.amx		
Processing method:	MS_standard_plot.pmx		





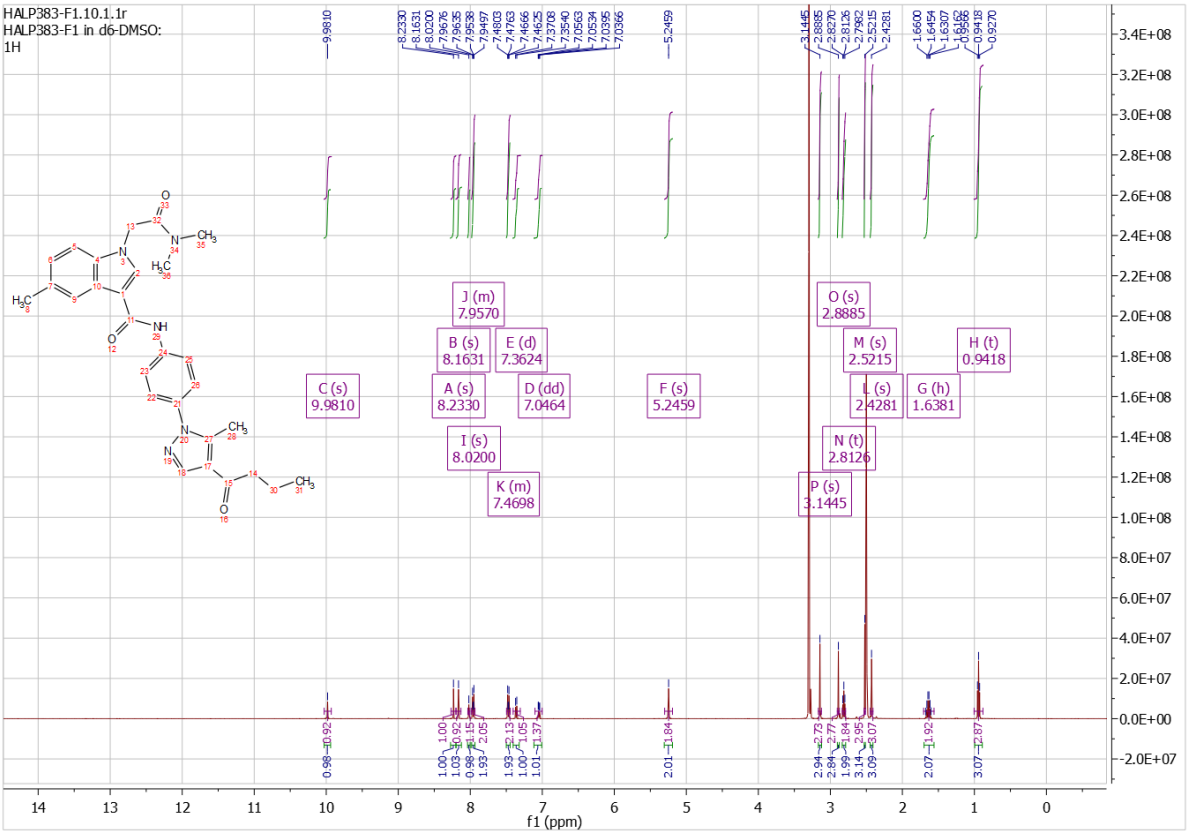


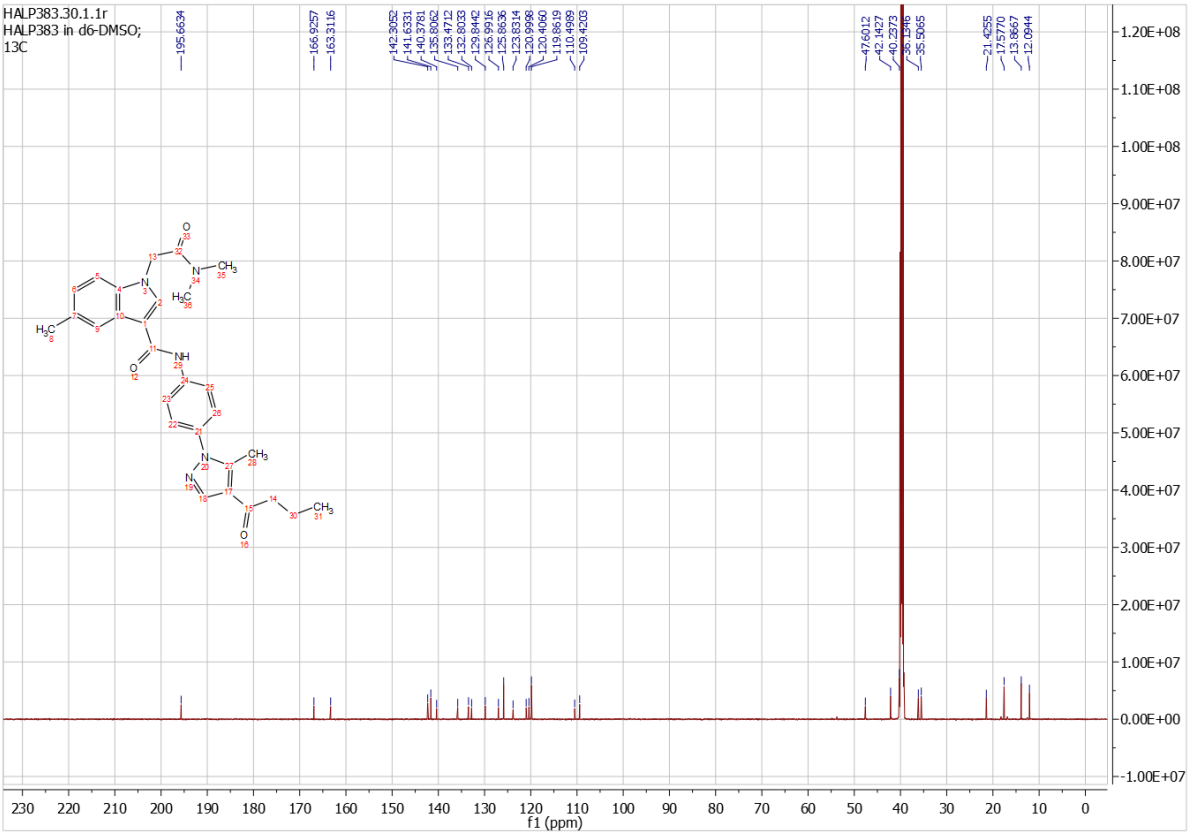


Signal: DAD1 Total WL (220.0:600.0 nm)

RT [min]	Peak MS Base Peak m/z	Area	Area%	Max Peak%	Height
7.276		138.8264	0.1636	0.171	22.716
7.895		644.3946	0.7593	0.792	114.179
8.398	484.400	81412.3986	95.9259	100.000	18649.637
8.666		2437.5904	2.8721	2.994	505.378
9.686		236.8471	0.2791	0.291	53.199
	Sum	84870.0571			

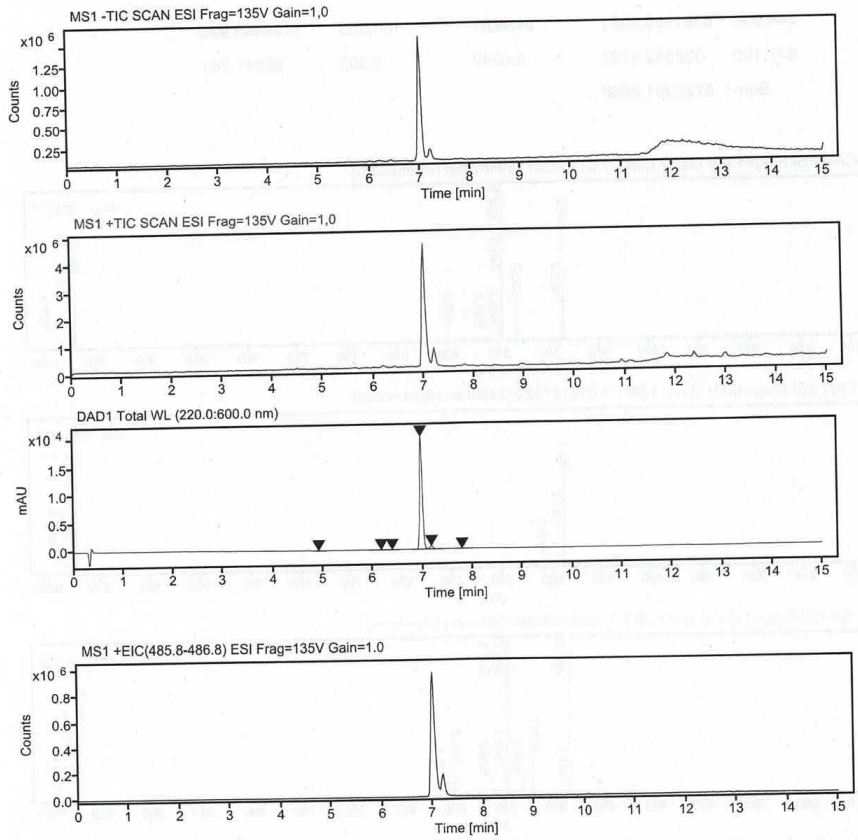
D:\CDSProjects\Default\0-standardplot+EIC.rdl [Rev. 8851] Printed: 2024-05-08 07:05:31+02:00 Page 1 of 2


HALP383-F1.10.1.1r
HALP383-F1 in d6-DMSO:
1H
J (m)
7.9570
B (s)
8.1631
E (d)
7.3624
C (s)
9.9810
A (s)
8.2330
D (dd)
7.0464
F (s)
5.2459
O (s)
2.8885
M (s)
2.5215
H (t)
0.9418
L (s)
2.4281
G (h)
1.6381
I (s)
8.0200
N (t)
2.8126
K (m)
7.4698
P (s)
3.1445
f1 (ppm)


HALP383.30.1.1r
HALP383 in d6-DMSO;
13C
f1 (ppm)

_N_-(4-(4-Butyryl-5-methyl-1_H_-pyrazol-1-yl)phenyl)-1-(2-(ethylamino)-2-oxoethyl)-5-methyl-1_H_-indole-3-carboxamide (20)

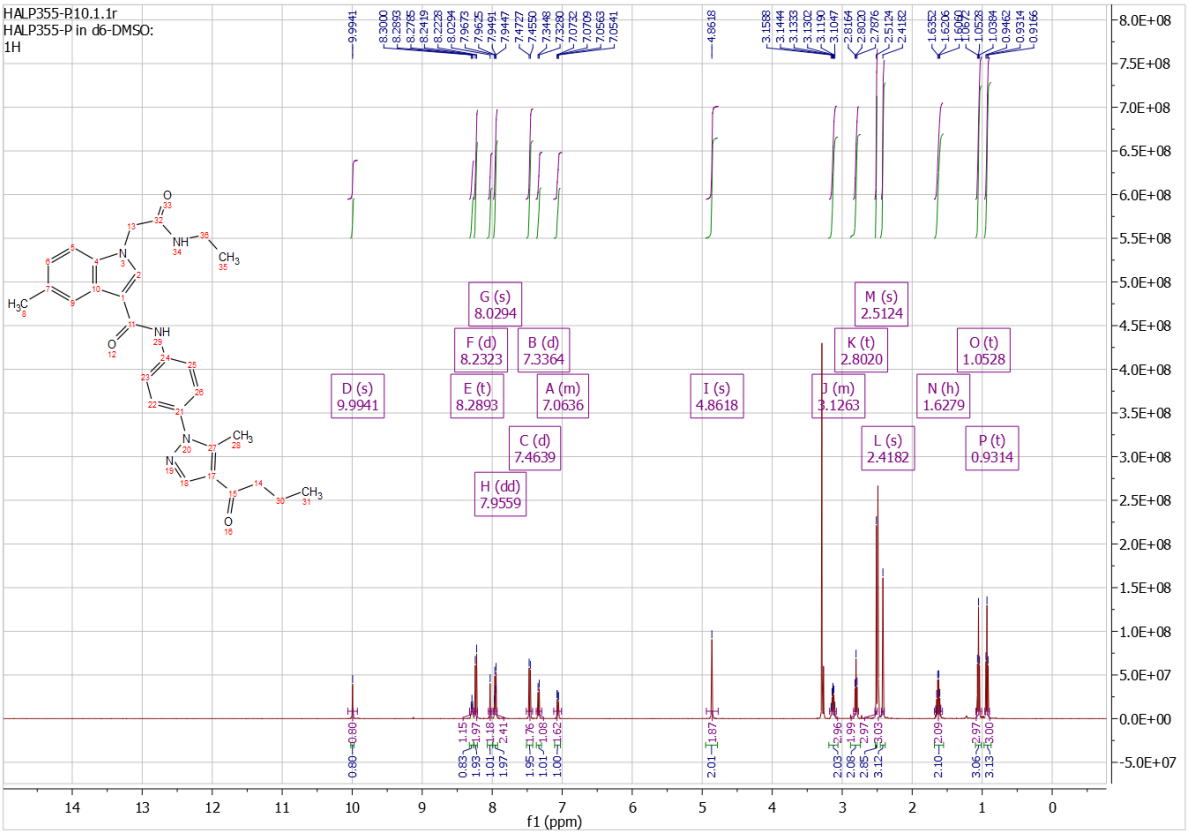
Sequence Name:	SingleSample		
Data file:	HALP355-P.dx	**Project Name:**	Single Quad
Sample name:	HALP355-P	**Operator :**	SYSTEM
Instrument:	Single Quad	**Acquired on:**	2024-02-19 16:06:04+01:00
Inj. volume:	2.000	**Location:**	P2-F8
Acq. method:	00-new_wasser-acn_standard_100-1000_BD-20min.amx		
Processing method:	MS_standard_plot.pmx		

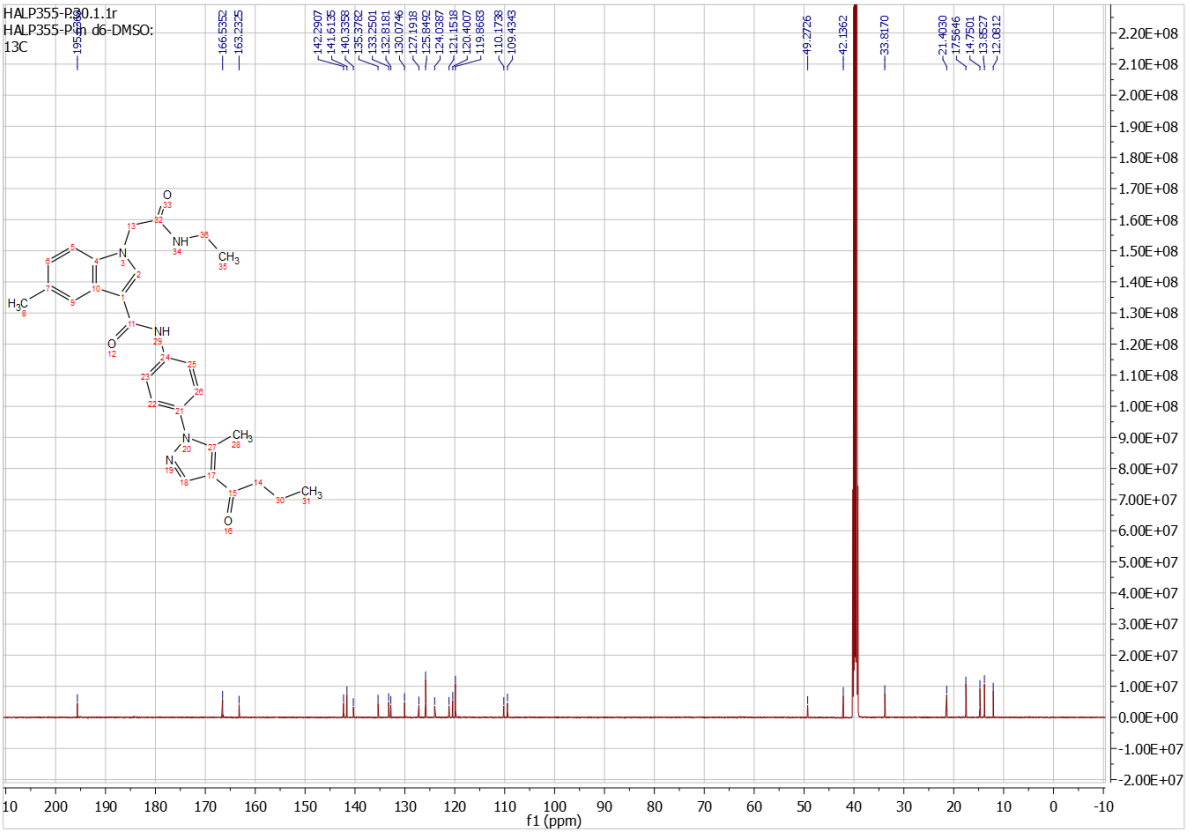


Signal: DAD1 Total WL (220.0:600.0 nm)

RT [min]	Peak MS Base Peak m/z	Area	Area%	Max Peak%	Height
4.916		75.2347	0.0907	0.094	20.246
6.164		240.0727	0.2894	0.301	35.345
6.390		128.4654	0.1549	0.161	38.077
6.977		79782.3153	96.1825	100.000	20245.473
7.175		2595.2805	3.1288	3.253	606.377
7.787		127.5075	0.1537	0.160	29.704
	Sum	82948.8762			

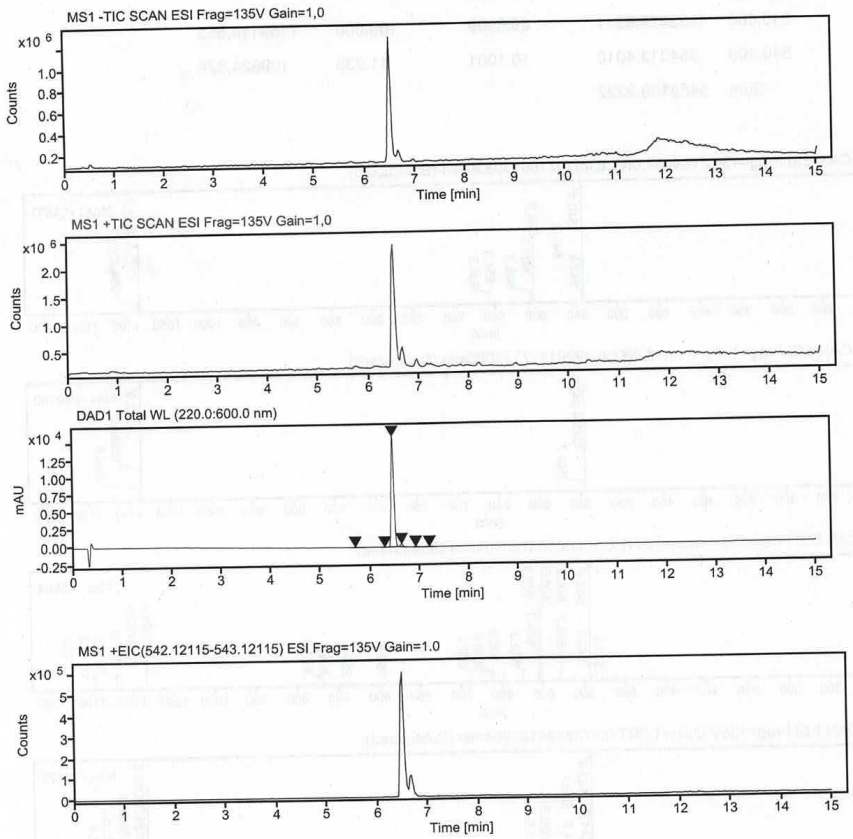
D:\CDSProjects\Default\0-standardplot+EIC.rdl [Rev. 7364] Printed: 2024-02-20 07:03:17+01:00 Page 1 of 2


HALP355-P.10.1.1r
HALP355-P in d6-DMSO:
1H
D (s)
9.9941
G (s)
8.0294
F (d)
8.2323
E (t)
8.2893
B (d)
7.3364
A (m)
7.0636
C (d)
7.4639
H (dd)
7.9559
I (s)
4.8618
M (s)
2.5124
K (t)
2.8020
J (m)
3.1263
N (h)
1.6279
O (t)
1.0528
L (s)
2.4182
P (t)
0.9314
f1 (ppm)


HALP355-P30.1.1r
HALP355-P in d6-DMSO:
13C
f1 (ppm)

_N_-(4-(4-Butyryl-5-methyl-1_H_-pyrazol-1-yl)phenyl)-1-(2-(4-hydroxypiperidin-1-yl)-2-oxoethyl)-5-methyl-1_H_-indole-3-carboxamide (21)

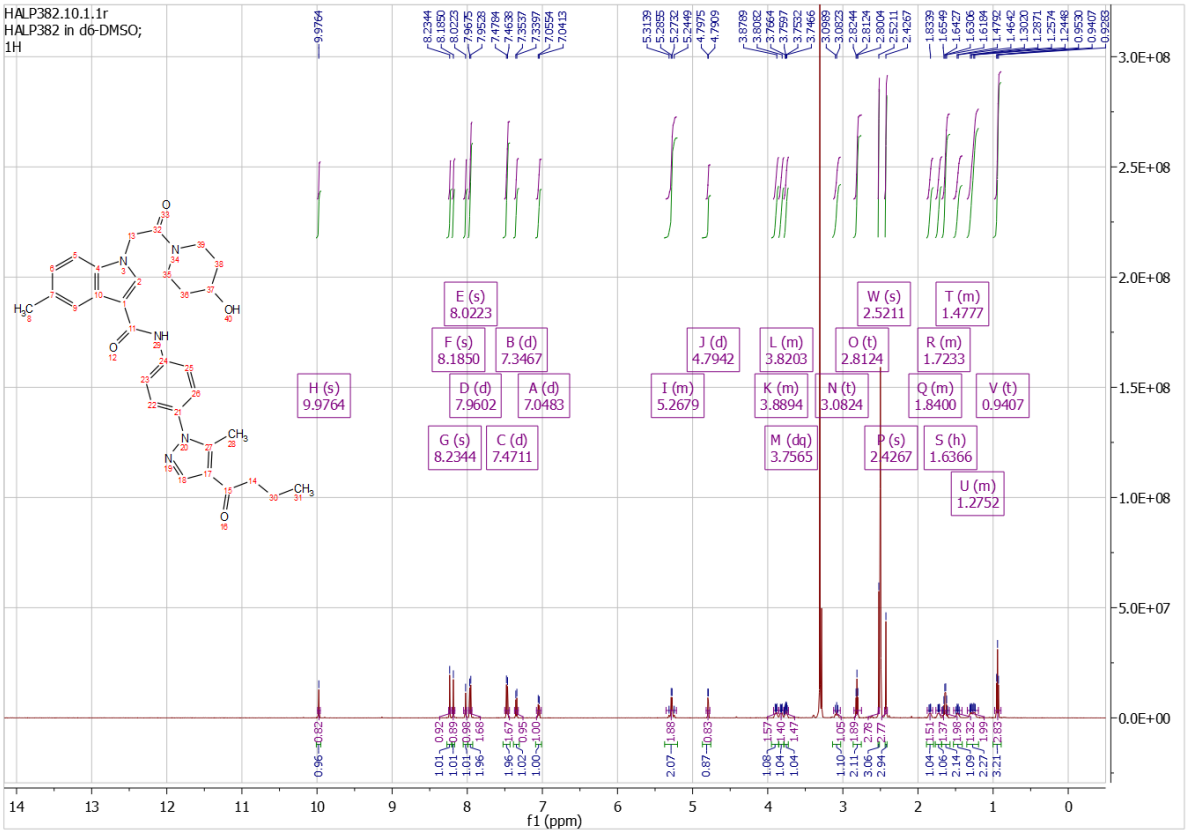
Sequence Name:	SingleSample		
Data file:	HALP382.dx	**Project Name:**	Single Quad
Sample name:	HALP382	**Operator :**	SYSTEM
Instrument:	Single Quad	**Acquired on:**	2024-03-18 13:27:58+01:00
Inj. volume:	2.000	**Location:**	P1-A10
Acq. method:	00-new_wasser-acn_standard_100-1500_BD-20min.amx		
Processing method:	MS_standard_plot.pmx		

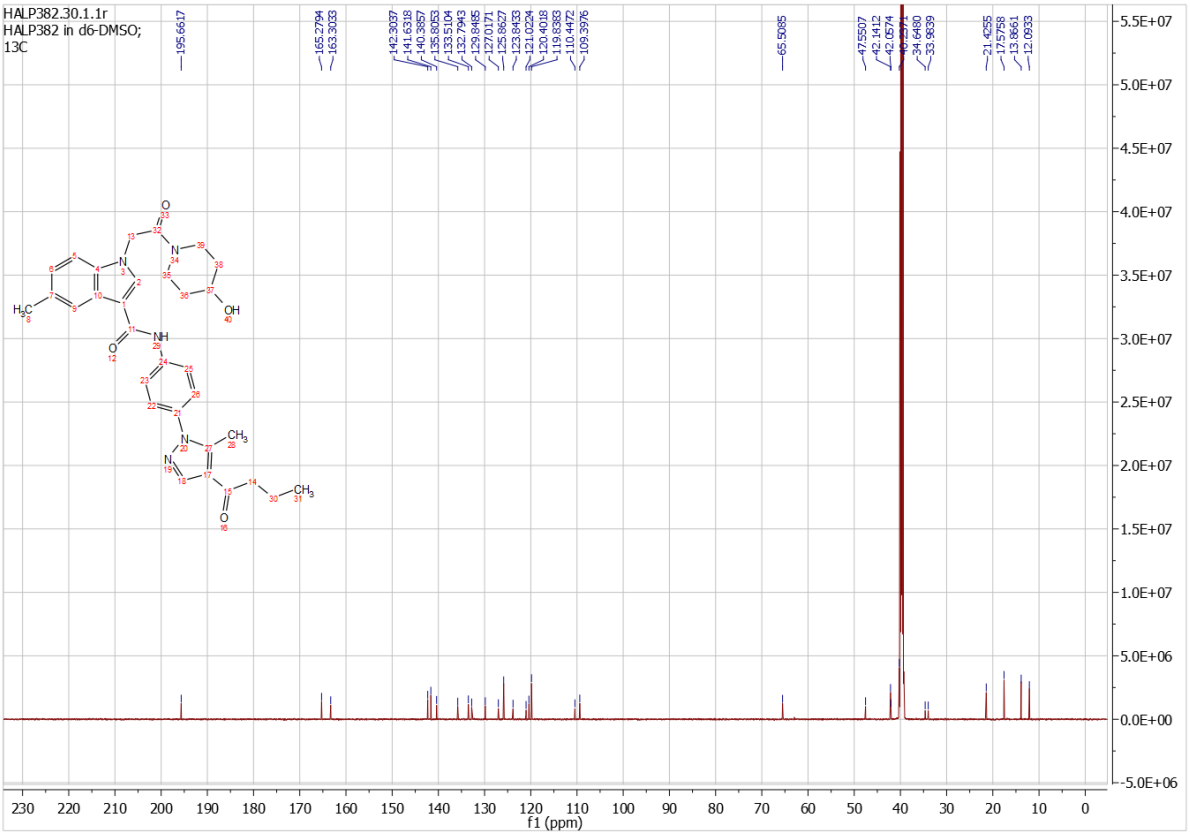


Signal: DAD1 Total WL (220.0:600.0 nm)

RT [min]	Peak MS Base Peak m/z	Area	Area%	Max Peak%	Height
5.705		109.1736	0.1759	0.182	21.273
6.297		26.2370	0.0423	0.044	9.546
6.463		60013.7424	96.6737	100.000	15873.249
6.640		1461.7990	2.3548	2.436	408.404
6.924		179.4202	0.2890	0.299	49.028
7.200		288.2937	0.4644	0.480	37.001
	Sum	62078.6659			

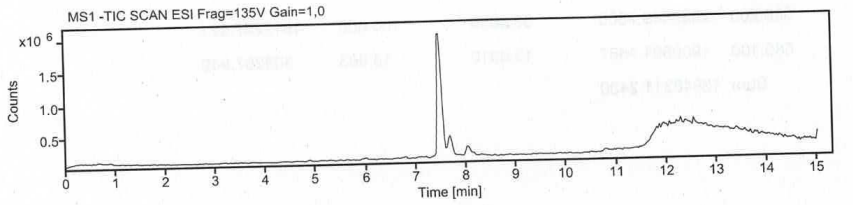
D:\CDSProjects\Default\0-standardplot+EIC.rdl [Rev. 8001] Printed: 2024-03-19 06:27:09+01:00 Page 1 of 2

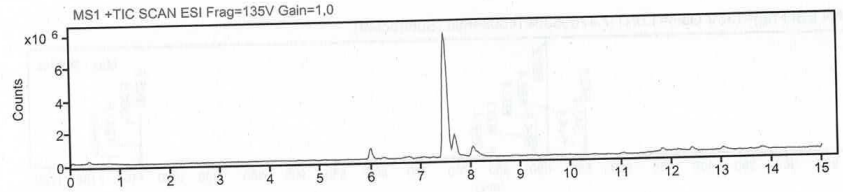

HALP382.10.1.1r
HALP382 in d6-DMSO;
1H
H (s) 9.9764
E (s) 8.0223
F (s) 8.1850
B (d) 7.3467
D (d) 7.9602
A (d) 7.0483
G (s) 8.2344
C (d) 7.4711
J (d) 4.7942
I (m) 5.2679
L (m) 3.8203
K (m) 3.8894
M (dq) 3.7565
W (s) 2.5211
O (t) 2.8124
N (t) 3.0824
P (s) 2.4267
T (m) 1.4777
R (m) 1.7233
Q (m) 1.8400
S (h) 1.6366
V (t) 0.9407
U (m) 1.2752
f1 (ppm)

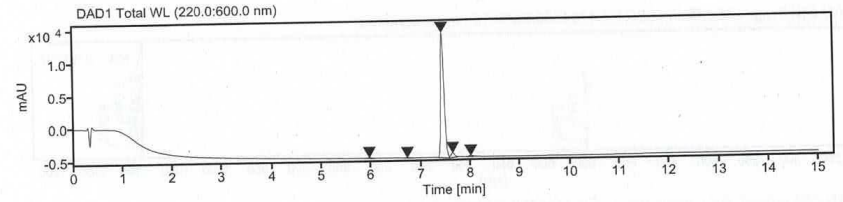

HALP382.30.1.1r
HALP382 in d6-DMSO;
13C
f1 (ppm)

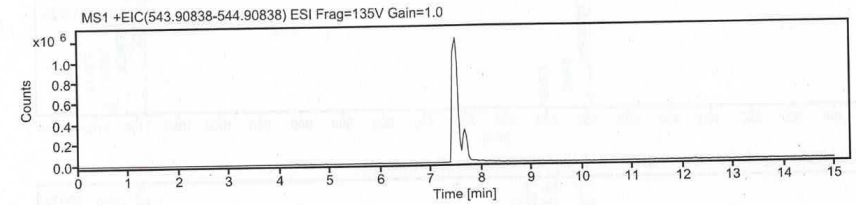
_N_-(4-(4-Butyryl-5-methyl-1_H_-pyrazol-1-yl)phenyl)-1-(2-(4-fluoropiperidin-1-yl)-2-oxoethyl)-5-methyl-1_H_-indole-3-carboxamide (22)

Sequence Name:	SingleSample		
Data file:	HALP422.dx	**Project Name:**	Single Quad
Sample name:	HALP422	**Operator :**	SYSTEM
Instrument:	Single Quad	**Acquired on:**	2024-09-23 09:22:19+02:00
Inj. volume:	2.000	**Location:**	P1-A1
Acq. method:	00-new_wasser-acn_standard_100-1500_BD-20min.amx		
Processing method:	MS_standard_plot.pmx		









Signal: DAD1 Total WL (220.0:600.0 nm)

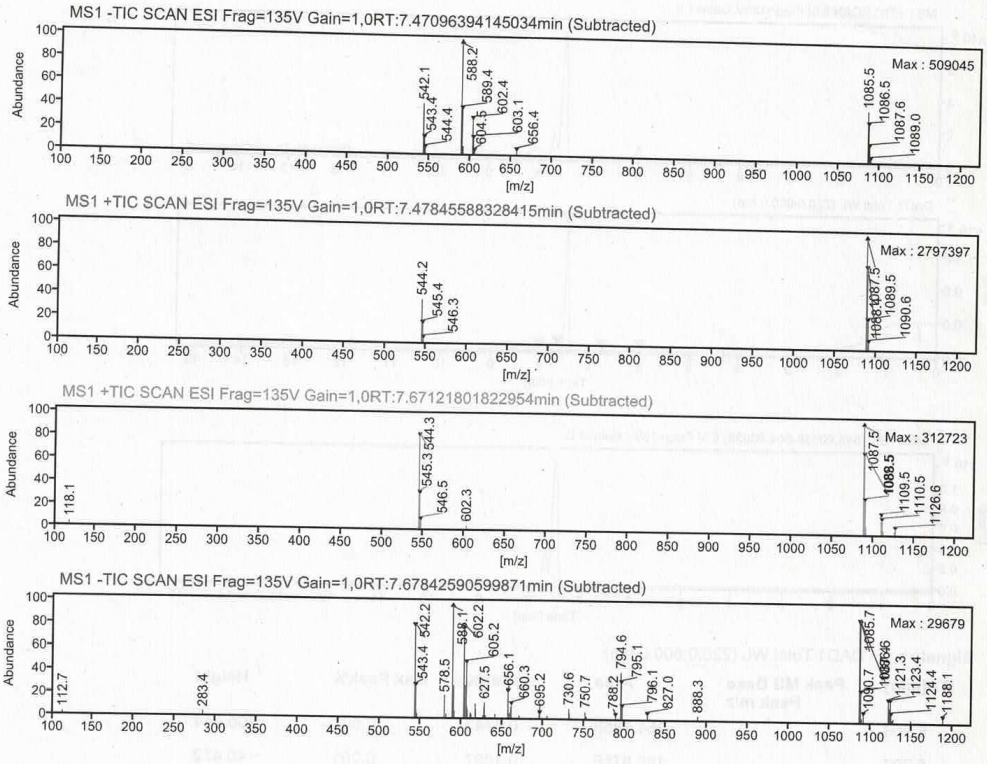
RT [min]	Peak MS Base Peak m/z	Area	Area%	Max Peak%	Height
5.958		464.7856	0.4743	0.502	105.244
6.727		185.8756	0.1897	0.201	40.472
7.442		92646.7336	94.5368	100.000	19179.277
7.639		3833.4110	3.9116	4.138	718.186
8.002		869.8956	0.8876	0.939	179.616
	Sum	98000.7015			

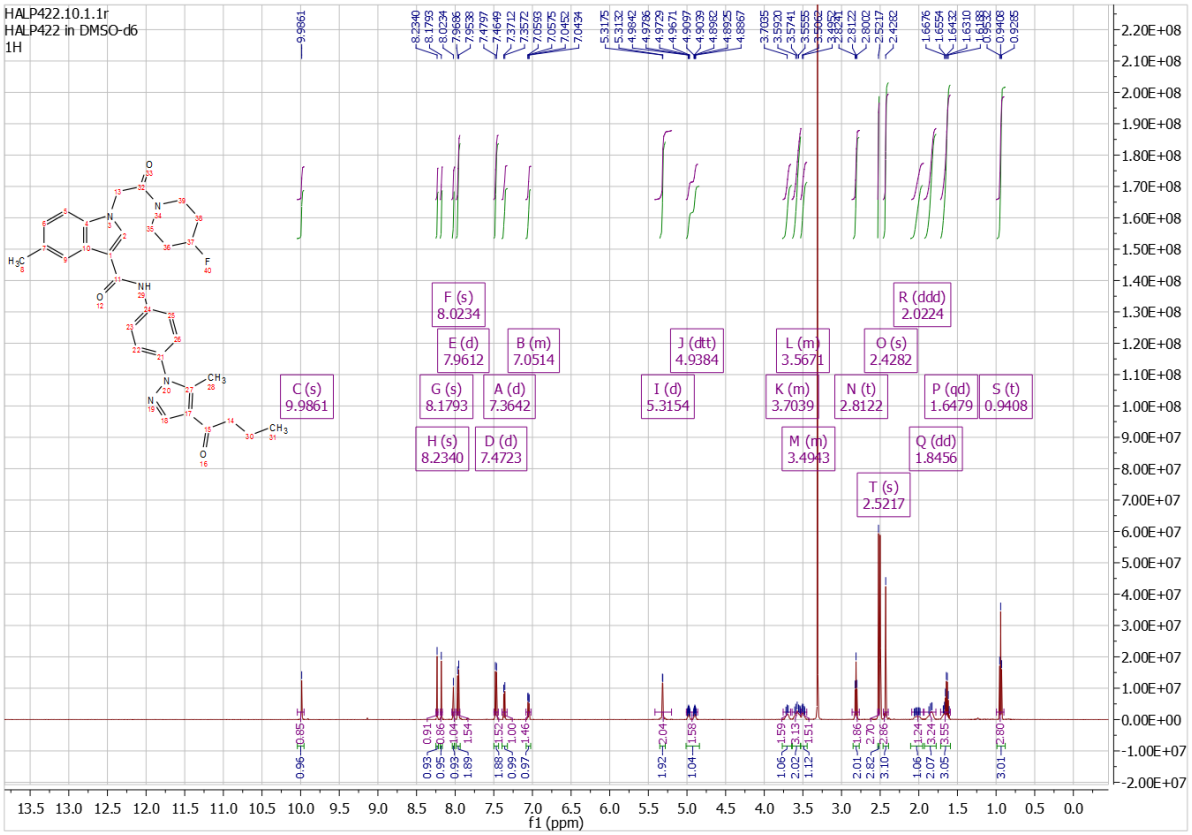
Signal: MS1 +TIC SCAN ESI Frag=135V Gain=1,0

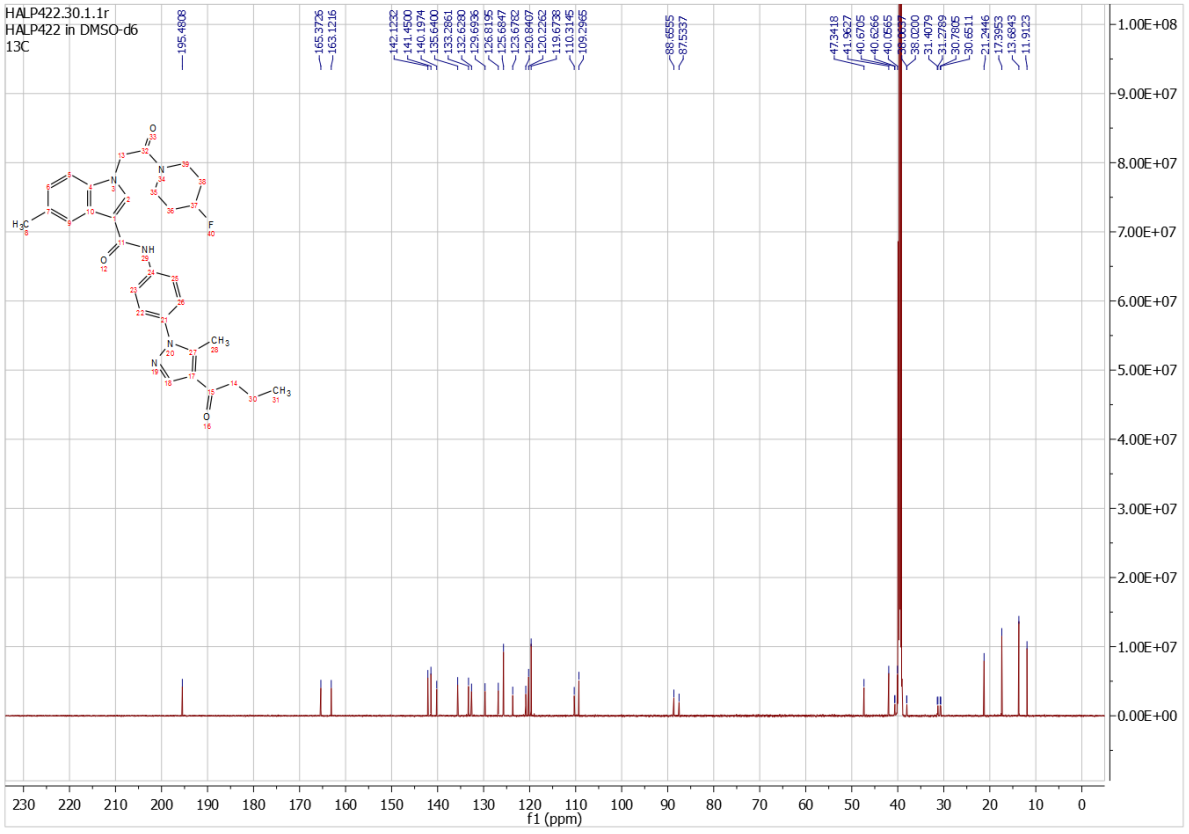
RT [min]	Peak MS Base Peak m/z	Area	Area%	Max Peak%	Height
7.478	1087.500	51085355.2929	87.2082	100.000	7719032.121
7.671	1087.500	7493274.4201	12.7918	14.668	1368412.093
	Sum	58578629.7130			

Signal: MS1 -TIC SCAN ESI Frag=135V Gain=1,0

RT [min]	Peak MS Base Peak m/z	Area	Area%	Max Peak%	Height
7.471	588.200	12038649.7563	86.3090	100.000	1912287.621
7.678	588.100	1909661.4867	13.6910	15.863	303267.949
	Sum	13948311.2430			

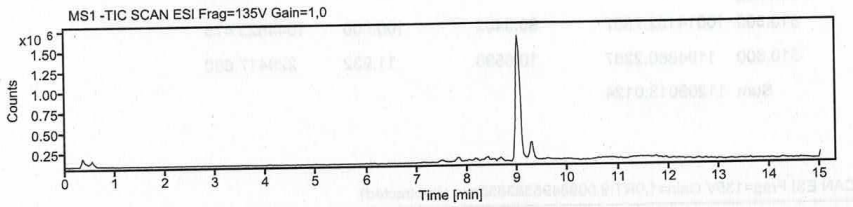


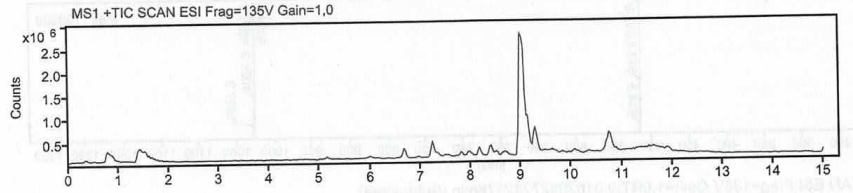

HALP422.10.1.1r
HALP422 in DMSO-d6
1H
F (s) 8.0234
E (d) 7.9612
B (m) 7.0514
J (dtt) 4.9384
L (m) 3.5671
R (ddd) 2.0224
O (s) 2.4282
C (s) 9.9861
G (s) 8.1793
A (d) 7.3642
I (d) 5.3154
K (m) 3.7039
N (t) 2.8122
P (qd) 1.6479
S (t) 0.9408
H (s) 8.2340
D (d) 7.4723
M (m) 3.4943
Q (dd) 1.8456
T (s) 2.5217
f1 (ppm)

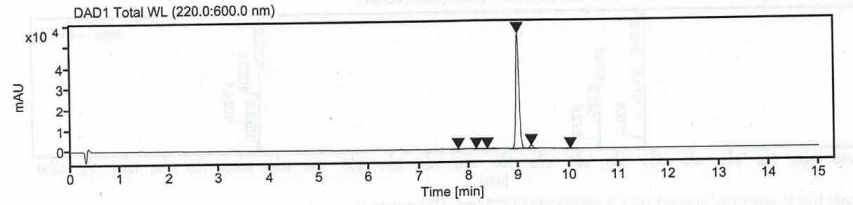

HALP422.30.1.1r
HALP422 in DMSO-d6
13C
f1 (ppm)

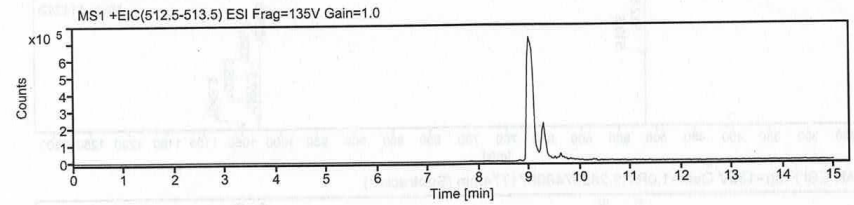
_N_-(4-(4-Butyryl-5-methyl-1_H_-pyrazol-1-yl)phenyl)-1-(2-(cyclopropyl(methyl)amino)-2-oxoethyl)-5-methyl-1_H_-indole-3-carboxamide (23)

Sequence Name:	SingleSample		
Data file:	HALP380-F1.dx	**Project Name:**	Single Quad
Sample name:	HALP380-F1	**Operator :**	SYSTEM
Instrument:	Single Quad	**Acquired on:**	2024-05-07 13:11:41+02:00
Inj. volume:	5.000	**Location:**	P2-A5
Acq. method:	00-new_wasser-acn_standard_100-1500_BD-20min.amx		
Processing method:	MS_standard_plot.pmx		





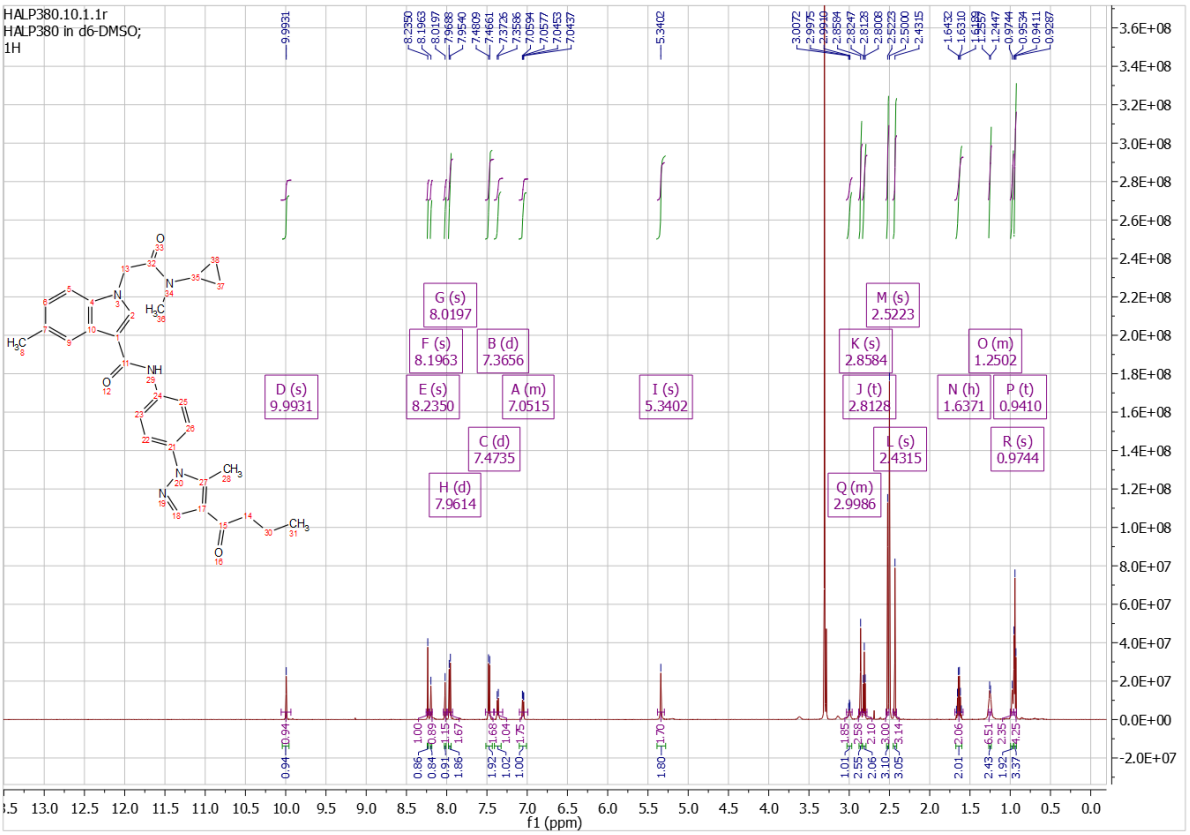


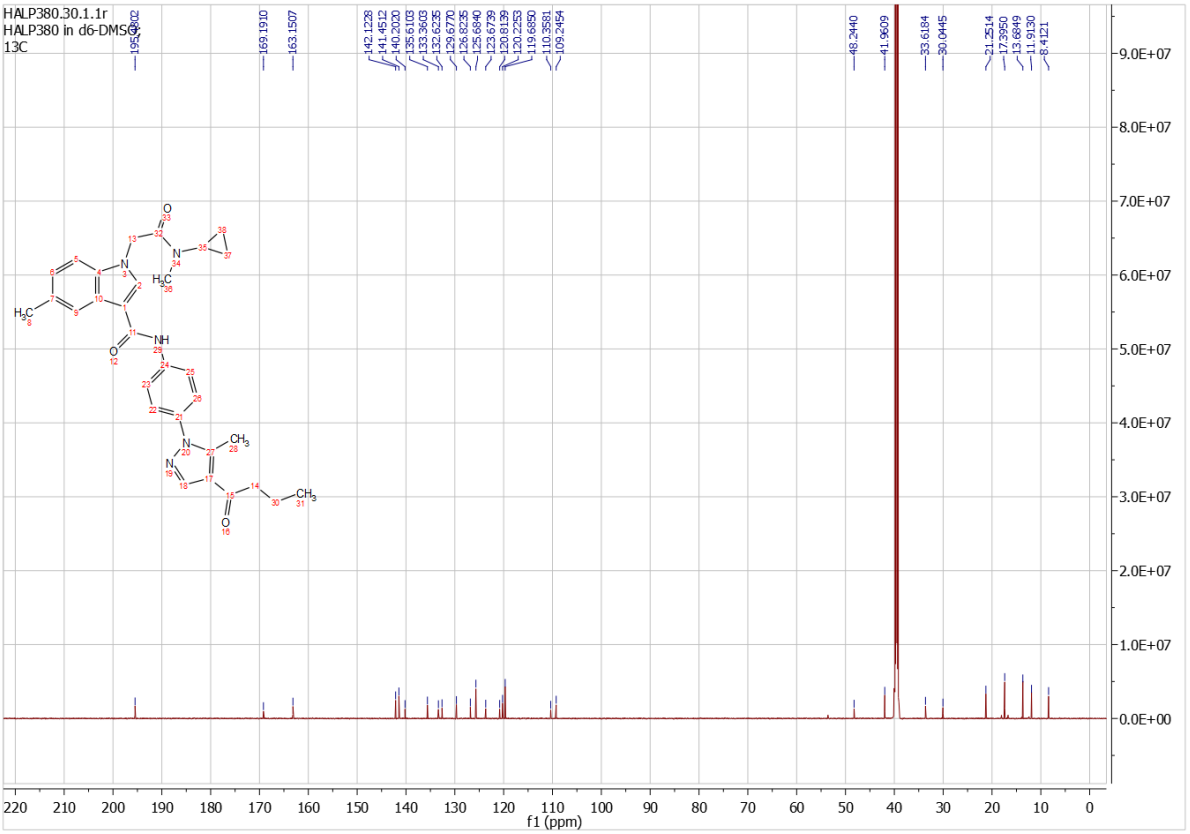


Signal: DAD1 Total WL (220.0:600.0 nm)

RT [min]	Peak MS Base Peak m/z	Area	Area%	Max Peak%	Height
7.785		901.4906	0.3425	0.356	205.109
8.144		686.5013	0.2608	0.271	178.157
8.366		1240.7517	0.4714	0.489	197.054
8.984	512.800	253534.1740	96.3333	100.000	55129.009
9.251		6516.1889	2.4759	2.570	1500.466
10.032		305.1247	0.1159	0.120	50.063
	Sum	263184.2313			

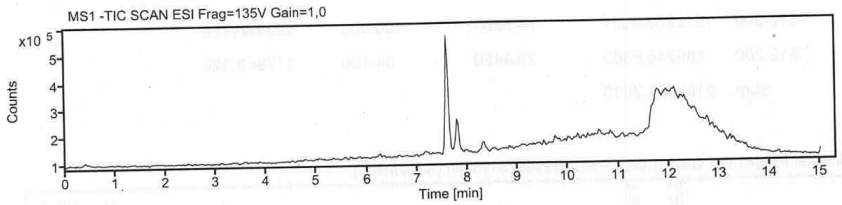
D:\CDSProjects\Default\0-standardplot+EIC.rdl [Rev. 8849] Printed: 2024-05-08 06:52:28+02:00 Page 1 of 2

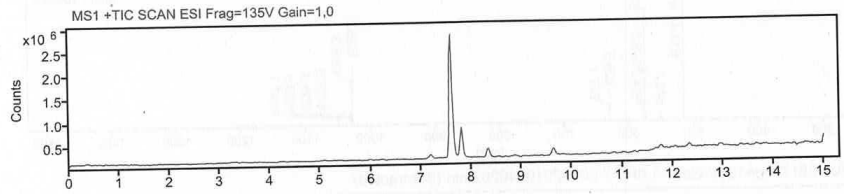

HALP380.10.1.1r
HALP380 in d6-DMSO;
1H
D (s)
9.9931
G (s)
8.0197
F (s)
8.1963
B (d)
7.3656
E (s)
8.2350
A (m)
7.0515
C (d)
7.4735
H (d)
7.9614
I (s)
5.3402
M (s)
2.5223
K (s)
2.8584
O (m)
1.2502
J (t)
2.8128
N (h)
1.6371
P (t)
0.9410
L (s)
2.4315
R (s)
0.9744
Q (m)
2.9986
f1 (ppm)

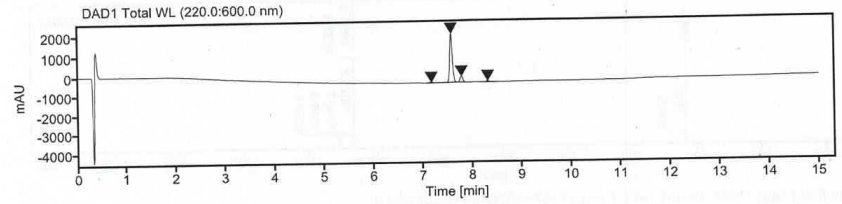

HALP380.30.1.1r
HALP380 in d6-DMSO;
13C
f1 (ppm)

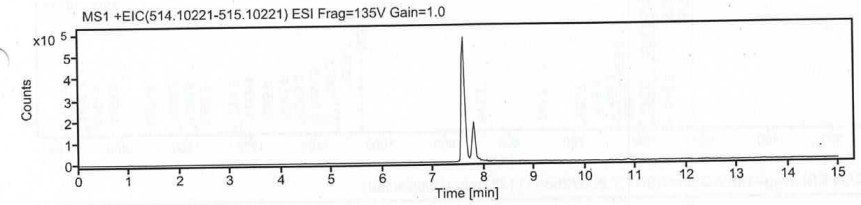
_N_-(4-(4-Butyryl-5-methyl-1_H_-pyrazol-1-yl)phenyl)-1-(2-(diethylamino)-2-oxoethyl)-5-methyl-1_H_-indole-3-carboxamide (24)

Sequence Name:	SingleSample		
Data file:	HALP410-F2.dx	**Project Name:**	Single Quad
Sample name:	HALP410-F2	**Operator :**	SYSTEM
Instrument:	Single Quad	**Acquired on:**	2024-07-04 13:21:05+02:00
Inj. volume:	3.000	**Location:**	P1-E3
Acq. method:	00-new_wasser-acn_standard_100-1500_BD-20min.amx		
Processing method:	MS_standard_plot.pmx		









Signal: DAD1 Total WL (220.0:600.0 nm)

RT [min]	Peak MS Base Peak m/z	Area	Area%	Max Peak%	Height
7.165		128.8941	1.1988	1.381	25.758
7.569	512.300	9336.6474	86.8397	100.000	2465.852
7.773	512.200	1150.4771	10.7005	12.322	307.120
8.303		135.5651	1.2609	1.452	53.795
	Sum	10751.5837			

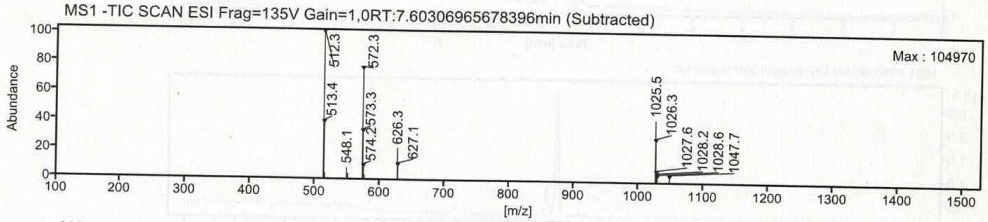
Signal: MS1 +TIC SCAN ESI Frag=135V Gain=1,0

RT [min]	Peak MS Base Peak m/z	Area	Area%	Max Peak%	Height
7.605	1027.800	11365034.5370	83.3882	100.000	2642597.380
7.808	514.400	2264035.6865	16.6118	19.921	607734.190
	Sum	13629070.2236			

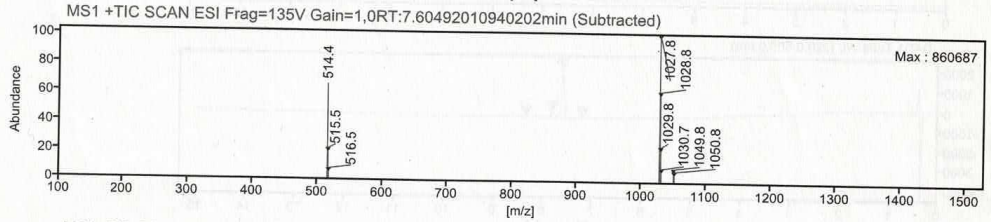
Signal: MS1 -TIC SCAN ESI Frag=135V Gain=1,0

RT [min]	Peak MS Base Peak m/z	Area	Area%	Max Peak%	Height
7.603	512.300	1612250.4307	74.5550	100.000	423928.125
7.804	512.200	550246.8303	25.4450	34.129	117946.320
	Sum	2162497.2610			

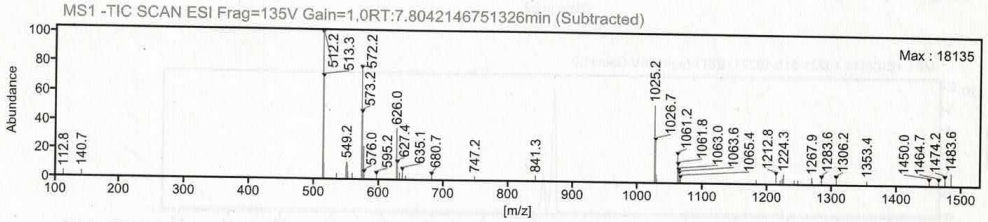
MS1 -TIC SCAN ESI Frag=135V Gain=1,0RT:7.60306965678396min (Subtracted)



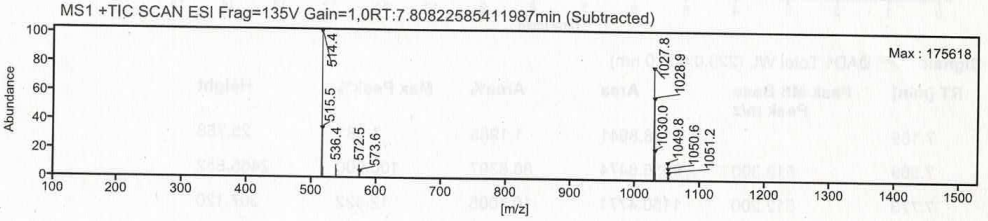
MS1 +TIC SCAN ESI Frag=135V Gain=1,0RT:7.60492010940202min (Subtracted)

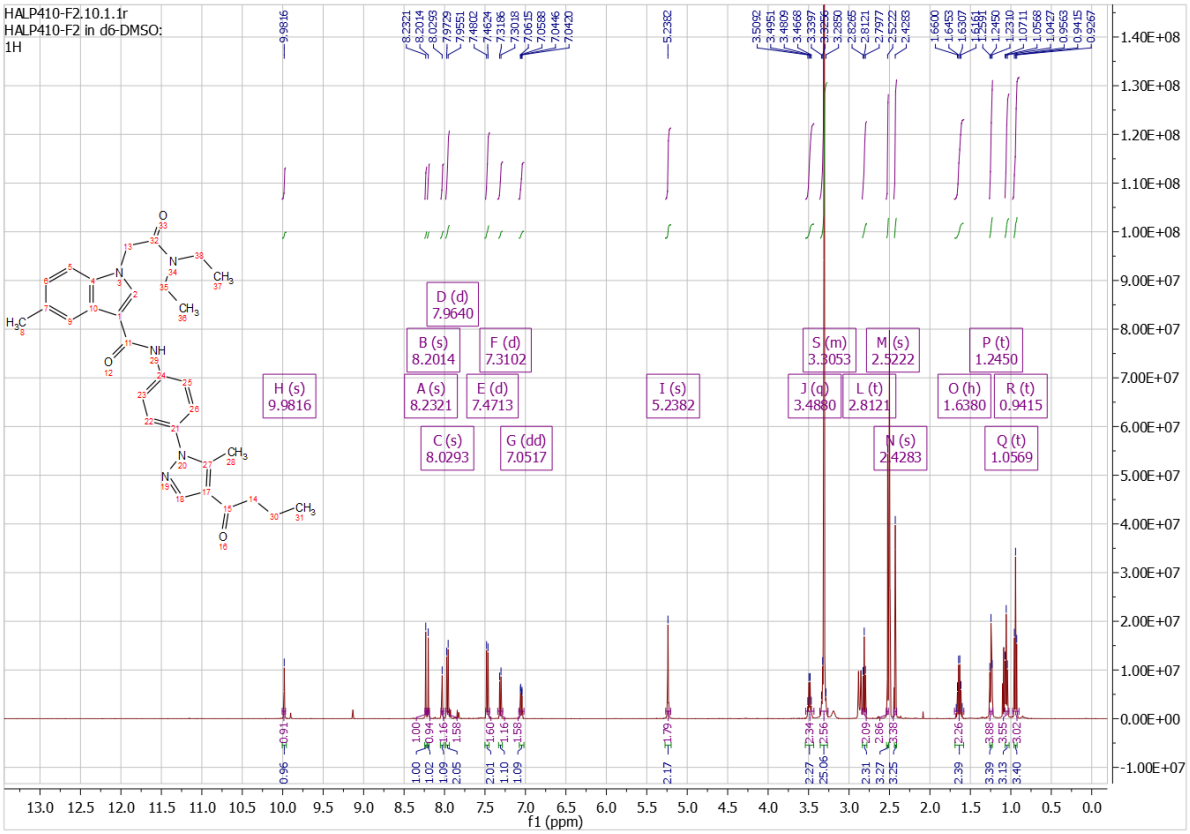


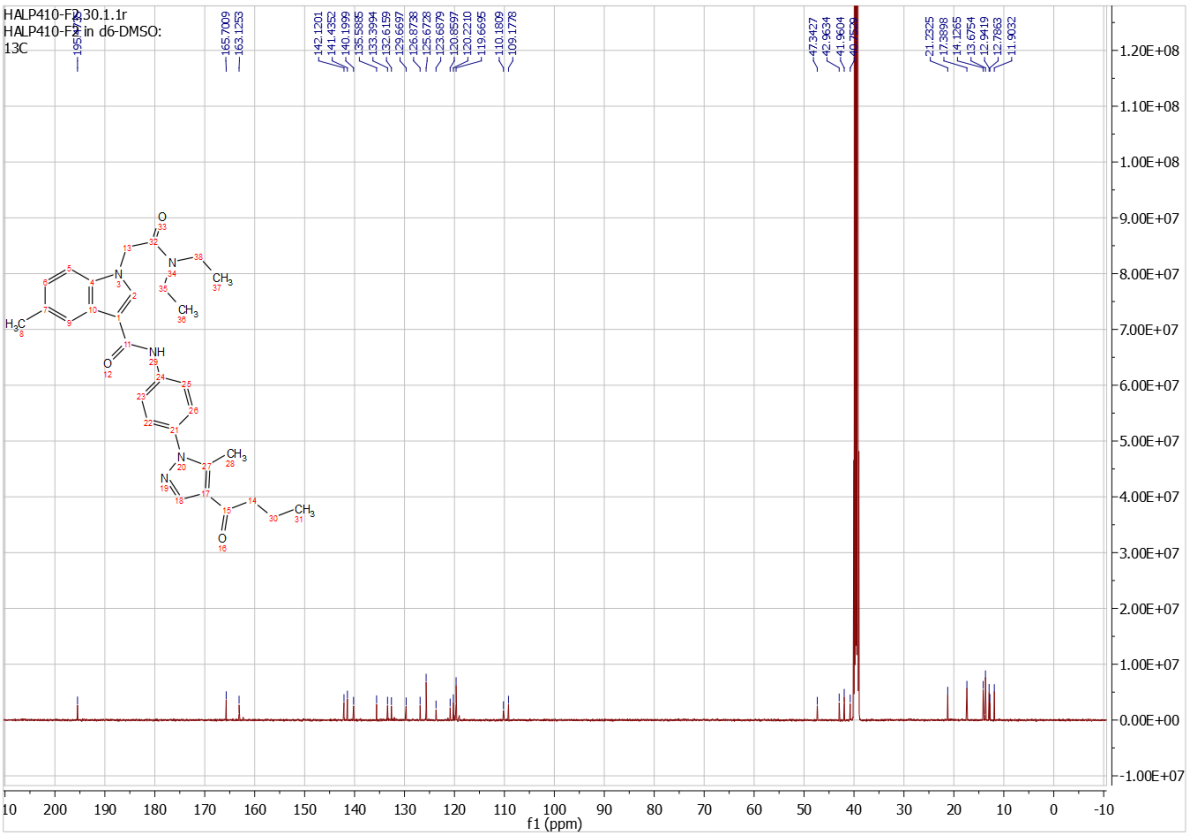
MS1 -TIC SCAN ESI Frag=135V Gain=1,0RT:7.8042146751326min (Subtracted)



MS1 +TIC SCAN ESI Frag=135V Gain=1,0RT:7.80822585411987min (Subtracted)

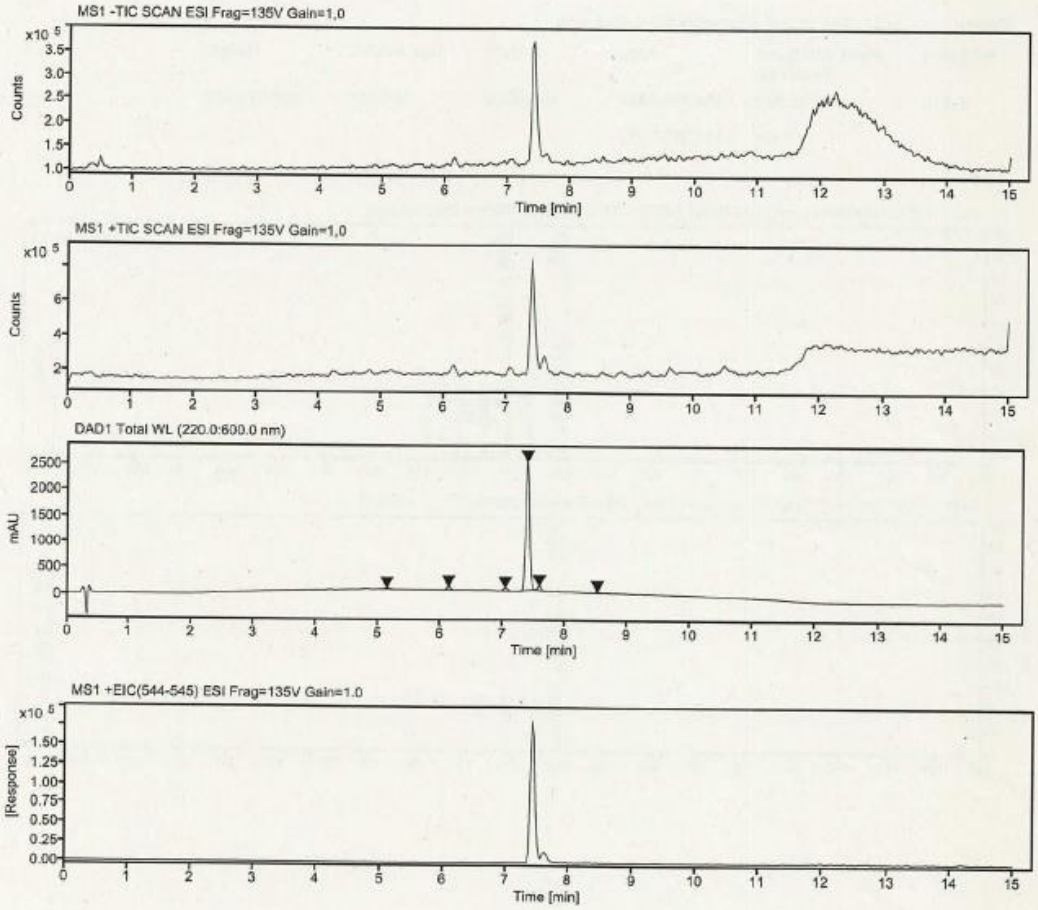



HALP410-F2.10.1.1r
HALP410-F2 in d6-DMSO:
1H
D (d)
7.9640
B (s)
8.2014
F (d)
7.3102
S (m)
3.3053
M (s)
2.5222
P (t)
1.2450
H (s)
9.9816
A (s)
8.2321
E (d)
7.4713
I (s)
5.2382
J (q)
3.4880
L (t)
2.8121
O (h)
1.6380
R (t)
0.9415
C (s)
8.0293
G (dd)
7.0517
N (s)
2.4283
Q (t)
1.0569
f1 (ppm)


HALP410-F2.30.1.1r
HALP410-F2 in d6-DMSO:
13C
f1 (ppm)

_N_-(4-(4-Butyryl-5-methyl-1_H_-pyrazol-1-yl)phenyl)-5-methyl-1-(2-oxo-2-thiomorpholinoethyl)-1_H_-indole-3-carboxamide (25)

Sequence Name:	SingleSample		
Data file:	HALP275.dx	**Project Name:**	Single Quad
Sample name:	HALP275	**Operator :**	SYSTEM
Instrument:	Single Quad	**Acquired on:**	2023-05-23 07:55:59+02:00
Inj. volume:	2.000	**Location:**	P1-E5
Acq. method:	00-new_wasser-acn_standard_100-1500_BD-20min.amx		
Processing method:	MS_standard_plot.pmx		



Signal: DAD1 Total WL (220.0:600.0 nm)

RT [min]	Peak MS Base Peak m/z	Area	Area%	Max Peak%	Height
5.130		109.0615	0.9360	1.024	23.186
6.123		226.2245	1.9414	2.124	61.827
7.031		260.5224	2.2358	2.446	56.816
7.386		10649.9540	91.3969	100.000	2478.782
7.581		318.1980	2.7307	2.988	84.933
8.513		88.4576	0.7591	0.831	19.438

D:\CDSProjects\Default\00-standardplot+EIC.rdl [Rev. 5269] Printed: 2023-05-23 08:40:38+02:00 Page 1 of 2

RT [min]	Peak MS Base Peak m/z	Area	Area%	Max Peak%	Height
	Sum	11652.4179			

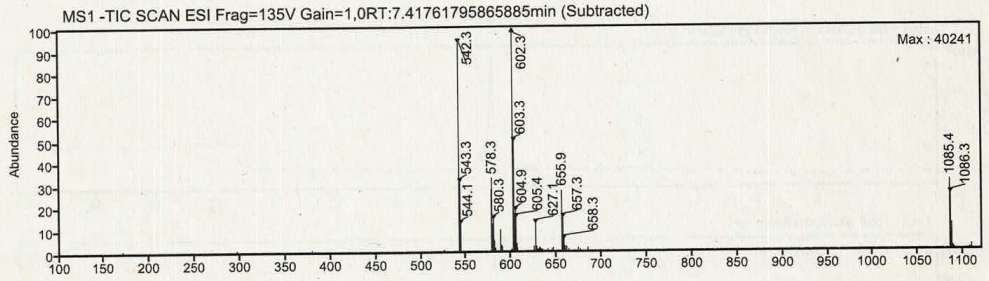
Signal: MS1 +TIC SCAN ESI Frag=135V Gain=1,0

RT [min]	Peak MS Base Peak m/z	Area	Area%	Max Peak%	Height
7.418	544.300	3304835.7936	100.0000	100.000	673567.769
	Sum	3304835.7936			

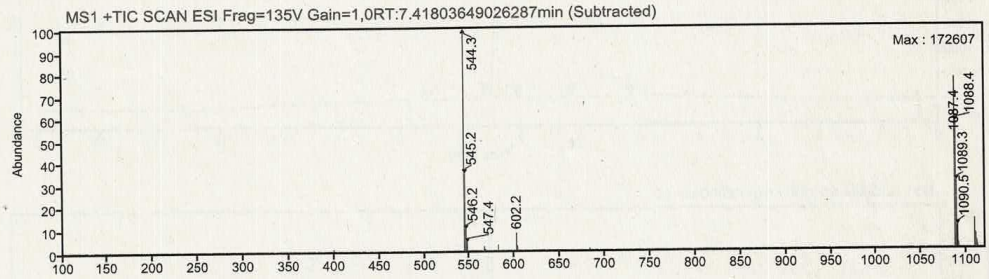
Signal: MS1 -TIC SCAN ESI Frag=135V Gain=1,0

RT [min]	Peak MS Base Peak m/z	Area	Area%	Max Peak%	Height
7.418	602.300	1464309.3957	100.0000	100.000	263626.444
	Sum	1464309.3957			

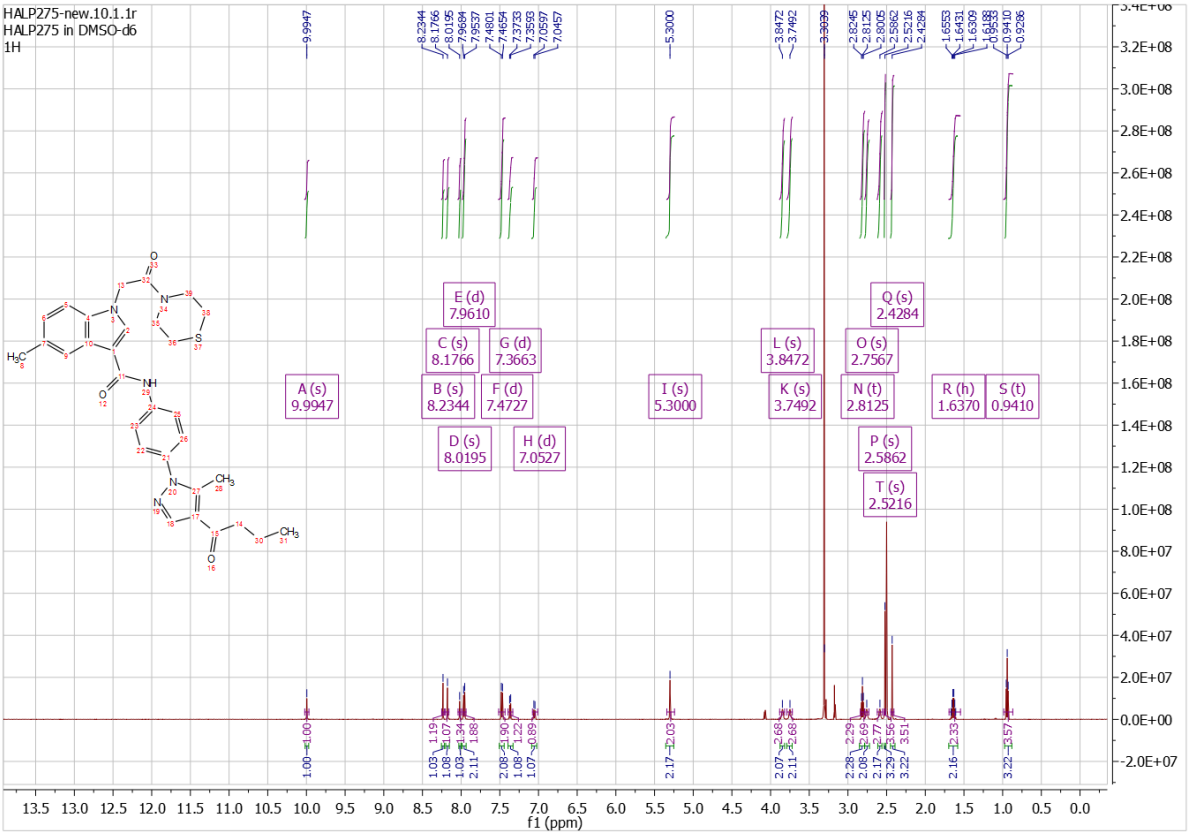
MS1 -TIC SCAN ESI Frag=135V Gain=1,0RT:7.41761795865885min (Subtracted)

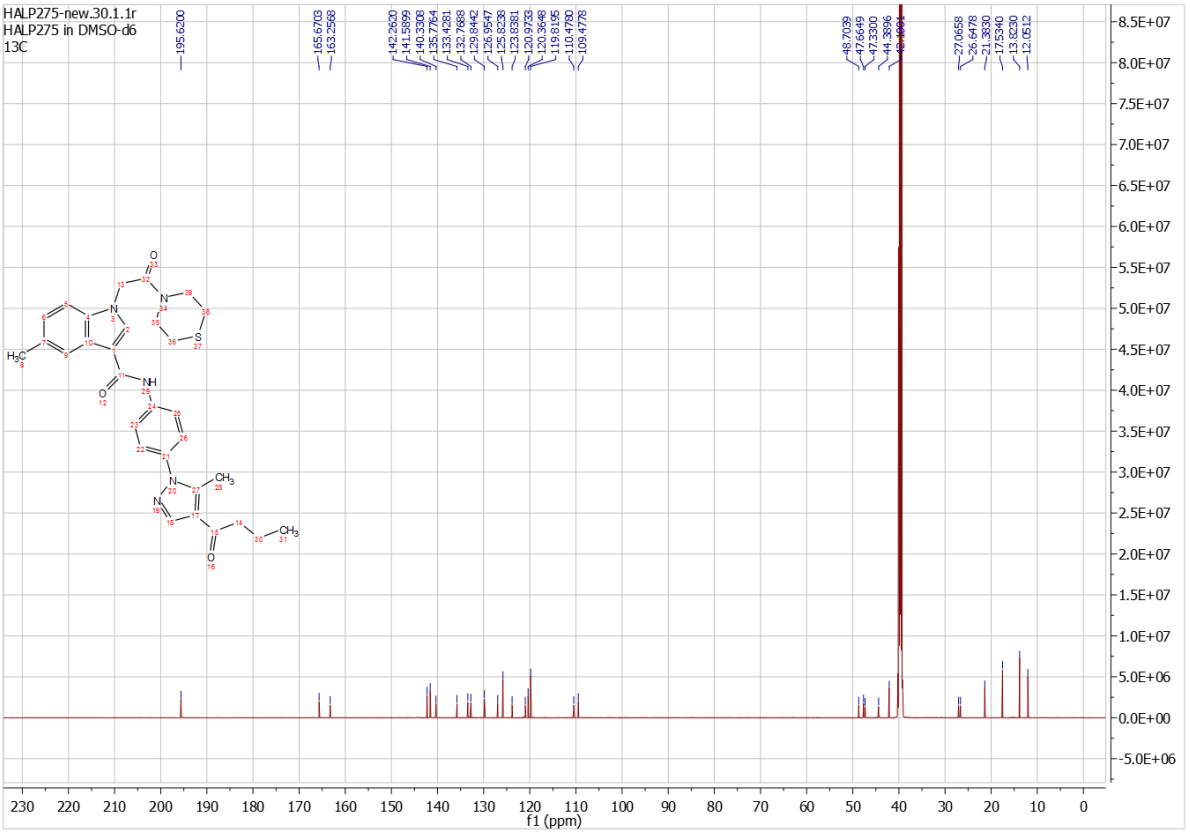


MS1 +TIC SCAN ESI Frag=135V Gain=1,0RT:7.41803649026287min (Subtracted)



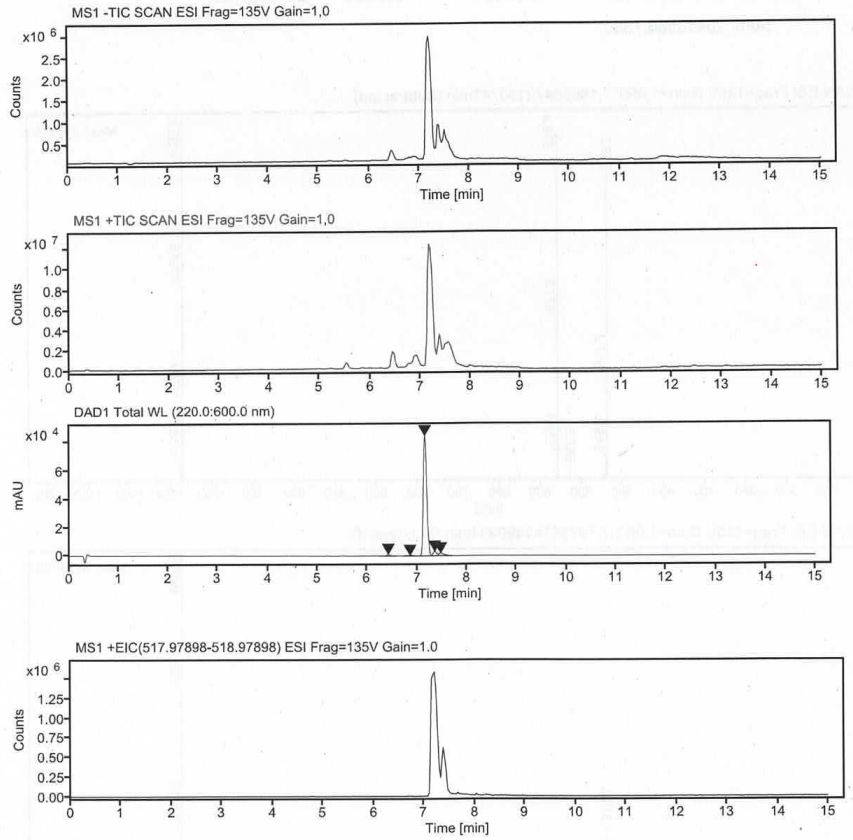
D:\CDSProjects\Default\00-standardplot+EIC.rdl [Rev. 5269] Printed: 2023-05-23 08:40:38+02:00 Page 2 of 2


HALP275-new.10.1.1r
HALP275 in DMSO-d6
1H
A (s) 9.9947
B (s) 8.2344
C (s) 8.1766
D (s) 8.0195
E (d) 7.9610
F (d) 7.4727
G (d) 7.3663
H (d) 7.0527
I (s) 5.3000
K (s) 3.7492
L (s) 3.8472
N (t) 2.8125
O (s) 2.7567
P (s) 2.5862
Q (s) 2.4284
R (h) 1.6370
S (t) 0.9410
T (s) 2.5216
f1 (ppm)


HALP275-new.30.1.1r
HALP275 in DMSO-d6
13C
f1 (ppm)

_N_-(4-(4-Butyryl-5-methyl-1_H_-pyrazol-1-yl)phenyl)-1-(2-((2-fluoroethyl)(methyl)amino)-2-oxoethyl)-5-methyl-1_H_-indole-3-carboxamide (26)

Sequence Name:	SingleSample		
Data file:	HALP420-F1.dx	**Project Name:**	Single Quad
Sample name:	HALP420-F1	**Operator :**	SYSTEM
Instrument:	Single Quad	**Acquired on:**	2024-09-27 07:14:57+02:00
Inj. volume:	4.000	**Location:**	P2-A10
Acq. method:	00-new_wasser-acn_standard_100-1500_BD-20min.amx		
Processing method:	MS_standard_plot.pmx		



Signal: DAD1 Total WL (220.0:600.0 nm)

RT [min]	Peak MS Base Peak m/z	Area	Area%	Max Peak%	Height
6.419		4953.3114	1.0883	1.179	1067.388
6.862		1973.4745	0.4336	0.470	280.081
7.161		420015.5662	92.2823	100.000	84819.404
7.356		14640.0319	3.2166	3.486	3015.880
7.475		13559.4459	2.9792	3.228	1804.239
	Sum	455141.8298			

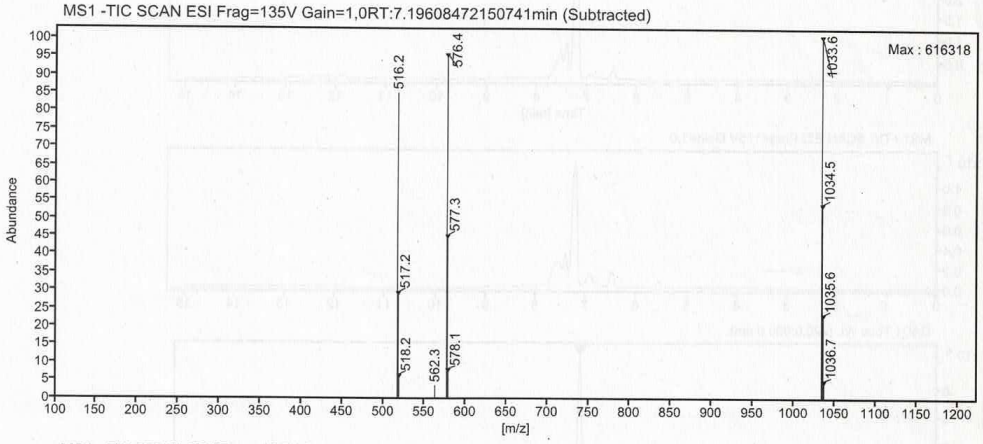
Signal: MS1 +TIC SCAN ESI Frag=135V Gain=1,0

RT [min]	Peak MS Base Peak m/z	Area	Area%	Max Peak%	Height
7.197	1035.500	77053727.2339	100.0000	100.000	11641449.708
	Sum	77053727.2339			

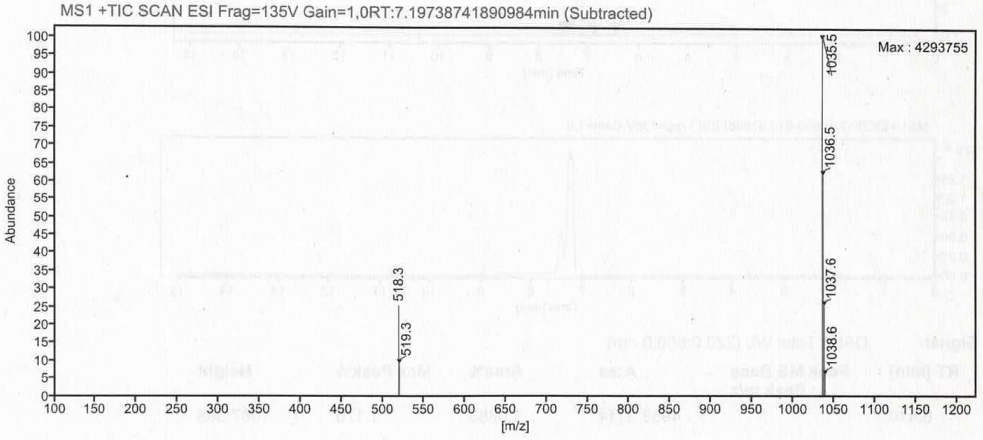
Signal: MS1 -TIC SCAN ESI Frag=135V Gain=1,0

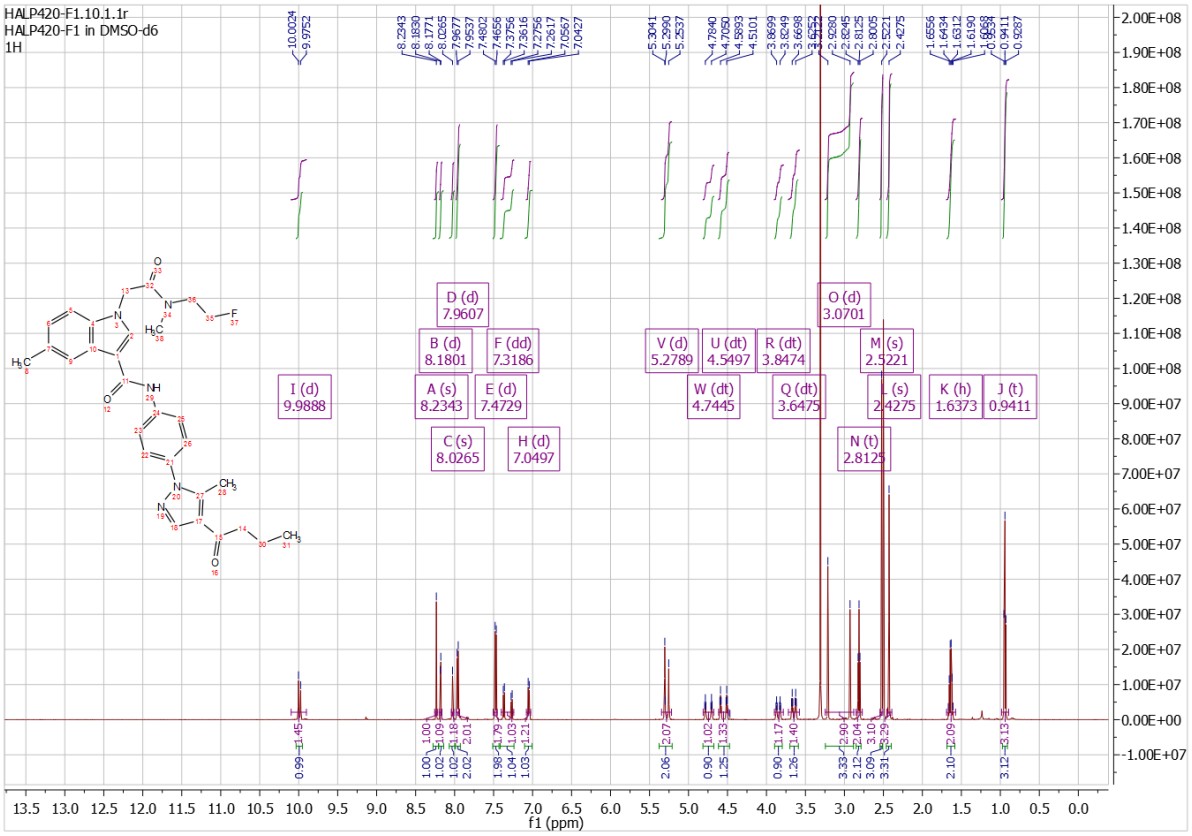
RT [min]	Peak MS Base Peak m/z	Area	Area%	Max Peak%	Height
7.196	1033.600	20448666.7320	100.0000	100.000	2848967.351
	Sum	20448666.7320			

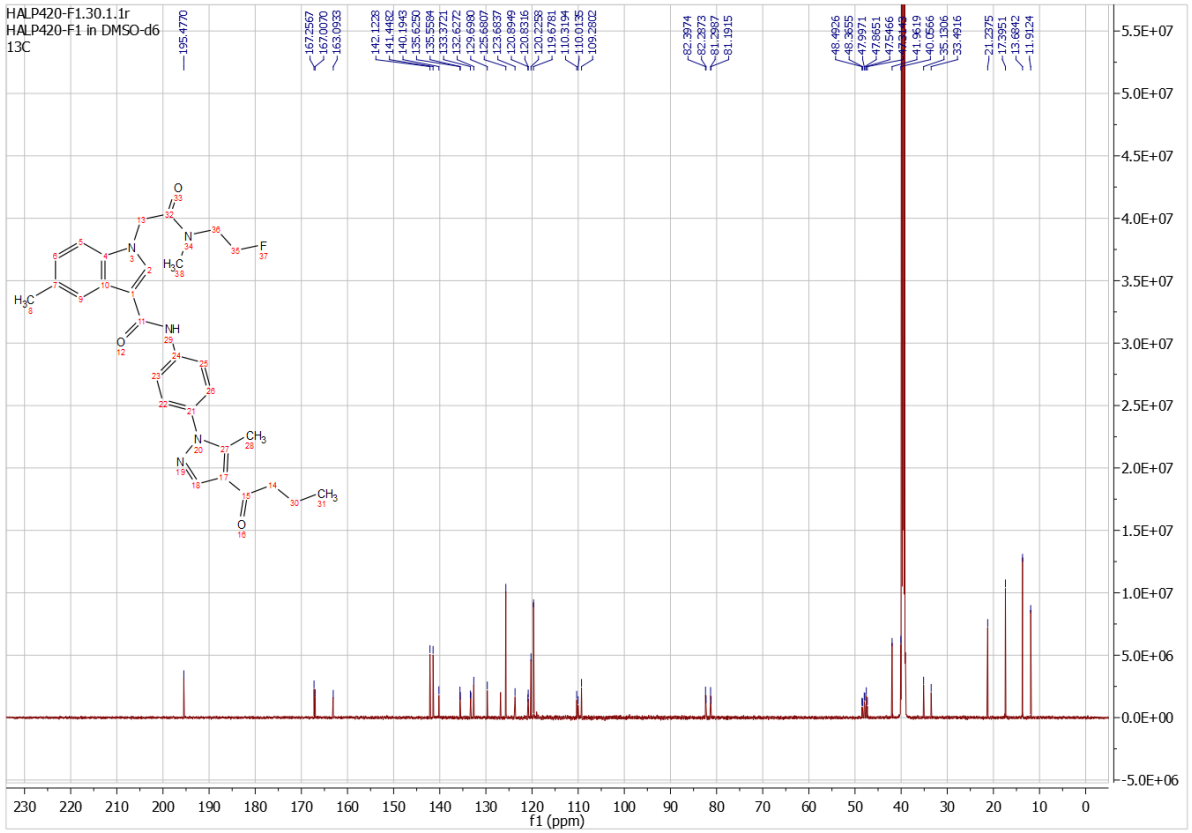
MS1 -TIC SCAN ESI Frag=135V Gain=1,0RT:7.19608472150741min (Subtracted)



MS1 +TIC SCAN ESI Frag=135V Gain=1,0RT:7.19738741890984min (Subtracted)

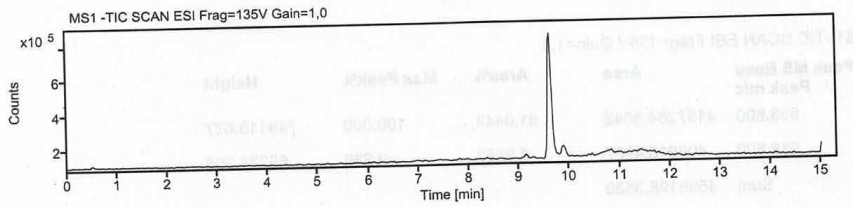


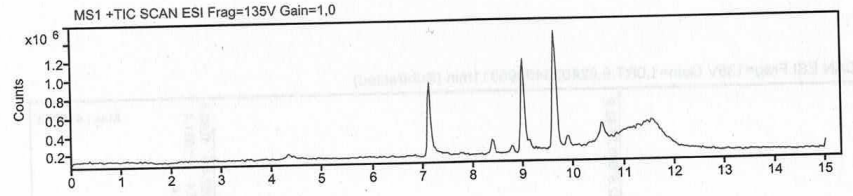

HALP420-F1.10.1.1r
HALP420-F1 in DMSO-d6
1H
I (d) 9.9888
A (s) 8.2343
B (d) 8.1801
C (s) 8.0265
D (d) 7.9607
E (d) 7.4729
F (dd) 7.3186
H (d) 7.0497
V (d) 5.2789
W (dt) 4.7445
U (dt) 4.5497
Q (dt) 3.6475
R (dt) 3.8474
O (d) 3.0701
N (t) 2.8125
M (s) 2.5221
L (s) 2.4275
K (h) 1.6373
J (t) 0.9411
f1 (ppm)

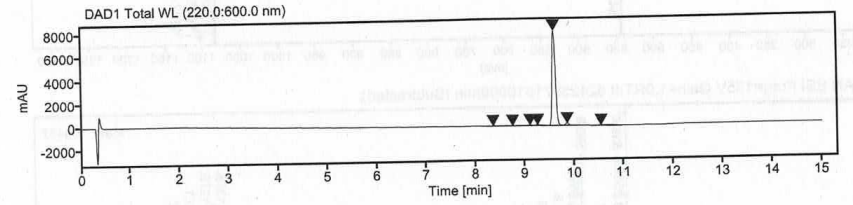

HALP420-F1.30.1.1r
HALP420-F1 in DMSO-d6
13C
f1 (ppm)

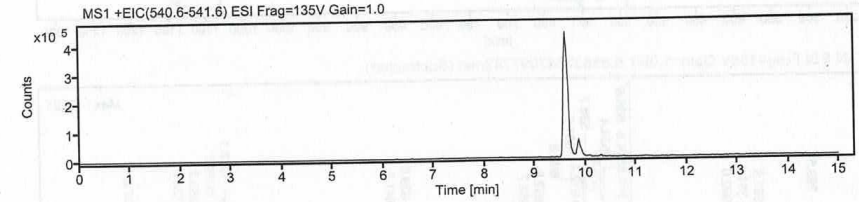
_N_-(4-(4-Butyryl-5-methyl-1_H_-pyrazol-1-yl)phenyl)-5-methyl-1-(2-(3-methylpiperidin-1-yl)-2-oxoethyl)-1_H_-indole-3-carboxamide (27)

Sequence Name:	SingleSample		
Data file:	HALP376-F1.dx	**Project Name:**	Single Quad
Sample name:	HALP376-F1	**Operator :**	SYSTEM
Instrument:	Single Quad	**Acquired on:**	2024-05-07 12:29:37+02:00
Inj. volume:	2.000	**Location:**	P2-A3
Acq. method:	00-new_wasser-acn_standard_100-1500_BD-20min.amx		
Processing method:	MS_standard_plot.pmx		









Signal: DAD1 Total WL (220.0:600.0 nm)

RT [min]	Peak MS Base Peak m/z	Area	Area%	Max Peak%	Height
8.350		102.2851	0.2617	0.276	23.113
8.747		102.8003	0.2630	0.277	15.104
9.098		188.8586	0.4831	0.509	48.712
9.253		338.4761	0.8659	0.913	68.545
9.590		37078.9756	94.8546	100.000	8125.545
9.852		814.2762	2.0831	2.196	198.898
10.540		464.6544	1.1887	1.253	31.974

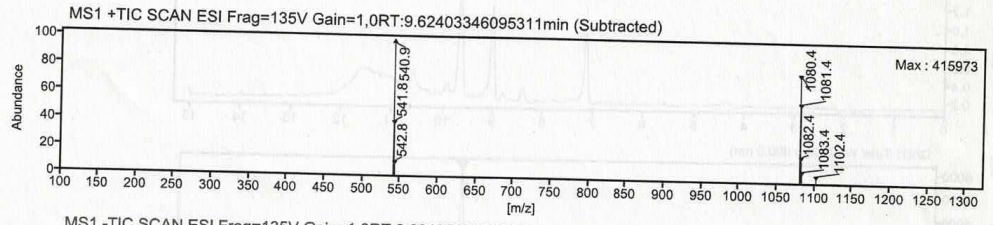
RT [min]	Peak MS Base Peak m/z	Area	Area%	Max Peak%	Height
	Sum	39090.3263			

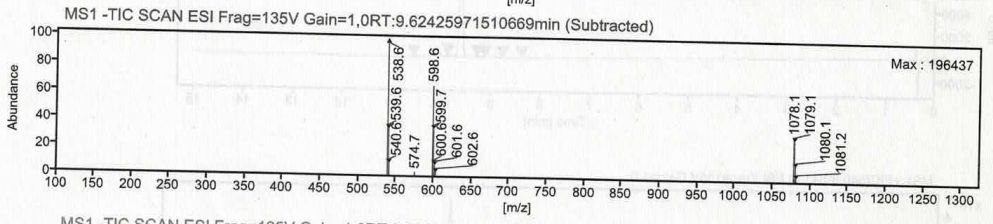
Signal: MS1 +TIC SCAN ESI Frag=135V Gain=1,0

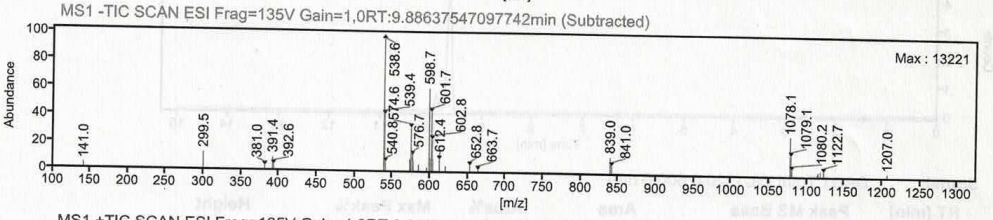
RT [min]	Peak MS Base Peak m/z	Area	Area%	Max Peak%	Height
9.624	540.900	6622535.6036	96.5613	100.000	1224947.653
9.888	540.800	235836.0019	3.4387	3.561	90214.892
	Sum	6858371.6056			

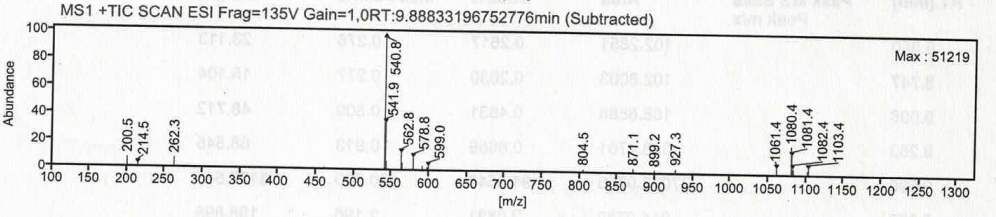
Signal: MS1 -TIC SCAN ESI Frag=135V Gain=1,0

RT [min]	Peak MS Base Peak m/z	Area	Area%	Max Peak%	Height
9.624	538.600	4157284.8542	91.0448	100.000	749113.677
9.886	538.600	408913.4987	8.9552	9.836	65224.206
	Sum	4566198.3530			

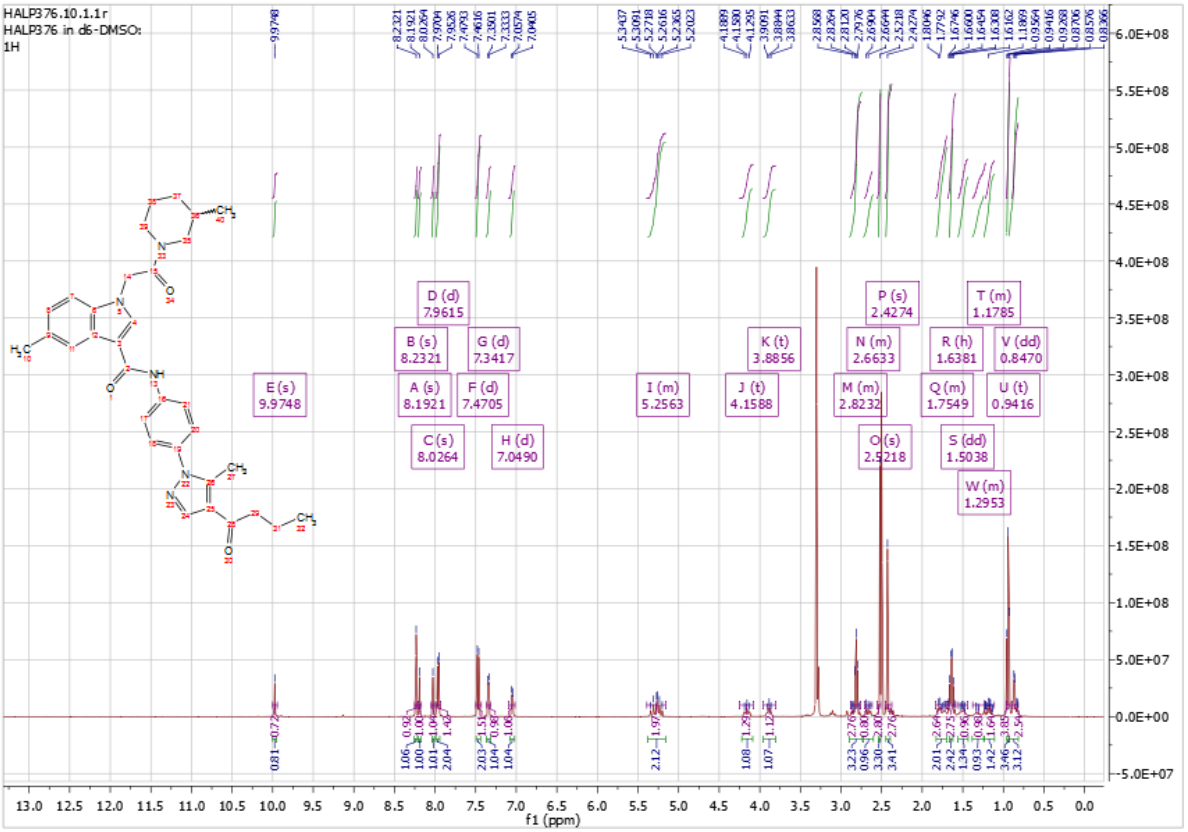


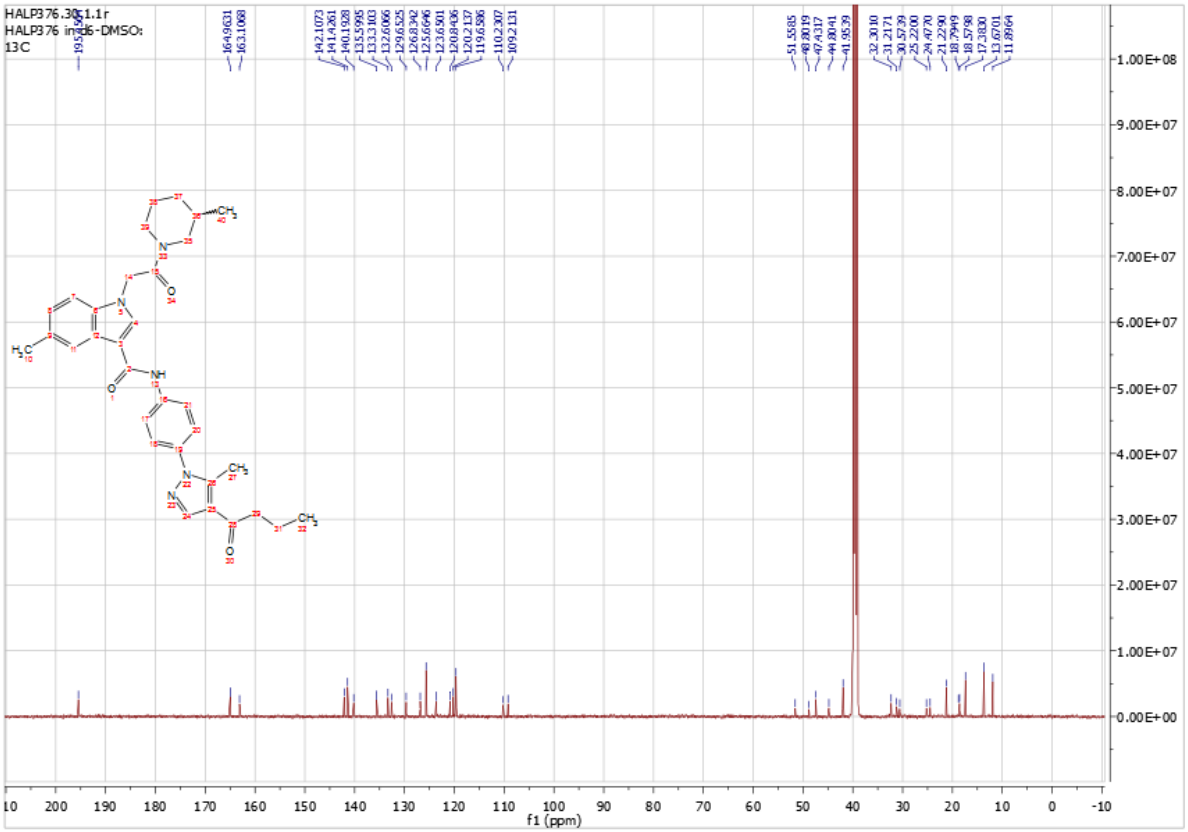






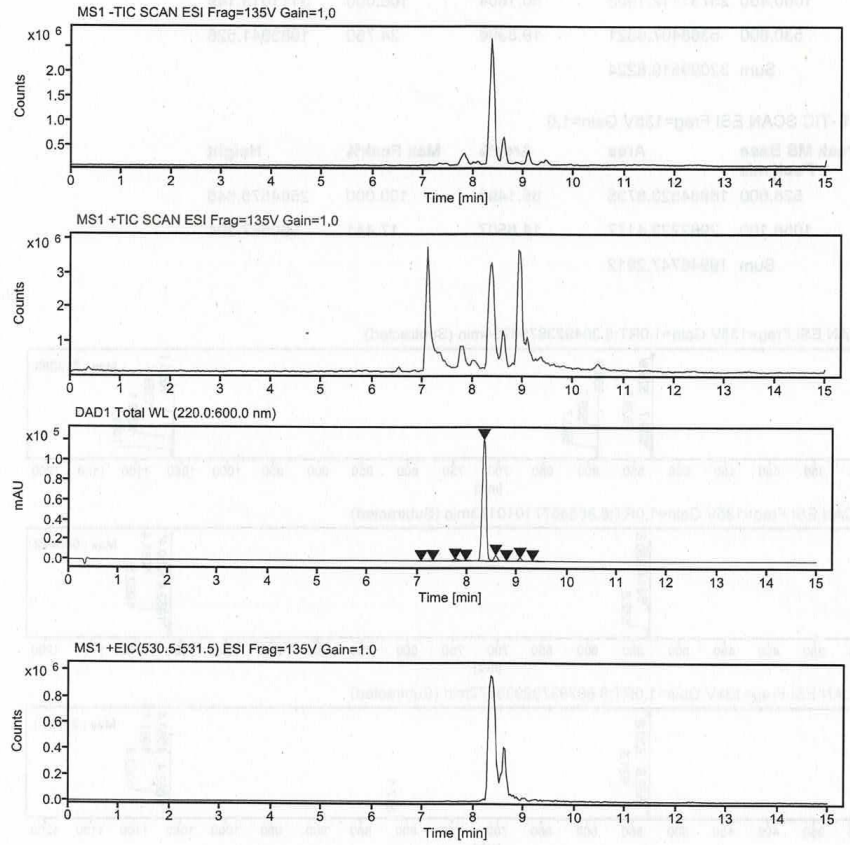
D:\CDSProjects\Default\0-standardplot+EIC.rdl [Rev. 8849] Printed: 2024-05-08 06:50:06+02:00 Page 2 of 2


HALP376.10.1.1r
HALP376 in d6-DMSO
1H
E (s) 9.9748
D (d) 7.9615
B (s) 8.2321
G (d) 7.3417
A (s) 8.1921
F (d) 7.4705
C (s) 8.0264
H (d) 7.0490
I (m) 5.2563
J (t) 4.1588
K (t) 3.8856
M (m) 2.8232
O (s) 2.5218
P (s) 2.4274
N (m) 2.6633
Q (m) 1.7549
R (h) 1.6381
S (dd) 1.5038
T (m) 1.1785
V (dd) 0.8470
U (t) 0.9416
W (m) 1.2953
f1 (ppm)


HALP376.30.1.1r
HALP376 in d6-DMSO
13C
f1 (ppm)

_N_-(4-(4-Butyryl-5-methyl-1_H_-pyrazol-1-yl)phenyl)-1-(2-((2-methoxyethyl)(methyl)amino)-2-oxoethyl)-5-methyl-1_H_-indole-3-carboxamide (28)

Sequence Name:	SingleSample		
Data file:	HALP375-F1.dx	**Project Name:**	Single Quad
Sample name:	HALP375-F1	**Operator :**	SYSTEM
Instrument:	Single Quad	**Acquired on:**	2024-05-07 04:32:28+02:00
Inj. volume:	4.000	**Location:**	P1-D6
Acq. method:	00-new_wasser-acn_standard_100-1500_BD-20min.amx		
Processing method:	MS_standard_plot.pmx		



Signal: DAD1 Total WL (220.0:600.0 nm)

RT [min]	Peak MS Base Peak m/z	Area	Area%	Max Peak%	Height
7.072		524.3731	0.0705	0.077	136.503
7.312		2760.0761	0.3710	0.404	314.624
7.756		12414.4529	1.6686	1.818	1586.782
7.969		2597.5828	0.3491	0.380	360.512
8.332	528.600	682789.1939	91.7703	100.000	121247.880
8.572		27578.7360	3.7067	4.039	5609.826
8.788		1129.7697	0.1518	0.165	151.381

D:\CDSProjects\Default\0-standardplot+EIC.rdl [Rev. 8827] Printed: 2024-05-07 11:00:50+02:00 Page 1 of 2

RT [min]	Peak MS Base Peak m/z	Area	Area%	Max Peak%	Height
9.061		12068.6280	1.6221	1.768	2780.792
9.312		2157.0796	0.2899	0.316	266.248
	Sum	744019.8922			

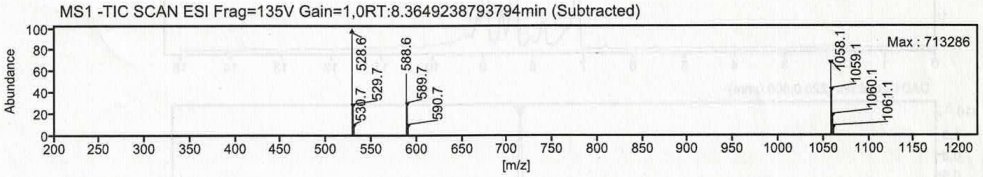
Signal: MS1 +TIC SCAN ESI Frag=135V Gain=1,0

RT [min]	Peak MS Base Peak m/z	Area	Area%	Max Peak%	Height
8.365	1060.400	25731112.1903	80.1604	100.000	3111013.149
8.608	530.800	6368407.6321	19.8396	24.750	1083841.526
	Sum	32099519.8224			

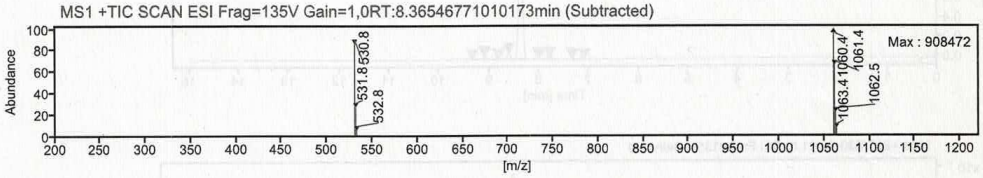
Signal: MS1 -TIC SCAN ESI Frag=135V Gain=1,0

RT [min]	Peak MS Base Peak m/z	Area	Area%	Max Peak%	Height
8.365	528.600	16984523.8735	85.1493	100.000	2564575.846
8.608	1058.100	2962223.4177	14.8507	17.441	560567.891
	Sum	19946747.2912			

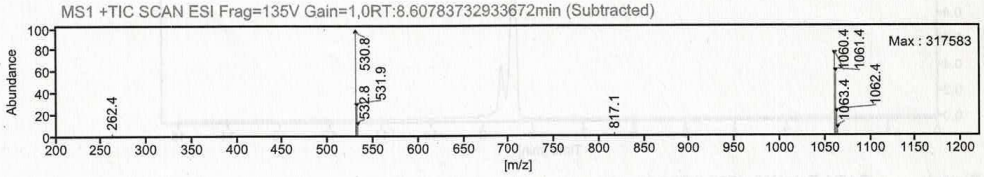
MS1 -TIC SCAN ESI Frag=135V Gain=1,0RT:8.3649238793794min (Subtracted)



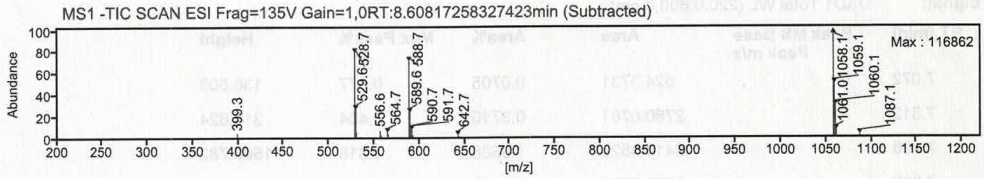
MS1 +TIC SCAN ESI Frag=135V Gain=1,0RT:8.36546771010173min (Subtracted)

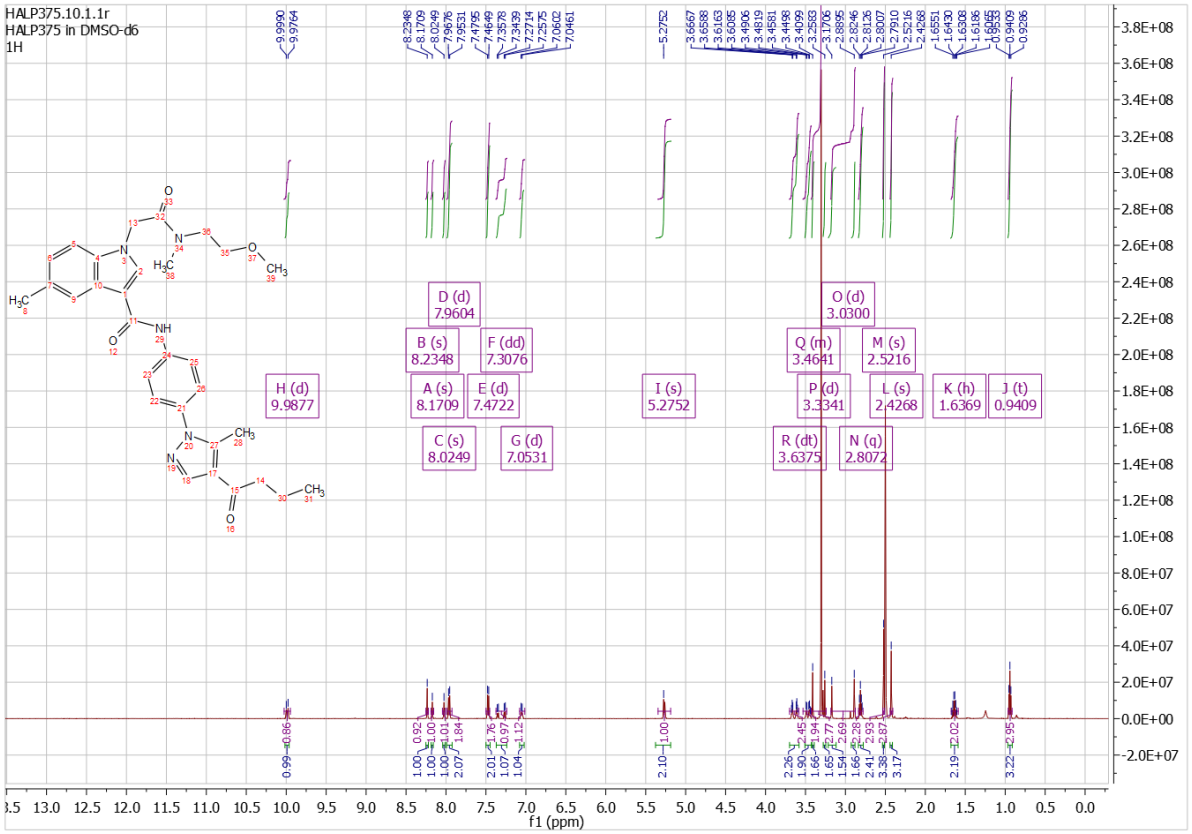


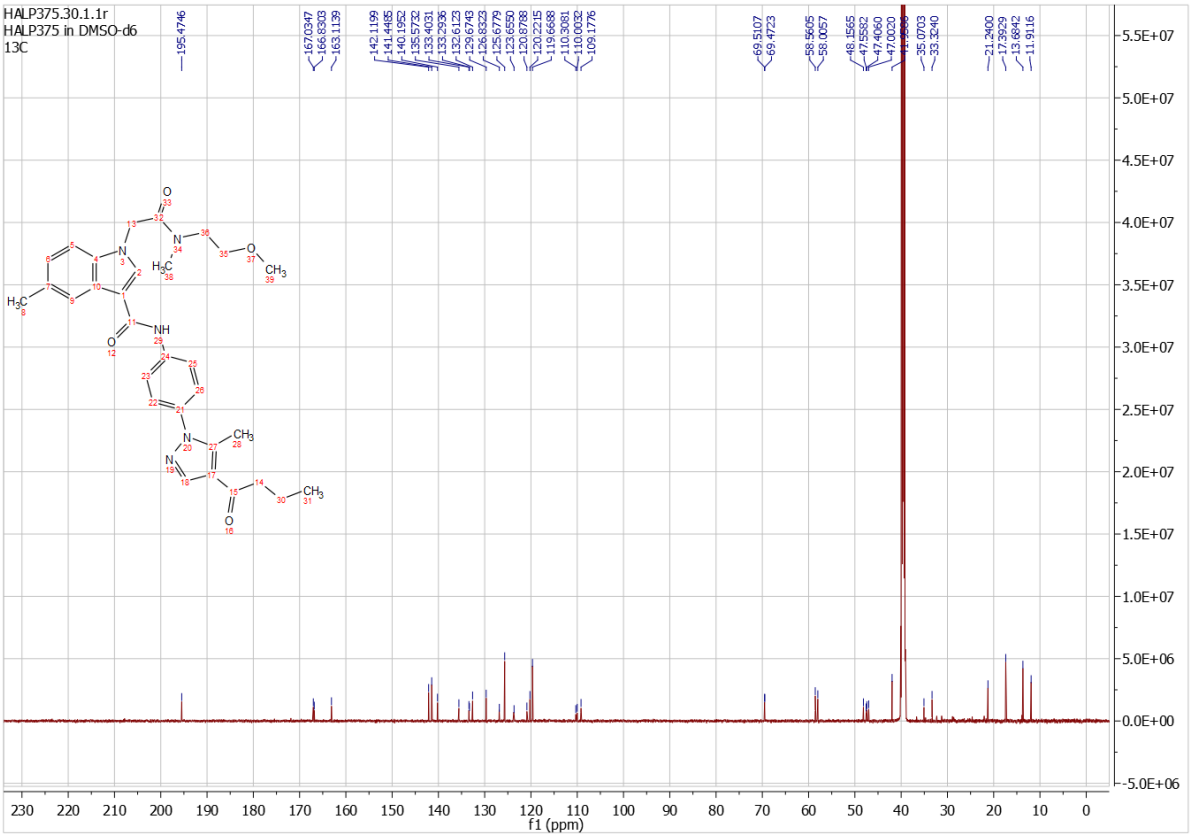
MS1 +TIC SCAN ESI Frag=135V Gain=1,0RT:8.60783732933672min (Subtracted)



MS1 -TIC SCAN ESI Frag=135V Gain=1,0RT:8.60817258327423min (Subtracted)

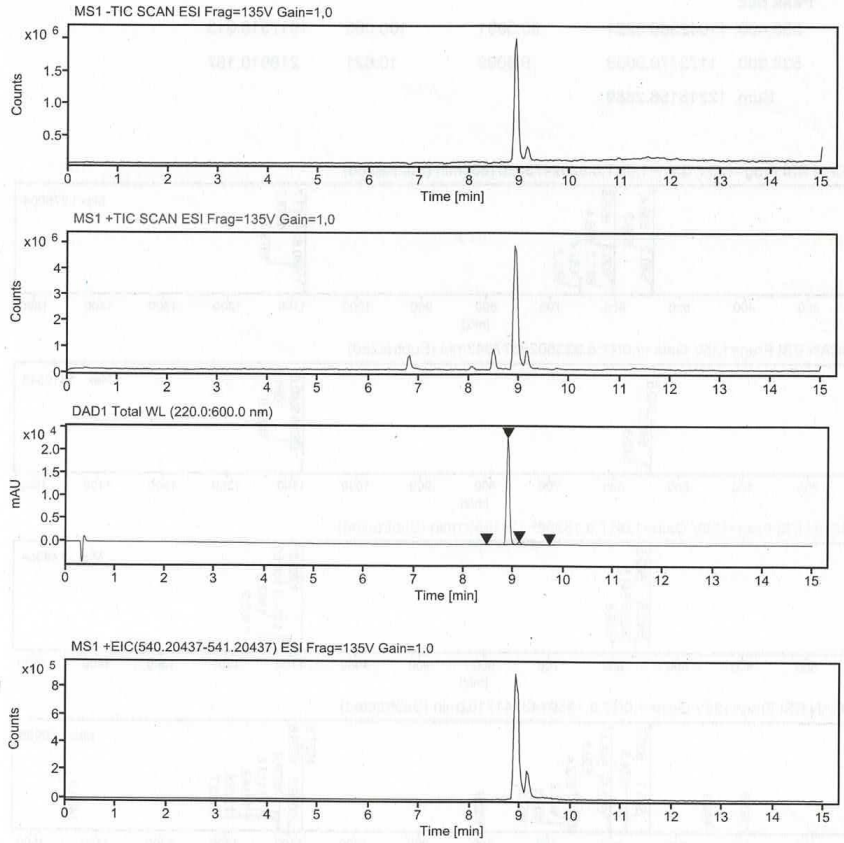



HALP375.10.1.1r
HALP375 in DMSO-d6
1H
D (d) 7.9604
B (s) 8.2348
F (dd) 7.3076
A (s) 8.1709
E (d) 7.4722
C (s) 8.0249
G (d) 7.0531
H (d) 9.9877
I (s) 5.2752
O (d) 3.0300
Q (m) 3.4641
M (s) 2.5216
P (d) 3.3341
L (s) 2.4268
K (h) 1.6369
J (t) 0.9409
R (dt) 3.6375
N (q) 2.8072
f1 (ppm)


HALP375.30.1.1r
HALP375 in DMSO-d6
13C
f1 (ppm)

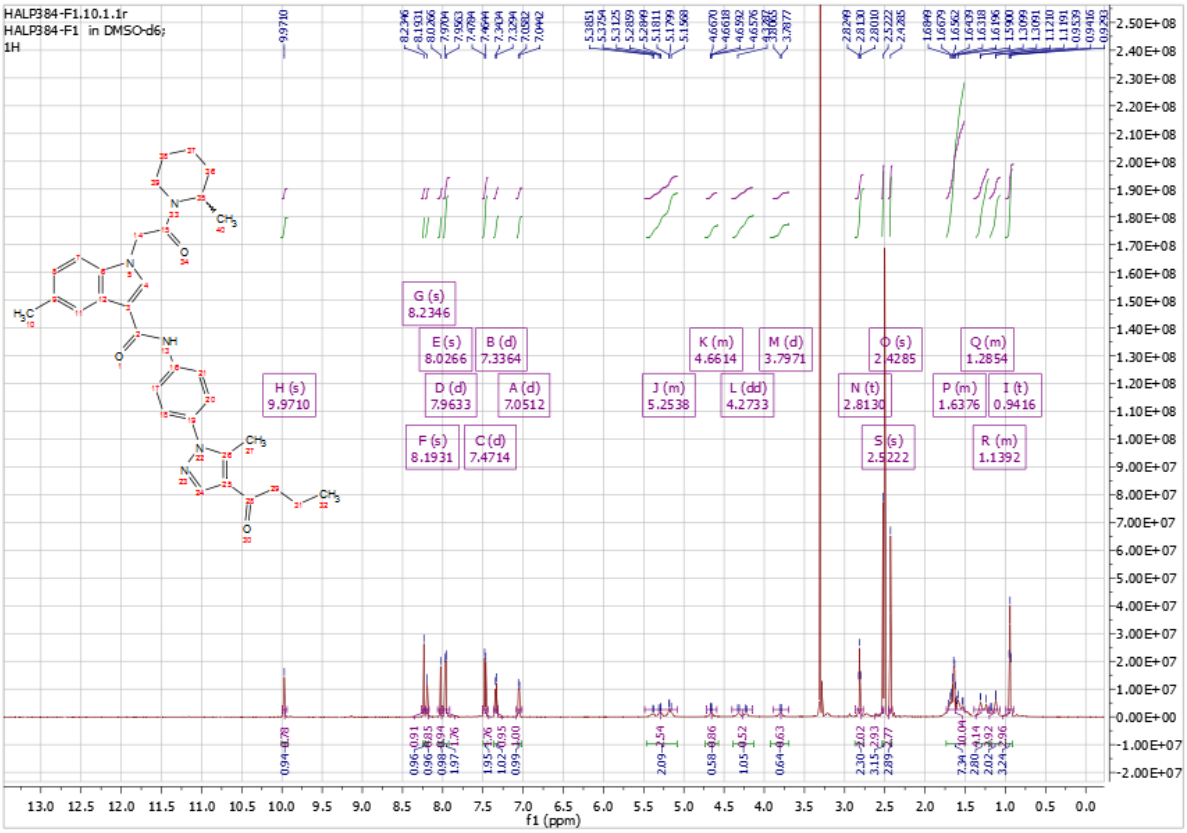
_N_-(4-(4-Butyryl-5-methyl-1_H_-pyrazol-1-yl)phenyl)-5-methyl-1-(2-(2-methylpiperidin-1-yl)-2-oxoethyl)-1_H_-indole-3-carboxamide (29)

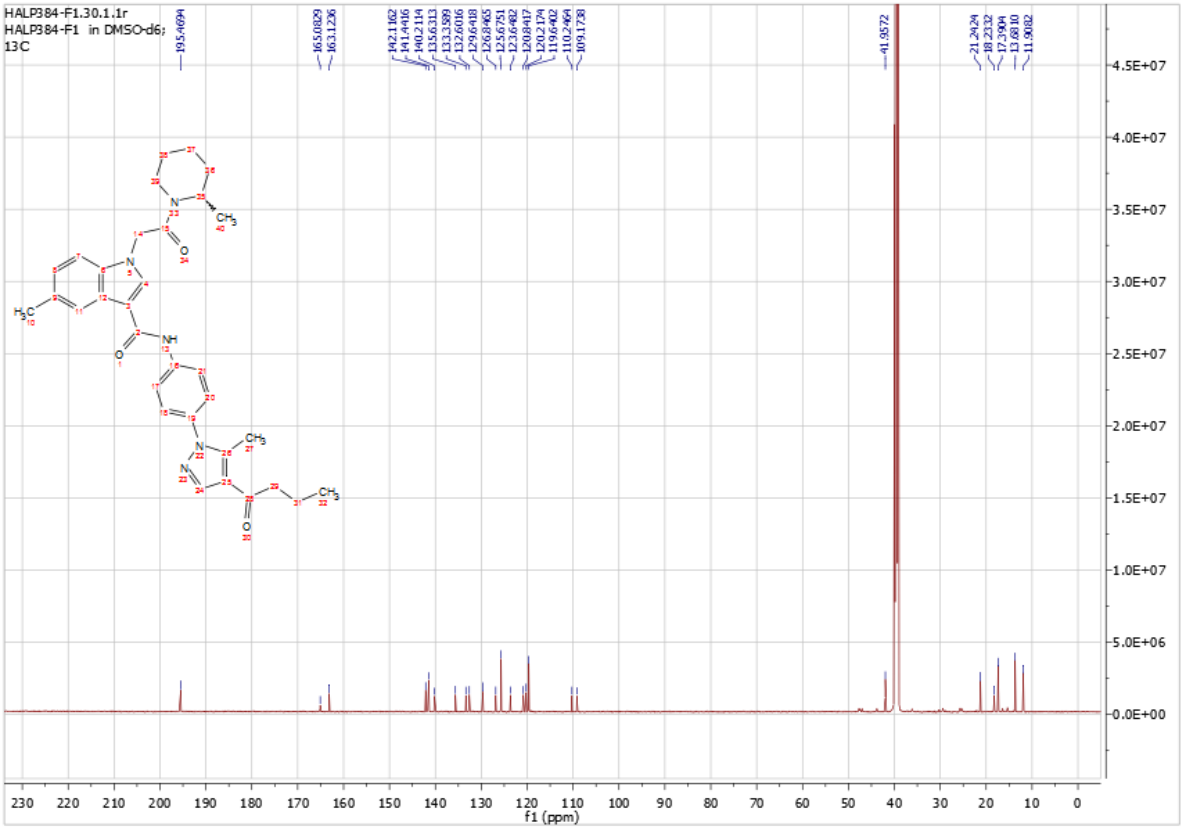
Sequence Name:	SingleSample		
Data file:	HALP384-F1.dx	**Project Name:**	Single Quad
Sample name:	HALP384-F1	**Operator :**	SYSTEM
Instrument:	Single Quad	**Acquired on:**	2024-05-23 14:50:24+02:00
Inj. volume:	3.000	**Location:**	P1-D6
Acq. method:	000-getauscht_Cwasser-Bacn_standard_100-1500_CB-20min.amx		
Processing method:	MS_standard_plot.pmx		



Signal: DAD1 Total WL (220.0:600.0 nm)

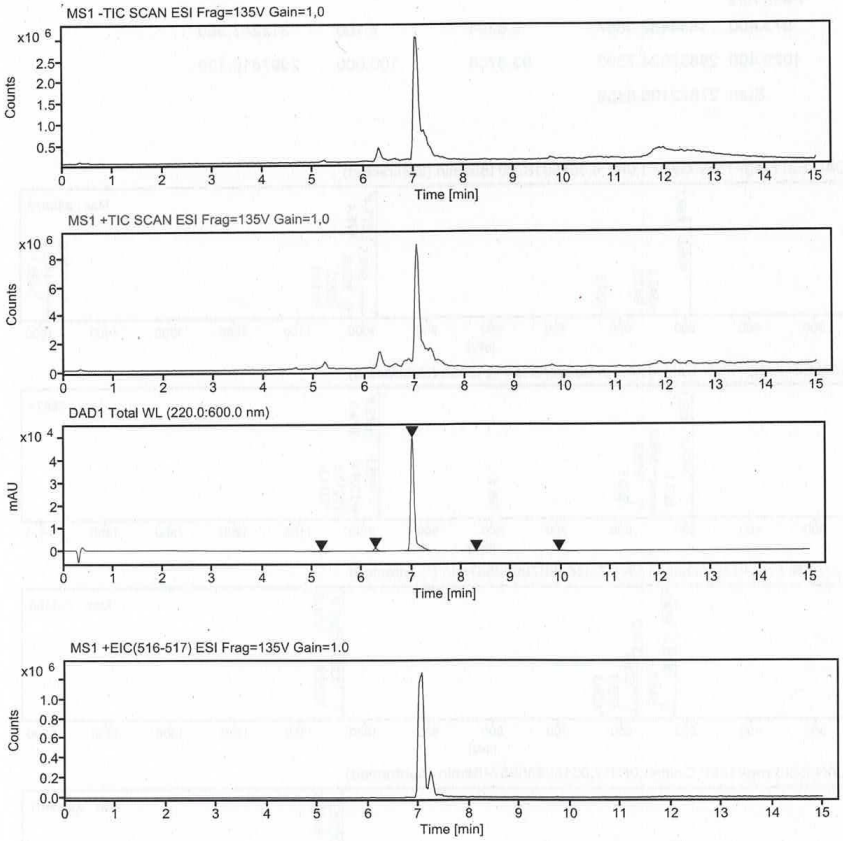
RT [min]	Peak MS Base Peak m/z	Area	Area%	Max Peak%	Height
8.458		166.3251	0.1691	0.173	33.897
8.888	538.400	96136.8980	97.7576	100.000	23087.383
9.119		1973.0951	2.0064	2.052	544.285
9.723		65.7748	0.0669	0.068	13.200
	Sum	98342.0929			


HALP384-F1.10.1.1r
HALP384-F1 in DMSO-d6;
1H
H (s)
9.9710
G (s)
8.2346
E (s)
8.0266
B (d)
7.3364
D (d)
7.9633
A (d)
7.0512
F (s)
8.1931
C (d)
7.4714
K (m)
4.6614
M (d)
3.7971
J (m)
5.2538
L (dd)
4.2733
O (s)
2.4285
N (t)
2.8130
S (s)
2.5222
Q (m)
1.2854
P (m)
1.6376
I (t)
0.9416
R (m)
1.1392
f1 (ppm)


HALP384-F1.30.1.1r
HALP384-F1 in DMSO-d6;
13C
f1 (ppm)

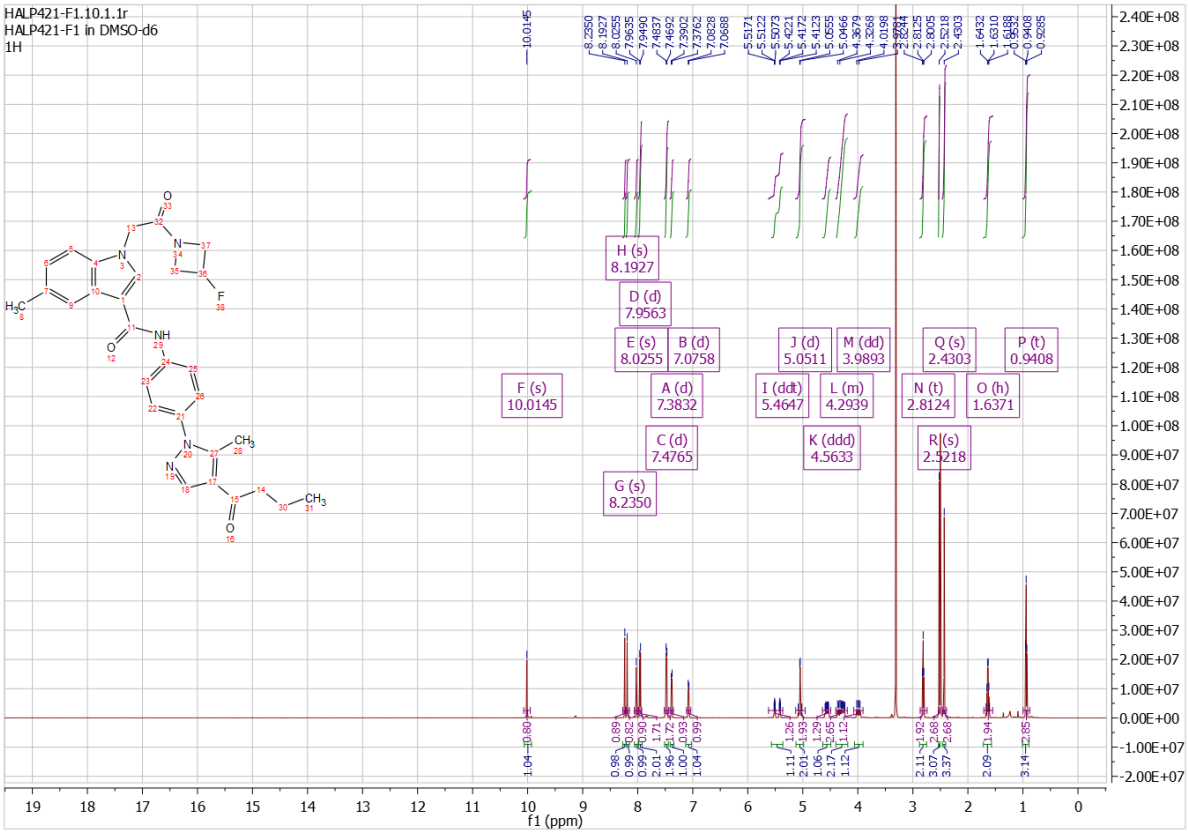
N-(4-(4-Butyryl-5-methyl-1*H*-pyrazol-1-yl)phenyl)-1-(2-(3-fluoroazetidin-1-yl)-2-oxoethyl)-5-methyl-1*H*-indole-3-carboxamide (30)

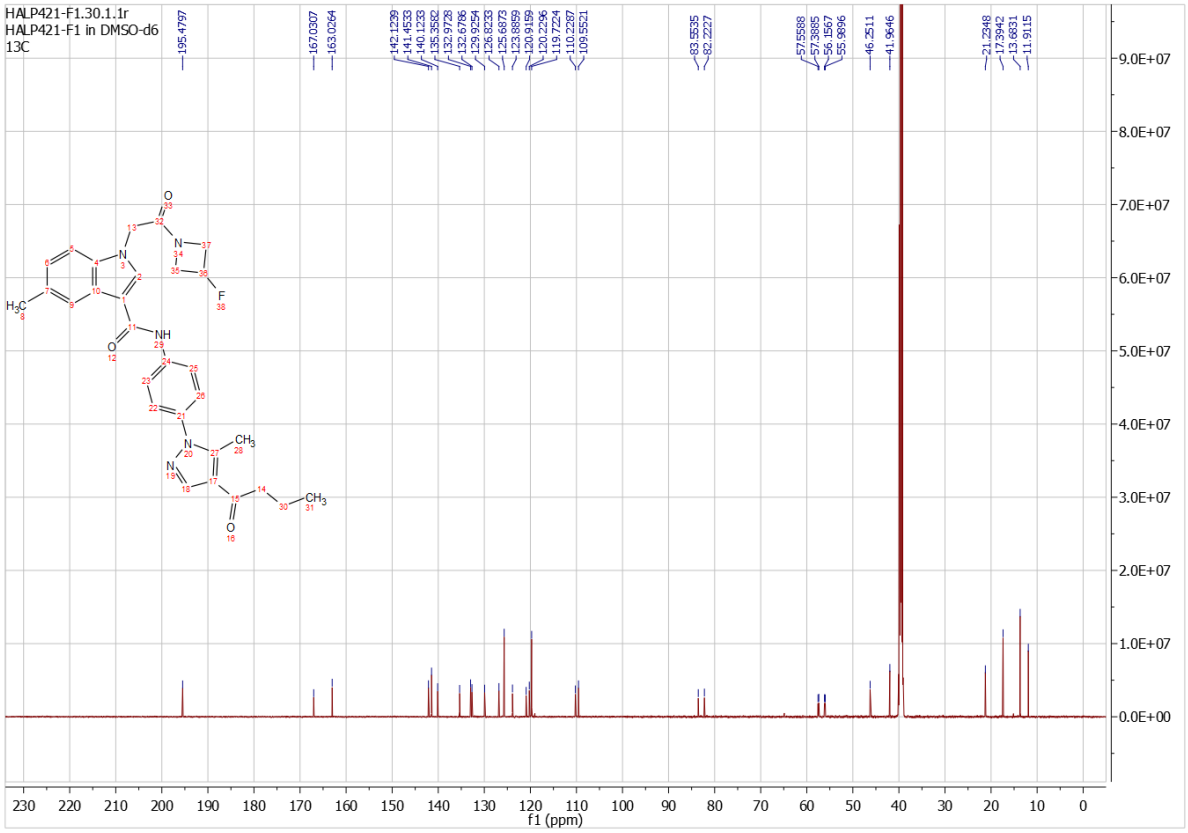
Sequence Name:	SingleSample		
Data file:	HALP421-F4.dx	**Project Name:**	Single Quad
Sample name:	HALP421-F4	**Operator :**	SYSTEM
Instrument:	Single Quad	**Acquired on:**	2024-09-30 10:16:49+02:00
Inj. volume:	8.000	**Location:**	P2-D6
Acq. method:	00-new_wasser-acn_standard_100-1500_BD-20min.amx		
Processing method:	*MS_standard_plot.pmx		



Signal: DAD1 Total WL (220.0:600.0 nm)

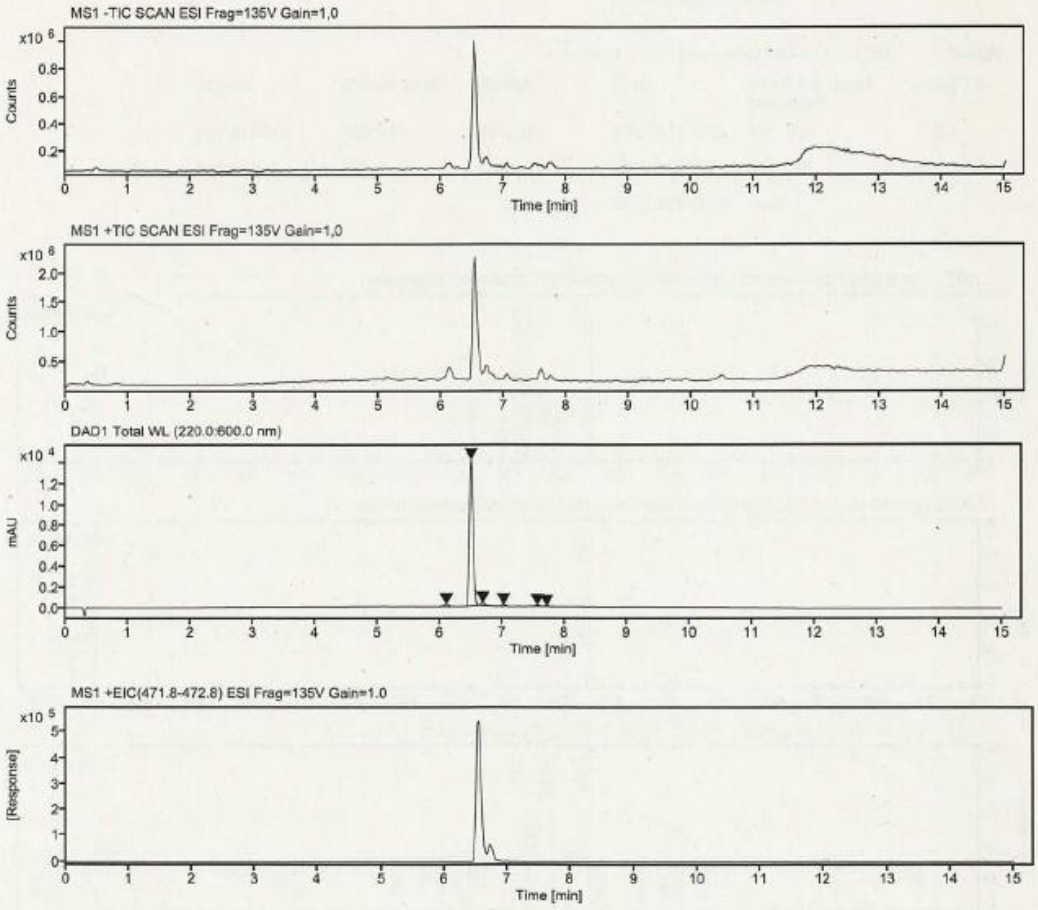
RT [min]	Peak MS Base Peak m/z	Area	Area%	Max Peak%	Height
5.184		561.0414	0.2027	0.208	110.287
6.272		6184.2321	2.2347	2.291	1211.888
7.015		269914.7431	97.5367	100.000	50452.572
8.299		43.6622	0.0158	0.016	2.643
9.963		27.7938	0.0100	0.010	7.742
	Sum	276731.4727			


HALP421-F1.10.1.1r
HALP421-F1 in DMSO-d6
1H
F (s) 10.0145
H (s) 8.1927
D (d) 7.9563
E (s) 8.0255
B (d) 7.0758
A (d) 7.3832
C (d) 7.4765
G (s) 8.2350
J (d) 5.0511
M (dd) 3.9893
I (ddt) 5.4647
L (m) 4.2939
K (ddd) 4.5633
Q (s) 2.4303
P (t) 0.9408
N (t) 2.8124
O (h) 1.6371
R (s) 2.5218
f1 (ppm)


HALP421-F1.30.1.1r
HALP421-F1 in DMSO-d6
13C
f1 (ppm)

_N_-(4-(4-Butyryl-5-methyl-1_H_-pyrazol-1-yl)phenyl)-5-methyl-1-(2-(methylamino)-2-oxoethyl)-1_H_-indole-3-carboxamide (31)

Sequence Name:	SingleSample		
Data file:	HALP272.dx	**Project Name:**	Single Quad
Sample name:	HALP272	**Operator :**	SYSTEM
Instrument:	Single Quad	**Acquired on:**	2023-05-22 13:56:13+02:00
Inj. volume:	2.000	**Location:**	P1-C3
Acq. method:	00-new_wasser-acn_standard_100-1000_BD-20min.amx		
Processing method:	MS_standard_plot.pmx		



Signal: DAD1 Total WL (220.0:600.0 nm)

RT [min]	Peak MS Base Peak m/z	Area	Area%	Max Peak%	Height
6.109		1026.1386	1.6493	1.752	219.332
6.506		58565.0766	94.1284	100.000	14244.681
6.692		1059.3908	1.7027	1.809	284.032
7.025		601.6043	0.9669	1.027	174.537
7.569		658.8649	1.0590	1.125	140.138
7.717		307.2267	0.4938	0.525	73.209

D:\CDSProjects\Default\00-standardplot+EIC.rdl [Rev. 5252] Printed: 2023-05-23 06:35:58+02:00 Page 1 of 2

RT [min]	Peak MS Base Peak m/z	Area	Area%	Max Peak%	Height
	Sum	62218.3019			

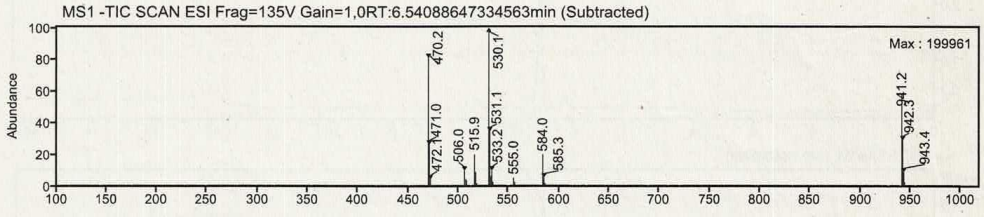
Signal: MS1 +TIC SCAN ESI Frag=135V Gain=1,0

RT [min]	Peak MS Base Peak m/z	Area	Area%	Max Peak%	Height
6.542	943.300	9621400.6606	98.3523	100.000	2028276.316
6.728	472.000	161184.4338	1.6477	1.675	106541.408
	Sum	9782585.0944			

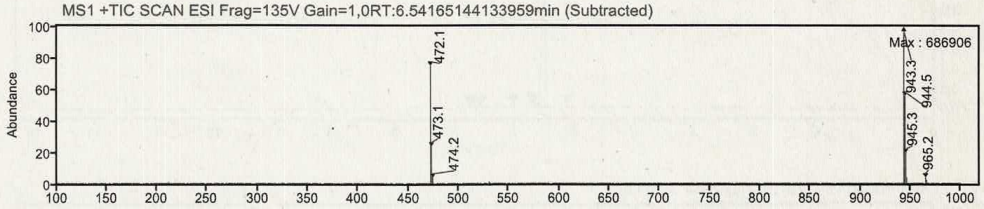
Signal: MS1 -TIC SCAN ESI Frag=135V Gain=1,0

RT [min]	Peak MS Base Peak m/z	Area	Area%	Max Peak%	Height
6.541	530.100	4390172.7608	96.3198	100.000	940645.481
6.724	470.100	167741.9542	3.6802	3.821	44813.499
	Sum	4557914.7150			

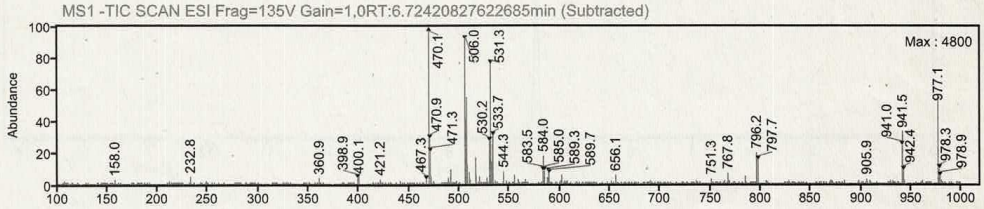
MS1 -TIC SCAN ESI Frag=135V Gain=1,0RT:6.54088647334563min (Subtracted)



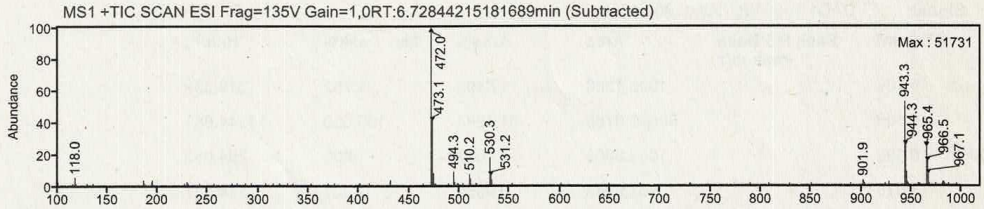
MS1 +TIC SCAN ESI Frag=135V Gain=1,0RT:6.54165144133959min (Subtracted)



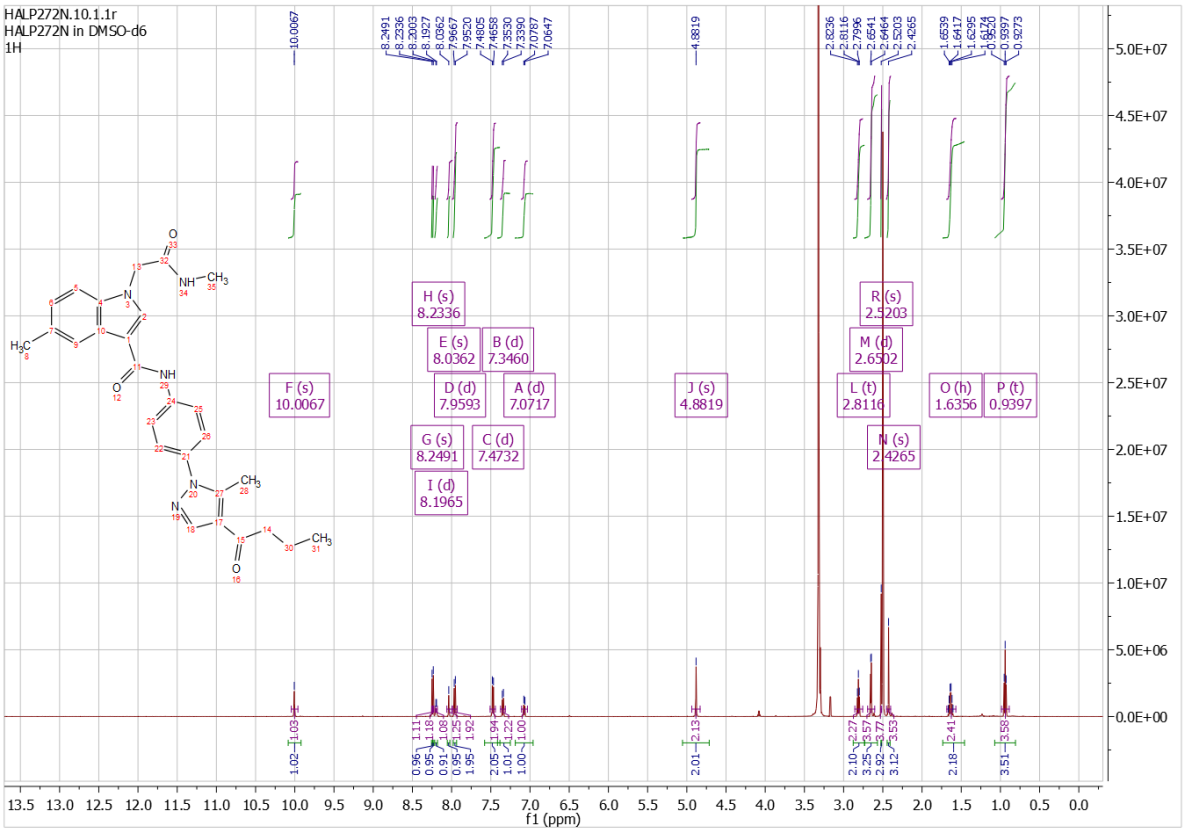
MS1 -TIC SCAN ESI Frag=135V Gain=1,0RT:6.72420827622685min (Subtracted)

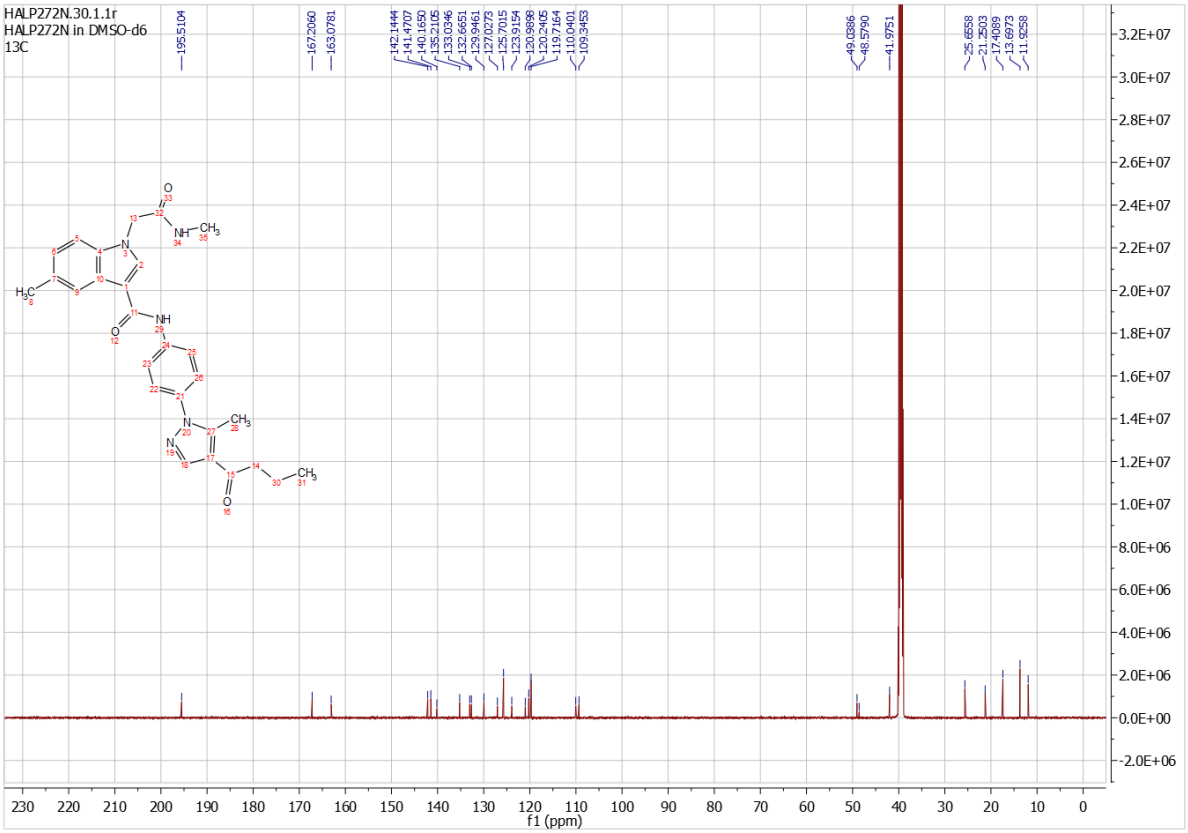


MS1 +TIC SCAN ESI Frag=135V Gain=1,0RT:6.72844215181689min (Subtracted)



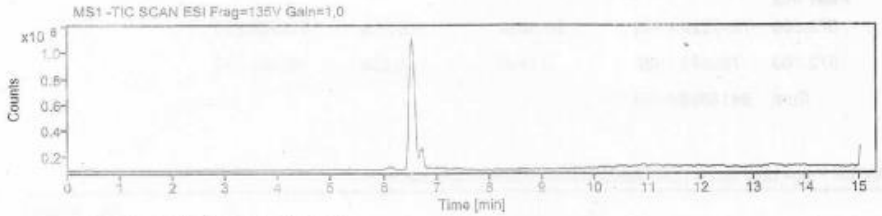
D:\CDSProjects\Default\00-standardplot+EIC.rdl [Rev. 5252] Printed: 2023-05-23 06:35:58+02:00 Page 2 of 2

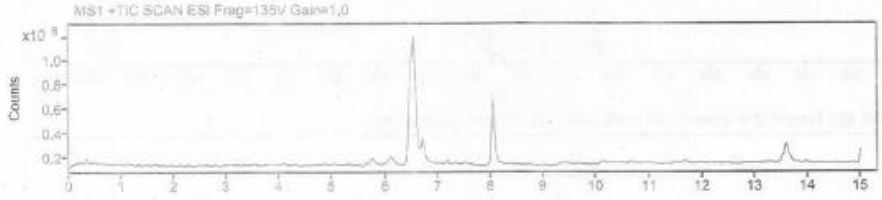

HALP272N.10.1.1r
HALP272N in DMSO-d6
1H
F (s) 10.0067
H (s) 8.2336
E (s) 8.0362
B (d) 7.3460
D (d) 7.9593
A (d) 7.0717
G (s) 8.2491
C (d) 7.4732
I (d) 8.1965
J (s) 4.8819
R (s) 2.5203
M (d) 2.6502
L (t) 2.8116
N (s) 2.4265
O (h) 1.6356
P (t) 0.9397
f1 (ppm)

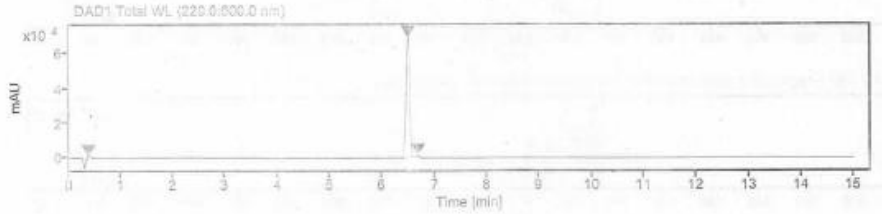

HALP272N.30.1.1r
HALP272N in DMSO-d6
13C
f1 (ppm)

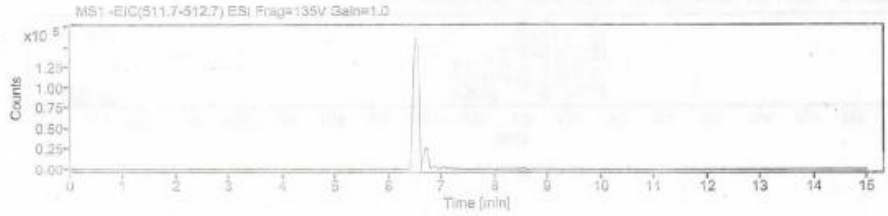
_N_-(4-(4-Butyryl-5-methyl-1_H_-pyrazol-1-yl)phenyl)-1-(2-(3-hydroxyazetidin-1-yl)-2-oxoethyl)-5-methyl-1_H_-indole-3-carboxamide (32)

Sequence Name:	SingleSample		
Data file:	HALP381-F1.dx	Project Name:	Single Quad
Sample name:	HALP381-F1	Operator :	SYSTEM
Instrument:	Single Quad	Acquired on:	2024-05-22 12:26:29+02:00
Inj. volume:	8.000	Location:	P1-A11
Acq. method:	000-getauscht_Cwasser-Bacn_standard_100-1500_CB-20min.amx		
Processing method:	MS_standard_plot.pmx		



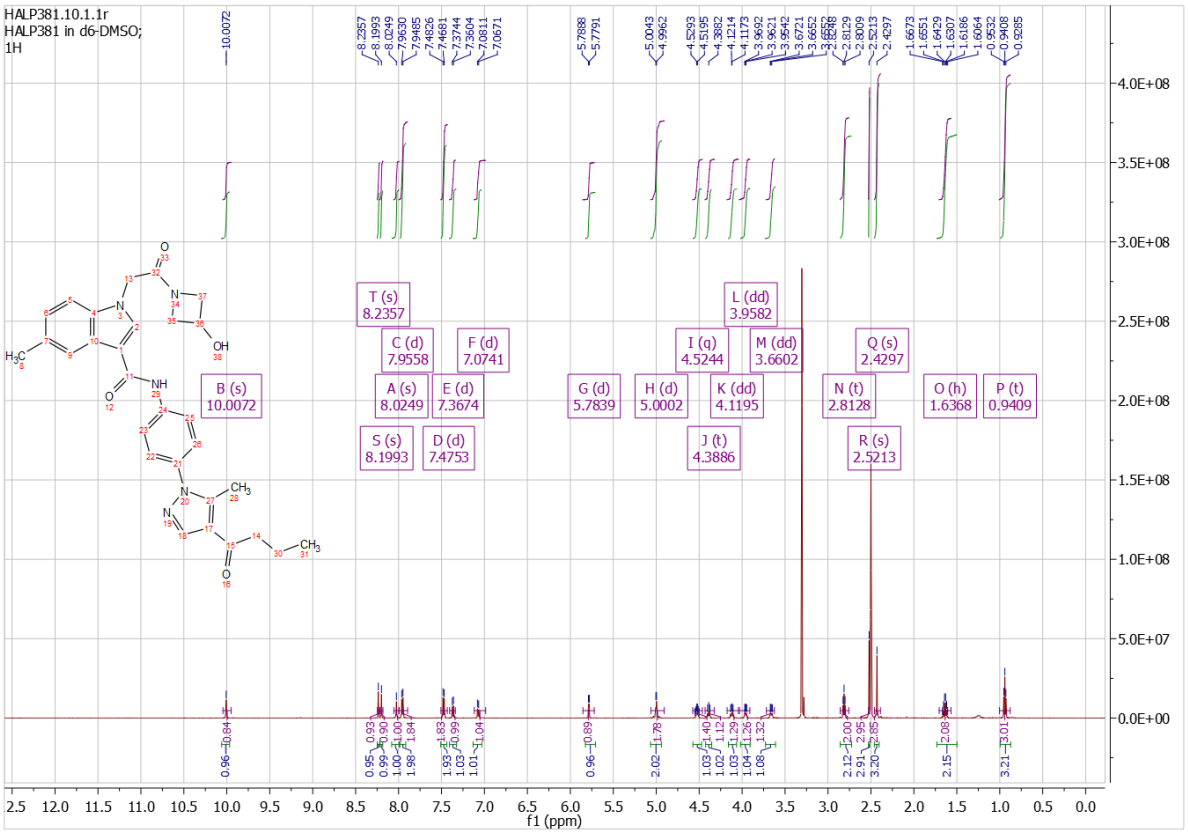


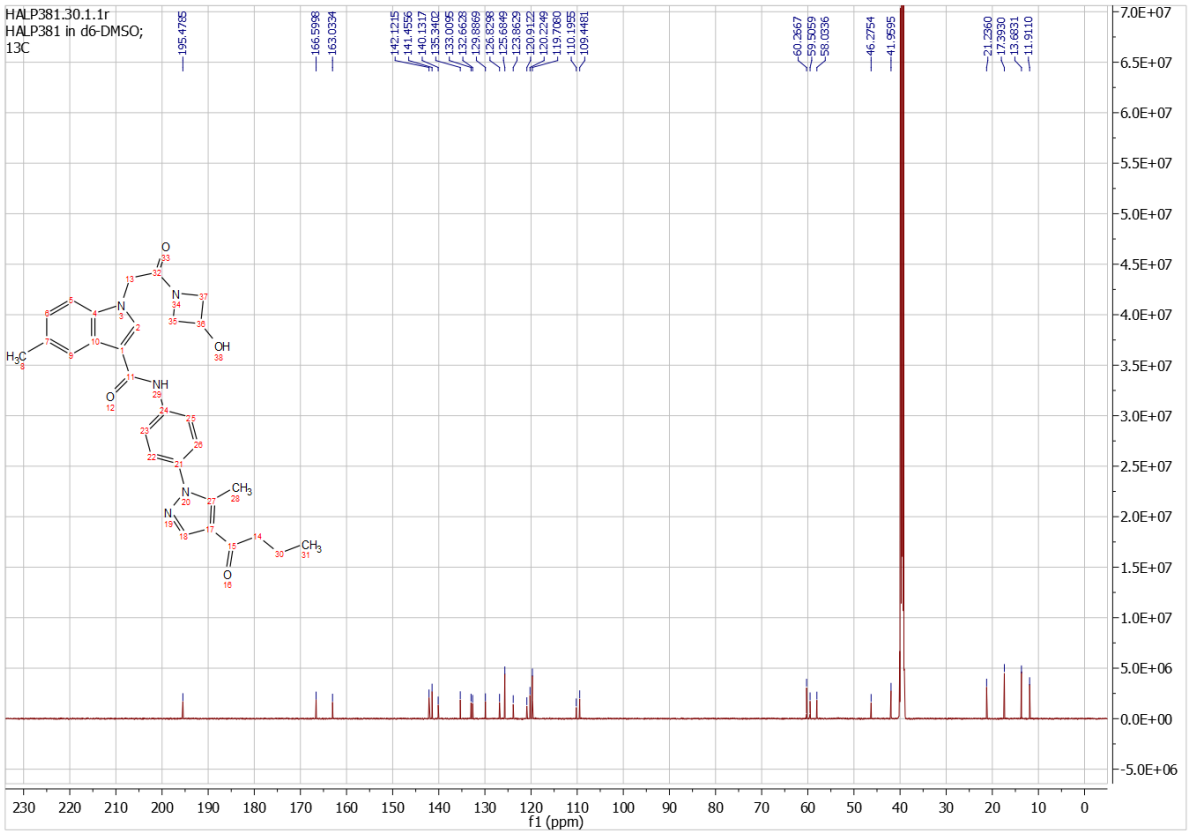




Signal: DAD1 Total WL (220.0:600.0 nm)

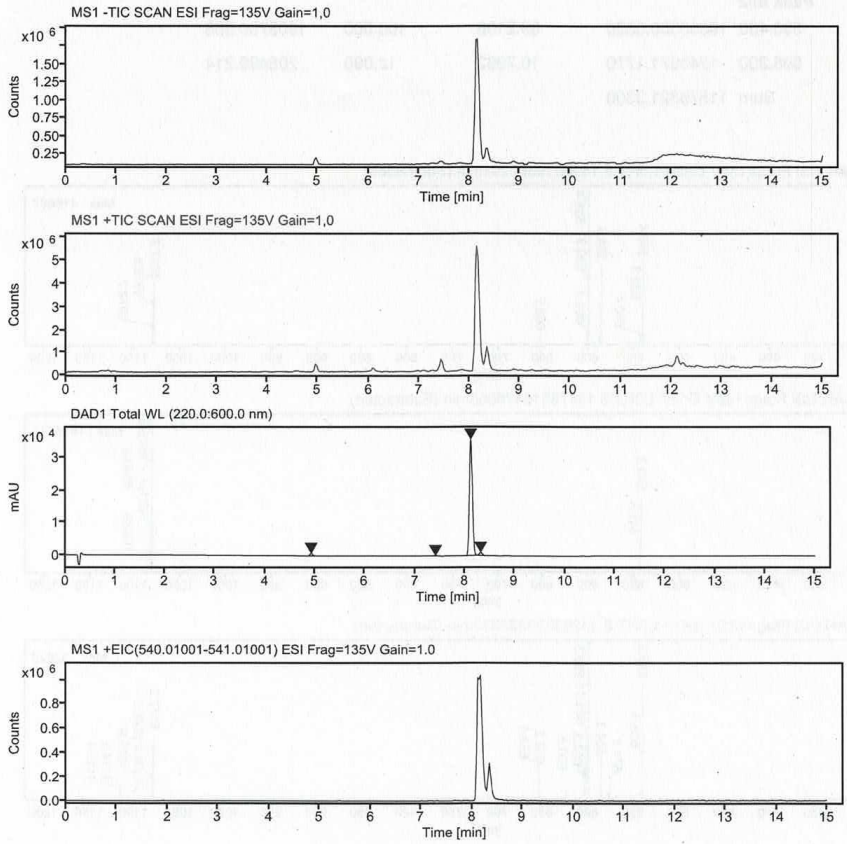
RT [min]	Peak MS Base Peak m/z	Area	Area%	Max Peak%	Height
0.384		2369.3721	0.6971	0.714	556.155
6.493	572.800	331995.6620	97.6740	100.000	69753.050
6.677		5536.7374	1.6289	1.668	1479.755
	Sum	339901.7715			


HALP381.10.1.1r
HALP381 in d6-DMSO;
1H
T (s)
8.2357
C (d)
7.9558
F (d)
7.0741
B (s)
10.0072
A (s)
8.0249
E (d)
7.3674
G (d)
5.7839
H (d)
5.0002
I (q)
4.5244
K (dd)
4.1195
L (dd)
3.9582
M (dd)
3.6602
N (t)
2.8128
Q (s)
2.4297
O (h)
1.6368
P (t)
0.9409
S (s)
8.1993
D (d)
7.4753
J (t)
4.3886
R (s)
2.5213
f1 (ppm)


HALP381.30.1.1r
HALP381 in d6-DMSO;
13C
f1 (ppm)

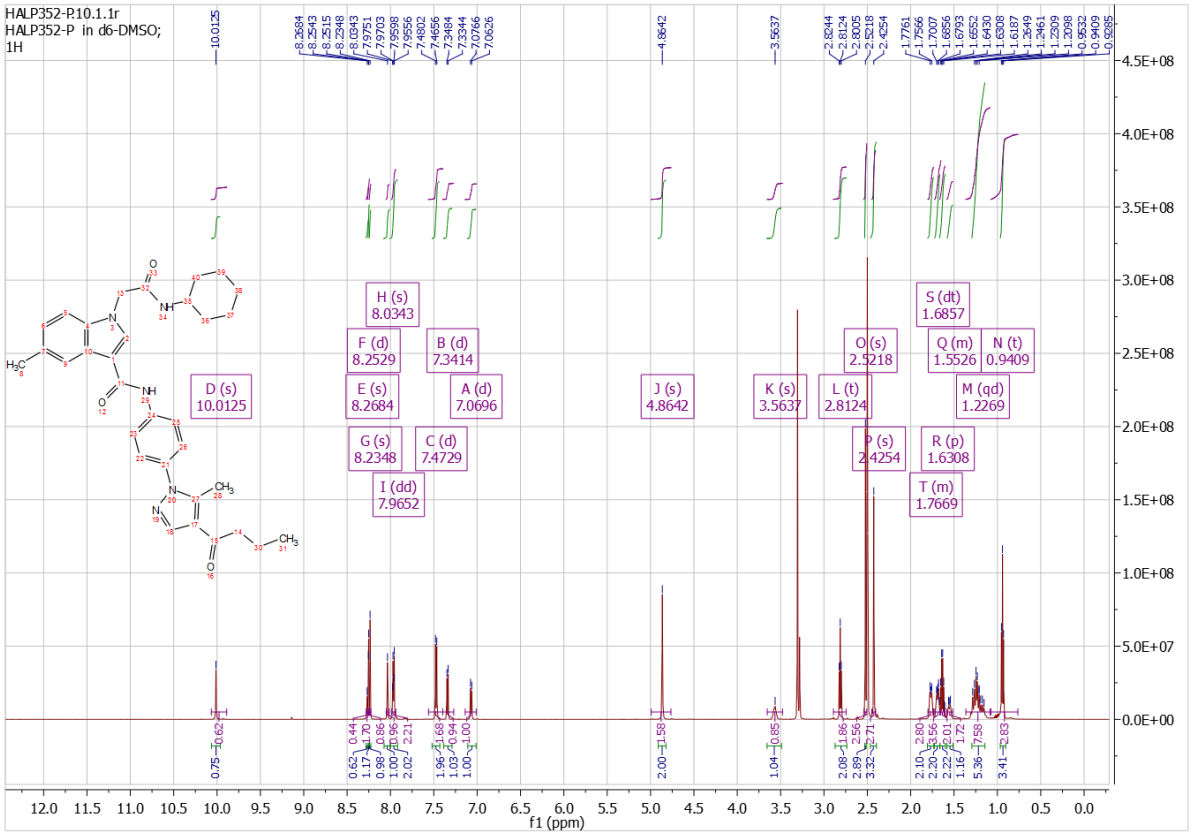
_N_-(4-(4-Butyryl-5-methyl-1_H_-pyrazol-1-yl)phenyl)-1-(2-(cyclohexylamino)-2-oxoethyl)-5-methyl-1_H_-indole-3-carboxamide (33)

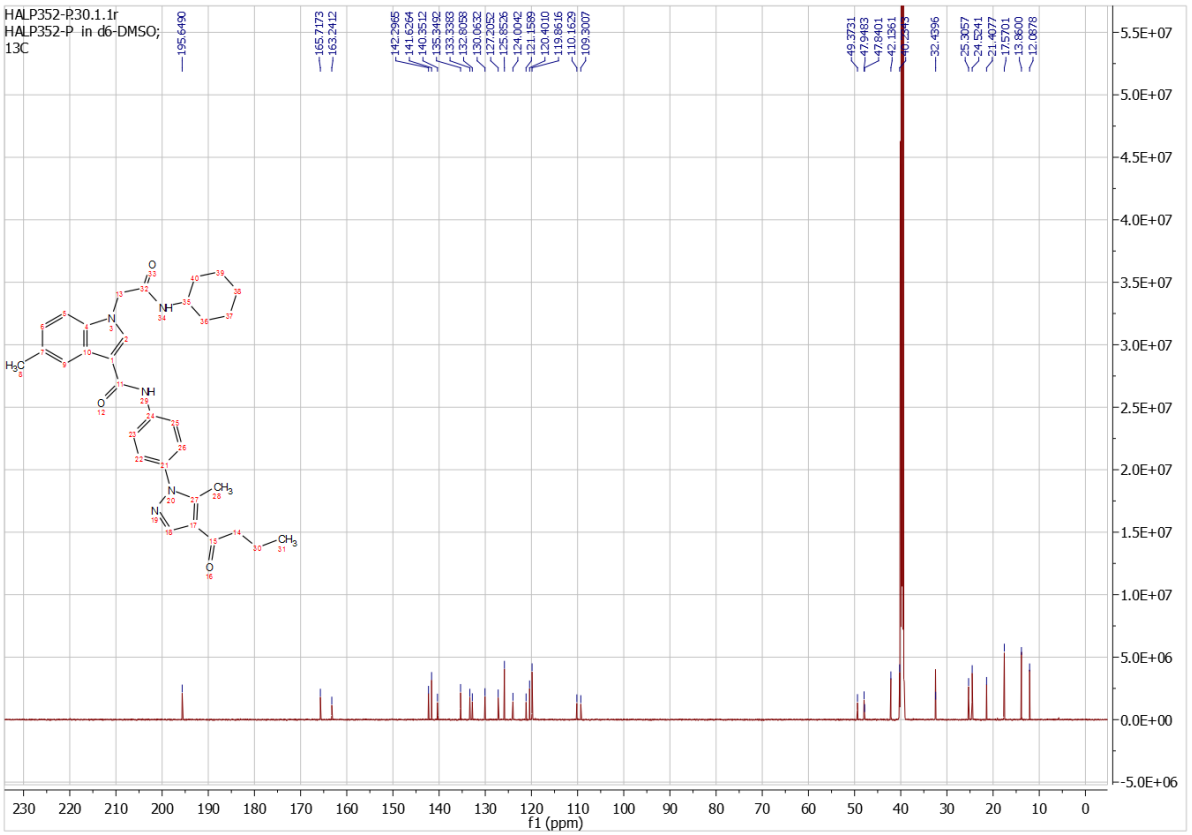
Sequence Name:	SingleSample		
Data file:	HALP352-P.dx	**Project Name:**	Single Quad
Sample name:	HALP352-P	**Operator :**	SYSTEM
Instrument:	Single Quad	**Acquired on:**	2024-02-19 16:48:05+01:00
Inj. volume:	4.000	**Location:**	P2-F10
Acq. method:	00-new_wasser-acn_standard_100-1500_BD-20min.amx		
Processing method:	MS_standard_plot.pmx		



Signal: DAD1 Total WL (220.0:600.0 nm)

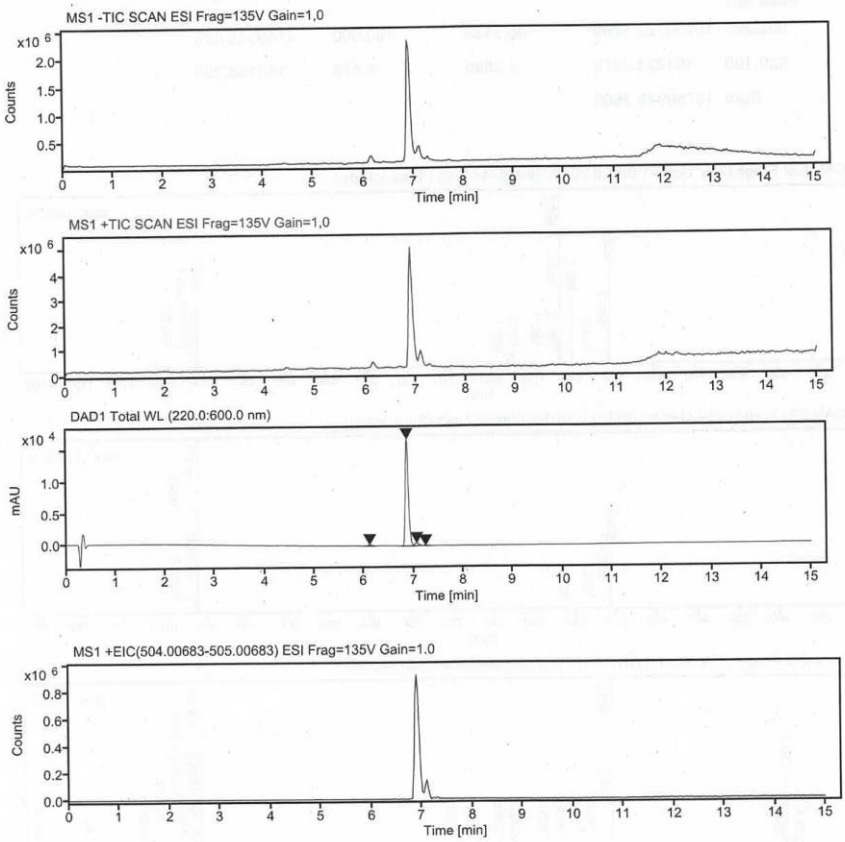
RT [min]	Peak MS Base Peak m/z	Area	Area%	Max Peak%	Height
4.928		2606.8983	1.6687	1.750	736.749
7.413		966.6549	0.6188	0.649	117.919
8.119		148942.4606	95.3381	100.000	35933.722
8.315		3709.4493	2.3744	2.491	947.151
	Sum	156225.4630			


HALP352-P.10.1.1r
HALP352-P in d6-DMSO;
1H
H (s) 8.0343
F (d) 8.2529
B (d) 7.3414
E (s) 8.2684
A (d) 7.0696
G (s) 8.2348
C (d) 7.4729
I (dd) 7.9652
D (s) 10.0125
J (s) 4.8642
K (s) 3.5637
L (t) 2.8124
O (s) 2.5218
P (s) 2.4254
S (dt) 1.6857
Q (m) 1.5526
N (t) 0.9409
R (p) 1.6308
M (qd) 1.2269
T (m) 1.7669
f1 (ppm)


HALP352-P.30.1.1r
HALP352-P in d6-DMSO;
13C
f1 (ppm)

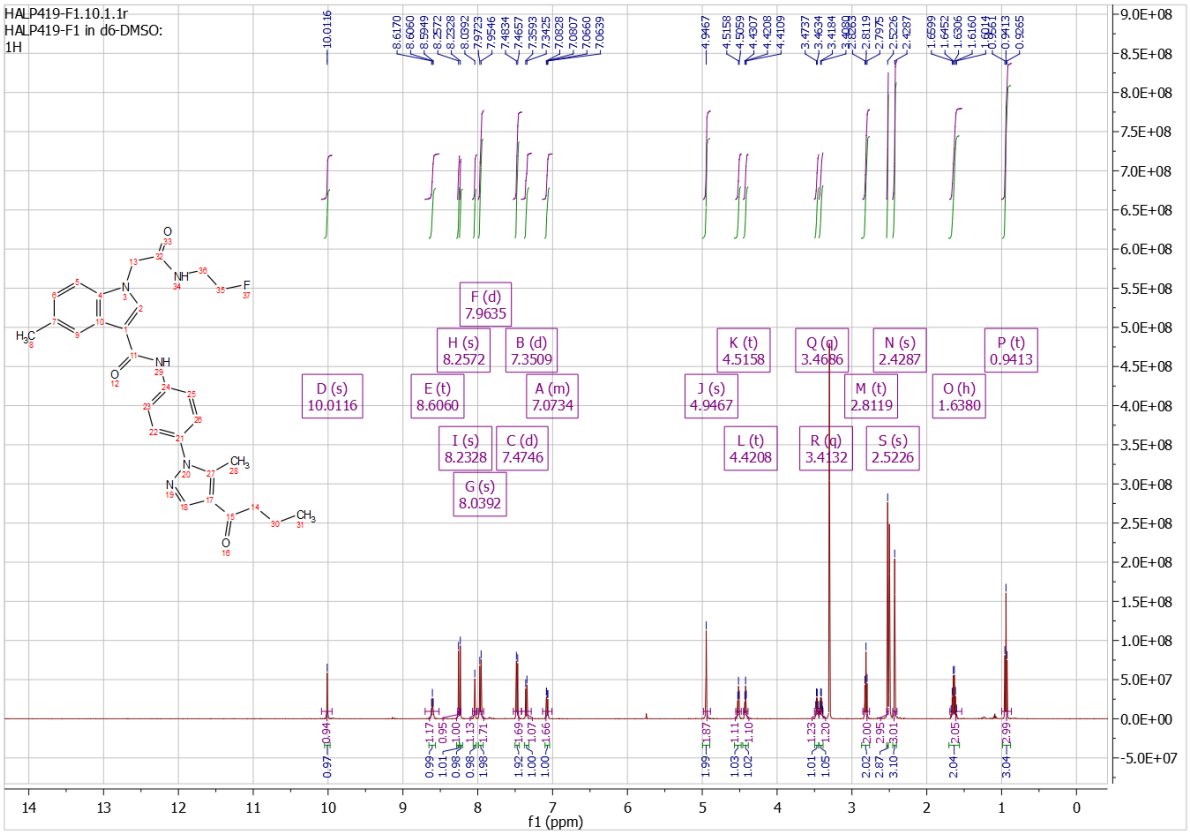
_N_-(4-(4-Butyryl-5-methyl-1_H_-pyrazol-1-yl)phenyl)-1-(2-((2-fluoroethyl)amino)-2-oxoethyl)-5-methyl-1_H_-indole-3-carboxamide (34)

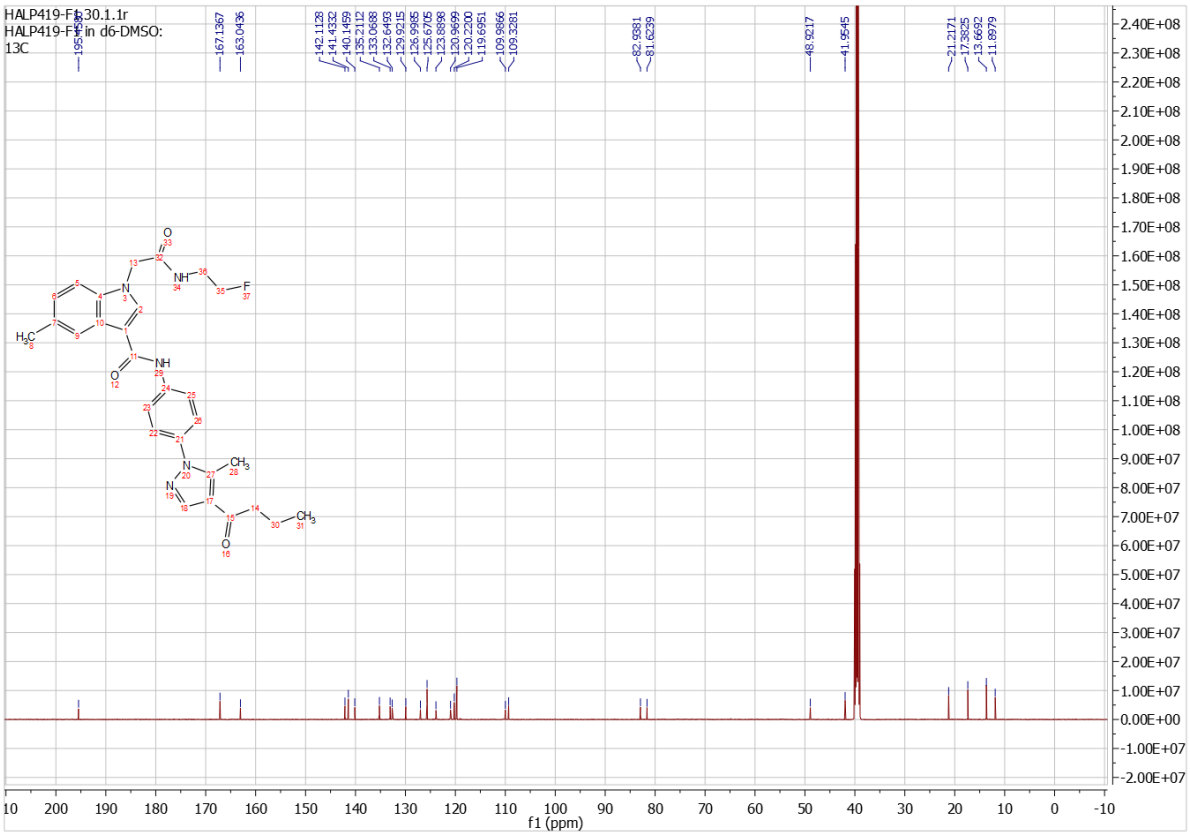
Sequence Name:	SingleSample		
Data file:	HALP419-F1.dx	**Project Name:**	Single Quad
Sample name:	HALP419-F1	**Operator :**	SYSTEM
Instrument:	Single Quad	**Acquired on:**	2024-10-04 07:21:34+02:00
Inj. volume:	2.000	**Location:**	P1-C3
Acq. method:	00-new_wasser-acn_standard_100-1500_BD-20min.amx		
Processing method:	MS_standard_plot.pmx		



Signal: DAD1 Total WL (220.0:600.0 nm)

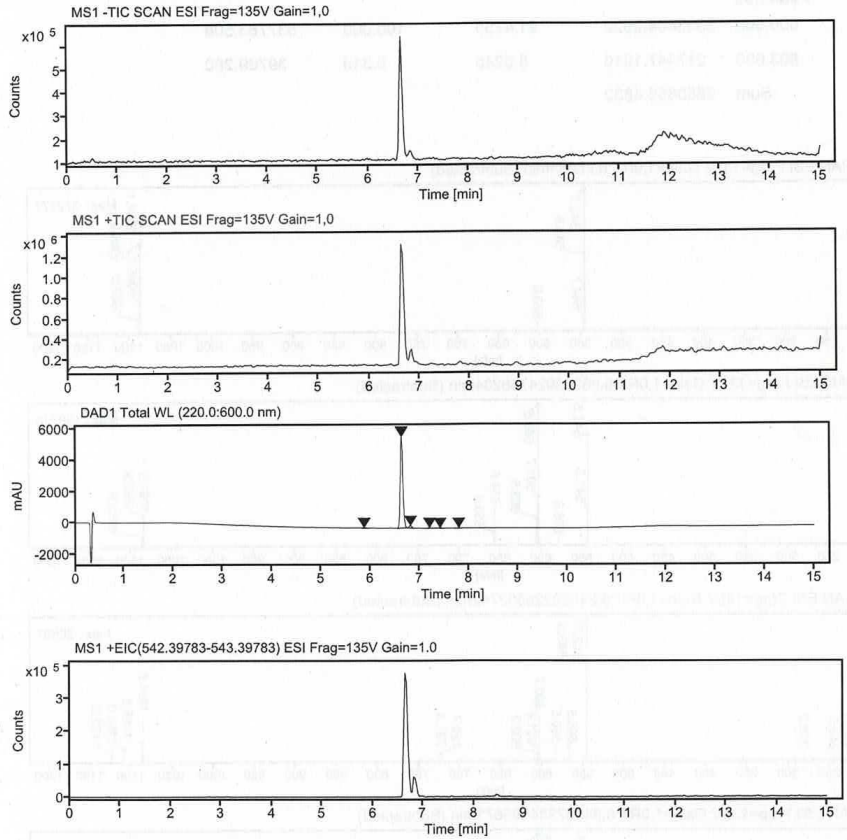
RT [min]	Peak MS Base Peak m/z	Area	Area%	Max Peak%	Height
6.115		834.3610	1.0584	1.107	194.589
6.870		75346.4960	95.5761	100.000	16967.854
7.066		2413.1621	3.0611	3.203	489.895
7.244		240.0406	0.3045	0.319	63.297
	Sum	78834.0597			


HALP419-F1.10.1.1r
HALP419-F1 in d6-DMSO:
1H
F (d)
7.9635
H (s)
8.2572
B (d)
7.3509
K (t)
4.5158
Q (q)
3.4636
N (s)
2.4287
P (t)
0.9413
D (s)
10.0116
E (t)
8.6060
A (m)
7.0734
J (s)
4.9467
M (t)
2.8119
O (h)
1.6380
I (s)
8.2328
C (d)
7.4746
L (t)
4.4208
R (q)
3.4132
S (s)
2.5226
G (s)
8.0392
f1 (ppm)


HALP419-F1.30.1.1r
HALP419-F1 in d6-DMSO:
13C
f1 (ppm)

N-(4-(4-Butyryl-5-methyl-1*H*-pyrazol-1-yl)phenyl)-1-(2-(3-hydroxypiperidin-1-yl)-2-oxoethyl)-5-methyl-1*H*-indole-3-carboxamide (35)

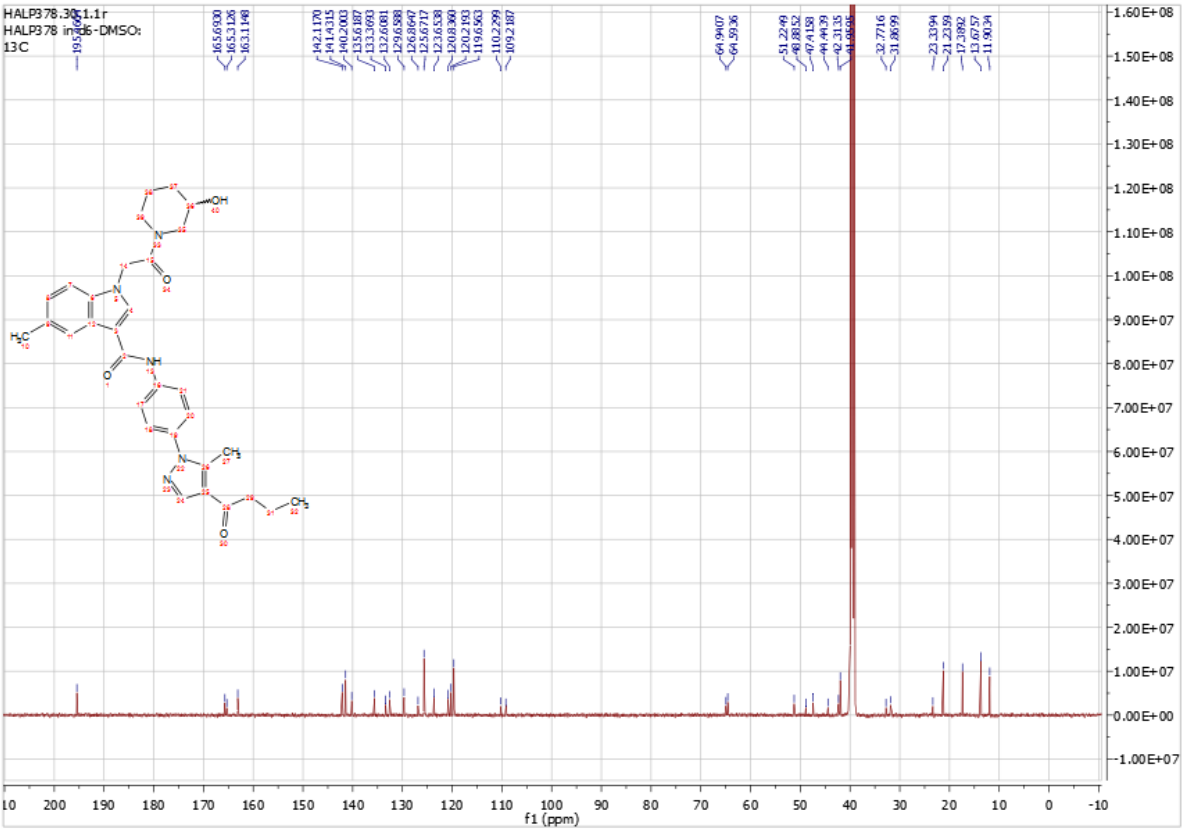
Sequence Name:	SingleSample		
Data file:	HALP378.dx	**Project Name:**	Single Quad
Sample name:	HALP378	**Operator :**	SYSTEM
Instrument:	Single Quad	**Acquired on:**	2024-03-18 12:03:53+01:00
Inj. volume:	2.000	**Location:**	P1-A6
Acq. method:	00-new_wasser-acn_standard_100-1500_BD-20min.amx		
Processing method:	MS_standard_plot.pmx		



Signal: DAD1 Total WL (220.0:600.0 nm)

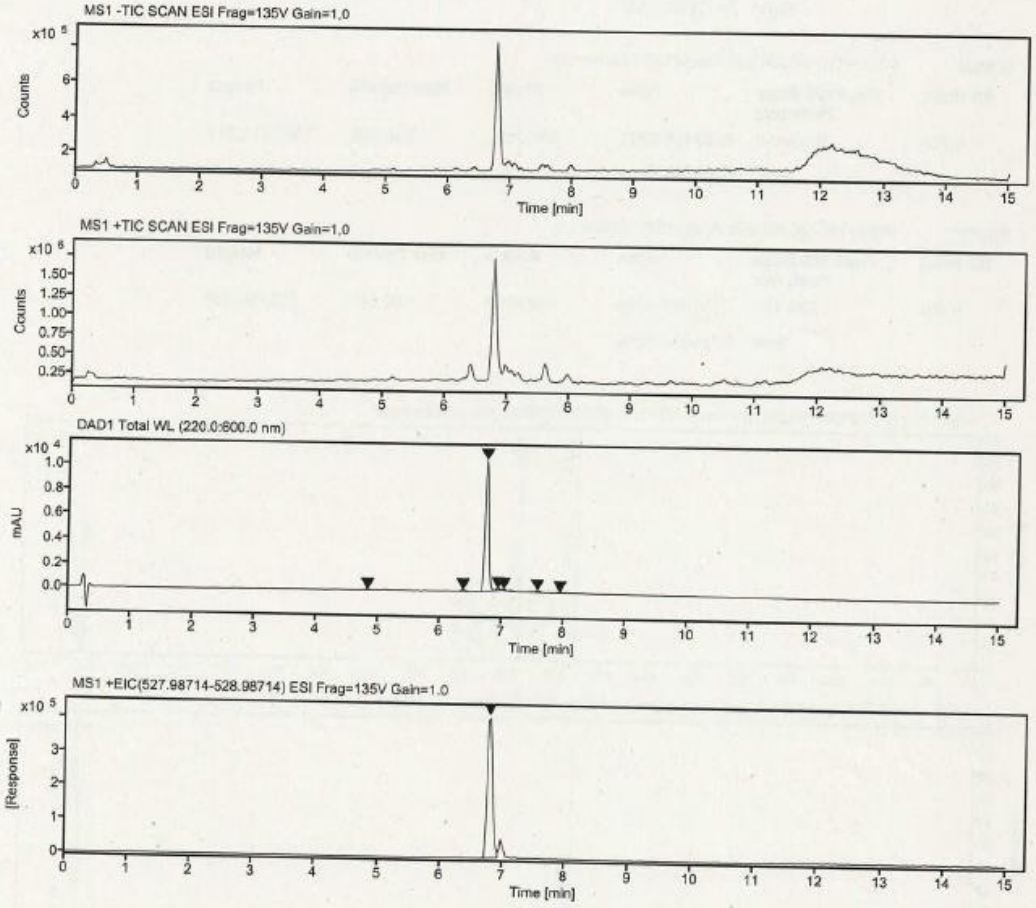
RT [min]	Peak MS Base Peak m/z	Area	Area%	Max Peak%	Height
5.865		47.5520	0.2081	0.214	8.400
6.629		22185.6316	97.0805	100.000	5820.189
6.809		499.0815	2.1839	2.250	142.761
7.194		55.3281	0.2421	0.249	13.174
7.407		23.3744	0.1023	0.105	5.663
7.787		41.8555	0.1832	0.189	9.479
	Sum	22852.8230			


HALP378.10.1.1r
HALP378 in d6-DMSO:
1H
D (s)
9.9736
E (d)
7.9622
B (d)
8.1837
F (d)
7.4711
A (s)
8.0279
G (t)
7.3327
C (s)
8.2321
H (d)
7.0445
B1 (dd)
4.9550
A1 (s)
5.2630
X (m)
3.6114
U (m)
3.1611
Q (s)
2.4276
L (h)
1.6382
V (dd)
3.4079
R (s)
2.5222
I (m)
1.7827
P (t)
0.9416
W (m)
3.4891
T (t)
2.8120
N (m)
1.4173
Y (d)
3.7517
f1 (ppm)


HALP378.30.1.1r
HALP378 in d6-DMSO:
13C
f1 (ppm)

_N_-(4-(4-Butyryl-5-methyl-1_H_-pyrazol-1-yl)phenyl)-5-methyl-1-(2-morpholino-2-oxoethyl)-1_H_-indole-3-carboxamide (36)

Sequence Name:	SingleSample		
Data file:	HALP274.dx	**Project Name:**	Single Quad
Sample name:	HALP274	**Operator :**	SYSTEM
Instrument:	Single Quad	**Acquired on:**	2023-05-23 07:34:55+02:00
Inj. volume:	5.000	**Location:**	P1-E4
Acq. method:	00-new_wasser-acn_standard_100-1500_BD-20min.amx		
Processing method:	MS_standard_plot.pmx		



Signal: DAD1 Total WL (220.0:600.0 nm)

RT [min]	Peak MS Base Peak m/z	Area	Area%	Max Peak%	Height
4.840		171.9260	0.3552	0.381	61.712
6.382		576.6378	1.1915	1.277	128.540
6.754	1055.400	45149.5705	93.2908	100.000	10615.347
6.944		610.4868	1.2614	1.352	189.592
7.041		587.9253	1.2148	1.302	121.239
7.585		947.0620	1.9569	2.098	172.869

D:\CDSProjects\Default\00-standardplot+EIC.rdl [Rev. 5269] Printed: 2023-05-23 08:40:48+02:00 Page 1 of 2

RT [min]	Peak MS Base Peak m/z	Area	Area%	Max Peak%	Height
7.948		353.0077	0.7294	0.782	75.212
	Sum	48396.6160			

Signal: MS1 +EIC(527.98714-528.98714) ESI Frag=135V Gain=1.0

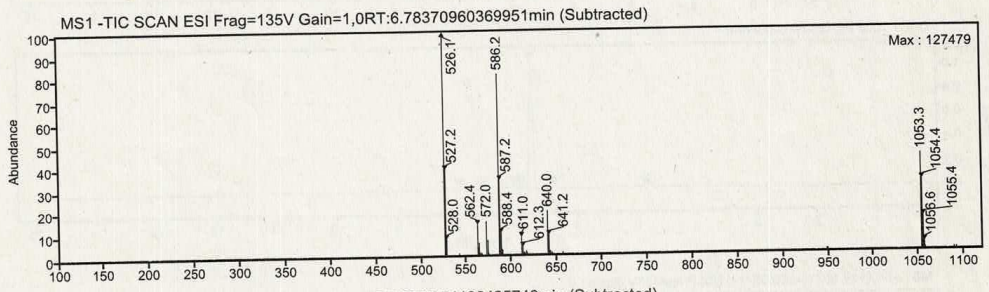
RT [min]	Peak MS Base Peak m/z	Area	Area%	Max Peak%	Height
6.779	1055.400	2465995.7200	100.0000	100.000	425298.432
	Sum	2465995.7200			

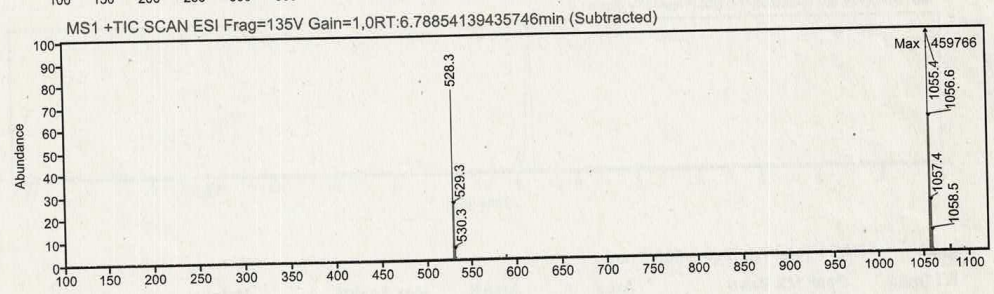
Signal: MS1 +TIC SCAN ESI Frag=135V Gain=1,0

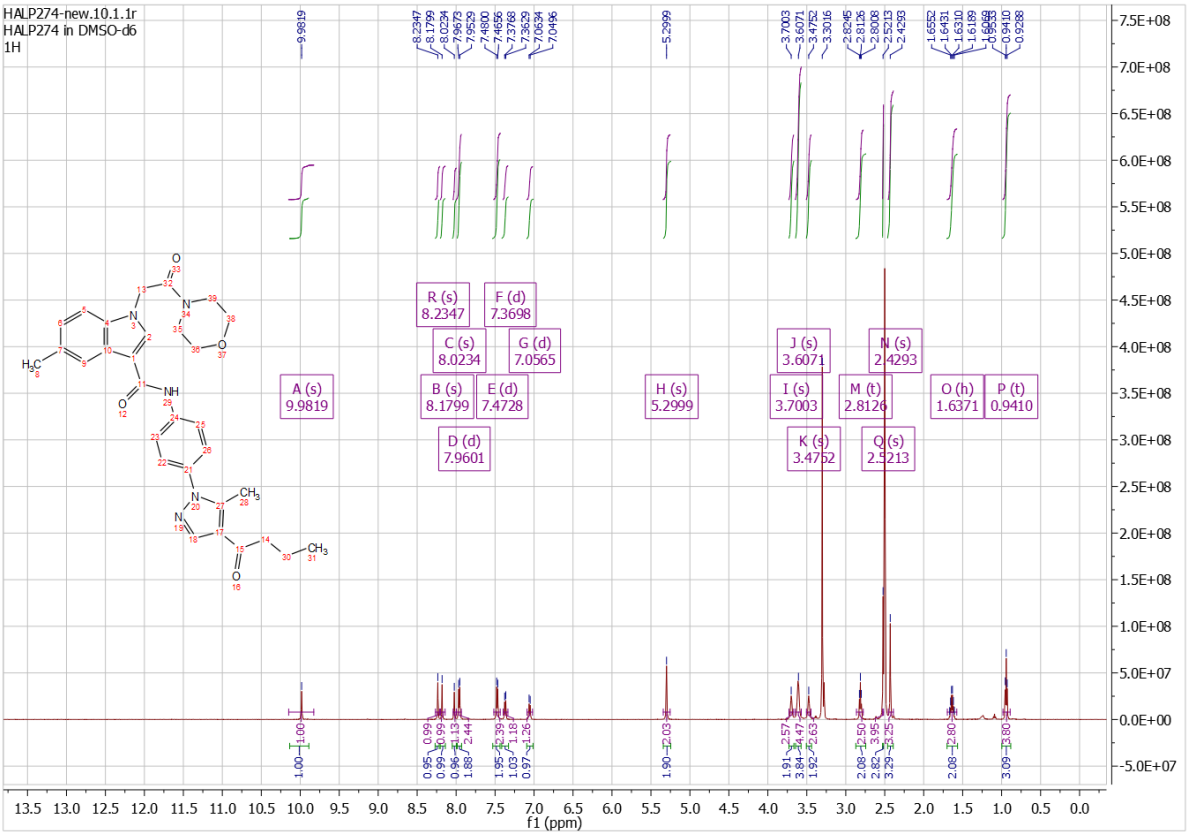
RT [min]	Peak MS Base Peak m/z	Area	Area%	Max Peak%	Height
6.789	1055.400	8063438.6711	100.0000	100.000	1559211.216
	Sum	8063438.6711			

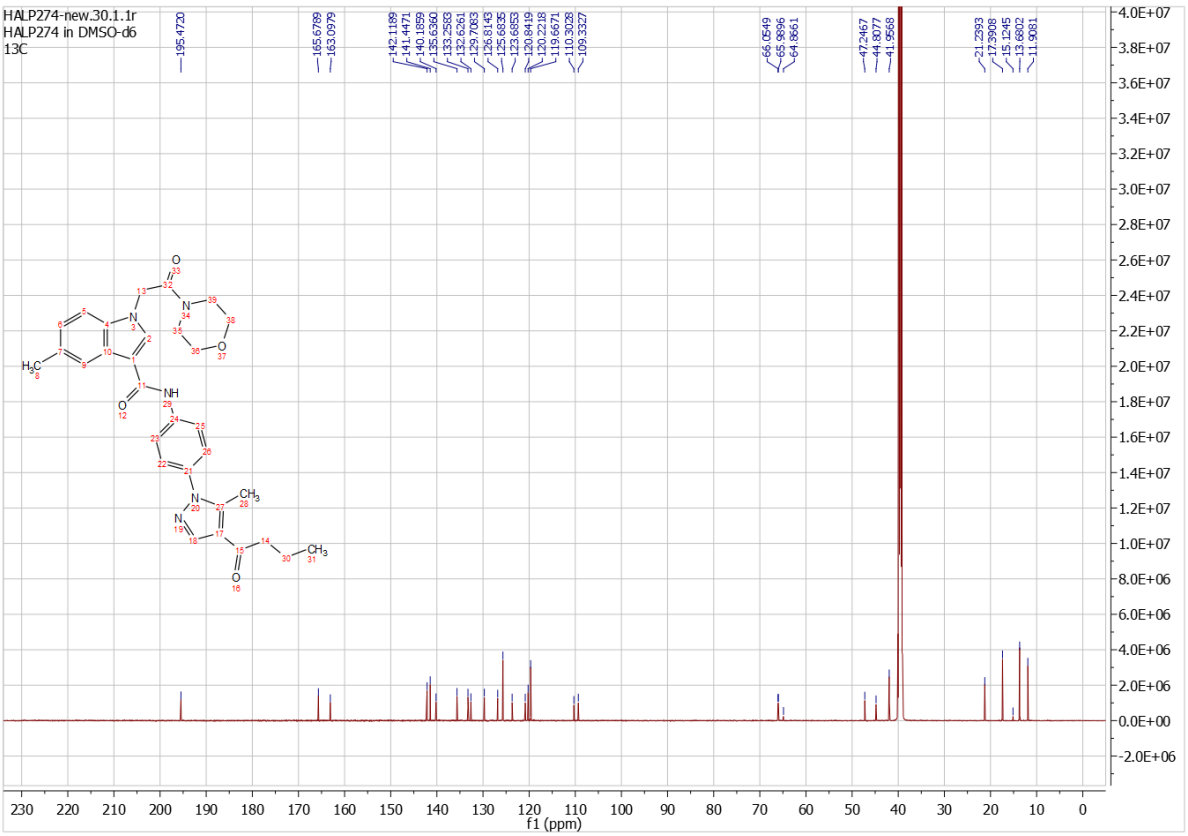
Signal: MS1 -TIC SCAN ESI Frag=135V Gain=1,0

RT [min]	Peak MS Base Peak m/z	Area	Area%	Max Peak%	Height
6.784	526.100	3136047.5288	100.0000	100.000	735159.269
	Sum	3136047.5288			



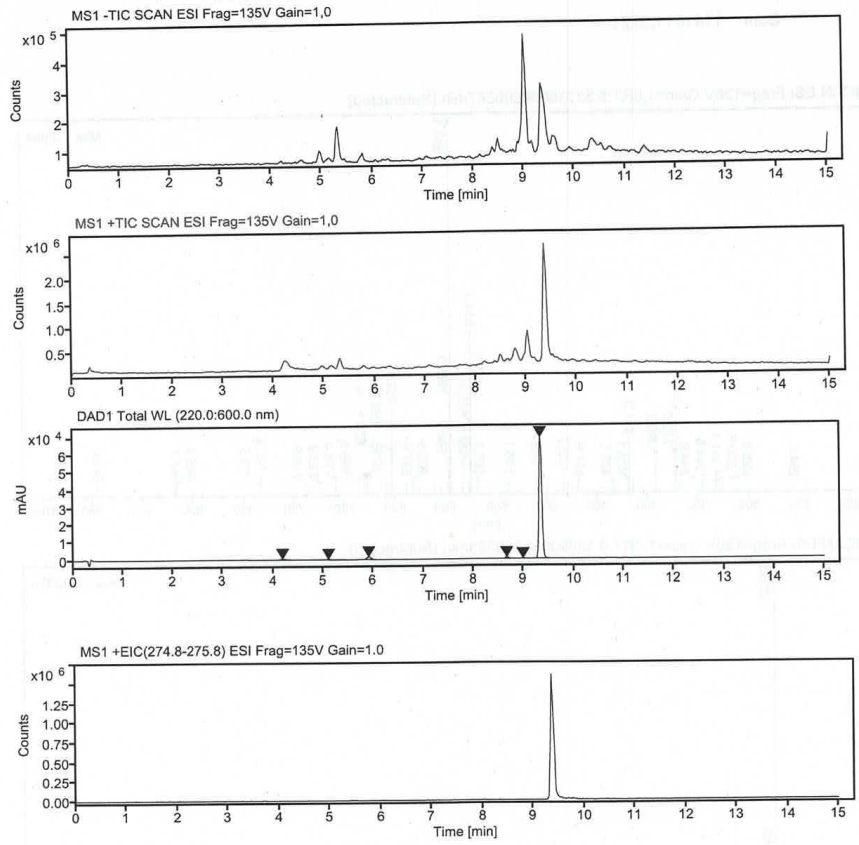



HALP274-new.10.1.1r
HALP274 in DMSO-d6
1H
A (s) 9.9819
B (s) 8.1799
C (s) 8.0234
D (d) 7.9601
E (d) 7.4728
F (d) 7.3698
G (d) 7.0565
H (s) 5.2999
I (s) 3.7003
J (s) 3.6071
K (s) 3.4752
M (t) 2.8126
N (s) 2.4293
O (s) 2.5213
O (h) 1.6371
P (t) 0.9410
f1 (ppm)


HALP274-new.30.1.1r
HALP274 in DMSO-d6
13C
f1 (ppm)

Ethyl 2-methyl-1-(4-nitrophenyl)-1*H*-pyrrole-3-carboxylate (37)

Sequence Name:	SingleSample		
Data file:	HALP367.dx	**Project Name:**	Single Quad
Sample name:	HALP367	**Operator :**	SYSTEM
Instrument:	Single Quad	**Acquired on:**	2024-03-26 11:22:24+01:00
Inj. volume:	2.000	**Location:**	P1-C4
Acq. method:	00-new_wasser-acn_standard_100-1000_BD-20min.amx		
Processing method:	MS_standard_plot.pmx		



Signal: DAD1 Total WL (220.0:600.0 nm)

RT [min]	Peak MS Base Peak m/z	Area	Area%	Max Peak%	Height
4.189		3706.8546	1.2568	1.341	444.908
5.109		2031.2342	0.6887	0.735	299.113
5.910		8688.8221	2.9460	3.142	1498.740
8.669		3434.8645	1.1646	1.242	798.811
8.995		564.2167	0.1913	0.204	169.928
9.345	594.100	276508.1368	93.7525	100.000	69380.876
	Sum	294934.1288			

D:\CDSProjects\Default\0-standardplot+EIC.rdl [Rev. 8201] Printed: 2024-03-26 13:46:25+01:00 Page 1 of 2

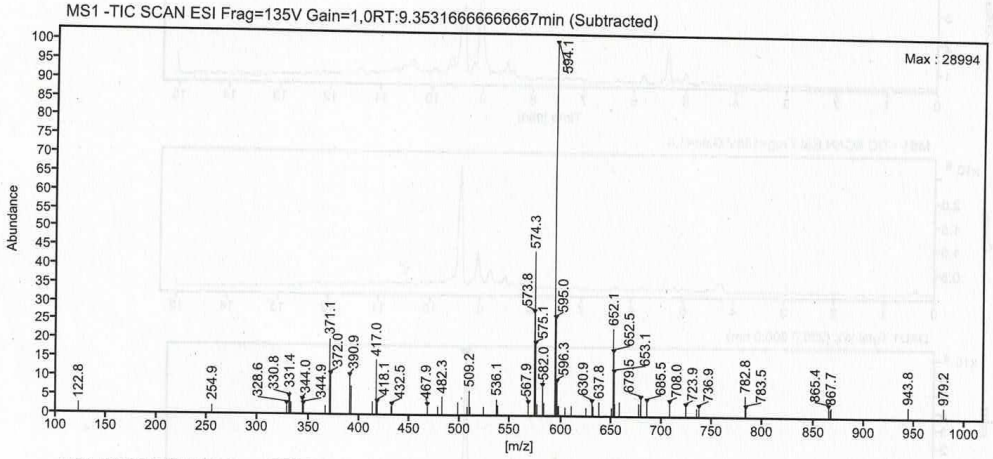
Signal: MS1 +TIC SCAN ESI Frag=135V Gain=1,0

RT [min]	Peak MS Base Peak m/z	Area	Area%	Max Peak%	Height
9.367	275.100	10635275.5702	100.0000	100.000	2320658.904
	Sum	10635275.5702			

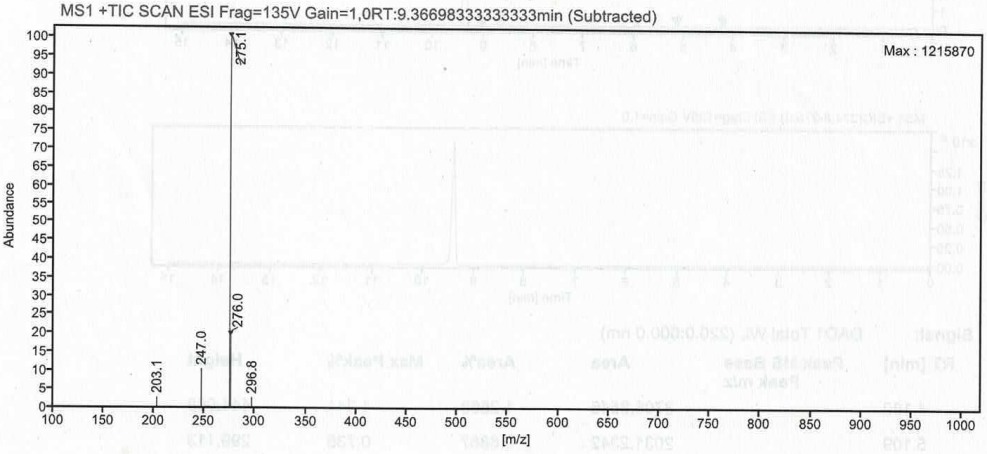
Signal: MS1 -TIC SCAN ESI Frag=135V Gain=1,0

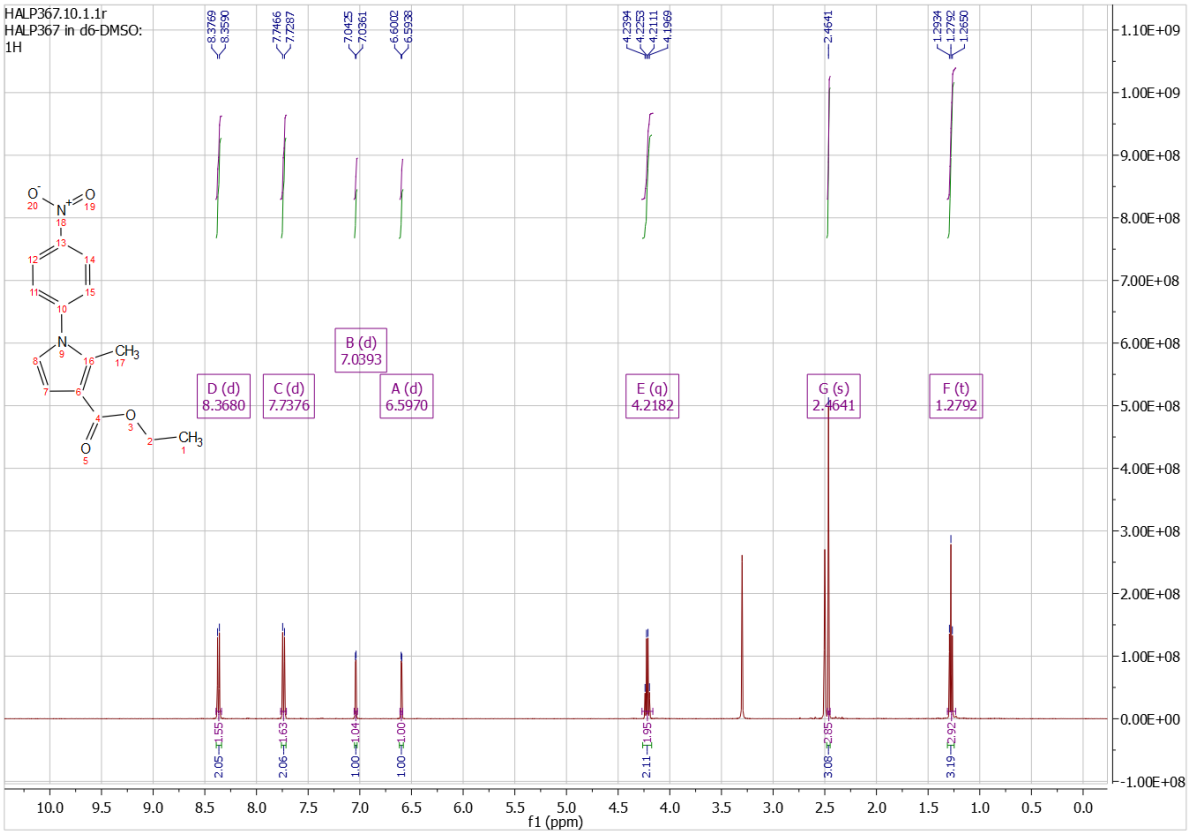
RT [min]	Peak MS Base Peak m/z	Area	Area%	Max Peak%	Height
9.353	594.100	1141811.3721	100.0000	100.000	191861.447
	Sum	1141811.3721			

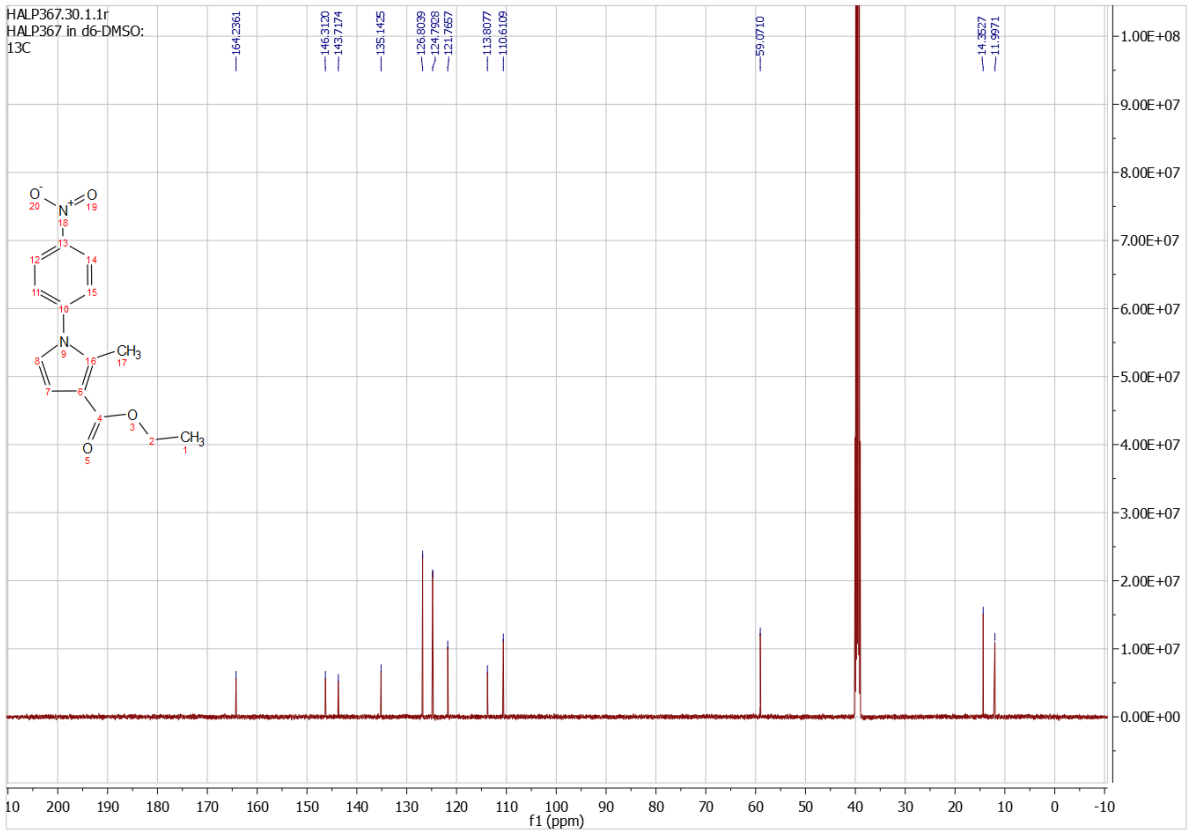
MS1 -TIC SCAN ESI Frag=135V Gain=1,0RT:9.35316666666667min (Subtracted)



MS1 +TIC SCAN ESI Frag=135V Gain=1,0RT:9.36698333333333min (Subtracted)

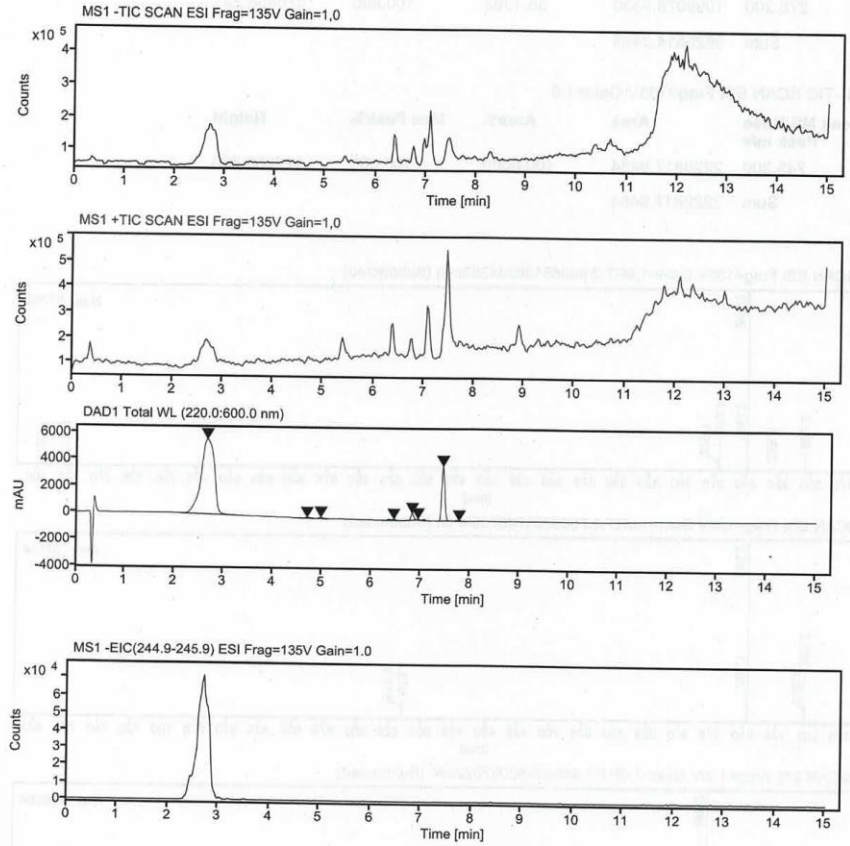



HALP367.10.1.1r
HALP367 in d6-DMSO:
1H
D (d)
8.3680
C (d)
7.7376
B (d)
7.0393
A (d)
6.5970
E (q)
4.2182
G (s)
2.4641
F (t)
1.2792
f1 (ppm)


HALP367.30.1.1r
HALP367 in d6-DMSO:
13C
f1 (ppm)

2-Methyl-1-(4-nitrophenyl)-1*H*-pyrrole-3-carboxylic acid (38)

Sequence Name:	SingleSample		
Data file:	HALP402-F2.dx	**Project Name:**	Single Quad
Sample name:	HALP402-F2	**Operator :**	SYSTEM
Instrument:	Single Quad	**Acquired on:**	2024-04-03 21:56:46+02:00
Inj. volume:	4.000	**Location:**	P1-C9
Acq. method:	00-new_wasser-acn_standard_100-1000_BD-20min.amx		
Processing method:	MS_standard_plot.pmx		



Signal: DAD1 Total WL (220.0:600.0 nm)

RT [min]	Peak MS Base Peak m/z	Area	Area%	Max Peak%	Height
2.664	247.300	103197.0558	82.7657	100.000	5564.032
4.690		434.1993	0.3482	0.421	72.344
4.968		531.8192	0.4265	0.515	113.581
6.445		694.2725	0.5568	0.673	90.107
6.821		1909.9170	1.5318	1.851	504.590
6.939		723.4330	0.5802	0.701	113.119
7.442		17095.9261	13.7112	16.566	4095.171

D:\CDSProjects\Default\0-standardplot+EIC.rdl [Rev. 8302] Printed: 2024-04-04 07:40:51+02:00 Page 1 of 2

RT [min]	Peak MS Base Peak m/z	Area	Area%	Max Peak%	Height
7.772		99.0969	0.0795	0.096	32.281
	Sum	124685.7198			

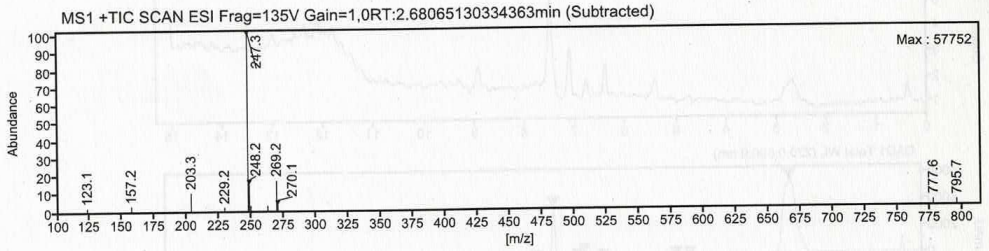
Signal: MS1 +TIC SCAN ESI Frag=135V Gain=1,0

RT [min]	Peak MS Base Peak m/z	Area	Area%	Max Peak%	Height
2.681	247.300	1626435.2665	44.8608	81.359	97167.922
7.467	275.200	1999078.9830	55.1392	100.000	376458.221
	Sum	3625514.2495			

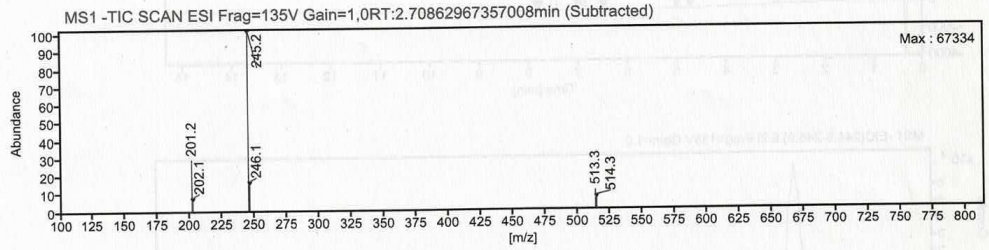
Signal: MS1 -TIC SCAN ESI Frag=135V Gain=1,0

RT [min]	Peak MS Base Peak m/z	Area	Area%	Max Peak%	Height
2.709	245.200	2220817.9484	100.0000	100.000	126656.220
	Sum	2220817.9484			

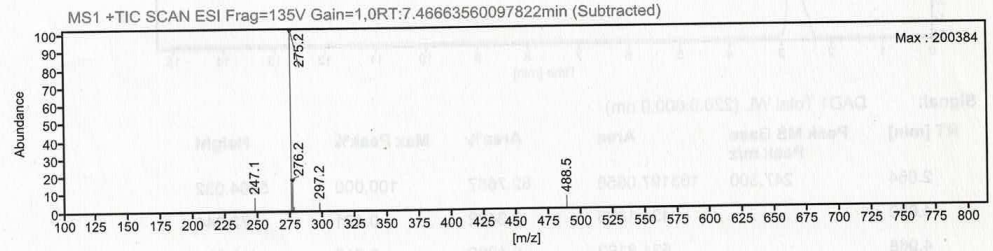
MS1 +TIC SCAN ESI Frag=135V Gain=1,0RT:2.68065130334363min (Subtracted)



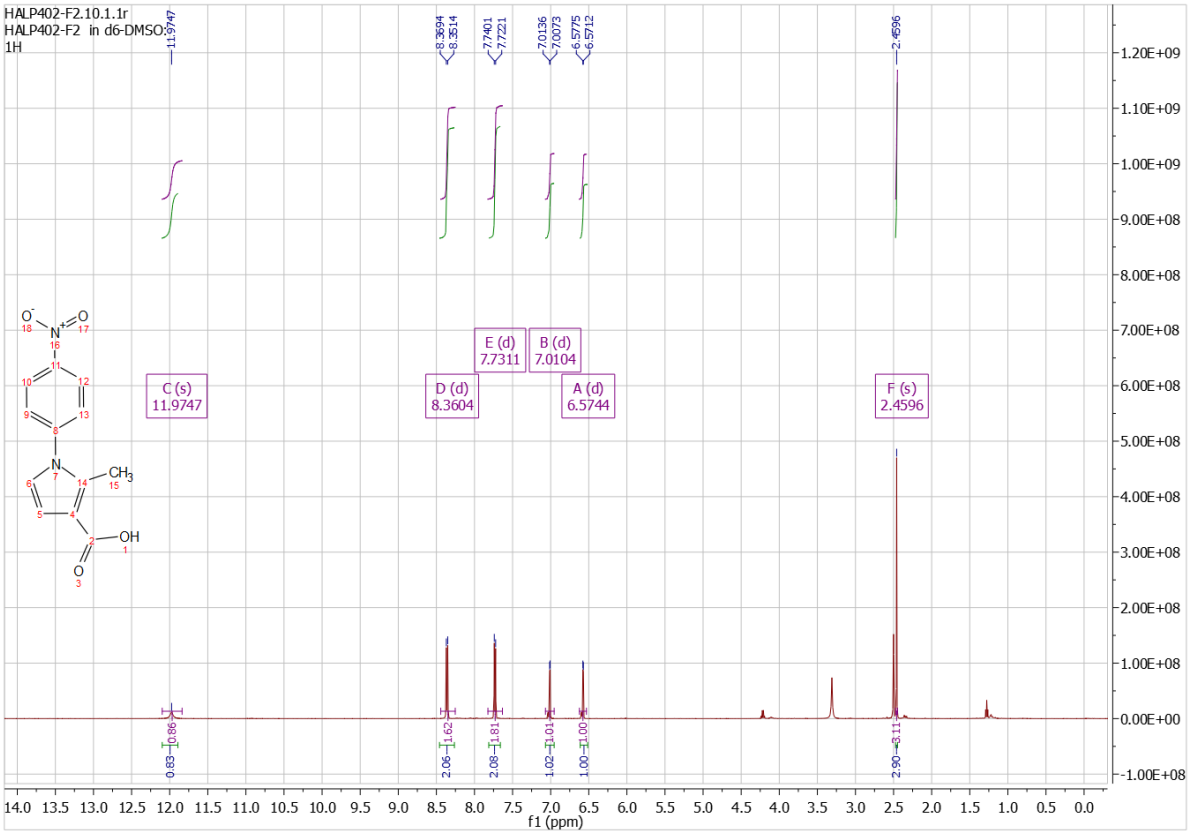
MS1 -TIC SCAN ESI Frag=135V Gain=1,0RT:2.70862967357008min (Subtracted)

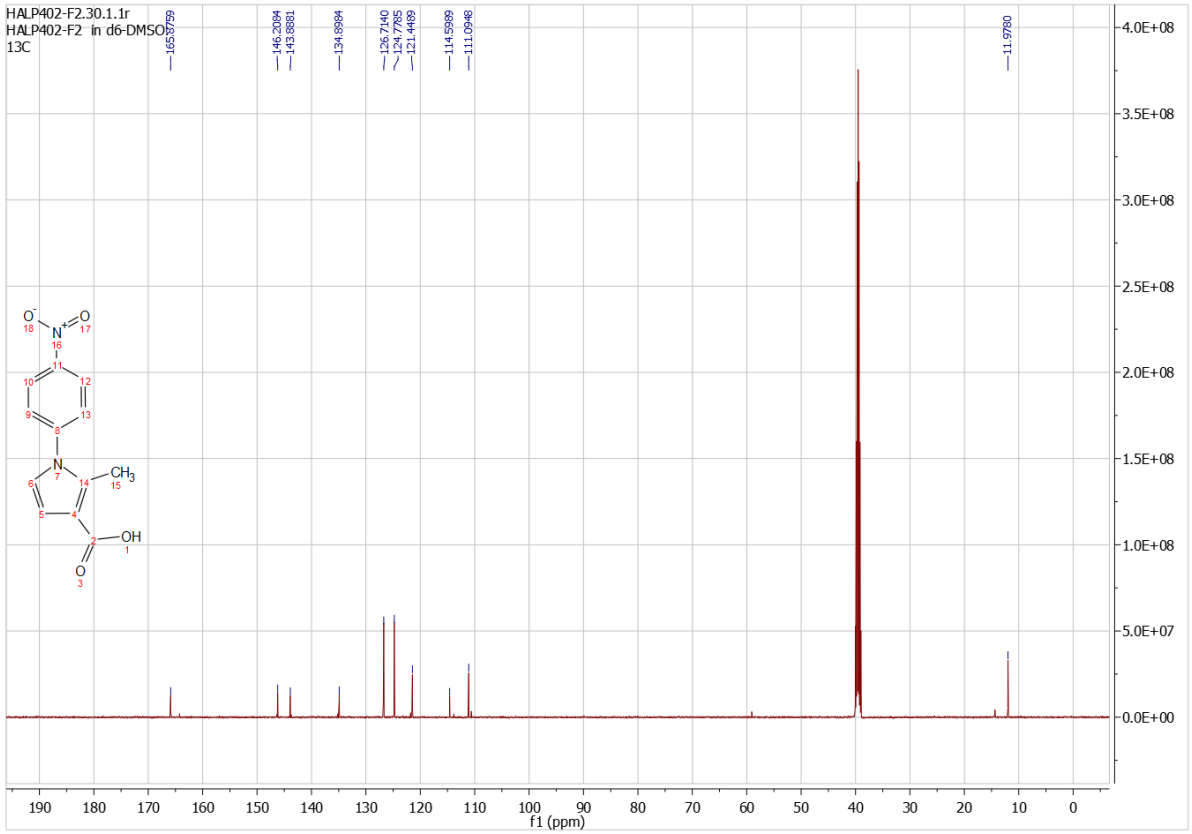


MS1 +TIC SCAN ESI Frag=135V Gain=1,0RT:7.46663560097822min (Subtracted)



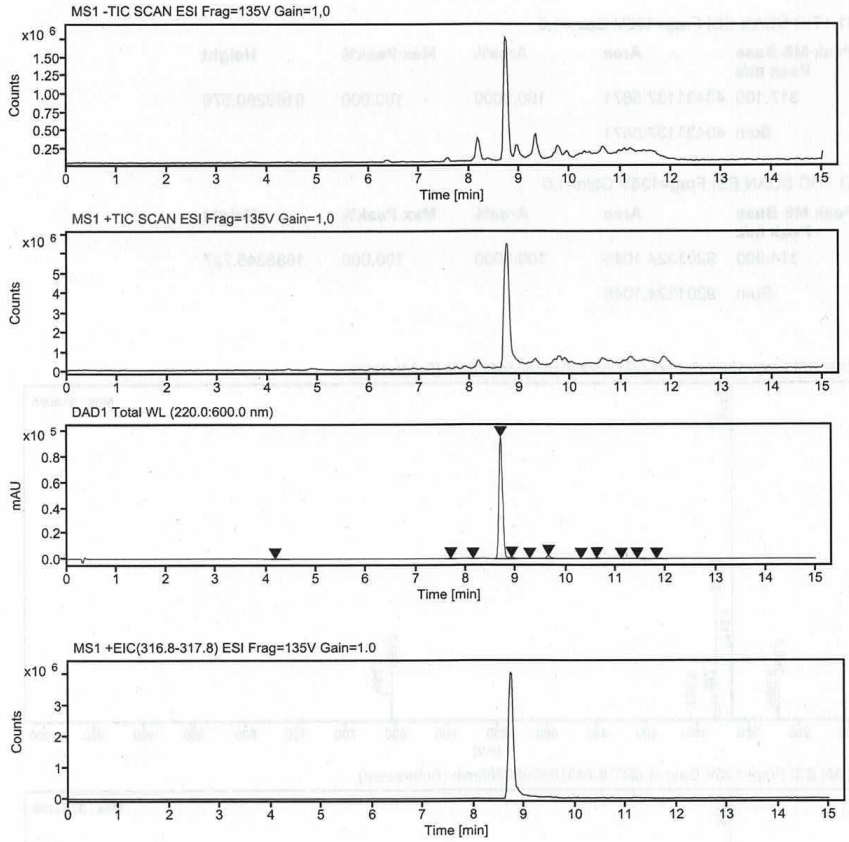
D:\CDSProjects\Default\0-standardplot+EIC.rdl [Rev. 8302] Printed: 2024-04-04 07:40:51+02:00 Page 2 of 2


HALP402-F2.10.1.1r
HALP402-F2 in d6-DMSO
1H
C (s)
11.9747
D (d)
8.3604
E (d)
7.7311
B (d)
7.0104
A (d)
6.5744
F (s)
2.4596
f1 (ppm)


HALP402-F2.30.1.1r
HALP402-F2 in d6-DMSO
13C
f1 (ppm)

Ethyl 3-(2-methyl-1-(4-nitrophenyl)-1*H*-pyrrol-3-yl)-3-oxopropanoate (39)

Sequence Name:	SingleSample		
Data file:	HALP403-F5.dx	**Project Name:**	Single Quad
Sample name:	HALP403-F5	**Operator :**	SYSTEM
Instrument:	Single Quad	**Acquired on:**	2024-05-02 18:28:27+02:00
Inj. volume:	2.000	**Location:**	P2-B4
Acq. method:	000-standard_ACN-H2O-CD-100-1000-20min.amx		
Processing method:	MS_standard_plot.pmx		



Signal: DAD1 Total WL (220.0:600.0 nm)

RT [min]	Peak MS Base Peak m/z	Area	Area%	Max Peak%	Height
4.179		1063.6289	0.2040	0.218	138.340
7.698		2959.4467	0.5677	0.607	626.156
8.142		1055.1349	0.2024	0.216	218.934
8.700		487761.0227	93.5608	100.000	96049.474
8.920		5945.6556	1.1405	1.219	893.994
9.280		446.8131	0.0857	0.092	104.030
9.655		13937.9226	2.6735	2.858	2459.606

D:\CDSProjects\Default\0-standardplot+EIC.rdl [Rev. 8776] Printed: 2024-05-03 07:26:04+02:00 Page 1 of 2

RT [min]	Peak MS Base Peak m/z	Area	Area%	Max Peak%	Height
10.304		436.5418	0.0837	0.089	54.293
10.624		3349.2289	0.6424	0.687	626.932
11.115		825.6596	0.1584	0.169	73.219
11.431		2174.6194	0.4171	0.446	215.839
11.819		1374.6244	0.2637	0.282	154.798
	Sum	521330.2986			

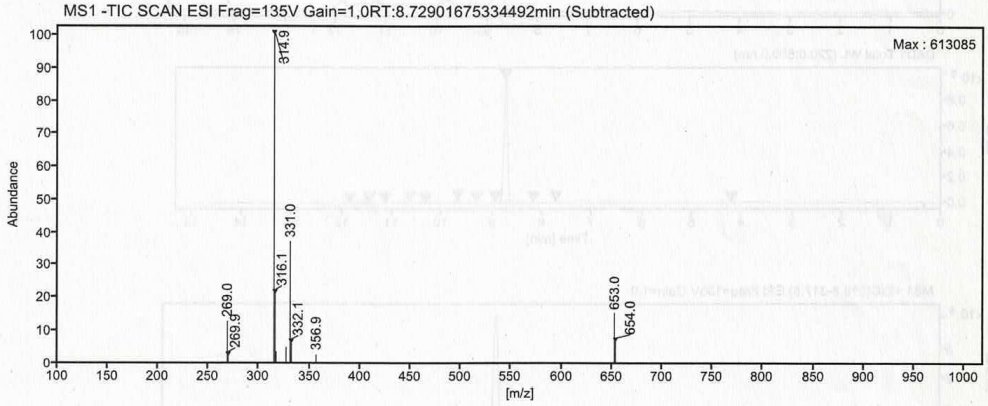
Signal: MS1 +TIC SCAN ESI Frag=135V Gain=1,0

RT [min]	Peak MS Base Peak m/z	Area	Area%	Max Peak%	Height
8.744	317.100	43431137.5871	100.0000	100.000	6180260.576
	Sum	43431137.5871			

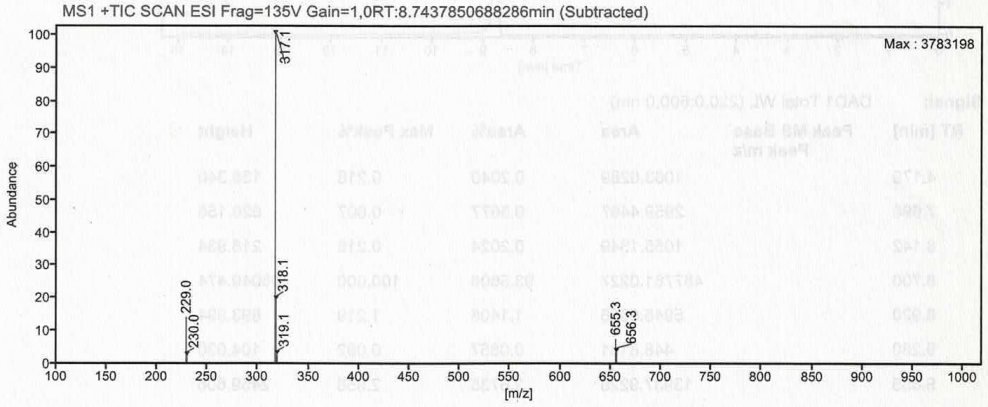
Signal: MS1 -TIC SCAN ESI Frag=135V Gain=1,0

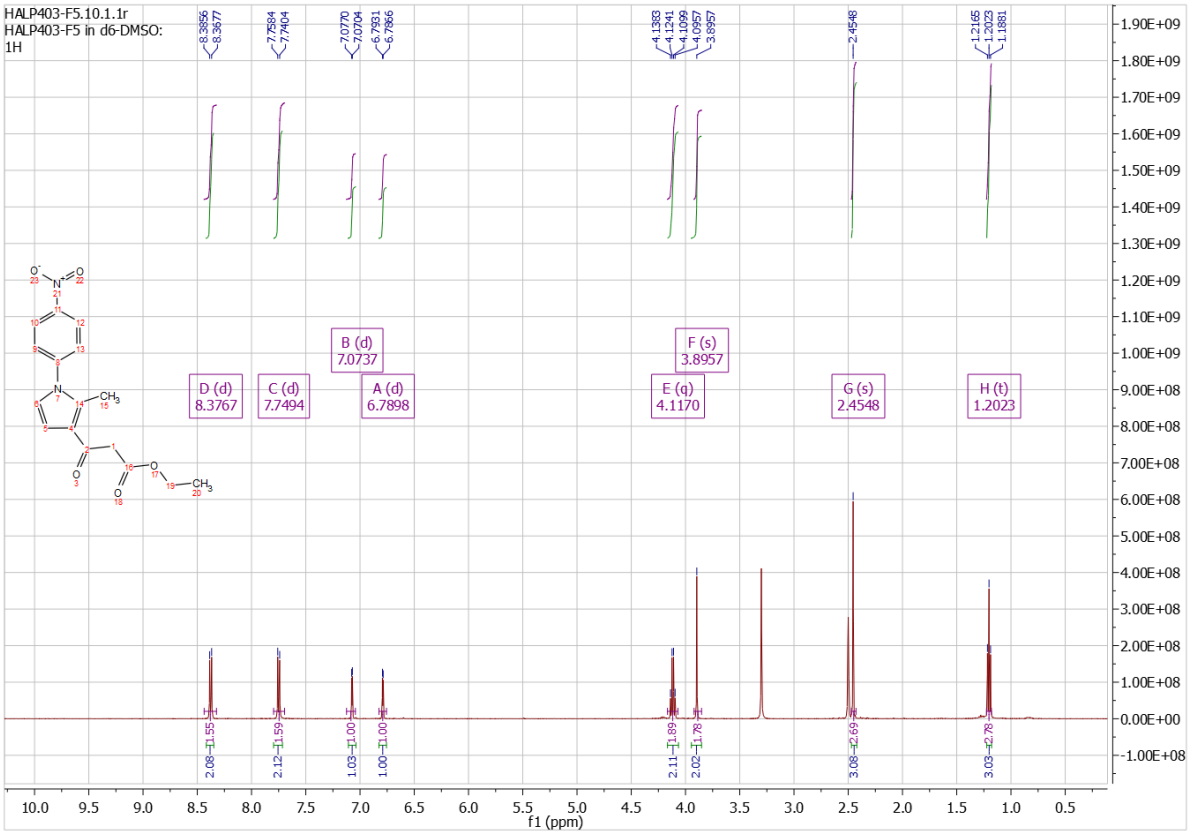
RT [min]	Peak MS Base Peak m/z	Area	Area%	Max Peak%	Height
8.729	314.900	9201324.1046	100.0000	100.000	1685345.727
	Sum	9201324.1046			

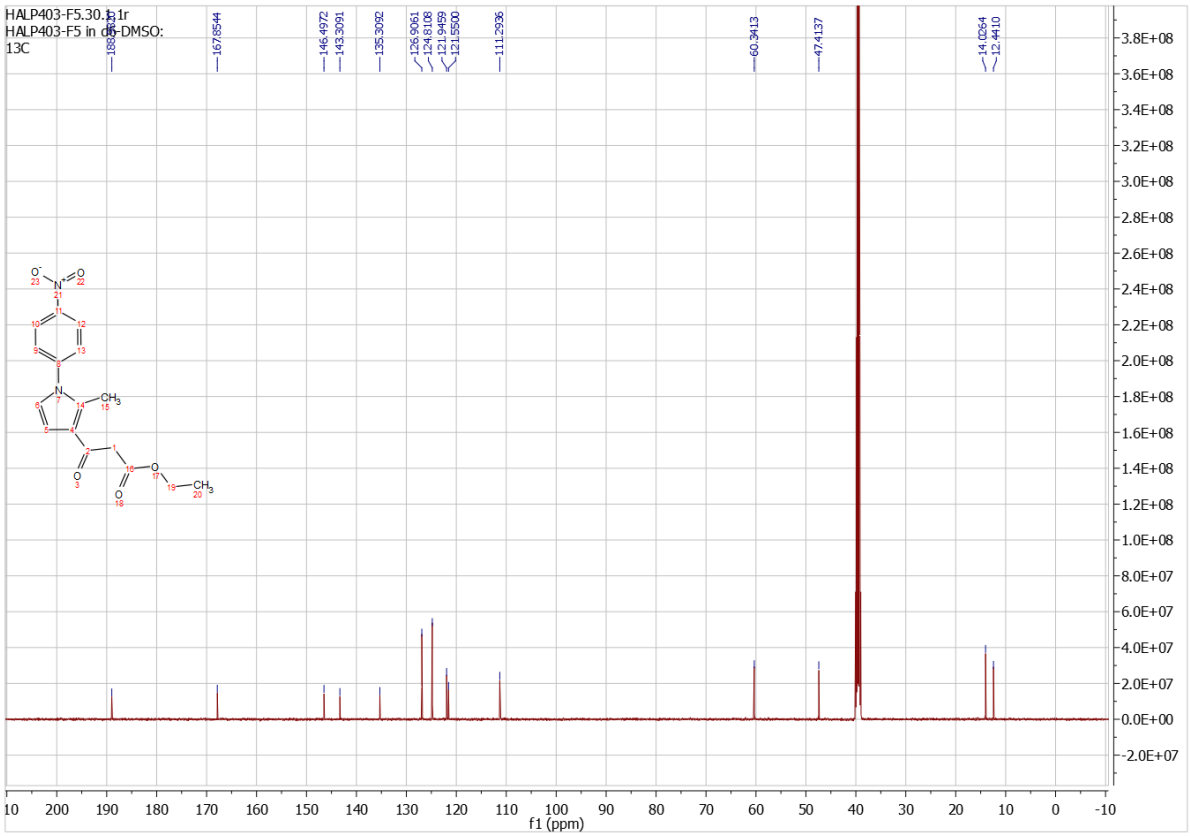
MS1 -TIC SCAN ESI Frag=135V Gain=1,0RT:8.72901675334492min (Subtracted)



MS1 +TIC SCAN ESI Frag=135V Gain=1,0RT:8.7437850688286min (Subtracted)

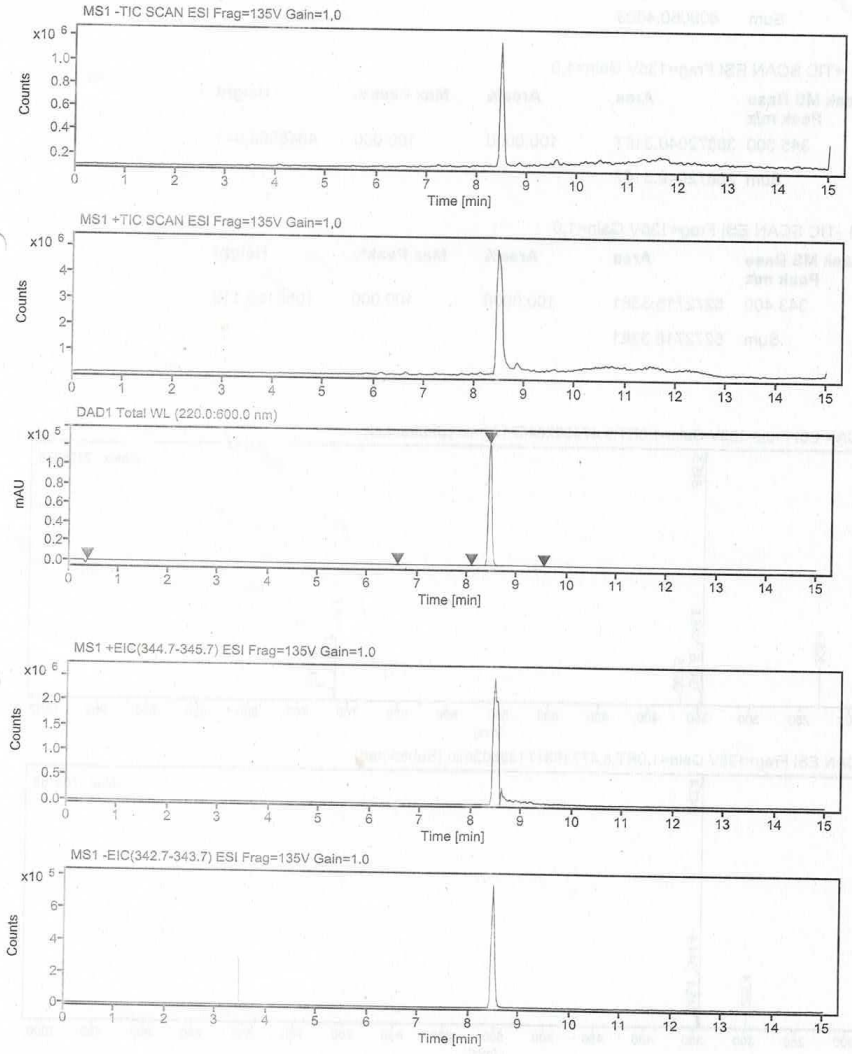



HALP403-F5.10.1.1r
HALP403-F5 in d6-DMSO:
1H
D (d)
8.3767
C (d)
7.7494
B (d)
7.0737
A (d)
6.7898
E (q)
4.1170
F (s)
3.8957
G (s)
2.4548
H (t)
1.2023
f1 (ppm)


HALP403-F5.30.1.1r
HALP403-F5 in d6-DMSO:
13C
f1 (ppm)

Ethyl 2-(2-methyl-1-(4-nitrophenyl)-1*H*-pyrrole-3-carbonyl)butanoate (40)

Sequence Name:	SingleSample		
Data file:	HALP404-F3.dx	**Project Name:**	Single Quad
Sample name:	HALP404-F3	**Operator :**	SYSTEM
Instrument:	Single Quad	**Acquired on:**	2024-05-14 23:30:15+02:00
Inj. volume:	2.000	**Location:**	P2-B6
Acq. method:	000-getauscht_Cwasser-Bacn_standard_100-1500_CB-20min.amx		
Processing method:	MS_standard_plot.pmx		



D:\CDSProjects\Default\0-standardplot+EIC.rdl [Rev. 8945] Printed: 2024-05-15 13:46:30+02:00 Page 1 of 2

Signal: DAD1 Total WL (220.0:600.0 nm)

RT [min]	Peak MS Base Peak m/z	Area	Area%	Max Peak%	Height
0.378		1355.6194	0.2226	0.226	714.348
6.602		2654.4962	0.4358	0.442	740.069
8.090		3482.1910	0.5717	0.579	838.805
8.447	345.500	600918.4749	98.6632	100.000	127511.252
9.545		649.7068	0.1067	0.108	204.584
	Sum	609060.4883			

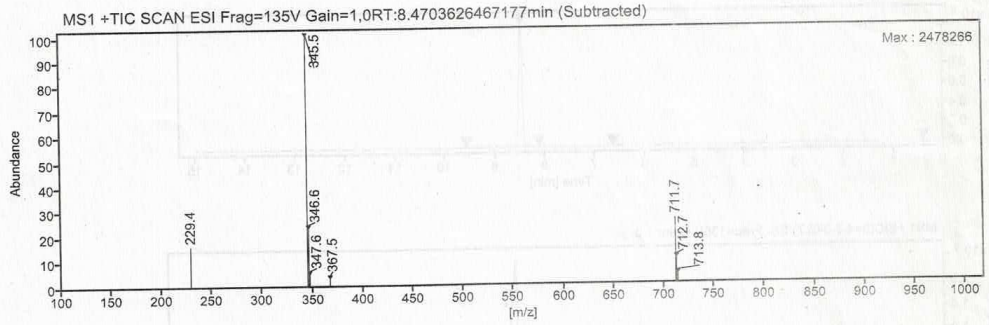
Signal: MS1 +TIC SCAN ESI Frag=135V Gain=1,0

RT [min]	Peak MS Base Peak m/z	Area	Area%	Max Peak%	Height
8.470	345.500	38872040.3167	100.0000	100.000	4848664.041
	Sum	38872040.3167			

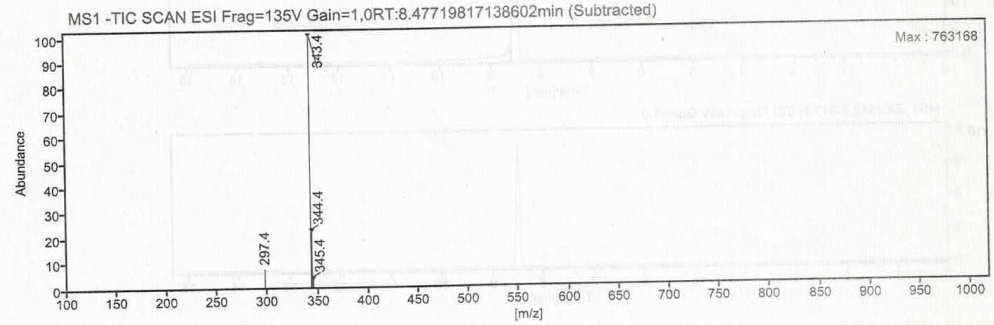
Signal: MS1 -TIC SCAN ESI Frag=135V Gain=1,0

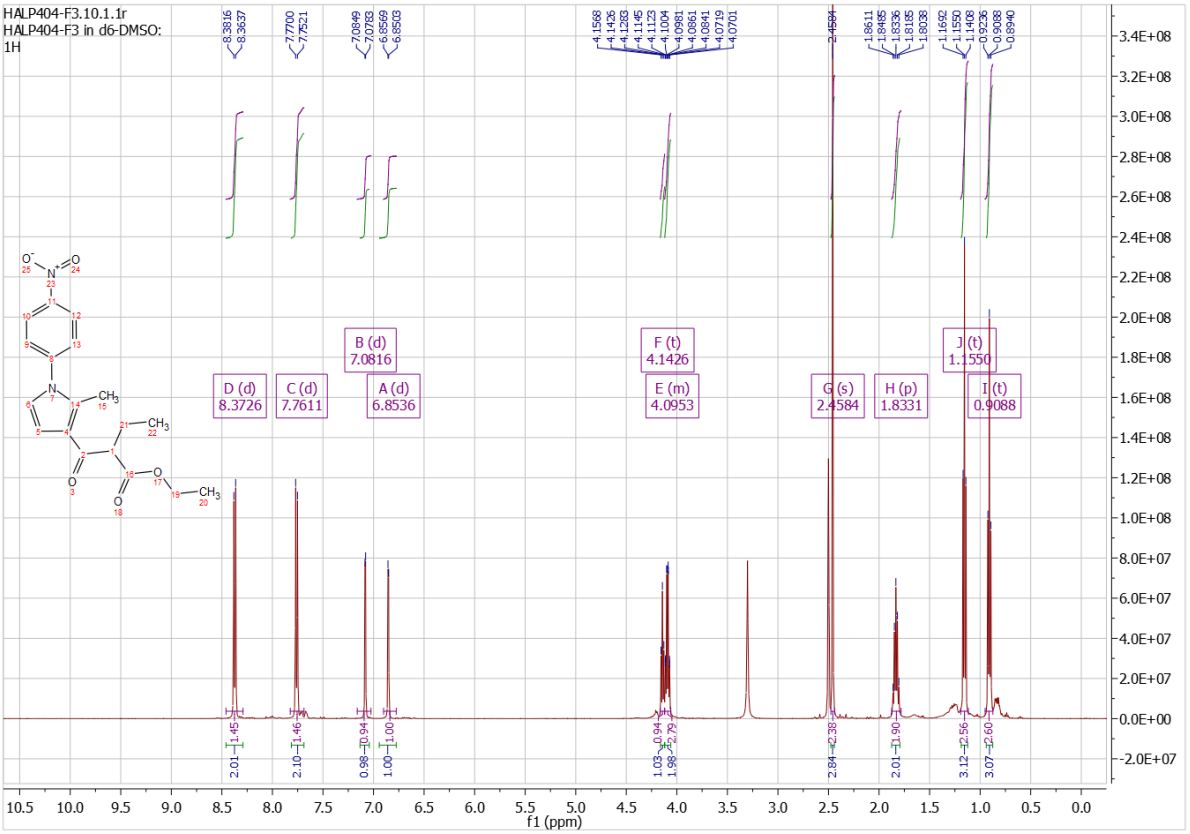
RT [min]	Peak MS Base Peak m/z	Area	Area%	Max Peak%	Height
8.477	343.400	5272718.3381	100.0000	100.000	1056109.119
	Sum	5272718.3381			

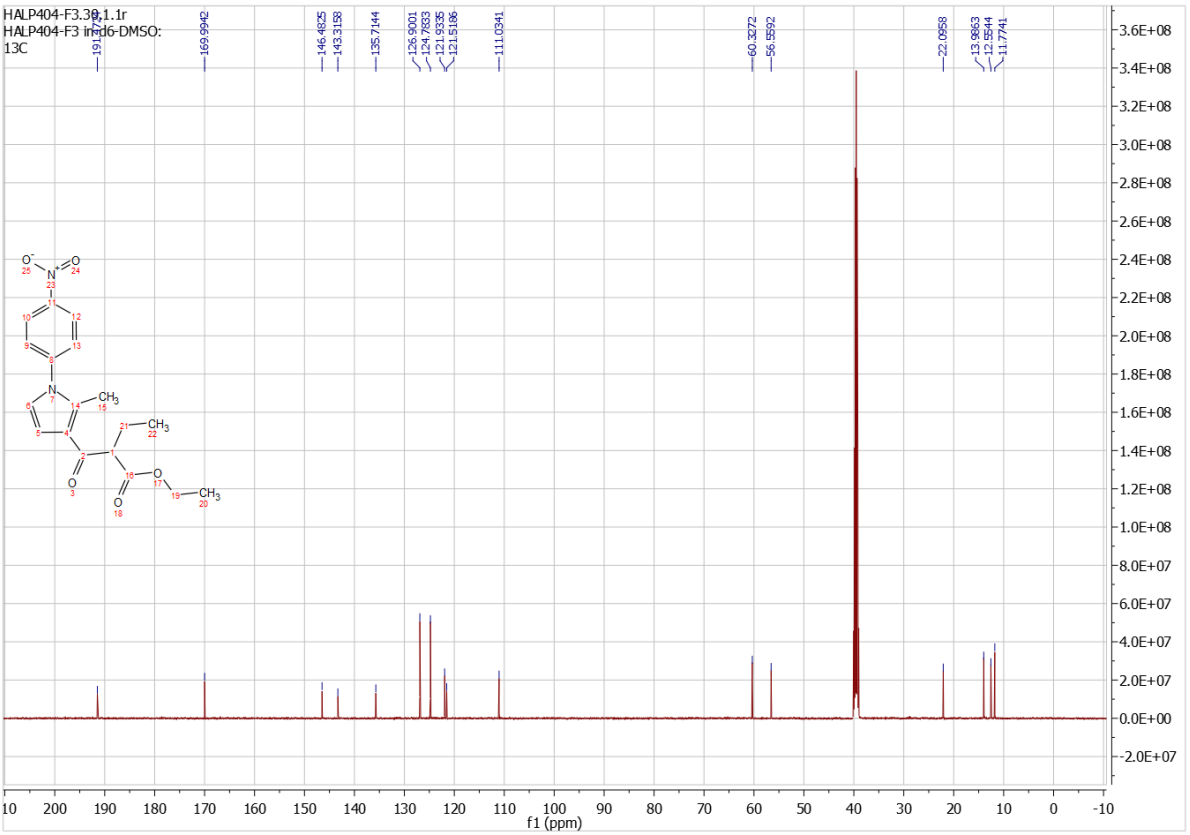
MS1 +TIC SCAN ESI Frag=135V Gain=1,0RT:8.4703626467177min (Subtracted)



MS1 -TIC SCAN ESI Frag=135V Gain=1,0RT:8.47719817138602min (Subtracted)

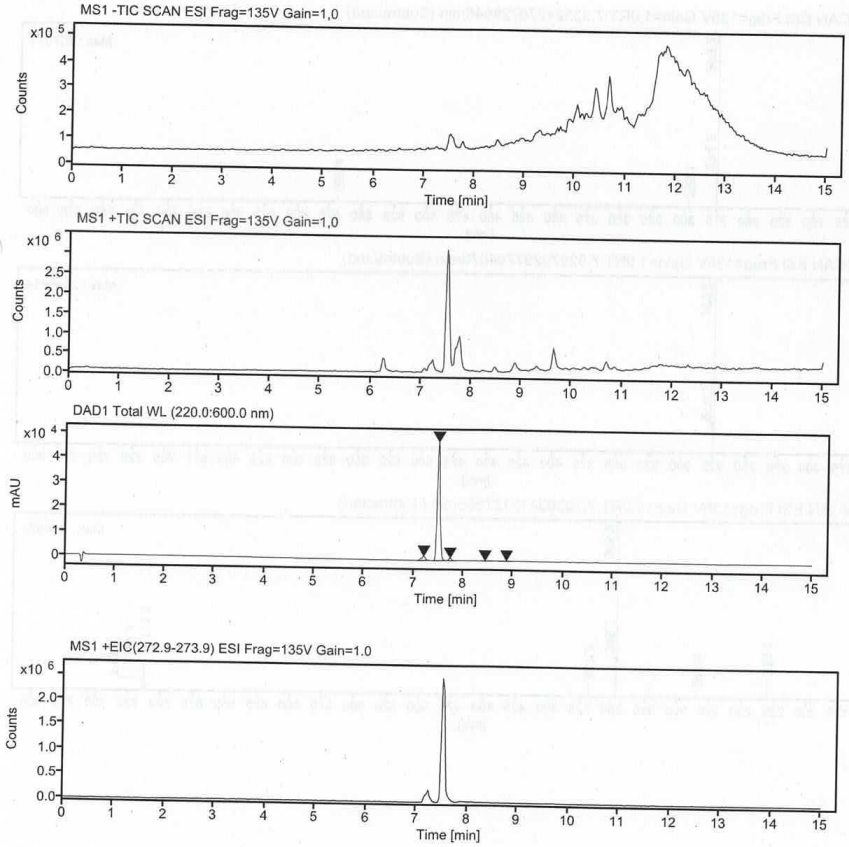



HALP404-F3.10.1.1r
HALP404-F3 in d6-DMSO:
1H
D (d)
8.3726
C (d)
7.7611
B (d)
7.0816
A (d)
6.8536
F (t)
4.1426
E (m)
4.0953
G (s)
2.4584
H (p)
1.8331
J (t)
1.1550
I (t)
0.9088
f1 (ppm)


HALP404-F3.30.1.1r
HALP404-F3 in d6-DMSO:
13C
f1 (ppm)

1-(2-Methyl-1-(4-nitrophenyl)-1*H*-pyrrol-3-yl)butan-1-one (41)

Sequence Name:	SingleSample		
Data file:	HALP405-F3.dx	**Project Name:**	Single Quad
Sample name:	HALP405-F3	**Operator :**	SYSTEM
Instrument:	Single Quad	**Acquired on:**	2024-05-27 19:01:44+02:00
Inj. volume:	2.000	**Location:**	P2-B6
Acq. method:	00-new_wasser-acn_standard_100-1000_BD-20min.amx		
Processing method:	MS_standard_plot.pmx		



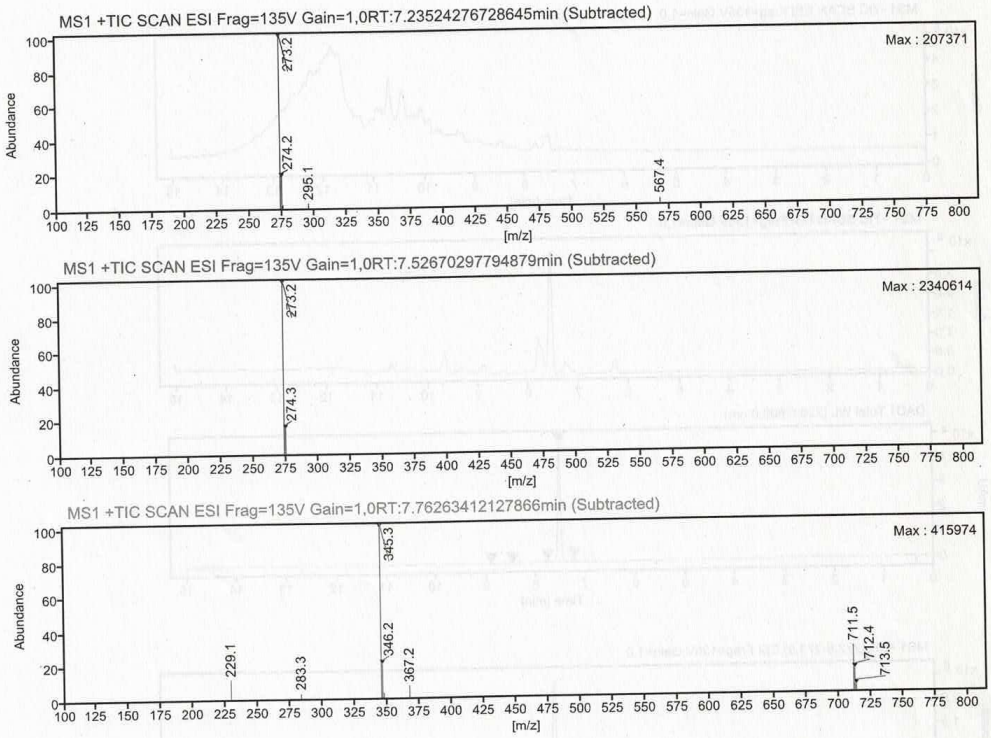
Signal: DAD1 Total WL (220.0:600.0 nm)

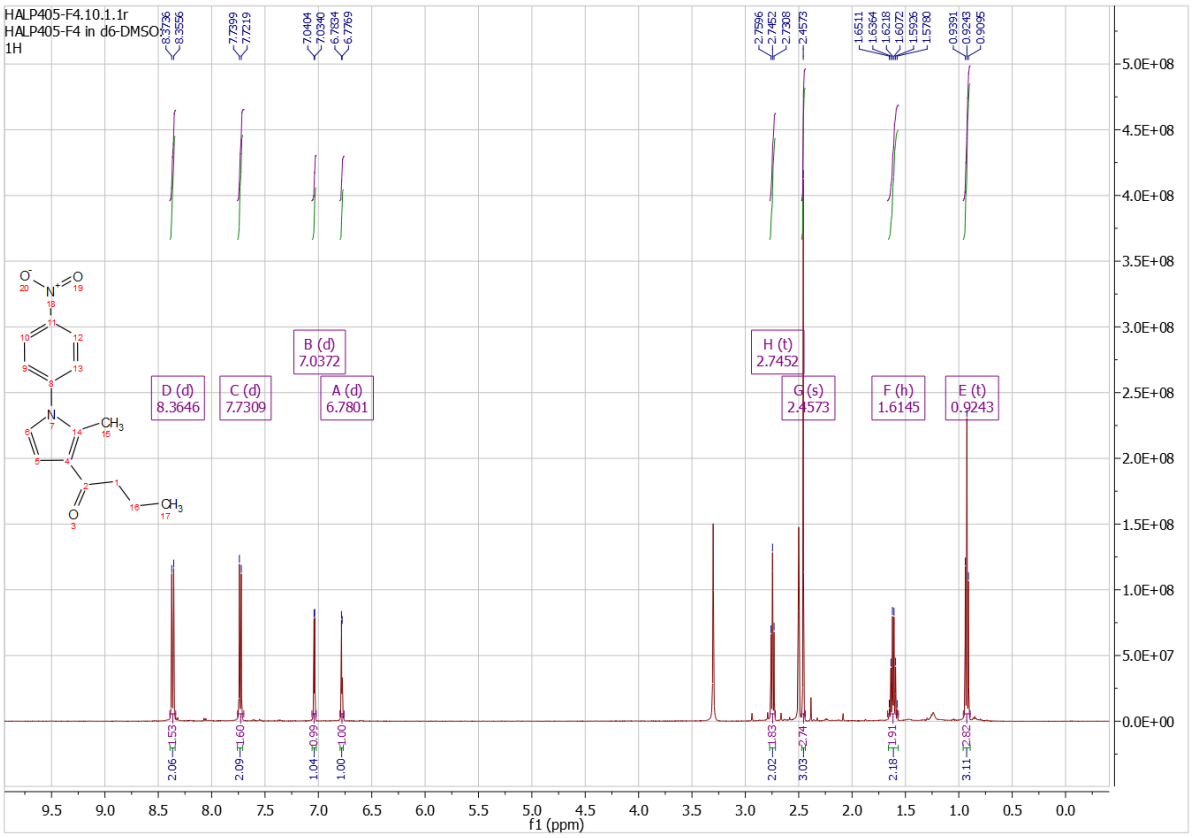
RT [min]	Peak MS Base Peak m/z	Area	Area%	Max Peak%	Height
7.209	273.200	9169.1907	4.3406	4.637	1725.180
7.493		197725.6905	93.6018	100.000	48750.451
7.737		3602.9040	1.7056	1.822	951.840
8.438		240.5938	0.1139	0.122	64.950
8.869		502.8953	0.2381	0.254	104.625
	Sum	211241.2743			

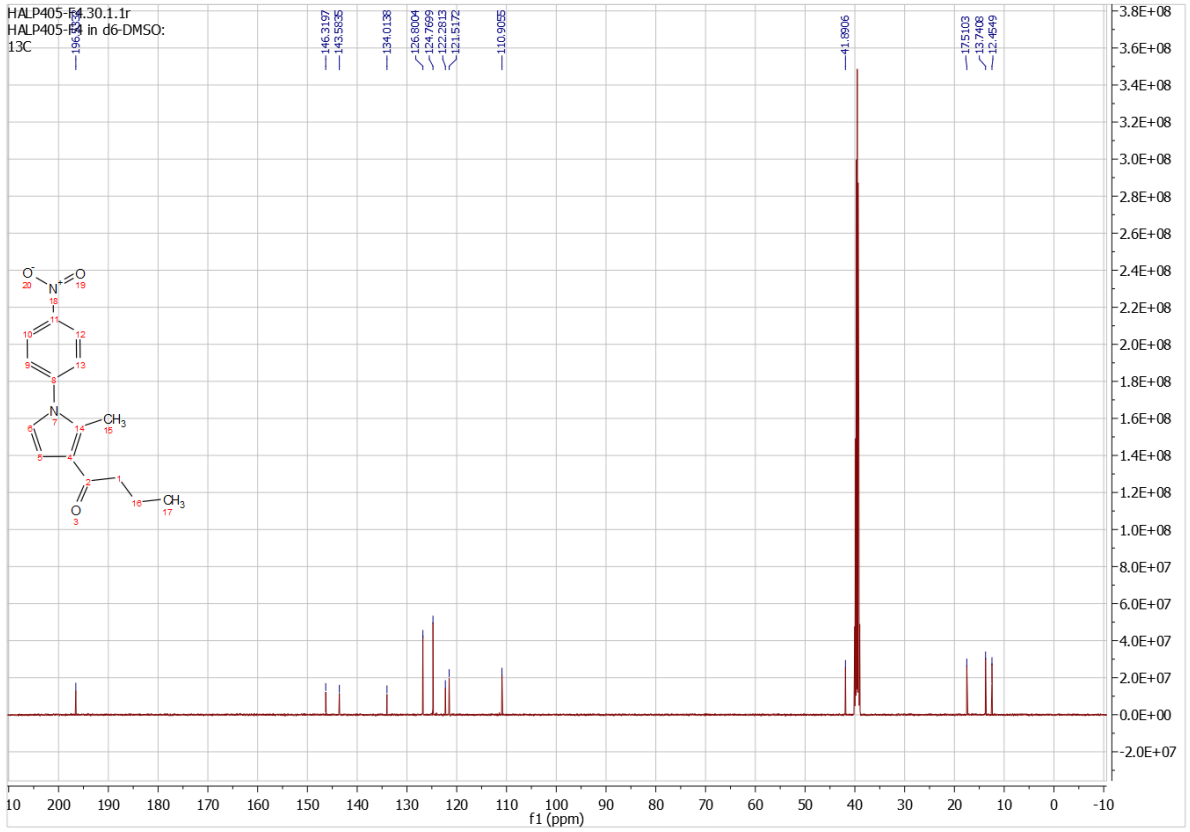
D:\CDSProjects\Default\0-standardplot+EIC.rdl [Rev. 9100] Printed: 2024-05-28 07:01:10+02:00 Page 1 of 2

Signal: MS1 +TIC SCAN ESI Frag=135V Gain=1,0

RT [min]	Peak MS Base Peak m/z	Area	Area%	Max Peak%	Height
7.235	273.200	1335135.5457	6.3134	9.135	265899.207
7.527	273.200	14615482.7462	69.1118	100.000	3100621.654
7.763	345.300	5196969.2401	24.5748	35.558	790369.706
	Sum	21147587.5321			

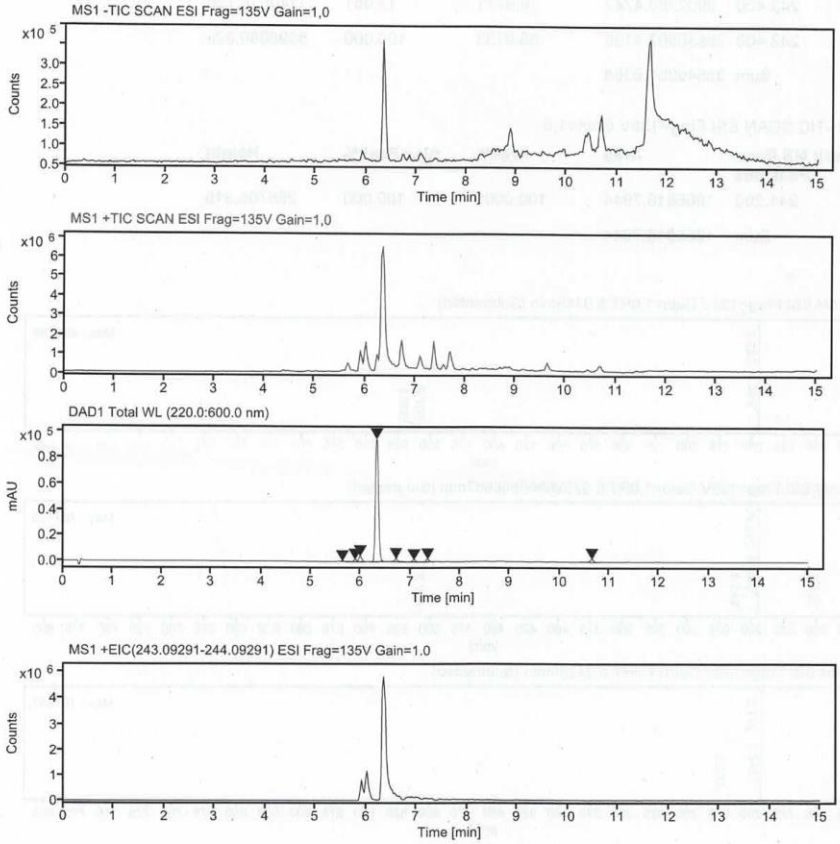



HALP405-F4.10.1.1r
HALP405-F4 in d6-DMSO:
1H
D (d)
8.3646
C (d)
7.7309
B (d)
7.0372
A (d)
6.7801
H (t)
2.7452
G (s)
2.4573
F (h)
1.6145
E (t)
0.9243
f1 (ppm)


HALP405-F4.30.1.1r
HALP405-F4 in d6-DMSO:
13C
f1 (ppm)

1-(1-(4-Aminophenyl)-2-methyl-1*H*-pyrrol-3-yl)butan-1-one (42)

Sequence Name:	SingleSample		
Data file:	HALP406.dx	**Project Name:**	Single Quad
Sample name:	HALP406	**Operator :**	SYSTEM
Instrument:	Single Quad	**Acquired on:**	2024-05-29 09:29:44+02:00
Inj. volume:	2.000	**Location:**	P1-B5
Acq. method:	00-new_wasser-acn_standard_100-1000_BD-20min.amx		
Processing method:	MS_standard_plot.pmx		



Signal: DAD1 Total WL (220.0:600.0 nm)

RT [min]	Peak MS Base Peak m/z	Area	Area%	Max Peak%	Height
5.632		1575.2022	0.3378	0.387	351.332
5.889		6101.1200	1.3085	1.498	1677.853
5.992		17142.6377	3.6766	4.208	4447.890
6.323		407399.2393	87.3755	100.000	94749.299
6.711		10106.4287	2.1675	2.481	2202.893
7.075		5932.4572	1.2723	1.456	1448.905
7.350		7551.1688	1.6195	1.854	1972.254

D:\CDSProjects\Default\0-standardplot+EIC.rdl [Rev. 9152] Printed: 2024-05-29 11:20:27+02:00 Page 1 of 2

RT [min]	Peak MS Base Peak m/z	Area	Area%	Max Peak%	Height
10.654		10454.3088	2.2422	2.566	2203.568
	Sum	466262.5626			

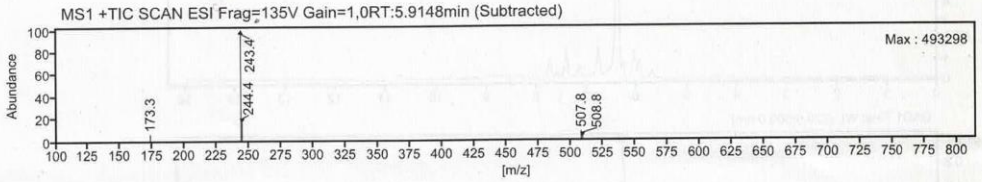
Signal: MS1 +TIC SCAN ESI Frag=135V Gain=1,0

RT [min]	Peak MS Base Peak m/z	Area	Area%	Max Peak%	Height
5.915	243.400	1816434.0509	5.1096	6.089	751860.420
6.025	243.400	3902260.4742	10.9771	13.081	1140618.729
6.357	243.400	29830507.4136	83.9133	100.000	5998080.325
	Sum	35549201.9388			

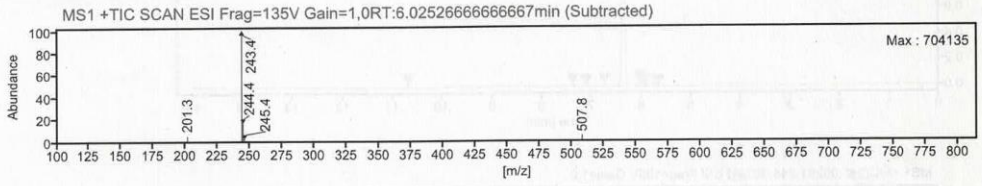
Signal: MS1 -TIC SCAN ESI Frag=135V Gain=1,0

RT [min]	Peak MS Base Peak m/z	Area	Area%	Max Peak%	Height
6.343	241.200	1065816.7944	100.0000	100.000	288705.315
	Sum	1065816.7944			

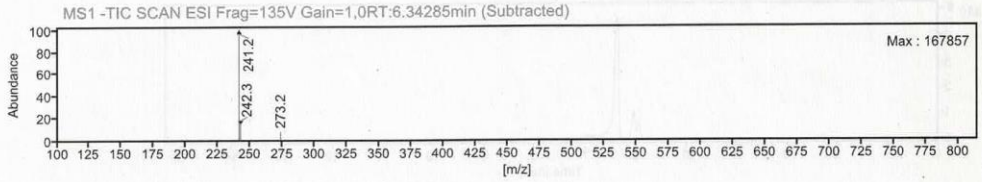
MS1 +TIC SCAN ESI Frag=135V Gain=1,0RT:5.9148min (Subtracted)



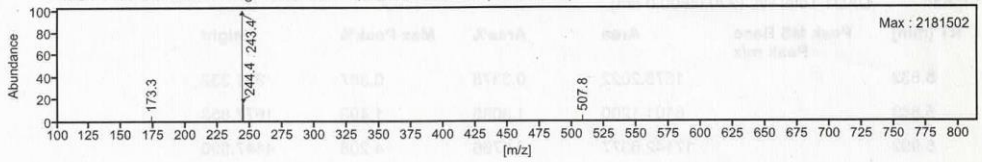
MS1 +TIC SCAN ESI Frag=135V Gain=1,0RT:6.02526666666667min (Subtracted)



MS1 -TIC SCAN ESI Frag=135V Gain=1,0RT:6.34285min (Subtracted)

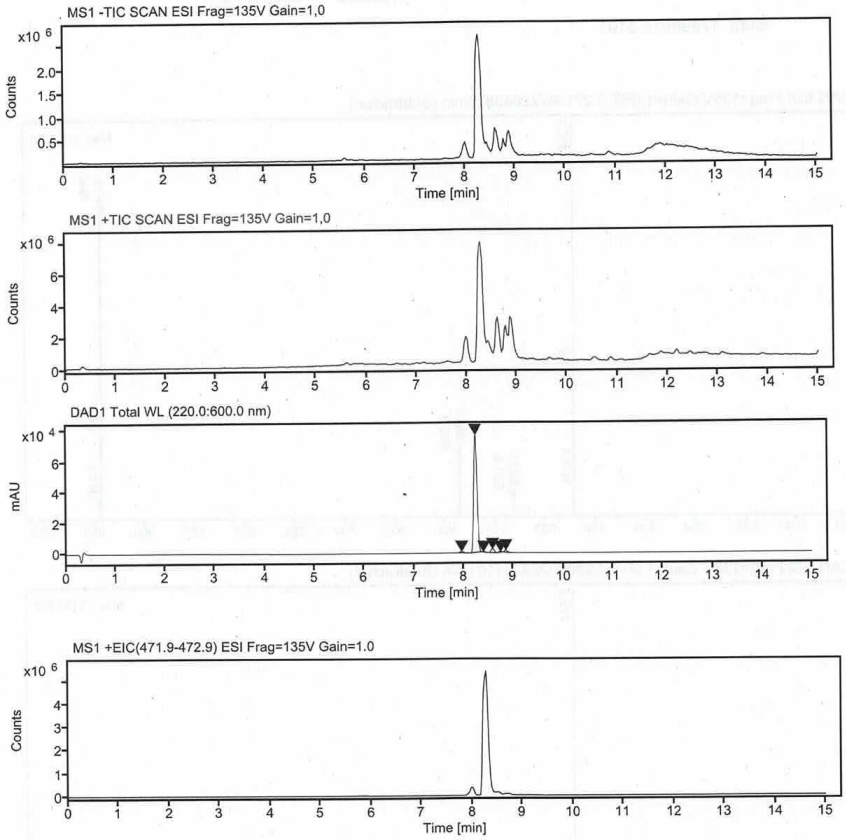


MS1 +TIC SCAN ESI Frag=135V Gain=1,0RT:6.35665min (Subtracted)



Methyl 2-(3-((4-(3-butyryl-2-methyl-1*H*-pyrrol-1-yl)phenyl)carbamoyl)-5-methyl-1*H*-indol-1-yl)acetate (43)

Sequence Name:	SingleSample		
Data file:	HALP417-F4.dx	**Project Name:**	Single Quad
Sample name:	HALP417-F4	**Operator :**	SYSTEM
Instrument:	Single Quad	**Acquired on:**	2024-10-23 16:21:15+02:00
Inj. volume:	5.000	**Location:**	P2-C7
Acq. method:	00-new_wasser-acn_standard_100-1000_BD-20min.amx		
Processing method:	MS_standard_plot.pmx		



Signal: DAD1 Total WL (220.0:600.0 nm)

RT [min]	Peak MS Base Peak m/z	Area	Area%	Max Peak%	Height
7.960		4285.6280	1.1012	1.173	940.685
8.240		365345.6616	93.8790	100.000	76153.998
8.403		982.0469	0.2523	0.269	278.839
8.585		11001.4071	2.8269	3.011	2467.701
8.747		1529.6278	0.3931	0.419	472.650
8.853		6022.2718	1.5475	1.648	1452.012
	Sum	389166.6432			

D:\CDSProjects\Default\0-standardplot+EIC.rdl [Rev. 11299] Printed: 2024-10-24 07:54:22+02:00 Page 1 of 2

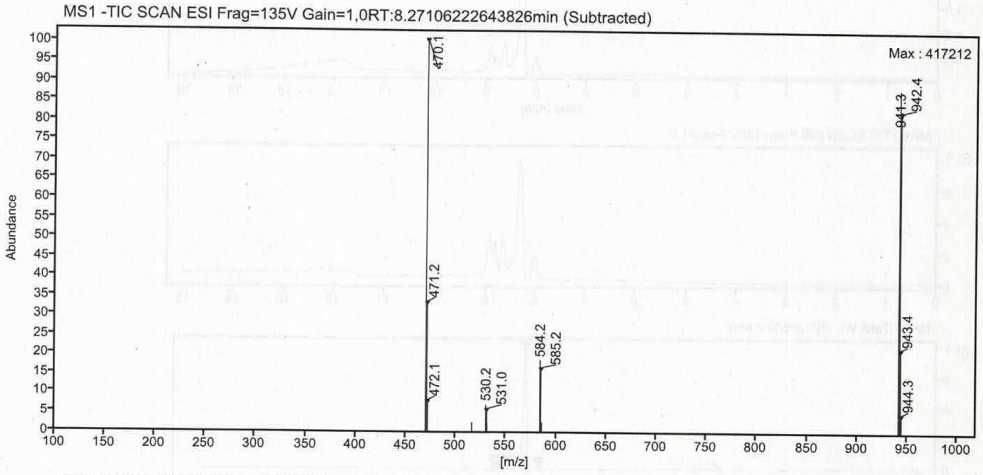
Signal: MS1 +TIC SCAN ESI Frag=135V Gain=1,0

RT [min]	Peak MS Base Peak m/z	Area	Area%	Max Peak%	Height
8.281	472.200	45925326.9025	100.0000	100.000	6852350.206
	Sum	45925326.9025			

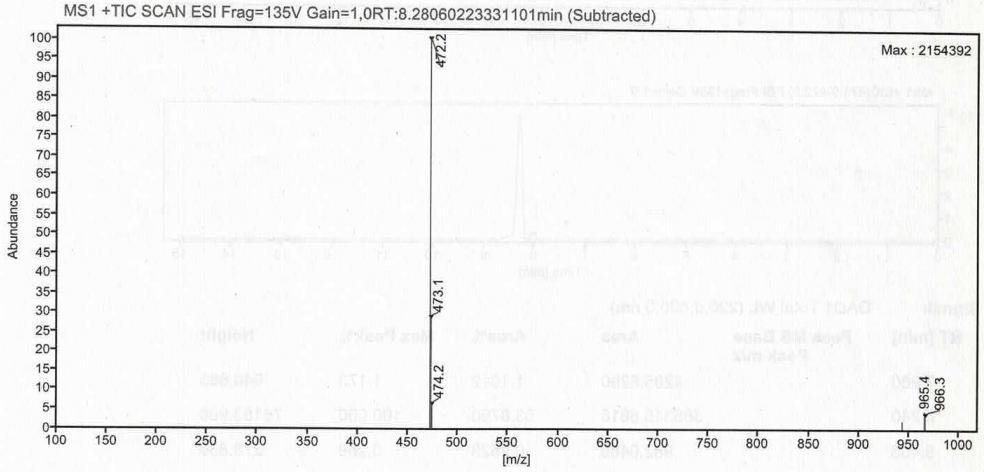
Signal: MS1 -TIC SCAN ESI Frag=135V Gain=1,0

RT [min]	Peak MS Base Peak m/z	Area	Area%	Max Peak%	Height
8.271	470.100	17898018.3101	100.0000	100.000	2492497.697
	Sum	17898018.3101			

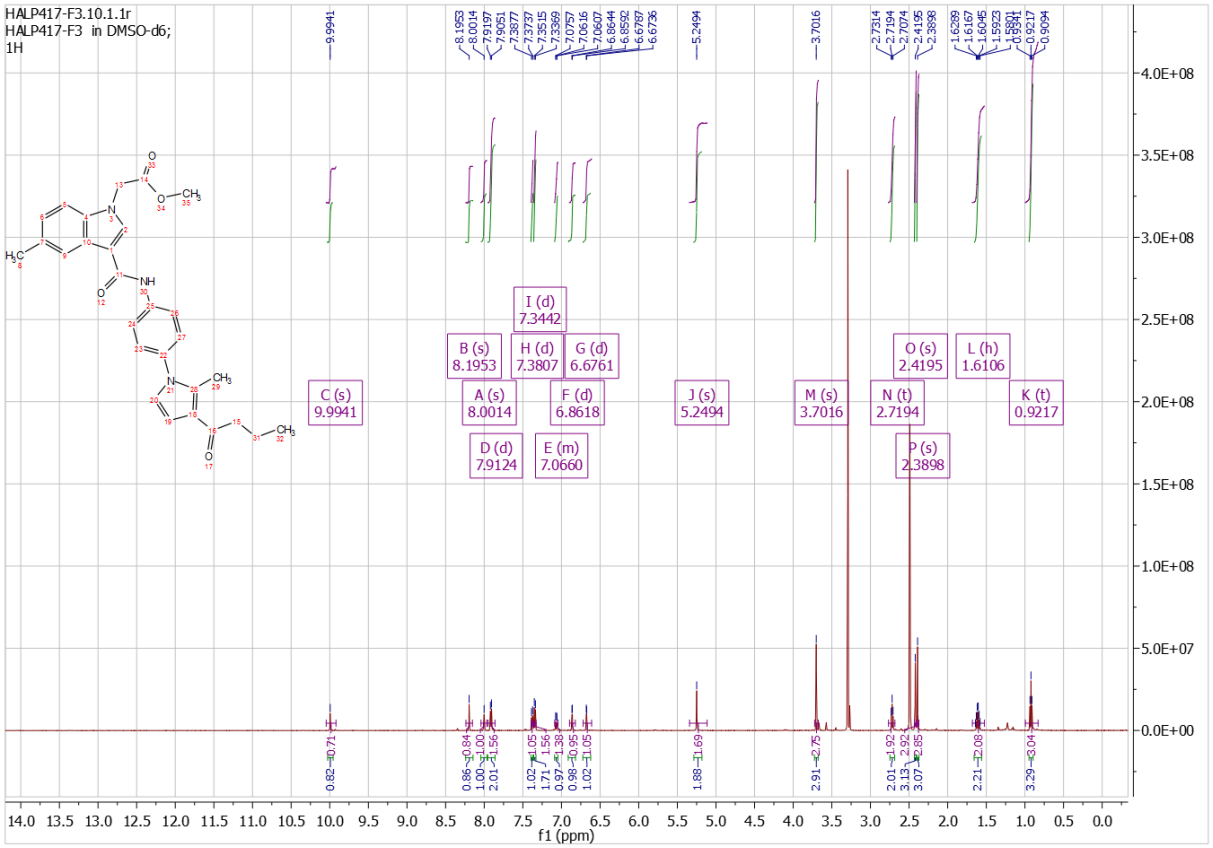
MS1 -TIC SCAN ESI Frag=135V Gain=1,0RT:8.27106222643826min (Subtracted)

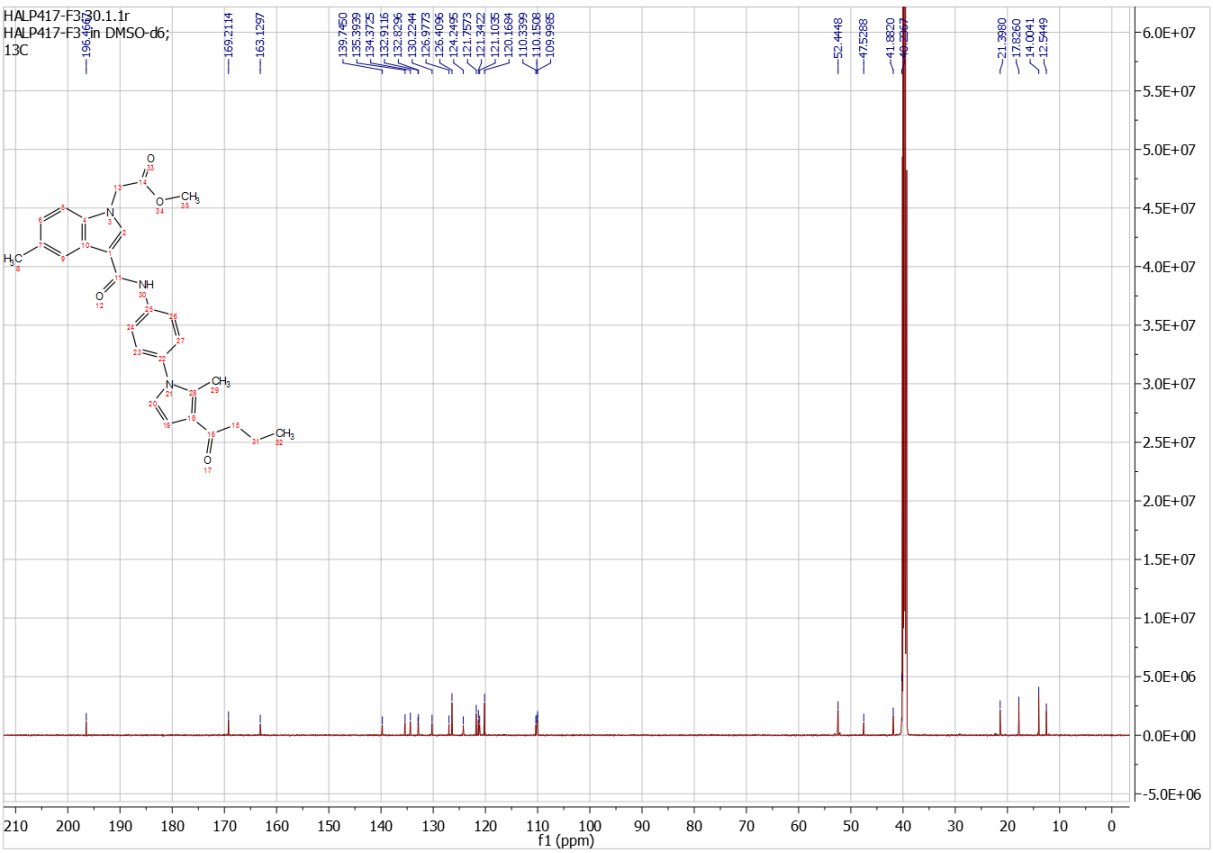


MS1 +TIC SCAN ESI Frag=135V Gain=1,0RT:8.28060223331101min (Subtracted)



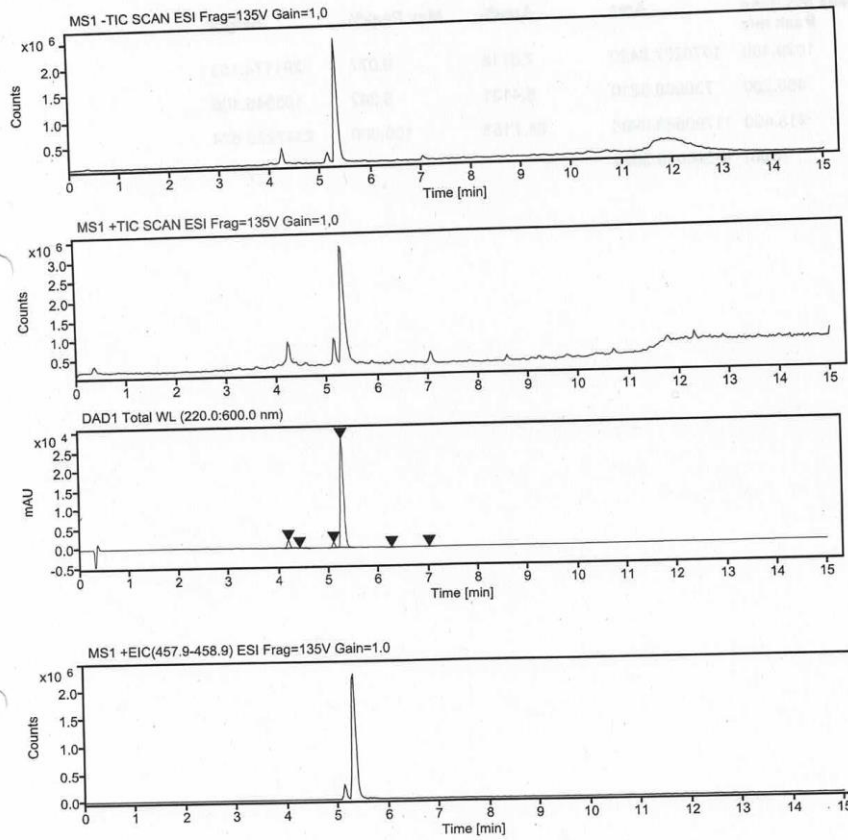
D:\CDSProjects\Default\0-standardplot+EIC.rdl [Rev. 11299] Printed: 2024-10-24 07:54:22+02:00 Page 2 of 2


HALP417-F3.10.1.1r
HALP417-F3 in DMSO-d6;
1H
C (s) 9.9941
B (s) 8.1953
A (s) 8.0014
D (d) 7.9124
I (d) 7.3442
H (d) 7.3807
E (m) 7.0660
G (d) 6.6761
F (d) 6.8618
J (s) 5.2494
M (s) 3.7016
O (s) 2.4195
N (t) 2.7194
P (s) 2.3898
L (h) 1.6106
K (t) 0.9217
f1 (ppm)


HALP417-F3c30.1.1r
HALP417-F3 in DMSO-d6;
13C
f1 (ppm)

2-(3-((4-(3-Butyryl-2-methyl-1*H*-pyrrol-1-yl)phenyl)carbamoyl)-5-methyl-1*H*-indol-1-yl)acetic acid (44)

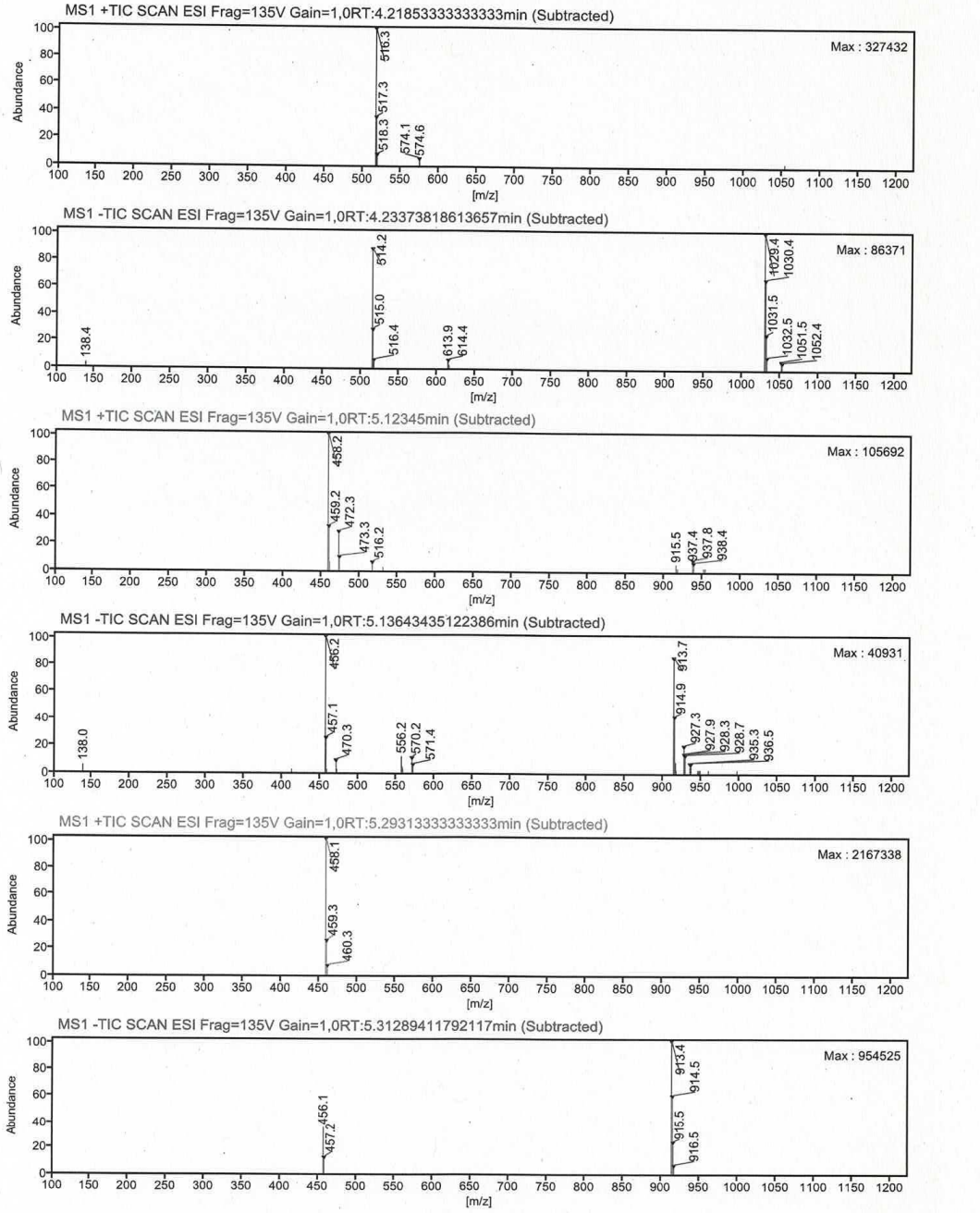
Sequence Name:	SingleSample	**Project Name:**	Single Quad
Data file:	HALP427.dx	**Operator :**	SYSTEM
Sample name:	HALP427	**Acquired on:**	2024-12-27 17:06:53+01:00
Instrument:	Single Quad	**Location:**	P1-B1
Inj. volume:	3.000		
Acq. method:	00-new_wasser-acn_standard_100-1500_BD-20min.amx		
Processing method:	MS_standard_plot.pmx		

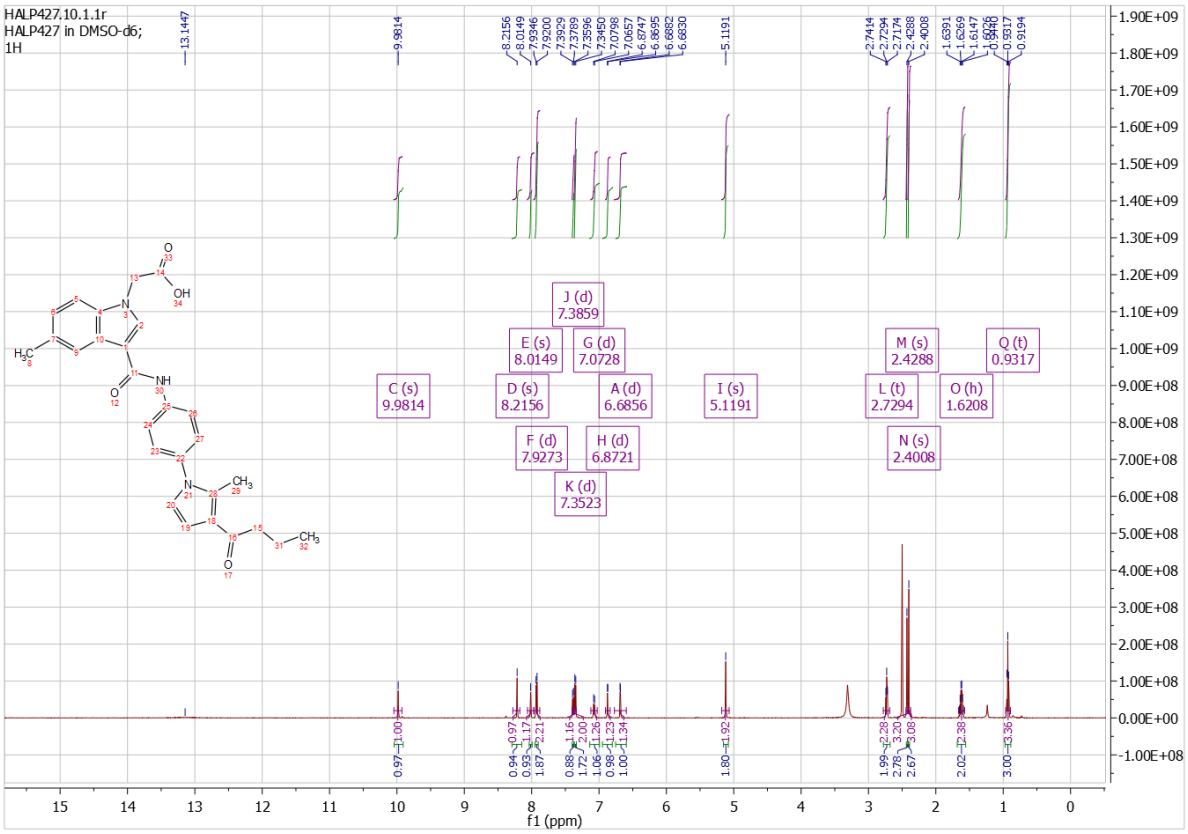


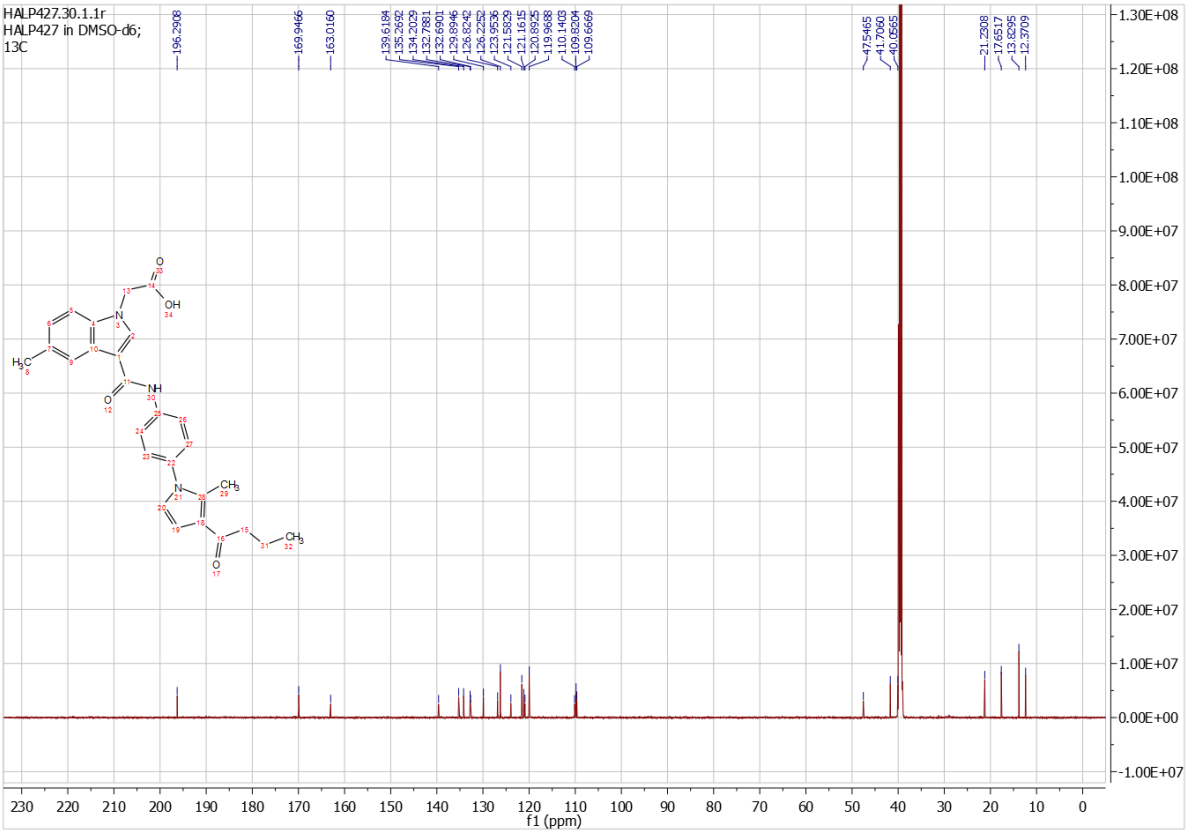
Signal: DAD1 Total WL (220.0:600.0 nm)

RT [min]	Peak MS Base Peak m/z	Area	Area%	Max Peak%	Height
4.197		7226.3545	5.1707	5.655	1939.593
4.419		3.5216	0.0025	0.003	51.178
5.101		4223.3262	3.0219	3.305	1356.833
5.278		127797.2092	91.4424	100.000	28019.237
6.267		107.7883	0.0771	0.084	30.791
7.018		398.8272	0.2854	0.312	90.960
	Sum	139757.0270			

D:\CDSProjects\Default\0-standardplot+EIC.rdl [Rev. 12194] Printed: 2025-01-02 12:25:39+01:00 Page 1 o


MS1 +TIC SCAN ESI Frag=135V Gain=1,0RT:4.21853333333333min (Subtracted)
Max : 327432
MS1 -TIC SCAN ESI Frag=135V Gain=1,0RT:4.23373818613657min (Subtracted)
Max : 86371
MS1 +TIC SCAN ESI Frag=135V Gain=1,0RT:5.12345min (Subtracted)
Max : 105692
MS1 -TIC SCAN ESI Frag=135V Gain=1,0RT:5.13643435122386min (Subtracted)
Max : 40931
MS1 +TIC SCAN ESI Frag=135V Gain=1,0RT:5.29313333333333min (Subtracted)
Max : 2167338
MS1 -TIC SCAN ESI Frag=135V Gain=1,0RT:5.31289411792117min (Subtracted)
Max : 954525
Abundance
[m/z]
D:\CDSProjects\Default\0-standardplot+EIC.rdl [Rev. 12194]
Printed: 2025-01-02 12:25:39+01:00
Page 3 of 3


HALP427.10.1.1r
HALP427 in DMSO-d6;
1H
C (s) 9.9814
J (d) 7.3859
E (s) 8.0149
G (d) 7.0728
D (s) 8.2156
A (d) 6.6856
I (s) 5.1191
M (s) 2.4288
Q (t) 0.9317
L (t) 2.7294
O (h) 1.6208
F (d) 7.9273
H (d) 6.8721
N (s) 2.4008
K (d) 7.3523
f1 (ppm)


HALP427.30.1.1r
HALP427 in DMSO-d6;
13C
f1 (ppm)

8 Acknowledgments

Whoever fails to show gratitude to people, has not truly shown gratitude to God

First and foremost, I would like to express my deepest gratitude to my supervisor, **Prof. Dr. Crista E. Müller**, for her outstanding scientific guidance, continuous support, and invaluable mentorship throughout my doctoral studies. Her encouragement, patience, and expertise have profoundly shaped my scientific growth and have been instrumental in the completion of this dissertation.

My sincere appreciation also goes to my second advisor, **Prof. Dr. Dirk Menche**, whose lectures in organic synthesis and analytical interpretation of NMR spectra have greatly deepened my understanding of chemical analysis and significantly supported the structural elucidation of my synthesized compounds.

I am deeply thankful to all my colleagues for their collaboration, assistance, and friendship. Their practical help and moral encouragement have enabled me to overcome the many challenges encountered during the experimental work and the revision of this dissertation. In particular, I would like to thank **Haneen Al-Hroub**, **Dr. Nader M. Boshta**, **Dr. Ahmed Elgokha**, **Angelo Oneto**, **Dr. Zahid Shafiq**, **Dr. Younis Baqi**, **Dr. Ahmed Temirak**, **Rasha Abu Shamleh**, and **Dr. Mahmud Rashid** for their dedication, teamwork, and scientific contributions.

Special recognition goes to our $P2Y_{12}$ receptor project team "PURImaging", including the working groups of **Dr. Alexandra Winkeler**, **Dr. Nadja Van Camp**, and **Dr. Bertrand Kuhnast** for their valuable collaboration, stimulating discussions, and productive exchange of ideas that greatly enriched this research.

I also wish to acknowledge all members of **Prof. Müller's research group**; whose commitment and collegiality created an inspiring and supportive working environment. My sincere thanks to our secretaries **Beate Ponatowski** and **Silke Hahn**, to our analytical experts **Marion Schneider**, **Christiane Bous**, **Sophie Kronisch**, and **Dr. Mariam Tahoun** for their assistance with LC/MS and NMR measurements, and to our safety and compound library authorizers **Dr. Ali El-Tayeb**, **Dr. Jörg Hockemeyer**, **Christin Vielmuth**, and **Nicole Florin** for ensuring a safe, organized, and efficient laboratory environment.

I am grateful to my colleagues who collaborated with me on side projects in both synthesis and biological testing, particularly **Dr. Andhika Mahardhika** for evaluating my synthesized GPR18 receptor ligands, **Dr. Jessica Nagel** for the cooperation in the P2X4 receptor project,

and **Dr. Filomena Perri** for our joint work on the synthesis of photoremovable protecting groups and caging molecules aimed at advancing antiepileptic drug development.

My thanks also go to my colleagues from the third-semester assistance group in the Organic Chemistry module for their cooperation and shared learning experiences that made this journey both productive and memorable.

I would also like to thank all my labmates, officemates, and students who carried out their practical courses or master's theses under my supervision. Their enthusiasm, curiosity, and contributions have enriched my research and teaching experience.

I gratefully acknowledge the generous financial and academic support provided by the **Saudi Ministry of Education**, the **Saudi Cultural Office**, and the **Embassy of the Kingdom of Saudi Arabia in Germany**, who made my doctoral studies possible through their scholarship program. I also extend my appreciation to the City of Bonn for their additional financial assistance and continuous support.

Finally, I wish to express my deepest gratitude to my family. To my father, for his unwavering encouragement and belief in me, and to my mother, whose sincere prayers and endless care have always accompanied me. My heartfelt thanks also go to my brothers and sister for their love, understanding, and shared support through every moment of this journey.

This dissertation is dedicated to my beloved family, whose love and presence remain the driving force behind all my efforts and achievements. At the heart of this family stands my beloved wife **Laila**, whose patience, resilience, and unwavering support have been my greatest source of strength throughout these years abroad. Her endurance through challenges and responsibilities has made this accomplishment possible.

My deepest love also goes to my courageous sons **Ali**, **Karrar**, and **Taj**, to my dear daughters **Fatimah** and **Zahra**, and to our youngest, **Mohammed**, whose arrival this year brought immense joy and a sense of completion to our family. May God bless and protect them all, grant them success in knowledge and virtue, and allow me the privilege of witnessing their continued growth and fulfillment in life.

To all who have contributed, directly or indirectly, to the success of this work - **thank you**.